LESSON BOOK



Near-Surface Wind Meteorology

Concepts, terminology and models for the wind between 10 and 150 metres

Thirty-one lessons · 701 pages

Ricardo Marquez, Ph.D.

ricardo-marquez.com

Near-Surface Wind Meteorology

Concepts, terminology and models for wind in the lowest part of the atmosphere

A lesson sequence, written up as a book

Ricardo Marquez

October 5, 2026 (work in progress: one chapter per lesson, added as the lessons proceed)

How to read this book

This book is about one question: why the wind at a given location, height and time is what it is. Each chapter expands one lesson of a sequence that answers it by following the wind downward,

large-scale forcing → boundary layer → surface layer → terrain and roughness → local flow → measured wind.

The heights of interest are those of engineering applications, from the 10 m of a weather station to the 150 m of a wind turbine: the heights at which a transmission line is cooled by the wind and a wind farm is driven by it.

The book is written for a reader who builds or uses wind models and wants the concepts and the vocabulary of meteorology stated precisely. Every new quantity is therefore introduced in the same order: its name, its physical meaning, its units, its equation, and how it is measured or modeled. Where the field uses a shorthand term, a *Jargon* box expands it once and the text then uses the expanded meaning. Every symbol is defined in the notation chapter that follows.

One distinction recurs in every chapter: what the atmosphere does, and what a model or an instrument represents of it. A weather model reports a wind for a grid cell several kilometers wide; an anemometer reports the wind at one point; neither is "the wind" without a statement of place, height, averaging time and scale. Statements that depend on the hemisphere are given for both. The numbers in the examples are illustrative, chosen to make each relation concrete.

Each chapter closes with a statement of what to retain, a table of its terms, and exercises.

Contents

How to read this book **ii**

Notation and vocabulary **x**

1 The atmosphere as a wind system **1**
1.1 The question and the framework . . . 1
1.2 Wind and its origin . . . 3
1.3 Pressure and the forces on air . . . 7
1.4 The layer near the surface . . . 11
1.5 Scales of atmospheric motion . . . 12
1.6 Model and measurement, forcing and response . . . 14
1.7 What to retain . . . 18
1.8 Exercises . . . 19

2 Pressure, geopotential and the pressure-gradient force **20**
2.1 Pressure and hydrostatic balance . . . 20
2.2 Pressure surfaces and geopotential . . . 24
2.3 Height gradients as pressure gradients . . . 26
2.4 Thickness and temperature . . . 29
2.5 Weather maps and their vocabulary . . . 32
2.6 Pressure field and near-surface wind . . . 35
2.7 What to retain . . . 37
2.8 Exercises . . . 37

3 Coriolis force and geostrophic wind **39**
3.1 The direction of large-scale wind . . . 39
3.2 The Coriolis force . . . 41
3.3 Geostrophic balance . . . 45
3.4 Computing the geostrophic wind . . . 49
3.5 Friction and the surface wind . . . 52
3.6 Geostrophic wind as forcing . . . 56
3.7 What to retain . . . 59
3.8 Exercises . . . 59

4 Gradient wind and curved flow **61**
4.1 From straight to curved flow . . . 61
4.2 The gradient wind balance . . . 63
4.3 Flow around lows and highs . . . 66
4.4 The limit on anticyclonic flow . . . 70
4.5 Vorticity . . . 73
4.6 Curvature at different scales . . . 76

4.7 What to retain . . . 80
4.8 Exercises . . . 80

5 Synoptic, mesoscale and microscale flow 83
5.1 Scale and the three ranges . . . 83
5.2 The synoptic scale and the mesoscale . . . 86
5.3 The microscale and terrain . . . 90
5.4 What a model resolves . . . 93
5.5 Kinds of model . . . 96
5.6 Dimensionless numbers and the scale of a wind value . . . 99
5.7 What to retain . . . 101
5.8 Exercises . . . 101

6 The atmospheric boundary layer 104
6.1 The layer that feels the surface . . . 104
6.2 The daily cycle and the convective layer . . . 107
6.3 The stable and residual layers . . . 110
6.4 Layers within the boundary layer . . . 112
6.5 Potential temperature and static stability . . . 116
6.6 Shear, turbulence and the wind profile . . . 120
6.7 What to retain . . . 124
6.8 Exercises . . . 124

7 The surface layer 127
7.1 The surface layer and its constant flux . . . 127
7.2 From stress to shear . . . 131
7.3 The logarithmic wind profile . . . 134
7.4 Roughness length and displacement height . . . 137
7.5 Fetch and internal boundary layers . . . 141
7.6 Stability and the limits of the theory . . . 144
7.7 What to retain . . . 147
7.8 Exercises . . . 148

8 Turbulence 149
8.1 Turbulence and turbulent transport . . . 149
8.2 Eddies and the energy cascade . . . 153
8.3 Turbulent kinetic energy and its budget . . . 157
8.4 Kinds of turbulence near the ground . . . 160
8.5 Turbulence statistics in engineering . . . 162
8.6 Turbulence in models . . . 165
8.7 What to retain . . . 169
8.8 Exercises . . . 171

9 Reynolds decomposition and turbulent fluxes 172
9.1 The decomposition of a measured record . . . 172
9.2 Covariance and the momentum flux . . . 175
9.3 Fluxes of heat and moisture . . . 180
9.4 Measuring fluxes by eddy covariance . . . 182
9.5 Averaging rules and the closure problem . . . 187
9.6 Correlation, quadrants and the wind profile . . . 190
9.7 What to retain . . . 194
9.8 Exercises . . . 194

10 Friction velocity **197**
10.1 Friction velocity as a velocity scale . . . 197
10.2 Friction velocity and the wind profile . . . 200
10.3 The drag coefficient . . . 203
10.4 Measuring and inferring friction velocity . . . 206
10.5 Scaling, similarity and limits . . . 209
10.6 The stress vector and calibration . . . 212
10.7 What to retain . . . 215
10.8 Exercises . . . 215

11 Aerodynamic roughness **217**
11.1 The roughness length as an aerodynamic property . . . 217
11.2 Roughness, the wind profile and the surface drag . . . 221
11.3 Displacement height and canopy layers . . . 223
11.4 Roughness by direction, fetch and time . . . 226
11.5 Roughness and terrain . . . 230
11.6 Estimating and using the roughness length . . . 231
11.7 What to retain . . . 235
11.8 Exercises . . . 235

12 The logarithmic wind profile **238**
12.1 The logarithmic profile and its origin . . . 238
12.2 Extrapolation between heights . . . 242
12.3 The power law . . . 244
12.4 Stability and the region of validity . . . 248
12.5 Failures of the profile and what they indicate . . . 250
12.6 The profile in models and practice . . . 254
12.7 What to retain . . . 257
12.8 Exercises . . . 257

13 Atmospheric stability **260**
13.1 Stability and the lapse rates . . . 260
13.2 Stability and potential temperature . . . 265
13.3 Stability and the wind profile . . . 267
13.4 The Richardson numbers . . . 270
13.5 Static and surface-layer stability . . . 273
13.6 Stability in space, time and models . . . 276
13.7 What to retain . . . 280
13.8 Exercises . . . 280

14 Monin–Obukhov similarity theory **283**
14.1 The similarity hypothesis . . . 283
14.2 The Obukhov length . . . 287
14.3 Dimensionless gradients . . . 290
14.4 Integrated profiles . . . 294
14.5 Use in a weather model . . . 298
14.6 Limits of the theory . . . 301
14.7 What to retain . . . 304
14.8 Exercises . . . 304

15 Obukhov length and the stability parameter **307**
15.1 Reading the Obukhov length . . . 307
15.2 The stability parameter at a height . . . 312
15.3 Stability and the wind profile . . . 315
15.4 Wind speed, heat flux and feedbacks . . . 318
15.5 Free convection and the whole boundary layer . . . 322
15.6 Stability in forecasts . . . 324
15.7 What to retain . . . 327
15.8 Exercises . . . 327

16 The daytime convective boundary layer **329**
16.1 Thermals and the mixed layer . . . 329
16.2 Growth and entrainment . . . 334
16.3 Velocity scales and flux profiles . . . 339
16.4 Convection and the near-surface wind . . . 342
16.5 Organized convection and local theory . . . 345
16.6 The surface beneath the convective layer . . . 348
16.7 What to retain . . . 351
16.8 Exercises . . . 351

17 The stable nocturnal boundary layer **354**
17.1 Formation and structure of the stable boundary layer . . . 354
17.2 Turbulence under stable stratification . . . 357
17.3 Regimes, collapse and bursts . . . 360
17.4 Wind above and across the stable layer . . . 365
17.5 Terrain at night . . . 369
17.6 Models, measurements and diagnosis . . . 371
17.7 What to retain . . . 373
17.8 Exercises . . . 375

18 Low-level jets **376**
18.1 The jet profile . . . 376
18.2 The nocturnal inertial jet . . . 379
18.3 The jet through the night and morning . . . 385
18.4 Other kinds of low-level jet . . . 387
18.5 Observing and detecting jets . . . 391
18.6 Consequences for applications . . . 394
18.7 What to retain . . . 396
18.8 Exercises . . . 398

19 Thermal circulations **399**
19.1 Differential heating as a source of wind . . . 399
19.2 Sea and land breezes . . . 403
19.3 Slope, valley and drainage winds . . . 409
19.4 Cities, convergence and density currents . . . 412
19.5 Large-scale flow and stability . . . 415
19.6 Climatology, models and diagnosis . . . 417
19.7 What to retain . . . 419
19.8 Exercises . . . 420

20 Terrain-induced flow **423**
20.1 Flow over a hill . . . 423
20.2 The magnitude of the speed-up . . . 427
20.3 Separation and sheltering . . . 430
20.4 Channeling, gap flow and exposure . . . 433
20.5 Stratified flow over terrain . . . 435
20.6 Terrain in models and practice . . . 438
20.7 What to retain . . . 441
20.8 Exercises . . . 441

21 Vegetation and urban canopies **444**
21.1 The canopy as a distributed momentum sink . . . 444
21.2 Wind in and above a canopy . . . 447
21.3 Vegetation canopies . . . 452
21.4 Urban canopies . . . 454
21.5 Representing canopies in models . . . 460
21.6 Canopies and wind measurements . . . 462
21.7 What to retain . . . 464
21.8 Exercises . . . 464

22 Wind measurements **466**
22.1 What a wind sensor reports . . . 466
22.2 In-situ wind instruments . . . 469
22.3 Sampling, response and averaging . . . 474
22.4 Mounting and flow distortion . . . 479
22.5 Wind profiling instruments . . . 481
22.6 Measurement errors and quality control . . . 484
22.7 What to retain . . . 490
22.8 Exercises . . . 490

23 Measurement height and exposure **493**
23.1 Height and the standard measurement . . . 493
23.2 Obstacles, fetch and footprint . . . 497
23.3 Terrain exposure . . . 501
23.4 Representativeness . . . 503
23.5 Comparing a station with a model . . . 506
23.6 Metadata, homogeneity and networks . . . 511
23.7 What to retain . . . 514
23.8 Exercises . . . 516

24 Wind statistics **517**
24.1 Means and variability of the wind . . . 517
24.2 Statistics of wind direction . . . 521
24.3 The distribution of wind speed . . . 523
24.4 Exceedance, quantiles and extremes . . . 527
24.5 Structure in time . . . 530
24.6 Verification of modeled wind . . . 535
24.7 What to retain . . . 538
24.8 Exercises . . . 538

25 Numerical weather prediction **541**
25.1 What a weather model solves . . . 541
25.2 The model grid . . . 544
25.3 The surface and the boundary layer . . . 549
25.4 Starting and bounding the forecast . . . 553
25.5 Interactions and limits . . . 557
25.6 Reading model wind . . . 559
25.7 What to retain . . . 562
25.8 Exercises . . . 562

26 Boundary-layer parameterizations **565**
26.1 The task of a boundary-layer scheme . . . 565
26.2 Orders of closure . . . 569
26.3 Convection and nonlocal schemes . . . 573
26.4 Stable boundary-layer closures . . . 578
26.5 The scheme inside the model . . . 581
26.6 Resolution and scale awareness . . . 584
26.7 What to retain . . . 588
26.8 Exercises . . . 588

27 Terrain and land-surface representation **591**
27.1 The effective surface of a grid cell . . . 591
27.2 Terrain in the model . . . 594
27.3 Land cover in the model . . . 599
27.4 Subgrid terrain . . . 603
27.5 The thermal state of the surface . . . 606
27.6 Consequences for validation and correction . . . 608
27.7 What to retain . . . 612
27.8 Exercises . . . 612

28 Statistical and dynamical downscaling **615**
28.1 The downscaling problem . . . 615
28.2 Simple statistical corrections . . . 617
28.3 Regression and model output statistics . . . 620
28.4 Machine-learning downscaling . . . 624
28.5 Dynamical and microscale downscaling . . . 628
28.6 Choosing and combining methods . . . 630
28.7 What to retain . . . 633
28.8 Exercises . . . 633

29 CFD and microscale wind modeling **636**
29.1 Computational fluid dynamics for local wind . . . 636
29.2 Reynolds-averaged models . . . 639
29.3 Large-eddy simulation . . . 643
29.4 Domain, boundary conditions and mesh . . . 646
29.5 Separation, stability and large-scale forcing . . . 650
29.6 From simulation to site prediction . . . 653
29.7 What to retain . . . 658
29.8 Exercises . . . 658

30 Building a defensible site wind model **661**
30.1 The site wind problem and its target 661
30.2 Physical hierarchy and atmospheric regime 665
30.3 Site characterization and observations 667
30.4 Baselines, predictors and model complexity 670
30.5 Validation and physical diagnosis 673
30.6 Uncertainty, decisions and the model report 677
30.7 What to retain 685
30.8 Exercises 686

Notation and vocabulary

Every symbol below has the same meaning in every chapter. SI units are used throughout; pressure is quoted in hectopascals ($1\,\mathrm{hPa} = 100\,\mathrm{Pa}$), as is usual in meteorology. Signs that depend on the hemisphere follow from the sign of the Coriolis parameter f, positive in the Northern Hemisphere and negative in the Southern.

Symbol	Unit	Meaning
x, y, z	m	Eastward, northward and upward coordinates; z is geometric height.
u, v, w	m/s	Eastward, northward and upward components of the air velocity.
$\mathbf{V}$	m/s	Horizontal wind vector, (u, v).
U	m/s	Horizontal wind speed, $\sqrt{u^2 + v^2}$.
U_{10}	m/s	Wind speed at 10 m above the ground.
β	degree	Wind direction: where the wind comes from, clockwise from true north; $u = -U\sin\beta$, $v = -U\cos\beta$.
$\mathbf{V}_g$, U_g	m/s	Geostrophic wind and its speed: the wind that balances the pressure-gradient and Coriolis forces.
U_{gr}	m/s	Gradient wind speed: the balanced wind on a curved path.
$\mathbf{V}_a$	m/s	Ageostrophic wind, $\mathbf{V} - \mathbf{V}_g$.
p	Pa, hPa	Atmospheric pressure.
p_{stn}, p_{msl}	Pa, hPa	Station pressure (measured at the instrument's elevation) and mean sea-level pressure (reduced to sea level).
ρ	kg/m^3	Air density.
T, T_v	K	Absolute temperature; virtual temperature, the temperature at which dry air has the density of the moist air.
$\overline{T_v}$	K	Mean virtual temperature of a layer between two pressure levels.
R_d	J/(kg K)	Specific gas constant of dry air, 287 J/(kg K).
g, g_0	m/s^2	Gravitational acceleration; its standard value 9.80665 m/s^2.
H	m	Pressure scale height, $R_d T/g$.
Φ	m^2/s^2	Geopotential: the work needed to raise a unit mass from sea level to height z.
Z	m	Geopotential height, Φ/g_0.
∇_h, ∇_p	1/m	Horizontal gradient at constant height; horizontal gradient along a constant-pressure surface.
Ω, $\boldsymbol{\Omega}$	rad/s	Rotation rate of the Earth, 7.292×10^{-5} rad/s, and its vector.

Symbol	Unit	Meaning
ϕ	degree, rad	Latitude, positive north of the equator.
f	1/s	Coriolis parameter, $2\Omega \sin\phi$.
$\mathbf{k}$	–	Unit vector pointing upward.
$\frac{\mathrm{D}}{\mathrm{D}t}$	1/s	Rate of change following an air parcel.
R	m	Radius of curvature of an air parcel's path.
ζ, η	1/s	Relative vorticity, $\partial v/\partial x - \partial u/\partial y$; absolute vorticity, $f + \zeta$.
L, H	m	Horizontal and vertical length scales of a flow feature. (The pressure scale height is written H.)
Δx	m	Grid spacing of a numerical model.
ν	m^2/s	Kinematic viscosity of air.
Ro	–	Rossby number, $U/(\lvert f\rvert L)$: inertia relative to the Coriolis force.
Re	–	Reynolds number, UL/ν: inertia relative to viscosity.
Ri	–	Richardson number: buoyancy relative to shear.
$\mathbf{a}_{\mathrm{PGF}}$, $\mathbf{a}_C$	$\mathrm{m/s}^2$	Pressure-gradient and Coriolis forces per unit mass (accelerations).
$\mathbf{F}$	$\mathrm{m/s}^2$	Friction force per unit mass: near the ground, the effect of turbulent momentum transfer.
α	degree	Angle between the surface wind and the isobars (Chapter 3); elsewhere a profile exponent or a slope angle, as stated.
K, δ	m^2/s, m	Eddy viscosity and Ekman length, $\delta = \sqrt{2K/\lvert f\rvert}$ (Chapter 3).
λ	1/s, m	Linear drag rate (Chapter 3); wavelength (Chapter 5).
$\mathbf{t}$, $\mathbf{n}$	–	Unit vectors along the flow and to its left (natural coordinates, Chapter 4).
Ro_R	–	Curvature Rossby number, $U_g/(\lvert f\rvert R)$.
$\mathcal{T}$	s	Time scale of a flow feature; the advective time is L/U.
θ, θ_v	K	Potential temperature, $T(p_0/p)^{R_d/c_p}$ with $p_0 = 1000\,\mathrm{hPa}$; virtual potential temperature.
c_p	J/(kg K)	Specific heat of air at constant pressure, 1004 J/(kg K).
z_i	m	Depth of the atmospheric boundary layer.
$\overline{a}$, a'	as a	Mean of a quantity a over the averaging period; its fluctuation, $a - \overline{a}$.
σ_u, σ_v, σ_w	m/s	Standard deviations of the along-wind, cross-wind and vertical velocity.
$\overline{u'w'}$, $\overline{v'w'}$	$\mathrm{m}^2/\mathrm{s}^2$	Kinematic vertical fluxes of along-wind and cross-wind momentum (covariances).
$\overline{w'\theta'}$, $\overline{w'T'}$	K m/s	Kinematic vertical heat flux, with potential temperature or temperature.
τ, τ_0	Pa	Turbulent shear stress, $-\rho\,\overline{u'w'}$ in along-wind coordinates; its value at the surface.
u_*	m/s	Friction velocity, $\sqrt{\tau_0/\rho}$: the velocity scale of the surface stress, not a wind speed.
w_*	m/s	Convective velocity scale, for buoyancy-driven turbulence.
κ	–	von Kármán constant, about 0.4.
l	m	Mixing length; near the ground $l = \kappa z$.

Symbol	Unit	Meaning
K_m, K_h	m^2/s	Eddy diffusivities for momentum and for heat: properties of the turbulence, not of the air.
z_0	m	Aerodynamic roughness length: the height at which the neutral logarithmic profile extrapolates to zero wind.
d, h_c	m	Zero-plane displacement height; height of the canopy or obstacles.
C_D	–	Drag coefficient, $\tau_0/(\rho U^2)$, for the wind at a stated height.
e	m^2/s^2	Turbulent kinetic energy per unit mass, $\frac{1}{2}(\overline{u'^2}+\overline{v'^2}+\overline{w'^2})$.
P_s, P_b, ε	m^2/s^3	Shear production, buoyancy production and dissipation rate of turbulent kinetic energy.
TI	–	Turbulence intensity, the standard deviation of wind speed divided by its mean.
H, LE	W/m^2	From Chapter 8 on: sensible and latent heat flux.
q, L_v	kg/kg, J/kg	Specific humidity; latent heat of vaporization of water.
r_{uw}	–	Correlation coefficient of the along-wind and vertical fluctuations, $\overline{u'w'}/(\sigma_u\sigma_w)$.
N	1/s	Buoyancy (Brunt–Väisälä) frequency, $N^2=(g/\theta)\,\mathrm{d}\theta/\mathrm{d}z$.
T_I	s	Inertial period, $2\pi/\lvert f\rvert$.
z_{jet}, U_{jet}	m, m/s	Height and wind speed of the core of a low-level jet.
B	–	Bowen ratio, H/LE: sensible over latent heat flux at the surface.
Fr	–	Froude number of stratified flow over terrain, $U/(Nh_m)$.
h_m, L_h	m	Height of a hill or mountain; its half-width, the horizontal distance from the crest to half the height.
S	–	Speed-up factor: wind at a point over terrain divided by the reference wind at the same height above ground upstream.
a, LAI, λ_f	1/m, –, –	Frontal area density of a canopy; leaf area index; frontal area index (frontal area of the obstacles per unit ground area).
G	–	Gust factor: gust speed divided by the mean speed of the same period.
f_s, f_N	Hz	Sampling frequency; Nyquist frequency, $f_s/2$.
c, k	m/s, –	Scale and shape parameters of the Weibull distribution of wind speed (in Chapter 24).
$\mathcal{T}_u$, Λ_u	s, m	Integral time scale and integral length scale of the along-wind turbulence.
RMSE, MAE	as the variable	Root-mean-square error and mean absolute error of a prediction.
ν_t	m^2/s	Eddy viscosity of a turbulence model (in Chapter 29; elsewhere K_m).
Ri_f	–	Flux Richardson number: buoyancy destruction of turbulent kinetic energy divided by its shear production.
$E(k)$, k	m^3/s^2, rad/m	Energy spectrum of turbulence and wavenumber.
η_K	m	Kolmogorov length, $(\nu^3/\varepsilon)^{1/4}$: the size of the smallest eddies.

Symbol	Unit	Meaning
L_{O}	m	Obukhov length, $-u_*^3\,\overline{\theta_v}/(\kappa\, g\,\overline{w'\theta_v'})$: the height scale at which buoyancy becomes as important as shear in producing or destroying turbulence. Negative in unstable, positive in stable conditions.
z/L_{O}	–	Stability parameter of the surface layer at height z (written ζ in much of the literature; this book keeps ζ for vorticity).
θ_*	K	Surface-layer temperature scale, $-\overline{w'\theta'}/u_*$.
ϕ_m, ϕ_h	–	Dimensionless wind shear, $(\kappa z/u_*)\,\partial U/\partial z$, and dimensionless potential-temperature gradient; functions of z/L_{O}, equal to one in neutral conditions.
ψ_m, ψ_h	–	Integrated stability corrections to the wind and temperature profiles.
Pr_t	–	Turbulent Prandtl number, K_m/K_h.
Γ_e, Γ_d	K/m	Environmental lapse rate, $-\partial T/\partial z$; dry adiabatic lapse rate, g/c_p.
Ri_g, Ri_B, Ri_c	–	Gradient and bulk Richardson numbers; critical value, about 0.25.
α, z_r	–, m	Exponent and reference height of the power-law wind profile, $U(z) = U(z_r)(z/z_r)^{\alpha}$.
α_c	–	Charnock parameter, in the roughness length of a water surface, $z_0 = \alpha_c\, u_*^2/g$.
δ	m	Also, in Chapter 7, the height of an internal boundary layer.

Vocabulary

Wind The motion of air relative to the Earth's surface; unless stated otherwise, its horizontal part.

Wind direction The direction the wind blows *from*: a southwesterly wind blows from the southwest toward the northeast.

Forcing and response A forcing is a physical driver imposed on the flow, such as a large-scale pressure gradient; the response is what the atmosphere does with it, which depends on friction, stability and terrain.

Free atmosphere The atmosphere above the layer that is directly influenced by the surface.

Atmospheric boundary layer (ABL) The part of the atmosphere that responds to the surface within about an hour or less.

Synoptic, mesoscale, microscale The three scale ranges of atmospheric motion: weather systems of about a thousand kilometers, circulations of one to a few hundred kilometers, and local flow below about one kilometer.

Resolved, parameterized A process a model's grid represents explicitly, against a process whose average effect the model computes from a formula.

Grid-cell value, point value The value a model reports for a whole grid cell, against the value an instrument measures at one place.

Measured, calculated, inferred A sensor reading; a quantity computed from readings by a known relation; a conclusion about a quantity that was not observed.

Chapter 1

The Atmosphere as a Wind System

1.1 The question and the framework

Every wind model, from a weather model with a grid of kilometers to the correction applied to a single anemometer, rests on a picture of why air moves. This chapter draws that picture in outline. Its question is

what causes wind, and why is the wind measured near the ground not simply the wind that the large-scale weather would produce?

The short answer is a chain of causes. The Sun heats the Earth unequally; unequal heating produces differences of air density; density differences produce differences of pressure; pressure differences accelerate the air; and the accelerated air is the wind. Wind is the atmosphere continuously working to remove pressure differences that unequal heating continuously creates. Near the surface, the result of that chain is then modified strongly by the rotation of the Earth, by friction against the ground, by turbulence, by terrain and by the stability of the air, which is whether vertical motions are damped or amplified by buoyancy. The rest of the chapter states each link of the chain once, with the depth needed to see the whole; Chapters 2 to 5 develop the first links in detail.

Jargon: free atmosphere, geostrophic forcing, stability, friction velocity, roughness length, roughness sublayer, fetch, nocturnal jet, parameterization

The *free atmosphere* is the atmosphere above the layer directly influenced by the surface (Section 1.4). *Geostrophic forcing* is the large-scale horizontal pressure gradient, expressed by the speed of the wind that would balance it against the Coriolis force, the geostrophic wind U_g in m/s (Chapter 3). *Stability* describes whether a parcel of air displaced vertically is pushed back (stable), left in place (neutral) or pushed further (unstable) by buoyancy; it is dimensionless in its usual measures and is treated in Chapter 13. The *friction velocity* u_*, in m/s, is a velocity scale built from the turbulent stress the surface exerts on the air, about a tenth of the mean wind near the ground over land. The *roughness length* z_0, in meters, is the height scale that characterizes how strongly a surface slows the wind; it ranges from about 10^{-4} m over calm water to about 1 m over forests and cities. The *roughness sublayer* is the layer within a few obstacle heights of the ground where the flow is dominated by individual trees and buildings. The *fetch* is the upstream distance over which the surface has been uniform, which sets how well the flow at a sensor has adjusted to that surface. A *nocturnal jet* (low-level jet) is a wind maximum a few hundred meters above the ground that forms at night when the air near the surface is stable. A *parameterization* is a formula with which a model computes the average effect of a process it cannot resolve on its grid, such as the turbulence of the boundary layer. Each of these terms receives its full treatment in a later chapter; they are named here because the framework below refers to them.

Key idea

Wind is the atmosphere's response to pressure differences created by unequal heating, turned by the Earth's rotation and slowed by friction; the wind measured at a point near the ground is the last link of a chain of transformations that starts in the large-scale pressure field and passes through the boundary layer, the surface and the terrain.

1.1.1 The organizing question

The question that organizes this book is: why is the wind at a given location, height and time what it is? The answer is built by following the wind downward through a sequence of layers and processes,

$$\text{synoptic forcing} \rightarrow \text{boundary layer} \rightarrow \text{surface layer} \rightarrow \text{terrain and roughness} \rightarrow \text{local flow} \rightarrow \text{measured wind},$$

in which each step receives the wind produced by the step above and transforms it. The first step is the large-scale pressure field of weather maps; the last is the reading of an instrument at a stated height above a particular piece of ground. The same decomposition can be written as a list of contributions,

$$\text{large-scale forcing} + \text{boundary-layer state} + \text{surface properties} + \text{terrain} + \text{local obstacles} = \text{local wind},$$

where the plus signs mean that each item contributes, not that the contributions add arithmetically. They do not: a rough surface reduces the wind by a fraction that depends on the stability, and a ridge accelerates whatever wind arrives at it. The precise statement is the functional relation of Section 1.5.1.

Every new quantity in the book is introduced in the same order: its name, its physical meaning, its units, its equation, and how it is measured or modeled. A second rule runs through every chapter: what the atmosphere does is kept apart from what a model or an instrument represents of it. Real turbulence is not the same object as a boundary-layer parameterization,

which is a formula for the average effect of that turbulence on a model grid. Real terrain is not the same object as the terrain of a model grid cell, which is an average elevation over several square kilometers. A wind value is therefore incomplete without a statement of where it applies, at what height, over what averaging time and at what spatial scale.

1.1.2 One anemometer reading

The framework is used by asking a fixed set of questions of every wind value. Take an illustrative anemometer at 20 m above the ground that reads $7\,\mathrm{m\,s^{-1}}$. Read through the framework, the reading raises these questions, from the top of the chain to the bottom:

- What is the geostrophic forcing, the wind that the large-scale pressure gradient would drive in the absence of friction?
- What is the stability of the boundary layer, and how deep is the boundary layer at this hour?
- What are the friction velocity u_* and the roughness length z_0 of the upstream surface?
- Is 20 m inside the roughness sublayer of nearby trees or buildings?
- How long and how uniform is the upstream fetch?
- Is the sensor on a slope or a crest where the terrain accelerates the flow?
- Is there a nocturnal jet above the sensor that the boundary layer may at times mix downward?
- Does the weather model used for comparison resolve any of these features, or does it represent them only through parameterizations and grid-cell averages?

None of these questions has the same answer at noon and at midnight, or over a forest and over a lake, and each of them changes how the $7\,\mathrm{m\,s^{-1}}$ should be interpreted and transferred to another height or another place.

The applications that motivate the book are all of this kind. A transmission line is cooled by the wind that crosses its conductors at heights of 10 to 50 m, so the current it can carry safely, its dynamic line rating, depends on the speed and direction of the wind along every span. A wind turbine is driven by the wind at 80 to 150 m. A sensor network is only as useful as the siting of its instruments, and the flow over hills and valleys decides whether a measurement at one place says anything about another. In each case the wind of interest is near-surface engineering wind, and in each case the large-scale weather is necessary but not sufficient to know it.

1.2 Wind and its origin

This section defines wind as a vector, with the convention used to report its direction, and follows the first links of the causal chain: unequal heating, the density differences it produces through the ideal gas law, and the way temperature acts on the wind only through pressure.

1.2.1 Wind as air in motion

Wind is the motion of air relative to the Earth's surface. At a point it is a velocity, a vector with three components, (u, v, w), in meters per second: u is the eastward component (positive toward the east, negative toward the west), v the northward component (positive toward the north), and w the upward component. The horizontal wind vector is

$$\mathbf{V} = (u, v), \tag{1.1}$$

and the horizontal wind speed is its magnitude,

$$U = |\mathbf{V}| = \sqrt{u^2 + v^2}. \tag{1.2}$$

Near the surface, the vertical velocity averaged over minutes is usually much smaller than the horizontal components, $|w| \ll |u|, |v|$; vertical velocities of weather systems are of the order of centimeters per second against horizontal winds of meters per second. For this reason "wind" means the horizontal motion unless stated otherwise. The instantaneous turbulent fluctuations of w near the ground are not small, often tenths of a meter per second and more in daytime convection, and they carry momentum and heat vertically; Chapters 8 and 9 treat them.

Direction. Meteorology reports wind direction as the direction the wind blows *from*, measured in degrees clockwise from true north. Writing β for that direction, a north wind ($\beta = 0°$ or $360°$) blows from the north toward the south, an east wind ($\beta = 90°$) from the east, and a southwesterly ($\beta = 225°$) from the southwest toward the northeast. The components follow from the speed and direction as

$$u = -U \sin\beta, \qquad v = -U \cos\beta, \tag{1.3}$$

where the minus signs express that the air moves toward the direction opposite to β. Inverting, β is the angle whose sine is proportional to $-u$ and whose cosine is proportional to $-v$, computed as the two-argument arctangent $\beta = \operatorname{atan2}(-u, -v)$ and mapped to $[0°, 360°)$; it is undefined in calm air, $U = 0$. For an illustrative southwesterly of $U = 10\,\mathrm{m\,s^{-1}}$,

$$u = -10 \sin 225° = -10 \times (-0.7071) = +7.07\,\mathrm{m\,s^{-1}}, \qquad v = -10 \cos 225° = +7.07\,\mathrm{m\,s^{-1}},$$

both positive because the air moves toward the northeast.

Figure 1.1 draws this example. The circle is a compass seen from above, with north at the top and east to the right. The thick arrow is the wind vector of the southwesterly; the two thin arrows are its eastward component u and northward component v; the arc measures the direction β clockwise from north to the side the wind comes from. The arrow points away from the direction it is named after, which is the usual source of sign errors when converting between components and directions.

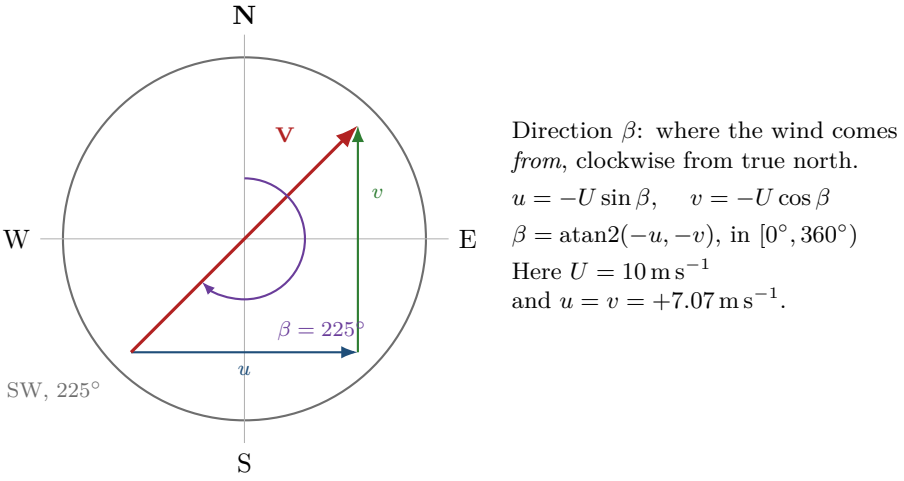


Figure 1.1: Components and direction of an illustrative southwesterly wind of $10\,\mathrm{m\,s^{-1}}$, seen from above, north at the top. The vector points toward the northeast; the direction $\beta = 225°$ names the southwest, where the wind comes from (equation (1.3)).

Measurement and modeling. A cup anemometer measures the speed U and a wind vane the direction β; a sonic anemometer measures the three components u, v and w directly, many times a second. A weather model carries u and v as variables at every grid point and level;

some models report them relative to the axes of their map projection, which then differ from east and north and must be rotated before equation (1.3) is applied. A direction measured with a magnetic compass must also be corrected to true north.

1.2.2 Unequal solar heating

The energy that drives the wind comes from the Sun, and the Sun does not heat the Earth evenly. The heating at a place depends on its latitude, which sets the angle of the sunlight; on the season and the time of day; on cloud cover; on the type of surface, since dark soil absorbs more than snow and a wet surface spends energy on evaporation that a dry one turns into heat; on soil moisture and vegetation; on elevation; and on whether the surface is ocean or land. Water heats and cools slowly because it mixes the absorbed energy through a deep layer and has a large heat capacity; land heats and cools quickly because only a thin layer takes part. A coast on a sunny afternoon therefore has warm air over the land beside cooler air over the sea, and a mountain slope in sunlight has warm air beside cooler air at the same height over the valley.

These differences act on every scale. Between the equator and the poles they drive the large-scale circulation and its weather systems; between land and sea they drive sea breezes; between a sunlit slope and the free air beside it they drive slope winds. In each case the heating is the original cause, but it is not the force that moves the air. The next two subsections follow how a difference of temperature becomes a force.

1.2.3 The ideal gas law and air density

Air behaves very nearly as an ideal gas, whose pressure, density and temperature are related by

$$p = \rho\, R_d\, T \qquad \Longleftrightarrow \qquad \rho = \frac{p}{R_d\, T}, \tag{1.4}$$

where p is the pressure in pascals, ρ the density in kilograms per cubic meter, T the absolute temperature in kelvin, and $R_d = 287\ \mathrm{J/(kg\,K)}$ the specific gas constant of dry air. Moist air is slightly less dense than dry air at the same pressure and temperature; Chapter 2 accounts for this with the virtual temperature, and here the dry form is enough. Equation (1.4) says that at equal pressure, warmer air is less dense: density is inversely proportional to absolute temperature.

For a worked example, take air at the standard sea-level pressure $p = 1013.25\,\mathrm{hPa} = 101\,325\,\mathrm{Pa}$. At $T = 15^\circ\mathrm{C} = 288.15\,\mathrm{K}$,

$$\rho = \frac{101\,325\,\mathrm{Pa}}{287\,\mathrm{J/(kg\,K)} \times 288.15\,\mathrm{K}} = \frac{101\,325}{82\,699} = 1.225\,\mathrm{kg/m^3}.$$

At $T = 35^\circ\mathrm{C} = 308.15\,\mathrm{K}$ and the same pressure, $\rho = 101\,325/(287 \times 308.15) = 101\,325/88\,439 = 1.146\,\mathrm{kg/m^3}$. The ratio of the two densities is $288.15/308.15 = 0.935$: a warming of 20 K makes the air 6.5 % less dense. A difference of this size between neighboring columns of air is ordinary over a sunny coast or a heated slope. Air temperature is measured by shielded thermometers; pressure by barometers; density is almost never measured directly but calculated from the two with equation (1.4).

1.2.4 Temperature acts through pressure

A temperature difference does not push air sideways. There is no horizontal force proportional to temperature in the equation of motion (Section 1.3); the only horizontal forces are pressure forces, the Coriolis force and friction. Temperature differences create wind indirectly, by changing how pressure is distributed in the vertical. The chain is

unequal heating → density differences → pressure differences → acceleration of the air → wind.

The middle link works as follows. Pressure decreases with height because it is the weight of the air above (Section 1.3.1), and it decreases more slowly in a column of less dense, warmer air. For an idealized column at a uniform temperature, the hydrostatic balance of Section 1.3.2 combined with equation (1.4) gives $\mathrm{d}p/p = -g\,\mathrm{d}z/(R_d T)$, and integrating from the ground, where $p = p_0$,

$$p(z) = p_0\, e^{-z/H}, \qquad H = \frac{R_d\, T}{g}, \tag{1.5}$$

where H is the pressure scale height, the height over which the pressure falls by a factor e; Chapter 2 develops this relation. Take two illustrative columns with the same surface pressure $p_0 = 1000\,\mathrm{hPa}$, a cold one at 10°C (283.15 K, $H = 287 \times 283.15/9.81 = 8284\,\mathrm{m}$) and a warm one at 20°C (293.15 K, $H = 8576\,\mathrm{m}$). At $z = 1000\,\mathrm{m}$,

$$p_{\mathrm{cold}} = 1000\, e^{-1000/8284} = 886.3\,\mathrm{hPa}, \qquad p_{\mathrm{warm}} = 1000\, e^{-1000/8576} = 889.9\,\mathrm{hPa}.$$

At the same height, the pressure over the warm column is 3.7 hPa higher than over the cold one, although the two surface pressures are equal. Equivalently, each pressure level lies higher in the warm column: the 900 hPa level is at 873 m in the cold column and at 904 m in the warm one.

Figure 1.2 draws the two columns in a vertical cross section. The horizontal axis is distance, with the cold column on the left and the warm column on the right; the vertical axis is height. The gray lines are levels of equal pressure, which rise from the cold to the warm column, with their vertical displacement exaggerated so that it is visible. At a fixed height above the ground the pressure is higher over the warm column, so the horizontal pressure difference aloft pushes air from the warm column toward the cold one (upper arrow). As air leaves the warm column aloft, the mass above its surface decreases and its surface pressure falls; the cold column gains mass and its surface pressure rises. The surface pressure difference then drives air near the ground from the cold side toward the warm side (lower arrow), and the circulation closes with rising air over the warm surface and sinking air over the cold one. This is the mechanism of the sea breeze, in which the cold column is over the sea and the warm one over the land. Temperature set up the circulation, but every arrow in the figure is driven by a pressure difference.

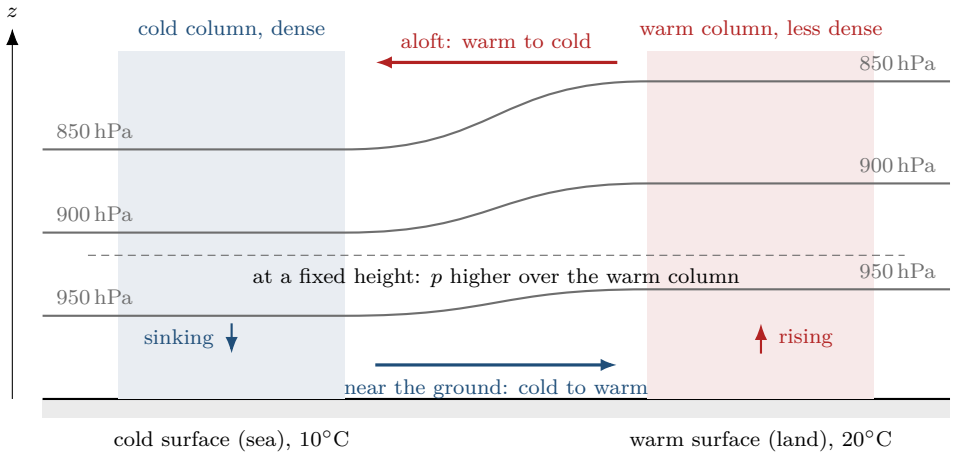


Figure 1.2: Vertical cross section of a cold and a warm column of air with equal surface pressure (schematic; vertical displacements of the pressure levels exaggerated). Gray lines: levels of equal pressure, higher in the warm column because pressure falls more slowly with height in less dense air. For uniform temperatures of 10 and 20°C and $p_0 = 1000\,\mathrm{hPa}$, equation (1.5) places the 900 hPa level at 873 and 904 m. Arrows: the circulation the resulting pressure differences drive.

1.3 Pressure and the forces on air

This section states what pressure is, writes the vertical balance that nearly always holds, derives the horizontal force that pressure differences exert, introduces the Coriolis force in outline, and assembles the three horizontal forces into one equation with the size of each term.

1.3.1 Pressure as the weight of the air above

Pressure is force per unit area, in pascals ($1\,\mathrm{Pa} = 1\,\mathrm{N/m^2}$); meteorology quotes it in hectopascals, $1\,\mathrm{hPa} = 100\,\mathrm{Pa}$. At any level in the atmosphere at rest, the pressure is very nearly the weight of the column of air above a unit area at that level. At sea level the standard pressure is $1013.25\,\mathrm{hPa} = 101\,325\,\mathrm{Pa}$, so the air above each square meter of sea surface has a mass of about

$$\frac{101\,325\,\mathrm{N/m^2}}{9.81\,\mathrm{m/s^2}} = 10\,330\,\mathrm{kg/m^2},$$

roughly ten metric tons per square meter. Going up, less air remains above, and the pressure decreases: by about half at 5.5 km, where the 500 hPa level is usually found.

Although pressure arises from the weight of the air above, it acts equally in all directions at a point: a small surface placed vertically feels the same pressure as one placed horizontally. This is why a pressure difference between two places at the same height exerts a horizontal force, even though the weight that produces the pressure acts vertically. Pressure is measured with barometers at stations (station pressure) and is reduced to a common reference, mean sea level, before horizontal comparisons are made; Chapter 2 treats that reduction.

1.3.2 Hydrostatic balance

Consider a thin horizontal slab of air of area A, between the heights z and $z + \mathrm{d}z$. Three vertical forces act on it: the pressure from below pushes up with $p(z)\,A$; the pressure from above pushes down with $p(z + \mathrm{d}z)\,A$; and gravity pulls the slab's mass $\rho A\,\mathrm{d}z$ down with the force $\rho g A\,\mathrm{d}z$. If the slab is not accelerating vertically, the three forces sum to zero,

$$p(z)\,A - p(z + \mathrm{d}z)\,A - \rho g A\,\mathrm{d}z = 0.$$

With $p(z + \mathrm{d}z) = p(z) + (\partial p/\partial z)\,\mathrm{d}z$, dividing by $A\,\mathrm{d}z$ gives

$$\frac{\partial p}{\partial z} = -\rho\, g, \tag{1.6}$$

the *hydrostatic balance*: the vertical pressure gradient balances gravity. Since ρ and g are positive, pressure decreases upward. Integrating equation (1.6) from a level z to the top of the atmosphere, where the pressure vanishes, gives $p(z) = \int_z^\infty \rho g\,\mathrm{d}z'$, which is exactly the weight per unit area of the air above z, the statement of Section 1.3.1.

Near sea level, with $\rho = 1.225\,\mathrm{kg/m^3}$ and $g = 9.81\,\mathrm{m/s^2}$, the pressure falls at

$$\rho g = 1.225 \times 9.81 = 12.0\,\mathrm{Pa/m}, \qquad \text{that is} \qquad 12.0 \times 100\,\mathrm{m} = 1202\,\mathrm{Pa} \approx 12\,\mathrm{hPa\ per\ 100\,m},$$

or about 1 hPa for every 8 m of ascent. (Over 100 m the density changes by about 1 %, so treating it as constant is accurate here.) A barometer carried from the base to the top of a 100 m tower reads about 12 hPa less at the top, which is three times the horizontal pressure difference across 100 km in a strong weather system (Section 1.3.3). The vertical pressure gradient is therefore thousands of times larger than the horizontal one, but it is almost exactly balanced by gravity, while the much smaller horizontal gradient is balanced by nothing of comparable size except the Coriolis force and friction. The atmosphere is usually very close to

hydrostatic balance; the balance fails in strong small-scale vertical motions, such as the updrafts of thunderstorms, and Chapter 2 builds on it.

Figure 1.3 shows the slab on the left. The box is the slab, between the heights z and $z + \mathrm{d}z$; the arrows on its lower and upper faces are the pressure forces, and the arrow from its center is its weight. In hydrostatic balance the upward arrow equals the sum of the two downward ones.

1.3.3 The pressure-gradient force

The same reasoning applied horizontally gives the force that starts the wind. Take a small box of air with sides $\mathrm{d}x$, $\mathrm{d}y$, $\mathrm{d}z$, and let the pressure vary in the x direction. The face at x is pushed in the $+x$ direction with the force $p(x)\,\mathrm{d}y\,\mathrm{d}z$; the face at $x + \mathrm{d}x$ is pushed in the $-x$ direction with $p(x + \mathrm{d}x)\,\mathrm{d}y\,\mathrm{d}z$. The net force in x is

$$\big[p(x) - p(x + \mathrm{d}x)\big]\,\mathrm{d}y\,\mathrm{d}z = -\frac{\partial p}{\partial x}\,\mathrm{d}x\,\mathrm{d}y\,\mathrm{d}z,$$

and dividing by the box's mass $\rho\,\mathrm{d}x\,\mathrm{d}y\,\mathrm{d}z$ gives the force per unit mass, an acceleration, $-(1/\rho)\,\partial p/\partial x$. Doing the same in y and collecting the two horizontal components,

$$\mathbf{a}_{\mathrm{PGF}} = -\frac{1}{\rho}\,\nabla_h p, \qquad \nabla_h p = \left(\frac{\partial p}{\partial x}, \frac{\partial p}{\partial y}\right), \tag{1.7}$$

the *pressure-gradient force* per unit mass, in $\mathrm{m/s^2}$. The gradient $\nabla_h p$ points toward increasing pressure, so the minus sign makes the force point toward decreasing pressure: from high to low pressure, perpendicular to the isobars (lines of equal pressure on a map), and stronger where the isobars are closer together. The right panel of Figure 1.3 draws the box with its two pressure forces; the higher pressure on the left face wins and the net force points to the right, toward the lower pressure. The pressure-gradient force is the first force of wind generation: without a horizontal pressure difference, air at rest stays at rest.

For an illustrative strong gradient of 4 hPa per 100 km and $\rho = 1.2\,\mathrm{kg/m^3}$,

$$|\nabla_h p| = \frac{400\,\mathrm{Pa}}{100\,000\,\mathrm{m}} = 4 \times 10^{-3}\,\mathrm{Pa/m}, \qquad |\mathbf{a}_{\mathrm{PGF}}| = \frac{4 \times 10^{-3}}{1.2} = 3.3 \times 10^{-3}\,\mathrm{m/s^2}.$$

Gradients of this size occur around vigorous storms; around 1 hPa per 100 km, giving $8 \times 10^{-4}\,\mathrm{m/s^2}$, is more common in midlatitude weather. The acceleration looks small, but acting alone on air initially at rest it would produce $3.3 \times 10^{-3} \times 3600 = 12\,\mathrm{m\,s^{-1}}$ after one hour and $72\,\mathrm{m\,s^{-1}}$ after six hours. Winds near the ground do not grow like this, because two other forces intervene: the Coriolis force turns the moving air, and friction slows it. The gradient is computed, not measured directly: it is the difference between barometer readings reduced to a common level, divided by their distance, or it is read from the analyzed pressure field of a weather model.

1.3.4 The Coriolis force

The wind is described in a frame of reference that rotates with the Earth, because that is the frame of every anemometer and every weather map. In a rotating frame, Newton's second law holds only if apparent forces are added. One of them, the centrifugal force, is folded into the observed gravity g. The other is the *Coriolis force*, which per unit mass is

$$\mathbf{a}_{\mathrm{C}} = -2\,\boldsymbol{\Omega} \times \mathbf{u}, \tag{1.8}$$

where $\boldsymbol{\Omega}$ is the Earth's rotation vector, of magnitude $\Omega = 7.292 \times 10^{-5}$ rad/s and pointing along the axis toward the North Pole, and $\mathbf{u} = (u, v, w)$ is the three-dimensional velocity relative to

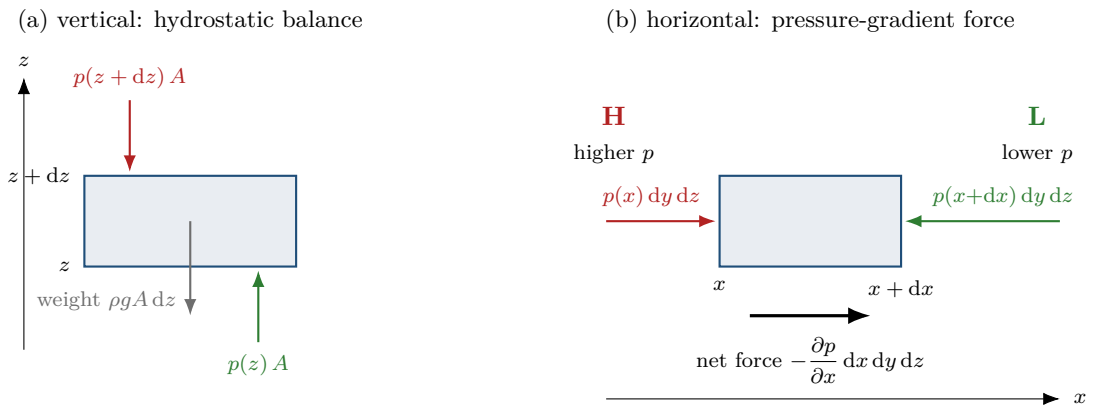


Figure 1.3: Pressure forces on a small volume of air. (a) A horizontal slab between z and $z+\mathrm{d}z$: the pressure force from below balances the pressure force from above plus the weight, which gives $\partial p/\partial z = -\rho g$ (equation (1.6)). (b) A box in a horizontal pressure gradient: the higher pressure on the left face exceeds the lower pressure on the right face, and the net force, per unit mass $-(1/\rho)\,\partial p/\partial x$, points from high to low pressure (equation (1.7)).

the Earth. At latitude ϕ, in the local east-north-up coordinates, $\boldsymbol{\Omega} = \Omega\,(0, \cos\phi, \sin\phi)$. Working out the cross product,

$$-2\,\boldsymbol{\Omega} \times \mathbf{u} = \big(2\Omega \sin\phi\, v - 2\Omega\cos\phi\, w,\ -2\Omega\sin\phi\, u,\ 2\Omega\cos\phi\, u\big).$$

For large-scale horizontal motion the term in w is negligible because $|w| \ll |u|$, and the vertical component is negligible against gravity. What remains is the horizontal Coriolis force,

$$\mathbf{a}_{\mathrm{C},h} = (fv, -fu) = -f\,\mathbf{k} \times \mathbf{V}, \qquad f = 2\Omega\sin\phi, \tag{1.9}$$

where $\mathbf{k}$ is the upward unit vector and f the *Coriolis parameter*, in s^{-1}. At 45°N, $f = 2 \times 7.292 \times 10^{-5} \times \sin 45^\circ = 1.03 \times 10^{-4}\,\mathrm{s}^{-1}$; at 23.5°S, near the Tropic of Capricorn in southern Brazil, $f = 2 \times 7.292 \times 10^{-5} \times \sin(-23.5^\circ) = -5.82 \times 10^{-5}\,\mathrm{s}^{-1}$; at the equator $f = 0$.

Three properties follow from equation (1.9). The force is perpendicular to the wind, so it changes the direction of the moving air but not its speed, and it does no work. Its magnitude is $|f|\,U$: zero for air at rest, $1.03 \times 10^{-3}\,\mathrm{m/s^2}$ for a $10\,\mathrm{m\,s^{-1}}$ wind at 45°N and $5.8 \times 10^{-4}\,\mathrm{m/s^2}$ at 23.5°S, comparable to the pressure-gradient force of Section 1.3.3. And its direction depends on the sign of f. For an eastward wind, $u > 0$ and $v = 0$, the force is $(0, -fu)$: toward the south when $f > 0$, which is to the right of the motion, and toward the north when $f < 0$, which is to the left. In the Northern Hemisphere moving air is deflected to the right of its direction of motion; in the Southern Hemisphere, to the left.

Figure 1.4 illustrates the consequence. Each panel is a map seen from above, north at the top, with straight east-west isobars and the low pressure to the north; the left panel is in the Northern Hemisphere and the right panel in the Southern. A parcel starts from rest at the dot, and the pressure-gradient force (black arrow) accelerates it northward, toward the low. As it gains speed the Coriolis force (purple arrow) pushes it sideways, to the right in the north and to the left in the south, and the path (red) turns until the air moves along the isobars rather than across them: toward the east with the low on its left in the Northern Hemisphere, toward the west with the low on its right in the Southern. Large-scale wind therefore does not blow straight from high to low pressure; it turns until it flows nearly parallel to the isobars. Chapter 3 derives that balanced state, the geostrophic wind, and shows that the exact path of a parcel released from rest oscillates about it rather than turning smoothly as drawn.

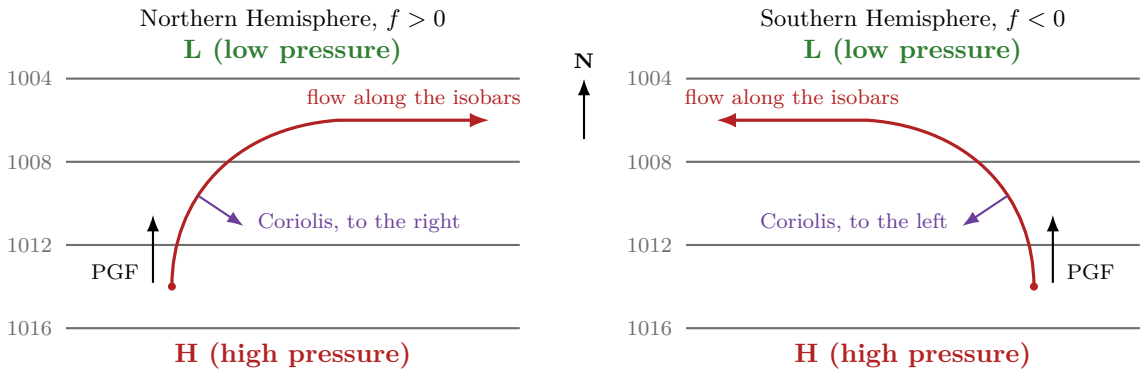


Figure 1.4: Deflection by the Coriolis force (schematic map view, north at the top, no friction). Gray: isobars, in hPa, with the low to the north. A parcel released from rest at the dot is accelerated toward the low by the pressure-gradient force (PGF) and deflected by the Coriolis force, equation (1.9), to the right in the Northern Hemisphere and to the left in the Southern, until it moves along the isobars. The smooth turn is schematic; the exact path oscillates about the final direction.

1.3.5 The horizontal momentum equation

The forces of this section combine into one equation for the horizontal wind following an air parcel,

$$\frac{\mathrm{D}\mathbf{V}}{\mathrm{D}t} = -\frac{1}{\rho}\nabla_h p \;-\; f\,\mathbf{k}\times\mathbf{V} \;+\; \mathbf{F}, \tag{1.10}$$

which reads, term by term,

acceleration following the parcel = pressure forcing + rotation + friction and turbulence.

The left-hand side, $\frac{\mathrm{D}\mathbf{V}}{\mathrm{D}t}$, is the rate of change of the wind of one parcel of air as it moves, in $\mathrm{m/s^2}$; it is not the rate of change at a fixed anemometer, which also changes when a different parcel arrives. The first term on the right is the pressure-gradient force of equation (1.7); the second the Coriolis force of equation (1.9); the third, $\mathbf{F}$, is the force per unit mass exerted by friction, which near the ground is the drag of the surface transmitted upward by turbulence. The equation omits small terms that arise from the curvature of the Earth and the vertical velocity, which do not matter at the scales of this book.

The importance of each term depends on where the air is. Table 1.1 gives illustrative orders of magnitude for a midlatitude weather system above the boundary layer, with a wind of $U = 10\,\mathrm{m\,s^{-1}}$ that changes over a distance of $L = 1000\,\mathrm{km}$, and for the air near the ground. Above the boundary layer, the pressure-gradient and Coriolis forces are both of order $10^{-3}\,\mathrm{m/s^2}$ and nearly cancel; the acceleration is about ten times smaller, of order $U^2/L = 10^{-4}\,\mathrm{m/s^2}$; friction is negligible. Their ratio $U/(|f|L) = 10^{-4}/10^{-3} = 0.1$ is the Rossby number, which measures how much the acceleration matters against rotation and which Chapters 4 and 5 develop. Near the surface the friction term becomes as large as the other two, so all three forces matter: the wind is slower, and it crosses the isobars toward low pressure instead of flowing along them.

Principle 1.1. *Air is pushed by the horizontal pressure gradient, from high toward low pressure; rotation turns the moving air, to the right in the Northern Hemisphere and to the left in the Southern; and friction near the surface slows it. Aloft the first two nearly balance; near the ground all three are of the same size.*

Table 1.1: Terms of the horizontal momentum equation, equation (1.10), with illustrative orders of magnitude. Above the boundary layer: $U = 10\,\mathrm{m\,s^{-1}}$, $L = 1000\,\mathrm{km}$, $f = 10^{-4}\,\mathrm{s^{-1}}$, a gradient of about 1 hPa per 100 km. Near the surface: the same gradient, a slower wind, and turbulent drag.

Term	Expression	Physical meaning	Above the boundary layer ($\mathrm{m/s^2}$)	Near the surface ($\mathrm{m/s^2}$)
Acceleration	$\frac{\mathrm{D}\mathbf{V}}{\mathrm{D}t}$	change of a parcel's wind; scale U^2/L	10^{-4}	10^{-4} to 10^{-3}
Pressure-gradient force	$-(1/\rho)\nabla_h p$	push from high to low pressure	10^{-3}	10^{-3}
Coriolis force	$-f\,\mathbf{k}\times\mathbf{V}$	deflection by rotation; scale $\lvert f\rvert U$	10^{-3}	a few 10^{-4}
Friction	$\mathbf{F}$	surface drag carried by turbulence	negligible	10^{-3}

1.4 The layer near the surface

The engineering heights of this book lie in the lowest part of the atmosphere, where the surface acts on the air directly. This section describes what the surface does to the flow, defines the atmospheric boundary layer and the surface layer, and places the heights of common instruments within them.

1.4.1 Drag and turbulence over a real surface

Above the boundary layer, the moving air is not in contact with any surface. Near the ground, it meets the surface and everything on it: trees, buildings, hills and mountains, crops, lakes and the sea, and patches of ground at different temperatures. Every obstacle exerts a drag on the flow, and the flow behind obstacles breaks into eddies of many sizes: turbulence. Turbulence mixes the air vertically, carrying slow air from near the ground upward and fast air from above downward, and in doing so it spreads the effect of the surface drag through a layer much deeper than the obstacles themselves.

The surface also heats and cools the air. In the afternoon a sunlit surface warms the air in contact with it, which rises in thermals and stirs the layer vigorously; at night the ground cools by radiation and chills the air above it, which then resists vertical motion and damps turbulence. The same surface drag can therefore be spread through two kilometers of air in the afternoon and through a hundred meters at night. This dependence on time of day and weather is what makes near-surface wind different from the wind aloft, and it is why the friction term $\mathbf{F}$ of equation (1.10) cannot be given a single value.

1.4.2 The atmospheric boundary layer

The *atmospheric boundary layer* (ABL), also called the planetary boundary layer (PBL), is the lowest part of the atmosphere, the part that feels the surface directly and responds to changes at the surface, such as heating, cooling and drag, within about an hour or less. Above it is the free atmosphere, where the surface is felt only indirectly. The ABL depth, written z_i and measured in meters, is not set by an equation but by a criterion, such as the height where turbulence vanishes or where a temperature inversion caps the mixing; Chapter 6 states the criteria. It is measured from profiles of temperature, humidity and wind (radiosondes, towers),

and remotely with lidars and ceilometers that detect the top of the turbid, mixed layer. In a weather model it is diagnosed by the boundary-layer parameterization.

The depth varies by more than an order of magnitude. Under strongly stable conditions, on a clear night with light wind, the ABL can be about 100 m deep or less; in vigorous daytime convection it can exceed 2 km; commonly it lies between about 500 and 2000 m. Over land it follows the daily cycle of heating, growing through the morning and collapsing near sunset; over the sea, whose temperature changes little during the day, it varies much less. A tower of 150 m is therefore deep inside the ABL in the afternoon and may reach above it at night.

1.4.3 The surface layer

The *surface layer* is the lowest part of the ABL, roughly its lowest 5 to 10 %, in which the vertical turbulent fluxes of momentum and heat are close to their surface values, varying with height by less than about ten percent. In this layer the surface controls the flow most directly, the wind speed increases rapidly with height, and the Coriolis force is unimportant against friction. Its depth follows from that of the ABL: 5 to 10 m under a 100 m deep stable layer, 50 to 100 m under a 1000 m layer, 100 to 200 m under a 2000 m convective layer. Below it, within a few obstacle heights of the ground, lies the roughness sublayer of the jargon box of Section 1.1, where the flow is shaped by the individual obstacles. Chapters 7, 9 and 12 develop the surface layer, its fluxes and its wind profile.

The engineering heights of this book fall in or near the surface layer: weather stations measure at 10 m, transmission-line sensors at about 20 to 50 m, wind-turbine hubs are at about 80 to 150 m, and meteorological towers span these heights. Whether a given height is inside the classical surface layer is not a property of the height. It depends on the conditions, and the same instrument can be inside it in the afternoon and above it at night.

1.4.4 Engineering heights in the boundary layer

Figure 1.5 places the engineering heights against the layers. The vertical axis is height above the ground on a logarithmic scale, from 1 m to 3 km. The three columns are three illustrative boundary layers: a strongly stable night with $z_i = 100$ m, a typical case with $z_i = 1000$ m (bracket: the common range of 500 to 2000 m), and vigorous daytime convection with $z_i = 2500$ m. In each column the light fill is the ABL and the darker fill the surface layer, drawn to 10 % of z_i with a dashed line at 5 %. The horizontal bands across all three columns are the instrument heights.

The figure shows the point of the previous subsection directly. On the convective afternoon, every engineering height up to the turbine hub lies in the surface layer. On the typical day the transmission-line sensors are inside it and the turbine hubs at or above its top. On the stable night only the 10 m station is at the top of the surface layer; the line sensors are above it, and the turbine rotor reaches the top of the ABL, where the wind can be decoupled from the surface and a nocturnal jet can form. One instrument can thus sample different layers at different hours, and a relation between heights fitted on daytime data does not transfer to the night.

1.5 Scales of atmospheric motion

The wind at one point is the sum of motions of very different sizes and durations. This section writes the near-surface wind as a function of the influences that act on it at once, and then sorts the motions of the atmosphere into the three scale ranges that meteorology uses.

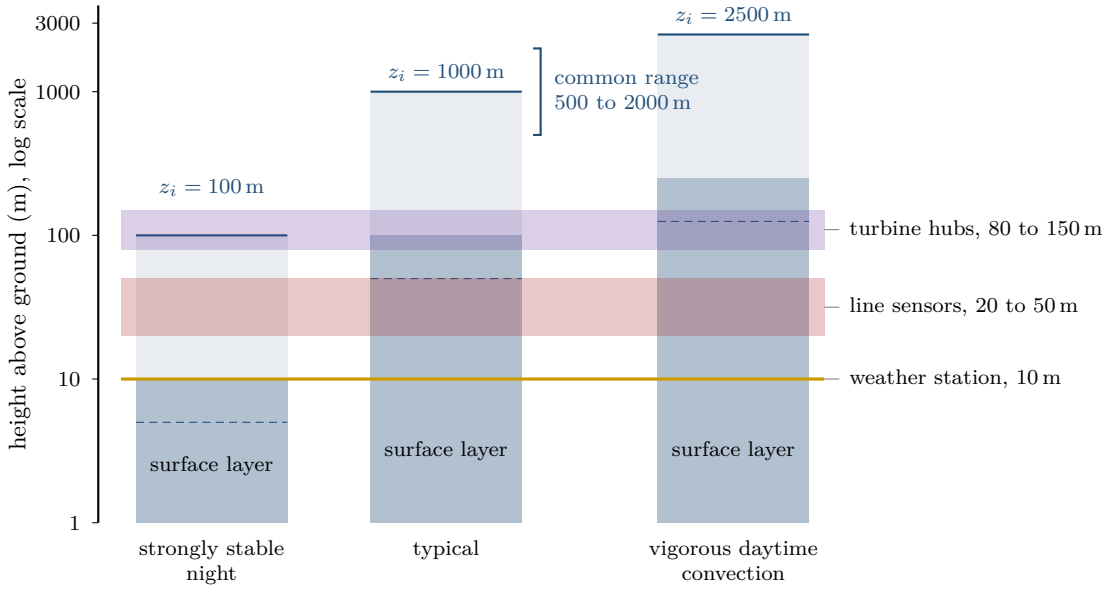


Figure 1.5: Engineering heights against three illustrative boundary layers, height on a logarithmic scale. Light fill: atmospheric boundary layer of depth z_i; darker fill: surface layer to 10 % of z_i, with a dashed line at 5 %. Bands: weather station (10 m), transmission-line sensors (20 to 50 m), wind-turbine hubs (80 to 150 m). The same height lies in different layers under different conditions.

1.5.1 The near-surface wind as a function of many influences

Consider the wind at 20 m at an illustrative site on a given afternoon. Several influences act on it at once. The large-scale weather sets the background: a synoptic system, say a high to the southeast and a low to the northwest in the Northern Hemisphere, drives a regional southwesterly wind. The boundary-layer structure decides how much of that wind reaches the ground: daytime convection mixes faster air from aloft downward. The surface roughness upstream slows the mean wind: a forest a kilometer upwind has reduced it. The terrain accelerates or decelerates the flow: a ridge on which the sensor stands speeds it up. And a local obstacle disturbs it: the wake of a building upwind adds turbulence and reduces the mean speed in certain directions.

The wind at 20 m is therefore not simply the synoptic wind, and no single one of these influences determines it. In functional form,

$$U_{20\mathrm{m}} = \mathcal{F}(\text{large-scale forcing},\ \text{stability},\ \text{roughness},\ \text{terrain},\ \text{obstacles},\ \text{height}), \qquad (1.11)$$

where $U_{20\mathrm{m}}$ is the wind speed at 20 m and $\mathcal{F}$ stands for the whole chain of transformations of Section 1.1.1, and the arguments interact: the speed-up over a ridge depends on the stability, and the slowing by a forest depends on the height and on the wind direction. Each argument belongs to a different scale of motion, which is the subject of the next subsection.

1.5.2 Synoptic, mesoscale and microscale

Meteorology sorts atmospheric motions into three ranges of horizontal size, each with a typical lifetime. The *synoptic scale*, of about 1000 km and more, contains the midlatitude cyclones and anticyclones (lows and highs) and the fronts between air masses; these systems last days, and they provide the background pressure forcing. The name comes from synoptic charts, on which observations made at the same time over a large area are plotted together. The *mesoscale*, from about 1 to 1000 km, contains sea breezes, mountain-valley circulations, thunderstorms, low-level

jets and urban circulations; these last minutes to hours. The *microscale*, below about 1 km, contains building wakes, the speed-up of the wind over hills, the turbulence inside and above forest canopies, local gusts and the flow around obstacles; these last seconds to minutes. The boundaries are conventions and differ between authors, particularly for the microscale. Table 1.2 lists the three ranges with their sizes, durations, examples and their role in near-surface wind.

Table 1.2: The three scales of atmospheric motion. Sizes and durations are approximate; the boundaries are conventions.

Scale	Horizontal size	Duration	Examples	Role for near-surface wind
Synoptic	about 1000 km and more	days	midlatitude cyclones, highs, fronts	background pressure forcing; the regional wind direction
Mesoscale	about 1 to 1000 km	minutes to hours	sea breezes, mountain-valley circulations, thunderstorms, low-level jets, urban circulations	regional modification and local forcing; the daily cycle
Microscale	below about 1 km	seconds to minutes	building wakes, hill speed-up, canopy turbulence, gusts, obstacle flow	the wind at one sensor or one span; gusts and turbulence

Figure 1.6 draws the same ranges as regions in a plane of size and duration. The horizontal axis is the horizontal size of a motion and the vertical axis its lifetime, both on logarithmic scales; the three shaded rectangles are the scale ranges, and the dots are examples placed at their typical size and lifetime. Larger motions live longer, so the examples lie along a band from the lower left to the upper right. Engineering wind needs all three ranges at once: the synoptic scale gives the forcing for days ahead, the mesoscale the regional and daily modification, and the microscale the wind that actually reaches a conductor, a rotor or an anemometer. Chapter 5 develops the scale ranges and the dimensionless numbers that decide which forces matter in each.

1.6 Model and measurement, forcing and response

This section separates two pairs of objects that the rest of the book keeps apart: the wind a weather model reports and the wind an instrument measures, and the large-scale forcing and the response of the near-surface air to it. It closes with the downward chain that organizes the book.

1.6.1 Grid-cell wind and point wind

A weather model divides the atmosphere into grid cells and computes one value of each variable per cell and level. Its 10 m wind, written U_{10}, is a *grid-scale wind*: the wind the model assigns to a whole cell, at 10 m above the cell's effective terrain elevation, over the cell's effective roughness, with turbulence and surface fluxes supplied by parameterizations. A model value of $U_{10} = 6.0\,\mathrm{m\,s^{-1}}$ is therefore not the wind measured by an anemometer 10 m above the ground at a particular spot inside that cell. With a grid spacing of $\Delta x = 3\,\mathrm{km}$ the cell covers $3\,\mathrm{km} \times 3\,\mathrm{km} = 9\,\mathrm{km}^2 = 9 \times 10^6\,\mathrm{m}^2$; with $\Delta x = 9\,\mathrm{km}$ it covers $81\,\mathrm{km}^2$. Features smaller than a

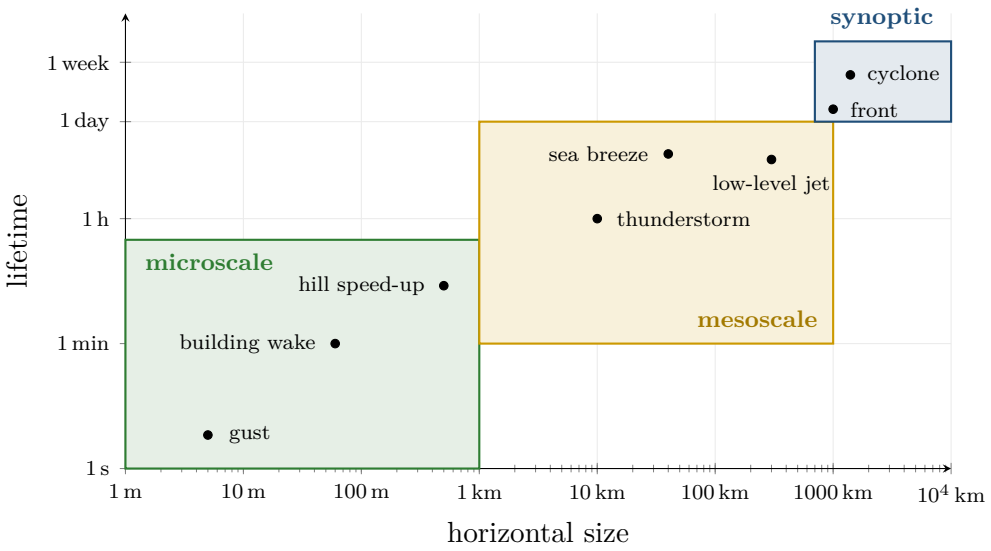


Figure 1.6: The three scales of atmospheric motion in a plane of horizontal size and lifetime, both logarithmic (schematic). Green: microscale, below about 1 km, seconds to minutes; gold: mesoscale, about 1 to 1000 km, minutes to hours; blue: synoptic, about 1000 km and more, days. Dots: illustrative examples at their typical size and lifetime.

few grid spacings, such as a single ridge or a patch of forest, are not represented at all, only their average effect on the cell.

A *point observation* is the value an instrument measures at one place: the anemometer samples the air passing through a volume of a few liters. Averaging over time widens what it sees: over a ten-minute average at $6\,\mathrm{m\,s^{-1}}$, about $6 \times 600 = 3600\,\mathrm{m}$ of air passes the instrument, but that air is a line upstream of the sensor along the wind direction, not the $9\,\mathrm{km^2}$ of the cell, and it carries the imprint of the obstacles and terrain right next to the sensor. The difference between the two is a difference of objects, not only an error of the model: one is a grid-scale atmospheric state, the other a point measurement. The part of their disagreement that comes from this difference of objects is called the *representativeness error*; it remains even when the model is perfect at its own scale and the instrument is perfect at its point.

Figure 1.7 draws the difference in a vertical cross section through three cells of a model with $\Delta x = 3\,\mathrm{km}$. The horizontal axis is distance in kilometers and the vertical axis elevation in meters, with a vertical exaggeration of about ten. The black line is the real terrain, with a ridge, a valley and a forest; the blue steps are the model terrain, one mean elevation per cell. The anemometer stands on a knoll in the middle cell, at 296 m, while the model ground of that cell is at its mean elevation of 272 m. The model's 10 m wind refers to 282 m above sea level over a flat cell with averaged roughness; the anemometer's 10 m is 306 m above sea level on a crest, where the terrain accelerates the flow. The two values describe different air.

1.6.2 Forcing and response

A *forcing* is a physical driver imposed on the flow from outside the layer of interest; the *response* is what the air does with it. For near-surface wind, the large-scale horizontal pressure gradient is the forcing, and terrain, turbulence, surface drag, heating and stability determine the response. The same forcing can produce very different winds near the ground. In an illustrative case, a synoptic pressure gradient sustains a wind of $15\,\mathrm{m\,s^{-1}}$ above the boundary layer. At night, with strong surface drag and a stable boundary layer that suppresses vertical mixing, the wind at 10 m is $5\,\mathrm{m\,s^{-1}}$, one third of the wind aloft. On a sunny afternoon with the same forcing, strong convective mixing brings fast air down from aloft, and the wind at 10 m is $9\,\mathrm{m\,s^{-1}}$, sixty

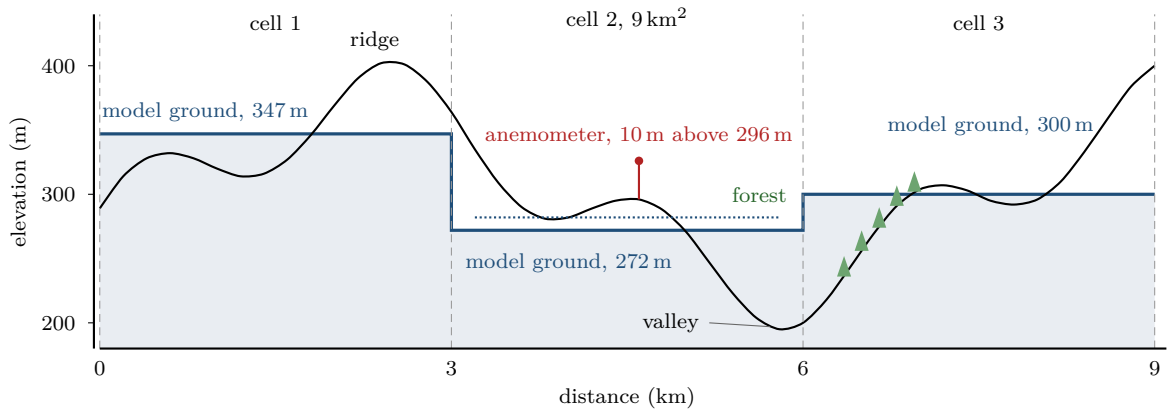


Figure 1.7: Real terrain against model terrain in a vertical cross section through three cells of a model with $\Delta x = 3\,\mathrm{km}$ (illustrative; vertical exaggeration about ten, mast not to scale). Black: real terrain; blue steps: model terrain, the mean elevation of each cell (347, 272 and 300 m). The anemometer stands on a knoll at 296 m in cell 2; the model's 10 m level in that cell (dotted) lies over a flat ground at 272 m. The grid-scale wind and the point wind refer to different air.

percent of it.

Figure 1.8 draws the two cases as wind profiles. The horizontal axis is wind speed and the vertical axis height above the ground on a logarithmic scale, from 10 to 2000 m; the red curve is the stable night and the blue curve the convective afternoon, with their 10 m values marked, and the vertical segment at the top is the $15\,\mathrm{m\,s^{-1}}$ wind aloft. Both curves reach the same wind aloft. The stable profile has strong shear, a large change of speed with height, over its lowest few hundred meters; the convective profile is faster at every height below 300 m and uniform above its lowest hundred meters, because the mixing has homogenized the layer and brought the momentum of the wind aloft close to the ground. The curves are illustrative shapes chosen to pass through the stated values, not solutions of a boundary-layer model; Chapters 7 and 14 derive the logarithmic profile of the surface layer and its dependence on stability.

The difference matters for every application. The power carried by the wind through a unit area is $\frac{1}{2}\rho U^3$, which at $\rho = 1.2\,\mathrm{kg/m^3}$ is $75\,\mathrm{W/m^2}$ at $5\,\mathrm{m\,s^{-1}}$ and $437\,\mathrm{W/m^2}$ at $9\,\mathrm{m\,s^{-1}}$, a factor of $(9/5)^3 = 5.8$ for the same forcing. Near-surface wind prediction is therefore not merely a problem of reading the pressure map: the map gives the forcing, and the boundary layer gives the response.

1.6.3 The downward chain

The chapter's ideas assemble into one mental model of near-surface wind, read from the free atmosphere down to the instrument:

synoptic atmosphere → mesoscale forcing → boundary layer → surface layer → terrain and roughness → sensor.

At each step the wind received from above is transformed, and the question to ask of any observed wind is which processes between the free atmosphere and the instrument transformed it into what was observed. The questions of Section 1.1.2 are this chain applied to one anemometer.

Figure 1.9 draws the chain. The boxes on the left are the six links, from the synoptic atmosphere at the top to the sensor at the bottom, joined by arrows in the direction in which the wind is passed down; the notes on the right state what each link contributes and what sets it. The upper links are the forcing; the lower links determine the response. Chapters 2 to 4 treat the top box, Chapter 5 the scales that separate the boxes, Chapters 6 to 21 the boundary layer, the surface layer and the terrain, and Chapters 22 and 23 the measurement.

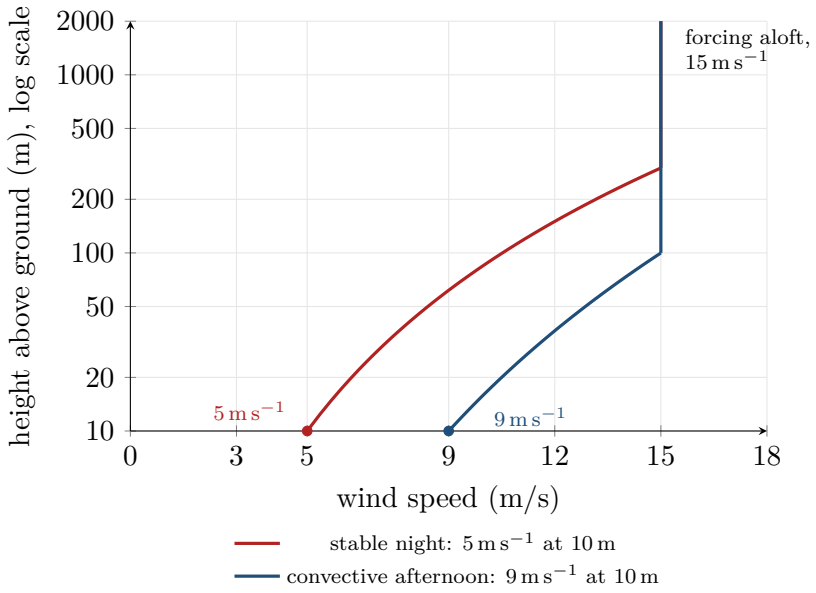


Figure 1.8: The same forcing, two responses (illustrative). Profiles $U(z) = 15\,\mathrm{m\,s^{-1}}\,(z/z_a)^{\alpha}$ below z_a and $15\,\mathrm{m\,s^{-1}}$ above it: stable night $z_a = 300\,\mathrm{m}$, $\alpha = 0.323$; convective afternoon $z_a = 100\,\mathrm{m}$, $\alpha = 0.222$; both values chosen so that the profiles pass through 5 and $9\,\mathrm{m\,s^{-1}}$ at 10 m. Above z_a both profiles equal the $15\,\mathrm{m\,s^{-1}}$ wind aloft.

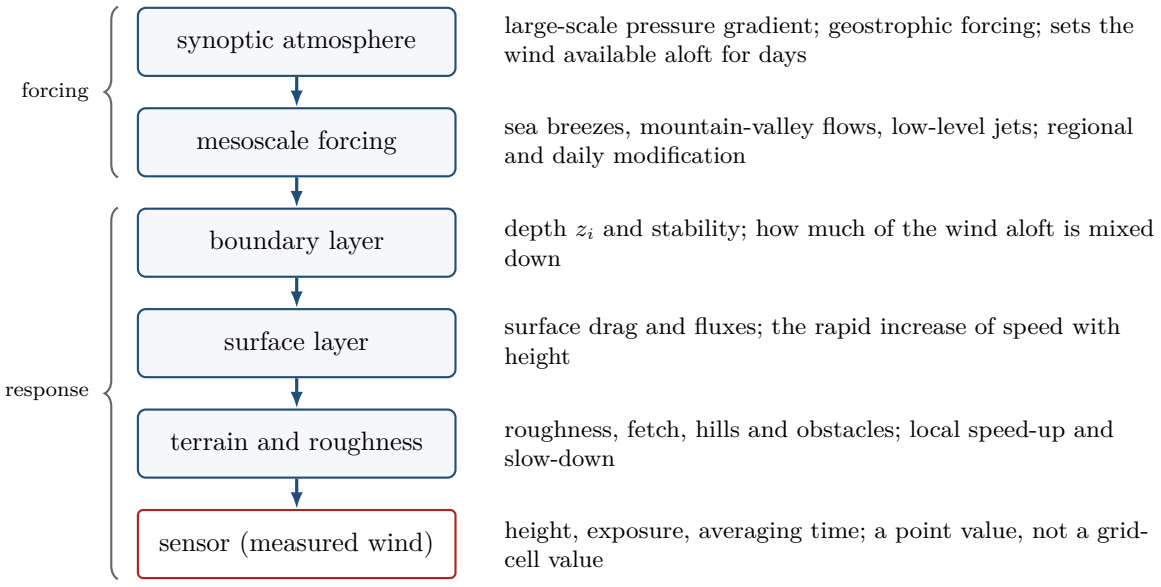


Figure 1.9: The downward chain from the free atmosphere to the instrument. Boxes: the links, from the synoptic atmosphere to the sensor; arrows: the direction in which the wind is passed down and transformed; notes: what each link contributes. The upper two links set the forcing; the lower four the response observed at the sensor.

Read as a sequence of causes, the chain is the takeaway of the chapter: differential heating creates the pressure field; the pressure field, turned by rotation, drives the large-scale wind; the boundary layer modifies that wind; the surface and the terrain modify it again; and the result is the local wind that an instrument measures at one point.

1.7 What to retain

Definition 1.1 (The atmosphere as a wind system)**.** Differential heating creates a pressure field; the pressure-gradient force, turned by the Coriolis force, drives the large-scale wind; the boundary layer, the surface and the terrain then modify that wind, so that the wind measured at one point and height is the end of a chain of transformations, not the large-scale wind itself.

Table 1.3 lists the chapter's terms with their meaning, their units and the subsection that defines each.

Table 1.3: Terms of the chapter and where each is defined.

Term	Meaning	Units	Defined in
Wind	motion of air relative to the surface; $\mathbf{V} = (u, v)$, speed $U = \sqrt{u^2 + v^2}$	m/s	1.2.1
Wind direction	where the wind comes from, clockwise from true north; $u = -U \sin\beta$, $v = -U \cos\beta$	degree	1.2.1
Pressure-gradient force	$-(1/\rho)\nabla_h p$; pushes air from high to low pressure	m/s^2	1.3.3
Hydrostatic balance	$\partial p/\partial z = -\rho g$; vertical pressure gradient balances gravity	Pa/m	1.3.2
Coriolis force	$-f\,\mathbf{k} \times \mathbf{V}$, $f = 2\Omega \sin\phi$; deflects moving air to the right (north) or left (south)	m/s^2	1.3.4
Atmospheric boundary layer	lowest layer, responding to the surface within about an hour; depth z_i from about 100 m to over 2 km	m (depth)	1.4.2
Surface layer	lowest 5 to 10 % of the ABL; fluxes near their surface values	m (depth)	1.4.3
Synoptic scale	about 1000 km and more, days; background forcing	km, days	1.5.2
Mesoscale	about 1 to 1000 km, minutes to hours	km, hours	1.5.2
Microscale	below about 1 km, seconds to minutes	m, s	1.5.2
Forcing and response	the imposed driver (large-scale pressure gradient) and what the near-surface air does with it	–	1.6.2
Grid-scale wind	the value a model assigns to a whole grid cell, e.g. U_{10} over 9 km^2	m/s	1.6.1
Point observation	the value an instrument measures at one place and height	m/s	1.6.1
Representativeness error	the part of a model-observation difference due to their different spatial support	m/s	1.6.1

1.8 Exercises

Exercise 1.1. (a) A wind vane at a station in southern Brazil reports a direction of $\beta = 300^\circ$ and the anemometer a speed of $8\,\mathrm{m\,s^{-1}}$. Compute u and v, and state toward which compass direction the air moves. (b) A sonic anemometer reports $u = -3\,\mathrm{m\,s^{-1}}$ and $v = +4\,\mathrm{m\,s^{-1}}$. Compute the speed and the meteorological direction, and name the wind (for example "northwesterly").

Exercise 1.2. A station at an elevation of about 1000 m reports $p = 900\,\mathrm{hPa}$ and $T = 30^\circ\mathrm{C}$. (a) Compute the air density from equation (1.4) and compare it with the sea-level value $1.225\,\mathrm{kg/m^3}$ of Section 1.2.3. (b) Using equation (1.6), compute the pressure difference between the base and the top of a 50 m mast at this station. (c) By what fraction is the force of a given wind speed on a conductor, which is proportional to ρU^2, smaller here than at sea level and 15°C?

Exercise 1.3. At a site at 30°S, the isobars run east-west and the pressure decreases toward the south by 2 hPa per 100 km; take $\rho = 1.2\,\mathrm{kg/m^3}$. (a) Compute the magnitude and direction of the pressure-gradient force per unit mass. (b) Compute f. (c) For air moving toward the south at $10\,\mathrm{m\,s^{-1}}$, compute the Coriolis force from equation (1.9), its magnitude and its compass direction, and check that it points to the left of the motion. (d) If the pressure-gradient force acted alone on air initially at rest, how long would it take to reach $10\,\mathrm{m\,s^{-1}}$? (e) Toward which compass direction does the large-scale wind eventually blow, and on which side is the low pressure when facing downwind?

Exercise 1.4. On a given day the boundary layer is 150 m deep at night and 1800 m deep in the afternoon. (a) Taking the surface layer as the lowest 10 % of the boundary layer, state for sensors at 10, 40 and 120 m whether each lies in the surface layer, in the boundary layer above it, or above the boundary layer, by night and by day. (b) With a wind of $15\,\mathrm{m\,s^{-1}}$ aloft, the 10 m wind is $5\,\mathrm{m\,s^{-1}}$ by night and $9\,\mathrm{m\,s^{-1}}$ by day. If the convective cooling of a conductor grows in proportion to $U^{0.5}$ (an illustrative exponent), by what factor is the cooling larger by day than by night for the same forcing? By what factor does the wind power density $\tfrac{1}{2}\rho U^3$ differ? (c) A model with $\Delta x = 3\,\mathrm{km}$ reports $U_{10} = 6.0\,\mathrm{m\,s^{-1}}$ for the cell in which a sensor stands. Name three reasons, from Section 1.6.1, why the sensor may read a different value even if both are correct.

Chapter 2

Pressure, Geopotential and the Pressure-Gradient Force

2.1 Pressure and hydrostatic balance

Chapter 1 introduced the horizontal pressure gradient as the force that sets air in motion. This chapter asks where that gradient comes from. The question is

how do temperature, density and height together create the pressure field that drives the wind?

The answer is a chain of three links. Hydrostatic balance fixes how pressure decreases with height, and it makes the rate of decrease depend on temperature. Because of that dependence, a surface of constant pressure lies higher above warm air than above cold air, and its height, the geopotential height, becomes the natural way to map the pressure field. A sloping pressure surface is, finally, the same thing as a horizontal pressure gradient, which accelerates the air. The chapter derives each link, gives the vocabulary of the weather maps that display them, and ends with the place of the pressure field in a model of the wind at 10 to 150 m above the ground.

Jargon: hectopascal, isobaric surface, heights, upper-air chart, thickness, contour interval, MSLP

The *hectopascal* (hPa) is 100 Pa; it is numerically equal to the millibar (mb) of older charts. An *isobaric surface* (also *constant-pressure surface* or *pressure level*) is the surface on which the pressure has one given value, for example the 500 hPa surface. On weather charts *heights* is short for the geopotential heights of an isobaric surface, in meters. An *upper-air chart* is a map of a quantity on an isobaric surface, named after its level: a "500 hPa chart" maps the height of the 500 hPa surface, usually with temperature and wind. *Thickness* is the difference in geopotential height between two isobaric surfaces; the "1000–500 hPa thickness" is $Z_{500} - Z_{1000}$. A *contour* is a line of equal value on a map, an *isobar* is a contour of pressure, and the *contour interval* is the step between adjacent contours. *MSLP* is mean sea-level pressure, the station pressure reduced to sea level (Section 2.5.1).

Key idea

Temperature controls the vertical spacing of pressure surfaces: warm columns are thick and cold columns thin. Differences in thickness tilt the pressure surfaces, a tilted pressure surface is a horizontal pressure gradient, and the pressure gradient accelerates the air.

2.1.1 Pressure as the weight of the air above

Pressure is a normal force per unit area,

$$p = \frac{F}{A}, \tag{2.1}$$

with F the force, in newtons, exerted on a surface of area A, in square meters. Its SI unit is the pascal, $1\,\mathrm{Pa} = 1\,\mathrm{N\,m^{-2}}$. Meteorology quotes pressure in hectopascals, $1\,\mathrm{hPa} = 100\,\mathrm{Pa}$, because the numbers are then of a convenient size: a typical sea-level pressure is about 1013 hPa (101 325 Pa in the standard atmosphere), and the differences between weather systems at sea level are a few to a few tens of hectopascals. Pressure is a scalar: at a point it acts equally in all directions, and it is the *difference* of pressure between two sides of a body of air that exerts a net force on it.

In air at rest, or nearly at rest, the pressure at a level is the weight of the air above that level, per unit area. A column of the atmosphere one square meter in cross section that stands on the sea surface contains about

$$\frac{p_0}{g} = \frac{101\,325\,\mathrm{Pa}}{9.81\,\mathrm{m\,s^{-2}}} \approx 10\,330\,\mathrm{kg}$$

of air, about ten tonnes, whose weight is what a barometer at sea level reads. Here p_0 is the sea-level pressure, a symbol used below for the pressure at a reference level. Rising through the column leaves progressively more of that air below, so the pressure decreases monotonically with height. Pressure is measured by a barometer: at a weather station, a fixed instrument at a surveyed elevation; aloft, a sensor carried by a radiosonde balloon or by an aircraft. Weather models compute it as a field from their equations.

2.1.2 Hydrostatic balance

Consider a thin horizontal slab of air with horizontal area A, bottom at height z and top at $z + \delta z$, where z is geometric height above mean sea level. Figure 2.1 draws the slab and the three vertical forces on it. The air below pushes up on the bottom face with the force $p(z)\,A$; the air above pushes down on the top face with $p(z+\delta z)\,A$; and gravity pulls the slab's mass $\rho A\,\delta z$ downward with the weight $\rho g A\,\delta z$, where ρ is the air density and g the gravitational acceleration. The horizontal pressure forces on the four side faces do not enter the vertical balance.

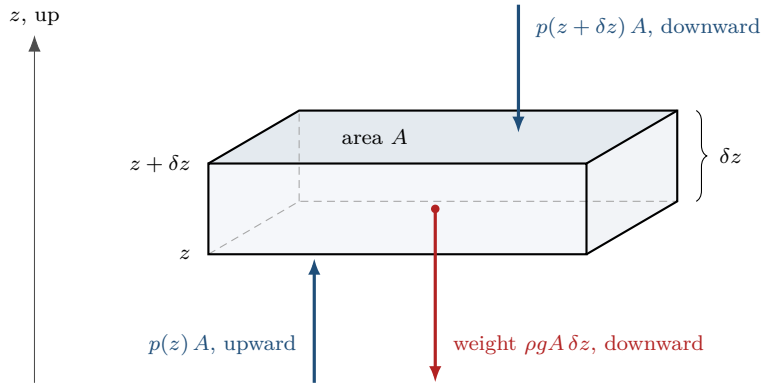


Figure 2.1: Vertical forces on a thin horizontal slab of air of area A and thickness δz. Blue: pressure forces of the air below and above; red: the slab's weight, applied at its center of mass. In hydrostatic balance the upward force exceeds the downward pressure force by exactly the weight.

Newton's second law for the vertical motion of the slab, with w its upward velocity, reads

$$\rho A\,\delta z\,\frac{\mathrm{D}w}{\mathrm{D}t} = p(z)\,A - p(z+\delta z)\,A - \rho g A\,\delta z. \tag{2.2}$$

Dividing by $A\,\delta z$ and letting $\delta z \to 0$, the pressure difference becomes a derivative, $[p(z) - p(z+\delta z)]/\delta z \to -\partial p/\partial z$, and

$$\rho\,\frac{\mathrm{D}w}{\mathrm{D}t} = -\frac{\partial p}{\partial z} - \rho g. \tag{2.3}$$

For most atmospheric motions the vertical acceleration is minute compared with g. In a large-scale weather system the vertical velocity is a few centimeters per second and changes over hours, giving accelerations below $10^{-5}\,\mathrm{m\,s^{-2}}$; even a thunderstorm updraft that gains $10\,\mathrm{m\,s^{-1}}$ in a few minutes accelerates at about $0.05\,\mathrm{m\,s^{-2}}$, half a percent of g. Dropping the left side of equation (2.3) leaves

$$\frac{\partial p}{\partial z} = -\rho g, \tag{2.4}$$

the *hydrostatic equation*. *Hydrostatic balance* is the state it describes: the upward pressure-gradient force on each layer of air balances the layer's weight. Since $\rho > 0$ and $g > 0$, the derivative is negative and pressure decreases upward everywhere. Integrating equation (2.4) from a height z to the top of the atmosphere, where the pressure vanishes, gives $p(z) = \int_z^\infty \rho g\,\mathrm{d}z'$, which is the statement of Section 2.1.1 in equation form: the pressure at a level is the weight of the air above it per unit area.

Near sea level, with $\rho \approx 1.225\,\mathrm{kg\,m^{-3}}$ (the density of dry air at 1013.25 hPa and 15°C), $\partial p/\partial z \approx -1.225 \times 9.81 = -12.0\,\mathrm{Pa\,m^{-1}}$: pressure falls by about 1 hPa for every 8 m of ascent. Weather models that resolve features of a few kilometers or less, such as convective cells and short mountain waves, keep the full equation (2.3) and are called non-hydrostatic; for the pressure field of weather systems hundreds of kilometers across, equation (2.4) holds to a fraction of a percent, and the rest of this chapter relies on it.

Principle 2.1. *In hydrostatic balance the pressure at a level is the weight per unit area of the air above it, and it decreases with height at the rate ρg.*

2.1.3 Pressure in an isothermal atmosphere

The hydrostatic equation contains the density, which itself depends on pressure and temperature. For dry air the ideal-gas law relates the three,

$$p = \rho\,R_d\,T, \tag{2.5}$$

with T the absolute temperature in kelvin and $R_d = 287\,\mathrm{J\,kg^{-1}\,K^{-1}}$ the specific gas constant of dry air. Solving for the density, $\rho = p/(R_d T)$, and substituting into equation (2.4) gives

$$\frac{\partial p}{\partial z} = -\frac{p\,g}{R_d T}. \tag{2.6}$$

The rate at which pressure decreases is proportional to the pressure itself and inversely proportional to the temperature. Dividing both sides by p separates the variables:

$$\frac{\mathrm{d}p}{p} = -\frac{g}{R_d T}\,\mathrm{d}z. \tag{2.7}$$

Equation (2.7) holds for any temperature profile. For a layer in which T is constant, and with g treated as constant, both sides can be integrated from a level z_1 with pressure p_1 to a level z_2 with pressure p_2:

$$\int_{p_1}^{p_2} \frac{\mathrm{d}p}{p} = -\frac{g}{R_d T}\int_{z_1}^{z_2} \mathrm{d}z \quad\Longrightarrow\quad \ln\frac{p_2}{p_1} = -\frac{g\,(z_2 - z_1)}{R_d T}. \tag{2.8}$$

Taking the exponential, and choosing $z_1 = 0$ with $p_1 = p_0$,

$$p(z) = p_0 \exp\!\left(-\frac{g\,z}{R_d T}\right). \tag{2.9}$$

In an isothermal atmosphere pressure decreases exponentially with height. Each further increment of height removes the same *fraction* of the pressure, not the same amount, because the air higher up is less dense and an equal height increment contains less mass.

2.1.4 Scale height

The group $R_d T/g$ in equation (2.9) has the dimension of a length. It is the *pressure scale height*,

$$H = \frac{R_d T}{g}, \qquad p(z) = p_0\, e^{-z/H}, \tag{2.10}$$

the height over which the pressure of an isothermal layer falls by a factor $e \approx 2.72$, to 37 % of its value at the base. It is a calculated quantity: it follows from the temperature, which is measured. Near the surface equation (2.6) reads $\partial p/\partial z = -p/H$, so the scale height also fixes the local rate of decrease.

For an illustrative warm column at $T = 290\,\mathrm{K}$ (17°C) and a cold column at $T = 250\,\mathrm{K}$ (−23°C),

$$H_{\mathrm{warm}} = \frac{287 \times 290}{9.81}\,\mathrm{m} = 8484\,\mathrm{m} \approx 8.5\,\mathrm{km},$$
$$H_{\mathrm{cold}} = \frac{287 \times 250}{9.81}\,\mathrm{m} = 7314\,\mathrm{m} \approx 7.3\,\mathrm{km}.$$

Starting from the same $p_0 = 1000\,\mathrm{hPa}$, the pressure 3 km up is $1000\,e^{-3000/8484} = 702\,\mathrm{hPa}$ in the warm column and $1000\,e^{-3000/7314} = 664\,\mathrm{hPa}$ in the cold one. The 500 hPa surface, where $p = p_0/2$, lies at $z = H \ln 2$: at $8484 \times 0.693 = 5881\,\mathrm{m}$ in the warm column and at $7314 \times 0.693 = 5070\,\mathrm{m}$ in the cold column, 811 m lower. Warmer air has the larger scale height, so its pressure falls more slowly with height, and a warm column is vertically thicker than a cold one.

Figure 2.2 draws the two profiles of equation (2.10). The horizontal axis is pressure, the vertical axis height. Both curves start at 1000 hPa at sea level; the dotted vertical line marks 500 hPa, and the two dots mark where each column reaches it. The cold profile lies to the left of the warm one at every height: at the same height the cold column has the lower pressure, and to reach the same pressure one rises less far in it.

Warm and cold columns. The comparison has a direct consequence for the pressure field aloft. Take two neighboring columns with equal surface pressure, one warm and one cold. Pressure falls faster with height in the cold column, so at any level aloft the cold column has the lower pressure, and every isobaric surface sits lower above cold air than above warm air. The 500 hPa surface is high over the warm column and low over the cold one. Horizontal differences of temperature, without any difference of surface pressure, are thus enough to create horizontal differences of pressure aloft, and they are the origin of much of the pressure pattern of the middle and upper troposphere. Section 2.4 makes the statement exact for a real atmosphere, in which temperature changes with height.

Virtual temperature. Moist air is less dense than dry air at the same pressure and temperature, because a molecule of water vapor (molar mass $18\,\mathrm{g\,mol^{-1}}$) is lighter than the average molecule of dry air ($29\,\mathrm{g\,mol^{-1}}$) that it replaces. The *virtual temperature* T_v, in kelvin, is the temperature dry air would need in order to have the density of the moist air at the same

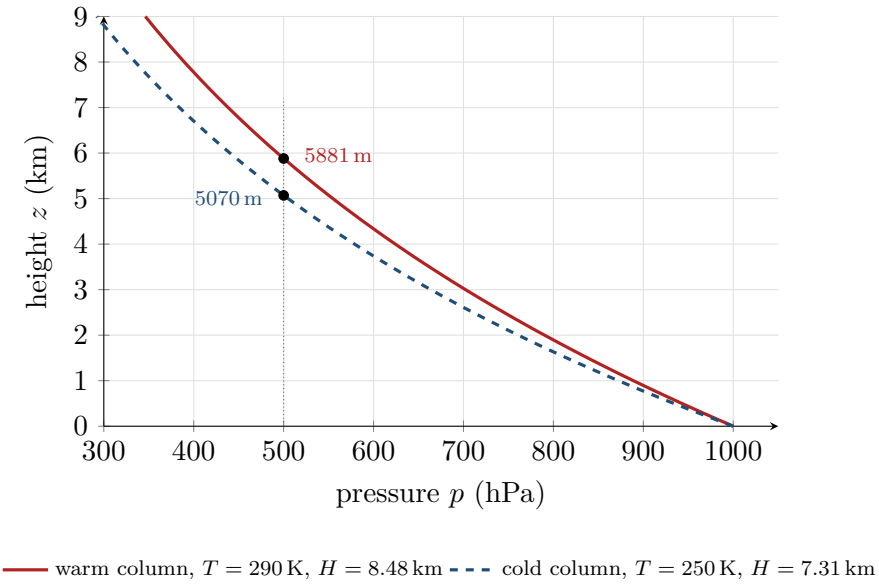


Figure 2.2: Pressure against height in two isothermal columns, $p(z) = p_0\, e^{-z/H}$ with $H = R_d T/g$ (equation (2.10)), $p_0 = 1000\,\mathrm{hPa}$, $R_d = 287\,\mathrm{J\,kg^{-1}\,K^{-1}}$, $g = 9.81\,\mathrm{m\,s^{-2}}$; temperatures illustrative. The 500 hPa surface is 811 m higher in the warm column.

pressure, so that the ideal-gas law keeps the dry form $p = \rho\, R_d\, T_v$. To a good approximation $T_v \approx T\,(1+0.61\,q)$, with q the specific humidity in kilograms of water vapor per kilogram of moist air. Humid tropical air at $T = 300\,\mathrm{K}$ with $q = 0.018\,\mathrm{kg\,kg^{-1}}$ has $T_v = 300 \times 1.011 = 303.3\,\mathrm{K}$, 3.3 K above its temperature; cold dry air at 250 K with $q = 0.001\,\mathrm{kg\,kg^{-1}}$ differs by only 0.15 K. The virtual temperature is calculated from measured temperature and humidity. Every relation of this section holds for moist air with T replaced by T_v, and the hypsometric equation of Section 2.4.1 is written with it.

2.2 Pressure surfaces and geopotential

Because pressure decreases monotonically with height, pressure itself can serve as the vertical coordinate. This section introduces the standard pressure levels, the isobaric surfaces they define, and the geopotential and geopotential height with which the heights of those surfaces are measured and mapped.

2.2.1 Pressure levels and isobaric surfaces

Meteorologists seldom ask what the pressure is at 5500 m. They ask the inverse question: at what height is the 500 hPa surface? An *isobaric surface* is the set of points at which the pressure has one given value. It is a surface in three dimensions that rises and falls from place to place and from hour to hour. Since pressure decreases monotonically upward in hydrostatic balance, every vertical column crosses a given isobaric surface exactly once, so the height of the surface is a single-valued function of horizontal position and time. That function is what an upper-air chart displays, and it is why pressure can replace height as the vertical coordinate.

Analyses and forecasts are exchanged on a fixed set of *standard pressure levels*: 1000, 925, 850, 700, 500, 300 and 250 hPa (with others, such as 200 and 100 hPa, higher up). Table 2.1 lists them with their geopotential heights and temperatures in the standard atmosphere, a reference profile with 1013.25 hPa and 15°C at sea level and a temperature decrease of 6.5 K per kilometer, and with the role each level plays in wind work. The actual heights depart from

these by up to several hundred meters with the temperature of the column below, which is the subject of Section 2.4. Over elevated terrain the lowest levels lie below the ground: a plateau at 1000 m has a surface pressure near 900 hPa, so the 1000 and 925 hPa surfaces do not exist above it, and the values a weather model reports there are extrapolations, not air.

Table 2.1: Standard pressure levels. Heights and temperatures are those of the standard atmosphere and are typical, not fixed; actual heights vary with the temperature of the column.

Level (hPa)	Typical height (m)	Standard temperature (°C)	Role in wind work
1000	111	14.3	near sea level; below the ground where surface pressure is under 1000 hPa
925	762	10.0	within or near the top of the daytime boundary layer over low terrain
850	1457	5.5	just above the boundary layer over low terrain; low-level forcing; below the ground over high plateaus
700	3012	−4.6	lower free troposphere, above most terrain
500	5574	−21.2	middle troposphere, with about half the atmosphere's mass above it; ridges and troughs of the large-scale pattern
300	9164	−44.6	upper troposphere; level of the midlatitude jet streams
250	10363	−52.4	jet-stream level, near the midlatitude tropopause

The heights on upper-air charts are obtained in two ways. A radiosonde, a balloon-borne instrument package, measures pressure, temperature and humidity as it rises, and the heights of the standard levels are calculated from those profiles with the hypsometric equation of Section 2.4.1. A weather model computes them from its own pressure and temperature fields and interpolates its output to the standard levels.

2.2.2 Geopotential

The gravitational acceleration g is not quite constant. At sea level it increases from about $9.780\,\mathrm{m\,s^{-2}}$ at the equator to about $9.832\,\mathrm{m\,s^{-2}}$ at the poles, because of the Earth's rotation and flattening, and it decreases with height, by about $0.003\,\mathrm{m\,s^{-2}}$ per kilometer near the surface. The *geopotential* Φ absorbs this variation into one quantity: it is the work needed to raise a unit mass against gravity from mean sea level to the height z,

$$\Phi(z) = \int_0^z g(z')\,\mathrm{d}z', \qquad \mathrm{d}\Phi = g\,\mathrm{d}z, \tag{2.11}$$

in joules per kilogram, which is $\mathrm{m^2\,s^{-2}}$. It is the gravitational potential energy per unit mass. Where g is treated as constant, $\Phi \approx gz$.

Surfaces of constant geopotential are the level surfaces of the Earth: gravity is everywhere perpendicular to them, so no work is done in moving along one, and a horizontal force is, exactly, a force along a surface of constant geopotential. This is the property that makes Φ the right vertical variable for the pressure-gradient force of Section 2.3.3. With $\mathrm{d}\Phi = g\,\mathrm{d}z$, the hydrostatic equation (2.4) takes the compact form

$$\mathrm{d}p = -\rho\,\mathrm{d}\Phi, \tag{2.12}$$

in which g no longer appears explicitly.

2.2.3 Geopotential height

Geopotential in $\mathrm{m^2\,s^{-2}}$ is not an intuitive number. The *geopotential height* converts it back to meters by dividing by a fixed standard gravity,

$$Z = \frac{\Phi}{g_0}, \qquad g_0 = 9.80665\,\mathrm{m\,s^{-2}}. \tag{2.13}$$

Wherever the actual g equals g_0, a meter of geopotential height is a meter of geometric height. Elsewhere the two differ slightly. At a geometric height of 5500 m, integrating equation (2.11) with the sea-level gravity of each latitude and its decrease with height gives $Z - z \approx -19\,\mathrm{m}$ at the equator, $-5\,\mathrm{m}$ at 45° latitude and $+10\,\mathrm{m}$ at the poles, differences of a few tenths of a percent. In the lower atmosphere $Z \approx z$ to within a few meters, and for reading a weather map the two can be taken as equal. The difference matters only where precision is at stake: the 30 m change of $Z - z$ from the equator to the pole means that a surface of constant geometric height is not quite a level surface, which is why charts use Z.

Like the heights of standard levels, geopotential height is calculated, not measured directly: from a radiosonde's pressure and temperature profile or from a model's fields. Upper-air charts label it in meters (or in decameters, tens of meters, on many charts: "570" for 5700 m).

2.2.4 Reading a 500 hPa chart

A 500 hPa chart shows the geopotential height Z_{500} of the 500 hPa surface as contours. A value $Z_{500} = 5700\,\mathrm{m}$ at a place means that one must rise about 5700 m above mean sea level there to reach the pressure of 500 hPa. A value of 5500 m elsewhere means that the 500 hPa surface is 200 m lower there, which, by Section 2.1.4, typically indicates a colder column beneath it. The height contours describe the shape of a constant-pressure surface in the same way as the contours of a topographic map describe the shape of terrain: high values are hills of the surface, low values are valleys, and closely spaced contours are steep slopes.

On the average the polar columns are colder than the tropical ones, so in both hemispheres the 500 hPa heights decrease from the tropics toward the pole, from about 5900 m in the subtropics to 5100 m or less over polar regions in winter. Contours are commonly drawn every 60 m. Superimposed on the poleward decrease are waves and closed centers, the ridges and troughs of Section 2.5.3, which are the features a forecaster reads first.

2.3 Height gradients as pressure gradients

The pressure on an isobaric surface is, by definition, the same everywhere, yet the force that drives the wind is a horizontal pressure gradient. This section resolves the apparent paradox: it shows that a sloping pressure surface is a horizontal pressure gradient, defines the pressure-gradient force, and derives its exact expression in terms of the slope of the surface.

2.3.1 Pressure differences at a fixed height

The horizontal pressure gradient that accelerates air is evaluated at fixed geometric height, between points side by side. Take an illustrative 500 hPa surface at $Z = 5800\,\mathrm{m}$ in the west that slopes down to 5500 m in the east, 1000 km away, and consider the fixed height of 5600 m. Figure 2.3 draws this vertical cross section. The horizontal axis is distance from west to east; the vertical axis is height. The thick blue line is the 500 hPa surface, the shaded region below it is air at more than 500 hPa, and the dashed line is the level of 5600 m. Two points on that level are marked, one in the west and one in the east.

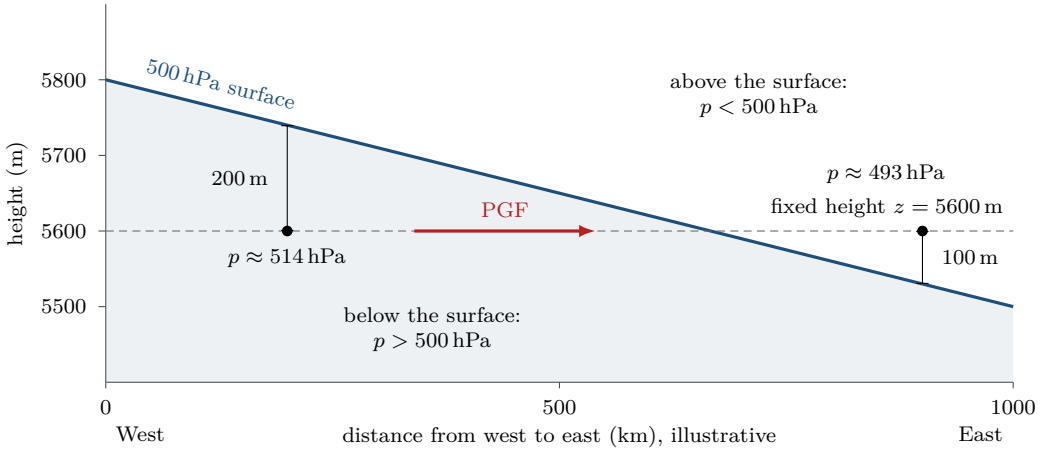


Figure 2.3: Vertical cross section through a sloping 500 hPa surface, illustrative: $Z = 5800$ m in the west, 5500 m in the east, 1000 km apart. At the fixed height of 5600 m the western point lies 200 m below the surface and the eastern point 100 m above it; pressures from $p = 500\,\text{hPa} \times e^{\Delta Z/H}$ with $H = 7.46$ km ($T = 255$ K). The pressure-gradient force (PGF) points from the higher to the lower pressure, toward the low side of the surface.

The western point lies 200 m *below* the 500 hPa surface, so it has air above it that the surface does not, and its pressure exceeds 500 hPa. With an illustrative temperature of 255 K near this level, $H = 287 \times 255/9.81 = 7460$ m, and equation (2.10) gives $p = 500\,e^{200/7460} = 513.6$ hPa. The eastern point lies 100 m *above* the surface, and its pressure is $500\,e^{-100/7460} = 493.3$ hPa. Along the fixed level the pressure therefore falls by about 20 hPa from west to east. The slope of the pressure surface and the horizontal pressure difference at fixed height are two descriptions of one fact: wherever an isobaric surface slopes, the pressure at fixed height changes horizontally, decreasing toward the side on which the surface is low.

2.3.2 The pressure-gradient force

Consider a small box of air with sides δx, δy, δz along the eastward, northward and upward directions, volume $\delta V = \delta x\,\delta y\,\delta z$ and mass $\rho\,\delta V$. The pressure on its western face pushes east with the force $p(x)\,\delta y\,\delta z$; the pressure on its eastern face pushes west with $p(x+\delta x)\,\delta y\,\delta z$. The net eastward force is

$$\left[p(x) - p(x+\delta x)\right]\delta y\,\delta z \approx -\frac{\partial p}{\partial x}\,\delta x\,\delta y\,\delta z = -\frac{\partial p}{\partial x}\,\delta V,$$

and the same argument applies in the northward direction. Dividing by the mass gives the force per unit mass, an acceleration. The horizontal *pressure-gradient force* per unit mass is

$$\mathbf{a}_{\text{PGF}} = -\frac{1}{\rho}\,\nabla_h p, \qquad \nabla_h p = \left(\frac{\partial p}{\partial x}, \frac{\partial p}{\partial y}\right), \tag{2.14}$$

where ∇_h is the horizontal gradient taken at constant height. Its unit is $\text{Pa m}^{-1}/(\text{kg m}^{-3}) = \text{N kg}^{-1} = \text{m s}^{-2}$. The minus sign makes the force point down the gradient, from high toward low pressure, perpendicular to the isobars. If pressure decreases eastward, $\partial p/\partial x < 0$, and the force points east. The vertical component of the same force, $-(1/\rho)\,\partial p/\partial z$, is the upward force that hydrostatic balance sets equal to g.

The pressure-gradient force does not depend on the Earth's rotation and is the same in both hemispheres: in each, it points toward low pressure. What differs between the hemispheres is the air's response to it, which is the subject of Chapter 3. In the example of

Section 2.3.1, with $\rho = 50\,000/(287 \times 255) = 0.683\,\mathrm{kg\,m^{-3}}$ near 500 hPa and a pressure difference of $513.6 - 493.3 = 20.3\,\mathrm{hPa} = 2030\,\mathrm{Pa}$ over 1000 km,

$$|\mathbf{a}_{\mathrm{PGF}}| = \frac{1}{0.683} \times \frac{2030\,\mathrm{Pa}}{10^6\,\mathrm{m}} \approx 3.0 \times 10^{-3}\,\mathrm{m\,s^{-2}},$$

directed east. Small as it looks, an acceleration of this size acting alone for one hour would add about $11\,\mathrm{m\,s^{-1}}$ to the wind.

2.3.3 The force from the slope of a pressure surface

The equivalence of slope and gradient can be made exact. Let pressure be a function of x and z, and move along an isobaric surface. Along the surface the pressure does not change, so

$$\mathrm{d}p = \left(\frac{\partial p}{\partial x}\right)_z \mathrm{d}x + \frac{\partial p}{\partial z}\,\mathrm{d}z = 0,$$

where the subscript z marks a derivative at constant height. The ratio $\mathrm{d}z/\mathrm{d}x$ along the surface is its slope, $(\partial z/\partial x)_p$, so

$$\left(\frac{\partial p}{\partial x}\right)_z = -\frac{\partial p}{\partial z}\left(\frac{\partial z}{\partial x}\right)_p = \rho g \left(\frac{\partial z}{\partial x}\right)_p, \tag{2.15}$$

using the hydrostatic equation (2.4) in the second step. The horizontal pressure gradient at fixed height equals the weight per unit volume times the slope of the pressure surface. Dividing by $-\rho$ and using $g\,\mathrm{d}z = \mathrm{d}\Phi = g_0\,\mathrm{d}Z$,

$$-\frac{1}{\rho}\left(\frac{\partial p}{\partial x}\right)_z = -g\left(\frac{\partial z}{\partial x}\right)_p = -\left(\frac{\partial \Phi}{\partial x}\right)_p = -g_0\left(\frac{\partial Z}{\partial x}\right)_p,$$

and with the same steps for y, in vector form,

$$-\frac{1}{\rho}\,\nabla_h p = -\nabla_p \Phi = -g_0\,\nabla_p Z, \tag{2.16}$$

where ∇_p is the horizontal gradient taken along the isobaric surface. To within the few-meter difference between Z and z of Section 2.2.3, the right-hand side is $-g\,\nabla_p z$.

Equation (2.16) is the reason upper-air charts show heights. On a height chart the density has disappeared: the pressure-gradient force per unit mass is gravity times the slope of the surface, whatever the density at that level. A 300 m fall of Z_{500} over 1000 km, the example of Figure 2.3, gives $g_0 \times 300/10^6 = 2.9 \times 10^{-3}\,\mathrm{m\,s^{-2}}$, the value of the fixed-height calculation of Section 2.3.2 without any need for ρ or T; the difference of about one percent between 2.94 and $2.97 \times 10^{-3}\,\mathrm{m\,s^{-2}}$ comes from evaluating the density at a single level across a 300 m interval in which it varies. Equal height gradients mean equal forces at every level, which is not true of equal pressure gradients, since ρ decreases upward.

Principle 2.2. *The slope of an isobaric surface is a horizontal pressure gradient: $-(1/\rho)\,\nabla_h p = -g_0\,\nabla_p Z$. The pressure-gradient force per unit mass is gravity times the slope, directed toward lower heights.*

2.3.4 Contour spacing

On a map, the magnitude of the gradient is read from the spacing of the contours: the closer the contours, the larger $|\nabla_h p|$ or $|\nabla_p Z|$ and the stronger the force. Figure 2.4 is a schematic surface map with north up. The blue lines are isobars at 1016, 1012, 1008 and 1004 hPa, with high pressure to the south and low pressure to the north; they are packed tightly on the west

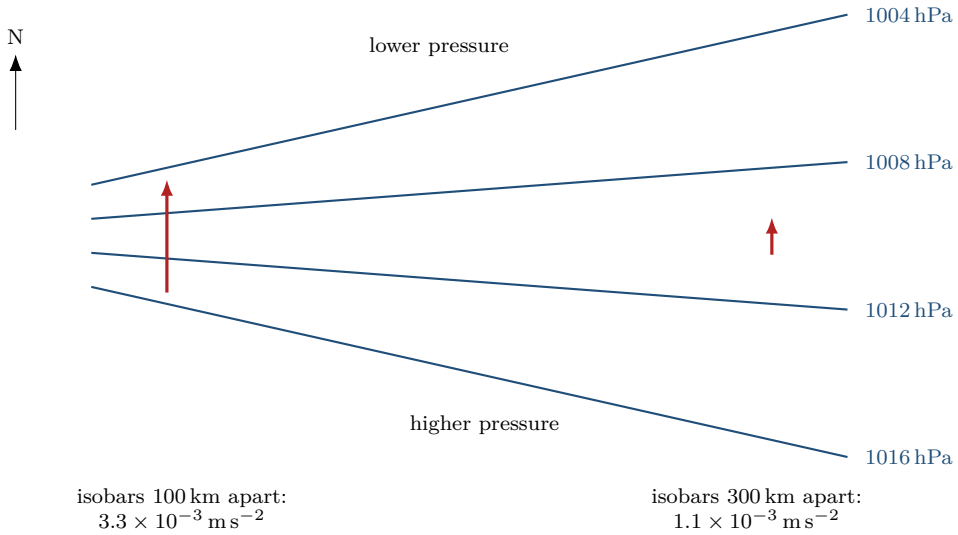


Figure 2.4: Contour spacing and the pressure-gradient force, schematic surface map with north up, valid in either hemisphere. Isobars every 4 hPa, about 100 km apart on the west side and 300 km apart on the east side (illustrative). Red: the pressure-gradient force, $|\nabla_h p|/\rho$ with $\rho = 1.2\,\mathrm{kg\,m^{-3}}$, perpendicular to the isobars toward low pressure and three times stronger where the isobars are three times closer.

side and spread on the east side. The red arrows are the pressure-gradient force at two places, drawn perpendicular to the isobars and with lengths proportional to the force.

With 4 hPa = 400 Pa between isobars and a near-surface density of $1.2\,\mathrm{kg\,m^{-3}}$, the force where the isobars are 100 km apart is $400/(1.2\times10^5) = 3.3\times10^{-3}\,\mathrm{m\,s^{-2}}$, and where they are 300 km apart it is $400/(1.2\times3\times10^5) = 1.1\times10^{-3}\,\mathrm{m\,s^{-2}}$. On a height chart the same reading applies to height contours: at 500 hPa, contours every 60 m that are 300 km apart give $g_0\times60/(3\times10^5) = 2.0\times10^{-3}\,\mathrm{m\,s^{-2}}$.

Closely spaced pressure or height contours therefore indicate a strong forcing and, other things equal, strong winds. The wind that results is not fixed by the force alone. For the same gradient the balanced wind of Chapter 3 is stronger at low latitudes than at high ones, because the Coriolis effect that balances the force is weaker there; curvature of the flow modifies it (Chapter 4); and near the ground friction, the stability of the air and terrain decide how much of it reaches the surface, topics of Chapters 3, 13 and 20. Contour spacing measures the forcing, not the wind at a site.

2.4 Thickness and temperature

Section 2.1.4 found that warm isothermal columns are thicker than cold ones. This section makes the statement exact for an atmosphere whose temperature varies with height, through the hypsometric equation, works through the thickness of the 1000–500 hPa layer, and shows how horizontal temperature gradients tilt the pressure surfaces more and more with height.

2.4.1 The hypsometric equation

Start from the hydrostatic equation in geopotential form, equation (2.12), $\mathrm{d}\Phi = -\mathrm{d}p/\rho$, and replace the density with the ideal-gas law for moist air, $\rho = p/(R_d T_v)$:

$$\mathrm{d}\Phi = -R_d\,T_v\,\frac{\mathrm{d}p}{p} = -R_d\,T_v\,\mathrm{d}(\ln p). \tag{2.17}$$

Integrate from a lower pressure level p_1 to an upper level $p_2 < p_1$:

$$\Phi_2 - \Phi_1 = -R_d \int_{p_1}^{p_2} T_v \, \mathrm{d}(\ln p) = R_d \int_{p_2}^{p_1} T_v \, \mathrm{d}(\ln p).$$

Define the layer-mean virtual temperature as the average of T_v weighted by $\ln p$,

$$\overline{T_v} = \frac{\int_{p_2}^{p_1} T_v \, \mathrm{d}(\ln p)}{\int_{p_2}^{p_1} \mathrm{d}(\ln p)} = \frac{\int_{p_2}^{p_1} T_v \, \mathrm{d}(\ln p)}{\ln(p_1/p_2)}. \tag{2.18}$$

Then $\Phi_2 - \Phi_1 = R_d \, \overline{T_v} \, \ln(p_1/p_2)$, and dividing by g_0 gives the *hypsometric equation*,

$$Z_2 - Z_1 = \frac{R_d \, \overline{T_v}}{g_0} \ln \frac{p_1}{p_2}. \tag{2.19}$$

The left side is the thickness of the layer between the two isobaric surfaces. The equation is exact under hydrostatic balance: the variation of gravity is absorbed by the geopotential and the variation of temperature with height by the definition of $\overline{T_v}$. For an isothermal layer it reduces to equation (2.8). For dry air $T_v = T$, and in most of the troposphere the two differ by less than a few kelvin (Section 2.1.4), so $\overline{T_v} \approx \bar{T}$ is often adequate for a first estimate.

The equation says that the thickness of a layer between two given pressures is proportional to its mean virtual temperature and to nothing else. It does not depend on the surface pressure or on how much air lies below the layer. This is how radiosonde heights are computed: the measured profile of T_v is integrated layer by layer upward from the surface, and each standard level's height is the surface elevation plus the sum of the thicknesses below it.

2.4.2 The thickness of the 1000–500 hPa layer

The most widely used thickness is that of the 1000–500 hPa layer, $Z_{500} - Z_{1000}$, which contains about half the mass of the atmosphere. For this layer $\ln(p_1/p_2) = \ln 2 = 0.693$, and the coefficient of equation (2.19) is

$$\frac{R_d \ln 2}{g_0} = \frac{287 \times 0.693}{9.80665} \,\mathrm{m\,K^{-1}} = 20.29 \,\mathrm{m\,K^{-1}} :$$

each kelvin of layer-mean virtual temperature adds about 20 m of thickness. For two illustrative columns,

$$\begin{aligned} \overline{T_v} = 283\,\mathrm{K}\ (10^\circ\mathrm{C}): &\quad Z_{500} - Z_{1000} = 20.29 \times 283 = 5741\,\mathrm{m}, \\ \overline{T_v} = 263\,\mathrm{K}\ (-10^\circ\mathrm{C}): &\quad Z_{500} - Z_{1000} = 20.29 \times 263 = 5335\,\mathrm{m}. \end{aligned}$$

A difference of 20 K in mean temperature makes the warm layer 406 m thicker. For comparison, the standard atmosphere of Table 2.1 has a thickness of $5574 - 111 = 5463$ m, which corresponds to $\overline{T_v} = 269$ K. Large thickness means warm air, small thickness cold air: a thickness chart is a chart of the mean temperature of the lower half of the atmosphere, read in meters.

Thinner layers follow the same rule with smaller coefficients. For the 1000–850 hPa layer, which over low terrain contains the boundary layer, $R_d \ln(1000/850)/g_0 = 4.76\,\mathrm{m\,K^{-1}}$, and the two columns above give 1346 m and 1251 m, a difference of 95 m.

2.4.3 Temperature gradients and the tilt of pressure surfaces

Consider now two columns 1500 km apart, the illustrative warm and cold columns of Section 2.4.2, and suppose the 1000 hPa surface is flat, at $Z_{1000} = 100$ m in both: there is no pressure gradient near the ground. The 500 hPa surface is at $100 + 5335 = 5435$ m over the cold column and $100 + 5741 = 5841$ m over the warm one. The difference of temperature has created

a slope of 406 m in 1500 km at 500 hPa, and by equation (2.16) a pressure-gradient force of $g_0 \times 406/(1.5 \times 10^6) = 2.7 \times 10^{-3}\,\mathrm{m\,s^{-2}}$, directed from the warm side toward the cold side. At 850 hPa the slope is only 95 m and the force $6.2 \times 10^{-4}\,\mathrm{m\,s^{-2}}$; at 700 hPa it is 209 m and $1.4 \times 10^{-3}\,\mathrm{m\,s^{-2}}$.

Figure 2.5 draws this situation as a schematic vertical cross section, not to scale. The cold column is on the left, on the poleward side, and the warm column on the right, on the equatorward side; the lines are the 1000, 850, 700 and 500 hPa surfaces. The vertical double arrows in the two columns are their 1000–500 hPa thicknesses, and the red arrows between the columns are the pressure-gradient force at each level. The 1000 hPa surface is flat and carries no force; every surface above it tilts down toward the cold side, and the tilt, and with it the force, grows with height.

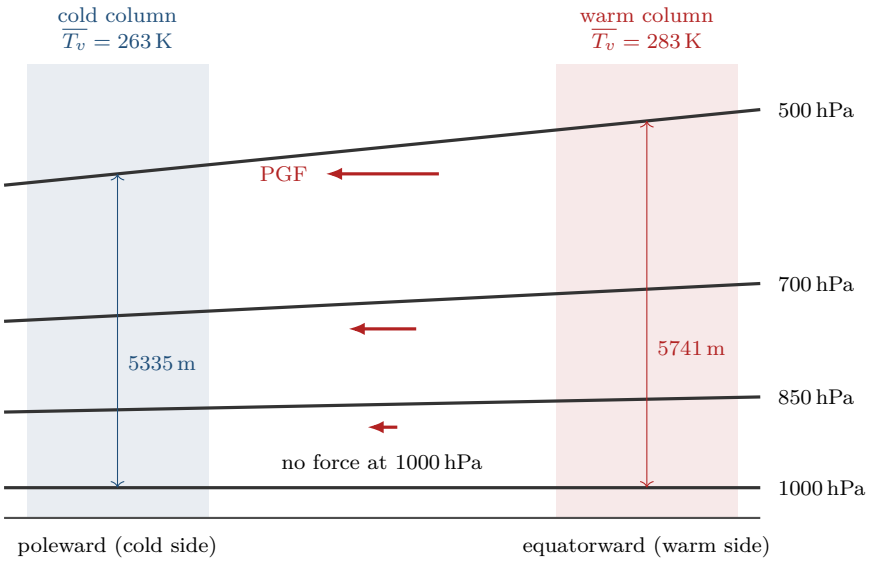


Figure 2.5: Pressure surfaces between a cold and a warm column, schematic and not to scale. With the 1000 hPa surface flat at $Z = 100$ m, the hypsometric equation (2.19) puts the 500 hPa surface at 5435 m over the cold column and 5841 m over the warm one (illustrative $\overline{T_v}$ of 263 and 283 K). The surfaces tilt toward the cold side, more steeply with height; red arrows: the pressure-gradient force, growing with height.

The general statement follows from writing the height of an upper surface as the height of a lower one plus the thickness between them. For the 500 hPa surface,

$$\nabla_p Z_{500} = \nabla_p Z_{1000} + \nabla_p (Z_{500} - Z_{1000}), \tag{2.20}$$

the height gradient aloft is the height gradient near the surface plus the thickness gradient, and by equation (2.19) the thickness gradient is $20.29\,\mathrm{m\,K^{-1}}$ times the gradient of layer-mean virtual temperature. Horizontal temperature gradients produce tilted pressure surfaces, tilted surfaces mean horizontal pressure gradients aloft, and those gradients accelerate the air. Where the poleward decrease of temperature is concentrated, in a front or a strong temperature contrast between land and sea, the height gradient aloft is concentrated with it.

Toward the thermal wind. Since the balanced wind of Chapter 3 is proportional to the height gradient, a pressure-gradient force that changes with height implies a wind that changes with height. A horizontal temperature gradient therefore implies vertical wind shear: the wind aloft differs from the wind below by an amount set by the thickness gradient between the levels. This relation is the thermal wind, developed in Chapter 18, and it is the reason that strong winds aloft lie above strong horizontal temperature contrasts.

Principle 2.3. *The thickness between two pressure levels is proportional to the layer-mean virtual temperature, $R_d\overline{T_v}\ln(p_1/p_2)/g_0$; horizontal temperature gradients tilt the pressure surfaces, increasingly with height, toward the cold side.*

2.5 Weather maps and their vocabulary

Weather charts display the pressure field in two ways: as sea-level pressure on surface maps and as heights of isobaric surfaces on upper-air maps. This section defines the pressures and the features those maps show, with the reduction of station pressure to sea level worked through, and explains why the contours of an upper-air chart resemble streamlines of the wind.

2.5.1 Station pressure and mean sea-level pressure

The *station pressure* p_{stn} is the pressure measured by a barometer at the elevation of the instrument. It is dominated by elevation. A station at 1500 m reads roughly 850 hPa while a station at sea level reads roughly 1013 hPa, a difference of more than 160 hPa that has nothing to do with the weather. The pressure differences between weather systems are ten times smaller, so a map of raw station pressures would be a map of the terrain.

The *mean sea-level pressure* p_{msl} removes the elevation effect. It is the station pressure reduced to sea level: the pressure that would be found at sea level below the station if the ground were replaced by a column of air of an assumed temperature. By the hypsometric equation (2.19) applied between sea level ($Z = 0$, pressure p_{msl}) and the station ($Z = z_{\mathrm{stn}}$, pressure p_{stn}),

$$p_{\mathrm{msl}} = p_{\mathrm{stn}} \exp\!\left(\frac{g_0\, z_{\mathrm{stn}}}{R_d\, \overline{T_v}}\right), \tag{2.21}$$

where z_{stn} is the station elevation and $\overline{T_v}$ the mean virtual temperature of the fictitious column. The station pressure is measured; the sea-level pressure is calculated, and the calculation depends on the assumption about the column.

Figure 2.6 draws the reduction. It is a vertical cross section of terrain, with height on the vertical axis and distance along the horizontal axis: a station A near sea level on the coast and a station B on a plateau at 1500 m. Below station B the dashed column is the fictitious air column of the reduction, extending from the station down to mean sea level, where the reduced pressure is reported.

For station B, take an illustrative air temperature of 15°C at the station and the standard decrease of 6.5 K per kilometer for the fictitious column, whose mean temperature, at its mid-height of 750 m, is then $288.2 + 0.0065 \times 750 \approx 293$ K; neglect humidity, so $\overline{T_v} \approx 293$ K. Then

$$\frac{g_0\, z_{\mathrm{stn}}}{R_d\, \overline{T_v}} = \frac{9.80665 \times 1500}{287 \times 293} = 0.1749, \qquad p_{\mathrm{msl}} = 850\,\mathrm{hPa} \times e^{0.1749} = 850 \times 1.1912 = 1012.5\,\mathrm{hPa}.$$

The 163 hPa difference between the two station pressures has become a difference of 0.5 hPa between the two sea-level pressures, and what remains on the map is the weather. The result is sensitive to the assumed column: with $\overline{T_v} = 283$ K, for example on a day 10 K colder, the same 850 hPa reduces to 1018.8 hPa. At a 1500 m station, an error of 10 K in the assumed column temperature moves the reduced pressure by about 6 hPa, more than one contour of a surface map. Operational reductions differ in how they choose the column temperature, and over high terrain the sea-level pressure field partly reflects that choice. Pressure gradients read from a sea-level map over mountains and high plateaus are therefore less reliable than those read over lowlands or from an upper-air chart.

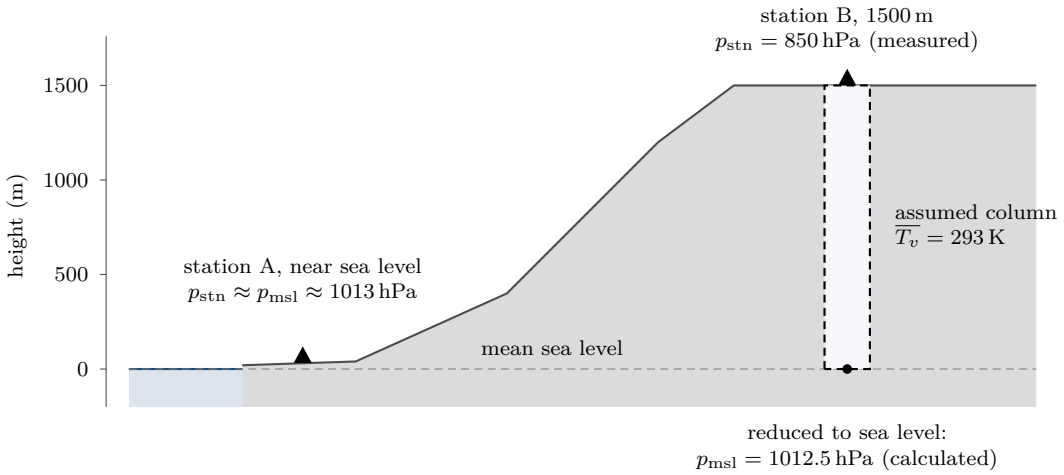


Figure 2.6: Reduction of station pressure to mean sea level, schematic cross section with illustrative values. Station B on a 1500 m plateau measures $p_{\mathrm{stn}} = 850\,\mathrm{hPa}$; replacing the ground beneath it by a column of air with an assumed $\overline{T_v} = 293\,\mathrm{K}$ and applying equation (2.21) gives $p_{\mathrm{msl}} = 1012.5\,\mathrm{hPa}$, comparable with the 1013 hPa of station A on the coast.

2.5.2 Surface maps and upper-air maps

A surface map contours the mean sea-level pressure, typically every 4 hPa (1000, 1004, 1008, 1012 hPa, ...): it shows pressure differences at approximately a common elevation, sea level. An upper-air map contours the geopotential height of an isobaric surface, at 500 hPa for example with contours such as 5400, 5520, 5640 and 5760 m (every 120 m in this list; 60 m is the common interval): it shows height differences of a common pressure surface. Table 2.2 sets the two side by side.

Table 2.2: Surface and upper-air maps compared. Both describe horizontal pressure gradients; they differ in which variable is held fixed.

	Surface map	Upper-air map (e.g. 500 hPa)
Quantity contoured	mean sea-level pressure p_{msl}	geopotential height Z
Held fixed	height (sea level)	pressure (500 hPa)
Typical contours	1000, 1004, 1008, 1012 hPa	5400, 5460, 5520, ... m
Force per unit mass	$-(1/\rho)\,\nabla_h p_{\mathrm{msl}}$	$-g_0\,\nabla_p Z$ (equation (2.16))
One contour interval equals	4 hPa $\approx$ 33 m of height of the 1000 hPa surface	60 m of height $\approx$ 4 hPa at a fixed height near 5.6 km
Main caveat	reduced (calculated) values over high terrain	interpolated or below ground at low levels over high terrain

The two kinds of map describe the same physical object, the horizontal pressure gradient, through different variables. Near sea level, with $\rho = 1.225\,\mathrm{kg\,m^{-3}}$, a pressure difference of 4 hPa corresponds to a height difference of the nearby isobaric surface of $400/(1.225 \times 9.80665) = 33\,\mathrm{m}$; at 500 hPa, with $\rho = 0.683\,\mathrm{kg\,m^{-3}}$, a height difference of 60 m corresponds to a pressure difference at fixed height of $0.683 \times 9.80665 \times 60 = 402\,\mathrm{Pa} \approx 4\,\mathrm{hPa}$. Dynamically, the isobars of a surface map and the height contours of an upper-air map are interchangeable descriptions of the forcing.

2.5.3 Ridges and troughs

A *ridge* is an elongated region of relatively high geopotential height on an isobaric surface (or of relatively high pressure on a surface map): the pressure surface bulges upward, and the contours bend toward the lower heights, which in both hemispheres means toward the pole. Ridges usually lie over relatively warm columns. A *trough* is an elongated region of relatively low geopotential height (or pressure): the surface dips, the contours bend toward the higher heights, that is toward the equator, and troughs usually lie over relatively cold columns. The line along which the contours bend most sharply is the ridge axis or trough axis. Both terms are descriptive and are read from the shape of the contours; on a 500 hPa chart they are the waves of the large-scale pattern.

Figure 2.7 draws one wave of 500 hPa height contours in each hemisphere, with north up in both panels. In the Northern Hemisphere panel the heights decrease northward, from 5760 m at the bottom to 5400 m at the top; in the Southern Hemisphere panel they decrease southward, from 5760 m at the top to 5400 m at the bottom. The contours have the same shape in both panels, but the labels swap: where the contours bulge northward the Northern Hemisphere has a ridge (high heights pushed poleward) and the Southern Hemisphere a trough (low heights pushed equatorward). The dashed lines are the ridge and trough axes and the black arrows the large-scale wind along the contours, from the west in both panels.

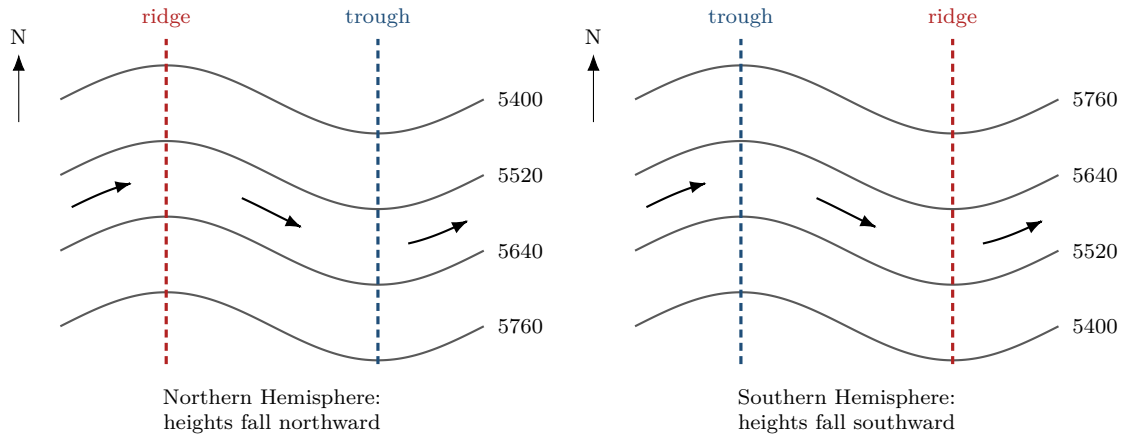


Figure 2.7: Ridge and trough on a 500 hPa chart, schematic, north up in both panels; contour labels are geopotential heights in meters. The same contour shape is a ridge where it bulges toward the pole and a trough where it bulges toward the equator, so the labels swap between the hemispheres. Arrows: the large-scale wind, nearly parallel to the contours with lower heights on its left in the Northern Hemisphere and on its right in the Southern Hemisphere; from the west in both.

For South America the consequence is practical: a 500 hPa ridge over the continent appears on the chart as contours bulging southward, toward Antarctica, and a trough as contours bulging northward, toward the tropics. The physical definitions, high heights over warm columns and low heights over cold ones, are the same in both hemispheres; only the direction of the pole on the map changes.

2.5.4 Height contours and streamlines

If the pressure-gradient force acted alone, air would accelerate straight down the gradient, across the contours, from high toward low heights. On the Earth, moving air is deflected by the Coriolis effect, to the right of its motion in the Northern Hemisphere and to the left in the Southern Hemisphere. The deflection continues until the Coriolis force nearly balances the pressure-

gradient force, which happens when the wind blows nearly parallel to the contours. Above the boundary layer, on scales of hundreds of kilometers, the large-scale wind is therefore close to parallel to the height contours, with lower heights to its left in the Northern Hemisphere and to its right in the Southern Hemisphere. Since heights fall toward the pole in both hemispheres, the mean wind aloft blows from the west in both, as in Figure 2.7.

This near-balance is geostrophic balance, the subject of Chapter 3; it is why the height contours of an upper-air chart look like the streamlines of the flow and why forecasters read the wind directly from them. The resemblance is approximate in two ways. The departures from balance are small but are what changes the pattern, and near the surface friction breaks the balance and turns the wind across the isobars toward low pressure, a topic of Chapter 3.

2.6 From the pressure field to near-surface wind

The pressure field is where a model of the wind at 10 to 150 m above the ground begins. This section places it in the modeling chain, separates the forcing it supplies from the response near the surface, and works through a quantitative 850 hPa example.

2.6.1 The modeling chain

A model of near-surface wind does not begin at 10 m. The wind at a site is the end of a chain of transformations: the pressure field aloft sets a large-scale wind; the boundary layer, the layer of air directly influenced by the ground, adjusts that wind through turbulent mixing and surface drag; and terrain and local surface features shape what finally arrives at the height of a conductor, an anemometer or a turbine hub. Figure 2.8 draws the chain. The four boxes are its stages, from left to right; the braces above group them into forcing and response, and the notes below say how a weather model and an instrument represent each stage.

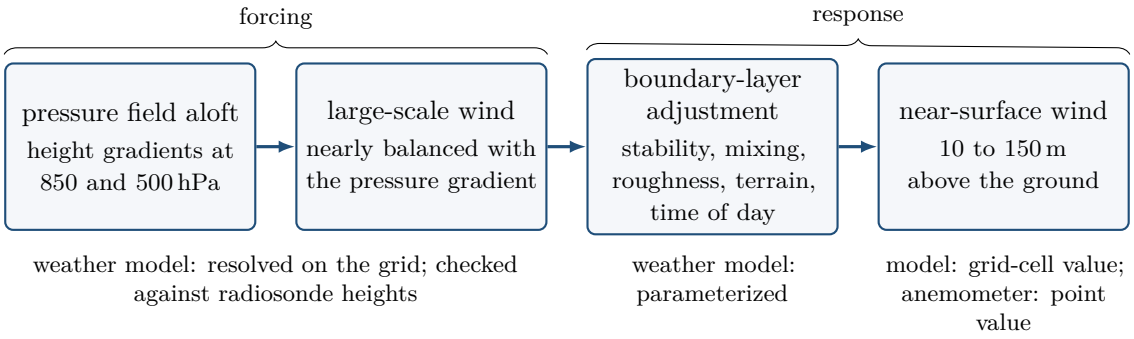


Figure 2.8: The modeling chain from the pressure field to the wind at a site. The pressure field aloft and the large-scale wind are the forcing, well resolved by a weather model; the boundary layer and the local features are the response, which a model parameterizes and an instrument samples at one point.

The distinction between what the atmosphere does and what a model represents runs along the chain. The height field at 850 or 500 hPa varies over hundreds to thousands of kilometers, much larger than the grid spacing of any current weather model, so a model represents it well, and radiosonde heights check it directly. The boundary-layer adjustment involves turbulent eddies far smaller than a grid cell; a model computes their average effect from a parameterization, a formula, rather than resolving them. The wind a model reports at 10 m is therefore a grid-cell value, a parameterized response to a well-resolved forcing, while an anemometer reports a point value at one place and height. A diagnosis of a wind event, or of a model's error, proceeds down the chain in the same order: first the forcing, then the response.

2.6.2 Forcing and response near the surface

A strong height gradient at 850 hPa means a strong forcing. Whether it produces $4\,\mathrm{m\,s^{-1}}$ or $12\,\mathrm{m\,s^{-1}}$ at 10 m depends on the response: on the stability of the lower atmosphere, on how vigorously turbulent mixing brings the faster air above down toward the surface, on the roughness of the surface, on the terrain, and on the time of day, which governs the first two over land. Under the same illustrative forcing, a well-mixed afternoon over open flat land can bring most of the momentum of the air above down to 10 m, while a calm, clear night lets the air near the ground cool, become stable and decouple from the flow aloft, so that the 10 m wind is a fraction of the wind a few hundred meters up. These mechanisms are the subject of Chapters 6 to 20.

The division of roles can be stated compactly: the upper-air forcing sets the wind available to the boundary layer, and the boundary layer controls how much of it appears near the surface. For engineering applications both halves matter. The convective cooling of an overhead conductor, and hence the current a transmission line can carry, depends on the speed and direction of the wind at conductor height, typically 10 to 30 m, where the response is most variable. A wind turbine hub at 100 to 150 m sits higher in the boundary layer, closer to the forcing, and its wind can behave differently from the 10 m wind at the same site, at night in particular.

2.6.3 An 850 hPa example

Take two illustrative locations A and B, $\Delta n = 300\,\mathrm{km}$ apart along the direction of the height gradient, with 850 hPa heights $Z_A = 1500\,\mathrm{m}$ and $Z_B = 1380\,\mathrm{m}$. The height difference is $\Delta Z = 120\,\mathrm{m}$, a slope of $120/(3\times10^5) = 4.0\times10^{-4}$. By equation (2.16) the pressure-gradient force per unit mass is

$$|\mathbf{a}_{\mathrm{PGF}}| = g_0\,\frac{\Delta Z}{\Delta n} = 9.80665 \times \frac{120\,\mathrm{m}}{3\times10^5\,\mathrm{m}} = 3.9\times10^{-3}\,\mathrm{m\,s^{-2}},$$

directed from A toward B. Expressed as a pressure difference at a fixed height near 1.5 km, with $\rho = 85\,000/(287\times280) = 1.06\,\mathrm{kg\,m^{-3}}$ for an illustrative 280 K, it is $\rho\, g_0\, \Delta Z = 1.06 \times 9.80665 \times 120 = 1245\,\mathrm{Pa}$, about 12 hPa in 300 km. Acting alone for one hour this force would add $3.9\times10^{-3}\times3600 = 14\,\mathrm{m\,s^{-1}}$ to the wind. It does not act alone: within a few hours the Coriolis effect turns the accelerating air until the two nearly balance.

Chapter 3 derives that balance. Anticipating its result, the Coriolis acceleration of a horizontal wind of speed U has magnitude $|f|\,U$, with $f = 2\Omega\sin\phi$ the Coriolis parameter, and the balanced, geostrophic, wind speed is the one at which it equals the pressure-gradient force:

$$U_g = \frac{g_0}{|f|}\,|\nabla_p Z|. \tag{2.22}$$

At an illustrative latitude of 45°, north or south, $|f| = 2\times7.292\times10^{-5}\times\sin 45^\circ = 1.03\times10^{-4}\,\mathrm{s^{-1}}$ and $U_g = 3.9\times10^{-3}/1.03\times10^{-4} = 38\,\mathrm{m\,s^{-1}}$. In the Northern Hemisphere ($f > 0$), with B to the north of A, this wind blows along the contours with the lower heights on its left, from the west. In the Southern Hemisphere ($f < 0$), with B to the south of A, it blows with the lower heights on its right, again from the west.

A geostrophic wind of $38\,\mathrm{m\,s^{-1}}$ at 850 hPa is strong; gradients of this size are found around intense cyclones and along fronts, and they are a substantial forcing. With a difference of only 10 m over the same 300 km the force is $g_0\times10/(3\times10^5) = 3.3\times10^{-4}\,\mathrm{m\,s^{-2}}$, twelve times weaker, and the geostrophic wind at 45° is about $3\,\mathrm{m\,s^{-1}}$. The 850 hPa height gradient, together with the 925 and 700 hPa gradients, is therefore one of the first quantities to inspect when diagnosing a windy day. It says how strong the forcing is; Section 2.6.2 says why it does not, by itself, give the wind at 10 m.

2.7 What to retain

Definition 2.1 (The pressure field as wind forcing)**.** Temperature sets density and, through hydrostatic balance, the rate at which pressure decreases with height; the mean temperature of a layer sets its thickness; differences of thickness tilt the pressure surfaces; and a tilted pressure surface is a horizontal pressure gradient, $-(1/\rho)\,\nabla_h p = -g_0\,\nabla_p Z$, which accelerates the air and forces the wind.

Table 2.3 lists the chapter's terms with their meaning, their units and the subsection that defines each.

Table 2.3: Terms of the chapter and where each is defined.

Term	Meaning	Units	Defined in
Hydrostatic balance	$\partial p/\partial z = -\rho g$: the pressure force on a layer balances its weight	–	2.1.2
Scale height	$H = R_d T/g$: height over which an isothermal layer's pressure falls by e	m	2.1.4
Virtual temperature	$T_v \approx T(1 + 0.61\,q)$: temperature of dry air with the moist air's density	K	2.1.4
Isobaric surface	surface of one constant pressure	–	2.2.1
Geopotential	$\Phi = \int_0^z g\,\mathrm{d}z'$: work to lift a unit mass from sea level	$\mathrm{m^2\,s^{-2}}$	2.2.2
Geopotential height	$Z = \Phi/g_0$; within a few meters of z in the lower atmosphere	m	2.2.3
Pressure-gradient force	$-(1/\rho)\,\nabla_h p = -g_0\,\nabla_p Z$, toward low pressure	$\mathrm{m\,s^{-2}}$	2.3.2, 2.3.3
Hypsometric equation	$Z_2 - Z_1 = (R_d\overline{T_v}/g_0)\ln(p_1/p_2)$	m	2.4.1
Thickness	height difference between two isobaric surfaces; $\propto \overline{T_v}$	m	2.4.1
Station pressure	p_{stn}: pressure measured at the instrument's elevation	hPa	2.5.1
Mean sea-level pressure	p_{msl}: station pressure reduced to sea level with an assumed column	hPa	2.5.1
Ridge	elongated region of relatively high height or pressure; often warm	–	2.5.3
Trough	elongated region of relatively low height or pressure; often cold	–	2.5.3

2.8 Exercises

Exercise 2.1. An isothermal column has $T = 270\,\mathrm{K}$ and a surface pressure of 1010 hPa at sea level. (a) Compute its scale height. (b) Compute the pressure at 1500 m and the height of the 700 hPa surface. (c) Repeat (a) and (b) for $T = 300\,\mathrm{K}$, and state in which column the 700 hPa surface is higher and by how much. (d) Using the hydrostatic equation, by how many meters must a barometer at sea level be raised in the 300 K column for its reading to fall by 1 hPa?

Exercise 2.2. (a) A radiosonde ascent gives a 1000–500 hPa thickness of 5460 m. Compute the layer-mean virtual temperature. (b) Compute the 1000–850 hPa thickness of a layer with $\overline{T_v} = 290\,\mathrm{K}$. (c) Across a front, the 1000–500 hPa thickness decreases by 240 m over 600 km

while the 1000 hPa surface is flat. Using equation (2.20), compute the pressure-gradient force per unit mass at 500 hPa and state its direction relative to the warm and the cold air. (d) What is the force at 1000 hPa?

Exercise 2.3. A station at an elevation of 800 m measures $p_{\mathrm{stn}} = 915\,\mathrm{hPa}$. (a) Reduce it to sea level with an assumed column $\overline{T_v} = 290\,\mathrm{K}$. (b) Repeat with $\overline{T_v} = 285\,\mathrm{K}$ and 295 K, and give the spread of the reduced pressure. (c) A neighboring coastal station reports $p_{\mathrm{msl}} = 1006\,\mathrm{hPa}$, 200 km away. With $\rho = 1.2\,\mathrm{kg\,m^{-3}}$, compute the range of sea-level pressure-gradient forces implied by (a) and (b), and say what the exercise shows about reading sea-level pressure gradients over elevated terrain.

Exercise 2.4. On an 850 hPa chart over southern South America at 35°S, the height is 1520 m at a point A and 1480 m at a point B 400 km due south of A. (a) Compute the magnitude of the pressure-gradient force per unit mass and its direction. (b) Compute the Coriolis parameter f, with its sign, and the geostrophic speed from equation (2.22). (c) State the direction from which the balanced wind blows, using the rule of Section 2.5.4, and check it against Figure 2.7. (d) A transmission line in the area runs east–west. Explain why the result of (b) does not give the wind speed or direction at the conductor height of 20 m, and name the factors that decide them.

Chapter 3

Coriolis Force and Geostrophic Wind

3.1 The direction of large-scale wind

Chapter 2 described the pressure field: how pressure is measured, how it is reduced to sea level, and how it is mapped, as isobars on a surface of constant height or as height contours on a surface of constant pressure. A horizontal difference of pressure pushes air from high toward low pressure. On a weather map, however, the wind of the large weather systems does not blow from the high to the low. It blows nearly along the contours, with high pressure on one side and low pressure on the other, and only near the ground does it cross them at an angle. The question of this chapter is

why does large-scale wind flow along the pressure contours instead of directly from high to low pressure, and why does the wind near the ground cross them?

The answer involves the rotation of the Earth. The pressure-gradient force starts the motion; the Coriolis force, which appears because the wind is described relative to a rotating Earth, turns it; and when the two forces balance, the result is the geostrophic wind. The chapter derives the Coriolis force, the balance and its consequences in both hemispheres; it shows how the geostrophic wind is computed from a weather map; it explains why friction near the ground makes the wind cross the isobars toward low pressure; and it places the geostrophic wind at the head of the chain of processes that produces the wind at the heights of engineering interest, 10 to 150 m above the ground.

Jargon: isobar, height contour, inertial and rotating frame, Coriolis force, Coriolis parameter, geostrophic balance, geostrophic wind, ageostrophic wind, cross-isobar flow, surface stress, Ekman spiral, free atmosphere

An *isobar* is a line of constant pressure on a map of a surface of constant height, usually sea level; a *height contour* is a line of constant geopotential height on a map of a surface of constant pressure (Chapter 2). Both are called *pressure contours* below. An *inertial frame* is a frame of reference that neither accelerates nor rotates, in which Newton's laws hold as written; a *rotating frame* turns with the Earth, and winds are measured in it. The *Coriolis force* is the apparent force per unit mass, in $\mathrm{m\,s^{-2}}$, that appears in the equation of motion written in the rotating frame; for horizontal motion it is $-f\mathbf{k}\times\mathbf{V}$, perpendicular to the wind, with magnitude $|f|U$. The *Coriolis parameter* $f = 2\Omega\sin\phi$, in $\mathrm{s^{-1}}$, sets its strength at latitude ϕ; it is calculated from the latitude, positive north of the equator and negative south of it. *Geostrophic balance* is the state in which the pressure-gradient force and the Coriolis force are equal and opposite, so that the air does not accelerate horizontally. The *geostrophic wind* $\mathbf{V}_g$, in $\mathrm{m\,s^{-1}}$, is the wind that would be in exact geostrophic balance with the pressure field; it is not measured but calculated from analyzed fields of pressure or geopotential height. The *ageostrophic wind* $\mathbf{V}_a = \mathbf{V} - \mathbf{V}_g$ is the part of the actual wind that departs from it. *Cross-isobar flow* is the component of the wind across the isobars, directed toward low pressure near the surface; the angle between the wind and the isobars is the *crossing angle*. *Surface stress*, in pascals, is the horizontal force per unit area that the surface and the atmosphere exert on each other, carried by the turbulent transfer of horizontal momentum. The *Ekman spiral* is the idealized strengthening and turning of the wind with height through the friction layer, from a slow cross-isobar wind at the surface to the geostrophic wind aloft. The *free atmosphere* is the atmosphere above the boundary layer, where the effect of surface friction is negligible.

Key idea

The pressure-gradient force accelerates air toward low pressure; as the air gains speed, the Coriolis force, perpendicular to the motion and proportional to the speed, turns it until the two forces balance and the wind blows along the contours, with low pressure to its left in the Northern Hemisphere and to its right in the Southern. Near the ground, surface stress slows the wind, the Coriolis force weakens with it, and the pressure-gradient force, no longer fully balanced, turns the wind across the contours toward low pressure.

3.1.1 Wind along the contours

Two observations frame the chapter. On a map of the 500 hPa surface, about 5.5 km above sea level, the wind reported by weather balloons blows almost exactly along the height contours, and it is strongest where the contours are closest together. On a sea-level map of the same day, the wind reported by surface stations blows at an angle to the isobars, toward the low-pressure side, and it is slower than the wind aloft. In both hemispheres the prevailing winds of middle latitudes are westerlies (wind direction is always the direction the wind blows *from*): in the Northern Hemisphere they blow with the low pressure of the polar side, to the north, on their left; in the Southern Hemisphere they blow with the low pressure of the polar side, to the south, on their right.

Neither observation follows from the pressure-gradient force alone, which points straight from high to low pressure, across the contours. Something turns the air through a right angle aloft and through a smaller angle near the ground. The sections that follow identify the turning force, show how it balances the pressure-gradient force in the free atmosphere, and show how friction near the ground upsets the balance in a way that produces the crossing angle.

3.1.2 The pressure-gradient force

Consider a small box of air with sides δx, δy, δz. The air on its western face pushes eastward with force $p(x)\,\delta y\,\delta z$; the air on its eastern face pushes westward with force $p(x+\delta x)\,\delta y\,\delta z$. The net eastward force is $-[p(x+\delta x)-p(x)]\,\delta y\,\delta z \approx -(\partial p/\partial x)\,\delta x\,\delta y\,\delta z$, and dividing by the mass $\rho\,\delta x\,\delta y\,\delta z$ gives an acceleration $-(1/\rho)\,\partial p/\partial x$. With the same argument in the northward direction, the horizontal *pressure-gradient force* per unit mass is

$$\mathbf{a}_{\mathrm{PGF}} = -\frac{1}{\rho}\nabla_h p, \tag{3.1}$$

in $\mathrm{m\,s^{-2}}$ (pascals per meter divided by kilograms per cubic meter). It points from high toward low pressure, perpendicular to the isobars, and its magnitude is inversely proportional to the isobar spacing. Only differences of pressure matter: a uniform pressure pushes equally on all faces and exerts no net force. Chapter 1 introduced this force and Chapter 2 how its gradient is read from maps.

For a gradient of 4 hPa per 100 km, that is $400\,\mathrm{Pa}/10^5\,\mathrm{m} = 4\times10^{-3}$ Pa/m, and a near-surface density $\rho = 1.2$ kg/m^3,

$$|\mathbf{a}_{\mathrm{PGF}}| = \frac{4\times10^{-3}}{1.2} = 3.3\times10^{-3}\,\mathrm{m\,s^{-2}}.$$

If this acceleration acted alone on air starting at rest, the air would reach $3.3\times10^{-3}\times3\times3600 = 36\,\mathrm{m\,s^{-1}}$ after three hours and $72\,\mathrm{m\,s^{-1}}$ after six, and it would keep accelerating straight toward the low. Large-scale winds near the ground rarely exceed a few tens of meters per second, and pressure gradients of this size persist for days. Another force must therefore act on moving air, and it must grow as the air speeds up.

3.1.3 The horizontal equation of motion

The forces of this chapter are terms of one equation, Newton's second law per unit mass for the horizontal wind, written in the frame that rotates with the Earth:

$$\frac{\mathrm{D}\mathbf{V}}{\mathrm{D}t} = -\frac{1}{\rho}\nabla_h p \;-\; f\mathbf{k}\times\mathbf{V} \;+\; \mathbf{F}. \tag{3.2}$$

The left-hand side is the acceleration of an air parcel, the rate of change of its velocity as it moves. On the right, the first term is the pressure-gradient force of equation (3.1); the second is the Coriolis force, derived in Section 3.2; the third, $\mathbf{F}$, is the friction force per unit mass, which near the ground is the effect of turbulent transfer of momentum (Section 3.5.3). All three are in $\mathrm{m\,s^{-2}}$. The vertical counterpart of equation (3.2) reduces at large scale to the hydrostatic balance of Chapter 2.

Every flow regime in this chapter is a special case of equation (3.2) in which some terms are kept and the others dropped. Table 3.1 lists the cases: the first column names the balance, the second the terms kept, the third where it applies, and the last where it is developed. The geostrophic wind keeps only the pressure-gradient and Coriolis forces; the surface wind adds friction; the adjustment toward balance keeps the acceleration; and curved flow keeps the centripetal part of the acceleration, which is the subject of Chapter 4.

3.2 The Coriolis force

This section derives the Coriolis force from the change of reference frame, gives the Coriolis parameter by latitude in both hemispheres, fixes the direction of the force in each hemisphere, and states in what sense it is an apparent force.

Table 3.1: Balances of the horizontal equation of motion, equation (3.2), treated in this and the next chapter.

Balance	Terms kept	Where it applies	Developed in
Geostrophic	pressure gradient, Coriolis	free atmosphere, nearly straight contours	Section 3.3.3
Inertial oscillation	acceleration, Coriolis acting on the departure from balance	air released from rest or disturbed	Section 3.3.2
Three-force balance	pressure gradient, Coriolis, friction	friction layer, steady flow	Section 3.5.1
Ekman balance	pressure gradient, Coriolis, vertical turbulent transfer	boundary layer, idealized	Section 3.5.4
Gradient wind	pressure gradient, Coriolis, centripetal acceleration	curved contours	Chapter 4

3.2.1 Acceleration in a rotating frame

The Earth rotates at $\Omega = 7.292 \times 10^{-5}$ rad/s about its axis; the rotation vector $\boldsymbol{\Omega}$ points along the axis toward the North Pole. A vector $\mathbf{A}$ fixed in the rotating Earth, seen from an inertial frame, changes at the rate $\boldsymbol{\Omega} \times \mathbf{A}$. For any vector, the rate of change seen in the inertial frame (subscript I) is therefore the rate seen in the rotating frame (subscript R) plus that rotation:

$$\left(\frac{\mathrm{d}\mathbf{A}}{\mathrm{d}t}\right)_I = \left(\frac{\mathrm{d}\mathbf{A}}{\mathrm{d}t}\right)_R + \boldsymbol{\Omega} \times \mathbf{A}. \tag{3.3}$$

Apply it first to the position $\mathbf{r}$ of an air parcel measured from the Earth's center: the inertial velocity is $\mathbf{u}_I = \mathbf{u} + \boldsymbol{\Omega} \times \mathbf{r}$, where $\mathbf{u} = (u, v, w)$ is the velocity relative to the Earth, the wind. Apply it again to $\mathbf{u}_I$, with $\boldsymbol{\Omega}$ constant:

$$\left(\frac{\mathrm{d}\mathbf{u}_I}{\mathrm{d}t}\right)_I = \left(\frac{\mathrm{d}\mathbf{u}}{\mathrm{d}t}\right)_R + \boldsymbol{\Omega} \times \mathbf{u} + \boldsymbol{\Omega} \times (\mathbf{u} + \boldsymbol{\Omega} \times \mathbf{r}) = \left(\frac{\mathrm{d}\mathbf{u}}{\mathrm{d}t}\right)_R + 2\,\boldsymbol{\Omega} \times \mathbf{u} + \boldsymbol{\Omega} \times (\boldsymbol{\Omega} \times \mathbf{r}).$$

Newton's law holds for the left-hand side, the acceleration in the inertial frame, which equals the real forces per unit mass. Solving for the acceleration relative to the Earth,

$$\left(\frac{\mathrm{d}\mathbf{u}}{\mathrm{d}t}\right)_R = (\text{real forces per unit mass}) \;-\; 2\,\boldsymbol{\Omega} \times \mathbf{u} \;-\; \boldsymbol{\Omega} \times (\boldsymbol{\Omega} \times \mathbf{r}). \tag{3.4}$$

Two terms have appeared that no physical agent exerts. The last is the centrifugal acceleration, at most $\Omega^2 a = 0.034\,\mathrm{m\,s^{-2}}$ at the equator for the Earth's radius $a = 6371$ km; it does not depend on the wind and is absorbed, together with true gravitation, into the gravity g that defines the local vertical. The middle term, $-2\,\boldsymbol{\Omega} \times \mathbf{u}$, is the *Coriolis acceleration*, and it depends on the wind.

To write its components, use local axes with x east, y north and z up at latitude ϕ. In these axes $\boldsymbol{\Omega} = \Omega\,(0,\ \cos\phi,\ \sin\phi)$: the rotation vector lies in the north–vertical plane, tilted up from the horizontal by the latitude. Expanding the cross product,

$$-2\,\boldsymbol{\Omega} \times \mathbf{u} = \big(\,2\Omega \sin\phi\; v - 2\Omega\cos\phi\; w,\ \ -2\Omega\sin\phi\; u,\ \ 2\Omega\cos\phi\; u\,\big). \tag{3.5}$$

Two terms are negligible for large-scale flow. The term $2\Omega\cos\phi\, w$ in the eastward component involves the vertical velocity, a few centimeters per second in large-scale weather systems: at 45° and $w = 0.1\,\mathrm{m\,s^{-1}}$ it is $1 \times 10^{-5}\,\mathrm{m\,s^{-2}}$, a hundred times smaller than the terms kept below. The vertical component $2\Omega\cos\phi\, u$, about $10^{-3}\,\mathrm{m\,s^{-2}}$ for $u = 10\,\mathrm{m\,s^{-1}}$, is ten thousand times smaller

than $g = 9.81\,\mathrm{m\,s^{-2}}$ and does not affect the hydrostatic balance. What remains acts in the horizontal and depends only on the horizontal wind. With the *Coriolis parameter* $f = 2\Omega \sin\phi$,

$$\mathbf{a}_C = -f\mathbf{k} \times \mathbf{V} = (\, fv,\ -fu\,), \tag{3.6}$$

since $\mathbf{k} \times \mathbf{V} = (-v,\ u)$. Equation (3.6) is the Coriolis term of equation (3.2). Only the local vertical component of the Earth's rotation, $\Omega \sin\phi$, turns horizontal winds; it is largest at the poles and vanishes at the equator.

3.2.2 The Coriolis parameter

The Coriolis parameter

$$f = 2\Omega \sin\phi \tag{3.7}$$

has units of $\mathrm{s^{-1}}$ and takes the sign of the latitude: positive in the Northern Hemisphere, zero at the equator, negative in the Southern Hemisphere. It is calculated, not measured; the latitude of a site fixes it. A related time scale is the *inertial period* $2\pi/|f|$, the time in which the Coriolis force alone would turn a moving parcel through a full circle; its meaning for the wind is shown in Section 3.3.2.

Table 3.2 gives both quantities by latitude. The first column is the magnitude of the latitude, the second $\sin|\phi|$, the third and fourth f at that latitude north and south, in units of $10^{-4}\,\mathrm{s^{-1}}$, and the last the inertial period in hours, which is the same in both hemispheres. In middle latitudes $|f| \approx 10^{-4}\,\mathrm{s^{-1}}$; at 30° it is half its polar value; near the equator it is small and the inertial period becomes days long. Brazil extends from about 5° N to 34° S, so across it f runs from $+0.13 \times 10^{-4}$ through zero to $-0.82 \times 10^{-4}\,\mathrm{s^{-1}}$, and most of the country lies at latitudes where $|f|$ is a third or less of its midlatitude value. Near 23.5° S, the latitude of São Paulo, $f = -0.58 \times 10^{-4}\,\mathrm{s^{-1}}$; near 30° S, in southern Brazil, $f = -0.73 \times 10^{-4}\,\mathrm{s^{-1}}$.

Table 3.2: Coriolis parameter $f = 2\Omega \sin\phi$ and inertial period $2\pi/|f|$ by latitude, with $\Omega = 7.292 \times 10^{-5}$ rad/s.

$\lvert\phi\rvert$	$\sin\lvert\phi\rvert$	f, north ($10^{-4}\,\mathrm{s^{-1}}$)	f, south ($10^{-4}\,\mathrm{s^{-1}}$)	inertial period (h)
0°	0.000	0	0	none
5°	0.087	+0.127	−0.127	137.3
10°	0.174	+0.253	−0.253	68.9
15°	0.259	+0.377	−0.377	46.2
20°	0.342	+0.499	−0.499	35.0
23.5°	0.399	+0.582	−0.582	30.0
30°	0.500	+0.729	−0.729	23.9
45°	0.707	+1.031	−1.031	16.9
60°	0.866	+1.263	−1.263	13.8
90°	1.000	+1.458	−1.458	12.0

3.2.3 Direction in both hemispheres

Three properties of the Coriolis force follow from equation (3.6). First, it is perpendicular to the wind: $\mathbf{a}_C \cdot \mathbf{V} = fvu - fuv = 0$. Second, its magnitude is $|f|$ times the speed, $|\mathbf{a}_C| = |f|\,U$, because $\mathbf{k} \times \mathbf{V}$ has the length of $\mathbf{V}$. Third, its side depends on the sign of f. The vector $\mathbf{k} \times \mathbf{V}$ is the wind rotated a quarter turn counterclockwise, seen from above, that is, pointing to the left of the motion. In the Northern Hemisphere $f > 0$, the minus sign reverses it, and the Coriolis force points to the *right* of the motion. In the Southern Hemisphere $f < 0$, $-f > 0$, and the force points to the *left* of the motion.

Two examples check the signs with equation (3.6). Air moving northward has $\mathbf{V} = (0, v)$ with $v > 0$, so $\mathbf{a}_C = (fv, 0)$: in the Northern Hemisphere $fv > 0$ and the air is accelerated toward the east, to its right; in the Southern Hemisphere $fv < 0$ and it is accelerated toward the west, to its left. Air moving eastward has $\mathbf{V} = (u, 0)$ with $u > 0$, so $\mathbf{a}_C = (0, -fu)$: toward the south in the Northern Hemisphere and toward the north in the Southern. At 45° a wind of $10\,\mathrm{m\,s^{-1}}$ feels a Coriolis acceleration of $1.03 \times 10^{-4} \times 10 = 1.0 \times 10^{-3}\,\mathrm{m\,s^{-2}}$, about a third of the pressure-gradient force of the 4 hPa per 100 km example; at 30° S the same wind feels $0.73 \times 10^{-3}\,\mathrm{m\,s^{-2}}$, directed to its left.

Figure 3.1 draws the rule. Each panel is a map view with north up, marked by the arrow labeled N. The black arrows are a parcel's wind in four directions, north, east, south and west; the red arrow at the tip of each is the Coriolis acceleration that wind receives. In the left panel, the Northern Hemisphere, every red arrow points to the right of its black arrow; in the right panel, the Southern Hemisphere, every red arrow points to the left. In both, the red arrows are perpendicular to the motion, so they change its direction without changing its speed.

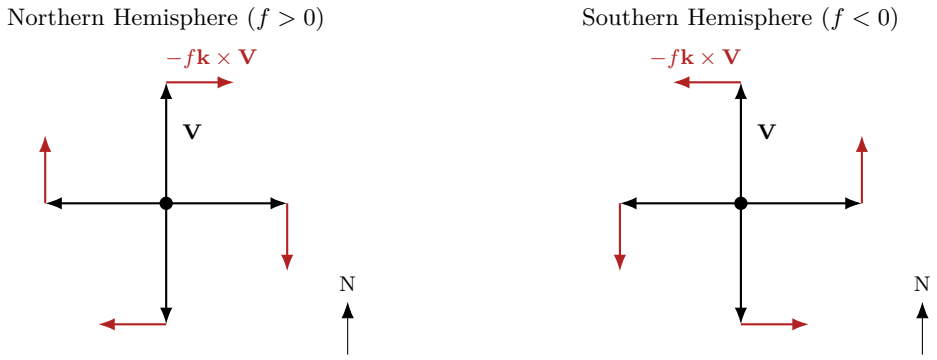


Figure 3.1: Direction of the Coriolis acceleration, map view, north up. Black: wind of a parcel moving north, east, south or west. Red: the Coriolis acceleration $-f\mathbf{k} \times \mathbf{V}$ it receives, drawn at the tip of the wind arrow. It points to the right of the motion in the Northern Hemisphere and to the left in the Southern. Lengths are schematic.

Because the Coriolis force is perpendicular to the wind, it does no work: the rate at which it changes the kinetic energy per unit mass, $\mathbf{V} \cdot \mathbf{a}_C$, is zero. The Coriolis force therefore does not create wind and cannot speed it up or slow it down; it only changes the direction of air that is already moving. The energy of the wind comes from the pressure field, through the pressure-gradient force.

Principle 3.1. *The Coriolis force acts perpendicular to the wind, with magnitude $|f|U$: to the right of the motion in the Northern Hemisphere and to the left in the Southern. It vanishes for air at rest and changes the direction of moving air, never its speed.*

3.2.4 An apparent force

The Coriolis force is not exerted by anything. It appears in equation (3.4) only because the motion is described relative to a rotating frame. A ball rolled across a turntable travels in a straight line as seen from the room, but relative to the turning table its path curves; an observer riding on the table, who insists on describing the motion relative to the table, must add a sideways force to Newton's law to account for the curve. In an inertial frame the Coriolis force is absent, the path is explained by the real forces alone, and the physics, and every prediction, is the same.

The atmosphere is described in the rotating frame because that is the frame in which winds are measured and used. An anemometer is fixed to the ground, which at the equator moves

eastward at $\Omega a = 7.292 \times 10^{-5} \times 6.371 \times 10^{6} = 465\,\mathrm{m\,s^{-1}}$ relative to an inertial frame; a wind of $10\,\mathrm{m\,s^{-1}}$ is a small difference between two large inertial velocities. Writing the equations relative to the Earth keeps the variables at the size of the wind itself, keeps the ground at rest as a boundary, and moves the effect of rotation into two terms: the centrifugal part, absorbed into gravity, and the Coriolis force.

3.3 Geostrophic balance

This section follows air from rest to balance: how the Coriolis force grows with speed, how a parcel released in a pressure gradient approaches the balanced state, what the balanced wind is, why it is parallel to the contours, and which side the low pressure lies on in each hemisphere.

3.3.1 Dependence on speed

The magnitude of the Coriolis force, $|f|U$, is zero for air at rest and grows in proportion to the speed. The pressure-gradient force, in contrast, does not depend on the motion at all; it is fixed by the pressure field. A pressure difference applied to still air therefore starts a sequence: the pressure-gradient force accelerates the air; the air moves; a Coriolis force appears, small at first; the wind turns; and as the air keeps gaining speed, the Coriolis force strengthens with it.

There is a speed at which the Coriolis force becomes as large as the pressure-gradient force. With the 4 hPa per 100 km gradient of Section 3.1.2 at 45° N, where $f = 1.031 \times 10^{-4}\,\mathrm{s^{-1}}$, the Coriolis force of a $10\,\mathrm{m\,s^{-1}}$ wind is $1.03 \times 10^{-3}\,\mathrm{m\,s^{-2}}$, less than the $3.33 \times 10^{-3}\,\mathrm{m\,s^{-2}}$ of the pressure gradient, and that of a $32.3\,\mathrm{m\,s^{-1}}$ wind is $1.031 \times 10^{-4} \times 32.3 = 3.33 \times 10^{-3}\,\mathrm{m\,s^{-2}}$, equal to it. This speed, at which the two forces can cancel, is the geostrophic wind speed of Section 3.3.3.

3.3.2 Adjustment from rest

Figure 3.2 shows the approach to balance as a sequence of force diagrams. Each row is one hemisphere, with the isobars drawn as horizontal lines, lower pressure along the upper line and higher pressure along the lower one, so that the pressure-gradient force (blue) points north in every panel. In each panel the dot is the parcel, the black arrow its wind and the red arrow the Coriolis force. In panel (a) the parcel is at rest and only the pressure-gradient force acts. In (b) the parcel moves slowly, mostly toward the low, and a small Coriolis force pushes it to the right in the Northern Hemisphere and to the left in the Southern. In (c) it is faster, the Coriolis force is larger, and the wind has turned further. In (d) the wind blows along the isobars and the Coriolis force is equal and opposite to the pressure-gradient force: the forces cancel and there is no further horizontal acceleration. The two rows are mirror images: the final wind blows along the isobars toward the east, with the low on its left, in the Northern Hemisphere, and toward the west, with the low on its right, in the Southern.

The staged diagram is the usual qualitative account, but the equation of motion says more, and the full answer contains an overshoot. Take a uniform pressure gradient with pressure falling northward, so that the pressure-gradient force is $(0, G)$ with $G = -(1/\rho)\,\partial p/\partial y > 0$, no friction, and air at rest at $t = 0$. The balanced wind is $u_g = G/f$, $v_g = 0$ (Section 3.3.3 derives it). Equation (3.2) in components reads $\mathrm{d}u/\mathrm{d}t = fv$ and $\mathrm{d}v/\mathrm{d}t = G - fu = -f(u - u_g)$. The departure from the balanced wind, $(u - u_g,\ v)$, therefore obeys $\mathrm{d}(u - u_g)/\mathrm{d}t = fv$ and $\mathrm{d}v/\mathrm{d}t = -f(u - u_g)$: it rotates at the angular rate f without changing its length. With the initial departure $(-u_g, 0)$, the solution is

$$u(t) = u_g\,(1 - \cos ft), \qquad v(t) = u_g \sin ft, \tag{3.8}$$

which can be checked by differentiation. The velocity runs around a circle of radius $|u_g|$ centered on the geostrophic wind. The parcel starts toward the low, is turned until it moves along the

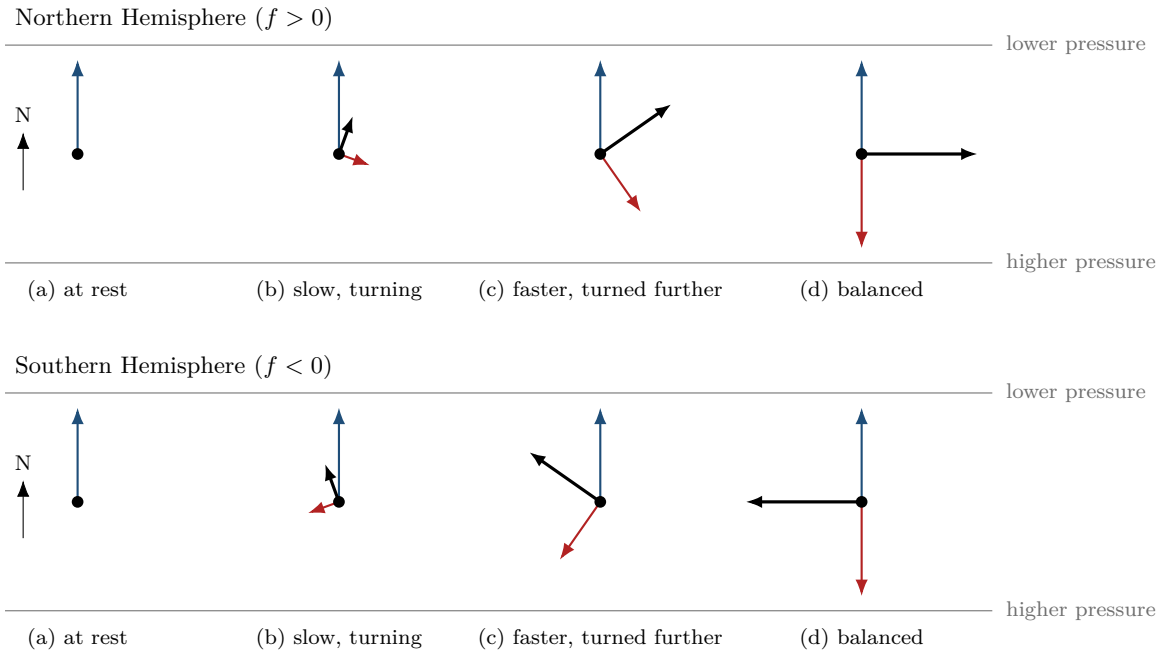


Figure 3.2: Approach to geostrophic balance, schematic force diagrams in map view, north up, with pressure decreasing northward. Blue: pressure-gradient force, the same in every panel. Black: wind. Red: Coriolis force, perpendicular to the wind with length proportional to its speed. Upper row: Northern Hemisphere, the wind turns right and ends blowing east. Lower row: Southern Hemisphere, the wind turns left and ends blowing west. The monotonic approach drawn here assumes the overshoot of Figure 3.3 has been damped.

isobars at $t = \pi/|f|$ with *twice* the geostrophic speed, is then turned back toward the high by a Coriolis force that now exceeds the pressure-gradient force, and comes to rest again after one inertial period $2\pi/|f|$, displaced along the isobars. Integrating equation (3.8) gives the path, $x = u_g\,(t - \sin(ft)/f)$ and $y = (u_g/f)(1 - \cos ft)$, a cycloid that never strays more than $2u_g/f$ toward the low. The motion is an *inertial oscillation* about the geostrophic wind, and its time average over a period is exactly the geostrophic wind.

Figure 3.3 draws these paths for an illustrative gradient of 1 hPa per 100 km with $\rho = 1.2$ kg/m^3, at 45° N and 45° S, where $|u_g| = 8.08\,\mathrm{m\,s^{-1}}$ and the inertial period is 16.9 h. The horizontal axis is the eastward distance from the release point and the vertical axis the northward distance, both in kilometers; the gray lines are two isobars 1 hPa apart, labeled with illustrative values. The solid curves are the frictionless paths of equation (3.8) over one inertial period, red for the Northern Hemisphere and blue for the Southern. The Northern Hemisphere parcel drifts east and the Southern one west, both first moving toward the low and reaching 157 km north of the start at half a period, where they move at $16.2\,\mathrm{m\,s^{-1}}$; each stops again 492 km from its start. The dashed curves are the same release with the departure from the geostrophic wind damped at the illustrative rate $0.3|f|$: after one period only 15 % of the initial departure remains, and the parcel is moving almost along the isobars at nearly the geostrophic speed, about 72 km north of its starting isobar.

The frictionless parcel never settles: in an exactly frictionless atmosphere with a fixed pressure field, air released from rest oscillates about the geostrophic wind indefinitely. The real atmosphere reaches balance because the oscillation is removed. Friction damps it near the ground, and, more importantly in the free atmosphere, the pressure field is not fixed: the initial imbalance is radiated away by gravity waves while the pressure field and the wind adjust toward each other. This process is called *geostrophic adjustment*, and it completes in a time of

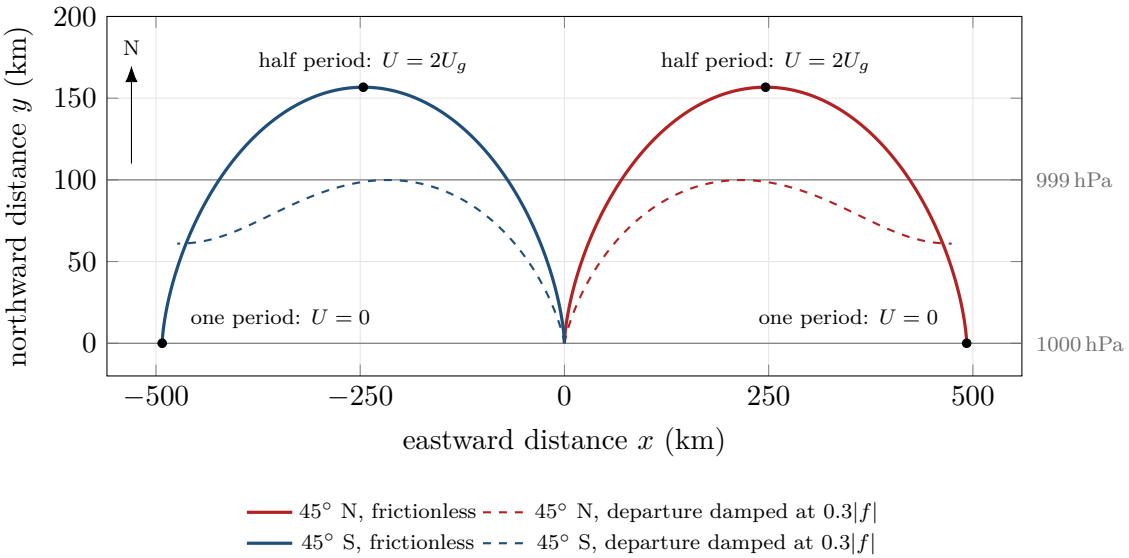


Figure 3.3: Paths of a parcel released from rest in a uniform pressure gradient of 1 hPa per 100 km falling northward, $\rho = 1.2$ kg/m^3, at 45° N ($f = +1.031 \times 10^{-4}\,\mathrm{s}^{-1}$, red) and 45° S ($f = -1.031 \times 10^{-4}\,\mathrm{s}^{-1}$, blue), over one inertial period of 16.9 h. Solid: frictionless, $x = u_g(t - \sin(ft)/f)$, $y = (u_g/f)(1 - \cos ft)$, $u_g = \pm 8.08\,\mathrm{m\,s}^{-1}$. Dashed: the departure from the geostrophic wind decaying at the illustrative rate $0.3|f|$. North–south distances are drawn at twice the scale of east–west distances. Computed by `scripts/ch03_data.py`.

the order of the inertial period, about a day or less in middle latitudes. Inertial oscillations are nonetheless real and observed: when the friction acting on the boundary layer drops abruptly at sunset, the wind above the surface layer oscillates about its balanced value with the inertial period, one origin of the nocturnal low-level jet treated in Chapter 18.

3.3.3 The balance and the geostrophic wind

Once the acceleration and friction are negligible, equation (3.2) reduces to a balance between two forces,

$$-\frac{1}{\rho}\nabla_h p \;-\; f\mathbf{k}\times\mathbf{V}_g = 0, \tag{3.9}$$

the *geostrophic balance*, and the wind that satisfies it is the *geostrophic wind* $\mathbf{V}_g$. To solve for it, take the cross product of $\mathbf{k}$ with every term. For a horizontal vector, $\mathbf{k}\times(\mathbf{k}\times\mathbf{V}_g) = -\mathbf{V}_g$, so

$$-\frac{1}{\rho}\,\mathbf{k}\times\nabla_h p + f\,\mathbf{V}_g = 0,$$

and, for $f \neq 0$,

$$\mathbf{V}_g = \frac{1}{f\rho}\,\mathbf{k}\times\nabla_h p. \tag{3.10}$$

Since $\mathbf{k}\times\nabla_h p = (-\partial p/\partial y,\ \partial p/\partial x)$, the components are

$$u_g = -\frac{1}{f\rho}\frac{\partial p}{\partial y}, \qquad v_g = \frac{1}{f\rho}\frac{\partial p}{\partial x}, \tag{3.11}$$

and the speed is

$$U_g = \frac{|\nabla_h p|}{|f|\,\rho}. \tag{3.12}$$

Substituting back confirms the balance; the eastward component of equation (3.9) becomes

$$-\frac{1}{\rho}\frac{\partial p}{\partial x} + f v_g = -\frac{1}{\rho}\frac{\partial p}{\partial x} + \frac{1}{\rho}\frac{\partial p}{\partial x} = 0.$$

Equation (3.10) is a diagnostic relation: given the pressure field at an instant, it returns a wind, with no time integration. The geostrophic wind is therefore a calculated quantity, the wind the pressure field would support in exact balance. Where the actual wind is measured, the difference between the two is the ageostrophic wind of Section 3.6.5.

3.3.4 Flow parallel to the contours

The geostrophic wind is perpendicular to the pressure gradient: $\mathbf{V}_g \cdot \nabla_h p = (1/f\rho)\,(\mathbf{k} \times \nabla_h p) \cdot \nabla_h p = 0$, because a cross product is perpendicular to each of its factors. The pressure gradient is perpendicular to the isobars, so the geostrophic wind blows along them. Air in geostrophic balance does not move from high to low pressure at all; it moves along lines of constant pressure, and its speed is set by how steep the pressure gradient across them is.

The same conclusion follows directly from the forces. Suppose pressure decreases toward the north. The pressure-gradient force then points north. For balance, the Coriolis force must point south. The Coriolis force is perpendicular to the wind, so a wind whose Coriolis force is north–south must itself blow east–west, along the isobars. In balance, both forces are perpendicular to the wind, equal in size and opposite in direction; neither has a component along the wind, which is why the speed stays constant.

3.3.5 The hemisphere rule

Which way along the isobars the wind blows depends on the sign of f. The vector $\mathbf{k} \times \nabla_h p$ is the pressure gradient, which points toward high pressure, rotated a quarter turn counterclockwise; it points along the isobars with high pressure on its right. In the Northern Hemisphere, $f > 0$, the geostrophic wind of equation (3.10) points the same way, so it blows with *low pressure to its left*. In the Southern Hemisphere, $f < 0$, it points the opposite way and blows with *low pressure to its right*. This is known as Buys Ballot's law: an observer standing with the wind at the back has low pressure on the left in the Northern Hemisphere and on the right in the Southern. A consequence for closed isobars is the sense of circulation. Around a low the geostrophic wind circulates counterclockwise in the Northern Hemisphere and clockwise in the Southern; around a high the senses are reversed. Rotation in the same sense as the Earth's, seen from above the hemisphere's own pole, is called *cyclonic*, and the opposite sense *anticyclonic*; lows are cyclonic in both hemispheres.

Figure 3.4 shows the rule on two schematic weather maps with the same pressure pattern, a low (L) to the west and a high (H) to the east, with isobars labeled in hectopascals. North is up in both panels, marked by the arrow labeled N; the left panel is in the Northern Hemisphere and the right panel in the Southern. The arrows are the balanced wind along the outer isobars. In the left panel they circulate counterclockwise around the low and clockwise around the high, and between the two systems the wind blows north; in the right panel every arrow is reversed, and between the systems the wind blows south. In every arrow the low is on the left in the Northern Hemisphere and on the right in the Southern. On closed, curved isobars the balanced wind is the gradient wind of Chapter 4, which differs in speed from the geostrophic wind but follows the same direction rule.

Principle 3.2. *The geostrophic wind blows along the pressure contours, with low pressure to its left in the Northern Hemisphere and to its right in the Southern; its speed is the pressure gradient divided by $|f|\rho$.*

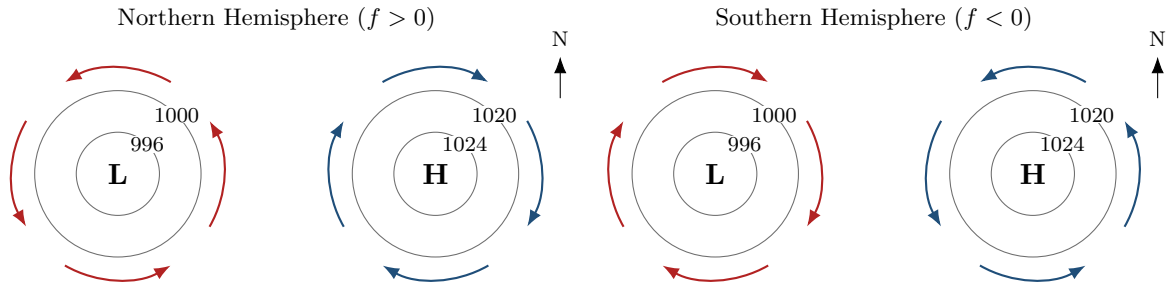


Figure 3.4: The hemisphere rule on two schematic weather maps with the same pressure field (isobars in hPa, illustrative), north up. Red: balanced wind around the low; blue: around the high. Northern Hemisphere (left): counterclockwise around the low, clockwise around the high, low pressure to the left of the wind. Southern Hemisphere (right): clockwise around the low, counterclockwise around the high, low pressure to the right of the wind.

3.4 Computing the geostrophic wind

This section turns equation (3.10) into numbers: from pressure on a map of constant height, from geopotential height on a map of constant pressure, from the spacing of the contours, and across latitudes; it closes with the conditions under which the result describes the real wind.

3.4.1 From pressure at constant height

On a map of constant height, such as a sea-level pressure analysis, equation (3.12) gives the speed and the hemisphere rule the direction. The density is that of the air at the map's height; a sea-level map with $\rho \approx 1.2$ kg/m^3 gives the *surface geostrophic wind*, the balanced wind for the pressure gradient at the ground, which the actual surface wind does not reach because of friction (Section 3.5).

Example 3.1 (The same gradient in both hemispheres)**.** Pressure decreases toward the north at 4 hPa per 100 km, so $\partial p/\partial x = 0$ and $\partial p/\partial y = -4 \times 10^{-3}$ Pa/m; take $\rho = 1.2$ kg/m^3.

At 45° *N*, $f = +1.031 \times 10^{-4}\,\mathrm{s}^{-1}$ and $f\rho = 1.238 \times 10^{-4}$ kg m^{-3} s^{-1}. By equation (3.11),

$$u_g = -\frac{-4 \times 10^{-3}}{1.238 \times 10^{-4}} = +32.3\,\mathrm{m\,s}^{-1}, \qquad v_g = 0.$$

The wind blows toward the east: a westerly of 32.3 m s^{-1}, with the low pressure to the north, on its left.

At 30° *S*, $f = -0.729 \times 10^{-4}\,\mathrm{s}^{-1}$ and $f\rho = -0.875 \times 10^{-4}$ kg m^{-3} s^{-1}, so

$$u_g = -\frac{-4 \times 10^{-3}}{-0.875 \times 10^{-4}} = -45.7\,\mathrm{m\,s}^{-1}, \qquad v_g = 0.$$

The wind blows toward the west: an easterly of 45.7 m s^{-1}, with the low to the north, on its right. The same pressure gradient gives a wind in the opposite direction and, because $|f|$ is smaller, 1.41 times faster.

In southern middle latitudes the pressure normally decreases toward the pole, that is, toward the south; with $\partial p/\partial y = +4 \times 10^{-3}$ Pa/m at 30° S, $u_g = +45.7$ m s^{-1}, a westerly with the low to the south, on its right, as in Section 3.1.1. A gradient of 4 hPa per 100 km is strong, found in vigorous midlatitude storms; a gradient of 1 hPa per 100 km gives 8.1 m s^{-1} at 45° and 11.4 m s^{-1} at 30°.

The density enters inversely. At the 850 hPa level, about 1.5 km above sea level, with a temperature near 280 K, $\rho = 85\,000/(287 \times 280) = 1.06$ kg/m^3, so the same gradient in pascals

per meter gives a geostrophic wind about 13 % faster than at sea level. Maps at upper levels are therefore usually drawn on constant-pressure surfaces, where the density drops out, as the next subsection shows.

3.4.2 From geopotential height

On a surface of constant pressure the pressure gradient is zero by construction, and the information is carried instead by the height of the surface, Z, which varies from place to place (Chapter 2). The two descriptions are linked by the hydrostatic balance. Along a surface of constant pressure, $\mathrm{d}p = (\partial p/\partial x)_z\,\mathrm{d}x + (\partial p/\partial z)\,\mathrm{d}z = 0$, so

$$\left(\frac{\partial p}{\partial x}\right)_z = -\frac{\partial p}{\partial z}\left(\frac{\partial z}{\partial x}\right)_p = \rho g\left(\frac{\partial z}{\partial x}\right)_p,$$

using $\partial p/\partial z = -\rho g$. Dividing by ρ, the pressure-gradient force at constant height equals g times the slope of the pressure surface: $(1/\rho)\nabla_h p = g\,\nabla_p z$. With the geopotential height, $\Phi = g_0 Z$, the exact form is $(1/\rho)\nabla_h p = \nabla_p \Phi = g_0 \nabla_p Z$, and equation (3.10) becomes

$$\mathbf{V}_g = \frac{g_0}{f}\,\mathbf{k}\times\nabla_p Z, \qquad u_g = -\frac{g_0}{f}\frac{\partial Z}{\partial y}, \quad v_g = \frac{g_0}{f}\frac{\partial Z}{\partial x}. \tag{3.13}$$

The density has disappeared: on a constant-pressure map the same height gradient gives the same geostrophic wind at every level. The geostrophic wind blows along the height contours, with low heights playing the role of low pressure in the hemisphere rule. Strong height gradients mean strong geostrophic winds, and tightly packed contours on an 850 or 500 hPa map indicate strong winds.

As an illustration, on a 500 hPa map drawn with contours every 60 m, let two contours be 300 km apart, with heights decreasing toward the pole. The height gradient is $60/(3\times 10^5) = 2\times 10^{-4}$. At 45° N, $U_g = 9.81\times 2\times 10^{-4}/1.031\times 10^{-4} = 19.0\,\mathrm{m\,s^{-1}}$; at 30° S, $U_g = 9.81\times 2\times 10^{-4}/0.729\times 10^{-4} = 26.9\,\mathrm{m\,s^{-1}}$. In both cases the wind is a westerly: in the Northern Hemisphere the low heights to the north lie on its left; in the Southern Hemisphere $\partial Z/\partial y > 0$, $f < 0$, and $u_g = -(g_0/f)\,\partial Z/\partial y > 0$, with the low heights to the south on its right.

3.4.3 Contour spacing and speed

For contours drawn at a fixed interval Δp and a local spacing Δn between neighboring contours, equation (3.12) reads

$$U_g \approx \frac{\Delta p}{|f|\,\rho\,\Delta n}, \tag{3.14}$$

and in the same way $U_g \approx g_0\,\Delta Z/(|f|\,\Delta n)$ on a constant-pressure map. The speed is inversely proportional to the spacing. With isobars every 4 hPa at 45° N and $\rho = 1.2$ kg/m^3, a spacing of 400 km gives $8.1\,\mathrm{m\,s^{-1}}$, 200 km gives $16.2\,\mathrm{m\,s^{-1}}$ and 100 km gives $32.3\,\mathrm{m\,s^{-1}}$. Reading the packing of the contours is how wind speed is estimated from a weather map at a glance.

The physical reading of equation (3.14) comes from the balance itself, $|f|\,U_g = |\nabla_h p|/\rho$: a stronger pressure gradient can be balanced only by a stronger Coriolis force, and since the Coriolis force is proportional to the speed, only by a faster wind. The pressure field does not push the air faster along the isobars; it requires a faster wind for the balance to hold, and the adjustment of Section 3.3.2 produces it.

3.4.4 Latitude and the equator

For a fixed pressure gradient, $U_g \propto 1/|f| = 1/(2\Omega|\sin\phi|)$: the smaller the Coriolis parameter, the faster the wind needed to produce a Coriolis force that balances the gradient. Figure 3.5

plots this dependence. The horizontal axis is latitude, negative in the Southern Hemisphere; the vertical axis is the geostrophic speed for a gradient of 1 hPa per 100 km at $\rho = 1.2$ kg/m^3; the shaded band marks latitudes within 10° of the equator. The curve is symmetric because U_g depends on $|f|$; the direction, not shown, reverses between the hemispheres. From the poles toward 30° the speed doubles, from 5.7 to 11.4 m s^{-1}; toward 10° it reaches 32.9 m s^{-1} and at 5° 65.6 m s^{-1}, and it grows without bound at the equator.

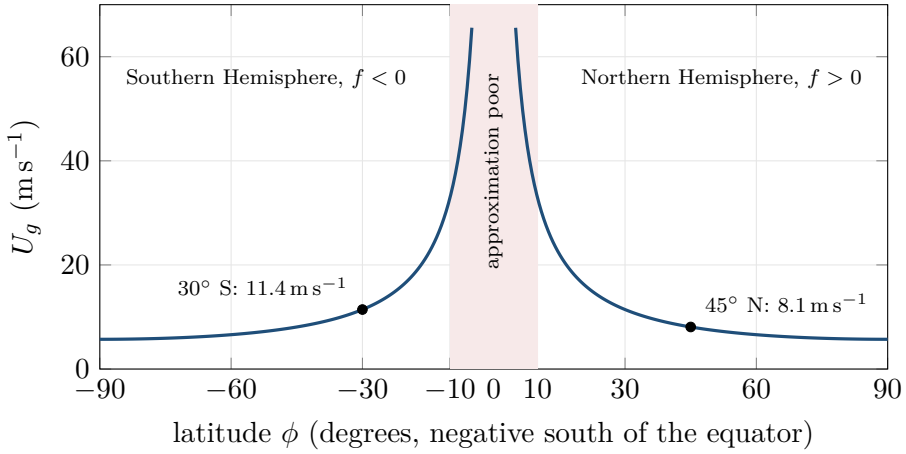


Figure 3.5: Geostrophic wind speed against latitude for a fixed pressure gradient, $U_g = |\nabla_h p|/(\rho\, 2\Omega|\sin\phi|)$ with $|\nabla_h p| = 1$ hPa per 100 km and $\rho = 1.2$ kg/m^3, so $U_g = 5.71\,\mathrm{m\,s^{-1}}/|\sin\phi|$; drawn for $|\phi| \geq 5°$. Shaded: within 10° of the equator, where the geostrophic approximation is of little use.

The divergence of the curve does not mean that equatorial winds are fast; it means that the geostrophic relation fails there. At the equator $f = 0$, the horizontal Coriolis force vanishes, and no balance with a pressure gradient exists; f also changes sign across the equator, so the direction rule flips. Close to it, $|f|$ is so small that the Coriolis force of a realistic wind is weaker than the other terms of equation (3.2) that geostrophic balance neglects. The ratio of the acceleration term to the Coriolis term is measured by the Rossby number $\mathrm{Ro} = U/(|f|L)$, developed in Chapter 5; for $U = 10\,\mathrm{m\,s^{-1}}$ and a horizontal scale $L = 1000$ km it is 0.10 at 45°, 0.26 at 15° and 0.79 at 5°. Geostrophic balance requires $\mathrm{Ro} \ll 1$. As a rough guide the approximation is of little use within 10 to 15 degrees of the equator, and tropical pressure gradients are correspondingly weak: a near-equatorial wind is not predicted from the isobars this way. For the northern part of Brazil this rules the geostrophic wind out as a forcing estimate; for the southern part, near 30° S, it is as useful as in other middle latitudes.

3.4.5 Conditions of validity

The geostrophic wind is an approximation obtained by dropping terms from equation (3.2), and it is accurate where those terms are small. Table 3.3 lists the conditions. The first column is the condition, the second the term it allows to be neglected, and the third where the condition fails. The approximation works best when the horizontal scale is large, the flow is slowly varying, friction is weak, the contours are only modestly curved and the latitude is not near the equator; these are the conditions of the *free atmosphere* of large weather systems, above the boundary layer, where the geostrophic wind typically agrees with the observed wind to within about ten to twenty percent. It is poorer near the surface, in strongly curved flow, around small-scale terrain and in rapidly evolving systems.

Table 3.3: Conditions under which the geostrophic wind approximates the actual wind, and where each fails.

Condition	Term it allows to neglect	Where it fails
Large horizontal scale, slow evolution (Ro $\ll 1$)	acceleration $\frac{\mathrm{D}\mathbf{V}}{\mathrm{D}t}$	fronts, sea breezes, convective storms, rapidly deepening systems
Weak friction	friction $\mathbf{F}$	the boundary layer, the lowest few hundred meters to a kilometer or two
Modest curvature of the contours	centripetal part of $\frac{\mathrm{D}\mathbf{V}}{\mathrm{D}t}$	tight lows, tropical cyclones (Chapter 4)
Latitude away from the equator	none; it keeps the Coriolis term large	within about 10 to 15 degrees of the equator
Smooth terrain at the scale considered	terrain-forced accelerations	flow over hills, through valleys, around coasts

3.5 Friction and the surface wind

Near the ground the geostrophic balance is upset by friction. This section shows how friction turns the wind across the isobars, how large the crossing angle is, what friction physically is in the atmosphere, and how the wind changes with height through the friction layer in the idealized Ekman solution.

3.5.1 Flow across the isobars

Above the boundary layer the pressure-gradient force and the Coriolis force nearly balance. Near the surface, friction slows the wind. The Coriolis force, $|f|U$, falls with the speed, but the pressure-gradient force does not depend on the wind and is unchanged. The pressure-gradient force now exceeds the Coriolis force, and the excess has a component toward low pressure. The chain is: surface friction, slower wind, weaker Coriolis force, flow across the isobars toward low pressure.

The steady balance of three forces makes this quantitative. Represent friction by a linear drag opposite to the wind, $\mathbf{F} = -\lambda\mathbf{V}$, with a drag rate λ in s^{-1}; this is the simplest model of the friction layer as a single slab. Equation (3.2) in steady state, with the pressure gradient written through the geostrophic wind, $-(1/\rho)\nabla_h p = f\mathbf{k}\times\mathbf{V}_g$, becomes

$$0 = f\mathbf{k}\times\mathbf{V}_g - f\mathbf{k}\times\mathbf{V} - \lambda\mathbf{V}. \tag{3.15}$$

Resolve the forces along the wind and across it, and let the wind make an angle α with the isobars. The pressure-gradient force has magnitude $|f|U_g$ and is perpendicular to the isobars, so its component along the wind is $|f|U_g\sin\alpha$ and across it $|f|U_g\cos\alpha$. The Coriolis force, $|f|U$, is entirely across the wind; friction, λU, is entirely along it, backward. Balance along and across the wind gives

$$|f|U_g\sin\alpha = \lambda U, \qquad |f|U_g\cos\alpha = |f|U,$$

so

$$\tan\alpha = \frac{\lambda}{|f|}, \qquad \frac{U}{U_g} = \cos\alpha. \tag{3.16}$$

The wind is slower than the geostrophic wind and crosses the isobars toward low pressure: rotated from $\mathbf{V}_g$ toward the low, to the left of $\mathbf{V}_g$ in the Northern Hemisphere and to the right in the Southern. The sign follows from equation (3.15), whose solution in complex notation,

$W = u + \mathrm{i}v$, is $W = W_g\, f(f + \mathrm{i}\lambda)/(f^2 + \lambda^2)$: a counterclockwise rotation by α for $f > 0$ and a clockwise one for $f < 0$, toward the low in both cases.

Figure 3.6 draws the balance for an illustrative crossing angle of 30°. Each panel is a map view with north up and lower pressure to the north. The dashed arrow is the geostrophic wind, along the isobars; the thick black arrow is the actual wind, $\cos 30° = 0.87$ times as fast, turned toward the low by α. The blue arrow is the pressure-gradient force, the red arrow the Coriolis force on the actual wind, and the green arrow the friction. Placed head to tail, the three force arrows would close: their sum is zero. In the Northern Hemisphere (left) the Coriolis force points to the right of the wind and the wind is turned left of $\mathbf{V}_g$; in the Southern Hemisphere (right) both are mirrored.

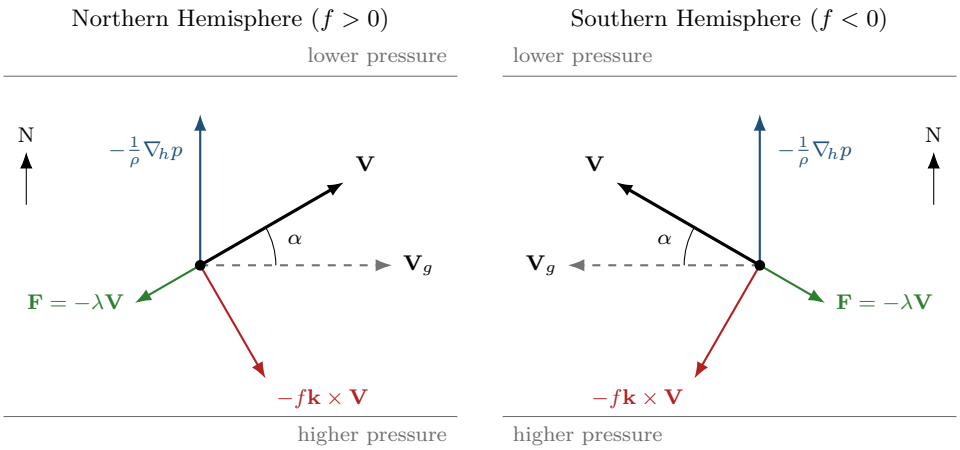


Figure 3.6: Three-force balance of the surface wind with linear drag, equation (3.15), for an illustrative crossing angle $\alpha = 30°$ ($\lambda = |f| \tan 30°$). Map view, north up, lower pressure to the north. Force arrows to scale with each other: pressure-gradient force 1, Coriolis force $\cos\alpha = 0.87$, friction $\sin\alpha = 0.5$; wind $U = U_g \cos\alpha$. The wind crosses the isobars toward low pressure in both hemispheres.

At 45° N, a 30° crossing angle requires $\lambda = 1.031 \times 10^{-4} \times \tan 30° = 5.95 \times 10^{-5}\,\mathrm{s}^{-1}$, a drag that would stop the wind in about $1/\lambda = 4.7$ h if nothing drove it. The model then gives $U = 0.87\,U_g$. Equation (3.16) ties the speed reduction to the crossing angle, and that tie is its main limitation: observed winds at 10 m over land are often less than half the geostrophic wind while crossing the isobars at well under 60°. Most of the reduction near the ground is a decrease of speed with height within the lowest tens of meters, the surface layer of Chapter 7, which a single slab cannot represent. The slab model is right about the direction of the effect and the order of the angle, not about the near-surface speed.

3.5.2 The crossing angle

The crossing angle is not a universal constant. It depends on the roughness of the surface, which sets how strongly the surface drags on the air; on the stability of the boundary layer, which sets how efficiently turbulence mixes momentum vertically; on the latitude, through f; and on the depth of the boundary layer over which the drag is spread. As a rough guide, the angle between the surface wind and the isobars is about 10 to 30° over smoother surfaces such as the sea and flat open land, and can be larger over rough land, forests or cities, sometimes 40° or more.

Equation (3.16) exposes the dependence on latitude: for the same drag, a smaller $|f|$ gives a larger angle. The drag $\lambda = 3.75 \times 10^{-5}\,\mathrm{s}^{-1}$ that produces a 20° crossing at 45° produces $\arctan(3.75/3.77) = 45°$ at 15° latitude. Stability acts through the mixing: in a stable boundary layer at night, weak mixing leaves the lowest layers more strongly influenced by the surface drag

and the turning between the surface and the geostrophic wind is usually larger; in a convective boundary layer by day, strong mixing brings momentum down from aloft and the turning is usually smaller. For an application that needs the wind direction at the ground, such as the angle between the wind and a transmission line conductor, which controls how effectively the wind cools the conductor, a direction estimated from the geostrophic wind therefore carries an uncertain rotation of tens of degrees that must be treated as a parameter, not a constant.

3.5.3 Friction as turbulent momentum transfer

Friction in the atmosphere is not molecular drag. The molecular viscosity of air, $\nu \approx 1.5 \times 10^{-5}$ m^2/s, could only influence a layer of the order of $\sqrt{2\nu/|f|} \approx 0.5$ m deep in a day, as Section 3.5.4 makes precise. The friction that slows the wind through hundreds of meters is the work of turbulence: eddies carry faster-moving air downward and slower-moving air upward, and the net effect is a downward vertical flux of horizontal momentum, from the free atmosphere toward the ground, where the surface absorbs it.

That flux, per unit area, is a stress $\boldsymbol{\tau}$, in pascals. At the ground it is the *surface stress* $\boldsymbol{\tau}_0$, the horizontal force per unit area exerted by the surface on the air (and, equal and opposite, by the air on the surface). The friction force per unit mass in equation (3.2) is the vertical divergence of the stress,

$$\mathbf{F} = \frac{1}{\rho}\frac{\partial \boldsymbol{\tau}}{\partial z}, \tag{3.17}$$

so a layer of air is decelerated when more momentum leaves it through its bottom than enters through its top. Because $\boldsymbol{\tau}$ decreases from $\boldsymbol{\tau}_0$ at the ground to nearly zero at the top of the boundary layer, the layer as a whole loses momentum to the surface, and the term $\mathbf{F}$ of the chapter means exactly this turbulent momentum transport. The surface stress is measured by eddy covariance, from the correlation of fast fluctuations of horizontal and vertical wind recorded by a sonic anemometer; in a weather model it is not resolved but computed by a surface-layer parameterization from the wind, the roughness and the stability, topics of Chapters 11 and 13. The simplest closure writes the stress as proportional to the vertical gradient of the wind,

$$\boldsymbol{\tau} = \rho K \frac{\partial \mathbf{V}}{\partial z}, \tag{3.18}$$

with an *eddy viscosity* K in m^2/s that plays for turbulence the role ν plays for molecules; in the boundary layer K is of order 1 to 10 m^2/s or more, about a million times ν. The linear drag of Section 3.5.1 is the vertical average of equation (3.17) over a slab, with the surface stress taken proportional to the wind.

3.5.4 The Ekman spiral

With equation (3.18) and a constant K, the steady, horizontally uniform balance of the boundary layer is

$$0 = f\mathbf{k} \times (\mathbf{V}_g - \mathbf{V}) + K\frac{\partial^2 \mathbf{V}}{\partial z^2}, \tag{3.19}$$

the pressure-gradient force written again through a geostrophic wind that is the same at all heights. In complex notation, $W = u + \mathrm{i}v$, the two components combine into $K\,W'' = \mathrm{i}f\,(W - W_g)$. Its solutions are $W - W_g \propto e^{-sz}$ with $s^2 = \mathrm{i}f/K$. For $f > 0$, $s = (1+\mathrm{i})/\delta$; for $f < 0$, $s = (1-\mathrm{i})/\delta$; in both,

$$\delta = \sqrt{\frac{2K}{|f|}} \tag{3.20}$$

is the Ekman length. Requiring the wind to vanish at the ground and to approach $\mathbf{V}_g$ far above it, and choosing the x axis along $\mathbf{V}_g$, gives

$$u = U_g \left(1 - e^{-z/\delta} \cos\frac{z}{\delta}\right), \qquad v = \operatorname{sgn}(f)\, U_g\, e^{-z/\delta} \sin\frac{z}{\delta}. \tag{3.21}$$

Near the ground $u \approx v \operatorname{sgn}(f) \approx U_g z/\delta$: the wind is weak and crosses the isobars at 45°, toward low pressure. With height it strengthens and turns toward the direction of $\mathbf{V}_g$. At $z = \pi\delta$ it first becomes parallel to $\mathbf{V}_g$, slightly faster than it, $(1+e^{-\pi})U_g = 1.04\,U_g$; above, it approaches $\mathbf{V}_g$ in ever smaller turns. The height $\pi\delta$ is called the Ekman depth. With an illustrative $K = 5$ m^2/s, $\delta = 311$ m and $\pi\delta = 978$ m at 45°, and $\delta = 370$ m, $\pi\delta = 1163$ m at 30° S; with the molecular ν in place of K, δ would be about half a meter.

Figure 3.7 plots equation (3.21) as a *hodograph*: the curve traced by the tips of the wind vectors at successive heights, drawn from a common origin. The horizontal axis is the wind component along $\mathbf{V}_g$ and the vertical axis the component across it, both divided by U_g; the dashed line from the origin to $(1, 0)$ is the geostrophic wind, taken toward the east. The red curve is the Northern Hemisphere, where the low lies on the left of $\mathbf{V}_g$ (up in the figure); the blue curve is the Southern, where the low lies on the right (down). The dots mark the heights $z = 0.5\delta$, δ, 2δ and $\pi\delta$, and the thin arrows are the wind vectors at $z = \delta$. Both curves leave the origin at 45° toward their low, bulge out to a maximum cross-isobar component of $0.32\,U_g$ at $z = (\pi/4)\delta$, and converge on $\mathbf{V}_g$; they are mirror images. In the Northern Hemisphere the wind turns clockwise with height, which is called *veering*; in the Southern Hemisphere it turns counterclockwise, *backing*.

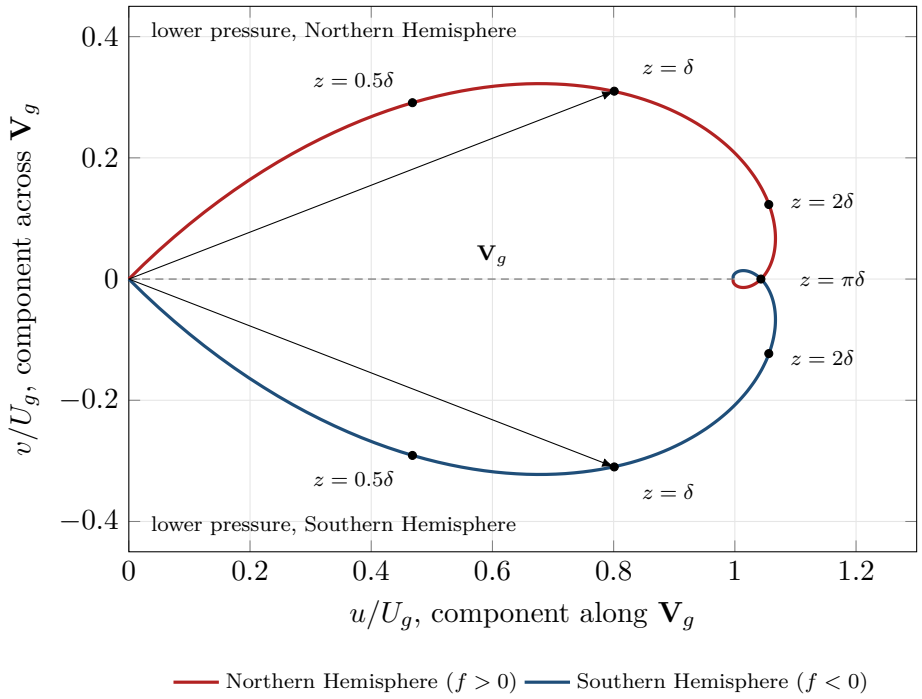


Figure 3.7: Ekman spiral as a hodograph, equation (3.21): $u/U_g = 1 - e^{-z/\delta}\cos(z/\delta)$, $v/U_g = \pm e^{-z/\delta}\sin(z/\delta)$, upper sign Northern Hemisphere, lower sign Southern, $\delta = \sqrt{2K/|f|}$, constant eddy viscosity K, geostrophic wind $\mathbf{V}_g$ along the horizontal axis. The wind crosses the isobars at 45° toward low pressure at the ground and turns with height to $\mathbf{V}_g$, clockwise (veering) in the Northern Hemisphere and counterclockwise (backing) in the Southern.

The Ekman solution is an idealization, and its limits are specific. It assumes a constant eddy viscosity, whereas real mixing is weak near the ground, strongest in the middle of the boundary

layer and dependent on stability; it assumes steady, horizontally uniform flow and a geostrophic wind that does not change with height, whereas horizontal temperature gradients make $\mathbf{V}_g$ vary with height and the boundary layer evolves through the day. Its surface crossing angle of 45° is larger than the 10 to 30° observed over smooth surfaces; matching it to a surface layer with a logarithmic profile, a topic of Chapters 7 and 12, reduces the angle. Observed profiles are therefore rarely a perfect spiral. What survives is the structure: surface stress produces both *speed shear*, the increase of wind speed with height, and *direction shear*, the turning of the wind with height, through the boundary layer, toward the low near the ground and toward the geostrophic wind aloft.

Principle 3.3. *Near the ground, surface stress slows the wind, the Coriolis force weakens with the speed, and the unbalanced pressure-gradient force turns the wind across the isobars toward low pressure: to the left of the geostrophic wind in the Northern Hemisphere and to the right in the Southern. With height the wind strengthens and turns toward the geostrophic wind.*

3.6 The geostrophic wind as forcing of the near-surface wind

This section separates the actual wind from the geostrophic wind, places the geostrophic wind at the top of the chain that produces the wind at engineering heights, works an example in which one forcing produces two different surface winds, and defines the ageostrophic wind that carries every departure from balance.

3.6.1 Actual and geostrophic wind

The two winds of this chapter are different objects. $\mathbf{V}$ is the actual wind, the velocity an instrument measures at a place, height and time. $\mathbf{V}_g$ is a hypothetical wind, the one that would exactly balance the pressure-gradient and Coriolis forces of the pressure field at that place; it is calculated from an analysis of the pressure or height field, not measured. In general $\mathbf{V} \neq \mathbf{V}_g$: in the free atmosphere the two are close, within the tolerances of Section 3.4.5, and near the ground they differ in speed and in direction.

Their roles also differ. The geostrophic wind describes the large-scale pressure forcing: the push the weather system applies, summarized as a wind. The actual wind near the ground is the response of the boundary layer to that forcing, and the boundary layer transforms $\mathbf{V}_g$ into a profile $\mathbf{V}(z)$ whose speed and direction at each height depend on the surface and on the state of the boundary layer. A model of the near-surface wind therefore needs both: the forcing, and a description of the transformation.

3.6.2 The modeling chain

Figure 3.8 lays out the transformation as a chain. Each box is one stage, from left to right: the pressure field, as pressure at constant height or geopotential height on pressure surfaces; the geostrophic wind it implies in the free atmosphere; the momentum transport of the boundary layer, governed by surface stress, stability and depth; and the near-surface wind at the heights of applications. The braces group the stages into the large-scale forcing and the boundary-layer response. The atmosphere above the boundary layer acts as a large-scale boundary condition for the layer below it: it supplies the momentum that turbulence carries down, and it sets the wind that the profile approaches at its top.

Weather models follow this chain. A model such as WRF, HRRR or ECMWF resolves the pressure field and, with it, the geostrophic forcing on its grid; the boundary-layer momentum

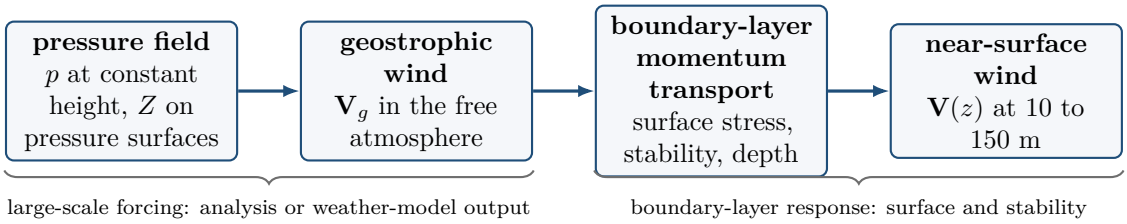


Figure 3.8: The modeling chain from pressure forcing to near-surface wind. The first two stages are set by the large-scale weather pattern; the last two by the boundary layer, which transforms the same geostrophic wind into different near-surface winds depending on the surface and the stability.

transport is turbulence on scales far below the grid spacing and is parameterized. The near-surface wind the model reports is therefore a grid-cell value produced by the last two stages of Figure 3.8 under a parameterization, not a point measurement; its errors at a site come mostly from those stages and from the terrain and obstacles that the grid does not represent, less from the large-scale pressure field.

3.6.3 One forcing, two boundary-layer states

A geostrophic wind of $20\,\mathrm{m\,s^{-1}}$ does not imply a wind of $20\,\mathrm{m\,s^{-1}}$ at 10 m. Consider, as an illustration, the same pressure field over the same site on one night and the following morning. At night the ground cools, the boundary layer becomes stable, turbulent mixing is weak, and little of the momentum aloft reaches the ground: the 10 m wind is $U_{10} = 4\,\mathrm{m\,s^{-1}}$, a fifth of the geostrophic wind. After sunrise the ground heats the air, convection mixes the boundary layer, and momentum is carried down efficiently: the 10 m wind rises to perhaps $U_{10} = 10\,\mathrm{m\,s^{-1}}$, half of it. The pressure forcing is identical; the boundary-layer state differs.

Figure 3.9 draws two illustrative profiles consistent with this example. The horizontal axis is wind speed and the vertical axis height above ground on a logarithmic scale, from 10 m to 1.5 km; the dashed vertical line is the geostrophic wind of $20\,\mathrm{m\,s^{-1}}$. The blue curve is the stable night, starting at $4\,\mathrm{m\,s^{-1}}$ at 10 m; the red curve is the convective morning, starting at $10\,\mathrm{m\,s^{-1}}$. Both approach the geostrophic wind aloft. The difference between them is largest near the ground, a factor of 2.5 at 10 m, and shrinks with height, to 13.5 against $17.8\,\mathrm{m\,s^{-1}}$ at 100 m in these illustrative shapes. The night profile also typically turns more with height, so the two states differ in direction as well as speed. For a transmission line at 10 to 30 m, whose convective cooling grows with the wind speed across the conductor, the two states give very different ratings under the same weather map; for a wind turbine near 100 m, the difference in speed is smaller but the shear across the rotor is larger at night. The shapes are illustrative: a stable profile above 100 m can increase faster than drawn and even exceed the geostrophic wind in a low-level jet, a topic of Chapter 18.

The slab model of Section 3.5.1 cannot reproduce these numbers: a ratio $U/U_g = 0.2$ would require $\cos\alpha = 0.2$, a crossing angle of 78°. The reduction at 10 m is mostly speed shear within the lowest layers, which the boundary-layer chapters describe with the surface layer and stability.

3.6.4 A conceptual decomposition

The chain of Figure 3.8 can be summarized by writing the wind at height z at a site as the geostrophic wind plus a sequence of modifications,

$$\mathbf{V}(z) = \mathbf{V}_g + \Delta\mathbf{V}_{\mathrm{ABL}}(z) + \Delta\mathbf{V}_{\mathrm{terrain}} + \Delta\mathbf{V}_{\mathrm{local}}, \tag{3.22}$$

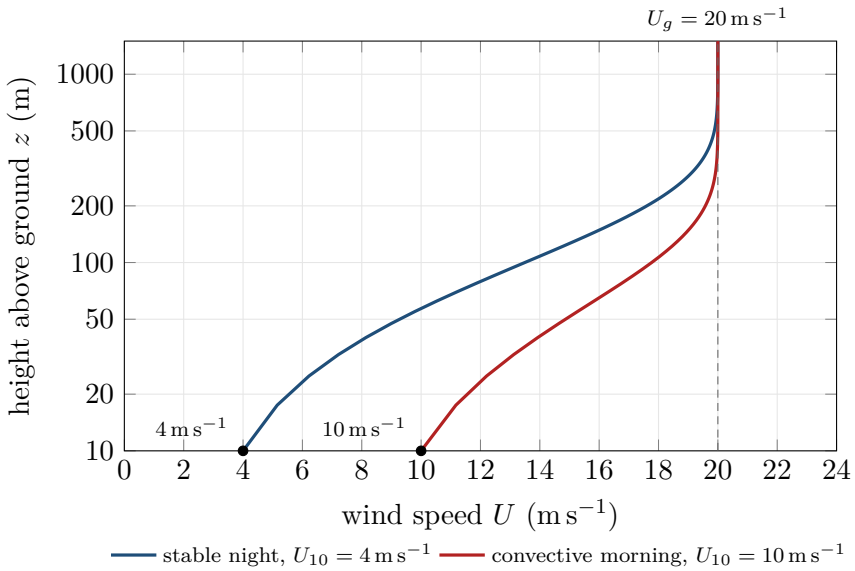


Figure 3.9: Two illustrative wind profiles under the same geostrophic wind of $20\,\mathrm{m\,s^{-1}}$: $U(z) = 20\,\mathrm{m\,s^{-1}}\,[1 - a\,e^{-(z-10\,\mathrm{m})/h}]$ with $a = 0.8$, $h = 100\,\mathrm{m}$ (stable night) and $a = 0.5$, $h = 60\,\mathrm{m}$ (convective morning). The shapes are not solutions of a boundary-layer model; they show that the same forcing yields different near-surface winds.

in which the geostrophic wind is the large-scale forcing, $\Delta\mathbf{V}_{\mathrm{ABL}}(z)$ is the change of speed and direction produced by boundary-layer physics, $\Delta\mathbf{V}_{\mathrm{terrain}}$ the change produced by terrain, and $\Delta\mathbf{V}_{\mathrm{local}}$ that produced by local obstacles such as buildings and trees near the sensor.

Equation (3.22) is conceptual, not a formal equation. Its terms are not independent and cannot be computed separately and added: the effect of a hill depends on the stability of the boundary layer flowing over it, and the boundary-layer profile depends on the roughness of the terrain. The geostrophic wind itself can change with height when the layer has horizontal temperature gradients, which the first term hides. The decomposition is useful as an inventory of what a model must represent between a weather map and a sensor, and of where each source of error enters; Chapters 6 to 23 take its terms in turn.

3.6.5 The ageostrophic wind

In exact geostrophic balance the wind does not change, $\frac{\mathrm{D}\mathbf{V}}{\mathrm{D}t} = 0$. Winds do change, and the change is tied to the departure from balance. Define the *ageostrophic wind*

$$\mathbf{V}_a = \mathbf{V} - \mathbf{V}_g, \tag{3.23}$$

in $\mathrm{m\,s^{-1}}$, computed as the difference between a measured or modeled wind and the geostrophic wind of the analyzed pressure field. Replacing the pressure-gradient force in equation (3.2) by $f\mathbf{k} \times \mathbf{V}_g$, as in Section 3.5.1,

$$\frac{\mathrm{D}\mathbf{V}}{\mathrm{D}t} = -f\mathbf{k} \times \mathbf{V}_a + \mathbf{F}. \tag{3.24}$$

Away from friction, every horizontal acceleration is the Coriolis force acting on the ageostrophic wind: no acceleration without an ageostrophic wind, and no ageostrophic wind, in frictionless flow, without acceleration. The inertial oscillation of Section 3.3.2 is the simplest case, an ageostrophic wind rotating at the rate f.

The ageostrophic wind is small in the free atmosphere but carries most of what makes the weather change. For constant f and ρ, the geostrophic wind of equation (3.11) has no horizontal divergence, $\partial u_g/\partial x + \partial v_g/\partial y = -\partial^2 p/(f\rho\,\partial x\,\partial y) + \partial^2 p/(f\rho\,\partial y\,\partial x) = 0$, so the convergence and

divergence that by mass continuity drive vertical motion come from the ageostrophic wind. In the friction layer the ageostrophic wind is the cross-isobar flow: in the slab model it is perpendicular to the actual wind, with magnitude $|\mathbf{V}_a| = U_g \sin\alpha$, $5\,\mathrm{m\,s^{-1}}$ for $U_g = 10\,\mathrm{m\,s^{-1}}$ and $\alpha = 30°$. Converging into lows and diverging out of highs, it forces rising air over lows and sinking air over highs, a process called *Ekman pumping*. The ageostrophic wind is associated with accelerating and decelerating flow, with fronts, with vertical motion, with boundary-layer friction and with systems that evolve rapidly; it is also, for near-surface applications, nearly all of the difference between the wind a weather map implies and the wind a sensor records.

3.7 What to retain

Definition 3.1 (Geostrophic wind and its surface departure)**.** The pressure-gradient force accelerates air, the Coriolis force grows with the speed, and the two balance in the geostrophic wind $\mathbf{V}_g = (1/f\rho)\,\mathbf{k} \times \nabla_h p$, which blows along the contours with low pressure to its left in the Northern Hemisphere and to its right in the Southern; near the ground, surface stress slows the wind, the Coriolis force weakens, and the wind crosses the isobars toward low pressure.

Table 3.4 lists the terms of the chapter with their meaning, units and the subsection that defines each.

3.8 Exercises

Exercise 3.1. (a) Compute f and the inertial period at 15° S, 35° S and 50° N. (b) Air moves toward the east at $12\,\mathrm{m\,s^{-1}}$. Give the magnitude and the compass direction of its Coriolis acceleration at 35° S and at 50° N. (c) At 15° S and at 35° S, pressure decreases toward the east at 2 hPa per 100 km, with $\rho = 1.15\ \mathrm{kg/m^3}$. Compute the geostrophic wind components, the speed and the wind direction (the direction it blows from), and check each against the hemisphere rule. (d) Comment on the result at 15° S.

Exercise 3.2. An 850 hPa map at 25° S shows height contours every 30 m, 250 km apart, with heights decreasing toward the south. (a) Compute the geostrophic wind speed and its direction, and state on which side of the wind the low heights lie. (b) Why is no density needed? (c) What contour spacing would give the same speed at 45° N, and from which direction would that wind blow if heights also decreased toward the pole?

Exercise 3.3. At 30° S the geostrophic wind is $12\,\mathrm{m\,s^{-1}}$ from the west, and surface observations show the wind crossing the isobars at 25°. Use the slab model of Section 3.5.1. (a) Compute the drag rate λ and the surface wind speed. (b) Give the direction of the surface wind as a compass bearing it blows from, and explain the side of the turn. (c) Compute the magnitude of the ageostrophic wind. (d) With the same λ, what crossing angle does the model give at 45° N? (e) An anemometer at 10 m reads $4\,\mathrm{m\,s^{-1}}$ under a $12\,\mathrm{m\,s^{-1}}$ geostrophic wind; what crossing angle would the slab model need to explain the ratio, and what does that say about the model?

Exercise 3.4. In a neutral boundary layer with $K = 8\ \mathrm{m^2/s}$, the geostrophic wind is $15\,\mathrm{m\,s^{-1}}$ from the west at 40° N and, on another occasion, at 40° S. (a) Compute δ and the Ekman depth $\pi\delta$. (b) From equation (3.21), compute the wind speed and the angle between the wind and $\mathbf{V}_g$ at $z = 100\,\mathrm{m}$ and $z = 400\,\mathrm{m}$. (c) Give the compass direction the wind blows from at 100 m in each hemisphere. (d) State whether the wind veers or backs with height in each hemisphere, and what the Ekman solution predicts for the crossing angle at the ground.

Table 3.4: Terms of the chapter and where each is defined.

Term	Meaning	Units	Defined in
Pressure-gradient force	$-(1/\rho)\nabla_h p$; from high toward low pressure	$\mathrm{m\,s^{-2}}$	3.1.2
Coriolis force	$-f\mathbf{k}\times\mathbf{V}$; apparent force of the rotating frame, perpendicular to the wind	$\mathrm{m\,s^{-2}}$	3.2.1
Coriolis parameter	$f = 2\Omega\sin\phi$; positive north, negative south	$\mathrm{s^{-1}}$	3.2.2
Inertial period	$2\pi/\lvert f\rvert$; period of the inertial oscillation	h	3.2.2
Geostrophic adjustment	approach of wind and pressure field to balance	–	3.3.2
Geostrophic balance	pressure-gradient force + Coriolis force = 0	–	3.3.3
Geostrophic wind	$\mathbf{V}_g = (1/f\rho)\,\mathbf{k}\times\nabla_h p = (g_0/f)\,\mathbf{k}\times\nabla_p Z$	$\mathrm{m\,s^{-1}}$	3.3.3, 3.4.2
Hemisphere rule	low pressure left of $\mathbf{V}_g$ (north), right (south)	–	3.3.5
Free atmosphere	above the boundary layer; friction negligible	–	3.4.5
Cross-isobar flow	wind component across the isobars, toward low pressure	$\mathrm{m\,s^{-1}}$	3.5.1
Crossing angle	α, angle between wind and isobars; $\tan\alpha = \lambda/\lvert f\rvert$ in the slab model	degree	3.5.1
Surface stress	$\boldsymbol{\tau}_0$; turbulent momentum transfer between atmosphere and surface	Pa	3.5.3
Eddy viscosity	K in $\boldsymbol{\tau} = \rho K\,\partial\mathbf{V}/\partial z$	$\mathrm{m^2\,s^{-1}}$	3.5.3
Ekman spiral	idealized turning and strengthening of the wind with height	–	3.5.4
Ekman depth	$\pi\delta$, $\delta = \sqrt{2K/\lvert f\rvert}$	m	3.5.4
Veering, backing	clockwise, counterclockwise turning with height	–	3.5.4
Ageostrophic wind	$\mathbf{V}_a = \mathbf{V} - \mathbf{V}_g$; carries acceleration, convergence, friction	$\mathrm{m\,s^{-1}}$	3.6.5

Chapter 4

Gradient Wind and Curved Flow Around Highs and Lows

4.1 From straight to curved flow

Chapter 3 explained why the large-scale wind above the boundary layer blows along the pressure contours rather than across them: the pressure-gradient force starts the motion, the Coriolis force turns it, and the two come into balance in the geostrophic wind. That balance has an assumption built into it that the weather map contradicts. The isobars and height contours on a map are rarely straight; they close around lows and highs and bend through troughs and ridges. The question of this chapter is

what changes when the wind follows curved pressure contours instead of straight ones?

The answer adds one ingredient to the balance, the acceleration that any curved path requires, and the result is the gradient wind. The chapter writes the balance along and across the flow, solves it around lows and highs in both hemispheres, derives the limit it places on anticyclonic flow, introduces vorticity as the measure of local rotation, and closes with the Rossby number, which says at which scales curvature and the Coriolis force matter and at which only curvature does.

Jargon: centripetal acceleration, natural coordinates, gradient wind, cyclonic, anticyclonic, subgeostrophic, supergeostrophic

The *centripetal acceleration* of a body moving at speed U on a path of radius of curvature R is the acceleration U^2/R, in $\mathrm{m\,s^{-2}}$, directed toward the center of curvature; it is the rate at which the direction of the velocity changes, and it is present even when the speed is constant. *Natural coordinates* are a local frame attached to the moving air: one axis along the flow, one across it. The *gradient wind* is the steady, frictionless, horizontal wind that blows along curved isobars with the pressure-gradient force, the Coriolis force and the centripetal acceleration in balance; its speed U_{gr} is in $\mathrm{m\,s^{-1}}$. It is not measured directly: it is computed from an analyzed pressure or geopotential-height field, and it is compared with winds measured above the boundary layer by radiosondes, aircraft or wind profilers. *Cyclonic* flow rotates in the same sense as the Earth seen from above the local hemisphere, the sense of the flow around a low: counterclockwise in the Northern Hemisphere, clockwise in the Southern. *Anticyclonic* flow rotates in the opposite sense, the sense of the flow around a high: clockwise in the Northern Hemisphere, counterclockwise in the Southern. A wind is *subgeostrophic* when its speed is less than the geostrophic speed U_g of the same pressure gradient, and *supergeostrophic* when it is greater.

Key idea

On a curved path the pressure-gradient force and the Coriolis force no longer cancel: their difference supplies the inward acceleration U^2/R. Around a low this makes the balanced wind slower than the geostrophic wind, around a high faster, in both hemispheres; and at the small scales of terrain, where U^2/R dwarfs the Coriolis acceleration, the balance that matters no longer involves the Coriolis force at all.

4.1.1 The straight-flow assumption of geostrophic balance

The geostrophic wind of Chapter 3 is defined by two horizontal forces per unit mass that cancel: the pressure-gradient force $-(1/\rho)\nabla_h p$, directed from high toward low pressure, and the Coriolis force $-f\mathbf{k}\times\mathbf{V}_g$, perpendicular to the wind. Its speed follows from equating their magnitudes,

$$U_g = \frac{|\nabla_h p|}{\rho\,|f|}, \tag{4.1}$$

with $f = 2\Omega\sin\phi$ the Coriolis parameter, positive in the Northern Hemisphere and negative in the Southern. Writing $|f|$ makes equation (4.1) a speed in both hemispheres.

If the two forces cancel exactly, the net horizontal force on the air is zero, and by Newton's second law in the Earth-fixed frame the air does not accelerate: it moves in a straight line at constant speed. The geostrophic balance is therefore, strictly, a statement about straight flow. A parcel that follows a closed isobar around a low, or the bend of a height contour through a trough, changes direction continuously. A change of direction is an acceleration even when the speed does not change, and an acceleration requires a net force. On a curved path the pressure-gradient and Coriolis forces cannot cancel exactly; something must be left over to turn the air. A two-force balance cannot describe such a path, and the size of the leftover is the subject of this chapter.

4.1.2 Centripetal acceleration

Consider a parcel moving at constant speed U along a circular arc of radius R. Figure 4.1 draws the situation. On the left, the gray arc is the parcel's path, turning to the left (counterclockwise seen from above), and the black dot at the top is the center of curvature; black arrows are the velocity at two positions Δt apart, $\mathbf{V}_1$ and $\mathbf{V}_2$, of equal length but different direction. On the right, the two velocity vectors are drawn from a common origin; the red arrow joining their tips is the velocity change $\Delta\mathbf{V} = \mathbf{V}_2 - \mathbf{V}_1$.

In the time Δt the parcel travels the distance $U\Delta t$ along the arc, and its direction turns through the angle $\Delta\theta = U\Delta t/R$, in radians. The two velocity vectors have length U and enclose the angle $\Delta\theta$, so for a small angle the change has magnitude $|\Delta\mathbf{V}| \approx U\,\Delta\theta$ and points perpendicular to the velocity, toward the center of curvature, as the figure shows. Dividing by Δt and letting it shrink,

$$a_c = \lim_{\Delta t\to 0}\frac{|\Delta\mathbf{V}|}{\Delta t} = U\,\frac{\mathrm{d}\theta}{\mathrm{d}t} = \frac{U^2}{R}, \tag{4.2}$$

the centripetal acceleration, directed toward the center. It grows with the square of the speed and falls with the radius: a tighter curve, or a faster parcel on the same curve, needs a larger inward acceleration.

For a sense of size, take an illustrative synoptic case, a wind of $U = 15\,\mathrm{m\,s^{-1}}$ circling a low at $R = 500\,\mathrm{km}$:

$$a_c = \frac{(15\,\mathrm{m\,s^{-1}})^2}{5\times10^5\,\mathrm{m}} = \frac{225}{5\times10^5}\,\mathrm{m\,s^{-2}} = 4.5\times10^{-4}\,\mathrm{m\,s^{-2}}.$$

At a latitude where $|f| = 10^{-4}\,\mathrm{s^{-1}}$ the Coriolis acceleration of the same wind is $|f|U = 1.5\times10^{-3}\,\mathrm{m\,s^{-2}}$, so the centripetal acceleration is 0.3 of it, too large to ignore and too

small to dominate. The same $10\,\mathrm{m\,s^{-1}}$ wind turning around a hill with $R = 1\,\mathrm{km}$ needs $a_c = 100/1000 = 0.1\,\mathrm{m\,s^{-2}}$, a hundred times its Coriolis acceleration of $10^{-3}\,\mathrm{m\,s^{-2}}$. The ratio of the two accelerations, $U/(|f|R)$, decides which of them controls the flow; it reappears as the Rossby number in Section 4.6.

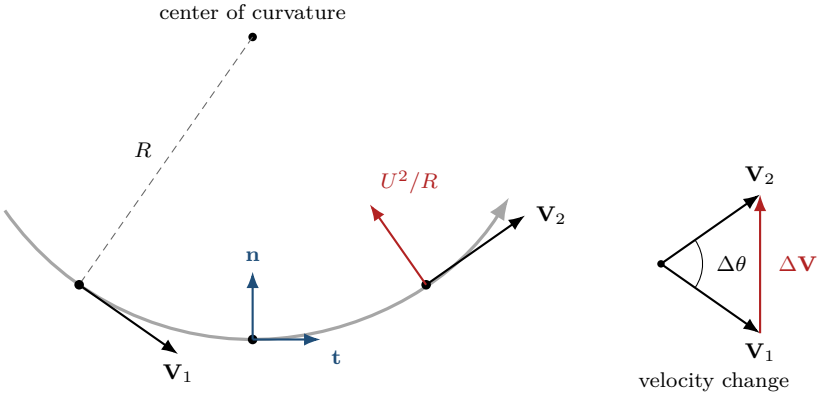


Figure 4.1: A parcel on a path that turns to the left (counterclockwise seen from above), schematic. Left: the path (gray), the center of curvature at distance R, the velocity $\mathbf{V}_1$ and $\mathbf{V}_2$ at two positions, the natural-coordinate unit vectors $\mathbf{t}$ (along the flow) and $\mathbf{n}$ (across it, to the left) at the middle position, and the centripetal acceleration U^2/R (red). Right: the two velocities from a common origin; their difference $\Delta\mathbf{V}$ has magnitude $U\Delta\theta$ with $\Delta\theta = U\Delta t/R$ and points toward the center of curvature.

4.2 The gradient wind balance

This section writes the horizontal momentum balance in coordinates attached to the flow, obtains the gradient wind balance and its geostrophic limit, defines cyclonic and anticyclonic flow precisely in both hemispheres, and relates the inward-acceleration description to the centrifugal force used in many texts.

4.2.1 Natural coordinates

At each point of a parcel's path define two horizontal unit vectors (Figure 4.1): $\mathbf{t}$, tangent to the path and pointing along the motion, and $\mathbf{n} = \mathbf{k} \times \mathbf{t}$, perpendicular to the path and pointing to the left of the motion. The coordinate s measures distance along the path and n distance across it. In these *natural coordinates* the horizontal velocity has one component only,

$$\mathbf{V} = U\,\mathbf{t}, \qquad U \geq 0,$$

and its direction is carried by $\mathbf{t}$. The radius of curvature R is given a sign: $R > 0$ when the path turns to the left, toward $+\mathbf{n}$, that is counterclockwise seen from above, and $R < 0$ when it turns to the right, clockwise. Its magnitude $|R|$ is the distance to the center of curvature. A straight path has $|R| \to \infty$.

The acceleration of the parcel follows from differentiating $\mathbf{V} = U\mathbf{t}$ along its path. Both factors change: the speed U and the direction $\mathbf{t}$. As the parcel advances by $\mathrm{d}s = U\mathrm{d}t$, the tangent turns by the angle $\mathrm{d}s/R$ toward $\mathbf{n}$, so $\frac{\mathrm{D}\mathbf{t}}{\mathrm{D}t} = (U/R)\,\mathbf{n}$, and

$$\frac{\mathrm{D}\mathbf{V}}{\mathrm{D}t} = \frac{\mathrm{D}U}{\mathrm{D}t}\,\mathbf{t} + \frac{U^2}{R}\,\mathbf{n}. \tag{4.3}$$

The first term changes the speed; the second, the centripetal acceleration of equation (4.2), changes the direction. With the sign convention for R, the second term points toward the center of curvature on either kind of turn.

4.2.2 The balance along and across the flow

Above the boundary layer friction is small, and the horizontal momentum equation per unit mass reads

$$\frac{\mathrm{D}\mathbf{V}}{\mathrm{D}t} = -\frac{1}{\rho}\nabla_h p - f\,\mathbf{k}\times\mathbf{V}, \tag{4.4}$$

acceleration equal to the pressure-gradient force plus the Coriolis force, both per unit mass, in $\mathrm{m\,s^{-2}}$. In natural coordinates the Coriolis term is $-f\,\mathbf{k}\times U\mathbf{t} = -fU\mathbf{n}$, entirely across the flow, and the pressure gradient splits into $\partial p/\partial s$ along the flow and $\partial p/\partial n$ across it. Taking the $\mathbf{t}$ and $\mathbf{n}$ components of equation (4.4) with equation (4.3) gives

$$\frac{\mathrm{D}U}{\mathrm{D}t} = -\frac{1}{\rho}\frac{\partial p}{\partial s}, \tag{4.5}$$

$$\frac{U^2}{R} = -\frac{1}{\rho}\frac{\partial p}{\partial n} - fU. \tag{4.6}$$

Term by term: in equation (4.5), $\frac{\mathrm{D}U}{\mathrm{D}t}$ is the rate of change of the speed following the parcel and $-(1/\rho)\,\partial p/\partial s$ the pressure-gradient force along the path; in equation (4.6), U^2/R is the centripetal acceleration, $-(1/\rho)\,\partial p/\partial n$ the pressure-gradient force across the path, positive when pressure falls to the left, and $-fU$ the Coriolis force, which points to the right of the motion ($-\mathbf{n}$) when $f > 0$ and to the left when $f < 0$.

The *gradient wind balance* is the steady case. If the speed does not change along the path, equation (4.5) requires $\partial p/\partial s = 0$: the wind blows along the isobars, as the geostrophic wind does. Equation (4.6) then fixes the speed. Writing the cross-flow pressure-gradient force in terms of the geostrophic speed of the same gradient, $fU_g = -(1/\rho)\,\partial p/\partial n$, it becomes

$$\frac{U^2}{R} + fU - fU_g = 0. \tag{4.7}$$

This is the gradient wind balance: centripetal acceleration, Coriolis force and pressure-gradient force in balance across the flow. Its positive root $U = U_{gr}$ is the gradient wind speed. Defined this way, U_g is positive whenever the low pressure lies on the side the hemisphere requires for geostrophic flow (to the left of the wind in the Northern Hemisphere, to the right in the Southern), and then $U_g = |\nabla_h p|/(\rho|f|)$, equation (4.1).

Assumptions. Equation (4.7) assumes steady speed, no friction, horizontal motion, and that R is the radius of curvature of the parcel's trajectory. A map shows the curvature of the contours and of the streamlines, which equals the trajectory curvature only when the pattern does not move; for a moving low or high the two differ, a correction not treated here.

4.2.3 The geostrophic limit

Dividing equation (4.7) by fU gives a compact form,

$$\frac{U_g}{U} = 1 + \frac{U}{fR}. \tag{4.8}$$

The last term is the ratio of the centripetal acceleration to the Coriolis acceleration, signed. On a straight path, $|R| \to \infty$, it vanishes and $U = U_g$: the gradient wind reduces to the geostrophic wind. The geostrophic wind is therefore the straight-flow limit of the gradient wind, and the

departure of the gradient wind from it is governed by $U/(|f||R|)$, which is small for broad, gently curved flow and large for tight curvature. Equation (4.8) also shows the direction of the departure before any quadratic is solved: it depends only on the sign of fR, which the next subsection interprets.

4.2.4 Cyclonic and anticyclonic flow in both hemispheres

The Earth rotates counterclockwise when seen from above the North Pole and clockwise when seen from above the South Pole. Flow that turns in the same sense as the Earth beneath it is *cyclonic*; flow that turns in the opposite sense is *anticyclonic*. Air circulating around a low is cyclonic and air circulating around a high is anticyclonic, in both hemispheres, because in both the Coriolis force must point away from a low and toward a high for the flow to be in balance (Section 4.3).

Figure 4.2 shows the four cases. Each panel draws three circular isobars around a center of low (L) or high (H) pressure, with blue arrows giving the sense of the wind; north is up in every panel. The top row is the Northern Hemisphere, the bottom row the Southern; the left column is a low, the right column a high. The low turns counterclockwise in the north and clockwise in the south; the high does the reverse. The sense of rotation of a low is not a property of lows; it is fixed by the sign of f.

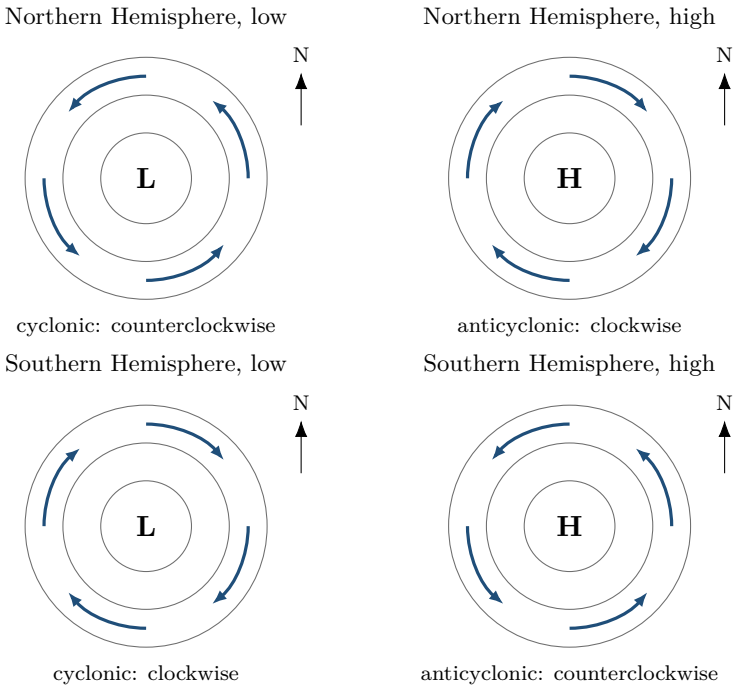


Figure 4.2: Cyclonic and anticyclonic flow in the two hemispheres, schematic. Gray circles: isobars around a low (L) or a high (H); blue arrows: sense of the balanced wind; north is up. Cyclonic flow turns with the Earth seen from above the local hemisphere (counterclockwise in the north, clockwise in the south); anticyclonic flow turns against it.

In the sign convention of Section 4.2.1 the two cases have a compact test. Cyclonic flow in the Northern Hemisphere turns counterclockwise, $R > 0$ with $f > 0$; in the Southern it turns clockwise, $R < 0$ with $f < 0$. In both, $fR > 0$. Anticyclonic flow has $fR < 0$ in both. Equation (4.8) then reads, without reference to the hemisphere,

$$\begin{aligned} &\text{cyclonic, } fR > 0: && U_g/U > 1, \quad U < U_g \text{ (subgeostrophic);} \\ &\text{anticyclonic, } fR < 0: && U_g/U < 1, \quad U > U_g \text{ (supergeostrophic).} \end{aligned}$$

The sign of f changes the sense in which a low turns, but not the fact that the balanced wind around it is slower than geostrophic.

Principle 4.1. *Whether a curved flow is cyclonic or anticyclonic is decided by the sign of fR, not by the sense of rotation alone: counterclockwise is cyclonic in the Northern Hemisphere and anticyclonic in the Southern.*

4.2.5 Centripetal acceleration and centrifugal force

The curvature term can be stated in two equivalent ways, and both appear in the literature. In the Earth-fixed frame used so far, in which the Coriolis force already appears because the frame rotates with the Earth, the parcel on a curved path has an inward acceleration U^2/R, and equation (4.6) says that the pressure-gradient and Coriolis forces together must supply it: their sum is not zero but equal to the centripetal acceleration.

Alternatively, the motion can be described in a frame that also turns with the parcel around the center of curvature. In that frame the parcel is at rest, and an apparent outward force per unit mass, the *centrifugal force* U^2/R, is added to the balance. Moving U^2/R to the other side of equation (4.6) gives the three-force form

$$\underbrace{-\frac{1}{\rho}\frac{\partial p}{\partial n}}_{\text{pressure gradient}} \quad \underbrace{-fU}_{\text{Coriolis}} \quad \underbrace{-\frac{U^2}{R}}_{\text{centrifugal}} = 0,$$

pressure-gradient force plus Coriolis force plus centrifugal force equal zero. The two statements are the same equation with one term on different sides; neither is more correct. This book uses the inward-acceleration description, because it keeps every term a real force or a real acceleration in one frame and makes plain that the curved flow is not in equilibrium in the sense of zero net force: the net force is exactly what turns the air.

4.3 Flow around lows and highs

This section applies the cross-flow balance to air circulating around a low and around a high, draws the forces on the parcel, solves the balance explicitly for the gradient wind speed, works one low in the Northern Hemisphere and one high in the Southern, and compares the results with the geostrophic wind as the radius of curvature shrinks. Throughout the section R denotes the radius as a positive distance, $|R|$ of Section 4.2.1; the sense of rotation is carried by the words low and high.

4.3.1 Forces around a low

Around a low the pressure increases outward, so the pressure-gradient force points inward, toward the center, with magnitude $(1/\rho)|\partial p/\partial n| = |f|U_g$. The flow is cyclonic. In the Northern Hemisphere it is counterclockwise, and the Coriolis force, to the right of the motion, points outward; in the Southern Hemisphere it is clockwise, and the Coriolis force, to the left of the motion, again points outward. In both hemispheres the Coriolis force around a low points away from the center, with magnitude $|f|U$.

The parcel needs a net inward acceleration U^2/R. The inward pressure-gradient force must therefore both cancel the outward Coriolis force and supply the centripetal acceleration:

$$|f|U_g = |f|U + \frac{U^2}{R}. \tag{4.9}$$

Since $U^2/R > 0$, the Coriolis force is smaller than the pressure-gradient force, $|f|U < |f|U_g$, and $U < U_g$: the balanced wind around a low is *subgeostrophic*. Part of the pressure gradient is used to turn the air and is not available to be balanced by the Coriolis force, so a smaller speed suffices.

Figure 4.3(a) draws this balance for an illustrative low in the Northern Hemisphere with $|f| = 10^{-4}\,\mathrm{s}^{-1}$, $U_g = 10\,\mathrm{m\,s}^{-1}$ and $R = 500\,\mathrm{km}$, at the northernmost point of a circular isobar. The gray arc is the isobar, the center of the low lies below (not to scale), north is up, and the black arrow is the wind, blowing toward the west. The blue arrow is the pressure-gradient force, the red arrow the Coriolis force and the green arrow their sum, all drawn to one scale. The blue arrow is longer than the red one, and the short green arrow, the net inward force, is exactly the centripetal acceleration the parcel needs.

4.3.2 Forces around a high

Around a high the pressure decreases outward, and the pressure-gradient force points outward with magnitude $|f|U_g$. The flow is anticyclonic: clockwise in the Northern Hemisphere, with the Coriolis force to the right of the motion, inward; counterclockwise in the Southern Hemisphere, with the Coriolis force to the left of the motion, again inward. In both hemispheres the Coriolis force around a high points toward the center, with magnitude $|f|U$.

Now the inward Coriolis force must both cancel the outward pressure-gradient force and supply the centripetal acceleration:

$$|f|U = |f|U_g + \frac{U^2}{R}. \tag{4.10}$$

The Coriolis force must exceed the pressure-gradient force, $|f|U > |f|U_g$, which requires $U > U_g$: the balanced wind around a high is *supergeostrophic*. The only inward force available is the Coriolis force, and it grows only by the air moving faster.

Figure 4.3(b) draws the same construction for a high in the Southern Hemisphere with the same $|f|$, U_g and R. The flow is counterclockwise, so at the northernmost point of the isobar it again blows toward the west; the Coriolis force, to the left of that motion in this hemisphere, points south, toward the center. The pressure-gradient force (blue) now points outward, the Coriolis force (red) inward and longer, and the net force (green) is again inward and equal to U^2/R. Comparing the two panels: the pressure-gradient force is the same, the sense of the Coriolis force is reversed relative to it, and the wind speed that makes the balance close is $8.54\,\mathrm{m\,s}^{-1}$ around the low and $13.82\,\mathrm{m\,s}^{-1}$ around the high (Section 4.3.3).

4.3.3 Solving for the gradient wind speed

Equations (4.9) and (4.10) are quadratic in U. Multiplying each by R and collecting terms,

$$\begin{aligned} \text{low:} \quad & U^2 + |f|RU - |f|RU_g = 0, \\ \text{high:} \quad & U^2 - |f|RU + |f|RU_g = 0. \end{aligned}$$

The quadratic formula gives the gradient wind speed in terms of the geostrophic speed, the radius and $|f|$:

$$\text{low:} \quad U_{gr} = -\frac{|f|R}{2} + \sqrt{\frac{f^2R^2}{4} + |f|RU_g}, \tag{4.11}$$

$$\text{high:} \quad U_{gr} = \frac{|f|R}{2} - \sqrt{\frac{f^2R^2}{4} - |f|RU_g}. \tag{4.12}$$

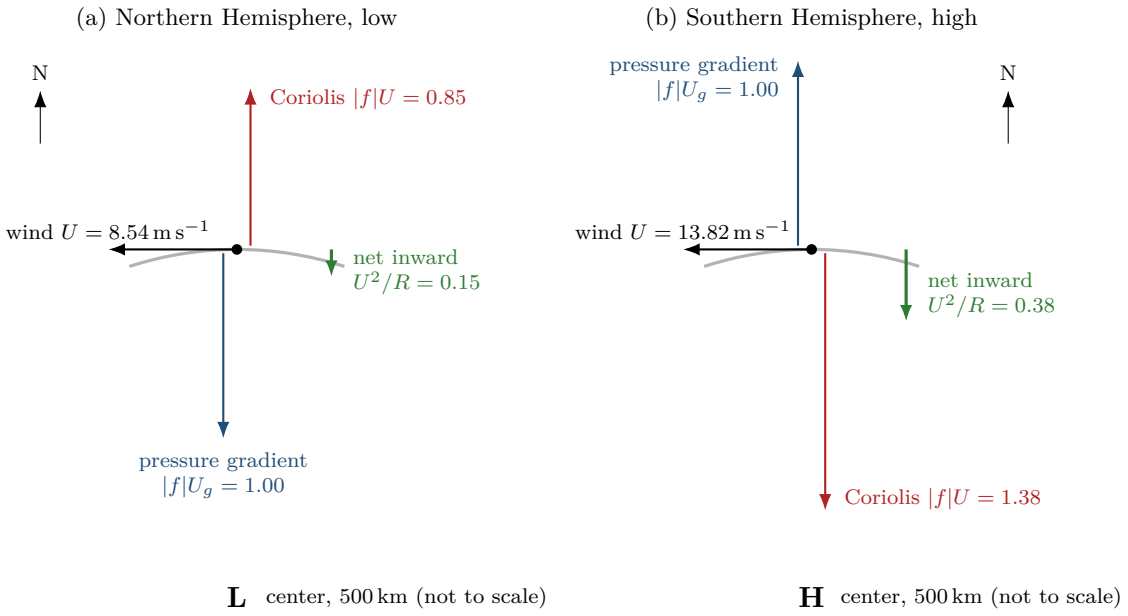


Figure 4.3: Forces per unit mass on a parcel at the northernmost point of a circular isobar, drawn to one scale, in units of $10^{-3}\,\mathrm{m\,s^{-2}}$. Both panels use illustrative $|f| = 10^{-4}\,\mathrm{s^{-1}}$ (about 43° latitude, north in (a), south in (b)), $U_g = 10\,\mathrm{m\,s^{-1}}$ and $R = 500\,\mathrm{km}$; the wind speeds are the gradient wind solutions of equations (4.11) and (4.12). (a) Around a low the pressure-gradient force (blue) points inward and exceeds the outward Coriolis force (red). (b) Around a high the Coriolis force points inward and exceeds the outward pressure-gradient force. In both the net force (green) is the inward centripetal acceleration U^2/R.

Each quadratic has two roots, and the physical one is selected by requiring a positive speed that tends to U_g as the curvature vanishes. For the low, the product of the roots is $-|f|RU_g < 0$, so exactly one root is positive, the one written. For the high, both roots are positive; as $R \to \infty$ the root with the minus sign tends to U_g and the one with the plus sign grows without bound, so the minus sign is the physical choice.

Both solutions depend on U_g, R and $|f|$ only through one dimensionless group, the *curvature Rossby number*

$$\mathrm{Ro}_R = \frac{U_g}{|f|R}, \tag{4.13}$$

the ratio of the geostrophic speed to the speed $|f|R$, or equivalently of a centripetal acceleration U_g^2/R to a Coriolis acceleration $|f|U_g$. Dividing equations (4.11) and (4.12) by U_g and rationalizing,

$$\text{low:}\quad \frac{U_{gr}}{U_g} = \frac{2}{1+\sqrt{1+4\mathrm{Ro}_R}}, \qquad \text{high:}\quad \frac{U_{gr}}{U_g} = \frac{2}{1+\sqrt{1-4\mathrm{Ro}_R}}. \tag{4.14}$$

For small Ro_R both reduce to $U_{gr}/U_g \approx 1 \mp \mathrm{Ro}_R$: the fractional departure from geostrophic balance is, to first order, the curvature Rossby number itself, minus around a low and plus around a high.

The other roots. The discarded root of the high, $U_{gr} = |f|R/2 + \sqrt{f^2R^2/4 - |f|RU_g}$, and a negative root of the low, which corresponds to anticyclonic rotation around a low, are mathematically valid balances. They are called anomalous, because they are not connected to the geostrophic wind as the curvature vanishes, and they are not observed in large-scale flow. Anticyclonic rotation around a low does occur in small vortices such as dust devils, where the Coriolis force is negligible and either sense of rotation is possible (Section 4.6.4).

4.3.4 A worked low

Take an illustrative low in the Northern Hemisphere at about 43° N, where $f = 2\Omega \sin\phi = 1.0 \times 10^{-4}\,\mathrm{s}^{-1}$, with a geostrophic speed $U_g = 20\,\mathrm{m\,s}^{-1}$ (about 2.4 hPa per 100 km at $\rho = 1.2\,\mathrm{kg/m}^3$, by equation (4.1)) and a radius of curvature $R = 500\,\mathrm{km}$. Then $|f|R = 10^{-4} \times 5 \times 10^5 = 50\,\mathrm{m\,s}^{-1}$, $\mathrm{Ro}_R = 20/50 = 0.4$, and equation (4.11) gives

$$U_{gr} = -25 + \sqrt{25^2 + 50 \times 20} = -25 + \sqrt{1625} = -25 + 40.31 = 15.31\,\mathrm{m\,s}^{-1},$$

or $U_{gr}/U_g = 0.766$ from equation (4.14). The check on the forces, in $\mathrm{m\,s}^{-2}$:

$$\underbrace{|f|U_g}_{2.00\times10^{-3}} = \underbrace{|f|U_{gr}}_{1.53\times10^{-3}} + \underbrace{U_{gr}^2/R}_{(15.31)^2/(5\times10^5)=0.47\times10^{-3}} .$$

The geostrophic estimate, $20\,\mathrm{m\,s}^{-1}$, overestimates the balanced wind by $4.7\,\mathrm{m\,s}^{-1}$, about 31 % of the balanced wind. The same check in the signed form of equation (4.8): the flow is counterclockwise, $R = +5 \times 10^5\,\mathrm{m}$, $f > 0$, so $U/(fR) = 15.31/50 = 0.306$ and $U_g/U = 1.306$, which gives $U = 20/1.306 = 15.31\,\mathrm{m\,s}^{-1}$.

4.3.5 A worked high in the Southern Hemisphere

Take an illustrative high over the South Atlantic at 30° S, where $f = 2\Omega\sin(-30°) = -\Omega = -7.29 \times 10^{-5}\,\mathrm{s}^{-1}$, with $U_g = 10\,\mathrm{m\,s}^{-1}$ and $R = 1000\,\mathrm{km}$. The flow is anticyclonic, which in this hemisphere is counterclockwise. With $|f|R = 7.29 \times 10^{-5} \times 10^6 = 72.9\,\mathrm{m\,s}^{-1}$ and $\mathrm{Ro}_R = 10/72.9 = 0.137$, equation (4.12) gives

$$U_{gr} = 36.46 - \sqrt{36.46^2 - 72.92 \times 10} = 36.46 - \sqrt{600.1} = 36.46 - 24.50 = 11.96\,\mathrm{m\,s}^{-1},$$

or $U_{gr}/U_g = 1.196$. The check on the forces, in $\mathrm{m\,s}^{-2}$:

$$\underbrace{|f|U_{gr}}_{0.872\times10^{-3}} = \underbrace{|f|U_g}_{0.729\times10^{-3}} + \underbrace{U_{gr}^2/R}_{(11.96)^2/10^6=0.143\times10^{-3}} .$$

The geostrophic estimate underestimates the balanced wind by about $2\,\mathrm{m\,s}^{-1}$, or 16 % of the balanced wind. In the signed form: counterclockwise means $R = +10^6\,\mathrm{m}$, and with $f < 0$, $fR = -72.9\,\mathrm{m\,s}^{-1}$ and $U/(fR) = 11.96/(-72.9) = -0.164$, so $U_g/U = 0.836$ and $U = 10/0.836 = 11.96\,\mathrm{m\,s}^{-1}$. The sign of fR identified the flow as anticyclonic without any rule specific to the hemisphere.

4.3.6 Comparison and the effect of the radius of curvature

Table 4.1 collects the three cases for one pressure gradient: the rows are cyclonic, straight and anticyclonic flow; the columns give the direction of the Coriolis force on the parcel, the balance across the flow, the resulting relation to the geostrophic speed, and the speed for an illustrative $U_g = 10\,\mathrm{m\,s}^{-1}$, $R = 500\,\mathrm{km}$ and $|f| = 10^{-4}\,\mathrm{s}^{-1}$ ($\mathrm{Ro}_R = 0.2$). The same isobar spacing, which fixes U_g, gives $8.54\,\mathrm{m\,s}^{-1}$ around the low, $10\,\mathrm{m\,s}^{-1}$ on a straight path and $13.82\,\mathrm{m\,s}^{-1}$ around the high: a factor of 1.6 between the balanced winds of identical pressure gradients.

The departure from geostrophic balance depends on the radius. For very large R the term U^2/R is negligible, and the gradient wind is the geostrophic wind. As R shrinks, the curvature term grows and the departure grows with it. For the illustrative $U_g = 10\,\mathrm{m\,s}^{-1}$ and $|f| = 10^{-4}\,\mathrm{s}^{-1}$:

Table 4.1: Balanced wind for one pressure gradient on three kinds of path, valid in both hemispheres. Last column: illustrative $U_g = 10\,\mathrm{m\,s^{-1}}$, $R = 500\,\mathrm{km}$, $|f| = 10^{-4}\,\mathrm{s^{-1}}$, from equations (4.11) and (4.12).

Path	Coriolis force	Balance across the flow	Speed	Example
Cyclonic, around a low	outward	$\lvert f\rvert U_g = \lvert f\rvert U + U^2/R$	$U < U_g$, subgeostrophic	$8.54\,\mathrm{m\,s^{-1}}$
Straight	opposite to the pressure gradient	$\lvert f\rvert U_g = \lvert f\rvert U$	$U = U_g$, geostrophic	$10.00\,\mathrm{m\,s^{-1}}$
Anticyclonic, around a high	inward	$\lvert f\rvert U = \lvert f\rvert U_g + U^2/R$	$U > U_g$, supergeostrophic	$13.82\,\mathrm{m\,s^{-1}}$

radius R (km)	2000	1000	500	400	250
Ro_R	0.05	0.10	0.20	0.25	0.40
around a low, U_{gr} ($\mathrm{m\,s^{-1}}$)	9.54	9.16	8.54	8.28	7.66
around a high, U_{gr} ($\mathrm{m\,s^{-1}}$)	10.56	11.27	13.82	20.00	none

At $R = 2000\,\mathrm{km}$ the balanced wind is within 6 % of the geostrophic speed on either side; at 500 km it differs from it by −15 % around the low and +38 % around the high. The geostrophic approximation therefore works well along broad, nearly straight parts of a flow and poorly near strongly curved lows and highs.

Figure 4.4 plots equation (4.14). The horizontal axis is the curvature Rossby number Ro_R; the vertical axis is the ratio of gradient to geostrophic speed. The blue curve is the low, the red curve the high, and the dashed horizontal line the straight-flow value of one. Dots mark the worked examples: (a) the low of Section 4.3.4, (b) and (c) the low and high of Table 4.1, (d) the Southern Hemisphere high of Section 4.3.5. The low curve falls slowly and continuously; at $\mathrm{Ro}_R = 1$ the balanced wind is still 62 % of geostrophic. The high curve rises faster and faster and ends at $\mathrm{Ro}_R = 1/4$, where $U_{gr} = 2U_g$; beyond that point the balance has no solution. The asymmetry is the subject of Section 4.4.

4.4 The limit on anticyclonic flow

The anticyclonic solution of equation (4.12) contains a square root that can become imaginary. This section derives the resulting limit, states it as a maximum pressure gradient and a maximum wind speed, works it with numbers, and draws its consequence for the pressure field near the center of a high.

4.4.1 The discriminant

The high's quadratic, $U^2 - |f|RU + |f|RU_g = 0$, has real roots only if its discriminant is not negative:

$$f^2R^2 - 4|f|RU_g \geq 0.$$

Dividing by $4|f|R > 0$ and using $U_g = |\nabla_h p|/(\rho|f|)$ gives the limit in two equivalent forms,

$$U_g \leq \frac{|f|R}{4} \qquad \Longleftrightarrow \qquad |\nabla_h p| \leq \frac{\rho f^2 R}{4}, \tag{4.15}$$

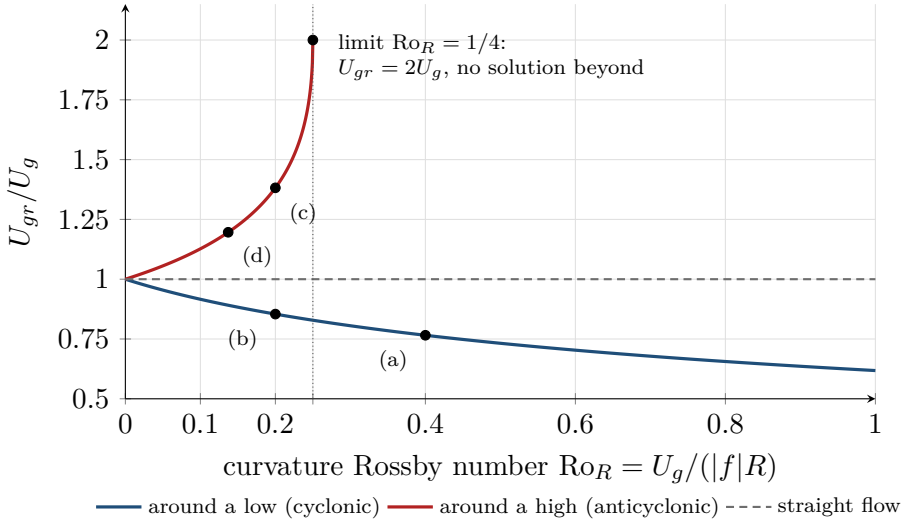


Figure 4.4: Ratio of the gradient wind speed to the geostrophic speed against the curvature Rossby number, equation (4.14): low $2/(1+\sqrt{1+4\mathrm{Ro}_R})$, high $2/(1+\sqrt{1-4\mathrm{Ro}_R})$, valid in both hemispheres. Dots: (a) worked low, $U_g = 20\,\mathrm{m\,s^{-1}}$, $R = 500\,\mathrm{km}$, $|f| = 10^{-4}\,\mathrm{s^{-1}}$; (b), (c) low and high with $U_g = 10\,\mathrm{m\,s^{-1}}$, $R = 500\,\mathrm{km}$, $|f| = 10^{-4}\,\mathrm{s^{-1}}$; (d) worked high at 30° S, $U_g = 10\,\mathrm{m\,s^{-1}}$, $R = 1000\,\mathrm{km}$. The anticyclonic curve ends at the limit $\mathrm{Ro}_R = 1/4$.

a maximum pressure gradient for anticyclonic gradient flow at a given radius and latitude, or equivalently $\mathrm{Ro}_R \le 1/4$. At the limit the two roots coincide at

$$U_{gr} = \frac{|f|R}{2} = 2U_g, \tag{4.16}$$

which is the largest anticyclonic gradient wind possible at radius R: the regular root of equation (4.12) rises from U_g toward $|f|R/2$ as U_g grows toward $|f|R/4$, and no larger gradient admits a balanced solution. In the Southern Hemisphere the limit is the same with $|f|$, since only f^2 and $|f|$ appear.

The physical reason lies in how the two sides of the balance grow with speed. Around a high, the net inward force available to turn the air is the excess of the Coriolis force over the pressure-gradient force, $|f|(U - U_g)$, which grows linearly with U. The inward acceleration the curve requires, U^2/R, grows quadratically. A balance is a speed at which the two are equal.

Figure 4.5 shows the two sides of equation (4.10) for $R = 500\,\mathrm{km}$ and $|f| = 10^{-4}\,\mathrm{s^{-1}}$. The horizontal axis is the wind speed; the vertical axis is acceleration in $10^{-3}\,\mathrm{m\,s^{-2}}$. The black parabola is the required centripetal acceleration U^2/R; the three straight lines are the available net inward force $|f|(U - U_g)$ for three geostrophic speeds. A gradient wind is an intersection. For $U_g = 8\,\mathrm{m\,s^{-1}}$ (blue) the line crosses the parabola twice, at the regular root $10\,\mathrm{m\,s^{-1}}$ and at the anomalous root $40\,\mathrm{m\,s^{-1}}$. For $U_g = 12.5\,\mathrm{m\,s^{-1}}$ (green, dashed) it touches the parabola at a single point, $25\,\mathrm{m\,s^{-1}}$: the limit. For $U_g = 16\,\mathrm{m\,s^{-1}}$ (red, dotted) the line stays below the parabola at every speed: no speed lets the Coriolis force grow fast enough to supply the required curvature, and no steady anticyclonic gradient wind exists.

For a low the corresponding construction never fails: the low's quadratic has the discriminant $f^2R^2 + 4|f|RU_g$, a sum of positive terms, so a cyclonic gradient wind exists for every pressure gradient and every radius. The pressure-gradient force itself supplies the inward acceleration, and a steeper gradient simply yields a faster wind.

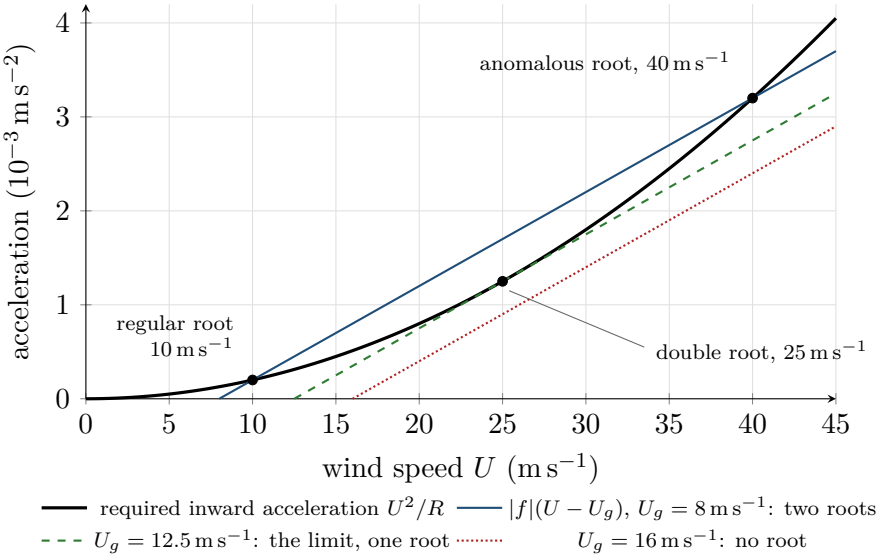


Figure 4.5: Graphical solution of the anticyclonic gradient wind balance, equation (4.10), for illustrative $R = 500\,\text{km}$ and $|f| = 10^{-4}\,\text{s}^{-1}$: required inward acceleration U^2/R (parabola) against the available net inward force $|f|(U - U_g)$ (lines) for three geostrophic speeds. Intersections are gradient wind solutions. The limit, $U_g = |f|R/4 = 12.5\,\text{m s}^{-1}$, is the tangent line, with the double root $U = |f|R/2 = 25\,\text{m s}^{-1}$.

4.4.2 A worked limit

At $R = 500\,\text{km}$ from the center of a high, with $|f| = 10^{-4}\,\text{s}^{-1}$ and $\rho = 1.2\,\text{kg/m}^3$, equation (4.15) gives

$$U_g \le \frac{10^{-4} \times 5 \times 10^5}{4} = 12.5\,\text{m s}^{-1},$$
$$|\nabla_h p| \le \frac{1.2 \times 10^{-8} \times 5 \times 10^5}{4} = 1.5 \times 10^{-3}\,\text{Pa m}^{-1} = 1.5\,\text{hPa per } 100\,\text{km},$$

and the balanced wind cannot exceed $|f|R/2 = 25\,\text{m s}^{-1}$. Closer to the center the limit tightens in proportion to R: at $R = 100\,\text{km}$ the largest admissible gradient is 0.3 hPa per 100 km and the largest balanced wind $5\,\text{m s}^{-1}$. Toward the equator it tightens with f^2: at 30° S, $|f| = 7.29 \times 10^{-5}\,\text{s}^{-1}$, and the maximum gradient at 500 km falls to $1.2 \times (7.29 \times 10^{-5})^2 \times 5 \times 10^5/4 = 8.0 \times 10^{-4}\,\text{Pa m}^{-1}$, about 0.8 hPa per 100 km, with a maximum balanced wind of $|f|R/2 = 18.2\,\text{m s}^{-1}$. By contrast, a pressure gradient of 3 hPa per 100 km at 500 km from the center of a low is unremarkable, and it has a gradient wind like any other.

An analysis that shows a steeper gradient than equation (4.15) allows on the anticyclonic side does not describe a steady balanced flow there: the air is accelerating, the flow is not circular about the assumed center, or the analysis is in error. The limit is therefore also a consistency check on a pressure or height analysis.

4.4.3 The flat centers of highs

Apply the limit at every radius of a circular high, with R the distance from the center. The pressure falls outward from the center, and at each radius R' its gradient obeys $|\mathrm{d}p/\mathrm{d}R'| \le \rho f^2 R'/4$. Integrating from the center to a radius R,

$$p(0) - p(R) = \int_0^R \left|\frac{\mathrm{d}p}{\mathrm{d}R'}\right| \mathrm{d}R' \le \frac{\rho f^2 R^2}{8}. \tag{4.17}$$

The pressure excess at the center of a balanced high is bounded by a quantity that grows only with the square of the distance. With $|f| = 10^{-4}\,\mathrm{s}^{-1}$ and $\rho = 1.2\,\mathrm{kg/m^3}$ the bound is $1.2 \times 10^{-8} \times (5 \times 10^5)^2/8 = 375\,\mathrm{Pa}$, that is 3.75 hPa within 500 km of the center, and about 2.0 hPa at 30° S. A low has no such bound: a central pressure 20 to 30 hPa below that of its surroundings 500 km away is common in a strong extratropical cyclone (illustrative).

This is why the centers of highs on weather maps are broad and flat, with widely spaced isobars and light winds, while the centers of lows can be deep, with tightly packed isobars and strong winds close to the center. Cyclonic flow has no restriction on its curvature in the idealized balance, and strongly curved cyclonic circulations, from extratropical cyclones to tropical cyclones, are dynamically more common than equally extreme anticyclonic ones. For near-surface wind applications the consequence is direct: under the center of a high the large-scale forcing of the wind is weak, and the local wind is left to local processes, thermal circulations and drainage flows among them, which Chapters 17 and 19 describe.

Principle 4.2. *Anticyclonic gradient flow is bounded: at radius R the geostrophic speed cannot exceed $|f|R/4$ and the balanced wind cannot exceed $|f|R/2$, so the pressure gradient must vanish toward the center of a high. Cyclonic flow has no such bound.*

4.5 Vorticity

Curvature describes how a single streamline bends; it does not by itself say whether the air rotates. This section defines relative vorticity, the measure of local rotation, computes it for two flows that rotate for different reasons, splits it into curvature and shear parts, and adds the Earth's own rotation to obtain absolute vorticity, with the sign conventions for both hemispheres.

4.5.1 Relative vorticity

The *relative vorticity* is the vertical component of the curl of the velocity relative to the Earth,

$$\zeta = \frac{\partial v}{\partial x} - \frac{\partial u}{\partial y}, \tag{4.18}$$

in s^{-1}, with u and v the eastward and northward wind components and x, y eastward and northward. Physically, ζ is twice the local angular velocity of a small fluid element about the vertical: a small paddle wheel with a vertical axis, carried with the flow, turns at the rate $\zeta/2$. By the mathematical convention, which is the same in both hemispheres, $\zeta > 0$ is counterclockwise rotation seen from above and $\zeta < 0$ clockwise.

Vorticity is not measured by an instrument at a point. It is computed: from a gridded wind analysis or a model output by finite differences of equation (4.18) across neighboring grid points, or from a ring of wind observations as the circulation around the ring divided by the enclosed area, which equals the mean vorticity inside it. Either way the value is an average over the grid spacing or the ring, and it depends on that scale: the same flow analyzed on a coarse grid shows smaller extremes of vorticity than on a fine one. This is the grid-cell-against-point distinction applied to a derivative of the wind.

Vorticity is related to curvature but not identical to it. Rotation of a fluid element can come from curved streamlines, from horizontal shear of the speed across straight streamlines, or from both; and the two can cancel, so that air moving on circles need not rotate at all (Section 4.5.3).

4.5.2 Solid-body rotation and pure shear

Two simple flows show the two sources of vorticity. Figure 4.6 draws them. Panel (a) is solid-body rotation: blue arrows on three dashed circles give the velocity, which grows in proportion to the distance from the center, as on a rotating turntable; the small cross with a curved arrow is a paddle wheel carried by the flow. Panel (b) is a straight shear flow: eastward velocity arrows whose length increases northward, from $5\,\mathrm{m\,s^{-1}}$ at the bottom to $20\,\mathrm{m\,s^{-1}}$ at the top, over an illustrative 300 km; north is up.

Solid-body rotation. A flow rotating counterclockwise as a rigid body with angular velocity ω has, at position (x, y) from the center, $u = -\omega y$ and $v = \omega x$, so

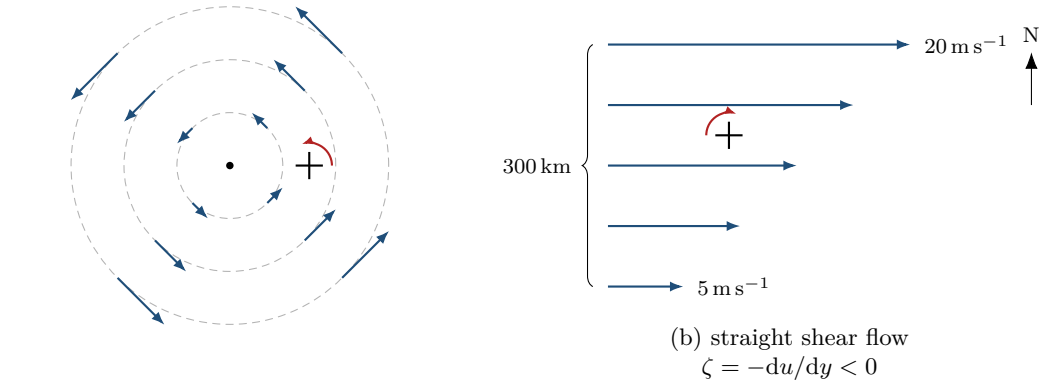
$$\zeta = \frac{\partial(\omega x)}{\partial x} - \frac{\partial(-\omega y)}{\partial y} = \omega + \omega = 2\omega. \tag{4.19}$$

The vorticity is uniform and equal to twice the angular velocity; the paddle wheel in panel (a) turns counterclockwise at the rate ω. An illustrative flow with $U = 10\,\mathrm{m\,s^{-1}}$ at 500 km from the center rotates at $\omega = U/R = 10/(5 \times 10^5) = 2 \times 10^{-5}\,\mathrm{s^{-1}}$ and has $\zeta = 4 \times 10^{-5}\,\mathrm{s^{-1}}$, positive.

Pure shear. A flow with straight, parallel streamlines, $u = u(y)$ and $v = 0$, has

$$\zeta = -\frac{\mathrm{d}u}{\mathrm{d}y}. \tag{4.20}$$

In panel (b) the eastward wind increases northward by $15\,\mathrm{m\,s^{-1}}$ over 300 km, so $\zeta = -15/(3 \times 10^5) = -5 \times 10^{-5}\,\mathrm{s^{-1}}$. The streamlines do not curve, yet the paddle wheel turns clockwise, because the faster air on its northern side pushes its top blades eastward faster than the slower air pushes its bottom blades.



(a) solid-body rotation, counterclockwise
$\zeta = 2\omega > 0$

(b) straight shear flow
$\zeta = -\mathrm{d}u/\mathrm{d}y < 0$

Figure 4.6: Two sources of relative vorticity, schematic. (a) Solid-body rotation, $u = -\omega y$, $v = \omega x$: curved streamlines and speed proportional to distance from the center; $\zeta = 2\omega$, with illustrative $\omega = 2 \times 10^{-5}\,\mathrm{s^{-1}}$ giving $\zeta = 4 \times 10^{-5}\,\mathrm{s^{-1}}$. (b) Straight shear flow, u rising from 5 to $20\,\mathrm{m\,s^{-1}}$ northward over an illustrative 300 km: $\zeta = -5 \times 10^{-5}\,\mathrm{s^{-1}}$. Red: sense in which a small paddle wheel carried by the flow turns.

4.5.3 Curvature and shear vorticity

In the natural coordinates of Section 4.2.1 the relative vorticity separates into two parts,

$$\zeta = \frac{U}{R} - \frac{\partial U}{\partial n}, \tag{4.21}$$

with R signed as in that section and $\mathbf{n}$ pointing to the left of the flow. The *curvature vorticity* U/R comes from the turning of the streamlines; the *shear vorticity* $-\partial U/\partial n$ comes from the change of speed across them. Both are in s^{-1}.

The two examples of Section 4.5.2 check the formula. In the shear flow the streamlines are straight, $U/R = 0$, and $\mathbf{n}$ points north, so $-\partial U/\partial n = -\mathrm{d}u/\mathrm{d}y$, equation (4.20). In solid-body rotation $U = \omega r$ at distance r from the center, the path turns left with $R = r$, so the curvature part is $U/R = \omega$; $\mathbf{n}$ points toward the center, where the speed falls, so $\partial U/\partial n = -\omega$ and the shear part is $+\omega$. The sum is 2ω, as in equation (4.19): in solid-body rotation half the vorticity is curvature and half is shear.

The two parts can also cancel. In a vortex whose speed falls off as $U = c/r$ with distance from the center, the curvature part is $U/R = c/r^2$ and the shear part is $-\partial U/\partial n = \mathrm{d}U/\mathrm{d}r = -c/r^2$, so $\zeta = 0$ everywhere except at the center: air moving on circles without rotating. Curved streamlines are therefore not the same as rotation, and air circulating around a low has cyclonic curvature vorticity whose total vorticity also depends on how its speed varies with distance from the center. In weather systems both parts are present: the flow around a low carries mainly curvature vorticity, the flanks of a jet stream mainly shear vorticity.

4.5.4 Planetary and absolute vorticity

The Earth itself rotates as a solid body with angular velocity Ω, and by equation (4.19) its vorticity is 2Ω about the polar axis. The component about the local vertical at latitude ϕ is $2\Omega \sin\phi = f$: the Coriolis parameter is the *planetary vorticity*, the vorticity that air at rest relative to the ground has because the ground rotates. It is positive in the Northern Hemisphere, where the Earth turns counterclockwise seen from above, and negative in the Southern. The *absolute vorticity* is the sum of planetary and relative vorticity,

$$\eta = f + \zeta, \tag{4.22}$$

in s^{-1}: the rotation of the air seen from an inertial frame. It is computed, like ζ, from analyzed winds, with f known from the latitude. In large-scale flow $|\zeta|$ is typically a fraction of $|f|$; the relative vorticity of the solid-body example, $4 \times 10^{-5}\,\mathrm{s}^{-1}$, is 0.4 of $f = 10^{-4}\,\mathrm{s}^{-1}$. Since $\zeta \sim U/L$ for a flow of speed U and size L, the ratio $|\zeta/f|$ is of the order of the Rossby number of Section 4.6.3. Absolute vorticity is introduced here as terminology; its role in the dynamics of weather systems is beyond the scope of this book.

Sign conventions. Cyclonic rotation is rotation in the sense of the Earth's, so cyclonic relative vorticity has the sign of f: positive in the Northern Hemisphere, negative in the Southern. The shear flow of Figure 4.6(b), with $\zeta = -5 \times 10^{-5}\,\mathrm{s}^{-1}$, is anticyclonic if it lies in the Northern Hemisphere and cyclonic if it lies in the Southern; the same southern flow is the poleward flank of a westerly jet, where the lows lie. Stated without reference to the hemisphere, vorticity is cyclonic when $f\zeta > 0$ and anticyclonic when $f\zeta < 0$, the same test as $fR > 0$ for curvature in Section 4.2.4.

The limiting anticyclone. The limit of Section 4.4 has a vorticity reading. A high in solid-body rotation at the limiting speed $U = |f|R/2$ rotates at $\omega = |f|/2$ in the anticyclonic sense, so its relative vorticity is $-f$ and its absolute vorticity $\eta = f - f = 0$. Flows whose absolute vorticity has the opposite sign to f are inertially unstable, a property not developed further here; the anticyclonic limit lies exactly at that boundary.

4.6 Curvature at different scales

Curved flow appears on a weather map as bent contours around lows, highs, troughs and ridges, and in terrain as streamlines bent over ridges and around obstacles. This section reads curvature on a map, separates synoptic from terrain-induced curvature, introduces the Rossby number as the measure of which balance applies at which scale, and closes with the chain of scales that ends at a sensor on a transmission line.

4.6.1 Curved contours on weather maps

On a map of isobars or of the height of a pressure surface, the spacing of the contours fixes the geostrophic speed through equation (4.1), and their shape fixes the radius of curvature. The results of Section 4.3 translate into a rule for reading the map: where the contours curve strongly around a low or through a trough, a straight-line geostrophic estimate overestimates the balanced wind; where they curve around a high or through a ridge, it underestimates it. The same contour spacing does not imply the same balanced wind.

Figure 4.7 illustrates the rule on a schematic 500 hPa height map of the Southern Hemisphere. North is up; the gray lines are height contours, labeled at the left in meters, with the lower heights to the south, toward the pole, so the westerlies blow from left to right with low heights on their right, as the Southern Hemisphere requires. The contours are equally spaced and undulate in a wave. Where they bulge northward, toward the equator, lies a trough, where the flow turns clockwise: cyclonic in this hemisphere. Where they dip southward lies a ridge, where the flow turns counterclockwise: anticyclonic. The blue arrows are the balanced wind in the channel between the second and third contours, drawn with length proportional to speed: shortest in the trough, longest in the ridge, and close to geostrophic where the contours are straight between them.

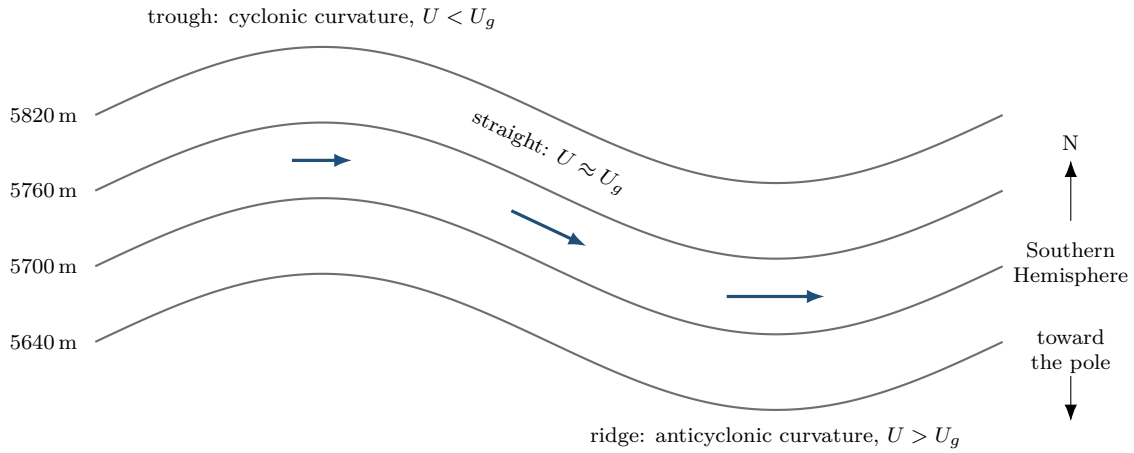


Figure 4.7: Schematic 500 hPa height map of the Southern Hemisphere (illustrative heights). Equally spaced contours (gray) with lower heights toward the pole; the westerly flow has the low heights on its right. Blue arrows: balanced wind between the 5700 and 5760 m contours, length proportional to speed. The same contour spacing gives a subgeostrophic wind in the trough (cyclonic curvature, clockwise in this hemisphere), a supergeostrophic wind in the ridge (counterclockwise), and nearly the geostrophic wind where the contours are straight.

A weather model does not apply this rule: it solves the momentum equations with all their terms, so curvature enters its winds without being singled out. The rule is a reading aid for maps, and a check: where a model's or an analysis's winds above the boundary layer differ from the geostrophic speed of its contours, the curvature of the contours should explain the sign and

roughly the size of the difference. A model also represents curvature only down to a few grid spacings: a grid of $\Delta x = 10\,\mathrm{km}$ cannot resolve a curve of radius 5 km, which in the model is smoothed into a gentler one.

4.6.2 Synoptic and terrain-induced curvature

Curved flow occurs at very different scales. *Synoptic curvature* is the curvature of the flow around highs and lows, troughs and ridges, with radii from about 100 km to more than 1000 km; it is the curvature of the gradient wind. *Terrain-induced curvature* is the bending of streamlines by ridges, valleys, escarpments and buildings, with radii from about 10 m to 10 km. Both are curvature in the sense of equation (4.2), and the same equations of motion govern both. The dominant balance is different: at synoptic scales the centripetal acceleration is a correction to the balance between the pressure-gradient and Coriolis forces; at terrain scales the Coriolis force is much less important than the centripetal acceleration and than the pressure perturbations that the terrain itself creates. The illustrative numbers of Section 4.1.2 already showed this: U^2/R is 0.3 of the Coriolis acceleration for a 500 km curve and a hundred times it for a 1 km curve.

4.6.3 The Rossby number

The ratio that decides between the two regimes is the *Rossby number*,

$$\mathrm{Ro} = \frac{U}{|f|L}, \tag{4.23}$$

dimensionless, where U is a typical speed of the flow and L a typical horizontal length scale, such as the radius of curvature or the size of the feature that perturbs the flow. It estimates the ratio of the inertial (advective or centripetal) acceleration, of order U^2/L, to the Coriolis acceleration, of order $|f|U$. It is also the ratio of two times: the time $1/|f|$ that the Coriolis force needs to turn a wind appreciably (about $10^4\,\mathrm{s}$, nearly three hours, at $|f| = 10^{-4}\,\mathrm{s^{-1}}$) to the time L/U that the air takes to cross the feature. The absolute value $|f|$ makes Ro positive in both hemispheres. When $\mathrm{Ro} \ll 1$ the Coriolis force is important and the flow is close to geostrophic or gradient balance; when $\mathrm{Ro} \gg 1$ inertia dominates and the Coriolis force is negligible. It is calculated from the scales of a flow, not measured; the curvature Rossby number of equation (4.13) is the special case with $L = R$ and $U = U_g$.

A synoptic example. For $U = 10\,\mathrm{m\,s^{-1}}$, $L = 1000\,\mathrm{km}$ and $|f| = 10^{-4}\,\mathrm{s^{-1}}$,

$$\mathrm{Ro} = \frac{10}{10^{-4} \times 10^6} = 0.1.$$

The Coriolis force is ten times the inertial acceleration, the flow is close to balance, and curvature is a correction of order 10 %: with $\mathrm{Ro}_R = 0.1$, equation (4.14) gives $U_{gr}/U_g = 0.92$ around a low and 1.13 around a high.

A hill example. For the same $U = 10\,\mathrm{m\,s^{-1}}$ and $|f| = 10^{-4}\,\mathrm{s^{-1}}$ but $L = 1000\,\mathrm{m}$, the size of a hill,

$$\mathrm{Ro} = \frac{10}{10^{-4} \times 10^3} = 100.$$

The air crosses the hill in $L/U = 100\,\mathrm{s}$, a hundredth of the time the Coriolis force needs to turn it. For the immediate flow over a 1 km hill the Coriolis force is negligible.

Figure 4.8 extends the two examples across all scales. Both axes are logarithmic: the horizontal axis is the length scale L from 10 m to 10 000 km, the vertical axis the Rossby number.

The solid blue line is Ro for $U = 10\,\mathrm{m\,s^{-1}}$ and $|f| = 10^{-4}\,\mathrm{s^{-1}}$; the dashed red line is the same speed at 23.5° latitude in either hemisphere, $|f| = 5.8 \times 10^{-5}\,\mathrm{s^{-1}}$, which raises Ro by a factor of 1.7. The dotted horizontal line is Ro = 1, and the labels at the top mark the approximate ranges of microscale, mesoscale and synoptic flow. The two dots are the examples. The line falls by a factor of ten per decade of L: Ro is below one only for features larger than about 100 km, near one in the mesoscale, and far above one at the scales of hills and buildings.

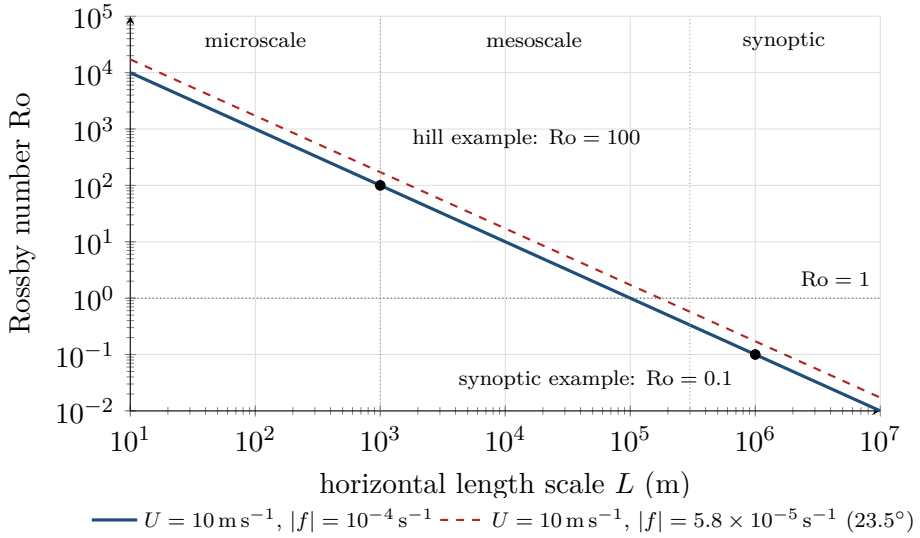


Figure 4.8: Rossby number $\mathrm{Ro} = U/(|f|L)$ against the horizontal length scale, for $U = 10\,\mathrm{m\,s^{-1}}$ with $|f| = 10^{-4}\,\mathrm{s^{-1}}$ (about 43° latitude) and $|f| = 5.8 \times 10^{-5}\,\mathrm{s^{-1}}$ (23.5° latitude), either hemisphere. Dots: the synoptic example ($L = 1000\,\mathrm{km}$, Ro = 0.1) and the hill example ($L = 1\,\mathrm{km}$, Ro = 100). Scale boundaries at 1 km and about 300 km are approximate.

4.6.4 Dominant balances by scale

The Rossby number sorts the forces that dominate at each scale. Table 4.2 lists, for the three traditional scale ranges, the typical length scale, the Rossby number for $U = 10\,\mathrm{m\,s^{-1}}$ and $|f| = 10^{-4}\,\mathrm{s^{-1}}$, the terms of the momentum balance that dominate, and the balanced-flow description that applies. At large scales the pressure-gradient force is balanced mainly by the Coriolis force, with curvature as a correction: the geostrophic and gradient winds. In the mesoscale the pressure-gradient force, inertia, buoyancy and the Coriolis force may all matter, and which dominates depends on the phenomenon. At the microscale the flow is governed by inertia, pressure perturbations, turbulence and the terrain, and the Coriolis force is weak. Chapter 5 develops the three ranges.

Cyclostrophic balance. At very large Rossby number the Coriolis term drops out of equation (4.6), and a steady curved flow balances the pressure-gradient force against the centripetal acceleration alone,

$$\frac{U^2}{R} = \frac{1}{\rho}\left|\frac{\partial p}{\partial n}\right|, \tag{4.24}$$

the *cyclostrophic balance*. It requires the pressure-gradient force to point toward the center of curvature, so it is possible only around low pressure, and since f no longer appears either sense of rotation is allowed. Dust devils and tornadoes are close to this balance. Most microscale flow over terrain is not a steady vortex at all, and no balanced-wind formula describes it; the speed-ups, separations and wakes it shows come from the pressure perturbations the terrain creates, which Chapter 20 treats.

Table 4.2: Dominant balances by scale. Rossby numbers for illustrative $U = 10\,\mathrm{m\,s^{-1}}$, $|f| = 10^{-4}\,\mathrm{s^{-1}}$; scale boundaries are approximate.

Scale	Length L	Ro	Dominant terms	Balanced-flow description
Synoptic	300 km to several 1000 km	about 0.02 to 0.3	pressure gradient and Coriolis; curvature as a correction	geostrophic wind; gradient wind
Mesoscale	1 to 300 km	0.3 to 100	pressure gradient, inertia, buoyancy and Coriolis, by phenomenon	none general; depends on the circulation
Microscale	below 1 km	above 100	inertia, pressure perturbations, turbulence, terrain; Coriolis weak	cyclostrophic in intense small vortices; otherwise none

4.6.5 Nesting of scales

The wind at a site is the product of several scales acting at once, each with its own dominant physics. Figure 4.9 draws the chain as a sequence of stages from top to bottom: the synoptic gradient wind, its mesoscale modification, the adjustment through the boundary layer, acceleration by the terrain, and local turbulence. Each box names a stage; the text beside it gives its typical scale and the physics that dominates there. The Coriolis force appears in the top two stages only; the boundary layer adds turbulent momentum transfer, which Chapters 8 and 9 develop; the terrain and turbulence stages are governed by inertia and pressure perturbations, at Rossby numbers of order one hundred and above.

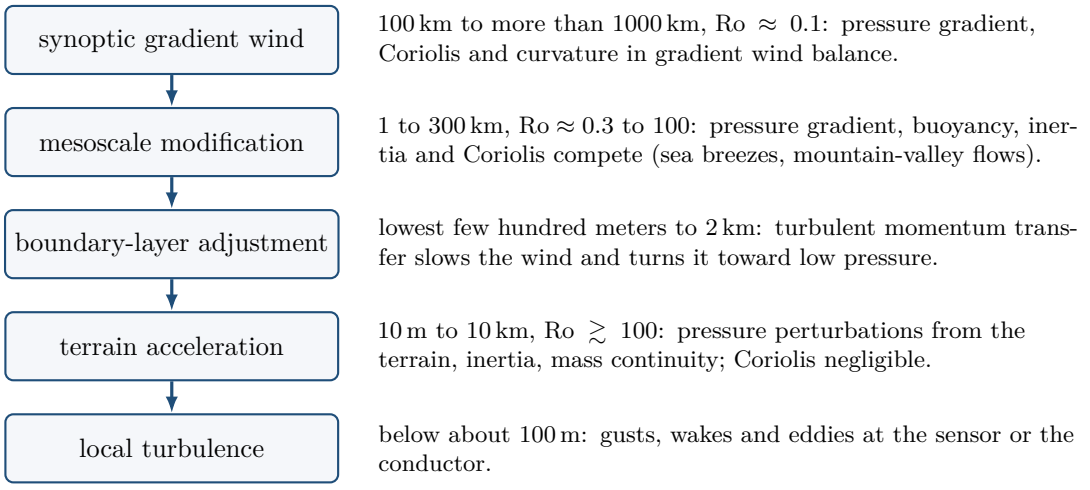


Figure 4.9: Nesting of scales from the large-scale forcing to the local wind, schematic. Each stage modifies the wind it receives, with different dominant physics; scale ranges and Rossby numbers (for $U = 10\,\mathrm{m\,s^{-1}}$, $|f| = 10^{-4}\,\mathrm{s^{-1}}$) are approximate.

The nesting explains why a single balanced-wind formula cannot give the wind at a site. The gradient wind is the right description of the top stage, and it sets the momentum available to the lower ones; each lower stage transforms it according to its own physics, with parameters of its own.

4.6.6 A ridge crossing

Consider an illustrative modeling case. A weather model predicts a wind of $12\,\mathrm{m\,s^{-1}}$ from the southwest at 100 m above the ground over a region; the value is a grid-cell value, an average over a cell several kilometers wide. Where a transmission line crosses a ridge within that cell, the terrain compresses the streamlines over the crest, and the local wind at the conductor height may be $16\,\mathrm{m\,s^{-1}}$, a speed-up factor of $16/12 = 1.33$.

The speed-up is not a Coriolis phenomenon, and the Rossby number shows why. The air crosses a 1 km ridge at $12\,\mathrm{m\,s^{-1}}$ in about $1000/12 \approx 83\,\mathrm{s}$; the Coriolis acceleration, $|f|U \approx 10^{-4} \times 12 = 1.2 \times 10^{-3}\,\mathrm{m\,s^{-2}}$, can change the velocity in that time by at most about $1.2 \times 10^{-3} \times 83 \approx 0.1\,\mathrm{m\,s^{-1}}$, forty times less than the $4\,\mathrm{m\,s^{-1}}$ observed. The speed-up comes instead from the pressure perturbations the ridge creates, the curvature of the streamlines over it, mass continuity (the same flow passing through a reduced effective cross-section must move faster) and turbulence. A rough size of the pressure perturbation involved follows from Bernoulli's relation along a streamline, a simplification that neglects friction and assumes steady flow:

$$\Delta p \approx -\tfrac{1}{2}\rho\,(U_2^2 - U_1^2) = -0.6 \times (16^2 - 12^2)\,\mathrm{Pa} \approx -67\,\mathrm{Pa}$$

with $\rho = 1.2\,\mathrm{kg/m^3}$, a pressure drop of about 0.7 hPa over the crest across a distance of order 1 km. A synoptic gradient of 2 hPa per 100 km changes the pressure by only 0.02 hPa over the same kilometer: locally, the terrain's own pressure field is some thirty times stronger than the large-scale one. Chapter 20 treats terrain flow properly.

The engineering consequence is large. The convective cooling of an overhead conductor increases with the wind speed across it, so the line's thermal rating at the crest is set by the $16\,\mathrm{m\,s^{-1}}$ local wind (and its direction relative to the conductor, which the terrain may also change), not by the model's $12\,\mathrm{m\,s^{-1}}$; the power available to a wind turbine on the crest, proportional to U^3, is $(16/12)^3 = 2.4$ times that of the grid-cell wind. The distinction to keep is between the large-scale gradient wind, which the model represents, and the local terrain-induced flow, which it does not resolve.

4.7 What to retain

Definition 4.1 (Gradient wind and curved flow)**.** When the flow curves, the pressure-gradient force, the Coriolis force and the centripetal acceleration U^2/R together set the balanced wind: subgeostrophic around lows, supergeostrophic and bounded by $|f|R/2$ around highs, in both hemispheres. This matters at large scales around highs and lows; at terrain scales $\mathrm{Ro} \gg 1$ and the Coriolis force is relatively unimportant.

Table 4.3 lists the chapter's terms with their meaning, units and the subsection that defines each.

4.8 Exercises

Exercise 4.1. A low in the Northern Hemisphere at 50° N has a pressure gradient of 2 hPa per 100 km at 400 km from its center, with $\rho = 1.1\,\mathrm{kg/m^3}$. (a) Compute f and the geostrophic speed U_g. (b) Compute the curvature Rossby number and the gradient wind speed. (c) Compute the pressure-gradient, Coriolis and centripetal accelerations and check that they balance. (d) By what percentage does the geostrophic speed overestimate the balanced wind, and does the flow turn clockwise or counterclockwise?

Exercise 4.2. A high is centered over the South Atlantic at 25° S. (a) State its sense of rotation and the direction from which the balanced wind blows at a site 600 km north of its center. (b)

Table 4.3: Terms of the chapter and where each is defined.

Term	Meaning	Units	Defined in
Centripetal acceleration	U^2/R toward the center of curvature; present on any curved path	$\mathrm{m\,s^{-2}}$	4.1.2
Natural coordinates	axes along ($\mathbf{t}$, s) and across ($\mathbf{n}$, n) the flow; $R > 0$ for a left turn	m	4.2.1
Gradient wind	steady frictionless wind along curved isobars, $U^2/R + fU - fU_g = 0$	$\mathrm{m\,s^{-1}}$	4.2.2
Cyclonic	turning with the Earth; around a low; $fR > 0$, $f\zeta > 0$	–	4.2.4
Anticyclonic	turning against the Earth; around a high; $fR < 0$, $f\zeta < 0$	–	4.2.4
Centrifugal force	apparent outward U^2/R in a frame turning with the parcel	$\mathrm{m\,s^{-2}}$	4.2.5
Subgeostrophic	$U < U_g$; balanced wind around a low	–	4.3.1
Supergeostrophic	$U > U_g$; balanced wind around a high	–	4.3.2
Curvature Rossby number	$\mathrm{Ro}_R = U_g/(\lvert f\rvert R)$; sets U_{gr}/U_g	–	4.3.3
Anticyclonic limit	$U_g \le \lvert f\rvert R/4$, $\lvert\nabla_h p\rvert \le \rho f^2 R/4$, $U_{gr} \le \lvert f\rvert R/2$	–	4.4.1
Relative vorticity	$\zeta = \partial v/\partial x - \partial u/\partial y$; local rotation, twice the angular velocity	$\mathrm{s^{-1}}$	4.5.1
Curvature and shear vorticity	U/R and $-\partial U/\partial n$, the two parts of ζ	$\mathrm{s^{-1}}$	4.5.3
Planetary vorticity	$f = 2\Omega \sin\phi$, the vorticity of the rotating Earth about the local vertical	$\mathrm{s^{-1}}$	4.5.4
Absolute vorticity	$\eta = f + \zeta$	$\mathrm{s^{-1}}$	4.5.4
Rossby number	$\mathrm{Ro} = U/(\lvert f\rvert L)$; inertia relative to Coriolis	–	4.6.3
Cyclostrophic balance	$U^2/R = (1/\rho)\lvert\partial p/\partial n\rvert$, at $\mathrm{Ro} \gg 1$	–	4.6.4

With $U_g = 6\,\mathrm{m\,s^{-1}}$ at that site, compute the gradient wind speed. (c) Compute the largest geostrophic speed, the largest pressure gradient (with $\rho = 1.2\,\mathrm{kg/m^3}$) and the largest gradient wind speed that a balanced anticyclonic flow can have at 600 km from the center. (d) An analysis shows a gradient of 1.2 hPa per 100 km at 300 km from the center. Show that no steady gradient wind exists there, and list what this can mean for the analysis or the flow.

Exercise 4.3. (a) A vortex rotates counterclockwise as a solid body with a speed of $8\,\mathrm{m\,s^{-1}}$ at 400 km from its center. Compute its relative vorticity, and state whether it is cyclonic if it lies at 35° N and if it lies at 35° S. (b) A westerly jet at 30° S has $30\,\mathrm{m\,s^{-1}}$ on its axis, falling to $10\,\mathrm{m\,s^{-1}}$ at 500 km north and at 500 km south of the axis. Compute the shear vorticity on each flank and identify the cyclonic flank. (c) Compute the absolute vorticity on each flank. (d) Verify the result of (a) from the curvature and shear parts of equation (4.21).

Exercise 4.4. A transmission line runs near 23.5° S. (a) Compute the Rossby number of a $15\,\mathrm{m\,s^{-1}}$ flow for $L = 2000$ km, 50 km and 2 km, and say which balance applies to each. (b) A weather model gives $12\,\mathrm{m\,s^{-1}}$ from the southwest at 100 m over the region, and a mast on a ridge crest crossed by the line records $16\,\mathrm{m\,s^{-1}}$. Compute the speed-up factor and the largest change of velocity the Coriolis force could produce while the air crosses the 1 km ridge. (c) Estimate the pressure perturbation over the crest from Bernoulli's relation with $\rho = 1.2\,\mathrm{kg/m^3}$, and compare it with the change of a synoptic gradient of 1.5 hPa per 100 km across 1 km. (d) Should the model's $12\,\mathrm{m\,s^{-1}}$ be corrected for curvature with equation (4.14) before it is used for the line's rating at the crest? Explain.

Chapter 5

Synoptic, Mesoscale and Microscale Flow

5.1 Scale and the three ranges

The atmosphere does not behave the same way at every size. A cyclone 2000 km across, a sea breeze 50 km wide, the flow over a ridge 2 km wide and the wake of a building 50 m long are all wind, and all obey the same equations of motion, but the terms of those equations that matter differ from one to the next. The pressure-gradient and Coriolis forces that balance in the cyclone (Chapter 3) are joined by buoyancy in the sea breeze, and the Coriolis force all but disappears over the ridge and behind the building, where inertia, pressure perturbations set up by the obstacle and turbulence take over. The question of this chapter is

which physical processes dominate the wind at which spatial and temporal scales, and which of them does a given model or instrument represent?

The chapter first defines the scales of a flow feature and the three traditional ranges, synoptic, mesoscale and microscale. It then describes what dominates in each range, with the sea breeze, slope winds and flow over a hill as worked cases; what a numerical model resolves at a given grid spacing; the kinds of model that operate on each range; and the dimensionless numbers that summarize all of this. It ends with the habit the chapter is meant to leave: every wind value belongs to a scale, a place, a height and an averaging time.

Jargon: scale of a phenomenon, advective time, synoptic scale, mesoscale, microscale, dominant balance, Rossby number

The *scales* of a flow feature are the orders of magnitude of its horizontal size L, its vertical size H (both in meters), its typical wind speed U (m/s) and its time scale $\mathcal{T}$ (s), the time over which it forms, changes or decays. The *advective time* $t_{\mathrm{adv}} = L/U$ is the time the wind takes to carry air across the feature. The *synoptic scale* is the range of weather systems of roughly 1000 to more than 5000 km that evolve over days, the systems drawn on a weather map (from the Greek for a view taken all together). The *mesoscale* is the intermediate range, roughly 1 to 1000 km and minutes to hours. The *microscale* is the range below about 1 km, with time scales of seconds to minutes. The *dominant balance* of a flow is the small set of terms of the equations of motion that are much larger than the rest and nearly cancel one another. The *Rossby number* $\mathrm{Ro} = U/(|f|L)$, dimensionless, is the ratio of the inertial acceleration of the flow to the Coriolis acceleration; it is computed from the scales, not measured.

Key idea

The scales of a flow decide which forces dominate it, and the forces decide how the wind responds: geostrophic balance at the synoptic scale, a competition of pressure, buoyancy, inertia and Coriolis at the mesoscale, and pressure perturbations, inertia and turbulence at the microscale. A wind value is therefore incomplete until its scale is stated, and a model represents only the scales its grid can resolve.

5.1.1 The scales of a phenomenon

Any flow feature, a cyclone, a sea breeze, the flow over a hill, can be described to an order of magnitude by four numbers. The horizontal length scale L is its width or the distance over which its wind changes appreciably. The vertical scale H is its depth. The velocity scale U is a typical wind speed within it, or a typical change of wind speed across it. The time scale $\mathcal{T}$ is how long it takes to form or to change appreciably. For an illustrative sea breeze these are $L \approx 50\,\mathrm{km}$, $H \approx 1\,\mathrm{km}$, $U \approx 5\,\mathrm{m\,s^{-1}}$ and $\mathcal{T} \approx 12\,\mathrm{h}$; for the flow over an illustrative hill they are $L \approx 1\,\mathrm{km}$, $H \approx 100\,\mathrm{m}$, $U \approx 10\,\mathrm{m\,s^{-1}}$ and $\mathcal{T}$ of minutes.

These scales are not precise measurements; they are the sizes that enter an estimate of each term of the equations of motion. A term built from them, such as an acceleration $U/\mathcal{T}$ or a pressure-gradient force per unit mass $\Delta p/(\rho L)$, is then compared with the others, and the terms that are an order of magnitude or more smaller are dropped. This procedure, *scale analysis*, is how the dominant balance of each range in this chapter is obtained.

Aspect ratio. The ratio H/L says whether the vertical momentum balance is hydrostatic. For a synoptic system, $H \approx 10\,\mathrm{km}$ and $L \approx 1000\,\mathrm{km}$ give $H/L \approx 0.01$: vertical accelerations are tiny compared with gravity, and the hydrostatic relation of Chapter 2 holds to high accuracy. For flow over a hill or around a building H and L are comparable, vertical accelerations are not small, and the flow is *nonhydrostatic*. The distinction reappears in the models of Section 5.5: a model of microscale flow must solve the vertical momentum equation in full.

5.1.2 The advective time

If the time scale of a feature is set by the wind carrying air through it, then

$$\mathcal{T} \sim t_{\mathrm{adv}} = \frac{L}{U}. \tag{5.1}$$

For $L = 100\,\mathrm{km} = 10^5\,\mathrm{m}$ and $U = 10\,\mathrm{m\,s^{-1}}$,

$$t_{\mathrm{adv}} = \frac{10^5\,\mathrm{m}}{10\,\mathrm{m\,s^{-1}}} = 10^4\,\mathrm{s} = \frac{10^4}{3600}\,\mathrm{h} \approx 2.8\,\mathrm{h}.$$

At the same wind speed, a synoptic length of 1000 km gives $10^5\,\mathrm{s}$, about 28 h or a little over a day, and a microscale length of 100 m gives 10 s. The advective time alone thus reproduces the time scales associated with the three ranges: days, hours, seconds.

The advective time also fixes the acceleration scale. A parcel crossing a feature in time L/U changes its velocity by an amount of order U, so its acceleration is of order

$$\left|\frac{\mathrm{D}\mathbf{V}}{\mathrm{D}t}\right| \sim \frac{U}{t_{\mathrm{adv}}} = \frac{U^2}{L}, \tag{5.2}$$

which is the inertial term against which the Coriolis force is compared in Section 5.2.1. Not every feature evolves at its advective time. Circulations driven by the daily cycle of heating, such as the sea breeze, have a time scale set by the sun, about half a day, whatever the wind speed; they last longer than the time the wind takes to cross them.

5.1.3 The synoptic, meso and micro ranges

Meteorology traditionally divides atmospheric motion into three ranges by horizontal scale. The *synoptic scale* covers roughly 1000 to more than 5000 km and time scales of days; the *mesoscale* roughly 1 to 1000 km and minutes to hours; the *microscale* less than about 1 km and seconds to minutes. Table 5.1 sets the three side by side. Its columns give the range, its horizontal and time scales, examples of its phenomena, the terms that dominate its momentum balance, and an order of magnitude of the Rossby number at $U = 10\,\mathrm{m\,s^{-1}}$ and $|f| = 10^{-4}\,\mathrm{s^{-1}}$, the value of the Coriolis parameter in middle latitudes of either hemisphere.

Table 5.1: The three traditional scale ranges of atmospheric motion. The boundaries are approximate. The Rossby numbers are orders of magnitude for $U = 10\,\mathrm{m\,s^{-1}}$ and $|f| = 10^{-4}\,\mathrm{s^{-1}}$.

Range	Horizontal scale	Time scale	Examples	Dominant terms	Ro
Synoptic	1000 to 5000 km and more	days	extratropical cyclones, anticyclones, fronts, jet-stream patterns, large troughs and ridges	pressure gradient and Coriolis; curvature and acceleration as corrections	0.1 to 1
Mesoscale	1 to 1000 km	minutes to hours	sea breezes, mountain-valley circulations, thunderstorms, squall lines, low-level jets	pressure, buoyancy, inertia and Coriolis, in proportions set by the phenomenon	about 1
Microscale	below 1 km	seconds to minutes	hill speed-up, building wakes, canopy turbulence, gusts, flow separation	pressure perturbations, inertia, turbulence; viscosity near surfaces	$\gg 1$

The boundaries are not exact, and different texts place them differently. Finer subdivisions exist: the mesoscale is often split into three sub-ranges, of a few kilometers, a few tens and a few hundreds of kilometers, and the microscale into the scales of terrain and obstacle flow and the much smaller scales of turbulence. What matters is not the name of a range but the dominant balance that goes with it, and that balance changes gradually across the boundaries rather than at them.

5.1.4 A space-time diagram

Figure 5.1 places named phenomena on a single diagram. The horizontal axis is the horizontal length scale L and the vertical axis the time scale $\mathcal{T}$, both logarithmic, each tick a factor of ten in L and labeled in familiar units of time on the vertical axis. The shaded vertical bands mark the three ranges of Table 5.1. Each numbered circle is one phenomenon at an illustrative typical size and lifetime, named in the key at the upper left. The dashed line is the advective time $\mathcal{T} = L/U$ of equation (5.1) for $U = 10\,\mathrm{m\,s^{-1}}$.

Two features of the diagram carry the argument of the chapter. First, the phenomena lie along a diagonal: large features live long and small features briefly, and the diagonal runs close to the advective line, because for most of them the time scale is the time the wind takes to cross them. Second, the departures from the line are informative. The sea breeze (7) and the mountain-valley circulation (6) lie well above it, because their time scale is the daily cycle of heating, not the crossing time; the low-level jet (9), a nocturnal feature hundreds of kilometers long, lies below it, because it forms and decays within a night while the wind would take longer than that to cross it. A phenomenon's position on the diagram already says what drives it: advection, the sun or the night.

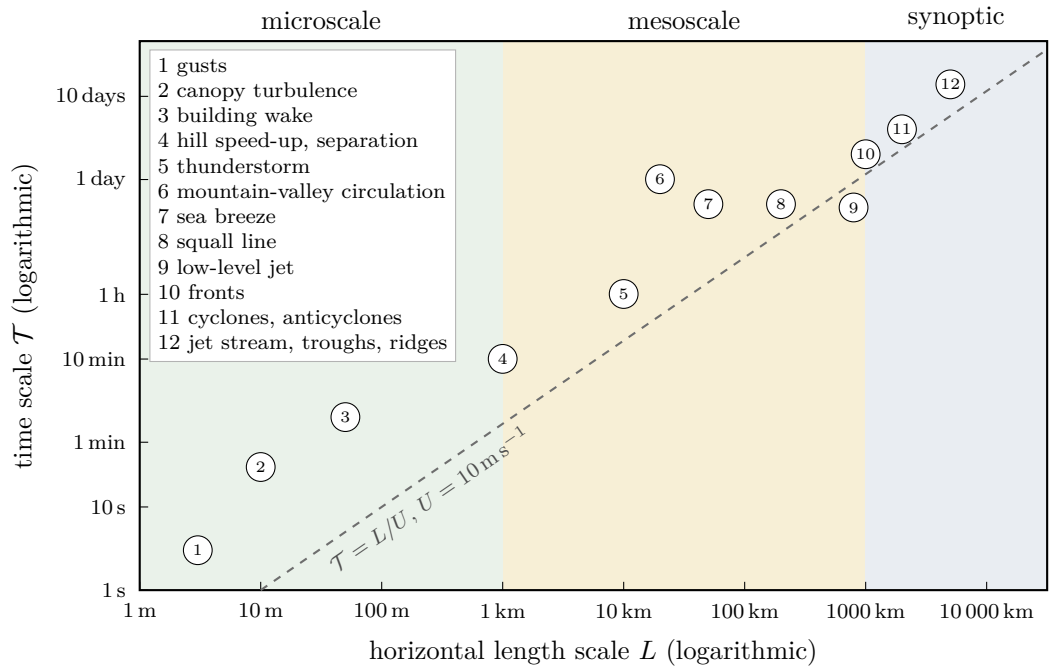


Figure 5.1: Space-time diagram of atmospheric phenomena. Both axes are logarithmic. The shaded bands are the microscale (below 1 km), the mesoscale (1 to 1000 km) and the synoptic scale (above 1000 km). Positions are illustrative typical sizes and lifetimes. The dashed line is the advective time $\mathcal{T} = L/U$ for $U = 10\,\mathrm{m\,s^{-1}}$.

5.2 The synoptic scale and the mesoscale

This section gives the dominant balance of the synoptic scale and what it does and does not fix in the local wind, then catalogues the mesoscale and works two of its circulations, the sea breeze and the slope and mountain-valley winds, through their mechanism and their magnitudes.

5.2.1 Dominant balance at the synoptic scale

The synoptic scale contains extratropical cyclones (the low-pressure systems of middle latitudes), anticyclones, fronts, the large troughs and ridges of the upper-level flow, and the patterns of the jet stream, the narrow band of strongest wind near the top of the troposphere. Their horizontal scale is $L \sim 10^6\,\mathrm{m}$.

Above the layer directly affected by the surface, the horizontal momentum equation reads

$$\frac{\mathrm{D}\mathbf{V}}{\mathrm{D}t} + f\,\mathbf{k}\times\mathbf{V} = -\frac{1}{\rho}\nabla_h p, \tag{5.3}$$

with the acceleration of a parcel on the left, the Coriolis term next to it and the pressure-gradient force per unit mass on the right. Scale each term. The acceleration is of order U^2/L by equation (5.2); the Coriolis term is of order $|f|\,U$. Their ratio is

$$\frac{U^2/L}{|f|\,U} = \frac{U}{|f|\,L} = \mathrm{Ro}. \tag{5.4}$$

With $U = 10\,\mathrm{m\,s^{-1}}$, $L = 10^6\,\mathrm{m}$ and $|f| = 10^{-4}\,\mathrm{s^{-1}}$, the acceleration is $10^{-4}\,\mathrm{m\,s^{-2}}$, the Coriolis term $10^{-3}\,\mathrm{m\,s^{-2}}$, and $\mathrm{Ro} = 0.1$. A pressure difference of 10 hPa = 1000 Pa across 1000 km at $\rho = 1.2\,\mathrm{kg\,m^{-3}}$ gives a pressure-gradient force of $1000/(1.2\times10^6) \approx 8.3\times10^{-4}\,\mathrm{m\,s^{-2}}$, the same

order as the Coriolis term. The acceleration, ten times smaller, is dropped at first order, and what remains is the geostrophic balance of Chapter 3,

$$f\,\mathbf{k}\times\mathbf{V}_g = -\frac{1}{\rho}\nabla_h p \qquad \Longleftrightarrow \qquad \mathbf{V}_g = \frac{1}{\rho f}\,\mathbf{k}\times\nabla_h p. \tag{5.5}$$

The second form follows from the first by taking $\mathbf{k}\times$ of both sides and using $\mathbf{k}\times(\mathbf{k}\times\mathbf{V}_g) = -\mathbf{V}_g$. With $f > 0$ the geostrophic wind keeps low pressure on its left in the Northern Hemisphere; with $f < 0$ it keeps low pressure on its right in the Southern Hemisphere. Its speed in the example is $U_g = 1000/(1.2\times10^{-4}\times10^{6}) \approx 8.3\,\mathrm{m\,s^{-1}}$.

For stronger winds or tighter systems, Ro rises toward 0.3 to 1 (for example $U = 20\,\mathrm{m\,s^{-1}}$, $L = 10^{6}\,\mathrm{m}$ and $|f| = 1.03\times10^{-4}\,\mathrm{s^{-1}}$ at 45° latitude give $\mathrm{Ro}\approx 0.19$), and the neglected terms come back as corrections: the centripetal acceleration of curved flow, which gives the gradient wind of Chapter 4, and the along-path acceleration of flow entering and leaving jet streaks. These, and the geostrophic relation applied to the height of pressure surfaces aloft (the upper-level height field), are the tools of the synoptic scale. Fronts, the boundaries between air masses, are synoptic in length but only tens to a hundred kilometers wide across, so across a front the Rossby number approaches one and the balance there is already mesoscale.

Principle 5.1. *The scale of a flow fixes its dominant balance. Where* $\mathrm{Ro}\ll 1$ *the pressure-gradient and Coriolis forces nearly balance; where* $\mathrm{Ro}\sim 1$ *inertia, pressure, Coriolis and often buoyancy compete; where* $\mathrm{Ro}\gg 1$ *the Coriolis force is negligible.*

5.2.2 What synoptic forcing gives the local wind

A strong low may produce a wind at the 850 hPa level, about 1.5 km above sea level, of $U_{850}\approx 20\,\mathrm{m\,s^{-1}}$ over hundreds of kilometers. That number does not fix the wind at 10 m above the ground at any particular site. Between the 850 hPa level and the ground, friction with the surface slows and turns the wind, the stability of the air decides how strongly the faster flow aloft is mixed down, and terrain and obstacles rearrange it locally; the near-surface wind under that $20\,\mathrm{m\,s^{-1}}$ flow may be anything from nearly calm in a sheltered valley at night to gusts above $20\,\mathrm{m\,s^{-1}}$ on an exposed ridge.

What the synoptic flow does set is the *large-scale momentum environment*: the direction and strength of the background wind, the pressure gradient that drives it, and the store of momentum aloft that the boundary layer can tap. It is the forcing; the smaller scales are the response, and they modify it rather than replace it. A forecast that gets the synoptic flow wrong cannot get the local wind right, but a correct synoptic flow is only the first of several steps between the weather map and the reading of an anemometer.

5.2.3 The mesoscale catalogue

The mesoscale holds the circulations between the weather map and the site, from about 1 km to 500 km for the phenomena that matter most to near-surface wind.

- *Sea and lake breezes*: daytime onshore flow driven by the contrast in heating between land and water, tens of kilometers inland (Section 5.2.4).
- *Mountain-valley circulations*: upslope and up-valley flow by day, downslope and down-valley flow at night (Section 5.2.5).
- *Thunderstorms*: convective cells about 10 km across whose cold outflow spreads along the ground as a gust front, an abrupt rise in wind and change in direction.

- *Squall lines*: lines of thunderstorms one to several hundred kilometers long that move as one system with a strong gust front ahead of them.
- *Low-level jets*: bands of maximum wind within the lowest kilometer, often forming at night; Chapter 18 treats them.
- *Urban heat-island circulations*: inflow toward a city that stays warmer than its surroundings, most often at night.
- *Downslope windstorms*: strong, gusty winds that descend the lee slope of a mountain range when stable air flows across it.

In this range several forces compete: the pressure gradient, buoyancy (the vertical force on air that is warmer or colder than its surroundings), the inertia of the flow, and the Coriolis force. With Ro ~ 1 none of them can be dropped in general, and which one leads depends on the phenomenon: buoyancy in a sea breeze or a thunderstorm, inertia and pressure in a downslope windstorm, Coriolis together with the decoupling of the surface in a nocturnal low-level jet.

5.2.4 The sea breeze

By day, land heats faster than water. The sun's energy is absorbed in a thin layer of soil whose heat capacity is small, while in water it penetrates meters deep and is mixed through a large volume; the land surface and the air above it warm by several kelvin while the sea surface hardly changes. The chain from there to the wind is

$$\text{heating} \;\rightarrow\; \text{density difference} \;\rightarrow\; \text{pressure difference} \;\rightarrow\; \text{circulation.}$$

Figure 5.2 draws the circulation in a vertical cross section through a coast, sea on the left and land on the right. The blue arrows are the circulation: an onshore branch near the surface, a rising branch over the heated land, a return branch aloft toward the sea, and a sinking branch over the water. The two dashed lines are surfaces of constant pressure, p_1 near the ground and $p_2 < p_1$ aloft; the letters H and L mark relatively high and low pressure at the same height.

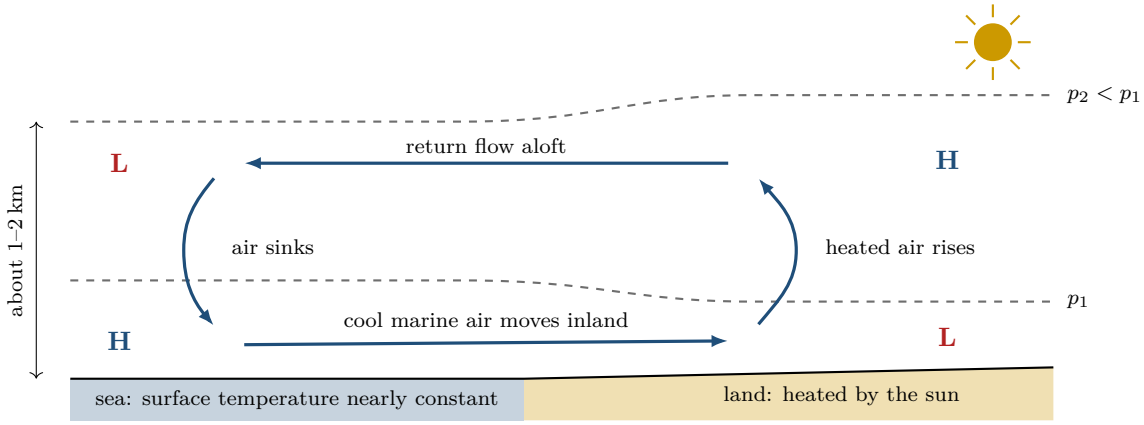


Figure 5.2: Vertical cross section of a sea breeze (schematic, not to scale; the circulation is typically one to two kilometers deep and tens of kilometers wide). Blue arrows: the circulation. Dashed lines: surfaces of constant pressure, bent down over the land near the ground and up over the land aloft. H and L: high and low pressure relative to the other side at the same height.

The pressure pattern in the figure follows from the hydrostatic relation of Chapter 2. Start from equal surface pressure over land and sea. The thickness of the layer between two pressure levels p_1 and p_2 is, by the hypsometric equation,

$$\Delta z = \frac{R_d \overline{T_v}}{g} \ln \frac{p_1}{p_2}, \tag{5.6}$$

proportional to the layer's mean virtual temperature. Take the layer from 1000 to 900 hPa, an illustrative mean temperature of 300 K over the sea and a contrast of 3 K over the land:

$$\Delta z_{\text{sea}} = \frac{287 \times 300}{9.81} \ln\frac{1000}{900} = 8777\,\text{m} \times 0.1054 \approx 925\,\text{m}, \qquad \Delta z_{\text{land}} = 925\,\text{m} \times \frac{303}{300} \approx 934\,\text{m}.$$

The heated column is about 9 m thicker. At the height where the pressure over the sea is 900 hPa, the land column still has 9 m of air above that level that the sea column does not, so its pressure there is higher by the weight of that slab,

$$\Delta p = \rho\, g\, \Delta z \approx 1.05\,\text{kg m}^{-3} \times 9.81\,\text{m s}^{-2} \times 9.2\,\text{m} \approx 95\,\text{Pa} \approx 1\,\text{hPa},$$

with $\rho = p/(R_d T) = 90\,000/(287 \times 300) \approx 1.05\,\text{kg m}^{-3}$ at that level. Aloft, then, pressure is higher over the land, and air there moves toward the sea: the return flow. Air leaving the land column aloft reduces the mass above the land surface, so the surface pressure over land falls, and the mass arriving over the sea raises the surface pressure there. The surface pressure difference that results is of the same order, a fraction of a hectopascal to about one, low over the land and high over the sea, and near the ground cool marine air moves inland.

A pressure difference of about 1 hPa looks small beside the 10 hPa differences of a weather map, but it acts over a short distance. Across an illustrative 20 km at $\rho = 1.15\,\text{kg m}^{-3}$ the pressure-gradient force per unit mass is $95/(1.15 \times 20\,000) \approx 4.1 \times 10^{-3}\,\text{m s}^{-2}$, five times the synoptic value of Section 5.2.1. Unopposed for an hour it would produce $4.1 \times 10^{-3} \times 3600 \approx 15\,\text{m s}^{-1}$; friction with the surface and the circulation's own adjustment of the pressure field hold the onshore wind to a few meters per second. The leading edge of the inflowing marine air, the sea-breeze front, can move tens of kilometers inland during the afternoon.

The sea breeze and the synoptic wind. The observed surface wind is the synoptic wind together with the sea-breeze circulation, and the two may reinforce or oppose each other. With a weak synoptic wind the sea breeze dominates the afternoon wind at the coast. With an offshore synoptic wind the two oppose: an illustrative offshore $3\,\text{m s}^{-1}$ against an onshore circulation of $5\,\text{m s}^{-1}$ leaves about $2\,\text{m s}^{-1}$ onshore by vector addition, and a stronger offshore wind holds the sea-breeze front at the coast or prevents it altogether. The addition is only approximate, because the synoptic wind also changes how the circulation develops, but it shows that the wind a coastal site experiences at 15:00 may owe more to the local land-sea contrast than to the weather map.

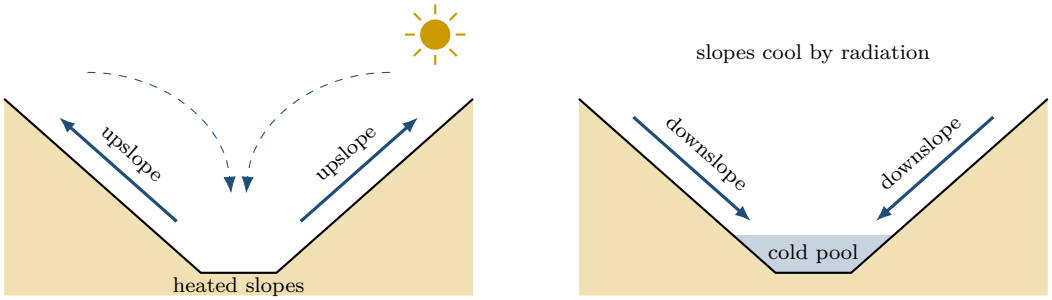
Turning with the Coriolis force. With $\text{Ro} \sim 1$ the Coriolis force acts on the sea breeze over the hours it lasts. It deflects moving air to the right of its motion in the Northern Hemisphere ($f > 0$) and to the left in the Southern ($f < 0$), so as the afternoon proceeds the sea-breeze wind turns clockwise (veers) in the Northern Hemisphere and counterclockwise (backs) in the Southern. On a coast with the sea to the east, the onshore wind starts from the east; it then turns toward the east-southeast in the Northern Hemisphere and toward the east-northeast in the Southern. The turning is a fraction of a full rotation, since a full turn would take an inertial period $2\pi/|f|$, about 17 h at 45° and 31 h at 23° latitude in either hemisphere.

5.2.5 Slope and mountain-valley winds

Terrain sets up its own thermally driven circulations. By day the sun heats sloping ground, and the air in contact with the slope becomes warmer than the air at the same height away from it, over the center of the valley. At the same height and pressure, warmer air is less dense: for an ideal gas $\Delta\rho/\rho = -\Delta T/T$. The warm air is therefore buoyant, and the component of its buoyancy along the slope drives it uphill: an *upslope* (anabatic) wind. At night the ground

cools by emitting infrared radiation, the air next to the slope becomes colder and denser than the air at the same height over the valley, and it drains downhill: a *downslope* (katabatic) wind.

Figure 5.3 shows the two regimes in a vertical cross section across a valley. In panel (a), by day, the solid arrows are the upslope flow along each side, and the dashed arrows the weaker return flow that closes the circulation by sinking over the valley center. In panel (b), at night, the solid arrows are the downslope drainage and the shaded layer is the cold air that collects on the valley floor.



(a) day: upslope (anabatic) flow (b) night: downslope (katabatic) flow

Figure 5.3: Slope winds in a cross section across a valley (schematic). (a) By day, air heated along the slopes rises up them and sinks over the valley center. (b) At night, air cooled along the slopes drains down them and pools on the valley floor. The along-valley component, perpendicular to the page, is up-valley by day and down-valley at night.

The along-slope driving force is easy to estimate. Air warmer by ΔT than its surroundings at the same height has an upward buoyancy acceleration $g\,\Delta T/T$; on a slope at angle α to the horizontal, its component along the slope is

$$a_{\parallel} = g\,\frac{\Delta T}{T}\,\sin\alpha. \tag{5.7}$$

For an illustrative night with $\Delta T = -3\,\mathrm{K}$, $T = 285\,\mathrm{K}$ and $\alpha = 10°$, $|a_{\parallel}| = 9.81 \times (3/285) \times 0.174 \approx 0.018\,\mathrm{m\,s^{-2}}$, directed downslope, about twenty times the synoptic pressure-gradient force of Section 5.2.1. Friction with the slope and mixing with the air above keep the resulting speeds to a few meters per second, but the force is local, persistent through the night and independent of the weather map.

Along the valley axis, the same contrast between the air in the valley and the air at the same height over the plain drives a *mountain-valley circulation*: up-valley wind by day, down-valley wind at night, perpendicular to the cross section of Figure 5.3. Slope and valley winds together can change the near-surface wind substantially, reversing its direction twice a day. They dominate when the large-scale forcing is weak, under a slack pressure gradient, clear skies and light synoptic wind; a strong synoptic wind mixes the heated or cooled air away and overrides them. For a transmission line along a valley, the night-time drainage wind may be the only wind the conductor sees, and it is a wind no synoptic chart shows.

5.3 The microscale and terrain

Below about a kilometer the Coriolis force drops out and the wind is shaped by the ground itself. This section catalogues microscale flow, gives the two physical arguments for why terrain accelerates and decelerates the wind, continuity and pressure perturbations, and then places the microscale in the chain of scales that a single near-surface reading carries.

5.3.1 The microscale catalogue

The microscale contains the speed-up of wind over hills and ridges, the wakes of buildings and other obstacles, the turbulence within and above vegetation canopies, gusts, flow separation (the detachment of the flow from a surface, usually on the lee side of an obstacle), recirculation (a region of reversed flow behind the separation), and shear layers (thin regions across which the wind speed changes sharply). Its scales run from millimeters, the size of the smallest turbulent eddies, where viscosity turns their motion into heat, to about a kilometer.

At these scales $\mathrm{Ro} \gg 1$. For $U = 10\,\mathrm{m\,s^{-1}}$, $L = 1\,\mathrm{km}$ and $|f| = 10^{-4}\,\mathrm{s^{-1}}$, equation (5.4) gives $\mathrm{Ro} = 100$; for a building wake with $L = 50\,\mathrm{m}$, $\mathrm{Ro} = 2000$. The Coriolis force is two to three orders of magnitude smaller than the inertial term and is negligible: air crosses a hill in about 100 s, a small fraction of the time the Coriolis force needs to turn it appreciably, which is of order $1/|f| \approx 3\,\mathrm{h}$. What remains is

$$\text{pressure perturbations} + \text{inertia} + \text{turbulence} + \text{viscous effects near surfaces.}$$

Turbulence carries momentum between layers of the flow; molecular viscosity matters only in the thin layers, millimeters thick, that touch solid surfaces, including the surface of a conductor, whose convective heat loss is controlled by such a layer.

5.3.2 Continuity and terrain speed-up

When wind flows over a ridge, the streamlines (lines everywhere tangent to the velocity) crowd together over the crest. Figure 5.4 shows the pattern in a vertical cross section: the wind arrives from the left, the curves are streamlines, the shaded shape is the hill of height h, and the dashed line is the top of the layer within which the flow is displaced, at an illustrative depth D above the upwind ground. The two vertical dimension arrows mark the depth available to the flow upwind, D, and over the crest, $D - h$. The signs near the ground mark where the pressure is raised (+) or lowered (−) by the hill, and the lee side shows a possible separated region with recirculation.

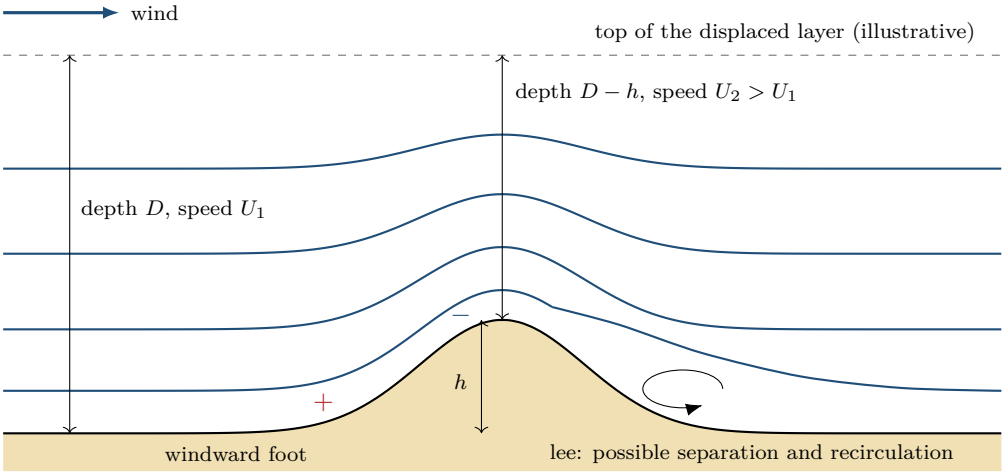


Figure 5.4: Flow over a two-dimensional hill (schematic). Streamlines (blue) are drawn as $z = z_u + h(x)\,(1 - z_u/D)$, with z_u the upwind height of each streamline, for the hill profile $h(x) = h\,e^{-(x/a)^2}$ and an illustrative layer depth D (here $D = 3.3\,h$), so that the displacement decreases to zero at the top of the layer; the lowest streamline is drawn separating on the lee side. The streamlines crowd over the crest, where the speed is highest and the pressure lowest (−); pressure is raised at the windward foot (+).

The crowding is a consequence of mass conservation. Over distances of a few kilometers or less and away from strong vertical motion, the density of air changes little, and conservation of

mass reduces to the condition that the velocity field has no divergence. Written for the full three-dimensional velocity (u, v, w),

$$\frac{\partial u}{\partial x} + \frac{\partial v}{\partial y} + \frac{\partial w}{\partial z} = 0. \tag{5.8}$$

The vertical term matters here: it is the upward motion on the windward slope and the downward motion on the lee that make room for the hill. For flow across a long ridge, integrate equation (5.8) over the depth of the displaced layer. Per unit length of ridge, the volume flow through a vertical section upwind, $U_1 D$, must equal the volume flow over the crest, $U_2(D - h)$, where U_1 and U_2 are the speeds averaged over each section. More generally, for a cross-sectional flow area A,

$$A_1 U_1 \approx A_2 U_2 \qquad \Longrightarrow \qquad \frac{U_2}{U_1} \approx \frac{A_1}{A_2}. \tag{5.9}$$

A smaller effective flow area gives a higher speed. For an illustrative displaced layer $D = 500\,\mathrm{m}$ deep over a ridge $h = 100\,\mathrm{m}$ high,

$$\frac{A_1}{A_2} = \frac{500\,\mathrm{m}}{500\,\mathrm{m} - 100\,\mathrm{m}} = 1.25, \qquad U_2 = 1.25 \times 10\,\mathrm{m\,s^{-1}} = 12.5\,\mathrm{m\,s^{-1}},$$

a 25 % speed-up over the crest for an upwind $10\,\mathrm{m\,s^{-1}}$.

The area argument is intuition for hilltop speed-up, not the full theory. It gives the average speed-up over the section and says nothing about how it is distributed with height, and it requires a depth D that the real atmosphere does not supply as a fixed lid. In practice the speed-up is concentrated near the ground, within a layer whose depth is of the order of the hill's half-width, so the fractional speed-up close to the crest can exceed the section average; the stability of the air and the roughness of the slope change it further. Chapter 20 gives the theory.

5.3.3 Pressure perturbations over a hill

Continuity says the flow must speed up over the crest; the momentum equation says what makes it do so. With the Coriolis force negligible and away from the thin layers where turbulence and viscosity act, steady flow along a streamline obeys Bernoulli's relation $p + \frac{1}{2}\rho U^2 = \text{constant}$: where the wind speeds up the pressure falls, and where it slows the pressure rises. In Figure 5.4 the flow decelerates as it approaches the windward foot of the hill, where the pressure is raised; it accelerates up the slope toward a minimum of pressure over the crest; and downwind it may accelerate again, decelerate, separate from the surface and recirculate, depending on the steepness of the lee slope and the stability of the air.

The size of these perturbations follows from the example of Section 5.3.2. A speed-up from 10 to $12.5\,\mathrm{m\,s^{-1}}$ at $\rho = 1.2\,\mathrm{kg\,m^{-3}}$ lowers the pressure by

$$\Delta p = -\tfrac{1}{2}\rho\,(U_2^2 - U_1^2) = -\tfrac{1}{2} \times 1.2 \times (156.25 - 100) \approx -34\,\mathrm{Pa},$$

and an illustrative slowing to $8\,\mathrm{m\,s^{-1}}$ at the windward foot raises it by $\frac{1}{2} \times 1.2 \times (100 - 64) \approx 22\,\mathrm{Pa}$. These differences occur within a few hundred meters. A synoptic pressure gradient of 1 hPa per 100 km, by contrast, changes the pressure by 1 Pa across a kilometer. Locally, the hill's own pressure perturbation is tens of times stronger than the synoptic gradient that drives the wind in the first place.

The consequence is that local terrain flow is governed by the pressure perturbations the terrain itself creates, not by the synoptic pressure gradient. The large-scale gradient sets the oncoming wind; the hill redistributes it. The same is true of buildings, tree lines and every other obstacle large enough to slow the flow: each creates its own pattern of raised pressure on its windward face and lowered pressure around and behind it.

5.3.4 Scale interaction

The scales act on a near-surface wind together. Consider a chain of influences on a single reading. A synoptic cyclone sets a regional southwesterly wind, blowing with the low to the northwest of the region in the Northern Hemisphere and to the southeast in the Southern. A mesoscale mountain circulation modifies that flow near a range, channeling it along valleys or adding a daytime upslope component. A ridge accelerates it locally. Vegetation adds roughness and turbulence near the ground. Finally the exposure of the sensor, its height and the obstacles around it, determines what the instrument records. A single observation at 10 m thus carries the influence of features of about 1000 km, 100 km, 1 km and 100 m at once, and of the instrument's immediate surroundings besides.

Imperfect separation. The influence also runs upward, from small scales to large. Stable air flowing over terrain generates gravity waves, oscillations of air displaced vertically against its stratification, that propagate upward and carry momentum to regions far larger than the terrain that launched them. Thunderstorms, as a group, transport heat and moisture vertically and alter the synoptic flow around them. Convection in the boundary layer influences where and when clouds develop, which in turn changes the heating at the surface. The ranges of Table 5.1 are therefore not independent layers of the flow, and a change at one scale can be felt at another. The hierarchy is still useful for modeling: it says which processes a model of a given extent and grid spacing must resolve, and which it may treat as an external input or a parameterized effect.

5.4 What a model resolves

A numerical model represents the atmosphere by values on a grid, and the grid decides which scales of this chapter appear explicitly in its output and which appear only through approximations. This section defines the distinction, the gap between grid spacing and the scale a model actually resolves, and applies both to a 3 km weather model.

Jargon: resolved process, parameterized process, grid spacing, effective resolution, subgrid

A process is *resolved* by a model when its grid is fine enough to represent the structure of the process explicitly, so that the model's equations compute its flow. A process is *parameterized* when the model represents only its average effect on the resolved variables, through a formula with adjustable coefficients. The *grid spacing* Δx, in meters, is the horizontal distance between neighboring grid points of the model. The *effective resolution*, also in meters, is the smallest horizontal scale the model represents with reasonable accuracy in amplitude and structure; it is several times Δx. A feature or process smaller than the grid can represent is *subgrid*.

5.4.1 Resolved and parameterized processes

A model with $\Delta x = 9\,\text{km}$ stores one value of each variable per $9\,\text{km} \times 9\,\text{km}$ cell. A hill 300 m across occupies about a thirtieth of the width of such a cell; it cannot appear in the model terrain, which is itself an average over each cell. Its influence on the flow is not lost entirely but is buried in other quantities: in the smoothed topography, whose cell average is raised a little by the hill; in a roughness parameter that represents the drag of all subgrid terrain and vegetation in the cell; and in subgrid parameterizations of the drag exerted by unresolved orography. None of these gives the speed-up over the hill's crest or the wake behind it; they give, at best, the hill's effect on the average wind of the cell.

With $\Delta x = 50\,\mathrm{m}$ the same hill spans six grid cells, and the model's equations may represent it explicitly: the windward rise, the crest speed-up and the lee deceleration appear in the computed flow. Whether a process is resolved is thus a property of the process and the grid together, not of the process alone. Turbulence that is subgrid at $\Delta x = 9\,\mathrm{km}$ is still subgrid at 50 m for its smaller eddies, and the model then parameterizes those while resolving the hill.

5.4.2 Grid spacing and effective resolution

A feature needs several grid cells to be represented. The shortest wave any grid can hold has a wavelength of $2\Delta x$: one grid point at a crest, the next at a trough. Even that wave is represented badly. Figure 5.5 shows why. The horizontal axis is position in units of grid cells; three waves of wavelength $\lambda = 2\Delta x$, $4\Delta x$ and $10\Delta x$ are drawn one above another, each as the true continuous wave (thin gray curve) and as the values the grid holds at its points (blue dots joined by straight segments). All three have the same amplitude and the same phase offset of one radian at $x = 0$.

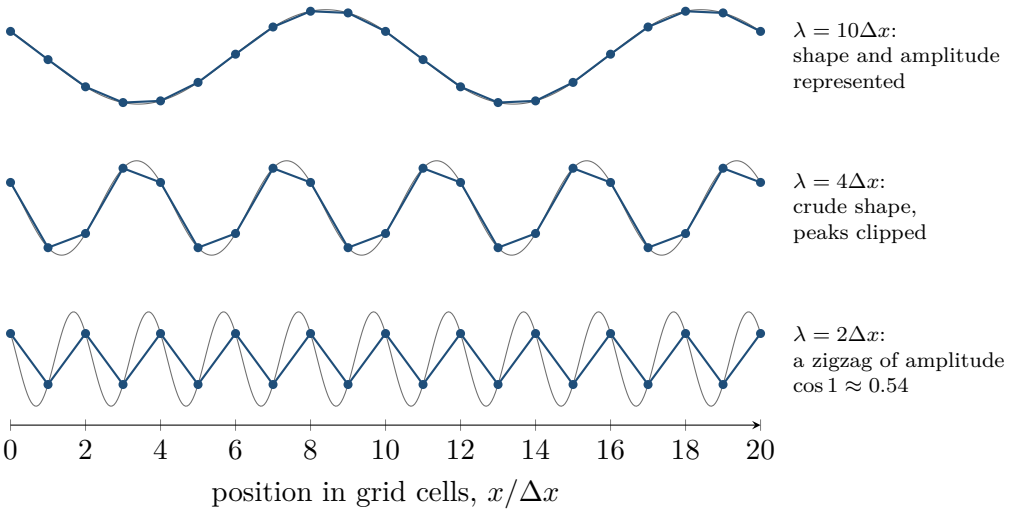


Figure 5.5: Three waves of unit amplitude, $\cos(2\pi x/\lambda + 1)$, of wavelength $\lambda = 2\Delta x$ (bottom), $4\Delta x$ (middle) and $10\Delta x$ (top), each shown as the continuous wave (gray) and as the values held at the grid points (blue). Only the longest wave is represented with its shape and amplitude.

At $\lambda = 10\Delta x$ the grid values trace the wave faithfully. At $\lambda = 4\Delta x$ they keep its wavelength but cut its peaks, because the grid points rarely fall on a crest. At $\lambda = 2\Delta x$ the grid holds only a zigzag whose amplitude depends on where the points happen to fall: 0.54 for this phase, and zero for a wave whose zero crossings coincide with the grid points. Two further effects make the shortest waves worse than this sampling picture suggests. The finite-difference approximations to derivatives that models use are accurate only for waves many grid cells long, so short waves travel at the wrong speed; and models deliberately add numerical diffusion or filtering to remove the noise that such waves generate. The result is a working rule,

$$L_{\mathrm{resolved}} \gtrsim 5 \text{ to } 10\,\Delta x, \tag{5.10}$$

where the factor depends on the model and its numerical methods. A model with $\Delta x = 1\,\mathrm{km}$ effectively resolves features of 5 to 10 km or larger; features between 1 and 5 km appear in its output damped and distorted, and features below 1 km not at all.

Principle 5.2. *Grid spacing is not resolvable scale. A model with grid spacing Δx represents features of about 5 to $10\,\Delta x$ and larger; everything smaller enters its output only through parameterizations.*

5.4.3 A 3 km weather model

Apply the rule to a weather model with $\Delta x = 3\,\text{km}$, whose effective resolution is 15 to 30 km. Table 5.2 lists five features of decreasing size. Its columns give the feature, an illustrative size L, the ratio $L/\Delta x$, and how the model represents the feature.

Table 5.2: Features of different size as represented by a weather model with $\Delta x = 3\,\text{km}$ (effective resolution about 15 to 30 km). Sizes are illustrative.

Feature	L	$L/\Delta x$	Status	What the model carries
Front	300 km	100	well resolved	position, temperature contrast and wind shift computed explicitly
Valley	30 km	10	partly resolved	the valley is present, its slopes and floor smoothed; channeling partly represented
Ridge	3 km	1	poorly resolved	at most a one-cell bump with a lowered crest; no realistic crest speed-up
Hill	300 m	0.1	unresolved	absent from the model terrain; effect only through roughness and subgrid drag
Building	30 m	0.01	absent	at most part of the roughness assigned to the cell's land use

Figure 5.6 shows what the grid does to terrain. The horizontal axis is distance along an illustrative 48 km transect and the vertical axis terrain height above sea level. The thin black curve is the terrain, built from a valley about 30 km wide, a ridge about 3 km wide, a hill about 300 m wide and small-scale roughness. The blue curve is the terrain averaged over 100 m cells and the thick red steps are the same terrain averaged over 3 km cells: the best terrain a model with that grid spacing could carry, before any further smoothing its numerics add.

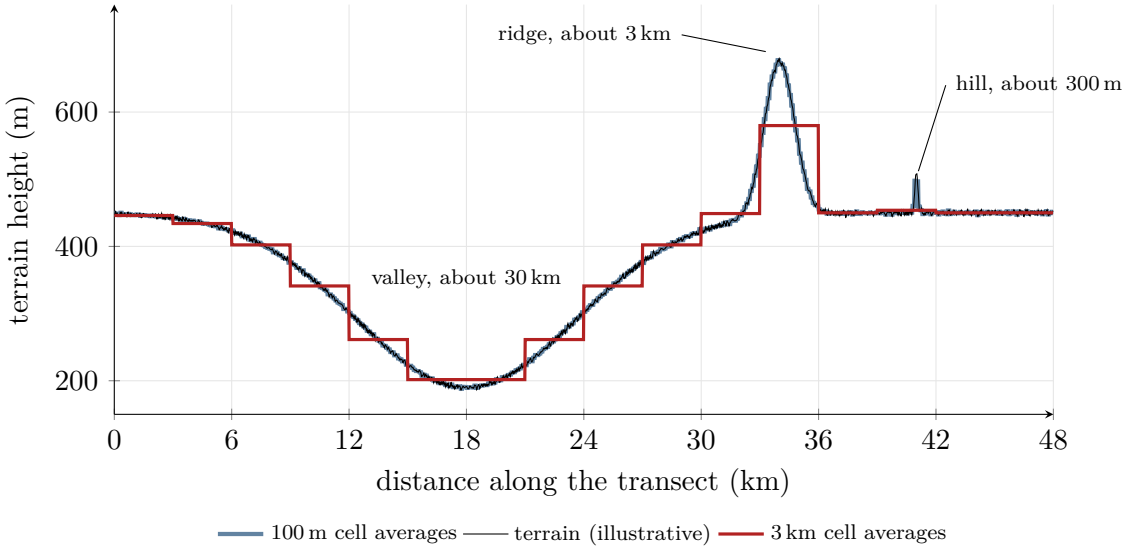


Figure 5.6: An illustrative terrain transect (thin black) and its averages over grid cells of 100 m (blue) and 3 km (red). On the 3 km grid the ridge crest at 678 m becomes a cell at 580 m and the hill crest at 508 m a cell at 454 m; the 100 m grid keeps the ridge crest to within 1 m and the hill crest to within 10 m. Data generated by `scripts/ch05_data.py`.

The 3 km steps follow the valley, which spans ten cells, but cut about 100 m off the ridge and erase the hill: the cell containing the hill crest sits about 50 m below it, at the height of the surrounding plain. The 100 m averages are almost indistinguishable from the terrain at this scale, losing only the small-scale roughness. By equation (5.10) even the 100 m grid would

represent the flow over the 300 m hill only roughly, three cells being fewer than five; but it carries the hill's shape, which the 3 km grid cannot.

A wind of $U_{10} = 7\,\mathrm{m\,s^{-1}}$ from the 3 km model is therefore the wind 10 m above the red terrain of Figure 5.6, averaged over a 3 km cell, with the hill and the ridge's crest absent. An anemometer on the hill's crest stands about 50 m above the model's ground, on terrain that accelerates the flow, among obstacles the model never saw. The model's $7\,\mathrm{m\,s^{-1}}$ does not see the terrain the anemometer sees, and a difference between the two is not by itself an error of either: they are values at different scales.

5.5 Kinds of model

Different models are built for different parts of the range of scales. This section describes the two families, numerical weather prediction and computational fluid dynamics, the two ways of treating turbulence, the range of grid spacing where neither treatment fits, and how the models are chained to produce the wind at a site.

Jargon: NWP, CFD, RANS, LES, gray zone

Numerical weather prediction (NWP) is the forecasting of the atmosphere by integrating the equations of atmospheric motion, thermodynamics and moisture on a three-dimensional grid forward in time from an observed initial state. *Computational fluid dynamics* (CFD) is the numerical solution of the equations of fluid flow, the Navier–Stokes equations, around a specified geometry. *RANS*, Reynolds-averaged Navier–Stokes, is a CFD formulation that solves for the mean flow and models the whole effect of turbulence. *LES*, large-eddy simulation, resolves the large turbulent eddies and models only the small ones. The *gray zone* is the range of grid spacing, for the boundary layer roughly 100 m to 1 km, at which turbulent structures are partly resolved and partly not.

5.5.1 Numerical weather prediction and computational fluid dynamics

NWP models cover the synoptic scale, the mesoscale and the larger scales of the boundary layer over large domains, up to the whole globe. Examples named in practice include WRF, HRRR and the ECMWF models. They start from an analysis of current observations, carry moisture, clouds, radiation and the exchange of heat and momentum with the land and the sea, and parameterize every process smaller than their effective resolution: cumulus convection on coarser grids, boundary-layer turbulence, the drag of unresolved terrain. Their output is a set of grid-cell values, including the 10 m wind of the model's smoothed terrain.

CFD models cover the microscale: flow over hills, around buildings, through industrial sites and urban areas. They resolve local geometry in detail, with grids of meters or less near surfaces, over domains of a few kilometers. They usually take the large-scale wind as a boundary condition, a prescribed inflow profile or values from an NWP model, and often omit moisture, radiation and the evolution of the weather within the domain. NWP gives the weather without the site; CFD gives the site without the weather.

5.5.2 Reynolds averaging and large-eddy simulation

Turbulent flow can be split into a mean and a fluctuation, $u = \overline{u} + u'$. Averaging the equations of motion removes the fluctuations from every term except one: products such as $\overline{u'w'}$ survive, because the average of a product of fluctuations is not zero. The term $-\rho\,\overline{u'w'}$ is the turbulent (Reynolds) stress, the vertical transport of horizontal momentum by eddies, and it has to be supplied by a model of turbulence, a closure, because the averaged equations do not determine it. RANS solves for the mean flow with such a closure. It is efficient and well suited to steady

terrain flow and engineering studies, such as the mean speed-up over a ridge for a given wind direction; it does not give the gusts and eddies themselves.

LES filters the equations in space at about the grid scale instead of averaging in time. Eddies larger than the filter are computed explicitly, and only those smaller than the grid are modeled. It is used for boundary-layer turbulence, flows around buildings and convective structures, and gives time series with gusts and turbulence statistics. The price is a much finer grid and much more computation: halving the grid spacing in all three dimensions multiplies the number of grid points by eight and, because the stable time step shrinks in proportion to the grid spacing, the number of time steps by two, so the cost by about sixteen. Table 5.3 summarizes the families. Its columns give the approach, what it resolves, what it parameterizes, an illustrative grid spacing and its typical use.

Table 5.3: Kinds of atmospheric flow model. Grid spacings are illustrative orders of magnitude.

Approach	Resolves	Parameterizes	Δx	Typical use
Global NWP	synoptic systems, large mesoscale features	convection, boundary-layer turbulence, subgrid terrain	10 to 25 km	large-scale state, forecasts of days
Regional NWP	mesoscale circulations, large terrain	boundary-layer turbulence, small terrain	1 to 4 km	mesoscale structure, near-surface forecasts
RANS CFD	steady mean flow around the geometry	all turbulence	1 to 20 m	mean terrain speed-up, siting studies
LES	large turbulent eddies, gusts	eddies smaller than the grid	1 to 50 m	turbulence, building flow, convective structure

5.5.3 The gray zone

Mesoscale NWP and LES rest on opposite assumptions about turbulence. A boundary-layer parameterization in NWP assumes that all turbulent eddies are much smaller than the grid, so that the grid sees only their average effect. The subgrid model of LES assumes the opposite: that the grid resolves the eddies carrying most of the turbulent energy and models only a small remainder. Both assumptions are valid only far from the scale of the energy-carrying eddies, whose size is comparable to the depth of the boundary layer, a few hundred meters to a couple of kilometers.

Between the two lies a range of grid spacing that is neither coarse enough for the parameterization's assumption nor fine enough to resolve the turbulence, called the gray zone or *terra incognita*. For the boundary layer it lies roughly between 100 m and 1 km, depending on the boundary layer's state: deeper in a convective afternoon, shallower in a stable night. There the largest turbulent structures, such as convective rolls and thermals, are partly resolved by the grid while the parameterization also represents them, so their effect may be counted twice or misrepresented. Boundary-layer parameterization at these spacings is complicated and an area of active development, and a model run at 500 m is not simply a better version of the same model at 3 km.

5.5.4 From a weather model to a transmission-line span

Consider the forecast of wind at a transmission-line span, the conductor between two towers, where the convective cooling of the conductor, and with it the current it can safely carry, depends on the wind speed and on its direction relative to the conductor. The available forecast

comes from a 3 km NWP model; next to the span stands a terrain feature about 200 m across, a fifteenth of a grid cell and far below the model's effective resolution of 15 to 30 km. The model cannot see the feature, nor the channeling or sheltering it produces at the span.

The forecast is therefore built in steps:

$$\text{NWP} \;\rightarrow\; \text{mesoscale background} \;\rightarrow\; \text{microscale correction.}$$

The NWP model supplies the mesoscale background: the wind of the 3 km cell, with the synoptic and mesoscale influences it resolves. A microscale correction then maps that background to the span. It may come from CFD runs of the terrain around the span for each wind direction, from statistical downscaling (a fitted relation between model output and past local measurements), from a terrain speed-up model that estimates the local acceleration from the shape of the terrain, or from local observations on or near the line. Each method corrects both speed and direction, and direction matters as much as speed for the conductor. Downscaling is the subject of Chapter 28.

5.5.5 A modeling hierarchy

The steps generalize into a hierarchy, each level supplying the next with the scales it resolves. Figure 5.7 draws it. The top row is the hierarchy: four boxes, left to right, with the arrows showing what each passes on; the notes below each box give an illustrative grid spacing and the scales it supplies. The bottom row maps the transmission-line example of Section 5.5.4 onto the last three levels.

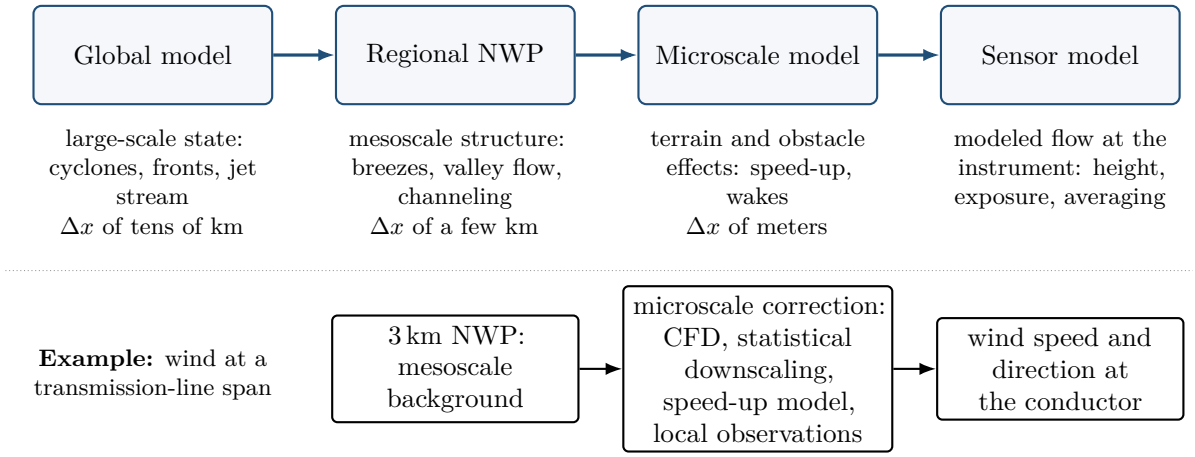


Figure 5.7: A modeling hierarchy for near-surface wind. Top: each level resolves a range of scales and passes its flow to the next. Bottom: the transmission-line example, in which a 200 m terrain feature lies far below the resolution of the 3 km model. Grid spacings are illustrative.

The global model gives the large-scale state; regional NWP gives the mesoscale structure; a microscale model gives the effects of terrain and obstacles; a sensor model connects the modeled flow to the measurement location, accounting for the instrument's height, its exposure to nearby obstacles and vegetation, and its averaging. Each level takes the output of the one before as its boundary condition, and each adds the scales the one before could not resolve.

The last level is the one most often omitted, and it is the one that connects any model to data. A model wind and a measured wind are comparable only after both are brought to the same place, height and averaging time. The difference that remains between a grid-cell value and a point measurement after that is the *representativeness* difference: the part of the point value made by scales the model does not carry. It is not an error of the instrument, nor necessarily of the model, and it does not shrink with better instruments.

5.6 Dimensionless numbers and the scale of a wind value

Three dimensionless numbers summarize which terms of the equations dominate a flow, and one worked chain of wind values shows why every wind number must carry its scale. This section gives both and ends with the questions to ask of any wind value.

5.6.1 Three dimensionless numbers

A dimensionless (or nondimensional) number is a ratio of two terms of the governing equations, each estimated from the scales of the flow. Its size says which of the two terms dominates and so which simplification is safe.

Rossby number. $\mathrm{Ro} = U/(|f|L)$, inertia against the Coriolis force, from equation (5.4). The absolute value of f is used because the number measures the size of the Coriolis term, whose direction, set by the sign of f, differs between the hemispheres. For an illustrative mesoscale flow at 30°S, with $f = 2\Omega \sin\phi = 2 \times 7.292 \times 10^{-5} \times \sin(-30^\circ) = -7.29 \times 10^{-5}\,\mathrm{s}^{-1}$, $U = 8\,\mathrm{m\,s}^{-1}$ and $L = 40\,\mathrm{km}$,

$$\mathrm{Ro} = \frac{8}{7.29 \times 10^{-5} \times 4 \times 10^{4}} \approx 2.7,$$

inertia and Coriolis comparable, and the flow, though not geostrophic, is turned by the Coriolis force over a few hours; to the left of its motion, since $f < 0$.

Reynolds number. $\mathrm{Re} = UL/\nu$, inertia against molecular viscosity, with the kinematic viscosity of air $\nu \approx 1.5 \times 10^{-5}\,\mathrm{m^2\,s^{-1}}$. For flow over a 100 m obstacle at $10\,\mathrm{m\,s}^{-1}$,

$$\mathrm{Re} = \frac{10 \times 100}{1.5 \times 10^{-5}} \approx 6.7 \times 10^{7}.$$

Atmospheric flows have enormous Reynolds numbers: molecular viscosity is negligible for the flow as a whole, which is turbulent, and the drag the ground exerts on the wind is carried by turbulent stresses, treated in Chapters 9 and 10. Viscosity matters only near surfaces and for small bodies. For a conductor 30 mm in diameter in a $2\,\mathrm{m\,s}^{-1}$ wind, $\mathrm{Re} = 2 \times 0.03/(1.5 \times 10^{-5}) = 4000$, and the convective heat loss of the conductor is a function of this number.

Richardson number. Ri compares the buoyancy forces of a stratified layer with the production of turbulence by wind shear. In its gradient form,

$$\mathrm{Ri} = \frac{(g/\theta_v)\,\partial\theta_v/\partial z}{(\partial U/\partial z)^2}, \tag{5.11}$$

where θ_v is the virtual potential temperature, the temperature air would have if brought without exchange of heat to 1000 hPa, corrected for its moisture; Chapter 13 develops it. A positive Ri means stable stratification, which suppresses turbulence; a negative Ri means unstable stratification, which feeds it. For an illustrative night-time layer 50 m deep in which θ_v rises by 1 K and the wind by $2\,\mathrm{m\,s}^{-1}$, at $\theta_v = 290\,\mathrm{K}$,

$$\mathrm{Ri} = \frac{(9.81/290) \times (1/50)}{(2/50)^2} = \frac{6.77 \times 10^{-4}}{1.6 \times 10^{-3}} \approx 0.42,$$

above the critical value of about 0.25 beyond which turbulence tends to die out, so turbulence in this layer is weak or intermittent.

Together the three numbers say which terms of the equations dominate: Ro whether the Coriolis force can be dropped or must be balanced, Re whether viscosity matters, Ri whether stratification controls the turbulence. They can be computed for any flow before any model is chosen.

5.6.2 One wind, four values

Consider an illustrative chain of wind values in one region at one time. A synoptic low gives a southwesterly wind of $15\,\mathrm{m\,s^{-1}}$ at 850 hPa; with $\mathbf{V}_g$ keeping low pressure on its left in the Northern Hemisphere and on its right in the Southern, the low lies to the northwest in the first case and to the southeast in the second. Mesoscale channeling through a valley raises the wind there to $18\,\mathrm{m\,s^{-1}}$. A local ridge adds 25 %, so that at the ridge top the wind is $18 \times 1.25 = 22.5\,\mathrm{m\,s^{-1}}$. A sensor behind vegetation, elsewhere in the same valley, reads $16\,\mathrm{m\,s^{-1}}$. Figure 5.8 draws the four values as bars; the labels under the bars give the level, place and scale of each, and the arrows above the first three bars mark the multiplicative steps between them.

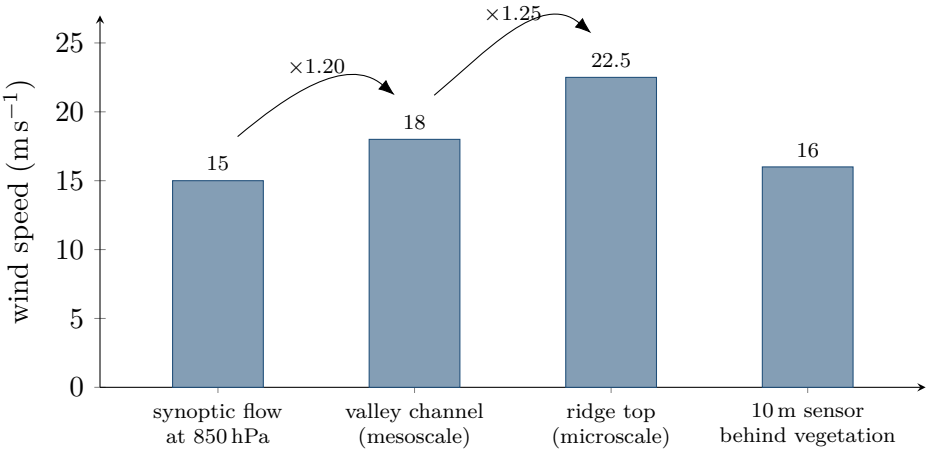


Figure 5.8: Four illustrative wind values in one region at one time: the synoptic flow at 850 hPa, the wind in a valley that channels it, the wind on a ridge top in that valley, and a 10 m anemometer reading behind vegetation at another place in the valley.

All four values are legitimate answers to the question of how strong the wind is, at different scales and places. The $15\,\mathrm{m\,s^{-1}}$ is a grid-scale value at about 1.5 km above sea level, representative of hundreds of kilometers. The $18\,\mathrm{m\,s^{-1}}$ is a valley-scale value, the $22.5\,\mathrm{m\,s^{-1}}$ a point value on an exposed crest, the $16\,\mathrm{m\,s^{-1}}$ a point value near the ground in a sheltered spot; the sensor's value is lower than the ridge-top value not because either is wrong but because it is measured at a different place, at a different height and among different obstacles. A statement of wind speed without its place, height, averaging time and spatial scale cannot be compared with any other.

5.6.3 The scale of a wind value

The example leads to a habit: for any wind value, ask what scale it represents. A value of $U = 8\,\mathrm{m\,s^{-1}}$ can be any of the six quantities in Table 5.4, whose columns give the source of the value, the spatial extent over which it is representative, the time over which it is averaged, and what it leaves out. The six are not interchangeable.

The first three rows are modeled and the last three measured, but the measured values differ among themselves as much as the modeled ones: a 3-second gust of $8\,\mathrm{m\,s^{-1}}$ and a 10-minute mean of $8\,\mathrm{m\,s^{-1}}$ describe different winds at the same point, since the gust is the largest short-period mean in the interval and the corresponding mean is lower. Before two wind values are compared, combined or used to correct one another, five questions should be answered for each: where (which point or which grid cell), at what height above which ground (real or model terrain), over what averaging time, at what spatial scale, and whether it is measured or modeled, and by what.

Table 5.4: Six meanings of a wind speed of $8\,\mathrm{m\,s^{-1}}$. Extents and averaging times are illustrative.

Source of the $8\,\mathrm{m\,s^{-1}}$	Spatial extent	Averaging time	What it leaves out
Global-model 10 m wind	a cell tens of kilometers wide, over smoothed terrain	model time step or output interval	valleys, ridges, local circulations, all terrain below the cell size
3 km regional-model output	a 3 km cell; features below about 15 km damped	model time step or output interval	ridges, hills and obstacles below the effective resolution
LES velocity at 100 m height	a point of an LES grid of meters to tens of meters	instantaneous	eddies smaller than the grid; the weather outside the domain
10 m anemometer reading	one point, with its exposure	the instrument's sampling interval	everything not at that point and height
3-second gust	one point	maximum of 3 s means within the reporting period	the mean wind, which is lower
10-minute mean	one point	10 min	the gusts within the 10 minutes

Principle 5.3. *A wind value is complete only with its place, its height, its averaging time and the spatial scale it represents. Values that differ in any of these are different quantities, and a difference between them is not by itself an error.*

5.7 What to retain

Definition 5.1 (The chain of scales)**.** Near-surface wind is the end of a chain: synoptic forcing, mesoscale circulation, the boundary layer, microscale terrain and obstacles, and the sensor, each link with its own dominant physics; different models operate on different parts of the chain, and each represents only the scales its grid resolves.

Table 5.5 lists the terms of the chapter, their meaning, their units and the subsection that defines each.

5.8 Exercises

Exercise 5.1. A coast at 23°S runs north to south with the ocean to the east. On an afternoon of weak synoptic forcing a sea breeze develops with $L = 40\,\mathrm{km}$ and $U = 5\,\mathrm{m\,s^{-1}}$. (a) Compute the advective time, the Coriolis parameter f (with its sign), the Rossby number and the inertial period $2\pi/|f|$. (b) The sea breeze starts as an easterly wind. In which sense does the Coriolis force turn it during the afternoon, and toward which direction does it move? Give the answer for the same coast at 23°N as well. (c) A synoptic westerly of $3\,\mathrm{m\,s^{-1}}$ blows offshore. Estimate the net early-afternoon surface wind by vector addition and say why the estimate is only approximate.

Exercise 5.2. Two weather models have $\Delta x = 1\,\mathrm{km}$ and $\Delta x = 4\,\mathrm{km}$. (a) Using equation (5.10) with a factor of 5 to 10, give the effective resolution of each. (b) Classify each of the following as well resolved, partly resolved, poorly resolved or unresolved in each model: a valley 40 km wide, a ridge 6 km wide, a hill 800 m wide, a building 30 m long. (c) Refining the horizontal grid from 4 to 1 km while keeping the vertical levels fixed multiplies the number of columns and the number of time steps; by about what factor does the cost rise?

Exercise 5.3. Wind of $9\,\mathrm{m\,s^{-1}}$ approaches a long ridge 120 m high, and the displaced layer is taken as 600 m deep. (a) Use equation (5.9) to estimate the speed over the crest. (b) Use

Table 5.5: The terms of the chapter and where each is defined.

Term	Meaning	Units	Defined in
Advective time	$t_{\text{adv}} = L/U$, time for the wind to cross a feature	s	5.1.2
Synoptic scale	weather systems of about 1000 to 5000 km and more, lasting days; pressure gradient and Coriolis balance	–	5.1.3, 5.2.1
Mesoscale	circulations of about 1 to 1000 km, minutes to hours; pressure, buoyancy, inertia and Coriolis compete	–	5.1.3, 5.2.3
Microscale	flow below about 1 km, seconds to minutes; Coriolis negligible	–	5.1.3, 5.3.1
Rossby number	$\text{Ro} = U/(\lvert f \rvert L)$, inertia relative to Coriolis	–	5.2.1, 5.6.1
Reynolds number	$\text{Re} = UL/\nu$, inertia relative to viscosity	–	5.6.1
Richardson number	Ri, buoyancy relative to shear, equation (5.11)	–	5.6.1
Resolved process	represented explicitly by the model's grid	–	5.4.1
Parameterized process	represented only by its average effect, through a formula	–	5.4.1
Grid spacing Δx	distance between neighboring grid points	m	5.4.1
Effective resolution	smallest scale represented accurately, about 5 to $10\,\Delta x$	m	5.4.2
NWP	numerical weather prediction: synoptic, mesoscale and large boundary-layer scales over large domains	–	5.5.1
CFD	computational fluid dynamics: microscale flow around a resolved geometry	–	5.5.1
RANS	mean flow solved, all turbulence modeled	–	5.5.2
LES	large eddies resolved, small eddies modeled	–	5.5.2
Gray zone	grid spacings, about 100 m to 1 km for the boundary layer, at which turbulence is partly resolved	m	5.5.3

Bernoulli's relation with $\rho = 1.2\,\mathrm{kg\,m^{-3}}$ to estimate the pressure change between the upwind flow and the crest. (c) A synoptic gradient of 2 hPa per 100 km acts across the 1.5 km from the ridge's foot to its crest. Compute the pressure change it produces over that distance and compare. (d) Give two reasons the speed-up near the ground at the crest may differ from (a).

Exercise 5.4. (a) Compute the Rossby number of flow at $8\,\mathrm{m\,s^{-1}}$ over a hill 1.5 km wide at 30°S, and state whether the Coriolis force matters. (b) Compute the Reynolds number of a conductor 28 mm in diameter in a $1.5\,\mathrm{m\,s^{-1}}$ wind with $\nu = 1.5 \times 10^{-5}\,\mathrm{m^2\,s^{-1}}$. (c) In a night-time layer 60 m deep, θ_v rises by 1.5 K and the wind by $1.5\,\mathrm{m\,s^{-1}}$, with $\theta_v = 288\,\mathrm{K}$. Compute Ri and say what it implies for turbulence. (d) A line operator receives $8\,\mathrm{m\,s^{-1}}$ from a 3 km model and $5\,\mathrm{m\,s^{-1}}$ from a 10 m anemometer near a span. List what must be known about each value before the difference can be called a model error.

Chapter 6

The Atmospheric Boundary Layer

6.1 The layer that feels the surface

The first five chapters followed the wind from the pressure field to the balanced flows of the synoptic scale and then down through the scales of motion to the microscale. In all of them the ground appeared mainly as a lower boundary that slows the wind. The air in contact with the ground is, however, a layer with its own physics: it is heated and cooled by the surface every day, stirred by turbulence that the surface generates, and deepened and thinned by the sun. It is the layer in which almost every engineering wind, at a weather station, on a transmission span or at the hub of a wind turbine, is measured and used. The question of this chapter is

what makes the lowest part of the atmosphere fundamentally different from the air above it, and how does that difference shape the wind near the ground?

The chapter defines the atmospheric boundary layer and the free atmosphere above it, follows the boundary layer through its daily cycle from the convective afternoon to the stable night, divides it into the layers that matter for near-surface wind, introduces potential temperature as the variable that measures static stability, and ends with what stability and turbulence do to the vertical profile of the wind, and therefore to the relation between a wind at 100 m and a wind at 10 m.

Jargon: atmospheric boundary layer (ABL), planetary boundary layer (PBL), free atmosphere, surface forcing, boundary-layer depth, diurnal cycle, stratification

The *atmospheric boundary layer* (ABL) is the lowest part of the atmosphere, the part that responds directly to the surface on time scales of about an hour or less. The *planetary boundary layer* (PBL) is the same layer under another name; the two terms and their abbreviations are interchangeable, and "PBL height" and "ABL depth" mean the same thing. The *free atmosphere* is the atmosphere above it, where the direct influence of the surface is weak and the flow is governed by the pressure-gradient force, the Coriolis force and the large-scale dynamics of the earlier chapters. A *surface forcing* is an exchange between the ground and the air that drives the boundary layer: of momentum, of heat, of moisture, and the drag and turbulence of roughness elements. The *boundary-layer depth* z_i, in meters, is the height of the top of the boundary layer above the ground; it is diagnosed from soundings, remote sensing or a model's profiles (Section 6.4.1). The *diurnal cycle* is the variation of a quantity over the 24 hours of a day, driven here by solar heating by day and radiative cooling at night. *Stratification* is the vertical arrangement of the air's density, and so of its buoyancy; it is *stable* when lighter air lies over denser air and *unstable* when the reverse holds.

Key idea

The atmospheric boundary layer translates the large-scale wind of the free atmosphere into the wind near the ground. The main control on that translation is whether turbulence can move momentum vertically, and that depends on the heating or cooling of the surface: by day, convection couples the surface to the flow aloft; at night, stable stratification can disconnect them.

6.1.1 Definition

The atmospheric boundary layer is the lowest part of the atmosphere that responds directly to surface forcing on time scales of about an hour or less. The definition is dynamical, not geometric: it names the layer by what it does, exchanging momentum, heat, moisture and sometimes pollutants or other scalars with the surface, not by a fixed height. Above it, a change at the ground, such as the morning heating of a field, reaches the air only over days and indirectly, through clouds, radiation and the large-scale circulation.

The one-hour figure follows from the speed of the eddies that do the exchanging. In a convective boundary layer the large eddies, the thermals of Section 6.2.2, have a velocity scale, the *convective velocity scale*,

$$w_* = \left(\frac{g}{\theta} \, z_i \, (\overline{w'\theta'})_0 \right)^{1/3}, \tag{6.1}$$

where $(\overline{w'\theta'})_0$ is the kinematic sensible heat flux at the surface in $\mathrm{K\,m\,s^{-1}}$ (its definition and measurement are in Chapter 9; multiplied by ρc_p it gives the sensible heat flux H in $\mathrm{W\,m^{-2}}$) and θ is the potential temperature of Section 6.5.1, here simply a representative absolute temperature. For an illustrative afternoon with $(\overline{w'\theta'})_0 = 0.2\,\mathrm{K\,m\,s^{-1}}$ (about $1.2 \times 1004 \times 0.2 \approx 240\,\mathrm{W\,m^{-2}}$), $z_i = 1500\,\mathrm{m}$ and $\theta = 300\,\mathrm{K}$,

$$w_* = \left(\frac{9.81 \times 1500 \times 0.2}{300} \right)^{1/3} \mathrm{m\,s^{-1}} = (9.81)^{1/3}\,\mathrm{m\,s^{-1}} \approx 2.1\,\mathrm{m\,s^{-1}},$$

and the time a thermal takes to cross the layer, the *eddy turnover time* $t_* = z_i / w_*$, is $1500/2.1 \approx 700\,\mathrm{s}$, about twelve minutes. A few turnovers, under an hour, are enough for a change of the surface heating to be felt through the whole layer. In a stable boundary layer the eddies are weaker and the layer thinner, and the response is slower and confined to a shallower depth.

Depth. The depth of the boundary layer varies continuously. It can be as little as 100 m, or less, on a strongly stable night with weak wind, and 2000 m or more in strong daytime convection; over hot, dry land in summer the afternoon layer can reach several kilometers. Over the ocean, whose surface temperature changes little between day and night, the boundary layer has a weak daily cycle and a depth that is often a few hundred meters to about a kilometer. The boundary layer is therefore not a fixed-height slab; it is a dynamical layer whose depth is one of the variables that describe its state. The simplest model of it, the Ekman layer of Chapter 3 with a constant eddy viscosity K, already shows the range: its depth scale $\delta = \sqrt{2K/|f|}$ at $|f| = 10^{-4}\,\mathrm{s^{-1}}$ is $\sqrt{2 \times 50/10^{-4}} = 1000\,\mathrm{m}$ for an illustrative daytime $K = 50\,\mathrm{m^2\,s^{-1}}$ and $\sqrt{2 \times 1/10^{-4}} \approx 140\,\mathrm{m}$ for an illustrative nighttime $K = 1\,\mathrm{m^2\,s^{-1}}$, the same in either hemisphere since only $|f|$ enters. The eddy viscosity is a property of the turbulence, and the turbulence changes by orders of magnitude between day and night; the rest of the chapter is about why.

6.1.2 Surface forcings

Four exchanges between the ground and the air drive the boundary layer. Figure 6.1 shows them as a schematic: the ground at the bottom, the boundary layer as the shaded band above it with its top at z_i, the free atmosphere above, and one arrow or symbol for each forcing.

- *Momentum exchange.* The ground slows the wind. At the surface the air is at rest relative to the ground, and the drag the surface exerts on the air, the surface stress, is transmitted upward as a downward flux of momentum carried by turbulent eddies (Chapters 9 and 10). The boundary layer is where the wind loses momentum to the ground.
- *Sensible heat exchange.* The surface heats the air above it by day and cools it at night. This exchange changes the buoyancy of the air near the ground and therefore, as Sections 6.2.2 and 6.3.2 show, the kind and the strength of the turbulence.
- *Moisture exchange.* Evaporation from soil and water and transpiration by plants add water vapor to the air; condensation and dew remove it. Water vapor makes air lighter, so moisture also affects buoyancy, and its condensation releases heat.
- *Roughness effects.* Trees, crops, buildings and terrain exert drag on the flow and shed wakes, generating turbulence directly from the wind (Section 6.4.3).

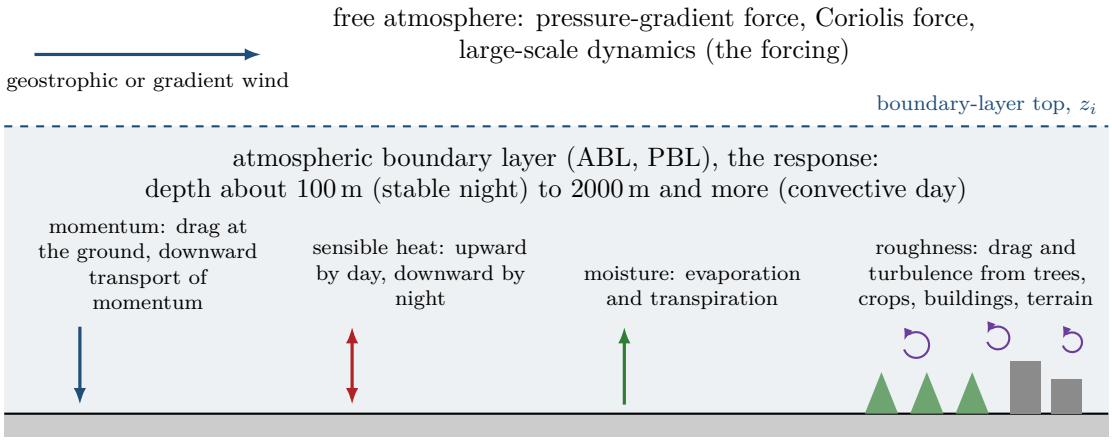


Figure 6.1: The four surface forcings of the atmospheric boundary layer (schematic, not to scale). The boundary layer (shaded) exchanges momentum, sensible heat and moisture with the ground and is stirred by the drag of roughness elements; the free atmosphere above carries the large-scale forcing.

The four forcings are not independent. The heat exchange decides how effectively the momentum exchange is spread through the layer: the same surface drag is communicated through 1500 m of air on a sunny afternoon and through less than 200 m on a clear night. The moisture exchange competes with the heat exchange for the energy the surface receives from the sun: a wet field turns more of it into evaporation and less into sensible heat than a dry one, and grows a shallower convective layer. The roughness elements set the drag, and with it the mechanical turbulence that persists when the heating stops.

6.1.3 The free atmosphere

Above the boundary layer the direct effect of the surface is much weaker. The flow there is governed by the pressure-gradient force, the Coriolis force and the large-scale dynamics treated in Chapters 2 to 5: it is close to geostrophic on straight isobars and close to the gradient wind on curved ones, and it changes with the weather systems over hours to days. Turbulence in the free atmosphere is intermittent and patchy, confined to clouds, jet-stream shear zones and breaking waves, rather than the continuous stirring of the boundary layer.

The two layers stand to each other as forcing and response. The free atmosphere carries the large-scale forcing: the pressure gradient and the wind it supports. The boundary layer is the

surface-modified response to that forcing: the same pressure gradient acts in it, but the wind it produces is slowed, turned toward low pressure, made gusty and made to vary with the time of day by the exchanges of Section 6.1.2. A forecast of the free-atmosphere wind is a forecast of the forcing; the wind at a sensor or a span is the response, and the boundary layer is the transformation between the two.

What a model represents. A weather model does not resolve the turbulent eddies of the boundary layer, whose sizes range from millimeters to about z_i; it represents their average effect by a boundary-layer parameterization, a formula for the vertical turbulent transport of momentum, heat and moisture given the model's mean profiles (the distinction between resolved and parameterized processes of Chapter 5). The free-atmosphere wind of a model is largely resolved; the boundary-layer wind is resolved only in its mean and depends on that parameterization. The difference between the two is one reason near-surface winds are harder to forecast than winds aloft.

6.2 The daily cycle and the convective boundary layer

Over land, the boundary layer goes through a daily cycle of growth and collapse driven by the sun. This section describes the cycle as a whole and then the daytime half of it: the convective boundary layer, the mixing of momentum it produces and the entrainment zone at its top.

6.2.1 The diurnal cycle

Solar heating by day and radiative cooling at night change the sign of the buoyancy at the ground and with it the structure of the turbulence. On a clear day over land the sequence is: at sunrise the ground begins to warm, and a convective layer begins to grow from the surface; through the morning it deepens, slowly at first and then rapidly; in the afternoon it is deep and nearly steady; at sunset the ground cools, convection stops, and a shallow stable layer forms at the surface while the air above is left behind as the remnant of the day's mixing. In short,

sunrise → convective growth → deep afternoon boundary layer → sunset → shallow stable boundary layer.

Figure 6.2 draws this cycle as a time-height diagram, the standard way of showing it. The horizontal axis is local time over 24 hours, with an illustrative sunrise at 06:00 and sunset at 18:00 (dotted vertical lines); the vertical axis is height above the ground in kilometers. Each shaded region is one of the layers named in this section and the next. The light gold region is the convective mixed layer, which grows from the ground after sunrise; the darker gold band at its top is the entrainment zone; the gray region is the residual layer, the air mixed on the previous day; the blue regions near the ground are the stable boundary layer of the night, before sunrise and after sunset; the green strip at the bottom of the daytime layer is the surface layer; the free atmosphere is the white region above. The solid line at 1.8 km is the capping inversion that separates the boundary layer from the free atmosphere at night and in the morning. All depths and times are illustrative.

Three features of the diagram carry the rest of the chapter. First, the depth of the boundary layer changes by an order of magnitude over the day, from about 0.2 km before sunrise to about 1.8 km in the afternoon. Second, the growth in the morning is not steady: the mixed layer first has to erode the stable layer left by the night, which takes a couple of hours (Section 6.3.5), and then grows quickly into the residual layer, whose air offers little resistance. Third, the collapse at sunset is abrupt at the ground and absent aloft: the turbulence stops, but the air mixed during the day stays where it is, so that at night the boundary layer of the time-height diagram

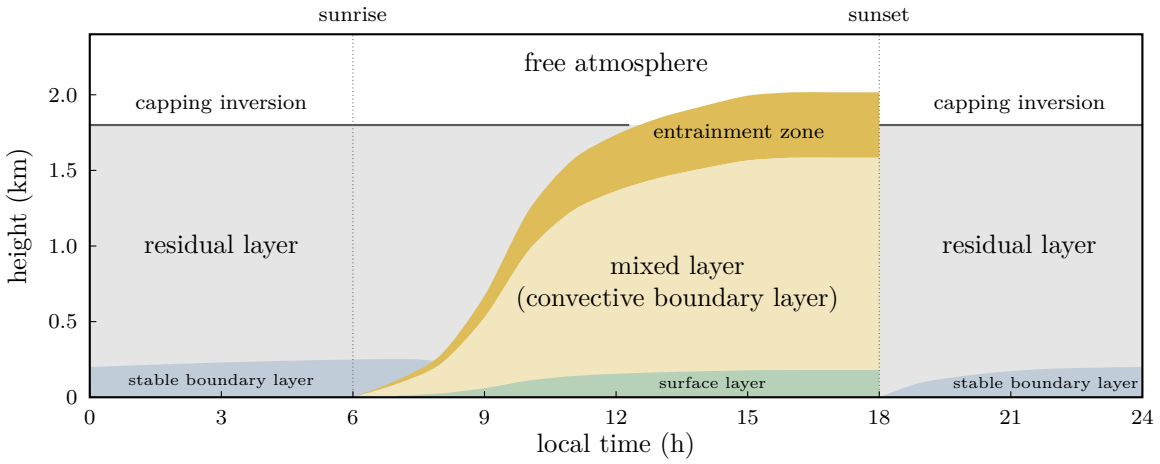


Figure 6.2: Time-height diagram of the boundary layer over land on a clear day (schematic, illustrative depths and times). The mixed layer grows after sunrise, under an entrainment zone, to about 1.8 km in the afternoon; after sunset a shallow stable boundary layer forms at the ground and the air above it becomes the residual layer, capped by the inversion left by the day's mixing.

has two parts, the thin stable layer that responds to the surface and the residual layer above it that no longer does.

6.2.2 The convective boundary layer

During the day, the ground absorbs sunlight and warms faster than the air above it. Once the surface is warmer than the air in contact with it, $T_{\text{surface}} > T_{\text{air}}$, the surface heats the lowest air, which becomes lighter than its surroundings, that is, buoyant, and rises. The rising plumes of warm air, called *thermals*, are typically a few hundred meters wide and reach the top of the layer; between them, cooler air sinks more slowly over a larger area. This buoyancy-driven overturning is *convective turbulence*, and the layer it fills is the *convective boundary layer* (CBL): the daytime boundary layer whose turbulence is produced mainly by surface heating. It is also called the *mixed layer*, because the convective turbulence mixes heat, momentum and moisture through most of its depth.

Why "mixed". The thermals carry warm air upward and the surrounding descent carries air downward, and in an hour or less every parcel of the layer has been exchanged with air from other heights several times (the turnover time of Section 6.1.1). Any conserved property is then nearly uniform with height. For heat the conserved property is not the temperature, which falls with height as air rises and expands, but the potential temperature θ, the temperature corrected for the change of pressure with height (Section 6.5.1); through most of the convective layer θ is nearly constant with height. Specific humidity is nearly uniform as well. Wind speed is not perfectly constant with height, because the surface keeps removing momentum at the bottom and the free atmosphere supplies it at the top, but its vertical gradients through the middle of the layer are much weaker than under stable conditions. The strong gradients are confined to a thin *surface layer* at the bottom (Section 6.4.2) and to the entrainment zone at the top (Section 6.2.4).

6.2.3 Daytime momentum mixing

Convective eddies do not only carry heat upward; they carry momentum in both directions. A thermal rising from the ground carries slow air upward; the compensating descent brings air with the higher momentum of the upper boundary layer down toward the surface. The net effect is a downward transport of momentum, from where the wind is strong to where it is weak, and the chain is

strong turbulence → strong vertical coupling → momentum transported downward.

The near-surface wind is then tied to the wind of the whole mixed layer, and that wind in turn to the free atmosphere through the entrainment zone.

Two consequences are visible in any record of near-surface wind over land. First, the surface wind often increases after the morning transition, the period after sunrise when the mixed layer erodes the nocturnal stable layer and reconnects the surface to the faster air aloft. On an illustrative day with a steady large-scale flow of $12\,\mathrm{m\,s^{-1}}$ at 300 m, the 10 m wind may be $3\,\mathrm{m\,s^{-1}}$ at sunrise and $7\,\mathrm{m\,s^{-1}}$ in the early afternoon without any change in the weather pattern. Second, the daytime surface wind is gustier: the thermals and the downward bursts of fast air make the wind at a point fluctuate strongly over seconds to minutes (gusts and their statistics are treated in Chapter 8). Daytime surface winds are therefore both stronger and gustier than nighttime surface winds under the same large-scale forcing.

The same mixing has the opposite effect higher up. Momentum moved downward to the surface is momentum removed from the upper part of the layer, so the wind at 100 to 200 m is often weaker by day than at night, when it is no longer drained to the ground (Section 6.3.3). Between the two, at a height that depends on the site and is often between about 50 and 100 m, the daily cycle of the wind speed reverses phase: below it the wind peaks in the afternoon; above it, at night. A daily wind cycle measured at a 10 m mast is not the daily cycle at a turbine hub, and neither is the daily cycle on a transmission line strung at an intermediate height.

6.2.4 The entrainment zone

At the top of the daytime convective layer the thermals overshoot into the stable air above, are slowed by their negative buoyancy there and sink back, dragging with them some of the free-atmosphere air they have disturbed. The layer in which this happens is the *entrainment zone*: the transition layer at the top of the convective boundary layer in which thermals interact with the free atmosphere and free-atmosphere air is incorporated into the boundary layer. Its thickness varies, but a few tenths of z_i is typical. The incorporation itself is *entrainment*.

Entrainment is how the convective layer grows. Its rate is written as an *entrainment velocity* w_e, the rate at which the top of the boundary layer advances into the free-atmosphere air, so that

$$\frac{\mathrm{d}z_i}{\mathrm{d}t} = w_e + w_s, \tag{6.2}$$

where w_s is the large-scale vertical velocity at z_i, negative under the subsidence of a high-pressure system. In Figure 6.2 the top of the layer rises from about 0.25 to 1.1 km between 08:00 and 10:00, a growth rate of $850\,\mathrm{m}/7200\,\mathrm{s} \approx 0.12\,\mathrm{m\,s^{-1}}$; with an illustrative subsidence of $w_s = -0.01\,\mathrm{m\,s^{-1}}$, the entrainment velocity is $w_e = 0.12 + 0.01 = 0.13\,\mathrm{m\,s^{-1}}$. In the afternoon the top is nearly steady at 1.8 km, and equation (6.2) then says that entrainment, about $0.01\,\mathrm{m\,s^{-1}}$, just balances the subsidence.

Entrainment sets more than the depth. The entrained air is warmer in potential temperature and usually drier than the mixed layer, so it warms and dries the boundary layer from the top while the surface warms and moistens it from the bottom; the downward heat flux at the top is typically about a fifth of the upward heat flux at the surface. It also carries the free-atmosphere

momentum into the mixed layer, which is how the wind of the free atmosphere reaches the boundary layer by day. The temperature, the moisture and the momentum of the whole layer are thus fixed jointly by the surface fluxes at the bottom and the entrainment fluxes at the top.

6.3 The stable boundary layer and the residual layer

After sunset the surface stops heating the air and begins to cool it. This section describes the stable boundary layer that results, why stable stratification suppresses turbulence, the decoupling of the surface from the flow above, the residual layer left by the day, and the memory that the boundary layer carries from one part of the cycle to the next.

6.3.1 The stable boundary layer

After sunset the ground loses heat by longwave radiation to the sky, and on a clear night it cools quickly, by several kelvin in the first hours. The air in contact with it is cooled from below, so that soon $T_{\text{surface}} < T_{\text{air}}$ and the air near the surface is colder and therefore denser than the air above. That arrangement, denser air below lighter air, is *stable stratification*: it resists vertical motion, and the layer in which it forms is the *stable boundary layer* (SBL), the nighttime boundary layer whose stratification is stable and whose turbulence is produced only by wind shear and is damped by the stratification.

The stable boundary layer is shallow, typically 50 to a few hundred meters, and its depth depends mainly on the wind: a strong wind keeps mechanical turbulence going through a deeper layer, while a calm, clear night produces a very shallow, very stable layer. Clouds reduce the radiative cooling and with it the stability, and a cloudy, windy night may produce a boundary layer close to neutral. Over the ocean the cycle is weak in both directions, because the sea surface temperature barely changes between day and night.

6.3.2 Suppression of turbulence by stability

Stable stratification suppresses turbulence because it opposes vertical displacement. Consider a parcel of air in a stable layer, displaced upward quickly enough that it exchanges no heat with its surroundings. It expands and cools as it rises into lower pressure, but in a stable layer the air it arrives in is warmer still, relative to the parcel, than the air it left. The parcel is then colder and denser than its new surroundings, negatively buoyant, and it sinks back toward its starting level. Displaced downward, it is compressed and warmed but arrives among air that is colder and denser still, is positively buoyant and rises back. In both directions the stratification exerts a restoring force, and the parcel oscillates about its original level instead of continuing to move. Section 6.5.4 makes the argument quantitative with potential temperature and gives the frequency of the oscillation.

A turbulent eddy is a set of such displacements. In a stable layer each vertical excursion is opposed by a restoring force that converts the kinetic energy of the eddy into potential energy, so the stratification drains energy from the vertical motions. The chain is

$$\text{stable stratification} \rightarrow \text{suppressed vertical motions} \rightarrow \text{weaker turbulence} \rightarrow \text{weaker vertical momentum exchange.}$$

The effect is selective: horizontal motions are not opposed by buoyancy, so a stable layer can still have horizontal meandering of the wind while its vertical exchange is nearly shut off. Whether the turbulence survives at all is decided by the competition between the shear that produces it and the stratification that destroys it, the competition measured by the Richardson number Ri of Chapter 5 and taken up in Section 6.6.3.

6.3.3 Decoupling

When the turbulence in the stable layer is weak, the air near the ground is no longer pulled along by the air above it. Strong winds can then exist just above the shallow stable layer without reaching the surface. An illustrative night with $15\,\mathrm{m\,s^{-1}}$ at 100 m and $2\,\mathrm{m\,s^{-1}}$ at 10 m has a mean shear of

$$\frac{\Delta U}{\Delta z} = \frac{15-2}{100-10}\,\frac{\mathrm{m\,s^{-1}}}{\mathrm{m}} = \frac{13}{90}\,\mathrm{s^{-1}} \approx 0.14\,\mathrm{s^{-1}}$$

between the two heights, against about $0.02\,\mathrm{s^{-1}}$ for an afternoon with $8\,\mathrm{m\,s^{-1}}$ at 10 m and $10\,\mathrm{m\,s^{-1}}$ at 100 m, a seven times weaker shear. This state is *surface decoupling*: the surface layer is dynamically disconnected from the flow above it, in the sense that the momentum of the flow aloft is no longer transmitted to the ground.

Figure 6.3 shows the two profiles. The horizontal axis is wind speed and the vertical axis height above the ground, from 0 to 300 m. The solid red curve is the illustrative night profile, with the stable boundary layer shaded blue up to an illustrative 150 m; the dashed gold curve is an illustrative afternoon profile. The dots mark the values at 10 and 100 m, listed in the box at the upper left. By day the wind is nearly uniform above a few tens of meters and the 10 m wind is most of the 100 m wind. At night the 10 m wind is a small fraction of the 100 m wind, and above the stable layer the wind exceeds the daytime value and reaches a maximum near the top of the stable layer, a feature treated in Chapter 18 as the low-level jet.

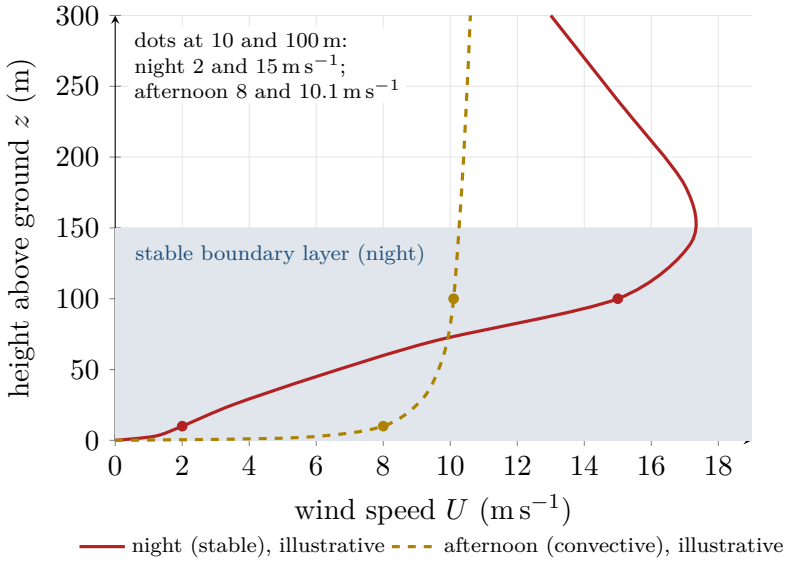


Figure 6.3: Surface decoupling (illustrative profiles drawn through chosen points). At night (solid) the stable boundary layer, shaded up to 150 m, separates a nearly calm surface, $2\,\mathrm{m\,s^{-1}}$ at 10 m, from a strong flow aloft, $15\,\mathrm{m\,s^{-1}}$ at 100 m, with a wind maximum near the top of the stable layer. In the afternoon (dashed) convective mixing keeps the profile nearly uniform above the lowest tens of meters.

Decoupling is one of the major difficulties of near-surface forecasting. The 100 m wind of a decoupled night can be well forecast, because it follows the large-scale forcing, while the 10 m wind depends on whether the weak turbulence of the stable layer manages to connect the two, which can switch on and off within an hour (Section 6.6.3). For a transmission line strung at 15 to 30 m, a decoupled night means that the conductor sits in nearly calm air, with little convective cooling, under a strong wind that the line never feels; a rating that assumes the wind at the span follows the wind aloft overstates the cooling exactly on those nights. For a turbine at 100 m the same night is a windy one.

6.3.4 The residual layer

After sunset the lower part of the boundary layer becomes stable, but the air above it, mixed during the afternoon, does not change at once. Its turbulence decays within an hour or so for lack of the thermals that drove it, but its potential temperature, its moisture and any pollutants mixed into it remain nearly uniform with height, as they were in the afternoon mixed layer. This layer is the *residual layer*: the remnant of the previous day's mixed layer, lying above the nocturnal stable boundary layer and below the free atmosphere, with the properties of the mixed layer but without its turbulence. Its stability is close to neutral, and it is capped by the inversion that capped the afternoon mixed layer.

The night structure is therefore, from top to bottom,

$$\text{free atmosphere / residual layer / stable boundary layer / surface,}$$

as in Figure 6.2 before sunrise and after sunset. The residual layer is not in contact with the surface, since the stable layer below insulates it, and in that sense it is no longer part of the boundary layer as defined in Section 6.1.1; it is kept in the picture because it is where the next morning's mixed layer will grow, and because its near-neutral stratification lets the wind in it accelerate once the drag of the ground is cut off.

6.3.5 Memory of the boundary layer

The boundary layer at any moment carries the history of the previous hours. After sunset the surface cools quickly while the air aloft keeps the daytime structure, which is why the residual layer exists. After sunrise the turbulence begins near the ground and takes time to erode the nighttime structure: the new mixed layer must warm the cold air of the stable layer up to the potential temperature of the residual layer before it can grow into it.

The time this takes can be estimated from a heat budget. Let the stable layer be 200 m deep, with a potential-temperature deficit relative to the residual layer of 7.5 K at the ground decreasing linearly to zero at its top (illustrative values). The heat, per unit area and divided by ρc_p, needed to remove the deficit is the area of the triangle,

$$\tfrac{1}{2} \times 7.5\,\mathrm{K} \times 200\,\mathrm{m} = 750\,\mathrm{K\,m}.$$

If the surface supplies, on average over the morning, a kinematic heat flux of $0.1\,\mathrm{K\,m\,s^{-1}}$ (a sensible heat flux of about $1.2 \times 1004 \times 0.1 \approx 120\,\mathrm{W\,m^{-2}}$), the erosion takes

$$\frac{750\,\mathrm{K\,m}}{0.1\,\mathrm{K\,m\,s^{-1}}} = 7500\,\mathrm{s} \approx 2.1\,\mathrm{h},$$

during which the mixed layer stays shallow and the surface wind stays weak. Only then does the layer grow rapidly into the residual layer and reconnect the ground to the wind aloft, as the steep rise of Figure 6.2 after 08:00 shows. A colder night, a deeper stable layer or a weaker morning sun delays the reconnection further.

Near-surface wind therefore depends on recent history, not only on the present large-scale forcing. Two mornings with the same pressure gradient and the same sunshine can have different 10 m winds at 09:00 because their nights were different. A model of near-surface wind that uses only the current forcing as input misses this memory; a model with the boundary-layer state as a variable carried from one hour to the next keeps it.

6.4 Layers within the boundary layer

The boundary layer is itself layered, and the layers differ in what governs the wind within them. This section defines the boundary-layer height and the ways it is diagnosed, the surface layer and its two sublayers, and assembles the vertical picture.

6.4.1 Boundary-layer height

The depth of the boundary layer is written z_i; other texts and model outputs write h, h_{PBL} or z_{PBL} for the same quantity. There is no single universal definition of it, because the top of the boundary layer is a transition, not a surface, and different properties change across it at slightly different heights. Table 6.1 lists the common diagnostics. Its columns give the property used, the instrument or the model field from which it is computed, and what the diagnostic locates.

Table 6.1: Common diagnostics of the boundary-layer height z_i. Thresholds in use vary between authors and models.

Property	Source	Height diagnosed as
Temperature gradient	radiosonde, model profile	base of the capping inversion, or height of the largest increase of θ with height; by day, the height where a surface parcel's θ meets the profile
Turbulence level	sonic anemometers on towers, aircraft, large-eddy simulation	height where the turbulent kinetic energy or the momentum flux falls to a small fraction of its near-surface value
Richardson number	radiosonde, model profile	lowest height where the bulk Richardson number, equation (6.3), exceeds a critical value, often 0.25
Aerosol backscatter	lidar, ceilometer	height of the sharp drop of aerosol concentration from the mixed layer to the cleaner free atmosphere
Vertical velocity variance	Doppler lidar, radar wind profiler	height where σ_w^2 falls below a threshold

The Richardson-number diagnostic is the one most weather models use. The *bulk Richardson number* between the surface and a height z compares the buoyancy difference across the layer with the wind speed at its top,

$$\mathrm{Ri}_b(z) = \frac{g}{\theta_v}\,\frac{\left(\theta_v(z) - \theta_v(0)\right) z}{U(z)^2}, \tag{6.3}$$

where θ_v is the virtual potential temperature, the potential temperature of dry air with the same density as the moist air (Section 6.5.1). In a layer where the potential temperature at 1000 m exceeds the surface value by 1 K and the wind at 1000 m is $10\,\mathrm{m\,s^{-1}}$, with $\theta_v \approx 300\,\mathrm{K}$, $\mathrm{Ri}_b = 9.81 \times 1 \times 1000/(300 \times 100) \approx 0.33$, above the critical 0.25; the top of the boundary layer lies below 1000 m.

The diagnostics agree when the top is sharp, as under a strong capping inversion in the afternoon, and differ when it is diffuse, as in the morning, in the evening and at night, where a temperature-based and a turbulence-based diagnostic can differ by a factor of two. "PBL height" is therefore partly a diagnostic quantity: a number defined by the method that computed it. A boundary-layer height in a model's output is computed from the model's profiles by the model's own criterion; one from a ceilometer is the top of the aerosol layer, which at night is often the top of the residual layer rather than of the stable layer. Before two values are compared, the diagnostic behind each must be known.

6.4.2 The surface layer

The *surface layer* is the lowest part of the boundary layer, roughly the lowest tenth of its depth, $z \lesssim 0.1\,z_i$. With $z_i = 1000\,\mathrm{m}$ it is the lowest 100 m, which contains most engineering measurements: weather-station anemometers at 10 m, transmission conductors at 10 to 40 m, and the lower half of a modern wind turbine rotor. At night the same rule gives much less:

with $z_i = 150\,\mathrm{m}$ the surface layer is only about 15 m deep, so a 10 m sensor is near its top and a 100 m hub lies well above it, inside the stable layer but outside the surface layer.

The surface layer is special because, within it, the turbulent fluxes of momentum, heat and moisture are approximately constant with height: they vary by less than about ten percent from the ground to its top, $\partial\tau/\partial z \approx 0$ for the turbulent shear stress τ. For that reason it is also called the *constant-flux layer*. The near constancy follows from the thinness of the layer: the fluxes change with height only as fast as the forces that the flux divergence must balance, the pressure gradient and the Coriolis force, can absorb, and over a tenth of the boundary-layer depth they absorb only a small fraction of the surface flux. The constant-flux property is the basis of the logarithmic wind profile, of the friction velocity u_* as the single velocity scale of the layer, and of the similarity theory that corrects the profile for stability, treated in Chapter 7, Chapter 10 and Chapter 14. In the convective boundary layer the surface layer is also where the strong wind shear and the superadiabatic temperature gradient of Section 6.5.5 are concentrated.

6.4.3 The roughness sublayer

Close to the obstacles that make up a rough surface, trees, buildings, crops, the flow is spatially heterogeneous: it accelerates through gaps, slows behind each element and separates in its wake. In this layer individual obstacles matter, the wakes of neighboring elements overlap, and the mean wind at a point depends on where the point is relative to the nearest elements; the flow is not horizontally homogeneous. This layer is the *roughness sublayer*: the lowest part of the surface layer, extending from the ground to about two to five times the obstacle height h_c, in which the flow is influenced by individual roughness elements. Over short grass it is a few tens of centimeters deep and of no practical consequence; over a forest or a city it is tens of meters deep and contains the measurement.

A forest. Over a forest with a canopy height $h_c = 20\,\mathrm{m}$ the roughness sublayer extends to about $2h_c = 40\,\mathrm{m}$ to $5h_c = 100\,\mathrm{m}$. An anemometer at 30 m, $1.5h_c$, is inside it: its readings may still be strongly influenced by canopy-scale structures, the gusts that penetrate the crowns and the gaps and clearings near the mast, and they depend on the mast's position relative to them. The simple logarithmic profile, which assumes a horizontally homogeneous flow over a uniform surface, is questionable there. Two corrections that apply over tall canopies are treated in Chapter 7: the height is measured from a displacement height d inside the canopy, often taken as about two thirds of h_c, here about 13 m, so that the anemometer's effective height is $30 - 13 = 17\,\mathrm{m}$ rather than 30 m; and within the roughness sublayer the measured shear is weaker than the logarithmic profile predicts, because the wakes of the crowns add mixing. With an illustrative daytime $z_i = 1000\,\mathrm{m}$ the surface layer extends to 100 m, and the roughness sublayer fills between 40 and all of those 100 m; at night, with $z_i = 150\,\mathrm{m}$, the surface layer of about 15 m lies entirely below the treetops.

6.4.4 The inertial sublayer

Above the roughness sublayer and within the surface layer lies the *inertial sublayer*: the part of the surface layer high enough that individual roughness elements are no longer distinguishable and low enough that the fluxes are still nearly constant. Its turbulence responds to the aggregate roughness of the surface, the combined drag of all the elements, rather than to any one of them, and the flow is horizontally homogeneous over a uniform surface. The inertial sublayer is where the logarithmic profile and Monin–Obukhov similarity theory (Chapters 12 and 14) apply best, and where a measurement is most representative of an area rather than of the obstacles nearest the sensor.

The inertial sublayer exists only when the surface layer is deeper than the roughness sublayer, that is, when $0.1\,z_i$ exceeds two to five times h_c. Over short vegetation that holds by day and

at night. Over the forest of Section 6.4.3 it holds marginally by day, between about 40 and 100 m, and not at all at night. Over a city with 20 m buildings it can fail by day as well. A site whose sensors sit where the inertial sublayer is thin or absent cannot be described by a single roughness length and a logarithmic profile.

6.4.5 The vertical picture

Assembled from the bottom, the layers of the boundary layer are

surface / roughness sublayer / inertial sublayer (together, the surface layer) / mixed or residual layer / entrainment zone / free atmosphere,

with a stable boundary layer replacing the lower part of the mixed layer at night. Figure 6.4 draws the picture for an illustrative afternoon and night side by side. The vertical axis is height above the ground on a logarithmic scale, from 0.5 m to 3000 m, so that each factor of ten in height takes the same space and the thin lower layers are visible. Each column is a stack of layers; the dotted lines mark 10 m, the height of a weather-station anemometer, and 100 m, an illustrative hub height. The obstacles are taken as $h_c = 1$ m (crops or shrubs), so that the roughness sublayer ends at about 3 m; the boundary-layer depth is 1000 m in the afternoon and 200 m at night.

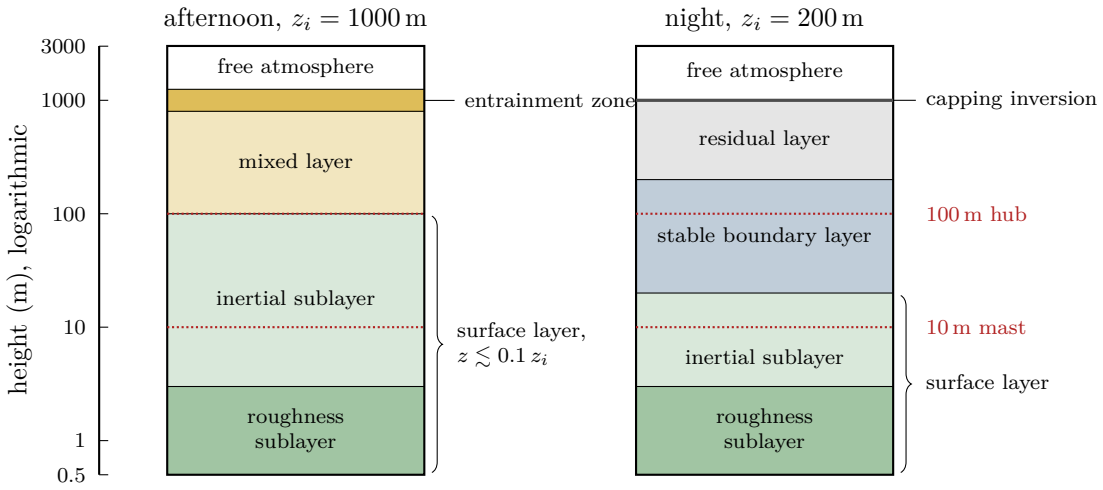


Figure 6.4: The layers of the boundary layer on a logarithmic height axis (schematic). Illustrative values: obstacle height $h_c = 1$ m, roughness sublayer to 3 m; afternoon $z_i = 1000$ m, surface layer to 100 m, entrainment zone 800 to 1250 m; night $z_i = 200$ m, surface layer to 20 m, residual layer to 1000 m. Dotted lines: 10 m and 100 m.

The figure shows why the same two heights mean different things at different times. In the afternoon the 10 m mast and the 100 m hub are both in the surface layer, the hub at its top, and both are tied to the mixed layer above. At night the mast is near the top of a 20 m surface layer and the hub is in the stable boundary layer above the surface layer, where the constant-flux assumption no longer holds and where the wind may be close to its nocturnal maximum. The picture depends on whether the boundary layer is convective, neutral or stable: a neutral boundary layer, on a cloudy and windy day or night, has a surface layer and an upper layer mixed by shear rather than by convection, without the sharp capping or the residual layer of the clear-sky cases.

6.5 Potential temperature and static stability

The stability of a layer is decided by how the buoyancy of a displaced parcel compares with that of its new surroundings, and temperature alone cannot make the comparison because air changes temperature when it moves vertically. This section derives the variable that removes that effect, potential temperature, uses it to classify stability, and describes the daytime and nighttime profiles and inversions.

6.5.1 Potential temperature

Air that moves vertically changes pressure, and with it temperature, even if no heat is added or removed. The first law of thermodynamics for a unit mass of dry air states that the heat added, δq in $\mathrm{J\,kg^{-1}}$, goes into internal energy and into work of expansion,

$$\delta q = c_v \,\mathrm{d}T + p\,\mathrm{d}\left(\frac{1}{\rho}\right), \tag{6.4}$$

where $c_v = 717\,\mathrm{J\,kg^{-1}\,K^{-1}}$ is the specific heat at constant volume and $1/\rho$ the specific volume. With the ideal-gas law $p/\rho = R_d T$, the work term is $p\,\mathrm{d}(1/\rho) = \mathrm{d}(p/\rho) - (1/\rho)\,\mathrm{d}p = R_d\,\mathrm{d}T - (1/\rho)\,\mathrm{d}p$, and since $c_v + R_d = c_p$ $(717 + 287 = 1004)$,

$$\delta q = c_p\,\mathrm{d}T - \frac{1}{\rho}\,\mathrm{d}p = c_p\,\mathrm{d}T - \frac{R_d T}{p}\,\mathrm{d}p.$$

For an *adiabatic* process, one with no heat exchanged, $\delta q = 0$ and

$$\frac{\mathrm{d}T}{T} = \frac{R_d}{c_p}\,\frac{\mathrm{d}p}{p}.$$

Integrating from the parcel's actual state (T, p) to the reference pressure $p_0 = 1000\,\mathrm{hPa}$, and calling θ the temperature the parcel has when it arrives there, $\ln(\theta/T) = (R_d/c_p)\ln(p_0/p)$, that is

$$\theta = T\left(\frac{p_0}{p}\right)^{R_d/c_p}, \qquad \frac{R_d}{c_p} = \frac{287}{1004} \approx 0.286. \tag{6.5}$$

The *potential temperature* θ, in kelvin, is the temperature a parcel of dry air would have if brought adiabatically from its pressure p to 1000 hPa. It is conserved by a parcel that moves vertically without exchanging heat, while its temperature T changes, so it removes the adiabatic effect of pressure and makes parcels at different heights comparable: two parcels with the same θ have the same density when brought to the same pressure, whatever their present temperatures. It is computed, not measured: a radiosonde or a tower measures T and p, and equation (6.5) gives θ. For moist air the comparison of densities uses the *virtual potential temperature* θ_v, the potential temperature computed from the virtual temperature T_v of Chapter 2 instead of T; it exceeds θ by about 0.6 times the specific humidity times θ, typically one or two kelvin, and is the variable used whenever buoyancy is computed.

6.5.2 The dry adiabatic lapse rate

The rate at which a parcel's temperature falls as it rises adiabatically follows from the hydrostatic relation. In a hydrostatic atmosphere, $\mathrm{d}p = -\rho g\,\mathrm{d}z$ (Chapter 2); a parcel takes the pressure of its surroundings, so with $\delta q = 0$, $c_p\,\mathrm{d}T = (1/\rho)\,\mathrm{d}p = -g\,\mathrm{d}z$ (taking the parcel's density equal to that of its surroundings, to within the small difference that produces buoyancy). The parcel's temperature therefore falls at the *dry adiabatic lapse rate*

$$\Gamma_d = -\left.\frac{\mathrm{d}T}{\mathrm{d}z}\right|_{\text{parcel}} = \frac{g}{c_p} = \frac{9.81\,\mathrm{m\,s^{-2}}}{1004\,\mathrm{J\,kg^{-1}\,K^{-1}}} = 9.77\times10^{-3}\,\mathrm{K\,m^{-1}} \approx 9.8\,\mathrm{K\,km^{-1}}. \tag{6.6}$$

(The units check: $\mathrm{J\,kg^{-1}} = \mathrm{m^2\,s^{-2}}$, so g/c_p is in $\mathrm{K\,m^{-1}}$.) Rising 1 km without exchanging heat, unsaturated air cools by almost 10 K; saturated air cools more slowly, because condensation releases heat, a refinement not needed in this chapter.

Taking the logarithm of equation (6.5) and differentiating with height relates the vertical gradient of θ to that of T in the environment:

$$\frac{1}{\theta}\frac{\mathrm{d}\theta}{\mathrm{d}z} = \frac{1}{T}\frac{\mathrm{d}T}{\mathrm{d}z} - \frac{R_d}{c_p}\frac{1}{p}\frac{\mathrm{d}p}{\mathrm{d}z} = \frac{1}{T}\frac{\mathrm{d}T}{\mathrm{d}z} + \frac{R_d}{c_p}\frac{\rho g}{p} = \frac{1}{T}\left(\frac{\mathrm{d}T}{\mathrm{d}z} + \frac{g}{c_p}\right),$$

using $\rho/p = 1/(R_d T)$ in the last step. So

$$\frac{\mathrm{d}\theta}{\mathrm{d}z} = \frac{\theta}{T}\left(\frac{\mathrm{d}T}{\mathrm{d}z} + \Gamma_d\right). \tag{6.7}$$

Potential temperature is constant with height exactly when the environment's temperature falls at the dry adiabatic rate. The standard atmosphere, with $\mathrm{d}T/\mathrm{d}z = -6.5\,\mathrm{K\,km^{-1}}$, has $\mathrm{d}\theta/\mathrm{d}z \approx 9.8 - 6.5 = 3.3\,\mathrm{K\,km^{-1}}$ (the factor θ/T is close to one in the lower atmosphere).

6.5.3 A worked value

Take a parcel at 850 hPa, about 1.4 km above the 1000 hPa level, with an illustrative temperature of 10°C = 283.15 K. Then

$$\left(\frac{1000}{850}\right)^{0.2859} = e^{\,0.2859\ln(1.1765)} = e^{\,0.2859\times 0.1625} = e^{\,0.0465} = 1.0476,$$

and

$$\theta = 283.15\,\mathrm{K} \times 1.0476 = 296.6\,\mathrm{K},$$

or 23.5°C: brought down to 1000 hPa without exchanging heat, the parcel would arrive at about 23.5°C. Compare it with surface air at 1000 hPa and 25°C, whose potential temperature equals its temperature, 298.15 K, since $p = p_0$. In temperature the air at 850 hPa is 15 K colder than the surface air; in potential temperature it is only 1.5 K colder. Most of the temperature difference is the adiabatic effect of the lower pressure aloft. The remaining 1.5 K means that θ decreases with height on average between the two levels: the layer is, on average, slightly unstable, which on a sunny afternoon is mostly the superadiabatic layer near the ground described in Section 6.5.5.

Highland stations. The same correction compares stations at different elevations. An illustrative station on a plateau at about 900 hPa reading 22°C has $\theta = 295.15\times(1000/900)^{0.286} = 295.15 \times 1.0306 \approx 304.2$ K; the coastal station at 1000 hPa and 25°C has 298.15 K. The plateau air is 3 K cooler in temperature but 6 K warmer in potential temperature: brought to the same pressure, it would be the lighter of the two.

6.5.4 Static stability

The sign of the vertical gradient of potential temperature classifies the *static stability* of a layer, its tendency to restore or to amplify a vertical displacement:

stable	$\mathrm{d}\theta/\mathrm{d}z > 0$	displacements are opposed;
neutral	$\mathrm{d}\theta/\mathrm{d}z \approx 0$	displacements are neither opposed nor amplified;
unstable	$\mathrm{d}\theta/\mathrm{d}z < 0$	displacements are amplified.

By equation (6.7) the same classes in temperature are a temperature falling more slowly than $9.8\,\mathrm{K\,km^{-1}}$ (stable), at that rate (neutral), and faster (unstable, or *superadiabatic*). For moist air θ_v replaces θ.

The displaced-parcel argument of Section 6.3.2 becomes quantitative with θ. Let a parcel start at height z_a with the potential temperature of its surroundings, and be displaced adiabatically by a small distance δz. It keeps its potential temperature $\theta(z_a)$; the surroundings at $z_a + \delta z$ have $\theta(z_a) + (\mathrm{d}\theta/\mathrm{d}z)\,\delta z$. At the same pressure the density of air is inversely proportional to its temperature, and so to its potential temperature, so the buoyancy acceleration of the parcel, $b = g(\rho_{\mathrm{env}} - \rho_{\mathrm{parcel}})/\rho_{\mathrm{parcel}}$, is

$$b \approx g\,\frac{\theta_{\mathrm{parcel}} - \theta_{\mathrm{env}}}{\theta_{\mathrm{env}}} = -\frac{g}{\theta}\,\frac{\mathrm{d}\theta}{\mathrm{d}z}\,\delta z.$$

Newton's second law for the displacement is then

$$\frac{\mathrm{d}^2\delta z}{\mathrm{d}t^2} = -N^2\,\delta z, \qquad N^2 = \frac{g}{\theta}\,\frac{\mathrm{d}\theta}{\mathrm{d}z}, \tag{6.8}$$

where N, in s^{-1}, is the *buoyancy frequency* (or Brunt–Väisälä frequency). If $N^2 > 0$ the parcel oscillates about z_a with period $2\pi/N$: the layer is stable. If $N^2 = 0$ it stays where it is put: neutral. If $N^2 < 0$ the displacement grows exponentially: unstable. For a nocturnal inversion with an illustrative $\mathrm{d}\theta/\mathrm{d}z = 3\,\mathrm{K}$ per 100 m and $\theta = 285\,\mathrm{K}$, $N^2 = 9.81{\times}0.03/285 = 1.03{\times}10^{-3}\,\mathrm{s}^{-2}$, $N = 0.032\,\mathrm{s}^{-1}$ and the period is $2\pi/0.032 \approx 195\,\mathrm{s}$, about three minutes. In the free atmosphere, with $\mathrm{d}\theta/\mathrm{d}z = 3\,\mathrm{K\,km}^{-1}$ and $\theta = 300\,\mathrm{K}$, $N \approx 0.0099\,\mathrm{s}^{-1}$ and the period is about 630 s, ten minutes. The stronger the stratification, the stiffer the restoring force and the faster the oscillation.

Figure 6.5 draws the argument. Each panel plots height against potential temperature for one stability class; the solid line is the environment's profile and the circle is a parcel starting on it at the middle height. The dashed arrows are adiabatic displacements up and down, vertical on this axis because the parcel keeps its θ; the short red arrows at their ends show the buoyancy force on the parcel in its new position. In the stable panel the parcel is colder (smaller θ) than the environment above and warmer below, and both forces point back toward the start; in the unstable panel both point away from it; in the neutral panel the parcel matches its surroundings everywhere and no force arises.

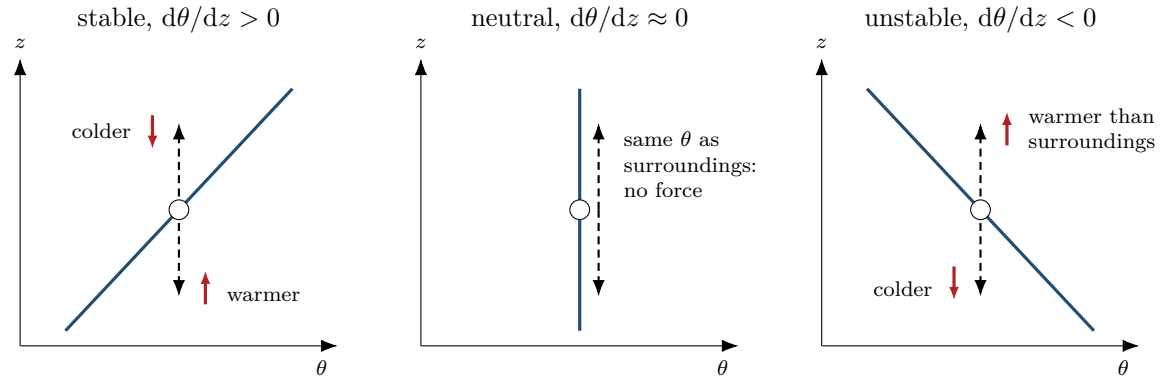


Figure 6.5: Static stability by the displaced-parcel argument. Solid line: the environment's potential temperature against height; circle: a parcel on it; dashed arrows: adiabatic displacements, at constant θ; red arrows: the buoyancy force on the displaced parcel, $b = -N^2\,\delta z$ with $N^2 = (g/\theta)\,\mathrm{d}\theta/\mathrm{d}z$ (equation (6.8)). Stable: restoring; neutral: none; unstable: amplifying.

Local and nonlocal stability. The local gradient is a good guide in the stable boundary layer and in the free atmosphere, but not everywhere in the convective layer. In the upper part of a mixed layer θ often increases slightly with height, which by the local rule is weakly stable,

yet the layer is vigorously turbulent, because thermals from the superadiabatic surface layer arrive with enough buoyancy and momentum to cross it. The stability of the convective layer as a whole is set by the surface heating, not by the gradient at one height; this is one reason the boundary-layer schemes of weather models treat convective and stable layers differently.

6.5.5 Daytime and nighttime profiles

The layers of Section 6.4 are visible in a profile of potential temperature. Figure 6.6 draws an illustrative afternoon profile and an illustrative night profile side by side. In each panel the horizontal axis is potential temperature from 288 to 308 K and the vertical axis is height from 0 to 2000 m; a dry adiabat is a vertical line on these axes, so any departure from the vertical is a departure from neutral.

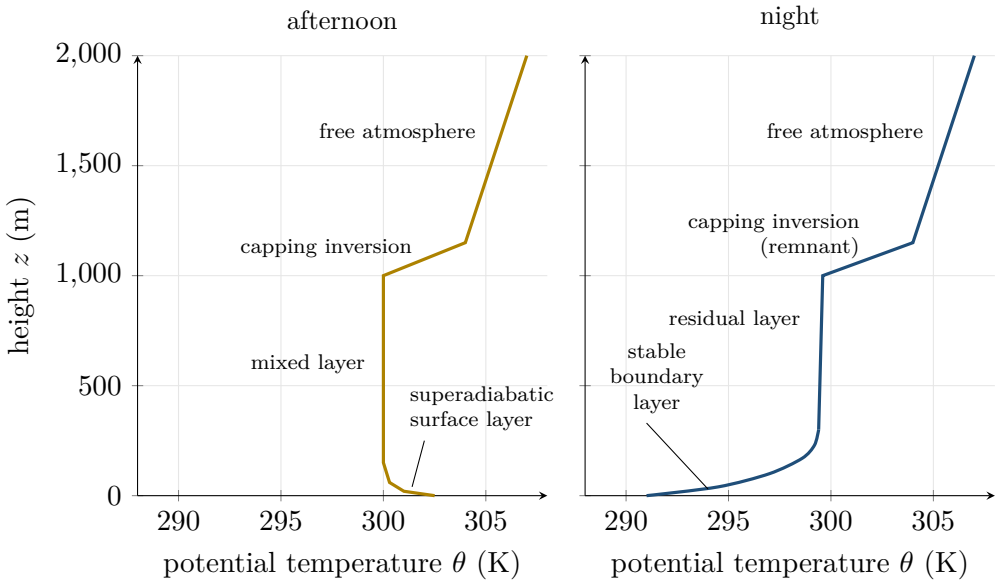


Figure 6.6: Illustrative profiles of potential temperature (drawn through chosen points). Afternoon: a superadiabatic surface layer ($\mathrm{d}\theta/\mathrm{d}z < 0$), a mixed layer with nearly constant θ to 1000 m, a capping inversion (+4 K in 150 m) and a stable free atmosphere. Night: a stable boundary layer (+8 K in the lowest 200 m or so), a nearly neutral residual layer and the remnant of the day's capping inversion.

The afternoon profile has three parts. Near the ground there is a very shallow *superadiabatic layer*, tens of meters deep, in which θ decreases with height: here 2.5 K in the lowest 150 m, most of it in the lowest 20 m. This is the surface layer of the convective boundary layer, where the surface heats the air faster than the thermals can carry the heat away. Above it, θ is nearly constant through the mixed layer, the signature of Section 6.2.2. At the top, θ increases sharply through the capping inversion, here by 4 K in 150 m, which limits the vertical mixing: thermals reaching it are colder than the air they enter and sink back, and only entrainment (Section 6.2.4) slowly lifts it.

The night profile reverses the bottom. Near the ground θ increases strongly with height through the stable boundary layer, here from 291 to about 299 K in the lowest 200 m; above it, θ is nearly constant through the residual layer at nearly the afternoon value, slightly lowered by radiative cooling; and the capping inversion of the afternoon remains above. The free atmosphere, above both, is the same in the two panels: it hardly changes between afternoon and night. The comparison is the boundary layer's daily cycle in one variable: everything that changes between the two panels is below the capping inversion.

6.5.6 Inversions and the capping inversion

An *inversion* is a layer in which the temperature itself, not only the potential temperature, increases with height, $\mathrm{d}T/\mathrm{d}z > 0$, the inverse of the usual decrease. By equation (6.7) an inversion has $\mathrm{d}\theta/\mathrm{d}z > (\theta/T)\,\Gamma_d$, about $10\,\mathrm{K\,km^{-1}}$, so it is strongly stable. Both inversions of Figure 6.6 qualify: the nocturnal surface layer, with θ rising about 8 K in 200 m, has $\mathrm{d}\theta/\mathrm{d}z \approx 40\,\mathrm{K\,km^{-1}}$, so its temperature rises by about $40 - 10 = 30\,\mathrm{K\,km^{-1}}$, some 6 K over the 200 m, a *surface inversion* or *radiation inversion*; the capping inversion, with 4 K in 150 m, has $\mathrm{d}\theta/\mathrm{d}z \approx 27\,\mathrm{K\,km^{-1}}$ and a temperature rise of about $17\,\mathrm{K\,km^{-1}}$.

An inversion suppresses turbulence, since its buoyancy frequency is large (Section 6.5.4), and therefore acts as a lid. It traps what is below it: pollutants emitted near the ground, which accumulate under a nocturnal inversion and under the capping inversion of a polluted afternoon; moisture, which may form fog or low cloud beneath it; and cold air, which pools in valleys and basins on clear nights. The *capping inversion* is the inversion, or more generally the strongly stable layer, at the top of the convective boundary layer that separates it from the free atmosphere; its base is the usual temperature-based diagnostic of z_i (Table 6.1). Not every capping layer is a true inversion: a layer in which θ increases strongly but T still decreases slightly caps the convection as effectively, and is often called an inversion in loose usage. The distinction that matters for the wind is the size of $\mathrm{d}\theta/\mathrm{d}z$, which sets the resistance to vertical mixing.

6.6 Shear, turbulence and the wind profile

The daily cycle of stability changes how the wind varies with height. This section defines vertical wind shear, names the two sources of boundary-layer turbulence, describes the intermittent turbulence of the stable layer, and then works out what all of this means for the relation between the wind at 100 m and the wind at 10 m and for the power-law profile used to connect them.

6.6.1 Vertical wind shear

Near the ground the wind speed $U(z)$ increases with height, from zero at the surface to the wind of the upper boundary layer. Its rate of change with height, $\partial U/\partial z$ in $\mathrm{s^{-1}}$, is the *vertical wind shear*; it is measured from anemometers at two or more heights on a mast, or from a lidar or a sodar profile, and it is largest near the ground. More generally the shear is the vertical derivative of the wind vector, $\partial \mathbf{V}/\partial z$, which includes a change of direction with height. In the boundary layer the wind turns with height because friction slows the wind near the surface, the Coriolis force weakens with it, and the pressure-gradient force then turns the slower air toward low pressure, as in the Ekman layer of Chapter 3. Low pressure lies to the left of the wind in the Northern Hemisphere and to its right in the Southern, so going up from the surface the wind turns clockwise, it *veers*, in the Northern Hemisphere and counterclockwise, it *backs*, in the Southern. The total turning across the boundary layer is illustratively 10 to 20° on a convective afternoon, when mixing keeps the surface wind close to the wind aloft, and 30 to 50° or more on a stable night.

Wind shear itself generates turbulence. A layer in which the wind changes with height is a layer in which neighboring parcels move at different speeds, and the velocity difference feeds eddies that mix the two, the mechanism treated next.

6.6.2 Mechanical and buoyant turbulence

Boundary-layer turbulence has two sources. *Mechanical turbulence* is turbulence produced by wind shear and by flow around obstacles: rough ground, a forest edge, buildings, and the strong shear near the surface itself. It needs no heating, it exists whenever the wind blows over a rough

surface, and it can persist at night if the shear is strong enough to overcome the stratification. *Buoyant turbulence*, or convective turbulence, is turbulence produced by unstable stratification: by day, the surface heating of Section 6.2.2 drives rising plumes that stir the whole mixed layer, and in strongly convective conditions, with a light wind and a strong sun, buoyancy dominates the production.

The two are the two production terms of the budget of turbulent kinetic energy derived in Chapter 8: shear production, $P_s = -\overline{u'w'}\,\partial U/\partial z$, positive wherever momentum is carried down the gradient of the wind, and buoyancy production, $P_b = (g/\theta)\,\overline{w'\theta'}$, positive when the heat flux is upward (unstable) and negative when it is downward (stable). By day both are positive and add; at night the buoyancy term is negative and destroys the turbulence the shear produces, which is the energy statement of Section 6.3.2. Which source dominates is a question of the wind speed and the surface heat flux together: a windy afternoon over a rough surface is mostly mechanical, a calm sunny one mostly buoyant, and the ratio of the two is the basis of the stability parameters treated in Chapters 13 and 15.

6.6.3 Intermittent turbulence in the stable layer

In a strongly stable boundary layer the turbulence is often not steady but *intermittent*: long periods of very weak turbulence, minutes to an hour, interrupted by short bursts of vigorous mixing. The bursts come from shear instabilities, gravity waves breaking in the stable layer, drainage flows of cold air down slopes, and the strong shear beneath low-level jets.

The shear-instability cycle can be followed with the gradient Richardson number of Chapter 5, $\mathrm{Ri} = (g/\theta_v)(\partial\theta_v/\partial z)/(\partial U/\partial z)^2$, whose critical value is about 0.25: turbulence is sustained below it and dies above it. Once the surface is decoupled, the air above it, relieved of the drag of the ground, accelerates; the shear across the stable layer grows until Ri falls below the critical value; a burst of turbulence mixes momentum and heat downward, reduces the shear and raises Ri; the turbulence dies, and the cycle starts again. For an illustrative layer 50 m deep with θ increasing by 3 K across it and $\theta_v \approx 288$ K, $\mathrm{Ri} = 0.25$ requires

$$\left(\frac{\Delta U}{\Delta z}\right)^2 = \frac{9.81}{288} \times \frac{3}{50} \times \frac{1}{0.25}\,\mathrm{s}^{-2} = 8.2 \times 10^{-3}\,\mathrm{s}^{-2}, \qquad \frac{\Delta U}{\Delta z} = 0.090\,\mathrm{s}^{-1},$$

a wind difference of $0.090 \times 50 = 4.5\,\mathrm{m\,s}^{-1}$ across the layer: below that, the layer stays quiet; once the acceleration aloft pushes the difference past it, the layer becomes turbulent.

The stable boundary layer is therefore qualitatively different from the daytime layer, not a weaker version of it. Its turbulence is patchy in time and in height, its fluxes are small and variable, its profiles depend on events such as a passing wave or a drainage flow, and the averaging assumptions that work by day (Chapter 8) work poorly. For near-surface wind it means that a decoupled night can produce sudden rises of the 10 m wind, by several meters per second for minutes, without any change in the large-scale weather.

6.6.4 From 100 meters to 10 meters

Let a model give $U_{100} = 12\,\mathrm{m\,s}^{-1}$ at 100 m. The wind at 10 m that goes with it depends on the state of the boundary layer. In a convective state, strong mixing keeps the profile flat above the lowest tens of meters and U_{10} is relatively large. In a neutral state, the shear is governed by the surface drag alone and the profile is logarithmic,

$$U(z) = \frac{u_*}{\kappa}\,\ln\frac{z}{z_0}, \tag{6.9}$$

with the friction velocity u_* (Chapter 10), the von Kármán constant $\kappa \approx 0.4$ and the roughness length z_0, derived in Chapter 7. In a stable state, weak mixing lets the air near the ground

slow down and U_{10} is much smaller. The mapping $U_{100} \to U_{10}$ is not geometric: it is not a fixed ratio set by the two heights, but a function of the boundary-layer state.

For the neutral case, equation (6.9) gives the ratio directly, independently of u_*:

$$\frac{U_{10}}{U_{100}} = \frac{\ln(10/z_0)}{\ln(100/z_0)} = \frac{\ln 333.3}{\ln 3333.3} = \frac{5.809}{8.112} = 0.716$$

for an illustrative grassland roughness $z_0 = 0.03\,\mathrm{m}$, so $U_{10} = 0.716 \times 12 = 8.6\,\mathrm{m\,s^{-1}}$. For the convective and stable cases the logarithmic profile is corrected for stability, by a method treated in Chapter 14; Figure 6.7 and Table 6.2 use that correction with illustrative parameters. In the figure the horizontal axis is wind speed and the vertical axis height on a logarithmic scale from 1 to 150 m, on which the neutral profile of equation (6.9) is a straight line. The three solid or dashed curves are the convective, neutral and stable profiles, all passing through $12\,\mathrm{m\,s^{-1}}$ at 100 m (the dotted horizontal lines mark 10 and 100 m); the gray curve is the fixed power law of Section 6.6.5 with the exponent 1/7.

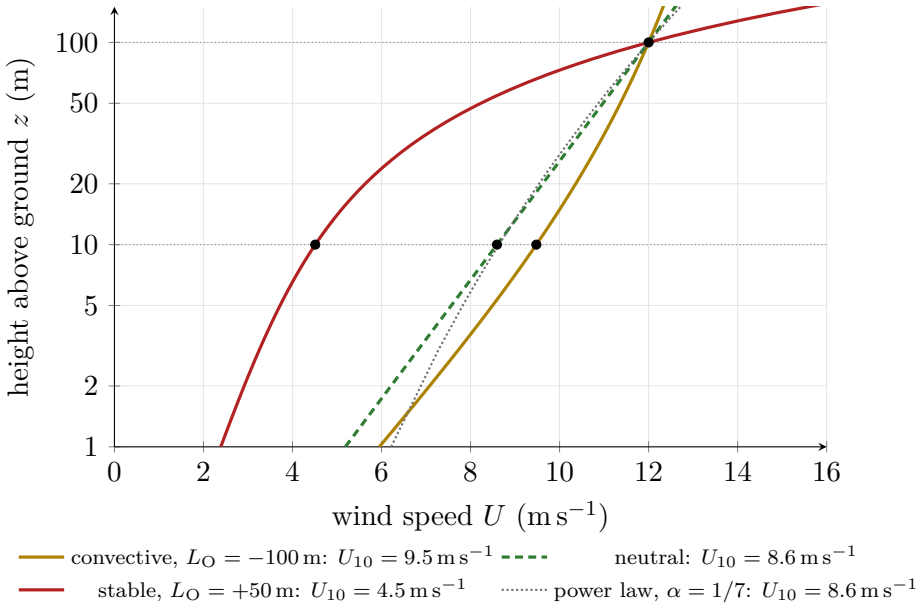


Figure 6.7: Three wind profiles with the same $U_{100} = 12\,\mathrm{m\,s^{-1}}$ over the same surface ($z_0 = 0.03\,\mathrm{m}$), computed from the stability-corrected logarithmic profile $U = (u_*/\kappa)[\ln(z/z_0) - \psi_m(z/L_O)]$ treated in Chapter 14, with Businger–Dyer forms of ψ_m and illustrative Obukhov lengths $L_O = -100\,\mathrm{m}$ (convective), infinite (neutral) and $+50\,\mathrm{m}$ (stable; the stable form is used beyond its usual range, as a shape). Gray dotted: $U = 12\,(z/100)^{1/7}$. Data: `scripts/ch06_data.py`.

Table 6.2: The 10 m wind implied by $U_{100} = 12\,\mathrm{m\,s^{-1}}$ in three states (Figure 6.7), and the decoupled night of Section 6.3.3 for comparison. The exponent is $\alpha = \ln(U_{100}/U_{10})/\ln 10$, equation (6.11).

State	U_{100} ($\mathrm{m\,s^{-1}}$)	U_{10} ($\mathrm{m\,s^{-1}}$)	U_{10}/U_{100}	α
Convective	12	9.5	0.79	0.10
Neutral	12	8.6	0.72	0.145
Stable	12	4.5	0.38	0.42
Decoupled night	15	2.0	0.13	0.88

The convective and neutral profiles are close: at a 100 m wind of $12\,\mathrm{m\,s^{-1}}$ the shear production is large, L_O is long and the convective correction is modest, giving 9.5 against $8.6\,\mathrm{m\,s^{-1}}$. The

stable profile is far from both: the same $12\,\mathrm{m\,s^{-1}}$ at 100 m comes with $4.5\,\mathrm{m\,s^{-1}}$ at 10 m, half the neutral value. Between day and night, then, the forecast at 100 m can be identical while the 10 m wind differs by a factor of two, and on a decoupled night by more. The stability of the boundary layer is a second input to the mapping, as necessary as the wind aloft.

6.6.5 The power-law profile

A common engineering shortcut connects the wind at two heights by a power law,

$$\frac{U(z_2)}{U(z_1)} = \left(\frac{z_2}{z_1}\right)^{\alpha}, \tag{6.10}$$

with a fixed *shear exponent* α, often $1/7 \approx 0.14$. It is a convenient empirical profile with no physical derivation: it is a curve with one parameter that can be fitted between two heights. Given speeds at two heights, the exponent they imply is

$$\alpha = \frac{\ln\big(U(z_2)/U(z_1)\big)}{\ln(z_2/z_1)}. \tag{6.11}$$

For the two illustrative profiles of Figure 6.7 that bracket the daily cycle, the convective with $U_{10} = 9.48\,\mathrm{m\,s^{-1}}$ and the stable with $U_{10} = 4.51\,\mathrm{m\,s^{-1}}$,

$$\alpha_{\mathrm{conv}} = \frac{\ln(12/9.48)}{\ln 10} = \frac{0.236}{2.303} = 0.10, \qquad \alpha_{\mathrm{stab}} = \frac{\ln(12/4.51)}{\ln 10} = \frac{0.979}{2.303} = 0.42,$$

and for the decoupled night of Section 6.3.3, $\alpha = \ln(15/2)/\ln 10 = 2.015/2.303 = 0.88$. Even the neutral exponent is not fixed: equation (6.9) gives $\alpha = \ln[\ln(100/z_0)/\ln(10/z_0)]/\ln 10$, which is 0.145 for $z_0 = 0.03\,\mathrm{m}$ but $\ln(5.298/2.996)/2.303 = 0.25$ for an illustrative rough surface with $z_0 = 0.5\,\mathrm{m}$.

The exponent is therefore not universal. It changes with stability, with roughness, with terrain and with the time of day, and nighttime stable profiles have much stronger shear than the daytime ones; the value 1/7 corresponds, roughly, to neutral flow over short grass. The error of a fixed exponent is largest exactly when stability departs most from neutral. With $\alpha = 1/7$ the forecast $U_{100} = 12\,\mathrm{m\,s^{-1}}$ gives $U_{10} = 12 \times 10^{-1/7} = 12 \times 0.720 = 8.6\,\mathrm{m\,s^{-1}}$: about $0.9\,\mathrm{m\,s^{-1}}$ too low against the convective $9.5\,\mathrm{m\,s^{-1}}$, and about $4.1\,\mathrm{m\,s^{-1}}$, or 90 percent, too high against the stable $4.5\,\mathrm{m\,s^{-1}}$. In the other direction, extrapolating a stable-night measurement of $4.5\,\mathrm{m\,s^{-1}}$ at 10 m upward with $\alpha = 1/7$ gives $4.5 \times 10^{1/7} = 6.3\,\mathrm{m\,s^{-1}}$ at 100 m instead of $12\,\mathrm{m\,s^{-1}}$; since the power in the wind scales with the cube of the speed, the available wind power at the hub is underestimated by a factor of $(6.3/12)^3 \approx 0.14$. For a transmission line rated from a forecast aloft, the stable-night error has the unsafe sign: it overstates the wind at the conductor, and with it the convective cooling.

> **Principle 6.1.** *The ratio between the wind at two heights in the boundary layer is a property of the boundary-layer state, not of the heights alone; a fixed profile exponent is wrong in proportion to how far the stability departs from neutral, and most wrong on stable nights.*

6.6.6 The coupling problem

The chapter's material can be assembled into one chain. Figure 6.8 draws it as a sequence of boxes from left to right: the free-atmosphere wind set by the large-scale pressure field; the boundary-layer coupling, the vertical transport of momentum by turbulence; the surface-layer wind at the heights of engineering interest; and the sensor or the equipment that experiences it.

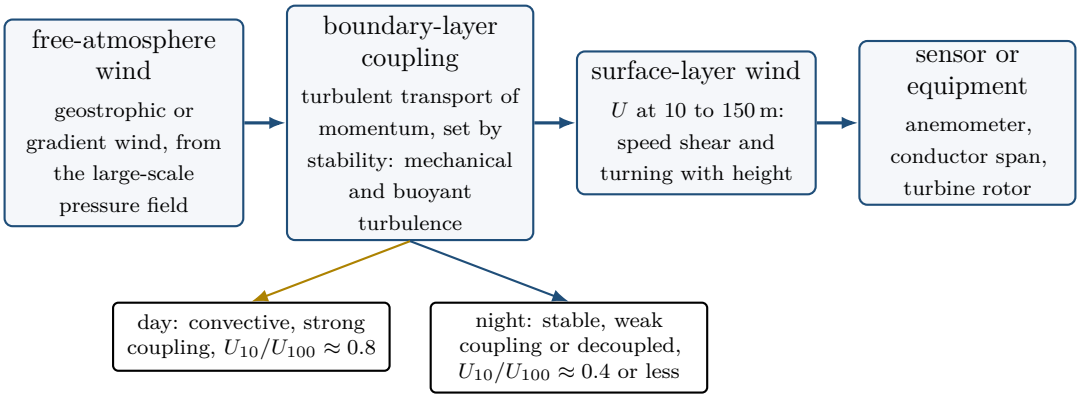


Figure 6.8: Near-surface wind as a coupling problem (schematic). The free-atmosphere wind is the forcing; the boundary layer transmits it to the surface layer with an efficiency set by stability and turbulence; the sensor or the equipment sees the result. Ratios are those of Table 6.2.

The two boxes below the coupling stage are its two regimes, day and night, with illustrative ratios of the 10 m to the 100 m wind from Table 6.2.

Read from left to right, the figure is the chapter's answer to its question. The free-atmosphere wind is what the large-scale forcing produces and what a weather model forecasts best. The surface-layer wind is what the ground, the sensor and the equipment experience. The boundary layer couples the two, and the strength of the coupling is set by stability and turbulence: strong by day, when buoyant and mechanical turbulence move momentum through the whole layer; weak at night, when stratification suppresses the vertical motions, and sometimes absent, when the surface decouples. Every quantity of the chapter is a piece of that coupling: the depth z_i over which it acts, the potential temperature gradient that measures its resistance, the shear that drives it, and the memory that carries it from one hour to the next.

6.7 What to retain

Definition 6.1 (The atmospheric boundary layer)**.** The atmospheric boundary layer is the lowest part of the atmosphere, 100 m to 2000 m and more deep, that responds to the surface within about an hour; it translates the large-scale wind of the free atmosphere into the near-surface wind, and the main control on that translation is whether turbulence can move momentum vertically, which the daily cycle of surface heating and cooling turns up by day and down at night.

Table 6.3 lists the terms of the chapter, their meaning, their units and the subsection that defines each.

6.8 Exercises

Exercise 6.1. A radiosonde launched in the early afternoon reports 24.0°C at 1000 hPa, 18.0°C at 925 hPa, 12.0°C at 850 hPa, 14.0°C at 800 hPa and 11.0°C at 750 hPa; the levels are about 0, 670, 1380, 1890 and 2430 m above the 1000 hPa level. (a) Compute θ at each level with $R_d/c_p = 0.286$. (b) Compute $\mathrm{d}\theta/\mathrm{d}z$ in $\mathrm{K\,km^{-1}}$ for each of the four layers and classify each as stable, near neutral or unstable. (c) Which layer is an inversion in the sense of Section 6.5.6? Estimate z_i and name the diagnostic of Table 6.1 on which the estimate rests. (d) Compute the buoyancy frequency and the oscillation period in the inversion layer.

Exercise 6.2. A forecast gives $U_{100} = 11\,\mathrm{m\,s^{-1}}$ at a site with $z_0 = 0.03\,\mathrm{m}$. Measurements on two days at the same forecast give $U_{10} = 8.5\,\mathrm{m\,s^{-1}}$ at 14:00 and $U_{10} = 3.0\,\mathrm{m\,s^{-1}}$ at 03:00. (a)

Table 6.3: The terms of the chapter and where each is defined.

Term	Meaning	Units	Defined in
ABL, PBL	atmospheric or planetary boundary layer: the layer that responds to the surface within about an hour	–	6.1.1
Free atmosphere	air above the boundary layer, governed by pressure gradient, Coriolis and large-scale dynamics	–	6.1.3
Convective boundary layer	daytime boundary layer whose turbulence is driven mainly by surface heating	–	6.2.2
Mixed layer	the convective layer, in which θ, humidity and wind are nearly uniform with height	–	6.2.2
Convective velocity scale w_*	velocity of the thermals, equation (6.1)	m/s	6.1.1
Entrainment zone	layer at the top of the convective boundary layer where free-atmosphere air is incorporated	m	6.2.4
Stable boundary layer	nighttime layer of stable stratification near the ground, turbulence from shear only	–	6.3.1
Decoupling	state in which the surface layer is dynamically disconnected from the flow above	–	6.3.3
Residual layer	remnant of the previous day's mixed layer above the stable boundary layer	–	6.3.4
Boundary-layer height z_i	depth of the boundary layer, defined by the diagnostic used	m	6.4.1
Surface layer	lowest tenth of the boundary layer, with nearly constant fluxes	m	6.4.2
Roughness sublayer	lowest part, to about 2 to 5 h_c, where individual obstacles shape the flow	m	6.4.3
Inertial sublayer	part of the surface layer above the roughness sublayer, responding to aggregate roughness	m	6.4.4
Potential temperature θ	$T(p_0/p)^{R_d/c_p}$, temperature brought adiabatically to 1000 hPa	K	6.5.1
Dry adiabatic lapse rate Γ_d	$g/c_p \approx 9.8\,\mathrm{K\,km^{-1}}$, cooling of a rising unsaturated parcel	K/m	6.5.2
Static stability	stable, neutral, unstable as $\mathrm{d}\theta/\mathrm{d}z > 0, \approx 0, < 0$	–	6.5.4
Buoyancy frequency N	$\sqrt{(g/\theta)\,\mathrm{d}\theta/\mathrm{d}z}$, oscillation frequency of a displaced parcel	1/s	6.5.4
Inversion	layer with $\mathrm{d}T/\mathrm{d}z > 0$; strongly stable; a lid on mixing	–	6.5.6
Vertical wind shear	$\partial U/\partial z$ or $\partial \mathbf{V}/\partial z$	1/s	6.6.1
Mechanical turbulence	turbulence produced by shear and obstacles	–	6.6.2
Buoyant turbulence	turbulence produced by unstable stratification	–	6.6.2
Shear exponent α	exponent of the power-law profile, equation (6.11); not universal	–	6.6.5

Compute the shear exponent implied by each pair. (b) Compute the 10 m wind that a fixed exponent $\alpha = 1/7$ predicts, and its error against each measurement in $\mathrm{m\,s^{-1}}$ and in percent. (c) Compute the neutral ratio U_{10}/U_{100} from equation (6.9) and compare. (d) A transmission line at 12 m is rated with the fixed-exponent wind. On which of the two occasions is the rating unsafe, and why?

Exercise 6.3. A wind-resource mast stands in a clearing of a forest with $h_c = 18\,\mathrm{m}$. Anemometers are mounted at 10, 30, 60 and 100 m. (a) Give the range of heights of the roughness sublayer. (b) With $z_i = 1200\,\mathrm{m}$ on an afternoon and $z_i = 120\,\mathrm{m}$ at night, give the depth of the surface layer in each case. (c) For each anemometer and each case, state whether it lies in the roughness sublayer, the inertial sublayer, or above the surface layer. (d) Which anemometer, if any, can be used with a simple logarithmic profile, and in which case? Take the displacement height as $\frac{2}{3}h_c$ and give the effective height of that anemometer.

Exercise 6.4. At a site at 30°S the free-atmosphere wind is a steady westerly of $14\,\mathrm{m\,s^{-1}}$ (blowing from 270°). (a) On which side of the wind does low pressure lie, and in which direction, toward north or south, is the surface wind turned? (b) The surface wind is turned by 20° from the free-atmosphere direction on a convective afternoon and by 45° on a stable night. Give the direction the surface wind blows from in each case, in degrees clockwise from north. (c) Going up from the surface, does the wind veer or back? Give the answers to (a) to (c) for the same situation at 30°N. (d) On the stable night the morning mixed layer must remove a θ deficit of 6 K at the ground decreasing linearly to zero at 180 m, with a mean surface kinematic heat flux of $0.08\,\mathrm{K\,m\,s^{-1}}$. Estimate how long after the heat flux turns upward the surface is recoupled to the flow aloft.

Chapter 7

The Surface Layer

7.1 The surface layer and its constant flux

The atmospheric boundary layer of Chapter 6 is the part of the atmosphere that feels the ground. Within it, one thin slice feels the ground directly: the lowest few tens of meters, where the drag of the surface and the exchange of heat with it control the wind more than the pressure gradient, the Coriolis force or the depth of the boundary layer do. Most engineering wind lives in that slice. A weather station anemometer at 10 m, a conductor of a transmission line at 15 to 40 m and the lower half of a wind turbine rotor are all in it. The question of this chapter is

why does the lowest part of the boundary layer have its own theory, and what does that theory give for the wind profile?

The chapter first locates the surface layer and shows, by an order-of-magnitude argument, that the vertical flux of momentum changes little across it. It then derives the wind shear from that constant flux and Prandtl's mixing length, integrates the shear into the logarithmic wind profile, and works the profile through with numbers. It explains the two surface parameters of the profile, the roughness length and the displacement height; the adjustment of the flow where the surface changes, through fetch and internal boundary layers; and the departures from the logarithmic profile caused by stability. It ends with the list of assumptions under which the theory holds and how real sites violate them. Three quantities, the friction velocity u_*, the roughness length z_0 and the dimensionless height $\ln(z/z_0)$, are the working tools of the chapter; two more, the Obukhov length L_O and the ratio z/L_O that measures stability, appear here only by name and are treated in Chapters 14 and 15.

Jargon: surface layer, constant-flux layer, Reynolds decomposition, momentum flux, surface stress, friction velocity

The *surface layer* is the lowest part of the atmospheric boundary layer, roughly its lowest 5 to 10 %, in which the turbulent exchange of momentum and heat with the surface dominates the wind. It is also called the *constant-flux layer*, because the vertical turbulent fluxes of momentum and heat change by only a small fraction of their surface values across it. The *Reynolds decomposition* writes each instantaneous variable as its mean over an averaging period plus a fluctuation, $u = \overline{u} + u'$. The *momentum flux* is the covariance $\overline{u'w'}$ ($\mathrm{m^2/s^2}$), the vertical transport of horizontal momentum per unit mass by turbulent eddies. The *surface stress* $\tau_0 = -\rho\,\overline{u'w'}$ (Pa) is the horizontal force per unit area that the air and the ground exert on each other. The *friction velocity* $u_* = \sqrt{\tau_0/\rho}$ (m/s) is the velocity scale of that stress; it is not a wind speed.

Key idea

Near the ground the momentum flux is nearly constant with height, while the size of the eddies that carry it grows in proportion to the distance from the ground. A constant flux carried by eddies of size κz requires a shear $u_*/(\kappa z)$, and integrating that shear gives the logarithmic wind profile, $U(z) = (u_*/\kappa)\ln[(z-d)/z_0]$ under neutral stability.

7.1.1 Position in the boundary layer

The surface layer occupies roughly the lowest 5 to 10 % of the boundary layer. With a boundary-layer depth $z_i = 1000\,\mathrm{m}$, a typical afternoon value over land, it extends to about 50 to 100 m. At night, when the boundary layer may be only $z_i = 200\,\mathrm{m}$ deep, it extends to only 10 to 20 m. The fraction is a rule of thumb, not a definition: the surface layer is defined by the behavior of the fluxes, described in the next subsection, and its top is the height at which that behavior stops being a good approximation.

Figure 7.1 places the surface layer in the boundary layer. The vertical axis is height from the ground to above z_i; the horizontal axis is the turbulent shear stress τ relative to its surface value τ_0. The blue line is an idealized stress profile that falls linearly from τ_0 at the ground to zero at the top of the boundary layer, a common approximation for a well-mixed boundary layer. The shaded band is the lowest 10 % of the boundary layer, and the dotted line marks $\tau = 0.9\,\tau_0$.

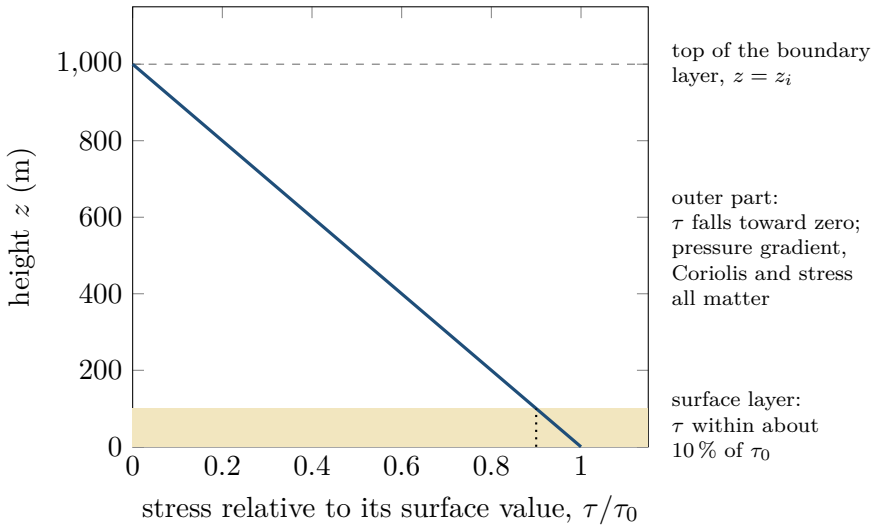


Figure 7.1: The surface layer within the boundary layer. Blue: idealized stress profile $\tau/\tau_0 = 1 - z/z_i$ for $z_i = 1000\,\mathrm{m}$. Shaded: the lowest 10 % of the boundary layer, $z < 100\,\mathrm{m}$, across which the stress stays within 10 % of its surface value (dotted line at 0.9).

The figure makes one point. Across the shaded band the stress changes from τ_0 to $0.9\,\tau_0$, a change of 10 %; across the rest of the boundary layer it changes from $0.9\,\tau_0$ to zero. The wind speed behaves the other way round: it rises from zero at the surface to most of its boundary-layer value within the shaded band, as Section 7.3 shows. Many engineering wind measurements, at 10, 20, 40 or 60 m, lie in the surface layer by day and in strong wind, and some of them lie above it at night, when the surface layer is thin.

7.1.2 Why the flux varies little with height

The near-constancy of the stress follows from the horizontal momentum balance. Take the mean flow to be steady and horizontally homogeneous, so that the mean wind does not change with

time or with horizontal position. The horizontal momentum equation of the boundary layer then reduces to a balance of three forces per unit mass: the pressure-gradient force, the Coriolis force and the vertical divergence of the turbulent momentum flux. Writing the pressure-gradient force through the geostrophic wind, $-(1/\rho)\nabla_h p = f\,\mathbf{k}\times\mathbf{V}_g$, the balance is

$$0 = -f\,\mathbf{k}\times(\mathbf{V}-\mathbf{V}_g) + \frac{1}{\rho}\frac{\partial \boldsymbol{\tau}}{\partial z}, \qquad \boldsymbol{\tau} = -\rho\left(\overline{u'w'},\ \overline{v'w'}\right), \tag{7.1}$$

where $\boldsymbol{\tau}$ is the turbulent stress vector and $\overline{u'w'}$ and $\overline{v'w'}$ are the vertical fluxes of the two horizontal velocity components. The difference $\mathbf{V}-\mathbf{V}_g = \mathbf{V}_a$ is the ageostrophic wind. Taking magnitudes, and treating ρ as constant over the depth considered,

$$\left|\frac{\partial(\boldsymbol{\tau}/\rho)}{\partial z}\right| = |f|\,|\mathbf{V}_a|, \tag{7.2}$$

which holds in both hemispheres because only $|f|$ appears. The stress changes with height only as fast as the Coriolis force acting on the ageostrophic wind allows.

Integrate equation (7.2) across the lowest layer of depth Δz. The change of the kinematic stress is at most

$$\Delta\left|\frac{\boldsymbol{\tau}}{\rho}\right| \le |f|\,|\mathbf{V}_a|\,\Delta z, \tag{7.3}$$

with $|\mathbf{V}_a|$ the largest ageostrophic speed in the layer. Take illustrative middle-latitude values: $|f| = 10^{-4}\,\mathrm{s^{-1}}$; a geostrophic wind of $10\,\mathrm{m\,s^{-1}}$ and a near-surface wind of $6\,\mathrm{m\,s^{-1}}$ crossing the isobars at 25°, which give $|\mathbf{V}_a| = \sqrt{10^2+6^2-2\times10\times6\cos25^\circ} \approx 5.2\,\mathrm{m\,s^{-1}}$, near the largest the ageostrophic wind becomes; and a surface friction velocity $u_* = 0.5\,\mathrm{m\,s^{-1}}$, so that $\tau_0/\rho = u_*^2 = 0.25\,\mathrm{m^2\,s^{-2}}$. For $\Delta z = 50\,\mathrm{m}$, the lowest 5 % of a 1000 m boundary layer,

$$\Delta\left|\frac{\boldsymbol{\tau}}{\rho}\right| \le 10^{-4}\,\mathrm{s^{-1}}\times 5.2\,\mathrm{m\,s^{-1}}\times 50\,\mathrm{m} = 0.026\,\mathrm{m^2\,s^{-2}},$$

about 10 % of u_*^2. For $\Delta z = 100\,\mathrm{m}$ the bound doubles, to about 20 %. Over the whole boundary layer the same balance must remove all of the surface stress, and it does so because $|\mathbf{V}_a|\Delta z$ accumulates over 1000 m: an average ageostrophic speed of $2.5\,\mathrm{m\,s^{-1}}$ over 1000 m gives $10^{-4}\times 2.5\times 1000 = 0.25\,\mathrm{m^2\,s^{-2}}$, the whole of u_*^2.

Across the same lowest 50 m, the wind speed changes from zero near the ground to about $7.8\,\mathrm{m\,s^{-1}}$ in the worked example of Section 7.3.3, a change of order 100 %. The stress is thus constant to within 10 to 20 % while the wind changes completely; that contrast is what "constant flux" means. It holds only as long as the assumptions behind equation (7.1) hold: a mean flow that is steady and horizontally homogeneous. The direction of the stress also changes little across the layer, so the wind direction in the surface layer turns by only a few degrees; most of the turning of the wind with height described in Chapter 3 happens above it.

Principle 7.1. *In the surface layer the turbulent fluxes are nearly independent of height, to within about* 10 *to* 20 %*, while the wind speed changes from zero to most of its boundary-layer value. A single surface value of each flux therefore characterizes the whole layer.*

The consequence is the reason the surface layer has its own theory. If the flux is the same at every height in the layer, then the flux at the surface, a single number, describes the turbulence at every height, and the wind profile can depend only on that number, on the height and on a few properties of the surface. Relations of this kind, in which a profile is fixed by a small set of scales, are called *similarity relations*; the logarithmic profile of Section 7.3 is the simplest of them.

7.1.3 Momentum flux, surface stress and friction velocity

The flux that is constant is a turbulent one, and it is defined through the Reynolds decomposition. Each instantaneous velocity component is split into its mean over an averaging period, typically 10 to 30 min, and a fluctuation about that mean,

$$u = \overline{u} + u', \qquad w = \overline{w} + w', \tag{7.4}$$

so that $\overline{u'} = \overline{w'} = 0$ by construction. In this chapter x points along the mean wind, so $\overline{u} = U$ and $\overline{v} = 0$. Near flat ground the mean vertical velocity $\overline{w}$ is nearly zero, since air cannot flow through the surface, but the fluctuation w' is not: eddies move air up and down continually. The average of the product $u'w'$, the covariance $\overline{u'w'}$, measures how these vertical motions transport horizontal momentum. It is the *turbulent momentum flux*, in kinematic units of $\mathrm{m^2/s^2}$. Chapter 9 treats the statistics and the measurement of such fluxes; this chapter needs only their sign and their magnitude.

The sign of the flux. When the wind increases with height, an eddy that moves air downward ($w' < 0$) brings air from a level where the mean wind is faster, so it arrives with $u' > 0$; an eddy that moves air upward ($w' > 0$) brings slower air, $u' < 0$. In both cases $u'w' < 0$, and on average $\overline{u'w'} < 0$ near the surface. With the sign convention of this book, fluxes positive upward, a negative $\overline{u'w'}$ is a downward flux of along-wind momentum: momentum is carried from the faster air aloft toward the ground, where it is removed by drag.

Surface stress. The rate at which momentum is delivered to the ground per unit area is a force per unit area, the surface stress

$$\tau_0 = -\rho\,\overline{u'w'}\big|_{\text{surface}}, \tag{7.5}$$

in pascals ($\mathrm{N\,m^{-2}} = \mathrm{kg\,m^{-1}\,s^{-2}}$), written here for the one-dimensional case with the stress aligned with the mean wind. In the constant-flux layer the value at the surface and the value at any height in the layer are the same to the accuracy of Section 7.1.2. The atmosphere transfers momentum to the ground, and the ground exerts an equal and opposite drag on the atmosphere.

Friction velocity. Stress has units of $\mathrm{kg\,m^{-1}\,s^{-2}}$; dividing by the density ($\mathrm{kg\,m^{-3}}$) leaves $\mathrm{m^2\,s^{-2}}$, the square of a velocity. Its square root is the *friction velocity*,

$$u_* = \sqrt{\frac{\tau_0}{\rho}} = \sqrt{-\overline{u'w'}}, \tag{7.6}$$

in m/s. It is not the speed of any air: it is a velocity scale derived from the surface stress, the characteristic strength of turbulent momentum transfer near the ground. A larger u_* means a stronger stress and a stronger turbulent exchange. Chapter 10 treats how u_* is measured or inferred, its relation to a drag coefficient, and its direction when the stress is a vector.

7.1.4 Typical values of the friction velocity

The friction velocity is about $0.1\,\mathrm{m\,s^{-1}}$ in weak winds and 0.5 to $1\,\mathrm{m\,s^{-1}}$ in strong winds over rough terrain. With $\rho = 1.2\,\mathrm{kg\,m^{-3}}$, equation (7.6) turns these into stresses:

$$\begin{aligned}
u_* = 0.1\,\mathrm{m\,s^{-1}}: &\quad \tau_0 = \rho\,u_*^2 = 1.2 \times 0.1^2\,\mathrm{Pa} = 0.012\,\mathrm{Pa},\\
u_* = 0.5\,\mathrm{m\,s^{-1}}: &\quad \tau_0 = 1.2 \times 0.5^2\,\mathrm{Pa} = 0.30\,\mathrm{Pa},\\
u_* = 1\,\mathrm{m\,s^{-1}}: &\quad \tau_0 = 1.2 \times 1^2\,\mathrm{Pa} = 1.2\,\mathrm{Pa}.
\end{aligned}$$

A stress of 1 Pa is small as a force, one newton on a square meter, but it acts on every square meter of the ground at once, and it is what the boundary layer has to supply by drawing momentum down from aloft.

The friction velocity is not a property of the surface alone. It depends on the wind speed, which sets how much momentum there is to transfer; on the roughness of the surface, which sets how efficiently the surface extracts it (Section 7.4); and on the stability of the air, which enhances or suppresses the turbulence that carries it (Section 7.6). The same field has a small u_* on a calm night and a large one in a windy afternoon. Roughly, for a given surface and stability, u_* is proportional to the wind speed at a fixed height; the profile of Section 7.3 makes the proportionality exact under neutral conditions.

7.2 From stress to shear

This section explains why the wind increases with height near the ground, introduces the mixing length that relates the turbulent flux to the shear, and derives the neutral shear relation in two ways: from the constant stress and the mixing length, and from dimensional analysis.

7.2.1 The origin of shear

At the ground the air is at rest relative to the surface; a few millimeters above a smooth surface viscosity enforces that, and among the elements of a rough surface the drag of grass blades, crops, trees and buildings does the same in an averaged sense. Higher up, the wind is driven by the pressure gradient and approaches the boundary-layer wind. The mean wind therefore increases with height, $\partial U/\partial z > 0$: there is *vertical wind shear*, the rate of change of the mean wind speed with height, in s^{-1}.

The shear and the stress maintain one another. Surface drag slows the lowest air and creates shear; shear feeds turbulence, because eddies moving vertically through a sheared mean flow carry fluctuations of horizontal velocity and extract energy from the mean flow (Chapter 8 gives the energy budget); turbulence carries momentum downward, which is the stress; and the stress, delivered to the ground, is the drag. The chain is

$$\text{surface drag} \;\rightarrow\; \text{wind shear} \;\rightarrow\; \text{turbulence} \;\rightarrow\; \text{downward momentum transfer} \;\rightarrow\; \text{surface drag}.$$

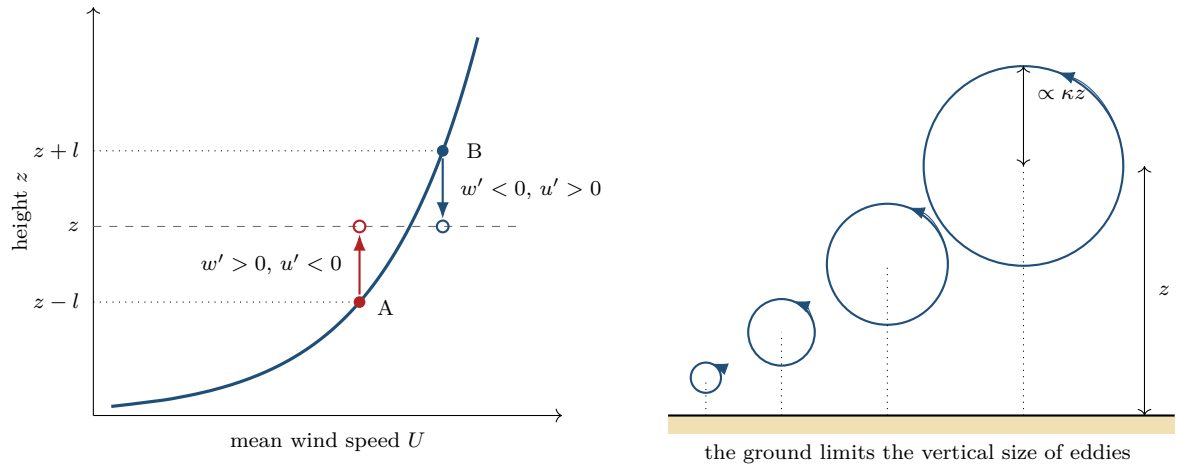
To close the loop quantitatively, the flux has to be related to the shear. The mixing length does that.

7.2.2 The mixing length

Prandtl's mixing-length argument treats an eddy as moving a parcel of air vertically over a characteristic distance before the parcel mixes with its new surroundings. Figure 7.2(a) draws the argument. The horizontal axis is the mean wind speed and the vertical axis height; the blue curve is the mean profile $U(z)$. The dashed line is a reference level z, and the dotted lines are the levels $z - l$ and $z + l$, one mixing length below and above it. Parcel A (red) starts at $z - l$ and rises to z; parcel B (blue) starts at $z + l$ and sinks to z. Each keeps the horizontal velocity of its starting level, marked by its vertical arrow. Panel (b) draws eddies whose size is proportional to their height above the ground, the subject of Section 7.2.3.

Write the argument out. A parcel displaced upward by a distance $l' > 0$ from level $z - l'$ to level z keeps the mean wind of its origin, $U(z - l') \approx U(z) - l'\,\partial U/\partial z$, by a first-order Taylor expansion. At level z it therefore differs from the mean wind by

$$u' = -l'\,\frac{\partial U}{\partial z}. \tag{7.7}$$



(a) the parcel argument

(b) eddy size grows with height

Figure 7.2: The mixing length (schematic). (a) Prandtl's argument: parcel A, displaced upward from $z-l$, arrives at z slower than the mean wind there; parcel B, displaced downward from $z+l$, arrives faster. Both give $u'w' < 0$. (b) Eddies near the ground: an eddy centered at height z cannot extend much farther vertically than its distance to the ground, so the mixing length grows in proportion to z.

The same expression holds for a downward displacement, with $l' < 0$ and $u' > 0$. The vertical velocity of the parcel has the sign of its displacement, and Prandtl assumed that its magnitude is of the same order as $|u'|$, since eddies stir the air in all directions with comparable speeds: $w' = c\,l'\,|\partial U/\partial z|$ with c a positive constant of order one. The product is

$$u'w' = -c\,l'^2 \left|\frac{\partial U}{\partial z}\right| \frac{\partial U}{\partial z},$$

negative whatever the sign of the displacement, as Figure 7.2(a) shows. Averaging over many parcels and collecting the unknown constant and the mean square displacement into a single length, $l^2 = c\,\overline{l'^2}$, gives

$$-\overline{u'w'} = l^2 \left|\frac{\partial U}{\partial z}\right| \frac{\partial U}{\partial z}. \tag{7.8}$$

The *mixing length* l, in meters, is the characteristic vertical distance over which eddies move air before it mixes. It is not measured directly; it is defined by equation (7.8) and estimated from measured fluxes and profiles.

7.2.3 Growth of the mixing length with height

Near the ground the eddies that carry momentum are limited in size by the ground itself. An eddy whose center is at 1 m cannot move air vertically over tens of meters, because the ground is 1 m below it; an eddy centered at 100 m can. Figure 7.2(b) shows this: each circle is an eddy whose size is a fixed fraction of the height of its center. The simplest assumption consistent with the picture is that the mixing length is proportional to height,

$$l = \kappa z, \tag{7.9}$$

with $\kappa \approx 0.4$, the *von Kármán constant*, a dimensionless number determined by experiment and taken as universal for neutral surface layers (published values lie between about 0.38 and 0.42). At 10 m, $l = 4$ m; at 50 m, $l = 20$ m.

Equation (7.9) is an idealization. It holds at heights large compared with the roughness elements and small compared with the boundary-layer depth. Above the surface layer the

mixing length stops growing in proportion to height, limited by the depth of the turbulent layer, and empirical forms that make l approach a constant aloft are used in that region; within a canopy, the size of the eddies is set by the canopy elements rather than by the height. Neither region is covered by the theory of this chapter.

7.2.4 Eddy viscosity

Equation (7.8) has the form of a diffusion law: the flux is proportional to the gradient of the mean wind, down the gradient. The proportionality factor is the *eddy viscosity*, or eddy diffusivity for momentum,

$$-\overline{u'w'} = K_m \frac{\partial U}{\partial z}, \qquad K_m = l^2 \left| \frac{\partial U}{\partial z} \right|, \tag{7.10}$$

in m^2/s. The analogy is with molecular viscosity, which relates the viscous stress to the shear in the same way, but K_m is not a property of the air. It is a property of the turbulence: it depends on height, on the shear and, through the shear, on the wind speed, the roughness and the stability. The magnitudes differ enormously. In the worked example of Section 7.3.3, $K_m = 2\,\mathrm{m}^2\,\mathrm{s}^{-1}$ at 10 m, while the kinematic viscosity of air is $\nu \approx 1.5 \times 10^{-5}\,\mathrm{m}^2\,\mathrm{s}^{-1}$, about 10^5 times smaller. Above the lowest millimeters, turbulence carries essentially all of the momentum. Representing the turbulent flux by an eddy viscosity is a first-order closure, one of the kinds of turbulence model described in Chapter 8.

7.2.5 The neutral shear

In a neutral surface layer, where buoyancy neither helps nor hinders the turbulence (Section 7.6.1), the shear follows from combining the two results of this chapter so far. By the constant-flux property and equation (7.6), the flux at every height in the layer equals its surface value,

$$-\overline{u'w'} = u_*^2.$$

By Prandtl's relation (7.8) with $\partial U/\partial z > 0$ and the mixing length (7.9),

$$-\overline{u'w'} = (\kappa z)^2 \left(\frac{\partial U}{\partial z} \right)^2 .$$

Equating the two and taking the positive square root,

$$\frac{\partial U}{\partial z} = \frac{u_*}{\kappa z}. \tag{7.11}$$

The shear is inversely proportional to height: large near the ground and small aloft. With $u_* = 0.5\,\mathrm{m\,s}^{-1}$ it is $1.25\,\mathrm{s}^{-1}$ at 1 m, $0.125\,\mathrm{s}^{-1}$ at 10 m and $0.025\,\mathrm{s}^{-1}$ at 50 m. The eddy viscosity of equation (7.10) becomes $K_m = (\kappa z)^2\, u_*/(\kappa z) = \kappa\, u_*\, z$, growing linearly with height.

The same result by dimensional analysis. The shear relation does not depend on the details of Prandtl's parcel picture; it follows from the list of quantities the shear can depend on. In a neutral surface layer, at heights well above the roughness elements, the shear $\partial U/\partial z$ (units s^{-1}) can depend only on the friction velocity u_* (m/s), which carries the flux, and on the height z (m), which limits the eddies. The other candidates drop out, each for a stated reason. The density enters only through $\tau_0/\rho = u_*^2$. The viscosity matters only within a distance of order $\nu/u_* = 1.5 \times 10^{-5}/0.5 = 3 \times 10^{-5}\,\mathrm{m}$ of the surface. The roughness length matters only near the roughness elements, which the flow at height $z \gg z_0$ no longer sees individually. The Coriolis parameter and the boundary-layer depth matter only for heights comparable with z_i or with $u_*/|f| = 0.5/10^{-4} = 5000\,\mathrm{m}$. Buoyancy is absent by the assumption of neutrality. Three

quantities built from two dimensions, length and time, form a single dimensionless group, and that group must be a constant:

$$\frac{z}{u_*}\frac{\partial U}{\partial z} = \text{constant} \equiv \frac{1}{\kappa}.$$

This is equation (7.11) again, with κ now defined as the constant that experiment must supply. The two routes agree; the dimensional route shows that the result rests on the list of relevant quantities, not on the parcel model.

Principle 7.2. *In a neutral surface layer the wind shear is $u_*/(\kappa z)$: set by the friction velocity, inversely proportional to height, and independent of the roughness of the surface at a given friction velocity.*

7.3 The logarithmic wind profile

This section integrates the neutral shear into the logarithmic wind profile, gives the integration constant its physical meaning, draws the profile, works it through with numbers, and compares it with the straight-line and power-law forms often used in its place.

7.3.1 Integration and the roughness length

Integrating equation (7.11) with respect to z gives

$$U(z) = \frac{u_*}{\kappa}\ln z + C,$$

with C a constant of integration. The logarithm of a dimensional height is not meaningful by itself; the constant must absorb a length. Writing $C = -(u_*/\kappa)\ln z_0$ with z_0 a length gives

$$U(z) = \frac{u_*}{\kappa}\ln\frac{z}{z_0}, \tag{7.12}$$

the *logarithmic wind profile*, or log law, of the neutral surface layer. The length z_0 is the *aerodynamic roughness length*. In equation (7.12) it is the height at which the profile, extrapolated downward, reaches zero: $U(z_0) = 0$ because $\ln 1 = 0$.

The division of roles is exact. The theory of Section 7.2 fixes the slope of the profile, u_*/κ per unit of $\ln z$; the surface fixes its offset, through z_0. The theory does not predict z_0. It is a property of the surface, determined by measurement or estimated from the surface type, as Section 7.4 describes.

7.3.2 The profile on linear and logarithmic axes

Figure 7.3 draws the profile of equation (7.12) for $u_* = 0.5\,\mathrm{m\,s^{-1}}$, $z_0 = 0.1\,\mathrm{m}$ and $\kappa = 0.4$ in two ways. Both panels have the wind speed on the horizontal axis and height on the vertical axis. In panel (a) the height axis is linear, from 0 to 100 m; in panel (b) it is logarithmic, from 0.1 to 100 m, each major tick a factor of ten. The two marked points are the wind speeds at 10 and 50 m worked out in Section 7.3.3.

On the linear axis the profile is a curve that rises steeply near the ground and bends over aloft: most of the increase in speed happens in the lowest few meters, and above 20 m the speed changes slowly. On the logarithmic axis the same profile is a straight line. Its slope is $u_*/\kappa = 1.25\,\mathrm{m\,s^{-1}}$ per unit of $\ln z$, or $1.25 \times \ln 10 = 2.88\,\mathrm{m\,s^{-1}}$ for every factor of ten in height, and it meets $U = 0$ at $z = z_0 = 0.1\,\mathrm{m}$. This straightness is the practical test of the log law. Wind speeds measured at several heights under neutral conditions and plotted against $\ln z$ should lie on a line; the slope of the line gives u_*/κ, and its intercept with $U = 0$ gives z_0. Curvature on such a plot is a sign that one of the assumptions of Section 7.6.4 fails.

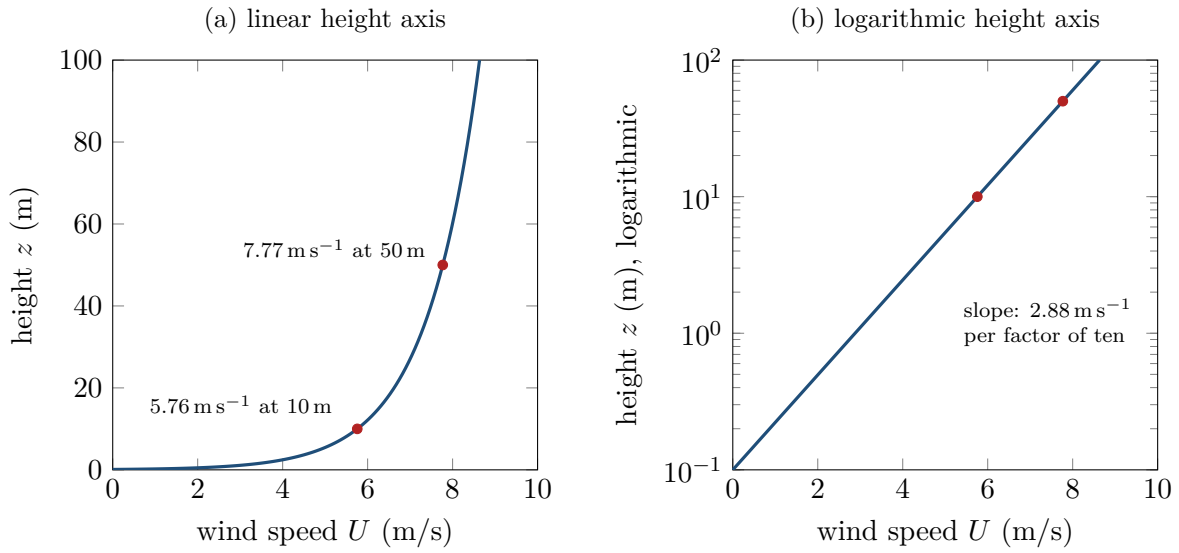


Figure 7.3: The neutral logarithmic wind profile $U(z) = (u_*/\kappa)\ln(z/z_0)$ with $u_* = 0.5\,\mathrm{m\,s^{-1}}$, $z_0 = 0.1\,\mathrm{m}$ and $\kappa = 0.4$, on a linear (a) and a logarithmic (b) height axis. Red points: the values at 10 and 50 m. In (b) the line meets $U = 0$ at $z = z_0$, the lower left corner of the panel.

7.3.3 A worked profile

Take $u_* = 0.5\,\mathrm{m\,s^{-1}}$, $z_0 = 0.1\,\mathrm{m}$ and $\kappa = 0.4$, so that $u_*/\kappa = 1.25\,\mathrm{m\,s^{-1}}$. At 10 m,

$$U(10\,\mathrm{m}) = 1.25\,\mathrm{m\,s^{-1}} \times \ln\frac{10}{0.1} = 1.25\,\mathrm{m\,s^{-1}} \times \ln 100 = 1.25 \times 4.605\,\mathrm{m\,s^{-1}} \approx 5.76\,\mathrm{m\,s^{-1}},$$

and at 50 m,

$$U(50\,\mathrm{m}) = 1.25\,\mathrm{m\,s^{-1}} \times \ln 500 = 1.25 \times 6.215\,\mathrm{m\,s^{-1}} \approx 7.77\,\mathrm{m\,s^{-1}}.$$

Raising the height five times raises the wind by a factor of $7.77/5.76 = 1.35$, an increase of $2.01\,\mathrm{m\,s^{-1}}$. Every doubling of height adds the same increment, $(u_*/\kappa)\ln 2 = 1.25 \times 0.693 \approx 0.87\,\mathrm{m\,s^{-1}}$, whether it is from 1 to 2 m or from 50 to 100 m.

Table 7.1 extends the example to five heights. Its columns give the height, the wind speed from equation (7.12), the mixing length κz, the shear from equation (7.11), the eddy viscosity $\kappa u_* z$, and the local power-law exponent $1/\ln(z/z_0)$ derived in Section 7.3.4.

Table 7.1: The worked neutral profile, $u_* = 0.5\,\mathrm{m\,s^{-1}}$, $z_0 = 0.1\,\mathrm{m}$, $\kappa = 0.4$. The kinematic stress $u_*^2 = 0.25\,\mathrm{m^2\,s^{-2}}$ is the same at every height.

Height z (m)	U (m/s)	$l = \kappa z$ (m)	$\partial U/\partial z$ (s^{-1})	K_m (m^2/s)	local exponent
1	2.88	0.4	1.25	0.2	0.434
2	3.74	0.8	0.625	0.4	0.334
10	5.76	4	0.125	2	0.217
50	7.77	20	0.025	10	0.161
100	8.63	40	0.0125	20	0.145

The table shows the structure of the layer at a glance. Across the heights, the shear falls by a factor of 100 and the eddy viscosity rises by a factor of 100, so that their product, the flux $K_m\,\partial U/\partial z = 0.25\,\mathrm{m^2\,s^{-2}}$, stays the same: weak eddies acting on a strong gradient near the ground carry the same momentum as strong eddies acting on a weak gradient aloft. The 100 m row lies at the top of the surface layer for a 1000 m boundary layer, and above it the log law should not be trusted without checking.

7.3.4 Logarithm, straight line and power law

The profile is neither linear in height, $U \propto z$, nor a power of height, $U \propto z^{\alpha}$; it is logarithmic, $U \propto \ln z$ plus a constant. The distinction matters because each form extrapolates differently from a measured height.

A linear profile through the 10 m value, $U = 0.576\,\mathrm{s}^{-1} \times z$, would give $28.8\,\mathrm{m\,s}^{-1}$ at 50 m, five times the 10 m value instead of 1.35 times; the rate of increase of a logarithmic profile falls with height, and that of a linear one does not. The power law $U(z) = U(z_r)\,(z/z_r)^{\alpha}$, with z_r a reference height and α an exponent, is widely used in wind energy because it is simple, and it can be made to agree with the log law over a limited range. The link between the two is the *local power-law exponent*, the exponent of the power law that has the same value and the same slope as the log profile at a given height:

$$\alpha(z) = \frac{\mathrm{d}\ln U}{\mathrm{d}\ln z} = \frac{z}{U}\frac{\partial U}{\partial z} = \frac{z}{(u_*/\kappa)\ln(z/z_0)} \cdot \frac{u_*}{\kappa z} = \frac{1}{\ln(z/z_0)}. \tag{7.13}$$

The exponent depends on height and on roughness, not on the wind speed. For $z_0 = 0.1$ m it is $1/\ln 100 = 0.217$ at 10 m, $1/\ln 500 = 0.161$ at 50 m and $1/\ln 1000 = 0.145$ at 100 m. The familiar value $\alpha = 1/7 \approx 0.143$ corresponds to $\ln(z/z_0) = 7$, that is $z \approx 1100\,z_0$: about 110 m over $z_0 = 0.1$ m, or 11 m over $z_0 = 0.01$ m. A single exponent for all heights and all surfaces is therefore an approximation even in neutral conditions.

Figure 7.4 compares the forms. Panel (a) has the wind speed on the horizontal axis and height on a linear vertical axis from 0 to 150 m; it shows the worked log profile, the power law that passes through its 10 and 50 m values, and the straight line through its 10 m value. Panel (b) has the local exponent of equation (7.13) on the horizontal axis and height on the vertical axis, for three roughness lengths, with the value 1/7 marked.

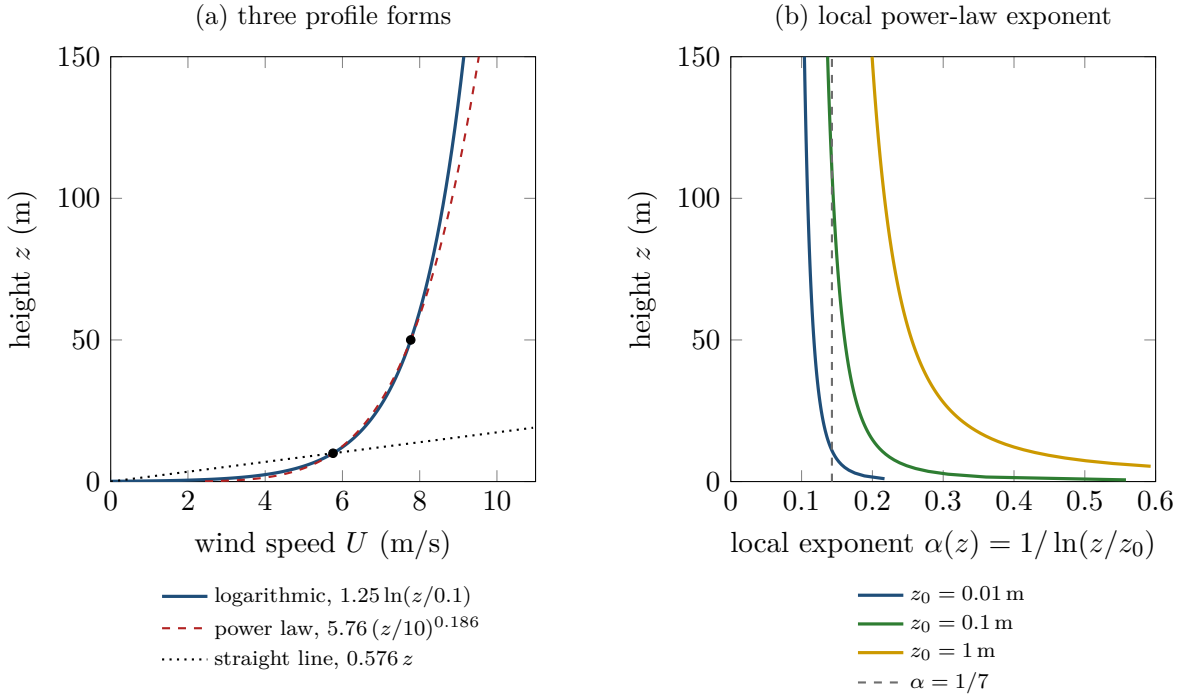


Figure 7.4: (a) The worked log profile ($u_* = 0.5\,\mathrm{m\,s}^{-1}$, $z_0 = 0.1$ m, $\kappa = 0.4$), the power law with $\alpha = 0.186$ fitted through its values at 10 and 50 m (black points), and the straight line through its 10 m value. (b) The local power-law exponent $\alpha(z) = 1/\ln(z/z_0)$ of the neutral log profile for three roughness lengths; dashed: $\alpha = 1/7$.

In panel (a) the straight line leaves the plot by 20 m; it is not a usable description of the surface layer. The power law and the log profile agree at the two fitting heights and lie close together between them, but they part outside that range. The power law with $\alpha = \ln(7.77/5.76)/\ln 5 = 0.186$ gives $8.84\,\mathrm{m\,s^{-1}}$ at 100 m against the log law's $8.63\,\mathrm{m\,s^{-1}}$, 2.4 % higher, and $4.27\,\mathrm{m\,s^{-1}}$ at 2 m against $3.74\,\mathrm{m\,s^{-1}}$, 14 % higher. Near the ground the power law cannot follow the steep logarithmic rise, and aloft it keeps growing faster than the logarithm. Panel (b) shows why: the exponent that a power law would need falls steadily with height and is larger over rougher surfaces at every height. An exponent fitted between two heights is valid between those heights; used to extrapolate from a 10 m station to a 100 m hub or down to a 2 m sensor, it carries an error that grows with the distance of the extrapolation, before stability is even considered.

7.4 Roughness length and displacement height

The log profile has two surface parameters. This section explains what the roughness length is and is not, lists typical values, shows how roughness changes the profile at the same friction velocity and at the same wind aloft, adds the displacement height needed over tall and dense obstacles, and ends with the layer just above such obstacles where the log law fails.

7.4.1 What the roughness length is and is not

The aerodynamic roughness length z_0 is an effective parameter of the surface that expresses how strongly it extracts momentum from the flow. It is defined by the log profile: it is the value of the length in equation (7.12) that makes the profile fit measured winds, and formally it is the height at which the neutral log profile extrapolates to zero wind. It is not the average height of the obstacles, the height of the grass or the height of the trees; for many vegetated surfaces it is roughly one tenth of the obstacle height, a rough rule whose factor varies with the density and shape of the elements.

Nor is z_0 the height at which the real wind vanishes. Within and just above the roughness elements the log law does not apply, and the real wind at height z_0 among grass blades or crops is in general not zero. The zero of the log profile is an extrapolation of the profile measured higher up, a way of encoding the surface's drag in a length. Over water z_0 also changes with the flow itself, because the waves that make the surface rough grow with the wind; an empirical relation of the form $z_0 \approx 0.015\,u_*^2/g$ (with a coefficient between about 0.011 and 0.018) gives $z_0 \approx 0.015 \times 0.3^2/9.81 \approx 1.4 \times 10^{-4}$ m for $u_* = 0.3\,\mathrm{m\,s^{-1}}$. Vegetation that bends in strong wind and snow that fills in the gaps between plants change z_0 in the same way.

7.4.2 Typical values

Table 7.2 lists approximate roughness lengths for common surfaces, with an illustrative obstacle height for each and the friction velocity that the log law gives for a $10\,\mathrm{m\,s^{-1}}$ wind at 10 m above the displacement height, $u_* = 0.4 \times 10/\ln(10/z_0)$, evaluated at a representative z_0 from the range. The values span four orders of magnitude, and they depend on the geometry of the obstacles and on the flow regime, so each range is a guide, not a constant.

The last column shows how strongly roughness controls the stress at a given wind: from water to forest, the same $10\,\mathrm{m\,s^{-1}}$ requires a friction velocity almost five times larger and a stress about 22 times larger, since $\tau_0 \propto u_*^2$. Over forest and cities the values assume that heights are measured above the displacement height of Section 7.4.4.

Table 7.2: Approximate aerodynamic roughness lengths. The last column is the neutral friction velocity for $U = 10\,\mathrm{m\,s^{-1}}$ at 10 m above the displacement height, at the representative z_0 given in parentheses. Obstacle heights are illustrative.

Surface	z_0 (m)	Obstacle height	u_* for $10\,\mathrm{m\,s^{-1}}$ at 10 m
Smooth water	10^{-4} to 10^{-3}	waves, centimeters	$0.37\,\mathrm{m\,s^{-1}}$ ($z_0 = 2\times10^{-4}$ m)
Short grass	0.01 to 0.05	0.05 to 0.2 m	$0.69\,\mathrm{m\,s^{-1}}$ ($z_0 = 0.03$ m)
Cropland	0.05 to 0.2	0.3 to 2 m	$0.87\,\mathrm{m\,s^{-1}}$ ($z_0 = 0.1$ m)
Shrubs	0.1 to 0.5	1 to 3 m	$1.06\,\mathrm{m\,s^{-1}}$ ($z_0 = 0.23$ m)
Forest	0.5 to 2	10 to 30 m	$1.74\,\mathrm{m\,s^{-1}}$ ($z_0 = 1$ m)
Dense urban	1 and more	10 to 50 m	$1.74\,\mathrm{m\,s^{-1}}$ or more ($z_0 \geq 1$ m)

7.4.3 Rougher surfaces and stronger shear

The effect of roughness on the profile depends on what is held fixed. Figure 7.5 shows the two cases. Both panels have the wind speed on the horizontal axis and the height above the zero plane, $z - d$, on a logarithmic vertical axis from 1 to 150 m, for three surfaces: water ($z_0 = 2\times10^{-4}$ m), grass ($z_0 = 0.03$ m) and forest ($z_0 = 1$ m), with the forest's height counted from its displacement height. In panel (a) the friction velocity is the same, $0.5\,\mathrm{m\,s^{-1}}$, over all three. In panel (b) the wind at 100 m is the same, $10\,\mathrm{m\,s^{-1}}$, as a stand-in for the same large-scale forcing above the surface layer, and each surface has the friction velocity that the log law then requires.

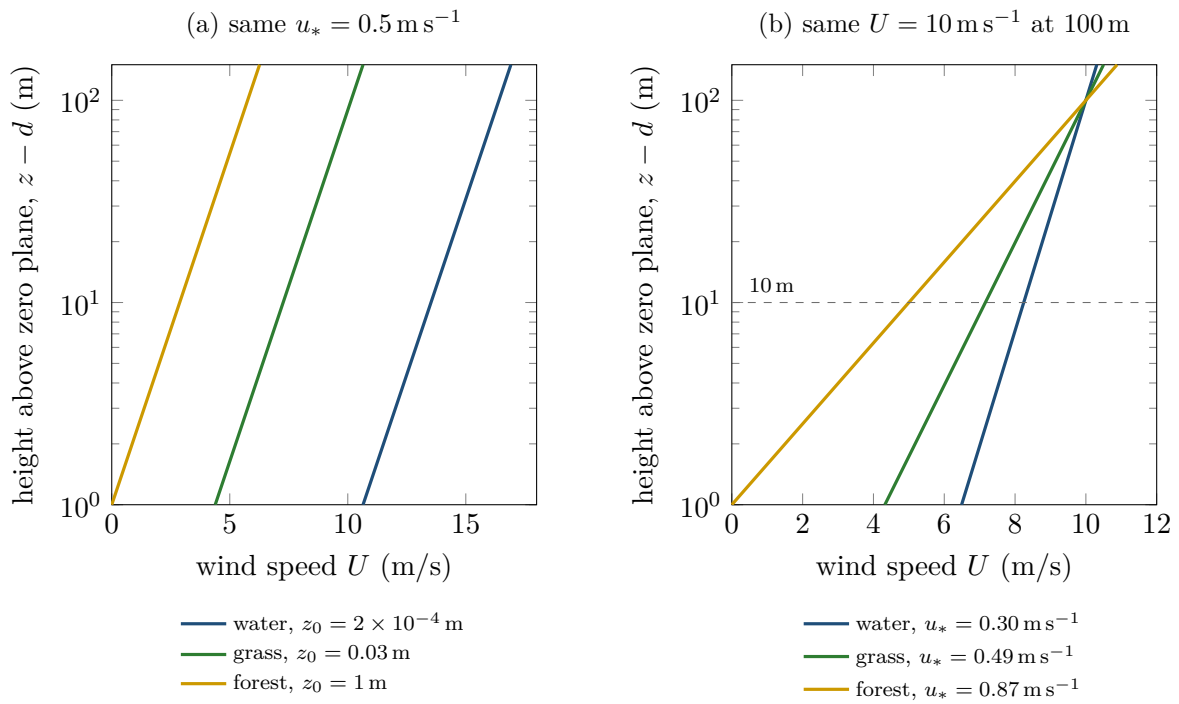


Figure 7.5: Neutral log profiles $U = (u_*/\kappa)\ln[(z-d)/z_0]$, $\kappa = 0.4$, over water, grass and forest. (a) Same friction velocity, $0.5\,\mathrm{m\,s^{-1}}$: parallel lines, the same shear at every height. (b) Same wind, $10\,\mathrm{m\,s^{-1}}$, at 100 m above the zero plane: the rougher surface has the larger friction velocity, the larger change of wind per factor of ten in height, the stronger shear and the weaker near-surface wind.

Panel (a) shows a result that follows directly from equation (7.11): at the same friction velocity the shear $u_*/(\kappa z)$ does not depend on z_0, and the three profiles are parallel lines on the logarithmic axis. Roughness only shifts them: the rougher the surface, the lower the wind

at every height. The same u_* over water and forest is not the same weather, though: it takes $13.5\,\mathrm{m\,s^{-1}}$ at 10 m over water but only $2.9\,\mathrm{m\,s^{-1}}$ over forest to produce a friction velocity of $0.5\,\mathrm{m\,s^{-1}}$.

Panel (b) is the comparison that corresponds to similar large-scale forcing, and there roughness does increase the shear. To carry the same $10\,\mathrm{m\,s^{-1}}$ at 100 m, the rougher surface draws more momentum out of the flow, so its friction velocity is larger: 0.30, 0.49 and $0.87\,\mathrm{m\,s^{-1}}$ over water, grass and forest. Its shear at 10 m, $u_*/(\kappa \times 10\,\mathrm{m})$, is larger in the same ratio: 0.076, 0.123 and $0.217\,\mathrm{s^{-1}}$. Its wind near the ground is lower: at 10 m above the zero plane, $8.2\,\mathrm{m\,s^{-1}}$ over water, $7.2\,\mathrm{m\,s^{-1}}$ over grass and $5.0\,\mathrm{m\,s^{-1}}$ over forest. A 10 m wind over open water and one over forest under similar forcing can thus differ by more than a third, and a rougher surface means stronger drag, stronger near-surface shear and a weaker wind near the ground. Fixing the wind at 100 m is itself a simplification: in reality the roughness also changes the wind higher up, more weakly, and the comparison is cleanest when made against the geostrophic wind, which the surface roughness does not change.

7.4.4 The zero-plane displacement

Over tall, dense obstacles, such as a forest or a city, the flow above the obstacles behaves as if the ground had been raised. The momentum is absorbed not at the ground but over the depth of the canopy, mostly in its upper part, and the log profile above the canopy fits measurements only if height is counted from a raised level. The *zero-plane displacement height* d, in meters, is that level, and the profile becomes

$$U(z) = \frac{u_*}{\kappa} \ln \frac{z-d}{z_0}, \qquad z - d \gg z_0. \tag{7.14}$$

Physically, d is close to the mean height at which the canopy absorbs momentum. For a forest of canopy height h_c, d is typically 0.6 to $0.8\,h_c$; over short grass or water d is negligible and is taken as zero. With d, the shear of equation (7.11) becomes $u_*/[\kappa(z-d)]$, and the eddies are limited by the distance to the effective surface rather than to the ground.

Figure 7.6 draws a worked forest profile. The axes are wind speed and height above the ground. The shaded band from the ground to h_c is the canopy and the lighter band above it the roughness sublayer of Section 7.4.6. The dashed horizontal line is the displacement height and the dotted one the level $d + z_0$. The blue curve is equation (7.14), solid where it applies and dashed where it is only an extrapolation; the gray curve inside the canopy is a schematic of the real wind there.

The numbers are illustrative: a forest $h_c = 20\,\mathrm{m}$ tall with $d = 0.7\,h_c = 14\,\mathrm{m}$ and $z_0 = 0.1\,h_c = 2\,\mathrm{m}$, at the top of the forest range of Table 7.2, in a wind with $u_* = 0.8\,\mathrm{m\,s^{-1}}$, so that $u_*/\kappa = 2\,\mathrm{m\,s^{-1}}$. At 40 m and 60 m, twice and three times the canopy height,

$$U(40\,\mathrm{m}) = 2\,\mathrm{m\,s^{-1}} \times \ln \frac{40-14}{2} = 2\,\mathrm{m\,s^{-1}} \times \ln 13 \approx 5.13\,\mathrm{m\,s^{-1}},$$
$$U(60\,\mathrm{m}) = 2\,\mathrm{m\,s^{-1}} \times \ln \frac{60-14}{2} = 2\,\mathrm{m\,s^{-1}} \times \ln 23 \approx 6.27\,\mathrm{m\,s^{-1}}.$$

Ignoring the displacement, with the same u_* and z_0, would give $2\ln 20 \approx 5.99\,\mathrm{m\,s^{-1}}$ at 40 m and $2\ln 30 \approx 6.80\,\mathrm{m\,s^{-1}}$ at 60 m, too high by 17 % and 8 %. The error is largest near the canopy, where d is a large fraction of z, and it fades with height as $z - d$ approaches z. The figure also shows that the extrapolated profile reaches zero at $d + z_0 = 16\,\mathrm{m}$, inside the canopy, where the real wind is weak but not zero.

7.4.5 Displacement and roughness are not interchangeable

The two parameters do different things. The displacement height d moves the origin of the height coordinate: it is the effective vertical displacement of the aerodynamic surface. The

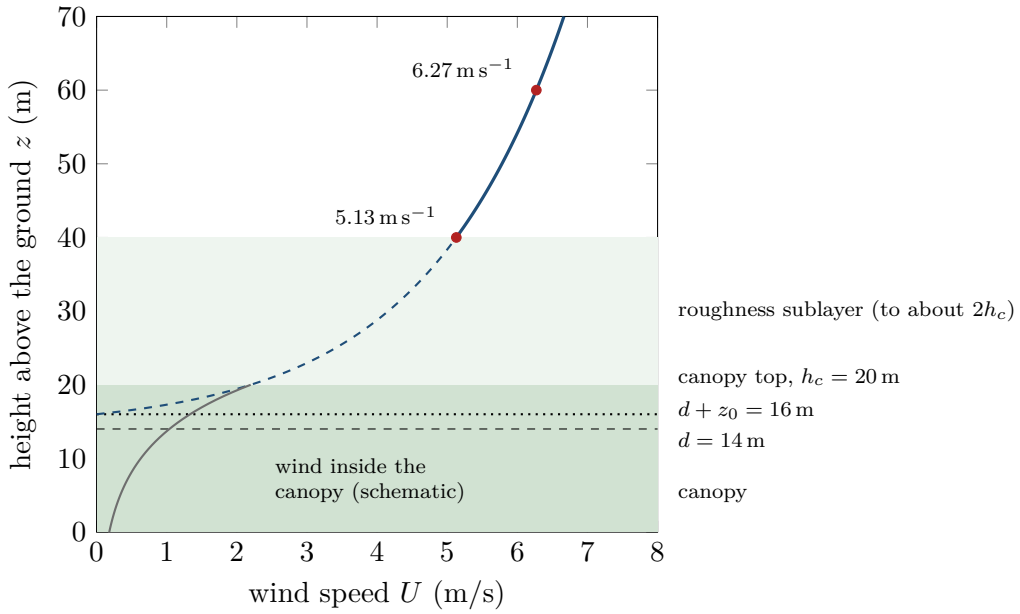


Figure 7.6: Neutral profile over an illustrative forest, $h_c = 20\,\mathrm{m}$, $d = 14\,\mathrm{m}$, $z_0 = 2\,\mathrm{m}$, $u_* = 0.8\,\mathrm{m\,s^{-1}}$: $U = 2\,\mathrm{m\,s^{-1}} \times \ln[(z - 14\,\mathrm{m})/2\,\mathrm{m}]$. Solid blue: above the roughness sublayer, where the log law applies. Dashed blue: its extrapolation, reaching zero at $z = d + z_0$. Gray: schematic wind inside the canopy, which is not zero at that level. Red points: values at 40 and 60 m.

roughness length z_0 sets the offset of the profile once the origin is fixed: it is the effective roughness that controls momentum extraction. On a plot against $\ln(z - d)$ the profile is a straight line whose intercept is set by z_0; on a plot against $\ln z$, a nonzero d makes the profile curve, steepest at the lowest heights.

A wrong d therefore cannot be compensated by a different z_0 without changing u_* too. Fit the profile $U = (u_*/\kappa)\ln(z/z_0)$, with $d = 0$, to the two forest values of Section 7.4.4. The slope per unit of $\ln z$ is

$$\frac{u_*}{\kappa} = \frac{6.27 - 5.13}{\ln(60/40)}\,\mathrm{m\,s^{-1}} = \frac{1.14}{0.405}\,\mathrm{m\,s^{-1}} \approx 2.81\,\mathrm{m\,s^{-1}},$$

so $u_* \approx 1.13\,\mathrm{m\,s^{-1}}$ instead of $0.8\,\mathrm{m\,s^{-1}}$, and $z_0 = 40\,\mathrm{m} \times \exp(-5.13/2.81) \approx 6.5\,\mathrm{m}$ instead of 2 m. The fit passes through both measured points, but it overstates the friction velocity by about 40 %, and hence the stress by about 100 %, and it assigns the forest a roughness length that is three times too large. Two heights cannot separate d from z_0 and u_*; three or more heights well above the roughness sublayer, a direct measurement of u_*, or an estimate of d from the canopy height are needed. Chapter 10 returns to this kind of non-uniqueness.

7.4.6 The roughness sublayer

The log law describes the flow over a surface that is horizontally homogeneous in aggregate: the individual trees or buildings are not seen, only their averaged drag. Close above the obstacles that is not true. Within the *roughness sublayer*, which extends from the canopy top to roughly two to three times the obstacle height (a rough rule, deeper over sparse or irregular obstacles), the wakes of individual trees, the coherent eddies that form at the canopy top, and the horizontal variation from one gap to the next all affect the flow. The mean wind there varies from place to place at the same height, and the measured shear near the canopy top is generally smaller than the log law predicts, because these eddies mix more efficiently than eddies of size $\kappa(z - d)$.

A sensor in the roughness sublayer, for example at 25 or 30 m above the 20 m forest of Figure 7.6, measures a wind that depends on its exact position relative to individual crowns and gaps. Fitting the log law to such data, or extrapolating from it with u_*, z_0 and d, makes simple similarity unreliable: the parameters obtained describe the sensor's surroundings, not the surface. Over a forest the log law should be applied above about $2h_c$, here 40 m, which is why the solid part of the curve in the figure starts there.

7.5 Fetch and internal boundary layers

A real surface changes from place to place, and the flow above it needs distance to adjust to each change. This section defines fetch, describes the internal boundary layer that grows downwind of a change in roughness, gives a rough rule for its growth, and applies the rule to a measurement mast near a forest edge.

7.5.1 Fetch

The *fetch* is the upwind distance, in meters, over which the air reaching a point has traveled across a given surface type. The log profile with the roughness length of that surface applies only if the fetch is long enough for the flow to have adjusted to it. A sensor over grass with a forest 50 m upwind does not measure a grass profile: the air at its height left the forest a few seconds earlier and still carries the profile, the turbulence and the momentum deficit of the forest. The surface that matters is the upwind one, over a distance that grows with the height of the measurement.

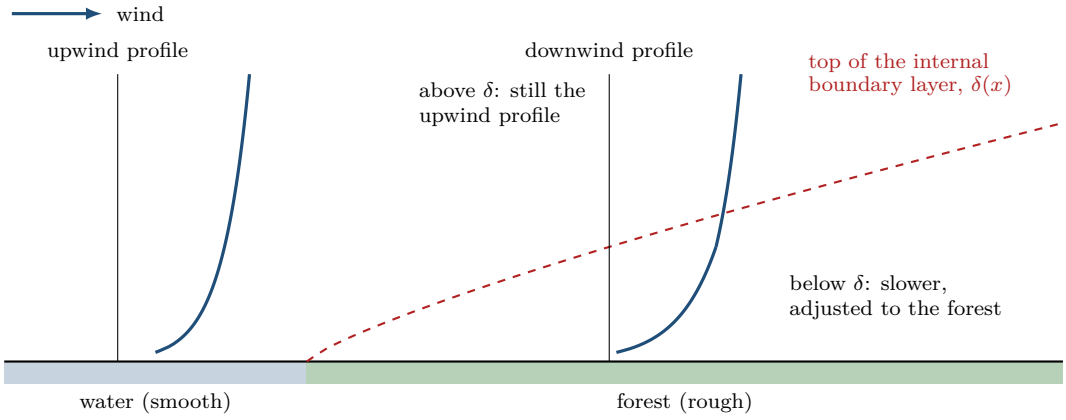
Fetch depends on the wind direction. A sensor at the edge of a field may have kilometers of grass upwind for one wind direction and a forest edge a hundred meters away for another. The roughness length that describes a site is therefore, in general, a function of direction, and the local land cover directly under the sensor is only one input to it. A weather model faces the same problem at a different scale: it diagnoses its 10 m wind from its lowest model level by a surface-layer relation with one effective roughness length for the whole grid cell, which is an average over many surface types and is not the roughness upwind of any particular instrument.

7.5.2 The internal boundary layer

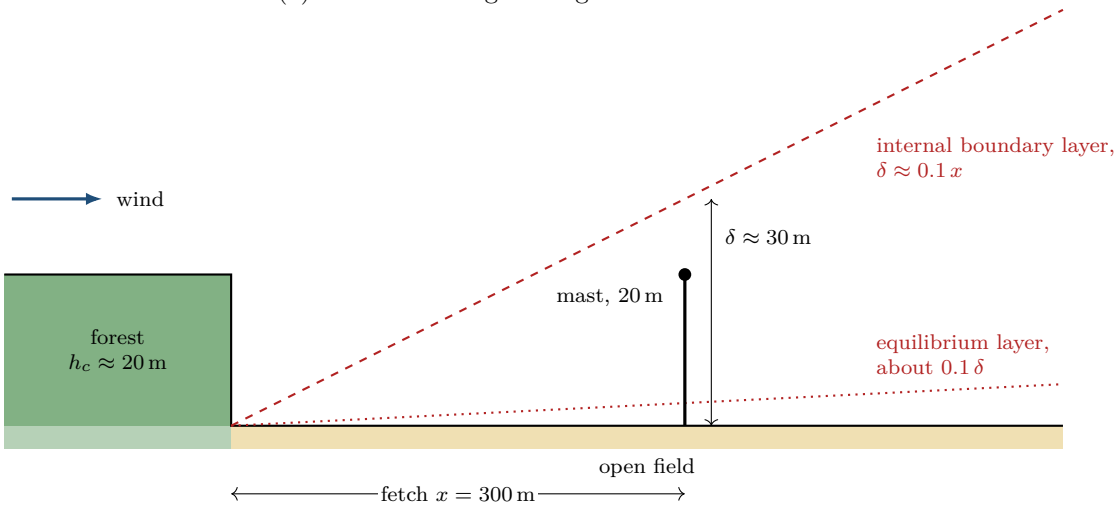
When air crosses a change in roughness, from water to forest for example, the lower atmosphere does not adjust at once. The air in contact with the new surface feels the new drag immediately; the air above it learns of the change only as turbulence carries the new stress upward. A layer adjusted to the new surface therefore grows with distance downwind of the change. This layer is the *internal boundary layer*: the layer, inside the existing boundary layer, whose flow has been modified by the surface downwind of a change in surface properties. Its top, at height δ, separates air that has felt the new surface from air that still carries the profile of the old one.

Figure 7.7(a) shows the structure in a vertical cross section, with the wind from the left. The strip on the left is water and the strip on the right forest; the dashed curve is the top of the internal boundary layer, growing from the shoreline. The two blue curves are wind profiles: one over the water, upwind of the change, and one over the forest, downwind of it. Panel (b) is the measurement site of Section 7.5.3. In both panels the vertical scale is exaggerated about five times relative to the horizontal.

The downwind profile in panel (a) has a kink at δ. Below it the wind is slower than upwind at the same height, because the forest extracts more momentum, and the shear near the ground is larger. Above it the profile is still the water profile. Near the surface the wind adjusts first; higher levels remember the old surface longer. Between the two lies a transition: only the lowest part of the internal boundary layer is fully in equilibrium with the new surface, in the sense



(a) smooth-to-rough change: water to forest



(b) a mast 300 m downwind of a forest edge

Figure 7.7: Internal boundary layers (schematic, vertical scale exaggerated about five times). (a) Downwind of a change from water to forest, a layer adjusted to the forest grows from the shoreline; below its top the wind is slower than upwind, above it the upwind profile persists. (b) A 20 m mast 300 m downwind of a forest edge, with the rough rules $\delta \approx 0.1\,x$ for the internal boundary layer and about $0.1\,\delta$ for the layer in equilibrium with the field.

that a log profile with the new z_0 describes it, and the rest is a blend. A common rough rule puts the top of this *equilibrium layer* at about one tenth of δ.

A rough growth rule. The height of the internal boundary layer grows less than linearly with the fetch x downwind of the change. A rough rule, adequate for order-of-magnitude estimates at distances of hundreds of meters to a few kilometers in near-neutral conditions, is

$$\delta \approx 0.1\, x, \tag{7.15}$$

so that the internal boundary layer rises about one meter for every ten meters of fetch. Empirical fits of the form $\delta \approx 0.28\, z_{0r}\, (x/z_{0r})^{0.8}$, with z_{0r} the larger of the two roughness lengths, give values of the same order: for $z_{0r} = 1\,\mathrm{m}$ and $x = 300\,\mathrm{m}$, $0.28 \times 300^{0.8} \approx 27\,\mathrm{m}$, against 30 m from equation (7.15). Both are rough rules. The growth is faster over rough surfaces and in unstable air, and much slower in stable air, when the turbulence that carries the new stress upward is weak; at night an internal boundary layer may stay only a few meters deep for kilometers. The same reasoning gives the rule of thumb used to site flux and profile instruments: the fetch of uniform surface upwind should be of order 100 times the measurement height, so that the instrument lies in the equilibrium layer, $0.1 \times 0.1\, x \geq z$.

7.5.3 A mast downwind of a forest edge

Consider the site of Figure 7.7(b): an anemometer at 20 m on an open field, with 300 m of field upwind and then a forest. The local land cover suggests a grass roughness length. The rough rule says otherwise. At $x = 300\,\mathrm{m}$,

$$\delta \approx 0.1 \times 300\,\mathrm{m} = 30\,\mathrm{m}, \qquad \text{equilibrium layer} \approx 0.1 \times 30\,\mathrm{m} = 3\,\mathrm{m}.$$

The anemometer lies inside the internal boundary layer of the field, below 30 m, but far above the 3 m layer that is in equilibrium with it. The wind it measures reflects both surfaces: the field below, which speeds the near-surface air up after the drag of the forest, and the forest upwind, whose momentum deficit the air at 20 m still carries. A log profile with the grass roughness length, used to extrapolate from 20 m to 10 m or to 60 m, would be wrong, and a roughness length inferred from the profile would lie between the grass and forest values and would change with height. For the 20 m anemometer to measure a wind in equilibrium with the field, the rough rule asks for $0.01\, x \geq 20\,\mathrm{m}$, a fetch of about 2000 m.

Two further effects make the site harder than the rule suggests. The forest edge itself, a step 20 m high, sheds a wake and may cause the flow to separate from the canopy top and reattach downwind, affecting the flow over a distance of order ten to twenty canopy heights, here 200 to 400 m, which includes the mast. And for a wind direction from which the field extends farther, the same mast would see a different fetch and a different effective roughness, as the exercises show. A single z_0 taken from the immediate land cover is therefore a poor description of such a site; a roughness length that depends on direction and on height, or a direct measurement of u_*, is needed.

> **Principle 7.3.** *The wind at a sensor reflects the surface upwind of it, over a fetch that grows with the sensor's height, roughly one hundred heights for full adjustment. A roughness length read from the land cover directly under the sensor is reliable only when that cover extends that far upwind in the direction of the wind.*

7.6 Stability and the limits of the theory

The logarithmic profile is the neutral case. This section states when neutral conditions occur, shows how heating and cooling of the surface change the profile, gives the general form that includes stability without deriving it, and lists the assumptions of surface-layer theory with the ways real sites violate them.

7.6.1 Neutral conditions

The simple log profile assumes *neutral stability*: a surface layer in which buoyancy neither enhances nor suppresses turbulence, so that the turbulence is produced mechanically, by the shear, alone. In terms of the potential temperature of Chapter 6, the layer is neutral when θ, strictly the virtual potential temperature θ_v, is nearly constant with height, $\partial\theta_v/\partial z \approx 0$, and the surface heat flux is near zero. A *neutral surface layer* is one in which these conditions hold and the log profile of equation (7.14) applies.

Neutral conditions are common in strong winds, when mechanical turbulence is so strong that any buoyancy effect is small by comparison; under overcast skies, which reduce both the daytime heating and the night-time cooling of the surface; and in general when heating or cooling is weak, including the short periods around the morning and evening transitions when the surface heat flux changes sign. They are not the typical state on a clear day or a clear night with light wind, which are often the conditions of greatest interest for the cooling of a transmission line.

7.6.2 Unstable and stable departures

When the sun heats the surface, the air in contact with it becomes warmer and lighter than the air above, and buoyancy adds to the turbulence: the surface layer is *unstable*. Mixing is more efficient, the faster air aloft is brought down more effectively, and the profile is flatter than the log law, with less shear. For the same wind aloft, the near-surface wind is stronger than the neutral log profile suggests.

When the surface cools, typically on clear nights, the air in contact with it becomes colder and denser than the air above, and buoyancy works against vertical motion: the surface layer is *stable*. Turbulence is suppressed, the lowest air is partly decoupled from the faster air aloft, and the shear is stronger. The 10 m wind may be much weaker than the 100 m wind, and in strongly stable conditions the near-surface air may be nearly calm while the wind a hundred meters up is strong.

Figure 7.8 shows the three cases. The horizontal axis is wind speed and the vertical axis height on a logarithmic scale from 1 to 150 m, over a surface with $z_0 = 0.1$ m. All three profiles have the same wind, $10\,\mathrm{m\,s^{-1}}$, at 100 m. The neutral profile is the straight line; the unstable and stable profiles are drawn from standard empirical stability corrections, stated in the caption, which Chapter 14 derives.

The three profiles meet at 100 m and part below it. At 10 m the neutral wind is $6.67\,\mathrm{m\,s^{-1}}$, the unstable wind $7.66\,\mathrm{m\,s^{-1}}$ and the stable wind $4.29\,\mathrm{m\,s^{-1}}$: the ratio of the 10 m wind to the 100 m wind is 0.67, 0.77 and 0.43. The unstable profile is curved to the right of the neutral line, flatter near the top; the stable profile is curved to the left, with a strong shear above 10 m. A 10 m measurement extrapolated to 100 m with the neutral log law would give $10\,\mathrm{m\,s^{-1}}$ only in neutral air; from the stable $4.29\,\mathrm{m\,s^{-1}}$ it would give $4.29 \times 6.908/4.605 \approx 6.4\,\mathrm{m\,s^{-1}}$, 36 % too low, and from the unstable $7.66\,\mathrm{m\,s^{-1}}$ it would give $11.5\,\mathrm{m\,s^{-1}}$, 15 % too high. Stability corrections are therefore essential whenever the air is not neutral.

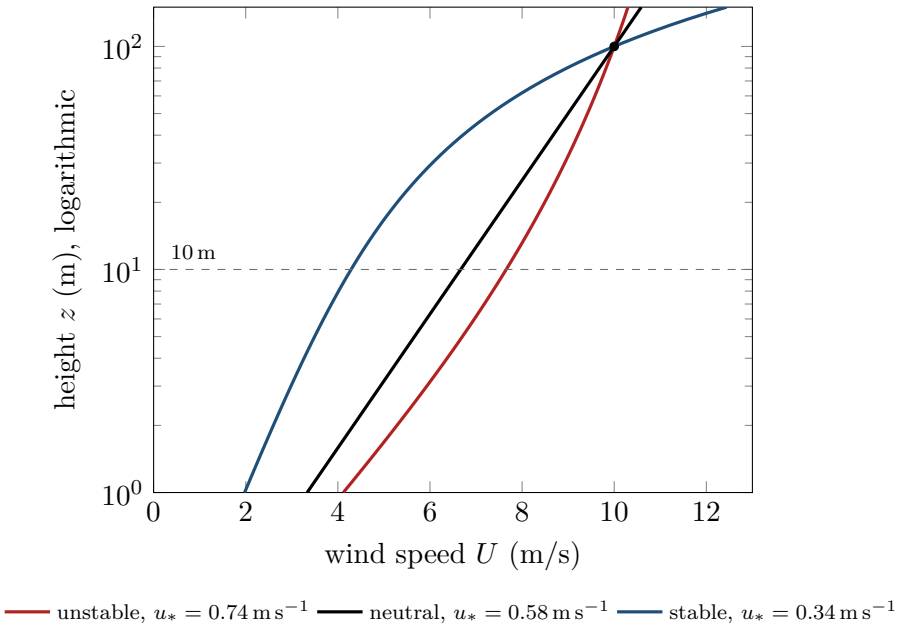


Figure 7.8: Wind profiles over $z_0 = 0.1\,\mathrm{m}$ with the same wind, $10\,\mathrm{m\,s^{-1}}$, at 100 m (black point), on a logarithmic height axis. $U = (u_*/\kappa)[\ln(z/z_0) - \psi_m]$ with $\kappa = 0.4$. Neutral: $\psi_m = 0$. Stable: $\psi_m = -5z/L_O$ with $L_O = 100\,\mathrm{m}$. Unstable: $\psi_m = 2\ln[(1+x)/2] + \ln[(1+x^2)/2] - 2\arctan x + \pi/2$, $x = (1 - 16z/L_O)^{1/4}$, with $L_O = -50\,\mathrm{m}$. The corrections are standard empirical forms, used here for illustration.

7.6.3 The general form

The neutral shear relation is one case of a general statement: in the surface layer the shear depends on the friction velocity, the height and the stability. Written in dimensionless form,

$$\frac{\kappa z}{u_*}\frac{\partial U}{\partial z} = \text{a function of stability}, \qquad \begin{cases} = 1 & \text{neutral}, \\ < 1 & \text{unstable}, \\ > 1 & \text{stable}, \end{cases} \tag{7.16}$$

and the integrated profile is

$$U(z) = \frac{u_*}{\kappa}\left[\ln\frac{z-d}{z_0} - \psi_m\right], \tag{7.17}$$

where ψ_m, dimensionless, is the *stability correction* to the log profile: zero in neutral conditions, positive in unstable conditions and negative in stable conditions, at a given friction velocity. The signs agree with Figure 7.8. At the same u_*, unstable air has less shear and therefore less wind at a given height than the log law gives; stable air has more. The stability enters through the ratio z/L_O of height to the Obukhov length, a length scale built from the friction velocity and the surface heat flux. The framework that defines L_O and gives ψ_m, Monin–Obukhov similarity theory, is the subject of Chapter 14.

7.6.4 Assumptions of surface-layer theory

The classic theory of this chapter rests on a set of assumptions. Table 7.3 lists them as a checklist. Its columns give each assumption, what it requires, how it typically fails at a real site, and a symptom in the data that the failure leaves.

Real sites often violate several assumptions at once. A mast on a wooded ridge at night is in non-flat terrain, near heterogeneous roughness, possibly in the roughness sublayer and in stable

Table 7.3: Assumptions of classic surface-layer theory, as a checklist for a measurement site.

Assumption	Requires	How it fails at a real site	Symptom in the data
Stationary flow	mean wind and fluxes steady over the averaging period	morning and evening transitions, passing fronts, gust fronts, sea-breeze onset	fluxes and means that change between consecutive averaging periods
Horizontal homogeneity	the same surface in every direction over a long distance	mixed land cover, field edges, coastlines, settlements	roughness length that depends on wind direction
Constant flux with height	the bound of equation (7.3) small	measurement heights near the top of a shallow (night-time) boundary layer	fluxes at two heights that differ by more than about 20 %
Sufficient fetch	sensor within the equilibrium layer of the local surface	a forest edge, a building or a shoreline a few hundred meters upwind	profile curved on a $\ln z$ plot; z_0 fitted from different height pairs disagrees
Above the roughness sublayer	z more than about 2 to 3 obstacle heights	short masts over forest or in towns	large scatter between nearby sensors at the same height
No terrain-induced pressure effects	flat terrain	hills, ridges, escarpments, valleys (Chapter 5)	speed-up or slow-down not explained by roughness; wind direction turned by terrain
Equilibrium turbulence	turbulence in balance with the local shear and surface	air just downwind of a change in surface, wakes of obstacles	turbulence intensity out of line with the measured shear
Known stability state	neutral, or a measured stability for ψ_m	clear days and nights with light wind	profile curved on a $\ln z$ plot even with long fetch; diurnal cycle in the fitted z_0

air. The symptoms column is the practical point of the table: a roughness length that changes with direction, with the time of day, or with the pair of heights used to fit it is not a property of the surface, and its variation names the assumption that has failed. The log law is the reference against which such departures are measured, not a description that can be assumed to hold.

7.7 What to retain

Definition 7.1 (The neutral surface layer)**.** Surface drag sets a turbulent momentum flux that is nearly constant in the lowest 5 to 10 % of the boundary layer; the flux defines the friction velocity u_*, and carried by eddies of size $\kappa(z-d)$ it requires the shear $u_*/[\kappa(z-d)]$. Under neutral conditions the wind profile is therefore $U(z) = (u_*/\kappa)\ln[(z-d)/z_0]$, valid with sufficient fetch and above the roughness sublayer.

Table 7.4 lists the terms of the chapter, their meaning, their units and the subsection that defines each.

Table 7.4: The terms of the chapter and where each is defined.

Term	Meaning	Units	Defined in
Surface layer	lowest 5 to 10 % of the boundary layer, dominated by exchange with the surface	–	7.1.1
Constant-flux layer	the surface layer seen through its fluxes, constant to within about 10 to 20 %	–	7.1.2
Reynolds decomposition	$u = \overline{u} + u'$: mean over an averaging period plus fluctuation	as u	7.1.3
Momentum flux	$\overline{u'w'}$, vertical turbulent transport of along-wind momentum; negative (downward) near the surface	$\mathrm{m^2/s^2}$	7.1.3
Surface stress τ_0	$-\rho\,\overline{u'w'}$ at the surface: drag between air and ground	Pa	7.1.3
Friction velocity u_*	$\sqrt{\tau_0/\rho}$, velocity scale of the surface stress; about 0.1 to 1 $\mathrm{m\,s^{-1}}$	m/s	7.1.3, 7.1.4
Mixing length l	vertical distance over which eddies move air before mixing; κz near the ground	m	7.2.2, 7.2.3
von Kármán constant κ	universal constant of the neutral surface layer, about 0.4	–	7.2.3
Eddy viscosity K_m	$-\overline{u'w'}/(\partial U/\partial z)$; $\kappa u_* z$ in the neutral surface layer	$\mathrm{m^2/s}$	7.2.4
Logarithmic wind profile	$U = (u_*/\kappa)\ln[(z-d)/z_0]$, the neutral surface-layer profile	m/s	7.3.1
Local power-law exponent	$1/\ln(z/z_0)$, exponent of the power law tangent to the log profile	–	7.3.4
Roughness length z_0	effective surface parameter for momentum extraction; zero of the extrapolated log profile	m	7.4.1
Zero-plane displacement d	raised origin of the profile over tall dense obstacles; 0.6 to 0.8 h_c for forests	m	7.4.4
Roughness sublayer	layer up to about 2 to 3 obstacle heights where individual obstacles matter	m	7.4.6
Fetch	upwind distance over a given surface type	m	7.5.1
Internal boundary layer	layer modified by the surface downwind of a change; top roughly $0.1\,x$	m	7.5.2
Neutral surface layer	surface layer with $\partial\theta_v/\partial z \approx 0$, turbulence from shear alone	–	7.6.1
Stability correction ψ_m	departure of the profile from the log law caused by buoyancy	–	7.6.3

7.8 Exercises

Exercise 7.1. Over short grass with $z_0 = 0.03\,\mathrm{m}$, in neutral conditions, the friction velocity is $0.35\,\mathrm{m\,s^{-1}}$; take $\kappa = 0.4$ and $\rho = 1.2\,\mathrm{kg\,m^{-3}}$. (a) Compute the surface stress. (b) Compute the wind speed at 2, 10 and 100 m. (c) At 10 m, compute the mixing length, the shear and the eddy viscosity, and compare the eddy viscosity with $\nu = 1.5 \times 10^{-5}\,\mathrm{m^2\,s^{-1}}$. (d) Compute the local power-law exponent at 10 m and the power-law exponent that joins the 10 and 100 m values. (e) The boundary layer is 800 m deep, $|f| = 10^{-4}\,\mathrm{s^{-1}}$, and the ageostrophic wind in the lowest 40 m is at most $4\,\mathrm{m\,s^{-1}}$. Use equation (7.3) to bound the relative change of the stress across those 40 m, and say whether the constant-flux approximation holds there.

Exercise 7.2. Two cup anemometers on a mast over flat, uniform farmland record $6.0\,\mathrm{m\,s^{-1}}$ at 10 m and $7.5\,\mathrm{m\,s^{-1}}$ at 40 m on an overcast, windy afternoon; take the displacement height as zero and $\kappa = 0.4$. (a) Compute u_* and z_0 from the two readings. (b) Which surface of Table 7.2 does z_0 correspond to? (c) Compute the surface stress for $\rho = 1.2\,\mathrm{kg\,m^{-3}}$ and the wind at 100 m. (d) Why does the calculation require the overcast, windy conditions, and what would a third anemometer at 20 m allow that two cannot?

Exercise 7.3. A forest has canopy height $h_c = 25\,\mathrm{m}$; take $d = 0.7\,h_c$ and $z_0 = 0.1\,h_c$. In neutral conditions the wind at 60 m above the ground is $7.0\,\mathrm{m\,s^{-1}}$. (a) Compute u_*. (b) Compute the wind at 40 and 80 m, and say which of the three heights lie within the roughness sublayer if it extends to $2h_c$. (c) An analyst ignores the displacement and fits $U = (u_*/\kappa)\ln(z/z_0)$ through the 60 and 80 m values. Compute the fitted u_* and z_0 and the error in the stress.

Exercise 7.4. A 20 m mast stands on an open grass field at 23°S. The forest edge around the field lies 300 m from the mast toward bearing 115° and 2.5 km from it toward bearing 065°. The geostrophic wind blows from 090°, and near the ground friction turns the wind 25° across the isobars toward low pressure. (a) On which side of the easterly geostrophic flow is low pressure in the Southern Hemisphere, and from which direction does the near-surface wind blow? (b) Using $\delta \approx 0.1\,x$ and an equilibrium layer of $0.1\,\delta$, decide whether the 20 m anemometer measures a wind in equilibrium with the grass. (c) Repeat (a) and (b) for the same site and the same geostrophic wind at 23°N. (d) Explain why the effective roughness length of this site must be specified by wind direction.

Chapter 8

Turbulence

8.1 Turbulence and turbulent transport

A cup anemometer on a mast does not show a steady wind. Its reading rises and falls by several meters per second within seconds, and a sonic anemometer beside it shows that the air also moves up and down and from side to side. This variability is often treated as noise around the "real" wind. It is not random noise in that sense: it is turbulence, an organized but chaotic motion that spans a wide range of sizes and that carries momentum, heat, moisture, pollutants and kinetic energy between the ground and the air above. The question of this chapter is

what is turbulence, and why is it the mechanism that sets the wind near the ground?

The chapter first separates a wind record into a mean and a fluctuation and shows how the fluctuations transport momentum and heat far faster than molecular diffusion could. It then describes the eddies that make up turbulence and the cascade that carries their energy from large to small sizes; the turbulent kinetic energy and the budget of its production and dissipation; the kinds of turbulence found near the ground; the statistics used in engineering, turbulence intensity, gusts and averaging periods; and the way weather and engineering models represent turbulence they cannot compute.

Jargon: turbulence, eddy, mean flow, fluctuation, Reynolds decomposition, turbulent flux, Reynolds number

Turbulence is three-dimensional, rotational and chaotic motion of a fluid that contains a continuous range of sizes of motion and mixes the fluid far faster than molecular diffusion. An *eddy* is one coherent swirling structure within that motion, with a size, a velocity and a lifetime. The *mean flow* is the average of the velocity over a stated averaging period, $\overline{u}$ for the along-wind component; the *fluctuation* is the departure of the instantaneous velocity from it, $u' = u - \overline{u}$, both in m/s. The *Reynolds decomposition* is the split of every variable into these two parts, $u = \overline{u} + u'$. A *turbulent flux* is the mean transport of a quantity by the fluctuations, measured as the covariance of the vertical velocity fluctuation with the fluctuation of the quantity, such as $\overline{w'\theta'}$ in K m/s or $\overline{u'w'}$ in $\mathrm{m^2/s^2}$. The *Reynolds number* $\mathrm{Re} = UL/\nu$, dimensionless, is the ratio of inertial to viscous forces in a flow of speed U and size L; a flow with a large Reynolds number is turbulent.

Key idea

Wind shear near the ground generates turbulent eddies; the eddies carry fast air down and slow air up, so that the covariance $\overline{u'w'}$ is negative and momentum flows toward the surface; and that downward transport is what shapes the mean wind profile. Turbulence is not noise around the near-surface wind but the mechanism that determines it.

8.1.1 Mean flow and fluctuation

Any measured velocity component can be written as the sum of a mean and a fluctuation,

$$u = \overline{u} + u', \qquad v = \overline{v} + v', \qquad w = \overline{w} + w', \tag{8.1}$$

the Reynolds decomposition. The mean is taken over an averaging period, typically ten to thirty minutes for turbulence work: long enough to contain many eddies, short enough that the weather does not change appreciably within it. By construction the fluctuations average to zero, $\overline{u'} = \overline{v'} = \overline{w'} = 0$. In this chapter, as in the chapters around it, u is the component along the mean wind, v the component across it and w the upward component, so that $\overline{v} = 0$ by the choice of axes and $\overline{w} \approx 0$ over flat ground, where air cannot flow through the surface. The statistics of such a record, its variances and covariances, are the subject of Chapter 9; here they are used as the language in which turbulence is described.

Figure 8.1 shows a synthetic ten-minute record of the kind a sonic anemometer at about 10 m above open ground produces. The horizontal axis is time in minutes; the upper panel is the along-wind component u and the lower panel the vertical component w, both in m/s. The red lines are the ten-minute means, $\overline{u} = 10\,\mathrm{m\,s^{-1}}$ and $\overline{w} = 0$. The record was generated from seeded random numbers shaped by a realistic turbulence spectrum and then fixed to illustrative statistics: standard deviations $\sigma_u = 2.0\,\mathrm{m\,s^{-1}}$, $\sigma_v = 1.6\,\mathrm{m\,s^{-1}}$ and $\sigma_w = 1.0\,\mathrm{m\,s^{-1}}$, and covariance $\overline{u'w'} = -0.64\,\mathrm{m^2\,s^{-2}}$. The along-wind speed ranges from about 3.5 to 16 $\mathrm{m\,s^{-1}}$ around its mean of 10 $\mathrm{m\,s^{-1}}$; the largest fluctuation, near the sixth minute, is $u' = +6\,\mathrm{m\,s^{-1}}$. The fluctuations are not white noise: they come in excursions lasting from a fraction of a second to tens of seconds, the signatures of eddies of different sizes passing the sensor. The vertical component swings between about -3.8 and $+3.4\,\mathrm{m\,s^{-1}}$ with a mean of zero.

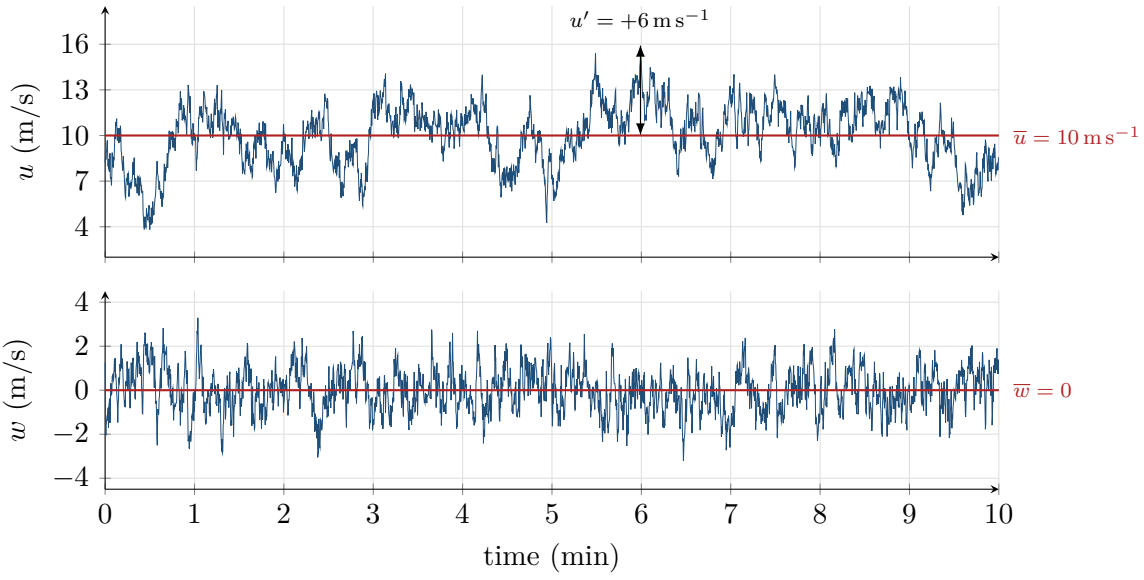


Figure 8.1: A synthetic ten-minute record at about 10 m above open ground, illustrative: along-wind component u (upper) and vertical component w (lower), generated at 20 Hz and plotted every 0.25 s. Red lines: ten-minute means. The record has $\overline{u} = 10\,\mathrm{m\,s^{-1}}$, $\sigma_u = 2.0\,\mathrm{m\,s^{-1}}$, $\sigma_v = 1.6\,\mathrm{m\,s^{-1}}$, $\sigma_w = 1.0\,\mathrm{m\,s^{-1}}$ and $\overline{u'w'} = -0.64\,\mathrm{m^2\,s^{-2}}$ (script `scripts/ch08_data.py`, von Kármán spectra, seed 8).

The decomposition is a statement about the flow, not about the instrument: the mean is the part of the wind that the weather pattern and the terrain organize over the averaging period, and the fluctuation is the part carried by eddies. Which part is which depends on the

averaging period, a dependence that returns in Section 8.5.4. A weather model with a grid of a few kilometers predicts only something like the mean; an anemometer measures the sum.

8.1.2 Three-dimensional fluctuations

Turbulence is three-dimensional. Even where the mean vertical velocity is essentially zero, as near flat ground, the vertical fluctuation w' is not: in Figure 8.1 its standard deviation is $1.0\,\mathrm{m\,s^{-1}}$, half that of the along-wind component. A parcel moving upward at $w' = +1\,\mathrm{m\,s^{-1}}$ for five seconds rises five meters before the eddy that carries it breaks up and another takes over, and in doing so it takes its properties, its temperature, its moisture and its horizontal velocity, with it. The vertical fluctuations are what connect one height to another. The cross-wind fluctuations v' make the wind direction meander about its mean, and the swirling of the eddies means that the flow is rotational: its fluctuations carry vorticity. Random variations confined to a plane, or random waves without rotation, are not turbulence in this sense and do not mix the air in the same way.

The transport by the vertical fluctuations is easiest to see for heat. On a sunny afternoon the ground heats the air in contact with it. An eddy that lifts air from near the surface ($w' > 0$) lifts air that is warmer than the average at the level it reaches ($T' > 0$), so the product $w'T'$ is positive. An eddy that brings air down from above ($w' < 0$) brings air that is cooler than the average ($T' < 0$), and the product is again positive. Averaged over many eddies, $\overline{w'T'} > 0$: heat is carried upward, even though no air is carried upward on average. The same reasoning applies to moisture, pollutants and, as Section 8.1.4 shows, horizontal momentum.

8.1.3 Fluxes as covariances

A flux is an amount of a quantity crossing a unit area per unit time. If air of density ρ moves upward at velocity w and carries a quantity s per kilogram of air, the instantaneous vertical flux is $\rho\, w\, s$. Writing $w = \overline{w} + w'$ and $s = \overline{s} + s'$ and averaging, with ρ treated as constant,

$$\overline{\rho\, w\, s} = \rho\left(\overline{w}\,\overline{s} + \overline{w}\,\overline{s'} + \overline{w'}\,\overline{s} + \overline{w's'}\right) = \rho\,\overline{w}\,\overline{s} + \rho\,\overline{w's'}, \tag{8.2}$$

because the means of the fluctuations vanish. The first term is transport by the mean vertical motion, negligible near flat ground. The second is the *turbulent flux*: the covariance of the vertical velocity fluctuation with the fluctuation of the quantity, multiplied by the density. It is non-zero only if the two fluctuations are correlated, that is, if upward-moving air systematically differs from downward-moving air.

For heat, $s = c_p\,\theta$, and the sensible heat flux is

$$H = \rho\, c_p\, \overline{w'\theta'}, \tag{8.3}$$

in $\mathrm{W/m^2}$, where $\overline{w'\theta'}$, in $\mathrm{K\,m/s}$, is the *kinematic* heat flux and θ the potential temperature (Chapter 6). An illustrative afternoon value of $\overline{w'\theta'} = 0.166\,\mathrm{K\,m\,s^{-1}}$ with $\rho = 1.2\,\mathrm{kg\,m^{-3}}$ and $c_p = 1004\,\mathrm{J\,kg^{-1}\,K^{-1}}$ gives $H = 1.2 \times 1004 \times 0.166 = 200\,\mathrm{W\,m^{-2}}$. For horizontal momentum, $s = u$, and the kinematic momentum flux is $\overline{u'w'}$, in $\mathrm{m^2/s^2}$. A covariance can be written as a correlation coefficient times two standard deviations, $\overline{u'w'} = r_{uw}\,\sigma_u\,\sigma_w$; in the record of Figure 8.1, $r_{uw} = -0.64/(2.0 \times 1.0) = -0.32$, a typical value near the ground. Most of the variance of u and w is therefore uncorrelated motion; only about a third of it, in correlation, does the transport.

8.1.4 Downward transport of momentum

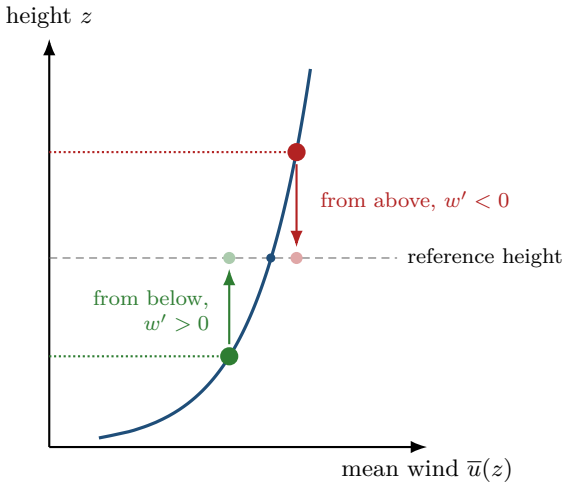
Near the ground the mean wind increases with height. An eddy that moves air downward ($w' < 0$) brings it from a level where the wind is faster, so the parcel arrives with more along-wind

momentum than its new surroundings ($u' > 0$). An eddy that moves air upward ($w' > 0$) brings slower air from below ($u' < 0$). In both cases the product $u'w'$ is negative, and on average

$$\overline{u'w'} < 0, \qquad \tau = -\rho\,\overline{u'w'} > 0, \tag{8.4}$$

where τ, in pascals, is the turbulent shear stress: the along-wind momentum carried downward per unit area per unit time. With the sign convention of this book, fluxes positive upward, a negative $\overline{u'w'}$ is a downward flux of momentum. For the record of Figure 8.1, $\tau = 1.2 \times 0.64 = 0.77\,\mathrm{Pa}$, and the velocity scale of this stress, $u_* = \sqrt{-\overline{u'w'}} = 0.8\,\mathrm{m\,s^{-1}}$, is the friction velocity of Chapter 10.

Figure 8.2 draws the argument. The blue curve is a mean wind profile, height upward and speed to the right; the dashed line is a reference height, and the blue dot on it is the mean wind there. One parcel (red) starts above the reference height, where the mean wind is faster, and is carried down; another (green) starts below, where it is slower, and is carried up. Each keeps, for the moment, the speed of its origin, shown by the dotted line from the axis, so at the reference height the red parcel arrives to the right of the profile and the green one to the left. Both parcels contribute a negative $u'w'$, so the average is negative without any parcel needing to carry momentum on purpose: the sign follows from the shear alone. The momentum carried down is eventually absorbed at the ground as drag on the surface, its roughness elements and its vegetation; this downward transport is the friction force of Chapter 3, written there as $\mathbf{F}$, and Section 8.6.1 shows that per unit mass it is $-\partial\overline{u'w'}/\partial z$. The fluxes of momentum, heat and moisture, and how they are measured, are treated in full in Chapter 9.



At the reference height
air from above: $w' < 0$, $u' > 0$, so $u'w' < 0$
air from below: $w' > 0$, $u' < 0$, so $u'w' < 0$
average: $\overline{u'w'} < 0$, a downward flux of momentum;
stress $\tau = -\rho\,\overline{u'w'} > 0$, absorbed at the ground as drag.

Figure 8.2: Downward transport of momentum in a wind that increases with height (schematic; the profile is drawn logarithmic in height). The dotted lines give each parcel's along-wind speed, the mean at its origin. Air moved down by an eddy arrives at the reference height to the right of the profile, faster than its surroundings; air moved up arrives to the left, slower; both give $u'w' < 0$.

8.1.5 Turbulent and molecular transport

Air at rest also transports momentum and heat, by the random motion of its molecules. The rates are set by the kinematic viscosity $\nu \approx 1.5 \times 10^{-5}\,\mathrm{m^2\,s^{-1}}$ for momentum and the thermal diffusivity, about $2.1 \times 10^{-5}\,\mathrm{m^2\,s^{-1}}$, for heat, both properties of air. Turbulent transport can be described by the same form with an *eddy diffusivity* K in place of the molecular one (Section 8.6.4); near the ground K ranges from about 1 to more than $100\,\mathrm{m^2\,s^{-1}}$. The ratio

$$\frac{K}{\nu} \approx \frac{1 \text{ to } 100\,\mathrm{m^2\,s^{-1}}}{1.5 \times 10^{-5}\,\mathrm{m^2\,s^{-1}}} \approx 7 \times 10^4 \text{ to } 7 \times 10^6 \tag{8.5}$$

says that turbulence moves momentum and heat five to seven orders of magnitude faster than molecular diffusion.

The difference is clearest as a time. A diffusive process spreads a quantity over a distance L in a time of order L^2/D, with D the diffusivity. Over $L = 100\,\mathrm{m}$, molecular viscosity would take $100^2/(1.5\times10^{-5}) \approx 6.7\times10^8\,\mathrm{s}$, about 21 years, while an eddy diffusivity of $10\,\mathrm{m^2\,s^{-1}}$ takes $100^2/10 = 1000\,\mathrm{s}$, about 17 minutes. Without turbulence, the surface would have no practical influence on the wind 100 m up. Molecular transport still matters in a layer a few millimeters thick against every surface, on the ground, on a leaf, on a conductor, where the eddies cannot reach; the final transfer of heat from a conductor to the air passes through such a layer. Above it, transport is turbulent. A second difference is that ν is a property of the air while K is a property of the flow: it depends on the wind, the height and the stability, and it changes by orders of magnitude between day and night.

8.1.6 The Reynolds number

Whether a flow is turbulent is decided by the Reynolds number. For a flow of speed U varying over a length L, the inertial acceleration is of order U^2/L and the viscous acceleration of order $\nu U/L^2$; their ratio is

$$\mathrm{Re} = \frac{U^2/L}{\nu U/L^2} = \frac{UL}{\nu}. \tag{8.6}$$

When Re is small, viscosity damps any disturbance and the flow is laminar, smooth and layered. When Re is large, disturbances grow faster than viscosity can damp them, and the flow becomes turbulent; flow in a pipe, for example, becomes turbulent at Reynolds numbers of a few thousand.

For near-surface wind with $U = 10\,\mathrm{m\,s^{-1}}$, $L = 100\,\mathrm{m}$ and $\nu = 1.5\times10^{-5}\,\mathrm{m^2\,s^{-1}}$,

$$\mathrm{Re} = \frac{10\,\mathrm{m\,s^{-1}}\times 100\,\mathrm{m}}{1.5\times10^{-5}\,\mathrm{m^2\,s^{-1}}} \approx 6.7\times10^7,$$

four orders of magnitude above the threshold. Even a light wind of $1\,\mathrm{m\,s^{-1}}$ over 10 m gives $\mathrm{Re}\approx 7\times10^5$. The near-surface atmosphere is therefore almost always strongly turbulent. The exception is not a low Reynolds number but strong stable stratification on clear, calm nights, when buoyancy suppresses the vertical motions that viscosity cannot (Section 8.4.3).

8.2 Eddies and the energy cascade

Turbulence is made of eddies of many sizes, and its energy passes from the largest to the smallest before it is lost. This section describes the eddies, the cascade of energy among them, the spectrum that results, and the smallest size the cascade reaches.

8.2.1 Eddies and their range of sizes

An eddy is a coherent turbulent motion: a swirling, organized parcel of air that moves as a unit within the larger flow for a while, with its own size, velocity and lifetime, before it is stretched and broken up. Eddies are not separate objects with sharp edges; they overlap, merge and sit inside one another, and a record such as Figure 8.1 is the sum of all of them passing the sensor. In the atmosphere their sizes range from about a millimeter to more than a kilometer: the largest are the thermals of a convective afternoon, as deep as the boundary layer, and the smallest are the eddies at which viscosity acts, computed in Section 8.2.4.

The size of the largest eddies is limited by the geometry. Near the ground an eddy cannot be much larger than its distance from the surface, because the ground blocks its vertical motion, so at height z the energy-containing eddies are of size of order z: a few meters at 2 m, tens of

meters at 20 m. Higher up the limit is the depth of the boundary layer, z_i. The lifetime of an eddy is of the order of its turnover time, its size divided by its velocity: an eddy of 20 m with a velocity of $1\,\mathrm{m\,s^{-1}}$ lives about 20 s, and an eddy of 1 cm with a velocity of about $0.1\,\mathrm{m\,s^{-1}}$ lives about a tenth of a second.

Large and small eddies. The large eddies hold most of the turbulent kinetic energy and do most of the transport of momentum, heat and moisture. They are generated directly by the processes that feed turbulence: wind shear, convection, flow over terrain and around obstacles. They therefore carry the imprint of their source: their shape and orientation depend on the direction of the shear, on gravity and on the obstacle. They are also unstable: each is stretched and sheared by its neighbors and breaks down into smaller eddies, which break down in turn. The small eddies hold little energy and transport little, but they are where the energy is finally converted into heat.

8.2.2 The Kolmogorov picture

The chain from large to small eddies is the *energy cascade*. Its standard description, due to Kolmogorov (1941), has three ranges of scale. In the *production range* the largest eddies draw energy from the mean flow, through shear, or from buoyancy. In the *inertial subrange* eddies of intermediate size receive energy from larger ones and pass it to smaller ones; neither production nor viscosity acts appreciably there, so energy is transferred without loss. In the *dissipation range* the eddies are small enough for viscosity to convert their kinetic energy into heat. In a steady state the rate at which energy enters at the large scales, passes through every intermediate scale and is dissipated at the small scales is one and the same number, the dissipation rate ε, in $\mathrm{m^2/s^3}$, which is watts per kilogram.

Figure 8.3 draws the cascade. From left to right are the mean flow, eddies of decreasing size, and heat. The arrows entering the largest eddy from above are the two sources of turbulent energy, shear production and buoyancy production (Section 8.3.5); the arrows between eddies are the transfer down the cascade, all at the rate ε; the braces below mark the three ranges with illustrative sizes for a height of about 10 m. The figure makes one feature explicit: the energy dissipated by the smallest eddies is set by the largest ones. A large eddy of velocity u_0 and size ℓ_0 passes on its kinetic energy, of order u_0^2, in about one turnover time, ℓ_0/u_0, so

$$\varepsilon \sim \frac{u_0^2}{\ell_0/u_0} = \frac{u_0^3}{\ell_0}, \tag{8.7}$$

independent of the viscosity. With $u_0 \approx \sigma_w = 1\,\mathrm{m\,s^{-1}}$ and $\ell_0 \approx 10\,\mathrm{m}$, $\varepsilon \sim 0.1\,\mathrm{m^2\,s^{-3}}$. Viscosity does not decide how much energy is dissipated, only the size at which it happens.

8.2.3 The spectrum and the $-5/3$ law

The distribution of turbulent energy over eddy sizes is described by the energy spectrum $E(k)$. Here $k = 2\pi/\lambda$ is the wavenumber, in rad/m, the inverse of a spatial scale λ: small k means large eddies, large k small eddies. $E(k)\,\mathrm{d}k$ is the turbulent kinetic energy per unit mass in eddies with wavenumbers between k and $k + \mathrm{d}k$, so $E(k)$ has units of $\mathrm{m^3\,s^{-2}}$ and its integral over all wavenumbers is the turbulent kinetic energy of Section 8.3.1. (The letter k is reserved for the wavenumber in this book; turbulent kinetic energy is e.)

In the inertial subrange the eddies have forgotten how they were produced and are not yet affected by viscosity, so the spectrum can depend only on the rate ε at which energy passes through and on the wavenumber k itself. Kolmogorov's form follows from units alone. Write $E(k) = C_K\,\varepsilon^a\,k^b$ with a dimensionless constant C_K. The units must match:

$$\mathrm{m^3\,s^{-2}} = \left(\mathrm{m^2\,s^{-3}}\right)^a \left(\mathrm{m^{-1}}\right)^b = \mathrm{m^{2a-b}\,s^{-3a}}.$$

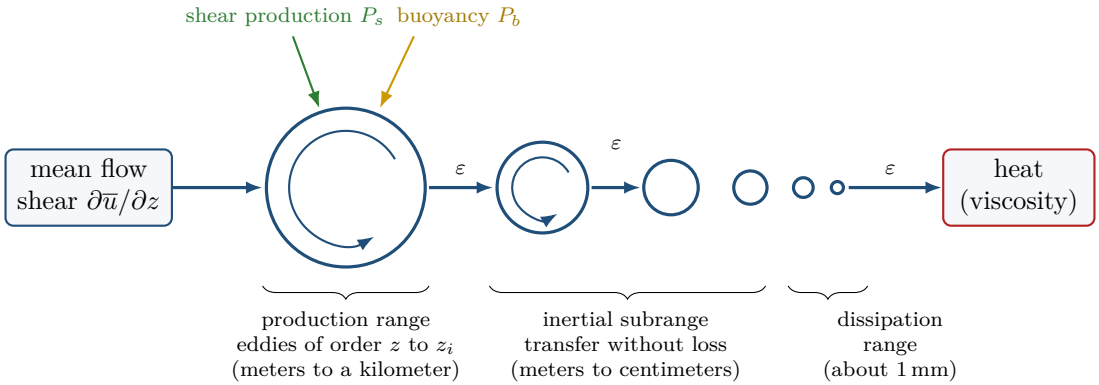


Figure 8.3: The energy cascade (schematic). Shear and buoyancy feed the largest eddies; energy passes to ever smaller eddies at the rate ε without loss through the inertial subrange and is converted into heat by viscosity at the smallest scales. Sizes are illustrative for a height of about 10 m.

The seconds give $-3a = -2$, so $a = 2/3$; the meters give $2a - b = 3$, so $b = 4/3 - 3 = -5/3$. Hence

$$E(k) = C_K \, \varepsilon^{2/3} \, k^{-5/3}, \tag{8.8}$$

with $C_K \approx 1.5$ from measurements: the $-5/3$ law. On log-log axes it is a straight line of slope $-5/3$, and its level gives ε. A sensor at a fixed point measures in time, not in space; if the eddies are carried past it by the mean wind faster than they change, an eddy of wavenumber k produces a signal of frequency $\overline{u}k/(2\pi)$ (Taylor's frozen-turbulence hypothesis), and the frequency spectrum of a sonic anemometer record shows the same $-5/3$ slope in its high-frequency part.

Figure 8.4 plots a model spectrum on log-log axes. The horizontal axis is the wavenumber k from 10^{-3} to about 4×10^3 rad m^{-1}, eddies from kilometers to millimeters; the vertical axis is $E(k)$. The dashed vertical lines divide the three ranges of Figure 8.3, and the gray line is the pure $-5/3$ law. At small k the spectrum rises to a peak near $k \approx 0.3$ rad m^{-1}, eddies of about 20 m, the energy-containing eddies at this height; through the inertial subrange it follows the $-5/3$ line over more than two decades; beyond $k \approx 250$ rad m^{-1}, eddies of a few centimeters and less, it falls steeply as viscosity removes the energy. Turbulence is a continuous range of scales, not a set of separate sizes.

8.2.4 The Kolmogorov length scale

The cascade ends where an eddy is small enough for viscosity to destroy it in about one turnover. In the inertial subrange an eddy of size ℓ has a velocity $v_\ell \sim (\varepsilon \, \ell)^{1/3}$, which follows from equation (8.7) applied at every scale. Its own Reynolds number is

$$\mathrm{Re}_\ell = \frac{v_\ell \, \ell}{\nu} = \frac{\varepsilon^{1/3} \, \ell^{4/3}}{\nu},$$

and setting $\mathrm{Re}_\ell = 1$, the size at which inertia and viscosity are equal, gives

$$\eta_K = \left(\frac{\nu^3}{\varepsilon} \right)^{1/4}, \tag{8.9}$$

the *Kolmogorov length scale*, often written η; the subscript here distinguishes it from the absolute vorticity. The units check: ν^3/ε is m^6 s^{-3}/(m^2 s^{-3}) = m^4, and its fourth root is a length.

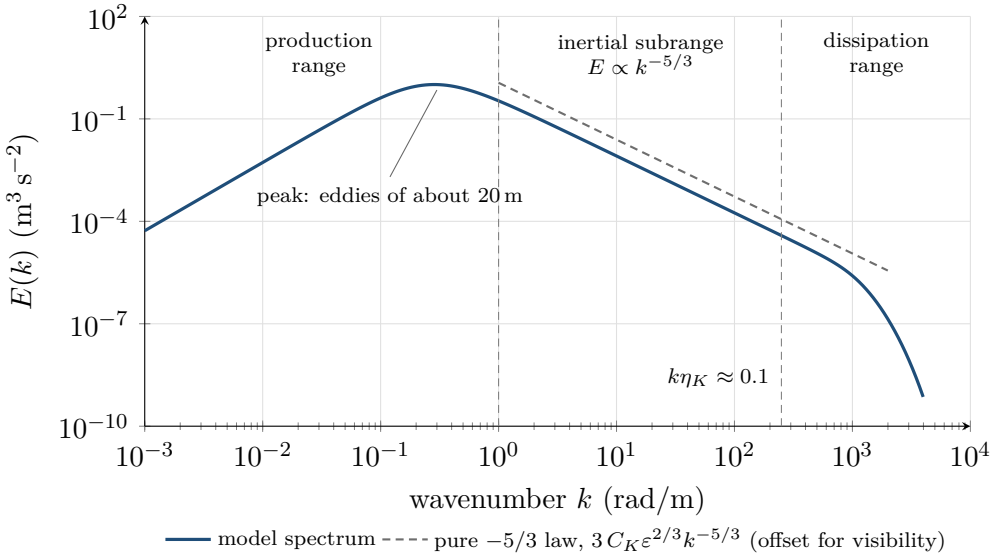


Figure 8.4: Model energy spectrum on log-log axes, illustrative, for $C_K = 1.5$, $\varepsilon = 0.128\,\mathrm{m^2\,s^{-3}}$, a large-eddy length $L = 10\,\mathrm{m}$ and $\eta_K = 0.40\,\mathrm{mm}$, from a standard model form, $E(k) = C_K\varepsilon^{2/3}k^{-5/3}f_L(kL)f_\eta(k\eta_K)$ with $f_L = [kL/((kL)^2 + 6.78)^{1/2}]^{11/3}$ and $f_\eta = \exp\{-5.2[((k\eta_K)^4 + 0.4^4)^{1/4} - 0.4]\}$. The range boundaries at $k = 1$ and $250\,\mathrm{rad\,m^{-1}}$ are approximate.

For an illustrative near-surface dissipation rate $\varepsilon = 0.128\,\mathrm{m^2\,s^{-3}}$, the value of the worked example in Section 8.3.2,

$$\eta_K = \left(\frac{(1.5\times10^{-5})^3}{0.128}\right)^{1/4} = \left(2.64\times10^{-14}\right)^{1/4}\ \mathrm{m} \approx 4.0\times10^{-4}\,\mathrm{m} = 0.40\,\mathrm{mm}.$$

Higher in the boundary layer, with $\varepsilon = 0.01\,\mathrm{m^2\,s^{-3}}$, $\eta_K \approx 0.76\,\mathrm{mm}$. Because of the fourth root, dissipation rates that differ by a factor of ten change η_K by less than a factor of two: the smallest eddies in the atmosphere are always of order a millimeter. At this scale the eddy velocity is $(\nu\varepsilon)^{1/4} \approx 3.7\,\mathrm{cm/s}$ and the turnover time $(\nu/\varepsilon)^{1/2} \approx 0.011\,\mathrm{s}$.

The ratio of the largest to the smallest eddies is $10\,\mathrm{m}/0.4\,\mathrm{mm} = 2.5\times10^4$ at this height, and more than 10^6 across a convective boundary layer. A simulation that resolved every eddy in one cubic kilometer of air at a spacing of η_K would need $(1000/0.0004)^3 \approx 1.6\times10^{19}$ grid points, far beyond any computer. Every atmospheric model therefore represents at least the small eddies, and usually all of them, by a formula; Section 8.6 describes how.

8.2.5 Local isotropy

The large eddies are anisotropic: they are shaped by the shear, by gravity and by the ground, and their statistics differ between the along-wind, cross-wind and vertical directions (Section 8.4.4). As energy passes down the cascade, each step of breakup scrambles the orientation a little more, and the small eddies retain progressively less memory of the direction of the mean flow and of the surface. Kolmogorov's hypothesis of *local isotropy* is that, at scales well inside the inertial subrange and below, the statistics of turbulence are approximately the same in every direction.

Local isotropy has a measurable consequence. In the inertial subrange the frequency spectra of the cross-wind and vertical components should be 4/3 of the along-wind spectrum at the same frequency, and sonic anemometer records near the ground approach this ratio at frequencies of a few hertz and above, though not at the low frequencies of the energy-containing eddies. It also justifies a practical method: because the inertial-subrange level of a spectrum depends only

on ε, equation (8.8) is used to estimate the dissipation rate from a fast velocity record, without resolving the millimeter scales at which dissipation actually occurs.

8.3 Turbulent kinetic energy and its budget

The intensity of turbulence is measured by its kinetic energy, and that energy is the balance of what shear and buoyancy produce, what the cascade dissipates and what the eddies carry from one height to another. This section defines the turbulent kinetic energy, derives each term of its budget with worked numbers, and assembles them.

8.3.1 Turbulent kinetic energy

The *turbulent kinetic energy* per unit mass is half the sum of the variances of the three velocity components,

$$e = \tfrac{1}{2}\left(\overline{u'^2} + \overline{v'^2} + \overline{w'^2}\right) = \tfrac{1}{2}\left(\sigma_u^2 + \sigma_v^2 + \sigma_w^2\right), \tag{8.10}$$

in $\mathrm{m^2\,s^{-2}}$, which is joules per kilogram. It is the kinetic energy of the fluctuations alone, the energy of the eddies, as distinct from the kinetic energy of the mean flow, $\frac{1}{2}\overline{u}^2$. It is measured by a three-component sonic anemometer, from the variances of a record such as Figure 8.1; a cup anemometer, which records only the horizontal speed, cannot give it. Many texts write turbulent kinetic energy as k and name models after it (the "k–ε" model of Section 8.6.3); in this book k is the wavenumber and the energy is e.

For the illustrative standard deviations of the record, $\sigma_u = 2.0\,\mathrm{m\,s^{-1}}$, $\sigma_v = 1.6\,\mathrm{m\,s^{-1}}$ and $\sigma_w = 1.0\,\mathrm{m\,s^{-1}}$,

$$e = \tfrac{1}{2}\left(2.0^2 + 1.6^2 + 1.0^2\right) = \tfrac{1}{2}\,(4.00 + 2.56 + 1.00) = 3.78\,\mathrm{m^2\,s^{-2}},$$

or 3.78 J/kg, about $4.5\,\mathrm{J/m^3}$ at $\rho = 1.2\,\mathrm{kg\,m^{-3}}$. The mean flow at $10\,\mathrm{m\,s^{-1}}$ carries $\frac{1}{2}\times 10^2 = 50\,\mathrm{J/kg}$, so the eddies hold about 8 % of the kinetic energy of the near-surface wind. More than half of e is in the along-wind component; the vertical component, the one that does the transport, holds only $0.5/3.78 = 13\,\%$.

8.3.2 Shear production

The main source of turbulence near the ground is the shear of the mean wind. Its rate follows from the energy of the mean flow. For horizontally uniform flow in along-wind coordinates, the averaged momentum equation of Section 8.6.1 contains the turbulent term $-\partial\overline{u'w'}/\partial z$. Multiplying it by $\overline{u}$ gives the rate at which turbulence changes the mean kinetic energy, and by the product rule

$$-\overline{u}\,\frac{\partial \overline{u'w'}}{\partial z} = -\frac{\partial\left(\overline{u}\,\overline{u'w'}\right)}{\partial z} + \overline{u'w'}\,\frac{\partial \overline{u}}{\partial z}. \tag{8.11}$$

The first term on the right is the divergence of a flux: it moves mean kinetic energy from one height to another and integrates to the boundary values over a column. The second term is a local loss: with $\overline{u'w'} < 0$ and $\partial\overline{u}/\partial z > 0$ it is negative, and the energy it removes from the mean flow appears, with the opposite sign, in the budget of the eddies. That gain is the *shear production*

$$P_s = -\overline{u'w'}\,\frac{\partial \overline{u}}{\partial z}, \tag{8.12}$$

in $\mathrm{m^2\,s^{-3}}$ or W/kg. (If the wind turns with height, a second term $-\overline{v'w'}\,\partial\overline{v}/\partial z$ adds to it.) Shear production is positive whenever the momentum flux runs down the gradient of the mean wind, which Section 8.1.4 showed it does: shear makes eddies, and the eddies are paid for with the energy of the mean wind.

For the record of Figure 8.1, $\overline{u'w'} = -0.64\,\mathrm{m^2\,s^{-2}}$, and with an illustrative shear at 10 m of $\partial\overline{u}/\partial z = 0.2\,\mathrm{s^{-1}}$, the value the neutral logarithmic profile of Chapter 7 gives there for $u_* = 0.8\,\mathrm{m\,s^{-1}}$,

$$P_s = -(-0.64\,\mathrm{m^2\,s^{-2}}) \times 0.2\,\mathrm{s^{-1}} = 0.128\,\mathrm{m^2\,s^{-3}},$$

0.128 W for every kilogram of air, about $0.15\,\mathrm{W/m^3}$. Dividing the energy by its rate of supply, $e/P_s = 3.78/0.128 \approx 30\,\mathrm{s}$: the eddies' energy is replaced in about half a minute. Turbulence near the ground is not a reservoir that persists on its own; if the shear stopped, it would decay within minutes.

8.3.3 Buoyancy production and destruction

The second source, or sink, is buoyancy. A parcel whose virtual potential temperature exceeds that of its surroundings by θ_v' is lighter and feels an upward buoyant acceleration $g\,\theta_v'/\theta_v$ (Chapter 6). The rate at which this force does work on the vertical fluctuations, per unit mass, is the average of force times velocity,

$$P_b = \overline{w'\,\frac{g\,\theta_v'}{\theta_v}} = \frac{g}{\theta_v}\,\overline{w'\theta_v'} \approx \frac{g}{\theta}\,\overline{w'\theta'}, \tag{8.13}$$

with the last form for dry air, in which θ_v and θ coincide; in moist air the flux of θ_v, which includes the buoyancy of water vapor, is the correct one. When warm air rises and cool air sinks, $\overline{w'\theta'} > 0$ and buoyancy feeds the eddies: *buoyancy production*. When the air is stably stratified, warmer above colder, an eddy that lifts air lifts it into warmer surroundings, where it is cooler and heavier ($w' > 0$, $\theta' < 0$), and one that lowers air brings it into cooler surroundings, where it is warmer and lighter. Then $\overline{w'\theta'} < 0$ and $P_b < 0$: the eddies work against gravity, and buoyancy destroys turbulent energy, converting it into potential energy of the stratification.

With $g/\theta = 9.81/300 = 0.0327\,\mathrm{m\,s^{-2}\,K^{-1}}$ for an illustrative $\theta = 300\,\mathrm{K}$, two heat fluxes give the two signs.

- *Day*: a sensible heat flux of $H = 200\,\mathrm{W\,m^{-2}}$ is, by equation (8.3), $\overline{w'\theta'} = 200/(1.2\times1004) = 0.166\,\mathrm{K\,m\,s^{-1}}$, and $P_b = 0.0327 \times 0.166 = 5.4 \times 10^{-3}\,\mathrm{m^2\,s^{-3}}$.
- *Night*: $H = -30\,\mathrm{W\,m^{-2}}$ gives $\overline{w'\theta'} = -0.0249\,\mathrm{K\,m\,s^{-1}}$ and $P_b = -8.1 \times 10^{-4}\,\mathrm{m^2\,s^{-3}}$.

Compared with the shear production of $0.128\,\mathrm{m^2\,s^{-3}}$ in the $10\,\mathrm{m\,s^{-1}}$ wind of Section 8.3.2, both are small, about 4 % and −0.6 %: in a strong wind the lowest ten meters are close to neutral whatever the sun does. Buoyancy matters when the wind is light or the height is greater, because shear production falls with the wind speed and with height while the heat flux does not; in the light-wind cases of Figure 8.5 it is comparable to or larger than shear production. Shear creates turbulence and stable stratification suppresses it; their competition is the subject of Section 8.3.6.

8.3.4 Dissipation

The energy produced by shear and buoyancy leaves the turbulence through the cascade of Section 8.2.2, and the rate at which viscosity converts it into heat at the Kolmogorov scale is the *dissipation rate* ε, in $\mathrm{m^2\,s^{-3}}$. It is always positive: dissipation only removes energy. Its value is set by the large eddies, $\varepsilon \sim u_0^3/\ell_0$ (equation (8.7)), even though the conversion happens at the smallest. It is not measured directly, because no practical sensor resolves millimeter eddies outdoors; it is inferred from the inertial-subrange level of a measured spectrum through equation (8.8), or from the budget as the term that closes it.

The heat produced is real but small in the energy balance of the ground. Near the surface in strong wind, $\varepsilon \approx 0.1\,\mathrm{W/kg}$ warms the air at only about $0.1/1004 \approx 10^{-4}\,\mathrm{K/s}$, and integrated

over the depth of the boundary layer the dissipation is of order 1 to $10\,\mathrm{W\,m^{-2}}$, against sensible heat fluxes of tens to hundreds. The energy dissipated ultimately comes from the large-scale pressure gradient that drives the wind, through the mean flow and the cascade. In a simple budget, the turbulent kinetic energy changes at the rate

$$\frac{\mathrm{d}e}{\mathrm{d}t} = \text{production} + \text{transport} - \text{dissipation},$$

which the next subsection writes term by term.

8.3.5 The budget equation

For horizontally uniform conditions in along-wind coordinates, the budget of turbulent kinetic energy is

$$\frac{\partial e}{\partial t} = \underbrace{-\overline{u'w'}\,\frac{\partial \overline{u}}{\partial z}}_{P_s} + \underbrace{\frac{g}{\theta_v}\,\overline{w'\theta_v'}}_{P_b} \underbrace{-\frac{\partial}{\partial z}\left(\tfrac{1}{2}\overline{w'(u'^2+v'^2+w'^2)} + \frac{\overline{w'p'}}{\rho}\right)}_{\mathrm{Tr}} - \varepsilon. \tag{8.14}$$

Term by term: the storage on the left is the rate of change of e at a fixed point; P_s is shear production, the transfer from the mean wind; P_b is buoyancy production when positive and buoyancy destruction when negative; Tr is transport, the divergence of the flux of turbulent kinetic energy carried by the eddies themselves and by pressure fluctuations, which moves energy between heights without creating or destroying it; and ε is dissipation. The equation is derived by subtracting the averaged momentum equations from the full ones, multiplying each fluctuation equation by its own velocity fluctuation and averaging; the derivation is long, but each term has the meaning just given, and the two production terms are the ones derived in Sections 8.3.2 and 8.3.3.

In steady, horizontally uniform conditions near the ground, storage is small and transport is often modest, and the budget reduces to a local balance, $P_s + P_b \approx \varepsilon$: turbulence is dissipated about as fast as it is produced. Figure 8.5 shows three illustrative budgets at 10 m in light to moderate wind. The horizontal axis groups the three conditions; for each, the four bars are shear production, buoyancy production, minus the dissipation, and transport, in units of $10^{-3}\,\mathrm{m^2\,s^{-3}}$, gains above the zero line and losses below. In each group the bars sum to zero, a steady state. The *neutral* budget (overcast, $u_* = 0.3\,\mathrm{m\,s^{-1}}$, $\partial\overline{u}/\partial z = 0.075\,\mathrm{s^{-1}}$) is shear production balanced by dissipation. The *convective* budget (afternoon, $u_* = 0.3\,\mathrm{m\,s^{-1}}$, $H = 200\,\mathrm{W\,m^{-2}}$) has buoyancy production larger than shear production, which is itself smaller than in the neutral case because convective mixing weakens the shear to $0.039\,\mathrm{s^{-1}}$; transport exports part of the energy upward. The *stable* budget (night, $u_* = 0.2\,\mathrm{m\,s^{-1}}$, $H = -30\,\mathrm{W\,m^{-2}}$) has a stronger shear of $0.15\,\mathrm{s^{-1}}$, because the suppressed mixing lets the wind change faster with height, and a negative buoyancy term that removes part of what shear produces.

Principle 8.1. *Turbulent kinetic energy is produced by shear, $P_s = -\overline{u'w'}\,\partial\overline{u}/\partial z$, produced or destroyed by buoyancy, $P_b = (g/\theta_v)\overline{w'\theta_v'}$, redistributed by transport and removed by dissipation ε; near the ground in steady conditions production and dissipation nearly balance.*

8.3.6 The flux Richardson number

The competition between shear and stratification is summarized by the ratio of buoyancy destruction to shear production, the *flux Richardson number*

$$\mathrm{Ri}_f = -\frac{P_b}{P_s} = \frac{-(g/\theta_v)\,\overline{w'\theta_v'}}{-\overline{u'w'}\,\partial\overline{u}/\partial z}. \tag{8.15}$$

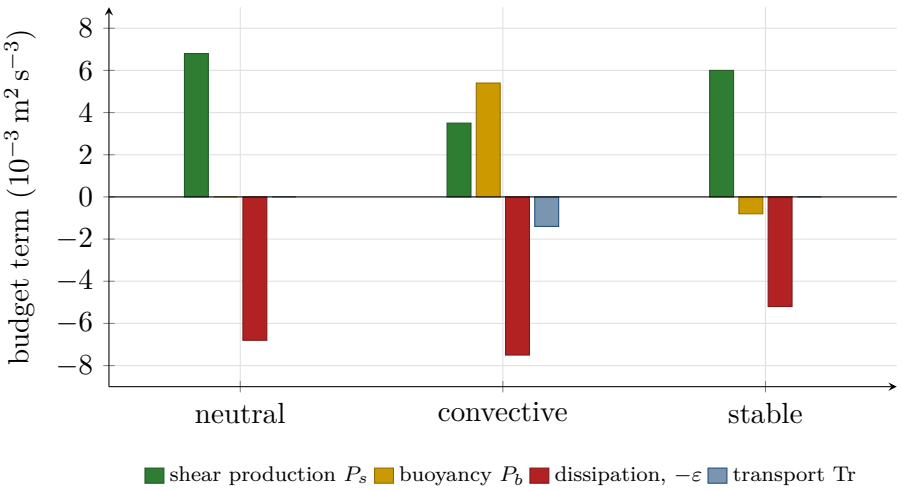


Figure 8.5: Illustrative budgets of turbulent kinetic energy at 10 m, equation (8.14) in steady state. Neutral: $P_s = 0.09 \times 0.075 = 6.8$, $\varepsilon = 6.8$. Convective: $P_s = 0.09 \times 0.039 = 3.5$, $P_b = 5.4$ ($H = 200\,\mathrm{W\,m^{-2}}$), $\varepsilon = 7.5$, $\mathrm{Tr} = -1.4$. Stable: $P_s = 0.04 \times 0.15 = 6.0$, $P_b = -0.8$ ($H = -30\,\mathrm{W\,m^{-2}}$), $\varepsilon = 5.2$. All values in $10^{-3}\,\mathrm{m^2\,s^{-3}}$; each group sums to zero.

It is positive in stable conditions, where buoyancy removes a fraction Ri_f of what shear produces; zero in neutral conditions; and negative in unstable conditions, where buoyancy adds to production. In the steady local balance with no transport, $\varepsilon = P_s + P_b = P_s\,(1 - \mathrm{Ri}_f)$, and since ε cannot be negative, shear-driven turbulence can be sustained only for $\mathrm{Ri}_f < 1$. Observations show that it fades well before that bound, at values of about 0.2 to 0.25, the critical flux Richardson number.

For the windy night of Section 8.3.3, $\mathrm{Ri}_f = 8.1 \times 10^{-4}/0.128 = 0.006$, negligible; for the stable budget of Figure 8.5, $\mathrm{Ri}_f = 0.8/6.0 = 0.13$, and the turbulence survives with a reduced dissipation; for the convective budget, $\mathrm{Ri}_f = -5.4/3.5 = -1.5$. The flux Richardson number is related to the gradient Richardson number Ri of Chapter 5, which uses the gradients of potential temperature and wind instead of the fluxes, by $\mathrm{Ri}_f = (K_h/K_m)\,\mathrm{Ri}$, with the eddy diffusivities of Section 8.6.4. Both measure whether shear production can overcome buoyant suppression; Chapter 13 takes them up in full.

8.4 Kinds of turbulence near the ground

The two production terms of the budget correspond to two kinds of turbulence, mechanical and convective, and the destruction term to a third regime in which turbulence is weak and intermittent. This section describes each and the anisotropy that the ground imposes on all three.

8.4.1 Mechanical turbulence

Mechanical turbulence is generated by shear production: by the shear of the wind near the ground, by drag on the surface, and by flow over and around obstacles and terrain, buildings, trees and forests, ridges and escarpments, where the flow separates and forms wakes. It occurs by day or by night whenever the wind is strong enough. Its eddies scale with the height above the ground in the surface layer and with the size of the obstacle in a wake. Figure 8.6 draws the three kinds side by side; each panel is a vertical cross section, the ground at the bottom and the mean wind from left to right. In the left panel the eddies grow with height and are tilted by the shear, and an obstacle sheds a wake of smaller eddies.

Because shear production scales with u_*^3 divided by height, and u_* is proportional to the wind speed for a given surface, the standard deviations of mechanical turbulence are proportional to the wind speed: $\sigma_u \approx 2.4\,u_*$ in neutral conditions (Section 8.4.4). With the logarithmic profile $\overline{u} = (u_*/\kappa)\ln(z/z_0)$ of Chapter 7,

$$\frac{\sigma_u}{\overline{u}} \approx \frac{2.4\,\kappa}{\ln(z/z_0)} \approx \frac{0.96}{\ln(z/z_0)},$$

independent of the wind speed. At 10 m over open land with hedges, $z_0 = 0.08$ m, this is $0.96/\ln 125 = 0.20$, the ratio of the record of Figure 8.1; over open sea, $z_0 \approx 0.0002$ m, it is $0.96/\ln(5\times10^4) = 0.09$. In neutral conditions the roughness of the ground, not the wind speed, sets the relative strength of mechanical turbulence.

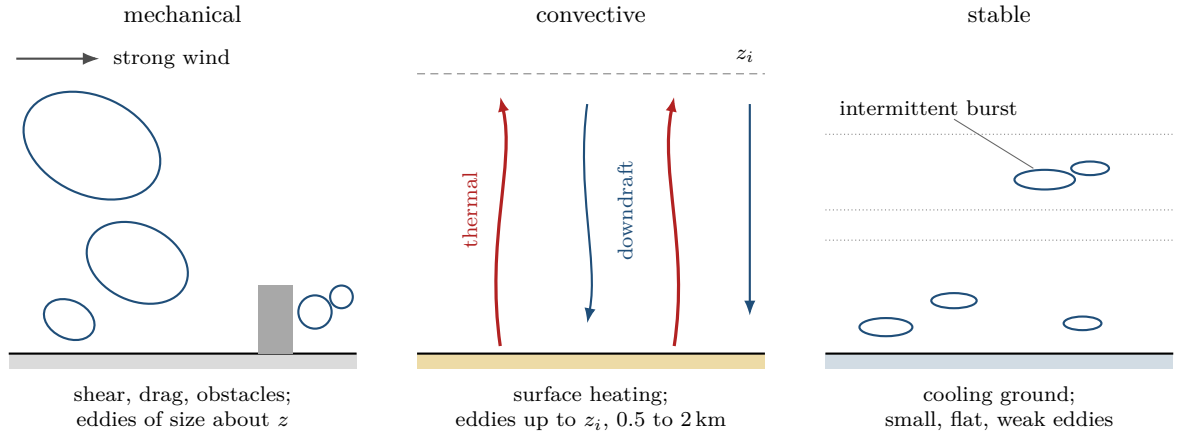


Figure 8.6: Three kinds of near-surface turbulence in vertical cross section (schematic; mean wind from left to right, ground at the bottom). Mechanical: eddies grow with height and tilt with the shear; an obstacle sheds a wake. Convective: thermals and downdrafts as deep as the boundary layer. Stable: small, flattened eddies, often confined to bursts, between layers (dotted) that barely exchange air.

8.4.2 Convective turbulence

Convective turbulence is generated by buoyancy production. When the sun heats the ground, the air in contact with it warms, becomes lighter and rises in plumes that merge into thermals; cooler air sinks between them in broader, slower downdrafts (middle panel of Figure 8.6). In a deep daytime boundary layer the largest of these motions span the whole depth, from hundreds of meters to more than a kilometer, and they dominate the vertical transport of heat, moisture and momentum in the layer. Their velocity scale is the *convective velocity scale*

$$w_* = \left(\frac{g}{\theta_v}\,\overline{w'\theta'_{v0}}\,z_i\right)^{1/3}, \tag{8.16}$$

in m/s, where the subscript 0 denotes the surface value of the kinematic heat flux. For the afternoon flux of Section 8.3.3, 0.166 K m s^{-1}, and $z_i = 1500$ m, $w_* = (0.0327\times0.166\times1500)^{1/3} = (8.14)^{1/3} \approx 2.0$ m s^{-1}; the standard deviation of the vertical velocity in the middle of such a layer is about $0.6\,w_* \approx 1.2$ m s^{-1}.

Convective turbulence differs from mechanical turbulence in two ways that matter near the ground. It does not need wind: on a calm sunny afternoon thermals mix the boundary layer vigorously even when the mean wind is 1 or 2 m s^{-1}, so the wind near the ground is variable in speed and direction with a large ratio of fluctuation to mean. And its large eddies take minutes

to pass a sensor, so a ten-minute average contains only a few of them, and the mean itself varies from one ten-minute period to the next. Convective turbulence is most important in the afternoon, in light wind, and over dry ground, where most of the sun's energy becomes sensible heat flux.

8.4.3 Stable and intermittent turbulence

On clear nights the ground cools by radiation, the air near it becomes colder than the air above, and the stratification is stable. Buoyancy then destroys turbulence. The eddies that survive are smaller, weaker and flatter, with more horizontal than vertical motion, because vertical excursions cost energy against gravity (right panel of Figure 8.6). Layers a few meters apart can slide past each other with little exchange, and the air near the ground becomes partly decoupled from the wind above.

Turbulence in stable conditions is often *intermittent*: quiet periods with almost no turbulence alternate with bursts lasting seconds to minutes. During a quiet period the reduced mixing lets the wind above accelerate and the shear grow; when shear production overcomes buoyant destruction, that is when the Richardson number falls below its critical value, turbulence breaks out, mixes momentum down, reduces the shear, and dies again. Whether turbulence survives at all is decided by the competition of Section 8.3.6: strong enough shear still generates turbulence in stable air, as on a windy night, and weak shear does not. A ten-minute statistic of an intermittent record mixes bursts and calm and may describe neither; flux and turbulence measurements are least reliable in these conditions.

8.4.4 Anisotropy near the surface

Near the ground the three standard deviations are unequal, approximately

$$\sigma_u > \sigma_v > \sigma_w, \tag{8.17}$$

which is *anisotropy*: turbulence that is not the same in every direction. The ground blocks vertical motion, so the largest eddies are flattened; the along-wind component also receives the shear production directly, since P_s enters the budget of $\overline{u'^2}$ and reaches the other components only by pressure fluctuations that redistribute energy among them. The anisotropy is strongest at the large, energy-containing scales and fades at the small scales, as Section 8.2.5 described.

Table 8.1 gives typical ratios of the standard deviations to the friction velocity over flat, uniform ground in neutral conditions, with each component's share of the turbulent kinetic energy. The columns are the component, the ratio σ/u_*, its square and the share; the last row is the total. With these values, $e \approx 5.5\,u_*^2$, and more than half of it is in the along-wind component, against one third each for isotropic turbulence. The record of Figure 8.1, with ratios $2.0/0.8 = 2.5$, $1.6/0.8 = 2.0$ and $1.0/0.8 = 1.25$, is close to these values. The ratios for σ_w are the most reliable; those for σ_u and σ_v vary more, because the horizontal components also include slow meanders and mesoscale motions unrelated to the local shear, which can inflate σ_v in particular at low wind speed and at night. In convective conditions σ_w scales with w_* rather than u_* and the ratios to u_* grow.

8.5 Turbulence statistics in engineering

Engineering use of wind data rarely works with spectra or budgets; it works with a few statistics of a record: a mean, a turbulence intensity, a gust. This section defines them, states what each does and does not say about the turbulence, and shows how strongly a wind value depends on the period over which it is averaged.

Table 8.1: Typical neutral values of the velocity standard deviations near the ground over flat, uniform terrain, and each component's share of the turbulent kinetic energy. The ratios vary by about ten percent between sites and are larger in unstable conditions.

Component	σ/u_* (typical neutral)	$(\sigma/u_*)^2$	Share of e
along-wind, σ_u	2.4	5.76	53 %
cross-wind, σ_v	1.9	3.61	33 %
vertical, σ_w	1.25	1.56	14 %
total, $e/u_*^2 = \frac{1}{2}\sum(\sigma/u_*)^2$	–	10.93	$e \approx 5.5\,u_*^2$

8.5.1 Turbulence intensity

The *turbulence intensity* is the standard deviation of the wind speed divided by its mean over the same period,

$$\mathrm{TI} = \frac{\sigma_U}{\overline{U}}, \tag{8.18}$$

dimensionless and often quoted in percent, where U is the horizontal wind speed and σ_U its standard deviation, usually over ten minutes. For a mean wind of $\overline{U} = 10\,\mathrm{m\,s^{-1}}$ with $\sigma_U = 2\,\mathrm{m\,s^{-1}}$,

$$\mathrm{TI} = \frac{2\,\mathrm{m\,s^{-1}}}{10\,\mathrm{m\,s^{-1}}} = 0.2 = 20\,\%.$$

Because the fluctuations of speed are mostly along-wind, σ_U is close to σ_u when TI is moderate; for the record of Figure 8.1, the horizontal speed has mean $10.13\,\mathrm{m\,s^{-1}}$ and standard deviation $1.99\,\mathrm{m\,s^{-1}}$, so TI = 0.196. Typical values at turbine and conductor heights in neutral conditions range from below 10 % offshore to 15 to 25 % over rough land and more near forests and buildings, consistent with the $0.96/\ln(z/z_0)$ of Section 8.4.1. Wind-turbine design classes, fatigue loads and the power-curve corrections of wind energy all use it.

Limits of the statistic. Turbulence intensity has three practical limits. It is undefined at calm and inflated at low speed: a standard deviation of $0.5\,\mathrm{m\,s^{-1}}$ is 50 % of a $1\,\mathrm{m\,s^{-1}}$ mean, so a night-time or convective record with a light wind shows a large TI that says more about the small denominator than about the turbulence. It depends on the averaging period and on the sensor: a longer period adds slower variations to σ_U, and a slower instrument, such as a cup anemometer with a response length of a few meters, removes the fastest ones. And it depends on how the record is treated: removing a trend within the period, caused by a front or a sea-breeze onset, reduces σ_U. A value of TI is meaningful only with its averaging period, sampling rate and processing.

8.5.2 Turbulence intensity is not turbulence

Turbulence intensity is useful but incomplete. It is one number, the relative variance of one component, and two flows with the same TI can differ in every other property of their turbulence: the sizes of their eddies and therefore their spectra; their anisotropy; their momentum flux; and their intermittency. Consider two records, both with TI = 0.2. The first is the record of Figure 8.1: $\overline{U} = 10\,\mathrm{m\,s^{-1}}$, mechanical turbulence with eddies of about 20 m passing in a couple of seconds, a momentum flux $\overline{u'w'} = -0.64\,\mathrm{m^2\,s^{-2}}$. The second is a convective afternoon with $\overline{U} = 2\,\mathrm{m\,s^{-1}}$ and $\sigma_U = 0.4\,\mathrm{m\,s^{-1}}$: the fluctuations come from thermals a kilometer across that take minutes to pass, the momentum flux is small, and much of the variance is in the vertical and cross-wind components.

The consequences differ. A wind turbine's fatigue depends on the spectrum and coherence of the eddies across its rotor, not only on TI; a conductor's cooling responds to the slow variations of speed and direction over minutes, which the second record has and the first averages out; a dispersion estimate depends on σ_w and the eddy sizes. TI is a summary of the amplitude of the fluctuations, to be read together with the stability, the averaging period and, where possible, the spectrum.

8.5.3 Gusts

A *gust* is a short-duration excursion of the wind speed well above its mean. It is not a separate phenomenon: it is the high tail of the turbulent fluctuations, sometimes enhanced by organized structures such as a convective downdraft reaching the ground or a burst of turbulence in stable air. Because every record has a highest value, a gust is defined as a statistic: the maximum, over a reference period, of the speed averaged over a short gust duration. The most common definition is the highest three-second running mean in a ten-minute or one-hour period. A three-second gust and a ten-minute mean are therefore different statistics of the same record, with $U_{\mathrm{gust}} > \overline{U}$ always.

Their ratio is the *gust factor* $G = U_{\mathrm{gust}}/\overline{U}$, and the excess of the gust over the mean, in units of the standard deviation, is the *peak factor* $g_{\mathrm{pk}} = (U_{\mathrm{gust}} - \overline{U})/\sigma_U$, so that

$$U_{\mathrm{gust}} = \overline{U} + g_{\mathrm{pk}}\,\sigma_U = \overline{U}\,(1 + g_{\mathrm{pk}}\,\mathrm{TI}). \tag{8.19}$$

In the record of Figure 8.1, the highest three-second mean of the horizontal speed is $14.1\,\mathrm{m\,s^{-1}}$, near the sixth minute, so $G = 14.1/10.13 = 1.39$ and $g_{\mathrm{pk}} = (14.12 - 10.13)/1.985 = 2.0$; the highest single 20 Hz sample is $16.0\,\mathrm{m\,s^{-1}}$. The peak factor grows slowly with the length of the reference period, since a longer record samples more extreme fluctuations, and falls with the gust duration, since a longer gust average smooths them; typical three-second peak factors over ten minutes to an hour are about 2 to 3.5. Equation (8.19) shows why rough sites are gusty: the gust factor grows with TI.

8.5.4 The averaging period

A wind record sampled at 20 Hz can be reported as individual samples, three-second gusts, one-minute means, ten-minute means or hourly means, and the numbers differ. Averaging over a period removes the fluctuations shorter than that period, so the longer the averaging, the smaller the spread of the averaged values and the lower their maximum. Table 8.2 shows this for the horizontal speed of the record of Figure 8.1. Its columns are the averaging period, the number of averaged values in the ten minutes (running means for three seconds, consecutive blocks for one minute), the highest and lowest averaged value, and the standard deviation of the averaged values. The same ten minutes of wind give a highest value of $16.0\,\mathrm{m\,s^{-1}}$ as samples, $14.1\,\mathrm{m\,s^{-1}}$ as three-second gusts, $11.4\,\mathrm{m\,s^{-1}}$ as one-minute means and $10.1\,\mathrm{m\,s^{-1}}$ as the ten-minute mean; the spread falls from 1.98 to $1.12\,\mathrm{m\,s^{-1}}$ between samples and one-minute means. An hourly mean, the usual output interval of a weather model, smooths further and also absorbs the variations between successive ten-minute periods.

Observing practice fixes conventions: the ten-minute mean and the highest three-second running mean are the most widely used for surface wind and gusts, and other periods, such as one- or two-minute means, are used in some national and aviation practices. A weather model's wind is different again: it is the value of a grid cell at a time step, a spatial average over the cell that corresponds roughly, not exactly, to a time average of tens of minutes at a point. None of these is "the" wind. Each is a different statistic of the same turbulent flow.

Table 8.2: The horizontal wind speed of the ten-minute record of Figure 8.1 averaged over four periods, illustrative (script `scripts/ch08_data.py`). Three-second values are running means; one-minute values are consecutive blocks.

Averaging period	Values in 10 min	Highest (m/s)	Lowest (m/s)	Std. dev. (m/s)
single sample, 0.05 s	12 000	16.0	3.5	1.98
3 s (running)	11 941	14.1	4.6	1.85
1 min (blocks)	10	11.4	8.4	1.12
10 min	1	10.1	10.1	–

The question to ask of any wind value. A report that "the wind was $15\,\mathrm{m\,s^{-1}}$" is incomplete until it states over what averaging period. In the record above, $15\,\mathrm{m\,s^{-1}}$ is exceeded by individual samples but by no three-second gust, and it is half again the ten-minute mean; a three-second gust of $15\,\mathrm{m\,s^{-1}}$ would be consistent with a ten-minute mean of about $10.8\,\mathrm{m\,s^{-1}}$ at this site's gust factor, and a ten-minute mean of $15\,\mathrm{m\,s^{-1}}$ would bring three-second gusts near $21\,\mathrm{m\,s^{-1}}$. With the averaging period go the height, the exposure of the site, the instrument or model and its sampling rate, the attributes that Chapter 5 required of every wind value.

> **Principle 8.2.** *A gust, a one-minute mean, a ten-minute mean and a grid-cell value are different statistics of one turbulent wind; a wind value is interpretable only with its averaging period, and comparing values of different periods mistakes turbulence for error.*

8.6 Turbulence in models

No atmospheric model resolves turbulence down to the Kolmogorov scale, so every model represents some or all of it by a formula. This section shows where the unknown turbulent terms come from, why they cannot be computed from the mean flow alone, how the main families of model handle them, and what follows for the wind a model predicts near the ground.

8.6.1 Reynolds averaging and the Reynolds stresses

The equations of motion, the Navier–Stokes equations, hold for the instantaneous turbulent flow. To obtain equations for the mean flow, every variable is split as in equation (8.1) and the equations are averaged, using three rules that follow from the definition of the mean: the mean of a fluctuation is zero; the mean of a mean times a fluctuation is zero; and the mean of a product is

$$\overline{a\,b} = \overline{a}\,\overline{b} + \overline{a'b'}. \tag{8.20}$$

Linear terms, such as the pressure gradient and the Coriolis term, simply become their means. The advection terms are products of velocities, and they leave behind averages of products of fluctuations that do not vanish. For the along-wind momentum equation, written in flux form for incompressible flow, the advection by the vertical velocity is $\partial(u\,w)/\partial z$, whose mean is $\partial(\overline{u}\,\overline{w})/\partial z + \partial\overline{u'w'}/\partial z$.

For horizontally uniform flow with $\overline{w} = 0$ and molecular viscosity negligible away from the surface, the averaged horizontal momentum equations are, in east–north components,

$$\frac{\partial \overline{u}}{\partial t} = -\frac{1}{\rho}\frac{\partial \overline{p}}{\partial x} + f\,\overline{v} - \frac{\partial \overline{u'w'}}{\partial z}, \qquad \frac{\partial \overline{v}}{\partial t} = -\frac{1}{\rho}\frac{\partial \overline{p}}{\partial y} - f\,\overline{u} - \frac{\partial \overline{v'w'}}{\partial z}. \tag{8.21}$$

The last terms are new: the friction force per unit mass of Chapter 3 is

$$\mathbf{F} = -\left(\frac{\partial \overline{u'w'}}{\partial z}, \; \frac{\partial \overline{v'w'}}{\partial z} \right), \tag{8.22}$$

the divergence of the turbulent momentum flux. In general the averaging leaves the nine correlations $\overline{u_i' u_j'}$, with $u_1, u_2, u_3 = u, v, w$, and $-\rho\, \overline{u_i' u_j'}$ are the *Reynolds stresses*: the effect of the unresolved turbulence on the mean flow, acting like stresses on the faces of a fluid element. Six are independent, since $\overline{u'w'} = \overline{w'u'}$; the three on the diagonal are $-\rho$ times the variances, whose sum is $-2\rho\, e$; and near the ground the important ones are $\overline{u'w'}$ and $\overline{v'w'}$, the vertical fluxes of horizontal momentum.

The friction term turns the near-surface wind toward low pressure in both hemispheres, since it opposes the wind and leaves the pressure gradient partly unbalanced by the Coriolis force. In the Northern Hemisphere ($f > 0$) low pressure lies to the left of the geostrophic wind, so the surface wind is turned to the left of the wind aloft, counterclockwise seen from above, and the wind veers (turns clockwise) with height. In the Southern Hemisphere ($f < 0$) low pressure lies to the right, the surface wind is turned clockwise, and the wind backs (turns counterclockwise) with height. The magnitude of the turning depends on how strongly the turbulence couples the layers: it is larger when the mixing is weak.

8.6.2 The closure problem

Averaging produces more unknowns than equations. The averaged equations of motion, continuity and heat have the mean velocity components, the mean pressure and the mean potential temperature as unknowns, matched by as many equations, but they also contain the six Reynolds stresses and the three turbulent heat fluxes, nine further unknowns for which the averaging supplies no equation. Equations for the stresses can be derived, in the same way as the budget of equation (8.14), but they contain new unknowns of their own: triple correlations such as $\overline{w'u'u'}$, correlations of pressure and velocity fluctuations, and dissipation terms. Equations for those contain still higher correlations. At every level of the hierarchy the number of unknowns exceeds the number of equations. This is the *turbulence closure problem.*

A model closes the hierarchy by expressing the unknowns at some level in terms of the known quantities, using assumptions calibrated on measurements. A first-order closure expresses the fluxes directly through the mean gradients, with an eddy diffusivity (Section 8.6.4). A one-and-a-half-order closure adds a prognostic equation for the turbulent kinetic energy, equation (8.14) with its transport and dissipation modeled, and builds the diffusivity from e and a length scale. A second-order closure carries equations for all the stresses and fluxes and models the third-order terms. Higher order is not automatically better: each level adds assumptions and constants. Closure is the point at which physics gives way to parameterization, and it is where models differ most.

8.6.3 RANS, LES and boundary-layer schemes

Every turbulence model decides which motions it resolves and which it models. Table 8.3 compares the three families met in wind work. Its columns give the approach, what it resolves explicitly, what it represents by a closure, examples of the closure, and what its output contains. *RANS* (Reynolds-averaged Navier–Stokes) models solve the averaged equations of Section 8.6.1 and model all the turbulence, typically with two prognostic equations, for the turbulent kinetic energy and for its dissipation rate (k–ε) or for a specific dissipation rate (k–ω), where k in these established names is the turbulent kinetic energy. They predict a mean flow and work well for the mean speed-up over terrain for a given wind direction, but they cannot reproduce individual eddies or gusts. *LES* (large-eddy simulation) filters the equations at about the grid

scale, resolves the large eddies, which carry most of the energy and transport, and models only the small ones with a subgrid model; it produces time series with gusts and turbulence statistics, at the cost of much finer grids, meters to tens of meters, and much more computation. *Boundary-layer schemes* in numerical weather prediction (NWP), also called planetary boundary layer (PBL) schemes, are the closures of weather models such as WRF, HRRR and ECMWF's: with grids of kilometers, the model cannot resolve most boundary-layer turbulence, and the scheme computes in each column the vertical turbulent fluxes of momentum, heat and moisture from the resolved profiles.

Table 8.3: Families of turbulence model and what each resolves and models. Chapter 5 compares the same families by grid spacing and use.

Approach	Resolves	Models	Closure examples	Output
RANS	the mean flow around the geometry	all turbulence	k–ε, k–ω	mean speed-up and turning; no gusts
LES	eddies larger than the filter (about the grid)	subgrid eddies	subgrid eddy diffusivity, often from a subgrid e	time series, gusts, turbulence statistics
NWP boundary-layer scheme	the mean profiles of a grid column, kilometers wide	all boundary-layer turbulence, as vertical fluxes	eddy diffusivity from stability, shear, height, mixing length or e	grid-cell mean wind, temperature and moisture profiles

The table carries the book's recurring distinction. Each family represents a different part of the real turbulence, and its wind is a different quantity: a RANS wind is an ensemble mean at a point, an LES wind is a filtered instantaneous wind, an NWP wind is a grid-cell mean. None of them is the wind an anemometer measures, and a comparison with a measurement has to account for what was resolved and what was averaged.

8.6.4 Eddy diffusivity

The simplest closure treats turbulent transport like molecular diffusion: the flux runs down the gradient of the mean, in proportion to it,

$$-\overline{u'w'} = K_m \frac{\partial \overline{u}}{\partial z}, \qquad -\overline{w'\theta'} = K_h \frac{\partial \overline{\theta}}{\partial z}, \tag{8.23}$$

where K_m and K_h, in $\mathrm{m^2\,s^{-1}}$, are the *eddy diffusivities* for momentum (also called eddy viscosity) and for heat. Unlike ν, they are properties of the turbulence, not of the air. For the record of Figure 8.1 with the shear of Section 8.3.2,

$$K_m = \frac{-\overline{u'w'}}{\partial \overline{u}/\partial z} = \frac{0.64\,\mathrm{m^2\,s^{-2}}}{0.2\,\mathrm{s^{-1}}} = 3.2\,\mathrm{m^2\,s^{-1}},$$

about 2×10^5 times the kinematic viscosity, and equal to $\kappa\, u_*\, z = 0.4 \times 0.8 \times 10$, the neutral surface-layer value that the mixing length of Chapter 7 gives.

The difficulty of the closure is all in K_m. It depends on the stability, through the sign and size of P_b; on the shear; on the height, since eddies near the ground are small; on a mixing length; and on the turbulent kinetic energy. Boundary-layer schemes specify it in different ways: as a prescribed profile across the boundary layer scaled by u_*, w_* and z_i; as $l^2\,|\partial \overline{u}/\partial z|$ with a stability correction; or as $c\,l\sqrt{e}$, with a dimensionless constant c and e from a prognostic budget (for the record, $l = \kappa z = 4\,\mathrm{m}$ and $\sqrt{e} = 1.94\,\mathrm{m\,s^{-1}}$ would require $c \approx 0.41$). The gradient form also fails in one important case: in a convective layer the large thermals carry heat upward even where the mean potential temperature gradient is zero or slightly positive, a counter-gradient flux no positive K_h can represent, which schemes handle with an added nonlocal term.

8.6.5 Why two models differ at 10 m

Two weather models can share nearly identical synoptic pressure fields, the same geostrophic wind and the same wind at a few hundred meters, and still predict different winds at 10 m. The reason is in the boundary-layer scheme. Through equation (8.23), the eddy diffusivity sets how strongly the fast air above is coupled to the slow air near the ground: a larger K_m mixes more momentum down and gives a stronger wind near the surface and a weaker shear; a smaller K_m leaves the low levels decoupled and slow. Two schemes that compute different K_m for the same profiles, especially at night and in transitions, therefore give different surface winds. An error in the predicted 10 m wind can be an error of the turbulence model even when the large-scale forecast is excellent.

Figure 8.7 shows the consequence for a transmission line. The horizontal axis is the mean wind speed and the vertical axis the height. Both curves have $15\,\mathrm{m\,s^{-1}}$ at 200 m; they differ only in how well the layer below is mixed. The blue curve, a well-mixed profile, gives $12\,\mathrm{m\,s^{-1}}$ at a conductor or a sensor at 20 m; the red curve, a weakly mixed, decoupled profile, gives $5\,\mathrm{m\,s^{-1}}$ at the same height. The dashed line marks 20 m. The difference is entirely in the vertical turbulent coupling.

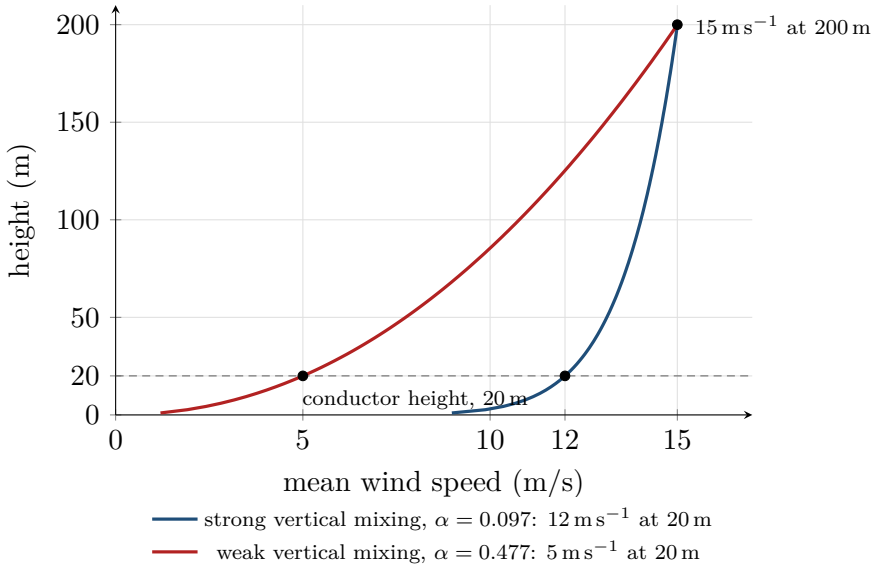


Figure 8.7: Two mean wind profiles with the same wind aloft and different vertical turbulent coupling, illustrative: $\overline{u}(z) = 15\,\mathrm{m\,s^{-1}}\,(z/200\,\mathrm{m})^{\alpha}$ with $\alpha = 0.097$ (well mixed) and $\alpha = 0.477$ (decoupled), chosen to give 12 and $5\,\mathrm{m\,s^{-1}}$ at 20 m.

For a line rated dynamically, the convective cooling of the conductor depends on the wind speed and on its direction relative to the conductor; in the usual rating methods the forced-convection term grows roughly as the wind speed to a power of about 0.5 to 0.6. At the same angle of attack, $12\,\mathrm{m\,s^{-1}}$ against $5\,\mathrm{m\,s^{-1}}$ gives a cooling ratio of $(12/5)^{0.6} \approx 1.7$, about seventy percent more heat removed and correspondingly more current allowed. Whether the line can carry it depends on the vertical turbulent coupling, not on the forecast of the wind aloft. Turbulence is not noise around the forecast; it is part of the mechanism that sets the mean near-surface wind.

8.6.6 Turbulence and the mean wind

The chapter's relations close into a loop. The shear of the mean wind produces turbulent kinetic energy (equation (8.12)); the eddies carry momentum downward as a negative $\overline{u'w'}$ (equation (8.4)); the divergence of that flux removes momentum from the upper part of the

layer and delivers it toward the ground, where the surface drag absorbs it (equation (8.21)); and the resulting mean profile sets the shear again. The mean flow creates turbulence, and turbulence modifies the mean flow.

Figure 8.8 draws the loop. The four boxes are the mean shear, the production of turbulent kinetic energy, the momentum flux, and the mean wind profile; the arrows between them are the relations just listed. Two external inputs enter it: the pressure-gradient forcing that keeps the wind aloft blowing, and the drag of the surface that absorbs the momentum at the bottom. Buoyancy acts on the production box, adding energy by day and removing it at night, and so changes the strength of the whole loop. A steady near-surface wind profile is the state in which this loop is in balance; a change in any part, a rougher surface, a cooling ground, a stronger pressure gradient, moves the profile to a new balance.

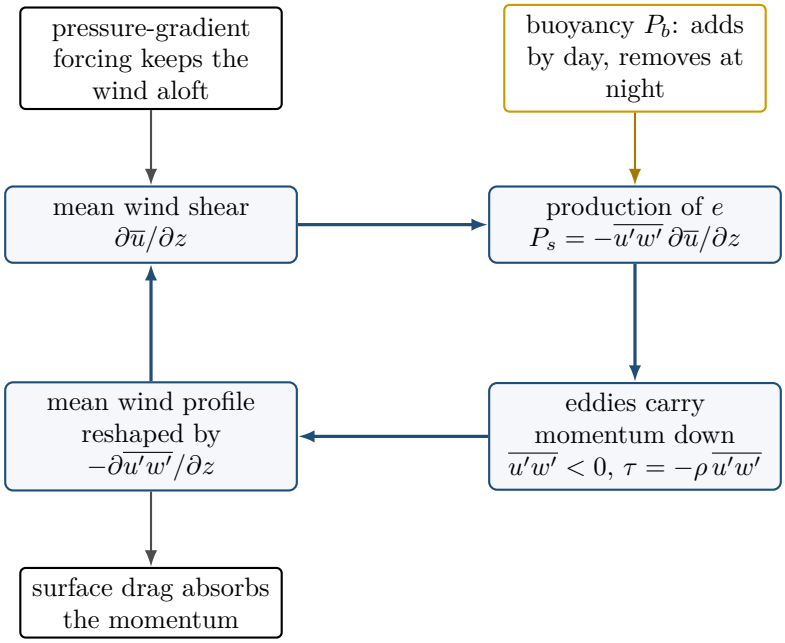


Figure 8.8: The feedback between the mean wind and turbulence (schematic). Shear produces turbulent kinetic energy, the eddies carry momentum downward, the flux divergence reshapes the mean profile, and the profile sets the shear. Forcing aloft and surface drag drive and close the loop; buoyancy strengthens it by day and weakens it at night.

The quantities that describe this loop are the ones a reader of boundary-layer data should recognize on sight: the fluctuations u', v', w'; their standard deviations σ_u, σ_v, σ_w; the momentum flux $\overline{u'w'}$; the kinematic heat flux $\overline{w'\theta'}$; the turbulent kinetic energy e; and the dissipation rate ε.

8.7 What to retain

Definition 8.1 (Turbulence near the ground)**.** Wind shear near the ground generates turbulent eddies, the eddies carry momentum downward as a negative covariance $\overline{u'w'}$, and that momentum transport determines the mean wind profile; turbulence is the mechanism that sets the near-surface wind, not noise around it.

Table 8.4 lists the terms of the chapter, their meaning, their units and the subsection that defines each.

Table 8.4: The terms of the chapter and where each is defined.

Term	Meaning	Units	Defined in
Turbulence	three-dimensional, rotational, chaotic motion over a continuous range of scales that mixes far faster than molecular diffusion	–	8.1
Eddy	coherent swirling structure within turbulence, millimeters to kilometers	m (size)	8.2.1
Reynolds decomposition	$u = \overline{u} + u'$: mean over an averaging period plus fluctuation	m/s	8.1.1
Turbulent flux	covariance of w' with a fluctuation, $\overline{w's'}$; $H = \rho c_p \overline{w'\theta'}$	K m/s, m^2/s^2	8.1.3
Reynolds number	$\mathrm{Re} = UL/\nu$; about 7×10^7 near the surface	–	8.1.6
Reynolds stress	$-\rho\,\overline{u_i' u_j'}$, effect of unresolved turbulence on the mean flow; $\tau = -\rho\overline{u'w'}$	Pa	8.1.4, 8.6.1
Energy cascade	transfer of energy from large to small eddies at the rate ε	–	8.2.2
Inertial subrange	scales between production and dissipation; $E(k) = C_K \varepsilon^{2/3} k^{-5/3}$	–	8.2.3
Kolmogorov length	$\eta_K = (\nu^3/\varepsilon)^{1/4}$, about 0.4 to 1 mm	m	8.2.4
Turbulent kinetic energy	$e = \frac{1}{2}(\sigma_u^2 + \sigma_v^2 + \sigma_w^2)$	m^2/s^2	8.3.1
Shear production	$P_s = -\overline{u'w'}\,\partial\overline{u}/\partial z$, energy from the mean wind	m^2/s^3	8.3.2
Buoyancy production	$P_b = (g/\theta_v)\overline{w'\theta_v'}$; destruction when negative	m^2/s^3	8.3.3
Dissipation	ε, conversion of turbulent energy into heat by viscosity	m^2/s^3	8.3.4
Flux Richardson number	$\mathrm{Ri}_f = -P_b/P_s$; turbulence fades above about 0.2 to 0.25	–	8.3.6
Anisotropy	unequal standard deviations, $\sigma_u > \sigma_v > \sigma_w$ near the ground	–	8.4.4
Turbulence intensity	$\mathrm{TI} = \sigma_U/\overline{U}$ over a stated period	–	8.5.1
Gust	highest short-duration mean (usually 3 s) in a reference period	m/s	8.5.3
Closure problem	averaging yields more unknowns (stresses, fluxes) than equations	–	8.6.2
Eddy diffusivity	K_m, K_h: flux divided by mean gradient; a property of the flow	m^2/s	8.6.4
RANS	averaged equations solved; all turbulence modeled	–	8.6.3
LES	large eddies resolved; subgrid eddies modeled	–	8.6.3

8.8 Exercises

Exercise 8.1. A sonic anemometer at 10 m over grassland records, over ten minutes in along-wind coordinates, $\overline{u} = 8\,\mathrm{m\,s^{-1}}$, $\sigma_u = 1.5\,\mathrm{m\,s^{-1}}$, $\sigma_v = 1.2\,\mathrm{m\,s^{-1}}$, $\sigma_w = 0.75\,\mathrm{m\,s^{-1}}$ and $\overline{u'w'} = -0.36\,\mathrm{m^2\,s^{-2}}$. The shear at 10 m is $0.15\,\mathrm{s^{-1}}$ and $\rho = 1.2\,\mathrm{kg\,m^{-3}}$. (a) Compute the turbulent kinetic energy, the turbulence intensity (taking $\sigma_U \approx \sigma_u$), the stress τ and the friction velocity. (b) Compute the ratios σ/u_* and compare them with Table 8.1. (c) Compute the shear production and the eddy diffusivity for momentum. (d) Assuming production and dissipation balance, compute the Kolmogorov length scale with $\nu = 1.5 \times 10^{-5}\,\mathrm{m^2\,s^{-1}}$, and the time in which shear production would replace the turbulent kinetic energy.

Exercise 8.2. At the same site, an afternoon has $H = 300\,\mathrm{W\,m^{-2}}$, $\theta = 305\,\mathrm{K}$, $\rho = 1.15\,\mathrm{kg\,m^{-3}}$ and a boundary layer 1800 m deep; the following night has $H = -40\,\mathrm{W\,m^{-2}}$, $\theta = 285\,\mathrm{K}$ and $\rho = 1.25\,\mathrm{kg\,m^{-3}}$. Use $c_p = 1004\,\mathrm{J\,kg^{-1}\,K^{-1}}$ and dry air. (a) Compute the kinematic heat flux and the buoyancy term P_b for each. (b) The shear production at 10 m is $4 \times 10^{-3}\,\mathrm{m^2\,s^{-3}}$ in the afternoon and $6 \times 10^{-3}\,\mathrm{m^2\,s^{-3}}$ at night. Compute the flux Richardson number for each and state which kind of turbulence dominates. (c) Compute w_* for the afternoon. (d) If at night the wind weakens so that shear production falls to $2 \times 10^{-3}\,\mathrm{m^2\,s^{-3}}$ with the same heat flux, what happens to Ri_f, and what behavior of the turbulence is to be expected?

Exercise 8.3. A site has a ten-minute mean wind of $9\,\mathrm{m\,s^{-1}}$ with $\sigma_U = 1.8\,\mathrm{m\,s^{-1}}$. (a) Compute TI. (b) With a three-second peak factor of 2.2, compute the expected three-second gust and the gust factor. (c) A newspaper reports that "the wind reached $15\,\mathrm{m\,s^{-1}}$". Which of the following could this value be, at this site: a single fast sample, a three-second gust, a one-minute mean, a ten-minute mean? Explain. (d) A weather model's grid-cell wind for the same hour is $9.5\,\mathrm{m\,s^{-1}}$ and the site's anemometer reports a gust of $13\,\mathrm{m\,s^{-1}}$. Is the difference an error of the model? State what must be known about both values before deciding.

Exercise 8.4. A transmission line at 23°S runs north to south. The wind at 200 m is $15\,\mathrm{m\,s^{-1}}$ from 300°. Two weather models, with different boundary-layer schemes, give at the conductor height of 20 m: model A, $12\,\mathrm{m\,s^{-1}}$ turned 15° toward low pressure; model B, $5\,\mathrm{m\,s^{-1}}$ turned 35° toward low pressure. (a) In which sense, clockwise or counterclockwise seen from above, does friction turn the wind in the Southern Hemisphere? Give the direction from which the 20 m wind blows in each model. (b) Compute the angle between each wind and the conductor and the component of each wind perpendicular to the conductor. (c) Repeat (a) and (b) for the same line and winds at 23°N. (d) Using a forced-convection cooling proportional to $U^{0.6}$ at the same angle, compare the cooling under the two models, and explain why the weaker-mixing model also has the larger turning.

Chapter 9

Reynolds Decomposition and Turbulent Fluxes

9.1 The decomposition of a measured record

A sonic anemometer on a tower near the ground reports the three components of the air velocity twenty times a second. Its record of the along-wind component jumps by one or two meters per second from one reading to the next, and its record of the vertical component swings between upward and downward many times a minute, although the mean vertical velocity over flat ground is essentially zero. Neither record, read as it stands, says how much momentum the air delivers to the ground, how much heat the ground gives to the air or how much water evaporates. Those transports are hidden in the way the fluctuations of different quantities move together. The question of this chapter is

how are rapidly fluctuating wind measurements turned into physically meaningful turbulent transport of momentum, heat and moisture?

The answer is the Reynolds decomposition, which separates each measured quantity into a mean and a fluctuation, together with the observation that the average of a product of two fluctuations, a covariance, does not vanish. The chapter defines the decomposition and the statistics built on it, mean, variance, standard deviation, covariance and correlation; derives the fluxes of momentum, heat and moisture and the friction velocity from them; describes how they are measured by eddy covariance and what the averaging window, stationarity and coordinate rotation do to the result; shows how the covariances enter the averaged equations of motion and why they must be modeled; and ends with quadrant analysis and the chain that leads from a covariance to the wind profile. What turbulence is, its energy and its cascade, is the subject of Chapter 8; this chapter treats its statistics and the transport they measure.

Jargon: Reynolds decomposition, mean, fluctuation (prime), variance, standard deviation, covariance, turbulent flux, kinematic flux

The *Reynolds decomposition* writes any measured quantity $a(t)$, a velocity component, a temperature, a humidity, as the sum of its *mean* over an averaging period, $\overline{a}$, and a *fluctuation* about that mean, $a' = a - \overline{a}$; the prime is read "prime" and always denotes such a departure, never a separate component of the flow. The *variance* $\overline{a'^2}$ is the mean square of the fluctuation, in the square of the units of a; its square root, the *standard deviation* σ_a, measures how strongly a fluctuates, in the units of a. The *covariance* $\overline{a'b'}$ of two quantities is the mean of the product of their fluctuations; its sign says whether the two tend to depart from their means in the same direction or in opposite directions. A *turbulent flux* is the rate at which turbulent motion carries a quantity across a surface, per unit area; the vertical turbulent flux of a quantity A is proportional to the covariance $\overline{w'A'}$ of the vertical velocity with A. Written as the covariance itself, without the density or the factor that converts it to energy or mass, it is a *kinematic flux*: in $\mathrm{m^2\,s^{-2}}$ for momentum and in $\mathrm{K\,m\,s^{-1}}$ for heat.

Key idea

A turbulent flux is not a measure of how variable the air is but of how two fluctuations move together. Over ground where the wind increases with height, the along-wind and vertical fluctuations are anticorrelated, $\overline{u'w'} < 0$, which means that momentum is carried downward to the surface; its magnitude defines the friction velocity, $u_* = \sqrt{-\overline{u'w'}}$, and through it the wind profile above.

9.1.1 A measured time series

Consider a record of the along-wind velocity $u(t)$ from a fast-response anemometer, of which five successive readings are, in meters per second,

$$8.1, \quad 7.6, \quad 8.9, \quad 8.4, \quad 7.9.$$

Each reading is the wind at one instant and one point; no two are equal, and none is "the" wind. The first step of every turbulence analysis is to split each reading into the part that persists over a chosen averaging period and the part that does not. With the average of u over the period written $\overline{u}$,

$$u(t) = \overline{u} + u'(t), \qquad u'(t) = u(t) - \overline{u}. \tag{9.1}$$

This is the Reynolds decomposition, named after Osborne Reynolds, who introduced it in 1895 to write averaged equations for turbulent flow in pipes. For a record of N samples $u_1, \ldots, u_N$ taken at equal intervals, the mean is the arithmetic average,

$$\overline{u} = \frac{1}{N} \sum_{i=1}^{N} u_i, \tag{9.2}$$

and for a continuous record over a period t_a it is $\overline{u} = t_a^{-1} \int_0^{t_a} u \, \mathrm{d}t$. The mean is a property of the whole period, a single number; the fluctuation is a new time series with one value per sample.

For illustration, take the mean over the period as $\overline{u} = 8\,\mathrm{m\,s^{-1}}$. A reading of $u = 9.2\,\mathrm{m\,s^{-1}}$ then has the fluctuation $u' = 9.2 - 8 = +1.2\,\mathrm{m\,s^{-1}}$: the air at that instant moves $1.2\,\mathrm{m\,s^{-1}}$ faster than the mean. A reading of $u = 6.9\,\mathrm{m\,s^{-1}}$ has $u' = 6.9 - 8 = -1.1\,\mathrm{m\,s^{-1}}$: the air moves $1.1\,\mathrm{m\,s^{-1}}$ slower. If the five readings above are themselves the whole record, their mean is $\overline{u} = (8.1 + 7.6 + 8.9 + 8.4 + 7.9)/5 = 40.9/5 = 8.18\,\mathrm{m\,s^{-1}}$, and their fluctuations are

$$-0.08, \quad -0.58, \quad +0.72, \quad +0.22, \quad -0.28\,\mathrm{m\,s^{-1}}.$$

The same reading of $8.1\,\mathrm{m\,s^{-1}}$ has a fluctuation of $+0.10\,\mathrm{m\,s^{-1}}$ about a mean of $8\,\mathrm{m\,s^{-1}}$ and of $-0.08\,\mathrm{m\,s^{-1}}$ about a mean of $8.18\,\mathrm{m\,s^{-1}}$: a fluctuation is defined only together with the mean it departs from, and therefore with the averaging period that produced the mean. Section 9.4.3 returns to the choice of that period.

9.1.2 The fluctuation and its notation

The decomposition applies to every quantity in the record, each with its own mean:

$$v' = v - \overline{v}, \qquad w' = w - \overline{w}, \qquad T' = T - \overline{T}, \qquad \theta' = \theta - \overline{\theta}. \tag{9.3}$$

The prime marks a departure from the mean, not a different component of the velocity: u' is the along-wind velocity's departure from its mean, w' the vertical velocity's departure from its mean, T' and θ' the departures of the temperature and the potential temperature (Chapter 6) from theirs. The fluctuations have the units of the quantities they come from: meters per second for the velocities, kelvin for the temperatures.

Throughout the chapter the velocity components are taken in along-wind coordinates: u along the direction of the mean horizontal wind, v across it, positive to the left of u so that (u, v, w) is right-handed, and w upward. In these coordinates $\overline{v} = 0$ by construction, $\overline{u}$ is the mean wind speed, and over flat, uniform ground $\overline{w} \approx 0$, so that $w' = w$ to a very good approximation. Section 9.4.5 shows how a measured record is brought into these coordinates.

9.1.3 The zero mean of a fluctuation

The mean of a fluctuation over the period that defines it is zero:

$$\overline{u'} = 0, \qquad \overline{v'} = 0, \qquad \overline{w'} = 0, \qquad \overline{T'} = 0. \tag{9.4}$$

The proof takes one line. For N samples,

$$\overline{u'} = \frac{1}{N}\sum_{i=1}^{N}(u_i - \overline{u}) = \frac{1}{N}\sum_{i=1}^{N} u_i - \frac{1}{N}\,N\,\overline{u} = \overline{u} - \overline{u} = 0,$$

because $\overline{u}$ is the same number for every sample of the period, so its average is itself. The five fluctuations of Section 9.1.1 confirm it: $-0.08 - 0.58 + 0.72 + 0.22 - 0.28 = 0.00$.

The property has a consequence that the rest of the chapter depends on. Fluctuations of one quantity cancel on average, so the mean of a single fluctuation carries no information. Products of fluctuations do not cancel. The mean of u'^2 is positive whenever u fluctuates at all, because every square is positive; and the mean of $u'w'$ is nonzero whenever u' and w' tend to have the same sign, or opposite signs, more often than not. The information about turbulence is in these second moments.

9.1.4 Variance and standard deviation

The *variance* of u is the mean square of its fluctuation,

$$\sigma_u^2 = \overline{u'^2} = \frac{1}{N}\sum_{i=1}^{N} u_i'^2, \tag{9.5}$$

in $\mathrm{m^2\,s^{-2}}$, and the *standard deviation* is its square root, $\sigma_u = \sqrt{\overline{u'^2}}$, in $\mathrm{m\,s^{-1}}$. The standard deviation is the typical size of a fluctuation: a large σ_u means strong fluctuations of the along-wind wind, a gusty record; a small σ_u, a steady one. The same definitions give σ_v and σ_w for the cross-wind and vertical components and σ_T for the temperature. Statistical texts divide

by $N-1$ rather than N to remove a small bias of the sample variance; for a turbulence record of tens of thousands of samples the difference is negligible, and the definition with N keeps the averaging rules of Section 9.5.1 exact.

For the five readings of Section 9.1.1, the squared fluctuations are 0.0064, 0.3364, 0.5184, 0.0484 and 0.0784, whose mean is

$$\sigma_u^2 = \frac{0.988}{5} = 0.1976\,\mathrm{m^2\,s^{-2}}, \qquad \sigma_u = \sqrt{0.1976} = 0.44\,\mathrm{m\,s^{-1}}.$$

Five readings are far too few for a reliable estimate; a real variance is computed from a record of 10 to 60 minutes at 10 to 20 samples per second. The three velocity variances together form the turbulent kinetic energy per unit mass, $e = \frac{1}{2}(\overline{u'^2} + \overline{v'^2} + \overline{w'^2})$, whose budget is treated in Chapter 8; the ratio $\sigma_u/\overline{u}$ is close to the turbulence intensity TI defined there.

9.1.5 A synthetic record

Figure 9.1 shows a two-minute record of u and w sampled at 20 Hz, 2400 samples per component, together with the product of their fluctuations. The record is synthetic: it was generated from seeded random processes with time scales of a fraction of a second to a few seconds and rescaled so that its statistics are exactly the illustrative values used throughout the chapter, $\overline{u} = 8\,\mathrm{m\,s^{-1}}$, $\overline{w} = 0$, $\sigma_u = 1.2\,\mathrm{m\,s^{-1}}$, $\sigma_w = 0.62\,\mathrm{m\,s^{-1}}$ and $\overline{u'w'} = -0.25\,\mathrm{m^2\,s^{-2}}$. The horizontal axis of all three panels is time in seconds. The top panel is u with its mean drawn as a red line, so that u' is the vertical distance from the red line to the trace; the middle panel is w, whose mean is zero, so that the trace is w' itself; the bottom panel is the instantaneous product $u'w'$ with its mean, $-0.25\,\mathrm{m^2\,s^{-2}}$, as a red line. The two dotted vertical lines mark two instants picked out for Section 9.2.2, at 42.55 s and 98.5 s.

Three features of the figure carry the chapter. First, the along-wind fluctuations are of the order of ±1 to $\pm3\,\mathrm{m\,s^{-1}}$ about a mean of $8\,\mathrm{m\,s^{-1}}$, and the vertical ones of ±0.5 to $\pm2\,\mathrm{m\,s^{-1}}$ about zero: turbulence near the ground is not a small perturbation. Second, the product $u'w'$ is negative most of the time and reaches large negative values in short bursts, such as the two marked instants, while its positive excursions are smaller and rarer; its mean is negative. Third, the mean of $u'w'$, $-0.25\,\mathrm{m^2\,s^{-2}}$, is small compared with the typical size of the product itself, of order 1 to $5\,\mathrm{m^2\,s^{-2}}$: the flux is a small systematic residual of large fluctuations of both signs, which is why it needs long records, fast sampling and care to measure.

9.2 Covariance and the momentum flux

The mean of a product of two fluctuations is the statistic that measures transport. This section defines the covariance, shows why the covariance of the along-wind and vertical velocities is a vertical flux of momentum, converts it to a stress and to the friction velocity, and works a four-sample example through by hand.

9.2.1 Covariance

The *covariance* of two quantities a and b over an averaging period is the mean of the product of their fluctuations,

$$\overline{a'b'} = \frac{1}{N}\sum_{i=1}^{N} a_i'\,b_i'. \tag{9.6}$$

For the along-wind and vertical velocities it is $\overline{u'w'}$, in $\mathrm{m^2\,s^{-2}}$. Its sign is physically meaningful. If u' and w' tend to have the same sign, fast air (positive u') moving up (positive w') and slow air moving down, most products are positive and $\overline{u'w'} > 0$. If they tend to have opposite signs, fast air moving down and slow air moving up, $\overline{u'w'} < 0$. If the sign of one fluctuation

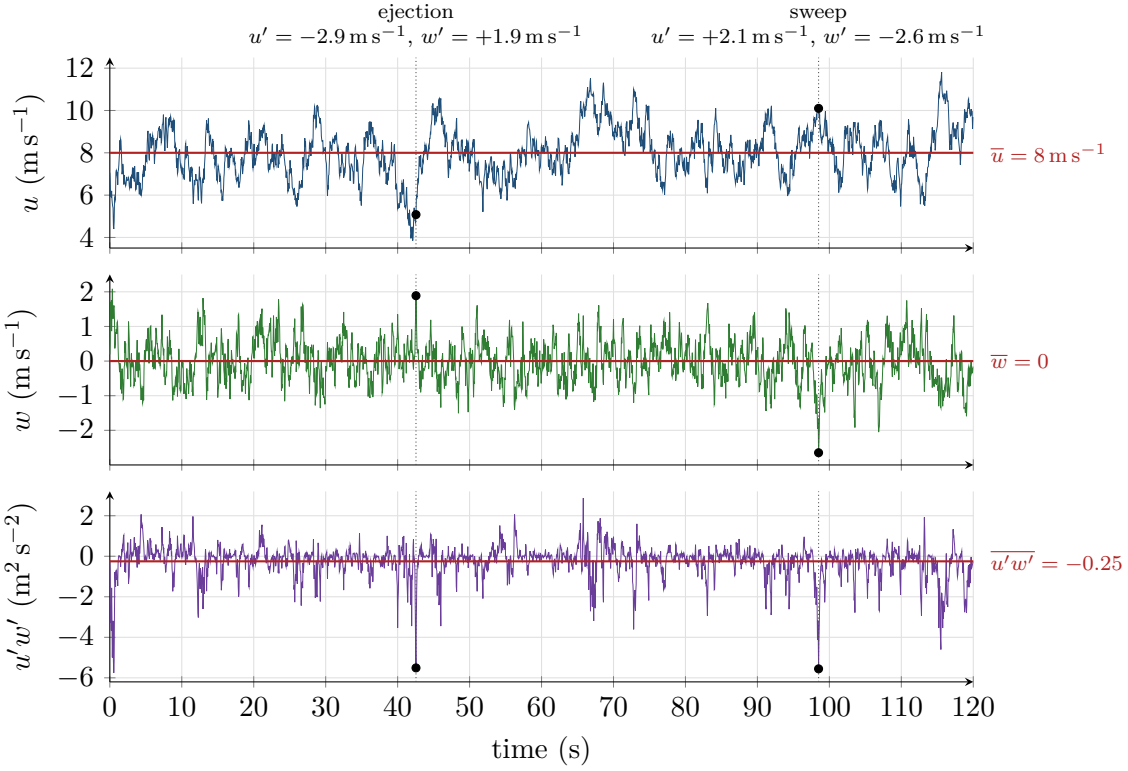


Figure 9.1: Synthetic two-minute record at 20 Hz (2400 samples) in along-wind coordinates, from `scripts/ch09_data.py`: seeded first-order autoregressive noise rescaled to the illustrative statistics $\overline{u} = 8\,\mathrm{m\,s^{-1}}$, $\overline{w} = 0$, $\sigma_u = 1.2\,\mathrm{m\,s^{-1}}$, $\sigma_w = 0.62\,\mathrm{m\,s^{-1}}$, $\overline{u'w'} = -0.25\,\mathrm{m^2\,s^{-2}}$ ($u_* = 0.5\,\mathrm{m\,s^{-1}}$). Top: along-wind velocity; middle: vertical velocity; bottom: the product of the fluctuations. Red lines: the means. Dots: one ejection ($t = 42.55\,\mathrm{s}$) and one sweep ($t = 98.5\,\mathrm{s}$).

says nothing about the sign of the other, positive and negative products cancel and $\overline{u'w'} \approx 0$, however large the fluctuations are. The variance of Section 9.1.4 is the special case $b = a$ of equation (9.6); it can never be negative, while a covariance can have either sign.

9.2.2 Momentum transport by exchanged parcels

Near the ground the mean wind increases with height, because the surface slows the air in contact with it. Picture turbulence as the exchange of small volumes of air, parcels, between levels, each parcel keeping for a while the along-wind velocity it had where it started. Figure 9.2 draws this. The horizontal axis is the mean along-wind speed and the vertical axis height; the blue curve is an illustrative mean profile that increases with height. The dotted horizontal line is a reference level at 15 m, where the mean speed is $7.13\,\mathrm{m\,s^{-1}}$, marked by a black dot. The red parcel starts at 40 m, where the mean wind is $8.36\,\mathrm{m\,s^{-1}}$, and moves down to the reference level; the green parcel starts at 5 m, where the mean wind is $5.76\,\mathrm{m\,s^{-1}}$, and moves up to it. The short horizontal segments at the reference level show each parcel's speed relative to the local mean.

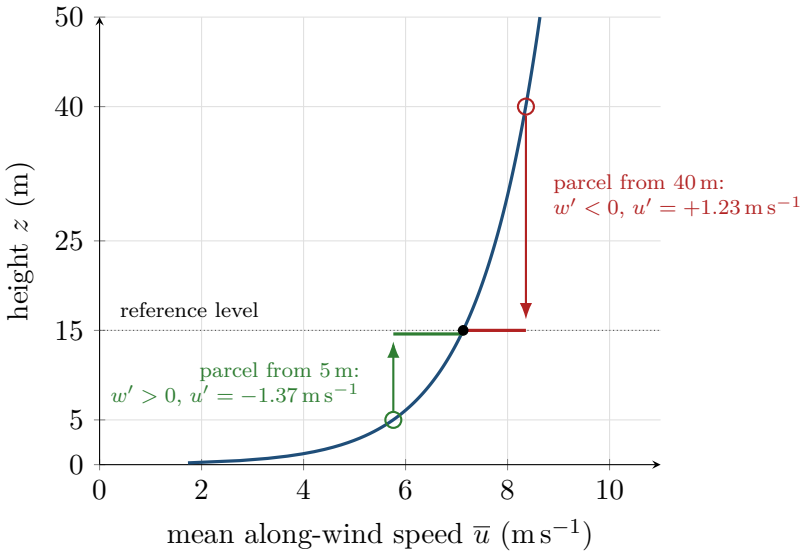


Figure 9.2: Momentum transport by the exchange of parcels in a mean wind that increases with height. Mean profile (illustrative): $\overline{u}(z) = (u_*/\kappa)\ln(z/z_0)$ with $u_* = 0.5\,\mathrm{m\,s^{-1}}$, $\kappa = 0.4$, $z_0 = 0.05\,\mathrm{m}$. A parcel arriving at the reference level (15 m) from above is faster than the local mean; one arriving from below is slower. Both give $u'w' < 0$.

The red parcel arrives moving down, $w' < 0$, and carrying the speed of the level it came from, $8.36\,\mathrm{m\,s^{-1}}$, which exceeds the local mean by $u' = 8.36 - 7.13 = +1.23\,\mathrm{m\,s^{-1}}$. The green parcel arrives moving up, $w' > 0$, with $5.76\,\mathrm{m\,s^{-1}}$, slower than the local mean by $u' = 5.76 - 7.13 = -1.37\,\mathrm{m\,s^{-1}}$. Both products are negative: $u'w' < 0$ for the descending fast parcel and for the ascending slow one. Averaged over many such exchanges,

$$\overline{u'w'} < 0 \quad \text{when} \quad \frac{\partial \overline{u}}{\partial z} > 0, \tag{9.7}$$

which means that horizontal momentum is carried downward: fast air is brought down toward the surface and slow air is carried up away from it, so that the layer near the ground continually receives momentum from above. That momentum is what the surface removes by friction; the downward momentum flux is the means by which the drag of the ground is felt hundreds of meters up, and the reason the friction force of Chapter 3 exists. The parcel picture is a heuristic,

since real eddies mix continuously with their surroundings and have no sharp starting level, but the sign it predicts is what measurements show: the anticorrelation of the two marked instants in Figure 9.1, an ejection of slow air upward and a sweep of fast air downward, is the typical case.

Why the product matters. A single fluctuation says little about transport. A reading with $u' = +2\,\mathrm{m\,s^{-1}}$ says only that the air is momentarily fast. If at the same instant $w' = -0.5\,\mathrm{m\,s^{-1}}$, then

$$u'w' = (+2\,\mathrm{m\,s^{-1}})(-0.5\,\mathrm{m\,s^{-1}}) = -1\,\mathrm{m^2\,s^{-2}},$$

and the reading describes fast air moving down: a contribution to the downward transport of momentum. The same $u' = +2\,\mathrm{m\,s^{-1}}$ with $w' = +0.5\,\mathrm{m\,s^{-1}}$ would be fast air moving up, a contribution of the opposite sign. Transport depends on coordinated fluctuations, on the joint behavior of u' and w', and not on the magnitude of either alone.

9.2.3 Kinematic flux and turbulent stress

The covariance $\overline{u'w'}$ is the *kinematic momentum flux*: the vertical flux of along-wind momentum per unit mass of air, in $\mathrm{m^2\,s^{-2}}$. The reasoning is direct. The momentum per unit volume of the air is ρu, and air crossing a horizontal surface with vertical velocity w carries momentum across it at the rate ρuw per unit area and unit time. Averaging, $\rho\,\overline{uw} = \rho\,\overline{u}\,\overline{w} + \rho\,\overline{u'w'}$ (Section 9.5.1); with $\overline{w} = 0$ only the turbulent part remains, $\rho\,\overline{u'w'}$, in $(\mathrm{kg\,m^{-3}})(\mathrm{m^2\,s^{-2}}) = \mathrm{kg\,m^{-1}\,s^{-2}} = \mathrm{N\,m^{-2}}$. A flux of momentum per unit area is a force per unit area, a stress. The *turbulent shear stress*, or *Reynolds stress*, is

$$\tau = -\rho\,\overline{u'w'}, \tag{9.8}$$

in $\mathrm{N\,m^{-2}} = \mathrm{Pa}$. It is the horizontal force per unit area that the air above a horizontal surface exerts on the air below it through turbulent exchange, and at the ground, where it is written τ_0, the drag of the air on the surface and, equal and opposite, of the surface on the air. It is called a stress because it acts like the viscous stress of a laminar flow, but it is carried by eddies, not by molecules, and near the ground it exceeds the viscous stress by several orders of magnitude.

For an illustrative surface-layer record with $\overline{u'w'} = -0.25\,\mathrm{m^2\,s^{-2}}$ and air density $\rho = 1.2\,\mathrm{kg\,m^{-3}}$,

$$\tau = -1.2\,\mathrm{kg\,m^{-3}} \times (-0.25\,\mathrm{m^2\,s^{-2}}) = 0.30\,\mathrm{N\,m^{-2}} = 0.30\,\mathrm{Pa}.$$

That is the weight of about 30 g spread over a square meter, small as a pressure, but acting continuously over every square meter of the ground it is the brake on the whole boundary layer.

The minus sign. In ordinary near-surface flow, with the wind increasing with height, $\overline{u'w'} < 0$ (equation (9.7)). The minus sign in equation (9.8) makes the stress positive in that case, so that τ is quoted as a magnitude in the direction of the mean wind: the air above drags the air below forward. The sign convention of the flux itself is unchanged, positive upward, so a negative kinematic flux is a downward transport of momentum and a positive stress (Section 9.3.4).

9.2.4 Friction velocity

The stress has units of a density times a velocity squared, so it defines a velocity scale,

$$u_* = \sqrt{\frac{\tau}{\rho}} = \sqrt{-\overline{u'w'}}, \tag{9.9}$$

the *friction velocity*, in $\mathrm{m\,s^{-1}}$, evaluated with the stress at the surface, τ_0, or in the surface layer, where the stress is nearly constant with height (Chapter 7). It is not the speed of any air; it is the velocity scale of the turbulent momentum transfer, and the velocity standard deviations of

the surface layer scale with it. For the record above, $u_* = \sqrt{0.25\,\mathrm{m^2\,s^{-2}}} = 0.5\,\mathrm{m\,s^{-1}}$. How the friction velocity is measured or inferred, and its relation to the drag coefficient, are the subject of Chapter 10.

Both horizontal components. The turbulent stress is a horizontal vector. Its two components are the vertical fluxes of the along-wind and the cross-wind momentum, $-\rho\,\overline{u'w'}$ and $-\rho\,\overline{v'w'}$, so its magnitude is $|\boldsymbol{\tau}| = \rho\sqrt{\overline{u'w'}^2 + \overline{v'w'}^2}$, and the friction velocity defined from the magnitude is

$$u_* = \sqrt{\frac{|\boldsymbol{\tau}|}{\rho}} = \left[\overline{u'w'}^2 + \overline{v'w'}^2\right]^{1/4}. \tag{9.10}$$

In along-wind coordinates the stress is usually nearly aligned with the mean wind and $\overline{v'w'}$ is small. With illustrative values $\overline{u'w'} = -0.25$ and $\overline{v'w'} = 0.06\,\mathrm{m^2\,s^{-2}}$,

$$u_* = \left[(-0.25)^2 + 0.06^2\right]^{1/4} = (0.0625 + 0.0036)^{1/4} = 0.0661^{1/4} = 0.507\,\mathrm{m\,s^{-1}},$$

1.4 % more than the $0.5\,\mathrm{m\,s^{-1}}$ of the along-wind component alone, with the stress turned by $\arctan(0.06/0.25) = 13.5°$ from the mean wind. The cross-wind flux matters little for the magnitude while it is small, which is why coordinates are rotated so that u lies along the mean wind (Section 9.4.5); but a large $\overline{v'w'}$ is a sign of a turning of the wind with height or of a misaligned coordinate system, and the full form of equation (9.10) is the safe definition.

9.2.5 A four-sample example

Table 9.1 works the covariance through by hand for four illustrative samples of the along-wind and vertical fluctuations. Its columns are the sample number, u', w', their product, the quadrant of the (u', w') plane the sample falls in (Section 9.6.4), and what the sample describes physically.

Table 9.1: Four illustrative samples of the along-wind and vertical fluctuations and their products. The mean of the product is the kinematic momentum flux.

Sample	u' ($\mathrm{m\,s^{-1}}$)	w' ($\mathrm{m\,s^{-1}}$)	$u'w'$ ($\mathrm{m^2\,s^{-2}}$)	Quadrant	Meaning
1	+2	−0.5	−1.0	sweep	fast air moving down
2	−1	+0.4	−0.4	ejection	slow air moving up
3	+1	−0.3	−0.3	sweep	fast air moving down
4	−2	+0.6	−1.2	ejection	slow air moving up
Sum	0	+0.2	−2.9		
Mean	0	+0.05	−0.725		$\overline{u'w'}$

All four products are negative, and

$$\overline{u'w'} = \frac{-1.0 - 0.4 - 0.3 - 1.2}{4} = \frac{-2.9}{4} = -0.725\,\mathrm{m^2\,s^{-2}}, \qquad u_* = \sqrt{0.725} \approx 0.85\,\mathrm{m\,s^{-1}},$$

with $\tau = 1.2 \times 0.725 = 0.87\,\mathrm{Pa}$ at $\rho = 1.2\,\mathrm{kg\,m^{-3}}$. Fast air moves downward and slow air upward in every sample, and the momentum flux is downward. Two remarks keep the example honest. First, the four values of w' average $+0.05\,\mathrm{m\,s^{-1}}$, not zero, so they are fluctuations about the mean of a longer record rather than of these four samples. The covariance is unaffected, because the u' values sum to zero: subtracting the four-sample mean 0.05 from every w' changes the sum of the products by $-0.05 \times \sum u' = 0$. Second, the four samples were chosen to fall in the sweep and ejection quadrants; their correlation coefficient (Section 9.6.1) is $-0.725/(1.58 \times 0.46) = -0.99$,

nearly perfect anticorrelation, whereas a real surface-layer record has a correlation near -0.3, with many samples of the opposite sign that partly cancel the flux, as in the bottom panel of Figure 9.1.

Principle 9.1. *The vertical flux of along-wind momentum is the covariance $\overline{u'w'}$; over ground where the wind increases with height it is negative, a downward transport, and it defines the turbulent stress $\tau = -\rho\,\overline{u'w'}$ and the friction velocity $u_* = \sqrt{-\overline{u'w'}}$.*

9.3 Fluxes of heat and moisture

The machinery that turns $\overline{u'w'}$ into a momentum flux applies to any quantity the air carries. This section applies it to heat and to water vapor, converts the kinematic fluxes to energy fluxes in watts per square meter, and states the general form and the sign convention shared by all of them.

9.3.1 Heat flux by day and by night

The covariance of the vertical velocity with the temperature, $\overline{w'T'}$, is the kinematic heat flux, in $\mathrm{K\,m\,s^{-1}}$. Its sign follows from the same parcel argument as for momentum, with temperature in place of velocity, and with one refinement. A parcel that moves vertically without exchanging heat changes its temperature by expansion or compression, by about 9.8 K per kilometer, but keeps its potential temperature θ (Chapter 6). The quantity a parcel carries unchanged between levels is therefore θ, and the heat flux that the parcel argument describes is $\overline{w'\theta'}$. Near the surface, over the few tens of meters in which fluxes are measured, θ' and T' differ by a factor within a few percent of one, so $\overline{w'T'}$ and $\overline{w'\theta'}$ are used interchangeably there, as in the definitions below.

Figure 9.3 draws the two cases. In each panel the horizontal axis is potential temperature and the vertical axis height; the curve is an illustrative mean profile, the dotted line a reference level at 20 m with the local mean marked by a black dot, and the two circles are parcels that arrive at the reference level, one from 4 m and one from 60 m, carrying the potential temperature of their starting level.

By day, left panel, the sun heats the ground, the ground heats the air in contact with it, and $\overline{\theta}$ decreases with height near the surface. The parcel rising from 4 m arrives with $\theta = 300.17$ K, 0.97 K warmer than the local mean of 299.20 K: $w' > 0$ and $\theta' > 0$. The parcel sinking from 60 m arrives with 298.54 K, 0.66 K cooler: $w' < 0$ and $\theta' < 0$. Both products are positive, so $\overline{w'\theta'} > 0$: warm air goes up and cool air comes down, an upward heat flux from the heated surface into the air.

At night, right panel, the ground cools by radiation, the air next to it cools, and $\overline{\theta}$ increases with height, a stable layer. The parcel rising from 4 m arrives 1.29 K cooler than the local mean, $w' > 0$ and $\theta' < 0$; the parcel sinking from 60 m arrives 0.88 K warmer, $w' < 0$ and $\theta' > 0$. Both products are negative, so $\overline{w'\theta'} < 0$: heat is carried downward, toward the colder surface. In stable air the vertical motions are also weaker, because each displaced parcel is pushed back toward its level by buoyancy, so the nighttime flux is small in magnitude as well as negative.

9.3.2 Sensible heat flux

The kinematic heat flux is converted to an energy flux by the heat content per unit volume and per kelvin, the density times the specific heat at constant pressure. The *sensible heat flux* is

$$H = \rho\, c_p\, \overline{w'T'}, \tag{9.11}$$

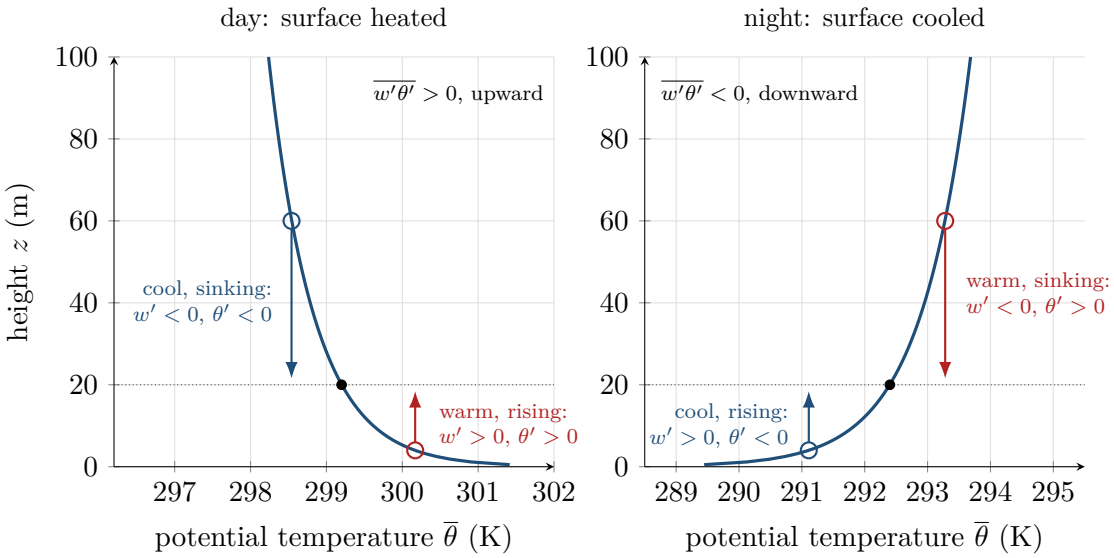


Figure 9.3: Sign of the turbulent heat flux. Illustrative mean profiles: day, $\overline{\theta} = 301\,\mathrm{K} - 0.6\,\mathrm{K}\,\ln(z/1\,\mathrm{m})$, decreasing with height over a heated surface; night, $\overline{\theta} = 290\,\mathrm{K} + 0.8\,\mathrm{K}\,\ln(z/1\,\mathrm{m})$, increasing with height over a cooled surface. Parcels from 4 m and 60 m arrive at the reference level (20 m) with the potential temperature of their starting level. By day both exchanges give $w'\theta' > 0$, by night both give $w'\theta' < 0$.

in $(\mathrm{kg\,m^{-3}})(\mathrm{J\,kg^{-1}\,K^{-1}})(\mathrm{K\,m\,s^{-1}}) = \mathrm{J\,m^{-2}\,s^{-1}} = \mathrm{W\,m^{-2}}$, with $c_p = 1004\,\mathrm{J\,kg^{-1}\,K^{-1}}$ for air. It is called sensible because it changes the temperature of the air, the heat that a thermometer senses, as distinct from the latent heat of Section 9.3.3, which is hidden in water vapor. With the positive-upward convention, $H > 0$ by day over a heated surface and $H < 0$ at night over a cooled one.

For an illustrative sunny midday over dry grassland, $\overline{w'T'} = 0.15\,\mathrm{K\,m\,s^{-1}}$ and $\rho = 1.2\,\mathrm{kg\,m^{-3}}$ give

$$H = 1.2\,\mathrm{kg\,m^{-3}} \times 1004\,\mathrm{J\,kg^{-1}\,K^{-1}} \times 0.15\,\mathrm{K\,m\,s^{-1}} = 181\,\mathrm{W\,m^{-2}},$$

an upward flux of energy comparable to a fifth of the midday solar radiation. An illustrative clear night with $\overline{w'T'} = -0.02\,\mathrm{K\,m\,s^{-1}}$ gives $H = 1.2 \times 1004 \times (-0.02) = -24\,\mathrm{W\,m^{-2}}$, a downward flux nearly an order of magnitude smaller. The asymmetry is typical: daytime heat fluxes over land reach a few hundred watts per square meter, nighttime ones a few tens. The heat flux is what makes the boundary layer convective by day and stable by night, and through it the stability that Chapter 14 adds to the wind profile.

Sonic anemometers measure temperature from the speed of sound, which depends on humidity as well as on temperature; their "sonic temperature" is close to the virtual temperature, and the flux they give is closer to a buoyancy flux than to $\overline{w'T'}$. The difference, a few percent over dry ground and more over wet ground, is removed by a standard correction that uses the measured humidity flux.

9.3.3 Moisture flux and latent heat flux

The same decomposition applies to the water vapor content of the air, measured by the *specific humidity* q, the mass of water vapor per unit mass of moist air, in $\mathrm{kg\,kg^{-1}}$: $q = \overline{q} + q'$. The covariance $\overline{w'q'}$ is the kinematic moisture flux, in $\mathrm{kg\,kg^{-1}\,m\,s^{-1}}$, and $\rho\,\overline{w'q'}$ is the mass of water vapor carried upward per unit area and unit time, in $\mathrm{kg\,m^{-2}\,s^{-1}}$: the evaporation rate. Evaporating a kilogram of water takes the *latent heat of vaporization* $L_v \approx 2.45 \times 10^6\,\mathrm{J\,kg^{-1}}$ at about 20°C (2.50×10^6 at 0°C), so the energy that leaves the surface in evaporated water, the

latent heat flux, is

$$LE = \rho\, L_v\, \overline{w'q'}, \tag{9.12}$$

in $\mathrm{W\,m^{-2}}$. The energy is released again, as sensible heat, wherever the vapor condenses, in a cloud or as dew.

For an illustrative well-watered crop at midday with $\overline{w'q'} = 5 \times 10^{-5}\,\mathrm{kg\,kg^{-1}\,m\,s^{-1}}$ and $\rho = 1.2\,\mathrm{kg\,m^{-3}}$,

$$LE = 1.2 \times 2.45 \times 10^{6} \times 5 \times 10^{-5} = 147\,\mathrm{W\,m^{-2}}.$$

The corresponding evaporation is $\rho\,\overline{w'q'} = 6 \times 10^{-5}\,\mathrm{kg\,m^{-2}\,s^{-1}} = 0.22\,\mathrm{kg\,m^{-2}}$ per hour, a layer of 0.22 mm of water per hour, since a kilogram of water spread over a square meter is a millimeter deep. Over a wet surface the latent heat flux often exceeds the sensible one; over a dry surface the reverse.

9.3.4 The unifying form

Momentum, heat and moisture are three cases of one form. The vertical turbulent flux of any quantity A carried by the air is proportional to

$$\text{vertical turbulent flux of } A \;\propto\; \overline{w'A'}, \tag{9.13}$$

and becomes a physical flux when multiplied by the density and, for heat and moisture, by the factor that converts the quantity per unit mass into energy. The same holds for any trace constituent of concentration c, a pollutant, carbon dioxide, a tracer: $\overline{w'c'}$ is its kinematic flux. Table 9.2 lists the cases. Its columns are the quantity transported, the fluctuation that multiplies w', the kinematic flux with its units, and the physical flux with its units.

Table 9.2: Vertical turbulent fluxes as covariances with the vertical velocity. Positive values are upward.

Quantity	With w'	Kinematic flux	Physical flux
Along-wind momentum	u'	$\overline{u'w'}$, $\mathrm{m^2\,s^{-2}}$	stress $\tau = -\rho\,\overline{u'w'}$, Pa (positive for downward transport)
Cross-wind momentum	v'	$\overline{v'w'}$, $\mathrm{m^2\,s^{-2}}$	cross-wind stress $-\rho\,\overline{v'w'}$, Pa
Heat	θ' or T'	$\overline{w'\theta'}$ or $\overline{w'T'}$, $\mathrm{K\,m\,s^{-1}}$	sensible heat flux $H = \rho\, c_p\, \overline{w'T'}$, $\mathrm{W\,m^{-2}}$
Water vapor	q'	$\overline{w'q'}$, $\mathrm{kg\,kg^{-1}\,m\,s^{-1}}$	latent heat flux $LE = \rho\, L_v\, \overline{w'q'}$, $\mathrm{W\,m^{-2}}$; evaporation $\rho\,\overline{w'q'}$, $\mathrm{kg\,m^{-2}\,s^{-1}}$
Trace constituent	c'	$\overline{w'c'}$, units of c times $\mathrm{m\,s^{-1}}$	mass or molar flux, e.g. of a pollutant or of carbon dioxide

Sign convention. Every flux in this book is positive upward, away from the surface. A positive $\overline{w'\theta'}$ is heat leaving the surface into the air, a positive $\overline{w'q'}$ is evaporation, a negative one is condensation or dew, and a negative $\overline{u'w'}$ is a downward transport of momentum toward the surface, which the stress of equation (9.8) reports as a positive τ. Surface energy-balance studies sometimes count fluxes positive toward the surface; values taken from such a source change sign.

9.4 Measuring fluxes by eddy covariance

The covariances of the previous sections can be computed directly from measured records, and that is how surface fluxes are measured. This section describes the method, why it needs fast

sampling, how the averaging window must sit in the gap between weather and turbulence, what a nonstationary record does to the statistics, and how the coordinates are rotated before any covariance is computed.

9.4.1 The eddy-covariance method

Eddy covariance is a measurement technique, not a model: fast instruments record the fluctuations of the vertical velocity and of the transported quantities at one point, and the fluxes are computed directly as the covariances of equation (9.6). A typical station has a three-dimensional sonic anemometer, which measures u, v, w and the sonic temperature from the transit times of sound pulses between pairs of transducers, and an open-path or closed-path infrared gas analyzer, which measures the concentrations of water vapor and carbon dioxide; both sample at 10 to 20 Hz from a mast a few meters above the surface. Over each averaging period the record gives

$$\tau = -\rho\,\overline{u'w'}, \qquad H = \rho\,c_p\,\overline{w'T'}, \qquad LE = \rho\,L_v\,\overline{w'q'},$$

and the carbon dioxide flux $\overline{w'c'}$. No assumption about the profile, the roughness or the stability is needed, which is why eddy covariance is the reference method for surface fluxes against which the profile and similarity methods of Chapters 12 and 14 are tested. The price is the set of conditions under which the computed covariance equals the physical flux: fast enough sampling, an averaging period that separates the mean from the turbulence, a stationary record, a correct coordinate system, and uniform terrain upwind, the *footprint* from which the measured air has come.

9.4.2 High-frequency sampling

The eddies that carry flux near the ground pass a sensor in seconds or less: at a height of 10 m and a wind of $8\,\mathrm{m\,s^{-1}}$, an eddy of the size of the measurement height passes in about $10/8 = 1.25$ s, and the smaller eddies that still carry part of the flux in a fraction of that. A record sampled once every ten minutes, the usual rate of a meteorological station, contains one value per period and no fluctuations at all; even a record sampled once a second blurs the smallest flux-carrying eddies. Resolving a fluctuation of period P requires at least two samples per period, and in practice several, so eddy-covariance systems sample at 10 to 20 Hz or more. At 20 Hz a thirty-minute period holds $20 \times 1800 = 36\,000$ samples per quantity. The closer to the ground and the stronger the wind, the smaller and faster the flux-carrying eddies, and the higher the rate required; the remaining loss at the high-frequency end, from the path length of the sonic and the separation between the sonic and the gas analyzer, is estimated and corrected for in standard processing.

9.4.3 The averaging window and scale separation

The fluctuation u' depends on how $\overline{u}$ is defined, and in practice $\overline{u}$ is the average over a block of fixed length, the *averaging window*, commonly 10, 30 or 60 minutes. The window decides which motions count as mean flow and which as turbulence. If it is too short, the largest eddies, which take minutes to pass, are partly absorbed into a mean that wanders from one window to the next, and their contribution to the variances and fluxes is lost. If it is too long, changes of the weather within the window, the passage of a front, the daily cycle, a sea breeze setting in, are counted as fluctuations and contaminate the statistics. The decomposition is meaningful only if there is a range of time scales, between the slowest eddies and the fastest weather, in which the atmosphere has little variability, so that a window placed in that range separates the two cleanly. This is the problem of *scale separation*.

Figure 9.4 sketches the energy spectrum of the near-surface wind speed over periods from ten days to a tenth of a second. The horizontal axis is frequency on a logarithmic scale, with

the corresponding periods marked along the top; the vertical axis is the spectral energy per logarithmic frequency interval, the frequency times the spectral density, in arbitrary units, so that equal areas under the curve are equal contributions to the variance. The curve is a schematic with three peaks, at the period of weather systems, at one day, and at the period of boundary-layer turbulence, and a trough between the second and the third, the *spectral gap*. The three vertical lines mark averaging windows of 10, 30 and 60 minutes, and the gray line at the right the highest frequency a 20 Hz record resolves.

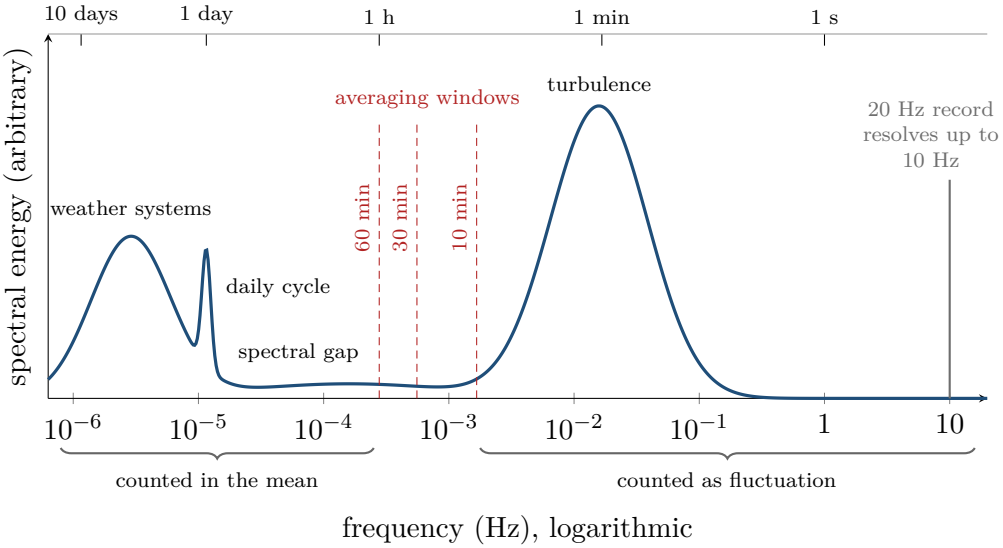


Figure 9.4: Schematic energy spectrum of the near-surface wind speed (illustrative), frequency times spectral density against frequency, of the form $0.55\,e^{-((x+5.54)/0.45)^2} + 0.4\,e^{-((x+4.94)/0.05)^2} + 0.05\,e^{-((x+3.8)/1.2)^2} + e^{-((x+1.8)/0.55)^2}$ with x the base-10 logarithm of the frequency in hertz: a weather-system peak near a period of four days, a daily peak, a turbulence peak near one minute, and a spectral gap between them. Dashed lines: averaging windows.

The averaging window acts as a dividing line on this axis. Variability at periods longer than the window, to the left, ends up in the differences between successive means; variability at shorter periods, to the right, ends up in the fluctuations. A window placed in the gap, where the curve is low, puts nearly all the turbulence on the right and nearly all the weather on the left, and the result is insensitive to the exact choice: 30 and 60 minutes give nearly the same flux. The 10-minute line sits on the low-frequency flank of the turbulence peak and cuts a little of it off, which is why flux measurements over land usually use 30 minutes, while 10 minutes remains the convention for wind statistics and turbulence intensity. Two cautions apply. The gap of the schematic is a feature of typical records, not a law; in convective afternoons the largest eddies have periods of tens of minutes, and at night mesoscale motions, gravity waves and meandering fill the gap, so that no window separates the scales cleanly. And the window must also be long enough to contain many independent eddies, or the covariance is a noisy estimate of the flux: with eddies of about ten seconds, a thirty-minute window holds of order two hundred of them.

9.4.4 Stationarity

Reynolds averaging over a time window assumes that the statistics of the record do not change within the window: that the mean, the variances and the covariances of the first and second halves are the same, apart from sampling noise. A record with this property is *stationary*. The assumption is what allows a time average at one point to stand for the average over many realizations of the same flow, the ensemble average for which the rules of Section 9.5.1 hold

exactly. If the mean wind changes within the window, part of what the decomposition calls u' is the changing mean, not turbulence.

Figure 9.5 makes the effect concrete with the case of a mean wind that climbs from 3 to $15\,\mathrm{m\,s^{-1}}$ within a thirty-minute window, as in the arrival of a gust front. The horizontal axis is time in minutes and the vertical axis the along-wind velocity. The blue trace is an illustrative record: turbulent fluctuations with a standard deviation of about $1.2\,\mathrm{m\,s^{-1}}$ about a mean that rises linearly, drawn as the dashed line. The dotted red line is the block mean of the whole window, $9\,\mathrm{m\,s^{-1}}$. The arrow at two minutes shows the "fluctuation" the decomposition assigns to that instant: almost all of it is the difference between the rising mean and the block mean.

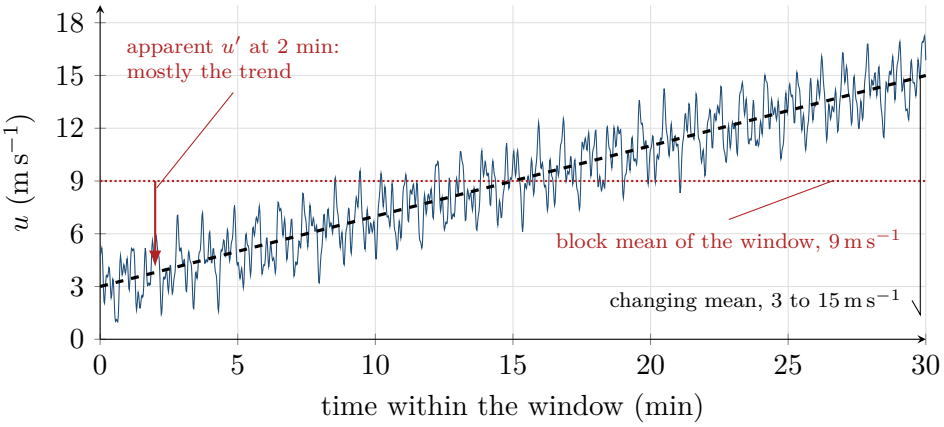


Figure 9.5: A nonstationary record (illustrative): $u(t) = 3 + 0.4\,t + \sum_k a_k \sin(2\pi t/P_k + \varphi_k)$ with t in minutes, $a_k = 1.1, 0.95, 0.7, 0.5\,\mathrm{m\,s^{-1}}$, $P_k = 0.93, 0.41, 0.23, 0.13\,\mathrm{min}$ and phases $\varphi_k = 1, 2, 0.5, 4\,\mathrm{rad}$ (turbulence standard deviation about $1.2\,\mathrm{m\,s^{-1}}$). The mean rises from 3 to $15\,\mathrm{m\,s^{-1}}$ within the window; the block mean is $9\,\mathrm{m\,s^{-1}}$.

The size of the contamination follows from the variance of a linear ramp. A mean rising linearly by ΔU over the window takes every value between its start and its end equally often, like a uniform distribution of width ΔU, whose variance is $\Delta U^2/12$:

$$\frac{1}{t_a}\int_0^{t_a}\Big(\frac{\Delta U\,t}{t_a}-\frac{\Delta U}{2}\Big)^2\mathrm{d}t = \Delta U^2\int_0^1 (s-\tfrac{1}{2})^2\mathrm{d}s = \frac{\Delta U^2}{12}.$$

If the turbulence is uncorrelated with the ramp, the two variances add. For $\Delta U = 15-3 = 12\,\mathrm{m\,s^{-1}}$, the ramp contributes $144/12 = 12\,\mathrm{m^2\,s^{-2}}$, while the turbulence of the figure contributes $1.2^2 = 1.44\,\mathrm{m^2\,s^{-2}}$. The apparent variance is $13.44\,\mathrm{m^2\,s^{-2}}$, more than nine times the true one, and the apparent standard deviation is $\sqrt{13.44} = 3.67\,\mathrm{m\,s^{-1}}$ instead of $1.2\,\mathrm{m\,s^{-1}}$; the apparent turbulence intensity is $3.67/9 = 0.41$ instead of $1.2/9 = 0.13$. The covariance $\overline{u'w'}$ is affected less, because w has no matching trend, but any simultaneous trend in w, in temperature or in humidity enters the fluxes the same way. Processing therefore tests every window: a common test computes the covariance over six five-minute sub-windows, averages them, and compares the result with the covariance of the whole thirty-minute window, flagging the window as nonstationary when the two differ by more than about thirty percent. Removing a fitted linear trend before computing the statistics, or shortening the window, reduces the contamination; neither recovers a record in which the flow itself changed regime.

9.4.5 Coordinate rotation

A sonic anemometer measures the velocity in its own axes, fixed by how it was mounted. If it is not exactly level, or if the ground slopes, its vertical axis is not perpendicular to the mean flow and part of the along-wind velocity appears in its w. The symptom is a measured mean

vertical velocity that is not zero, and the consequence is a covariance that mixes in the variance of u. Suppose the sensor's vertical axis is tilted by a small angle γ in the along-wind direction, so that the measured components are $u_m = u\cos\gamma - w\sin\gamma$ and $w_m = u\sin\gamma + w\cos\gamma$. Then $\overline{w_m} = \overline{u}\sin\gamma$ and

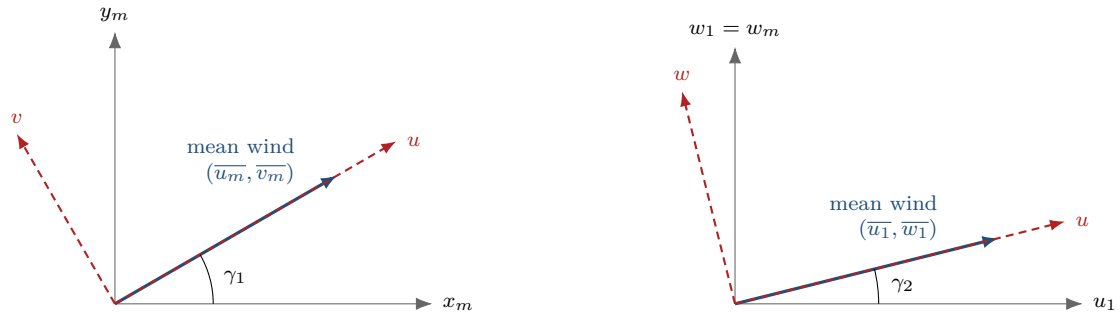
$$\overline{u'_m w'_m} = \overline{u'w'}\cos 2\gamma + \tfrac{1}{2}(\sigma_u^2 - \sigma_w^2)\sin 2\gamma.$$

For an illustrative tilt of $\gamma = 2^\circ$ in the record of Figure 9.1, $\overline{w_m} = 8 \times \sin 2^\circ = 0.28\,\mathrm{m\,s^{-1}}$, an implausible mean vertical velocity over flat ground, and

$$\overline{u'_m w'_m} = -0.25 \times 0.9976 + \tfrac{1}{2}(1.44 - 0.384) \times 0.0698 = -0.2494 + 0.0368 = -0.213\,\mathrm{m^2\,s^{-2}},$$

a flux 15 % too small in magnitude and a friction velocity of 0.461 instead of $0.500\,\mathrm{m\,s^{-1}}$, 8 % low, from a tilt that is hard to see by eye.

The remedy is to rotate the measured velocities into a coordinate system aligned with the mean flow of each window, in which $\overline{v} = 0$ and $\overline{w} = 0$; the along-wind direction is then u, as assumed in the rest of the chapter. Figure 9.6 shows the two rotations of the usual *double rotation*. Panel (a) looks down from above: the thin axes are the sensor's horizontal axes x_m and y_m, the blue arrow is the mean horizontal wind of the window, and the dashed axes are the rotated u and v. Panel (b) looks from the side, across the mean wind: the thin axes are the along-wind axis after the first rotation and the sensor's vertical axis, the blue arrow is the mean wind vector, tilted out of that plane, and the dashed axes are the final u and w. The angles are exaggerated.



(a) first rotation, seen from above

(b) second rotation, seen from the side

Figure 9.6: Double rotation of sonic-anemometer coordinates (angles exaggerated). (a) A rotation by γ_1 about the vertical axis brings u along the mean horizontal wind, so that $\overline{v} = 0$. (b) A rotation by γ_2 about the new cross-wind axis brings u along the mean wind vector, so that $\overline{w} = 0$.

In equations, with (u_m, v_m, w_m) the measured components, the first rotation uses the angle of the mean horizontal wind in the sensor's axes,

$$\gamma_1 = \arctan\frac{\overline{v_m}}{\overline{u_m}}, \qquad \begin{aligned} u_1 &= u_m\cos\gamma_1 + v_m\sin\gamma_1, \\ v_1 &= -u_m\sin\gamma_1 + v_m\cos\gamma_1, \qquad w_1 = w_m, \end{aligned} \tag{9.14}$$

after which $\overline{v_1} = \cos\gamma_1(-\overline{u_m}\tan\gamma_1 + \overline{v_m}) = 0$. The second uses the inclination of the mean wind vector in the (u_1, w_1) plane,

$$\gamma_2 = \arctan\frac{\overline{w_1}}{\overline{u_1}}, \qquad \begin{aligned} u &= u_1\cos\gamma_2 + w_1\sin\gamma_2, \\ w &= -u_1\sin\gamma_2 + w_1\cos\gamma_2, \qquad v = v_1, \end{aligned} \tag{9.15}$$

after which $\overline{w} = 0$ by the same argument. In words: first turn around the vertical until the mean horizontal wind lies along the first axis, then tilt around the new cross-wind axis until the

mean wind has no vertical component. The fluctuations and covariances are computed from the rotated components. For the tilted sensor of the example, $\gamma_2 = \arctan(0.28/7.99) = 2.0^\circ$ recovers the tilt and with it the flux of $-0.25\,\mathrm{m^2\,s^{-2}}$. The double rotation forces $\overline{w} = 0$ in every window, which also removes any real mean vertical motion and, on sloping ground, follows the local streamline direction from window to window; the *planar-fit* alternative fits one tilted plane to the mean winds of many windows from all directions and rotates every window into it, which keeps the coordinate system fixed to the terrain. Neither rotation forces $\overline{v'w'}$ to zero; the cross-wind flux that remains is the cross-wind stress of equation (9.10).

Principle 9.2. *An eddy-covariance flux is defined only together with its averaging window and its coordinate system: the window must separate turbulence from weather and see a stationary record, and the coordinates must be rotated so that the mean vertical velocity vanishes, or the covariance mixes in trends and the along-wind variance.*

9.5 Averaging rules and the closure problem

Covariances are not only measured; they appear in the equations of motion as soon as those equations are averaged. This section derives the rules of Reynolds averaging, shows where the covariance enters the mean momentum equation, states why that makes the averaged equations incomplete, and describes the simplest way of completing them, the flux-gradient relationship, with a case where it fails.

9.5.1 The averaging rules

For two quantities a and b, a constant c and a coordinate s (a space coordinate or time), the Reynolds average obeys

$$\overline{\overline{a}} = \overline{a}, \quad \overline{a'} = 0, \quad \overline{a+b} = \overline{a} + \overline{b}, \quad \overline{c\,a} = c\,\overline{a}, \quad \overline{\overline{a}\,b} = \overline{a}\,\overline{b}, \quad \overline{\frac{\partial a}{\partial s}} = \frac{\partial \overline{a}}{\partial s}. \tag{9.16}$$

The first holds because the mean of a period is a constant over that period; the second was proved in Section 9.1.3; the third and fourth are properties of any sum; the fifth follows from the first and fourth, since $\overline{a}$ is a constant within the period; the last holds exactly for a time average and a space derivative, and for a time derivative only when the record is stationary. An ensemble average satisfies all six exactly, which is the formal reason for the stationarity condition of Section 9.4.4.

The rule that matters is the one for a product. With $a = \overline{a} + a'$ and $b = \overline{b} + b'$,

$$a\,b = \overline{a}\,\overline{b} + \overline{a}\,b' + \overline{b}\,a' + a'b'.$$

Averaging term by term with the rules above, the first term is a constant and stays $\overline{a}\,\overline{b}$; the second is $\overline{a}\,\overline{b'} = 0$ and the third $\overline{b}\,\overline{a'} = 0$, because a constant times a fluctuation averages to zero; the fourth has no reason to vanish. Hence

$$\overline{a\,b} = \overline{a}\,\overline{b} + \overline{a'b'}, \tag{9.17}$$

and in general $\overline{a\,b} \neq \overline{a}\,\overline{b}$. For the velocity components, $\overline{uv} = \overline{u}\,\overline{v} + \overline{u'v'}$ and $\overline{uw} = \overline{u}\,\overline{w} + \overline{u'w'}$. The mean of a product is the product of the means plus the covariance, and the covariance is where turbulence enters every averaged equation that contains a product. The variance is the special case $\overline{u^2} = \overline{u}^2 + \overline{u'^2}$.

9.5.2 The Reynolds-stress term in the mean momentum equation

The equation for the eastward velocity u, in east-north-up coordinates and with density treated as constant, is

$$\frac{\partial u}{\partial t} + u\frac{\partial u}{\partial x} + v\frac{\partial u}{\partial y} + w\frac{\partial u}{\partial z} = -\frac{1}{\rho}\frac{\partial p}{\partial x} + fv + \nu\nabla^2 u.$$

Its advection terms are products of velocities and their derivatives. Mass continuity for constant density, $\partial u/\partial x + \partial v/\partial y + \partial w/\partial z = 0$, allows them to be rewritten as derivatives of products,

$$u\frac{\partial u}{\partial x} + v\frac{\partial u}{\partial y} + w\frac{\partial u}{\partial z} = \frac{\partial(uu)}{\partial x} + \frac{\partial(uv)}{\partial y} + \frac{\partial(uw)}{\partial z} - u\Big(\frac{\partial u}{\partial x} + \frac{\partial v}{\partial y} + \frac{\partial w}{\partial z}\Big),$$

where the last bracket is zero. Take one of these terms and average it with the rules of equation (9.16) and the product rule of equation (9.17):

$$\overline{\frac{\partial(uw)}{\partial z}} = \frac{\partial\,\overline{uw}}{\partial z} = \frac{\partial(\overline{u}\,\overline{w})}{\partial z} + \frac{\partial\,\overline{u'w'}}{\partial z}. \tag{9.18}$$

The first term on the right is the transport of mean momentum by the mean vertical motion; the second is new, the vertical divergence of the turbulent momentum flux. The other two advection terms give $\partial\,\overline{u'u'}/\partial x$ and $\partial\,\overline{u'v'}/\partial y$ in the same way. For a mean flow that is horizontally uniform, with $\overline{w} = 0$, these horizontal derivatives vanish and the averaged equation, with the viscous term negligible away from the surface, becomes

$$\frac{\partial\overline{u}}{\partial t} = -\frac{1}{\rho}\frac{\partial\overline{p}}{\partial x} + f\,\overline{v} - \frac{\partial\,\overline{u'w'}}{\partial z} = -\frac{1}{\rho}\frac{\partial\overline{p}}{\partial x} + f\,\overline{v} + \frac{1}{\rho}\frac{\partial\tau_x}{\partial z}, \tag{9.19}$$

with $\tau_x = -\rho\,\overline{u'w'}$ the eastward component of the stress. The last term is the friction force per unit mass of Chapter 3, now with its physical content: the vertical divergence of the turbulent momentum flux. Near the ground the stress decreases with height from its surface value toward zero at the top of the boundary layer, so $\partial\tau_x/\partial z$ has the sign opposite to the stress, and the term decelerates the mean wind. The equation is written for the eastward component, but the term has the same form for any horizontal direction, in either hemisphere; only the Coriolis term $f\,\overline{v}$ changes sign with f.

9.5.3 The closure problem

Equation (9.19) is one equation for the mean velocity, but it contains a second unknown, the covariance $\overline{u'w'}$, and its companion for $\overline{v}$ contains $\overline{v'w'}$; the averaged heat equation contains $\overline{w'\theta'}$ in the same way. Averaging a nonlinear equation always produces such terms: the term $\overline{uw}$ becomes $\overline{u}\,\overline{w} + \overline{u'w'}$, and the covariance is a quantity the mean equations do not determine. One can derive equations for the covariances themselves, but those contain triple products of fluctuations, and the equations for the triple products contain fourth-order products; at every order there are more unknowns than equations. This is the *closure problem* of turbulence: the averaged equations cannot be closed without a relation, from outside the equations, that expresses the unknown covariances in terms of known mean quantities.

The covariances that close the momentum equation are the Reynolds stresses, and every model of the mean wind near the ground, from a weather model to a computational-fluid-dynamics simulation of a hill, contains a choice of how to express them. The kinds of closure, first order, turbulent-kinetic-energy based and higher order, are described in Chapter 8. The next subsection gives the simplest.

9.5.4 Flux-gradient relationships

The simplest closure assumes that turbulence acts on the mean flow the way molecular diffusion does: the flux is proportional to the mean gradient and directed down it. For momentum and heat,

$$-\overline{u'w'} = K_m \frac{\partial \overline{u}}{\partial z}, \qquad -\overline{w'\theta'} = K_h \frac{\partial \overline{\theta}}{\partial z}, \tag{9.20}$$

where K_m and K_h, in $\mathrm{m^2\,s^{-1}}$, are the *eddy diffusivities* for momentum and for heat (the first is also called the eddy viscosity). These are *flux-gradient relationships*, also called first-order or K-theory closure. The form is that of molecular diffusion, but the coefficients are properties of the turbulence, not of the air: they depend on the size and speed of the eddies, and therefore on height, wind speed, stability and the surface. The heat flux is related to the gradient of θ, not of T, because a parcel carries its potential temperature unchanged (Section 9.3.1); in a neutral layer $\overline{\theta}$ is uniform while $\overline{T}$ falls by 9.8 K per kilometer, and a relation written with T would predict an upward heat flux where there is none.

In the neutral surface layer the eddy viscosity grows linearly with height, $K_m = \kappa\, z\, u_*$, the product of the mixing length $l = \kappa z$ and the velocity scale u_* (Chapter 7). For $u_* = 0.5\,\mathrm{m\,s^{-1}}$, $\kappa = 0.4$ and $z = 10\,\mathrm{m}$,

$$K_m = 0.4 \times 10\,\mathrm{m} \times 0.5\,\mathrm{m\,s^{-1}} = 2\,\mathrm{m^2\,s^{-1}}, \qquad \frac{\partial \overline{u}}{\partial z} = \frac{u_*}{\kappa z} = \frac{0.5}{4} = 0.125\,\mathrm{s^{-1}},$$

and equation (9.20) returns $-\overline{u'w'} = 2 \times 0.125 = 0.25\,\mathrm{m^2\,s^{-2}}$, the flux of the record of Figure 9.1. The molecular viscosity of air is $\nu \approx 1.5 \times 10^{-5}\,\mathrm{m^2\,s^{-1}}$, so the eddy viscosity at 10 m is about 1.3×10^5 times larger: near the ground, molecular diffusion of momentum is negligible except within millimeters of the surface. For heat, an illustrative daytime flux of $\overline{w'\theta'} = 0.15\,\mathrm{K\,m\,s^{-1}}$ across a gradient of $-0.05\,\mathrm{K\,m^{-1}}$ implies $K_h = 0.15/0.05 = 3\,\mathrm{m^2\,s^{-1}}$.

9.5.5 Down-gradient transport and where it fails

With positive diffusivities, equation (9.20) always sends the flux down the gradient. If $\partial\overline{u}/\partial z > 0$, then $\overline{u'w'} < 0$: momentum moves down, from the fast air above to the slow air below, which is the sign found from the parcel exchange of Section 9.2.2. If $\partial\overline{\theta}/\partial z < 0$, as over a heated surface, then $\overline{w'\theta'} > 0$: heat moves up, from the warm air below to the cooler air above. Turbulence in this picture mixes gradients away, and near the surface, where the eddies are small compared with the distances over which the mean profiles change, the picture is accurate.

It fails where the eddies that carry the flux are as large as the layer, so that the flux at a level is set by what happens far from it rather than by the local gradient. The standard case is the upper part of the convective boundary layer. Figure 9.7 shows it schematically, with height scaled by the boundary-layer depth z_i on the vertical axis of both panels. The left panel is the mean potential temperature: decreasing with height in the surface layer, nearly uniform through the mixed layer with a slight decrease in its lower half and a slight increase in its upper half, then a sharp increase across the capping inversion. The right panel is the heat flux divided by its surface value: it decreases linearly with height, from 1 at the surface to a negative value of about -0.2 at z_i, crossing zero at about $0.83\,z_i$. The shaded band, from about $0.5\,z_i$ to $0.83\,z_i$, is where the two disagree with equation (9.20).

In the shaded band $\partial\overline{\theta}/\partial z$ is slightly positive, so equation (9.20) with $K_h > 0$ predicts a downward heat flux, yet the measured flux is upward. Heat moves from cooler air below to warmer air above, a *counter-gradient* flux. The explanation is that the flux there is carried by thermals, plumes of warm air that rise from the heated surface across the whole depth of the mixed layer, keeping their excess temperature from near the ground; they respond to the surface heating, not to the weak local gradient they pass through. Where the gradient is nearly zero, in the middle of the mixed layer, the flux-gradient relation would require an infinite diffusivity,

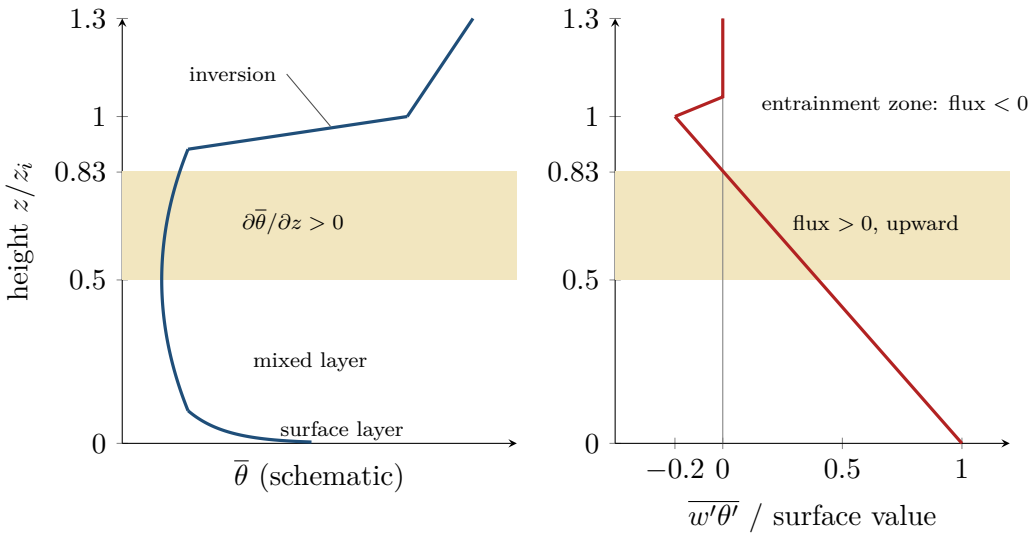


Figure 9.7: Counter-gradient heat flux in the convective boundary layer (schematic, not to scale). Left: mean potential temperature. Right: kinematic heat flux divided by its surface value, $\overline{w'\theta'}/\overline{w'\theta'}_0 = 1 - 1.2\,z/z_i$, the linear profile typical of a convective mixed layer with entrainment at its top. Shaded: the upper mixed layer, where the gradient is weakly positive and the flux is still upward, against the sign that a positive eddy diffusivity requires.

and where the gradient changes sign it would require a negative one: the diffusivity has lost its meaning. Schemes for convective boundary layers therefore add a nonlocal term to the flux that does not depend on the local gradient, or represent the thermals explicitly as a mass flux. Momentum transport shows similar failures inside plant canopies and near the maximum of a low-level jet, which Chapters 18 and 21 treat.

Principle 9.3. *Averaging the equations of motion turns every product into a product of means plus a covariance, and the covariances must be supplied by a closure; the flux-gradient relation is the simplest closure, accurate near the surface, but it fails where large eddies carry the flux across the layer, as in the upper convective mixed layer.*

9.6 Correlation, quadrants and the wind profile

A covariance mixes two things: how large the fluctuations are and how well they are coordinated. This section separates the two with the correlation coefficient, shows that strong turbulence need not carry flux, decomposes the flux of the synthetic record into the four quadrants of the (u', w') plane, and closes with the chain that leads from a measured covariance to the wind profile and with what models estimate in place of the covariance.

9.6.1 The correlation coefficient

The *correlation coefficient* of u and w is the covariance divided by the product of the standard deviations,

$$r_{uw} = \frac{\overline{u'w'}}{\sigma_u\,\sigma_w}, \qquad -1 \le r_{uw} \le 1, \tag{9.21}$$

dimensionless. It measures coordination alone: $r_{uw} = -1$ means that every fluctuation of u is matched by a proportional fluctuation of w of opposite sign, $r_{uw} = 0$ that the signs are unrelated. The bounds follow from the Cauchy–Schwarz inequality, $|\overline{u'w'}| \le \sqrt{\overline{u'^2}}\sqrt{\overline{w'^2}}$. Read

the other way, $\overline{u'w'} = r_{uw}\,\sigma_u\,\sigma_w$: the flux is the product of the fluctuation magnitudes and their coordination, and either factor can make it small.

In the neutral surface layer the standard deviations scale with the friction velocity, typically $\sigma_u \approx 2.4\,u_*$ and $\sigma_w \approx 1.25\,u_*$, so that

$$r_{uw} = \frac{-u_*^2}{(2.4\,u_*)(1.25\,u_*)} = -\frac{1}{3.0} \approx -0.33.$$

A typical correlation of u and w near the ground in neutral conditions is thus about -0.3: turbulence is only loosely coordinated, and the flux is a modest fraction of the largest value the same fluctuations could carry. The synthetic record of Figure 9.1 was built with this typical value, $r_{uw} = -0.25/(1.2 \times 0.62) = -0.336$.

9.6.2 Variance is not flux

Strong fluctuations do not imply a large flux. Consider illustrative turbulence with $\sigma_u = 2\,\mathrm{m\,s^{-1}}$ and $\sigma_w = 1\,\mathrm{m\,s^{-1}}$, both large, but with fluctuations whose signs are unrelated, $r_{uw} = 0$. Then

$$\overline{u'w'} = r_{uw}\,\sigma_u\,\sigma_w = 0 \times 2 \times 1 = 0,$$

and there is no net vertical transport of momentum, however gusty the record. With the same standard deviations and the typical $r_{uw} = -0.3$ the flux would be $-0.3 \times 2 \times 1 = -0.6\,\mathrm{m^2\,s^{-2}}$, a friction velocity of $\sqrt{0.6} = 0.77\,\mathrm{m\,s^{-1}}$. The variances say how much the air fluctuates; only the covariance says how much it transports. Records with large variance and small covariance occur where the fluctuations are produced by something other than local shear: horizontal meandering of the wind at night, wakes of upwind obstacles whose eddies have lost their coordination, or waves, in which u' and w' are a quarter period out of phase and their product averages to nearly zero.

9.6.3 Flux and turbulence intensity

The turbulence intensity TI, the standard deviation of the wind speed divided by its mean (Chapter 8), is the engineering measure of gustiness used in wind-turbine design and in loads on structures. It is a fluctuation amplitude; it does not contain $\overline{u'w'}$. Two flows with the same TI can have very different surface stress. Take two illustrative records, both with $\overline{u} = 10\,\mathrm{m\,s^{-1}}$ and $\sigma_u = 1.5\,\mathrm{m\,s^{-1}}$, so TI = 0.15 in both. In the first, shear-driven turbulence over rough ground, $\sigma_w = 0.8\,\mathrm{m\,s^{-1}}$ and $r_{uw} = -0.35$:

$$\overline{u'w'} = -0.35 \times 1.5 \times 0.8 = -0.42\,\mathrm{m^2\,s^{-2}}, \qquad \tau = 1.2 \times 0.42 = 0.50\,\mathrm{Pa}, \qquad u_* = 0.65\,\mathrm{m\,s^{-1}}.$$

In the second, a night with slow horizontal meandering, $\sigma_w = 0.5\,\mathrm{m\,s^{-1}}$ and $r_{uw} = -0.10$:

$$\overline{u'w'} = -0.10 \times 1.5 \times 0.5 = -0.075\,\mathrm{m^2\,s^{-2}}, \qquad \tau = 1.2 \times 0.075 = 0.09\,\mathrm{Pa}, \qquad u_* = 0.27\,\mathrm{m\,s^{-1}}.$$

The surface stresses differ by a factor of $0.504/0.090 = 5.6$ at equal turbulence intensity. Engineering turbulence metrics and meteorological flux metrics describe different aspects of the same record: the first how variable the wind is at a point, the second how much momentum, heat or moisture the turbulence moves. A wind profile, a surface drag or an evaporation rate depends on the second.

9.6.4 Quadrant analysis

The flux is an average over events of both signs. *Quadrant analysis* sorts the samples by the signs of u' and w' and asks how much of the flux each kind of event carries. The four quadrants of the (u', w') plane are

- Q1, *outward interaction*: $u' > 0$, $w' > 0$, fast air moving up, $u'w' > 0$;
- Q2, *ejection*: $u' < 0$, $w' > 0$, slow air moving up, $u'w' < 0$;
- Q3, *inward interaction*: $u' < 0$, $w' < 0$, slow air moving down, $u'w' > 0$;
- Q4, *sweep*: $u' > 0$, $w' < 0$, fast air moving down, $u'w' < 0$.

Sweeps and ejections both contribute negative products, that is, downward momentum transport; the two interaction quadrants contribute positive products that partly cancel it. The share of quadrant i is the sum of $u'w'$ over its samples, divided by N and by the total flux, $S_i = N^{-1} \sum_{\mathrm{Q}i} u'w' / \overline{u'w'}$; the four shares sum to one.

Figure 9.8 plots the 2400 samples of the synthetic record as points, with u' on the horizontal axis and w' on the vertical axis. The axes through the origin divide the plane into the four quadrants, labeled in the corners. The dashed red curves are the hyperbolas $|u'w'| = 3\,|\overline{u'w'}| = 0.75\,\mathrm{m^2\,s^{-2}}$: samples outside them, away from the axes, are strong events, whose product is more than three times the mean flux. Table 9.3 lists the shares computed by the script that generated the record. Its columns are the quadrant, its name, the share of the flux, and the fraction of the samples, that is, of the time.

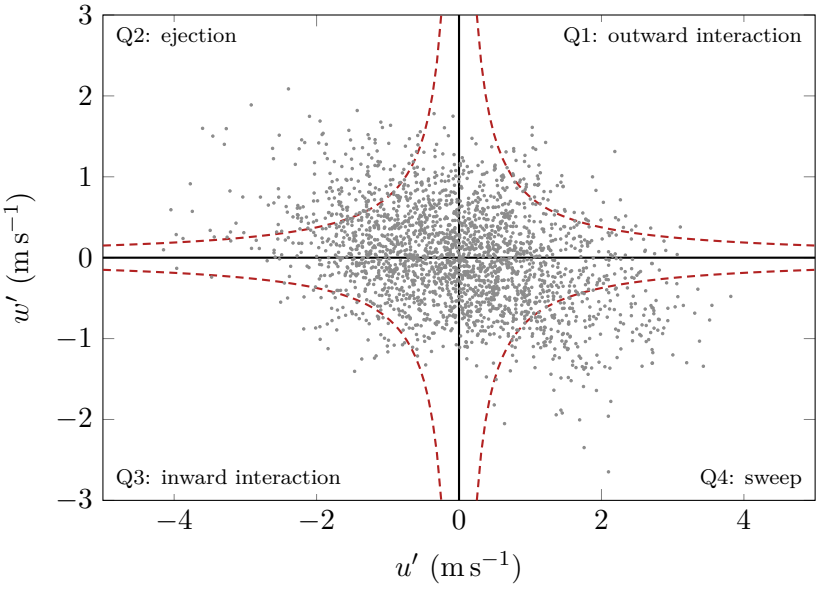


Figure 9.8: Quadrant plot of the synthetic 20 Hz record of Figure 9.1: each point is one sample (u', w'); $\overline{u'w'} = -0.25\,\mathrm{m^2\,s^{-2}}$, $r_{uw} = -0.34$. The cloud is tilted from upper left to lower right, the sign of a downward momentum flux. Dashed: the hyperbolas $|u'w'| = 0.75\,\mathrm{m^2\,s^{-2}}$, three times the mean flux; points beyond them are strong events.

The cloud of points in Figure 9.8 is elongated from upper left to lower right, the ejection and sweep quadrants, which is the visual form of a negative correlation. The table puts numbers on it. Sweeps and ejections together carry $0.80 + 0.70 = 1.50$ of the flux in 60 % of the time; the interactions, 40 % of the time, carry -0.50, cancelling a third of it. The strong events beyond the hyperbolas, 21 % of the samples, carry 86 % of the flux. The flux is thus made mostly by a minority of large, coordinated events of the two kinds, set against a background of weaker samples of both signs.

Sweeps and ejections near the ground. In a sweep, high-momentum air from above is brought down to the surface; in an ejection, low-momentum air from near the surface is

Table 9.3: Quadrant decomposition of the momentum flux of the synthetic record (Figure 9.8), computed by `scripts/ch09_data.py`. Shares of the flux sum to one; a negative share opposes the mean flux.

Quadrant	Event	Share of flux	Share of time
Q1	outward interaction, $u' > 0$, $w' > 0$	-0.26	0.20
Q2	ejection, $u' < 0$, $w' > 0$	$+0.70$	0.30
Q3	inward interaction, $u' < 0$, $w' < 0$	-0.24	0.20
Q4	sweep, $u' > 0$, $w' < 0$	$+0.80$	0.30
Strong events	$\lvert u'w' \rvert > 3\,\lvert\overline{u'w'}\rvert$, all quadrants	$+0.86$	0.21

carried away upward. Near the ground much of the momentum transport occurs in such intermittent events, organized in coherent structures that pass the sensor every few tens of seconds, rather than as a steady drizzle of small exchanges. Real records are more intermittent than the synthetic one, whose fluctuations were generated from Gaussian random processes: in measurements a few percent of the time can carry half of the flux. The Gaussian construction also makes sweeps and ejections nearly symmetric by design. Over real surfaces they are not: in the surface layer above the roughness elements ejections usually carry the larger share, while within and just above tall roughness, such as a forest canopy, sweeps dominate. The surface stress, and with it the wind that acts on a conductor or a rotor, is delivered largely by sweeps reaching down to the ground.

9.6.5 From covariance to the wind profile

The covariance connects to the mean wind profile through a short chain. The kinematic flux gives the stress, $\tau = -\rho\,\overline{u'w'}$; the stress gives the friction velocity, $u_* = \sqrt{\tau/\rho}$; in the neutral surface layer the friction velocity sets the shear,

$$\frac{\partial \overline{u}}{\partial z} = \frac{u_*}{\kappa z}, \tag{9.22}$$

and the shear integrated in height gives the profile, the logarithmic law $\overline{u}(z) = (u_*/\kappa)\ln(z/z_0)$ derived in Chapter 7:

$$\overline{u'w'} \;\rightarrow\; \tau \;\rightarrow\; u_* \;\rightarrow\; \partial\overline{u}/\partial z \;\rightarrow\; \overline{u}(z).$$

With the record's $u_* = 0.5\,\mathrm{m\,s^{-1}}$ and an illustrative $z_0 = 0.05\,\mathrm{m}$, the profile of Figure 9.2 gives $\overline{u} = 1.25\ln(10/0.05) = 1.25 \times 5.30 = 6.62\,\mathrm{m\,s^{-1}}$ at 10 m and $1.25\ln(30/0.05) = 8.00\,\mathrm{m\,s^{-1}}$ at 30 m, a typical conductor height. For a fixed roughness length the whole profile scales with u_*, so a 10 % error in the friction velocity is a 10 % error in the wind at every height; and the 8 % error of the tilted sensor of Section 9.4.5 would carry straight into the inferred profile. The covariance at one height thus determines the shape of the wind in the whole surface layer, once the roughness length and, outside neutral conditions, the stability are known; the friction velocity in this chain is the subject of Chapter 10.

9.6.6 What models estimate

Models of the near-surface wind do not compute the covariance from eddies, except in part. A weather model's boundary-layer scheme estimates $\overline{u'w'}$, $\overline{v'w'}$, $\overline{w'\theta'}$ and $\overline{w'q'}$ from the resolved

mean profiles and the surface conditions, without resolving any of the eddies that carry them, through a closure of the kinds named in Section 9.5.3; its surface-layer scheme supplies the surface values from the wind, temperature and humidity at the lowest model level. A Reynolds-averaged (RANS) computational model of flow over terrain does the same at finer scale: it solves for the mean flow and models every covariance. A large-eddy simulation (LES) resolves the larger, flux-carrying eddies explicitly and models only the covariance of the eddies smaller than its grid. In all three, the quantities of this chapter are present, either computed from resolved fluctuations or prescribed by a closure, and they are rarely shown to the user, who sees only the wind they produce.

These covariances are the hidden quantities behind almost every near-surface wind prediction. The stress decides how much the surface slows the flow, the heat flux decides the stability that bends the profile, and an error in either propagates into the forecast wind at 10 to 150 m. They are also where a model and a measurement can be compared at the level of mechanism rather than outcome: an eddy-covariance station measures the covariances directly, as a point statistic over its averaging window, while the model supplies them as grid-cell values from its closure.

Principle 9.4. *A turbulent flux is a covariance, the product of fluctuation magnitudes and their coordination; strong turbulence with poorly coordinated fluctuations carries little flux, and the flux at one height fixes the friction velocity and through it the shape of the near-surface wind profile.*

9.7 What to retain

Definition 9.1 (Turbulent flux)**.** A turbulent flux is not how variable the air is but how two fluctuations move together: the vertical flux of a quantity A is the covariance $\overline{w'A'}$ over a stated averaging window and coordinate system, and $\overline{u'w'} < 0$ means momentum carried downward, with $u_* = \sqrt{-\overline{u'w'}}$.

Table 9.4 lists the terms of the chapter, their meaning, their units and the subsection that defines each.

9.8 Exercises

Exercise 9.1. Six simultaneous samples of the along-wind and vertical velocity, in $\mathrm{m\,s^{-1}}$, are u: 7.4, 8.6, 9.1, 6.8, 7.9, 8.2 and w: 0.3, −0.2, −0.5, 0.4, 0.1, −0.1. (a) Compute $\overline{u}$, $\overline{w}$ and the fluctuations, and verify that each set of fluctuations sums to zero. (b) Compute σ_u, σ_w and $\overline{u'w'}$. (c) Compute τ at $\rho = 1.2\,\mathrm{kg\,m^{-3}}$, u_* and r_{uw}. (d) Classify each sample by quadrant, and say why six samples cannot give a reliable flux even though the arithmetic is exact.

Exercise 9.2. A sonic anemometer on the coast of Brazil at 22°S reports, for one thirty-minute window, mean east and north velocity components of $-6.0\,\mathrm{m\,s^{-1}}$ and $+4.0\,\mathrm{m\,s^{-1}}$ and, in the same east-north-up axes, kinematic fluxes $\overline{u'_E w'} = +0.155$ and $\overline{v'_N w'} = -0.128\,\mathrm{m^2\,s^{-2}}$; its mean vertical velocity is zero. (a) Compute the mean wind speed and the direction the wind blows from, and say whether this is consistent with the southeasterly trade winds of the Southern Hemisphere. (b) Rotate the fluxes into along-wind coordinates, u along the mean wind and v to its left, and give $\overline{u'w'}$ and $\overline{v'w'}$. (c) Compute u_* from the along-wind flux alone and from equation (9.10), and the angle between the stress and the mean wind. (d) Toward which compass direction does the stress of the air act on the ground?

Exercise 9.3. Over an irrigated field at midday, $\rho = 1.15\,\mathrm{kg\,m^{-3}}$, $\overline{w'T'} = 0.08\,\mathrm{K\,m\,s^{-1}}$ and $\overline{w'q'} = 1.2 \times 10^{-4}\,\mathrm{kg\,kg^{-1}\,m\,s^{-1}}$. At night over the same field, $\overline{w'T'} = -0.015\,\mathrm{K\,m\,s^{-1}}$. (a)

Table 9.4: The terms of the chapter and where each is defined.

Term	Meaning	Units	Defined in
Reynolds decomposition	$a = \overline{a} + a'$: mean over a window plus fluctuation	as a	9.1.1
Prime	$a' = a - \overline{a}$, the departure from the mean; $\overline{a'} = 0$	as a	9.1.2, 9.1.3
Variance	$\overline{a'^2}$, mean square fluctuation	units of a squared	9.1.4
Standard deviation	$\sigma_a = \sqrt{\overline{a'^2}}$, typical size of a fluctuation	as a	9.1.4
Covariance	$\overline{a'b'}$, mean product of two fluctuations; its sign is physical	product of units	9.2.1
Momentum flux	$\overline{u'w'}$ (kinematic); $\overline{u'w'} < 0$ is downward transport	$\mathrm{m^2\,s^{-2}}$	9.2.2, 9.2.3
Reynolds stress	$\tau = -\rho\,\overline{u'w'}$, turbulent shear stress; the covariance terms of the averaged equations	Pa	9.2.3, 9.5.2
Friction velocity	$u_* = [\overline{u'w'}^2 + \overline{v'w'}^2]^{1/4}$, velocity scale of the stress	$\mathrm{m\,s^{-1}}$	9.2.4
Heat flux	$\overline{w'\theta'}$ or $\overline{w'T'}$ (kinematic); $H = \rho\,c_p\,\overline{w'T'}$	$\mathrm{K\,m\,s^{-1}}$; $\mathrm{W\,m^{-2}}$	9.3.1, 9.3.2
Latent heat flux	$LE = \rho\,L_v\,\overline{w'q'}$, energy in evaporated water	$\mathrm{W\,m^{-2}}$	9.3.3
Eddy covariance	fluxes computed directly as covariances of fast records	–	9.4.1
Averaging window	block over which means are taken; must lie in the spectral gap	s, min	9.4.3
Stationarity	statistics unchanged within the window; a trend ΔU adds $\Delta U^2/12$ to the variance	–	9.4.4
Coordinate rotation	rotation to $\overline{v} = 0$, $\overline{w} = 0$ before computing covariances	–	9.4.5
Closure problem	averaged equations contain covariances they do not determine	–	9.5.3
Flux-gradient relationship	$-\overline{u'w'} = K_m\,\partial\overline{u}/\partial z$, $-\overline{w'\theta'} = K_h\,\partial\overline{\theta}/\partial z$	$\mathrm{m^2\,s^{-1}}$ for K_m, K_h	9.5.4
Correlation coefficient	$r_{uw} = \overline{u'w'}/(\sigma_u\sigma_w)$, about -0.3 near the ground (typical)	–	9.6.1
Sweep	Q4: $u' > 0$, $w' < 0$, fast air moving down	–	9.6.4
Ejection	Q2: $u' < 0$, $w' > 0$, slow air moving up	–	9.6.4

Compute H and LE at midday with $c_p = 1004\,\mathrm{J\,kg^{-1}\,K^{-1}}$ and $L_v = 2.45 \times 10^6\,\mathrm{J\,kg^{-1}}$, and the evaporation in millimeters per hour. (b) Compute H at night and describe, with the signs of w' and θ', the parcel exchanges that produce it. (c) A station reports one temperature and one vertical velocity every ten minutes. Explain why its covariance cannot be used as a heat flux.

Exercise 9.4. (a) Within a thirty-minute window the mean wind rises linearly from 6 to $10\,\mathrm{m\,s^{-1}}$, and the turbulence has $\sigma_u = 0.9\,\mathrm{m\,s^{-1}}$. Compute the apparent variance, standard deviation and turbulence intensity of the window, and compare them with the turbulent values. (b) A sonic is tilted by 3° in the along-wind direction in a flow with $\overline{u} = 6\,\mathrm{m\,s^{-1}}$, $\sigma_u = 1.0\,\mathrm{m\,s^{-1}}$, $\sigma_w = 0.5\,\mathrm{m\,s^{-1}}$ and $\overline{u'w'} = -0.12\,\mathrm{m^2\,s^{-2}}$. Compute the measured mean vertical velocity, the measured covariance and the error in u_*. (c) In a neutral surface layer with $u_* = 0.4\,\mathrm{m\,s^{-1}}$, compute K_m and $\partial\overline{u}/\partial z$ at 20 m. (d) In the upper part of a convective mixed layer, $\overline{w'\theta'} = 0.03\,\mathrm{K\,m\,s^{-1}}$ and $\partial\overline{\theta}/\partial z = +0.001\,\mathrm{K\,m^{-1}}$. Compute the diffusivity K_h that equation (9.20) would require and explain what its sign means.

Chapter 10

Friction Velocity

10.1 Friction velocity as a velocity scale for surface stress

The previous chapters built the description of the surface layer from averages and fluctuations. Chapter 9 showed that the covariance $\overline{u'w'}$ of the along-wind and vertical velocity fluctuations is a vertical flux of horizontal momentum, and that at the ground this flux is the force per unit area that the air exerts on the surface. Chapter 7 wrote the neutral wind profile in terms of a velocity u_* and a length z_0. This chapter takes the velocity u_* as its object. The question of the chapter is

what does the friction velocity mean physically, how is it related to the wind speed, the surface and the drag on the surface, and how is it measured, inferred and checked?

The chapter first defines the friction velocity from the surface stress and works out what its values mean as forces. It then places it in the wind profile, relates it to the drag coefficient used in bulk formulas, describes the ways of measuring and inferring it, and shows how it scales the turbulence and where that scaling stops. It ends with the stress as a vector and with a consequence for model evaluation: two models can agree on the wind at 10 m and disagree by a factor of five on the surface stress.

Jargon: surface stress, friction velocity, velocity scale, drag coefficient, stress vector, constant-stress layer, mechanical turbulence, convective velocity scale

The *surface stress* τ_0 is the horizontal force per unit area that the air exerts on the ground, in pascals ($\mathrm{N\,m^{-2}}$); it is carried by turbulence, $\tau_0 = -\rho\,\overline{u'w'}$ at the surface in coordinates aligned with the mean wind, and it is measured by eddy covariance or calculated from a wind profile. The *friction velocity* $u_* = \sqrt{\tau_0/\rho}$, in m/s, is that stress expressed as a velocity; it is not a wind speed. A *velocity scale* is a velocity built from the governing quantities of a flow that sets the size of its velocity differences and fluctuations, so that they become comparable from one flow to another once divided by it. The *drag coefficient* $C_D = \tau_0/(\rho U^2)$, dimensionless, is the ratio of the surface stress to the dynamic pressure scale of the mean wind U at a stated reference height; bulk formulas in models use it to compute the stress from the wind. The *stress vector* $\boldsymbol{\tau}_0 = (\tau_x, \tau_y)$, in pascals, is the surface stress with its direction, from the two covariances $\overline{u'w'}$ and $\overline{v'w'}$. The *constant-stress layer* (constant-flux layer) is the lowest part of the boundary layer, roughly its lowest tenth, in which the stress changes by less than about ten percent with height, so that one u_* describes it. *Mechanical turbulence* is turbulence produced by wind shear, drawing its energy from the mean flow; its velocity scale is u_*. The *convective velocity scale* w_*, in m/s, is the velocity scale of turbulence produced by buoyancy when the ground heats the air, built from the surface heat flux and the boundary-layer depth z_i.

Key idea

The friction velocity measures how strongly the surface and the atmosphere exchange horizontal momentum. The chain is turbulent covariance → surface stress → u_* → wind shear: u_* is the stress in velocity units, it sets the slope of the near-surface wind profile and the size of the turbulence, and it is a fundamental scaling variable of near-surface wind, distinct from the wind speed itself.

10.1.1 Surface stress in velocity units

In coordinates with u along the mean wind, v across it and w upward, Chapter 9 identified the turbulent shear stress at height z as

$$\tau(z) = -\rho\,\overline{u'w'}(z), \tag{10.1}$$

positive when momentum flows downward ($\overline{u'w'} < 0$), which is the normal case over the ground: air arriving from above ($w' < 0$) carries the faster flow aloft ($u' > 0$), and air arriving from below ($w' > 0$) carries the slower flow near the ground ($u' < 0$). At the surface, $\tau(0) = \tau_0$. The friction velocity is defined by

$$u_* = \sqrt{\frac{\tau_0}{\rho}} = \sqrt{-\,\overline{u'w'}\,\Big|_{\text{surface}}}, \tag{10.2}$$

so that $\tau_0 = \rho\,u_*^2$. Nothing new has been measured: equation (10.2) rewrites the surface stress in another unit. In practice "at the surface" means at a height inside the constant-stress layer of Section 10.2.4, where the stress is close to its surface value, typically a few meters above the ground and above the roughness elements.

Why a velocity. The units follow in three steps. A stress is a force per unit area, $\mathrm{N\,m^{-2}} = \mathrm{kg\,m^{-1}\,s^{-2}}$. Dividing by the density, in $\mathrm{kg\,m^{-3}}$, gives the kinematic stress τ_0/ρ in $\mathrm{m^2\,s^{-2}}$, the same unit as the covariance $\overline{u'w'}$. The square root of a quantity in $\mathrm{m^2\,s^{-2}}$ is in m/s. The result is a velocity, and a velocity is the convenient form because the quantities the stress controls are velocities: the change of wind speed with height, the standard deviations σ_u, σ_v, σ_w of the turbulent fluctuations, and the gusts. Each of them can be divided by u_* to give a dimensionless number, and those numbers are what Section 10.5 compares from site to site.

10.1.2 What the friction velocity measures

A friction velocity of $0.5\,\mathrm{m\,s^{-1}}$ does not mean that the wind is $0.5\,\mathrm{m\,s^{-1}}$, nor that any parcel of air moves at that speed. The ratio u_*/U at 10 m ranges from about 0.04 over the sea to about 0.13 over rough land (Table 10.1), so $u_* = 0.5\,\mathrm{m\,s^{-1}}$ goes with a 10 m wind of roughly 4 to $12\,\mathrm{m\,s^{-1}}$. The friction velocity measures how strongly momentum is exchanged between the atmosphere and the surface: it is the square root of the rate, per unit area and per unit density, at which horizontal momentum is delivered downward to the ground and lost there. Two flows with the same wind speed can have very different friction velocities, and one with a weaker wind can have the larger u_*, as Section 10.2.3 shows.

The distinction is the book's recurring one between a quantity of the flow and a quantity a model or an instrument reports. A cup anemometer reports U, a property of the mean flow at one height. No instrument reports u_* directly: a sonic anemometer reports fast velocity samples from which the covariance $\overline{u'w'}$ is computed (Section 10.4.1), and a weather model computes u_* from its lowest-level wind, an assumed roughness and a stability function (Section 10.4.5). The friction velocity is always calculated or inferred.

10.1.3 Stress and the square of the friction velocity

Since $\tau_0 = \rho u_*^2$, the stress grows with the square of the friction velocity. With $\rho = 1.2\,\mathrm{kg\,m^{-3}}$,

$$u_* = 0.4\,\mathrm{m\,s^{-1}}: \quad \tau_0 = 1.2 \times 0.4^2 = 1.2 \times 0.16 = 0.192\,\mathrm{Pa},$$

$$u_* = 0.8\,\mathrm{m\,s^{-1}}: \quad \tau_0 = 1.2 \times 0.8^2 = 1.2 \times 0.64 = 0.768\,\mathrm{Pa}.$$

Doubling the friction velocity quadruples the stress, since $0.768/0.192 = 4$. Conversely, a stress known to $\pm 20\,\%$ gives the friction velocity to about $\pm 10\,\%$, because a relative error in τ_0 is halved by the square root. Both stresses are small compared with the atmospheric pressure of about $10^5\,\mathrm{Pa}$, and they are not small in their effect, as the next subsection shows.

Figure 10.1 draws the relation. The horizontal axis is the friction velocity in m/s, the vertical axis the surface stress in pascals. The curve is $\tau_0 = \rho u_*^2$ with $\rho = 1.2\,\mathrm{kg\,m^{-3}}$; the two marked points are the examples above, with dotted lines to the axes. The curve is flat near the origin and steepens: the same increase of $0.4\,\mathrm{m\,s^{-1}}$ in u_* adds 0.192 Pa from 0 to $0.4\,\mathrm{m\,s^{-1}}$ and 0.576 Pa from 0.4 to $0.8\,\mathrm{m\,s^{-1}}$.

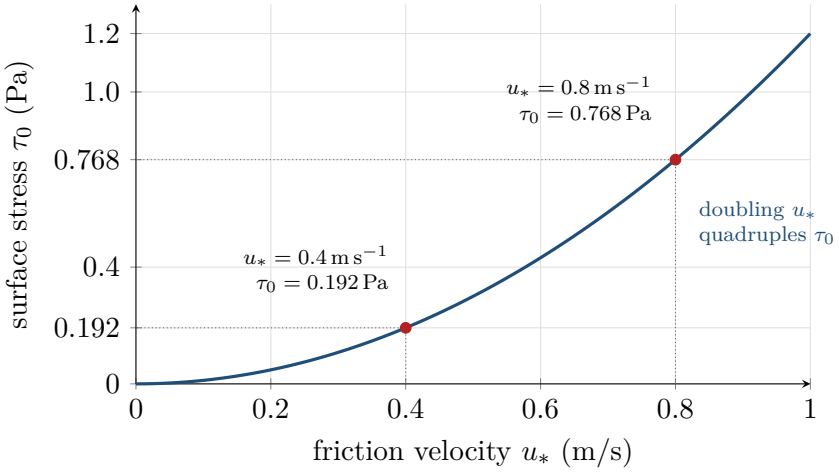


Figure 10.1: Surface stress against friction velocity, $\tau_0 = \rho u_*^2$ (equation (10.2)) with $\rho = 1.2\,\mathrm{kg\,m^{-3}}$. The marked points are the worked examples of Section 10.1.3.

10.1.4 The force on a square kilometer

A stress becomes concrete when multiplied by an area. Over one square kilometer, $10^6\,\mathrm{m^2}$, of level ground, the horizontal force is

$$\tau_0 \times 10^6\,\mathrm{m^2} = 0.192\,\mathrm{Pa} \times 10^6\,\mathrm{m^2} = 1.92 \times 10^5\,\mathrm{N} = 192\,\mathrm{kN}$$

for $u_* = 0.4\,\mathrm{m\,s^{-1}}$, and 768 kN for $u_* = 0.8\,\mathrm{m\,s^{-1}}$. The first is about the weight of a mass of $1.92 \times 10^5/9.81 \approx 19.6$ tonnes. It acts horizontally, downwind on the ground and upwind on the air, and it is spread over the ground's grass, crops, trees and buildings. Equivalently, every second the air above that square kilometer loses $1.92 \times 10^5\,\mathrm{kg\,m\,s^{-1}}$ of horizontal momentum to the surface.

What the loss would do. Suppose, for illustration, that the loss were shared evenly by a boundary layer $z_i = 1000\,\mathrm{m}$ deep, with nothing to replace it. The column above one square meter holds $\rho z_i = 1.2 \times 1000 = 1200\,\mathrm{kg}$ of air, and it would decelerate at

$$\frac{\tau_0}{\rho z_i} = \frac{0.192\,\mathrm{Pa}}{1200\,\mathrm{kg\,m^{-2}}} = 1.6 \times 10^{-4}\,\mathrm{m\,s^{-2}} \approx 0.58\,\mathrm{m\,s^{-1}} \text{ per hour.}$$

At that rate a boundary-layer wind of $6\,\mathrm{m\,s^{-1}}$ would be stopped in about ten hours. It is not, because the large-scale pressure gradient keeps resupplying momentum: friction slows the wind below its geostrophic value, the Coriolis force weakens with it, and the unbalanced pressure-gradient force drives a cross-isobaric flow toward low pressure (Chapter 3). Integrating the steady momentum balance over the depth of the layer gives the size of that flow: the depth-integrated ageostrophic mass transport has magnitude $\tau_0/|f|$ and points perpendicular to the surface stress, to its left in the Northern Hemisphere and to its right in the Southern. With $\tau_0 = 0.192\,\mathrm{Pa}$, $|f| = 10^{-4}\,\mathrm{s^{-1}}$ and $z_i = 1000\,\mathrm{m}$, its mean velocity is $\tau_0/(\rho\,|f|\,z_i) = 0.192/(1.2 \times 10^{-4} \times 1000) = 1.6\,\mathrm{m\,s^{-1}}$. The surface stress is the sink, the pressure gradient acting on that cross-isobaric flow the source.

10.1.5 The name

The word "friction" suggests molecular friction, the viscous stress of a fluid sliding over a surface. Near the ground that stress is negligible. The viscous stress is $\rho\,\nu\,\partial U/\partial z$; with $\nu = 1.5 \times 10^{-5}\,\mathrm{m^2\,s^{-1}}$ and the shear $\partial U/\partial z = 0.1\,\mathrm{s^{-1}}$ found at 10 m for $u_* = 0.4\,\mathrm{m\,s^{-1}}$ in Section 10.2.1, it is $1.2 \times 1.5 \times 10^{-5} \times 0.1 = 1.8 \times 10^{-6}\,\mathrm{Pa}$, about 10^5 times smaller than the turbulent stress of 0.192 Pa in the same flow. The momentum transfer that u_* measures is turbulent: eddies carry it, as the covariance of equation (10.1) expresses. Only in a sublayer millimeters thick over a very smooth surface, such as calm water, does molecular viscosity carry the stress.

The name comes from the study of turbulent flow along walls and in pipes, where the stress at the wall is called wall friction, or skin friction, and the velocity built from it was named after it. The atmospheric meaning is the same, with the ground as the wall. The physically accurate reading is a *surface-stress velocity scale*, and the book uses "friction velocity" only in that sense.

10.2 Friction velocity and the wind profile

The friction velocity enters the wind profile as the factor that sets the shear. This section recalls the neutral profile, works out two profiles that differ only in u_*, shows what controls u_*, and states where in the boundary layer a single value of u_* describes the flow.

10.2.1 The shear relation and the logarithmic profile

Chapter 7 derived the neutral surface-layer profile from a constant stress and a mixing length proportional to height. The result in differential form is

$$\frac{\partial U}{\partial z} = \frac{u_*}{\kappa\, z}, \tag{10.3}$$

with the von Kármán constant $\kappa \approx 0.4$. The friction velocity sets the magnitude of the shear at every height, and the height sets how the shear decreases away from the ground. At 10 m with $u_* = 0.4\,\mathrm{m\,s^{-1}}$, $\partial U/\partial z = 0.4/(0.4 \times 10) = 0.1\,\mathrm{s^{-1}}$, a change of $1\,\mathrm{m\,s^{-1}}$ per 10 m; at 50 m it is $0.02\,\mathrm{s^{-1}}$. Integrating equation (10.3) from the height z_0 at which the extrapolated wind vanishes,

$$U(z) - U(z_0) = \frac{u_*}{\kappa}\int_{z_0}^{z}\frac{\mathrm{d}z'}{z'} = \frac{u_*}{\kappa}(\ln z - \ln z_0),$$

and with $U(z_0) = 0$,

$$U(z) = \frac{u_*}{\kappa}\ln\frac{z}{z_0}, \qquad \text{or} \qquad U(z) = \frac{u_*}{\kappa}\ln\frac{z-d}{z_0} \tag{10.4}$$

over tall vegetation or buildings, where the displacement height d shifts the origin of the profile. The two parameters play distinct roles: u_* is the strength of the momentum exchange, a property

of the flow; z_0 is the aerodynamic character of the surface, a property of the ground. In this sense u_* is the natural velocity scale of the surface layer: the profile written as $U/u_* = (1/\kappa)\ln(z/z_0)$ contains no other velocity.

10.2.2 Two neutral profiles

Take $z_0 = 0.05\,\mathrm{m}$, typical of farmland with low crops, and $\kappa = 0.4$. With $u_* = 0.4\,\mathrm{m\,s^{-1}}$ the prefactor is $u_*/\kappa = 1\,\mathrm{m\,s^{-1}}$, and

$$U(10\,\mathrm{m}) = 1 \times \ln\frac{10}{0.05} = \ln 200 \approx 5.30\,\mathrm{m\,s^{-1}}, \qquad U(50\,\mathrm{m}) = \ln\frac{50}{0.05} = \ln 1000 \approx 6.91\,\mathrm{m\,s^{-1}}.$$

With $u_* = 0.8\,\mathrm{m\,s^{-1}}$ over the same surface the prefactor is $2\,\mathrm{m\,s^{-1}}$, and

$$U(10\,\mathrm{m}) = 2\ln 200 \approx 10.60\,\mathrm{m\,s^{-1}}, \qquad U(50\,\mathrm{m}) = 2\ln 1000 \approx 13.82\,\mathrm{m\,s^{-1}}.$$

For fixed z_0 and neutral stratification, doubling u_* doubles the wind at every height, because U is proportional to u_* in equation (10.4). The ratio $U(50)/U(10) = \ln 1000/\ln 200 = 1.30$ is the same for both, since it depends only on the heights and on z_0.

Figure 10.2 draws the two profiles. The horizontal axis is the wind speed in m/s and the vertical axis the height in meters, on a linear scale from the ground to 100 m. Each curve starts from zero at $z = z_0$; the marked points are the values computed above. On the linear height axis the profiles bend sharply in the lowest few meters, where the shear $u_*/(\kappa z)$ is largest, and become nearly vertical aloft. The profile for $u_* = 0.8\,\mathrm{m\,s^{-1}}$ lies at twice the speed of the other at every height, so the gap between them widens upward from zero at z_0 to $6.9\,\mathrm{m\,s^{-1}}$ at 50 m.

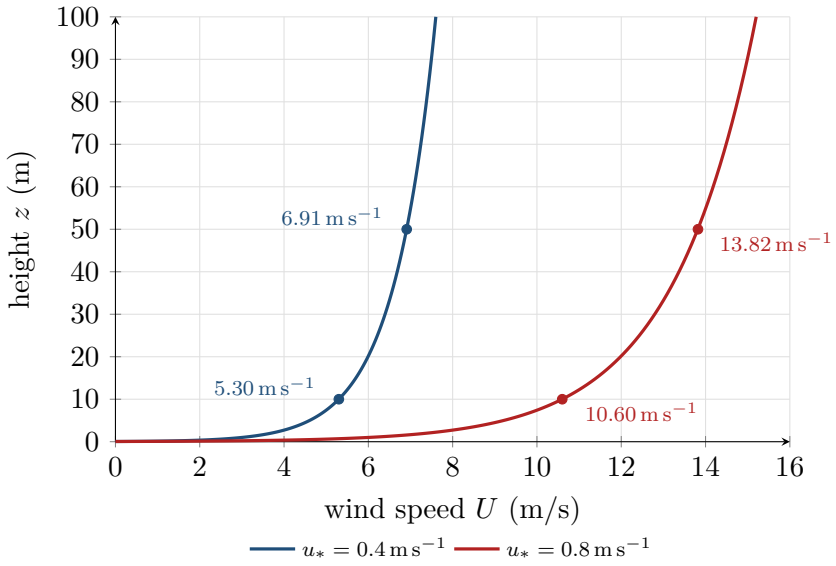


Figure 10.2: Neutral logarithmic profiles $U(z) = (u_*/\kappa)\ln(z/z_0)$ (equation (10.4)) with $z_0 = 0.05\,\mathrm{m}$ and $\kappa = 0.4$, for $u_* = 0.4$ and $0.8\,\mathrm{m\,s^{-1}}$. Marked points at 10 and 50 m. Values illustrative.

10.2.3 Dependence on wind speed, roughness and stability

Equation (10.4) can be read the other way, as an expression for u_* given a wind at one height,

$$u_* = \frac{\kappa\, U(z)}{\ln(z/z_0)}, \tag{10.5}$$

which shows that the friction velocity is not independent of the wind speed. It grows in proportion to the wind at fixed roughness, grows with the roughness at fixed wind, and, outside neutral conditions, depends on stability: $u_* = f(U, z_0, \text{stability})$. Over the farmland of the previous subsection, $U_{10} = 3\,\mathrm{m\,s^{-1}}$ gives $u_* = 0.4 \times 3/5.30 = 0.23\,\mathrm{m\,s^{-1}}$ and $U_{10} = 12\,\mathrm{m\,s^{-1}}$ gives $0.91\,\mathrm{m\,s^{-1}}$. A weak wind over a rough surface can produce a smaller u_* than a strong wind over a smooth one: $U_{10} = 2\,\mathrm{m\,s^{-1}}$ over a surface with $z_0 = 0.5\,\mathrm{m}$ gives $0.4 \times 2/\ln 20 = 0.27\,\mathrm{m\,s^{-1}}$, whereas $U_{10} = 12\,\mathrm{m\,s^{-1}}$ over a smooth surface with $z_0 = 0.001\,\mathrm{m}$ gives $0.4 \times 12/\ln 10^4 = 0.52\,\mathrm{m\,s^{-1}}$.

The friction velocity is therefore not a property of the terrain. The terrain contributes z_0; the weather contributes the wind speed and the stability; u_* is the combination that results, and it changes from hour to hour at a fixed site. Stability enters because buoyancy changes the shear for a given stress. In unstable air (ground warmer than the air above) rising thermals mix momentum vertically more efficiently, the profile is more uniform, and a given U_{10} goes with a larger u_* than in neutral air. In stable air (ground colder than the air above) vertical motion is suppressed, the profile is steeper, and the same U_{10} goes with a smaller u_*. Section 10.4.4 puts numbers on both.

10.2.4 Constant stress near the surface and its decrease aloft

Equation (10.4) uses one u_* for every height. That is legitimate only where the stress does not change appreciably with height. In the classical surface layer it does not: the stress there equals its surface value to within about ten percent, which is why the layer is also called the constant-stress or constant-flux layer (Chapter 7). Above it the stress decreases with height. At the top of the boundary layer, $z = z_i$, the turbulence fades and the stress is much smaller than τ_0, close to zero in the simplest case. Across the full boundary layer $\tau(z)$ is not constant, and the constant-flux approximation holds only near the ground.

The decrease is not arbitrary. In a steady, horizontally uniform boundary layer the vertical change of stress, divided by the density, balances the difference between the pressure-gradient and Coriolis forces at each height; in the idealization in which that difference is the same at every height, the stress falls linearly,

$$\tau(z) \approx \tau_0 \left(1 - \frac{z}{z_i}\right), \tag{10.6}$$

and its gradient $-\tau_0/z_i$ is the deceleration of Section 10.1.4 distributed evenly through the layer. Real profiles are curved and their stress also turns in direction with height (Section 10.6.2), but the linear form shows the proportions. If the surface layer is taken as the lowest tenth of the layer, the stress at its top is $0.9\,\tau_0$. For $\tau_0 = 0.192\,\mathrm{Pa}$ and $z_i = 1000\,\mathrm{m}$, the stress at 100 m is $0.173\,\mathrm{Pa}$, and the local friction velocity $\sqrt{\tau/\rho}$ there is $\sqrt{0.9} \times 0.4 = 0.38\,\mathrm{m\,s^{-1}}$, only 5 % below the surface value: the square root halves the relative change.

Figure 10.3 draws equation (10.6). The horizontal axis is the stress divided by its surface value, and the vertical axis the height divided by the boundary-layer depth. The solid line is τ/τ_0; the dashed curve is the corresponding local friction velocity divided by its surface value, $\sqrt{1 - z/z_i}$. The shaded band is the lowest tenth of the layer, and the dotted vertical line at 1 is the constant-stress approximation. Inside the band the solid line stays within ten percent of the dotted one; above it the two separate, and at mid-depth the stress is half its surface value.

Principle 10.1. *One friction velocity describes the wind profile only within the constant-stress layer, roughly the lowest tenth of the boundary layer. Above it the stress decreases toward the top of the layer, and a profile written with the surface u_* is an extrapolation.*

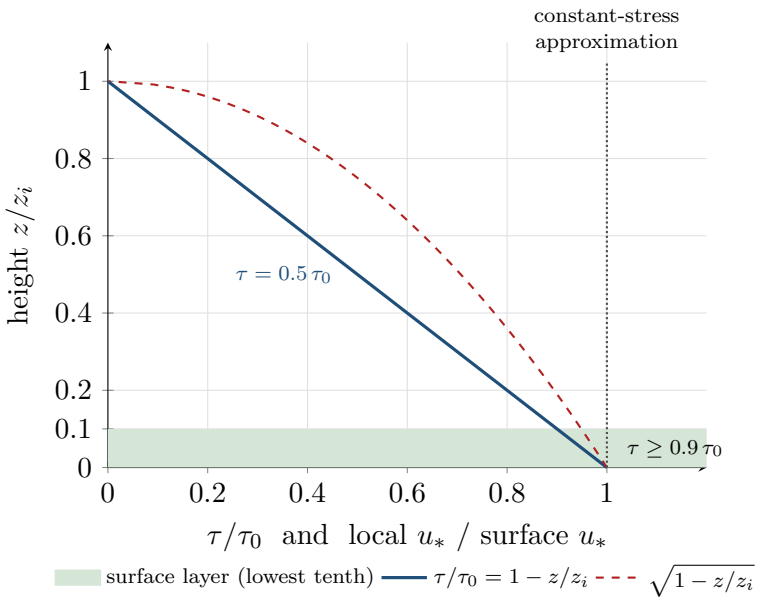


Figure 10.3: Stress and local friction velocity across the boundary layer in the linear idealization $\tau = \tau_0(1 - z/z_i)$ (equation (10.6)). Real profiles are curved and rotate with height; the figure shows only the proportions.

10.3 The drag coefficient

Weather models, ocean models and engineering codes rarely carry u_* as an input; they compute the surface stress from the wind with a drag coefficient. This section defines the coefficient, relates it to the friction velocity, derives its neutral form, and shows that a drag coefficient is meaningful only together with the surface, the reference height and the stability it was computed for.

10.3.1 Definition and relation to the friction velocity

The bulk formula for the surface stress is

$$\tau_0 = \rho\, C_D\, U(z)^2, \tag{10.7}$$

where $U(z)$ is the mean wind speed at a reference height z, usually 10 m, and C_D is the drag coefficient for that height. Equating it with $\tau_0 = \rho\, u_*^2$ gives

$$C_D = \frac{u_*^2}{U(z)^2}, \qquad u_* = U(z)\sqrt{C_D}. \tag{10.8}$$

The drag coefficient is the square of the ratio of the friction velocity to the wind speed. Equation (10.7) has the form of the drag on a body in a stream, a coefficient times the dynamic pressure $\frac{1}{2}\rho U^2$; by meteorological convention the factor $\frac{1}{2}$ is absorbed into C_D.

For $U_{10} = 8\,\mathrm{m\,s^{-1}}$ and $C_D = 0.004$,

$$\sqrt{0.004} \approx 0.063, \qquad u_* = 8 \times 0.063 \approx 0.51\,\mathrm{m\,s^{-1}}, \qquad \tau_0 = 1.2 \times 0.004 \times 8^2 = 0.31\,\mathrm{Pa}.$$

The friction velocity is 6 % of the wind speed. Since C_D near the ground lies typically between 0.001 and 0.02, $\sqrt{C_D}$ lies between 0.03 and 0.14, and $u_* \ll U$ in practically every case: the friction velocity is a small fraction of the wind it is associated with.

10.3.2 The neutral drag coefficient

The drag coefficient changes with the roughness of the surface, with the measurement height and with stability. Its neutral form follows from the logarithmic profile. Divide equation (10.4), without a displacement height, by u_*:

$$\frac{U(z)}{u_*} = \frac{1}{\kappa}\ln\frac{z}{z_0} \quad \Longrightarrow \quad \frac{u_*}{U(z)} = \frac{\kappa}{\ln(z/z_0)},$$

and square, using equation (10.8):

$$C_D = \left[\frac{\kappa}{\ln(z/z_0)}\right]^2. \tag{10.9}$$

With a displacement height, z is replaced by $z - d$. The neutral drag coefficient depends only on the ratio of the reference height to the roughness length.

At $z = 10\,\mathrm{m}$ over a smooth surface, $z_0 = 0.001\,\mathrm{m}$,

$$\ln\frac{10}{0.001} = \ln 10^4 \approx 9.21, \qquad C_D \approx \left(\frac{0.4}{9.21}\right)^2 = 0.0434^2 \approx 0.0019.$$

Over a rough surface, $z_0 = 0.5\,\mathrm{m}$,

$$\ln\frac{10}{0.5} = \ln 20 \approx 3.00, \qquad C_D \approx \left(\frac{0.4}{3.00}\right)^2 = 0.133^2 \approx 0.0178.$$

The rough surface has a drag coefficient $0.0178/0.0019 \approx 9.5$ times larger, almost ten times. For the same $U_{10} = 8\,\mathrm{m\,s^{-1}}$ the friction velocities are $8 \times 0.0434 = 0.35\,\mathrm{m\,s^{-1}}$ and $8 \times 0.134 = 1.07\,\mathrm{m\,s^{-1}}$, and the stresses 0.145 and 1.37 Pa. At $z_0 = 0.5\,\mathrm{m}$ a reference height of 10 m is only twenty roughness lengths above the ground; over such a surface the obstacles are several meters tall, a displacement height belongs in the formula, and the reference height should lie well above the obstacles, so the value illustrates the trend rather than a recommended design figure.

Figure 10.4 plots equation (10.9). The horizontal axis is the roughness length on a logarithmic scale from 10^{-4} to 0.5 m; the vertical axis is the drag coefficient multiplied by 1000. The solid curve is for a reference height of 10 m, the dashed curve for 100 m. The two blue points are the smooth and rough examples at 10 m; the red point is the rough surface with the reference height raised to 100 m. Both curves rise with roughness, the 10 m curve more steeply: as z_0 grows, $\ln(z/z_0)$ shrinks, and it shrinks faster in relative terms when z is small.

10.3.3 Surfaces from sea to rough land

The physical reading of equation (10.9) is that a rougher surface takes more momentum out of the same wind. Ocean, grassland, cropland, forest and dense city form a sequence of increasing roughness: larger and more closely spaced obstacles produce more form drag, the pressure difference between their windward and lee faces, and stronger eddies in their wakes. For a comparable mean wind the rougher surface carries the larger stress and the larger u_*.

Table 10.1 puts numbers on the sequence. Its columns give an illustrative surface, a typical roughness length (Chapter 11 treats roughness lengths in detail), the neutral drag coefficient at 10 m from equation (10.9), and the friction velocity and stress that go with $U_{10} = 8\,\mathrm{m\,s^{-1}}$ and $\rho = 1.2\,\mathrm{kg\,m^{-3}}$. Across the table the drag coefficient grows thirteenfold and the stress with it, while the wind at 10 m is held fixed. Over water the roughness length is not a fixed property of the surface: it grows with the wind as the waves grow, so the sea entry is one point of a wind-dependent relation. Forest and dense city are left out of the table because for them a reference height of 10 m lies inside or just above the canopy, where equation (10.9) does not apply without a displacement height and a higher reference height.

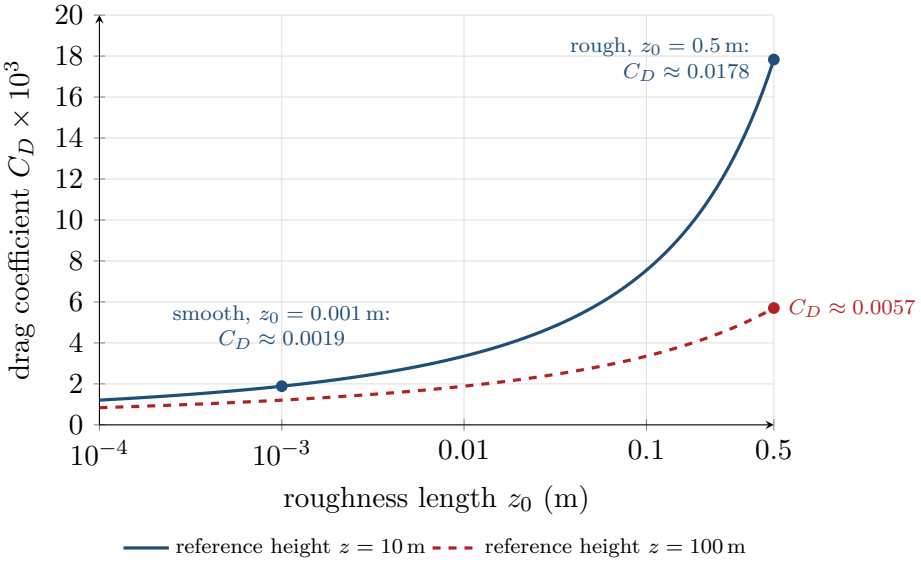


Figure 10.4: Neutral drag coefficient against roughness length, $C_D = [\kappa/\ln(z/z_0)]^2$ (equation (10.9)) with $\kappa = 0.4$ and no displacement height, for reference heights of 10 and 100 m.

Table 10.1: Neutral drag coefficient at 10 m, friction velocity and surface stress for $U_{10} = 8\,\mathrm{m\,s^{-1}}$ over surfaces of increasing roughness, from equations (10.8) and (10.9). Roughness lengths typical; values illustrative.

Surface	z_0 (m)	C_D at 10 m	u_* (m/s)	τ_0 (Pa)
Open sea, moderate wind	0.0002	0.0014	0.30	0.11
Very smooth land (mud flat, snow)	0.001	0.0019	0.35	0.14
Mown grass	0.01	0.0034	0.46	0.26
Farmland with low crops	0.05	0.0057	0.60	0.44
Rough land, scattered trees and buildings	0.5	0.0178	1.07	1.37

10.3.4 Dependence on reference height and stability

Equation (10.9) makes the dependence on reference height explicit. For one surface and one flow the friction velocity is the same at all heights within the constant-stress layer, but the wind speed that C_D is defined against is not. Two drag coefficients for the same flow at heights z_1 and z_2 are related by

$$\frac{C_D(z_2)}{C_D(z_1)} = \frac{U(z_1)^2}{U(z_2)^2} = \left[\frac{\ln(z_1/z_0)}{\ln(z_2/z_0)}\right]^2 . \tag{10.10}$$

Over farmland with $z_0 = 0.05\,\mathrm{m}$ the drag coefficient for 10 m is $(0.4/\ln 200)^2 = 0.0057$ and the one for 100 m is $(0.4/\ln 2000)^2 = (0.4/7.60)^2 = 0.0028$, half as large, because the wind at 100 m is $\ln 2000/\ln 200 = 1.43$ times the wind at 10 m and $1.43^2 \approx 2$. A drag coefficient quoted without its height is therefore incomplete, and one taken from a 10 m formula and applied to a model's lowest level at another height gives the wrong stress. Figure 10.4 shows the same point as the gap between its two curves.

Stability. Outside neutral conditions the profile carries the stability correction ψ_m of Section 10.4.4, and the same steps give

$$C_D = \left[\frac{\kappa}{\ln(z/z_0) - \psi_m}\right]^2 . \tag{10.11}$$

Unstable air ($\psi_m > 0$) raises the drag coefficient and stable air ($\psi_m < 0$) lowers it. A drag coefficient is thus a property of the surface, the reference height and the stability together, and a single fixed value for a site is a neutral, one-height approximation.

10.4 Measuring and inferring the friction velocity

The friction velocity is never read from a dial. It is computed from fast turbulence measurements, inferred from mean winds with a profile model, or taken from a model that computes it internally. This section describes each route, works examples, and compares what each needs and assumes.

10.4.1 Eddy covariance

The direct method uses a sonic anemometer, which measures the three velocity components ten to twenty times per second. Over an averaging period of typically 30 minutes the covariances $\overline{u'w'}$ and $\overline{v'w'}$ are computed as Chapter 9 describes, including the rotation of the coordinates into the mean wind and the quality checks. The kinematic stress has two horizontal components, $-\overline{u'w'}$ and $-\overline{v'w'}$, and its magnitude is $\sqrt{\overline{u'w'}^2 + \overline{v'w'}^2}$. The friction velocity is the square root of that magnitude:

$$u_* = \left[\,\overline{u'w'}^2 + \overline{v'w'}^2\,\right]^{1/4} . \tag{10.12}$$

When the stress is exactly aligned with the mean wind, $\overline{v'w'} = 0$ and equation (10.12) reduces to $u_* = \sqrt{-\overline{u'w'}}$. Including $\overline{v'w'}$ makes the result independent of the angle between the stress and the wind, which Section 10.6.2 discusses.

For an illustrative half-hour with $\overline{u'w'} = -0.12\,\mathrm{m^2\,s^{-2}}$ and $\overline{v'w'} = 0.03\,\mathrm{m^2\,s^{-2}}$,

$$\sqrt{0.12^2 + 0.03^2} = \sqrt{0.0144 + 0.0009} = \sqrt{0.0153} = 0.124\,\mathrm{m^2\,s^{-2}},$$

$$u_* = \sqrt{0.124\,\mathrm{m^2\,s^{-2}}} = 0.352\,\mathrm{m\,s^{-1}},$$

and $\tau_0 = 1.2 \times 0.124 = 0.148\,\mathrm{Pa}$. The along-wind component alone gives $\sqrt{0.12} = 0.346\,\mathrm{m\,s^{-1}}$, 1.5 % low. The method assumes that the instrument is inside the constant-stress layer, high enough above the roughness elements to see their combined effect, over reasonably flat and uniform ground, and that the averaging period captures the eddies that carry the flux.

10.4.2 A mean profile at two heights

Without a sonic anemometer, mean wind speeds at two heights within the surface layer give u_* under the neutral logarithmic profile. Subtracting equation (10.4) at z_1 from the same equation at z_2 eliminates the roughness length:

$$U_2 - U_1 = \frac{u_*}{\kappa}\left(\ln\frac{z_2}{z_0} - \ln\frac{z_1}{z_0}\right) = \frac{u_*}{\kappa}\ln\frac{z_2}{z_1},$$

so that

$$u_* = \frac{\kappa\,(U_2 - U_1)}{\ln(z_2/z_1)}, \qquad z_0 = z_1 \exp\!\left(-\frac{\kappa\,U_1}{u_*}\right), \tag{10.13}$$

where the second expression is equation (10.4) at z_1 solved for z_0. Two heights return both parameters of the profile.

For an illustrative mast with $U_1 = 6.0\,\mathrm{m\,s^{-1}}$ at $z_1 = 10\,\mathrm{m}$ and $U_2 = 7.6\,\mathrm{m\,s^{-1}}$ at $z_2 = 40\,\mathrm{m}$,

$$u_* = \frac{0.4 \times 1.6}{\ln 4} = \frac{0.64}{1.386} = 0.462\,\mathrm{m\,s^{-1}}, \qquad z_0 = 10\exp\!\left(-\frac{0.4 \times 6.0}{0.462}\right) = 10\,e^{-5.20} = 0.055\,\mathrm{m}.$$

The result is sensitive to the speed difference. If the upper anemometer reads $0.1\,\mathrm{m\,s^{-1}}$ high or low, $U_2 - U_1$ becomes 1.7 or $1.5\,\mathrm{m\,s^{-1}}$, the friction velocity becomes 0.491 or $0.433\,\mathrm{m\,s^{-1}}$ (about $\pm 6\,\%$), and the roughness length becomes 0.075 or 0.039 m, a range of almost a factor of two. Small errors in a difference of two similar numbers grow in u_*, and grow again, exponentially, in z_0.

Figure 10.5 shows the construction. The horizontal axis is the wind speed in m/s; the vertical axis is the height on a logarithmic scale, on which the logarithmic profile is a straight line. The two dots are the measurements. The solid line through them is the fitted profile; its slope, the change of U per unit change of $\ln z$, is u_*/κ, and its intercept with the axis $U = 0$ is z_0. The two dashed lines are the profiles obtained when the upper reading is changed by $\pm 0.1\,\mathrm{m\,s^{-1}}$. All three pass through the lower point; above it they spread only slightly, below it they fan out, and at $U = 0$ their intercepts lie at 0.039, 0.055 and 0.075 m.

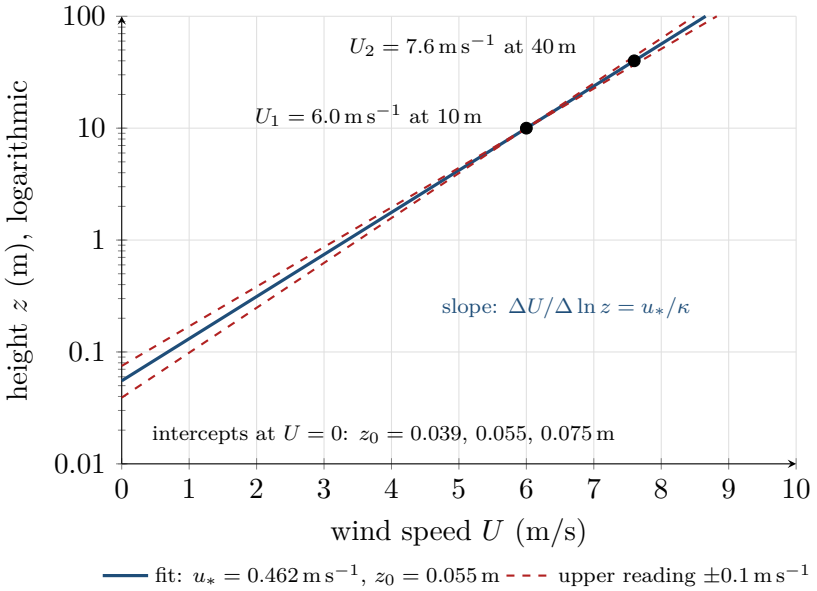


Figure 10.5: Friction velocity and roughness length from winds at two heights, equation (10.13), neutral profile $U = (u_*/\kappa)\ln(z/z_0)$ with $\kappa = 0.4$. On a logarithmic height axis the profile is a straight line. Dashed: the upper reading changed by $\pm 0.1\,\mathrm{m\,s^{-1}}$. Values illustrative.

10.4.3 One height and a known roughness length

With a wind at one height only, the friction velocity follows from equation (10.5) if the roughness length is known and the air is neutral: $u_* = \kappa U(z)/\ln(z/z_0)$. For $U_{10} = 8\,\mathrm{m\,s^{-1}}$ over farmland, $z_0 = 0.05\,\mathrm{m}$,

$$u_* = \frac{0.4 \times 8}{\ln 200} = \frac{3.2}{5.30} = 0.604\,\mathrm{m\,s^{-1}}.$$

The answer is as good as the roughness length. Since u_* depends on z_0 through a logarithm, a relative error in z_0 produces a much smaller relative error in u_*, but not a negligible one: with $z_0 = 0.1\,\mathrm{m}$ instead, $u_* = 3.2/\ln 100 = 0.695\,\mathrm{m\,s^{-1}}$ (+15 %), and with $z_0 = 0.025\,\mathrm{m}$, $u_* = 3.2/\ln 400 = 0.534\,\mathrm{m\,s^{-1}}$ (−12 %). A factor of two in the roughness length is a common uncertainty when z_0 is read from a land-cover map, and at this height it is worth +15 and −12 % in u_* and, squared, +32 and −22 % in the stress.

10.4.4 Stability correction

In stable or unstable air the logarithmic profile is corrected,

$$U(z) = \frac{u_*}{\kappa}\left[\ln\frac{z}{z_0} - \psi_m\right], \qquad u_* = \frac{\kappa\,U(z)}{\ln(z/z_0) - \psi_m}, \tag{10.14}$$

where ψ_m is the stability correction for momentum, dimensionless. It is zero in neutral air, positive in unstable air and negative in stable air, and it depends on the height and on a stability parameter that Chapter 14 defines through Monin–Obukhov similarity. With the stability unknown, the inference of u_* from one wind measurement is more uncertain than the neutral formula suggests.

To see how much, take the farmland example, $U_{10} = 8\,\mathrm{m\,s^{-1}}$ and $z_0 = 0.05\,\mathrm{m}$, with two illustrative corrections. In unstable air with $\psi_m = +0.6$, $u_* = 3.2/(5.30 - 0.6) = 3.2/4.70 = 0.681\,\mathrm{m\,s^{-1}}$; the neutral estimate of $0.604\,\mathrm{m\,s^{-1}}$ is 11 % low. In stable air with $\psi_m = -2.0$, $u_* = 3.2/(5.30 + 2.0) = 3.2/7.30 = 0.438\,\mathrm{m\,s^{-1}}$; the neutral estimate is 38 % high, and the stress it implies, $\propto u_*^2$, is $(0.604/0.438)^2 = 1.90$ times the true one. Ignoring stability errs most at night, in stable air, which is also when the near-surface wind is weakest and most variable.

10.4.5 Weather-model output and flux-tower datasets

A weather model computes u_* internally at every grid cell and time step. Its land-surface and boundary-layer schemes take the wind, temperature and humidity at the lowest model level, the roughness length assigned to the cell from its land cover, and the surface temperature, and solve a stability-corrected relation of the form of equation (10.14) for u_* and the heat fluxes together. The output u_* is a grid-cell value: it represents a cell several kilometers wide with one effective roughness, and it inherits every error of the assigned z_0, of the modeled stability and of the modeled wind. It is a model quantity, not a measurement, and comparing it with a tower u_* is a comparison of a grid-cell value with a point value.

Flux-tower datasets are the other common source. Networks of eddy-covariance towers, operated over forests, crops, grasslands and cities to measure the exchange of heat, water vapor and carbon dioxide, report u_* as a standard variable from equation (10.12). Their values are point measurements with the assumptions of Section 10.4.1, and they are often used in turn to screen the other fluxes: half-hours with very low u_* at night are flagged, because weak turbulence makes the covariances unreliable.

10.4.6 Comparison of the routes

Table 10.2 compares the five routes. Its columns give what each route needs as input, what it assumes, what it returns besides u_*, and its main source of error. Only eddy covariance

measures the stress itself; every other route infers it from mean winds through a profile relation, and inherits the assumptions of that relation.

Table 10.2: Routes to the friction velocity: what each needs and assumes.

Route	Needs	Assumes	Also returns	Main error
Eddy covariance, eq. (10.12)	sonic anemometer at 10–20 Hz, 30 min averages	constant-stress layer, flat uniform fetch, stationarity	stress direction, heat flux	weak or intermittent turbulence; tilt and averaging choices
Two heights, eq. (10.13)	two calibrated anemometers in the surface layer	neutral log profile, constant stress, both heights above the roughness elements	z_0	small speed differences; stability
One height and z_0, eq. (10.5)	one anemometer, a roughness length	neutral log profile, known z_0	–	z_0 from land cover; stability
One height, z_0, ψ_m, eq. (10.14)	as above, plus a heat-flux or temperature-gradient measurement	Monin–Obukhov similarity	stability	form of ψ_m; z_0
Weather model	model run	assigned z_0, modeled stability and wind	heat fluxes	grid-cell average; errors in z_0 and stability

The flux-tower dataset is not a separate row: it is the first route, carried out by someone else, with that route's assumptions applied to the tower's site. The table also shows which routes can test each other. A tower with a sonic anemometer and two cup anemometers yields u_* by the first two routes at once; agreement supports the neutral profile assumption, and a systematic difference at night points to stability.

10.5 Scaling, similarity and limits

The friction velocity is a scale for the turbulence as well as for the stress. This section shows how turbulence statistics normalized by u_* become comparable from site to site, explains the idea of similarity behind that, and marks two limits of the scaling: nearly decoupled stable flow, where u_* almost vanishes under a strong wind, and convective flow, where a different velocity scale takes over.

10.5.1 Normalized turbulence statistics

Since $u_*^2 = -\overline{u'w'}$ at the surface, the friction velocity is the size of the velocity covariance that carries the stress, and the standard deviations of the velocity components scale with it. In the neutral surface layer over flat, uniform terrain the ratios

$$\frac{\sigma_u}{u_*} \approx 2.4, \qquad \frac{\sigma_v}{u_*} \approx 1.9, \qquad \frac{\sigma_w}{u_*} \approx 1.25 \tag{10.15}$$

are typical values, with a spread of roughly ten percent among experiments. The vertical ratio is the most reliable, because vertical motion near the ground is limited by the ground itself; the horizontal ratios also depend on the boundary-layer depth and on slow meandering of the wind, and vary more from site to site. With $u_* = 0.4\,\mathrm{m\,s^{-1}}$ they give $\sigma_u \approx 0.96\,\mathrm{m\,s^{-1}}$, $\sigma_v \approx 0.76\,\mathrm{m\,s^{-1}}$ and $\sigma_w \approx 0.50\,\mathrm{m\,s^{-1}}$.

Combined with the logarithmic profile, the first ratio gives the neutral turbulence intensity at height z,

$$\mathrm{TI} = \frac{\sigma_u}{U} = \frac{2.4\,u_*}{(u_*/\kappa)\ln(z/z_0)} = \frac{2.4\,\kappa}{\ln(z/z_0)},$$

which for $z = 10\,\mathrm{m}$ and $z_0 = 0.05\,\mathrm{m}$ is $0.96/5.30 = 0.18$. The friction velocity has cancelled: in neutral air the turbulence intensity depends only on height and roughness, not on the wind speed. This is why turbulence intensity is a useful site descriptor for wind energy, and why a turbulence intensity that changes strongly with wind speed at one site is a sign of changing stability or of upwind features.

10.5.2 Similarity

Sites with different wind speeds and roughness have different turbulence in absolute terms, and the same turbulence once each is normalized by its own u_*. Figure 10.6 shows this for three illustrative neutral sites, open sea ($z_0 = 0.0002\,\mathrm{m}$), farmland ($0.05\,\mathrm{m}$) and rough land ($0.5\,\mathrm{m}$). The left panel plots σ_u against U_{10}: three straight lines of different slopes, $\sigma_u = 2.4\,\kappa\,U_{10}/\ln(10/z_0)$, with markers at $U_{10} = 4$, 8 and $12\,\mathrm{m\,s^{-1}}$. The right panel plots the same nine points against u_* instead: all fall on the single line $\sigma_u = 2.4\,u_*$. In the left panel the sites look like three different flows; in the right they are one flow at different strengths.

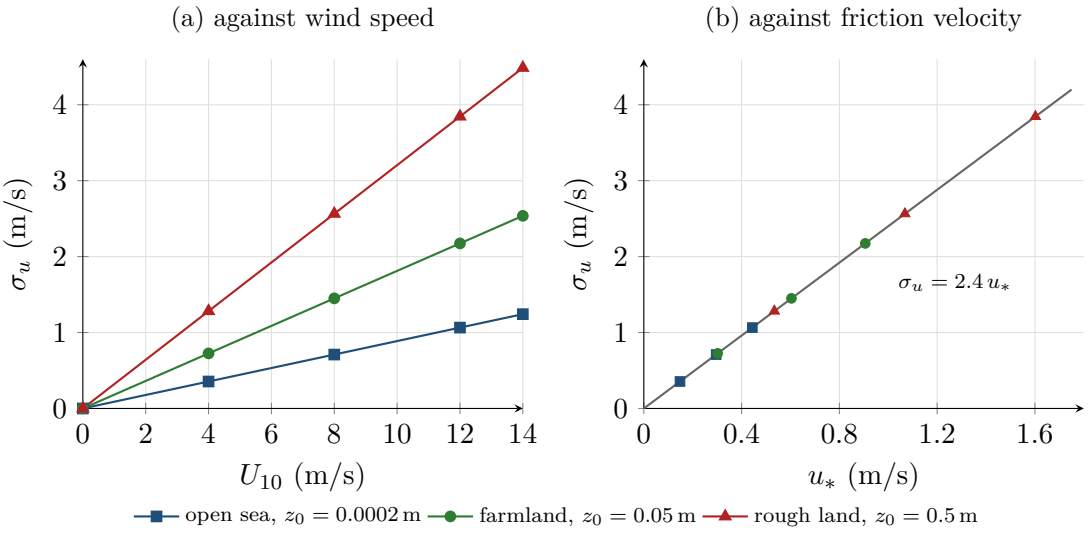


Figure 10.6: Similarity scaling in neutral flow, illustrative. (a) $\sigma_u = 2.4\,\kappa\,U_{10}/\ln(10/z_0)$ for three roughness lengths, $\kappa = 0.4$; markers at $U_{10} = 4$, 8, $12\,\mathrm{m\,s^{-1}}$. (b) The same points against $u_* = \kappa\,U_{10}/\ln(10/z_0)$ collapse onto $\sigma_u = 2.4\,u_*$ (equation (10.15), typical neutral value).

The collapse is the idea of similarity theory: find the right scales, and flows that differ in their dimensional quantities behave alike in dimensionless form. In the neutral surface layer the right scales are u_* for velocity and z for length, and every dimensionless statistic, σ_u/u_*, σ_w/u_*, $(\kappa z/u_*)\,\partial U/\partial z$, is a constant. Real data collapse less cleanly than Figure 10.6, with scatter from sampling, terrain and stability, and the collapse is the test of whether the scaling holds at a site. Monin–Obukhov similarity, the subject of Chapter 14, extends the idea to stable and unstable air by adding a length that measures buoyancy, so that each dimensionless statistic becomes a function of one stability parameter instead of a constant.

10.5.3 Decoupling and a vanishing friction velocity

A friction velocity close to zero does not mean that the wind is close to zero. On a clear night with weak synoptic forcing, the ground cools by radiation, the air above it becomes strongly stable, and turbulence near the ground can nearly cease. The layer above then loses its contact with the surface: it is decoupled, and it can accelerate, because the surface drag that slowed it

during the day is gone. In such an extremely stable state a wind of $10\,\mathrm{m\,s^{-1}}$ at 100 to 200 m can sit above a near-calm surface layer with u_* of a few centimeters per second.

With $u_* = 0.05\,\mathrm{m\,s^{-1}}$, the surface stress is $1.2 \times 0.05^2 = 0.003\,\mathrm{Pa}$, one sixty-fourth of the stress at $u_* = 0.4\,\mathrm{m\,s^{-1}}$. A strong wind aloft therefore does not imply strong coupling to the surface, and a neutral profile scaled to the strong wind aloft implies a large u_* and overstates both the wind and the turbulence near the ground. For near-surface engineering wind this is the regime of greatest uncertainty: a conductor at 15 m may sit in nearly still air beneath a jet of strong wind, and its convective cooling depends on which side of the transition it lies. Turbulence in this state is also weak and intermittent, which makes the eddy-covariance u_* itself uncertain (Section 10.4.5).

10.5.4 The convective velocity scale

On a sunny afternoon the opposite limit applies. Thermal turbulence, driven by buoyant plumes rising from the heated ground, can be vigorous with only a modest mean wind, and then u_*, which characterizes the momentum flux, does not measure the turbulence. For strongly convective conditions the velocity scale is built from the buoyancy supplied at the surface and the depth over which it acts:

$$w_* = \left[\frac{g}{\theta_0} \, (\overline{w'\theta'})_0 \, z_i \right]^{1/3}, \tag{10.16}$$

where θ_0 is a reference potential temperature of the layer in kelvin, $(\overline{w'\theta'})_0$ the kinematic heat flux at the surface in $\mathrm{K\,m\,s^{-1}}$, positive upward, and z_i the boundary-layer depth. Strictly the virtual potential temperature and its flux enter; over land in daytime the difference is small. The units are $(\mathrm{m\,s^{-2}\,K^{-1}})(\mathrm{K\,m\,s^{-1}})(\mathrm{m}) = \mathrm{m^3\,s^{-3}}$, and the cube root is in m/s. The scale is defined only when the surface heat flux is upward.

For an illustrative afternoon with $\theta_0 = 300\,\mathrm{K}$, $(\overline{w'\theta'})_0 = 0.2\,\mathrm{K\,m\,s^{-1}}$ (a sensible heat flux $H = \rho\, c_p\, (\overline{w'\theta'})_0 = 1.2 \times 1004 \times 0.2 \approx 240\,\mathrm{W\,m^{-2}}$) and $z_i = 1500\,\mathrm{m}$,

$$w_* = \left[\frac{9.81}{300} \times 0.2 \times 1500 \right]^{1/3} = [9.81]^{1/3} \approx 2.14\,\mathrm{m\,s^{-1}}.$$

The convective velocity scale sets the size of the vertical velocity fluctuations in the middle of the convective boundary layer, where σ_w reaches typically about $0.6\,w_* \approx 1.3\,\mathrm{m\,s^{-1}}$, and the speed of the thermals. Chapter 16 treats the convective boundary layer and this scaling in depth.

10.5.5 Mechanical and convective scales compared

The two velocity scales describe two sources of turbulence. Table 10.3 sets them side by side: their definition, the source of turbulence each measures, where each applies, and typical values. The friction velocity is the scale of mechanically driven turbulence, tied to the surface stress and to the shear; the convective velocity scale is the scale of buoyancy-driven turbulence in the convective boundary layer, tied to the surface heat flux and the layer depth.

The ratio of the two says which source dominates. In the example of Section 10.5.4 with a light wind and $u_* = 0.3\,\mathrm{m\,s^{-1}}$, $w_*/u_* = 2.14/0.3 \approx 7$: buoyancy dominates the turbulence of the layer, and the near-neutral ratios of equation (10.15) underestimate the vertical mixing everywhere above the lowest few tens of meters. With a strong wind, $u_* = 0.8\,\mathrm{m\,s^{-1}}$, and the same heat flux the ratio falls to about 2.7, and mechanical and convective turbulence are comparable. Both scales are needed to describe a sunny, windy day; neither alone is.

Table 10.3: The friction velocity and the convective velocity scale. Typical values illustrative.

	Friction velocity u_*	Convective velocity scale w_*
Definition	$\sqrt{\tau_0/\rho} = [\overline{u'w'}^2 + \overline{v'w'}^2]^{1/4}$	$[(g/\theta_0)(\overline{w'\theta'})_0\, z_i]^{1/3}$
Source of turbulence	shear of the mean wind against the surface (mechanical)	buoyancy of air heated at the surface (convective)
Applies where	surface layer; any stability, best in near-neutral air	convective boundary layer, heat flux upward
Scales	stress, shear, σ_u, σ_v, σ_w near the ground	σ_w and thermal speeds through the layer
Typical values	0.1 to 1 m s^{-1}; near 0 under decoupling	1 to 3 m s^{-1} on sunny afternoons; undefined at night

10.6 The stress vector and calibration

The surface stress has a direction as well as a magnitude, and the friction velocity summarizes only the magnitude. This section treats the stress as a vector, its angle to the wind in both hemispheres, and then a consequence of everything above for model evaluation: matching the 10 m wind does not fix the friction velocity, and a model can reach the right wind for the wrong reason.

10.6.1 The stress vector

In horizontal coordinates x and y, whether along-wind and cross-wind or east and north, the surface stress is the vector

$$\boldsymbol{\tau}_0 = (\tau_x, \tau_y) = (-\rho\,\overline{u'w'},\ -\rho\,\overline{v'w'}), \qquad |\boldsymbol{\tau}_0| = \rho\, u_*^2, \tag{10.17}$$

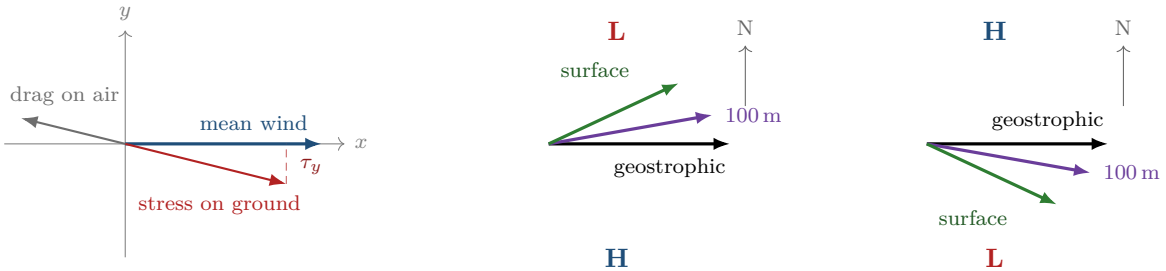
where u and v are now the velocity components along x and y. It is the force per unit area of the air on the ground, and its magnitude reproduces equation (10.12). The direction is $\arctan(\tau_y/\tau_x)$, taken in the quadrant of the components. In the example of Section 10.4.1, in along-wind coordinates with y to the left of the wind, $\tau_x = 1.2 \times 0.12 = 0.144$ Pa and $\tau_y = -1.2 \times 0.03 = -0.036$ Pa: the stress points downwind and $\arctan(0.036/0.144) = 14°$ to the right of the mean wind.

The direction matters whenever the wind direction changes with height. A single value of u_* then hides a rotation that a profile model, a pollutant-transport model or a comparison of wind directions between heights needs. In east-north coordinates the vector form also avoids an error: computing $\sqrt{-\overline{u'w'}}$ from the eastward component alone is correct only if the mean wind blows exactly from the west.

10.6.2 Direction of the stress relative to the wind

The stress the air exerts on the ground points approximately along the near-surface wind; the equal and opposite drag the ground exerts on the air approximately opposes it. The alignment is approximate, not exact, for three reasons. The wind turns with height through the boundary layer, and turbulent eddies connect levels with different wind directions, so the momentum delivered to the surface carries some of the direction of the wind above. Horizontal temperature gradients make the geostrophic wind itself change with height (strongly baroclinic conditions), which adds to the turning. And terrain deflects the flow near the ground differently from the flow aloft. Over flat, uniform ground in near-neutral air the angle between the surface stress and the surface wind is small, a few degrees; in strongly baroclinic conditions or complex terrain angles of ten to twenty degrees occur.

Figure 10.7 shows the vectors. Panel (a) is drawn in along-wind coordinates, viewed from above: the mean wind points along x; the stress on the ground is the example of the previous subsection, at 14° to the right of the wind, with its two components; the drag on the air is the opposite vector. Panels (b) and (c) are plan views with north at the top, for a geostrophic wind from the west, in the Northern and the Southern Hemisphere. Each shows the geostrophic wind, the wind at 100 m and the surface wind, with illustrative angles of 10° and 25° between them, and the side of low pressure. In the Northern Hemisphere the surface wind is turned to the left of the geostrophic wind, toward the low to the north, and the wind turns clockwise (veers) with height. In the Southern Hemisphere it is turned to the right, toward the low to the south, and the wind turns counterclockwise (backs) with height. In both, the surface stress lies close to the surface wind.



(a) along-wind frame angle 14°, illustrative

(b) Northern Hemisphere veers with height

(c) Southern Hemisphere backs with height

Figure 10.7: The stress vector and the turning of the wind, viewed from above. (a) Stress on the ground from $\overline{u'w'} = -0.12$ and $\overline{v'w'} = 0.03\,\mathrm{m^2\,s^{-2}}$, 14° to the right of the mean wind; the drag on the air is opposite. (b), (c) Geostrophic wind from the west with low pressure to the north (Northern Hemisphere) and to the south (Southern Hemisphere); the surface wind is turned toward the low by an illustrative 25° and the 100 m wind by 10°. The surface stress lies close to the surface wind.

10.6.3 Two models with the same 10 m wind

Consider two weather models that both give $U_{10} = 8\,\mathrm{m\,s^{-1}}$ at a site. Model A has $u_* = 0.3\,\mathrm{m\,s^{-1}}$ and model B has $u_* = 0.7\,\mathrm{m\,s^{-1}}$. Their surface momentum fluxes are very different: $\tau_0 = 1.2 \times 0.3^2 = 0.108\,\mathrm{Pa}$ for A and $1.2 \times 0.7^2 = 0.588\,\mathrm{Pa}$ for B, a factor of 5.4. The difference is concrete when each pair is translated, through equation (10.4) at 10 m under neutral stratification, into the roughness length it implies, $z_0 = z\exp(-\kappa U_{10}/u_*)$:

$$\text{A:}\quad z_0 = 10\exp\left(-\frac{0.4\times 8}{0.3}\right) = 10\,e^{-10.67} = 2.3\times 10^{-4}\,\mathrm{m},$$

$$\text{B:}\quad z_0 = 10\exp\left(-\frac{0.4\times 8}{0.7}\right) = 10\,e^{-4.57} = 0.10\,\mathrm{m}.$$

Model A behaves as if the site were open sea, model B as if it were farmland with tall crops: four hundred times different in roughness, with the same 10 m wind. Their drag coefficients at 10 m are $(0.3/8)^2 = 0.0014$ and $(0.7/8)^2 = 0.0077$.

The two models differ in everything that depends on u_*. Their turbulence differs: $\sigma_u \approx 2.4\,u_*$ gives 0.72 against $1.68\,\mathrm{m\,s^{-1}}$ near the ground. Their profiles above 10 m differ: extending the neutral logarithmic profile, the wind at 100 m is $(0.3/0.4)\ln(100/2.3\times 10^{-4}) = 9.7\,\mathrm{m\,s^{-1}}$ for A and $(0.7/0.4)\ln(100/0.10) = 12.0\,\mathrm{m\,s^{-1}}$ for B, a difference that matters at a turbine hub. Their heat fluxes differ, because turbulent transfer of heat scales with u_* as momentum does. And their boundary-layer depths differ: in neutral conditions the depth scales with $u_*/|f|$, so B's

layer is about $0.7/0.3 \approx 2.3$ times deeper than A's at the same latitude, in either hemisphere. Matching the 10 m wind does not show that the surface-layer physics is right.

10.6.4 Non-uniqueness in calibration

The same ambiguity affects calibration. A model calibrated only on U_{10} can compensate a wrong roughness length with a wrong friction velocity and still fit. Under the neutral profile every pair (z_0, u_*) on the curve

$$u_* = \frac{\kappa U_{10}}{\ln(10\,\mathrm{m}/z_0)} \tag{10.18}$$

reproduces the same 10 m wind exactly. The 10 m wind identifies one combination of the two parameters, not each of them; the parameters are non-unique. In a full model the compensating parameter need not be u_* itself: a wrong roughness can be offset by a wrong mixing scheme, a wrong stability or a wrong large-scale forcing, all of which change the computed u_*.

A wind at a second height separates them, because it constrains a different combination. Suppose the truth is $z_0 = 0.05\,\mathrm{m}$ and $u_* = 0.604\,\mathrm{m\,s^{-1}}$, so that $U_{10} = 8.0\,\mathrm{m\,s^{-1}}$ and $U(40\,\mathrm{m}) = (0.604/0.4)\ln 800 = 10.09\,\mathrm{m\,s^{-1}}$. Figure 10.8 plots the plane of the two parameters: the horizontal axis is the roughness length on a logarithmic scale, the vertical axis the friction velocity. The solid curve is equation (10.18) for $U_{10} = 8\,\mathrm{m\,s^{-1}}$; models A and B of Section 10.6.3 are marked on it. The dashed curve is the set of pairs that reproduce $U(40\,\mathrm{m}) = 10.09\,\mathrm{m\,s^{-1}}$, and the shaded band around it the set that reproduces it within $\pm 0.2\,\mathrm{m\,s^{-1}}$. The two curves cross at one point, the true pair. With an exact upper wind, the crossing identifies both parameters. With the $\pm 0.2\,\mathrm{m\,s^{-1}}$ band, the solid curve stays inside the band for z_0 from 0.029 to 0.079 m and u_* from 0.55 to $0.66\,\mathrm{m\,s^{-1}}$: bounded, though not sharply. The curves meet at a shallow angle, which is the geometric form of the sensitivity found in Section 10.4.2, and a third height or a direct u_* would narrow the range further.

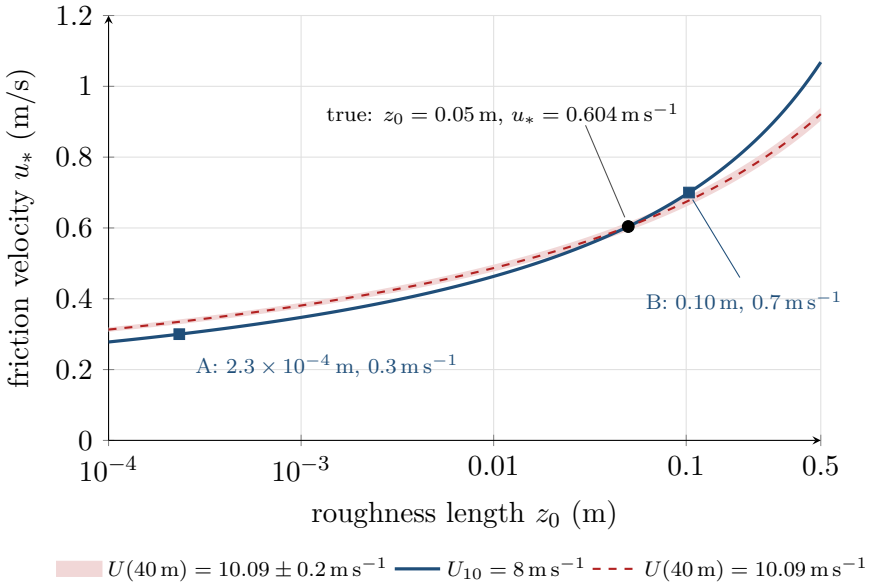


Figure 10.8: Non-uniqueness in calibration under the neutral profile $U(z) = (u_*/\kappa)\ln(z/z_0)$, $\kappa = 0.4$. Solid: pairs (z_0, u_*) giving $U_{10} = 8\,\mathrm{m\,s^{-1}}$ (equation (10.18)); dashed and shaded: pairs giving $U(40\,\mathrm{m}) = 10.09\,\mathrm{m\,s^{-1}}$ exactly and within $\pm 0.2\,\mathrm{m\,s^{-1}}$. Values illustrative.

10.6.5 Data that constrain the mechanism

The remedy is to validate a model against data that constrain the mechanism and not only the output. In order of how directly they bear on the surface momentum exchange:

- **Wind at several heights.** A mast or a remote-sensing profiler with three or more levels in the surface layer fixes the shear and with it u_* and z_0, as Figure 10.8 shows for two levels.
- **Turbulence measurements.** A sonic anemometer gives u_* directly through equation (10.12), and the standard deviations σ_u, σ_v, σ_w test the scaling of equation (10.15).
- **Surface fluxes.** The same instrument gives the heat flux, which tests the stability the model assumed and the convective scale of equation (10.16).
- **Stability information.** A temperature difference between two heights, or the heat flux with u_*, places each period in the stable, neutral or unstable regime, so that the comparison of profiles is made with the right ψ_m.

Each of these cuts across the curve of equation (10.18) in a different direction. A model that matches all of them has the right wind for the right reason; a model that matches only U_{10} has been shown to match U_{10}.

> **Principle 10.2.** *A wind at one height identifies one combination of friction velocity and roughness length, not each of them. Validation that is to support the surface-layer physics needs a second, independent constraint: a second height, a direct turbulence measurement, or a surface flux.*

10.7 What to retain

Definition 10.1 (Friction velocity)**.** The friction velocity $u_* = \sqrt{\tau_0/\rho}$ measures how strongly the surface and the atmosphere exchange horizontal momentum: turbulent covariance gives the surface stress, the stress gives u_*, and u_* sets the wind shear and the turbulence near the ground, which makes it a fundamental scaling variable of near-surface wind and not a wind speed.

Table 10.4 lists the terms of the chapter, their meaning, their units and the subsection that defines each.

10.8 Exercises

Exercise 10.1. A sonic anemometer at 8 m over grassland gives, for one half-hour in along-wind coordinates, $\overline{u'w'} = -0.09\,\mathrm{m^2\,s^{-2}}$ and $\overline{v'w'} = -0.02\,\mathrm{m^2\,s^{-2}}$, with $\rho = 1.15\,\mathrm{kg\,m^{-3}}$. (a) Compute u_* from equation (10.12), the stress magnitude, and the u_* obtained from $\overline{u'w'}$ alone. (b) Compute the angle between the stress on the ground and the mean wind, and say on which side of the wind it lies. (c) The mean wind at 10 m is $6.5\,\mathrm{m\,s^{-1}}$. Compute the drag coefficient. (d) At noon on the same day the kinematic heat flux is $0.15\,\mathrm{K\,m\,s^{-1}}$, $\theta_0 = 300\,\mathrm{K}$ and $z_i = 1200\,\mathrm{m}$. Compute w_* and the ratio w_*/u_*, and say which source of turbulence dominates.

Exercise 10.2. Cup anemometers at 20 and 60 m on a mast over farmland read 7.0 and $8.2\,\mathrm{m\,s^{-1}}$ in neutral conditions. (a) Compute u_* and z_0 with equation (10.13). (b) Predict the wind at 100 m and the drag coefficient for 20 m. (c) The upper anemometer is found to read $0.1\,\mathrm{m\,s^{-1}}$ low. Recompute u_* and z_0 and state the relative change of each. (d) Which of the two parameters is the more sensitive to anemometer error, and why?

Table 10.4: The terms of the chapter and where each is defined.

Term	Meaning	Units	Defined in
Friction velocity u_*	$\sqrt{\tau_0/\rho} = [\overline{u'w'}^2 + \overline{v'w'}^2]^{1/4}$: the surface stress in velocity units; scale of mechanical turbulence and of the shear	m/s	10.1.1, 10.4.1
Surface stress τ_0	horizontal force per unit area of the air on the ground, $-\rho\,\overline{u'w'}$ at the surface, $= \rho\,u_*^2$	Pa	10.1.1, 10.1.3
Drag coefficient C_D	$\tau_0/(\rho U^2)$ at a stated height; neutral form $[\kappa/\ln(z/z_0)]^2$	–	10.3.1, 10.3.2
Stress vector $\boldsymbol{\tau}_0$	$(-\rho\,\overline{u'w'}, -\rho\,\overline{v'w'})$: magnitude and direction of the surface stress	Pa	10.6.1
Velocity scale	a velocity built from the governing quantities that makes velocity statistics comparable across flows	m/s	10.1.1, 10.5.2
Constant-stress layer	lowest part of the boundary layer, about its lowest tenth, where τ is within about 10 % of τ_0	–	10.2.4
Mechanical turbulence	turbulence produced by wind shear; scaled by u_*	–	10.5.1, 10.5.5
Convective velocity scale w_*	$[(g/\theta_0)(\overline{w'\theta'})_0\,z_i]^{1/3}$: scale of buoyancy-driven turbulence in the convective boundary layer	m/s	10.5.4
Similarity	collapse of dimensionless statistics onto common relations once normalized by the right scales	–	10.5.2
Non-uniqueness	different parameter pairs (z_0, u_*) reproducing the same wind at one height	–	10.6.4

Exercise 10.3. A station at 30°S over flat farmland records, in east-north-up coordinates, a mean wind from the west ($u = 6\,\mathrm{m\,s^{-1}}$, $v = 0$) and the covariances $\overline{u'w'} = -0.10$ and $\overline{v'w'} = 0.02\,\mathrm{m^2\,s^{-2}}$, with $\rho = 1.2\,\mathrm{kg\,m^{-3}}$. (a) Compute the components and magnitude of the stress vector on the ground and u_*. (b) In which compass direction does the stress on the ground point, and by how many degrees is it turned from the mean wind, to the left or to the right? (c) Compute the Coriolis parameter. The surface wind is turned by 20° from the geostrophic wind toward low pressure. Is the low to the north or to the south, from which direction does the geostrophic wind blow, and does the wind veer or back with height? (d) Give the answers to (c) for the same surface wind at 30°N.

Exercise 10.4. Two weather models both give $U_{10} = 6\,\mathrm{m\,s^{-1}}$ at a site. Model A has $u_* = 0.25\,\mathrm{m\,s^{-1}}$ and model B $u_* = 0.5\,\mathrm{m\,s^{-1}}$. (a) Under the neutral profile, compute the roughness length each implies, and its drag coefficient at 10 m. (b) Compute the wind each implies at 80 m and the standard deviation σ_u near the ground from equation (10.15). (c) A sonic anemometer at the site measures $u_* = 0.46\,\mathrm{m\,s^{-1}}$ in neutral conditions with the same 10 m wind. Which model is closer, and which roughness length does the measurement imply? (d) At night the u_* of model B is twice the measured one while its 10 m wind is correct. Name two model errors that could produce this, and one measurement that would distinguish them.

Chapter 11

Aerodynamic Roughness

11.1 The roughness length as an aerodynamic property

Chapter 7 derived the neutral logarithmic wind profile and found that the theory fixes its slope, through the friction velocity u_*, but not its offset, which the surface supplies through a length z_0. Chapter 10 showed that the same length sets the drag coefficient and with it the surface stress for a given wind. Every wind model that uses a surface-layer relation, from an extrapolation between two anemometer heights to the diagnosis of the 10 m wind in a weather model, therefore needs a value of z_0, and most of them take it from a table of land-cover types. The question of this chapter is

what does the aerodynamic roughness length represent physically, what does it depend on, and how is it estimated and used?

The chapter first states what the roughness length is, by its definition in the profile, and what it is not, by comparison with the height of the obstacles that cause it. It then shows how roughness enters the profile and the drag, adds the displacement height and the layers above a tall canopy, and describes how the roughness of one site changes with wind direction, with the distance to a change of surface, with the waves on water and with the seasons. It separates roughness from terrain relief, and it ends with the ways the roughness length is estimated, why one height cannot determine it, how an error in it becomes a forecast bias, and how a roughness assigned to a weather-model grid cell relates to the roughness around one instrument.

Jargon: aerodynamic roughness length, obstacle height, form drag, wake, aerodynamic and geometric roughness

The *aerodynamic roughness length* z_0 (m) is the length in the neutral logarithmic profile $U(z) = (u_*/\kappa)\ln[(z-d)/z_0]$: the height above the zero plane at which the profile, extrapolated downward, reaches zero wind. It is obtained by fitting the profile to measured winds or by estimating it from the surface, and weather models assign it to each grid cell from land-cover data. The *obstacle height* h_c (m), also canopy height, is the mean height of the elements that make up the surface: grass, crops, trees, buildings. It is measured directly, by survey, by airborne laser scanning or from building databases. *Form drag*, or pressure drag, is the force a flow exerts on a body through the pressure difference between its windward and lee faces; it dominates the drag of grass blades, trees and buildings, whereas skin friction, the viscous drag along a surface, dominates only over very smooth surfaces. A *wake* is the region of slowed, turbulent flow downwind of an obstacle. *Aerodynamic roughness* is the drag a surface exerts on the flow, expressed by z_0; *geometric roughness* is the size of the surface elements, expressed by heights and spacings. The two are related but not the same.

Key idea

The roughness length is not the height of the obstacles: it is an effective parameter that describes how strongly a surface removes momentum from the flow above it, and it depends on the height, density, shape, arrangement and flexibility of the obstacles, on the wind direction, on the upwind fetch, on the season and, over water, on the wind itself.

11.1.1 The roughness length as an extrapolated zero

In the neutral surface layer over a flat, uniform surface the wind profile is

$$U(z) = \frac{u_*}{\kappa} \ln \frac{z-d}{z_0}, \tag{11.1}$$

with $\kappa \approx 0.4$ the von Kármán constant and d the displacement height of Section 11.3.1, zero over short vegetation and water. Chapter 7 obtained equation (11.1) by integrating the shear $\partial U/\partial z = u_*/[\kappa(z-d)]$; the roughness length entered as the constant of integration, the length that makes the argument of the logarithm dimensionless. Setting $z - d = z_0$ gives $\ln 1 = 0$ and $U = 0$: the roughness length is the height above the zero plane at which the logarithmic profile, extrapolated downward from the heights where it holds, reaches zero wind.

The definition makes z_0 an extrapolated parameter, not a physical height. Near and among the roughness elements the logarithmic profile does not hold, and the real wind at the height z_0 is in general not zero; among grass blades or inside a forest it is weak but finite. What z_0 encodes is the offset of the profile measured higher up. Solving equation (11.1) for z_0 makes that explicit:

$$z_0 = (z-d)\, \exp\!\left(-\frac{\kappa\, U(z)}{u_*}\right) = (z-d)\, \exp\!\left(-\frac{\kappa}{\sqrt{C_D}}\right), \tag{11.2}$$

where the second form uses the drag coefficient $C_D = u_*^2/U^2$ at the height z (Chapter 10). At a given height, a surface that carries a large stress for a given wind, a small ratio U/u_* and a large C_D, has a large z_0; a surface that lets the wind blow with little stress has a small one. The roughness length is thus a measure of drag expressed as a length. With $C_D = 0.0034$ at 10 m, $\sqrt{C_D} = 0.058$ and $z_0 = 10\,\mathrm{m} \times e^{-0.4/0.058} = 10\,\mathrm{m} \times e^{-6.91} \approx 0.01\,\mathrm{m}$, the value of mown grass.

11.1.2 Roughness length and obstacle height

The roughness length is much smaller than the height of the obstacles that produce it. Grass $h_c = 0.1\,\mathrm{m}$ tall typically has $z_0 \approx 0.01\,\mathrm{m}$, a ratio $z_0/h_c = 0.1$. A forest canopy $h_c = 20\,\mathrm{m}$ tall typically has $z_0 \approx 1\,\mathrm{m}$, a ratio of 0.05. In general $z_0 \ll h_c$, and ratios between about 0.03 and 0.15 cover most vegetation. The ratio is not a constant, because the height is only one of the properties that set the drag.

The obstacle height still influences z_0: for surfaces of the same kind, taller elements produce more drag and a larger roughness length. But z_0 is not a property of any single element. It summarizes the aggregate drag of many elements, averaged over an area large enough to contain many of them, as felt by the flow at heights well above them. A single tree in a field does not have a roughness length; a forest does, and a field with scattered trees does, and the two values differ because the number and arrangement of the trees differ.

11.1.3 The sources of roughness

The elements of a surface (grass blades, crops, shrubs, trees, buildings, small irregularities of the ground) remove momentum from the air flowing over and between them. Each element is a bluff body in the flow. Air piles up against its windward face and separates at its edges, leaving a region of low pressure and slow, turbulent air behind it, the wake. The pressure difference

between the windward and the lee face is the form drag. Summed over all elements in a unit area of ground, the form drag is the momentum the surface removes from the flow per unit time and area: it is the surface stress τ_0, and it is delivered to the elements by the turbulent momentum flux of Chapter 9.

The wakes are also sources of turbulence. Each one generates eddies of about the size of the element, which mix the air near the surface and add to the shear-produced turbulence above it. The chain is: surface elements, pressure drag and wakes, turbulence, momentum loss of the mean flow. The more effective the drag of the elements is, the larger the stress for a given wind aloft and, by equation (11.2), the larger z_0.

11.1.4 Aerodynamic against geometric roughness

Two surfaces with obstacles of the same height can have very different roughness lengths. Figure 11.1 draws two examples in side view and one curve. Panel (a) shows thin vertical poles of height h_c spaced widely; panel (b) shows block-like obstacles of the same height, wider and more closely spaced. In both, the wind blows from the left, and the dashed outlines mark wakes. Panel (c) has on its horizontal axis the *frontal area index* $\lambda_f = A_f/A_T$, the total area of the obstacle faces that face the wind (A_f) divided by the ground area they stand on (A_T), dimensionless; on its vertical axis is the ratio z_0/h_c. The solid curve is an illustrative form of the dependence; the dashed line is the rule $z_0/h_c = 0.5\,\lambda_f$ of Section 11.6.

The poles of panel (a) present little face to the wind: their wakes are narrow, most of the air passes between them untouched, and the aggregate drag is small. The blocks of panel (b) present a large face, their wakes are wide, and eddies form in the spaces between them. With the same height, the blocks have a roughness length about eight times larger in panel (c), $0.091\,h_c$ against $0.010\,h_c$ on the illustrative curve. Panel (c) also shows a less obvious result. The roughness length does not grow without limit as the elements crowd together. At small λ_f (isolated roughness) each element adds its own wake, and z_0 grows in proportion to λ_f. At intermediate values the wakes overlap (wake interference) and each added element adds less. At large values the elements are so close that the flow skims over their tops and the air between them is trapped (skimming flow); the surface then behaves more like a raised, smoother floor, z_0 falls, and the displacement height of Section 11.3.1 rises. The maximum of z_0/h_c, about 0.1, lies at λ_f between about 0.2 and 0.4 in wind-tunnel and field data; the exact form of the curve differs among studies, which is why the one in the figure is labeled illustrative.

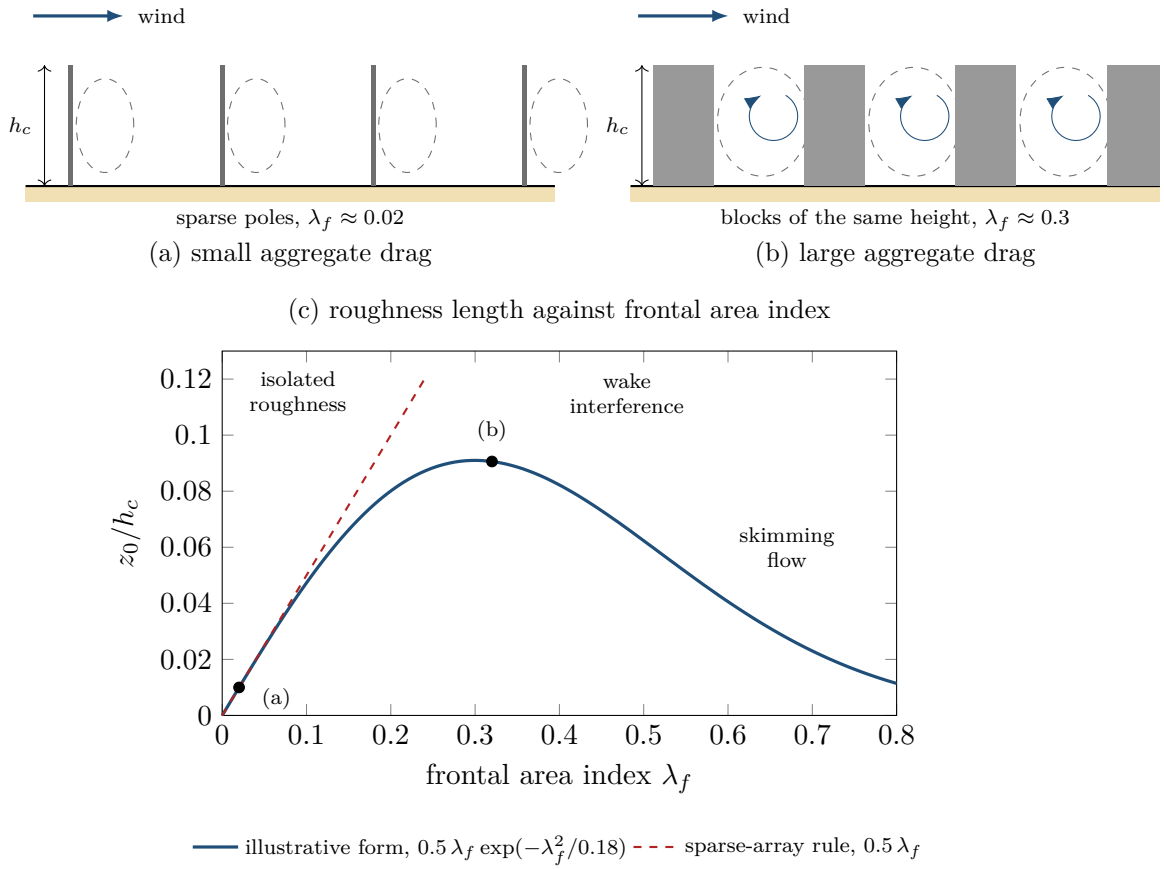
The roughness length is therefore not a function of the obstacle height alone. It depends on the density of the elements and their spacing, on their shape (a block, a cylinder, a cone of foliage), on their arrangement (aligned rows against a staggered pattern), on their porosity (a tree crown lets part of the air through, a building does not) and on their flexibility (grass and crops bend and streamline in strong wind, reducing their drag). Roughness is aerodynamic, not geometric.

> **Principle 11.1.** *The roughness length measures the drag of a surface, not the size of its elements. Two surfaces of the same obstacle height can differ in z_0 by an order of magnitude, through the density, spacing, shape, porosity and flexibility of the elements.*

11.1.5 Typical values

Table 11.1 lists representative ranges of the roughness length for common surfaces, with an illustrative obstacle height and the main properties that move a surface within its range. The ranges span more than four orders of magnitude, from smooth ice to dense city centers.

The table is a guide for first estimates, not a lookup of constants. There is no universal value for “forest” or “city”. A young, open pine stand and a dense mature broadleaf forest



(a) small aggregate drag

(b) large aggregate drag

(c) roughness length against frontal area index

Figure 11.1: Aerodynamic against geometric roughness (schematic). (a) Sparse thin poles and (b) blocks of the same height h_c, wind from the left; dashed: wakes; circular arrows in (b): eddies trapped between the blocks. (c) Roughness length relative to obstacle height against the frontal area index λ_f: the curve $z_0/h_c = 0.5\,\lambda_f \exp(-\lambda_f^2/0.18)$ is illustrative, chosen to follow the sparse-array rule $z_0/h_c = 0.5\,\lambda_f$ (dashed) at small λ_f and to fall when the elements crowd together; the two points mark surfaces (a) and (b).

Table 11.1: Representative aerodynamic roughness lengths. Ranges, not constants; obstacle heights illustrative.

Surface	z_0 (m)	Obstacle height	What moves z_0 within the range
Smooth snow, ice	10^{-4} to 10^{-3}	millimeters	surface texture, sastrugi (wind-carved snow ridges)
Open water	10^{-4} to 10^{-2}	waves	wind stress and wave age (Section 11.4.3); the upper end only in very strong wind or steep coastal waves
Short grass	0.01 to 0.05	0.05 to 0.2 m	grass height, mowing, bending in strong wind
Agricultural land	0.03 to 0.3	0.2 to 2.5 m	crop type and growth stage, hedges and scattered trees
Shrubs	0.1 to 0.5	1 to 3 m	height and density of the bushes
Forest	0.5 to 2	10 to 30 m	canopy height, density, leaf area, leaf-on or leaf-off
Suburban	0.5 to 2	5 to 10 m	building density, trees between houses
Dense urban	1 to 3 and more	10 to 100 m	building heights and their variation, street layout

are both forest; an area of detached houses with gardens and a center of high-rise towers are both urban. Each entry stands for a family of surfaces whose roughness lengths differ by a factor of three or more, and the rest of the chapter shows that the same surface also changes its roughness with the wind direction, the fetch and the season.

11.2 Roughness, the wind profile and the surface drag

This section shows how the roughness length changes the wind profile, first with the friction velocity held fixed and then with the wind aloft held fixed, and how it sets the drag coefficient and the stress. The derivations of the profile and of the drag coefficient are those of Chapters 7 and 10; this section uses them to compare surfaces.

11.2.1 Profiles at the same friction velocity

Take two surfaces with $z_0 = 0.01\,\mathrm{m}$ (short grass) and $z_0 = 1.0\,\mathrm{m}$ (a forest, heights counted from its zero plane), and the same friction velocity $u_* = 0.5\,\mathrm{m\,s^{-1}}$, so that $u_*/\kappa = 1.25\,\mathrm{m\,s^{-1}}$. At 10 m above the zero plane equation (11.1) gives

$$z_0 = 0.01\,\mathrm{m}: \quad U(10\,\mathrm{m}) = 1.25\,\mathrm{m\,s^{-1}} \times \ln 1000 = 1.25 \times 6.908\,\mathrm{m\,s^{-1}} = 8.63\,\mathrm{m\,s^{-1}},$$
$$z_0 = 1.0\,\mathrm{m}: \quad U(10\,\mathrm{m}) = 1.25\,\mathrm{m\,s^{-1}} \times \ln 10 = 1.25 \times 2.303\,\mathrm{m\,s^{-1}} = 2.88\,\mathrm{m\,s^{-1}}.$$

At the same friction velocity the rougher surface has the smaller mean wind at every height, here three times smaller at 10 m. The shear $u_*/[\kappa(z-d)]$ is the same over both, so on a logarithmic height axis the two profiles are parallel lines displaced by $(u_*/\kappa)\ln(1.0/0.01) = 1.25 \times 4.605 = 5.76\,\mathrm{m\,s^{-1}}$. The rougher surface extracts momentum more strongly, and it takes a weaker wind to produce the same stress over it.

The comparison is useful for reading the profile formula, but it is not a comparison of two weathers. A friction velocity of $0.5\,\mathrm{m\,s^{-1}}$ is a strong stress over grass, reached with an $8.6\,\mathrm{m\,s^{-1}}$ wind at 10 m, and a weak one over forest, reached with $2.9\,\mathrm{m\,s^{-1}}$. Holding u_* fixed treats the stress as given and the wind as the response, whereas in the atmosphere the large-scale flow is given and both the stress and the wind near the ground respond to the surface.

11.2.2 Profiles under the same wind aloft

When the same large-scale flow passes over two surfaces, the friction velocity itself changes: roughness affects both the stress and the profile. A simple way to represent the same forcing is to hold the wind fixed at a reference height z_r high in the surface layer and let each surface set its own u_*. From equation (11.1) at z_r,

$$u_* = \frac{\kappa\, U(z_r)}{\ln[(z_r - d)/z_0]}, \qquad \frac{U(z)}{U(z_r)} = \frac{\ln[(z-d)/z_0]}{\ln[(z_r-d)/z_0]}. \tag{11.3}$$

With $U = 10\,\mathrm{m\,s^{-1}}$ at $z_r = 100\,\mathrm{m}$ above the zero plane, and $\kappa\,U(z_r) = 4\,\mathrm{m\,s^{-1}}$, the logarithms are $\ln 10^4 = 9.210$ and $\ln 10^3 = 6.908$ for the smooth surface and $\ln 100 = 4.605$ and $\ln 10 = 2.303$ for the rough one, so that

$$z_0 = 0.01\,\mathrm{m}: \quad u_* = \frac{4}{9.210}\,\mathrm{m\,s^{-1}} = 0.434\,\mathrm{m\,s^{-1}}, \quad U(10\,\mathrm{m}) = 10\,\mathrm{m\,s^{-1}} \times \frac{6.908}{9.210} = 7.50\,\mathrm{m\,s^{-1}},$$
$$z_0 = 1.0\,\mathrm{m}: \quad u_* = \frac{4}{4.605}\,\mathrm{m\,s^{-1}} = 0.869\,\mathrm{m\,s^{-1}}, \quad U(10\,\mathrm{m}) = 10\,\mathrm{m\,s^{-1}} \times \frac{2.303}{4.605} = 5.00\,\mathrm{m\,s^{-1}}.$$

The rougher surface now has twice the friction velocity and still the weaker 10 m wind, but the difference in the 10 m wind is a factor of 1.5, not 3.

Figure 11.2 draws both comparisons. The horizontal axis is the wind speed and the vertical axis the height above the zero plane on a logarithmic scale from 1 to 100 m. Blue lines are the smooth surface ($z_0 = 0.01$ m), gold lines the rough one ($z_0 = 1.0$ m). Dashed lines hold $u_* = 0.5\,\mathrm{m\,s^{-1}}$ fixed; solid lines hold $U = 10\,\mathrm{m\,s^{-1}}$ at 100 m fixed. The points mark the 10 m values worked out above.

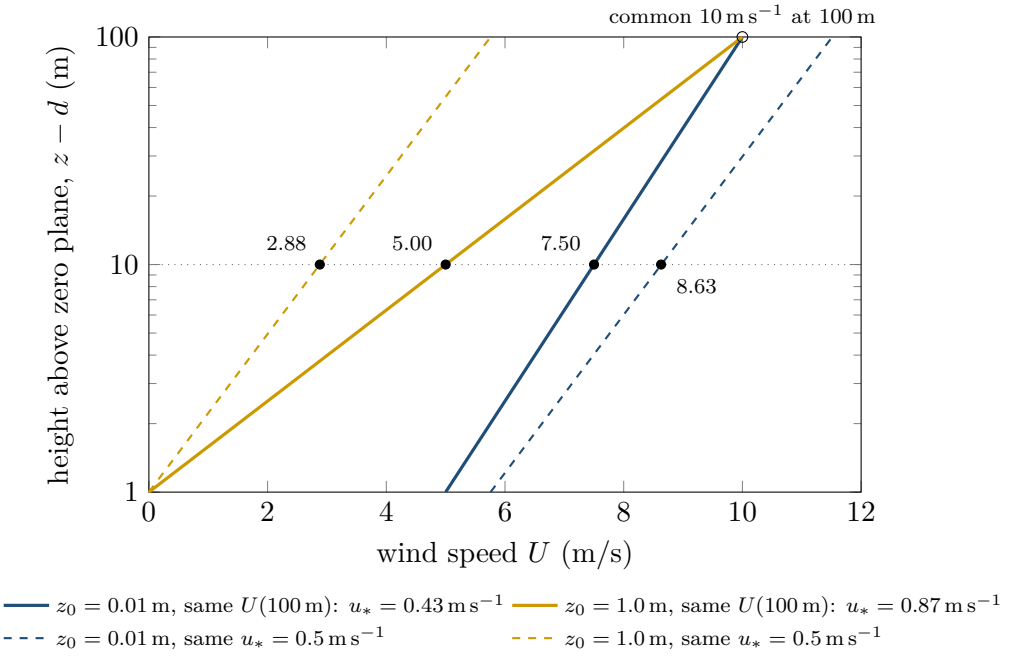


Figure 11.2: Neutral profiles $U = (u_*/\kappa)\ln[(z-d)/z_0]$, $\kappa = 0.4$, over a smooth ($z_0 = 0.01$ m) and a rough ($z_0 = 1.0$ m) surface. Dashed: the same friction velocity, $0.5\,\mathrm{m\,s^{-1}}$. Solid: the same wind, $10\,\mathrm{m\,s^{-1}}$, at 100 m above the zero plane (open circle). Points: values at 10 m, in m/s. Values illustrative.

The dashed lines are parallel and far apart; the solid lines meet at 100 m and diverge downward; the rough-surface line spans the wider range of speeds between 1 and 100 m, which is the larger change of wind per factor of ten in height and the stronger shear. Holding u_* fixed is mathematically convenient and physically incomplete: it exaggerates the effect of roughness on the near-surface wind, here by a factor of two in the ratio of the 10 m winds, because it ignores that a rougher surface draws a larger stress out of the same flow. Holding the wind at 100 m fixed is closer to the atmosphere but is itself a simplification: over a long fetch the rougher surface also slows the wind at 100 m, less than near the ground, and the cleanest comparison is against the geostrophic wind, which the surface does not change.

11.2.3 Roughness and the drag coefficient

The bulk formula of Chapter 10 gives the surface stress from the wind at a reference height, $\tau_0 = \rho C_D U(z)^2$, and in neutral air the drag coefficient follows from the logarithmic profile:

$$C_D = \left[\frac{\kappa}{\ln[(z-d)/z_0]}\right]^2. \tag{11.4}$$

A larger z_0 makes the logarithm smaller and C_D larger. The chain is roughness length, drag coefficient, surface stress: $z_0 \to C_D \to \tau_0$.

For the two surfaces of Section 11.2.2, at 10 m,

$$z_0 = 0.01\,\mathrm{m}: \quad C_D = (0.4/6.908)^2 = 0.00335, \quad \tau_0 = 1.2 \times 0.00335 \times 7.50^2\,\mathrm{Pa} = 0.226\,\mathrm{Pa},$$

$$z_0 = 1.0\,\mathrm{m}: \quad C_D = (0.4/2.303)^2 = 0.0302, \quad \tau_0 = 1.2 \times 0.0302 \times 5.00^2\,\mathrm{Pa} = 0.905\,\mathrm{Pa},$$

with $\rho = 1.2\,\mathrm{kg\,m^{-3}}$. The stresses equal $\rho\,u_*^2$ with the friction velocities found above, $1.2 \times 0.434^2 = 0.226\,\mathrm{Pa}$ and $1.2 \times 0.869^2 = 0.905\,\mathrm{Pa}$, as they must. Under the same wind aloft the drag coefficient at 10 m is nine times larger over the rough surface, the 10 m wind is a third smaller, and the stress, the product of the two effects, is four times larger. The rougher surface takes more momentum out of the same flow, and the near-surface wind is lower because of it.

11.3 Displacement height and the layers above a canopy

Over tall and dense obstacles the roughness length alone does not describe the surface. This section gives the displacement height its physical meaning, separates its role from that of the roughness length, works a canopy example with numbers, and describes the two layers above a canopy: the roughness sublayer, where the logarithmic profile fails, and the inertial sublayer above it, where it holds.

11.3.1 The zero-plane displacement as a level of momentum absorption

Over a forest, a field of tall crops or a city, the flow above the obstacles behaves as if the ground had been raised. The *zero-plane displacement height* d (m) is the height of that apparent ground: the level from which heights must be counted for the logarithmic profile, equation (11.1), to fit the winds measured above the obstacles. It is needed over forests, tall crops and urban canopies, and is negligible over short grass, bare soil and water.

Its physical meaning comes from where the drag acts. Over a 20 m forest, most of the momentum is absorbed by the crowns, branches and leaves of the upper canopy, not by the soil, which lies in still air under them. Let $D(z)$ be the drag force of the canopy elements per unit volume at height z ($\mathrm{N/m^3}$). The total stress is the integral of the drag over the canopy depth, and the displacement height is the height of its centroid,

$$\tau_0 = \int_0^{h_c} D(z)\,\mathrm{d}z, \qquad d = \frac{\int_0^{h_c} z\,D(z)\,\mathrm{d}z}{\int_0^{h_c} D(z)\,\mathrm{d}z}\,: \tag{11.5}$$

the mean level of momentum absorption. The flow far above the canopy cannot distinguish a drag spread through the canopy from the same total drag acting at this one level, which is why the logarithmic profile above the canopy fits with heights counted from d. The interpretation is supported by wind-tunnel and field measurements of drag profiles in canopies.

A two-layer illustration shows how the centroid falls well inside the canopy. Suppose that 90 % of the drag of a 20 m forest acts in the crown layer from 10 to 20 m, spread evenly so that its centroid is at 15 m, and 10 % in the trunk space and understory, with centroid at 5 m. Then

$$d = 0.9 \times 15\,\mathrm{m} + 0.1 \times 5\,\mathrm{m} = 13.5\,\mathrm{m} + 0.5\,\mathrm{m} = 14.0\,\mathrm{m},$$

which is $0.7\,h_c$, the usual rule of thumb for dense canopies, $d \approx 0.6$ to $0.8\,h_c$. A canopy whose foliage is concentrated near the top has a higher displacement; a sparse one, whose drag reaches the ground between the trees, has a lower one. The ground has not moved; the origin of the momentum exchange has.

11.3.2 Displacement height against roughness length

The two surface parameters answer different questions. The displacement height d says where the effective aerodynamic origin of the profile is. The roughness length z_0 says how rough the aerodynamic surface at that origin is: how much stress it carries for a given wind. On a plot of U against $\ln(z - d)$ the profile is a straight line; d fixes which plot to use, and z_0 is where that line meets $U = 0$.

For a canopy, d is usually much larger than z_0: about $0.7\,h_c$ against about 0.05 to $0.1\,h_c$, so 14 m against 1 to 2 m for a 20 m forest. The two parameters are linked through the canopy geometry (panel (c) of Figure 11.1 shows that as elements crowd together z_0 falls while d rises), but they are not interchangeable: Chapter 7 showed that a profile fitted with the wrong displacement returns a wrong friction velocity and a wrong roughness length together.

11.3.3 A canopy example

Take an illustrative forest with $h_c = 20\,\mathrm{m}$, $d = 14\,\mathrm{m}$ and $z_0 = 1.5\,\mathrm{m}$, and a sensor at $z = 40\,\mathrm{m}$. The aerodynamic height of the sensor, its height above the zero plane, is $z - d = 26\,\mathrm{m}$, and the profile gives

$$U(40\,\mathrm{m}) = \frac{u_*}{\kappa} \ln \frac{40 - 14}{1.5} = \frac{u_*}{\kappa} \ln 17.33 = 2.853\,\frac{u_*}{\kappa}.$$

Ignoring the displacement height would use $\ln(40/1.5) = \ln 26.67 = 3.283$ instead, a factor that is 15 % larger. With an illustrative friction velocity $u_* = 0.8\,\mathrm{m\,s^{-1}}$, so that $u_*/\kappa = 2\,\mathrm{m\,s^{-1}}$, the two give 5.71 and $6.57\,\mathrm{m\,s^{-1}}$.

The error works in both directions. Predicting the wind from a known u_* without d overstates it by 15 % at 40 m. Inferring u_* from a measured $5.71\,\mathrm{m\,s^{-1}}$ at 40 m without d gives $u_* = 0.4 \times 5.71/3.283 = 0.695\,\mathrm{m\,s^{-1}}$ instead of $0.8\,\mathrm{m\,s^{-1}}$, 13 % low, and the stress $\rho\,u_*^2$ 24 % low. The error shrinks with height as $z - d$ approaches z: the ratio of the two logarithms is 1.27 at 30 m, 1.15 at 40 m, 1.08 at 60 m and 1.04 at 100 m. Panel (b) of Figure 11.3, described in the next subsection, draws the two profiles.

11.3.4 The roughness sublayer and the inertial sublayer

Close to the canopy top the flow does not see a uniform surface. It sees individual trees or buildings: wakes behind each crown, gaps between them, coherent eddies that form in the strong shear at the canopy top and sweep into and out of the canopy. The *roughness sublayer* is the layer just above the obstacles in which these effects make the flow vary from place to place at the same height and the turbulence heterogeneous. In it the logarithmic profile with d and z_0 may not work; the measured shear is usually smaller than the logarithmic value $u_*/[\kappa(z - d)]$, because the canopy-top eddies mix more efficiently than surface-layer eddies of the same height. Its depth is about 2 to $5\,h_c$, depending on the geometry: near the low end for dense, uniform canopies and toward the high end for sparse or irregular ones. Over a 20 m forest that is 40 to 100 m. A sensor at 30 m above such a forest, $1.5\,h_c$, is inside the roughness sublayer by any estimate, and its readings depend on its position relative to individual crowns and gaps.

Above the roughness sublayer lies the *inertial sublayer*, the part of the surface layer where the effects of the individual obstacles have blended into an aggregate drag. There the flow responds to the surface only through d and z_0, the stress is nearly constant with height, and the logarithmic profile and the similarity theory of Chapters 12 and 14 are most defensible. Over short grass the roughness sublayer is a few tenths of a meter deep and the inertial sublayer begins almost at the ground; over a forest or a city it may begin only at 50 to 100 m, and in a shallow night-time surface layer it may not exist at all.

Figure 11.3 draws these levels. Panel (a) is a schematic cross section of the illustrative forest, with height above the ground on the vertical axis (to scale): the canopy up to $h_c = 20\,\mathrm{m}$, the displacement height at 14 m, the band from $2\,h_c$ to $5\,h_c$ in which the top of the roughness sublayer lies, the inertial sublayer above it, and masts with sensors at 30 and 60 m. Panel (b) has wind speed on the horizontal axis and height above the ground on the vertical axis; it draws the profile of Section 11.3.3 with and without the displacement height, both for $u_* = 0.8\,\mathrm{m\,s^{-1}}$ and $z_0 = 1.5\,\mathrm{m}$.

Panel (a) shows that the sensor at 30 m lies in the roughness sublayer whatever its depth, and the sensor at 60 m lies in it if the roughness sublayer is deeper than $3\,h_c$, which a sparse

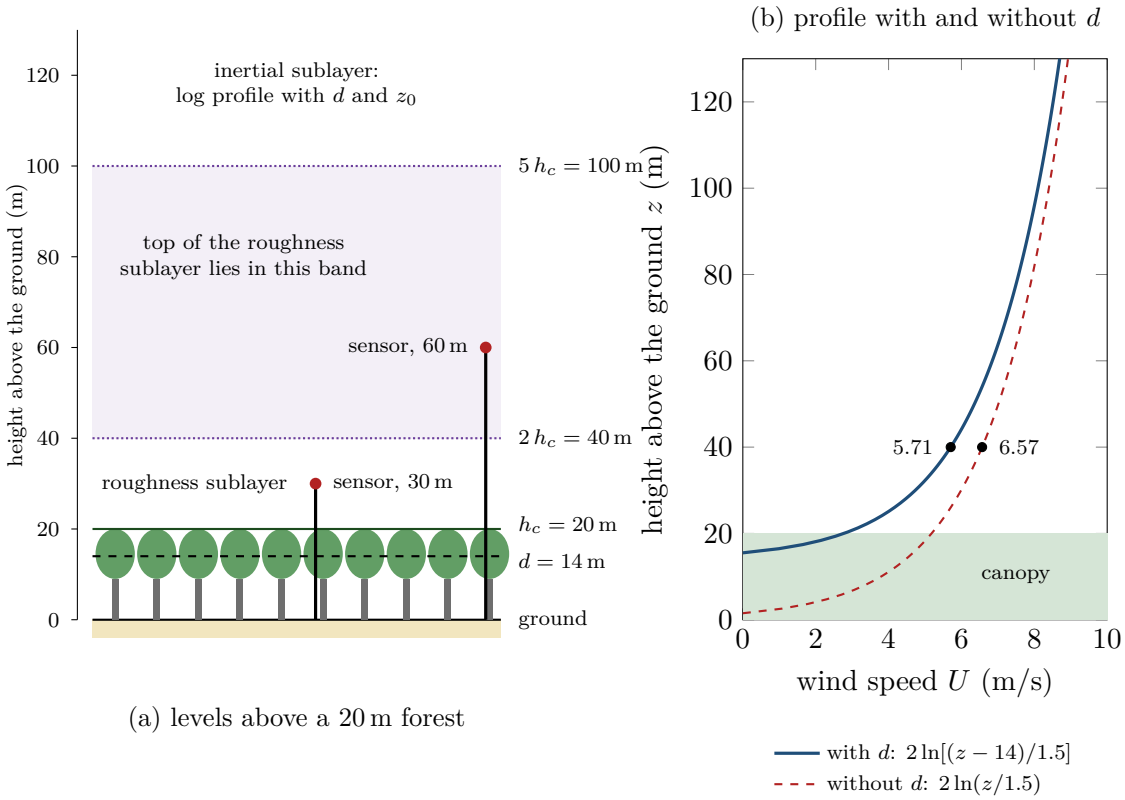


Figure 11.3: Levels and profiles above an illustrative forest, $h_c = 20\,\text{m}$, $d = 14\,\text{m}$, $z_0 = 1.5\,\text{m}$. (a) Schematic to scale in height: the canopy, the displacement height (dashed), the canopy top, the band $2\,h_c$ to $5\,h_c$ in which the top of the roughness sublayer lies (shaded), and two sensors. (b) Neutral profiles for $u_* = 0.8\,\text{m}\,\text{s}^{-1}$, $\kappa = 0.4$, with the displacement height (solid) and without it (dashed); points: values at 40 m, in m/s. Neither curve describes the wind inside the canopy (shaded).

or irregular forest makes likely. Only above 100 m is a sensor in the inertial sublayer by every estimate. Panel (b) shows that the profile without d is too fast at every height, by the most near the canopy. Both panels together make the practical point: over a tall canopy the logarithmic profile, with or without d, is reliable only well above the canopy, and the heights at which engineering wind is usually needed, 10 to 60 m, are those at which it is least reliable.

Principle 11.2. *Over a tall canopy the logarithmic profile holds only in the inertial sublayer, above a roughness sublayer about* 2 *to* 5 *canopy heights deep, and only with heights counted from the displacement height, the mean level at which the canopy absorbs momentum.*

11.4 Roughness that depends on direction, fetch and time

A real site has not one roughness length but many: one for each wind direction, each distance to the nearest change of surface, each sea state and each season. This section treats directional roughness, fetch and internal boundary layers, the roughness of water, and the changes of vegetation, forests and cities over time and space.

11.4.1 Directional roughness

Consider a sensor with open fields to the west, a forest to the east and suburban development to the south. Air arriving from the west has crossed grass; air from the east has crossed forest. The profile at the sensor therefore has a different roughness length for each wind direction, $z_0 = z_0(\beta)$, with β the direction from which the wind blows. This is *directional roughness*, also called roughness-sector dependence: the roughness length of a site as a function of the upwind direction, usually tabulated for sectors of 30° or 45°. A plot of such a table is a *roughness rose*.

Figure 11.4 is the roughness rose of this illustrative site. Each wedge is a sector of 30° centered on the direction from which the wind comes, with north at the top and east to the right; its radius is proportional to $\log_{10} z_0$ on the scale of the three dotted circles, 0.01, 0.1 and 1 m, and its shade indicates the surface type. The rose describes the site, not the weather, and holds in either hemisphere.

The rose spans a factor of 33, from 0.03 m over the open grass to the west to 1.0 m over the forest to the east. Take a westerly and an easterly wind with the same wind aloft, $10\,\mathrm{m\,s^{-1}}$ at 100 m, in neutral air, with heights counted from the ground at the sensor, which stands in the open. By equation (11.3), with $\ln(100/0.03) = 8.112$ and $\ln(10/0.03) = 5.809$ for the westerly and the values of Section 11.2.2 for the easterly,

$$z_0(270°) = 0.03\,\mathrm{m}: \quad u_* = \frac{4}{8.112}\,\mathrm{m\,s^{-1}} = 0.493\,\mathrm{m\,s^{-1}}, \quad U(10\,\mathrm{m}) = 7.16\,\mathrm{m\,s^{-1}};$$
$$z_0(90°) = 1.0\,\mathrm{m}: \quad u_* = \frac{4}{4.605}\,\mathrm{m\,s^{-1}} = 0.869\,\mathrm{m\,s^{-1}}, \quad U(10\,\mathrm{m}) = 5.00\,\mathrm{m\,s^{-1}},$$

the westerly value from $U(10\,\mathrm{m}) = 10\,\mathrm{m\,s^{-1}} \times 5.809/8.112$. The same synoptic wind gives a 10 m wind 30 % lower when it blows from the east. Wind direction thus controls the near-surface wind speed indirectly, through the roughness of the upwind surface. For a transmission line whose rating depends on the wind at the conductor, an easterly and a westerly of equal strength aloft are not equal cooling conditions at this site.

Direction relative to the geostrophic wind. The surface wind does not blow from the same direction as the geostrophic wind: friction turns it toward low pressure (Chapter 3), by an angle that is larger over rougher surfaces and in more stable air, typically 10 to 20° over the sea and 20 to 40° over land. Low pressure lies to the left of the geostrophic flow in the Northern

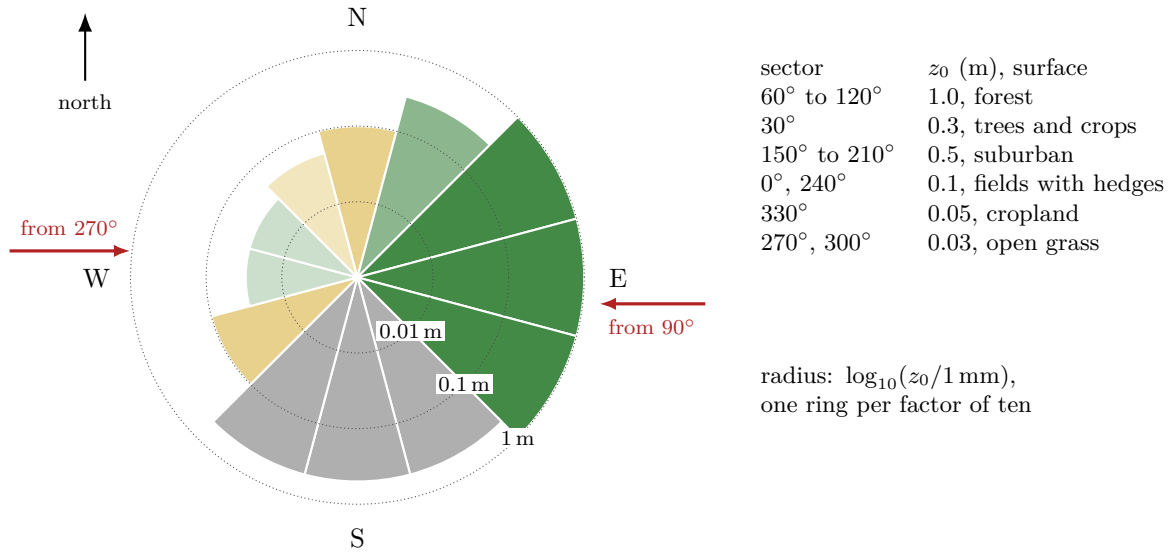


Figure 11.4: Roughness rose of an illustrative site (valid in either hemisphere): roughness length by 30° sector of the direction from which the wind blows, radius proportional to $\log_{10} z_0$ (rings at 0.01, 0.1 and 1 m). Arrows: the westerly and easterly cases of the worked example. Values illustrative.

Hemisphere ($f > 0$) and to its right in the Southern Hemisphere ($f < 0$). With β measured clockwise from north, the surface direction is therefore $\beta_g - \alpha$ in the Northern Hemisphere and $\beta_g + \alpha$ in the Southern, where β_g is the geostrophic direction and α the turning angle. For the site of Figure 11.4 with a geostrophic wind from 250° and an illustrative $\alpha = 20°$, the surface wind comes from 270° if the site is at 23°S and from 230° if it is at 23°N. The first falls in the open-grass sector, $z_0 = 0.03$ m; the second in the 240° sector, $z_0 = 0.1$ m, and with 10 m s^{-1} at 100 m the 10 m wind is 7.16 against 6.67 m s^{-1}. The roughness sector that matters is the one the surface wind comes from, and finding it from a forecast of the flow aloft requires the hemisphere.

11.4.2 Fetch and internal boundary layers

The sector a wind comes from is not the only geometry that matters; the distance over which the air has crossed each surface matters too. Chapter 7 defined the fetch, the upwind distance over which the air has traveled across a given surface, and the internal boundary layer, the layer adjusted to a new surface that grows upward downwind of a change in roughness from $z_{0,1}$ to $z_{0,2}$. Near the ground the wind adjusts to the new surface quickly; aloft, the profile of the old surface persists until the internal boundary layer reaches it. With the rough rule of that chapter, the top of the internal boundary layer is at $\delta \approx 0.1\,x$ at a distance x downwind of the change, and only its lowest tenth or so is in equilibrium with the new surface.

Consider a sensor at 10 m over grass, with only 100 m of grass between it and a forest upwind. The internal boundary layer of the grass reaches about $\delta \approx 10$ m at the sensor, and the layer in equilibrium with the grass only about 1 m. The flow at 10 m has not adjusted to the grass. The effective roughness it reflects is a mixture of the upwind forest and the local grass, between 0.03 and 1 m and, at this height, closer to the forest value. A land-cover lookup of the pixel under the sensor would return grass and would be wrong for this direction. In the picture of a water-to-land transition, just past the shoreline the lowest meters adjust to the land while the air above is still marine; farther inland the adjustment layer deepens, $\delta(x)$ growing with the distance x from the coast, to about 50 m at 500 m inland by the same rule.

Coastlines. A coastline is geometrically simple, a line between water and land, and physically complex. Marine air with its own temperature and humidity crosses a roughness transition of two to four orders of magnitude; the land heats and cools daily while the sea does not, which drives sea and land breezes and changes the stability across the coast between day and night; and coasts often rise into cliffs or hills. The roughness change, the stability change and the terrain all act at once, and a single roughness length for a coastal site is a weak description. Thermal circulations and terrain flow are the subjects of Chapters 19 and 20.

11.4.3 Water surfaces and the Charnock relation

Water is not a surface of fixed roughness. Its roughness elements are waves, and the short waves that carry most of the stress grow with the wind. A dimensional argument gives the form of the dependence. Over open water in strong enough wind, where the waves are in equilibrium with the local wind and viscosity is unimportant, the roughness length can depend only on the stress that raises the waves, through u_* (m/s), and on gravity, which restores them, through g (m/s^2). The only length that can be formed from these two is u_*^2/g, so

$$z_0 = \alpha_c \frac{u_*^2}{g}, \tag{11.6}$$

the *Charnock relation*, in which the dimensionless *Charnock parameter* α_c is determined by experiment: about 0.011 for open ocean and up to about 0.018 or more near coasts and in fetch-limited water, where the waves are young and steep. Ocean roughness increases with the wind stress. In light wind the water surface becomes aerodynamically smooth, the roughness is set by the viscous sublayer, and a viscous term $0.11\,\nu/u_*$ is often added: $z_0 = \alpha_c\, u_*^2/g + 0.11\,\nu/u_*$.

Because z_0 depends on u_* and u_* on z_0, the roughness for a given wind is found by iteration. Start from a guess of z_0, compute $u_* = \kappa U_{10}/\ln(10\,\mathrm{m}/z_0)$, compute a new z_0 from the Charnock relation with the viscous term, and repeat. Table 11.2 carries out the iteration for $U_{10} = 5$ and $15\,\mathrm{m\,s^{-1}}$, with $\alpha_c = 0.011$, $\nu = 1.5 \times 10^{-5}\,\mathrm{m^2\,s^{-1}}$, $g = 9.81$ m/s^2 and a first guess $z_0 = 10^{-4}\,\mathrm{m}$. Each row gives the roughness length used, the friction velocity it implies and the roughness length that friction velocity implies in turn.

Table 11.2: Iteration of the Charnock relation with the viscous term, $z_0 = \alpha_c u_*^2/g + 0.11\,\nu/u_*$, $\alpha_c = 0.011$, and the neutral log law at 10 m. The last two rows give the converged drag coefficient at 10 m and the surface stress for $\rho = 1.2\,\mathrm{kg\,m^{-3}}$.

	$U_{10} = 5\,\mathrm{m\,s^{-1}}$			$U_{10} = 15\,\mathrm{m\,s^{-1}}$		
Step	z_0 in (m)	u_* (m/s)	z_0 out (m)	z_0 in (m)	u_* (m/s)	z_0 out (m)
1	1.00×10^{-4}	0.174	4.33×10^{-5}	1.00×10^{-4}	0.521	3.08×10^{-4}
2	4.33×10^{-5}	0.162	3.96×10^{-5}	3.08×10^{-4}	0.578	3.77×10^{-4}
3	3.96×10^{-5}	0.161	3.92×10^{-5}	3.77×10^{-4}	0.589	3.92×10^{-4}
4	3.92×10^{-5}	0.161	3.92×10^{-5}	3.92×10^{-4}	0.591	3.95×10^{-4}
C_D at 10 m		1.03×10^{-3}			1.56×10^{-3}	
τ_0 (Pa)		0.031			0.42	

The iteration converges in three or four steps. Tripling the wind raises the friction velocity from 0.161 to $0.592\,\mathrm{m\,s^{-1}}$, a factor of 3.7, and the roughness length tenfold, from 3.9×10^{-5} to 4.0×10^{-4} m. At $5\,\mathrm{m\,s^{-1}}$ the viscous term is about a quarter of z_0 (1.0×10^{-5} m); at $15\,\mathrm{m\,s^{-1}}$ it is under 1 %. The drag coefficient rises by half, from 1.03×10^{-3} to 1.56×10^{-3}, and the stress, proportional to $C_D\,U^2$, rises fourteenfold for a threefold wind. Over land, with fixed z_0, the same tripling would leave C_D unchanged and multiply the stress by nine.

Figure 11.5 shows the whole relation. Both panels have the 10 m wind speed on the horizontal axis. Panel (a) has the roughness length on a logarithmic vertical axis; panel (b) has the drag

coefficient at 10 m, multiplied by 1000. Solid curves include the viscous term; dashed curves are the Charnock term alone. The points are the two converged cases of Table 11.2.

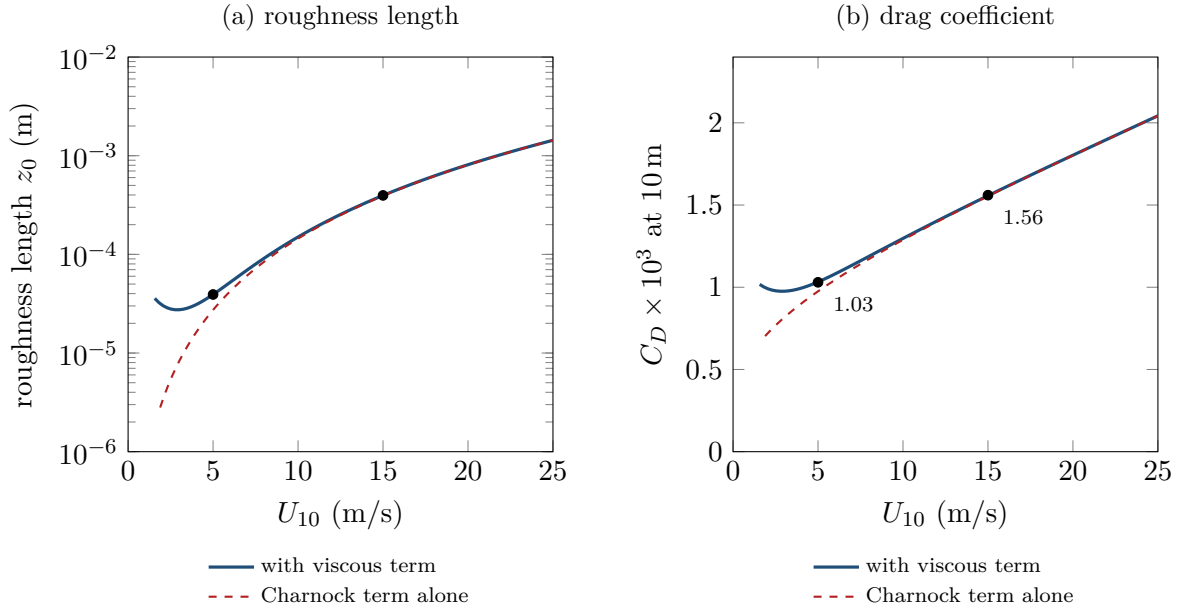


Figure 11.5: Roughness length (a) and neutral drag coefficient at 10 m (b) of a water surface against the 10 m wind, from $z_0 = \alpha_c u_*^2/g + 0.11\,\nu/u_*$ (solid) or $z_0 = \alpha_c u_*^2/g$ (dashed), with $\alpha_c = 0.011$ and a kinematic viscosity $\nu = 1.5 \times 10^{-5}\,\mathrm{m^2\,s^{-1}}$, each combined with the neutral profile $U_{10} = (u_*/\kappa)\ln(10\,\mathrm{m}/z_0)$, $\kappa = 0.4$. Points: the converged cases of Table 11.2.

Above about $5\,\mathrm{m\,s^{-1}}$ the two curves agree and the roughness length grows roughly as the square of the wind, so that it rises from about 4×10^{-5} m at $5\,\mathrm{m\,s^{-1}}$ to above 10^{-3} m at $25\,\mathrm{m\,s^{-1}}$. Below about $3\,\mathrm{m\,s^{-1}}$ the viscous term takes over: the surface is smooth, the roughness length grows again as the wind weakens, and the drag coefficient has a minimum of about 1.0×10^{-3} near $3\,\mathrm{m\,s^{-1}}$. A roughness length fixed at a single value for the sea, as a land-cover table would give, misses this wind dependence, and with it a factor of one and a half in the drag coefficient between light and strong wind. The upper end of the range for water in Table 11.1, 10^{-2} m, needs $u_* \approx 3\,\mathrm{m\,s^{-1}}$ with $\alpha_c = 0.011$, which the log law places at a 10 m wind of about $50\,\mathrm{m\,s^{-1}}$, or steep young waves with a larger α_c.

11.4.4 Seasonal and dynamic roughness of vegetation

Vegetation roughness changes in time. A crop field is bare soil after sowing and a canopy of maize two or more meters tall a few months later; a deciduous forest loses its leaves in winter; snow fills the gaps between plants and buries low vegetation; and plants bend and streamline in strong wind, lowering their drag exactly when the wind is strongest. A field in April is not the same surface as the field in August, in the Northern Hemisphere; for a summer crop in the Southern Hemisphere the same contrast falls around October and February.

Take an illustrative field with $z_0 = 0.01$ m when bare and $z_0 = 0.25$ m under a mature crop 2.5 m tall (the displacement height of the crop, about 1.7 m, is neglected here for simplicity). With $10\,\mathrm{m\,s^{-1}}$ at 100 m in neutral air, equation (11.3) gives a 10 m wind of $7.50\,\mathrm{m\,s^{-1}}$ over the bare field and

$$U(10\,\mathrm{m}) = 10\,\mathrm{m\,s^{-1}} \times \frac{\ln 40}{\ln 400} = 10 \times \frac{3.689}{5.991}\,\mathrm{m\,s^{-1}} = 6.16\,\mathrm{m\,s^{-1}}$$

over the crop, 18 % less. A wind model calibrated on spring data and applied in summer, with the same roughness length, carries this error as a seasonal bias. A deciduous forest often changes

less in z_0 between leaf-on and leaf-off than its foliage suggests, because the branches and trunks still produce drag, but its displacement height falls when the leaves are off, because the drag then reaches deeper into the canopy.

11.4.5 Forests and urban areas

A forest is described by its canopy height, density and leaf area, the leaf surface per unit ground area; each changes z_0 and d. Forest edges add a further effect: the flow meeting an edge is deflected upward, may separate from the canopy top and reattach downwind, and the edge sheds strong local turbulence and starts an internal boundary layer. Close to edges, clearings and roads the roughness of the forest is not defined in the sense of this chapter. A generic $z_0 = 1\,\mathrm{m}$ for every forest is a simplification: sometimes acceptable for a first estimate over a large uniform stand, often wrong by a factor of two or more for a particular site and direction.

An urban area mixes buildings of different heights, street canyons, isolated towers and open spaces such as parks and squares. A single z_0 and d for a city district is an aggregate approximation of a surface whose drag is concentrated on a few tall buildings and whose flow at street level is governed by the local geometry. Where the aggregate is not enough, more detailed descriptions are used: urban canopy models that represent streets and roofs explicitly in a weather model, computational fluid dynamics of the actual buildings, and morphology-based parameterizations that compute z_0 and d from building heights, frontal areas and plan areas (Section 11.6).

> **Principle 11.3.** *The roughness length of a site is a function of wind direction, fetch, season and, over water, wind speed. A single value for a site is an approximation that must be justified for the directions and periods to which it is applied.*

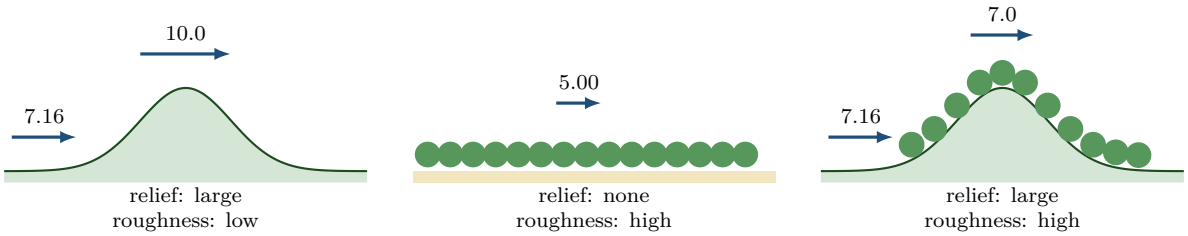
11.5 Roughness and terrain

Roughness and terrain relief are often confused, because both are properties of "the ground" that change the wind. This section separates them and shows, on a forested ridge, how they can act on the near-surface wind in opposite directions.

11.5.1 Relief against roughness

Terrain relief is the shape of the ground surface on scales of hundreds of meters and more: hills, ridges, valleys, escarpments. *Roughness* is the drag of the elements on the surface, on scales of the elements themselves. A smooth grass-covered hill has large relief and low roughness. A flat forest has no relief and high roughness. The two act through different physics: relief changes the pressure field and the geometry of the flow, forcing air over and around obstacles, accelerating it over crests and slowing it in hollows; roughness changes the surface drag and the turbulence. In a weather model or a flow model they are also different inputs: relief enters through the terrain height of each grid cell, roughness through z_0 and d, and small-scale relief that the grid cannot resolve is sometimes added to the roughness length as an effective orographic roughness, a practice that mixes the two on purpose.

Figure 11.6 illustrates the distinction with three schematic cross sections, wind from the left. Panel (a) is a smooth grassy hill, panel (b) a flat forest, panel (c) a forested ridge of the same shape as the hill. Each arrow is the wind at 10 m above the ground or, over forest, above the zero plane, its length proportional to the speed printed above it. The numbers are illustrative: the upstream grass wind of $7.16\,\mathrm{m\,s^{-1}}$ and the forest wind of $5.00\,\mathrm{m\,s^{-1}}$ are those of Section 11.4.1, for $10\,\mathrm{m\,s^{-1}}$ at 100 m, and the hill is assumed to raise the wind at its crest by a factor of 1.4 at this height.



(a) smooth grassy hill (b) flat forest (c) forested ridge

Figure 11.6: Relief against roughness (schematic), wind from the left. Arrows: the wind at 10 m above the ground, or above the zero plane over forest, in m/s, for an illustrative $10\,\mathrm{m\,s^{-1}}$ at 100 m in neutral air, with $z_0 = 0.03\,\mathrm{m}$ for grass, $z_0 = 1.0\,\mathrm{m}$ for forest and an assumed crest speed-up factor of 1.4. Vertical scale exaggerated.

On the grassy hill the relief raises the wind from 7.16 to $10.0\,\mathrm{m\,s^{-1}}$. Over the flat forest the roughness lowers it to $5.00\,\mathrm{m\,s^{-1}}$ with no relief at all. Neither panel alone predicts panel (c).

11.5.2 A forested ridge

On a forested ridge the two effects compete. The ridge accelerates the flow near the crest; the forest slows the near-surface wind and increases the turbulence. Multiplying the forest wind by the crest factor gives $5.00 \times 1.4 = 7.0\,\mathrm{m\,s^{-1}}$ at 10 m above the zero plane, about the same as the $7.16\,\mathrm{m\,s^{-1}}$ over the flat grass upstream: in this illustration the speed-up of the ridge and the drag of the forest nearly cancel. A sensor on the forested crest would read the same mean wind as one on the open plain, for opposite reasons, and with much stronger turbulence.

The multiplication is a simplification. The speed-up over a hill is not independent of the roughness: a rough surface reduces the speed-up near the ground and can cause the flow to separate on the lee slope, so the two effects interact rather than multiply. The case is common at real sites, where transmission lines and wind turbines are often placed on forested ridges, and it is the reason why a terrain model run with the wrong roughness, or a roughness correction applied without the terrain, gives a wrong near-surface wind. Terrain flow is the subject of Chapter 20; this chapter's point is that relief and roughness are separate inputs, each to be stated.

11.6 Estimating and using the roughness length

The roughness length is not measured directly; it is estimated, and the estimate is then used in profiles, models and corrections. This section compares the methods of estimation, shows what one and several heights can identify, and follows a roughness length into a forecast: as a source of bias, as a grid-cell average, and in the correction of a wind from one exposure to another.

11.6.1 Four ways to estimate the roughness length

Four methods are in common use. *Land-cover classification* assigns each land-cover class of a map a tabulated z_0, as in Table 11.1; it is fast and covers any area, and it is crude. *Wind-profile fitting* fits equation (11.1) to mean winds at several heights on a mast, in neutral periods, and returns u_* and z_0 (Chapter 10 gives the two-height formula). *Eddy covariance* measures u_* directly with a sonic anemometer and infers z_0 from the mean wind at the same height by equation (11.2). *Morphometric methods* compute z_0 and d from the geometry of the obstacles (heights, frontal areas, plan areas, density), and are used where the geometry is known and measurements are not, as over cities and canopies. Table 11.3 compares them. Its columns give

what each method needs, what it returns, its typical error in z_0 (indicative orders of magnitude, not guarantees) and its main limitation.

Table 11.3: Methods of estimating the roughness length. Errors indicative, as a multiplicative factor on z_0.

Method	Needs	Returns	Typical error in z_0	Main limitation
Land-cover classification	land-cover map, lookup table	z_0 (sometimes d) per class	factor 2 to 3, more at mixed sites	no direction, fetch or season unless added by hand
Wind-profile fitting	two or more calibrated heights in the inertial sublayer, neutral periods, sorted by direction	z_0, u_* (with three heights, d)	factor about 1.4 for $\pm 0.1\,\mathrm{m\,s^{-1}}$ on a 10/40 m pair	anemometer error, stability, roughness sublayer
Eddy covariance	sonic anemometer, mean wind at the same height	u_* measured, z_0 inferred	factor about 1.7 for 10 % in u_* (one half-hour)	needs many neutral periods; flux footprint upwind
Morphometric	obstacle heights, frontal and plan areas (survey, laser scanning, building database)	z_0, d by direction	factor about 2; rules differ among themselves	empirical rules; porosity and flexibility of vegetation

The eddy-covariance error follows from equation (11.2): $\ln z_0 = \ln z - \kappa U/u_*$, so a relative error ϵ in u_* changes $\ln z_0$ by about $(\kappa U/u_*)\,\epsilon = \ln(z/z_0)\,\epsilon$. For grass at 10 m, $\ln(10/0.03) = 5.81$, and $\epsilon = \pm 10\,\%$ moves z_0 by a factor of $e^{0.53} = 1.7$ upward or $e^{-0.65} = 0.52$ downward. The roughness length sits in an exponent, and every method that infers it from winds amplifies the errors of those winds; averaging many neutral periods by direction sector is what makes the profile and eddy-covariance methods precise.

A morphometric rule of thumb. For sparse arrays of obstacles, the rule of Lettau gives

$$z_0 \approx 0.5\, h_c\, \lambda_f, \qquad \lambda_f = \frac{A_f}{A_T}, \tag{11.7}$$

with h_c the mean obstacle height and λ_f the frontal area index of Section 11.1.4. It is the dashed line of Figure 11.1(c) and applies only while the elements are sparse, λ_f below about 0.2; for denser arrays it overestimates, because of wake interference and skimming flow. For an illustrative suburb of houses 8 m tall, each presenting a face 10 m wide to the wind and standing on a plot of 20 m × 20 m, $\lambda_f = 80/400 = 0.2$ and $z_0 \approx 0.5 \times 8\,\mathrm{m} \times 0.2 = 0.8\,\mathrm{m}$, inside the suburban range of Table 11.1. Since A_f depends on which faces meet the wind, the rule gives a roughness that depends on direction for elongated buildings or aligned rows. A cruder rule for dense vegetation uses the height alone, $z_0 \approx 0.1\, h_c$ and $d \approx 0.67\, h_c$.

11.6.2 Identifiability from one and from several heights

One measurement cannot determine the roughness length. With $U(10\,\mathrm{m}) = 6\,\mathrm{m\,s^{-1}}$ in neutral air, equation (11.1) is one equation in two unknowns, u_* and z_0, and every pair on the curve $u_* = 0.4 \times 6\,\mathrm{m\,s^{-1}}/\ln(10\,\mathrm{m}/z_0)$ reproduces the measurement: $z_0 = 0.01$ m with $u_* = 0.347\,\mathrm{m\,s^{-1}}$, $z_0 = 0.1$ m with $0.521\,\mathrm{m\,s^{-1}}$, $z_0 = 1.0$ m with $1.042\,\mathrm{m\,s^{-1}}$. The pairs differ by a factor of three in the friction velocity and nine in the stress, and the 10 m wind cannot choose among them. Chapter 10 treats this non-uniqueness for model calibration.

A second height carries the missing information, because the shear depends on the pair. The three pairs above predict 7.20, 7.81 and $9.61\,\mathrm{m\,s^{-1}}$ at 40 m; a measured $U(40\,\mathrm{m})$ selects

one, and with two heights both u_* and z_0 are determined, within the sensitivity to anemometer error of Table 11.3. A direct stress measurement constrains the pair much better: a sonic anemometer reading $u_* = 0.52\,\mathrm{m\,s^{-1}}$ with the same $6\,\mathrm{m\,s^{-1}}$ at 10 m gives, by equation (11.2), $z_0 = 10\,\mathrm{m} \times e^{-0.4\times 6/0.52} = 10\,\mathrm{m} \times e^{-4.62} = 0.099\,\mathrm{m}$. Three or more heights, or a stress measurement plus two heights, are needed when the displacement height is also unknown.

11.6.3 Roughness error as forecast bias

A weather model that consistently underpredicts the observed 10 m wind at a site may have the right large-scale flow and the wrong surface. Suppose the model assigns the site's grid cell $z_0 = 0.5\,\mathrm{m}$ while the true effective roughness for the prevailing directions is 0.05 m, and suppose the model's wind at 100 m, $10\,\mathrm{m\,s^{-1}}$, is correct. By equation (11.3), with $\ln 20 = 2.996$, $\ln 200 = 5.298$ and $\ln 2000 = 7.601$, the model (first line) and the site (second line) give

$$z_0 = 0.5\,\mathrm{m}: \quad u_* = \frac{4}{5.298}\,\mathrm{m\,s^{-1}} = 0.755\,\mathrm{m\,s^{-1}}, \quad U(10\,\mathrm{m}) = \frac{2.996}{5.298}\times 10\,\mathrm{m\,s^{-1}} = 5.65\,\mathrm{m\,s^{-1}};$$
$$z_0 = 0.05\,\mathrm{m}: \quad u_* = \frac{4}{7.601}\,\mathrm{m\,s^{-1}} = 0.526\,\mathrm{m\,s^{-1}}, \quad U(10\,\mathrm{m}) = \frac{5.298}{7.601}\times 10\,\mathrm{m\,s^{-1}} = 6.97\,\mathrm{m\,s^{-1}}.$$

The model's 10 m wind is $1.32\,\mathrm{m\,s^{-1}}$, or 19 %, too low, and its friction velocity 44 % too high. The bias comes from the land-surface representation, not from the synoptic forcing. Correcting it by adjusting the large-scale wind, or by a statistical scaling of the output, would make the 10 m wind right for the wrong reason and leave the stress, the turbulence and the extrapolation to other heights wrong. A bias that depends on wind direction, larger for the sectors whose true roughness differs most from the grid value, points to roughness as its source.

11.6.4 Effective roughness of a grid cell

A weather-model grid cell of 1 km × 1 km may contain forest, roads, grass and buildings, but the model uses one roughness length for it. That value is an *effective roughness*: the roughness length of a uniform surface that would exert the same total stress on the flow at a height above the cell where the patches' influences have merged. It is a grid-scale property, not the roughness at any sensor in the cell.

Averaging roughness is not linear, because what adds up over patches is the stress, the momentum flux, and the stress depends on z_0 through the square of a logarithm. Let the patches have area fractions f_i and roughness lengths $z_{0,i}$, and let z_b be a *blending height*, a height at which the wind is nearly the same over all patches while each patch still carries its own stress. With the common wind $U(z_b)$, patch i carries $\rho\, C_{D,i}(z_b)\, U(z_b)^2$; requiring the effective surface to carry the area-weighted mean stress gives

$$\left[\frac{\kappa}{\ln(z_b/z_{0,\mathrm{eff}})}\right]^2 = \sum_i f_i \left[\frac{\kappa}{\ln(z_b/z_{0,i})}\right]^2, \tag{11.8}$$

an average of drag coefficients, not of roughness lengths. For a cell half forest ($z_0 = 1.0\,\mathrm{m}$, displacement neglected) and half grass ($z_0 = 0.03\,\mathrm{m}$), with $z_b = 60\,\mathrm{m}$,

$$C_D^{\mathrm{forest}} = \left(\frac{0.4}{\ln 60}\right)^2 = 0.00954, \quad C_D^{\mathrm{grass}} = \left(\frac{0.4}{\ln 2000}\right)^2 = 0.00277, \quad \overline{C_D} = 0.00616,$$

$$\ln\frac{60}{z_{0,\mathrm{eff}}} = \frac{0.4}{\sqrt{0.00616}} = 5.10, \qquad z_{0,\mathrm{eff}} = 60\,\mathrm{m} \times e^{-5.10} = 0.37\,\mathrm{m}.$$

The arithmetic mean of the two roughness lengths is 0.515 m; their geometric mean, the average of $\ln z_0$, is 0.17 m. The effective value lies between them. The choice of z_b matters little: 40, 100 and 200 m give 0.39, 0.35 and 0.33 m.

Figure 11.7 shows the effective roughness as the forest fraction of the cell varies. The horizontal axis is the forest fraction from 0 to 1, the vertical axis the roughness length on a logarithmic scale. The solid curve is equation (11.8) with $z_b = 60\,\mathrm{m}$; the dashed and dotted curves are the arithmetic and geometric means.

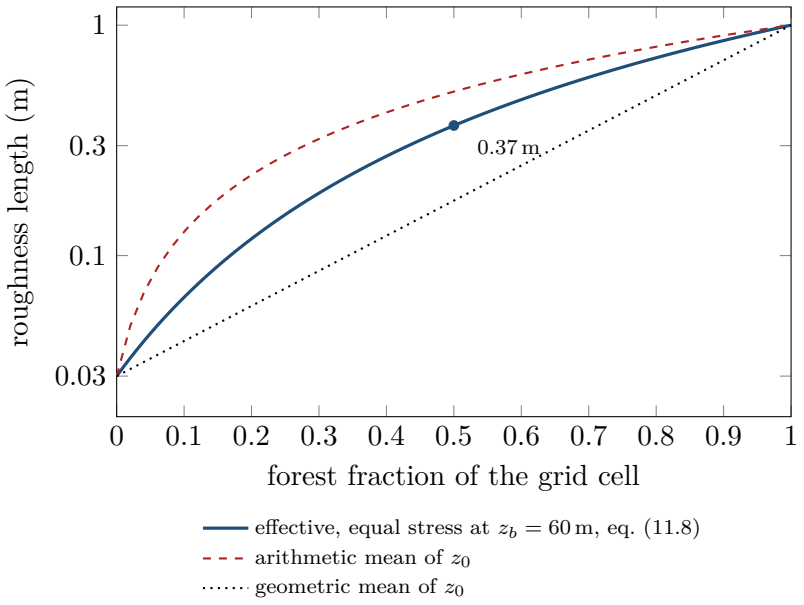


Figure 11.7: Effective roughness length of a grid cell of forest ($z_0 = 1.0\,\mathrm{m}$) and grass ($z_0 = 0.03\,\mathrm{m}$) against the forest fraction: equal area-weighted stress at a blending height of 60 m (solid, equation (11.8), $\kappa = 0.4$, displacement neglected), the arithmetic mean (dashed) and the geometric mean (dotted). Point: the half-and-half case. Values illustrative.

The effective roughness rises quickly with the first patches of forest: a quarter of forest already gives 0.15 m, five times the grass value, because the rough patches carry a disproportionate share of the stress. Between the two pure cases the geometric mean underestimates it and the arithmetic mean overestimates it. A model that averages $\ln z_0$ over the land-cover classes in a cell gives the cell less drag than its patches exert together.

11.6.5 Representativeness and roughness correction

A model cell with $z_{0,\mathrm{model}} = 0.3\,\mathrm{m}$ may contain a sensor in an open corridor where the local roughness is $z_{0,\mathrm{local}} = 0.03\,\mathrm{m}$. The model's 10 m wind and the measured 10 m wind are then not strictly comparable: the model gives the wind over the effective surface of the cell, the sensor the wind over its own exposure. This is a problem of *representativeness*, the degree to which a point measurement stands for the area a model value describes, and it recurs in every comparison of grid-cell and point winds. Before a model is judged against a station, the exposure of the station has to be accounted for.

The usual tool is a *roughness correction*. If the friction velocity is the same over both surfaces, dividing equation (11.1) written for surface 2 by the same equation for surface 1 gives

$$\frac{U_2(z)}{U_1(z)} = \frac{\ln[(z-d_2)/z_{0,2}]}{\ln[(z-d_1)/z_{0,1}]}, \tag{11.9}$$

with d_1 and d_2 the displacement heights of the two surfaces. For a model wind of $5.0\,\mathrm{m\,s^{-1}}$ at 10 m over $z_{0,1} = 0.3\,\mathrm{m}$, converted to the open corridor, $z_{0,2} = 0.03\,\mathrm{m}$, both with zero displacement,

$$U_2(10\,\mathrm{m}) = 5.0\,\mathrm{m\,s^{-1}} \times \frac{\ln 333}{\ln 33.3} = 5.0\,\mathrm{m\,s^{-1}} \times \frac{5.809}{3.507} = 8.28\,\mathrm{m\,s^{-1}}.$$

The same-friction-velocity assumption is often poor, and this example shows by how much. A local patch of smoother ground under the same flow does not keep the stress of the rougher surroundings: its stress falls, as Section 11.2.2 showed. If instead the wind is taken as common at a blending height, 60 m here, and each surface carries its own u_*, equation (11.3) applied to each surface gives

$$\frac{U_2(10\,\mathrm{m})}{U_1(10\,\mathrm{m})} = \frac{\ln(10/0.03)/\ln(60/0.03)}{\ln(10/0.3)/\ln(60/0.3)} = \frac{5.809/7.601}{3.507/5.298} = \frac{0.764}{0.662} = 1.155,$$

and $U_2(10\,\mathrm{m}) = 5.77\,\mathrm{m\,s^{-1}}$. The two corrections differ by a factor of 1.43: 66 % against 15 %. The same-u_* form is the right one only when the stress really is shared, for example when correcting between two heights or two instruments over the same surface; for a change of exposure under a common flow, the form with a common wind aloft is the better approximation, and it too assumes neutral air, a well-chosen blending height and a fetch long enough for the local surface to have set its own stress. Every roughness correction is to be applied with its assumption stated.

11.6.6 Effective roughness as a conditional description

The results of the chapter replace a lookup by a conditional statement. Not "grass has $z_0 = 0.03\,\mathrm{m}$", but: for this wind direction, this season, this obstacle geometry, this fetch and this measurement height, the surface behaves approximately like a homogeneous aerodynamic surface with an effective roughness length z_0, and with a displacement height d if the obstacles are tall. Each condition in the statement corresponds to a section of the chapter: the direction to the roughness rose, the season to the growth of vegetation, the geometry to the frontal area index, the fetch to the internal boundary layer, and the height to the roughness and inertial sublayers.

The conditional form also states what the roughness length is for. It is a parameter of the logarithmic profile, valid where that profile is valid, and it carries the surface's drag into every quantity computed from the profile: the stress, the drag coefficient, the wind at another height and the wind over another exposure. How the profile itself is used to move a wind between heights, and where it stops being valid, is the subject of Chapter 12.

11.7 What to retain

Definition 11.1 (Aerodynamic roughness length)**.** The aerodynamic roughness length z_0 is not the physical height of the obstacles; it is an effective measure of how strongly a surface modifies momentum transport, defined as the height above the zero plane at which the neutral logarithmic profile extrapolates to zero, and it depends on wind direction, fetch, surface geometry, season and flow regime.

Table 11.4 lists the terms of the chapter, their meaning, their units and the subsection that defines each.

11.8 Exercises

Exercise 11.1. An urban district has buildings of mean height $h_c = 12\,\mathrm{m}$, each presenting a face 15 m wide to the wind and standing on a plot of $30\,\mathrm{m} \times 30\,\mathrm{m}$. (a) Compute the frontal area index and the roughness length from the rule of equation (11.7), and say whether the rule applies. (b) Take $d = 7.2\,\mathrm{m}$ and $u_* = 0.6\,\mathrm{m\,s^{-1}}$ in neutral air. Compute the wind at 50 m above the ground with and without the displacement height, and the drag coefficient at 50 m. (c) A sensor on a 20 m roof mast reads the wind at 32 m above the ground. Is it likely to be in the inertial sublayer? Give the range of roughness-sublayer depths for this district.

Table 11.4: The terms of the chapter and where each is defined.

Term	Meaning	Units	Defined in
Aerodynamic roughness length z_0	height above the zero plane at which the neutral log profile extrapolates to zero; measure of surface drag, $z_0 = (z-d)\exp(-\kappa/\sqrt{C_D})$	m	11.1.1
Obstacle height h_c	mean height of the surface elements (canopy height); z_0 is typically 0.03 to 0.15 h_c	m	11.1.2
Frontal area index λ_f	frontal area of the obstacles facing the wind per unit ground area	–	11.1.4
Zero-plane displacement d	height of the apparent ground of the log profile; the mean level of momentum absorption in a canopy, about 0.7 h_c	m	11.3.1
Roughness sublayer	layer above the obstacles, about 2 to 5 h_c deep, where individual wakes make the flow heterogeneous and the log law may fail	m (depth)	11.3.4
Inertial sublayer	layer above the roughness sublayer where the flow sees only the aggregate z_0 and d and the log law holds	m (depth)	11.3.4
Directional roughness $z_0(\beta)$	roughness length of a site as a function of the upwind direction; plotted as a roughness rose	m	11.4.1
Fetch	upwind distance over which the air has crossed a given surface	m	11.4.2
Internal boundary layer	layer adjusted to a new surface, growing with distance downwind of a roughness change	m (depth δ)	11.4.2
Charnock relation	roughness of water, $z_0 = \alpha_c u_*^2/g$, $\alpha_c \approx 0.011$ to 0.018; plus $0.11\,\nu/u_*$ in light wind	m	11.4.3
Effective roughness	roughness of a uniform surface that exerts the same total stress as a mixed area; a grid-scale property	m	11.6.4
Morphometric roughness	z_0 and d computed from obstacle geometry, e.g. $z_0 \approx 0.5\,h_c\,\lambda_f$ for sparse arrays	m	11.6.1
Roughness correction	conversion of a wind between two exposures by the ratio of log-profile factors, with a stated assumption on u_*	–	11.6.5

Exercise 11.2. A coastal station records $U_{10} = 10\,\mathrm{m\,s^{-1}}$ over the sea in neutral air. (a) Iterate the Charnock relation with the viscous term, starting from $z_0 = 10^{-4}\,\mathrm{m}$, with $\alpha_c = 0.011$, and give z_0, u_* and C_D at 10 m after convergence. (b) Repeat with $\alpha_c = 0.018$ for young waves in an offshore wind with short fetch. (c) By what fraction does the stress differ between (a) and (b)? (d) The same $10\,\mathrm{m\,s^{-1}}$ blows over short grass with $z_0 = 0.03\,\mathrm{m}$. Compute C_D and the ratio of the grass stress to the sea stress of (a).

Exercise 11.3. A weather station at 25°S has the roughness rose of Figure 11.4. The geostrophic wind blows from 60° and the surface wind is turned from it by 25° toward low pressure. (a) On which side of the geostrophic flow does the low pressure lie, and from which direction does the surface wind blow? Which roughness sector applies? (b) With $9\,\mathrm{m\,s^{-1}}$ at 100 m in neutral air, compute u_* and U_{10} for that sector. (c) Repeat (a) and (b) for the same station geometry at 25°N. (d) By what percentage does U_{10} differ between the two hemispheres, and why does the difference not come from the Coriolis force acting on the 10 m wind directly?

Exercise 11.4. A 1 km grid cell is 30 % forest ($z_0 = 1.0\,\mathrm{m}$) and 70 % grass ($z_0 = 0.03\,\mathrm{m}$); displacement heights are neglected. (a) Compute the effective roughness with equation (11.8) and $z_b = 60\,\mathrm{m}$, and compare it with the arithmetic and geometric means. (b) The model gives $U_{10} = 5.5\,\mathrm{m\,s^{-1}}$ for the cell. A station in the cell stands in an open grass corridor. Convert the model wind to the station's exposure with equation (11.9) and with the common-wind-at-60 m form of Section 11.6.5. (c) The station measures $6.3\,\mathrm{m\,s^{-1}}$ on average in neutral conditions. Which correction makes the model look unbiased, and which assumption behind it is more defensible for this station? (d) Name one measurement at the station that would test the answer to (c).

Chapter 12

The Logarithmic Wind Profile

12.1 The logarithmic profile and its origin

Chapter 7 derived the neutral logarithmic wind profile from a constant momentum flux and a mixing length that grows with height, and Chapter 11 described the two surface parameters that enter it, the roughness length and the displacement height. This chapter is about using the profile: carrying a measured wind from one height to another, comparing it with the power law that engineering practice often uses in its place, stating where it holds, reading the evidence when measurements refuse to fit it, and recognizing it inside the output of a weather model. The question of the chapter is

why does the mean wind often increase logarithmically with height near the surface, and under which conditions can that profile be used to move a wind from one height to another?

The profile is

$$U(z) = \frac{u_*}{\kappa} \ln \frac{z - d}{z_0}, \tag{12.1}$$

with the friction velocity u_*, the von Kármán constant $\kappa \approx 0.4$, the displacement height d and the roughness length z_0. It holds only under specific assumptions, and the aim of the chapter is the equation together with its limits. The first section restates its derivation compactly, explains why the function is a logarithm, shows what each of its three controlling quantities does, and works it through with numbers.

Jargon: logarithmic wind profile, wind shear, wind extrapolation, equilibrium surface layer, representativeness

The *logarithmic wind profile* (log law) is equation (12.1): the mean wind speed U (m/s) in a neutral surface layer as a function of height, increasing with the logarithm of the height above the displacement height. *Wind shear* is the rate of change of the mean wind with height, $\partial U/\partial z$, in s^{-1}; in wind-energy usage the word also names the speed difference between two heights or the exponent of the power law of Section 12.3.1, and this chapter states which is meant. *Wind extrapolation* is the estimation of the mean wind at a height where it was not measured from the wind measured at another height, through an assumed profile; upward extrapolation, from a 10 m station to a 100 m hub, is the common case. An *equilibrium surface layer* is a surface layer whose turbulence and mean profile are in balance with the local surface and the local fluxes: the flow is stationary, horizontally homogeneous over a long enough fetch, and the flux is nearly constant with height, so that the profile depends only on u_*, z_0, d and the stability. *Representativeness* is the degree to which a measured or modeled value stands for the quantity it is used for: whether a wind measured at one point and height, or reported for a grid cell, describes the wind at the place, height, area and averaging time of the application.

Key idea

In a neutral equilibrium surface layer the surface stress fixes the velocity scale u_* and the distance from the effective surface fixes the size of the eddies, so the shear is $u_*/[\kappa(z-d)]$ and the profile is a logarithm. The profile is a consequence of that turbulence structure; it is reliable exactly as far as the atmosphere behaves as a stationary, homogeneous, constant-flux surface layer, and every use of it, from extrapolation to the 10 m wind of a weather model, inherits that condition.

12.1.1 The profile from constant stress and the mixing length

The derivation has four steps, each stated in full in Chapter 7; here they are written with the displacement height from the start.

Constant stress. In the surface layer the turbulent stress changes little with height, $\tau(z) \approx \tau_0$, so the kinematic momentum flux equals its surface value at every height of the layer,

$$-\overline{u'w'} = u_*^2, \tag{12.2}$$

and the friction velocity is constant with height. Under neutral stability the turbulence that carries this flux is generated mechanically, by the shear, and buoyancy plays no part.

Mixing length. The eddies that carry the flux are limited in size by their distance from the surface that absorbs the momentum. Over tall, dense obstacles that surface is raised to the displacement height, and the mixing length is

$$l = \kappa\,(z-d), \tag{12.3}$$

so that the closer a point is to the effective surface, the smaller the eddies that fit.

Flux and shear. Prandtl's mixing-length relation ties the flux to the shear, $-\overline{u'w'} = l^2\,(\partial U/\partial z)^2$ for $\partial U/\partial z > 0$. Substituting equations (12.2) and (12.3),

$$u_*^2 = \kappa^2\,(z-d)^2 \left(\frac{\partial U}{\partial z}\right)^2,$$

and taking the positive square root,

$$\frac{\partial U}{\partial z} = \frac{u_*}{\kappa\,(z-d)}. \tag{12.4}$$

Integration. Since u_* does not depend on height, equation (12.4) integrates to

$$U(z) = \frac{u_*}{\kappa}\,\ln(z-d) + C.$$

The constant is fixed by requiring $U = 0$ at $z - d = z_0$, which gives $C = -(u_*/\kappa)\ln z_0$ and hence equation (12.1). The condition is a definition of z_0, not a statement that the real wind vanishes at that height; a later subsection, Section 12.4.3, returns to the difference.

12.1.2 Why a logarithm

The logarithm is not an empirical curve chosen because it fits measurements. It follows from two physical statements: the momentum flux is constant with height, and the mixing length is proportional to the distance from the effective surface. Together they give a shear inversely proportional to that distance, $\partial U/\partial z \propto 1/(z-d)$, and the function whose derivative is $1/(z-d)$ is $\ln(z-d)$. Chapter 7 reached the same shear by dimensional analysis alone: in a neutral surface layer the only quantities that can set the shear are u_* and the height, and the only combination of them with units of s^{-1} is u_*/z times a constant.

The shape has a direct reading. The shear is strongest near the surface and decreases with height; the wind keeps increasing, but more and more slowly. Equal ratios of height add equal increments of wind: between heights z_1 and z_2 above the displacement height, the increase is $(u_*/\kappa)\ln[(z_2-d)/(z_1-d)]$, which depends only on the ratio of the two heights. Every doubling of height adds $(u_*/\kappa)\ln 2 = 0.69\,u_*/\kappa$, whether it is from 1 to 2 m or from 50 to 100 m.

12.1.3 The three controlling quantities

Equation (12.1) has three parameters, and each does a different thing to the profile.

- The friction velocity u_* is the velocity scale. It multiplies the whole profile: a larger u_* gives a larger shear at every height and, for a fixed z_0, a higher wind at every height.
- The roughness length z_0 is the aerodynamic roughness of the surface. At a fixed u_* it shifts the profile without changing its shear: a rougher surface gives a lower wind at every height.
- The displacement height d shifts the origin of the height coordinate upward, over tall canopies and cities; it moves the whole profile up by d and matters most near the obstacles.

Figure 12.1 varies each in turn from a common illustrative baseline, $u_* = 0.4\,\mathrm{m\,s^{-1}}$, $z_0 = 0.05\,\mathrm{m}$, $d = 0$. All three panels have the wind speed on the horizontal axis and the height above the ground on a linear vertical axis from 0 to 100 m. Panel (a) varies the friction velocity, 0.2, 0.4 and $0.6\,\mathrm{m\,s^{-1}}$, at $z_0 = 0.05\,\mathrm{m}$. Panel (b) varies the roughness length, 0.01, 0.05 and 0.5 m, at $u_* = 0.4\,\mathrm{m\,s^{-1}}$. Panel (c) varies the displacement height, 0, 5 and 10 m, at $u_* = 0.4\,\mathrm{m\,s^{-1}}$ and $z_0 = 0.5\,\mathrm{m}$, a roughness typical of the tall obstacles that produce a displacement.

In panel (a) the three profiles start from zero at the same height, z_0, and fan out: the friction velocity scales the whole curve, so at 100 m the winds are 3.8, 7.6 and $11.4\,\mathrm{m\,s^{-1}}$, in the ratio $1:2:3$ of the friction velocities, and the shear at each height is in the same ratio. In panel (b) the profiles are the same curve displaced sideways: at a fixed u_* the shear $u_*/(\kappa z)$ does not depend on z_0, and each profile has the same increase of wind between any two heights, while the rough surface sits $3.9\,\mathrm{m\,s^{-1}}$ to the left of the smooth one ($\ln(0.5/0.01) = 3.91$). In panel (c) the profiles are the same curve displaced upward by d: at 100 m they differ by only $0.1\,\mathrm{m\,s^{-1}}$, 5.30, 5.25 and $5.19\,\mathrm{m\,s^{-1}}$, but at 20 m they read 3.69, 3.40 and $3.00\,\mathrm{m\,s^{-1}}$. The displacement height matters near the obstacles and fades aloft, the roughness length shifts the whole profile, and the friction velocity scales it.

12.1.4 A worked profile

Take $u_* = 0.4\,\mathrm{m\,s^{-1}}$, $z_0 = 0.05\,\mathrm{m}$ and $d = 0$, the baseline of Figure 12.1. Then $u_*/\kappa = 1\,\mathrm{m\,s^{-1}}$ and the profile is simply

$$U(z) = 1\,\mathrm{m\,s^{-1}} \times \ln\frac{z}{0.05\,\mathrm{m}}.$$

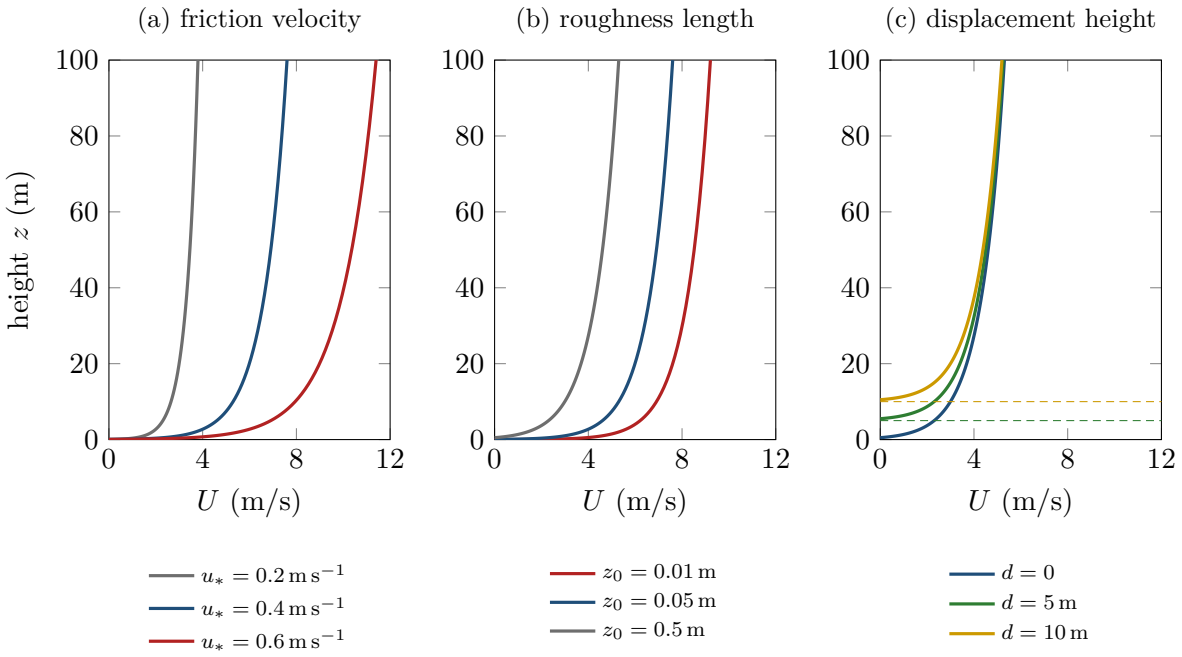


Figure 12.1: The three controlling quantities of the neutral profile $U = (u_*/\kappa)\ln[(z-d)/z_0]$, $\kappa = 0.4$, varied one at a time (illustrative values). (a) $z_0 = 0.05\,\mathrm{m}$, $d = 0$ and three friction velocities. (b) $u_* = 0.4\,\mathrm{m\,s^{-1}}$, $d = 0$ and three roughness lengths. (c) $u_* = 0.4\,\mathrm{m\,s^{-1}}$, $z_0 = 0.5\,\mathrm{m}$ and three displacement heights, marked by dashed lines of the same color.

At four heights,

$$U(2\,\mathrm{m}) = \ln 40 \approx 3.69\,\mathrm{m\,s^{-1}}, \qquad U(10\,\mathrm{m}) = \ln 200 \approx 5.30\,\mathrm{m\,s^{-1}},$$
$$U(50\,\mathrm{m}) = \ln 1000 \approx 6.91\,\mathrm{m\,s^{-1}}, \quad U(100\,\mathrm{m}) = \ln 2000 \approx 7.60\,\mathrm{m\,s^{-1}}.$$

Table 12.1 lists these values with the increase from the height below, the increase per meter of height, the mixing length κz and the shear $u_*/(\kappa z)$.

Table 12.1: The worked neutral profile, $u_* = 0.4\,\mathrm{m\,s^{-1}}$, $z_0 = 0.05\,\mathrm{m}$, $d = 0$, $\kappa = 0.4$, so that $U = \ln(z/0.05\,\mathrm{m})$ in m/s (illustrative).

Height z (m)	U (m/s)	Increase from the height below (m/s)	Increase per meter of height (m/s)	$l = \kappa z$ (m)	$\partial U/\partial z$ ($\mathrm{s^{-1}}$)
2	3.69	–	–	0.8	0.50
10	5.30	1.61	0.20	4	0.10
50	6.91	1.61	0.040	20	0.020
100	7.60	0.69	0.014	40	0.010

From 2 to 10 m the wind increases by $1.6\,\mathrm{m\,s^{-1}}$ over 8 m; from 50 to 100 m it increases by only $0.7\,\mathrm{m\,s^{-1}}$ over 50 m. The increase per meter falls from 0.20 to $0.014\,\mathrm{m\,s^{-1}}$ per meter, a factor of fourteen. The increments are diminishing, but they are not zero: from 10 to 50 m the wind still gains the same $1.61\,\mathrm{m\,s^{-1}}$ as from 2 to 10 m, because both intervals span a factor of five in height. The table also shows why the shear falls: the eddies that carry the same flux, $u_*^2 = 0.16\,\mathrm{m^2\,s^{-2}}$ at every height, grow from 0.8 to 40 m, and larger eddies need a weaker gradient to carry it.

Principle 12.1. *The logarithmic profile is the consequence of a constant momentum flux carried by eddies whose size is proportional to the distance from the effective surface. The friction velocity scales it, the roughness length shifts it, the displacement height moves its origin, and equal ratios of height add equal increments of wind.*

12.2 Extrapolation between heights

The most common use of the profile is to carry a wind measured at one height to another. This section derives the ratio formula that does so without the friction velocity, works an example, and computes how much the result depends on the assumed roughness length and on whether a displacement height is included.

12.2.1 The height ratio

Write equation (12.1) at two heights z_1 and z_2 and divide one by the other. The factor u_*/κ is the same at both heights and cancels:

$$\frac{U(z_2)}{U(z_1)} = \frac{\ln\!\left[(z_2 - d)/z_0\right]}{\ln\!\left[(z_1 - d)/z_0\right]}. \tag{12.5}$$

The friction velocity, which is rarely measured, is not needed. A wind measured at z_1 gives the wind at z_2 as soon as z_0 and d are known and the conditions are neutral. These are the three things the ratio still depends on, and each is an assumption: z_0 and d must describe the surface upwind of the site in the direction of the wind (Chapter 11), and the air must be neutral, or the ratio must be corrected for stability (Section 12.4.1). The ratio also requires that both heights lie in the same equilibrium surface layer, which Section 12.4.5 makes precise.

12.2.2 Extrapolation from 10 to 40 meters

Let an anemometer at 10 m over farmland read $U(10\,\mathrm{m}) = 6\,\mathrm{m\,s^{-1}}$ in neutral conditions, with $z_0 = 0.1\,\mathrm{m}$ and $d = 0$. The wind at 40 m follows from equation (12.5):

$$U(40\,\mathrm{m}) = 6\,\mathrm{m\,s^{-1}} \times \frac{\ln(40/0.1)}{\ln(10/0.1)} = 6\,\mathrm{m\,s^{-1}} \times \frac{\ln 400}{\ln 100} = 6\,\mathrm{m\,s^{-1}} \times \frac{5.99}{4.61} \approx 7.8\,\mathrm{m\,s^{-1}}.$$

The same formula gives $U(100\,\mathrm{m}) = 6 \times \ln 1000/\ln 100 = 6 \times 1.5 = 9.0\,\mathrm{m\,s^{-1}}$. Quadrupling the height raises the wind by 30 %; ten times the height raises it by 50 %. The friction velocity is implied, $u_* = 0.4 \times 6/4.61 = 0.52\,\mathrm{m\,s^{-1}}$, but it was never used.

12.2.3 Sensitivity to the assumed roughness length

The roughness length is the parameter most often guessed: read from a land-cover class or a table, it is commonly uncertain by a factor of two or three. Repeat the extrapolation with z_0 three times smaller, 0.033 m, and three times larger, 0.3 m:

$$\begin{aligned}
z_0 = 0.033\,\mathrm{m}: \qquad U(40\,\mathrm{m}) &= 6\,\mathrm{m\,s^{-1}} \times \frac{\ln 1200}{\ln 300} = 6 \times \frac{7.09}{5.70} = 7.46\,\mathrm{m\,s^{-1}},\\
U(100\,\mathrm{m}) &= 6\,\mathrm{m\,s^{-1}} \times \frac{\ln 3000}{\ln 300} = 6 \times \frac{8.01}{5.70} = 8.42\,\mathrm{m\,s^{-1}};\\
z_0 = 0.3\,\mathrm{m}: \qquad U(40\,\mathrm{m}) &= 6\,\mathrm{m\,s^{-1}} \times \frac{\ln 133}{\ln 33.3} = 6 \times \frac{4.89}{3.51} = 8.37\,\mathrm{m\,s^{-1}},\\
U(100\,\mathrm{m}) &= 6\,\mathrm{m\,s^{-1}} \times \frac{\ln 333}{\ln 33.3} = 6 \times \frac{5.81}{3.51} = 9.94\,\mathrm{m\,s^{-1}}.
\end{aligned}$$

Against the 7.81 and 9.00 m s^{-1} of the base case, a factor of three in z_0 changes the 40 m wind by -4.5 and $+7.2$ % and the 100 m wind by -6.4 and $+10.4$ %. The power carried by the wind through a unit area, $\frac{1}{2}\rho U^3$, scales with the cube of the speed, so at 100 m it changes by factors of 0.82 and 1.35.

Figure 12.2 draws the dependence. The horizontal axis is the assumed roughness length on a logarithmic scale from 0.01 to 1 m; the vertical axis is the extrapolated wind. The two curves are the extrapolated winds at 40 and 100 m from the same 6 m s^{-1} at 10 m; the dotted line is the measured 6 m s^{-1}, and the shaded band is the factor-of-three range around $z_0 = 0.1$ m, with the three computed values marked on each curve.

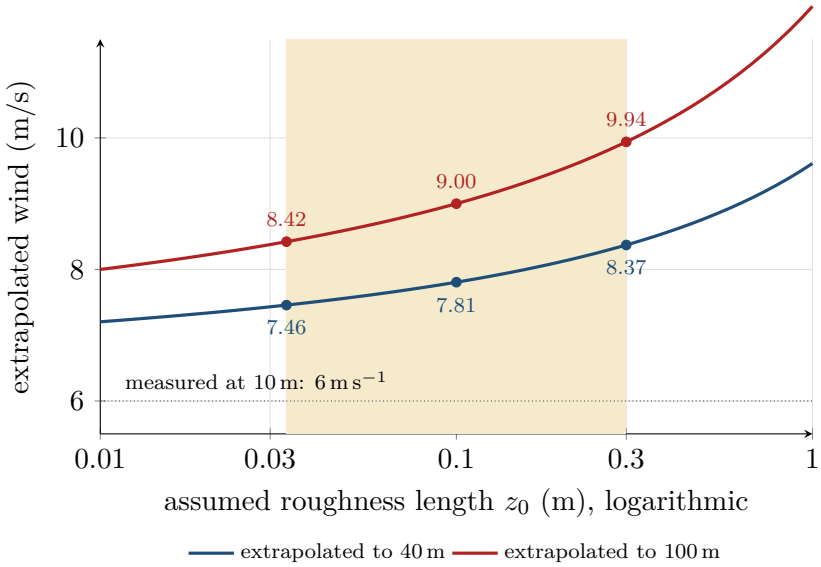


Figure 12.2: Neutral extrapolation of a 10 m wind of 6 m s^{-1} to 40 and 100 m, $U(z_2) = U(10\,\mathrm{m})\ln(z_2/z_0)/\ln(10\,\mathrm{m}/z_0)$ (equation (12.5) with $d = 0$), as a function of the assumed roughness length. Shaded: a factor of three either way of the illustrative $z_0 = 0.1$ m.

Both curves rise with z_0: a rougher surface implies more shear for the same 10 m wind, so more wind aloft. The 100 m curve is steeper than the 40 m curve, because the error grows with the distance of the extrapolation. The curves are also steeper on the right than on the left: the dependence on z_0 enters through $\ln(10\,\mathrm{m}/z_0)$ in the denominator, which shrinks as z_0 grows, so an overestimated roughness costs more than an underestimated one. Over the shaded band the dependence is moderate, because z_0 enters through a logarithm; a factor of three in z_0 is worth less than 10 % in the wind at 100 m, but cubed it is worth a third of the wind power.

12.2.4 Ignoring a displacement height

Over a forest or a city the displacement height is often left out, either because it is unknown or because a land-cover table supplies only a roughness length. Take the illustrative forest of Chapter 7: canopy height $h_c = 20$ m, $d = 14$ m, $z_0 = 2$ m and $u_* = 0.8$ m s^{-1}, with a mast at 40 m, twice the canopy height and so at the lower edge of the height range where the log law applies above a forest. The mast reads $U(40\,\mathrm{m}) = 2\ln(26/2) = 5.13$ m s^{-1}. With the displacement height, the wind at 100 m is

$$U(100\,\mathrm{m}) = 5.13\,\mathrm{m\,s^{-1}} \times \frac{\ln[(100-14)/2]}{\ln[(40-14)/2]} = 5.13\,\mathrm{m\,s^{-1}} \times \frac{\ln 43}{\ln 13} = 5.13 \times \frac{3.76}{2.56} = 7.52\,\mathrm{m\,s^{-1}}.$$

Without it, with the same z_0,

$$U(100\,\mathrm{m}) = 5.13\,\mathrm{m\,s^{-1}} \times \frac{\ln(100/2)}{\ln(40/2)} = 5.13 \times \frac{3.91}{3.00} = 6.70\,\mathrm{m\,s^{-1}},$$

10.9 % too low, and the wind power at 100 m is underestimated by a factor of $(6.70/7.52)^3 = 0.71$, about 29 %. The sign follows from the geometry. Counting heights from the ground instead of from the zero plane makes the measurement height look farther from the effective surface than it is, 40 instead of 26 m, where the profile is flatter, so the profile is extrapolated upward with too little shear. The error is largest when the measurement is close to the canopy and the target far above it, which is the usual geometry of a short mast in a forested wind-energy site.

Principle 12.2. *The ratio of the winds at two heights removes the friction velocity but not the roughness length, the displacement height or the stability. Its error grows with the distance of the extrapolation and, through the cube of the speed, is tripled in the wind power.*

12.3 The power law

Engineering practice often replaces the logarithmic profile by a power of height. This section defines the power law, compares the two laws, states what the exponent represents, derives the exponent that makes a power law agree with a log profile between two heights, shows why the fixed exponent 1/7 is dangerous on a stable night, and explains why a power law can still fit measurements well over a limited range.

12.3.1 Definition

The *power law* (power-law wind profile) is

$$U(z) = U(z_r)\left(\frac{z}{z_r}\right)^{\alpha}, \tag{12.6}$$

where z_r (m) is a *reference height* at which the wind is known, usually the height of a measurement, and α (dimensionless) is the *wind-shear exponent*, often called simply the shear exponent. The value $\alpha = 1/7 \approx 0.143$ gives the *one-seventh power law*, a long-standing default in wind engineering. Given winds at two heights, the exponent they imply is

$$\alpha = \frac{\ln\left[U(z_2)/U(z_1)\right]}{\ln(z_2/z_1)}, \tag{12.7}$$

which follows from taking the logarithm of equation (12.6) written at z_2 with $z_r = z_1$. The power law is convenient: one parameter, no roughness length, no friction velocity, and a closed form that is easy to invert and to integrate over a rotor. It is also more empirical: it is not derived from any statement about the flux or the turbulence.

12.3.2 Two laws compared

Table 12.2 compares the two laws point by point. Its columns give the logarithmic and the power law; its rows give the origin of each, its parameters, how it treats roughness and stability, its behavior near the ground and aloft, its link to the surface stress, and where each is typically used.

The log law is tied to the surface stress, includes roughness explicitly and connects directly to surface-layer theory, including its stability corrections. The power law is simple and convenient, and it often fits observations over a limited range of heights well, but its exponent is not universal. The rest of this section makes the second statement quantitative.

Table 12.2: The logarithmic profile and the power law compared.

Aspect	Logarithmic profile	Power law
Origin	derived from constant flux and a mixing length (surface-layer theory)	empirical curve, no derivation
Parameters	u_*, z_0, d; L_O when corrected for stability	α and a reference wind $U(z_r)$
Roughness	explicit, through z_0 and d	implicit, absorbed into α
Stability	explicit correction ψ_m, from surface-layer theory	absorbed into α, which must be refitted
Near the ground	falls to zero at $z - d = z_0$, steep shear	falls to zero at $z = 0$, too little shear close to the ground
Aloft	keeps growing as $\ln z$; not valid above the surface layer	keeps growing as z^α, faster than $\ln z$
Surface stress	tied to it: the slope is u_*/κ	none
Exponent	local exponent varies with height and z_0	one exponent for all heights
Typical use	surface-layer analysis, weather-model surface schemes, extrapolation with known z_0	wind-resource and structural engineering, quick extrapolation, fits to mast data

12.3.3 What the exponent represents

The exponent measures shear in relative terms. From equation (12.6), $\alpha = \mathrm{d}\ln U/\mathrm{d}\ln z = (z/U)\,\partial U/\partial z$: it is the fractional increase of wind per fractional increase of height. A large α means strong shear, a wind that grows quickly with height; a small α means a flat profile. A 10 % increase in height raises the wind by about 1.4 % for $\alpha = 0.14$ and by about 4 % for $\alpha = 0.4$.

Because it measures shear, the exponent inherits everything that controls shear. Approximately, unstable air, in which buoyancy enhances the mixing, gives a small exponent; neutral air a moderate one; stable air, in which buoyancy suppresses the mixing, a large one. Roughness matters too: a rougher surface extracts more momentum and steepens the profile, which raises the exponent. And for a log-like profile the exponent falls with height, so the height range over which it is measured matters. In short,

$$\alpha = \text{a function of stability, roughness and height range,}$$

and a single number stands for all three only in one particular state.

12.3.4 The exponent equivalent to a log profile

Chapter 7 derived the local exponent of the neutral profile, the exponent of the power law tangent to it at one height, $1/\ln(z/z_0)$. For extrapolation the relevant number is different: the exponent of the power law that passes through the log profile at two heights z_1 and z_2. Equating the power-law ratio $(z_2/z_1)^\alpha$ with the log-law ratio of equation (12.5) at $d = 0$ and taking logarithms,

$$\alpha_{\mathrm{eq}}(z_1, z_2) = \frac{\ln\left[\ln(z_2/z_0)/\ln(z_1/z_0)\right]}{\ln(z_2/z_1)}, \tag{12.8}$$

with $z - d$ in place of z where a displacement height applies. The equivalent exponent depends on z_0 and on both heights, and not on the wind speed. It lies between the local exponents at z_1 and z_2: for $z_0 = 0.1\,\mathrm{m}$ these are 0.217 at 10 m and 0.145 at 100 m, and the equivalent exponent between the two heights is 0.176.

Table 12.3 evaluates equation (12.8) for seven roughness lengths, from open water to forest, over three height ranges: 10 to 50 m, 10 to 100 m (station to hub) and 50 to 150 m (across a large rotor).

Table 12.3: Power-law exponent equivalent to the neutral log profile between two heights, equation (12.8), $d = 0$. Surface descriptions are indicative.

Surface	z_0 (m)	10 to 50 m	10 to 100 m	50 to 150 m
Open water	0.0002	0.086	0.084	0.077
Smooth open land	0.01	0.130	0.125	0.110
Short grass	0.03	0.152	0.145	0.126
Farmland	0.05	0.165	0.157	0.134
Cropland	0.1	0.186	0.176	0.148
Shrubs, scattered trees	0.3	0.235	0.219	0.177
Forest	1.0	0.329	0.301	0.225

Two patterns stand out. Down each column, the exponent grows with roughness, from 0.08 over water to 0.3 over forest; across each row, it falls as the height range moves up. Even in strictly neutral air, therefore, no single exponent fits all surfaces and all height ranges. The value 1/7 between 10 and 100 m corresponds to $z_0 \approx 0.027$ m, short grass; over farmland it is already too small, and over water too large.

12.3.5 Why one-seventh is dangerous

As a rough first approximation, the one-seventh law is acceptable. It is dangerous because it hides the roughness, the stability, the fetch and the regime of the flow behind a constant, and stability alone can move the true exponent far from 0.143: a stable night may have much stronger shear, a convective afternoon much less.

To quantify it, take a 10 m anemometer over farmland, $z_0 = 0.05$ m, $d = 0$, reading $U(10\,\mathrm{m}) = 5\,\mathrm{m\,s^{-1}}$, and a wind turbine hub at 100 m. Let the night be stable with an illustrative Obukhov length $L_O = 200$ m, a length scale defined in Chapter 14 that is positive in stable air, with the standard stable correction of Section 12.4.1, $\psi_m = -5\,z/L_O$. The profile is then $U(z) = (u_*/\kappa)[\ln(z/z_0) + 5\,z/L_O]$, and the ratio of the hub wind to the 10 m wind is

$$\frac{U(100\,\mathrm{m})}{U(10\,\mathrm{m})} = \frac{\ln 2000 + 5 \times 100/200}{\ln 200 + 5 \times 10/200} = \frac{7.601 + 2.5}{5.298 + 0.25} = \frac{10.10}{5.548} = 1.821,$$

so $U(100\,\mathrm{m}) = 9.10\,\mathrm{m\,s^{-1}}$, and by equation (12.7) the true exponent is $\ln 1.821/\ln 10 = 0.26$. The one-seventh law gives

$$U(100\,\mathrm{m}) = 5\,\mathrm{m\,s^{-1}} \times 10^{1/7} = 5 \times 1.390 = 6.95\,\mathrm{m\,s^{-1}},$$

24 % too low. The available wind power, $\frac{1}{2}\rho U^3$ with $\rho = 1.2\,\mathrm{kg\,m^{-3}}$, is $0.6 \times 9.10^3 = 452\,\mathrm{W\,m^{-2}}$ in the stable profile and $0.6 \times 6.95^3 = 201\,\mathrm{W\,m^{-2}}$ by the one-seventh law: a factor of $(6.95/9.10)^3 = 0.44$, an underestimate of 56 %. The neutral log law does better but not well: it gives $5 \times 7.601/5.298 = 7.17\,\mathrm{m\,s^{-1}}$ and $221\,\mathrm{W\,m^{-2}}$, half the stable value.

The same correction for a convective afternoon with an illustrative $L_O = -50$ m, with the unstable form of Section 12.4.1, gives $\psi_m = 0.46$ at 10 m and 1.49 at 100 m, a hub wind of $5 \times (7.601 - 1.495)/(5.298 - 0.461) = 6.31\,\mathrm{m\,s^{-1}}$ and an exponent of 0.10; there the one-seventh law overestimates the wind power by a factor of $(6.95/6.31)^3 = 1.33$. The same 10 m reading thus corresponds to hub winds from 6.3 to $9.1\,\mathrm{m\,s^{-1}}$ depending on the state of the air, and the fixed exponent is wrong in opposite directions by day and by night.

The error has the unsafe sign for a transmission line rated from a forecast aloft. Extrapolating the stable $9.10\,\mathrm{m\,s^{-1}}$ at 100 m down to a conductor at 30 m with the one-seventh law gives

$9.10 \times 0.3^{1/7} = 7.66\,\mathrm{m\,s^{-1}}$, while the stable profile gives $5 \times (\ln 600 + 0.75)/5.548 = 6.44\,\mathrm{m\,s^{-1}}$: the fixed exponent overstates the wind at the conductor, and with it the convective cooling, by 19 %.

Figure 12.3 draws the four profiles that share the $5\,\mathrm{m\,s^{-1}}$ at 10 m. The horizontal axis is wind speed and the vertical axis height on a linear scale from 0 to 150 m. The gray dashed curve is the one-seventh law, the black curve the neutral log profile, the blue curve the stable and the red curve the unstable profile; the dotted horizontal line marks the hub at 100 m, and the legend gives each profile's wind there.

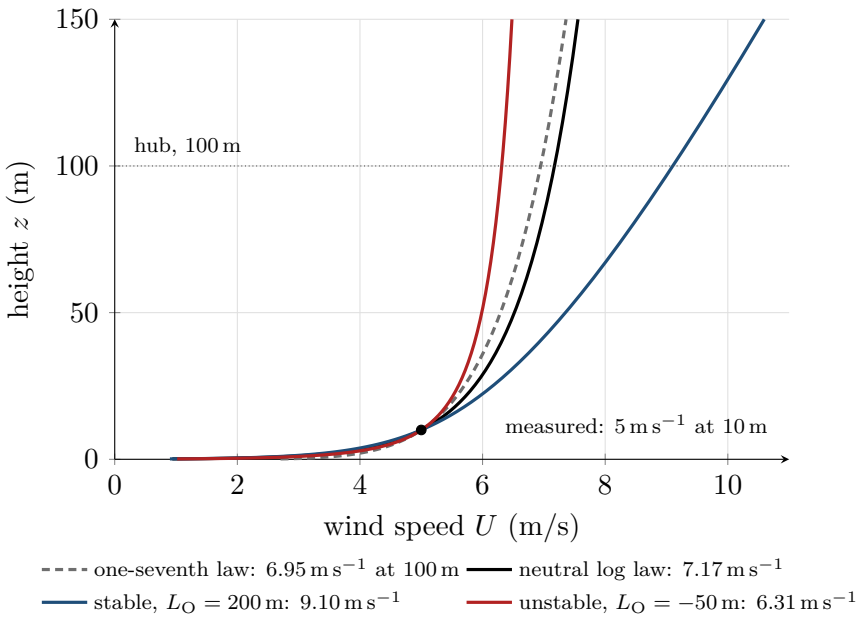


Figure 12.3: Four profiles through the same 10 m wind of $5\,\mathrm{m\,s^{-1}}$ over $z_0 = 0.05$ m (illustrative). One-seventh law: $U = 5\,(z/10)^{1/7}$. Log law: $U = (u_*/\kappa)[\ln(z/z_0) - \psi_m]$ with $\kappa = 0.4$; neutral $\psi_m = 0$; stable $\psi_m = -5\,z/L_O$, $L_O = 200$ m; unstable $\psi_m = 2\ln[(1+x)/2] + \ln[(1+x^2)/2] - 2\arctan x + \pi/2$, $x = (1 - 16\,z/L_O)^{1/4}$, $L_O = -50$ m.

The four curves meet at the measured point and spread above it; by 100 m they span 6.3 to $9.1\,\mathrm{m\,s^{-1}}$. The stable profile leans furthest to the right, its shear above 10 m sustained by the linear term $5\,z/L_O$, and the one-seventh curve lies between the unstable and the neutral profiles, close to neither the day nor the night. One caution applies to the stable curve itself: at night the surface layer may be only a few tens of meters deep (Section 12.4.5), and the stable correction is then carried to 100 m beyond the layer where it was established. The real night-time shear above the surface layer can be larger still, a subject of Chapter 17.

Principle 12.3. *The shear exponent is a property of the state of the air, the surface and the height range, not a constant. A fixed exponent of* 1/7 *is wrong in opposite directions by day and by night, and its largest errors, on stable nights, underestimate the wind power at a hub and overestimate the wind at a low conductor.*

12.3.6 A local fit

Over a restricted range of heights a logarithm and a weak power law are hard to tell apart, which is why fitted power laws often describe mast data well. Take the neutral worked profile of Section 12.1.4, $U = \ln(z/0.05\,\mathrm{m})$, and fit a power law through its values at 20 and 80 m, 5.99

and $7.38\,\mathrm{m\,s^{-1}}$. By equation (12.7), or equivalently equation (12.8), the exponent is

$$\alpha = \frac{\ln(7.378/5.991)}{\ln 4} = \frac{0.208}{1.386} = 0.150,$$

close to 1/7. Between 20 and 80 m the two curves differ by at most 0.54 %, at 40 m, less than the accuracy of a good cup anemometer. Outside the range they part: the power law is 1.9 % high at 10 m, 15 % high at 2 m and 28 % high at 1 m, and above the range it is 1.3 % high at 150 m and 3.4 % high at 300 m.

Figure 12.4 shows the comparison. The horizontal axis is wind speed; the vertical axis is height on a logarithmic scale from 1 to 300 m, on which the log profile is a straight line and the power law a curve. The shaded band is the fitting range, 20 to 80 m, and the two marked points are the values through which the power law was fitted.

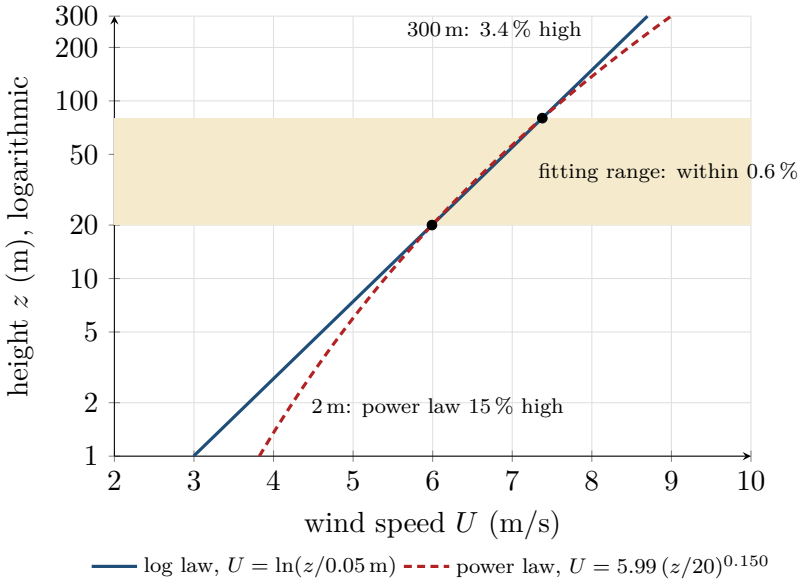


Figure 12.4: A power law fitted through a neutral log profile at 20 and 80 m. Log law: $U = (u_*/\kappa)\ln(z/z_0)$ with $u_* = 0.4\,\mathrm{m\,s^{-1}}$, $z_0 = 0.05\,\mathrm{m}$, $\kappa = 0.4$. Power law: exponent 0.150 from equation (12.8). Shaded: the fitting range.

Inside the shaded band the two curves cannot be separated by eye; below it the power law bends away to the right, unable to follow the steep logarithmic shear near the ground, and above it the power law slowly outruns the logarithm. A good power-law fit over 20 to 80 m is therefore an empirical approximation over that range, not a law. It carries no information about the roughness or the stability that produced the profile, and it should not be used outside the range of the data that fixed its exponent.

12.4 Stability and the region of validity of the profile

Neutral stability is the major assumption behind equation (12.1), and height is limited at both ends. This section states the stability-corrected profile, describes how it departs from the neutral one, and draws the region of heights and conditions in which the profile can be trusted.

12.4.1 The stability-corrected profile

In general the surface-layer profile is

$$U(z) = \frac{u_*}{\kappa}\left[\ln\frac{z-d}{z_0} - \psi_m\!\left(\frac{z-d}{L_O}\right)\right], \tag{12.9}$$

where L_O (m) is the Obukhov length, the height scale at which buoyancy becomes as important as shear in producing or destroying turbulence, negative in unstable and positive in stable air, and ψ_m (dimensionless) is the *stability correction for momentum*: the integrated departure of the profile from the logarithm caused by buoyancy. Its argument is the stability parameter z/L_O, written with $z-d$ in place of z where a displacement height applies (the literature writes it ζ; this book keeps ζ for vorticity). A term $\psi_m(z_0/L_O)$ that belongs in the exact integral is omitted, since $z_0 \ll |L_O|$ makes it negligible: 0.004 for $z_0 = 0.05\,\mathrm{m}$ and $L_O = -50\,\mathrm{m}$.

As $|L_O| \to \infty$ the buoyancy effect vanishes, $\psi_m \to 0$, and the neutral log law returns. Chapter 14 defines L_O and derives ψ_m from the dimensionless shear of Monin–Obukhov similarity theory. This chapter uses the standard empirical (Businger–Dyer) forms,

$$\begin{aligned} \psi_m &= -5\,\frac{z}{L_O} && \text{stable, } L_O > 0, \\ \psi_m &= 2\ln\frac{1+x}{2} + \ln\frac{1+x^2}{2} - 2\arctan x + \frac{\pi}{2}, \quad x = \left(1 - 16\,\frac{z}{L_O}\right)^{1/4} && \text{unstable, } L_O < 0, \end{aligned} \tag{12.10}$$

the first usually trusted up to $z/L_O \approx 1$. Equation (12.9) turns the ratio formula into

$$\frac{U(z_2)}{U(z_1)} = \frac{\ln[(z_2-d)/z_0] - \psi_m((z_2-d)/L_O)}{\ln[(z_1-d)/z_0] - \psi_m((z_1-d)/L_O)}, \tag{12.11}$$

which needs L_O in addition to z_0 and d; the friction velocity still cancels.

12.4.2 Unstable and stable departures

When $L_O < 0$, the surface heats the air, buoyancy enhances the turbulence and the mixing is stronger: momentum is carried down more efficiently, the shear is smaller, and the profile is flatter than the neutral one; $\psi_m > 0$. In the convective afternoon of Section 12.3.5, the wind increases from $5\,\mathrm{m\,s^{-1}}$ at 10 m to $6.31\,\mathrm{m\,s^{-1}}$ at 100 m, against $7.17\,\mathrm{m\,s^{-1}}$ in neutral air.

When $L_O > 0$, the surface cools the air, buoyancy suppresses the turbulence and the mixing is weaker: the lowest air is partly decoupled from the air above, the shear is stronger, and $\psi_m < 0$. The neutral log law then substantially underestimates the speed difference between lower and upper levels. In the stable night of Section 12.3.5 the difference between 10 and 100 m is $9.10 - 5 = 4.10\,\mathrm{m\,s^{-1}}$; the neutral law gives $7.17 - 5 = 2.17\,\mathrm{m\,s^{-1}}$, 47 % too small. Chapter 13 treats the static stability that sets the sign of L_O, and Chapter 15 the interpretation of its numerical values.

12.4.3 Not down to the ground

The condition $U = 0$ at $z - d = z_0$ is formal. It fixes the constant of integration and defines z_0; it does not describe the air at that height. The profile holds above the roughness elements, at heights large compared with z_0 and above the roughness sublayer, the layer of two to three obstacle heights in which the wakes of individual plants, trees or buildings affect the flow (Chapter 7). Below that, within a canopy, the wind is set by the drag of the canopy elements and is weak but not zero at $z = d + z_0$; over a smooth surface the lowest fraction of a millimeter, of order ν/u_*, is a viscous sublayer in which molecular viscosity carries the stress. Neither region is described by equation (12.1), and the profile should not be extrapolated into them: a log-law wind at 0.5 m over a 1 m crop, or at 10 m inside a 20 m forest, is a number with no physical counterpart.

12.4.4 Not indefinitely upward

The profile is a surface-layer relation. With a boundary-layer depth $z_i = 1000\,\mathrm{m}$, the surface layer reaches roughly 100 m, and extrapolating from 10 to 800 m with the log law is not justified. Over

farmland with $z_0 = 0.05\,\mathrm{m}$ it would give $U(800\,\mathrm{m}) = U(10\,\mathrm{m}) \times \ln 16\,000/\ln 200 = 1.83\,U(10\,\mathrm{m})$, so $11\,\mathrm{m\,s^{-1}}$ from a 10 m wind of $6\,\mathrm{m\,s^{-1}}$, with no change of direction. Above the surface layer three things that the derivation excluded take over. The stress decreases with height toward zero at z_i, so the flux is no longer the constant u_*^2. The Coriolis force, absent from the surface-layer balance, turns the wind with height toward the geostrophic direction: clockwise with increasing height (veering) in the Northern Hemisphere and counterclockwise (backing) in the Southern Hemisphere. And the structure of the boundary layer controls the profile: a convective mixed layer has nearly uniform wind over most of its depth, a stable boundary layer may carry a wind maximum near its top. The log law keeps growing as $\ln z$ through all of it and is wrong in speed and in direction.

12.4.5 The region of validity

The two limits define a band of heights: above the roughness sublayer and below the top of the surface layer. Within that band the profile still needs a set of conditions on the flow:

- a horizontally homogeneous surface upwind of the site;
- stationary flow over the averaging period;
- adequate fetch, so that the heights of interest lie in the layer in equilibrium with the local surface;
- an approximately constant flux with height;
- a known stability, neutral or measured, to evaluate ψ_m.

These conditions are more restrictive than a rule such as "below 100 m", because both ends of the band move: the bottom with the height of the obstacles, the top with the depth of the boundary layer, which changes by a factor of five or more between day and night.

Figure 12.5 draws the band for an illustrative crop surface, canopy height $h_c = 1\,\mathrm{m}$, $d = 0.7\,\mathrm{m}$ and $z_0 = 0.1\,\mathrm{m}$, on a day and a night. The vertical axis is height above the ground on a logarithmic scale from 1 cm to 3 km. Each column is a stack of layers: the canopy, the roughness sublayer to about $3h_c$, the surface layer taken as the lowest 10 % of the boundary layer, the rest of the boundary layer, and the air above. The blue band is the region of validity. The dashed horizontal lines are three common measurement heights, 10, 40 and 100 m; the dotted line inside the canopy is $z = d + z_0$, where the extrapolated profile reaches zero.

By day the band runs from about 3 to 100 m and contains all three measurement heights, with the 100 m line at its upper edge. At night it runs from about 3 to 20 m and contains only the 10 m height; the 40 and 100 m heights lie in the stable boundary layer above the surface layer, where neither the neutral profile nor its stability correction is established. A hub-height extrapolation that is defensible at noon can thus be indefensible at midnight at the same site, and the condition is set by the depth of the boundary layer, not by a fixed height. The other conditions of the list are not drawn: they are properties of the site and the weather, and the next section shows how their failure appears in data.

12.5 Failures of the profile and what they indicate

Measured profiles often do not fit the log law. This section describes the common situations in which it fails, works a two-height diagnostic that turns a misfit into information, and states the rule that follows: a misfit is evidence about the flow, not a reason to adjust the parameters until the theory fits.

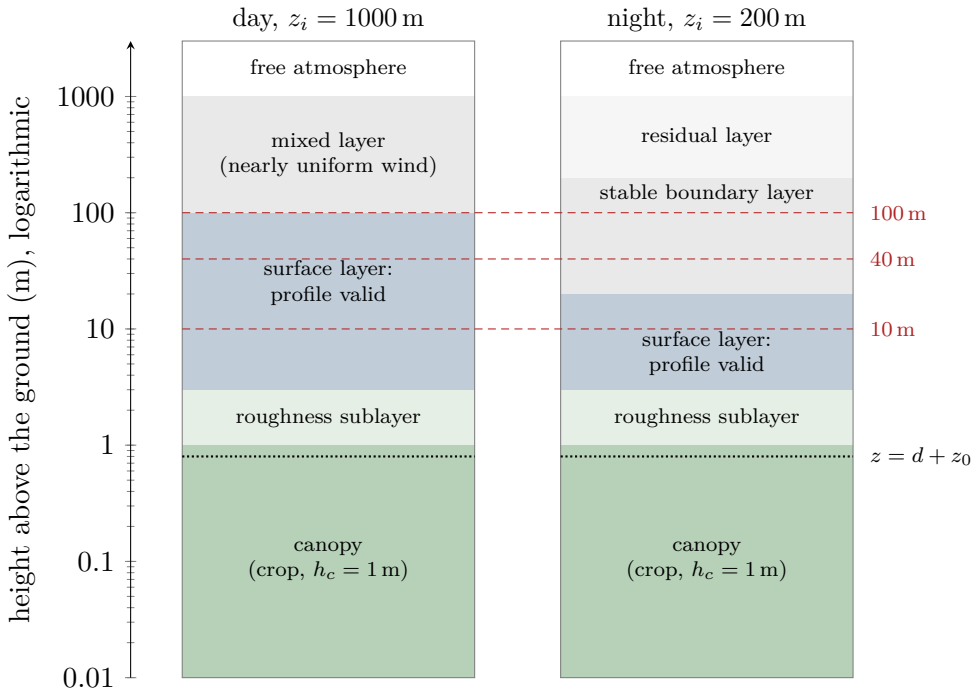


Figure 12.5: Region of validity of the logarithmic profile (blue) over an illustrative crop surface, $h_c = 1\,\mathrm{m}$, $d = 0.7\,\mathrm{m}$, $z_0 = 0.1\,\mathrm{m}$: above the roughness sublayer (to about $3h_c$) and below the top of the surface layer (taken as $0.1\,z_i$), on a day with $z_i = 1000\,\mathrm{m}$ and a night with $z_i = 200\,\mathrm{m}$. Dashed: measurement heights; dotted: the formal zero of the profile. Layer depths are illustrative and vary from day to day.

12.5.1 Complex terrain

On a ridge or a hilltop the flow is accelerated by a pressure gradient that the terrain itself creates: air forced over the obstacle speeds up, and the pressure is lower over the crest than upwind. The shear at the crest is then no longer controlled by the surface stress alone, since a horizontal pressure gradient that varies with height adds a term the surface-layer balance does not contain. The flow is also out of equilibrium, because the air passes over the crest in a few minutes, too quickly for the turbulence to adjust to the local surface; horizontally heterogeneous, because the slope, the roughness and the exposure change along its path; possibly separated, on a steep lee slope where the flow leaves the surface and a recirculating eddy forms; and curved, so that centrifugal effects enter.

Figure 12.6 sketches the situation in a vertical cross section, with the wind from the left and the vertical scale exaggerated. The gray shape is the ridge. At the left, upwind on flat ground, the blue curve is an equilibrium log profile. Above the crest, the red curve is the speeded-up profile, with the upwind profile copied as a dashed blue curve for comparison; on the steep lee slope a dashed loop marks a possible separated, recirculating flow.

The crest profile is faster than the upwind one at every height, and the difference is largest close to the ground, where the fractional speed-up is greatest; higher up the two profiles converge. Plotted against the logarithm of height, the crest profile is not a straight line: its shear near the ground is smaller than the log law predicts, and a log law fitted to two crest anemometers gives a friction velocity and a roughness length that describe neither the surface nor the stress. A sensor on a ridge therefore measures a wind for which the log law may fail entirely. Terrain-specific modeling, by computational fluid dynamics (CFD) or by an empirical speed-up correction, is needed; Chapter 20 treats terrain-induced flow.

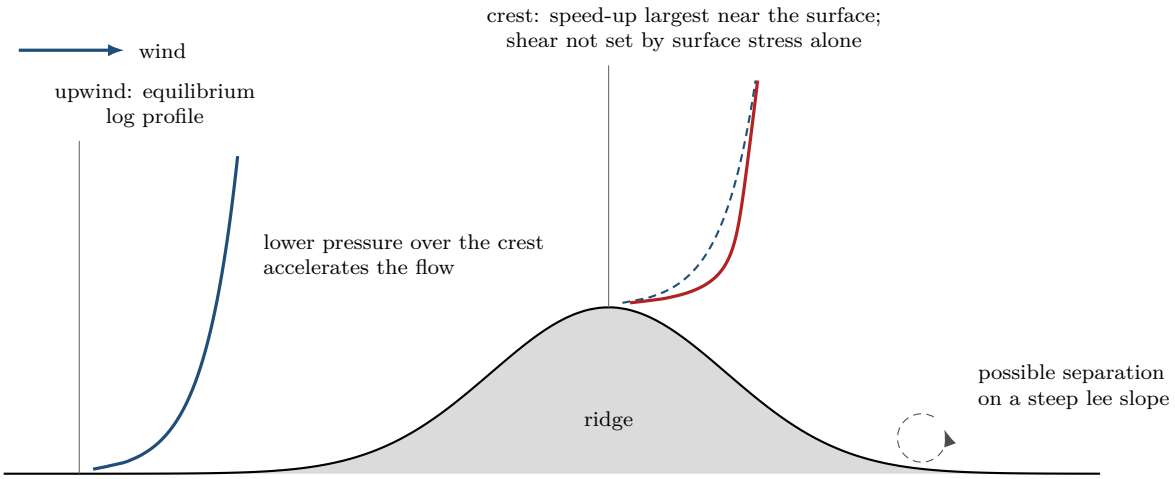


Figure 12.6: Flow over a ridge (schematic, vertical scale exaggerated). Blue: the upwind equilibrium log profile, repeated dashed above the crest. Red: the crest profile, illustratively $U_{\mathrm{crest}}(\Delta z) = U_{\mathrm{up}}(\Delta z)\,[1 + 0.6\,e^{-\Delta z/\ell}]$ with Δz the height above the local ground and ℓ an illustrative decay height, small compared with the width of the ridge. The fractional speed-up is largest close to the ground.

12.5.2 Forest edges

Air passing from a field into a forest meets a sudden increase in drag. The flow is developing: an internal boundary layer grows from the edge (Chapter 7), below whose top the wind adjusts to the forest and above which it still carries the profile of the field. The profile changes with distance downstream, so it is not vertically self-similar: no single set of u_*, z_0 and d describes it at every height, and the parameters fitted at one distance from the edge differ from those fitted at another. Even over perfectly flat terrain, then, a mast within a few hundred meters of an edge does not see a clean log profile; it sees a blend of two surfaces whose proportions depend on the height of the instrument and on the wind direction. The reverse transition, from forest to field, has the same character, with the added wake of the canopy.

12.5.3 Low wind speeds

With weak winds and stable conditions, common at night, the turbulence becomes intermittent: quiet periods with almost no turbulent exchange alternate with bursts. Averaged over 10 to 30 minutes, the fluxes collapse toward zero and are poorly defined, the constant-flux approximation fails, and the profile no longer represents a quasi-steady balance between stress and shear. A log fit to such data gives strange friction velocities and roughness lengths. For an illustrative calm-night pair, $1.0\,\mathrm{m\,s^{-1}}$ at 10 m and $2.5\,\mathrm{m\,s^{-1}}$ at 40 m, the two-height formulas of Chapter 10 give $u_* = 0.4 \times 1.5/\ln 4 = 0.43\,\mathrm{m\,s^{-1}}$, as large as on a windy afternoon, and $z_0 = 10\,\mathrm{m} \times \exp(-0.4 \times 1.0/0.433) = 4.0\,\mathrm{m}$, the roughness of a city, over what may be a meadow. Neither number is a property of the site: both are artifacts of fitting a neutral equilibrium law to a flow that is neither neutral nor in equilibrium.

12.5.4 A two-height diagnostic

The misfit can be turned into a test. Let a mast over what is described as open grassland record $U(10\,\mathrm{m}) = 4.5\,\mathrm{m\,s^{-1}}$ and $U(40\,\mathrm{m}) = 6.5\,\mathrm{m\,s^{-1}}$, and assume $d = 0$. If the neutral log law holds, the ratio of the two winds fixes the roughness length through equation (12.5):

$$\frac{6.5}{4.5} = \frac{\ln(40/z_0)}{\ln(10/z_0)}.$$

Write $r = U(z_2)/U(z_1)$. Expanding the logarithms, $r \ln z_1 - r \ln z_0 = \ln z_2 - \ln z_0$, so

$$\ln z_0 = \frac{r \ln z_1 - \ln z_2}{r - 1}. \tag{12.12}$$

With $r = 1.444$, $\ln 10 = 2.303$ and $\ln 40 = 3.689$,

$$\ln z_0 = \frac{1.444 \times 2.303 - 3.689}{0.444} = \frac{3.326 - 3.689}{0.444} = -0.817, \qquad z_0 = 0.44\,\mathrm{m},$$

and the slope gives $u_* = 0.4 \times (6.5 - 4.5)/\ln 4 = 0.58\,\mathrm{m\,s^{-1}}$. The two routes of Chapter 10 agree: $10\,\mathrm{m} \times \exp(-0.4 \times 4.5/0.577) = 0.44\,\mathrm{m}$.

An effective roughness length of 0.44 m is not a number of several meters, as a guess from the size of the speed difference might suggest; the logarithm compresses it. It is nonetheless implausible for open grassland, whose roughness length lies between about 0.01 and 0.05 m (Chapter 11): it is ten to forty times too large, the value of shrubland or scattered trees. The fit has returned a number that is absurd for the site, and the absurdity is the result. It says that something in the assumptions is wrong, and there are four candidates: stability matters; the terrain influences the flow; the measurements are unrepresentative, for example because the lower anemometer is sheltered or the upper one sees a different fetch; or the surface is not what the description says.

The first candidate can be tested by the same data. Keep the grassland value $z_0 = 0.03\,\mathrm{m}$ and ask what stable Obukhov length reproduces the observed ratio with the stable correction $\psi_m = -5\,z/L_\mathrm{O}$:

$$\frac{\ln(40/0.03) + 5 \times 40/L_\mathrm{O}}{\ln(10/0.03) + 5 \times 10/L_\mathrm{O}} = \frac{7.196 + 200/L_\mathrm{O}}{5.809 + 50/L_\mathrm{O}} = 1.444,$$

which gives $127.8/L_\mathrm{O} = 1.444 \times 5.809 - 7.196 = 1.195$ and $L_\mathrm{O} = 107\,\mathrm{m}$, with $u_* = 0.29\,\mathrm{m\,s^{-1}}$. A moderately stable surface layer with $40/L_\mathrm{O} = 0.37$, well inside the range of the stable correction, explains the two winds with the roughness of grass. A neutral profile with the same grass roughness through the 10 m value would have given only $4.5 \times 7.196/5.809 = 5.57\,\mathrm{m\,s^{-1}}$ at 40 m.

Figure 12.7 draws the three readings of the data. The horizontal axis is wind speed; the vertical axis is height on a logarithmic scale from 1 cm to 100 m. The two black points are the measurements. The blue line is the neutral fit, which passes through both points and reaches zero at $z_0 = 0.44\,\mathrm{m}$; the red curve is the stable profile over grass, which also passes through both points and reaches zero at $z_0 = 0.03\,\mathrm{m}$; the gray dashed line is the neutral grass profile through the 10 m point, which misses the 40 m point.

Both solid curves pass through both measurements; two heights cannot choose between them. They differ where there are no data: below 10 m, where the neutral fit reaches zero at 0.44 m and the stable profile at 0.03 m, and above 40 m, where the stable profile curves to the right. A third anemometer, at 2 or at 80 m, or a measurement of the stability, would separate them; so would a sonic anemometer measuring u_* directly, 0.58 against $0.29\,\mathrm{m\,s^{-1}}$, a factor of four in the stress.

12.5.5 Not forcing the theory onto the data

When observations disagree with a neutral log profile, the response "estimate a different roughness until it fits" is wrong. The fitted $z_0 = 0.44\,\mathrm{m}$ of the diagnostic reproduces the two winds, but it attributes to the surface an effect of the atmosphere; used at another time, under neutral or unstable conditions, it would overpredict the shear, and used to infer the stress it would be wrong by a factor of four. The disagreement may be evidence that an assumption of the model is wrong, and the list of Section 12.4.5 names the candidates: stability, terrain, fetch, roughness sublayer, stationarity. A parameter that comes out of a fit outside its physical range, or that changes with the time of day, with the wind direction or with the pair of heights used, is a symptom to be explained, not a value to be adopted.

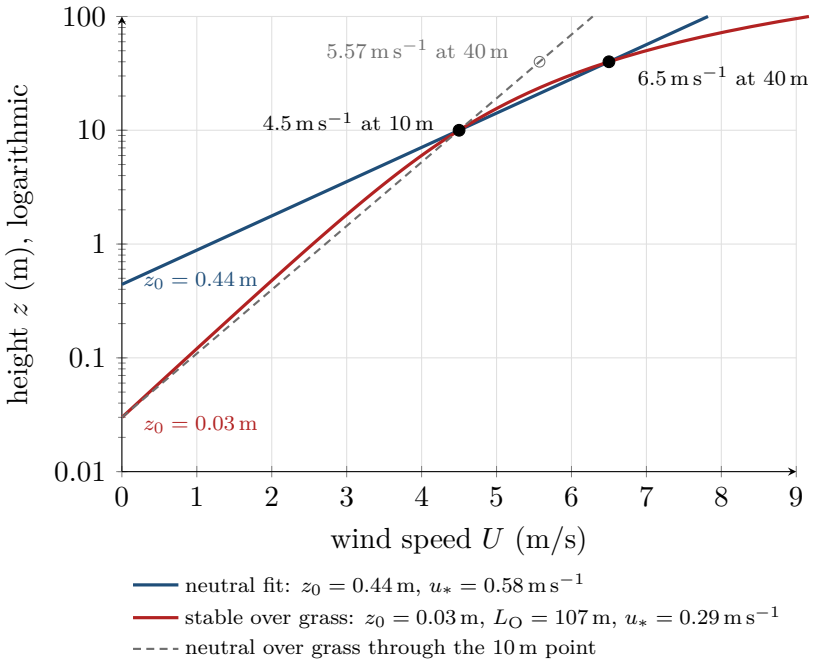


Figure 12.7: The two-height diagnostic. Measurements (illustrative): 4.5 m s^{-1} at 10 m and 6.5 m s^{-1} at 40 m over open grassland, $\kappa = 0.4$, $d = 0$. Blue: neutral log law fitted through both points, equation (12.12). Red: stable profile $U = (u_*/\kappa)[\ln(z/z_0) + 5\,z/L_O]$ with the grassland roughness. Gray dashed: neutral grassland profile through the 10 m point.

Principle 12.4. *A log-law parameter fitted to data and found outside its physical range is a diagnostic: it indicates which assumption of the equilibrium surface layer has failed. The response is to identify the failure, not to adjust the parameter until the profile fits.*

12.6 The profile in models and practice

The logarithmic profile is built into the tools that produce most near-surface wind data. This section arranges the profile and its extensions as a hierarchy of models, shows how a weather model uses surface-layer similarity to produce its 10 m wind and its 2 m temperature, and closes with a checklist for extrapolation.

12.6.1 A hierarchy of profile models

The relations of this chapter form four levels, each adding physics and inputs to the one below. Figure 12.8 draws them as a stack read from the bottom up. Each box gives the level, its formula or its content, and the assumptions it keeps; the arrows between boxes name what is added.

Levels 1 to 3 differ in their parameters but share their foundation: an equilibrium surface layer, stationary, homogeneous and of constant flux. Moving up through them adds realism at the price of inputs that must themselves be measured or estimated: a displacement height from the canopy, an Obukhov length from fluxes or from temperature profiles. Level 4 is a different kind of step. It drops the foundation, and with it the closed-form profile: the flow over a ridge, across a forest edge or in an intermittent stable night must be modeled or measured, not written down. The practical skill is to decide which level a site and a time require, and the checklist of Section 12.6.4 serves that decision.

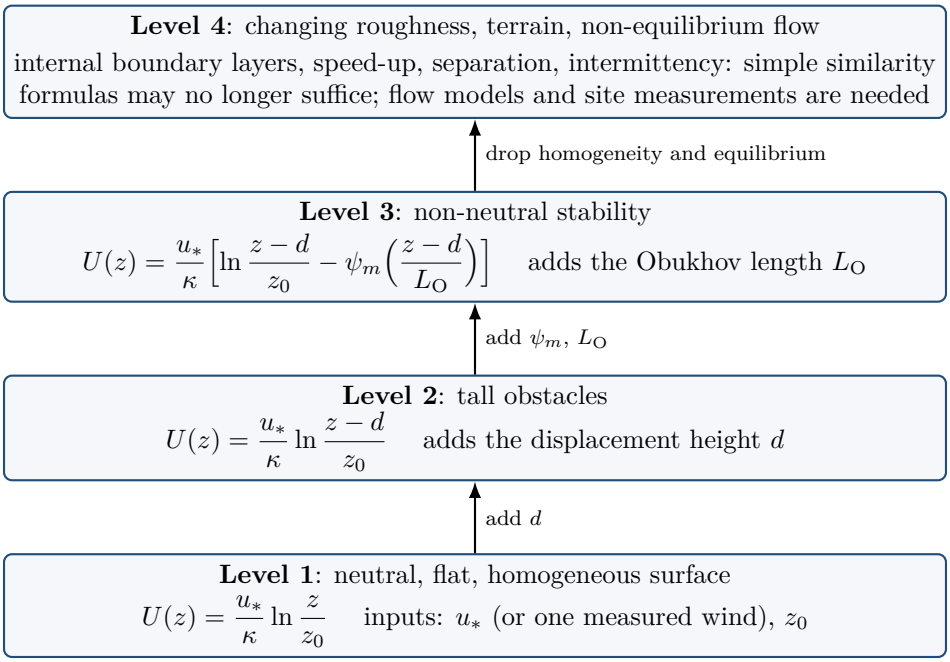


Figure 12.8: A hierarchy of near-surface wind profile models. Levels 1 to 3 are similarity relations of the equilibrium surface layer, each adding one parameter; level 4 is where the equilibrium surface layer itself no longer holds.

12.6.2 The 10 m wind of a weather model

Many weather models do not compute the wind at 10 m directly. Their lowest computational level lies at some height z_1 above the ground, commonly a few tens of meters, and the 10 m wind is diagnosed from the wind at that level with surface-layer similarity theory. The steps are:

1. take the wind speed U_1 and the temperature at the lowest level z_1, and the temperature of the ground;
2. take the roughness length z_0 assigned to the grid cell from its land cover;
3. solve the stability-corrected profile, equation (12.9), together with its counterpart for temperature, for u_* and L_O, iteratively because L_O depends on u_* (Chapter 14);
4. evaluate the same profile at 10 m.

With $d = 0$, as in most models, the result is

$$U_{10} = U_1 \,\frac{\ln(10\,\mathrm{m}/z_0) - \psi_m(10\,\mathrm{m}/L_O)}{\ln(z_1/z_0) - \psi_m(z_1/L_O)}, \tag{12.13}$$

the ratio formula of equation (12.11) applied downward. The direction of the 10 m wind is usually taken to be that of the lowest level, since the wind turns only a few degrees across the surface layer.

Take an illustrative grid cell in southern Brazil whose lowest level is at $z_1 = 30$ m, with $U_1 = 8\,\mathrm{m\,s^{-1}}$ from 040° and a cell roughness length $z_0 = 0.1$ m. In neutral air,

$$U_{10} = 8\,\mathrm{m\,s^{-1}} \times \frac{\ln 100}{\ln 300} = 8 \times \frac{4.605}{5.704} = 6.46\,\mathrm{m\,s^{-1}}, \qquad u_* = \frac{0.4 \times 8}{5.704} = 0.56\,\mathrm{m\,s^{-1}}.$$

Table 12.4: The 10 m wind diagnosed by equation (12.13) from $U_1 = 8\,\mathrm{m\,s^{-1}}$ at $z_1 = 30\,\mathrm{m}$, $\kappa = 0.4$, $d = 0$, with the corrections of equation (12.10) (illustrative).

State	z_0 (m)	L_O (m)	$\psi_m(30\,\mathrm{m})$	$\psi_m(10\,\mathrm{m})$	u_* (m/s)	U_{10} (m/s)
Neutral	0.1	∞	0	0	0.56	6.46
Stable	0.1	100	−1.50	−0.50	0.44	5.67
Unstable	0.1	−50	0.87	0.46	0.66	6.86
Neutral, smoother cell	0.03	∞	0	0	0.46	6.73
Neutral, rougher cell	0.5	∞	0	0	0.78	5.85

Table 12.4 repeats the diagnosis for a stable and an unstable state and for two other roughness lengths. Its columns give the roughness length, the Obukhov length, the two stability corrections, the friction velocity and the diagnosed 10 m wind, all from the same $8\,\mathrm{m\,s^{-1}}$ at 30 m.

From the same wind at the lowest level, the diagnosed 10 m wind ranges from 5.67 to $6.86\,\mathrm{m\,s^{-1}}$ with stability and from 5.85 to $6.73\,\mathrm{m\,s^{-1}}$ with the cell roughness. The 10 m wind of the model is therefore partly a diagnostic product of surface-layer theory: it is the wind at the lowest level, carried down by an assumed profile with an assumed roughness and a modeled stability. It is not the wind at a grid node located 10 m above the ground, and it is a grid-cell value: the roughness is that of the cell, a blend of fields, forest and buildings several kilometers wide, not the roughness upwind of any particular anemometer. The direction carries the same caveat. The model reports 040° at 10 m; the real wind near the ground is turned slightly toward low pressure, which in the Southern Hemisphere is a clockwise turn as height decreases, toward perhaps 043°, and in the Northern Hemisphere a counterclockwise one.

This matters when a model is validated against stations. A difference between the model's U_{10} and an anemometer can come from the wind at the lowest level, from the cell roughness against the station's upwind roughness, from the modeled stability, or from the representativeness of the station; comparing the two numbers alone cannot say which. Validation at the lowest model level, against a mast or a profiler at that height, removes the surface-layer diagnosis from the comparison.

12.6.3 The 2 m temperature

The 2 m temperature of a weather model is diagnosed in the same way. The temperature profile of the surface layer has the same structure as the wind profile,

$$\theta(z) = \theta_s + \frac{\theta_*}{\kappa}\left[\ln\frac{z}{z_{0h}} - \psi_h\!\left(\frac{z}{L_\mathrm{O}}\right)\right], \tag{12.14}$$

where θ_s is the potential temperature at the surface, $\theta_* = -\overline{w'\theta'}/u_*$ is the surface-layer temperature scale, z_{0h} is a roughness length for heat, usually smaller than z_0, and ψ_h is the stability correction for heat; Chapter 14 defines all three. The model knows the temperature of its ground and of its lowest level, and the flux relationship between the two, solved together with the wind profile, gives θ_* and L_O; the 2 m temperature is then equation (12.14) evaluated at $z = 2\,\mathrm{m}$. Like the 10 m wind, it is an interpolation by a parameterization between two levels the model does compute, and both diagnostics inherit the assumptions of the equilibrium surface layer. On a calm, clear night, when those assumptions fail, both are least reliable.

12.6.4 A checklist for extrapolation

Before a simple log-law extrapolation is trusted, seven questions have to be answered. Table 12.5 lists them with the reason each matters, a way to check it, and what to do if the answer is no.

Only when every answer is yes is a simple log-law extrapolation justified; each no moves the problem up the hierarchy of Figure 12.8.

Table 12.5: Seven questions before a log-law extrapolation.

Question	Why it matters	How to check	If no
1. Are both heights in the surface layer?	the profile is a surface-layer relation	compare with $0.1\,z_i$; at night z_i may be 200 m or less	do not extrapolate across the top; use profile measurements
2. Is the terrain reasonably homogeneous?	the profile assumes one surface	land-cover map by direction sector	use a directional z_0 or a flow model
3. Are both heights above the roughness sublayer?	the profile fails among and just above obstacles	heights above about 2 to $3\,h_c$	raise the measurement, or model the canopy flow
4. Is there enough fetch?	the profile needs equilibrium with the local surface	fetch of about 100 times the height	account for the internal boundary layer
5. Is the stability known?	stable and unstable profiles depart strongly	heat flux, temperature difference between heights, time of day	use equation (12.9) with a measured L_{O}
6. Is the flow approximately stationary?	the profile is an average of a steady state	consecutive averages agree; no front or transition	shorten the period, or exclude it
7. Is terrain acceleration negligible?	a terrain pressure gradient adds shear the profile lacks	site on flat ground, away from ridges and escarpments	speed-up correction or flow model

The checklist restates the physical interpretation of the whole chapter. Under neutral equilibrium conditions the surface stress fixes the friction velocity, and the distance from the surface fixes the turbulent length scale; together they give

$$\frac{\partial U}{\partial z} = \frac{u_*}{\kappa z},$$

and the logarithm follows. The profile is a consequence of that turbulence structure, not the result of curve fitting, and each question of the checklist asks whether the structure is present: a single stress, eddies limited by a single surface, and no buoyancy, terrain or history to disturb them. Of those conditions, the one that fails most often and most strongly is neutrality, and its physical basis, the static stability of the air, is the subject of Chapter 13.

12.7 What to retain

Definition 12.1 (The logarithmic wind profile)**.** The neutral profile $U(z) = (u_*/\kappa)\ln[(z-d)/z_0]$ is physically grounded, a consequence of a constant momentum flux carried by eddies whose size grows with the distance from the surface, but it is not universal: its reliability, for extrapolation and for model diagnosis alike, depends on whether the atmosphere behaves as a stationary, horizontally homogeneous, constant-flux surface layer of known stability.

Table 12.6 lists the terms of the chapter, their meaning, their units and the subsection that defines each.

12.8 Exercises

Exercise 12.1. Over smooth open land, $z_0 = 0.02$ m and $d = 0$, in neutral conditions, the friction velocity is $0.3\,\mathrm{m\,s^{-1}}$; take $\kappa = 0.4$. (a) Compute the wind at 2, 10, 50 and 100 m and

Table 12.6: The terms of the chapter and where each is defined.

Term	Meaning	Units	Defined in
Logarithmic wind profile	$U = (u_*/\kappa)\ln[(z-d)/z_0]$, the neutral surface-layer profile	m/s	12.1, 12.1.1
Wind shear	$\partial U/\partial z$; in wind energy also a speed difference or the exponent α	s^{-1}	12.1
Wind extrapolation	estimation of the wind at an unmeasured height through an assumed profile	–	12.1, 12.2.1
Height ratio	$U(z_2)/U(z_1)$ from the profile; independent of u_*	–	12.2.1
Power law	$U(z) = U(z_r)(z/z_r)^\alpha$, an empirical profile	m/s	12.3.1
Wind-shear exponent α	fractional increase of wind per fractional increase of height; depends on stability, roughness and height range	–	12.3.1, 12.3.3
Equivalent exponent	exponent of the power law through the log profile at two heights	–	12.3.4
Stability correction ψ_m	integrated departure of the profile from the logarithm caused by buoyancy; > 0 unstable, < 0 stable	–	12.4.1
Equilibrium surface layer	stationary, homogeneous, constant-flux surface layer whose profile depends only on u_*, z_0, d, L_O	–	12.1
Region of validity	heights above the roughness sublayer and below the top of the surface layer, under the conditions of the list	m	12.4.5
Effective roughness length	z_0 returned by a two-height neutral fit; a diagnostic when outside the surface's range	m	12.5.4
Diagnosed 10 m wind	model U_{10} obtained from the lowest model level by surface-layer similarity	m/s	12.6.2
Representativeness	degree to which a measured or modeled value stands for the quantity it is used for	–	12.1, 12.6.2

the increase over each interval. (b) Compute the shear at 2 and at 100 m and their ratio. (c) Over a plantation with $d = 12\,\mathrm{m}$, $z_0 = 1.5\,\mathrm{m}$ and $u_* = 0.6\,\mathrm{m\,s^{-1}}$, compute the wind at 40 and 60 m, then again ignoring the displacement height with the same z_0 and u_*, and give the error in percent at each height.

Exercise 12.2. A 10 m anemometer over farmland reads $7\,\mathrm{m\,s^{-1}}$ in neutral conditions; the land-cover table gives $z_0 = 0.05\,\mathrm{m}$, $d = 0$. (a) Extrapolate the wind to 60 and to 120 m. (b) Repeat with z_0 three times smaller and three times larger, and give the percentage change of the 120 m wind and the factor on the wind power at 120 m. (c) Compute the power-law exponent equivalent to the base case between 10 and 120 m, and the wind at 120 m given by the one-seventh law.

Exercise 12.3. On a clear night a 10 m anemometer over farmland, $z_0 = 0.05\,\mathrm{m}$, reads $6\,\mathrm{m\,s^{-1}}$, and the Obukhov length is estimated at $L_\mathrm{O} = 150\,\mathrm{m}$. (a) Using $\psi_m = -5\,z/L_\mathrm{O}$, compute the wind at a 100 m hub and the shear exponent it implies. (b) Compute the hub wind by the neutral log law and by the one-seventh law, and the ratio of the wind power each gives to the stable value. (c) Use Table 12.3 to say over which surface the one-seventh law would be right in neutral air between 10 and 100 m. (d) State one reason why the stable estimate of (a) may itself understate the hub wind.

Exercise 12.4. A mast at 22°S carries anemometers at 10 and 40 m; take $d = 0$. With the wind from 030°, over open pasture, it records 5.0 and $6.1\,\mathrm{m\,s^{-1}}$; with the wind from 150°, with a eucalyptus plantation 300 m upwind, it records 3.6 and $6.0\,\mathrm{m\,s^{-1}}$. (a) For each direction, solve equation (12.12) for the effective roughness length and compute u_*. (b) Which result is plausible for pasture, and what are two physical explanations of the other? (c) Keeping $z_0 = 0.02\,\mathrm{m}$ for pasture, compute the stable Obukhov length that would explain the 150° readings, and say whether the stable correction is within its usual range at 40 m. (d) A weather model reports 040° at its lowest level and the same direction at 10 m. In which sense, clockwise or counterclockwise, is the real near-surface wind turned with respect to the lowest-level wind at this site, and in which sense would it be turned at 22°N?

Chapter 13

Atmospheric Stability

13.1 Stability and the lapse rates

Chapter 6 introduced potential temperature, the dry adiabatic lapse rate and the displaced-parcel argument, and used them to describe the daily cycle of the boundary layer. Chapters 8 to 10 then showed that the wind near the ground is shaped by turbulent transport of momentum, and Chapters 11 and 12 treated the neutral profile that results when the turbulence is produced by shear alone. This chapter takes up the property that decides whether buoyancy adds to that turbulence, leaves it alone or removes it. The question of the chapter is

will a parcel of air displaced vertically keep moving, return, or remain where it was moved, and what does the answer do to the turbulence and to the wind near the ground?

The chapter first states stability as a comparison of two lapse rates and then restates it with potential temperature. It describes what each stability state does to the wind shear, defines the gradient and bulk Richardson numbers that weigh stratification against shear, and separates static stability, a property of a profile, from surface-layer stability, a property of the surface fluxes. It ends with how stability varies in height and in time and with what it does to the extrapolation of winds and to the errors of weather models.

Jargon: atmospheric stability, stratification, lapse rate, environmental lapse rate, dry adiabatic lapse rate, inversion, superadiabatic, Richardson number, static stability, surface-layer stability

Atmospheric stability is the tendency of the atmosphere to suppress or to amplify a vertical displacement of air; it controls how easily turbulence mixes heat and momentum vertically. *Stratification* is the vertical arrangement of density, described by the vertical gradient of potential temperature $\mathrm{d}\theta/\mathrm{d}z$ in $\mathrm{K\,m^{-1}}$; stable, neutral and unstable stratification have $\mathrm{d}\theta/\mathrm{d}z$ positive, near zero and negative. A *lapse rate* is a rate of decrease of temperature with height, in $\mathrm{K\,km^{-1}}$. The *environmental lapse rate* $\Gamma_e = -\mathrm{d}T/\mathrm{d}z$ is the observed one, measured by a radiosonde, a tower or an aircraft, or taken from a model's temperature profile. The *dry adiabatic lapse rate* $\Gamma_d = g/c_p \approx 9.8\,\mathrm{K\,km^{-1}}$ is the rate at which an unsaturated parcel cools when it rises without exchanging heat; it is computed, not observed. An *inversion* is a layer in which temperature increases with height, $\Gamma_e < 0$. A *superadiabatic* layer is one in which temperature decreases faster than the dry adiabatic rate, $\Gamma_e > \Gamma_d$. The *Richardson number* Ri, dimensionless, is the ratio of buoyant suppression to shear production of turbulence; it is computed from measured or modeled gradients of potential temperature and wind. *Static stability* is stability judged from the stratification alone; *surface-layer stability* is stability judged from the surface heat flux together with the mechanical turbulence, through the Obukhov length.

Key idea

Stability is the link in the chain thermal stratification → buoyancy → turbulence → vertical momentum mixing → wind profile: the same forcing aloft gives a strong, well-coupled surface wind when the air is unstable and a weak, sheared one when it is stable.

13.1.1 Three states of a displaced parcel

Consider a small parcel of air pushed upward or downward by a short distance and then released, quickly enough that it exchanges no heat with its surroundings. Three outcomes are possible. In a *stable* atmosphere the parcel returns toward its original level: vertical motion is suppressed, and the parcel oscillates about its starting height with the buoyancy frequency N derived in Chapter 6, $N^2 = (g/\theta)\,\mathrm{d}\theta/\mathrm{d}z$. In a *neutral* atmosphere the parcel has little tendency either way: it stays where it was moved. In an *unstable* atmosphere the parcel keeps moving away from its starting level: a small displacement grows, and vertical motion is amplified.

The three states matter for near-surface wind because turbulence is a collection of such displacements. An eddy that lifts slow air from near the ground and brings fast air down from above is the mechanism that transports momentum downward (Chapter 9). In stable air every such excursion is opposed and the eddies lose energy to the stratification; in unstable air the excursions are reinforced and the eddies gain energy from it; in neutral air the eddies depend on the wind shear alone. Stability therefore sets how efficiently the faster wind aloft reaches the ground, which is why it appears in every relation between the wind at two heights.

13.1.2 Environmental and dry adiabatic lapse rates

Temperature normally decreases with height in the lower atmosphere, and it is tempting to read that decrease as instability: the air below is warmer, so it should rise. It is not necessarily so, because a rising parcel does not keep its temperature. It moves into lower pressure, expands, does work on its surroundings and cools. Whether it ends up warmer or colder than the air around it depends on how fast it cools compared with how fast the surrounding air is colder at greater height. Two rates must therefore be compared, one describing the atmosphere and one describing the parcel.

The *environmental lapse rate*

$$\Gamma_e = -\frac{\partial T}{\partial z} \tag{13.1}$$

describes how the temperature of the actual atmosphere changes with height at one place and time. It is an observed property, measured by thermometers at two or more heights on a tower, by a radiosonde, or by a remote sensor, and in a model it is the slope of the temperature profile between two model levels. It is positive when temperature falls with height; the average of the lower atmosphere, used in the standard atmosphere, is $6.5\,\mathrm{K\,km^{-1}}$. It varies from hour to hour and from layer to layer, and near the ground it can take any sign.

The *dry adiabatic lapse rate* describes the parcel. Chapter 6 derived it from the first law of thermodynamics and the hydrostatic relation: an unsaturated parcel lifted without exchanging heat cools at

$$\Gamma_d = \frac{g}{c_p} = \frac{9.81\,\mathrm{m\,s^{-2}}}{1004\,\mathrm{J\,kg^{-1}\,K^{-1}}} = 9.77\,\mathrm{K\,km^{-1}} \approx 9.8\,\mathrm{K\,km^{-1}}. \tag{13.2}$$

It is a fixed number, the same everywhere in the lower atmosphere, because it depends only on gravity and the heat capacity of air. The two rates are different kinds of quantity: Γ_e is a property of the environment and changes all the time; Γ_d is a property of the process a displaced parcel undergoes and does not change. Stability is the comparison of the two. This chapter uses $\Gamma_d = 9.8\,\mathrm{K\,km^{-1}}$ in worked examples, as the rounded value.

13.1.3 The three comparisons

Let a parcel start at a height z_0 with the temperature T_0 of its surroundings and be lifted by δz. It cools at Γ_d, so its temperature is $T_0 - \Gamma_d\,\delta z$; the environment at the new height has $T_0 - \Gamma_e\,\delta z$. The parcel's temperature excess over its new surroundings is

$$T_{\text{parcel}} - T_{\text{env}} = (\Gamma_e - \Gamma_d)\,\delta z. \tag{13.3}$$

The parcel takes the pressure of its surroundings, and at equal pressure the density of air is inversely proportional to its temperature, so the buoyant acceleration b on the parcel, in $\mathrm{m\,s^{-2}}$, is

$$b = g\,\frac{\rho_{\text{env}} - \rho_{\text{parcel}}}{\rho_{\text{parcel}}} = g\,\frac{T_{\text{parcel}} - T_{\text{env}}}{T_{\text{env}}} = -\frac{g}{T}\,(\Gamma_d - \Gamma_e)\,\delta z, \tag{13.4}$$

positive upward. Three cases follow, for unsaturated air.

- *Stable*, $\Gamma_e < \Gamma_d$: the environment cools with height more slowly than the rising parcel. The lifted parcel is colder and denser than its new surroundings and sinks back; a parcel pushed down is warmer and rises back. The acceleration opposes the displacement.
- *Neutral*, $\Gamma_e = \Gamma_d$: a dry adiabatic atmosphere. The parcel has the temperature of its surroundings at every height and no buoyant force arises.
- *Unstable*, $\Gamma_e > \Gamma_d$: the environment cools with height faster than the parcel. The lifted parcel stays warmer than its surroundings and keeps rising; the acceleration is in the direction of the displacement.

Equation (13.4) is the parcel oscillation of Chapter 6 in lapse-rate form: $b = -N^2\,\delta z$ with $N^2 = (g/T)(\Gamma_d - \Gamma_e)$, which Section 13.2.2 shows is the same as $(g/\theta)\,\mathrm{d}\theta/\mathrm{d}z$.

A worked parcel. Take a parcel at 15°C (288.15 K) lifted $\delta z = 100\,\mathrm{m}$ in three illustrative environments with the same starting temperature. The parcel cools by $9.8 \times 0.1 = 0.98\,\mathrm{K}$, to 14.02°C, in all three.

- $\Gamma_e = 6.5\,\mathrm{K\,km^{-1}}$: the environment at 100 m is $15 - 0.65 = 14.35$°C. The excess is $(6.5 - 9.8) \times 0.1 = -0.33\,\mathrm{K}$ and $b = 9.81 \times (-0.33)/287.50 = -0.0113\,\mathrm{m\,s^{-2}}$: the parcel is pushed back down.
- $\Gamma_e = 9.8\,\mathrm{K\,km^{-1}}$: the environment is 14.02°C, the excess is zero and $b = 0$.
- $\Gamma_e = 12\,\mathrm{K\,km^{-1}}$: the environment is $15 - 1.2 = 13.80$°C. The excess is $(12 - 9.8) \times 0.1 = +0.22\,\mathrm{K}$ and $b = 9.81 \times 0.22/286.95 = +0.0075\,\mathrm{m\,s^{-2}}$: the parcel is pushed further up.

The accelerations are about a thousandth of g, but they act continuously. In the stable case $N^2 = (9.81/288.15)(3.3 \times 10^{-3}) = 1.12 \times 10^{-4}\,\mathrm{s^{-2}}$, $N = 0.0106\,\mathrm{s^{-1}}$, and a released parcel returns to its level in a quarter of the period $2\pi/N = 593\,\mathrm{s}$, about two and a half minutes. In the unstable case the displacement grows as $e^{\sigma t}$ with $\sigma = \sqrt{(9.81/288.15)(2.2 \times 10^{-3})} = 0.0087\,\mathrm{s^{-1}}$, by a factor e every two minutes.

Figure 13.1 draws the comparison on a temperature–height diagram. The horizontal axis is temperature and the vertical axis height above the starting level, from 0 to 200 m. The dashed black line is the dry adiabat through 15°C, the path of any unsaturated parcel that starts there; a neutral environment coincides with it. The three solid lines are environments: a superadiabatic one ($\Gamma_e = 12\,\mathrm{K\,km^{-1}}$), the standard lapse rate ($6.5\,\mathrm{K\,km^{-1}}$) and an inversion ($\mathrm{d}T/\mathrm{d}z = +5\,\mathrm{K\,km^{-1}}$). The dots mark the four temperatures at 100 m.

The reading is horizontal: at any height, an environment line to the right of the adiabat is warmer than the parcel, which sinks back (stable); one to the left is colder, and the parcel

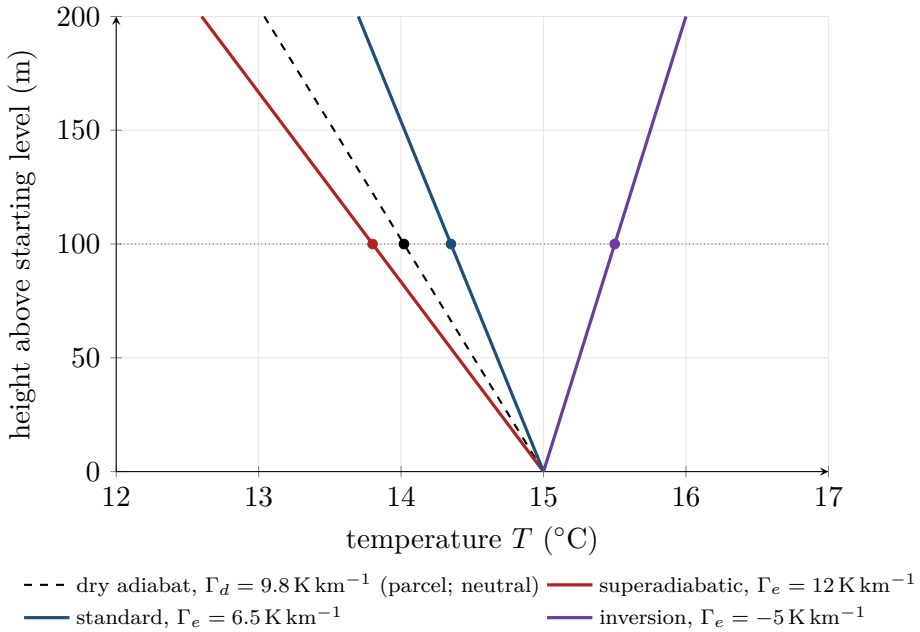


Figure 13.1: Temperature against height for a parcel and three environments, all starting at 15°C. Lines: $T = 15°\mathrm{C} - \Gamma z$ with the lapse rates in the legend. Dots at 100 m: parcel 14.02°C; superadiabatic environment 13.80°C (parcel 0.22 K warmer: unstable); standard environment 14.35°C (parcel 0.33 K colder: stable); inversion 15.50°C (parcel 1.48 K colder: strongly stable). Illustrative values.

keeps rising (unstable). The angle between the environment line and the adiabat grows with the strength of the stability or instability, and the inversion, tilted the other way, is the farthest from the adiabat of the three. Table 13.1 collects the same comparison for six environments, from superadiabatic to inversion; its columns give the lapse rate, the potential-temperature gradient that goes with it (Section 13.2.2), the excess temperature and the acceleration of a parcel lifted 100 m from 15°C, and the resulting class.

Table 13.1: Stability of six illustrative environments for an unsaturated parcel lifted 100 m from 15°C. The gradient of θ is $\Gamma_d - \Gamma_e$ with $\theta/T \approx 1$ (near 1000 hPa); the acceleration is equation (13.4).

Environment	Γ_e ($\mathrm{K\,km^{-1}}$)	$\mathrm{d}\theta/\mathrm{d}z$ ($\mathrm{K\,km^{-1}}$)	excess (K)	b ($\mathrm{m\,s^{-2}}$)	Class
Superadiabatic	12.0	−2.2	+0.22	+0.0075	unstable
Dry adiabatic	9.8	0	0	0	neutral
Standard atmosphere	6.5	+3.3	−0.33	−0.0113	stable
Weak lapse rate	5.0	+4.8	−0.48	−0.0164	stable, no inversion
Isothermal	0	+9.8	−0.98	−0.0334	stable
Inversion	−5.0	+14.8	−1.48	−0.0503	strongly stable

Principle 13.1. *For unsaturated air, stability is the comparison of the environmental lapse rate with the dry adiabatic lapse rate: $\Gamma_e < \Gamma_d$ is stable, $\Gamma_e = \Gamma_d$ neutral and $\Gamma_e > \Gamma_d$ unstable. The sign of $\mathrm{d}T/\mathrm{d}z$ alone does not decide it.*

13.1.4 Inversions, isothermal and superadiabatic layers

Three cases in Table 13.1 are worth stating separately, because each corrects a common misreading of a temperature profile.

Inversion. In an inversion, $\mathrm{d}T/\mathrm{d}z > 0$ and $\Gamma_e < 0$. A rising parcel cools at Γ_d while the environment warms with height, so the two rates act in opposite directions and the parcel falls behind its surroundings fastest: in Table 13.1 the inversion of $5\,\mathrm{K\,km^{-1}}$ gives a parcel lifted 100 m a deficit of 1.48 K and an acceleration of $-0.050\,\mathrm{m\,s^{-2}}$, four and a half times that of the standard atmosphere. Inversions are strongly stable; the nocturnal surface inversion and the capping inversion of the convective boundary layer (Chapter 6) are the two that matter most for near-surface wind.

Neutral is not isothermal. A neutral dry layer does not have constant temperature: its potential temperature is constant, $\mathrm{d}\theta/\mathrm{d}z = 0$, while its temperature falls at about $9.8\,\mathrm{K\,km^{-1}}$. An isothermal layer, $\mathrm{d}T/\mathrm{d}z = 0$, is stable, with $\mathrm{d}\theta/\mathrm{d}z = 9.8\,\mathrm{K\,km^{-1}}$, three times the potential-temperature gradient of the standard atmosphere. Reading a temperature profile that does not change with height as "neutral" confuses the temperature with the potential temperature.

Stable without an inversion. Stability does not require an inversion. With $\Gamma_e = 5\,\mathrm{K\,km^{-1}}$ the temperature decreases with height, yet $5 < 9.8$ and the layer is stable, with $\mathrm{d}\theta/\mathrm{d}z \approx 4.8\,\mathrm{K\,km^{-1}}$. Most of the free troposphere is in this state: temperature falls with height and the air is stable. An inversion is strongly stable; a decrease of temperature slower than Γ_d is stable; only a decrease faster than Γ_d is unstable.

Superadiabatic layers. A layer with $\Gamma_e > \Gamma_d$ is *superadiabatic*: its temperature falls faster than the dry adiabatic rate, and it is unstable for every parcel, unsaturated or saturated, since a saturated parcel cools more slowly still (Section 13.1.5). Such a layer is called *absolutely unstable*. It cannot persist through a deep layer, because the convection it drives mixes it toward neutral within minutes. It is common, however, in a very shallow layer over a strongly heated surface by day, where the ground heats the air faster than the convection can remove the heat. An illustrative sunny afternoon with the air 1.5 K warmer at 2 m than at 10 m has $\Gamma_e = 1.5/8 = 0.19\,\mathrm{K\,m^{-1}} = 190\,\mathrm{K\,km^{-1}}$, about twenty times the adiabatic rate, in the lowest meters. Above a few tens of meters the convective boundary layer is close to neutral.

13.1.5 Moisture and the saturated adiabatic lapse rate

The comparisons above hold for unsaturated air. Moisture changes them in two ways. First, water vapor is lighter than dry air, so in unsaturated moist air the comparison of densities uses the virtual potential temperature θ_v of Chapter 6 instead of θ; the correction is a kelvin or two in θ_v itself and usually small in its vertical gradient, but it matters over warm humid surfaces when the temperature gradient is weak. Second, a rising *saturated* parcel condenses water as it cools, and the latent heat released offsets part of the cooling by expansion. Its temperature falls at the *saturated adiabatic lapse rate* Γ_s (also called the moist or pseudo-adiabatic lapse rate), which depends on temperature and pressure because warm air holds more water to condense. At 1000 hPa it is about $3.5\,\mathrm{K\,km^{-1}}$ at 30°C, $4.2\,\mathrm{K\,km^{-1}}$ at 20°C and $6.5\,\mathrm{K\,km^{-1}}$ at 0°C, approaching Γ_d in very cold air; roughly 4 to $7\,\mathrm{K\,km^{-1}}$ over the range of the lower atmosphere.

With two parcel rates, the comparison has three outcomes instead of two. A layer with $\Gamma_e < \Gamma_s$ is *absolutely stable*, stable for unsaturated and saturated parcels alike. A layer with $\Gamma_e > \Gamma_d$ is absolutely unstable. A layer between the two, $\Gamma_s < \Gamma_e < \Gamma_d$, is *conditionally unstable*:

stable for an unsaturated parcel, unstable for a saturated one. The standard lapse rate of $6.5\,\mathrm{K\,km^{-1}}$ is conditionally unstable in warm humid air, where $\Gamma_s \approx 4\,\mathrm{K\,km^{-1}}$: this is the setting of deep tropical and summer convection over much of South America, where a parcel lifted to saturation can rise freely into a thunderstorm. *Moist static stability* is the stability of a layer judged against the saturated rate, or equivalently by the vertical gradient of the equivalent potential temperature, the potential temperature a parcel would have if all its vapor were condensed and the latent heat retained.

For near-surface wind the dry analysis is usually enough at first. Below cloud base the air near the ground is unsaturated, and its stability is described by the gradient of θ, or of θ_v, and by the surface heat flux of Section 13.5.2. Moisture enters through other routes, such as fog, which forms in the stable layer and then alters its cooling, and the outflow of thunderstorms, whose gusts and gust fronts are treated in Chapter 19.

13.2 Stability in terms of potential temperature

Comparing two lapse rates works, but it requires two numbers and a moving parcel; potential temperature combines both into one profile. This section restates the criterion with θ, derives the exact link between the potential-temperature gradient and the two lapse rates, converts the worked lapse rates into gradients of θ, and shows how surface heating and cooling produce the unstable and stable stratification.

13.2.1 The potential-temperature criterion

The potential temperature, derived in Chapter 6,

$$\theta = T\left(\frac{p_0}{p}\right)^{R_d/c_p}, \qquad p_0 = 1000\,\mathrm{hPa}, \tag{13.5}$$

is the temperature a parcel would have if brought adiabatically to 1000 hPa. It removes the warming and cooling caused by adiabatic compression and expansion: an unsaturated parcel that moves vertically without exchanging heat keeps its θ, while its T changes at Γ_d. On a θ–height diagram the dry adiabat of Figure 13.1 becomes a vertical line, and the comparison of a parcel with its surroundings becomes a comparison of one number, the parcel's θ, with the profile of the environment. For dry air the criterion is

$$\frac{\mathrm{d}\theta}{\mathrm{d}z} > 0 \text{ stable}, \qquad \frac{\mathrm{d}\theta}{\mathrm{d}z} = 0 \text{ neutral}, \qquad \frac{\mathrm{d}\theta}{\mathrm{d}z} < 0 \text{ unstable}, \tag{13.6}$$

with θ_v in place of θ for moist unsaturated air. It needs no reference to a parcel's path and no second lapse rate, which is why it is the form used in practice.

The meaning of an increasing θ is the parcel argument in one line. A parcel moved upward adiabatically keeps its potential temperature. If θ increases with height, the surroundings at the new height have a larger θ than the parcel; at the same pressure a larger θ means a higher temperature and a lower density, so the parcel is colder and denser than its surroundings and sinks back. A parcel moved downward arrives among air of smaller θ, is lighter and rises back. A profile of θ that increases with height is therefore a stack of layers each lighter than the one below, the stable arrangement; one that decreases with height has heavier air over lighter, and overturns.

13.2.2 Lapse rates and the potential-temperature gradient

The two forms of the criterion are linked exactly. Taking the logarithm of equation (13.5), $\ln\theta = \ln T + (R_d/c_p)(\ln p_0 - \ln p)$, and differentiating with height in the environment,

$$\frac{1}{\theta}\frac{\mathrm{d}\theta}{\mathrm{d}z} = \frac{1}{T}\frac{\mathrm{d}T}{\mathrm{d}z} - \frac{R_d}{c_p}\,\frac{1}{p}\frac{\mathrm{d}p}{\mathrm{d}z}.$$

The environment is hydrostatic, $\mathrm{d}p/\mathrm{d}z = -\rho g$, and by the ideal-gas law $\rho/p = 1/(R_d T)$, so the last term is $+(R_d/c_p)\,g/(R_d T) = g/(c_p T) = \Gamma_d/T$. With $\mathrm{d}T/\mathrm{d}z = -\Gamma_e$,

$$\frac{\mathrm{d}\theta}{\mathrm{d}z} = \frac{\theta}{T}\,(\Gamma_d - \Gamma_e). \tag{13.7}$$

The potential-temperature gradient is the difference of the two lapse rates, scaled by θ/T, which is 1 at 1000 hPa and a few percent larger at lower pressures. Its sign is the sign of $\Gamma_d - \Gamma_e$, so equations (13.6) and the three comparisons of Section 13.1.3 are the same statement. Multiplying by g/θ gives $(g/\theta)\,\mathrm{d}\theta/\mathrm{d}z = (g/T)(\Gamma_d - \Gamma_e)$: the squared buoyancy frequency is the same whether computed from θ or from the two lapse rates, as used in Section 13.1.3.

Worked conversions. Near 1000 hPa, $\theta/T \approx 1$ and the gradient is simply $\Gamma_d - \Gamma_e$. The standard lapse rate gives $\mathrm{d}\theta/\mathrm{d}z = 9.8 - 6.5 = 3.3\,\mathrm{K\,km^{-1}}$, or 0.33 K per 100 m: stable. The weak lapse rate of $5\,\mathrm{K\,km^{-1}}$ gives $9.8 - 5 = 4.8\,\mathrm{K\,km^{-1}}$, 0.48 K per 100 m: more stable, although the temperature still falls with height. At 850 hPa, with the illustrative $T = 283.15$ K used in Chapter 6, $\theta = 296.6$ K and $\theta/T = 1.048$, so the same two lapse rates give $1.048 \times 3.3 = 3.46$ and $1.048 \times 4.8 = 5.03\,\mathrm{K\,km^{-1}}$. The factor changes the size of the gradient by a few percent and never its sign. The superadiabatic $12\,\mathrm{K\,km^{-1}}$ gives $-2.2\,\mathrm{K\,km^{-1}}$ near 1000 hPa, and the inversion of $-5\,\mathrm{K\,km^{-1}}$ gives $+14.8\,\mathrm{K\,km^{-1}}$, as listed in Table 13.1.

Measuring the gradient. A tower measures T at two heights, not θ. Over a height difference Δz of tens of meters the pressure changes by only a few hectopascals, and equation (13.7) integrated over the layer gives the working rule

$$\Delta\theta \approx \Delta T + \Gamma_d\,\Delta z, \tag{13.8}$$

with ΔT the measured difference, upper minus lower. Between 10 and 80 m, $\Gamma_d\,\Delta z = 0.00977 \times 70 = 0.68$ K: a measured temperature decrease of 0.5 K is a potential-temperature increase of 0.18 K, a stable layer. Since the stability depends on a difference of a few tenths of a kelvin, the two thermometers must agree to better than about 0.1 K, which requires matched, ventilated and radiation-shielded sensors; an unshielded sensor in sunshine can be in error by more than the whole difference.

13.2.3 Surface heating and cooling

Near the ground the stratification is set by the surface. By day, sunlight absorbed by the ground warms it above the air temperature, and the ground heats the air in contact with it. The lowest air then has a higher potential temperature than the air above, $\theta_{\mathrm{low}} > \theta_{\mathrm{above}}$, so $\mathrm{d}\theta/\mathrm{d}z < 0$: the layer near the ground is unstable, warm air rises in plumes and thermals, and the turbulence is fed by buoyancy as well as by shear. This is *convective turbulence*, the subject of the convective boundary layer of Chapter 6.

At night, and most strongly under clear skies with light wind, the ground loses heat by longwave radiation to space and cools below the air temperature. The air in contact with it is cooled from below, so $\theta_{\mathrm{low}} < \theta_{\mathrm{above}}$ and $\mathrm{d}\theta/\mathrm{d}z > 0$: the layer is stable, often with a surface

inversion, and turbulence is suppressed. The heat flux between the ground and the air carries the information: upward by day ($\overline{w'\theta'} > 0$), downward at night ($\overline{w'\theta'} < 0$).

Figure 13.2 draws the two cases. Each panel shows the ground as a gray strip, the radiation that heats or cools it as a labeled arrow, the turbulent heat flux between the ground and the air as red arrows, and, on the right, a sketch of potential temperature against height in the lowest hundred meters, with θ on the horizontal axis.

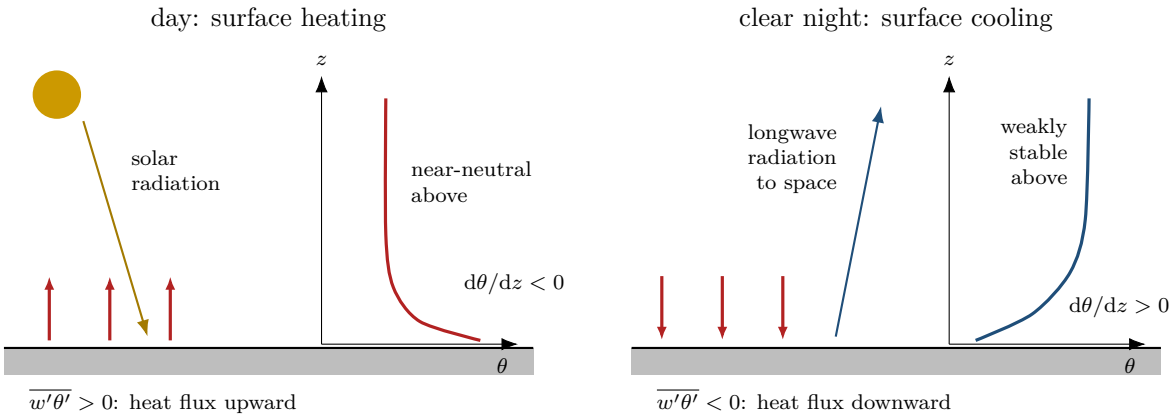


Figure 13.2: Surface heating and cooling (schematic). Day: absorbed sunlight heats the ground, the heat flux is upward and θ decreases with height near the ground (unstable). Clear night: the ground radiates to space, the heat flux is downward and θ increases with height near the ground (stable). The θ sketches span roughly the lowest 100 m.

The two θ sketches are the near-ground parts of the daytime and nighttime profiles: the daytime one bends to the left toward the ground, warmest at the surface, and the nighttime one bends to the right, coldest at the surface. In both, the departure from the vertical is concentrated in the lowest tens of meters, where the surface exchange is strongest; above it the daytime air is nearly neutral and the nighttime air weakly stable. The same ground thus switches the stratification above it from unstable to stable twice a day, and with it the coupling between the surface and the wind aloft treated next.

Principle 13.2. *For dry air,* $\mathrm{d}\theta/\mathrm{d}z$ *classifies static stability: positive is stable, zero neutral, negative unstable; it equals* $(\theta/T)(\Gamma_d - \Gamma_e)$*, and near the ground its sign follows the sign of the surface heat flux.*

13.3 Stability and the wind profile

Stability matters for wind because it sets how strongly turbulence mixes momentum between heights. This section describes the wind shear in each stability state, works one example in which the same wind aloft gives very different surface winds, places stability within the energy balance of turbulence, and describes the acceleration of the air above a stable layer.

13.3.1 Shear in each stability state

The vertical wind shear $\partial U/\partial z$ is set by a balance: the surface removes momentum at the bottom, and turbulence replaces it from above. The stronger the vertical mixing, the smaller the shear needed to carry the same downward flux of momentum, since $-\overline{u'w'} = K_m\,\partial U/\partial z$ with the eddy diffusivity K_m of Chapter 8. Stability changes K_m, and so the shear.

In *unstable* conditions, buoyant plumes add to the mechanical eddies, K_m is large, and momentum is mixed efficiently through a deep layer. The profile is flatter than the neutral

logarithmic one above the lowest meters, the shear is small, and the wind at 10 m is a large fraction of the wind at 100 m. In *neutral* conditions the shear is set by the surface drag alone and the profile is the logarithmic law of Chapter 7. In *stable* conditions, buoyancy removes energy from the eddies, K_m is small, the momentum of the flow aloft is not efficiently carried down, and the shear is large; the wind at 10 m can be a small fraction of the wind at 100 m, and large differences between the two heights are the norm on clear nights. The order is fixed: at a given wind aloft, shear increases from unstable to neutral to stable.

13.3.2 Same forcing, different surface wind

Consider a site where the wind at 200 m is $15\,\mathrm{m\,s^{-1}}$ both on a convective afternoon and on a stable night, under similar large-scale pressure gradients. On the afternoon, strong mixing couples the surface to the flow aloft and the wind at 10 m may be about $9\,\mathrm{m\,s^{-1}}$. On the stable night the surface is weakly coupled and the 10 m wind may be only about $3\,\mathrm{m\,s^{-1}}$. The forcing is similar; the coupling differs. Figure 13.3 draws the two illustrative profiles. The horizontal axis is wind speed and the vertical axis height above the ground from 0 to 250 m; the dots mark the values at 10 and 200 m.

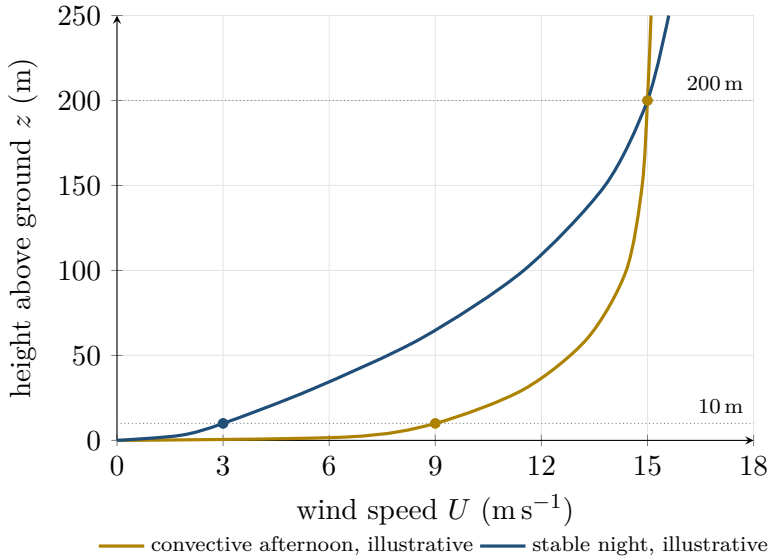


Figure 13.3: The same $15\,\mathrm{m\,s^{-1}}$ at 200 m on a convective afternoon and on a stable night (illustrative profiles drawn through chosen points). Afternoon: $U_{10} = 9\,\mathrm{m\,s^{-1}}$, mean shear between 10 and 200 m of $0.032\,\mathrm{s^{-1}}$. Night: $U_{10} = 3\,\mathrm{m\,s^{-1}}$, mean shear $0.063\,\mathrm{s^{-1}}$.

The afternoon profile rises steeply in the lowest tens of meters and is nearly uniform above about 100 m: the mixing has spread the momentum through the layer. The night profile increases steadily all the way up. Between 10 and 200 m the mean shear is $(15 - 9)/190 = 0.032\,\mathrm{s^{-1}}$ in the afternoon and $(15 - 3)/190 = 0.063\,\mathrm{s^{-1}}$ at night, twice as large. Expressed as the exponent of a power law between the two heights, $\alpha = \ln(U_{200}/U_{10})/\ln 20$, the afternoon gives $\ln(15/9)/2.996 = 0.17$ and the night $\ln 5/2.996 = 0.54$. The 10 m wind differs by a factor of three with the same forcing aloft. For a transmission line, whose convective cooling increases with the wind across the conductor, the night is the critical case: a rating that assumes the afternoon coupling at night overstates the wind at the conductor threefold.

13.3.3 Mechanical and buoyant turbulence

The physical reason is the budget of turbulent kinetic energy derived in Chapter 8. Turbulence near the ground has two production terms. *Shear production*, $P_s = -\overline{u'w'}\,\partial\overline{u}/\partial z$, converts

kinetic energy of the mean wind into eddies wherever the wind changes with height; it is always positive near the ground. *Buoyancy production*, $P_b = (g/\theta_v)\,\overline{w'\theta_v'}$, is positive when the heat flux is upward and convection feeds the eddies, and negative when the heat flux is downward: then it is *buoyancy destruction*, the work the eddies do lifting cold air and lowering warm air against the stratification. The stability state is therefore not a property of the temperature profile alone but of the balance between shear, which creates turbulence, and stratification, which either helps it or destroys it. Figure 13.4 draws that balance as a chain of boxes from the two sources on the left to the wind profile on the right; the dashed arrow at the top is the feedback by which the mixing changes the shear that produced it.

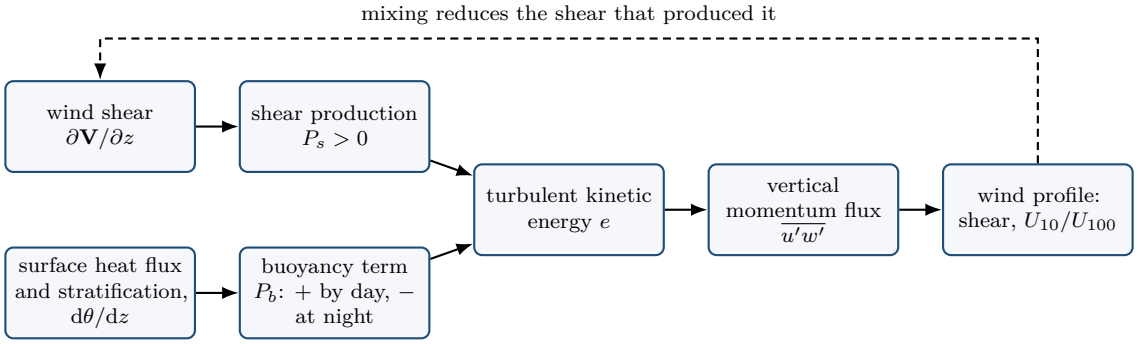


Figure 13.4: Stability in the turbulence budget (schematic). Shear and the buoyancy term set the turbulent kinetic energy; the turbulence carries momentum downward and shapes the profile; the profile's shear feeds back on shear production. By day both sources add; at night the buoyancy term subtracts.

Read from left to right, the figure is the key idea of the chapter. By day both sources feed the turbulence, the momentum flux is carried by vigorous eddies, and the shear needed is small. At night the buoyancy term subtracts from shear production; to keep a given momentum flux the shear must be larger, and if the buoyancy destruction wins, the turbulence weakens and the flux falls. The feedback arrow explains why stable layers can be self-reinforcing: weaker mixing lets the surface cool further and the stratification strengthen. It also explains why they can break down: weaker mixing lets the shear grow, and a large enough shear can restore the turbulence. Which effect wins is measured by the Richardson number of Section 13.4.

13.3.4 Acceleration above the stable layer

By day the whole boundary layer feels the drag of the ground: turbulence transmits the surface stress upward through the mixed layer, and the wind there stays below the geostrophic wind and turned toward low pressure (Chapter 3). After sunset the stable layer that forms near the ground transmits the drag upward much less efficiently. The air above it, in the residual layer, is suddenly relieved of most of its friction, while the pressure-gradient force that drives it is unchanged. It accelerates toward a more nearly geostrophic state.

The acceleration does not stop at the geostrophic wind. Once friction is removed, the ageostrophic part of the wind is no longer balanced and rotates with the inertial period $2\pi/|f|$, clockwise in the Northern Hemisphere and counterclockwise in the Southern, and the wind speed overshoots the geostrophic value some hours after sunset. The result is a wind maximum a few hundred meters above the ground, faster than the wind both above and below it: a *low-level jet*, treated in Chapter 18. The inertial period is about 18.6 h at 40° latitude ($|f| = 9.4 \times 10^{-5}\,\mathrm{s}^{-1}$) and about 30.6 h at 23° ($|f| = 5.7 \times 10^{-5}\,\mathrm{s}^{-1}$), so the timing of the maximum depends on latitude. For near-surface wind the consequence is that a stable night can bring the strongest winds of the day at turbine heights while the conductor of a transmission line, below the stable

layer, sits in nearly calm air.

13.4 The Richardson numbers

The competition between shear and stratification is measured by the Richardson number. This section derives the gradient Richardson number from the turbulence budget, states its interpretation and the meaning and limits of the critical value, defines the bulk Richardson number used with two measurement levels, and maps the regimes of shear and stratification.

13.4.1 The gradient Richardson number

Chapter 8 defined the *flux Richardson number* as the ratio of buoyancy destruction to shear production,

$$\mathrm{Ri}_f = -\frac{P_b}{P_s} = \frac{-(g/\theta)\,\overline{w'\theta'}}{-\overline{u'w'}\,\partial\overline{u}/\partial z - \overline{v'w'}\,\partial\overline{v}/\partial z}, \tag{13.9}$$

written here with both components of the momentum flux so that it holds when the wind turns with height (for moist air, θ_v replaces θ). It requires the fluxes, which only a fast-response instrument measures. The fluxes can be replaced by gradients with the flux–gradient closure of Chapter 8, which writes each flux as an eddy diffusivity times the mean gradient:

$$\overline{u'w'} = -K_m \frac{\partial\overline{u}}{\partial z}, \qquad \overline{v'w'} = -K_m \frac{\partial\overline{v}}{\partial z}, \qquad \overline{w'\theta'} = -K_h \frac{\partial\overline{\theta}}{\partial z}.$$

Substituting, the shear production becomes $P_s = K_m\left[(\partial\overline{u}/\partial z)^2 + (\partial\overline{v}/\partial z)^2\right]$ and the buoyancy destruction $-P_b = (g/\theta)\,K_h\,\partial\overline{\theta}/\partial z$, so

$$\mathrm{Ri}_f = \frac{K_h}{K_m}\,\frac{(g/\theta)\,\partial\overline{\theta}/\partial z}{(\partial\overline{u}/\partial z)^2 + (\partial\overline{v}/\partial z)^2} = \frac{\mathrm{Ri}_g}{\mathrm{Pr}_t}. \tag{13.10}$$

The second factor is the *gradient Richardson number*

$$\mathrm{Ri}_g = \frac{(g/\theta)\,\partial\overline{\theta}/\partial z}{(\partial\overline{u}/\partial z)^2 + (\partial\overline{v}/\partial z)^2} = \frac{N^2}{|\partial\mathbf{V}/\partial z|^2}, \tag{13.11}$$

and $\mathrm{Pr}_t = K_m/K_h$ is the turbulent Prandtl number. The gradient Richardson number is the squared buoyancy frequency divided by the square of the vector wind shear: the stabilizing effect of the stratification over the destabilizing effect of the shear. It is dimensionless (both terms are in s^{-2}), it uses only mean profiles, which towers, radiosondes, lidars and models all provide, and it is related to the flux form by $\mathrm{Ri}_g = \mathrm{Pr}_t\,\mathrm{Ri}_f$. Near neutral, $\mathrm{Pr}_t \approx 1$ and the two are nearly equal.

Two details of equation (13.11) matter in practice. The denominator is the square of the shear of the wind *vector*, not of the wind speed: when the wind turns with height, as it does across the stable layer, the vector shear exceeds the speed shear and the Richardson number computed from speeds alone is too large. And the numerator uses θ (or θ_v), not T: a temperature gradient must be converted with equation (13.8) before it enters.

13.4.2 Interpretation and the critical value

The sign of Ri_g is the sign of $\mathrm{d}\theta/\mathrm{d}z$, since the denominator is positive.

- $\mathrm{Ri}_g < 0$: unstable stratification; buoyancy helps the turbulence, and the more negative Ri_g, the larger the share of buoyancy in it.
- $\mathrm{Ri}_g \approx 0$: approximately neutral; the turbulence is produced by shear.

- $\mathrm{Ri}_g > 0$: stable stratification; buoyancy suppresses the turbulence, although strong enough shear can maintain it.

The size matters as well as the sign. A stable layer with $\mathrm{Ri}_g = 0.05$ is turbulent almost as if neutral; one with $\mathrm{Ri}_g = 1$ has the shear outweighed by the stratification.

Classic theory places the boundary at the *critical Richardson number* $\mathrm{Ri}_c \approx 0.25$. The value comes from the linear stability of a smooth, laminar, stratified shear flow: such a flow can become unstable to small waves, which grow into turbulence, only where $\mathrm{Ri}_g < 1/4$; where $\mathrm{Ri}_g \geq 1/4$ everywhere, small disturbances do not grow. In the turbulence budget a similar limit appears: with $\mathrm{Pr}_t \approx 1$, shear-driven turbulence fades when Ri_f reaches about 0.2 to 0.25 (Chapter 8). Turbulence is therefore hard to sustain for $\mathrm{Ri}_g \gtrsim 0.25$.

The value is a reference, not a universal threshold. First, it is a criterion for the *onset* of turbulence in a laminar flow; flow that is already turbulent can stay turbulent up to Ri_g of order one, so the transition shows hysteresis. Second, in stable conditions Pr_t rises above one, because waves continue to carry momentum where heat transport is suppressed, so $\mathrm{Ri}_g = \mathrm{Pr}_t\,\mathrm{Ri}_f$ can exceed 0.25 while Ri_f stays below it. Third, turbulence observed at a height need not be produced there: it can be intermittent, in bursts separated by quiet periods, or nonlocal, carried in from a more strongly sheared layer above or generated by breaking waves. A measured Ri_g of 0.4 therefore indicates weak or intermittent turbulence, not its absence.

13.4.3 The bulk Richardson number

Gradients are rarely measured; differences between two levels are. Replacing each derivative in equation (13.11) by a finite difference across a layer of depth Δz gives the *bulk Richardson number*

$$\mathrm{Ri}_B = \frac{g}{\theta_0}\,\frac{\Delta\theta\,\Delta z}{(\Delta\overline{u})^2 + (\Delta\overline{v})^2}, \tag{13.12}$$

with $\Delta\theta$, $\Delta\overline{u}$ and $\Delta\overline{v}$ the differences, upper minus lower, of the mean potential temperature and of the two wind components, and θ_0 a reference potential temperature, the layer mean. It is widely used in observations, from two levels of a mast or of a radiosonde, and in models, where the surface-layer schemes compute it between the ground and the lowest model level and the boundary-layer schemes use it to find the top of the boundary layer (Chapter 6). The wind difference is that of the vectors: with speeds U_1, U_2 and a turning $\Delta\beta$ between the two levels, $(\Delta\overline{u})^2 + (\Delta\overline{v})^2 = U_1^2 + U_2^2 - 2U_1U_2\cos\Delta\beta$.

Bulk and gradient values. Near the ground the profiles are curved, so a difference across a finite layer does not equal the gradient at either end. If both the wind and θ vary as $\ln z$, as in the neutral surface layer, a difference between z_1 and z_2 equals the gradient at the height $z_m = (z_2 - z_1)/\ln(z_2/z_1)$, and the bulk number equals the gradient number there. For levels at 10 and 80 m, $z_m = 70/\ln 8 = 33.7$ m. A bulk value is thus a value for a layer, assigned to a height inside it; the critical values used with bulk numbers in models differ from 0.25 and depend on the layer depth.

A worked mast. A 80 m mast at an illustrative site near sea level at 23°S has thermometers and anemometers at 10 and 80 m. Table 13.2 lists three half-hour averages: a sunny afternoon, an early night and a late night. Its columns give the temperatures, speeds and directions at the two levels and the quantities computed from them.

In the afternoon the temperature falls by 1.0 K between the two levels, but $\Delta\theta = -1.0{+}0.68 = -0.32$ K: the layer is superadiabatic on average. The wind does not turn, so $|\Delta\mathbf{V}| = 7.0 - 6.0 = 1.0\,\mathrm{m\,s^{-1}}$ and

$$\mathrm{Ri}_B = \frac{9.81}{302.7} \times \frac{(-0.316)\times 70}{1.0^2} = 0.0324 \times (-22.1) = -0.72,$$

Table 13.2: Bulk Richardson number from a two-level mast at 10 and 80 m, $\Delta z = 70$ m, at an illustrative site at 23°S. $\Delta\theta = \Delta T + 0.68$ K (equation (13.8)); $|\Delta\mathbf{V}|$ is the vector difference; Ri_B from equation (13.12), and from speeds alone in the last column.

Case	T_{10} (°C)	T_{80} (°C)	U_{10}, β_{10} ($\mathrm{m\,s^{-1}}$, °)	U_{80}, β_{80} ($\mathrm{m\,s^{-1}}$, °)	$\Delta\theta$ (K)	θ_0 (K)	$\lvert\Delta\mathbf{V}\rvert$ ($\mathrm{m\,s^{-1}}$)	Ri_B	speeds
Afternoon	30.0	29.0	6.0, 160	7.0, 160	−0.32	302.7	1.00	−0.72	−0.72
Early night	12.0	14.0	3.0, 160	9.0, 135	+2.68	286.2	6.41	+0.16	+0.18
Late night	10.0	12.8	1.0, 160	5.0, 135	+3.48	284.6	4.12	+0.50	+0.53

strongly unstable: with a weak shear, buoyancy dominates. In the early night the temperature rises by 2.0 K (an inversion) and $\Delta\theta = 2.68$ K. The wind increases from 3 to 9 $\mathrm{m\,s^{-1}}$ and backs from 160 to 135°, counterclockwise with height, as expected in the Southern Hemisphere where friction turns the surface wind toward low pressure on the right of the flow. The vector difference is $\sqrt{9 + 81 - 2 \times 3 \times 9 \times \cos 25^\circ} = \sqrt{41.06} = 6.41\ \mathrm{m\,s^{-1}}$, and

$$\mathrm{Ri}_B = \frac{9.81}{286.2} \times \frac{2.684 \times 70}{41.06} = 0.0343 \times 4.58 = 0.157.$$

The layer is stable, with an inversion, but below the critical value: the strong shear keeps it turbulent. Using the speed difference alone, 6.0 $\mathrm{m\,s^{-1}}$, would give 0.179, 14 % too large. In the late night the wind aloft has weakened to 5 $\mathrm{m\,s^{-1}}$, the 10 m wind is 1 $\mathrm{m\,s^{-1}}$ and the inversion has strengthened; $\mathrm{Ri}_B = 0.50$, twice the critical value, and the surface layer is close to decoupled. At the same site in the Northern Hemisphere the same profiles would veer, turning clockwise with height, and the Richardson numbers would be unchanged, since only the size of the turning enters.

13.4.4 Regimes of shear and stratification

The Richardson number places every layer on a plane of shear against stratification. Figure 13.5 draws that plane. The horizontal axis is the magnitude of the vector shear $|\partial\mathbf{V}/\partial z|$ from 0 to 0.12 $\mathrm{s^{-1}}$; the vertical axis is the squared buoyancy frequency $N^2 = (g/\theta)\,\mathrm{d}\theta/\mathrm{d}z$ in $10^{-3}\,\mathrm{s^{-2}}$, negative below the horizontal axis for unstable layers. The curve is $\mathrm{Ri}_g = 0.25$, the parabola $N^2 = 0.25\,|\partial\mathbf{V}/\partial z|^2$. The three shaded regions are the unstable half-plane, the stable region below the curve, and the stable region above it. The three dots are the mast layers of Table 13.2, with shear $|\Delta\mathbf{V}|/\Delta z$ and $N^2 = (g/\theta_0)\,\Delta\theta/\Delta z$.

A layer moves on this plane as conditions change. Moving up means stronger stratification, moving right stronger shear, and the Richardson number is constant along parabolas through the origin. The afternoon layer lies just below the axis, with little shear and little stratification, but in the unstable region. The early-night layer is well above the axis, with an inversion, yet to the right of the curve: stable and turbulent. The late-night layer has slightly stronger stratification and much weaker shear, and lies above the curve.

Stable does not mean no turbulence. The early-night layer shows that stability does not by itself suppress turbulence. Strong enough shear can overcome buoyant suppression: the same inversion of 2 K across 70 m is turbulent under a 6.4 $\mathrm{m\,s^{-1}}$ wind difference and nearly quiet under 2 $\mathrm{m\,s^{-1}}$. The Richardson number is therefore more informative than the temperature gradient alone. A forecaster who sees an inversion on a sounding and concludes that the surface is calm will be wrong on windy nights, when strong shear keeps the Richardson number low and the surface wind well mixed; the inversion says the layer is stable, and the Richardson number says whether the stability wins.

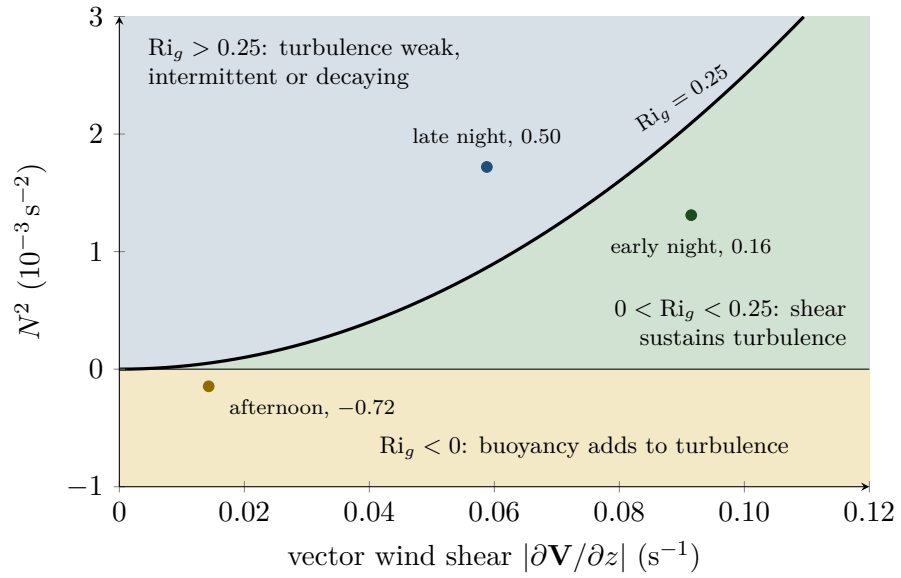


Figure 13.5: Regimes of shear and stratification. The curve $N^2 = 0.25\,|\partial \mathbf{V}/\partial z|^2$ is $\mathrm{Ri}_g = 0.25$; below the horizontal axis $N^2 < 0$ (unstable). Dots: the three mast layers of Table 13.2, labeled with their bulk Richardson numbers. Region boundaries are reference values, not sharp thresholds.

13.4.5 Very stable conditions

When Ri_g is well above the critical value, the boundary layer enters a regime that differs in kind from the weakly stable one. The turbulence is weak, intermittent and shallow: it may be confined to the lowest few meters, or to a layer aloft below a low-level jet, with nearly laminar air in between. Its typical history is a cycle of collapse and burst described in Chapter 6: the turbulence collapses, the surface decouples, the air aloft accelerates and the shear grows, the Richardson number falls below the critical value, a burst of mixing transfers momentum and heat down, the shear is reduced and the turbulence collapses again. Each burst can raise the 10 m wind by a few meters per second for minutes.

Very stable conditions are hard to model for three reasons. The averages over which turbulence theory is written lose their meaning when the flux is carried by a few events per hour. Processes usually negligible, such as gravity waves, drainage of cold air down gentle slopes and radiative cooling within the air itself, become comparable to the turbulent fluxes. And the result is sensitive to small differences: whether a night stays coupled or decouples can depend on a few tenths of a meter per second of wind aloft. Weather models therefore usually keep a minimum level of mixing in stable conditions to avoid unrealistic decoupling, which is one source of the nighttime errors of Section 13.6.4.

13.5 Static stability and surface-layer stability

"The surface layer is stable" can mean two different things. This section separates the stability read from a profile from the stability read from the surface fluxes, explains why the flux is the more informative of the two, previews the Obukhov length and the stability parameter, and relates the gradient Richardson number to the stability parameter.

13.5.1 Two meanings of stability

Static stability is a property of the stratification: the sign and size of $\mathrm{d}\theta/\mathrm{d}z$, or of N^2, in a layer. It is what the parcel argument of Sections 13.1 and 13.2 describes, and it is read from a temperature profile alone. It says what would happen to a displaced parcel; it does not say how much turbulence there is.

Surface-layer stability is a property of the turbulence near the ground: the combined effect of the surface heat flux, which produces or destroys turbulent energy by buoyancy, and of the mechanical turbulence, which shear produces from the surface stress. It is characterized by the stability parameter z/L_O of Section 13.5.3, which compares the two. In surface-layer meteorology and in the surface schemes of weather models, a statement such as "the surface layer is stable" usually means that the Obukhov length is positive, that is, that the heat flux is downward, rather than that a positive gradient of θ has been observed. Both are usually true together, but they are different measurements, and they can disagree in the cases that matter: near the transitions at sunrise and sunset, in the convective mixed layer, and when the gradient is too small to measure.

13.5.2 The heat flux and the gradient

The surface heat flux is the more informative of the two because it is the process, not its trace. A cooling surface has $\overline{w'\theta'} < 0$, and by the buoyancy term of the turbulence budget, $P_b = (g/\theta)\,\overline{w'\theta'} < 0$: buoyancy is *actively* removing energy from the eddies at that moment, at a rate that can be compared directly with shear production. A gradient $\mathrm{d}\theta/\mathrm{d}z > 0$ says only that a stratification exists; how much it suppresses the turbulence depends on how much turbulence there is to work against, which the gradient does not contain.

Three situations show the difference. In the upper part of a convective mixed layer, θ often increases slightly with height (statically stable by the local criterion), yet the layer is vigorously turbulent because the heat flux at the surface drives thermals through it (Chapter 6). Just after sunset the heat flux has already turned downward while the gradient near the ground is still close to zero; the buoyancy destruction has started before the profile shows it. And in strong wind the gradient can be too small to measure reliably while the heat flux, measured by eddy covariance (Chapter 9), is clear. Monin–Obukhov similarity theory, the framework of the next chapter, therefore characterizes the stability of the surface layer by the turbulent fluxes of momentum and heat, not by the gradients alone; the gradients become outputs of the theory.

13.5.3 The Obukhov length and the stability parameter

The comparison of buoyancy with mechanical turbulence is made by one length. The *Obukhov length* is

$$L_\mathrm{O} = -\frac{u_*^3\,\theta_v}{\kappa\, g\, \overline{w'\theta'_v}} \approx -\frac{u_*^3\,\theta}{\kappa\, g\, \overline{w'\theta'}}, \tag{13.13}$$

in meters, built from the friction velocity u_*, which measures the mechanical turbulence (Chapter 10), and the surface heat flux, which measures the buoyancy; the second form is for dry air. Its magnitude is, roughly, the height above which buoyancy becomes as important as shear in producing or destroying turbulence: below $|L_\mathrm{O}|$ the turbulence is mainly mechanical, above it mainly buoyant. Chapter 14 derives it and Chapter 15 interprets its values; here it is a preview.

Its sign follows the heat flux, because of the minus sign in its definition:

- unstable, $\overline{w'\theta'} > 0$: $L_\mathrm{O} < 0$;
- stable, $\overline{w'\theta'} < 0$: $L_\mathrm{O} > 0$;

- neutral, heat flux $\to 0$: $|L_{\mathrm{O}}| \to \infty$.

The *stability parameter* z/L_{O} is the measurement height divided by the Obukhov length, written ζ in much of the literature (this book keeps ζ for vorticity). It is negative in unstable conditions, near zero in neutral conditions and positive in stable conditions, and its magnitude says how far from neutral the surface layer is at that height.

Three illustrative half-hours, with $\theta = 300\,\mathrm{K}$ and $\overline{w'\theta'} = H/(\rho c_p)$ for a sensible heat flux H and $\rho c_p = 1.2 \times 1004\,\mathrm{J\,m^{-3}\,K^{-1}}$, show the range:

- sunny afternoon, $u_* = 0.3\,\mathrm{m\,s^{-1}}$, $H = 200\,\mathrm{W\,m^{-2}}$, $\overline{w'\theta'} = 0.166\,\mathrm{K\,m\,s^{-1}}$: $L_{\mathrm{O}} = -0.027 \times 300/(0.4 \times 9.81 \times 0.166) = -12.4\,\mathrm{m}$, and at 10 m, $z/L_{\mathrm{O}} = -0.80$;
- clear night with light wind, $u_* = 0.2\,\mathrm{m\,s^{-1}}$, $H = -30\,\mathrm{W\,m^{-2}}$, $\overline{w'\theta'} = -0.0249\,\mathrm{K\,m\,s^{-1}}$: $L_{\mathrm{O}} = +24.6\,\mathrm{m}$ and $z/L_{\mathrm{O}} = +0.41$;
- windy night, $u_* = 0.8\,\mathrm{m\,s^{-1}}$, the same $H = -30\,\mathrm{W\,m^{-2}}$: $L_{\mathrm{O}} = +1570\,\mathrm{m}$ and $z/L_{\mathrm{O}} = +0.006$, practically neutral.

The two nights have the same downward heat flux and the same sign of static stability, but the windy one is neutral for practical purposes: its mechanical turbulence, which grows as u_*^3, outweighs the buoyancy destruction.

13.5.4 Richardson number and the stability parameter

The two descriptions are connected. In the surface layer the gradients of wind and potential temperature are written, in Monin–Obukhov theory, as $\partial U/\partial z = (u_*/\kappa z)\,\phi_m$ and $\partial\theta/\partial z = (\theta_*/\kappa z)\,\phi_h$, with the temperature scale $\theta_* = -\overline{w'\theta'}/u_*$ and the dimensionless gradients ϕ_m and ϕ_h, functions of z/L_{O} equal to one in neutral conditions (Chapter 14). Substituting into equation (13.11), with the wind not turning in the surface layer,

$$\mathrm{Ri}_g = \frac{(g/\theta)\,\theta_*\,\phi_h/(\kappa z)}{u_*^2\,\phi_m^2/(\kappa z)^2} = \frac{\kappa g\,\theta_*\,z}{\theta\,u_*^2}\,\frac{\phi_h}{\phi_m^2},$$

and since equation (13.13) with $\overline{w'\theta'} = -u_*\theta_*$ gives $L_{\mathrm{O}} = \theta\,u_*^2/(\kappa g\,\theta_*)$, the first factor is z/L_{O}:

$$\mathrm{Ri}_g = \frac{z}{L_{\mathrm{O}}}\,\frac{\phi_h}{\phi_m^2}. \tag{13.14}$$

With the standard empirical (Businger–Dyer) forms, stable $\phi_m = \phi_h = 1 + 5\,z/L_{\mathrm{O}}$ and unstable $\phi_m = (1 - 16\,z/L_{\mathrm{O}})^{-1/4}$, $\phi_h = (1 - 16\,z/L_{\mathrm{O}})^{-1/2}$, the relation becomes

$$\mathrm{Ri}_g = \frac{z}{L_{\mathrm{O}}} \quad \text{(unstable)}, \qquad \mathrm{Ri}_g = \frac{z/L_{\mathrm{O}}}{1 + 5\,z/L_{\mathrm{O}}} \quad \text{(stable)}. \tag{13.15}$$

In unstable conditions the gradient Richardson number equals the stability parameter exactly with these forms; in stable conditions it grows more slowly and approaches 0.2 as z/L_{O} grows without bound. The stable relation can be inverted, $z/L_{\mathrm{O}} = \mathrm{Ri}_g/(1 - 5\,\mathrm{Ri}_g)$, only for $\mathrm{Ri}_g < 0.2$.

Table 13.3 tabulates the relation, with the turbulent Prandtl number $\mathrm{Pr}_t = \phi_h/\phi_m$ that the same forms imply and the flux Richardson number $\mathrm{Ri}_f = \mathrm{Ri}_g/\mathrm{Pr}_t$ of equation (13.10).

Two readings follow. For the illustrative cases of Section 13.5.3, the afternoon with $z/L_{\mathrm{O}} = -0.80$ has $\mathrm{Ri}_g = -0.80$; the light-wind night with $z/L_{\mathrm{O}} = 0.41$ has $\mathrm{Ri}_g = 0.407/(1 + 2.03) = 0.134$; the windy night has $\mathrm{Ri}_g = 0.006$. And the stable forms cannot represent a layer with $\mathrm{Ri}_g \geq 0.2$: the late-night mast layer of Table 13.2, with a bulk value of 0.50, lies outside their range. That is the very stable regime of Section 13.4.5, and it is where the theory of the next two chapters needs other forms or fails.

Table 13.3: Gradient Richardson number, turbulent Prandtl number and flux Richardson number against the stability parameter, from equation (13.14) with the Businger–Dyer forms stated in the text.

z/L_{O}	ϕ_m	ϕ_h	Ri_g	Pr_t	Ri_f
−2.0	0.417	0.174	−2.00	0.42	−4.79
−1.0	0.492	0.243	−1.00	0.49	−2.03
−0.5	0.577	0.333	−0.50	0.58	−0.87
−0.1	0.788	0.620	−0.10	0.79	−0.13
0	1.000	1.000	0	1.00	0
+0.1	1.500	1.500	0.067	1.00	0.067
+0.2	2.000	2.000	0.100	1.00	0.100
+0.5	3.500	3.500	0.143	1.00	0.143
+1.0	6.000	6.000	0.167	1.00	0.167
+2.0	11.00	11.00	0.182	1.00	0.182

13.6 Stability in space, time and models

Stability is not one number for a site. This section shows how it changes with height and through the day, what it does to the extrapolation of a wind from one height to another, how it shows up in the errors of weather models, and the diagnostic habit that follows.

13.6.1 Stability varies with height

The boundary layer is stratified differently at different heights, and a single label for it is ambiguous. Figure 13.6 draws an illustrative day column and night column side by side, not to scale. Each column is a stack of layers from the ground to the free atmosphere, colored by stability class as in the key below the columns; the labels on the right of each column name the layer and give its typical depth.

By day the column has an unstable surface layer, a well-mixed layer of nearly neutral stratification above it, a strongly stable capping inversion at its top and a stable free atmosphere. At night the order near the ground is reversed: a strongly stable layer in the lowest fifty meters or so, a less stable layer above it, a nearly neutral residual layer left from the afternoon, and the remnant of the inversion aloft. Each column contains every class. “The atmosphere is stable” is incomplete until it says where: a night can be strongly stable at 10 m and nearly neutral at 300 m, and an afternoon unstable at 10 m and strongly stable at 1 km. For near-surface wind the question is the stability of the layer between the ground and the height of interest, and, for the coupling to the wind aloft, of the layers above it.

13.6.2 Stability varies with time

Stability can change rapidly: at sunrise and sunset, when clouds arrive or clear, when rain wets and cools the ground, and when a front passes and replaces one air mass by another. The largest regular change is the evening transition. Around sunset the surface heat flux changes sign within an hour, from upward to downward, while the profile reorganizes over several hours: the stable layer grows from the ground up, the surface wind falls, and the wind above the stable layer accelerates. The morning transition reverses the sequence, with a lag while the new mixed layer erodes the night’s stable layer (Chapter 6). The result is a strong diurnal cycle of the near-surface wind at most land sites.

Figure 13.7 draws that cycle schematically for a clear day. The upper panel is the surface sensible heat flux H against the hour of the day; the lower panel, on the same time axis, is the wind at 10 m and at 100 m. The dotted vertical lines mark the hours at which the heat flux changes sign.

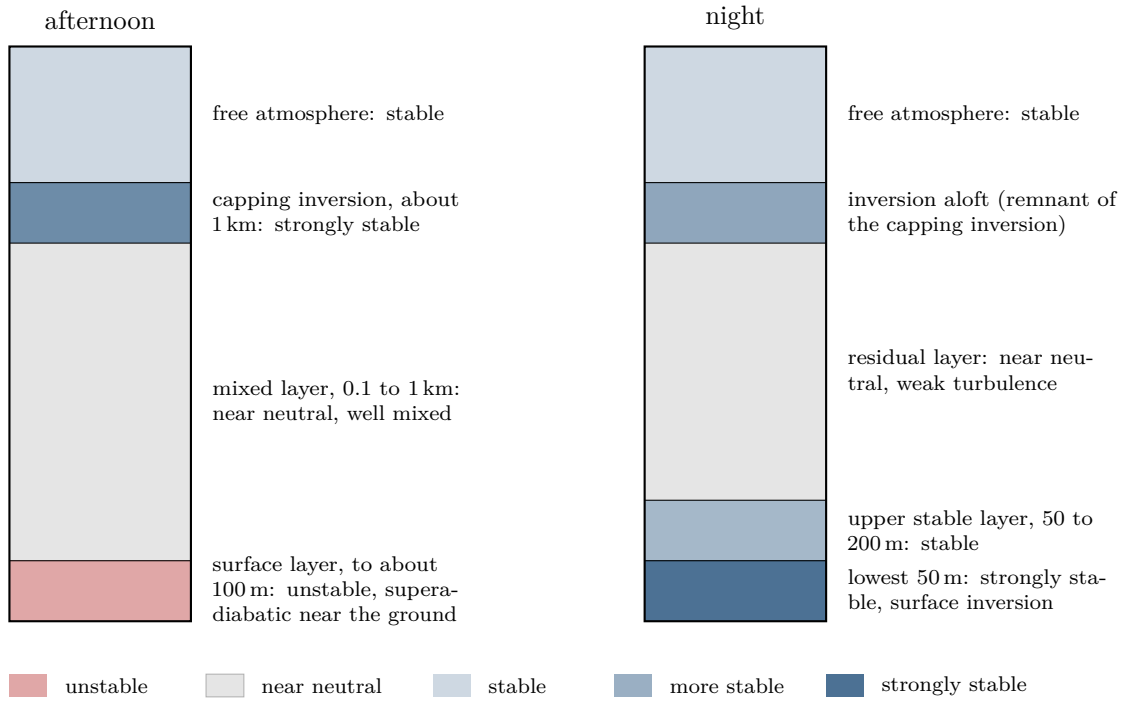


Figure 13.6: Stability by height in an illustrative afternoon and night column (schematic, not to scale). Darker blue means a larger positive $\mathrm{d}\theta/\mathrm{d}z$. Depths are typical values over land on a clear day and night.

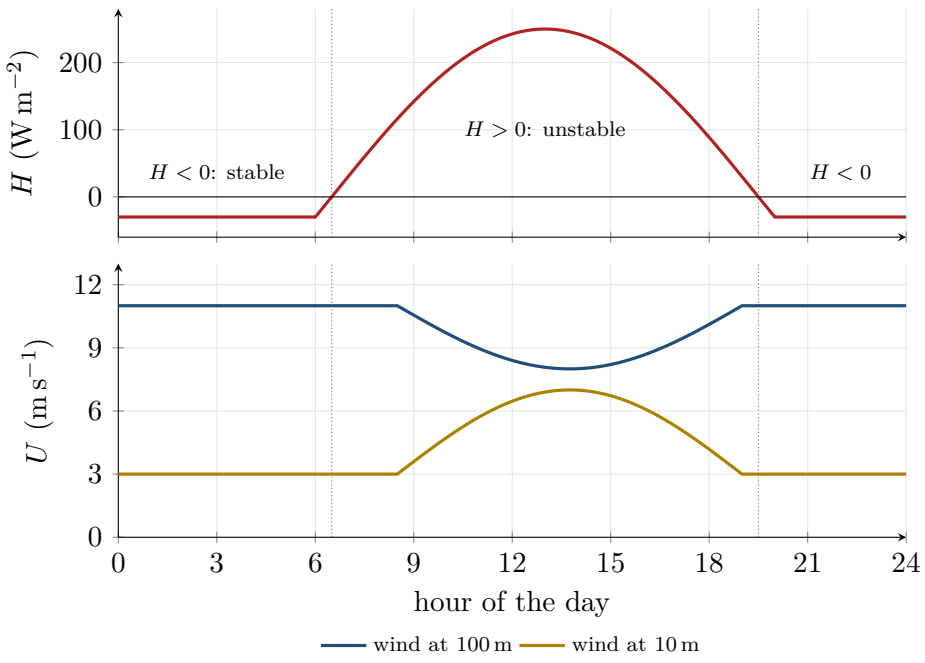


Figure 13.7: Schematic daily course on a clear day over land. Upper: $H = \max\{250\sin[\pi(t - 6.5)/13], -30\}\,\mathrm{W\,m^{-2}}$, with t the hour. Lower: $U_{100} = 11 - 3c$ and $U_{10} = 3 + 4c\ \mathrm{m\,s^{-1}}$, with the coupling factor $c = \max\{0, \sin[\pi(t - 8.5)/10.5]\}$, which starts two hours after the heat flux turns positive. Illustrative forms and values.

The heat flux is positive from about 06:30 to 19:30, peaking at $250\,\mathrm{W\,m^{-2}}$ at midday, and small and negative at night. The two winds move in opposite directions. At night the 10 m wind is $3\,\mathrm{m\,s^{-1}}$ and the 100 m wind $11\,\mathrm{m\,s^{-1}}$: the surface is weakly coupled and the air above the stable layer runs fast. After the morning erosion of the stable layer the two converge, to 7 and $8\,\mathrm{m\,s^{-1}}$ in the afternoon, when convective mixing couples the whole layer; the 100 m wind slows because its momentum is now shared with the air below. Around the evening sign change of the heat flux they separate again within an hour or two. A site's diurnal cycle therefore depends on height: the afternoon maximum of the 10 m wind is a nighttime minimum at hub height, and a 100 m measurement and a 10 m measurement at the same mast can show opposite cycles.

13.6.3 Extrapolation needs stability

A wind measured at one height is often extrapolated to another, for example from a 10 m station to the 100 m hub of a turbine. The extrapolation depends on stability. Take $U_{10} = 5\,\mathrm{m\,s^{-1}}$ over a surface with an illustrative $z_0 = 0.1$ m. Chapter 12 treats the extrapolation in detail; here the stability-corrected profile $U(z) = (u_*/\kappa)[\ln(z/z_0) - \psi_m(z/L_\mathrm{O})]$ of Chapter 7 is evaluated with the Businger–Dyer forms, stable $\psi_m = -5\,z/L_\mathrm{O}$ and unstable $\psi_m = 2\ln[(1+x)/2] + \ln[(1+x^2)/2] - 2\arctan x + \pi/2$ with $x = (1 - 16\,z/L_\mathrm{O})^{1/4}$, both derived in Chapter 14. The ratio U_{100}/U_{10} is independent of u_*:

$$\frac{U_{100}}{U_{10}} = \frac{\ln(100/z_0) - \psi_m(100/L_\mathrm{O})}{\ln(10/z_0) - \psi_m(10/L_\mathrm{O})}.$$

- Neutral: $\ln 1000/\ln 100 = 6.908/4.605 = 1.500$, so $U_{100} = 7.5\,\mathrm{m\,s^{-1}}$.
- Unstable, $L_\mathrm{O} = -100$ m: $\psi_m(-1) = 1.116$ and $\psi_m(-0.1) = 0.284$, so the ratio is $(6.908 - 1.116)/(4.605 - 0.284) = 5.792/4.321 = 1.340$ and $U_{100} = 6.7\,\mathrm{m\,s^{-1}}$.
- Stable, $L_\mathrm{O} = +100$ m: $\psi_m(1) = -5$ and $\psi_m(0.1) = -0.5$, so the ratio is $(6.908+5)/(4.605+0.5) = 11.908/5.105 = 2.332$ and $U_{100} = 11.7\,\mathrm{m\,s^{-1}}$.

The same $5\,\mathrm{m\,s^{-1}}$ at 10 m is therefore about $7\,\mathrm{m\,s^{-1}}$ at 100 m in unstable air and about $12\,\mathrm{m\,s^{-1}}$ in strongly stable air. Figure 13.8 draws the three profiles. The horizontal axis is wind speed and the vertical axis height on a logarithmic scale from 1 to 150 m, on which the neutral profile is a straight line; all three pass through $5\,\mathrm{m\,s^{-1}}$ at 10 m.

The unstable and neutral profiles are close, and the stable one parts from both above about 20 m. The neutral log law, applied without regard to stability, gives $7.5\,\mathrm{m\,s^{-1}}$ at 100 m: about 12 % too high for the unstable case and 36 % too low for the stable one. In terms of wind power, which scales with the cube of speed, the stable-case error is a factor $(7.5/11.7)^3 = 0.27$. A fixed shear exponent has the same defect, since the implied exponents, $\log_{10}(6.7/5) = 0.13$ and $\log_{10}(11.7/5) = 0.37$, differ by a factor of three. A wind measured at one height cannot be carried to another without knowing the stability between them.

13.6.4 Stability and model wind errors

Because stability controls the coupling, the pattern of a model's wind errors through the day is evidence about its turbulence and stability physics, not only about its large-scale forcing. Two patterns are classic. A forecast that matches the observed 10 m wind in the afternoon but overpredicts it at night suggests too much nocturnal mixing: the model's stable boundary layer transfers too much momentum from aloft to the surface, a *stable-boundary-layer mixing bias*. It is a long-standing weather-model problem, partly a consequence of the minimum mixing that models keep in stable conditions (Section 13.4.5). Conversely, a forecast that underpredicts the surface wind by day while the wind aloft is good suggests that the model underestimates

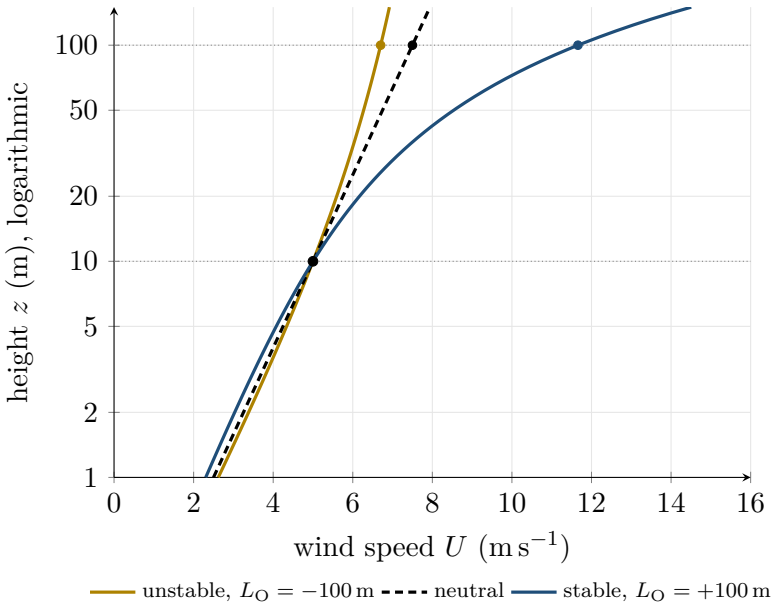


Figure 13.8: Three profiles through $U_{10} = 5\,\mathrm{m\,s^{-1}}$ over $z_0 = 0.1\,\mathrm{m}$: $U = (u_*/\kappa)[\ln(z/z_0) - \psi_m(z/L_O)]$ with $\kappa = 0.4$ and the Businger–Dyer ψ_m stated in the text. Unstable, $L_O = -100\,\mathrm{m}$, $u_* = 0.46\,\mathrm{m\,s^{-1}}$: $U_{100} = 6.7\,\mathrm{m\,s^{-1}}$. Neutral, $u_* = 0.43\,\mathrm{m\,s^{-1}}$: $7.5\,\mathrm{m\,s^{-1}}$. Stable, $L_O = +100\,\mathrm{m}$, $u_* = 0.39\,\mathrm{m\,s^{-1}}$: $11.7\,\mathrm{m\,s^{-1}}$; above 100 m the stable form is used beyond $z/L_O = 1$, as a shape. Illustrative parameters.

convective mixing: too small a surface heat flux, too shallow a mixed layer, or a mixing scheme that does not carry momentum down efficiently enough.

Table 13.4 lists these and related patterns as a diagnostic checklist. Its columns give the symptom in a comparison of model and observations, the likely cause, and the check that confirms or rejects it.

The table reads from symptom to cause, but each row is a hypothesis to be tested with the measurement in its last column. A nighttime overprediction of the 10 m wind could also come from a roughness length that is too small. The checks separate the two: a roughness length that is too small raises the modeled 10 m wind by day as well as at night and varies with wind direction, while excessive nocturnal mixing appears only at night and comes with a modeled shear and a modeled inversion weaker than the observed ones. A wind error is thus a diagnostic of turbulence and stability physics: its timing says which process is wrong.

13.6.5 A diagnostic habit

The relations of the chapter can be turned into a habit for reading wind data. Strong shear between two heights suggests stable stratification and weak mixing; weak shear suggests convective mixing and strong turbulence. In numbers, with the measurements at 10 and 100 m of Section 13.6.3, an exponent near 0.1 to 0.15 fits unstable or neutral air over short vegetation, and one above 0.3 points to stable air; a value above 0.5, like the night of Figure 13.3, points to strong stability or decoupling. Before trusting the reading, the other evidence should agree: the time of day, the sign of the heat flux if it is measured, the temperature difference between two heights converted to $\Delta\theta$, and the cloud cover.

The habit has limits. Terrain changes the shear by itself: flow over a hill speeds up near the crest and can flatten the profile in any stability. A low-level jet puts a wind maximum near or below the upper measurement height, so that the shear between two levels can be small, or even negative, in very stable air. Changes of surface roughness upwind create internal

Table 13.4: Patterns of near-surface wind error and their stability interpretation.

Symptom	Likely cause	Check
10 m wind good in the afternoon, too high at night	too much mixing in the stable boundary layer; excessive minimum mixing	observed and modeled shear between 10 and 100 m at night; strength of the observed surface inversion against the model's; nighttime u_*
10 m wind too low by day while the wind aloft is good	convective mixing too weak: surface heat flux or mixed-layer depth too small	modeled against observed sensible heat flux and z_i; daytime ratio U_{10}/U_{100}
100 m wind too low at night, wind maximum too weak or too high	too much mixing erodes the acceleration above the stable layer	lidar or profiler height and speed of the nighttime wind maximum
Largest errors around sunrise and sunset	wrong timing of the heat-flux sign change: cloud cover, soil moisture, radiation	modeled against observed hour at which H changes sign; cloud observations
Bias with no diurnal pattern	large-scale forcing, roughness or siting rather than stability	wind aloft against a radiosonde or a profiler; bias by wind direction (roughness, Chapter 11)

boundary layers with their own profiles (Chapter 7). The shear is evidence about stability, not a measurement of it. Turning these observations into a quantitative description of the surface layer, with the shear and the temperature gradient expressed as functions of the stability parameter, is the task of Monin–Obukhov similarity theory in Chapter 14.

13.7 What to retain

Definition 13.1 (Atmospheric stability)**.** Atmospheric stability is the tendency of the stratification to suppress or amplify vertical motion. It is set by the comparison of the environmental and dry adiabatic lapse rates, or equivalently by the sign of $\mathrm{d}\theta/\mathrm{d}z$, and it acts on the wind through the chain thermal stratification $\rightarrow$ buoyancy $\rightarrow$ turbulence $\rightarrow$ vertical momentum mixing $\rightarrow$ wind profile.

Table 13.5 lists the terms of the chapter, their meaning, their units and the subsection that defines each.

13.8 Exercises

Exercise 13.1. A tower near sea level measures, at dawn, $T = 8.0^\circ$C at 2 m, 9.5°C at 50 m and 9.2°C at 150 m; in the afternoon, 27.0°C at 2 m, 25.9°C at 50 m and 24.9°C at 150 m. Take $\Gamma_d = 9.8\,\mathrm{K\,km^{-1}}$ and $\theta/T \approx 1$. (a) For each time and each of the two layers compute Γ_e and $\mathrm{d}\theta/\mathrm{d}z$, and classify the layer. (b) Which layers are inversions, which are stable without an inversion, and which are superadiabatic? (c) For the upper dawn layer, compute the temperature excess and the buoyant acceleration of a parcel lifted 50 m from 50 m, and the buoyancy period $2\pi/N$. (d) In the afternoon the air is saturated at cloud base in a layer where $\Gamma_e = 6\,\mathrm{K\,km^{-1}}$ and $\Gamma_s = 4.5\,\mathrm{K\,km^{-1}}$. Classify the layer for an unsaturated and for a saturated parcel.

Exercise 13.2. A mast at 15°S has thermometers and wind vanes at 10 and 60 m. At 22:00 it records $T_{10} = 18.0^\circ$C, $T_{60} = 19.2^\circ$C, a wind of $4.0\,\mathrm{m\,s^{-1}}$ from 090° at 10 m and $8.0\,\mathrm{m\,s^{-1}}$ from 070° at 60 m. Take $\theta_0 = 292\,\mathrm{K}$ and $\Gamma_d = 9.77\,\mathrm{K\,km^{-1}}$. (a) Compute $\Delta\theta$. (b) Compute the vector wind difference and the bulk Richardson number, and the value obtained from the speeds alone. (c) Is the turning with height the one expected in the Southern Hemisphere? Which way

Table 13.5: The terms of the chapter and where each is defined.

Term	Meaning	Units	Defined in
Atmospheric stability	tendency of the atmosphere to suppress or amplify a vertical displacement	–	13.1.1
Environmental lapse rate Γ_e	$-\partial T/\partial z$ of the actual atmosphere; observed	K/km	13.1.2
Dry adiabatic lapse rate Γ_d	$g/c_p \approx 9.8\,\mathrm{K\,km^{-1}}$, cooling rate of a rising unsaturated parcel	K/km	13.1.2
Stable, neutral, unstable stratification	Γ_e less than, equal to, greater than Γ_d; $\mathrm{d}\theta/\mathrm{d}z$ positive, zero, negative	–	13.1.3, 13.2.1
Inversion	layer with $\mathrm{d}T/\mathrm{d}z > 0$; strongly stable	–	13.1.4
Superadiabatic	$\Gamma_e > \Gamma_d$; absolutely unstable; shallow over heated ground	–	13.1.4
Saturated adiabatic lapse rate Γ_s	cooling rate of a rising saturated parcel, about 4 to $7\,\mathrm{K\,km^{-1}}$	K/km	13.1.5
Conditional instability	$\Gamma_s < \Gamma_e < \Gamma_d$: stable when unsaturated, unstable when saturated	–	13.1.5
Potential temperature θ	$T(p_0/p)^{R_d/c_p}$; conserved in adiabatic motion; $\mathrm{d}\theta/\mathrm{d}z = (\theta/T)(\Gamma_d - \Gamma_e)$	K	13.2.1, 13.2.2
Gradient Richardson number Ri_g	$N^2/\lvert\partial\mathbf{V}/\partial z\rvert^2$: stratification against vector shear; $= \mathrm{Pr}_t\,\mathrm{Ri}_f$	–	13.4.1
Critical Richardson number Ri_c	about 0.25: reference value above which turbulence is hard to sustain; not a sharp threshold	–	13.4.2
Bulk Richardson number Ri_B	$(g/\theta_0)\Delta\theta\,\Delta z/\lvert\Delta\mathbf{V}\rvert^2$ from two levels	–	13.4.3
Static stability	stability of the stratification, from $\mathrm{d}\theta/\mathrm{d}z$	–	13.5.1
Surface-layer stability	stability from the surface heat flux and mechanical turbulence, through L_O and z/L_O	–	13.5.1, 13.5.3
Obukhov length L_O	$-u_*^3\theta_v/(\kappa g\,\overline{w'\theta_v'})$; negative unstable, positive stable	m	13.5.3

would the wind turn with height at 15°N, and would the Richardson number change? (d) At 03:00 the 60 m wind has dropped to $5.0\,\mathrm{m\,s^{-1}}$ from 070°, the 10 m wind to $1.0\,\mathrm{m\,s^{-1}}$ from 090°, and $T_{60} - T_{10} = 2.5\,\mathrm{K}$. Recompute Ri_B and describe the expected turbulence at each time.

Exercise 13.3. An eddy-covariance station at 10 m reports three half-hours with $\theta = 295\,\mathrm{K}$ and $\rho c_p = 1200\,\mathrm{J\,m^{-3}\,K^{-1}}$: (i) $u_* = 0.45\,\mathrm{m\,s^{-1}}$, $H = 150\,\mathrm{W\,m^{-2}}$; (ii) $u_* = 0.15\,\mathrm{m\,s^{-1}}$, $H = -20\,\mathrm{W\,m^{-2}}$; (iii) $u_* = 0.60\,\mathrm{m\,s^{-1}}$, $H = -20\,\mathrm{W\,m^{-2}}$. Take $\kappa = 0.4$. (a) Compute $\overline{w'\theta'}$, L_{O} and z/L_{O} for each. (b) Compute Ri_g at 10 m from equation (13.15). (c) Cases (ii) and (iii) have the same heat flux. Explain why their stability differs, and which of them static stability alone would distinguish. (d) A two-level profile in a fourth period gives $\mathrm{Ri}_g = 0.3$ at 10 m. What value of z/L_{O} do the stable Businger–Dyer forms assign to it, and what does the answer imply?

Exercise 13.4. A weather model gives $U_{10} = 6\,\mathrm{m\,s^{-1}}$ at a site with $z_0 = 0.1\,\mathrm{m}$. (a) Using the profile and the Businger–Dyer ψ_m of Section 13.6.3 with $\kappa = 0.4$, compute U_{100} for neutral air, for $L_{\mathrm{O}} = -100\,\mathrm{m}$ and for $L_{\mathrm{O}} = +100\,\mathrm{m}$, and the implied shear exponent between 10 and 100 m in each case. (b) A lidar at the site measures $U_{100} = 13\,\mathrm{m\,s^{-1}}$ and $U_{10} = 4\,\mathrm{m\,s^{-1}}$ on a clear night, when the model gives $U_{100} = 12.5\,\mathrm{m\,s^{-1}}$ and $U_{10} = 6\,\mathrm{m\,s^{-1}}$. Compute the observed and modeled exponents and use Table 13.4 to name the most likely model error. (c) Name one measurement that would distinguish that error from a roughness length that is too small in the model.

Chapter 14

Monin–Obukhov Similarity Theory

14.1 The similarity hypothesis

Chapter 7 derived the neutral logarithmic wind profile from a constant stress and a mixing length proportional to height, and showed, without deriving them, that the profile bends one way when the ground heats the air and the other way when it cools it. Chapter 13 described static stability and its effect on shear in qualitative and bulk terms. This chapter supplies the theory that turns those observations into formulas. The question of the chapter is

how is the neutral logarithmic law modified when the surface layer is stable or unstable, and how are the wind shear, the temperature gradient, the surface stress and the surface heat flux related to one another?

The answer is Monin–Obukhov similarity theory. The chapter first states its hypothesis and shows, by a dimensional argument, why one length and one dimensionless number are enough. It then derives that length, the Obukhov length, from the budget of turbulent kinetic energy; introduces the dimensionless gradients and their standard empirical forms; integrates them into stability-corrected profiles; shows how a weather model uses the result to compute fluxes and the 10 m wind; and closes with the conditions under which the theory fails.

Jargon: similarity theory, Monin–Obukhov similarity theory (MOST), Obukhov length, stability parameter, temperature scale, dimensionless gradient, stability correction, turbulent Prandtl number, local equilibrium

A *similarity theory* is a description of a class of flows in which suitably scaled, dimensionless quantities obey the same relations in every member of the class, whatever the dimensional values of wind, heat flux or roughness. *Monin–Obukhov similarity theory* (MOST) is the similarity theory of the atmospheric surface layer: it states that dimensionless gradients and turbulence statistics there depend on height only through one ratio. The *Obukhov length* L_{O}, in meters, $L_{\mathrm{O}} = -u_*^3\overline{\theta}/(\kappa\, g\, \overline{w'\theta'})$ for dry air, is the length built from the friction velocity and the surface buoyancy flux; it is calculated from eddy-covariance fluxes or, in a model, from the modeled fluxes, and it is negative in unstable and positive in stable conditions. The *stability parameter* z/L_{O}, dimensionless, is the height divided by the Obukhov length. The *temperature scale* $\theta_* = -\overline{w'\theta'}/u_*$, in kelvins, is the surface heat flux expressed as a temperature. A *dimensionless gradient* is a vertical gradient of mean wind or mean potential temperature multiplied by κz and divided by the matching scale: ϕ_m for wind, ϕ_h for potential temperature; both equal one in neutral air. A *stability correction* ψ_m or ψ_h, dimensionless, is the term that an integrated profile subtracts from the logarithm to account for buoyancy. The *turbulent Prandtl number* $\mathrm{Pr}_t = K_m/K_h$, dimensionless, is the ratio of the eddy diffusivity for momentum to that for heat. *Local equilibrium* is the condition in which the turbulence at a height is fully determined by the fluxes and the height there, with no memory of upwind surfaces, earlier times or distant eddies.

Key idea

In the surface layer, the wind shear at height z is $\partial U/\partial z = (u_*/\kappa z)\,\phi_m(z/L_{\mathrm{O}})$: the neutral shear multiplied by a universal function of one number. Negative z/L_{O} means unstable air and enhanced mixing, $\phi_m < 1$; z/L_{O} near zero means neutral air, $\phi_m = 1$; positive z/L_{O} means stable air and suppressed mixing, $\phi_m > 1$.

14.1.1 The neutral case and what buoyancy changes

In neutral air, Chapter 7 showed that the shear and the profile are

$$\frac{\partial U}{\partial z} = \frac{u_*}{\kappa\, z}, \qquad U(z) = \frac{u_*}{\kappa} \ln \frac{z}{z_0}, \tag{14.1}$$

with the friction velocity u_*, the von Kármán constant $\kappa \approx 0.4$ and the roughness length z_0. The derivation used two facts: the stress is constant with height in the surface layer, so that $-\overline{u'w'} = u_*^2$ at every height; and the eddies that carry it have a size proportional to the distance from the ground, the mixing length $l = \kappa z$. Neither fact refers to temperature. The neutral profile is the special case in which buoyancy does no work on the eddies.

When the ground is warmer than the air, rising parcels are lighter than their surroundings and are accelerated upward: buoyancy adds energy to the vertical motions, the eddies grow larger and more vigorous than κz suggests, and they mix momentum more efficiently. The same stress u_*^2 is then carried by a weaker shear. When the ground is colder than the air, vertical motions work against gravity, the eddies are smaller and weaker, and the same stress needs a stronger shear. Buoyancy therefore changes the shear for a given stress, and the factor by which it changes it is what this chapter derives. The constant stress survives; the mixing length κz does not.

14.1.2 The governing quantities

The central idea of the theory is that, in the surface layer over flat, uniform ground in steady conditions, the mean gradients and the turbulence statistics at height z are controlled by a small set of quantities:

- the height z above the ground (above the displacement height d over tall vegetation or buildings);
- the kinematic momentum flux at the surface, represented by u_*, in m/s;
- the kinematic heat flux at the surface, $\overline{w'\theta'}$, in K m/s;
- the buoyancy parameter $g/\overline{\theta}$, in $\mathrm{m\,s^{-2}\,K^{-1}}$, which converts a temperature fluctuation into a buoyant acceleration.

Heat flux and buoyancy parameter enter the dynamics of the eddies only through their product, the buoyancy flux $(g/\overline{\theta})\,\overline{w'\theta'}$, which is the buoyancy production of turbulent kinetic energy of Chapter 8. In moist air the flux of virtual potential temperature, $\overline{w'\theta'_v}$, replaces $\overline{w'\theta'}$, because water vapor also makes air lighter; over dry land the difference is small, over water and wet vegetation it can be important. This chapter writes the dry form.

Equally important is what the list leaves out. The roughness length z_0 is absent: it fixes where the profile starts but, once $z \gg z_0$, not how the gradient varies. The boundary-layer depth z_i is absent: the surface layer is assumed to be shallow enough that the eddies do not feel the top of the layer. The Coriolis parameter f is absent: the surface layer is too thin and its eddies too short-lived for the Earth's rotation to act on them. The relations of this chapter therefore hold identically in both hemispheres. Earth's rotation acts on the surface-layer wind only through what lies outside the theory: the turning of the wind direction with height (to the right with increasing height in the Northern Hemisphere, to the left in the Southern), the depth z_i, and the large-scale flow that sets u_*. Two derived scales are used throughout: u_* for velocity, and the temperature scale

$$\theta_* = -\frac{\overline{w'\theta'}}{u_*}, \tag{14.2}$$

in kelvins, for temperature, defined in Section 14.3.4.

14.1.3 The dimensional argument

The Buckingham pi theorem states that a physical relation among n quantities whose dimensions involve r independent base units can be rewritten as a relation among $n - r$ dimensionless groups. Apply it to the shear. Table 14.1 lists the four quantities assumed to govern it, with their dimensions in the base units of length (m) and time (s); the bottom rows list quantities assumed *not* to matter.

With $n = 4$ and $r = 2$, there are two dimensionless groups. Choose z and u_* as the repeating quantities, because together they supply a length and a time (z/u_*). The shear made dimensionless is

$$\Pi_1 = \frac{z}{u_*}\frac{\partial U}{\partial z}.$$

The buoyancy flux has dimensions $\mathrm{m^2\,s^{-3}}$; to cancel them, multiply by z (m) and divide by u_*^3 $(\mathrm{m^3\,s^{-3}})$:

$$\Pi_2 = \frac{z\,(g/\overline{\theta})\,\overline{w'\theta'}}{u_*^3}.$$

The theorem then says $\Pi_1 = F(\Pi_2)$ for some function F that dimensional analysis cannot supply. Equivalently, Π_2 is z divided by the only length that can be built from u_* and the

Table 14.1: Quantities of the dimensional argument for the shear in the surface layer. The last three rows are excluded by hypothesis.

Quantity	Symbol	Dimensions	Role
Wind shear	$\partial U/\partial z$	s^{-1}	the quantity to be predicted
Height	z	m	distance to the boundary; sets eddy size
Friction velocity	u_*	$\mathrm{m\,s}^{-1}$	momentum flux, mechanical source
Buoyancy flux	$(g/\overline{\theta})\,\overline{w'\theta'}$	$\mathrm{m}^2\,\mathrm{s}^{-3}$	buoyant source or sink
Roughness length	z_0	m	excluded for $z \gg z_0$
Boundary-layer depth	z_i	m	excluded for $z \ll z_i$
Coriolis parameter	f	s^{-1}	excluded: rotation too slow

buoyancy flux, $u_*^3/[(g/\overline{\theta})\,\overline{w'\theta'}]$. If the heat flux and the buoyancy parameter are kept as separate quantities, the kelvin becomes a third base unit, $n = 5$ and $r = 3$, and the count of groups is still two: the kelvin cancels only in the product.

Two conventions fix the groups in their standard form. The first group is multiplied by κ, so that it equals one in neutral air by equation (14.1):

$$\phi_m \equiv \frac{\kappa\, z}{u_*}\,\frac{\partial U}{\partial z}. \tag{14.3}$$

The length is multiplied by $-1/\kappa$, so that it is positive in stable air (downward heat flux) and so that its meaning in the energy budget is exact (Section 14.2.1):

$$L_{\mathrm{O}} = -\frac{u_*^3\,\overline{\theta}}{\kappa\, g\,\overline{w'\theta'}}. \tag{14.4}$$

The similarity hypothesis is then the statement

$$\frac{\kappa\, z}{u_*}\,\frac{\partial U}{\partial z} = \phi_m\!\left(\frac{z}{L_{\mathrm{O}}}\right), \tag{14.5}$$

with ϕ_m a universal function, the same at every site, to be found from measurements. Monin and Obukhov proposed it in the 1950s; the literature writes the stability parameter as $\zeta = z/L_{\mathrm{O}}$, and this book writes z/L_{O} because ζ denotes vorticity. The same argument applied to the potential-temperature gradient, with θ_* as the temperature scale, gives the second universal function ϕ_h of Section 14.3.4, and applied to the standard deviations of the velocity components gives σ_w/u_*, σ_u/u_* as functions of z/L_{O}.

14.1.4 What similarity means

The hypothesis makes a testable prediction: measurements taken at sites with different wind speeds, heat fluxes, roughness and temperatures, at different heights, must collapse onto one curve when the shear is divided by $u_*/(\kappa z)$ and plotted against z/L_{O} computed from the measured fluxes. Figure 14.1 illustrates the test with four illustrative runs: a light-wind afternoon (run A, $u_* = 0.35\,\mathrm{m\,s}^{-1}$, $L_{\mathrm{O}} = -20\,\mathrm{m}$), a calm night (run B, $0.25\,\mathrm{m\,s}^{-1}$, $+40\,\mathrm{m}$), a windy afternoon (run C, $0.6\,\mathrm{m\,s}^{-1}$, $-150\,\mathrm{m}$) and a windy night (run D, $0.5\,\mathrm{m\,s}^{-1}$, $+200\,\mathrm{m}$), each sampled at 2, 5, 10, 20 and 40 m, with a scatter of a few percent added to imitate measurement error. Panel (a) plots the measured shear in s^{-1} (horizontal, logarithmic) against height (vertical, logarithmic). Panel (b) plots the same twenty points as ϕ_m against z/L_{O}, with the standard empirical curve of Section 14.3.2 as the solid line.

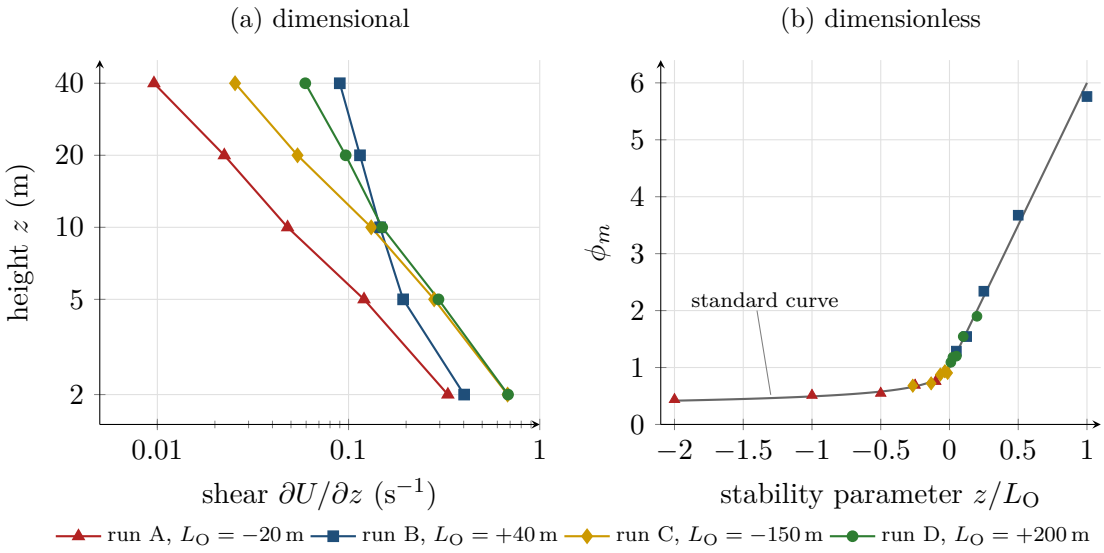


Figure 14.1: Similarity collapse, illustrative. Four runs at heights of 2 to 40 m, with shear computed from $\partial U/\partial z = (u_*/\kappa z)\,\phi_m(z/L_O)$ and multiplied by a deterministic scatter of $\pm 5\,\%$. (a) Shear against height. (b) The same points as ϕ_m against z/L_O, with the standard forms $\phi_m = (1 - 16\,z/L_O)^{-1/4}$ for $z/L_O < 0$ and $1 + 5\,z/L_O$ for $z/L_O \geq 0$ (equations (14.12) and (14.11)), $\kappa = 0.4$.

In panel (a) the four runs look like four unrelated flows: their shears at 10 m range from 0.048 to 0.150 s^{-1}, the night runs keep a strong shear far up while the afternoon runs lose it quickly, and no single profile describes them. In panel (b) the twenty points fall on one curve, below one for the two afternoons and above one for the two nights. Each run occupies a different stretch of the curve: the windy runs C and D stay near $z/L_O = 0$, because a large u_* makes $|L_O|$ long; the light-wind runs A and B reach far into the unstable and stable branches. Real field data collapse with more scatter than the figure shows, and the scatter grows at large $|z/L_O|$; the collapse of data from flat, uniform sites onto one curve is the evidence on which the theory rests, and a failure to collapse at a particular site is the evidence that the site violates one of its assumptions (Section 14.6).

14.2 The Obukhov length

The dimensional argument produced a length but gave no reason for its sign or for the factor κ. This section derives the Obukhov length from the budget of turbulent kinetic energy, checks its units, states its sign convention and physical meaning, computes a day and a night value from heat fluxes in W/m^2, and explains why the stability parameter, not the length alone, measures how much stability matters at a height.

14.2.1 Derivation from the turbulent kinetic energy budget

Chapter 8 wrote the two production terms of the budget of turbulent kinetic energy in along-wind coordinates:

$$P_s = -\overline{u'w'}\,\frac{\partial U}{\partial z}, \qquad P_b = \frac{g}{\overline{\theta}}\,\overline{w'\theta'}, \tag{14.6}$$

both in $\mathrm{m^2\,s^{-3}}$. In the surface layer the stress is constant, $-\overline{u'w'} = u_*^2$. If the shear had its neutral value $u_*/(\kappa z)$, the shear production would be

$$P_s^{\mathrm{n}} = u_*^2 \cdot \frac{u_*}{\kappa\, z} = \frac{u_*^3}{\kappa\, z}, \tag{14.7}$$

where the superscript n marks the neutral reference. This term falls off as $1/z$: mechanical production is concentrated near the ground, where the shear is largest. The buoyancy term does not depend on height in the surface layer, because the heat flux there is constant like the stress. Form the ratio of buoyancy *destruction*, $-P_b$, to the neutral shear production:

$$\frac{-P_b}{P_s^{\mathrm{n}}} = \frac{-(g/\overline{\theta})\,\overline{w'\theta'}}{u_*^3/(\kappa\, z)} = -\frac{\kappa\, g\,\overline{w'\theta'}}{u_*^3\,\overline{\theta}}\; z = \frac{z}{L_{\mathrm{O}}}, \tag{14.8}$$

with L_{O} as in equation (14.4). This is the derivation: the stability parameter is the ratio of buoyant destruction of turbulent kinetic energy to its neutral shear production, with its sign. It is positive when buoyancy destroys turbulence (stable air), negative when buoyancy produces it (unstable air), and zero when the heat flux vanishes. The factor κ in the definition is what makes the ratio exact, and the minus sign is what makes stable air positive.

The ratio uses the neutral shear, not the actual one. With the actual shear, $P_s = u_*^3\phi_m/(\kappa z)$, and the true ratio of the two production terms is the flux Richardson number of Chapter 8,

$$\mathrm{Ri}_f = \frac{-P_b}{P_s} = \frac{z/L_{\mathrm{O}}}{\phi_m(z/L_{\mathrm{O}})}. \tag{14.9}$$

The stability parameter is preferred because it is built from the fluxes alone, which a sonic anemometer measures and a model computes, without needing the shear, which is the unknown the theory is meant to predict.

Units. The friction velocity cubed is in $\mathrm{m^3\,s^{-3}}$. The kinematic heat flux $\overline{w'\theta'}$ is in $\mathrm{K\,m/s}$, and the buoyancy flux is $(g/\overline{\theta})\,\overline{w'\theta'}$ in $(\mathrm{m\,s^{-2}/K}) \times (\mathrm{K\,m\,s^{-1}}) = \mathrm{m^2\,s^{-3}}$, the unit of a production of turbulent kinetic energy per unit mass, W/kg. Their ratio, $\mathrm{m^3\,s^{-3}/(m^2\,s^{-3})} = \mathrm{m}$, is a length, and κ is dimensionless. The Obukhov length is therefore, in words, the cube of the mechanical velocity scale divided by the buoyancy flux: mechanically generated turbulence against buoyancy, expressed as a height.

14.2.2 Physical meaning and sign convention

Setting $z = |L_{\mathrm{O}}|$ in equation (14.8) gives $|P_b| = P_s^{\mathrm{n}}$: the magnitude of the Obukhov length is the height at which buoyancy production or destruction equals the neutral shear production. Below that height shear dominates the production of turbulence, and the flow is close to neutral, the more so the closer to the ground; above it buoyancy dominates. The statement is approximate in one respect: at $z = |L_{\mathrm{O}}|$ the actual shear is not the neutral shear, so the actual ratio of the two terms is $1/\phi_m$, equal to $1/6$ at $z/L_{\mathrm{O}} = 1$ and $1/0.49 = 2.0$ at $z/L_{\mathrm{O}} = -1$ with the standard forms. "The height at which buoyancy becomes comparable to shear" is the correct reading in order of magnitude.

Figure 14.2 draws the derivation for an illustrative sunny afternoon, $u_* = 0.4\,\mathrm{m\,s^{-1}}$ and $H = 200\,\mathrm{W\,m^{-2}}$ (Section 14.2.3). The horizontal axis is a production rate in $\mathrm{m^2\,s^{-3}}$ and the vertical axis height, both logarithmic. The solid blue curve is the neutral shear production $u_*^3/(\kappa z)$; the dashed blue curve is the actual shear production $u_*^3\phi_m/(\kappa z)$ with the unstable form of ϕ_m; the vertical gold line is the buoyancy production, constant with height. The solid curve crosses the gold line at $z = |L_{\mathrm{O}}| = 29.5\,\mathrm{m}$. Below the crossing the shear term is the larger; above it buoyancy is. The dashed curve lies left of the solid one at every height, because convective mixing reduces the shear, and crosses the gold line lower, at about 17 m.

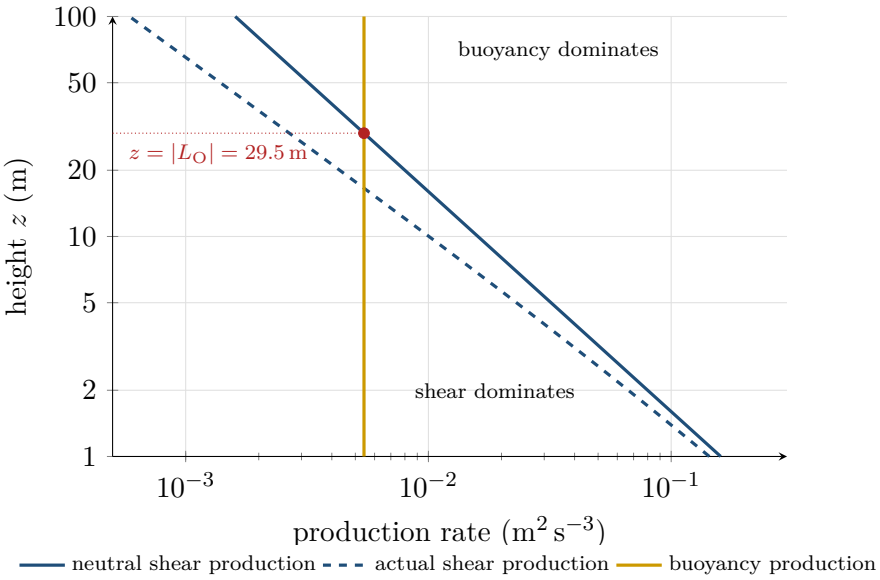


Figure 14.2: Production of turbulent kinetic energy against height for an illustrative afternoon: $u_* = 0.4\,\mathrm{m\,s^{-1}}$, $\kappa = 0.4$, $\overline{w'\theta'} = 0.166\,\mathrm{K\,m\,s^{-1}}$, $g/\overline{\theta} = 9.81/300$. Neutral shear production $u_*^3/(\kappa z) = 0.16/z$; actual shear production with $\phi_m = (1 - 16\,z/L_O)^{-1/4}$, $L_O = -29.5\,\mathrm{m}$; buoyancy production $5.43 \times 10^{-3}\,\mathrm{m^2\,s^{-3}}$.

Sign. The sign of L_O is the opposite of the sign of the heat flux, because u_*^3, $\overline{\theta}$, κ and g are all positive. Table 14.2 collects the three regimes. In unstable air the ground heats the air, $\overline{w'\theta'} > 0$, and $L_O < 0$. In stable air the ground cools the air, $\overline{w'\theta'} < 0$, and $L_O > 0$. As the heat flux tends to zero, $|L_O|$ grows without bound, and neutral air has $|L_O| \to \infty$ and $z/L_O = 0$. A large magnitude of L_O, of the order of a kilometer, therefore means nearly neutral air at the heights of interest, and a small magnitude, of ten meters or less, means strong stable or unstable effects close to the ground. The interpretation of particular numerical values is taken up in Chapter 15.

Table 14.2: Sign convention of the Obukhov length and its consequences.

Regime	Typical situation	$\overline{w'\theta'}$	L_O	z/L_O	ϕ_m	Shear for given u_*
Unstable	sunny day, ground warmer than air	> 0	< 0	< 0	< 1	weaker than neutral
Neutral	overcast, strong wind	0	$\pm\infty$	0	1	$u_*/(\kappa z)$
Stable	clear night, ground colder than air	< 0	> 0	> 0	> 1	stronger than neutral

14.2.3 A day value and a night value

Heat fluxes are usually reported as an energy flux H, the sensible heat flux in $\mathrm{W\,m^{-2}}$, related to the kinematic flux by $H = \rho\, c_p\, \overline{w'\theta'}$ (Chapter 9). With the illustrative values $\rho = 1.2\,\mathrm{kg\,m^{-3}}$, $c_p = 1004\,\mathrm{J\,kg^{-1}\,K^{-1}}$ and $\overline{\theta} = 300\,\mathrm{K}$, so that $\rho\, c_p = 1205\,\mathrm{J\,m^{-3}\,K^{-1}}$ and $g/\overline{\theta} = 0.0327\,\mathrm{m\,s^{-2}\,K^{-1}}$:

Example 14.1 (Afternoon)**.** A sunny afternoon over farmland, $H = 200\,\mathrm{W\,m^{-2}}$ and $u_* =$

$0.4\,\mathrm{m\,s^{-1}}$. The kinematic heat flux is $\overline{w'\theta'} = 200/1205 = 0.166\,\mathrm{K\,m\,s^{-1}}$. Then

$$L_\mathrm{O} = -\frac{0.4^3 \times 300}{0.4 \times 9.81 \times 0.166} = -\frac{0.064 \times 300}{0.651} = -\frac{19.2}{0.651} = -29.5\,\mathrm{m}.$$

At 10 m, $z/L_\mathrm{O} = 10/(-29.5) = -0.34$; at 80 m, -2.7.

Example 14.2 (Night)**.** A clear night, $H = -30\,\mathrm{W\,m^{-2}}$ and $u_* = 0.2\,\mathrm{m\,s^{-1}}$. The kinematic heat flux is $\overline{w'\theta'} = -30/1205 = -0.0249\,\mathrm{K\,m\,s^{-1}}$. Then

$$L_\mathrm{O} = -\frac{0.2^3 \times 300}{0.4 \times 9.81 \times (-0.0249)} = \frac{0.008 \times 300}{0.0977} = \frac{2.4}{0.0977} = +24.6\,\mathrm{m}.$$

At 10 m, $z/L_\mathrm{O} = 0.41$; at 80 m, 3.3, beyond the range in which the standard stable form was fitted (Section 14.3.2).

The two lengths are of similar magnitude although the heat fluxes differ by a factor of almost seven, because the night has half the friction velocity and u_* enters cubed: 0.2^3 is one eighth of 0.4^3. The same night flux with a windy $u_* = 0.4\,\mathrm{m\,s^{-1}}$ gives $L_\mathrm{O} = +197\,\mathrm{m}$, eight times longer, and the afternoon flux with $u_* = 0.3\,\mathrm{m\,s^{-1}}$ gives $L_\mathrm{O} = -12.4\,\mathrm{m}$. The friction velocity is as important as the heat flux in setting the stability: a strong wind keeps the surface layer close to neutral even under a large heat flux, and a weak wind lets a small heat flux dominate. The second pair of values, $u_* = 0.3\,\mathrm{m\,s^{-1}}$ with $H = 200\,\mathrm{W\,m^{-2}}$ and $u_* = 0.2\,\mathrm{m\,s^{-1}}$ with $H = -30\,\mathrm{W\,m^{-2}}$, are the convective and stable conditions of the illustrative energy budgets of Chapter 8; with the standard forms of Section 14.3.2 they give shears at 10 m of 0.039 and $0.152\,\mathrm{s^{-1}}$, the values used there.

14.2.4 The stability parameter and the role of height

The stability parameter, not L_O alone, measures how strongly buoyancy affects the flow at a height, because the neutral shear production decreases as $1/z$ while the buoyancy flux stays constant (Figure 14.2). The same atmosphere, with one L_O, is nearly neutral near the ground and strongly stratified higher up. With $L_\mathrm{O} = 100\,\mathrm{m}$, an illustrative moderately stable evening,

$$z = 2\,\mathrm{m}:\ z/L_\mathrm{O} = 0.02,\ \phi_m = 1.1; \qquad z = 50\,\mathrm{m}:\ z/L_\mathrm{O} = 0.5,\ \phi_m = 3.5.$$

A thermometer pair at 2 m sees an almost neutral profile, while a wind-turbine hub or a transmission conductor on a tall tower at 50 m sits where stability triples the shear. Statements such as “the atmosphere is stable” are therefore incomplete without a height.

The magnitude of z/L_O carries the degree of stability. Values near -0.01 are weakly unstable and practically neutral; values near -2 are strongly unstable, where convection dominates mechanical turbulence; values near $+0.01$ are weakly stable, and values near or above $+1$ are strongly stable. The neutral case is not a point but a band around zero, conventionally $|z/L_\mathrm{O}|$ below a few hundredths, in which the corrections to the logarithmic law are a few percent. Chapter 15 develops these ranges and their use in diagnosis; this chapter uses z/L_O as the argument of the universal functions.

14.3 Dimensionless gradients

The similarity hypothesis leaves the functions ϕ_m and ϕ_h to measurement. This section defines them, gives the standard empirical forms and their ranges of validity, works two examples, introduces the temperature scale and the heat function, explains why momentum and heat are mixed differently, and derives the relation between the gradient Richardson number and the stability parameter.

14.3.1 The dimensionless wind shear

The dimensionless wind shear, equation (14.3), is the measured shear divided by the neutral shear at the same height and friction velocity. Read the other way, the hypothesis gives the shear

$$\frac{\partial U}{\partial z} = \frac{u_*}{\kappa\, z}\,\phi_m\!\left(\frac{z}{L_{\mathrm{O}}}\right), \tag{14.10}$$

which is the neutral shear of equation (14.1) multiplied by a correction factor. In neutral air $\phi_m = 1$ and the neutral law is recovered. The factor can also be read as a correction to the mixing length: the effective mixing length is $\kappa z/\phi_m$, shorter than κz in stable air and longer in unstable air.

ϕ_m is measured by combining a profile and a flux: cup or sonic anemometers at several heights give the shear, a sonic anemometer gives u_* and $\overline{w'\theta'}$, and hence L_{O}. Field experiments over flat, uniform ground, beginning in the late 1960s, provided the data to which the standard forms below were fitted.

14.3.2 Standard empirical forms

In stable air turbulence is suppressed, and the same momentum flux needs more shear: $\phi_m > 1$. The data are well fitted by a linear function,

$$\phi_m = 1 + 5\,\frac{z}{L_{\mathrm{O}}}, \qquad 0 \le z/L_{\mathrm{O}} \lesssim 1, \tag{14.11}$$

so that $z/L_{\mathrm{O}} = 0.2$ gives $\phi_m = 1 + 5 \times 0.2 = 2$, twice the neutral shear. In unstable air buoyancy enhances mixing, and the same momentum flux needs less shear: $\phi_m < 1$. The standard form is

$$\phi_m = \left(1 - 16\,\frac{z}{L_{\mathrm{O}}}\right)^{-1/4}, \qquad -2 \lesssim z/L_{\mathrm{O}} < 0. \tag{14.12}$$

These are the Businger–Dyer forms, the standard empirical forms used throughout this book. The stated ranges are those over which the underlying data extend; outside them the forms are extrapolations. The coefficients 5 and 16 are the most widely used values; individual experiments have given somewhat different values, partly because they also differ in the value assumed for κ.

Figure 14.3 plots both branches. The horizontal axis is z/L_{O} from -2 to 1, the vertical axis the dimensionless gradient. The solid blue curve is ϕ_m; the dashed red curve is the dimensionless temperature gradient ϕ_h of Section 14.3.4, which coincides with ϕ_m on the stable side; the dotted horizontal line is the neutral value one. The two marked points are the worked examples of Section 14.3.3.

The figure shows the asymmetry of the two branches. On the stable side ϕ_m rises steeply and without bound: at $z/L_{\mathrm{O}} = 1$ the shear is six times the neutral value. On the unstable side it falls slowly: even at $z/L_{\mathrm{O}} = -2$ the shear is 0.42 of the neutral value, because the exponent $-1/4$ flattens the curve. Stable stratification changes the profile much more, per unit of $|z/L_{\mathrm{O}}|$, than unstable stratification does. The heat gradient falls faster than the momentum gradient on the unstable side: heat is mixed more efficiently than momentum there, the subject of Section 14.3.5.

Interpretation. The three regimes read directly off the figure. Stable, $\phi_m > 1$: more shear for a given stress, a wind that increases rapidly with height. Neutral, $\phi_m = 1$: the logarithmic law. Unstable, $\phi_m < 1$: less shear for a given stress, a wind that is nearly uniform with height above the lowest meters.

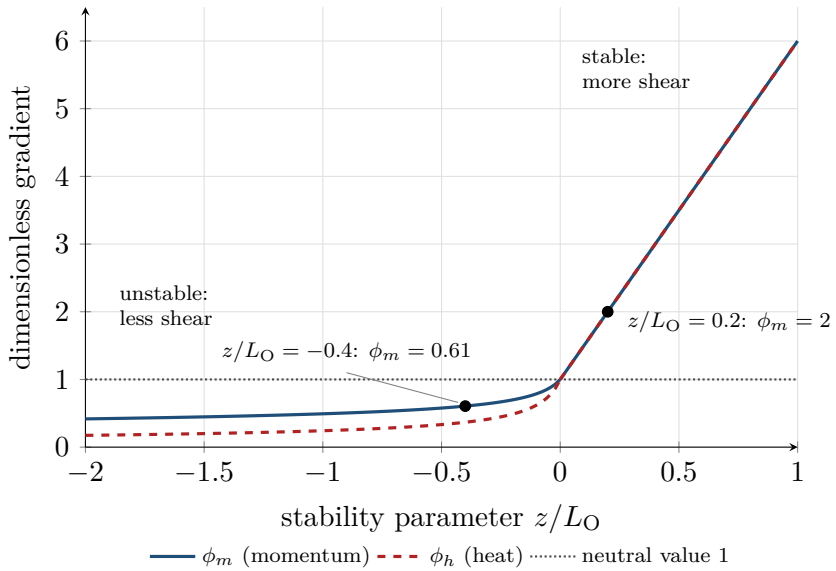


Figure 14.3: Dimensionless gradients against the stability parameter, from the standard Businger–Dyer forms: $\phi_m = (1 - 16\,z/L_{\mathrm{O}})^{-1/4}$ and $\phi_h = (1 - 16\,z/L_{\mathrm{O}})^{-1/2}$ for $z/L_{\mathrm{O}} < 0$; $\phi_m = \phi_h = 1 + 5\,z/L_{\mathrm{O}}$ for $z/L_{\mathrm{O}} \geq 0$ (equations (14.11), (14.12) and (14.15)).

14.3.3 Two worked examples

Example 14.3 (Stable shear)**.** $u_* = 0.4\,\mathrm{m\,s^{-1}}$, $z = 20\,\mathrm{m}$, $L_{\mathrm{O}} = 100\,\mathrm{m}$. Then $z/L_{\mathrm{O}} = 0.2$ and $\phi_m = 1 + 5 \times 0.2 = 2$. The shear is

$$\frac{\partial U}{\partial z} = \frac{0.4}{0.4 \times 20} \times 2 = 0.05 \times 2 = 0.1\,\mathrm{s^{-1}},$$

against the neutral $0.05\,\mathrm{s^{-1}}$: a change of $1\,\mathrm{m\,s^{-1}}$ over $10\,\mathrm{m}$ of height instead of $0.5\,\mathrm{m\,s^{-1}}$.

Example 14.4 (Unstable shear)**.** $u_* = 0.4\,\mathrm{m\,s^{-1}}$, $z = 20\,\mathrm{m}$, $L_{\mathrm{O}} = -50\,\mathrm{m}$. Then $z/L_{\mathrm{O}} = -0.4$, $1 - 16 \times (-0.4) = 1 + 6.4 = 7.4$, and

$$\phi_m = 7.4^{-1/4} = \frac{1}{\sqrt{\sqrt{7.4}}} = \frac{1}{\sqrt{2.720}} = \frac{1}{1.649} = 0.606.$$

The shear is $0.05 \times 0.606 = 0.030\,\mathrm{s^{-1}}$, 61 % of the neutral value.

With the same friction velocity and at the same height, the stable shear is $0.1/0.030 = 3.3$ times the unstable one. The two examples also show the asymmetry of Figure 14.3: a stability parameter of $+0.2$ changes the shear by $+100\,\%$, one of -0.4, twice as large in magnitude, by $-39\,\%$.

14.3.4 The temperature scale and the dimensionless temperature gradient

The temperature scale of equation (14.2), $\theta_* = -\overline{w'\theta'}/u_*$, is the heat flux expressed as a temperature, in the same way that u_* is the stress expressed as a velocity. Its sign is that of L_{O}: negative in unstable air, positive in stable air. In terms of it, the Obukhov length is

$$L_{\mathrm{O}} = \frac{u_*^2\,\overline{\theta}}{\kappa\, g\, \theta_*}, \tag{14.13}$$

obtained by substituting $\overline{w'\theta'} = -u_*\,\theta_*$ into equation (14.4). The dimensionless potential-temperature gradient is defined in parallel with equation (14.3),

$$\phi_h \equiv \frac{\kappa\, z}{\theta_*}\,\frac{\partial\overline{\theta}}{\partial z}, \qquad \frac{\partial\overline{\theta}}{\partial z} = \frac{\theta_*}{\kappa\, z}\,\phi_h\!\left(\frac{z}{L_{\mathrm{O}}}\right), \tag{14.14}$$

and its standard forms are

$$\phi_h = 1 + 5\,\frac{z}{L_{\mathrm{O}}} \quad (0 \le z/L_{\mathrm{O}} \lesssim 1), \qquad \phi_h = \left(1 - 16\,\frac{z}{L_{\mathrm{O}}}\right)^{-1/2} \quad (-2 \lesssim z/L_{\mathrm{O}} < 0). \tag{14.15}$$

Both forms equal one in neutral air, which assumes that heat and momentum are mixed alike there; some fits give a neutral value somewhat below one. Parallel relations hold for water vapor, with a humidity scale formed in the same way from the moisture flux, and for any other scalar carried by the eddies.

For the afternoon of Section 14.2.3, $\theta_* = -0.166/0.4 = -0.415\,\mathrm{K}$. At 10 m, $z/L_{\mathrm{O}} = -0.339$, $\phi_h = (1 + 5.43)^{-1/2} = 0.394$, and

$$\frac{\partial\overline{\theta}}{\partial z} = \frac{-0.415}{0.4 \times 10} \times 0.394 = -0.041\,\mathrm{K\,m^{-1}},$$

a potential temperature that falls by 4.1 K per 100 m, a strongly superadiabatic layer. For the night, $\theta_* = 0.0249/0.2 = 0.125\,\mathrm{K}$; at 10 m, $z/L_{\mathrm{O}} = 0.407$, $\phi_h = 3.04$, and $\partial\overline{\theta}/\partial z = 0.125 \times 3.04/4 = 0.095\,\mathrm{K\,m^{-1}}$, an inversion of almost 1 K per 10 m.

14.3.5 Why momentum and heat differ: the turbulent Prandtl number

The eddy diffusivities of Chapter 8 follow from the two gradients. For momentum, $u_*^2 = -\overline{u'w'} = K_m\,\partial U/\partial z = K_m\,u_*\phi_m/(\kappa z)$, so that

$$K_m = \frac{\kappa\, z\, u_*}{\phi_m}, \qquad K_h = \frac{\kappa\, z\, u_*}{\phi_h}, \tag{14.16}$$

the second from $\overline{w'\theta'} = -K_h\,\partial\overline{\theta}/\partial z$ with $\overline{w'\theta'} = -u_*\theta_*$. Their ratio is the turbulent Prandtl number,

$$\mathrm{Pr}_t = \frac{K_m}{K_h} = \frac{\phi_h}{\phi_m}. \tag{14.17}$$

With the standard forms, $\mathrm{Pr}_t = 1$ in stable air, and in unstable air $\mathrm{Pr}_t = (1 - 16\,z/L_{\mathrm{O}})^{-1/2}/(1 - 16\,z/L_{\mathrm{O}})^{-1/4} = (1 - 16\,z/L_{\mathrm{O}})^{-1/4} = \phi_m$, less than one: 0.61 at $z/L_{\mathrm{O}} = -0.4$, 0.42 at $z/L_{\mathrm{O}} = -2$. For the afternoon example at 10 m, $K_m = 0.4 \times 10 \times 0.4/0.628 = 2.55\,\mathrm{m^2\,s^{-1}}$ and $K_h = 1.6/0.394 = 4.1\,\mathrm{m^2\,s^{-1}}$.

The physical reason is that momentum and heat are not transported identically. A parcel carries its heat with it until it mixes; its horizontal momentum, in contrast, can be changed on the way by pressure fluctuations, which push on the parcel and exchange momentum with its surroundings without any mixing. In unstable air, buoyant plumes rise as coherent structures that carry heat efficiently and lose momentum to pressure forces, so that heat is transported more efficiently than momentum, $K_h > K_m$. This is why the theory needs two functions, ϕ_m and ϕ_h, and why a model that assumes the same diffusivity for both errs in convective conditions. In stable air the standard forms set $\mathrm{Pr}_t = 1$; observations in very stable air suggest values above one, with momentum still transported by waves when heat transport has nearly stopped (Section 14.6.3).

14.3.6 The gradient Richardson number and the stability parameter

The gradient Richardson number of Chapter 13,

$$\mathrm{Ri}_g = \frac{(g/\overline{\theta})\,\partial\overline{\theta}/\partial z}{(\partial U/\partial z)^2}, \tag{14.18}$$

uses gradients, whereas z/L_{O} uses fluxes; the theory connects them. Substitute the two gradients of equations (14.10) and (14.14):

$$\mathrm{Ri}_g = \frac{(g/\overline{\theta})\,\theta_*\,\phi_h/(\kappa z)}{u_*^2\phi_m^2/(\kappa z)^2} = \frac{g\,\kappa\,z\,\theta_*}{\overline{\theta}\,u_*^2}\cdot\frac{\phi_h}{\phi_m^2}.$$

By equation (14.13), the first factor is $z\,\kappa g\theta_*/(\overline{\theta}u_*^2) = z/L_{\mathrm{O}}$. Hence

$$\mathrm{Ri}_g = \frac{z}{L_{\mathrm{O}}}\,\frac{\phi_h(z/L_{\mathrm{O}})}{\phi_m(z/L_{\mathrm{O}})^2}. \tag{14.19}$$

For the standard unstable forms, $\phi_h/\phi_m^2 = (1-16\,z/L_{\mathrm{O}})^{-1/2}/(1-16\,z/L_{\mathrm{O}})^{-1/2} = 1$, and

$$\mathrm{Ri}_g = z/L_{\mathrm{O}} \qquad (z/L_{\mathrm{O}} < 0),$$

exactly. For the stable forms, $\phi_h/\phi_m^2 = 1/(1+5\,z/L_{\mathrm{O}})$, and

$$\mathrm{Ri}_g = \frac{z/L_{\mathrm{O}}}{1+5\,z/L_{\mathrm{O}}}, \qquad z/L_{\mathrm{O}} = \frac{\mathrm{Ri}_g}{1-5\,\mathrm{Ri}_g} \qquad (z/L_{\mathrm{O}} \geq 0).$$

For the stable example, $z/L_{\mathrm{O}} = 0.2$ gives $\mathrm{Ri}_g = 0.2/2 = 0.1$; for the unstable one, $\mathrm{Ri}_g = -0.4$. The stable relation has a consequence: as $z/L_{\mathrm{O}} \to \infty$, $\mathrm{Ri}_g \to 1/5 = 0.2$. The linear form cannot represent a layer whose gradient Richardson number exceeds 0.2; such a layer lies beyond the theory's standard stable branch, close to the critical value $\mathrm{Ri}_c \approx 0.25$ at which continuous turbulence is no longer sustained (Chapter 13). With $\mathrm{Pr}_t = 1$, the flux Richardson number of equation (14.9) equals Ri_g on the stable side, consistent with the relation $\mathrm{Ri}_f = \mathrm{Ri}_g/\mathrm{Pr}_t$ of Chapter 8.

14.4 Integrated stability corrections and profiles

Engineering questions concern the wind at given heights, not its gradient. This section integrates the dimensionless gradients into profiles, deriving the stability corrections ψ_m and ψ_h for the standard forms; contrasts the gradient and integrated corrections; writes the wind and temperature profiles; works an extrapolation from 10 to 50 m; and shows why the power-law exponent varies with stability.

14.4.1 Derivation of the stability correction

Start from equation (14.10) and split ϕ_m into its neutral value and a departure, $\phi_m = 1-(1-\phi_m)$:

$$\frac{\partial U}{\partial z} = \frac{u_*}{\kappa\,z} - \frac{u_*}{\kappa\,z}\big[1-\phi_m(z/L_{\mathrm{O}})\big].$$

Integrate from z_0, where the extrapolated wind vanishes, to z:

$$U(z) = \frac{u_*}{\kappa}\left[\ln\frac{z}{z_0} - \int_{z_0}^{z}\big[1-\phi_m(z'/L_{\mathrm{O}})\big]\frac{\mathrm{d}z'}{z'}\right].$$

Change the variable of integration to $s = z'/L_{\mathrm{O}}$, for which $\mathrm{d}z'/z' = \mathrm{d}s/s$, and define the *stability correction for momentum*

$$\psi_m(z/L_{\mathrm{O}}) \equiv \int_0^{z/L_{\mathrm{O}}} \frac{1-\phi_m(s)}{s}\,\mathrm{d}s. \tag{14.20}$$

The integral from z_0/L_{O} to z/L_{O} equals $\psi_m(z/L_{\mathrm{O}}) - \psi_m(z_0/L_{\mathrm{O}})$. Since z_0/L_{O} is tiny, of order 10^{-3} for $z_0 = 0.05\,\mathrm{m}$ and $|L_{\mathrm{O}}| = 50\,\mathrm{m}$, the second term is negligible and is dropped. The integrand is finite at $s = 0$ because $\phi_m(0) = 1$. The result is the stability-corrected profile

$$U(z) = \frac{u_*}{\kappa}\left[\ln\frac{z}{z_0} - \psi_m\!\left(\frac{z}{L_{\mathrm{O}}}\right)\right]. \tag{14.21}$$

Stable branch. With $\phi_m = 1 + 5s$, the integrand is $(1 - 1 - 5s)/s = -5$, and

$$\psi_m = -5\,\frac{z}{L_{\mathrm{O}}} \qquad (z/L_{\mathrm{O}} \geq 0). \tag{14.22}$$

Unstable branch. With $\phi_m = (1-16s)^{-1/4}$, substitute $x = (1-16s)^{1/4}$, so that $\phi_m = 1/x$, $s = (1-x^4)/16$ and $\mathrm{d}s = -(x^3/4)\,\mathrm{d}x$; the limit $s = 0$ becomes $x = 1$. The integrand transforms as

$$\frac{1-1/x}{s}\,\mathrm{d}s = \frac{x-1}{x}\cdot\frac{16}{1-x^4}\cdot\left(-\frac{x^3}{4}\right)\mathrm{d}x = \frac{4x^2(1-x)}{1-x^4}\,\mathrm{d}x = \frac{4x^2}{(1+x)(1+x^2)}\,\mathrm{d}x,$$

using $1 - x^4 = (1-x)(1+x)(1+x^2)$. Partial fractions give $4x^2/[(1+x)(1+x^2)] = 2/(1+x) + (2x-2)/(1+x^2)$, as multiplying out confirms: $2(1+x^2) + (2x-2)(1+x) = 4x^2$. The three terms integrate to $2\ln(1+x)$, $\ln(1+x^2)$ and $-2\arctan x$. Evaluating from 1 to x, with $\arctan 1 = \pi/4$,

$$\psi_m = 2\ln\frac{1+x}{2} + \ln\frac{1+x^2}{2} - 2\arctan x + \frac{\pi}{2}, \qquad x = \left(1 - 16\,\frac{z}{L_{\mathrm{O}}}\right)^{1/4} \qquad (z/L_{\mathrm{O}} < 0). \tag{14.23}$$

For $z/L_{\mathrm{O}} = -0.4$, $x = 7.4^{1/4} = 1.649$, and $\psi_m = 2\ln 1.325 + \ln 1.860 - 2\times 1.026 + 1.571 = 0.562 + 0.621 - 2.052 + 1.571 = 0.702$ (arctangent in radians).

Heat. The same steps with ϕ_h give ψ_h. On the stable side $\psi_h = -5\,z/L_{\mathrm{O}}$. On the unstable side, with $y = (1-16s)^{1/2}$, $\phi_h = 1/y$, $s = (1-y^2)/16$ and $\mathrm{d}s = -(y/8)\,\mathrm{d}y$, the integrand becomes $2(1-y)/(1-y^2)\,\mathrm{d}y = 2\,\mathrm{d}y/(1+y)$, and

$$\psi_h = 2\ln\frac{1+y}{2}, \qquad y = \left(1 - 16\,\frac{z}{L_{\mathrm{O}}}\right)^{1/2} \qquad (z/L_{\mathrm{O}} < 0). \tag{14.24}$$

14.4.2 Gradient correction and integrated correction

The two functions answer different questions. ϕ_m corrects the gradient $\partial U/\partial z$ at one height; ψ_m corrects the wind $U(z)$ itself, and by equation (14.20) it accumulates the departure $1 - \phi_m$ over all heights below z, weighted by $1/s$. A stable layer with $z/L_{\mathrm{O}} = 0.2$ at the top has twice the neutral shear there ($\phi_m = 2$), but the shear was closer to neutral lower down, and the wind at the top is reduced, relative to the logarithmic term, by only one unit of ln: $\psi_m = -5\times 0.2 = -1$. In the profile formula a negative ψ_m is subtracted, which *adds* to the logarithm; this is the larger wind increase between the surface and z that stable air produces for a given u_*.

Figure 14.4 plots the corrections. The axes are as in Figure 14.3, with the vertical axis now the dimensionless correction. The solid blue curve is ψ_m, the dashed red curve ψ_h; on the stable side both are the line $-5\,z/L_{\mathrm{O}}$. The two marked points are the values for the worked examples.

The corrections have the sign of $1 - \phi_m$: positive in unstable air, negative in stable air. At a given u_*, a positive ψ_m lowers the wind at height z and a negative one raises it. Their sizes

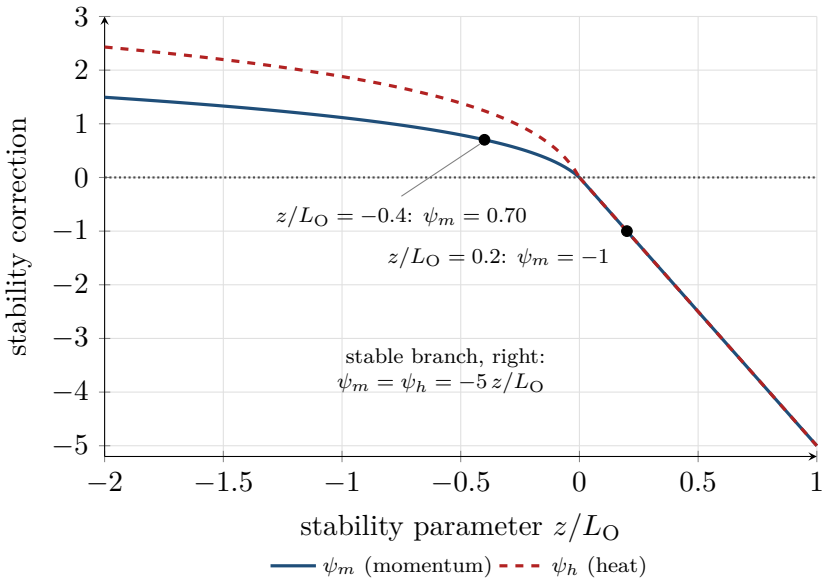


Figure 14.4: Integrated stability corrections against the stability parameter: ψ_m from equation (14.23) and ψ_h from equation (14.24) for $z/L_O < 0$; $\psi_m = \psi_h = -5\, z/L_O$ for $z/L_O \geq 0$ (equation (14.22)).

are to be compared with the logarithmic term. At 10 m over $z_0 = 0.05$ m, $\ln(z/z_0) = 5.30$; a correction of $+0.7$ removes 13 % of it and one of -1 adds 19 %. On the unstable side ψ_m grows slowly, reaching only 1.49 at $z/L_O = -2$; on the stable side it decreases without bound, and at $z/L_O = 1$ it is -5, nearly as large as the logarithm itself.

14.4.3 Wind and temperature profiles

The wind profile is equation (14.21). Over tall vegetation or buildings the height is measured from the displacement height d, in the logarithm and in the stability parameter alike,

$$U(z) = \frac{u_*}{\kappa}\left[\ln\frac{z-d}{z_0} - \psi_m\!\left(\frac{z-d}{L_O}\right)\right], \tag{14.25}$$

because the eddies scale with the distance from the effective surface, not from the ground. Over a forest with $d = 15$ m and $L_O = 100$ m, a sensor at 30 m has $(z-d)/L_O = 0.15$, not 0.30.

The potential-temperature profile follows in the same way from equation (14.14). Between two heights z_1 and z_2 in the surface layer,

$$\overline{\theta}(z_2) - \overline{\theta}(z_1) = \frac{\theta_*}{\kappa}\left[\ln\frac{z_2}{z_1} - \psi_h\!\left(\frac{z_2}{L_O}\right) + \psi_h\!\left(\frac{z_1}{L_O}\right)\right]. \tag{14.26}$$

Referred to the surface, the profile reads $\overline{\theta}(z) - \theta_s = (\theta_*/\kappa)[\ln(z/z_{0h}) - \psi_h(z/L_O)]$, where θ_s is the potential temperature at the surface and z_{0h} is a roughness length for heat, the height at which the extrapolated temperature profile reaches the surface value. Heat leaves the surface by molecular conduction through the thin layers of air on leaves and soil grains, without an analog of the form drag that transfers momentum, so z_{0h} is usually smaller than z_0, often by a factor of ten or more. Both profiles are logarithmic with corrections. On the stable side the two corrections are equal; on the unstable side $\psi_h > \psi_m$, and the temperature profile departs further from the logarithm than the wind profile, because heat is mixed more efficiently (Section 14.3.5).

14.4.4 Extrapolation from 10 to 50 meters

The practical use of the profile is to carry a measured wind to another height. Take an illustrative mast over farmland with $z_0 = 0.05\,\mathrm{m}$ and $U_{10} = 5\,\mathrm{m\,s^{-1}}$, to be extrapolated to 50 m, in three conditions. In each, the friction velocity is first found from the 10 m wind, $u_* = \kappa U_{10}/[\ln(10/z_0) - \psi_m(10/L_O)]$, and the profile is then evaluated at 50 m.

- *Neutral.* $u_* = 0.4 \times 5/5.298 = 0.378\,\mathrm{m\,s^{-1}}$ and $U(50) = (0.378/0.4)\ln 1000 = 0.944 \times 6.908 = 6.52\,\mathrm{m\,s^{-1}}$.
- *Stable,* $L_O = 100\,\mathrm{m}$. $\psi_m(0.1) = -0.5$, $\psi_m(0.5) = -2.5$. $u_* = 2/(5.298 + 0.5) = 0.345\,\mathrm{m\,s^{-1}}$ and $U(50) = 0.862 \times (6.908 + 2.5) = 8.11\,\mathrm{m\,s^{-1}}$.
- *Unstable,* $L_O = -50\,\mathrm{m}$. $\psi_m(-0.2) = 0.461$, $\psi_m(-1) = 1.116$. $u_* = 2/(5.298 - 0.461) = 0.414\,\mathrm{m\,s^{-1}}$ and $U(50) = 1.034 \times (6.908 - 1.116) = 5.99\,\mathrm{m\,s^{-1}}$.

The same 10 m wind gives 50 m winds of 5.99, 6.52 and $8.11\,\mathrm{m\,s^{-1}}$. A neutral extrapolation is 20 % low in the stable case and 9 % high in the unstable case. For wind energy, where the available power scales with the cube of the speed, the stable error is a factor $(8.11/6.52)^3 = 1.93$ in power density. Roughness alone is not enough to extrapolate: the same z_0 gives three different winds.

Figure 14.5 draws the three profiles. The horizontal axis is the wind speed, the vertical axis the height on a logarithmic scale from 1 to 100 m. On this axis the neutral profile is a straight line; all three pass through $5\,\mathrm{m\,s^{-1}}$ at 10 m (open circle); the filled points mark the 50 m values. The stable profile curves to the right with height, accelerating aloft; the unstable profile curves to the left, nearly vertical above 30 m; the departures grow with height because $|z/L_O|$ does.

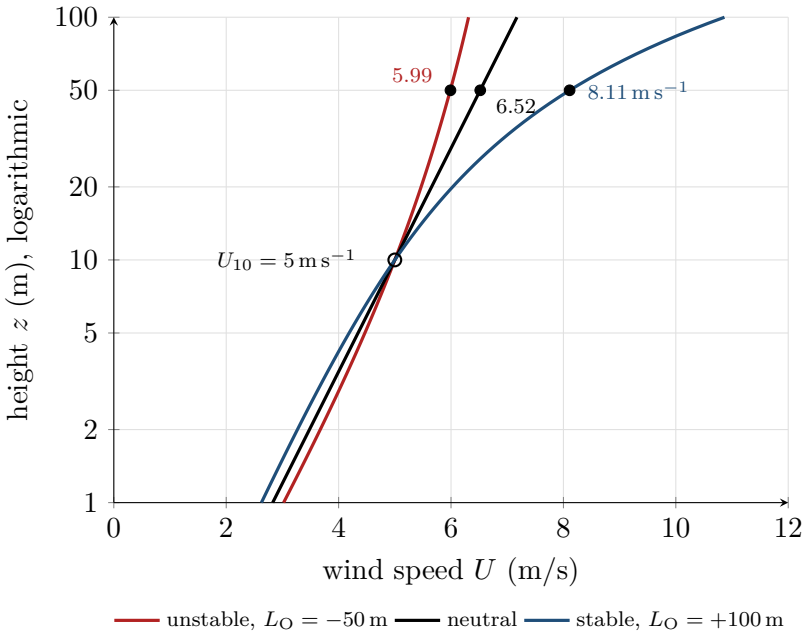


Figure 14.5: Wind profiles through the same 10 m wind of $5\,\mathrm{m\,s^{-1}}$ over $z_0 = 0.05\,\mathrm{m}$, illustrative. $U = (u_*/\kappa)[\ln(z/z_0) - \psi_m(z/L_O)]$ with $\kappa = 0.4$: neutral, $u_* = 0.378\,\mathrm{m\,s^{-1}}$; stable, $\psi_m = -5\,z/L_O$, $L_O = 100\,\mathrm{m}$, $u_* = 0.345\,\mathrm{m\,s^{-1}}$; unstable, equation (14.23) with $L_O = -50\,\mathrm{m}$, $u_* = 0.414\,\mathrm{m\,s^{-1}}$. Filled points: the 50 m values.

14.4.5 The variable power-law exponent

The power law $U(z) = U(z_r)(z/z_r)^{\alpha}$, widely used in wind engineering, has a constant exponent α. The local exponent of any profile is its logarithmic slope, $\alpha(z) = \mathrm{d}\ln U/\mathrm{d}\ln z = (z/U)\,\partial U/\partial z$. For a Monin–Obukhov profile, using equations (14.10) and (14.21),

$$\alpha(z) = \frac{z}{U}\cdot\frac{u_*\,\phi_m}{\kappa\, z} = \frac{\phi_m(z/L_{\mathrm{O}})}{\ln(z/z_0) - \psi_m(z/L_{\mathrm{O}})}. \tag{14.27}$$

The friction velocity cancels: the exponent depends on height, roughness and stability. Table 14.3 gives it for the three profiles of Figure 14.5, at 10 and 50 m, together with the bulk exponent $\ln[U(50)/U(10)]/\ln 5$ that a power law through the two heights would use. Its columns are the condition, the friction velocity, the 50 m wind, the bulk exponent and the local exponent at the two heights.

Table 14.3: Extrapolation of $U_{10} = 5\,\mathrm{m\,s^{-1}}$ over $z_0 = 0.05\,\mathrm{m}$ and the power-law exponents implied, from equations (14.21) and (14.27). Values illustrative.

Condition	u_* (m/s)	$U(50)$ (m/s)	bulk α, 10–50 m	α(10 m)	α(50 m)
Unstable, $L_{\mathrm{O}} = -50\,\mathrm{m}$	0.414	5.99	0.112	0.144	0.085
Neutral	0.378	6.52	0.165	0.189	0.145
Stable, $L_{\mathrm{O}} = +100\,\mathrm{m}$	0.345	8.11	0.301	0.259	0.372

Over one surface the bulk exponent ranges from 0.11 to 0.30, a factor of almost three. In neutral and unstable air the local exponent decreases with height, because the logarithm in the denominator grows; in stable air it increases, because ϕ_m grows faster than the denominator. The commonly quoted exponent $1/7 \approx 0.14$ is the neutral value near 50 m over this surface, or the unstable value near 10 m. A fitted power-law exponent is therefore partly an empirical proxy for stability, and an exponent fitted on a sample of mixed conditions averages over a diurnal cycle of stability; its use outside the conditions of the sample inherits the errors of Section 14.4.4.

14.5 Using the theory in a weather model

Weather models do not resolve the surface layer: their lowest level lies tens of meters above the ground, and everything below it is computed from Monin–Obukhov relations. This section describes how a model diagnoses its 10 m wind, derives the stability-dependent transfer coefficients, writes the coupled problem as an iteration with a worked example, and draws the hierarchy from inputs to profiles.

14.5.1 From the lowest model level to 10 meters

Consider a model, such as WRF, whose lowest level is at $z_1 = 30\,\mathrm{m}$. It carries the wind $U(z_1)$ there, it has assigned a roughness length z_0 to the grid cell, and its surface scheme computes u_*, the surface heat flux and hence L_{O}. The wind at 10 m is not a model level; it is diagnosed by applying equation (14.21) at both heights with the same u_* and dividing:

$$U_{10} = U(z_1)\,\frac{\ln(10/z_0) - \psi_m(10/L_{\mathrm{O}})}{\ln(z_1/z_0) - \psi_m(z_1/L_{\mathrm{O}})}. \tag{14.28}$$

With $U(z_1) = 6\,\mathrm{m\,s^{-1}}$ and $z_0 = 0.05\,\mathrm{m}$, the neutral diagnosis is $6 \times 5.298/6.397 = 4.97\,\mathrm{m\,s^{-1}}$. With $L_{\mathrm{O}} = +100\,\mathrm{m}$ it is $6 \times (5.298 + 0.5)/(6.397 + 1.5) = 4.41\,\mathrm{m\,s^{-1}}$; with $L_{\mathrm{O}} = +50\,\mathrm{m}$, $4.02\,\mathrm{m\,s^{-1}}$; with $L_{\mathrm{O}} = -50\,\mathrm{m}$, $5.25\,\mathrm{m\,s^{-1}}$.

Every error in L_O or z_0 therefore becomes an error in the diagnosed 10 m wind. A model that halves the Obukhov length of a stable night, from 100 to 50 m, lowers its 10 m wind by 9 %; one that doubles the roughness length to 0.1 m at $L_O = 100$ m lowers it from 4.41 to 4.25 m s^{-1}, 3.5 %. The diagnosed value is a grid-cell value, built on one effective roughness and one stability for a cell kilometers wide; comparing it with a station's 10 m wind compares a grid-cell value with a point value. The diagnosis also gives no direction of its own: the simplest schemes keep the direction of the lowest level, while the real wind turns with height across the layer, to the right with increasing height in the Northern Hemisphere and to the left in the Southern, most strongly in stable air.

14.5.2 Stability-dependent transfer coefficients

The bulk aerodynamic formulas of Chapter 10 compute the surface fluxes from the wind and temperature at one height,

$$\tau_0 = \rho\, C_D\, U(z)^2, \qquad H = -\rho\, c_p\, C_H\, U(z)\,[\overline{\theta}(z) - \theta_s], \tag{14.29}$$

with the drag coefficient C_D and the heat transfer coefficient C_H, both dimensionless. Monin–Obukhov theory supplies them. From equation (14.21), $u_*/U(z) = \kappa/[\ln(z/z_0) - \psi_m]$, and since $C_D = u_*^2/U^2$,

$$C_D = \left[\frac{\kappa}{\ln(z/z_0) - \psi_m(z/L_O)}\right]^2, \qquad C_H = \frac{\kappa^2}{[\ln(z/z_0) - \psi_m(z/L_O)]\,[\ln(z/z_{0h}) - \psi_h(z/L_O)]}, \tag{14.30}$$

the second from $H = \rho c_p \overline{w'\theta'} = -\rho c_p u_* \theta_*$ with θ_* from the surface-referred temperature profile. The transfer coefficients are functions of z/z_0 (and z/z_{0h}) and of z/L_O: the roughness sets their neutral value and the stability multiplies it.

Figure 14.6 plots C_D at $z = 10$ m, multiplied by 1000, against z/L_O from -2 to 1 for three roughness lengths: 0.001 m (very smooth land), 0.01 m (mown grass) and 0.1 m (farmland with tall crops). The dotted vertical line marks neutral air. Each curve is highest on the unstable side and falls steeply on the stable side.

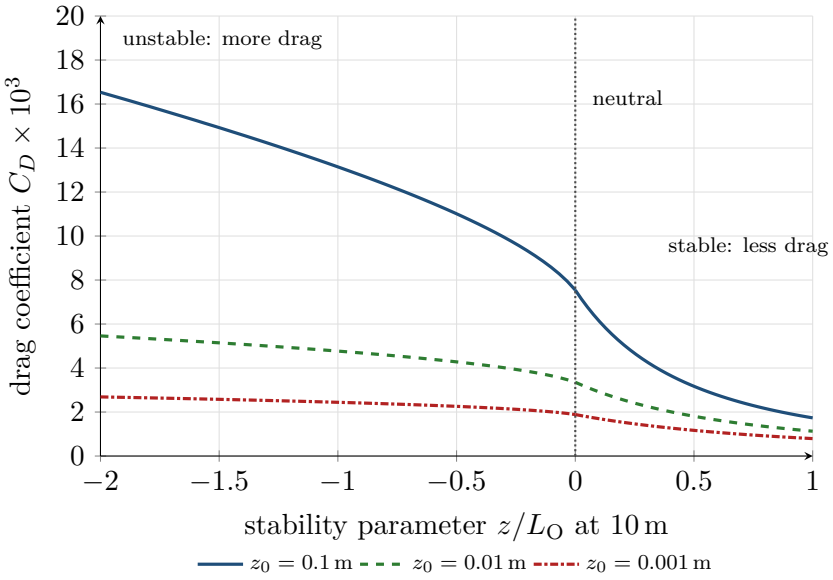


Figure 14.6: Drag coefficient at 10 m against the stability parameter, $C_D = \{\kappa/[\ln(10/z_0) - \psi_m(z/L_O)]\}^2$ (equation (14.30)) with $\kappa = 0.4$, the standard forms of ψ_m and no displacement height, for three roughness lengths.

For $z_0 = 0.1\,\mathrm{m}$ the neutral value is $(0.4/4.605)^2 = 7.5 \times 10^{-3}$; at $z/L_\mathrm{O} = -1$ it is $(0.4/3.489)^2 = 13.1 \times 10^{-3}$, and at $z/L_\mathrm{O} = 1$, $(0.4/9.605)^2 = 1.7 \times 10^{-3}$: a factor of 7.6 between a convective afternoon and a stable night over the same surface. The stability dependence is larger than the factor of four between the neutral values over the smoothest and the roughest of the three surfaces. A model that uses a neutral drag coefficient in stable air overestimates the stress, and the coupling of the surface to the air above, by a large factor, as Chapter 10 found for the friction velocity.

14.5.3 The coupled problem and its iterative solution

The relations form a closed loop. The Obukhov length needs u_* and the heat flux; u_* needs $\psi_m(z/L_\mathrm{O})$, which needs L_O; the heat flux needs $\psi_h(z/L_\mathrm{O})$, which also needs L_O. The inputs a model actually has are the wind and potential temperature at a reference height z_r (the lowest model level), the surface potential temperature θ_s from the land-surface scheme, and z_0 and z_{0h} (with humidity for the moist case). The unknowns u_*, θ_* and L_O satisfy three equations:

$$u_* = \frac{\kappa\, U(z_r)}{\ln(z_r/z_0) - \psi_m(z_r/L_\mathrm{O})}, \quad \theta_* = \frac{\kappa\,[\overline{\theta}(z_r) - \theta_s]}{\ln(z_r/z_{0h}) - \psi_h(z_r/L_\mathrm{O})}, \quad L_\mathrm{O} = \frac{u_*^2\,\overline{\theta}}{\kappa\, g\, \theta_*}.$$

They are solved by fixed-point iteration:

1. Start with a neutral first estimate: $\psi_m = \psi_h = 0$.
2. Compute u_* and θ_* from the first two equations, and the heat flux $\overline{w'\theta'} = -u_*\theta_*$, $H = \rho c_p \overline{w'\theta'}$.
3. Compute L_O from the third equation.
4. Update the stability corrections $\psi_m(z_r/L_\mathrm{O})$ and $\psi_h(z_r/L_\mathrm{O})$.
5. Recompute u_*, θ_* and L_O with the updated corrections.
6. Repeat steps 4 and 5 until L_O changes by less than a set tolerance between iterations.

Models often replace the iteration by a direct relation between z/L_O and the bulk Richardson number $\mathrm{Ri}_B = (g/\overline{\theta})\,[\overline{\theta}(z_r) - \theta_s]\, z_r/U(z_r)^2$, which is computed from the inputs alone, or by a few fixed iterations; the converged answer is the same.

14.5.4 A worked iteration

Take an illustrative clear evening at a site at 23°S, where the Coriolis parameter is $f = 2 \times 7.292 \times 10^{-5} \times \sin(-23^\circ) = -5.70 \times 10^{-5}\,\mathrm{s^{-1}}$. The lowest model level is $z_r = 30\,\mathrm{m}$ with $U = 6\,\mathrm{m\,s^{-1}}$; the air there is 1.5 K warmer in potential temperature than the surface, $\overline{\theta}(30\,\mathrm{m}) - \theta_s = +1.5\,\mathrm{K}$; over farmland $z_0 = 0.05\,\mathrm{m}$, and for simplicity $z_{0h} = z_0$; $\overline{\theta} = 300\,\mathrm{K}$. Then $\ln(30/0.05) = 6.397$ and $\mathrm{Ri}_B = 0.0327 \times 1.5 \times 30/36 = 0.041$. Nothing in the iteration depends on f: the same inputs at 23°N give the same fluxes.

The first pass is neutral: $u_* = 0.4 \times 6/6.397 = 0.375\,\mathrm{m\,s^{-1}}$, $\theta_* = 0.4 \times 1.5/6.397 = 0.0938\,\mathrm{K}$, and

$$L_\mathrm{O} = \frac{0.375^2 \times 300}{0.4 \times 9.81 \times 0.0938} = \frac{42.2}{0.368} = 114.7\,\mathrm{m},$$

so $z_r/L_\mathrm{O} = 0.261$ and $\psi_m = \psi_h = -5 \times 0.261 = -1.307$. The second pass uses these corrections: $u_* = 2.4/(6.397 + 1.307) = 0.312\,\mathrm{m\,s^{-1}}$, $\theta_* = 0.6/7.704 = 0.0779\,\mathrm{K}$, $L_\mathrm{O} = 95.3\,\mathrm{m}$. Table 14.4 lists the passes. Its columns are the pass number, the stability parameter used in the pass, the corresponding correction, the friction velocity, temperature scale and sensible heat flux that result, and the new Obukhov length and stability parameter.

Table 14.4: Fixed-point iteration for an illustrative stable case: $z_r = 30\,\mathrm{m}$, $U = 6\,\mathrm{m\,s^{-1}}$, $\overline{\theta}(z_r) - \theta_s = 1.5\,\mathrm{K}$, $z_0 = z_{0h} = 0.05\,\mathrm{m}$, $\overline{\theta} = 300\,\mathrm{K}$, $\rho c_p = 1205\,\mathrm{J\,m^{-3}\,K^{-1}}$, $\kappa = 0.4$, stable forms $\psi_m = \psi_h = -5\,z/L_\mathrm{O}$.

Pass	z_r/L_O used	$\psi_m = \psi_h$	u_* (m/s)	θ_* (K)	H (W/m^2)	new L_O (m)	new z_r/L_O
1	0	0	0.3752	0.0938	−42.4	114.7	0.261
2	0.261	−1.307	0.3115	0.0779	−29.2	95.3	0.315
3	0.315	−1.575	0.3011	0.0753	−27.3	92.1	0.326
4	0.326	−1.629	0.2990	0.0748	−26.9	91.4	0.328
5	0.328	−1.640	0.2986	0.0747	−26.9	91.3	0.329
6	0.329	−1.643	0.2985	0.0746	−26.8	91.3	0.329

The iteration converges in five or six passes to $L_\mathrm{O} = 91.3\,\mathrm{m}$, $z_r/L_\mathrm{O} = 0.329$, $u_* = 0.299\,\mathrm{m\,s^{-1}}$ and $H = -26.8\,\mathrm{W\,m^{-2}}$. The neutral first estimate was wrong by 26 % in u_* and 58 % in the heat flux: neglecting stability overstates both the stress and the cooling of the air by the ground. The converged state satisfies the bulk Richardson relation, $z/L_\mathrm{O}\,[\ln(z_r/z_{0h}) - \psi_h]/[\ln(z_r/z_0) - \psi_m]^2 = 0.329/8.040 = 0.041 = \mathrm{Ri}_B$. With it the diagnosed 10 m wind is $(0.299/0.4)[\ln 200 + 5 \times 10/91.3] = 0.746 \times 5.846 = 4.36\,\mathrm{m\,s^{-1}}$, against $4.97\,\mathrm{m\,s^{-1}}$ from a neutral diagnosis, and the drag coefficient at 30 m is $(0.299/6)^2 = 2.5 \times 10^{-3}$ against the neutral 3.9×10^{-3}. The same inputs with the air 1.5 K *cooler* than the surface, an unstable case, converge in two passes to $L_\mathrm{O} = -116\,\mathrm{m}$, $u_* = 0.410\,\mathrm{m\,s^{-1}}$ and $H = +54.7\,\mathrm{W\,m^{-2}}$; the unstable corrections change slowly with z/L_O, so the iteration settles faster.

14.5.5 The hierarchy from inputs to profiles

Figure 14.7 draws the structure of the computation. Each box is a level of the hierarchy, read from the top: the inputs at a reference height and at the surface; the fluxes they imply; the Obukhov length; the stability parameter at each height of interest; the dimensionless functions; and the profiles and transfer coefficients that are the outputs. The notes on the left say which levels are model state, which are calculated and which are diagnosed. The black downward arrows are the forward computation; the red arrow on the right is the iteration of Section 14.5.3, which feeds the corrections back to the fluxes until the loop closes.

This chain is the backbone of the surface-layer schemes of weather, climate, air-quality and land-surface models: almost every model quantity near the ground, from the 10 m wind to the evaporation from a field, passes through it. Its weak links are the inputs that are not measured at a grid cell, z_0, z_{0h} and θ_s, and the functions themselves outside their fitted ranges.

14.6 Limits of the theory

A similarity theory is only as general as its hypothesis. This section states the local-equilibrium assumption behind Monin–Obukhov theory, lists the conditions under which it fails, treats the two limits of stability in which it breaks down even over ideal terrain, and explains why it nevertheless remains the standard language of the surface layer.

14.6.1 A local-equilibrium theory

The theory assumes that the turbulence at a point is controlled by the local surface stress, the local heat flux and the height, and by nothing else (Table 14.1). This is an assumption of local equilibrium: the eddies at height z have adjusted to the fluxes at that place and time, have no

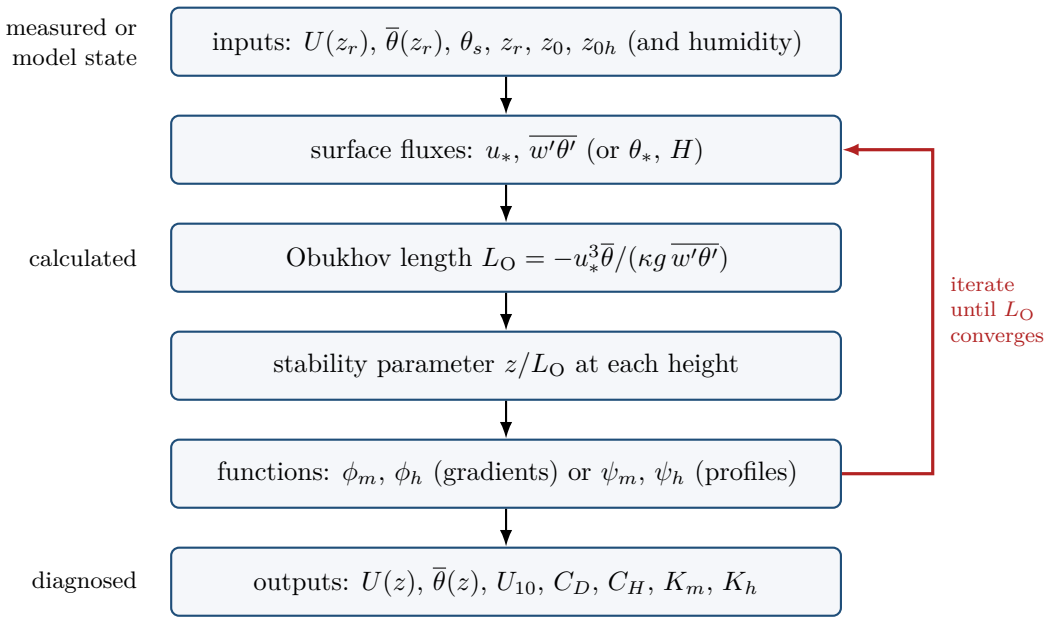


Figure 14.7: The Monin–Obukhov hierarchy from inputs to profiles. Each level is computed from the one above; the stability corrections feed back to the fluxes, and the loop is solved by iteration (Table 14.4).

memory of other surfaces or earlier states, and are not influenced by structures much larger than z. It holds best under four conditions:

- horizontally homogeneous terrain, flat and of uniform roughness and surface heating;
- adequate fetch, so that the surface layer at the measurement height has adjusted to the local surface (Chapter 7);
- stationary conditions, with fluxes that change slowly compared with the averaging period of about thirty minutes;
- heights well above the roughness elements and well below the top of the surface layer, roughly $z \gg z_0$, above the roughness sublayer, and $z \lesssim 0.1\,z_i$.

Under nonlocal influences, such as eddies generated elsewhere, flow adjusting to a new surface, or a boundary-layer top close to the ground, the relations still apply approximately and with growing error.

14.6.2 Where the theory fails

Table 14.5 lists the common failures. Its columns give the situation, the assumption it violates and the symptom in the data, a profile or flux that does not collapse onto the universal functions.

The first six rows are failures of the site or of the weather; they are avoided by choosing a homogeneous, stationary sample, and they are common in the places where near-surface wind matters most: transmission corridors that cross ridges and forest edges, wind farms on hills, and sensors on urban rooftops. The last two rows are failures of the theory itself, which occur even over ideal terrain, at the two ends of the stability range; the next two subsections treat them.

14.6.3 Very stable conditions

In weak to moderate stability, up to z/L_O of about 1, the linear forms of equation (14.11) describe the data reasonably. In very stable conditions, on clear nights with light wind, the

Table 14.5: Situations in which Monin–Obukhov similarity fails.

Situation	Assumption violated	Symptom
Steep or complex terrain	horizontal homogeneity; flat ground	speed-up and pressure gradients set the profile; shear not related to u_*
Forest edges, coastlines	homogeneity; adequate fetch	internal boundary layers; profile kinks at their tops
Urban canopies, tall vegetation	$z \gg z_0$; above the roughness sublayer	wakes of individual obstacles; profile not logarithmic near the roof or canopy level
Strong advection	homogeneity; constant flux with height	heat flux changing with height, as when warm air flows over a cold surface
Rapidly changing weather	stationarity	fronts, evening transition: fluxes and profiles out of step
Flow separation	local equilibrium	recirculation behind hills and buildings; reversed or near-zero shear
Intermittent stable turbulence	stationarity; continuous turbulence	bursts separated by quiet periods; averages that represent no actual state
Strongly convective eddies	locality; z as the only length	thermals scaled by z_i; horizontal variances not functions of z/L_O

assumptions break down. Turbulence becomes intermittent: quiet periods with almost no mixing alternate with bursts triggered by shear instabilities aloft. Gravity waves, oscillations of the stratified air that carry momentum without mixing it, contribute to the measured covariances. On sloping ground, cold air drains downhill in shallow drainage flows whose structure is set by the slope, not by the local fluxes. The flux at the surface no longer controls the turbulence at z; local equilibrium is lost, and a function of z/L_O no longer captures the flow.

The standard form also has an internal limit. By Section 14.3.6 it implies $\mathrm{Ri}_g < 0.2$ at every z/L_O, and its ϕ_m grows without bound, so that a model using it predicts a vanishing stress as the stability increases: the surface decouples from the air above, the ground cools without limit, and the modeled near-surface wind collapses. Observed very stable layers keep some mixing at gradient Richardson numbers above 0.2. Some model schemes therefore use stable functions that grow more slowly than linearly beyond z/L_O of about 1, or impose a lower bound on the mixing; these choices keep the model coupled to the surface and are tuned to results, not derived from the theory. In very stable conditions both the theory and the measurements that would test it are at their least reliable, which makes the stable night the regime of largest uncertainty for near-surface engineering wind.

14.6.4 Strong convection is nonlocal

In strongly unstable conditions the dominant eddies are thermals that span much of the boundary layer, hundreds of meters to a few kilometers deep. The turbulence at 20 m is then influenced by structures far larger than 20 m: downdrafts that bring fast air from aloft, and horizontal inflow toward the base of the thermals. These structures scale with the boundary-layer depth z_i and the convective velocity scale w_* of Chapter 10, not with z and u_*. The mean gradients still follow the standard forms reasonably, because near the ground they are dominated by local production, but the horizontal velocity variances depend on z_i/L_O, a ratio that contains the length the theory excludes. The heat flux at a height can even be carried against the local gradient, in the upper part of the convective layer, by thermals that originate at the surface.

This nonlocality is why weather models use nonlocal boundary-layer parameterizations in convective conditions, in which the mixing at a height depends on the whole layer and not only on the local gradient; Chapter 26 describes them. The limit of free convection, in which the wind vanishes and u_* ceases to be a relevant scale, is treated in Chapter 15.

14.6.5 Why the theory remains the standard

Despite these limits, Monin–Obukhov similarity is the standard language of surface-layer meteorology. Its quantities, u_*, L_{O}, z/L_{O}, ϕ_m, ϕ_h, ψ_m and ψ_h, are the vocabulary in which measurements are reported, models are formulated and their disagreements are diagnosed. It connects what can be measured or modeled at the surface, the momentum and heat fluxes, to the mean wind and temperature profiles that engineering needs, with two universal functions and two roughness lengths. It is used in weather prediction for surface fluxes and diagnosed 10 m and 2 m values; in micrometeorology to process flux-tower data; in wind energy to extrapolate wind to hub height and to classify stability; in air-quality models to set the dispersion near the ground; and in land-surface models to couple soil, vegetation and atmosphere. Where it fails, the failure is itself informative: a departure from the universal functions identifies a site or a period in which nonlocal physics dominate. The next chapter turns from the theory to its numbers: what particular values of the Obukhov length and the stability parameter mean, how they arise from feedbacks between stability and turbulence, how the free-convection limit behaves, and how they diagnose model behavior (Chapter 15).

14.7 What to retain

Definition 14.1 (Monin–Obukhov similarity)**.** In the surface layer, the wind shear is the neutral shear multiplied by a universal function of the stability parameter, $\partial U/\partial z = [u_*/(\kappa z)]\,\phi_m(z/L_{\mathrm{O}})$, with $L_{\mathrm{O}} = -u_*^3\overline{\theta}/(\kappa g\,\overline{w'\theta'})$: $z/L_{\mathrm{O}} < 0$ is unstable with enhanced mixing ($\phi_m < 1$), $z/L_{\mathrm{O}} \approx 0$ is neutral ($\phi_m = 1$), and $z/L_{\mathrm{O}} > 0$ is stable with suppressed mixing ($\phi_m > 1$).

Table 14.6 lists the terms of the chapter, their meaning, their units and the subsection that defines each.

14.8 Exercises

Exercise 14.1. A flat grassland site has $\overline{\theta} = 303\,\mathrm{K}$ and $\rho = 1.15\,\mathrm{kg\,m^{-3}}$, with $c_p = 1004\,\mathrm{J\,kg^{-1}\,K^{-1}}$. (a) In the afternoon, $H = 250\,\mathrm{W\,m^{-2}}$ and $u_* = 0.35\,\mathrm{m\,s^{-1}}$. Compute $\overline{w'\theta'}$, θ_* and L_{O}, and the stability parameter, ϕ_m and the shear at 10 and 80 m. (b) At night, $H = -20\,\mathrm{W\,m^{-2}}$ and $u_* = 0.15\,\mathrm{m\,s^{-1}}$. Repeat (a), and say at which height the standard stable form leaves its fitted range. (c) For each case, compute the height at which buoyancy production equals the neutral shear production. (d) Compute Pr_t, K_m and K_h at 10 m in each case.

Exercise 14.2. (a) Starting from $\phi_h = (1 - 16\,z/L_{\mathrm{O}})^{-1/2}$, derive equation (14.24) step by step. (b) A different fit for stable air gives $\phi_m = \phi_h = 1 + 6\,z/L_{\mathrm{O}}$. Derive ψ_m, the relation between Ri_g and z/L_{O}, and the limit of Ri_g as $z/L_{\mathrm{O}} \to \infty$. (c) With the standard forms, a tower measures $\mathrm{Ri}_g = 0.12$ at 15 m. Compute z/L_{O} and L_{O}. (d) What do the standard forms imply for a layer with a measured $\mathrm{Ri}_g = 0.25$, and what does that say about the layer?

Exercise 14.3. A weather model has its lowest level at 25 m, where the wind is $7\,\mathrm{m\,s^{-1}}$, over a cell with $z_0 = 0.1$ m. (a) Diagnose U_{10} in neutral air with equation (14.28). (b) Repeat with $L_{\mathrm{O}} = +40$ m and with $L_{\mathrm{O}} = -40$ m. (c) On the stable night the true Obukhov length is 80 m. Compute the error of the model's 10 m wind in m/s and percent. (d) Compute the drag coefficient at 10 m in the three cases of (a) and (b), and the ratio of the stable to the unstable value.

Exercise 14.4. A mast at 20°S stands 3 km inland from an east-facing coast. The roughness length depends on the wind direction β: for winds from the land sector, $225° < \beta < 315°$, $z_0(\beta) = 0.05$ m; for onshore winds from the sea sector, $45° < \beta < 135°$, an effective $z_0(\beta) = 0.01$ m after the flow has adjusted to the coastal plain. On one afternoon the wind at 10 m is

Table 14.6: The terms of the chapter and where each is defined.

Term	Meaning	Units	Defined in
Similarity theory	description in which scaled, dimensionless quantities obey the same relations in every flow of a class	–	14.1.3, 14.1.4
Monin–Obukhov similarity theory (MOST)	the similarity theory of the surface layer: dimensionless gradients and statistics are functions of z/L_O alone	–	14.1.3
Obukhov length L_O	$-u_*^3\overline{\theta}/(\kappa g\,\overline{w'\theta'})$; $\lvert L_\mathrm{O}\rvert$ is the height at which buoyancy production equals neutral shear production; <0 unstable, >0 stable	m	14.2.1, 14.2.2
Stability parameter z/L_O	buoyant destruction over neutral shear production of turbulent kinetic energy at height z; ζ in the literature	–	14.2.1, 14.2.4
Dimensionless shear ϕ_m	$(\kappa z/u_*)\,\partial U/\partial z$; $1+5\,z/L_\mathrm{O}$ stable, $(1-16\,z/L_\mathrm{O})^{-1/4}$ unstable	–	14.3.1, 14.3.2
Dimensionless temperature gradient ϕ_h	$(\kappa z/\theta_*)\,\partial\overline{\theta}/\partial z$; $1+5\,z/L_\mathrm{O}$ stable, $(1-16\,z/L_\mathrm{O})^{-1/2}$ unstable	–	14.3.4
Stability correction ψ_m	$\int_0^{z/L_\mathrm{O}}(1-\phi_m)\,\mathrm{d}s/s$; correction to the integrated wind profile	–	14.4.1, 14.4.2
Stability correction ψ_h	the same for the potential-temperature profile	–	14.4.1
Temperature scale θ_*	$-\overline{w'\theta'}/u_*$; the surface heat flux as a temperature	K	14.3.4
Turbulent Prandtl number Pr_t	$K_m/K_h=\phi_h/\phi_m$; below one in unstable air	–	14.3.5
Local equilibrium	turbulence fully set by the local fluxes and height, without memory of other places, times or larger eddies	–	14.6.1

$6\,\mathrm{m\,s^{-1}}$ from 90°, with air arriving from the cooler ocean and $L_{\mathrm{O}} = +150\,\mathrm{m}$; on another it is $6\,\mathrm{m\,s^{-1}}$ from 270° over heated land, with $L_{\mathrm{O}} = -40\,\mathrm{m}$. (a) Compute u_* and the wind at 80 m for each afternoon. (b) Compute the ratio of the wind power densities at 80 m, proportional to U^3. (c) Compute the Coriolis parameter. Does the wind direction turn clockwise or counterclockwise, seen from above, between 10 and 80 m, and does Monin–Obukhov theory give that turning? (d) Which assumption of Section 14.6.1 is most doubtful for the onshore case, and what would a profile from the mast show if it is violated?

Chapter 15

The Obukhov Length and the Stability Parameter

15.1 Reading the Obukhov length

Chapter 13 described static stability through the lapse rate, the potential-temperature gradient and the Richardson numbers. Chapter 14 built Monin–Obukhov similarity theory on top of it: it defined the Obukhov length L_{O}, derived the dimensionless wind shear ϕ_m and temperature gradient ϕ_h as functions of the stability parameter z/L_{O}, integrated them into the stability corrections ψ_m and ψ_h, and showed how the coupled problem of fluxes and stability is solved by iteration. That chapter supplies the machinery. This chapter supplies the intuition for the numbers that the machinery produces. Its question is

what do values such as $L_{\mathrm{O}} = -50\,\mathrm{m}$ *or* $z/L_{\mathrm{O}} = 0.3$ *mean physically, and what do they imply for the wind at the heights where the wind is used?*

The chapter first reads the Obukhov length as a ratio of mechanical to buoyant turbulence, explains its sign and why it is a length, and tabulates it for typical friction velocities and heat fluxes. It then turns the length into the stability parameter at a stated height and gives rough bands for reading it, works out what the parameter does to the shear and to the wind at 10 and 50 m, and follows the feedbacks by which wind speed and heat flux set the stability. It ends with the convective limit, the boundary layer as a whole, and the use of the Obukhov length to diagnose wind forecasts.

Jargon: Obukhov length, stability parameter, weakly and strongly stable or unstable, free convection, convective velocity scale, mechanical mixing, buoyant suppression

The *Obukhov length* L_{O}, in meters, is the surface-layer length scale $-u_*^3\,\overline{\theta}/(\kappa\, g\,\overline{w'\theta'})$ built from the friction velocity and the surface kinematic heat flux; it compares the strength of shear-generated turbulence with the strength of buoyancy, is negative when the surface heats the air and positive when it cools it, and is calculated from eddy-covariance fluxes or inferred by a model from mean profiles. The *stability parameter* z/L_{O}, dimensionless, is the height of interest divided by the Obukhov length; it says how important buoyancy is at that height. Conditions are *weakly stable* or *weakly unstable* when $|z/L_{\mathrm{O}}| \ll 1$, in practice $|z/L_{\mathrm{O}}|$ below about 0.1, and *strongly stable* or *strongly unstable* when $|z/L_{\mathrm{O}}|$ is of order one or larger. *Free convection* is the limit in which buoyancy, not shear, produces nearly all the turbulence: a strong upward heat flux with a weak mean wind, $z/L_{\mathrm{O}} \ll -1$. The *convective velocity scale* w_*, in m/s, is the velocity scale of buoyancy-driven turbulence in the whole convective boundary layer, built from the surface heat flux and the boundary-layer depth z_i. *Mechanical mixing* is vertical mixing by turbulence that the shear of the mean wind produces. *Buoyant suppression* is the removal of turbulent kinetic energy by a stable stratification, in which eddies must work against gravity to move air vertically.

Key idea

The sign of the Obukhov length says which way buoyancy acts: $L_{\mathrm{O}} < 0$ is unstable and $L_{\mathrm{O}} > 0$ is stable. Its size says nothing on its own; the ratio z/L_{O} says how important that stability is at the height of interest. For the wind at 20 m, the question is what $20\,\mathrm{m}/L_{\mathrm{O}}$ is.

15.1.1 The definition and its parts

The Obukhov length is defined from surface-layer quantities as

$$L_{\mathrm{O}} = -\frac{u_*^3\,\overline{\theta}}{\kappa\, g\,\overline{w'\theta'}}, \tag{15.1}$$

where u_* is the friction velocity, $\overline{\theta}$ a reference potential temperature of the surface layer in kelvin, $\kappa \approx 0.4$ the von Kármán constant, g the gravitational acceleration and $\overline{w'\theta'}$ the kinematic heat flux at the surface, positive upward. Strictly, the virtual potential temperature θ_v and its flux enter, so that moisture, which makes air lighter, counts toward buoyancy; over dry land by day the difference is small, and over water or wet ground it is not. Chapter 14 gives the derivation; this chapter uses the definition.

The kinematic heat flux is the sensible heat flux H, in $\mathrm{W\,m^{-2}}$, divided by $\rho\, c_p$. Substituting $\overline{w'\theta'} = H/(\rho\, c_p)$,

$$L_{\mathrm{O}} = -\frac{\rho\, c_p\,\overline{\theta}\, u_*^3}{\kappa\, g\, H}. \tag{15.2}$$

With the illustrative values $\rho = 1.2\,\mathrm{kg\,m^{-3}}$, $c_p = 1004\,\mathrm{J\,kg^{-1}\,K^{-1}}$, $\overline{\theta} = 300\,\mathrm{K}$, $\kappa = 0.4$ and $g = 9.81\,\mathrm{m\,s^{-2}}$, the prefactor is $1.2 \times 1004 \times 300/(0.4 \times 9.81) = 361\,440/3.924 \approx 92\,110$, and

$$L_{\mathrm{O}} \approx -92\,110\,\frac{u_*^3}{H} \qquad (u_* \text{ in m/s},\ H \text{ in } \mathrm{W\,m^{-2}},\ L_{\mathrm{O}} \text{ in m}). \tag{15.3}$$

For $u_* = 0.4\,\mathrm{m\,s^{-1}}$ and $H = 100\,\mathrm{W\,m^{-2}}$: $u_*^3 = 0.064\,\mathrm{m^3\,s^{-3}}$ and $L_{\mathrm{O}} = -92\,110 \times 0.064/100 \approx -59\,\mathrm{m}$. Every Obukhov length in this chapter that is computed from a heat flux uses equation (15.3).

The stability parameter at height z is the ratio z/L_{O}, or $(z-d)/L_{\mathrm{O}}$ where a displacement height applies. Much of the literature writes it ζ; this book keeps ζ for the relative vorticity and writes the ratio out. The standard empirical (Businger–Dyer) forms of the dimensionless shear, derived and discussed in Chapter 14, are

$$\phi_m = 1 + 5\,\frac{z}{L_{\mathrm{O}}} \quad (L_{\mathrm{O}} > 0), \qquad \phi_m = \left(1 - 16\,\frac{z}{L_{\mathrm{O}}}\right)^{-1/4} \quad (L_{\mathrm{O}} < 0), \tag{15.4}$$

and the corresponding integrated corrections are $\psi_m = -5\,z/L_{\mathrm{O}}$ in stable air and, in unstable air,

$$\psi_m = 2\ln\frac{1+x}{2} + \ln\frac{1+x^2}{2} - 2\arctan x + \frac{\pi}{2}, \qquad x = \left(1 - 16\,\frac{z}{L_{\mathrm{O}}}\right)^{1/4}. \tag{15.5}$$

Every profile in this chapter is computed with these forms, so that its numbers agree with those of the neighboring chapters.

15.1.2 Mechanical against buoyant turbulence

Equation (15.1) is a ratio of two rates. The numerator u_*^3 measures mechanical turbulence: near the ground the shear production of turbulent kinetic energy in neutral air is $u_*^3/(\kappa z)$, so u_*^3 is that production rate times a length. The denominator contains $(g/\overline{\theta})\,\overline{w'\theta'}$, the buoyancy production of turbulent kinetic energy per unit mass, P_b in the notation of Chapter 8. Ignoring the sign and the constant κ,

$$|L_{\mathrm{O}}| \sim \frac{\text{strength of mechanical turbulence}}{\text{strength of buoyancy}} = \frac{u_*^3}{\kappa\,(g/\overline{\theta})\,|\overline{w'\theta'}|}.$$

The units confirm that the ratio is a length: u_*^3 is in $\mathrm{m^3\,s^{-3}}$; $(g/\overline{\theta})\,\overline{w'\theta'}$ is in $(\mathrm{m\,s^{-2}/K}) \times (\mathrm{K\,m\,s^{-1}}) = \mathrm{m^2\,s^{-3}}$; their ratio is in meters.

Stronger shear-driven turbulence, a larger u_*, makes $|L_{\mathrm{O}}|$ larger, and it does so with the cube: doubling u_* multiplies $|L_{\mathrm{O}}|$ by eight. A stronger heat flux in either direction makes $|L_{\mathrm{O}}|$ smaller in proportion: doubling $|\overline{w'\theta'}|$ halves $|L_{\mathrm{O}}|$. A large $|L_{\mathrm{O}}|$ therefore means that buoyancy is weak compared with mechanical mixing, and a small $|L_{\mathrm{O}}|$ that buoyancy is important, either as a source of turbulence (heating) or as buoyant suppression of it (cooling).

15.1.3 The sign

The minus sign in equation (15.1) makes the length negative when the heat flux is upward. Over a surface heated by the sun, $\overline{w'\theta'} > 0$ and $L_{\mathrm{O}} < 0$: the surface layer is unstable and buoyancy adds turbulence. Over a surface cooled by radiation at night, $\overline{w'\theta'} < 0$ and $L_{\mathrm{O}} > 0$: the surface layer is stable and buoyancy removes turbulence. As the heat flux goes to zero, $|L_{\mathrm{O}}| \to \infty$: the neutral case, in which buoyancy plays no part, sits at infinity. The sign convention is the same in both hemispheres; it depends on the direction of the heat flux, not on the rotation of the Earth.

Because neutral conditions sit at infinity, L_{O} itself jumps from $-\infty$ to $+\infty$ as the heat flux changes sign in the evening. Its reciprocal does not:

$$\frac{1}{L_{\mathrm{O}}} = -\,\frac{\kappa\, g\,\overline{w'\theta'}}{u_*^3\,\overline{\theta}} \tag{15.6}$$

is proportional to the heat flux, passes smoothly through zero at neutral, and is negative when unstable and positive when stable. Two consequences follow for working with data. Averaging Obukhov lengths across a transition is meaningless, since the mean of $-5000\,\mathrm{m}$ and $+5000\,\mathrm{m}$ is zero, the most extreme value possible, while both half-hours were nearly neutral; averaging $1/L_{\mathrm{O}}$ or z/L_{O} is sound. And a time series of stability is plotted as $1/L_{\mathrm{O}}$ or z/L_{O}, as Section 15.6.3 does.

15.1.4 Why a length

The Obukhov length is roughly the height at which buoyancy becomes as important as mechanical turbulence. The statement follows from the budget of turbulent kinetic energy. In the surface layer the shear production is

$$P_s = -\overline{u'w'}\,\frac{\partial U}{\partial z} = u_*^2\,\frac{\partial U}{\partial z} = \frac{u_*^3}{\kappa z}\,\phi_m,$$

and the buoyancy production is $P_b = (g/\overline{\theta})\,\overline{w'\theta'}$. The stress, and with it u_*, is constant with height in the surface layer, and so is the heat flux. The shear production therefore falls as $1/z$ while the buoyancy production does not change with height. Their ratio, with the neutral shear $\phi_m = 1$, is

$$\left.\frac{P_b}{P_s}\right|_{\phi_m=1} = \frac{(g/\overline{\theta})\,\overline{w'\theta'}\,\kappa z}{u_*^3} = -\,\frac{z}{L_{\mathrm{O}}}. \tag{15.7}$$

The magnitude of the ratio grows in proportion to height and equals one at $z = |L_{\mathrm{O}}|$. Below that height shear dominates the production or destruction of turbulence; above it buoyancy does. The length is not a hard boundary. The ratio passes through one smoothly, and nothing in the air changes at $z = |L_{\mathrm{O}}|$. With the actual shear ϕ_m instead of the neutral one, the ratio becomes the flux Richardson number of Chapter 8,

$$\mathrm{Ri}_f = -\,\frac{P_b}{P_s} = \frac{z/L_{\mathrm{O}}}{\phi_m(z/L_{\mathrm{O}})}, \tag{15.8}$$

positive in stable air, where buoyancy destroys turbulence, and negative in unstable air.

Figure 15.1 draws the ratio against height for an Obukhov length of magnitude 20 m. The horizontal axis is the magnitude of the ratio of buoyant to shear production, the vertical axis the height, both logarithmic. The dashed line is equation (15.7), $z/|L_{\mathrm{O}}|$, the same for both signs. The solid curves use the actual ϕ_m of equation (15.4): gold for $L_{\mathrm{O}} = -20$ m, blue for $L_{\mathrm{O}} = +20$ m. The vertical dotted line marks equal production, the horizontal dotted line the height $z = |L_{\mathrm{O}}|$. The dashed line crosses equal production exactly at 20 m. The unstable curve lies to the right of it, because $\phi_m < 1$ reduces the shear production: at 20 m the buoyant production is already about twice the shear production ($1 \times 17^{1/4} = 2.03$). The stable curve lies to the left and bends upward: since ϕ_m grows in proportion to z/L_{O}, the ratio Ri_f approaches $1/5$ and never exceeds it. With the linear stable form, buoyancy never destroys more than a fifth of the shear production, however stable the air; that property matters in Section 15.5.5.

15.1.5 The Obukhov length for typical fluxes

Equation (15.3) turns a pair of friction velocity and heat flux into a length. Table 15.1 evaluates it on a grid. Its rows are friction velocities from 0.1 to 0.8 m s^{-1}, a range from nearly calm to strong wind over land; its columns are sensible heat fluxes, negative (downward, night) on the left and positive (upward, day) on the right, from -100 to $+300$ W m^{-2}. Each entry is L_{O} in meters. The entries in bold are the combinations that give lengths close to the four values used throughout this chapter: about -20, -500, $+20$ and $+500$ m.

The table shows which weather produces which length. A length of about -20 m needs strong heating with a moderate wind ($u_* = 0.4$ m s^{-1} with 300 W m^{-2}, a clear summer midday) or modest heating with a light wind (0.2 m s^{-1} with 40 W m^{-2}). A length of about -500 m needs a strong wind with weak heating (0.6 m s^{-1} with 40 W m^{-2}, an overcast or windy day). On the stable side, $+20$ m comes from a light wind with a moderate downward flux (0.2 m s^{-1} with -40 W m^{-2}) or from a nearly calm night with a very small one (0.1 m s^{-1} with only -5 W m^{-2}); $+500$ m comes from a strong wind with a large downward flux (0.8 m s^{-1} with -100 W m^{-2}) or a

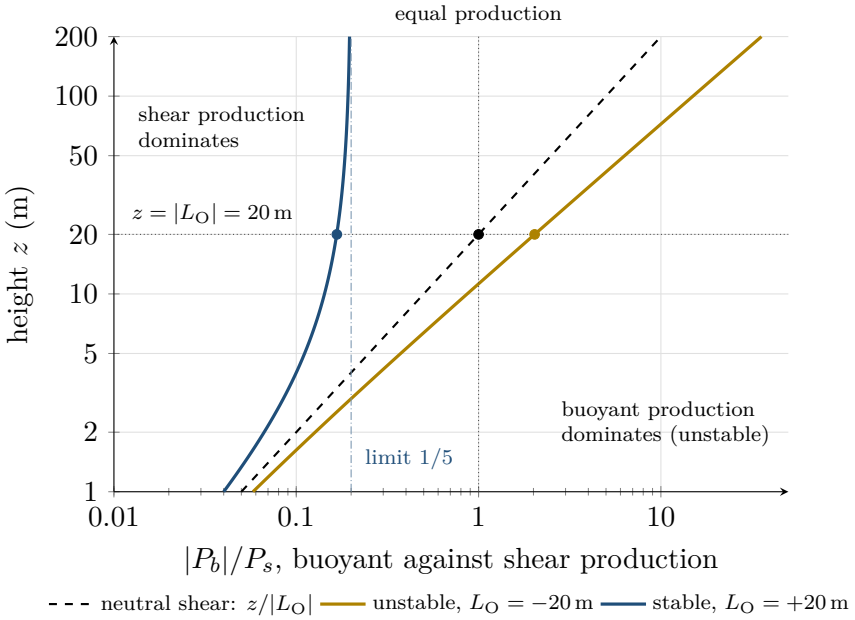


Figure 15.1: Magnitude of the ratio of buoyant to shear production of turbulent kinetic energy against height, for $|L_O| = 20\,\mathrm{m}$. Dashed: neutral shear, $z/|L_O|$ (equation (15.7)). Solid: $|z/L_O|/\phi_m$ with the Businger–Dyer ϕ_m of equation (15.4), for $L_O = -20\,\mathrm{m}$ and $+20\,\mathrm{m}$. The dash-dotted line is the stable limit 1/5. Values illustrative.

Table 15.1: Obukhov length L_O in meters from equation (15.3) for a grid of friction velocities and sensible heat fluxes ($\rho = 1.2\,\mathrm{kg\,m^{-3}}$, $c_p = 1004\,\mathrm{J\,kg^{-1}\,K^{-1}}$, $\overline{\theta} = 300\,\mathrm{K}$). Bold: entries near ± 20 and $\pm 500\,\mathrm{m}$. Values illustrative.

	stable: H ($\mathrm{W\,m^{-2}}$)				unstable: H ($\mathrm{W\,m^{-2}}$)		
u_* (m/s)	−100	−40	−10	−5	+40	+100	+300
0.1	0.9	2.3	9.2	**18**	−2.3	−0.9	−0.3
0.2	7.4	**18**	74	147	**−18**	−7.4	−2.5
0.3	25	62	249	**497**	−62	−25	−8.3
0.4	59	147	590	1179	−147	−59	**−20**
0.6	199	**497**	1990	3979	**−497**	−199	−66
0.8	**472**	1179	4716	9432	−1179	**−472**	−157

moderate wind with a very small one. The table is antisymmetric: reversing the sign of the flux reverses the sign of the length and keeps its magnitude, as the columns for $\pm 40\,\mathrm{W\,m^{-2}}$ show.

The wind enters through its cube, and it dominates: along any column the length changes by a factor of $8^3 = 512$ from the first row to the last, whereas across the realistic range of nighttime fluxes, about -5 to $-60\,\mathrm{W\,m^{-2}}$, it changes by about a factor of twelve. Not every cell is equally likely. Daytime fluxes over land reach 300 to $500\,\mathrm{W\,m^{-2}}$ under a clear sky; nighttime fluxes rarely exceed about $-60\,\mathrm{W\,m^{-2}}$. The upper-left corner of the table, a large downward flux with weak turbulence, is seldom observed, because weak turbulence cannot carry a large downward flux; Section 15.4.3 gives the limit.

15.2 The stability parameter at a height

An Obukhov length describes the surface layer as a whole; the stability parameter describes it at one height. This section evaluates four lengths at four heights, explains why the ratio and not the length is the useful number, gives rough bands and a mental scale for reading it, summarizes the readings for a sensor at 20 m, and states what the Obukhov length is not.

15.2.1 Four Obukhov lengths at four heights

Table 15.2 evaluates z/L_O for the four lengths -500, -20, $+500$ and $+20$ m at the heights 10, 20, 50 and 100 m, which span the wind measurements at weather stations, the heights of transmission conductors and the hubs of wind turbines. Each cell gives z/L_O and, below it, the dimensionless shear ϕ_m from equation (15.4): the factor by which the shear differs from its neutral value at the same friction velocity. Values in parentheses lie beyond $z/L_\mathrm{O} = 1$, where the linear stable form is used outside its range (Section 15.3.4).

Table 15.2: Stability parameter z/L_O (upper line) and dimensionless shear ϕ_m (lower line, equation (15.4)) for four Obukhov lengths at four heights. Parentheses: stable form beyond $z/L_\mathrm{O} = 1$. Values illustrative.

Obukhov length	$z = 10$ m	$z = 20$ m	$z = 50$ m	$z = 100$ m
$L_\mathrm{O} = -500$ m	-0.02	-0.04	-0.1	-0.2
	0.93	0.88	0.79	0.70
$L_\mathrm{O} = -20$ m	-0.5	-1	-2.5	-5
	0.58	0.49	0.40	0.33
$L_\mathrm{O} = +500$ m	0.02	0.04	0.1	0.2
	1.1	1.2	1.5	2.0
$L_\mathrm{O} = +20$ m	0.5	1	2.5	5
	3.5	6.0	(13.5)	(26)

$L_\mathrm{O} = -500$ m. At 10 m, $z/L_\mathrm{O} = -0.02$: weakly unstable, with mechanical turbulence dominating and a shear only 7 % below neutral. At 100 m, $z/L_\mathrm{O} = -0.2$: buoyancy is now noticeable and the shear is 30 % below neutral. The same mildly convective afternoon is near-neutral at a weather station and moderately unstable at a turbine hub.

$L_\mathrm{O} = -20$ m. At 10 m, $z/L_\mathrm{O} = -0.5$: substantially unstable, the shear 42 % below neutral. At 20 m, $z/L_\mathrm{O} = -1$: buoyancy and mechanical turbulence are of comparable importance in the scaling sense of equation (15.7). At 50 m, $z/L_\mathrm{O} = -2.5$: strongly unstable, with buoyancy the main source of turbulence.

$L_O = +500$ m. At 10 m, $z/L_O = 0.02$: the effect of stability is weak, a shear 10 % above neutral. At 100 m, $z/L_O = 0.2$: the shear is twice the neutral value and buoyant suppression matters. The air is stable, but weakly so at low heights.

$L_O = +20$ m. At 10 m, $z/L_O = 0.5$: by the bands of Section 15.2.3 this is in the moderate range, toward its upper end, and its effect on the profile is already strong, a shear three and a half times neutral. At 20 m, $z/L_O = 1$: buoyant suppression is very important, the shear is six times neutral, and the turbulence may be weak or intermittent. At 50 and 100 m the linear form gives shears of 13.5 and 26 times neutral, numbers that should not be trusted (Section 15.3.4).

15.2.2 The ratio, not the length

The same Obukhov length means different things at different heights, which is why the stability parameter is the more useful number. Take $L_O = 100$ m. At 2 m, $z/L_O = 0.02$ and $\phi_m = 1.1$: nearly neutral. At 80 m, $z/L_O = 0.8$ and $\phi_m = 5.0$: strongly affected by stability. The atmosphere is the same; only the height differs. The reason is the one behind Figure 15.1: the shear production of turbulence falls as $1/z$ while the buoyancy term is the same at every height of the surface layer, so the farther from the ground, the larger the share of buoyancy.

For an engineering question the height is fixed by the application: a weather station at 10 m, a transmission conductor at 15 to 30 m, a turbine hub at 80 to 150 m. The relevant question is therefore not *what is L_O?* but *what is z/L_O at the height of interest?* A single Obukhov length reported for a site carries a different stability at each of these heights, and a statement such as "the night was slightly stable" is incomplete until the height is named.

15.2.3 Rough bands

Table 15.3 gives rough bands for reading z/L_O. Its rows are three degrees of stability, weak, moderate and strong; its columns give the range of z/L_O on the unstable side, the range on the stable side, and what the band means for turbulence and the wind profile. The bands are conceptual guides, not thresholds: nothing physical happens at $z/L_O = 0.1$ or 1, and other authors draw the lines elsewhere. Their logic is that each band is a decade in $|z/L_O|$.

Table 15.3: Rough bands of the stability parameter. Conceptual guides, not thresholds.

Band	Unstable	Stable	Meaning
Weak	$-0.1 < z/L_O < 0$	$0 < z/L_O < 0.1$	mechanical turbulence dominates; shear between about 0.8 and 1.5 times neutral ($\phi_m = 0.79$ and 1.5 at the band edges)
Moderate	$-1 < z/L_O < -0.1$	$0.1 < z/L_O < 1$	buoyancy clearly modifies the turbulence; shear from about half to six times neutral
Strong	$z/L_O < -1$	$z/L_O > 1$	buoyancy dominates: convective turbulence on the unstable side, weak or intermittent turbulence on the stable side; simple forms questionable on the stable side

Figure 15.2 draws the bands on a number line. The six colored segments, gold for unstable and blue for stable, darker for stronger, are drawn with equal widths, so the line is not to scale: each segment spans a decade of $|z/L_O|$ except the two weak bands, which run to zero. The ticks mark the boundaries -1, -0.1, 0, 0.1 and 1. The dots below the line are the six readings of a sensor at 20 m from Section 15.2.4, labeled by their Obukhov length. The figure shows the symmetry of the scheme: the sign of z/L_O picks the side, convection to the left and suppression to the right; the magnitude picks the band.

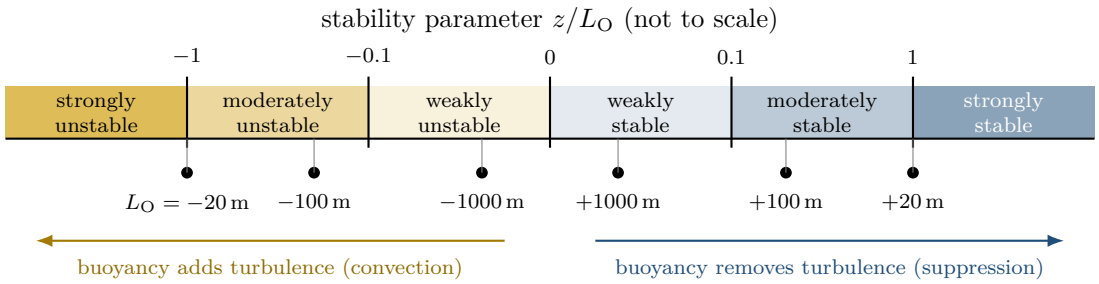


Figure 15.2: Rough bands of the stability parameter z/L_O on a number line whose segments are drawn with equal widths (not to scale). Dots: a sensor at $z = 20$ m under the six Obukhov lengths of Table 15.4. Bands are conceptual guides, not thresholds.

The boundary at one. A sensor at 20 m with $L_O = -20$ m reads $z/L_O = -1$, exactly on the boundary between the moderate and the strong band. Since the bands are guides, it is read as strongly unstable, the regime in which buoyant and shear production of turbulence are of the same order, and the same holds for $z/L_O = +1$ on the stable side.

15.2.4 A mental scale and a sensor at 20 meters

The bands condense into a mental scale that compares $|L_O|$ with the observation height z:

- $|L_O| \gg z$: approximately neutral; shear-generated turbulence controls the profile;
- $|L_O| \sim z$: stability matters strongly;
- $|L_O| \ll z$: buoyancy dominates, as the main source of turbulence when unstable and as its main sink when stable;

and the sign says which: convection for $L_O < 0$, suppression for $L_O > 0$. A ten-meter mast and a sixty-meter Obukhov length are a factor of six apart, inside the moderate band; a hub at 120 m under the same length is two lengths up, in the strong band.

Table 15.4 applies the scale to a sensor at $z = 20$ m. Its columns give six Obukhov lengths, the stability parameter, the dimensionless shear from equation (15.4), and the reading. The six rows are symmetric in pairs; the shear is not. The same $|z/L_O|$ changes the shear far more on the stable side than on the unstable side: at $|z/L_O| = 1$ the shear is about half of neutral when unstable and six times neutral when stable. Stable stratification acts on the wind profile more strongly than convection does at the same $|z/L_O|$, which is why nighttime extrapolation is the harder problem.

Table 15.4: Readings of a sensor at $z = 20$ m for six Obukhov lengths. ϕ_m from equation (15.4). Values illustrative.

L_O (m)	z/L_O at 20 m	ϕ_m	Reading
−1000	−0.02	0.93	nearly neutral, slightly unstable
−100	−0.2	0.70	moderately unstable
−20	−1	0.49	strongly unstable
+1000	+0.02	1.1	nearly neutral, slightly stable
+100	+0.2	2.0	moderately stable
+20	+1	6.0	strongly stable; turbulence may be weak or intermittent

15.2.5 What the Obukhov length is not

Two misreadings are common. The first treats the length as a boundary in the air. A length $L_O = -20\,\mathrm{m}$ does not mean that the air is unstable below 20 m and neutral above. It means that at heights comparable to 20 m buoyancy and mechanical turbulence are of comparable importance. The effect of stability varies continuously with height through z/L_O, and it is present, smaller, below 20 m and larger above; Figure 15.1 shows the continuous variation.

The second confuses the Obukhov length with the other lengths of the boundary layer. It is not the boundary-layer depth z_i, the height to which surface-driven turbulence reaches; not the inversion height, the base of the layer in which temperature increases with height; not the mixing height, the depth through which pollutants and heat released at the ground are mixed; and not the roughness length z_0, a property of the surface. It is a surface-layer stability scale. The numbers make the distinction plain. On a convective afternoon with a light wind the Obukhov length may be $-10\,\mathrm{m}$ while the boundary layer is 1500 m deep (Section 15.5.3), and over farmland the roughness length is about 0.05 m.

A stable example in the Southern Hemisphere. On a stable night the boundary-layer depth and the Obukhov length are related but still different. A widely used estimate of the depth of a stationary stable boundary layer is $z_i \approx 0.4\,\sqrt{u_*\,L_O/|f|}$, which combines the surface-layer length with the Coriolis parameter. Near São Paulo, at 23°S, $f = 2 \times 7.292 \times 10^{-5} \times \sin(-23^\circ) = -5.70 \times 10^{-5}\,\mathrm{s^{-1}}$, negative as in every Southern Hemisphere case, and the estimate uses its magnitude. With the illustrative night values $u_* = 0.25\,\mathrm{m\,s^{-1}}$ and $L_O = 50\,\mathrm{m}$,

$$z_i \approx 0.4\sqrt{\frac{0.25 \times 50}{5.70 \times 10^{-5}}} = 0.4\sqrt{2.19 \times 10^5} = 0.4 \times 468 \approx 187\,\mathrm{m},$$

almost four times the Obukhov length. The same night at 23°N gives the same depth, since only $|f|$ enters. What differs between the hemispheres is the turning of the wind through the layer: the wind turns toward the direction of the geostrophic wind with height, clockwise (veering) in the Northern Hemisphere and counterclockwise (backing) in the Southern, and in a shallow stable layer the turning from the surface to the top is commonly several tens of degrees.

15.3 What the stability parameter does to the wind profile

The stability parameter matters for wind because it sets the shear. This section recalls the relation, works the shear at 20 m for one friction velocity in three states, recomputes the wind at 10 and 50 m for three states with the standard functions, and states how far the stable form can be trusted.

15.3.1 Flatter and steeper profiles

In the surface layer, Chapter 14 gives the shear as

$$\frac{\partial U}{\partial z} = \frac{u_*}{\kappa z}\,\phi_m(z/L_O)\,, \tag{15.9}$$

and its integral as

$$U(z) = \frac{u_*}{\kappa}\left[\ln\frac{z}{z_0} - \psi_m(z/L_O)\right], \tag{15.10}$$

with z replaced by $z - d$ over tall vegetation or buildings, and the small term $\psi_m(z_0/L_O)$ neglected. When $z/L_O < 0$, $\phi_m < 1$: convective eddies mix momentum vertically more efficiently than shear alone would, less shear is needed to carry the same stress, and the profile is flatter than neutral. When $z/L_O > 0$, $\phi_m > 1$: buoyant suppression weakens the eddies, more

shear is needed to carry the same stress, and the profile is steeper. Because z/L_{O} grows with height, the departure from the neutral profile grows with height too.

15.3.2 Same friction velocity, different stability

Take $u_* = 0.4\,\mathrm{m\,s^{-1}}$ and $z = 20\,\mathrm{m}$. In neutral air,

$$\frac{\partial U}{\partial z} = \frac{0.4}{0.4 \times 20} = 0.05\,\mathrm{s^{-1}}.$$

In stable air with $z/L_{\mathrm{O}} = 0.2$ ($L_{\mathrm{O}} = 100\,\mathrm{m}$), $\phi_m = 1 + 5 \times 0.2 = 2$ and the shear doubles to $0.10\,\mathrm{s^{-1}}$. In unstable air with $z/L_{\mathrm{O}} = -0.4$ ($L_{\mathrm{O}} = -50\,\mathrm{m}$), $1 - 16 \times (-0.4) = 7.4$, $\phi_m = 7.4^{-1/4} = 0.606$, and the shear is $0.05 \times 0.606 = 0.030\,\mathrm{s^{-1}}$. Over a 10 m layer centered at 20 m, the three states give wind differences of about 0.3, 0.5 and $1.0\,\mathrm{m\,s^{-1}}$ for the same surface stress. A conductor span that rises 10 m across a slope sees these differences along its length, and a wind-turbine rotor 100 m across sees much larger ones.

15.3.3 The wind at 10 and 50 meters

The integrated profile turns the stability into wind at a height. Suppose a 10 m wind of $5\,\mathrm{m\,s^{-1}}$ over farmland with the illustrative roughness length $z_0 = 0.05\,\mathrm{m}$, and three states: weakly unstable, $z/L_{\mathrm{O}} \approx -0.05$; strongly unstable, $z/L_{\mathrm{O}} \approx -1$; strongly stable, $z/L_{\mathrm{O}} \approx +1$. Rough estimates often given for the 50 m wind in these states are about 6.5, 5.8 and $9\,\mathrm{m\,s^{-1}}$, with the remark that the exact numbers depend on the similarity functions while the qualitative behavior is robust. The standard functions test that remark. For each state, equation (15.10) at 10 m gives the friction velocity that produces $5\,\mathrm{m\,s^{-1}}$, and the same equation at 50 m then gives the wind there:

$$U(50\,\mathrm{m}) = 5\,\mathrm{m\,s^{-1}} \times \frac{\ln(50/z_0) - \psi_m(50\,\mathrm{m}/L_{\mathrm{O}})}{\ln(10/z_0) - \psi_m(10\,\mathrm{m}/L_{\mathrm{O}})}.$$

In neutral air the ratio is $\ln 1000/\ln 200 = 6.908/5.298 = 1.304$ and $U(50\,\mathrm{m}) = 6.52\,\mathrm{m\,s^{-1}}$.

A statement such as "$z/L_{\mathrm{O}} \approx -1$" does not say at which height the parameter is meant. Table 15.5 therefore computes each state twice: with the stated z/L_{O} at 10 m, and with it at 50 m, which gives an Obukhov length five times longer. Its columns are the state, the stated parameter, then for each reading the Obukhov length and the resulting $U(50\,\mathrm{m})$, and finally the rough estimate. For the strongly stable state with $z/L_{\mathrm{O}} = 1$ at 10 m the arithmetic is

$$L_{\mathrm{O}} = 10\,\mathrm{m}: \quad \frac{\ln 1000 + 5 \times 5}{\ln 200 + 5 \times 1} = \frac{6.908 + 25}{5.298 + 5} = \frac{31.91}{10.30} = 3.10, \qquad U(50\,\mathrm{m}) = 15.5\,\mathrm{m\,s^{-1}},$$

and with $z/L_{\mathrm{O}} = 1$ at 50 m, $L_{\mathrm{O}} = 50\,\mathrm{m}$: $(6.908 + 5)/(5.298 + 1) = 11.91/6.30 = 1.89$ and $U(50\,\mathrm{m}) = 9.45\,\mathrm{m\,s^{-1}}$.

Figure 15.3 draws the profiles. The horizontal axis is the wind speed in m/s; the vertical axis is the height from 2 to 60 m on a logarithmic scale, on which the neutral profile is a straight line. All curves pass through $5\,\mathrm{m\,s^{-1}}$ at 10 m (the black point). The dashed black line is neutral; the solid gold curve ($L_{\mathrm{O}} = -200\,\mathrm{m}$) and the dash-dotted dark gold curve ($L_{\mathrm{O}} = -10\,\mathrm{m}$) are the unstable states with z/L_{O} read at 10 m; the solid red curve is the stable state with $z/L_{\mathrm{O}} = 1$ at 50 m and the dotted red curve the stable state with $z/L_{\mathrm{O}} = 1$ at 10 m. The open circles at 50 m are the rough estimates. Above 10 m the unstable curves lie to the left of the neutral line and the stable curves to the right; below 10 m the order reverses, since each curve is pinned at 10 m.

The comparison is mixed and should be stated plainly. On the unstable side the rough estimates hold up under either reading: the strongly unstable $5.8\,\mathrm{m\,s^{-1}}$ matches the $L_{\mathrm{O}} = -10\,\mathrm{m}$ case almost exactly, and the weakly unstable $6.5\,\mathrm{m\,s^{-1}}$ is essentially the neutral value $6.52\,\mathrm{m\,s^{-1}}$,

Table 15.5: Wind at 50 m implied by $U_{10} = 5\,\mathrm{m\,s^{-1}}$ over $z_0 = 0.05\,\mathrm{m}$, from equation (15.10) with the Businger–Dyer corrections, for three states, each with the stated z/L_O read at 10 m and at 50 m. Last column: rough estimates for comparison. Data: `scripts/ch15_data.py`. Values illustrative.

		z/L_O at 10 m		z/L_O at 50 m		
State	z/L_O	L_O (m)	$U(50\,\mathrm{m})$	L_O (m)	$U(50\,\mathrm{m})$	Estimate
Neutral	0	∞	6.52	∞	6.52	–
Weakly unstable	−0.05	−200	6.21	−1000	6.41	6.5
Strongly unstable	−1	−10	5.79	−50	5.99	5.8
Strongly stable	+1	+10	15.5	+50	9.45	9

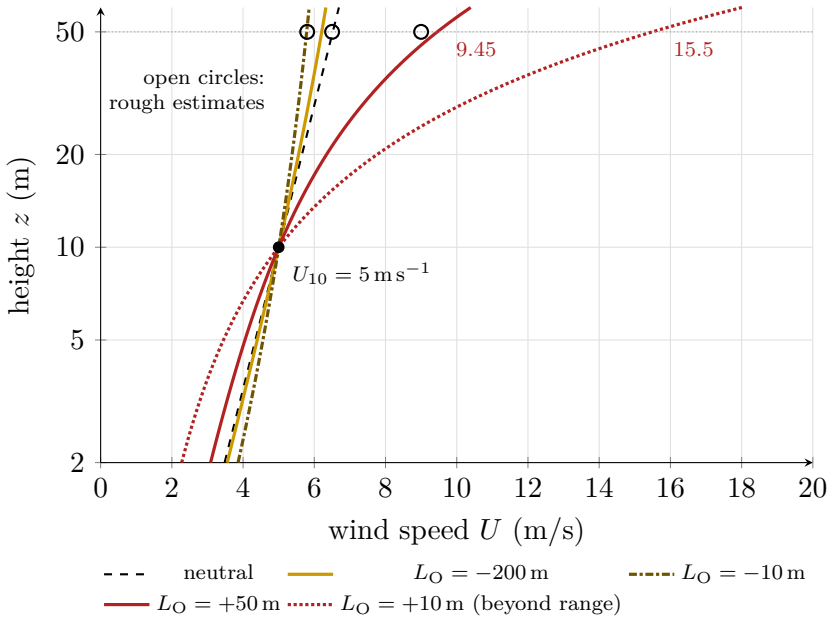


Figure 15.3: Wind profiles with the same $U_{10} = 5\,\mathrm{m\,s^{-1}}$ over $z_0 = 0.05\,\mathrm{m}$, on a logarithmic height axis, from $U = (u_*/\kappa)[\ln(z/z_0) - \psi_m(z/L_O)]$ (equation (15.10)) with $\kappa = 0.4$ and the Businger–Dyer ψ_m of equation (15.5); u_* is set in each case so that the 10 m wind is $5\,\mathrm{m\,s^{-1}}$. Open circles: rough estimates of 6.5, 5.8 and $9\,\mathrm{m\,s^{-1}}$ at 50 m. Dotted red: the linear stable form used at z/L_O up to 6, far beyond its range. Data: `scripts/ch15_data.py`. Values illustrative.

while the standard functions place the weakly unstable wind slightly below it, at 6.2 to 6.4 m s^{-1}. On the stable side the estimate of 9 m s^{-1} matches the reading with $z/L_O = 1$ at 50 m, which gives 9.45 m s^{-1}, but not the reading with $z/L_O = 1$ at 10 m, which gives 15.5 m s^{-1}, a tripling of the wind over 40 m. The qualitative behavior is robust: weakly unstable air sits just below neutral, strongly unstable air well below, stable air well above. The stable number is not robust, and the next subsection says why.

The friction velocities that the five profiles need are themselves informative: 0.377 m s^{-1} for neutral air, 0.390 and 0.478 m s^{-1} for the two unstable states, and 0.318 and 0.194 m s^{-1} for the two stable ones. The same 10 m wind goes with a stress that differs by a factor of $(0.478/0.194)^2 \approx 6$ between the strongly unstable and the strongly stable state. The power-law exponent between 10 and 50 m, $\ln(U_{50}/U_{10})/\ln 5$, is 0.165 in neutral air, 0.09 in the strongly unstable state and 0.40 in the stable state with $L_O = +50$ m: the exponent is in large part a proxy for stability, as Chapter 12 discusses.

15.3.4 The stable form at stability parameters of order one

The linear stable form $\phi_m = 1 + 5\,z/L_O$ was fitted to observations mostly with z/L_O below about 0.5 to 1. Within that range it works well. Beyond it, two things go wrong. First, the formula keeps increasing the shear without limit: at $z/L_O = 5$, at 50 m under $L_O = 10$ m, it gives $\phi_m = 26$, a shear twenty-six times neutral. Observations at such stabilities show smaller shears, and forms that grow more slowly than linearly beyond $z/L_O \approx 1$ are used in many weather models for that reason. Second, for $z/L_O \gg 1$ the linear form becomes $\phi_m \approx 5\,z/L_O$, so that

$$\frac{\partial U}{\partial z} \approx \frac{u_*}{\kappa z}\,\frac{5z}{L_O} = \frac{5\,u_*}{\kappa\,L_O},$$

independent of height: the eddies are limited in size by the stratification, through L_O, rather than by the distance to the ground. This "z-less" regime is plausible in the abstract, but in practice the air at such stabilities is governed by processes outside the theory, which Section 15.5.5 lists.

The 15.5 m s^{-1} of Table 15.5 is therefore an artifact of using a formula beyond its range, and even the 9.45 m s^{-1} is indicative rather than reliable, since at 50 m under $L_O = 50$ m the parameter is $z/L_O = 1$, the edge of the range, and at night 50 m may lie near the top of a shallow surface layer. The working rule is to treat stable profiles beyond $z/L_O \approx 1$ as shapes, not as numbers.

> **Principle 15.1.** *At the same magnitude of the stability parameter, stable stratification changes the wind profile far more than convection does. Stable corrections are reliable up to z/L_O of order one; beyond it they give the direction of the effect, not its size.*

15.4 Wind speed, heat flux and the feedbacks of stability

The Obukhov length combines the wind, through u_*, with the heat flux. This section shows how strongly the wind controls the result, why the turbulent heat flux and not a temperature difference enters, and how stability feeds back on itself, in opposite directions by night and by day.

15.4.1 Strong wind drives conditions toward neutral

Since $|L_O|$ grows with u_*^3, the wind dominates the stability. Hold the heat flux at an illustrative nighttime $H = -30$ W m^{-2} and vary the friction velocity. From equation (15.3),

$$u_* = 0.1,\ 0.2,\ 0.4,\ 0.6,\ 0.8\,\text{m s}^{-1}: \qquad L_O = 3.1,\ 24.6,\ 196,\ 663,\ 1572\,\text{m},$$

and the stability parameter at 10 m is 3.3, 0.41, 0.051, 0.015 and 0.006. Each doubling of the friction velocity multiplies the length by eight and divides z/L_O by eight. A night with a strong wind, u_* above about $0.4\,\mathrm{m\,s^{-1}}$, is near-neutral at 10 m even under the same surface cooling that makes a calm night strongly stable: mechanical turbulence overwhelms the buoyant suppression. The same holds by day: a sunny but windy afternoon has a long negative Obukhov length and a nearly neutral surface layer.

Figure 15.4 draws the relation. Both axes are logarithmic: the horizontal axis is the friction velocity from 0.05 to $1\,\mathrm{m\,s^{-1}}$, the vertical axis the Obukhov length from 1 to 10 000 m. The three lines are equation (15.3) for downward heat fluxes of 10, 30 and $100\,\mathrm{W\,m^{-2}}$; the points are the five values above. The horizontal dotted lines at 10 and 100 m separate the bands of stability at a height of 10 m, labeled at the right. On logarithmic axes each line is straight with slope three, and the three lines are parallel, offset by the ratio of the fluxes: tripling the flux moves a line down by a factor of three, while tripling the friction velocity moves a point up by a factor of twenty-seven.

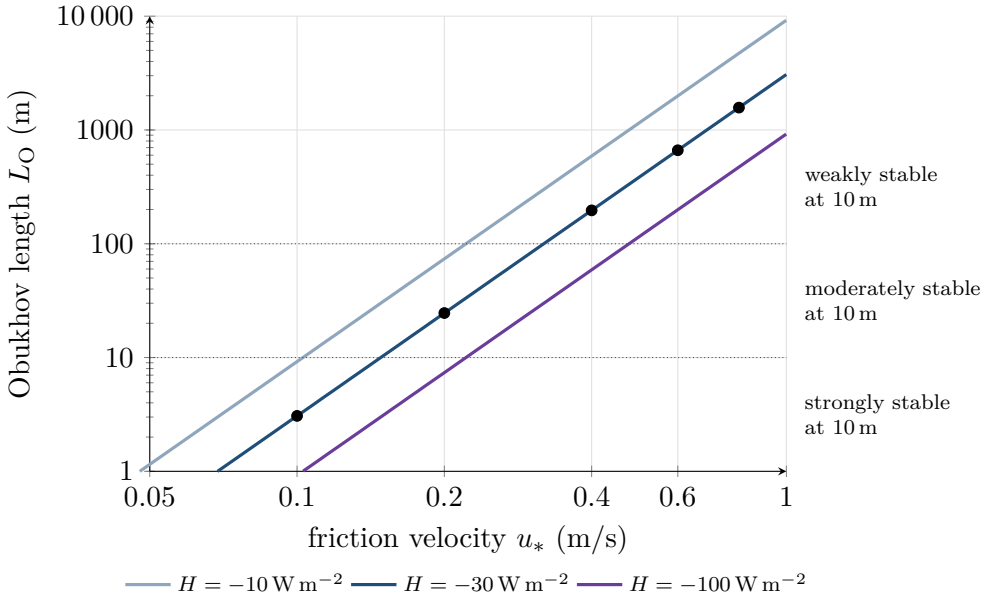


Figure 15.4: Obukhov length against friction velocity for three downward heat fluxes, $L_O = 92\,110\,u_*^3/|H|$ (equation (15.3)). Points: $H = -30\,\mathrm{W\,m^{-2}}$ with $u_* = 0.1$ to $0.8\,\mathrm{m\,s^{-1}}$. Dotted lines: $L_O = 10\,\mathrm{m}$ and 100 m, where z/L_O at 10 m equals 1 and 0.1. Values illustrative.

15.4.2 Weak wind and the two-night pattern

The converse follows from the same cube. When the wind is weak, u_* is small and u_*^3 very small, so the Obukhov length is short and a modest surface cooling is enough for strongly stable conditions. Calm, clear nights develop strong surface inversions for this reason: the sky lets the ground radiate, and nothing mechanical opposes the stratification that results.

The forecasting consequence is a pattern of two nights with similar radiative cooling of the surface. On night A a strong synoptic pressure gradient keeps the wind up; on night B the wind is weak. With the same illustrative downward flux $H = -20\,\mathrm{W\,m^{-2}}$ on both nights, night A with $u_* = 0.5\,\mathrm{m\,s^{-1}}$ has

$$L_O = 92\,110 \times \frac{0.125}{20} = 576\,\mathrm{m}, \qquad z/L_O = 0.017 \text{ at } 10\,\mathrm{m},$$

near-neutral or weakly stable, while night B with $u_* = 0.1\,\mathrm{m\,s^{-1}}$ has

$$L_\mathrm{O} = 92\,110 \times \frac{0.001}{20} = 4.6\,\mathrm{m}, \qquad z/L_\mathrm{O} = 2.2 \text{ at } 10\,\mathrm{m},$$

strongly stable, with mechanical mixing collapsed. The surface cooling is the same and the stability differs by a factor of 125 in the length. On night B the turbulent flux would in fact be smaller than on night A, since weak turbulence carries less heat, the surface would cool further, and the stratification would be stronger still. The surface temperature, or the surface cooling, does not determine the stability on its own; the wind does as much.

15.4.3 Heat flux, not temperature difference

The Obukhov length uses the turbulent heat flux $\overline{w'\theta'}$, not the temperature difference between the surface and the air. What matters for the turbulence is the heat that eddies actually move, since that is what buoyancy produces or destroys turbulent kinetic energy with. A temperature difference is a gradient; the flux is the gradient times an eddy diffusivity, $\overline{w'\theta'} = -K_h\,\partial\overline{\theta}/\partial z$, and the diffusivity is itself a property of the turbulence. With weak turbulence a large gradient goes with a small flux.

Two illustrative nights over the same field show the size of the effect, with a potential-temperature difference measured between 2 and 10 m. On a windy night the difference is 0.5 K and the flux $-40\,\mathrm{W\,m^{-2}}$, that is $\overline{w'\theta'} = -40/(1.2 \times 1004) = -0.0332\,\mathrm{K\,m\,s^{-1}}$; on a calm night the difference is 4 K and the flux $-8\,\mathrm{W\,m^{-2}}$, $\overline{w'\theta'} = -0.0066\,\mathrm{K\,m\,s^{-1}}$. The eddy diffusivities are

$$K_h = \frac{0.0332}{0.5/8} = 0.53\,\mathrm{m^2\,s^{-1}} \qquad \text{and} \qquad K_h = \frac{0.0066}{4/8} = 0.013\,\mathrm{m^2\,s^{-1}},$$

forty times apart. The calm night has the eight times larger gradient and the five times smaller flux. A stability measure built on the gradient alone would rank the calm night as more strongly forced; the flux shows how little heat the turbulence is actually moving, which is the information the Obukhov length needs. This matters most in very stable conditions, where the gradients are largest and the fluxes smallest and hardest to measure.

A maximum downward heat flux. The weakness of the flux in calm air has a sharper consequence. Hold the wind at 10 m fixed, as an idealization, and ask how large a downward heat flux the turbulence can carry. With the stable profile, $u_* = \kappa U/(a + 5x)$, where $a = \ln(z/z_0)$ and $x = z/L_\mathrm{O}$. Substituting into equation (15.1) solved for the flux,

$$\overline{w'\theta'} = -\frac{u_*^3\,\overline{\theta}}{\kappa\, g\, L_\mathrm{O}} = -\frac{\overline{\theta}\,\kappa^2\,U^3}{g\,z}\,\frac{x}{(a+5x)^3}.$$

As the stability x grows from zero, the factor $x/(a + 5x)^3$ first rises, because a stronger stratification drives more heat, and then falls, because it suppresses the turbulence that carries the heat. Its derivative vanishes where $a + 5x = 15x$, at $x = a/10$, and its maximum is $1/(33.75\,a^2)$. For $z = 10\,\mathrm{m}$ and $z_0 = 0.05\,\mathrm{m}$, $a = 5.30$, the maximum occurs at $z/L_\mathrm{O} = 0.53$, and with $\overline{\theta} = 300\,\mathrm{K}$ and $U = 3\,\mathrm{m\,s^{-1}}$,

$$|\overline{w'\theta'}|_\mathrm{max} = \frac{300 \times 0.16 \times 27}{9.81 \times 10} \times \frac{1}{33.75 \times 28.07} = \frac{13.2}{947} = 0.0139\,\mathrm{K\,m\,s^{-1}},$$

or $|H|_\mathrm{max} \approx 17\,\mathrm{W\,m^{-2}}$. At $U = 6\,\mathrm{m\,s^{-1}}$ the maximum is eight times larger, about $134\,\mathrm{W\,m^{-2}}$. A clear sky can draw more heat from the ground than $17\,\mathrm{W\,m^{-2}}$ even after the heat conducted up from the soil is counted. When it does, the turbulence cannot supply the difference, the surface cools faster, the stratification strengthens, the flux falls further, and the turbulence collapses. The existence of this maximum, which depends on the wind through its cube, is the reason weak-wind clear nights decouple while windy ones do not, and why the upper-left corner of Table 15.1 is seldom observed.

15.4.4 The stable feedback

The calm-night collapse is one outcome of a feedback. Figure 15.5 draws it. Each box is a state of the surface layer and each arrow a causal link; the external driver, surface cooling by longwave radiation, enters from the top, and the way out of the loop, turbulence generated by shear or by a disturbance, enters from the bottom. Following the loop: a stable stratification weakens the turbulence; weaker turbulence mixes less heat vertically; with less heat brought down from above, the air near the surface cools further; and colder air near the surface means a stronger stratification. Every link strengthens the next, so the loop is self-reinforcing, a positive feedback. It runs until something outside it generates turbulence: an increase of the wind aloft, the shear at the base of a low-level jet, a passing gravity wave or a change of cloud.

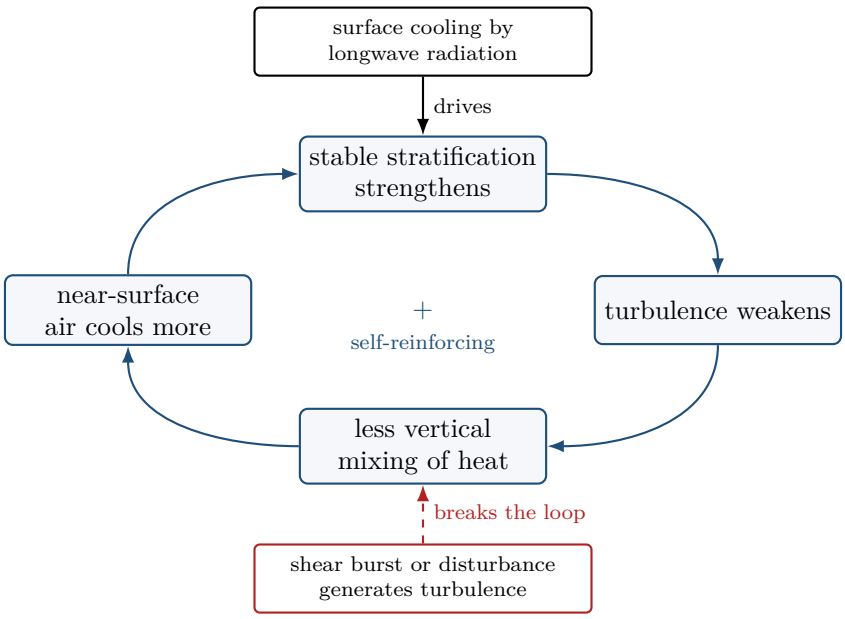


Figure 15.5: The stable feedback near the surface at night. Solid arrows: each state strengthens the next (positive feedback). The loop is driven by radiative cooling of the surface and is broken only by turbulence generated from outside it.

15.4.5 The unstable feedback

By day the corresponding loop runs the other way. Figure 15.6 uses the same layout: surface heating by sunlight is the external driver; the boxes are an unstable stratification, stronger turbulence, heat mixed upward, and a smaller near-surface gradient. The last link closes the loop with the opposite sign: a smaller gradient weakens the instability that started the chain. Convection erases the instability that created it, a negative, self-limiting feedback. The surface layer therefore does not run away by day as it can by night; it settles into a near-steady state in which the heating maintains a small superadiabatic gradient near the ground and a well-mixed layer above, as long as the sun keeps supplying heat.

> **Principle 15.2.** *Stability feeds back on itself in opposite directions. At night, stratification suppresses the turbulence that would destroy it, and the near-surface layer can run away to decoupling; by day, convection mixes away the gradient that drives it, and the surface layer settles. The wind, through* u_*^3*, decides how far either loop goes.*

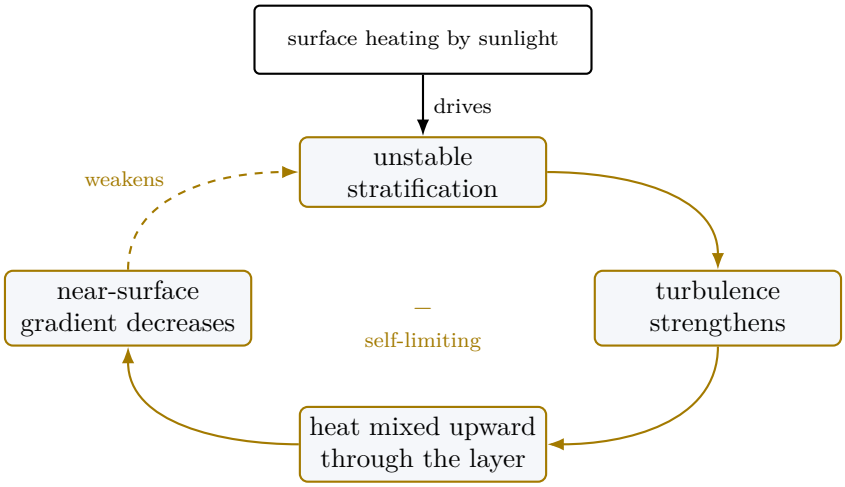


Figure 15.6: The unstable feedback near the surface by day. The dashed arrow closes the loop with the opposite sign: mixing removes the gradient that drives it (negative feedback). The loop is driven by solar heating of the surface.

15.5 Free convection and the whole boundary layer

The surface-layer parameter z/L_{O} describes stability near the ground. This section follows it to its convective limit, introduces the velocity scale that takes over there, compares the Obukhov length with the depth of the boundary layer, and explains why the opposite, strongly stable limit strains the theory.

15.5.1 Very negative stability parameter and free convection

A strong upward heat flux with a weak mean wind gives a small u_*, a large positive $\overline{w'\theta'}$, and therefore a small negative Obukhov length: the free-convection limit. For $u_* = 0.1\,\mathrm{m\,s^{-1}}$ and $H = 300\,\mathrm{W\,m^{-2}}$, Table 15.1 gives $L_{\mathrm{O}} = -0.3\,\mathrm{m}$, and at 10 m the parameter is $z/L_{\mathrm{O}} \approx -33$. In this limit buoyancy dominates the production of turbulence and $|z/L_{\mathrm{O}}| \gg 1$ on the unstable side through most of the surface layer. The friction velocity is no longer the sole useful turbulence scale, nor even the main one: the turbulence would persist with no mean wind at all, driven by plumes of warm air rising from the ground.

In the layer between $|L_{\mathrm{O}}|$ and roughly a tenth of the boundary-layer depth, the free-convection layer, the velocity scale that replaces u_* is built from the buoyancy flux and the height alone, $[(g/\overline{\theta})\,\overline{w'\theta'}\,z]^{1/3}$. At 10 m with $H = 300\,\mathrm{W\,m^{-2}}$, $\overline{w'\theta'} = 300/(1.2 \times 1004) = 0.249\,\mathrm{K\,m\,s^{-1}}$ and

$$\left[\frac{9.81}{300} \times 0.249 \times 10\right]^{1/3} = (0.0814)^{1/3} = 0.43\,\mathrm{m\,s^{-1}},$$

more than four times the friction velocity. The Businger–Dyer ϕ_m still returns a number, $(1 + 16 \times 33)^{-1/4} = 0.21$, but its meaning has changed: the mean wind near the ground in free convection is weak and gusty, and its profile is set by the convective eddies rather than by the stress.

15.5.2 The convective velocity scale

Above the free-convection layer the thermals span the whole boundary layer, and the height scale becomes the depth z_i itself. The convective velocity scale of Chapter 10,

$$w_* = \left[\frac{g}{\overline{\theta}}\,(\overline{w'\theta'})_0\,z_i\right]^{1/3}, \tag{15.11}$$

is the velocity of the buoyant thermals in the convective boundary layer. For the illustrative afternoon used in earlier chapters, $(\overline{w'\theta'})_0 = 0.2\,\mathrm{K\,m\,s^{-1}}$ ($H \approx 240\,\mathrm{W\,m^{-2}}$), $\overline{\theta} = 300\,\mathrm{K}$ and $z_i = 1500\,\mathrm{m}$,

$$w_* = \left[\frac{9.81}{300} \times 0.2 \times 1500\right]^{1/3} = (9.81)^{1/3} = 2.14\,\mathrm{m\,s^{-1}}.$$

The two velocity scales have different roles: u_* for the mechanically driven turbulence of the surface layer, w_* for the deep convection of the whole layer.

The two scales and the Obukhov length are linked. From equation (15.1), $(g/\overline{\theta})\,\overline{w'\theta'} = -u_*^3/(\kappa\, L_\mathrm{O})$; substituting into equation (15.11),

$$w_*^3 = -\frac{u_*^3\, z_i}{\kappa\, L_\mathrm{O}} \qquad \Longrightarrow \qquad \frac{w_*}{u_*} = \left(-\frac{z_i}{\kappa\, L_\mathrm{O}}\right)^{1/3}. \tag{15.12}$$

The ratio of the convective to the mechanical velocity scale depends only on the ratio of the boundary-layer depth to the Obukhov length.

15.5.3 The Obukhov length against the boundary-layer depth

The Obukhov length is a surface-layer stability length; z_i is the depth of the boundary layer. On the afternoon of the previous subsection, with a light wind, $u_* = 0.3\,\mathrm{m\,s^{-1}}$, the Obukhov length is

$$L_\mathrm{O} = -\frac{0.3^3 \times 300}{0.4 \times 9.81 \times 0.2} = -\frac{8.1}{0.785} = -10.3\,\mathrm{m},$$

tens of meters at most, while the boundary layer is 1500 m deep. Buoyancy is important from about 10 m up, very near the surface, and it drives the turbulence through a layer one hundred and fifty times deeper. With a strong wind, $u_* = 0.8\,\mathrm{m\,s^{-1}}$, and the same heat flux, $L_\mathrm{O} = -0.512 \times 300/0.785 = -196\,\mathrm{m}$: shear dominates the whole surface layer, and buoyancy takes over only above it.

Figure 15.7 draws the two afternoons. The vertical axis is the height on a logarithmic scale from 1 to 3000 m; each column is one afternoon, with the same heat flux and the same depth $z_i = 1500\,\mathrm{m}$. The colored layers mark where shear dominates (blue, below $|L_\mathrm{O}|$), the free-convection layer (light gold, from $|L_\mathrm{O}|$ to about $0.1\,z_i$, present only in the light-wind case), the mixed layer scaled by w_* (darker gold), and the entrainment zone at the top (gray). The dotted line at 150 m is the top of the surface layer. In the light wind almost the whole surface layer is convective; in the strong wind none of it is.

15.5.4 The ratio of boundary-layer depth to Obukhov length

The ratio $-z_i/L_\mathrm{O}$ condenses the comparison into one number. For the two afternoons,

$$-\frac{z_i}{L_\mathrm{O}} = \frac{1500}{10.3} = 145 \qquad \text{and} \qquad \frac{1500}{196} = 7.7,$$

and equation (15.12) turns them into $w_*/u_* = (145/0.4)^{1/3} = 7.1$ and $(7.7/0.4)^{1/3} = 2.7$, which agree with 2.14/0.3 and 2.14/0.8. Large values of $-z_i/L_\mathrm{O}$ mean strong convective forcing relative to surface shear; values above about ten are a common working boundary for a boundary layer whose turbulence is predominantly convective, and values of a few or less mark a layer in which shear and convection share the work.

The ratio differs in kind from z/L_O. The stability parameter is local: it describes the balance of shear and buoyancy at one height in the surface layer. The ratio $-z_i/L_\mathrm{O}$ is a whole-boundary-layer measure: it says how the turbulence of the entire layer is driven, which governs the vertical transport of momentum from the wind aloft down to the surface. A forecast of the wind at 100 m on a sunny afternoon needs both: z/L_O for the profile near the ground and $-z_i/L_\mathrm{O}$ for how strongly the layer as a whole is mixed.

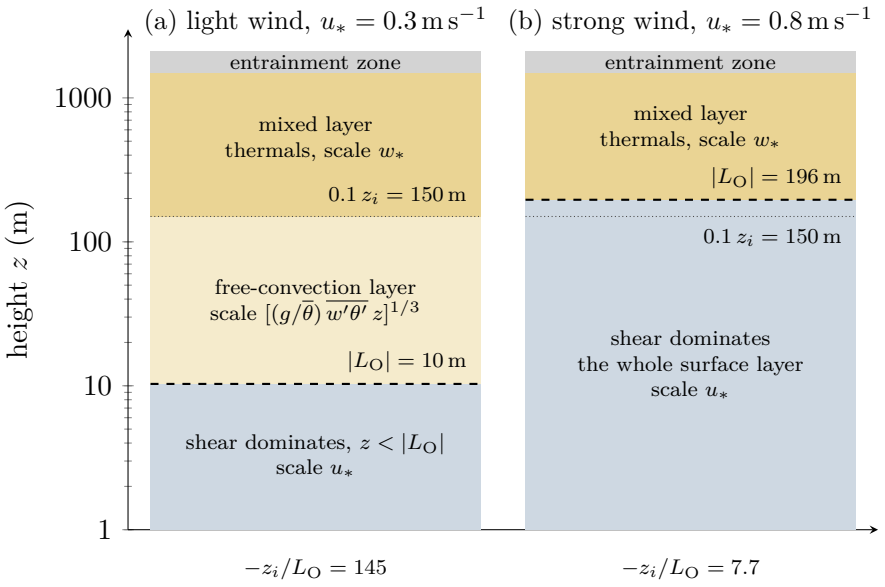


Figure 15.7: Schematic convective boundary layers on two afternoons with the same surface heat flux, $(\overline{w'\theta'})_0 = 0.2\,\mathrm{K\,m\,s^{-1}}$, and depth $z_i = 1500\,\mathrm{m}$, on a logarithmic height axis. (a) Light wind: $L_\mathrm{O} = -10\,\mathrm{m}$. (b) Strong wind: $L_\mathrm{O} = -196\,\mathrm{m}$. Layer boundaries are approximate. Values illustrative.

15.5.5 Why strongly stable conditions strain the theory

The unstable limit has a replacement theory, convective scaling with w_* and z_i. The strongly stable limit has none as simple. With strong stability the assumptions of Monin–Obukhov theory weaken one by one. The turbulence becomes intermittent, with quiet periods broken by bursts, so that a half-hour average mixes two regimes. The flow becomes nonstationary, changing within the averaging period. Gravity waves, oscillations of the stable stratification itself, carry momentum without being turbulence and contaminate the covariances. On sloping ground, cold air drains downhill and the flow is controlled by the drainage rather than by the local surface fluxes. And the turbulence at a sensor is influenced by events above it, such as shear at the base of a low-level jet, which a surface-based theory cannot see: the turbulence becomes nonlocal.

The formulas show the strain as well. With the linear form the flux Richardson number never exceeds 1/5 (Figure 15.1), which implies that turbulence survives at any stability; real very stable layers do not behave that way, and the collapse of Section 15.4.3 happens. The fluxes themselves become small, of the order of $u_* = 0.05$ to $0.1\,\mathrm{m\,s^{-1}}$ and a few $\mathrm{W\,m^{-2}}$, which is where eddy-covariance measurements are least reliable. For $z/L_\mathrm{O} \gg 1$, therefore, simple formulas should not be trusted, and a large positive z/L_O is partly a signal that the regime is one in which the theory itself is less reliable, not only a number to be inserted into it.

15.6 Stability in forecasts

The Obukhov length is not only a diagnostic of the atmosphere; it is a quantity every weather model computes, and errors in it show up in the forecast wind. This section traces the chain of errors, gives two diagnostic cases, and shows how quickly the length changes through a day.

15.6.1 The error chain

A wrong Obukhov length gives a wrong stability parameter, which gives a wrong ϕ_m, which gives a wrong shear, which gives errors in the wind at every height above the reference: U_{10}, U_{20}, U_{50}, U_{100}. In physical terms, a stability error is a mixing error, and a mixing error is a wind-profile error. Figure 15.8 draws the chain. The upper row lists the quantities in the order the calculation passes through them; the lower row gives the same chain in physical terms. Each arrow is a function of the previous quantity, so an error at the left propagates to the right with no opportunity to be corrected.

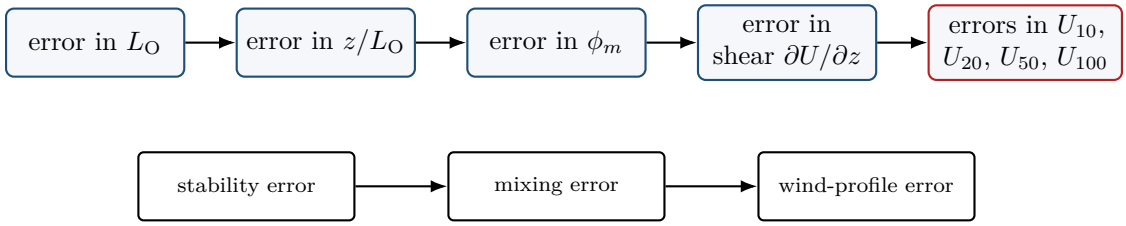


Figure 15.8: The chain by which an error in the Obukhov length becomes an error in the forecast wind. Upper row: the quantities of the calculation. Lower row: the same chain in physical terms.

An illustrative night puts numbers on it. Over farmland with $z_0 = 0.05\,\mathrm{m}$, the wind at 50 m is $8\,\mathrm{m\,s^{-1}}$ and correctly forecast. The true Obukhov length is 50 m; the model's is 200 m, too weakly stable. At 20 m the true ϕ_m is $1 + 5 \times 0.4 = 3.0$ and the model's $1 + 5 \times 0.1 = 1.5$: the model has half the true shear for a given stress. Equation (15.10), fitted to the 50 m wind, gives the 10 m wind

$$U_{10} = 8\,\mathrm{m\,s^{-1}} \times \frac{\ln 200 + 5 \times 10/L_O}{\ln 1000 + 5 \times 50/L_O} = \begin{cases} 8 \times 6.30/11.91 = 4.23\,\mathrm{m\,s^{-1}} & L_O = 50\,\mathrm{m\ (true)}, \\ 8 \times 5.55/8.16 = 5.44\,\mathrm{m\,s^{-1}} & L_O = 200\,\mathrm{m\ (model)}. \end{cases}$$

The model's 10 m wind is $1.2\,\mathrm{m\,s^{-1}}$, or 29 %, too strong, with the wind aloft exactly right. Its friction velocity, 0.39 against $0.27\,\mathrm{m\,s^{-1}}$, is too large as well, and so is its surface stress, by a factor of two.

15.6.2 Two diagnostic cases

The chain can be read backward, from a pattern of forecast errors to the physics behind it. Table 15.6 gives two cases. Its columns are the symptom in the verification, the likely cause in the model's turbulence and stability, and what to check to confirm it.

In the first case the forcing is fine; the error lies in how the model transmits it to the ground at night. The error chain of Section 15.6.1 is exactly this pattern: an Obukhov length four times too long produced a 29 % overprediction at 10 m with the wind aloft correct. The likely culprits are an Obukhov length that is too large, a stable function that suppresses mixing too weakly, or a boundary-layer scheme that is too diffusive by design. Several weather models add mixing in stable conditions deliberately, to avoid runaway surface cooling, and pay for it in the nighttime wind. In the second case the wind aloft is again correct, and the surface wind is too weak because the model does not convect strongly enough to bring that wind down: the sensible heat flux is too small, the Obukhov length not negative enough, the convective turbulence and the downward transport of momentum too weak. Either diagnosis is more informative than "surface wind bias", because it names the process to fix and the measurement that would confirm it.

Table 15.6: Two diagnostic cases: forecast-error patterns read as stability and mixing errors.

Symptom	Likely cause	What to check
Winds at 500 and 100 m correct; 10 m wind overpredicted at night	forcing correct; too much vertical mixing in stable conditions: L_O too large, stable function too weak, boundary-layer scheme too diffusive	model L_O, u_* and heat flux against flux-tower values on clear, light-wind nights; modeled against observed θ difference between 2 and 50 m; the stable function and any minimum mixing the scheme imposes
Strong winds aloft correct; surface wind underpredicted on sunny afternoons	underestimated sensible heat flux, hence too little convective turbulence and too little downward transport of momentum: L_O not negative enough	model sensible heat flux and surface energy balance (soil moisture, cloud); modeled z_i against soundings or remote sensing; $-z_i/L_O$ and the vertical profile of mixing

15.6.3 Rapid variation through a day

The Obukhov length depends on u_*^3 and on the heat flux, and both change quickly around sunrise and sunset, at cloud transitions and with changes of the wind. The length can therefore change sign and magnitude within an hour. A typical sequence over land is $L_O \approx -30$ m at midday, $|L_O| \to \infty$ near sunset as the heat flux passes through zero, and $L_O \approx +50$ m later in the evening.

Figure 15.9 draws a schematic daily course. All three panels share the horizontal axis, local time from midnight to midnight. The upper panel is the sensible heat flux, the middle panel the friction velocity, and the lower panel the reciprocal Obukhov length $1/L_O$ in inverse kilometers, plotted instead of L_O because L_O passes through infinity (Section 15.1.3). The curves come from the closed-form schematic given in the caption, chosen to reproduce the sequence above. The lower panel shows the sign change: $1/L_O$ is positive (stable) through the night, crosses zero at the moment the heat flux turns positive in the morning, reaches about -33 per kilometer ($L_O \approx -30$ m) in the early afternoon, and crosses zero again near 19 h, after which it settles at about $+20$ per kilometer ($L_O \approx +50$ m). The crossings are brief: within less than an hour on either side of each, $|1/L_O|$ exceeds five per kilometer and L_O is shorter than 200 m.

For a forecast the consequence is that stability is a fast variable. The hours around the evening transition are those in which the wind profile reorganizes, the near-surface wind drops and the wind aloft accelerates, and a model that is an hour late in turning the heat flux negative is an hour late in all of these.

15.6.4 Neutral as a transient

Exactly zero heat flux is brief: in Figure 15.9 it lasts for an instant twice a day. In practice "neutral" means $|z/L_O| \ll 1$, not $\overline{w'\theta'} = 0$, and that condition is met in two different ways. Near the transitions it is met briefly because the heat flux is small. Under strong wind or a thick overcast it is met for long periods because the friction velocity is large or the heat flux stays small all day. Only the second kind justifies the neutral logarithmic profile for more than an hour, and a site whose wind climate is dominated by light winds and clear skies spends most of its time away from neutral, in either direction.

The neutral profile is therefore the reference, not the typical state: it is what the profile reduces to when the stability parameter at the height of interest is small, and the Obukhov length is the quantity that says whether it is. The next chapter takes up the daytime convective boundary layer, where the convective velocity scale and the ratio of boundary-layer depth to

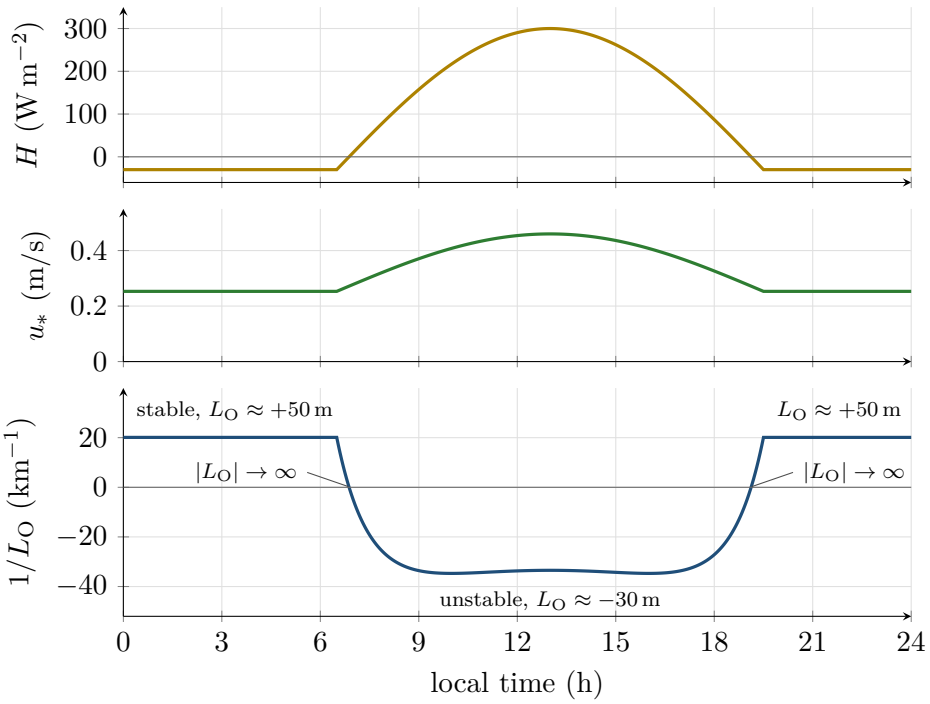


Figure 15.9: Schematic daily course of the sensible heat flux, the friction velocity and the reciprocal Obukhov length. Closed form: $s(t) = \max[0, \sin(\pi(t - 6.5)/13)]$, $H = 330\, s - 30\,\mathrm{W\,m^{-2}}$, $u_* = 0.253 + 0.207\, s$ m/s, $1/L_O$ from equation (15.3). Values illustrative.

Obukhov length introduced here become the governing quantities.

15.7 What to retain

Definition 15.1 (Reading the Obukhov length)**.** The sign of the Obukhov length gives the direction of the buoyancy effect, $L_O < 0$ unstable and $L_O > 0$ stable; the magnitude of the stability parameter z/L_O gives how important that effect is at the height of interest. For the wind at 20 m, the number to ask for is $20\,\mathrm{m}/L_O$.

Table 15.7 lists the terms of the chapter, their meaning, their units and the subsection that defines each.

15.8 Exercises

Exercise 15.1. On a summer afternoon over grassland an eddy-covariance station measures $u_* = 0.35\,\mathrm{m\,s^{-1}}$ and a sensible heat flux $H = 150\,\mathrm{W\,m^{-2}}$. Take $\rho = 1.2\,\mathrm{kg\,m^{-3}}$, $c_p = 1004\,\mathrm{J\,kg^{-1}\,K^{-1}}$ and $\overline{\theta} = 300\,\mathrm{K}$. (a) Compute the kinematic heat flux and the Obukhov length. (b) Compute z/L_O at 10, 20 and 80 m and place each in a band of Table 15.3. (c) Compute ϕ_m and the shear at 20 m, and compare with the neutral shear for the same u_*. (d) A transmission conductor runs at 20 m. State in one sentence how strongly stability matters for the wind at the conductor.

Exercise 15.2. Two clear nights over farmland ($z_0 = 0.05$ m) have the same downward heat flux, $H = -25\,\mathrm{W\,m^{-2}}$, with $u_* = 0.15\,\mathrm{m\,s^{-1}}$ on the first and $0.45\,\mathrm{m\,s^{-1}}$ on the second. (a) Compute L_O and z/L_O at 10 m for each night and name the band. (b) By what factor does L_O differ, and why is it the cube of the ratio of friction velocities? (c) With the formula of Section 15.4.3, compute the maximum downward heat flux that the turbulence can carry with

Table 15.7: The terms of the chapter and where each is defined.

Term	Meaning	Units	Defined in
Obukhov length L_{O}	$-u_*^3\overline{\theta}/(\kappa g\,\overline{w'\theta'})$: mechanical turbulence against buoyancy; height at which buoyant and neutral shear production are equal; <0 unstable, >0 stable	m	15.1.1, 15.1.4
Stability parameter z/L_{O}	height of interest divided by the Obukhov length; sets ϕ_m and the shear	–	15.1.1, 15.2.2
Weakly stable, weakly unstable	$\lvert z/L_{\mathrm{O}}\rvert \ll 1$, roughly below 0.1; close to neutral	–	15.2.3
Strongly stable, strongly unstable	$\lvert z/L_{\mathrm{O}}\rvert$ of order one or larger; buoyancy dominates	–	15.2.3
Free convection	buoyancy produces nearly all the turbulence; strong heating, weak wind, $z/L_{\mathrm{O}} \ll -1$	–	15.5.1
Convective velocity scale w_*	$[(g/\overline{\theta})(\overline{w'\theta'})_0\, z_i]^{1/3}$: velocity of thermals in the convective boundary layer; $w_*/u_* = [-z_i/(\kappa L_{\mathrm{O}})]^{1/3}$	m/s	15.5.2
Ratio $-z_i/L_{\mathrm{O}}$	whole-boundary-layer measure of convective against shear forcing	–	15.5.4
Mechanical mixing	vertical mixing by turbulence produced by the shear of the mean wind; scaled by u_*	–	15.1.2
Buoyant suppression	removal of turbulent kinetic energy by stable stratification	–	15.1.2, 15.4.4
Flux Richardson number Ri_f	$z/L_{\mathrm{O}}/\phi_m$: buoyant destruction over shear production; at most 1/5 with the linear stable form	–	15.1.4

a 10 m wind of $2.5\,\mathrm{m\,s^{-1}}$ and of $7\,\mathrm{m\,s^{-1}}$. (d) If the net radiative loss of the surface less the heat conducted from the soil is $40\,\mathrm{W\,m^{-2}}$, which wind risks decoupling, and which stage of the stable feedback of Figure 15.5 would follow?

Exercise 15.3. On a dry-season afternoon the surface heat flux is $H = 300\,\mathrm{W\,m^{-2}}$, the boundary layer is $z_i = 2000\,\mathrm{m}$ deep and the wind is light, $u_* = 0.25\,\mathrm{m\,s^{-1}}$. Use ρ, c_p and $\overline{\theta}$ of Exercise 1. (a) Compute w_* and L_{O}. (b) Compute $-z_i/L_{\mathrm{O}}$ and check equation (15.12) by computing w_*/u_* both ways. (c) Between which heights does the free-convection layer lie, approximately? (d) Compute z/L_{O} at 10 m and the free-convection velocity scale there, and compare it with u_*.

Exercise 15.4. A mast in southern Brazil, at 25°S over farmland ($z_0 = 0.05\,\mathrm{m}$), records on a clear night $u_* = 0.2\,\mathrm{m\,s^{-1}}$ and $H = -20\,\mathrm{W\,m^{-2}}$; the 10 m wind blows from 100°. (a) Compute L_{O}, and z/L_{O} at 10 and 50 m. (b) Compute the winds at 10 and 50 m from equation (15.10) with the linear stable form, and say how far the 50 m value can be trusted. (c) Compute the Coriolis parameter and the stable boundary-layer depth from $z_i \approx 0.4\sqrt{u_* L_{\mathrm{O}}/|f|}$, and compare it with L_{O}. (d) The wind turns by 30° between 10 m and the top of the layer. Does it turn clockwise or counterclockwise with height, and from which direction does it blow at the top? Give both answers for the same night at 25°N.

Chapter 16

The Daytime Convective Boundary Layer

16.1 Thermals and the mixed layer

Chapter 6 described the daily cycle of the boundary layer over land: a convective mixed layer that grows after sunrise under an entrainment zone, a stable layer that forms at the ground after sunset, and a residual layer left between them. Chapter 8 introduced the convective velocity scale w_* as the velocity of buoyancy-driven turbulence, Chapter 9 showed that the heat flux in the upper mixed layer runs against the local gradient, and Chapter 15 used the ratio of the boundary-layer depth to the Obukhov length to say how convective a layer is as a whole. This chapter assembles these pieces into one description of the daytime layer. Its question is

how does heating of the ground by the sun reorganize the whole boundary layer, and what does that reorganization do to the wind at the heights where the wind is used?

The chapter first describes the structures of the daytime layer: thermals, the downdrafts between them, the well-mixed interior, the superadiabatic layer at the ground and the capping inversion at the top. It then derives a slab model of how the layer grows through the day, builds the convective velocity scale and the vertical profiles of the heat and momentum fluxes, and follows the consequences for the wind near the ground, including the morning and evening transitions. It ends with the organized forms that convection takes, the limits they set for local theories and for weather models, and the surface energy balance that decides how strong the convection is in the first place.

Jargon: convective boundary layer, thermal, mixed layer, capping inversion, entrainment, convective velocity scale, morning and evening transition, horizontal convective rolls, nonlocal transport, Bowen ratio

The *convective boundary layer* (CBL) is the daytime boundary layer whose turbulence is produced mainly by heating of the ground; its depth z_i, in meters, is measured by radiosondes, lidars and wind profilers as the height of the capping inversion, and is computed by every weather model. A *thermal* is a rising plume of buoyant air, warmer than its surroundings, that carries heat upward ($w' > 0$ with $\theta' > 0$). The *mixed layer* is the interior of the CBL, in which potential temperature, humidity and, less perfectly, wind are nearly uniform with height. The *capping inversion* is the stable layer at the top of the CBL, across which θ increases sharply, in kelvin over tens to a few hundred meters. *Entrainment* is the incorporation of free-atmosphere air into the CBL by thermals that overshoot its top; its rate is the entrainment velocity w_e, in m/s. The *convective velocity scale* $w_* = [(g/\overline{\theta})(\overline{w'\theta'})_0\, z_i]^{1/3}$, in m/s, is the velocity of the thermals, calculated from the surface heat flux and the depth. The *morning transition* is the period after sunrise in which a growing convective layer erodes the stable nighttime structure; the *evening transition* is the period around sunset in which convection decays and a stable layer forms. *Horizontal convective rolls* are pairs of counter-rotating circulations with axes roughly along the mean wind, kilometers wide and tens of kilometers long. *Nonlocal transport* is vertical transport by eddies as large as the layer, which does not depend on the local gradient; models represent it by added terms in their boundary-layer schemes. The *Bowen ratio* $B = H/LE$, dimensionless, is the sensible heat flux divided by the latent heat flux at the surface.

Key idea

Heating of the ground does not change the large-scale forcing of the wind; it changes the coupling. Thermals and downdrafts mix the whole layer, and the wind near the ground then draws on the momentum of the air hundreds of meters above it.

A running example. The chapter follows one illustrative clear day over farmland with a roughness length $z_0 = 0.05\,\mathrm{m}$, at a site where the wind at 200 m stays near 13 to $14\,\mathrm{m\,s^{-1}}$ all day. At 13:00 the surface kinematic heat flux is $(\overline{w'\theta'})_0 = 0.198\,\mathrm{K\,m\,s^{-1}}$, a sensible heat flux $H = \rho\, c_p\, (\overline{w'\theta'})_0 = 1.2 \times 1004 \times 0.198 \approx 240\,\mathrm{W\,m^{-2}}$; the mixed layer is $z_i = 1270\,\mathrm{m}$ deep (Section 16.2.4); the wind at 20 m is $9\,\mathrm{m\,s^{-1}}$. Solving the unstable profile of Chapter 14 for this wind gives $u_* = 0.65\,\mathrm{m\,s^{-1}}$ and, from the definition of Chapter 15, $L_\mathrm{O} = -92\,110 \times 0.65^3/240 \approx -106\,\mathrm{m}$. All numbers of the running example are illustrative.

16.1.1 The daytime sequence

The air absorbs little of the sunlight that passes through it; the ground absorbs most of it. The atmosphere is therefore heated from below, and on a clear day over land the sequence after sunrise is

solar heating → surface warming → unstable near-surface air → buoyant thermals → shallow unstable layer → deep convective boundary layer.

Once the ground is warmer than the air touching it, the sensible heat flux turns upward and the lowest air becomes statically unstable in the sense of Chapter 13: a parcel displaced upward is lighter than its new surroundings and keeps rising. Over dry ground at midday the surface can be 10 to 20 K warmer than the air at 2 m (typical values), and buoyant plumes leave it continuously.

The layer stirred by these plumes is shallow at first, a few tens of meters an hour after sunrise and a few hundred meters by mid-morning, and it grows through the day to 1000 to

2000 m or more by the afternoon; over deserts and dry plains in summer it reaches 3 to 4 km (typical values). The *convective boundary layer* is this layer: the part of the atmosphere whose turbulence is produced mainly by heating of the ground. Its depth z_i is the height of its top, where the stable capping inversion begins. It is measured as the height of the jump in potential temperature on a radiosonde profile, as the height at which the aerosol backscatter of a lidar or ceilometer drops, since the mixed layer holds the aerosol emitted at the ground, or as the height of the peak in the return of a wind profiler; weather models diagnose it from their profiles of θ or of a bulk Richardson number. The rest of this section describes what fills the layer.

16.1.2 Thermals

A *thermal* is a rising plume, or a coherent rising region, of buoyant warm air. Inside it $\theta' > 0$ and $w' > 0$, so its contribution to the covariance $\overline{w'\theta'}$ is positive: a thermal carries sensible heat upward. Thermals start in the superadiabatic layer at the ground (Section 16.1.5) as small plumes over the warmest patches of ground, merge as they rise, and widen with height, from about a hundred meters across near the ground to several hundred meters in the middle of the layer; neighboring thermals are spaced about one to one and a half times z_i apart (typical values). The largest of them reach the top of the layer.

Their driving force is the buoyancy per unit mass, $b = g\,\theta'/\overline{\theta}$. A thermal 0.3 K warmer than its surroundings at $\overline{\theta} = 300\,\mathrm{K}$ has $b = 9.81 \times 0.3/300 = 0.0098\,\mathrm{m\,s^{-2}}$, about a thousandth of gravity. Without drag it would reach $\sqrt{2 \times 0.0098 \times 500} = 3.1\,\mathrm{m\,s^{-1}}$ after rising 500 m. Mixing with the surrounding air and the pressure forces needed to push that air aside hold real thermals to about 1 to $3\,\mathrm{m\,s^{-1}}$, the range of w_* (Section 16.3.2). Thermals are the dominant structure of the CBL: they carry most of its heat flux and much of its vertical transport of moisture and momentum. They are seen as fair-weather cumulus clouds where they rise above the condensation level, are used by glider pilots and soaring birds, are mapped by Doppler lidar and research aircraft, and appear in tower records as short intervals of strong upward velocity and high temperature.

16.1.3 Compensating downdrafts

Air that rises in thermals must be replaced. At any height, averaged over an area containing many thermals, the mean vertical mass flux is nearly zero: the large-scale vertical velocity is millimeters to centimeters per second, negligible against the meters per second of the thermals, and the density is nearly uniform across a horizontal level. If a fraction a_u of the area rises with mean velocity w_u and the rest sinks with mean velocity w_d, mass conservation requires

$$a_u\,w_u + (1 - a_u)\,w_d = 0 \qquad \Longrightarrow \qquad w_d = -\,\frac{a_u}{1 - a_u}\,w_u. \tag{16.1}$$

Updrafts in a CBL occupy less than half the area, typically about 40 %. With $a_u = 0.4$ and $w_u = 1.5\,\mathrm{m\,s^{-1}}$, $w_d = -0.4 \times 1.5/0.6 = -1.0\,\mathrm{m\,s^{-1}}$: the downdrafts are broader and weaker than the updrafts. The two-state picture also gives the variance and the asymmetry of the vertical velocity. Its variance is $\sigma_w^2 = 0.4 \times 1.5^2 + 0.6 \times 1.0^2 = 0.90 + 0.60 = 1.50\,\mathrm{m^2\,s^{-2}}$, so $\sigma_w = 1.22\,\mathrm{m\,s^{-1}}$; its third moment is $0.4 \times 1.5^3 - 0.6 \times 1.0^3 = 1.35 - 0.60 = 0.75\,\mathrm{m^3\,s^{-3}}$, positive. A vertical-velocity record in a CBL is therefore positively skewed: brief strong updrafts and longer, gentler descent.

Figure 16.1 draws the circulation in a vertical cross section. The horizontal direction is distance along the ground and the vertical direction height, from the heated ground to the free atmosphere above the layer. The gold plumes are thermals with upward arrows; the blue arrows between them are the compensating downdrafts; the gray band at the top is the entrainment zone, which the domes of the largest thermals push into, with small arrows marking free-atmosphere air drawn down at their flanks; the green strip at the bottom is the

superadiabatic surface layer. The figure shows the overturning that mixes the layer: warm air goes up in narrow columns, cooler air comes down over the larger area between them, and both motions carry heat upward.

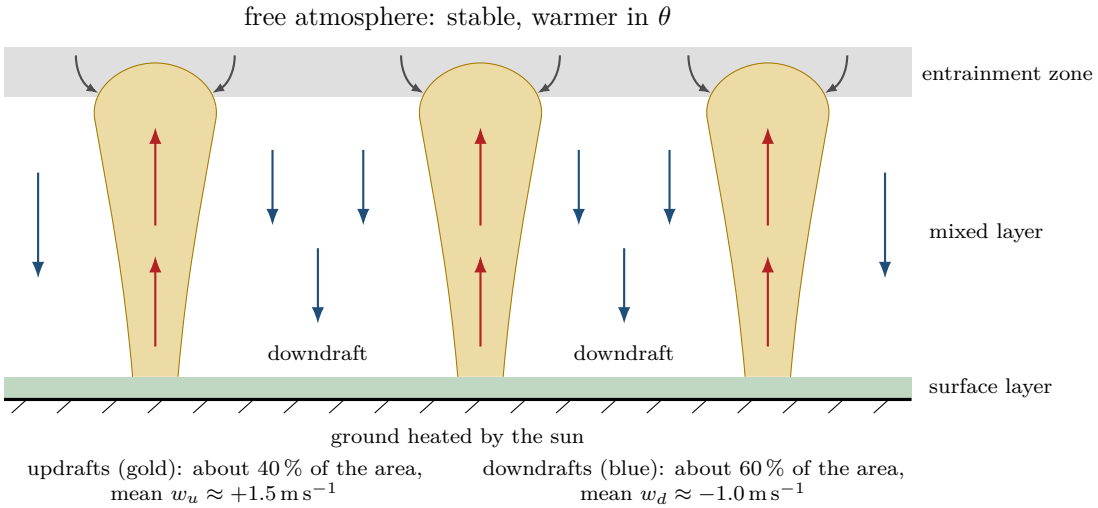


Figure 16.1: Thermals and compensating downdrafts in the convective boundary layer (vertical cross section, schematic, not to scale). Gold: thermals rising from the heated ground; blue arrows: compensating downdrafts; black arrows: free-atmosphere air entrained at the flanks of thermal domes. Area fractions and speeds are those of the illustrative two-state example, linked by mass conservation, equation (16.1).

The heat carried by the two branches follows from the same picture. Let the updrafts be warmer than the horizontal mean by θ'_u and the downdrafts cooler by θ'_d, with $a_u\,\theta'_u + (1-a_u)\,\theta'_d = 0$. With $\theta'_u = +0.12\,\mathrm{K}$ and $\theta'_d = -0.08\,\mathrm{K}$ (illustrative), the flux is

$$\overline{w'\theta'} = 0.4 \times 1.5 \times 0.12 + 0.6 \times (-1.0) \times (-0.08) = 0.072 + 0.048 = 0.12\,\mathrm{K\,m\,s^{-1}},$$

about 60 % of the surface value of the running example, which is the fraction the linear flux profile of Section 16.3.4 gives at a third of the depth. Both branches contribute: warm air rising and cool air sinking are both upward transport of heat. This vigorous overturning, warm air up and cooler air down, is what mixes the layer.

16.1.4 The mixed layer

The overturning is fast compared with the day. The convective turnover time $t_* = z_i/w_*$ of Chapter 6 is, for the running example, $1270/2.02 \approx 630\,\mathrm{s}$, about ten minutes (Section 16.3.1 computes w_*). In an hour every parcel of the layer is carried from the ground to the top and back several times. Any property that a parcel keeps as it moves is then made nearly uniform with height: the potential temperature θ, which a parcel keeps under dry adiabatic motion, and the specific humidity q, which it keeps until it condenses. The interior of the CBL in which this holds is the *mixed layer*, and $\theta(z) \approx \theta_m$, a constant, through it. Aerosol and pollutants emitted at the ground are mixed the same way, which is why a lidar sees the top of the mixed layer as the height where the backscatter drops.

The uniformity holds for θ, not for temperature. In the running example the mixed layer has $\theta_m \approx 300.4\,\mathrm{K}$ from about 100 to 1200 m; the temperature over the same 1100 m falls at the dry adiabatic lapse rate $\Gamma_d = g/c_p = 9.8\,\mathrm{K\,km^{-1}}$, by about 10.8 K. Nor is θ exactly constant: it decreases slightly with height in the lower half of the mixed layer and increases slightly in the upper half (the counter-gradient region of Chapter 9), by a few tenths of a kelvin over a

kilometer, against the several kelvin per kilometer of the free atmosphere above. The wind is the least well mixed of the three, because the ground removes momentum at the bottom continuously; Section 16.4.4 returns to it.

16.1.5 The superadiabatic surface layer

Very close to the ground the potential temperature decreases with height, $\partial\theta/\partial z < 0$: the temperature falls faster than the dry adiabatic lapse rate, which is what *superadiabatic* means. This layer is the surface layer of the CBL. Its strong gradients are confined to the lowest meters to tens of meters, and it is where the instability is strongest and where thermals are born. Above it the gradient weakens to the nearly neutral mixed layer.

Monin–Obukhov theory (Chapter 14) gives the gradient with the standard empirical (Businger–Dyer) form for heat in unstable air,

$$\frac{\partial\theta}{\partial z} = \frac{\theta_*}{\kappa z}\,\phi_h, \qquad \phi_h = \left(1 - 16\,\frac{z}{L_\mathrm{O}}\right)^{-1/2}, \qquad \theta_* = -\,\frac{(\overline{w'\theta'})_0}{u_*}, \tag{16.2}$$

with the integrated correction $\psi_h = 2\ln[(1+x^2)/2]$, $x = (1-16\,z/L_\mathrm{O})^{1/4}$, and the turbulent Prandtl number taken as one. For the running example, $\theta_* = -0.198/0.65 = -0.305\,\mathrm{K}$ and $L_\mathrm{O} = -106\,\mathrm{m}$. At 2 m, $\phi_h = (1 + 16\times 2/106)^{-1/2} = 1.302^{-1/2} = 0.876$ and the gradient is $-0.305\times 0.876/(0.4\times 2) = -0.33\,\mathrm{K\,m^{-1}}$: the potential temperature falls by a third of a kelvin per meter, and the temperature by 0.34 K per meter, about thirty-five times the dry adiabatic rate. At 50 m, $\phi_h = 8.55^{-1/2} = 0.342$ and the gradient is $-0.305\times 0.342/20 = -5.2\,\mathrm{K\,km^{-1}}$, still superadiabatic but weakly. Integrated between 2 and 100 m,

$$\theta(2\,\mathrm{m}) - \theta(100\,\mathrm{m}) = \frac{0.305}{0.4}\,[\ln 50 - \psi_h(100\,\mathrm{m}) + \psi_h(2\,\mathrm{m})] = 0.763\times 2.211 = 1.69\,\mathrm{K},$$

with $\ln 50 = 3.912$, $\psi_h(100\,\mathrm{m}) = 1.837$ and $\psi_h(2\,\mathrm{m}) = 0.136$. More than half of that difference, 0.94 K, lies below 10 m. A temperature sensor at 2 m on a sunny afternoon therefore reads well above the air at the height of a transmission conductor or a turbine hub, and neither reading is the temperature of the mixed layer.

16.1.6 The capping inversion and the vertical structure

At the top of the mixed layer the potential temperature increases sharply. This stable layer is the *capping inversion*: it separates the mixed layer from the warmer, stable free atmosphere and suppresses the growth of the layer, because a thermal that reaches it is colder than the air around it and decelerates. Strictly, an inversion is a layer in which temperature increases with height; at the top of a CBL the temperature often still decreases slightly while θ increases sharply, and the name is used for both. In the running example the jump in θ across the top is about 0.9 K (Section 16.2.3) and the free atmosphere above has a potential-temperature gradient $\gamma = \partial\theta/\partial z = 5\,\mathrm{K\,km^{-1}}$, a buoyancy frequency $N = \sqrt{(g/\bar\theta)\,\gamma} = \sqrt{0.0327\times 0.005} = 0.0128\,\mathrm{s^{-1}}$. Stronger caps, 2 to 5 K under a subsiding high-pressure system, are common.

The CBL therefore has four layers, from the ground up:

$$\text{surface layer} \to \text{mixed layer} \to \text{entrainment zone} \to \text{free atmosphere}.$$

Figure 16.2 draws the four layers of the running example at 13:00 as three profiles side by side, against the same height axis from the ground to 1800 m. The left panel is the potential temperature, the middle panel the wind speed and the right panel the specific humidity. The colored bands are shared: green for the surface layer, up to about $0.1\,z_i$; light gold for the mixed layer; gray for the entrainment zone, from about 1180 to 1360 m; white for the free atmosphere. In the surface layer θ and q decrease with height and the wind increases rapidly. Through the

mixed layer θ and q are constant, and the wind increases slowly. Across the entrainment zone θ increases by about 1.4 K, the air becomes drier by $3.5\,\mathrm{g\,kg^{-1}}$, and the wind increases by about $1\,\mathrm{m\,s^{-1}}$ to the free-atmosphere value. The profiles are constructed to be consistent with the slab model and the surface-layer formulas of this chapter.

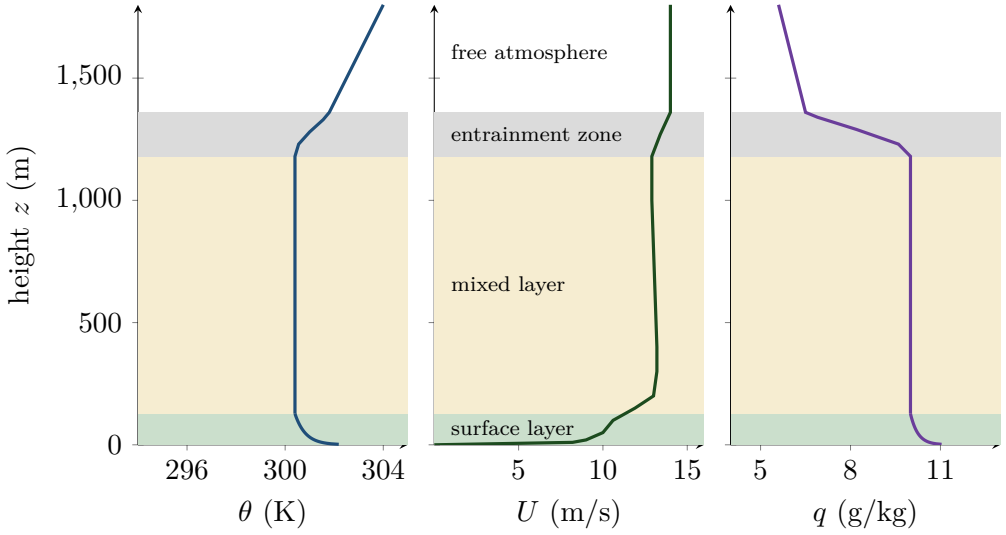


Figure 16.2: Vertical structure of the convective boundary layer of the running example at 13:00 ($z_i = 1270\,\mathrm{m}$). Left: potential temperature; middle: wind speed; right: specific humidity. Bands: surface layer (green, to $0.1\,z_i$), mixed layer (gold), entrainment zone (gray), free atmosphere (white). Surface-layer curves are logarithmic shapes matching the superadiabatic difference of Section 16.1.5; the free atmosphere has $\partial\theta/\partial z = 5\,\mathrm{K\,km^{-1}}$. Values illustrative.

16.2 Growth and entrainment

The depth of the convective layer changes by an order of magnitude over the morning. This section describes entrainment, the process by which the layer grows, derives a slab model of the growth from the heat budget, solves it for an illustrative day, and lists the factors that set the rate and the afternoon maximum.

16.2.1 Entrainment

The largest thermals arrive at the top of the layer with upward velocities of the order of w_* and overshoot into the stable air above. There they are colder than their surroundings, decelerate, and sink back, pulling some of the free-atmosphere air they have disturbed down with them. This is *entrainment*: the incorporation of free-atmosphere air into the boundary layer, which takes place in the entrainment zone at the top of the CBL. A rough estimate of how far a thermal overshoots is the distance over which a stable layer of buoyancy frequency N stops a parcel of vertical velocity w, about w/N; for $w = 2\,\mathrm{m\,s^{-1}}$ and $N = 0.0128\,\mathrm{s^{-1}}$ this is about 160 m, a little over a tenth of the depth of the running example, the order of the observed thickness of the entrainment zone. A sharp jump in θ at the top shortens the overshoot.

The entrained air differs from the mixed-layer air in every property, and entrainment changes all of them. Its potential temperature is higher by the jump $\Delta\theta$, so mixing it in warms the layer from the top; the heat flux at the top is $-w_e\,\Delta\theta$, downward. It is usually drier, by $\Delta q < 0$, so mixing it in dries the layer, with an upward moisture flux $-w_e\,\Delta q$ at the top. Its wind differs by ΔU, usually faster, so the momentum flux at the top is $-w_e\,\Delta U$, downward. For the running example at 13:00, with the entrainment velocity $w_e = 0.044\,\mathrm{m\,s^{-1}}$ of Section 16.2.4, $\Delta\theta = 0.91\,\mathrm{K}$,

$\Delta q = -3.5\,\mathrm{g\,kg^{-1}}$ and $\Delta U = 1\,\mathrm{m\,s^{-1}}$, the three fluxes at the top are $-0.040\,\mathrm{K\,m\,s^{-1}}$ (a sensible heat flux of about $-48\,\mathrm{W\,m^{-2}}$), $+1.5\times10^{-4}\,\mathrm{m\,s^{-1}}$ of specific humidity (equivalent to a latent heat flux of $1.2\times2.5\times10^{6}\times1.5\times10^{-4}\approx460\,\mathrm{W\,m^{-2}}$, which can exceed the evaporation at the ground, so that the mixed layer dries during the day), and $-0.044\,\mathrm{m^2\,s^{-2}}$ of momentum. Entrainment also deepens the layer, and it is one of the main controls on how fast the layer grows.

16.2.2 The growth mechanism

Growth proceeds in three steps that repeat continuously: surface heating generates convective turbulence; the turbulence reaches the inversion; entrainment incorporates air from above into the layer, whose top moves up. As Chapter 6 wrote it, the depth changes as

$$\frac{\mathrm{d}z_i}{\mathrm{d}t} = w_e + w_s, \tag{16.3}$$

where w_s is the large-scale vertical velocity at the top, negative under subsidence. Through the morning and early afternoon, w_e exceeds $|w_s|$ and $\mathrm{d}z_i/\mathrm{d}t > 0$.

The process is a heat budget. To deepen the layer by $\mathrm{d}z_i$, the air that joins it must be brought to the potential temperature of the mixed layer; since the air above is warmer in θ, the whole mixed layer must first warm up to the θ of the air it is about to absorb. The layer can deepen only as fast as the surface heat flux, helped by the entrainment flux, warms it, and the more strongly θ increases with height above the top, the more heat each meter of growth costs. The next subsection writes this budget down.

16.2.3 A slab model of mixed-layer growth

A *slab model* treats the mixed layer as a single slab with uniform potential temperature $\theta_m(t)$ from the ground to $z_i(t)$, with a jump $\Delta\theta(t)$ at the top. Its assumptions are: at the start of the day the profile is linear, $\theta(z,0) = \theta_s + \gamma z$, with a constant gradient γ; above the slab the air keeps that initial profile; there is no subsidence, no horizontal advection and no radiative heating; and the heat flux just below the top is a fixed fraction A of the surface flux,

$$(\overline{w'\theta'})_{z_i} = -\,w_e\,\Delta\theta = -A\,(\overline{w'\theta'})_0, \qquad A \approx 0.2. \tag{16.4}$$

The *entrainment ratio* A is an empirical closure, observed to be about 0.2 in convective layers with weak shear; it states that the turbulence spends a fixed share of the energy the surface supplies on lifting dense air across the top. The linear initial profile ignores the nighttime stable layer and the residual layer; Section 16.4.6 treats them.

Step 1: the column heat budget. The averaged heat equation without advection is $\partial\theta/\partial t = -\partial\overline{w'\theta'}/\partial z$. Integrated from the ground to a height above the top where the flux vanishes, and then in time from the start of the day,

$$\int_0^\infty [\theta(z,t) - \theta(z,0)]\,\mathrm{d}z = Q(t) \equiv \int_0^t (\overline{w'\theta'})_0\,\mathrm{d}t'. \tag{16.5}$$

The accumulated surface heat input Q, in K m, equals the area between the current and the initial profiles. For the slab profile that area is $\int_0^{z_i}(\theta_m - \theta_s - \gamma z)\,\mathrm{d}z = z_i(\theta_m - \theta_s) - \gamma z_i^2/2$; with $\theta_m = \theta_s + \gamma z_i - \Delta\theta$ (the jump brings the slab back to the initial profile at the top),

$$\frac{\gamma\, z_i^2}{2} - z_i\,\Delta\theta = Q(t). \tag{16.6}$$

Step 2: the slab heat budget. Integrating the heat equation from the ground to just below the top, where the flux is that of equation (16.4),

$$z_i \frac{\mathrm{d}\theta_m}{\mathrm{d}t} = (\overline{w'\theta'})_0 - (\overline{w'\theta'})_{z_i} = (1+A)\,(\overline{w'\theta'})_0. \tag{16.7}$$

Step 3: the solution. Without entrainment ($A = 0$, $\Delta\theta = 0$) equation (16.6) gives at once $z_i = \sqrt{2Q/\gamma}$: the layer deepens by warming up to the initial profile, a growth called *encroachment*. With entrainment, try a jump proportional to the depth, $\Delta\theta = c\,\gamma z_i$. Equation (16.6) becomes $\gamma z_i^2(\frac{1}{2} - c) = Q$, so that $\mathrm{d}z_i^2/\mathrm{d}t = (\overline{w'\theta'})_0/[\gamma(\frac{1}{2} - c)]$. Equation (16.7), with $\theta_m = \theta_s + \gamma z_i(1-c)$, becomes $\mathrm{d}z_i^2/\mathrm{d}t = 2(1+A)(\overline{w'\theta'})_0/[\gamma(1-c)]$. The two agree when $2(1+A)(\frac{1}{2} - c) = 1 - c$, that is, when $c = A/(1+2A)$. Then $\frac{1}{2} - c = 1/[2(1+2A)]$ and

$$z_i(t) = \sqrt{\frac{2\,(1+2A)\,Q(t)}{\gamma}}, \qquad \Delta\theta = \frac{A}{1+2A}\,\gamma\,z_i, \qquad w_e = \frac{\mathrm{d}z_i}{\mathrm{d}t} = \frac{(1+2A)\,(\overline{w'\theta'})_0}{\gamma\,z_i}. \tag{16.8}$$

The solution is exact for a layer that starts from zero depth when the flux turns positive. With $A = 0.2$, $1 + 2A = 1.4$: entrainment makes z_i^2 forty percent larger than encroachment and z_i eighteen percent larger, and the jump is $0.2/1.4 = 0.143$ of the potential temperature difference γz_i across the depth. The depth grows with the square root of the accumulated heat and falls with the square root of the stratification it grows into.

Figure 16.3 draws the slab profile of the running example at 13:00. The horizontal axis is potential temperature and the vertical axis height. The dashed line is the initial profile; the solid line is the slab, with the mixed layer at θ_m and the jump at z_i. The gold triangle is the heat added to the lower part of the layer, where the slab is warmer than the initial profile; the small blue triangle is the heat removed from the air between 1089 m and z_i, which was warmer than θ_m before it was entrained. Their difference is Q, equation (16.6). With $\gamma = 5\,\mathrm{K\,km^{-1}}$, $z_i = 1270\,\mathrm{m}$ and $Q = 2880\,\mathrm{K\,m}$ (computed in the next subsection): $\Delta\theta = 0.143 \times 0.005 \times 1270 = 0.91\,\mathrm{K}$; $\theta_m - \theta_s = \gamma z_i - \Delta\theta = 6.35 - 0.91 = 5.44\,\mathrm{K}$; and the check $0.005 \times 1270^2/2 - 1270 \times 0.907 = 4032 - 1152 = 2880\,\mathrm{K\,m}$ closes the budget.

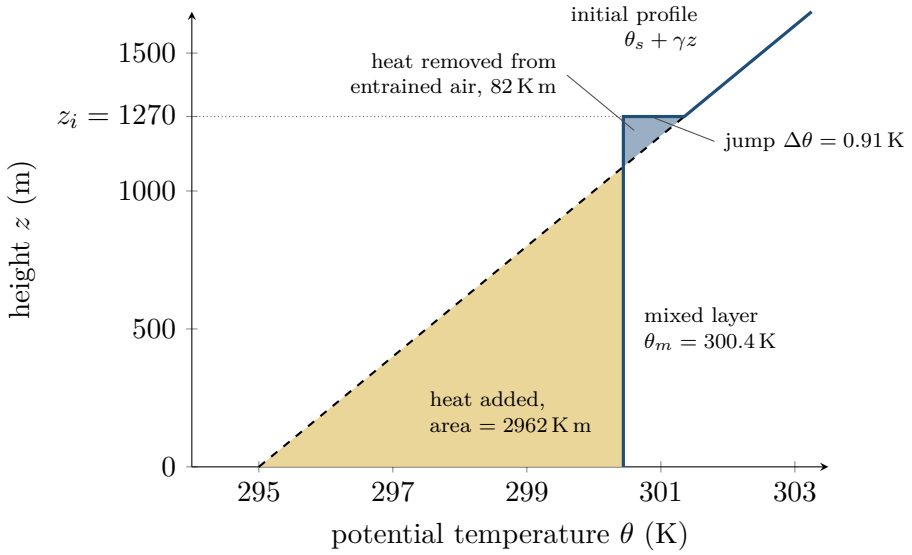


Figure 16.3: The slab model of the mixed layer, for the running example at 13:00. Dashed: initial profile $\theta_s + \gamma z$ with $\theta_s = 295\,\mathrm{K}$ and $\gamma = 5\,\mathrm{K\,km^{-1}}$. Solid: slab with $\theta_m = 300.44\,\mathrm{K}$ and a jump of 0.91 K at $z_i = 1270\,\mathrm{m}$ (equation (16.8), $A = 0.2$). Gold minus blue area equals the accumulated surface heat input, $Q = 2880\,\mathrm{K\,m}$. Values illustrative.

16.2.4 Growth through an illustrative day

To solve equation (16.8) for a day, the surface flux is needed as a function of time. An illustrative clear day has

$$(\overline{w'\theta'})_0(t) = 0.2\,\mathrm{K\,m\,s^{-1}} \times \sin\frac{\pi\,(t - 7\,\mathrm{h})}{11\,\mathrm{h}}, \qquad 7\,\mathrm{h} \le t \le 18\,\mathrm{h}, \tag{16.9}$$

positive from 07:00 to 18:00 with its maximum, $H \approx 240\,\mathrm{W\,m^{-2}}$, at 12:30. Its integral is

$$Q(t) = 0.2 \times \frac{11 \times 3600\,\mathrm{s}}{\pi}\left[1 - \cos\frac{\pi\,(t - 7\,\mathrm{h})}{11\,\mathrm{h}}\right] = 2521\,\mathrm{K\,m} \times \left[1 - \cos\frac{\pi\,(t - 7\,\mathrm{h})}{11\,\mathrm{h}}\right].$$

At 13:00 the bracket is $1 - \cos(6\pi/11) = 1.142$ and $Q = 2880\,\mathrm{K\,m}$; with $\gamma = 5\,\mathrm{K\,km^{-1}}$ and $A = 0.2$, $z_i = \sqrt{2.8 \times 2880/0.005} = 1270\,\mathrm{m}$, the depth of the running example. The flux at 13:00 is $0.2\sin(6\pi/11) = 0.198\,\mathrm{K\,m\,s^{-1}}$ and the entrainment velocity $w_e = 1.4 \times 0.198/(0.005 \times 1270) = 0.044\,\mathrm{m\,s^{-1}}$, about 160 m per hour.

Figure 16.4 plots the day. The upper panel is the surface kinematic heat flux of equation (16.9) against local time; the lower panel is the depth z_i from equation (16.8) for three cases: the base case ($A = 0.2$, $\gamma = 5\,\mathrm{K\,km^{-1}}$, blue), encroachment alone ($A = 0$, dashed), and a twice stronger stratification ($A = 0.2$, $\gamma = 10\,\mathrm{K\,km^{-1}}$, green). The dot marks the running example at 13:00. In the base case the depth is 240 m at 08:00, 470 m at 09:00, 700 m at 10:00, 1270 m at 13:00 and 1610 m at 16:00, and it ends the day at 1680 m. The growth rate is nearly constant through the morning, about $0.06\,\mathrm{m\,s^{-1}}$ (about 230 m per hour), and falls in the afternoon as the flux declines and the layer deepens. Encroachment alone is 16 % shallower at every time ($1/\sqrt{1.4} = 0.85$); doubling γ makes the layer 29 % shallower ($1/\sqrt{2} = 0.71$).

The model omits the nighttime stable layer. A real morning first spends an hour or two eroding it, during which the mixed layer stays shallow, and then grows quickly into the nearly neutral residual layer, for which $\gamma \approx 0$ and growth is limited only by the time the thermals take to reach its top; Section 16.4.6 returns to this. The slab curve is the growth into air that has not been mixed before.

16.2.5 Factors that change the growth rate

The growth rate depends on the surface heat flux, the strength of the inversion and of the stratification above, large-scale subsidence, wind shear and cloud cover. Equation (16.8) puts numbers on the first two. Since $z_i \propto \sqrt{Q/\gamma}$, halving the surface heat flux all day shrinks the depth by the factor $1/\sqrt{2}$, from 1270 to 900 m at 13:00; doubling the stratification does the same. The surface flux in turn depends on the sunshine and on how the surface divides its energy between sensible and latent heat (Section 16.6.4).

The other three act through terms the model leaves out. Subsidence lowers the top at the rate w_s in equation (16.3); a subsidence of $0.01\,\mathrm{m\,s^{-1}}$ removes 36 m of growth every hour, which is small against the morning growth rate of about 230 m per hour and decisive in the afternoon, when w_e falls to the same size. Wind shear across the top produces turbulent kinetic energy there and raises the entrainment ratio; raising A from 0.2 to 0.3 deepens the layer by the factor $\sqrt{1.6/1.4} = 1.07$. Cloud cover reduces the sunshine reaching the ground and with it the surface flux; a thick overcast can hold the layer to a few hundred meters all day.

16.2.6 The afternoon maximum

The depth peaks in the mid to late afternoon, well after the peak of solar radiation near noon. The reason is in equation (16.8): the depth depends on the accumulated heat Q, not on the instantaneous flux, and Q keeps increasing as long as the flux is positive. In the illustrative day the flux peaks at 12:30, when the depth is 1190 m; by 16:00 the flux has fallen to half its peak

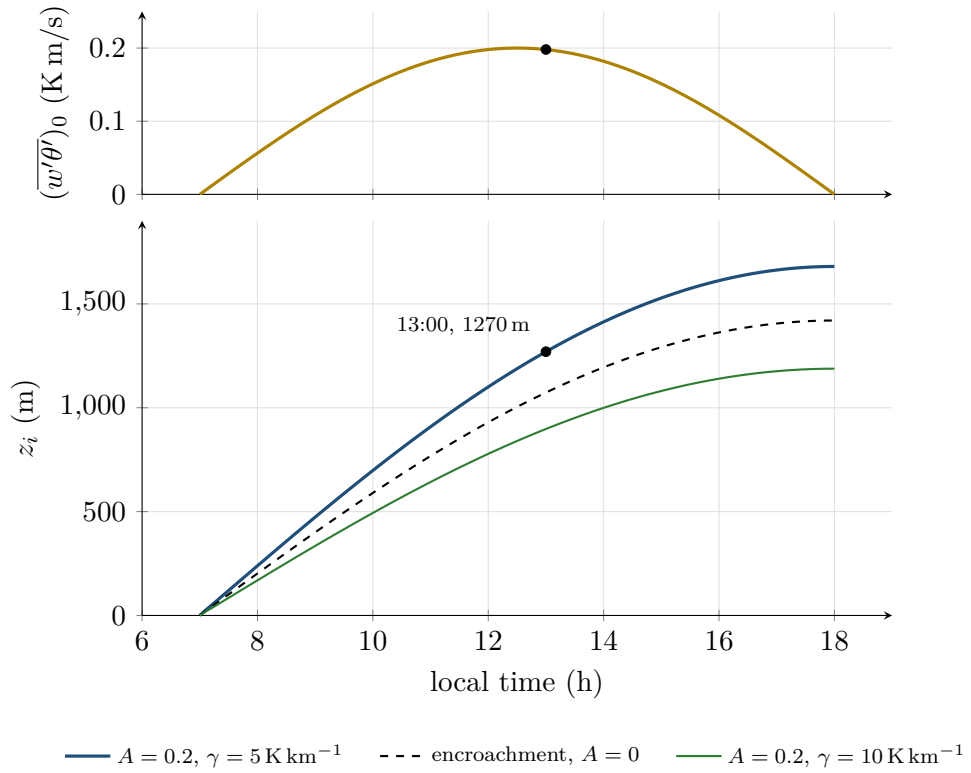


Figure 16.4: Growth of the convective boundary layer on an illustrative day. Upper: surface kinematic heat flux, $0.2 \sin[\pi(t-7)/11]$ K m s^{-1} for t in hours (equation (16.9)). Lower: depth from the slab model, $z_i = \sqrt{2(1+2A)Q/\gamma}$ (equation (16.8)), starting from zero depth at 07:00, without subsidence. Values illustrative.

value and the layer has grown by another 36 %, to 1610 m. The layer continues to be mixed while it grows, and the turbulence of the large eddies persists for a time after the flux declines.

What stops the growth is the balance in equation (16.3). Without subsidence the slab model grows until the flux reaches zero at 18:00. With subsidence the growth stops when w_e falls to $|w_s|$. In the base case $w_e = 1.4 \times 0.2 \sin[\pi(t-7)/11]/(0.005\, z_i)$ is $0.014\,\mathrm{m\,s^{-1}}$ at 16:30 and $0.0095\,\mathrm{m\,s^{-1}}$ at 17:00, so under a subsidence of $0.01\,\mathrm{m\,s^{-1}}$ the depth reaches its maximum near 17:00, lower than the curve of Figure 16.4 because the subsidence has acted all day. The afternoon depth is nearly steady for an hour or two before the evening transition (Section 16.4.7).

16.3 The convective velocity scale and the flux profiles

Convective turbulence has its own velocity scale and its own vertical profiles of the fluxes. This section derives the scale, interprets it, compares it with the friction velocity, and draws the heat and momentum flux profiles that follow from the mixed-layer budgets.

16.3.1 The convective velocity scale

The velocity of the thermals follows from their buoyancy and the depth over which it acts. A thermal with excess potential temperature θ' accelerates at $b = g\,\theta'/\overline{\theta}$ over a distance of order z_i, so its velocity satisfies $w^2 \sim b\, z_i$. The heat flux the thermals carry is of order $w\,\theta'$, and near the ground it equals the surface flux, so $\theta' \sim (\overline{w'\theta'})_0/w$. Eliminating θ', $w^3 \sim (g/\overline{\theta})\,(\overline{w'\theta'})_0\, z_i$, which defines the *convective velocity scale*

$$w_* = \left[\frac{g}{\overline{\theta}}\,(\overline{w'\theta'})_0\, z_i\right]^{1/3}, \tag{16.10}$$

in m/s; with moisture, the virtual potential temperature and its flux replace θ and $\overline{w'\theta'}$. The same scale follows from the energy budget: convective eddies with kinetic energy per unit mass of order w_*^2 turn over in a time of order z_i/w_*, so they need a supply of order w_*^3/z_i, which is the buoyancy production $P_b = (g/\overline{\theta})\,\overline{w'\theta'}$ of Chapter 8 at its surface value. Units: $(\mathrm{m\,s^{-2}\,K^{-1}}) \times (\mathrm{K\,m\,s^{-1}}) \times \mathrm{m} = \mathrm{m^3\,s^{-3}}$, whose cube root is a velocity.

For the running example at 13:00,

$$w_* = \left[\frac{9.81}{300} \times 0.198 \times 1270\right]^{1/3} = (0.0327 \times 0.198 \times 1270)^{1/3} = (8.22)^{1/3} = 2.02\,\mathrm{m\,s^{-1}}.$$

Earlier in the day the scale is smaller: at 09:00, with $(\overline{w'\theta'})_0 = 0.108\,\mathrm{K\,m\,s^{-1}}$ and $z_i = 473\,\mathrm{m}$, $w_* = (0.0327 \times 0.108 \times 473)^{1/3} = (1.67)^{1/3} = 1.19\,\mathrm{m\,s^{-1}}$. On a hot afternoon over dry ground, with $(\overline{w'\theta'})_0 = 0.35\,\mathrm{K\,m\,s^{-1}}$ ($H \approx 420\,\mathrm{W\,m^{-2}}$) and $z_i = 2500\,\mathrm{m}$, $w_* = (28.6)^{1/3} = 3.06\,\mathrm{m\,s^{-1}}$.

16.3.2 What the convective velocity scale measures

The scale is the characteristic speed of the thermals, and through them of the whole convective turbulence. A larger surface heat flux gives more buoyant thermals, and a deeper layer lets them accelerate over a longer distance; both raise w_*, but only with the cube root. Doubling either the flux or the depth raises the scale by $2^{1/3} = 1.26$. The cube root makes w_* a robust number: the three cases above span a factor of eleven in $(\overline{w'\theta'})_0\, z_i$ and less than a factor of three in w_*. Typical values are 1 to $3\,\mathrm{m\,s^{-1}}$ in moderate to strong convection.

The turbulence statistics of the mixed layer scale with w_*. The standard deviation of the vertical velocity is typically about $0.6\,w_*$ through the middle of the mixed layer, $1.2\,\mathrm{m\,s^{-1}}$ for the running example, consistent with the $1.22\,\mathrm{m\,s^{-1}}$ of the two-state picture of Section 16.1.3; the horizontal standard deviations are of the same order and nearly uniform with height. The

turnover time z_i/w_* sets how fast the layer responds: about ten minutes in the running example, so the mixed layer adjusts to a change of surface heating within half an hour, while a stable layer at night takes hours. The convective velocity scale is calculated, not measured: it needs the surface heat flux from an eddy-covariance station or a model and the depth from a profile.

16.3.3 Friction velocity against convective velocity scale

The daytime layer has two velocity scales. The friction velocity u_* (Chapter 10) measures mechanically generated turbulence, produced by the shear of the wind over the rough ground; the convective velocity scale w_* measures buoyancy-driven turbulence, produced by heating. When $w_* \gg u_*$ the layer is strongly convective; when u_* is comparable to or larger than w_*, the turbulence is mainly shear-driven. Chapter 15 showed that their ratio depends only on the ratio of depth to Obukhov length,

$$\frac{w_*}{u_*} = \left(-\frac{z_i}{\kappa\, L_{\mathrm{O}}} \right)^{1/3} . \tag{16.11}$$

Table 16.1 evaluates three afternoons with the surface flux and depth of the running example at 13:00 and three winds over the same farmland. Its columns are the friction velocity, the wind at 20 m that goes with it (from the unstable profile of Chapter 14), the Obukhov length, the ratio $-z_i/L_{\mathrm{O}}$, the ratio w_*/u_* and the regime. The convective velocity scale is $2.02\,\mathrm{m\,s^{-1}}$ in every row; only the wind changes. In a light wind the layer is strongly convective, with w_* eight times u_*; in the running example it is moderately convective, with a ratio of three; in a strong wind the two scales are equal and shear and buoyancy share the work. The last column anticipates Section 16.5.1.

Table 16.1: The two velocity scales on three afternoons with $(\overline{w'\theta'})_0 = 0.198\,\mathrm{K\,m\,s^{-1}}$ ($H = 240\,\mathrm{W\,m^{-2}}$), $z_i = 1270\,\mathrm{m}$ and $w_* = 2.02\,\mathrm{m\,s^{-1}}$, over farmland ($z_0 = 0.05\,\mathrm{m}$). L_{O} from $-92\,110\,u_*^3/H$. Values illustrative.

u_* (m/s)	U_{20} (m/s)	L_{O} (m)	$-z_i/L_{\mathrm{O}}$	w_*/u_*	Regime
0.25	2.6	−6	211	8.1	strongly convective; cells
0.65	9.0	−106	12	3.1	moderately convective; rolls likely
1.00	14.6	−386	3.3	2.0	shear and convection comparable

16.3.4 The heat flux profile

The heat flux varies strongly with height in a CBL, and its profile follows from the mixed-layer budget. In a well-mixed layer θ_m warms at the same rate at every height, so $\partial\theta/\partial t = -\partial\overline{w'\theta'}/\partial z$ is independent of height, and the flux is a straight line between its surface value and its value at the top:

$$\frac{\overline{w'\theta'}(z)}{(\overline{w'\theta'})_0} = 1 - (1+A)\,\frac{z}{z_i} = 1 - 1.2\,\frac{z}{z_i} \qquad (0 \le z \le z_i). \tag{16.12}$$

It is positive at the surface, decreases upward, crosses zero at $z = z_i/1.2 = 0.83\,z_i$, and is negative above, reaching $-0.2\,(\overline{w'\theta'})_0$ at the top. The negative part is the *entrainment heat flux*: in the entrainment zone, warmer free-atmosphere air is mixed downward, so heat moves down. For the running example at 13:00 the surface flux is $+240\,\mathrm{W\,m^{-2}}$, the flux at the top $-48\,\mathrm{W\,m^{-2}}$, the zero crossing at 1060 m, and the layer warms at $1.2 \times 0.198/1270 = 1.87 \times 10^{-4}\,\mathrm{K\,s^{-1}}$, about 0.67 K per hour.

Figure 16.5 draws this profile, left, beside the momentum flux profile of the next subsection, right. In both panels the vertical axis is height divided by z_i and the horizontal axis the flux

divided by its surface value; the vertical dashed line at one is what a constant flux would be, and the green band is the lowest tenth of the layer. The heat flux leaves the dashed line immediately: it is within 10 % of its surface value only below $0.083\,z_i$, about 105 m in the running example. Across the entrainment zone it returns from its minimum to zero in the free atmosphere, where there is no turbulence.

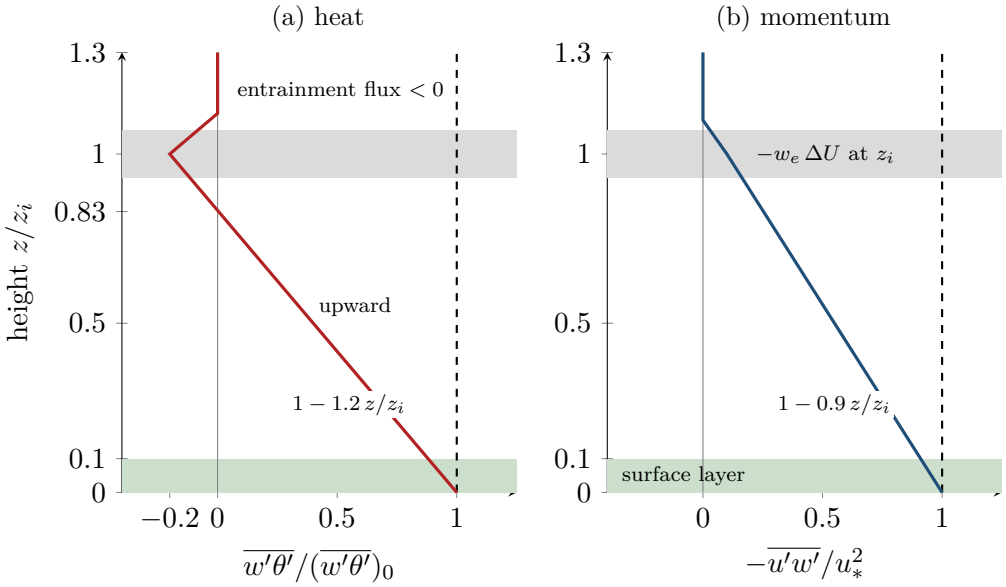


Figure 16.5: Flux profiles in the convective boundary layer, normalized by their surface values. (a) Kinematic heat flux, $1 - (1 + A)\,z/z_i$ with $A = 0.2$ (equation (16.12)). (b) Kinematic along-wind momentum flux, $1 - 0.9\,z/z_i$, reaching the entrainment value $w_e\Delta U/u_*^2 \approx 0.1$ at the top (running example: $w_e = 0.044\,\mathrm{m\,s^{-1}}$, $\Delta U = 1\,\mathrm{m\,s^{-1}}$, $u_* = 0.65\,\mathrm{m\,s^{-1}}$). Dashed: constant flux. Green: lowest tenth of the layer. Gray: entrainment zone. Schematic; values illustrative.

16.3.5 The momentum flux profile

The magnitude of the momentum flux, $|\overline{u'w'}|$, is largest near the surface and decreases toward the top of the layer. The same argument as for heat gives its shape. The along-wind momentum budget of the mixed layer is $\partial U/\partial t = F_p - \partial\overline{u'w'}/\partial z$, where F_p is the along-wind part of the pressure-gradient force, nonzero because the wind in the boundary layer crosses the isobars (the Coriolis force has no component along the wind). If the mixed-layer wind is uniform with height and F_p is nearly uniform, $\partial\overline{u'w'}/\partial z$ is nearly constant and the stress falls linearly from its surface value $-u_*^2$ to the entrainment value $-w_e\,\Delta U$ at the top. For the running example the top value is $-0.044 \times 1.0 = -0.044\,\mathrm{m^2\,s^{-2}}$ and the surface value $-0.65^2 = -0.42\,\mathrm{m^2\,s^{-2}}$, so the stress at the top is about a tenth of that at the ground, the profile of Figure 16.5(b).

The momentum flux is negative throughout: momentum moves downward everywhere in the layer. The ground is the sink; the pressure-gradient force across the depth of the layer and the entrainment of faster air at the top are the sources. The real profile is less tidy than the line in the figure. The wind direction changes with height, so the cross-wind flux $\overline{v'w'}$ is not zero, and the mixed-layer wind is not perfectly uniform; but the decrease of the stress from the ground to the top is a robust property of the daytime layer.

16.3.6 Constant flux only near the ground

The surface-layer theories of Chapters 12 to 15 assume that the stress and the heat flux are constant with height, so that u_* and $(\overline{w'\theta'})_0$ describe the whole layer in which they are applied.

Figure 16.5 shows how far that assumption holds in a CBL. The heat flux is within 10 % of its surface value up to $0.083\,z_i$ and the stress up to $0.11\,z_i$; both fall to half their surface values at 0.42 and $0.56\,z_i$. In the running example the constant-flux layer is therefore about 100 to 140 m deep, the lowest tenth of the layer, which is the usual definition of the surface layer.

Two consequences follow for the wind. Below about $0.1\,z_i$ the profile formulas of Chapter 14 apply with the surface fluxes, and a 20 m wind sensor or a transmission conductor sits well inside that layer. Above it they do not: at a hub height of 150 m in a 1270 m layer, the heat flux has already fallen by 14 % and the stress by 11 %, and the wind profile there belongs to the mixed layer rather than to the surface layer. The constant-flux assumption is a property of the lowest tenth of the boundary layer, not of the boundary layer.

16.4 Convection and the near-surface wind

The consequences of convection that matter most for engineering are those for the wind near the ground. This section explains why the daytime surface wind is stronger and gustier, why the wind aloft can weaken, how uniform the mixed-layer wind is, and how the transitions at either end of the day change the wind, with a worked morning and afternoon profile.

16.4.1 Downward mixing of momentum

Convection mixes higher-momentum air downward. A downdraft starting hundreds of meters up carries the faster wind of that height toward the ground, and a thermal rising from the ground carries slow air upward; the net effect is a downward flux of momentum through the whole layer (Section 16.3.5). The chain is

daytime heating → stronger vertical mixing → downward momentum transport → stronger near-surface wind,

and it operates with little or no change in the synoptic pressure gradient. The pressure gradient sets how much momentum the boundary layer receives; the mixing sets how it is shared between heights.

The near-surface wind therefore has a daily cycle over land even when the large-scale flow is steady: weak at night, when a stable layer decouples the ground from the air above, strong in the afternoon, when convection couples them. Chapter 6 described this cycle and the height, often between 50 and 100 m, above which its phase reverses. The rest of this section quantifies it.

16.4.2 Gustiness

Convective eddies are large and energetic, and a point at the ground sees them pass as alternations of downdrafts, which bring fast air down, and updraft bases, where slower air converges. The daytime near-surface wind is therefore stronger in the mean, with larger gusts, larger vertical velocity fluctuations and a higher turbulence intensity than the nighttime wind. This combination is the signature of turbulent coupling between the ground and the air aloft.

The horizontal fluctuations near the ground depend on both velocity scales. A standard empirical form for unstable conditions is

$$\sigma_u \approx u_* \left(12 + 0.5\,\frac{z_i}{|L_{\mathrm{O}}|}\right)^{1/3}, \tag{16.13}$$

which reduces to $\sigma_u \approx 2.3\,u_*$ in neutral conditions. For the running example, $\sigma_u = 0.65 \times (12 + 0.5 \times 12)^{1/3} = 0.65 \times 2.62 = 1.70\,\mathrm{m\,s^{-1}}$ and $\mathrm{TI} = 1.70/9.0 = 0.19$; the neutral value with the same u_* would be $1.49\,\mathrm{m\,s^{-1}}$. With the gust relation of Chapter 8, $U_{\mathrm{gust}} = \overline{U}(1 + g_{\mathrm{pk}}\,\mathrm{TI})$, and

a peak factor of 3, the three-second gust is $9.0 \times (1 + 3 \times 0.19) = 14.1\,\mathrm{m\,s^{-1}}$. In the light-wind afternoon of Table 16.1, $\sigma_u = 0.25 \times (12 + 0.5 \times 211)^{1/3} = 0.25 \times 4.90 = 1.22\,\mathrm{m\,s^{-1}}$ on a mean of $2.6\,\mathrm{m\,s^{-1}}$, a turbulence intensity of 0.47: the wind is weak in the mean and dominated by the convective eddies, with gusts more than twice the mean. At 08:00 on the stable morning of Section 16.4.5, with $u_* \approx 0.2\,\mathrm{m\,s^{-1}}$ and $\sigma_u \approx 2.3\,u_* = 0.46\,\mathrm{m\,s^{-1}}$ on a mean of $4\,\mathrm{m\,s^{-1}}$, the intensity is about 0.12 and the gust about $5.4\,\mathrm{m\,s^{-1}}$. The vertical fluctuations behave similarly: σ_w near the ground grows with height in a CBL, toward the typical $0.6\,w_*$ of the mixed layer.

16.4.3 Wind aloft can decrease

Mixing redistributes momentum; it does not create it. If the near-surface wind gains momentum by mixing, some layer above must lose it, and the wind at some upper levels decreases slightly when convection starts. In the running example the wind at 200 m falls from 14 to $13\,\mathrm{m\,s^{-1}}$ between 08:00 and 13:00 while the wind at 20 m more than doubles.

This conservation view gives a useful check on any explanation of a daytime surface-wind increase. If the wind near the ground increases and the wind aloft does not decrease, the extra momentum came from somewhere else: a change in the pressure gradient, advection, or a thermally driven circulation (Chapter 19). If the wind aloft decreases by about as much momentum as the surface layer gains, mixing is the explanation. Section 16.4.5 carries out the check on two profiles.

16.4.4 Mixed-layer wind

Through part of the mixed layer, wind speed and direction become more uniform with height. The shear is concentrated in the surface layer at the bottom and in the entrainment zone at the top, and it is much smaller in between than on a stable night, when the wind can change by $10\,\mathrm{m\,s^{-1}}$ and tens of degrees across a few hundred meters. The mixed-layer wind is usually somewhat weaker than the geostrophic wind and turned slightly toward low pressure, because the friction at the ground is communicated through the whole layer.

The uniformity is not perfect. The ground removes momentum continuously, so the wind still increases with height through the lower part of the mixed layer, and the wind direction still turns through the layer, in the sense set by the hemisphere (clockwise with height in the Northern Hemisphere, counterclockwise in the Southern, as in the Ekman spiral of Chapter 3), though by less than at night. In the running example the wind increases from $10.6\,\mathrm{m\,s^{-1}}$ at 100 m to $13.0\,\mathrm{m\,s^{-1}}$ at 200 m and then stays within $0.3\,\mathrm{m\,s^{-1}}$ of $13\,\mathrm{m\,s^{-1}}$ up to 1180 m (Figure 16.2).

16.4.5 A morning and an afternoon profile

An illustrative pair of profiles shows the redistribution. At 08:00 the wind is $U_{200} = 14\,\mathrm{m\,s^{-1}}$ at 200 m and $U_{20} = 4\,\mathrm{m\,s^{-1}}$ at 20 m: a stable surface layer, with $u_* \approx 0.2\,\mathrm{m\,s^{-1}}$ and $L_\mathrm{O} \approx 50\,\mathrm{m}$, is weakly coupled to strong wind left aloft by the night, with a maximum of $15.5\,\mathrm{m\,s^{-1}}$ near 300 m. At 13:00 the wind is $U_{200} = 13\,\mathrm{m\,s^{-1}}$ and $U_{20} = 9\,\mathrm{m\,s^{-1}}$: the running example. The large-scale wind barely changed; the coupling did.

Figure 16.6 plots both profiles. The horizontal axis is wind speed and the vertical axis height, from the ground to 1000 m. The blue line is 08:00 and the gold line 13:00; dots mark the values at 20 and 200 m. The gold shading below about 140 m, where the two profiles cross, is where the afternoon wind is faster; the blue shading above is where the morning wind was faster. The gold area is the momentum gained near the ground, and the blue area the momentum lost aloft.

Table 16.2 integrates the two profiles. Its rows are the lowest 100 m, the layer from 100 to 1000 m, and the lowest kilometer; its columns are the integrated speed $\int U\,\mathrm{d}z$ at each time, the momentum per unit area divided by the air density, in $\mathrm{m^2\,s^{-1}}$, by the trapezoidal rule on

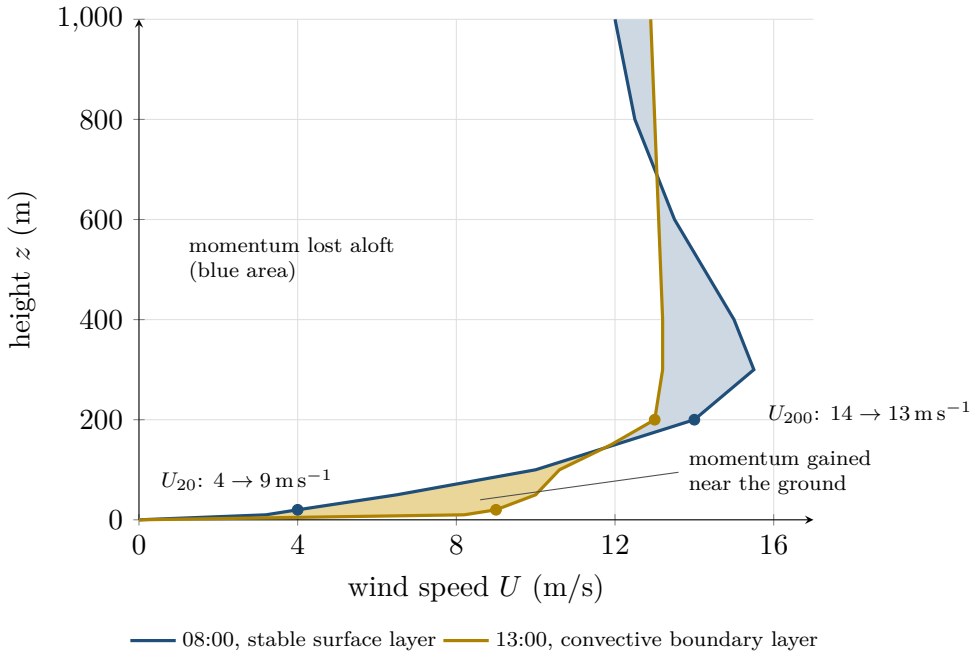


Figure 16.6: Wind profiles at 08:00 (stable surface layer under the wind left aloft by the night) and 13:00 (convective boundary layer of the running example). Gold: where the 13:00 wind is faster; blue: where the 08:00 wind was faster. Profiles are piecewise linear between tabulated heights; values illustrative.

the tabulated profile, the change, and the layer-mean wind at each time. The lowest 100 m gains $305\,\mathrm{m^2\,s^{-1}}$, half again its morning value; the layer above loses $455\,\mathrm{m^2\,s^{-1}}$, about 4 %; the kilometer as a whole changes by about 1 %. The gain near the ground is matched by a loss aloft: the afternoon wind at 20 m is morning wind from higher up, not new momentum.

Table 16.2: Layer-integrated speed $\int U\,\mathrm{d}z$ (momentum per unit area divided by density) for the profiles of Figure 16.6, trapezoidal rule. Values illustrative.

Layer	08:00 ($\mathrm{m^2/s}$)	13:00 ($\mathrm{m^2/s}$)	Change	Mean wind, 08:00 / 13:00 (m/s)
0 to 100 m	622	927	+305	6.2 / 9.3
100 to 1000 m	12 100	11 645	−455	13.4 / 12.9
0 to 1000 m	12 722	12 572	−150	12.7 / 12.6

The total is not exactly conserved in a real case, because the along-wind pressure force adds momentum and the surface drag removes it; over five hours each of these is several thousand $\mathrm{m^2\,s^{-1}}$ (the drag alone, $\int u_*^2\,\mathrm{d}t$, is about $3600\,\mathrm{m^2\,s^{-1}}$ for a friction velocity rising steadily from 0.2 to $0.65\,\mathrm{m\,s^{-1}}$ over the five hours). With steady large-scale forcing the two nearly cancel, and the profiles here are constructed so that they do, to about 1 %. The comparison also ignores the turning of the wind with height; with direction included, the same budget applies to each horizontal component of the vector momentum. A forecast that gets U_{20} right at 13:00 by raising the wind everywhere, instead of moving momentum down, is right for the wrong reason, and it will be wrong at 200 m.

16.4.6 The morning transition and the morning wind jump

At sunrise the boundary layer consists of a stable surface layer, often 100 to 300 m deep, under a residual layer: the remnant of the previous afternoon's mixed layer, nearly neutral and often carrying strong wind, since it was decoupled from the ground all night (Chapter 18 treats the jet that can form there). The *morning transition* is the period in which a shallow turbulent layer forms at the ground, grows, and erodes this structure. Wind speed, direction, turbulence and temperature all change quickly during it. Chapter 6 estimated the erosion time from a heat budget: a 200 m stable layer with a deficit of 7.5 K at the ground needs 750 K m of heat, which a mean morning flux of $0.1\,\mathrm{K\,m\,s^{-1}}$ supplies in about two hours.

Until the stable layer is gone, the surface stays decoupled and the near-surface wind weak. When the mixed layer breaks through into the residual layer, whose γ is close to zero, it grows by hundreds of meters within an hour (equation (16.8) with small γ), and the ground is reconnected to the momentum stored aloft:

$$\text{morning mixing} \rightarrow \text{recoupling} \rightarrow \text{sudden surface wind increase.}$$

This is the *morning wind jump*. In the example of Section 16.4.5, the 20 m wind can rise from about 4 to about $8\,\mathrm{m\,s^{-1}}$ within an hour in the middle of the morning, when the mixed layer reaches the $15\,\mathrm{m\,s^{-1}}$ air near 300 m. The convective cooling of an overhead conductor rises with the wind, so the rating of a line at 20 m can change as quickly.

The direction changes too. In the stable morning layer the wind turns strongly with height: clockwise with height in the Northern Hemisphere ($f > 0$), counterclockwise in the Southern ($f < 0$). As the ground couples to the air aloft, the near-surface direction moves toward the direction aloft. At a site in southern Brazil (Southern Hemisphere) with the 20 m wind from 060° and the 200 m wind from 020° at 08:00 (backed by 40° with height), a midday difference of about 10° means that the surface wind has backed by about 30°, to about 030°, during the morning. At the mirror site in the Northern Hemisphere the surface wind veers by the same amount. A wind-direction record that turns by tens of degrees in an hour after sunrise, together with a jump in speed, is the signature of recoupling.

16.4.7 The evening transition

Near sunset, typically within an hour or so before it, the net radiation falls below what the ground loses to the soil and to evaporation, and the surface heat flux passes through zero. Convective turbulence then loses its source and decays, and the cooling ground begins to build a stable stratification from below. The *evening transition* is this sequence: heat flux to zero, decay of the convective eddies, formation of a stable surface layer. Near the ground the wind drops as the surface is decoupled from the air above; aloft the wind is released from the drag of the ground and begins to accelerate, the start of the nighttime jet of Chapter 18.

Turbulence does not vanish at once. The large eddies take several turnover times to decay, and the turnover time grows as the heating weakens: in the illustrative day, at 17:00, $(\overline{w'\theta'})_0 = 0.056\,\mathrm{K\,m\,s^{-1}}$, $z_i = 1660\,\mathrm{m}$, $w_* = (0.0327 \times 0.056 \times 1660)^{1/3} = 1.45\,\mathrm{m\,s^{-1}}$, and $z_i/w_* \approx 19$ minutes. The mixed layer above the new stable layer does not disappear: it keeps its potential temperature, humidity and much of its momentum and becomes the residual layer, the memory of the day that the next morning's convection will reconnect to. The transition is therefore gradual, over one to two hours, and it begins at the ground and spreads upward.

16.5 Organized convection and the limits of local theory

Convection is not purely random. This section describes the organized forms it takes and what they mean for a point measurement, then explains why local similarity theory and local closures fail in a deep convective layer, and how weather models represent the transport they miss.

16.5.1 Convective cells and horizontal convective rolls

The thermals and downdrafts of a CBL often organize. In weak wind they form *convective cells*, polygonal patterns of rising and sinking air a few times z_i across, with updrafts at the cell walls (open cells) or in the cell centers. With moderate wind and shear they form *horizontal convective rolls*: elongated pairs of counter-rotating circulations with axes roughly aligned with the mean wind, or with the shear vector of the layer, within about 10 to 20° in either hemisphere. A roll is about as wide as the layer is deep, a counter-rotating pair two to three times z_i, so rolls are about 1 to 5 km wide and tens of kilometers long. Rolls form when both buoyancy and shear matter: buoyancy drives the overturning and shear organizes it into lines along the wind. Where the updraft branches reach the condensation level they produce parallel lines of cumulus, *cloud streets*, visible in satellite images.

Which form appears depends on the balance of buoyancy and shear in the whole layer, measured by $-z_i/L_O$ (Chapter 15). Rolls are most often observed when $-z_i/L_O$ is between a few and about 25; cells dominate above about 25; below a few, shear dominates and the convection is weak and poorly organized. These are typical ranges with wide scatter between studies. In Table 16.1 the running example ($-z_i/L_O = 12$) lies in the roll range, the light-wind afternoon (211) in the cell range.

Figure 16.7 draws rolls in a vertical cross section perpendicular to the mean wind, which blows into the page. The horizontal axis is cross-wind distance in kilometers and the vertical axis height up to the top of the layer. The six ellipses are counter-rotating rolls, each with its sense of rotation marked by an arrow; where two neighbors both turn upward there is an updraft branch, with a cumulus cloud above it, and where both turn downward a downdraft branch. The lower panel is the near-surface wind along the same line: stronger beneath the downdraft branches, which bring fast air down, and weaker beneath the updraft branches, where slow air from the ground converges. The bands of enhanced up- and downdraft and of locally stronger surface wind run along the wind for tens of kilometers.

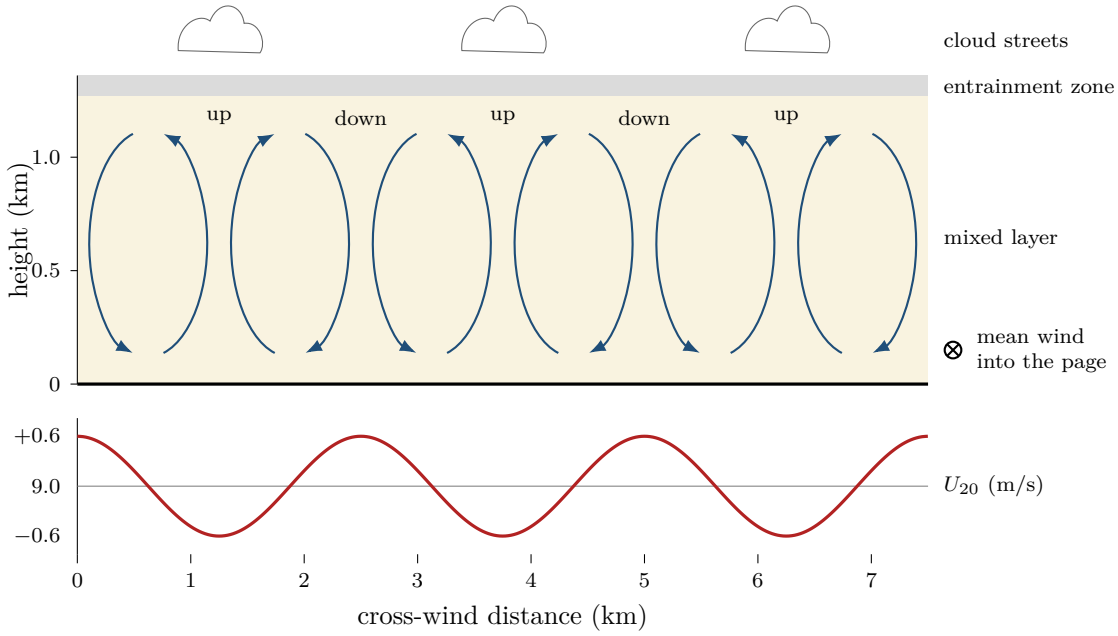


Figure 16.7: Horizontal convective rolls in a vertical cross section perpendicular to the mean wind (schematic). Upper: six counter-rotating rolls in a mixed layer 1.27 km deep, wavelength of a pair 2.5 km; cumulus clouds form over the updraft branches. Lower: wind at 20 m along the same line, $9.0 \pm 0.6\,\mathrm{m\,s^{-1}}$, strongest under the downdraft branches. Values illustrative.

16.5.2 Point measurements in organized convection

A sensor at a fixed point samples whatever part of the convective structure is over it. It may sit for a time beneath a downdraft, an updraft or the convergence line of a roll, and its record can then depart substantially from the mean over the surrounding area, even over flat, uniform terrain. Rolls are particularly persistent: they drift slowly across the wind and can keep a mast under the same branch for an hour or more, so that a mast under a downdraft band reads, in the illustrative numbers of Figure 16.7, about $0.6\,\mathrm{m\,s^{-1}}$ above the area mean, and a mast 1.25 km away the same amount below, for the whole period.

Unorganized thermals add sampling noise to the averages. With thermals spaced about $1.5\,z_i \approx 1.9\,\mathrm{km}$ apart and carried by a mixed-layer wind of $13\,\mathrm{m\,s^{-1}}$, one passes a point every 150 s, about four in a ten-minute average. A ten-minute mean then rests on few independent samples, and its sampling error is roughly $\sigma_u/\sqrt{4} = 1.70/2 \approx 0.85\,\mathrm{m\,s^{-1}}$, about 9 % of the $9\,\mathrm{m\,s^{-1}}$ mean of the running example (a rough estimate). Comparing a point measurement with the grid-cell wind of a weather model, which averages over many thermals or rolls, requires longer averages on convective afternoons than on windy overcast days, and differences of this size are not model errors.

16.5.3 Limits of local similarity

Monin–Obukhov similarity describes the surface layer with local quantities: the height z, the surface fluxes and the Obukhov length. In a deep CBL the large eddies span much of z_i, and a sensor at 20 m is influenced by eddies hundreds of meters deep that reach it from above as downdrafts. Quantities that these eddies dominate depend on z_i, which local similarity does not contain. The horizontal velocity variance is the clearest case: equation (16.13) contains $z_i/|L_\mathrm{O}|$, and on the light-wind afternoon of Table 16.1 it makes σ_u more than twice the $2.3\,u_*$ that local scaling gives. Two sites with the same u_* and L_O but different depths have different horizontal turbulence near the ground.

The mean wind and temperature gradients near the ground follow local similarity more closely, because they are set by the small eddies near the surface, and the profile formulas remain useful below about $0.1\,z_i$. What fails is the assumption that the flow at a height is determined by what happens at that height. In a convective layer the turbulence is *nonlocal*: the flux and the variance at a point are set by eddies that span the whole layer.

16.5.4 Nonlocal transport

A *local closure* writes a flux as an eddy diffusivity times the local gradient, $\overline{w'\theta'} = -K_h\,\partial\theta/\partial z$ (Chapter 9). Thermals carry heat, moisture and momentum over large vertical distances regardless of the local gradient: they leave the ground warm and keep their excess temperature as they rise through the nearly neutral mixed layer. Where the gradient is zero a local closure gives no flux; where it is slightly positive, in the upper mixed layer, it gives a downward flux, while the real flux is upward. *Nonlocal transport* is this transport by eddies as large as the layer, which depends on the surface forcing and the depth rather than on the local gradient.

Many boundary-layer schemes therefore add a nonlocal term. One widely used form is

$$\overline{w'\theta'} = -K_h\left(\frac{\partial\theta}{\partial z} - \gamma_c\right), \qquad \gamma_c \approx 6.5\,\frac{(\overline{w'\theta'})_0}{w_*\,z_i}, \qquad K_h(z) = \kappa\,w_*\,z\left(1-\frac{z}{z_i}\right)^2, \tag{16.14}$$

where γ_c is the counter-gradient correction, in K/m, and the coefficient 6.5 and the use of w_* as the velocity scale are simplifications of the published form. For the running example, $\gamma_c = 6.5 \times 0.198/(2.02 \times 1270) = 5.0 \times 10^{-4}\,\mathrm{K\,m^{-1}}$, half a kelvin per kilometer, and at mid-depth $K_h = 0.4 \times 2.02 \times 635 \times 0.25 = 128\,\mathrm{m^2\,s^{-1}}$. Where the mixed layer has no gradient the nonlocal term alone carries $128 \times 5.0 \times 10^{-4} = 0.064\,\mathrm{K\,m\,s^{-1}}$, the same order as the

$0.4 \times 0.198 = 0.079\,\mathrm{K\,m\,s^{-1}}$ of the linear profile at mid-depth, while the local term carries nothing. Another family of schemes represents the thermals explicitly as a mass flux of updrafts added to an eddy diffusivity for the small eddies. Either way the scheme adds to the local diffusion a transport that responds to the surface heating directly.

16.5.5 Convective boundary-layer schemes

A weather model cannot resolve thermals unless its grid spacing is tens of meters; at kilometer spacing they are parameterized. Its convective boundary-layer scheme must supply: the depth z_i, usually diagnosed from a bulk Richardson number or a parcel rising from the surface; the nonlocal mixing of the previous subsection; the entrainment at the top, explicitly through a prescribed entrainment flux or implicitly through the diffusivity profile; the surface fluxes, from the land-surface model and the surface-layer formulas; and the profile of the eddy diffusivities through the layer.

Different schemes make different choices for each, and they give different daytime wind profiles, temperatures and depths from the same large-scale forcing: depths that differ by hundreds of meters and winds at 100 m that differ by 1 to $2\,\mathrm{m\,s^{-1}}$ are possible between schemes (illustrative). The diagnostic of Chapter 15 applies: a model that is too weakly mixed by day underpredicts the surface wind with the wind aloft correct, and the cause may lie in the scheme as much as in the surface heat flux. Boundary-layer parameterizations are the subject of Chapter 26.

16.6 The surface beneath the convective layer

The strength of convection is set at the ground. This section describes how terrain and surface heterogeneity make the heating uneven, writes the surface energy balance, uses the Bowen ratio to compare a dry and a wet surface, and follows the chain from soil moisture to the wind.

16.6.1 Terrain and uneven heating

Over sloping ground the heating is not uniform. Slopes facing the sun receive more direct sunlight per unit area than flat ground, and slopes facing away receive less, because the irradiance on a surface is proportional to the cosine of the angle between the sun and the normal to the surface. At 25°S at the June solstice, when the noon sun is 41.6° above the northern horizon, the noon direct beam falls on flat ground at a zenith angle of 48.4° ($\cos = 0.663$), on a north-facing 20° slope at 28.4° ($\cos = 0.879$) and on a south-facing one at 68.4° ($\cos = 0.367$). The sunny slope receives 1.33 times the direct beam of flat ground, the shaded slope 0.55 times, a ratio of 2.4 between them. In the Southern Hemisphere the equator-facing slopes are those facing north; in the Northern Hemisphere, at 25°N in December, the same numbers hold for south-facing slopes.

Uneven heating drives circulations: air rises along heated slopes as upslope winds, valleys develop along-valley winds, and ridges and sunny slopes become preferred sources of thermal plumes. The daytime wind in complex terrain therefore reflects convection and terrain-driven mesoscale circulation together. Chapter 19 treats slope and valley winds, and Chapter 20 the mechanical effects of terrain on the flow.

16.6.2 Surface heterogeneity

Flat ground is not uniform either. Dry soil, irrigated crops, forest, urban surfaces and water divide the energy they receive differently between heating the air, evaporating water and warming the ground. Over a dry field most of the energy heats the air; over an irrigated field or a forest in leaf most of it evaporates water; over water little of it heats the air at all by day.

Neighboring boundary layers can therefore differ in heat flux by a factor of several, and in depth and convective velocity accordingly.

The differences drive their own circulations and structures. Contrasts in heating over a few kilometers or more produce thermal circulations, with flow from the cooler toward the warmer surface near the ground, the same mechanism as the sea breeze (Chapter 19). Air crossing from one surface to another develops an internal boundary layer (Chapter 7), whose depth grows with distance from the change. And the wind near the ground varies horizontally, since the coupling to the air aloft differs from patch to patch. The scale of the heterogeneity matters: patches much smaller than z_i are blended by the thermals, while patches larger than a few times z_i develop boundary layers of their own.

16.6.3 The surface energy balance

The energy that drives convection is the part of the net radiation that the surface passes to the air as sensible heat. The *surface energy balance* states that the net radiation absorbed by the surface is divided among three fluxes:

$$R_n = H + LE + G_s, \tag{16.15}$$

with every term in $\mathrm{W\,m^{-2}}$. R_n is the net radiation, absorbed sunlight plus absorbed longwave radiation minus emitted longwave radiation, positive into the surface. H is the sensible heat flux and LE the latent heat flux, the evaporation rate times the latent heat of vaporization $L_v = 2.5 \times 10^6\,\mathrm{J\,kg^{-1}}$, both positive upward. G_s is the ground heat flux, positive into the soil. Storage in vegetation and buildings and the energy used by photosynthesis are neglected. The available energy $R_n - G_s$ is what the surface divides between H and LE.

The terms are measured at flux stations: R_n by a net radiometer, G_s by heat-flux plates in the soil, H and LE by eddy covariance (Chapter 9); measured terms typically leave a residual of ten to thirty percent that does not close the balance. A weather model computes all four in its land-surface scheme, from the radiation, the soil moisture, the vegetation and the surface temperature. The sensible heat flux H, divided by $\rho\, c_p$, is the $(\overline{w'\theta'})_0$ that drives every quantity of this chapter.

16.6.4 The Bowen ratio and a dry and a wet surface

The *Bowen ratio* is the ratio of the sensible to the latent heat flux,

$$B = \frac{H}{LE}, \qquad H = \frac{B}{1+B}\,(R_n - G_s), \qquad LE = \frac{1}{1+B}\,(R_n - G_s). \tag{16.16}$$

It is large over dry surfaces, which have little water to evaporate, and small over moist ones; typical values are above 5 over deserts, 1 to 3 over dry grassland, 0.2 to 0.5 over well-watered crops and forest in leaf, and about 0.1 over the sea. It is measured directly by the *Bowen-ratio method*: with the same eddy diffusivity for heat and water vapor, $B = (c_p/L_v)\,\Delta\theta/\Delta q$ from the differences of potential temperature and specific humidity between two heights. A drop of 0.60 K and of $0.80\,\mathrm{g\,kg^{-1}}$ between 1 and 4 m gives $B = (1004/2.5 \times 10^6) \times 0.60/0.00080 = 0.30$, a wet surface.

Consider the same available energy over two surfaces: a peak of $R_n - G_s = 450\,\mathrm{W\,m^{-2}}$ at 12:30 on the illustrative day, a dry surface with $B = 3$ and a wet one with $B = 0.25$. Figure 16.8 shows the partition. Each bar is the available energy, divided into sensible heat (gold) and latent heat (blue), with the scale in $\mathrm{W\,m^{-2}}$ below. The dry surface sends $338\,\mathrm{W\,m^{-2}}$ into sensible heat and $113\,\mathrm{W\,m^{-2}}$ into evaporation; the wet surface sends $90\,\mathrm{W\,m^{-2}}$ into sensible heat and $360\,\mathrm{W\,m^{-2}}$ into evaporation. The same sunshine heats the air nearly four times as strongly over the dry surface.

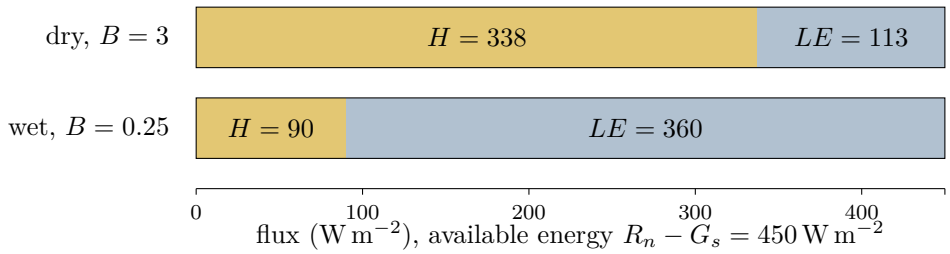


Figure 16.8: Partition of the same available energy, $R_n - G_s = 450\,\mathrm{W\,m^{-2}}$, between sensible heat H (gold) and latent heat LE (blue) over a dry surface ($B = 3$) and a wet surface ($B = 0.25$), from equation (16.16). Values illustrative.

Table 16.3 carries the two partitions through the slab model and the velocity scales. Its rows are the peak fluxes, the depth at 13:00 and at the end of the day from equation (16.8) (same day shape, $\gamma = 5\,\mathrm{K\,km^{-1}}$, $A = 0.2$; the depth scales with the square root of the peak flux, from the 1270 m of the base case with a peak of $0.2\,\mathrm{K\,m\,s^{-1}}$), the convective velocity scale at 13:00, and, for a wind with $u_* = 0.5\,\mathrm{m\,s^{-1}}$ on both days, the Obukhov length, the ratio $-z_i/L_\mathrm{O}$ and the expected organization. The dry surface gives a layer 1500 m deep at 13:00 with $w_* = 2.39\,\mathrm{m\,s^{-1}}$; the wet surface a layer half as deep, 780 m, with $w_* = 1.23\,\mathrm{m\,s^{-1}}$. The dry day is strongly convective and organized in cells; the wet day, under the same wind, is in the roll range near its weak end.

Table 16.3: A dry and a wet surface under the same available energy, peak $450\,\mathrm{W\,m^{-2}}$ at 12:30, on the illustrative day of Section 16.2.4. Values illustrative.

Quantity	Dry	Wet
Bowen ratio B	3	0.25
Peak sensible heat flux H (W m^{-2})	338	90
Peak latent heat flux LE (W m^{-2})	113	360
Peak kinematic heat flux $(\overline{w'\theta'})_0$ (K m s^{-1})	0.280	0.075
Depth z_i at 13:00 (m)	1500	780
Depth z_i at 18:00 (m)	1990	1030
Convective velocity scale w_* at 13:00 (m/s)	2.39	1.23
Obukhov length L_O at 13:00, $u_* = 0.5\,\mathrm{m\,s^{-1}}$ (m)	−35	−129
Ratio $-z_i/L_\mathrm{O}$ at 13:00	44	6.0
Organization (Section 16.5.1)	cells	rolls

The table uses the sensible heat flux alone. Water vapor is lighter than dry air, so evaporation also makes the air near the ground buoyant, and the buoyancy flux is that of the virtual potential temperature, approximately $\overline{w'\theta'} + 0.61\,\overline{\theta}\,\overline{w'q'}$. Over the wet surface the peak moisture flux is $LE/(\rho L_v) = 360/(1.2 \times 2.5 \times 10^6) = 1.2 \times 10^{-4}\,\mathrm{m\,s^{-1}}$, which adds $0.61 \times 300 \times 1.2 \times 10^{-4} = 0.022\,\mathrm{K\,m\,s^{-1}}$ to the 0.075 of sensible heat, a buoyancy flux 29 % larger; over the dry surface it adds 2 %. The correction raises w_* over the wet surface by $1.29^{1/3} = 1.09$ and leaves the comparison intact: the dry surface makes more sensible heat, stronger heating, a deeper layer and stronger convection; the wet surface makes more latent heat and a shallower, cooler and moister layer.

16.6.5 From soil moisture to wind

The chapter's results combine into one chain from the ground to the wind:

soil moisture → surface energy partition → sensible heat flux → convection → momentum mixing → near-surface wind.

Each link has been quantified. Soil moisture sets the Bowen ratio; the Bowen ratio divides the available energy (Figure 16.8); the sensible heat flux sets the growth of the layer and its convective velocity (Table 16.3); the depth and the strength of the convection set how much momentum is brought down from aloft (Section 16.4.5) and how gusty the surface wind is (Section 16.4.2). A drought, an irrigation season or a wet spell after rain therefore changes the daytime wind near the ground without any change in the large-scale weather.

For forecasting this makes land-surface modeling part of wind forecasting. A model with soils that are too wet produces too little sensible heat, a mixed layer too shallow and too weakly convective, and an afternoon surface wind that is too weak with the wind aloft correct; too dry soils produce the opposite error. Checking the modeled Bowen ratio and boundary-layer depth against flux stations and profiles is therefore part of diagnosing a daytime wind bias. After sunset the heat flux reverses, convection stops, and the layer left near the ground is the stable nocturnal boundary layer of Chapter 17.

16.7 What to retain

Definition 16.1 (The convective boundary layer)**.** Surface heating produces thermals, thermals produce deep turbulence, and deep turbulence redistributes heat and momentum vertically through the whole boundary layer; strong daytime convection couples the ground to the faster air aloft, which strengthens the near-surface wind and makes it gusty without any change in the large-scale forcing.

Table 16.4 lists the terms of the chapter, their meaning, their units and the subsection that defines each.

16.8 Exercises

Exercise 16.1. In a convective boundary layer the updrafts occupy 35 % of the area and rise at a mean $2.0\,\mathrm{m\,s^{-1}}$. (a) Find the mean downdraft velocity from mass conservation. (b) Compute σ_w and the sign of the third moment of the vertical velocity in the two-state picture. (c) The surface sensible heat flux is $300\,\mathrm{W\,m^{-2}}$ and $z_i = 1800\,\mathrm{m}$; take $\rho = 1.2\,\mathrm{kg\,m^{-3}}$, $c_p = 1004\,\mathrm{J\,kg^{-1}\,K^{-1}}$ and $\overline{\theta} = 300\,\mathrm{K}$. Compute $(\overline{w'\theta'})_0$, w_* and the turnover time. (d) Compare σ_w from (b) with the typical $0.6\,w_*$.

Exercise 16.2. A layer starts from zero depth at 08:00 and is heated by a constant kinematic flux of $0.15\,\mathrm{K\,m\,s^{-1}}$ into air with $\gamma = 4\,\mathrm{K\,km^{-1}}$; take $A = 0.2$. (a) Write $Q(t)$ and compute z_i at 10:00, 12:00 and 14:00 from the slab model. (b) Compute the jump $\Delta\theta$ and the entrainment velocity at 12:00, and check that $w_e\Delta\theta = A(\overline{w'\theta'})_0$. (c) Compute the warming rate of the mixed layer in kelvin per hour. (d) Under a subsidence of $0.015\,\mathrm{m\,s^{-1}}$, at what depth does the layer stop growing?

Exercise 16.3. At a site near 23°S at 08:00, the layer from 0 to 200 m has a mean wind of $6\,\mathrm{m\,s^{-1}}$ from 060° and the layer from 200 to 1000 m a mean wind of $14\,\mathrm{m\,s^{-1}}$ from 020°. By 13:00 convection has mixed the lowest kilometer to a uniform wind, with no net source or sink of momentum. (a) Is the turning of the wind with height at 08:00 consistent with the hemisphere? (b) Compute the eastward and northward components of each layer's wind, and the thickness-weighted mean vector. (c) Give the speed and direction of the mixed wind, and compare the speed with the thickness-weighted mean of the speeds. (d) By how much, and in which sense, has the wind direction near the ground turned during the morning? What would the answer be at the mirror site at 23°N?

Table 16.4: The terms of the chapter and where each is defined.

Term	Meaning	Units	Defined in
Convective boundary layer	daytime boundary layer whose turbulence is produced mainly by surface heating; depth z_i	m	16.1.1
Thermal	rising plume of buoyant warm air, $w' > 0$ with $\theta' > 0$; carries heat upward	–	16.1.2
Compensating downdraft	broader, weaker sinking between thermals, $w_d = -a_u w_u/(1-a_u)$	m/s	16.1.3
Mixed layer	interior of the CBL with nearly uniform θ and q	–	16.1.4
Superadiabatic layer	lowest meters to tens of meters, $\partial\theta/\partial z < 0$	–	16.1.5
Capping inversion	stable layer at the top of the CBL across which θ increases sharply	K	16.1.6
Entrainment	incorporation of free-atmosphere air at the top; rate w_e; heat flux at the top $-w_e\Delta\theta = -A(\overline{w'\theta'})_0$, $A \approx 0.2$	m/s	16.2.1, 16.2.3
Slab model	$z_i = \sqrt{2(1+2A)Q/\gamma}$: depth from accumulated heat and stratification	m	16.2.3
Convective velocity scale w_*	$[(g/\overline{\theta})(\overline{w'\theta'})_0 z_i]^{1/3}$: speed of thermals; 1 to $3\,\mathrm{m\,s^{-1}}$; $\sigma_w \approx 0.6\,w_*$	m/s	16.3.1, 16.3.2
Entrainment heat flux	negative heat flux near the top; heat flux profile $1 - 1.2\,z/z_i$	K m/s	16.3.4
Morning transition	erosion of the nighttime structure by a growing convective layer; recoupling and wind jump	–	16.4.6
Evening transition	heat flux to zero, decay of convection, stable layer forms; mixed layer becomes residual layer	–	16.4.7
Horizontal convective rolls	counter-rotating circulations along the wind, 1 to 5 km wide, tens of km long; $-z_i/L_O$ from a few to about 25	–	16.5.1
Nonlocal transport	transport by layer-sized eddies independent of the local gradient; counter-gradient term γ_c	–	16.5.4
Bowen ratio B	H/LE; large over dry, small over wet surfaces	–	16.6.4

Exercise 16.4. On a summer day the available energy peaks at $R_n - G_s = 510\,\mathrm{W\,m^{-2}}$. (a) Compute H and LE for a Bowen ratio of 4 (after a dry month) and of 0.3 (after a week of rain). (b) Using the slab model of Section 16.2.4 with the same day shape, $\gamma = 5\,\mathrm{K\,km^{-1}}$ and $A = 0.2$, compute z_i at 13:00 for each case by scaling from the base case. (c) Compute w_* at 13:00 for each case. (d) With $u_* = 0.4\,\mathrm{m\,s^{-1}}$, compute L_O and $-z_i/L_\mathrm{O}$ and state which organization of the convection to expect on each day, and on which day a mast at 20 m should show the larger turbulence intensity.

Chapter 17

The Stable Nocturnal Boundary Layer

17.1 Formation and structure of the stable boundary layer

Chapter 6 described the daily cycle of the boundary layer and introduced the stable layer that forms near the ground at night, the residual layer above it and the decoupling of the surface from the flow aloft. Chapters 13 to 15 then gave the tools that measure stable stratification: the potential-temperature gradient, the Richardson numbers, the Obukhov length and the stable feedback. This chapter assembles those pieces into a description of the nocturnal boundary layer as a whole. Its question is

why does the near-surface wind become so difficult to predict at night?

The answer is a chain: the surface cools, the air near it becomes stably stratified, the turbulence weakens, the surface decouples from the flow above, and the wind varies strongly with height and in time, with mixing that switches on and off. The stable layer is often much harder to model than the daytime convective layer of Chapter 16, and the reasons are physical, not only numerical.

The chapter first describes how the layer forms and what it looks like. It then treats the turbulence that survives under stable stratification, the two regimes of the stable layer with the collapse of turbulence, the bursts that interrupt it, shear instability and gravity waves, the wind above and across the layer with its turning with height, the drainage of cold air over terrain, and finally what the stable layer does to weather models, to measurements and to the diagnosis of a weak nighttime wind.

Jargon: stable boundary layer, nocturnal boundary layer, residual layer, decoupling, intermittent turbulence, turbulence collapse

The *stable boundary layer* (SBL) is the layer next to the ground in which the potential temperature increases with height, $\mathrm{d}\theta/\mathrm{d}z > 0$, because the surface is colder than the air above it; its turbulence is produced by wind shear alone and is damped by the stratification. Its depth, written z_i as for any boundary layer, is tens to a few hundred meters, measured as the height at which the turbulence (or the downward heat flux) falls to a small fraction of its surface value, or estimated from the top of the surface inversion on a radiosonde, tower or lidar profile. Formed by nighttime cooling, it is also called the *nocturnal boundary layer*. The *residual layer* is the remnant of the previous afternoon's mixed layer, above the stable layer and below the free atmosphere: nearly neutral, with nearly uniform θ, but with decaying turbulence. *Decoupling* is the state in which the turbulent transport of momentum between the surface layer and the flow above is too weak to carry the faster wind down: the two layers move nearly independently. *Intermittent turbulence* is turbulence that is not continuous in time but occurs in bursts of minutes separated by quiet periods of minutes to an hour; it is seen in the record of a fast-response anemometer as alternating low and high values of the standard deviation σ_w of the vertical velocity. *Turbulence collapse* is the near-disappearance of turbulence near the ground when buoyant destruction outweighs shear production and the stable feedback runs away.

Key idea

The stable boundary layer is not a weaker version of the daytime layer but a different regime: surface cooling → stable stratification → weak, intermittent turbulence → decoupling → strong shear, with terrain, gravity waves and the inertial oscillation of the wind aloft playing a far larger part than they do by day.

17.1.1 Radiative cooling of the surface

After sunset the surface no longer receives solar radiation but keeps emitting longwave (infrared) radiation, as every body at its temperature does. A surface at 285 K with an emissivity close to one emits $\sigma T^4 = 5.67 \times 10^{-8} \times 285^4 = 374\,\mathrm{W\,m^{-2}}$, with σ the Stefan–Boltzmann constant. It also receives longwave radiation from the atmosphere above, mostly from water vapor, carbon dioxide and clouds. Under a clear, fairly dry sky that downward flux is illustratively $314\,\mathrm{W\,m^{-2}}$, so the surface loses a net $60\,\mathrm{W\,m^{-2}}$. Under a low overcast the cloud base radiates almost like a black body at a temperature close to that of the surface, the downward flux rises toward the emitted one, and the net loss falls to a few tens or even a few $\mathrm{W\,m^{-2}}$. Clear skies give strong cooling; cloud largely prevents it.

The surface cannot store heat, so the net loss must be supplied by the neighbors of the surface: by conduction from the warmer soil below (the ground heat flux), by condensation of dew, and by a downward turbulent flux of sensible heat from the air above. The ground and the air in contact with it therefore cool. The air is cooled from below, so the coldest air lies at the bottom: $\theta_{\mathrm{low}} < \theta_{\mathrm{above}}$, $\mathrm{d}\theta/\mathrm{d}z > 0$, and the layer is stably stratified. In the stable layer a displaced parcel is pushed back toward its level (Chapter 13), so vertical motion is suppressed.

An order-of-magnitude cooling rate. Suppose, illustratively, that one third of the net loss of $60\,\mathrm{W\,m^{-2}}$ is drawn from the air as a downward sensible heat flux, $H = -20\,\mathrm{W\,m^{-2}}$, the rest coming from the soil, and that this heat is removed uniformly from a layer of depth h. The heat budget of the layer, per unit area, is

$$\rho\, c_p\, h\, \frac{\mathrm{d}\overline{\theta}}{\mathrm{d}t} = H, \qquad \text{so} \qquad \frac{\mathrm{d}\overline{\theta}}{\mathrm{d}t} = \frac{H}{\rho\, c_p\, h}.$$

With $\rho c_p = 1.2 \times 1004 = 1205\,\mathrm{J\,m^{-3}\,K^{-1}}$ and $h = 100\,\mathrm{m}$,

$$\frac{\mathrm{d}\overline{\theta}}{\mathrm{d}t} = \frac{-20}{1205 \times 100} = -1.66 \times 10^{-4}\,\mathrm{K\,s^{-1}} = -0.60\,\mathrm{K\,h^{-1}}.$$

If the same flux is drawn from a calm night's layer only 20 m deep, the rate is five times larger, $3.0\,\mathrm{K\,h^{-1}}$. A cooling of the order of one kelvin per hour, concentrated in the lowest tens of meters, is the typical result on a clear night: the shallower the layer over which the loss is spread, the faster and the more strongly it cools. Over a ten-hour night a flux of $-20\,\mathrm{W\,m^{-2}}$ removes $20 \times 36\,000/1205 \approx 600\,\mathrm{K\,m}$ of heat per unit area divided by ρc_p, the size of the potential-temperature deficit that the next morning's heating must erase before the mixed layer can grow (Chapter 6). The air also cools by its own longwave emission, a smaller contribution not included in this estimate.

17.1.2 A shallow layer

The daytime convective boundary layer is typically 1000 to 2000 m deep (Chapter 16), because buoyant thermals carry the surface heating through it. The actively turbulent part of the stable layer is typically 50 to 300 m deep, and sometimes less than 50 m on a calm, clear night. It is shallow because nothing lifts the cooled air: the only source of turbulence is shear, and the stratification that the cooling creates opposes the vertical excursions that would deepen the layer. Its depth increases with the wind, which supplies the shear, and decreases with the cooling, which strengthens the stratification.

The stable layer is therefore both shallower and more strongly stratified than the daytime layer. A potential-temperature increase of several kelvin over the lowest 100 to 200 m is common, against a nearly constant θ through a kilometer or more of daytime mixed layer. The depth of the surface inversion, the layer in which the temperature itself increases with height, can exceed the depth of the actively turbulent layer: the cooling reaches upward partly by radiation and by slow mixing in earlier hours, so the top of the inversion seen on a sounding is often higher than the top of the turbulence measured by a sonic anemometer or a sodar.

17.1.3 The residual layer above

The stable layer forms beneath the air that was mixed during the afternoon. That air keeps its nearly uniform potential temperature, moisture and pollutant content after sunset, while its turbulence decays within about an hour for lack of thermals: it becomes the residual layer (Chapter 6). The nighttime column has four parts, from top to bottom:

free atmosphere / residual layer / stable boundary layer / surface.

Figure 17.1 draws illustrative profiles of that column on a clear night. Both panels have height above the ground on the vertical axis, from 0 to 1200 m. The left panel shows potential temperature, with the stable boundary layer shaded blue up to an illustrative 200 m and the residual layer shaded gray above it up to the remnant of the afternoon's capping inversion near 1000 m. The right panel shows the wind speed over the same heights, with dots at 10, 50, 150 and 300 m, the heights of a profile used again in Section 17.4.5.

The two panels are read together, height by height. Within the stable boundary layer the potential temperature increases steeply, by about 8 K in 200 m, and so does the wind: from $2\,\mathrm{m\,s^{-1}}$ at 10 m to $14\,\mathrm{m\,s^{-1}}$ at 150 m. Both gradients are concentrated in the same shallow layer, and both are far larger than by day. Above the stable layer the potential temperature is nearly constant through the residual layer, and the wind there has a maximum faster than the large-scale wind both above and below it, before falling back toward the geostrophic value. The residual layer is no longer in contact with the ground; insulated from it by the stable layer, it has lost the drag that slowed it in the afternoon, which is the origin of the wind maximum treated in Section 17.4.1. The free atmosphere above is nearly the same as in the afternoon.

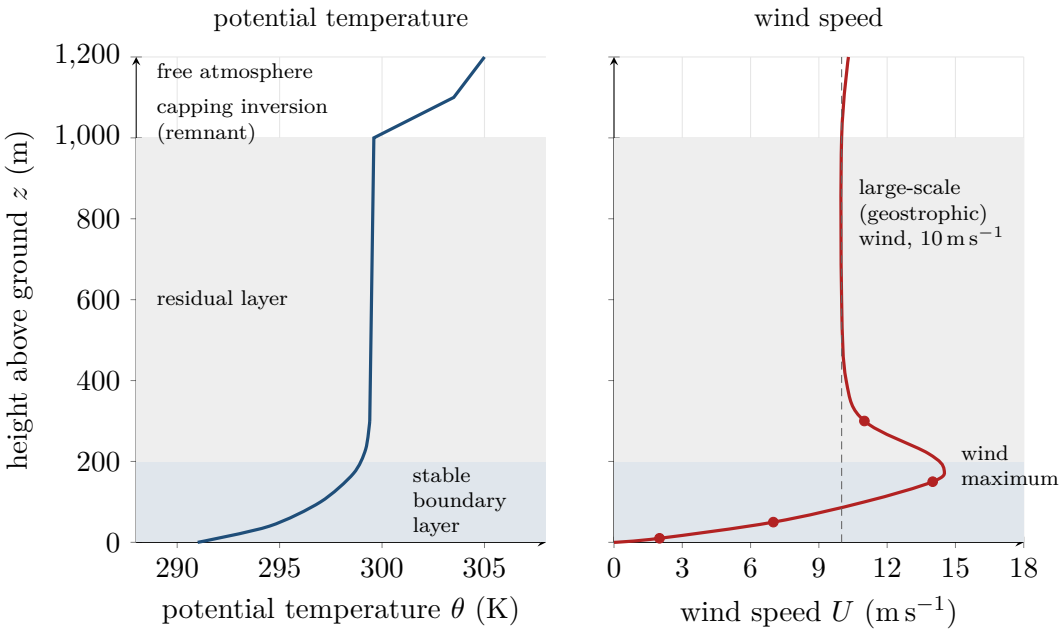


Figure 17.1: Illustrative night profiles (drawn through chosen points). Left: potential temperature, rising by about 8 K through a stable boundary layer of about 200 m, nearly constant through the residual layer, and rising again through the remnant of the afternoon's capping inversion. Right: wind speed, 2, 7, 14 and 11 m s^{-1} at 10, 50, 150 and 300 m (dots), with a maximum near the top of the stable layer above an illustrative geostrophic wind of 10 m s^{-1} (dashed).

17.2 Turbulence under stable stratification

The stratification of the stable layer acts on the turbulence through the buoyancy term of the turbulent kinetic energy budget. This section recalls that term, shows how shear production keeps turbulence alive against it, uses the Richardson number to weigh the two, and describes the decoupling and the steep wind profile that follow when buoyancy wins.

17.2.1 Buoyancy as a sink of turbulent kinetic energy

Chapter 8 derived the budget of the turbulent kinetic energy per unit mass e. In horizontally homogeneous conditions, with the transport terms omitted,

$$\frac{\partial e}{\partial t} = P_s + P_b - \varepsilon, \qquad P_s = -\overline{u'w'}\,\frac{\partial \overline{u}}{\partial z} - \overline{v'w'}\,\frac{\partial \overline{v}}{\partial z}, \qquad P_b = \frac{g}{\overline{\theta}}\,\overline{w'\theta'}, \tag{17.1}$$

all terms in m^2 s^{-3}, with ε the dissipation rate. In the stable layer the heat flux is downward, $\overline{w'\theta'} < 0$: eddies carry warm air down and cold air up. Every such exchange lifts dense air and lowers light air against the stratification, which costs energy, and the energy is taken from the eddies. A displaced parcel is pushed back toward its level, and the kinetic energy of its excursion is converted into potential energy of the stratification. The buoyancy term is therefore negative, $P_b < 0$: buoyancy is a sink of turbulent kinetic energy, *buoyant destruction*. Turbulence survives only if shear production exceeds buoyant destruction by enough to also cover dissipation.

A worked budget. With an illustrative downward heat flux $H = -20\,\mathrm{W\,m^{-2}}$, the kinematic flux is $\overline{w'\theta'} = -20/1205 = -0.0166\,\mathrm{K\,m\,s^{-1}}$, and with $\overline{\theta} = 285\,\mathrm{K}$, $P_b = (9.81/285) \times (-0.0166) = -5.7 \times 10^{-4}\,\mathrm{m^2\,s^{-3}}$. A friction velocity of $u_* = 0.2\,\mathrm{m\,s^{-1}}$, so $-\overline{u'w'} = 0.04\,\mathrm{m^2\,s^{-2}}$, in a shear of

$0.1\,\mathrm{s}^{-1}$ gives $P_s = 0.04 \times 0.1 = 4.0 \times 10^{-3}\,\mathrm{m^2\,s^{-3}}$, seven times larger: the turbulence survives, with a flux Richardson number $\mathrm{Ri}_f = -P_b/P_s = 0.14$. With a five times weaker friction velocity and shear, P_s falls by a factor of 125 to $3.2 \times 10^{-5}\,\mathrm{m^2\,s^{-3}}$, and the same heat flux would destroy the turbulence eighteen times faster than the shear produces it: such a flux cannot be sustained, the heat flux falls, and the surface layer moves toward collapse (Section 17.3.3).

17.2.2 Shear production and the Richardson number

Mechanical turbulence can survive at night if the shear is strong. The shear production $P_s = -\overline{u'w'}\,\partial U/\partial z$ (in along-wind coordinates) does not depend on the stratification directly, and the stable layer has strong shear, since the wind aloft is not slowed by the ground. The question at every height is whether shear production is strong enough to overcome the stable suppression.

The competition is measured by the gradient Richardson number of Chapter 13,

$$\mathrm{Ri}_g = \frac{N^2}{|\partial \mathbf{V}/\partial z|^2}, \qquad N^2 = \frac{g}{\overline{\theta}}\frac{\partial \overline{\theta}}{\partial z}, \qquad |\partial \mathbf{V}/\partial z|^2 = \left(\frac{\partial \overline{u}}{\partial z}\right)^2 + \left(\frac{\partial \overline{v}}{\partial z}\right)^2, \tag{17.2}$$

the ratio of buoyant suppression to shear production: N is the buoyancy frequency of Section 17.3.6 and $|\partial \mathbf{V}/\partial z|$ the magnitude of the vector shear of Section 17.4.4. When $\mathrm{Ri}_g \ll 1$ shear dominates and the turbulence is continuous; when Ri_g is large, above the critical value $\mathrm{Ri}_c \approx 0.25$ and especially well above it, the turbulence is weak or intermittent. Section 17.3.5 explains where the value 0.25 comes from.

The same inversion, two shears. Take an illustrative layer between 10 and 100 m with $\Delta\theta = 4\,\mathrm{K}$ and $\overline{\theta} = 285\,\mathrm{K}$, so $N^2 = (9.81/285) \times 4/90 = 1.53 \times 10^{-3}\,\mathrm{s^{-2}}$. With $3\,\mathrm{m\,s^{-1}}$ at 10 m and $12\,\mathrm{m\,s^{-1}}$ at 100 m, in the same direction, the vector shear is $9/90 = 0.10\,\mathrm{s^{-1}}$ and the bulk Richardson number is $\mathrm{Ri}_B = 1.53 \times 10^{-3}/0.010 = 0.15$: stable, yet the shear sustains the turbulence. If the wind at 100 m drops to $8\,\mathrm{m\,s^{-1}}$, the shear is $5/90 = 0.056\,\mathrm{s^{-1}}$, its square $3.09 \times 10^{-3}\,\mathrm{s^{-2}}$ and $\mathrm{Ri}_B = 0.50$: the same inversion now suppresses the turbulence. The stratification alone does not decide; the shear acting against it does as much.

17.2.3 Decoupling

When the turbulence of the stable layer is weak, the downward flux of momentum is too small to bring the momentum of the wind aloft to the ground. An illustrative night has $12\,\mathrm{m\,s^{-1}}$ at 100 m and only $2\,\mathrm{m\,s^{-1}}$ at 10 m: the mean shear between them is

$$\frac{\Delta U}{\Delta z} = \frac{12-2}{100-10}\,\mathrm{s^{-1}} = 0.11\,\mathrm{s^{-1}},$$

the ratio of the two winds is 0.17, and the power-law exponent between the two heights is $\ln(12/2)/\ln 10 = 0.78$, against about 0.1 to 0.2 by day. The turbulent transport is too weak to bring the momentum down: the surface layer is decoupled from the flow above. The strong wind aloft is real and can be forecast well, because it follows the large-scale forcing; the weak surface wind depends on how much of that momentum the weak turbulence transmits, which can change within minutes.

Decoupling is a statement about transport, not about the absence of wind: the two layers each keep their own wind, and the surface wind then follows local influences that are negligible by day, such as a gentle slope draining cold air (Section 17.5.1). For a transmission line at 15 to 30 m it means that the conductor can sit in nearly calm air, with little convective cooling, under a wind aloft that it never feels.

17.2.4 The steep stable profile

Monin–Obukhov theory (Chapter 14) expresses the steepening through the dimensionless shear ϕ_m,

$$\frac{\partial U}{\partial z} = \frac{u_*}{\kappa z}\,\phi_m(z/L_{\mathrm{O}})\,, \qquad \phi_m = 1 + 5\,z/L_{\mathrm{O}} \quad (z/L_{\mathrm{O}} \geq 0), \tag{17.3}$$

the second form being the standard empirical Businger–Dyer form for stable conditions. In stable air $L_{\mathrm{O}} > 0$ and $\phi_m > 1$: at the same friction velocity the shear is larger than the neutral $u_*/(\kappa z)$, by the factor ϕ_m. Integrating equation (17.3) from z_0 gives the log-linear profile

$$U(z) = \frac{u_*}{\kappa}\left[\ln\frac{z}{z_0} + 5\,\frac{z}{L_{\mathrm{O}}}\right], \tag{17.4}$$

with the term $5\,z/L_{\mathrm{O}}$ (the small term $-5\,z_0/L_{\mathrm{O}}$ dropped) adding a part that grows linearly with height to the logarithm.

The $0.10\,\mathrm{s}^{-1}$ example. An illustrative night has $U_{10} = 3\,\mathrm{m\,s}^{-1}$ and $U_{100} = 12\,\mathrm{m\,s}^{-1}$, a mean shear of $(12-3)/90 = 0.10\,\mathrm{s}^{-1}$ and an exponent of $\ln 4/\ln 10 = 0.60$. Equation (17.4) reproduces both winds with $u_* = 0.20\,\mathrm{m\,s}^{-1}$: the difference between the two heights is $U_{100} - U_{10} = (u_*/\kappa)\,[\ln 10 + 5 \times 90/L_{\mathrm{O}}]$, so $9 = 0.5\,[2.303 + 450/L_{\mathrm{O}}]$ gives $L_{\mathrm{O}} = 28.7\,\mathrm{m}$, and $U_{10} = 3\,\mathrm{m\,s}^{-1}$ then gives $\ln(10/z_0) = 6 - 50/28.7 = 4.26$, $z_0 = 0.14\,\mathrm{m}$, the roughness of a crop. At 10 m, $z/L_{\mathrm{O}} = 0.35$, $\phi_m = 2.74$ and the shear is $0.05 \times 2.74 = 0.137\,\mathrm{s}^{-1}$, against $0.05\,\mathrm{s}^{-1}$ for the neutral profile with the same u_*.

Figure 17.2 draws the two profiles that pass through $U_{10} = 3\,\mathrm{m\,s}^{-1}$ over the same surface: the stable log-linear profile of the example and the neutral logarithmic profile. The horizontal axis is wind speed and the vertical axis height from 0 to 120 m; the dotted line marks the height $z = L_{\mathrm{O}} = 28.7\,\mathrm{m}$.

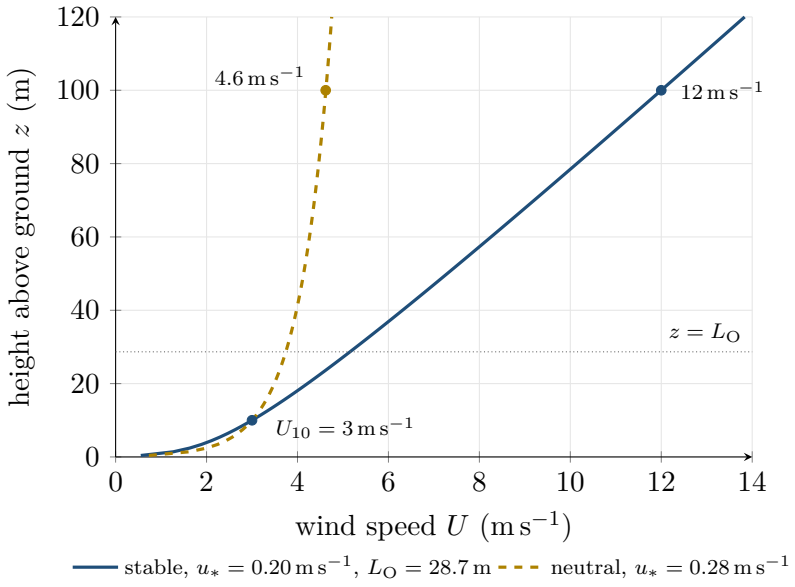


Figure 17.2: Stable and neutral profiles through the same $U_{10} = 3\,\mathrm{m\,s}^{-1}$ over $z_0 = 0.14\,\mathrm{m}$. Stable (solid): $U = (u_*/\kappa)[\ln(z/z_0) + 5z/L_{\mathrm{O}}]$ with $u_* = 0.20\,\mathrm{m\,s}^{-1}$, $L_{\mathrm{O}} = 28.7\,\mathrm{m}$, $\kappa = 0.4$. Neutral (dashed): $U = (u_*/\kappa)\ln(z/z_0)$ with $u_* = 0.28\,\mathrm{m\,s}^{-1}$. Illustrative values; above $z = L_{\mathrm{O}}$ the log-linear form is outside its tested range.

Near the ground the two curves nearly coincide; above a few meters they separate. The neutral profile bends over and reaches only $4.6\,\mathrm{m\,s}^{-1}$ at 100 m, a mean shear of $0.018\,\mathrm{s}^{-1}$; the

stable one keeps increasing, almost linearly above L_O, and reaches $12\,\mathrm{m\,s^{-1}}$. The same surface wind is thus consistent with very different winds aloft, and the stability decides which. The figure also shows a warning used in Section 17.6.1: to reproduce the observed $12\,\mathrm{m\,s^{-1}}$ the profile must be used up to $z/L_O = 100/28.7 = 3.5$, far beyond the range $z/L_O \lesssim 1$ in which the log-linear form has been tested. The steep profile is real; the formula that reproduces it at 100 m is being stretched.

17.3 Regimes, collapse and bursts

The stable layer does not have a single behavior. This section distinguishes its two regimes, describes the nonstationarity of the very stable one, follows the collapse of turbulence and the bursts that interrupt it, and treats the two wave phenomena that stratification makes possible: the Kelvin–Helmholtz instability of a sheared layer and the internal gravity wave, whose frequency scale is the buoyancy frequency.

17.3.1 Weakly stable and very stable regimes

Observations of nocturnal boundary layers fall into two broad regimes that differ in kind, not only in degree. In the *weakly stable* regime, typical of windy or cloudy nights, the wind is moderate, the turbulence is continuous, the surface is well coupled to the flow above, and Monin–Obukhov similarity describes the profiles. In the *very stable* regime, typical of clear nights with weak wind, the inversion is strong, the turbulence is weak and intermittent, the surface is decoupled, and processes negligible by day (drainage flows, gravity waves, radiative cooling of the air itself) carry fluxes comparable to the turbulent ones. Table 17.1 sets the two side by side; its rows are the properties of the layer and its two columns the regimes, with indicative values that are illustrative, not thresholds.

Table 17.1: The two regimes of the stable boundary layer. Numbers are indicative values for a site over short vegetation (illustrative), not thresholds; nights move between the regimes.

Property	Weakly stable	Very stable
Typical night	windy, or cloudy	clear, weak large-scale wind
Wind at 10 m	moderate, a few $\mathrm{m\,s^{-1}}$ or more	weak, often below $2\,\mathrm{m\,s^{-1}}$
Inversion	weak: $\Delta\theta$ of 1 to 2 K over 100 m	strong: 5 to 10 K or more over 100 m
Turbulence	continuous; σ_w steady	weak and intermittent; quiet periods and bursts
Coupling	well coupled to the flow aloft	decoupled; surface and flow aloft move nearly independently
Stability parameters	$z/L_O \lesssim 1$; Ri_g below about 0.25	$z/L_O \gg 1$; Ri_g above 0.25, often well above
Similarity theory	applies with the stable forms	fails or is unreliable
Drainage and waves	minor	important, can dominate the surface wind
Depth z_i	a few hundred meters	tens of meters

The two columns are qualitatively different regimes, and a night can move from one to the other: a weakly stable evening becomes very stable when the wind aloft slackens, and a very stable night can return to weakly stable when the wind aloft strengthens or cloud arrives. The transition between them is sharp rather than gradual, for the reason given in Section 17.3.3: the maximum downward heat flux that turbulence can carry depends on the cube of the wind, and once the cooling exceeds it the turbulence collapses.

17.3.2 Nonstationarity and intermittency

Very stable nights are not continuously quiet. They show long quiet periods, sudden bursts of turbulence, rapid shifts of wind direction, and wave-like oscillations of wind and temperature. Their turbulence is intermittent rather than continuously weak, and their statistics change within the averaging period: they are *nonstationary*, in the sense that the mean and variance computed over one half-hour differ from those of the next by more than sampling error.

Figure 17.3 sketches the record of such a night at a mast. The three panels share a time axis from 18:00 to 06:00. The top panel shows the wind speed at 10 m (solid) and 100 m (dashed); the middle panel the air temperature at 2 m; the bottom panel the standard deviation of the vertical velocity σ_w at 10 m, a measure of the turbulence. The two shaded bands mark bursts.

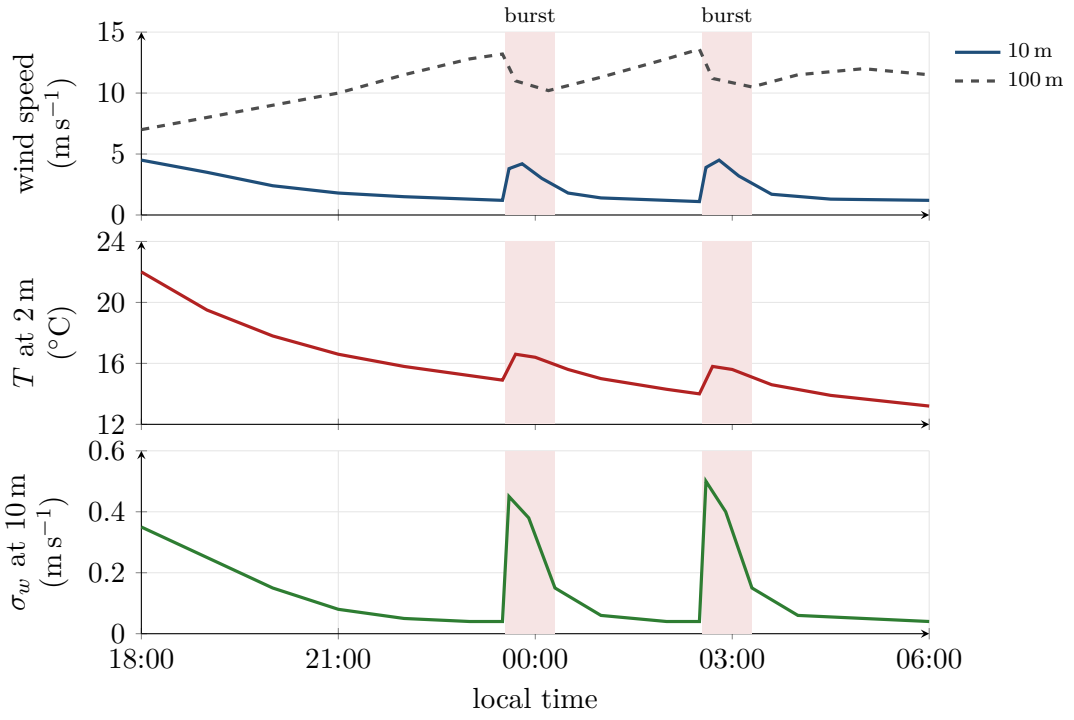


Figure 17.3: Schematic record of an intermittent night at a mast (illustrative values drawn by hand, not a measurement). Top: wind speed at 10 m (solid) and 100 m (dashed). Middle: air temperature at 2 m. Bottom: standard deviation of the vertical velocity at 10 m. Shaded: two bursts of turbulence, near 23:30 and 02:30.

The evening part of the record is the decay of the day's turbulence: σ_w falls from 0.35 to about 0.05 m s^{-1}, the 10 m wind falls from 4.5 to below 1.5 m s^{-1}, the temperature at 2 m falls by about 7 K, and the 100 m wind rises: the surface has decoupled. Then the three panels change together at each burst. The 10 m wind jumps by about 3 m s^{-1} within minutes, the 100 m wind drops by about 2 m s^{-1}, the 2 m temperature rises by about 1.7 K, and σ_w rises tenfold. Momentum and heat have been mixed down: the surface gains wind and warmth, the air aloft loses wind. Within about an hour each signal returns to its quiet trend, and the 100 m wind starts to build again. An average over the whole night, or even over a half-hour that contains a burst, describes neither the quiet periods nor the bursts.

17.3.3 Turbulence collapse

The quiet periods are the product of the stable feedback of Chapter 15: surface cooling strengthens the stratification, the stratification weakens the turbulence, the weaker turbulence

brings less heat down from the warmer air above, and the air near the surface cools further. Each link strengthens the next,

$$\text{cooling} \rightarrow \text{stability} \rightarrow \text{less mixing} \rightarrow \text{more cooling},$$

so the mixing near the ground can become very weak: the turbulence collapses.

The same chapter showed why the collapse can be abrupt. With the wind at a reference height held fixed, the downward heat flux that the stable surface layer can carry has a maximum, reached near $z/L_O = 0.5$ for $z = 10\,\mathrm{m}$ and $z_0 = 0.05\,\mathrm{m}$, and that maximum grows with the cube of the wind: about $17\,\mathrm{W\,m^{-2}}$ at $3\,\mathrm{m\,s^{-1}}$ and $134\,\mathrm{W\,m^{-2}}$ at $6\,\mathrm{m\,s^{-1}}$. A clear sky that demands more heat from the air than the maximum cannot be served by the turbulence; the surface cools faster than the turbulence can resupply it, the stratification strengthens, the flux falls further, and the turbulence collapses. This is why weak-wind clear nights collapse into the very stable regime while windy nights with the same sky stay weakly stable, and why the transition between the regimes of Table 17.1 is sharp.

17.3.4 Bursts and the collapse–burst cycle

The collapse does not have to last. Once the surface is decoupled, the air above it is relieved of the drag of the ground and accelerates (Section 17.4.1), while the air near the ground does not. The shear across the stable layer grows, and with it the shear production, until the Richardson number in some layer falls below its critical value. Shear instability then sets in (Section 17.3.5), and a *turbulent burst* follows: a short episode, minutes long, of vigorous turbulence that mixes momentum down and heat down, from the warm air aloft toward the cold surface. The mixing reduces the shear that produced it and warms the surface air, the Richardson number rises, and the turbulence weakens again. The night oscillates between quiet periods and bursts.

Figure 17.4 draws the cycle. Each box is a state of the lowest hundred meters and each arrow a step; the cycle runs clockwise from the quiet, decoupled state at the top. The external driver, radiative cooling, enters at the left and keeps returning the layer to the quiet state.

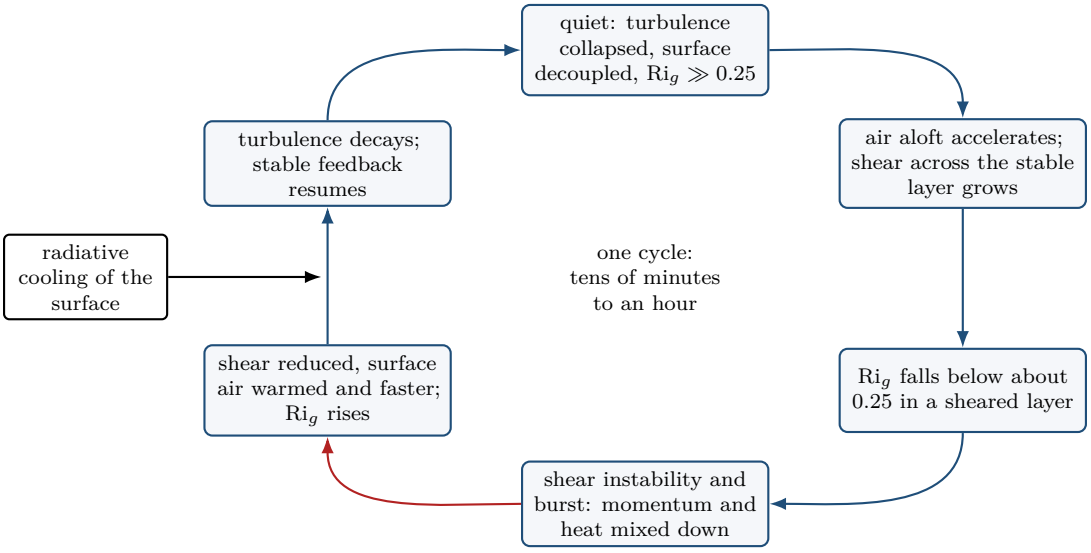


Figure 17.4: The collapse–burst cycle of a very stable night (schematic). Blue arrows: the slow steps, in which shear builds while the turbulence is weak; red arrow: the fast step, the burst. Radiative cooling drives the layer back toward collapse after each burst.

The upper half of the cycle is slow: the shear builds over tens of minutes while nothing happens at the surface. The burst at the bottom is fast, minutes long, and it is the only step that the surface instruments notice. The cycle reproduces the record of Figure 17.3: the 100 m

wind rising before each burst, the simultaneous jumps at the burst, and the relaxation afterward. Bursts are also triggered from outside the cycle, by a gravity wave breaking, a drainage flow arriving from a slope, or the shear beneath a low-level jet. In every case the surface wind can rise by several meters per second for minutes with no change in the large-scale weather, a gust that a model of the mean flow does not contain.

17.3.5 Kelvin–Helmholtz instability

Kelvin–Helmholtz instability is the instability of a sheared, stratified layer: when the shear across the layer is strong enough relative to its stratification, small wave-like disturbances of the layer grow, steepen, roll up and overturn into *billows*, which break down into turbulence. It is the main route from a quiet, sheared stable layer to a burst.

Where the critical value comes from. An energy argument gives the condition. Take two parcels of equal mass at heights z and $z+\delta z$ in a layer where the wind increases by δU and the buoyancy frequency is N, and let a disturbance exchange their heights and mix their momentum, so that both end with the mean wind of the pair. Their kinetic energy per unit mass, averaged over the two, falls from $[U^2+(U+\delta U)^2]/4$ to $(U+\delta U/2)^2/2$; the difference, released to the disturbance, is

$$\frac{2U^2+2U\,\delta U+\delta U^2}{4}-\frac{2U^2+2U\,\delta U+\delta U^2/2}{4}=\frac{\delta U^2}{8}.$$

Exchanging the two parcels' heights costs work against buoyancy. A parcel moved by a distance s in a stable layer feels a restoring acceleration $N^2 s$ (Chapter 6), so moving it by δz costs $\int_0^{\delta z} N^2 s\,\mathrm{d}s = N^2\delta z^2/2$ per unit mass, the same for the parcel moved up and for the parcel moved down. The disturbance can grow only if the released kinetic energy covers this cost:

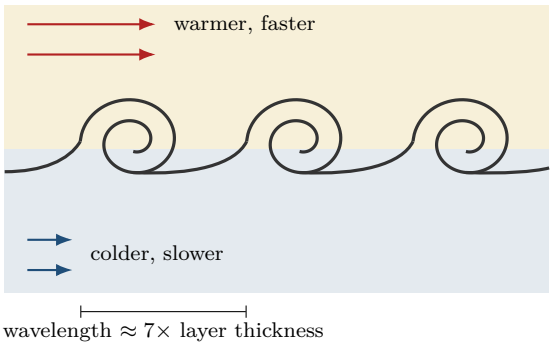
$$\frac{\delta U^2}{8} > \frac{N^2\,\delta z^2}{2} \quad\Longleftrightarrow\quad \frac{N^2}{(\delta U/\delta z)^2} < \frac{1}{4}. \tag{17.5}$$

The left side of the second form is the gradient Richardson number. The heuristic reproduces the result of the linear stability theory of a smooth, laminar, stratified shear flow: such a flow can be unstable only if $\mathrm{Ri}_g < 1/4$ somewhere in it. The condition is necessary, not sufficient, and it applies to the onset of instability in a laminar flow; already turbulent flow can persist above 0.25 (Chapter 13). This is the origin of the critical Richardson number $\mathrm{Ri}_c \approx 0.25$ of classical theory.

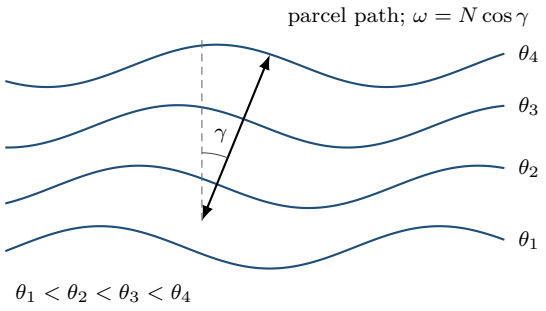
A worked layer. A shear layer 30 m deep near the top of the stable layer has $\Delta\theta = 1\,\mathrm{K}$ across it and $\overline{\theta} = 285\,\mathrm{K}$, so $N^2 = (9.81/285)\times 1/30 = 1.15\times10^{-3}\,\mathrm{s}^{-2}$. Instability requires $|\partial\mathbf{V}/\partial z|^2 > 4N^2 = 4.59\times10^{-3}\,\mathrm{s}^{-2}$, a shear above $0.068\,\mathrm{s}^{-1}$, a wind difference of more than $0.068\times30 = 2.0\,\mathrm{m\,s}^{-1}$ across the layer. Linear theory also gives the size of the billows: the fastest-growing wavelength is about seven times the thickness of the shear layer, here about 200 m. Billows of this size pass a mast in tens of seconds to a minute and are seen by sodars and lidars as regular, braided patterns in the shear layer.

Figure 17.5(a) sketches the billows in a vertical cross section. The upper layer, warmer and faster, moves to the right relative to the lower one, as the arrows show; the line is the interface between the two, rolled up into billows that turn clockwise in this view, the sense of the shear. Panel (b) is treated in Section 17.3.6.

In panel (a) each billow carries cold air from below up over its crest and warm air from above down under its trough. As the billows roll up, the interface is stretched into thin braids between them, and the billows break down into turbulence that mixes the two layers. The shear layer is thicker and less sheared afterward, its Richardson number is larger, and the instability stops: the burst has consumed its own cause.



(a) Kelvin–Helmholtz billows



(b) internal gravity wave

Figure 17.5: Waves in the stable layer (schematic vertical cross sections). (a) Kelvin–Helmholtz billows: the interface between a faster, warmer upper layer and a slower, colder lower layer rolls up into billows when $\mathrm{Ri}_g < 0.25$ in the shear layer. (b) An internal gravity wave: surfaces of constant potential temperature oscillate up and down; air parcels oscillate along paths tilted at the angle γ from the vertical, at the frequency $\omega = N\cos\gamma \le N$.

17.3.6 Internal gravity waves and the buoyancy frequency

A stratified fluid supports waves in which buoyancy is the restoring force. An *internal gravity wave* is such a wave inside the atmosphere (as opposed to a wave on the surface of water): a parcel displaced from its level is pushed back by buoyancy, overshoots, and oscillates, and the oscillation propagates through the stable layer as a wave. Gravity waves in the stable layer are excited by flow over terrain, by shear instability, by drainage flows and by convection in the distance. They produce oscillations of wind and temperature at a mast, with periods of minutes to tens of minutes, and where they steepen and break they generate intermittent turbulence.

The buoyancy frequency. The frequency scale of these waves is the buoyancy frequency, also called the *Brunt–Väisälä frequency*,

$$N^2 = \frac{g}{\overline{\theta}}\,\frac{\mathrm{d}\overline{\theta}}{\mathrm{d}z}, \tag{17.6}$$

in s^{-2}, derived in Chapter 6 as the frequency at which a parcel displaced vertically oscillates: $\mathrm{d}^2\delta z/\mathrm{d}t^2 = -N^2\,\delta z$. It is computed from a measured or modeled potential-temperature profile. $N^2 > 0$ when the layer is stable, and N is then real; the larger N, the stronger the restoring buoyancy. N measures the strength of the static stability: a larger $\mathrm{d}\theta/\mathrm{d}z$ gives a faster parcel oscillation.

Waves on tilted paths. In a wave the parcels need not move vertically. Let a parcel move a distance s along a straight path tilted at the angle γ from the vertical, as in Figure 17.5(b). Its vertical displacement is $s\cos\gamma$, the buoyant acceleration on it is $-N^2 s\cos\gamma$, vertical, and the component of that acceleration along the path is $-N^2 s\cos^2\gamma$. The parcel therefore oscillates along its path with

$$\omega = N\cos\gamma \le N. \tag{17.7}$$

Panel (b) of the figure draws this: the lines are surfaces of constant potential temperature, increasing upward, displaced by the wave; the double arrow is a parcel path at the angle γ from the vertical. Vertical oscillation, $\gamma = 0$, has the highest frequency, N; nearly horizontal paths oscillate slowly. The buoyancy period $2\pi/N$ is therefore the shortest period an internal gravity wave in the layer can have.

Worked values. Table 17.2 lists N and the buoyancy period for four illustrative layers: the free atmosphere, a weak and a moderate nocturnal inversion, and a strong one. Its columns give the temperature change, the potential-temperature gradient ($\Delta\theta \approx \Delta T + 0.0098\,\Delta z$, Chapter 13), the reference potential temperature, N and the period $2\pi/N$.

Table 17.2: Buoyancy frequency and period for illustrative layers, $N^2 = (g/\theta)\,\mathrm{d}\theta/\mathrm{d}z$ with $g = 9.81\,\mathrm{m\,s^{-2}}$.

Layer	Temperature change	$\mathrm{d}\theta/\mathrm{d}z$ ($\mathrm{K\,m^{-1}}$)	θ (K)	N ($\mathrm{s^{-1}}$)	$2\pi/N$
Free atmosphere	−6.8 K per km	0.003	300	0.0099	10.6 min
Weak inversion	+0.5 K per 100 m	0.0148	285	0.0226	4.6 min
Moderate inversion	+2.0 K per 100 m	0.030	285	0.0321	3.3 min
Strong inversion	+5 K per 50 m	0.110	285	0.0615	1.7 min

For the weak inversion, $N^2 = 9.81 \times 0.0148/285 = 5.09 \times 10^{-4}\,\mathrm{s^{-2}}$, $N = 0.0226\,\mathrm{s^{-1}}$ and $2\pi/N = 278\,\mathrm{s}$; for the strong one, $\mathrm{d}\theta/\mathrm{d}z = (5 + 0.49)/50 = 0.110\,\mathrm{K\,m^{-1}}$, $N^2 = 3.78 \times 10^{-3}\,\mathrm{s^{-2}}$, $N = 0.0615\,\mathrm{s^{-1}}$ and $2\pi/N = 102\,\mathrm{s}$. The table reads from top to bottom as a stiffening of the layer: a strong surface inversion restores a displaced parcel six times faster than the free atmosphere, and its gravity waves can have periods as short as two minutes, while the waves of a weak inversion have periods of about five minutes or more. Oscillations of wind and temperature with periods of a few minutes in a nighttime record are thus consistent with gravity waves in the surface inversion; slower ones, tens of minutes, with waves on tilted paths or in weaker stratification aloft.

17.4 Wind above and across the stable layer

The stable layer changes the wind above it as well as within it. This section describes the acceleration of the air above the stable layer and its inertial oscillation, the turning of the wind with height and the words used for it, the vector shear that combines speed and direction, and the wind profile with a maximum that results.

17.4.1 Acceleration aloft and the inertial oscillation

By day turbulence transmits the drag of the ground through the whole mixed layer, and the wind there stays below the geostrophic wind and turned toward low pressure (Chapter 3). At night the stable layer no longer transmits the drag upward. The air above it, in the residual layer, keeps the same pressure-gradient force but loses most of its friction, and it accelerates toward a more nearly geostrophic state. This is one ingredient of the low-level jet.

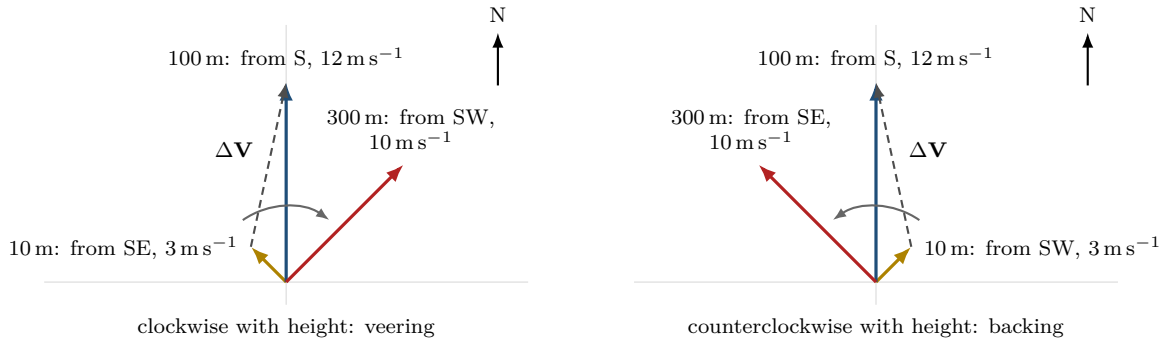
The acceleration does not settle on the geostrophic wind. At sunset the wind aloft is subgeostrophic and turned toward low pressure; its departure from the geostrophic wind, the ageostrophic wind $\mathbf{V}_a$, was balanced by friction. Once the turbulence weakens that balance is gone, and the ageostrophic wind rotates under the Coriolis force without changing its magnitude, as in the inertial oscillation of a parcel released from rest (Chapter 3). The total wind $\mathbf{V} = \mathbf{V}_g + \mathbf{V}_a$ then accelerates and turns through the night, and some hours after sunset, when $\mathbf{V}_a$ points along $\mathbf{V}_g$, it exceeds the geostrophic wind: a wind maximum forms a few hundred meters above the ground, as in Figure 17.1. This is the inertial oscillation mechanism of the nocturnal low-level jet, often named after Blackadar, who proposed it. The rotation is clockwise in the Northern Hemisphere ($f > 0$) and counterclockwise in the Southern ($f < 0$), with the inertial period $T_I = 2\pi/|f|$: about 18.6 h at 40°N ($|f| = 9.4 \times 10^{-5}\,\mathrm{s^{-1}}$) and 30.6 h at 23°S ($|f| = 5.7 \times 10^{-5}\,\mathrm{s^{-1}}$). A night lasts only a fraction of a period, so the wind aloft

accelerates and turns through the night without completing a rotation. Chapter 18 derives the oscillation of the ageostrophic wind and draws its hodograph for both hemispheres.

17.4.2 Directional shear

The wind changes direction with height as well as speed. The surface air is slowed by friction more than the air aloft. The Coriolis force is proportional to the wind speed, so it is weaker on the slow air near the ground, while the pressure-gradient force is nearly the same at all heights in the lowest few hundred meters; the slower air is therefore turned further toward low pressure. Since low pressure lies to the left of the flow in the Northern Hemisphere and to its right in the Southern (Chapter 3), going up from the surface the wind turns clockwise in the Northern Hemisphere and counterclockwise in the Southern. At night the friction is confined to the shallow stable layer, so the turning is concentrated there, and the turning across the lowest few hundred meters is larger than by day (illustratively 30 to 50° or more, against 10 to 20° on a convective afternoon, Chapter 6); the inertial oscillation aloft can add to it.

An illustrative Northern Hemisphere night has a southeasterly wind at 10 m (from 135°, 3 m s^{-1}), a southerly wind at 100 m (from 180°, 12 m s^{-1}) and a southwesterly wind at 300 m (from 225°, 10 m s^{-1}): the direction changes by 90° across 300 m, clockwise with height. The Southern Hemisphere counterpart is the mirror image: southwesterly at 10 m, southerly at 100 m, southeasterly at 300 m, counterclockwise with height. Figure 17.6 draws both. Each panel is a plan view with north at the top; each arrow starts at a common origin and points the way the wind blows (toward), with its length proportional to the speed, and is labeled with its height. The dashed arrow is the vector difference between the 10 and 100 m winds, used in Section 17.4.4.



(a) Northern Hemisphere (b) Southern Hemisphere

Figure 17.6: Turning of the wind with height on a stable night, plan views with north at the top (illustrative). Arrows point the way the wind blows, length 0.22 cm per m s^{-1}. (a) Northern Hemisphere: southeasterly at 10 m, southerly at 100 m, southwesterly at 300 m; the wind veers with height. (b) Southern Hemisphere: the mirror image; the wind backs with height. Dashed: the vector difference $\Delta\mathbf{V}$ between 10 and 100 m.

The arrows grow and turn from the bottom up: in panel (a) the tips move clockwise from northwest through north to northeast, in panel (b) counterclockwise from northeast through north to northwest. The arrows point toward the northwest, north and northeast because the winds come from the southeast, south and southwest; a wind is named for where it blows from. The dashed difference vector is longer than the difference of the arrow lengths, because it includes the change of direction.

17.4.3 Veering and backing

Two words name the sense of a change of wind direction. *Veering* is a clockwise rotation of the wind direction, seen from above: an increase of the direction angle β, for example from south through southwest to west ($180^\circ \to 225^\circ \to 270^\circ$). *Backing* is a counterclockwise rotation, a decrease of β, for example from south through southeast to east ($180^\circ \to 135^\circ \to 90^\circ$). Both words apply to a change with time at one height and to a change with height at one time, and the definitions are geometric: they are the same in both hemispheres. What differs between hemispheres is which one usually occurs.

- *With height, in the boundary layer*: the wind usually veers with height in the Northern Hemisphere and backs with height in the Southern, for the frictional reason of Section 17.4.2.
- *With time, above the stable layer at night*: the inertial oscillation of Section 17.4.1 turns the wind clockwise in the Northern Hemisphere and counterclockwise in the Southern, so the wind aloft usually veers through the night in the Northern Hemisphere and backs in the Southern.
- *With time, at a frontal passage*: the wind usually veers as a cold front passes in the Northern Hemisphere (for example from southwest to northwest) and backs in the Southern (for example from northwest to southwest, the shift that accompanies the cold fronts crossing southern Brazil).

Above the boundary layer, turning with height is also produced by horizontal temperature gradients, which this chapter does not treat. A wind direction measured at two heights is therefore evidence about friction and stability as well as about the large-scale flow: a large turning across a shallow layer at night is a signature of a decoupled stable layer.

17.4.4 Shear is a vector

Because the wind turns with height, the shear is the vertical derivative of the wind vector, not of the speed. Its magnitude is

$$\left|\frac{\partial \mathbf{V}}{\partial z}\right| = \sqrt{\left(\frac{\partial u}{\partial z}\right)^2 + \left(\frac{\partial v}{\partial z}\right)^2}, \tag{17.8}$$

in s^{-1}, and it is this quantity that enters the shear production of equation (17.1) and the gradient Richardson number of equation (17.2). Between two measurement levels, with speeds U_1 and U_2 and a turning $\Delta\beta$, $|\Delta\mathbf{V}|^2 = U_1^2 + U_2^2 - 2U_1U_2\cos\Delta\beta$, by the law of cosines; it equals the squared speed difference $(U_2 - U_1)^2$ only if $\Delta\beta = 0$.

Worked example. Take the 10 and 100 m winds of Figure 17.6(a). With $u = -U\sin\beta$ and $v = -U\cos\beta$, the 10 m wind from 135° at $3\,\mathrm{m\,s^{-1}}$ is $(u, v) = (-2.12, +2.12)\,\mathrm{m\,s^{-1}}$ and the 100 m wind from 180° at $12\,\mathrm{m\,s^{-1}}$ is $(0, +12.00)\,\mathrm{m\,s^{-1}}$. The difference is $(\Delta u, \Delta v) = (2.12, 9.88)\,\mathrm{m\,s^{-1}}$, with magnitude

$$|\Delta\mathbf{V}| = \sqrt{2.12^2 + 9.88^2} = \sqrt{102.1} = 10.10\,\mathrm{m\,s^{-1}},$$

the same as from the law of cosines, $\sqrt{9 + 144 - 72\cos 45^\circ} = 10.10\,\mathrm{m\,s^{-1}}$. The vector shear over 90 m is $0.112\,\mathrm{s^{-1}}$, against a speed shear of $(12 - 3)/90 = 0.100\,\mathrm{s^{-1}}$: 12 % larger. Since the Richardson number contains the square of the shear, the speed shear overestimates it by the factor $(0.112/0.100)^2 = 1.26$: with the $\Delta\theta = 4\,\mathrm{K}$ of Section 17.2.2, $\mathrm{Ri}_B = 0.153$ from the speeds and 0.121 from the vectors. The Southern Hemisphere mirror of panel (b) gives the same magnitudes, since only the size of the turning enters.

The turning matters most when the speeds are low. A weak-wind night with $2\,\mathrm{m\,s^{-1}}$ from 135° at 10 m and $4\,\mathrm{m\,s^{-1}}$ from 225° at 100 m has a speed shear of $2/90 = 0.022\,\mathrm{s^{-1}}$, but the two vectors are perpendicular, so $|\Delta\mathbf{V}| = \sqrt{4+16} = 4.47\,\mathrm{m\,s^{-1}}$ and the vector shear is $0.050\,\mathrm{s^{-1}}$, more than twice as large; a Richardson number computed from the speeds would be five times too large. On such nights a stable layer that looks shear-free from speeds alone can be sheared enough to be turbulent.

17.4.5 A profile with a jet

The acceleration aloft and the strong shear below it produce a wind profile that is not even monotonic: the wind increases with height to a maximum and then decreases. An illustrative night profile has

$$U_{10} = 2\,\mathrm{m\,s^{-1}}, \quad U_{50} = 7\,\mathrm{m\,s^{-1}}, \quad U_{150} = 14\,\mathrm{m\,s^{-1}}, \quad U_{300} = 11\,\mathrm{m\,s^{-1}},$$

the dots of Figure 17.1. The mean shear is $0.125\,\mathrm{s^{-1}}$ between 10 and 50 m, $0.070\,\mathrm{s^{-1}}$ between 50 and 150 m, and $-0.020\,\mathrm{s^{-1}}$ between 150 and 300 m, where the wind decreases. The maximum, here an illustrative $14.5\,\mathrm{m\,s^{-1}}$ near 180 m, is the core of a low-level jet, with height z_{jet} and speed U_{jet}.

No logarithmic or power-law profile fits it, because both increase monotonically with height. Figure 17.7 compares the profile with three such curves. The horizontal axis is wind speed and the vertical axis height from 0 to 320 m; the dots are the four values above and the solid curve a profile drawn through them. The dashed curve is a power law through the 10 and 50 m values, the dotted curve a logarithmic law through the same two values, and the gray curve a power law with a daytime exponent $\alpha = 0.14$ through the 10 m value.

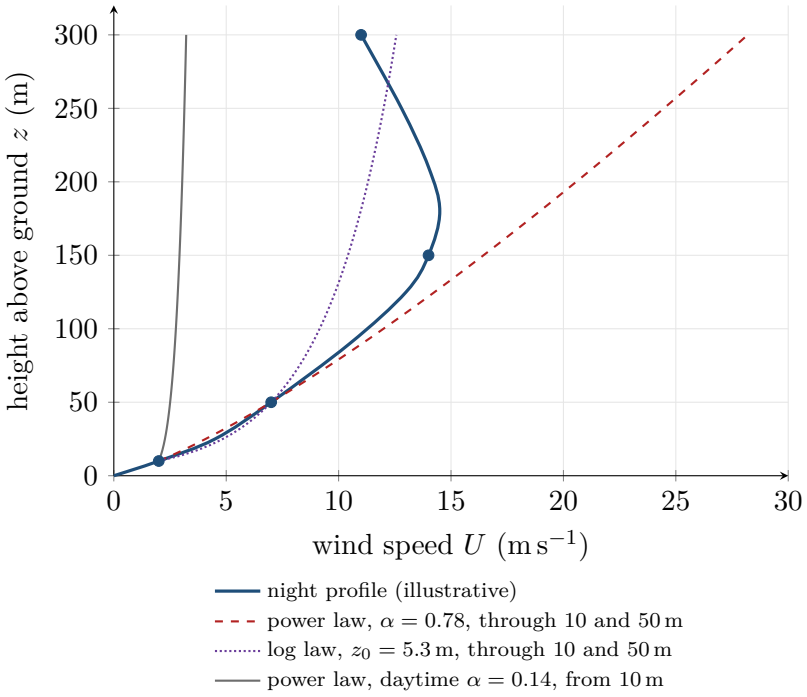


Figure 17.7: A night profile with a wind maximum and three monotonic fits. Dots: 2, 7, 14 and $11\,\mathrm{m\,s^{-1}}$ at 10, 50, 150 and 300 m (illustrative); the solid curve drawn through them has its maximum, the jet core, near 180 m. Dashed: $U = 2(z/10)^{0.78}$. Dotted: $U = 3.11\ln(z/5.25)$, in $\mathrm{m\,s^{-1}}$ with z in m. Gray: $U = 2(z/10)^{0.14}$.

Each fit fails in its own way. The power law through the two lowest values has the very large exponent $\ln 3.5/\ln 5 = 0.78$ and gives $16.5\,\mathrm{m\,s^{-1}}$ at 150 m and $28.2\,\mathrm{m\,s^{-1}}$ at 300 m, against

14 and 11 m s^{-1}: it cannot turn back. The logarithmic law through the same values needs a roughness length of 5.3 m, physically meaningless over a field, and gives 10.4 and 12.6 m s^{-1}, too slow at the core and still increasing above it. A least-squares power law through all four values (exponent 0.55) gives 2.4, 5.7, 10.4 and 15.3 m s^{-1}, wrong at every height and in the wrong direction at 300 m. The daytime power law gives 2.9 m s^{-1} at 150 m, a fifth of the observed wind. A profile with a maximum is outside the family of every formula built on a monotonic shape; it must be measured, or computed by a model that represents the stable layer and the acceleration aloft.

17.5 Terrain at night

Over sloping ground the cooling of the surface does more than stratify the air: it sets it in motion. This section describes the drainage of cold air down slopes, its accumulation in valleys, and the surface winds it produces against the large-scale flow. Thermally driven terrain circulations as a whole are the subject of Chapter 19.

17.5.1 Cold-air drainage

On a slope, the air in contact with the cooling ground becomes colder and denser than the air at the same height away from the slope. At the same height and pressure a temperature deficit ΔT gives a downward buoyant acceleration $g\,|\Delta T|/T$, and on a slope at angle α to the horizontal its component along the slope is (Chapter 5)

$$a_{\parallel} = g\,\frac{|\Delta T|}{T}\,\sin\alpha, \tag{17.9}$$

directed downslope. The cold air flows downhill: a *drainage flow*, a wind driven by the weight of cold air on sloping ground. When the flow is driven by cooling of the slope surface itself, it is called a *katabatic flow* (from the Greek for "going down"); the two terms are often used interchangeably, drainage flow being the more general one, including cold air that has pooled upslope and spills down. Drainage flows are measured as a shallow layer of downslope wind, typically 1 to 3 m s^{-1} and a few to a few tens of meters deep, with a speed maximum close to the ground and a temperature deficit at the surface; in models they are resolved only where the grid represents the slope.

Drainage occurs even when the large-scale wind is weak, and in fact mostly then, since a strong wind mixes the cooled air away. Its forcing is small but persistent. On a gentle valley floor with $\alpha = 2^\circ$ and an illustrative deficit of 2 K at $T = 285$ K, $a_{\parallel} = 9.81 \times (2/285) \times \sin 2^\circ = 0.0024$ m s^{-2}, about twice the pressure-gradient force of a typical synoptic gradient (about 10^{-3} m s^{-2}, the Coriolis force on a 10 m s^{-1} geostrophic wind at $|f| = 10^{-4}$ s^{-1}); on a 10° slope with a 3 K deficit it is 0.018 m s^{-2}. Over the slopes and valleys of a few kilometers that matter for a sensor or a span, the Coriolis force has little time to act, so drainage follows the terrain in both hemispheres alike.

17.5.2 Valley cold pools

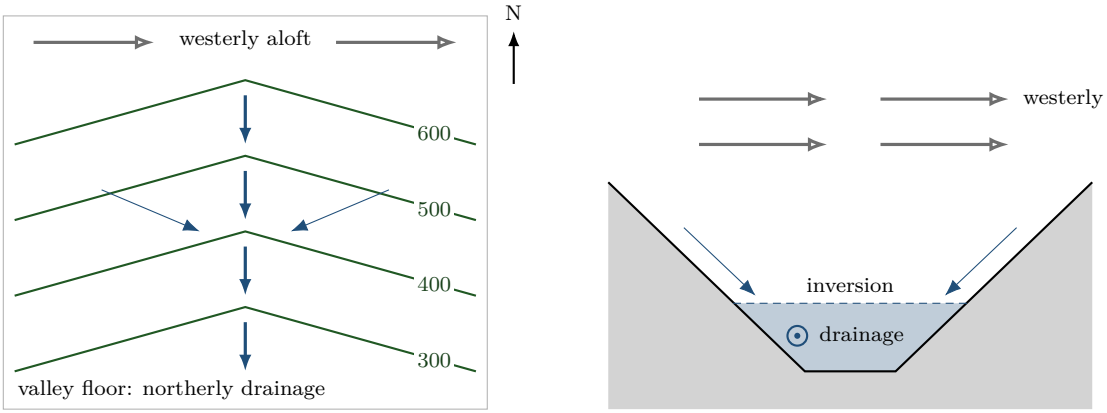
Drainage air collects where the terrain stops it: valley floors, basins and hollows. A *cold-air pool* is a layer of cold air trapped in a topographic low, with a strong inversion at its top (or through it), measured by thermometers at different heights on the valley floor and slopes, or seen on a model temperature field that resolves the valley. Within it the air is the coldest and densest in the area, the stratification is strong, and the wind on the valley floor is weak, often directed differently from the flow aloft and decoupled from it. A cold pool can be several kelvin colder at the valley floor than at the same height over the adjacent plain or on the upper slopes, and it can persist through the next day in winter when the sun is too weak to erode it.

For near-surface wind a cold pool is a place where the large-scale wind does not reach the ground. A sensor on a valley floor under a cold pool measures the drainage or a near calm, while a sensor a hundred meters higher on the slope measures the regional wind; both are correct, and neither represents the other.

17.5.3 Drainage against the synoptic wind

Drainage can produce a surface wind with no relation to the large-scale flow. Consider a region under a westerly synoptic wind, blowing from the west at the ridge tops, and a valley whose floor slopes down toward the south. At night the cold air drains down the valley, toward the south. A wind is named for where it comes from, so the drainage at the valley floor is a *northerly* wind (from about 360°), at right angles to the westerly aloft. A surface observation in the valley then looks nothing like the free-atmosphere flow, and a model or a forecaster that assumes the surface wind follows the large-scale wind, slowed and turned by a few tens of degrees, will be wrong in direction by about 90°.

Figure 17.8 draws the situation. Panel (a) is a plan view with north at the top: the contours are lines of equal ground elevation, in meters, whose points face up-valley, toward the north; the open gray arrows are the westerly wind above the ridges and the blue arrows the drainage along the valley floor and down the side slopes. Panel (b) is a vertical cross section across the valley, looking north with west on the left: the shaded layer is the cold pool, its top, the dashed line, an inversion; the gray arrows are the westerly above it, the blue arrows the drainage down the side slopes, and the symbol on the valley floor the drainage along the valley flowing toward the viewer, out of the page.



(a) plan view (b) cross section, looking north

Figure 17.8: Drainage against the synoptic wind (schematic; the drainage is a local, terrain-following flow, the same in both hemispheres). (a) Plan view, north at the top: a valley whose floor descends toward the south (contours in meters); the cold air drains down the side slopes and along the floor toward the south, a northerly surface wind, under a westerly wind above the ridges. (b) Cross section across the valley, looking north: the cold pool fills the valley floor under an inversion; the drainage flows out of the page, toward the south.

In panel (a) the contour values decrease from north to south, so the floor descends southward and the blue arrows along it point south; the side-slope arrows feed it from east and west. The gray arrows above the ridges point east, the way a westerly blows. Panel (b) shows why the two winds coexist: the cold pool fills the valley up to its inversion, the westerly passes above the inversion without mixing down into it, and the valley floor feels only the drainage. Neither panel contains the Coriolis force, so the same picture holds at the same terrain in either hemisphere.

Chapter 19 treats slope and valley winds as part of the thermally driven circulations, by day as well as by night.

17.6 Models, measurements and diagnosis of the stable layer

The physics of the previous sections is what makes the stable layer hard to represent. This section explains why similarity theory struggles at night, how weather models parameterize stable mixing and what their choice does to the surface wind and temperature, what the stable layer means for low sensors and for the extrapolation of winds with height, and closes with a sequence of checks for diagnosing an unexpectedly weak night wind.

17.6.1 Why similarity theory struggles

Monin–Obukhov similarity (Chapter 14) assumes a surface layer in which the turbulence is continuous, stationary, horizontally homogeneous, and determined locally by the surface fluxes and the height. In the very stable regime each assumption fails. The turbulence is not continuous but intermittent (Section 17.3.2). Transport is partly nonlocal: turbulence measured near the ground can be produced in a sheared layer aloft, at the base of a jet, and carried down, so it does not depend on the local fluxes. Gravity waves carry momentum without carrying much heat and produce wind and temperature fluctuations that are not turbulence. Drainage flows have their own shear, set by the slope, not by the surface stress. And the layer is nonstationary, so a half-hour average mixes quiet periods and bursts. The profile functions, such as $\phi_m = 1+5\,z/L_{\mathrm{O}}$, are fitted to data from the weakly stable regime; values of $z/L_{\mathrm{O}} \gg 1$, like the 3.5 of Figure 17.2, are a warning that the theory is being used outside its domain, not a measurement of how stable the layer is.

17.6.2 Stable parameterizations in weather models

A weather model does not resolve the eddies of the stable layer; it parameterizes their effect with eddy diffusivities K_m and K_h that depend on the stability. A common form, in a first-order scheme, is

$$K_m = l^2\,|\partial \mathbf{V}/\partial z|\,F_m(\mathrm{Ri}_g), \tag{17.10}$$

with l a mixing length, $|\partial \mathbf{V}/\partial z|$ the vector shear of the model profile and F_m a stability function that equals one in neutral air and decreases as Ri_g grows; K_h has a similar form. The model must decide how fast the turbulence collapses as the stability increases, and the choice of F_m is that decision. Two families illustrate it. A *short-tail* function such as $F_m = (1 - \mathrm{Ri}_g/\mathrm{Ri}_c)^2$ for $\mathrm{Ri}_g < \mathrm{Ri}_c$, and zero above, shuts the mixing off at the critical value: at $\mathrm{Ri}_g = 0.15$ with $\mathrm{Ri}_c = 0.25$ it gives $F_m = 0.16$, and at $\mathrm{Ri}_g = 0.5$ none. A *long-tail* function such as $F_m = 1/(1 + 10\,\mathrm{Ri}_g)$ never reaches zero: it gives 0.40 at $\mathrm{Ri}_g = 0.15$ and 0.17 at $\mathrm{Ri}_g = 0.5$. Both are illustrative forms of the two families, not the functions of a particular model.

Too much suppression lets the model's surface layer decouple entirely: the surface winds come out too weak and the surface too cold. Too much mixing keeps the surface coupled to the wind aloft: the surface winds come out too strong. Real stable layers lie between the two, and their intermittent turbulence is not represented by either.

17.6.3 The too-much-mixing problem

Many weather models keep more mixing in stable conditions than is observed, typically through a long-tailed stability function or a minimum eddy diffusivity. The reason is numerical and practical: when the model's turbulence collapses completely, its surface layer cools without limit, its near-surface shear and decoupling become unrealistically strong, and the forecasts of

temperature and of the larger-scale flow degrade. A background mixing prevents this runaway. Its cost is a systematic overprediction of the nighttime surface wind, together with an inversion that is too weak and a stable layer that is too deep.

The errors come in pairs, because one cause, the strength of the vertical mixing, moves heat and momentum together. Table 17.3 lists the pattern for too much and for too little mixing. Its rows are the modeled quantities that can be compared with observations, and its two columns give the sign of the model error in each case.

Table 17.3: Paired errors of a weather model's stable layer. Each column has one cause, the strength of the parameterized vertical mixing at night.

Modeled quantity	Too much mixing	Too little mixing
Temperature at 2 m	too warm (heat mixed down)	too cold
Wind at 10 m	too strong (momentum mixed down)	too weak
Shear between 10 and 100 m	too weak	too strong
Surface inversion	too weak	too strong
Depth of the stable layer	too deep	too shallow
Low-level jet	too weak, too high	too strong, too low

The pairing is the diagnostic. A model whose nights are both too warm at 2 m and too windy at 10 m has one error, too much mixing, not two, and correcting the wind by a statistical adjustment alone leaves the cause in place. The opposite pattern, a 2 m temperature too cold, a 10 m wind too low and a shear too strong, points to too little mixing, often a collapsed model surface layer on a night whose real turbulence was intermittent but present. An error in the wind with no matching error in the temperature points elsewhere: to the roughness length, the terrain, or the forcing aloft.

17.6.4 Consequences for a low sensor

For engineering measurements the stable layer means that a weak wind at a low sensor does not mean calm air in the column. A wind of $2\,\mathrm{m\,s^{-1}}$ at 20 m can sit under $10\,\mathrm{m\,s^{-1}}$ at 100 m: a mean shear of $8/80 = 0.10\,\mathrm{s^{-1}}$ and an exponent of $\ln 5/\ln 5 = 1.0$, a wind that grows in proportion to height. Both readings are correct. For a conductor at 20 m the low reading is the one that matters, and it is the conductor's convective cooling that suffers; for a turbine hub at 100 m the night is windy. A forecast or a sensor at one height describes that height. The wind at another height on a stable night must be measured there, or computed with the stability known.

17.6.5 Extrapolation failure

Extrapolating a wind from one height to another with a fixed power law carries the stability of the conditions in which the exponent was fitted. A daytime exponent, $\alpha = 0.14$, extrapolated upward from $U_{10} = 2\,\mathrm{m\,s^{-1}}$ gives $2 \times 10^{0.14} = 2.8\,\mathrm{m\,s^{-1}}$ at 100 m and $2 \times 15^{0.14} = 2.9\,\mathrm{m\,s^{-1}}$ at 150 m, against $14\,\mathrm{m\,s^{-1}}$ observed in the profile of Figure 17.7. Extrapolated downward from $U_{100} = 12\,\mathrm{m\,s^{-1}}$ in the decoupling example of Section 17.2.3, it gives $U_{10} = 12/10^{0.14} = 8.7\,\mathrm{m\,s^{-1}}$, four times the observed $2\,\mathrm{m\,s^{-1}}$: the error that overstates the cooling of a low conductor on a stable night.

Stable shear is stronger than daytime shear, so any fixed daytime exponent misses the nighttime profile, and a fixed nighttime exponent has the opposite problem by day. Even an exponent fitted at night fails above the jet core, because the profile may have a maximum and is then not even monotonic (Section 17.4.5). Extrapolation on a stable night needs the stability as

an input, through the log-linear profile within its range of validity, and above it a measurement or a model of the stable layer.

17.6.6 A diagnostic sequence for a weak night wind

When a measured nighttime wind near the ground is unexpectedly weak, compared with a forecast or with the wind aloft, the chapter's chain gives an ordered set of questions. Table 17.4 lists them. Its rows follow the chain from the cause, the surface cooling, to its terrain-specific outcomes; its columns give the question and what to check to answer it, with the measurement or model field that provides the evidence.

Table 17.4: Diagnostic sequence for an unexpectedly weak nighttime near-surface wind. Thresholds are indicative.

	Question	What to check
1	Strong surface cooling?	Cloud cover (clear or cloudy), net longwave radiation if measured, the rate of fall of the 2 m temperature after sunset (of the order of $1\,\mathrm{K\,h^{-1}}$ or more on a clear night)
2	An inversion?	Temperature at two or more heights, converted with $\Delta\theta \approx \Delta T + 0.0098\,\Delta z$; a temperature that rises with height; a sounding or model profile
3	A large Richardson number?	Ri_B between two levels with the vector wind difference; values above about 0.25 point to suppressed turbulence
4	Weak turbulence?	σ_w and u_* from a sonic anemometer; σ_w of a few centimeters per second; bursts in the record
5	A stronger wind aloft?	Lidar, sodar or tall-mast winds at 100 m and above, or the model's wind there; a ratio U_{10}/U_{100} well below 0.5 indicates decoupling
6	A low-level jet?	A wind maximum in the lowest few hundred meters, with the wind decreasing above it; turning of the wind with time aloft
7	Drainage flow from terrain?	The slope around the site; a surface wind directed down the local slope or valley, unrelated to the synoptic direction; a shallow cold layer
8	A cold-air pool?	A valley or basin site; a valley floor much colder than the slopes at the same time; very weak, variable wind; fog

The order matters. Questions 1 to 4 establish whether the site is in the stable regime at all, and how deeply; question 5 separates a weak wind everywhere, a slack night, from a weak wind only near the ground, a decoupled one; questions 6 to 8 identify which of the stable layer's own phenomena controls the surface wind. A weak wind with a cloudy sky, no inversion and continuous turbulence is not a stable-layer problem, and the explanation must be sought in the forcing or the exposure of the sensor. A weak wind with a clear sky, a strong inversion, a large Richardson number, a strong wind aloft and a wind maximum near 150 m is the decoupled night of this chapter, and its most prominent feature, the jet above it, is the subject of the next chapter, on low-level jets (Chapter 18).

17.7 What to retain

Definition 17.1 (The stable nocturnal boundary layer)**.** The stable boundary layer is not a weaker daytime layer but a different regime: surface cooling → stable stratification → weak, intermittent turbulence → decoupling → strong shear, in speed and in direction; in it terrain, gravity waves and the inertial oscillation of the wind aloft become disproportionately important.

Table 17.5 lists the terms of the chapter, their meaning, their units and the subsection that defines each.

Table 17.5: The terms of the chapter and where each is defined.

Term	Meaning	Units	Defined in
Stable boundary layer	layer next to the ground with $\mathrm{d}\theta/\mathrm{d}z > 0$ from surface cooling; turbulence from shear only; tens to a few hundred meters deep	m (depth z_i)	17.1, 17.1.2
Residual layer	remnant of the afternoon mixed layer above the stable layer; nearly neutral, decaying turbulence	m	17.1.3
Decoupling	turbulent momentum transport too weak to bring the wind aloft down; e.g. $12\,\mathrm{m\,s^{-1}}$ at 100 m over $2\,\mathrm{m\,s^{-1}}$ at 10 m	–	17.2.3
Weakly and very stable regimes	continuous turbulence and coupling, against intermittent turbulence and decoupling	–	17.3.1
Intermittent turbulence	bursts of turbulence separated by quiet periods	–	17.3.2
Turbulence collapse	near-disappearance of turbulence through the stable feedback	–	17.3.3
Turbulent burst	minutes-long episode of strong mixing of momentum and heat down	–	17.3.4
Kelvin–Helmholtz instability	growth and overturning of waves in a sheared stratified layer; requires $\mathrm{Ri}_g < 0.25$	–	17.3.5
Internal gravity wave	wave inside the stratified air with buoyancy as restoring force; $\omega = N\cos\gamma \le N$	$\mathrm{s^{-1}}$	17.3.6
Brunt–Väisälä frequency N	$N^2 = (g/\theta)\,\mathrm{d}\theta/\mathrm{d}z$; strength of static stability	$\mathrm{s^{-1}}$	17.3.6
Directional shear	change of wind direction with height	°/m	17.4.2
Veering	clockwise turning of the wind direction, with time or height	°	17.4.3
Backing	counterclockwise turning of the wind direction, with time or height	°	17.4.3
Vector shear $\lvert\partial\mathbf{V}/\partial z\rvert$	$\sqrt{(\partial u/\partial z)^2 + (\partial v/\partial z)^2}$; enters P_s and Ri_g	$\mathrm{s^{-1}}$	17.4.4
Drainage flow	downslope flow of cold, dense air	m/s	17.5.1
Katabatic flow	drainage flow driven by cooling of the slope surface	m/s	17.5.1
Cold-air pool	cold air trapped in a valley or basin under a strong inversion	–	17.5.2
Too-much-mixing problem	excess stable mixing in models: surface wind too strong, 2 m temperature too warm	–	17.6.3

17.8 Exercises

Exercise 17.1. On a clear night the surface emits $380\,\mathrm{W\,m^{-2}}$ and receives $325\,\mathrm{W\,m^{-2}}$ of longwave radiation from the sky. Take $\rho c_p = 1200\,\mathrm{J\,m^{-3}\,K^{-1}}$ and $\theta = 288\,\mathrm{K}$. (a) Compute the net longwave loss. (b) If $40\,\%$ of it is drawn from the air as a downward sensible heat flux and removed uniformly from a layer $60\,\mathrm{m}$ deep, compute the cooling rate of the layer in $\mathrm{K\,h^{-1}}$. (c) At 03:00 a tower measures $T = 6.0^\circ\mathrm{C}$ at $2\,\mathrm{m}$ and $9.0^\circ\mathrm{C}$ at $52\,\mathrm{m}$. Compute $\mathrm{d}\theta/\mathrm{d}z$, the buoyancy frequency N and the shortest gravity-wave period in the layer. (d) A gravity wave in the same layer has parcels moving along paths tilted 60° from the vertical. What is its period?

Exercise 17.2. A mast in the Northern Hemisphere has anemometers and thermometers at 10 and $90\,\mathrm{m}$, $\Delta z = 80\,\mathrm{m}$, $\overline{\theta} = 285\,\mathrm{K}$. At 21:00 it records $U_{10} = 3.5\,\mathrm{m\,s^{-1}}$, $U_{90} = 8.0\,\mathrm{m\,s^{-1}}$, both from 200°, and $\Delta\theta = 1.0\,\mathrm{K}$; at 02:00 it records $U_{10} = 1.2\,\mathrm{m\,s^{-1}}$, $U_{90} = 10.0\,\mathrm{m\,s^{-1}}$, both from 200°, and $\Delta\theta = 8.0\,\mathrm{K}$. (a) Compute the mean shear, the ratio U_{10}/U_{90} and Ri_B at each time. (b) Classify each time as weakly or very stable using Table 17.1, and state which time is decoupled. (c) Between 21:00 and 02:00 the $90\,\mathrm{m}$ wind has increased with no change in the large-scale pressure gradient. Name the mechanism, and state which way the $90\,\mathrm{m}$ wind direction is expected to turn with time. (d) A burst at 02:30 raises U_{10} to $4.0\,\mathrm{m\,s^{-1}}$ and lowers U_{90} to $8.0\,\mathrm{m\,s^{-1}}$, with $\Delta\theta = 5.0\,\mathrm{K}$. Recompute Ri_B, and use Figure 17.4 to explain why it has increased and what follows.

Exercise 17.3. A site at $25^\circ\mathrm{S}$ records at 23:00 a wind of $2.0\,\mathrm{m\,s^{-1}}$ from 250° at $10\,\mathrm{m}$ and $9.0\,\mathrm{m\,s^{-1}}$ from 200° at $80\,\mathrm{m}$, with $\Delta\theta = 3.0\,\mathrm{K}$ and $\overline{\theta} = 290\,\mathrm{K}$. (a) Does the wind veer or back with height? Is that the sense expected from friction in this hemisphere? (b) Compute the (u, v) components of both winds, the vector difference, the vector shear and the speed shear. (c) Compute Ri_B from the vectors and from the speeds, and the ratio of the two. (d) Over the next three hours the $80\,\mathrm{m}$ wind turns to 185° and then 170°. Is this veering or backing, and is it consistent with the inertial oscillation at this latitude? Compute the inertial period.

Exercise 17.4. A transmission line runs along the floor of a valley whose floor descends toward the east. On a clear night with a regional southerly wind of $8\,\mathrm{m\,s^{-1}}$ above the ridges, a sensor at $10\,\mathrm{m}$ on the valley floor reads $1.5\,\mathrm{m\,s^{-1}}$ from 270° and a lidar at the site reads $6\,\mathrm{m\,s^{-1}}$ at $50\,\mathrm{m}$, $12\,\mathrm{m\,s^{-1}}$ at $120\,\mathrm{m}$ and $9\,\mathrm{m\,s^{-1}}$ at $250\,\mathrm{m}$. (a) From which direction is a drainage wind on the valley floor expected to blow, and what is it called in the book's convention? Is the sensor's reading consistent with drainage or with the regional wind? (b) Extrapolate the $10\,\mathrm{m}$ reading to $120\,\mathrm{m}$ with a daytime exponent $\alpha = 0.14$ and compare with the lidar. (c) Compute the exponent of a power law through the 10 and $50\,\mathrm{m}$ readings and the speed it predicts at $250\,\mathrm{m}$; explain the failure. (d) Go through the eight questions of Table 17.4 and state which are answered by the data given and what each answer is.

Chapter 18

Low-Level Jets

18.1 The jet profile

The wind profiles of the earlier chapters all increase with height: the logarithmic profile, the power law and their stability-corrected forms give a wind that grows from zero at the roughness length toward the wind of the free atmosphere and never decreases on the way. Chapter 13 noted that on stable nights the air above a shallow stable layer accelerates, and Chapter 6 showed a night profile whose wind peaked near the top of that layer. The question of this chapter is

why can the wind become strongest a few hundred meters above the ground at night, and what does such a maximum do to the wind at the heights where it is used?

The chapter first describes the profile with a maximum and the quantities that characterize it. It then derives the classic nocturnal mechanism, an inertial oscillation of the ageostrophic wind released when friction collapses at sunset, follows the jet through the night and its breakdown in the morning, and catalogues the other mechanisms that produce low-level wind maxima. It ends with how jets are observed and detected and with their consequences for wind energy, transmission-line rating and forecasts.

Jargon: low-level jet, jet core, ageostrophic wind, inertial oscillation, Blackadar mechanism, supergeostrophic wind

A *low-level jet* is a local maximum of the horizontal wind speed in the lowest one to two kilometers of the atmosphere: a height below which the wind increases with height and above which it decreases. It is a feature of the measured or modeled profile $U(z)$, observed with profiling instruments and represented by a model on its vertical levels. The *jet core* is the height of that maximum, z_{jet} in meters, and the speed there, U_{jet} in $\mathrm{m\,s^{-1}}$. The *ageostrophic wind* $\mathbf{V}_a = \mathbf{V} - \mathbf{V}_g$, in $\mathrm{m\,s^{-1}}$, is the vector difference between the actual horizontal wind and the geostrophic wind of Chapter 3; it is calculated, not measured, from a measured wind and a geostrophic wind computed from the pressure field. An *inertial oscillation* is the rotation of the ageostrophic wind under the Coriolis force alone, at the angular rate $|f|$ and with the *inertial period* $T_I = 2\pi/|f|$. The *Blackadar mechanism*, named after the meteorologist who proposed it in 1957, is the explanation of the nocturnal low-level jet as such an oscillation, started when the friction acting on the lower atmosphere collapses at sunset. A *supergeostrophic wind* is a wind faster than the local geostrophic wind, $|\mathbf{V}| > |\mathbf{V}_g|$.

Key idea

At sunset the stable layer cuts the air above it off from the drag of the ground. The ageostrophic wind that friction had maintained during the day is then no longer balanced and rotates under the Coriolis force with the inertial period, so that some hours later it points along the geostrophic wind and adds to it: the wind aloft becomes supergeostrophic, while the wind near the ground stays weak. The profile then has a maximum, and no profile that increases monotonically with height can represent it.

18.1.1 A wind maximum above the ground

A low-level jet is defined by the shape of the profile, not by the speed of the wind. An illustrative night profile reads

$$U_{10} = 3\,\mathrm{m\,s^{-1}}, \quad U_{50} = 7\,\mathrm{m\,s^{-1}}, \quad U_{150} = 14\,\mathrm{m\,s^{-1}}, \quad U_{300} = 11\,\mathrm{m\,s^{-1}},$$

with the subscript giving the height in meters. The wind more than quadruples between 10 and 150 m and then decreases by $3\,\mathrm{m\,s^{-1}}$ between 150 and 300 m: a maximum, then a decrease. The maximum is not a measurement error or a gust; it is a layer of fast-moving air a few hundred meters thick, with slower air both above and below it.

The surface-layer profiles of the earlier chapters cannot reproduce it. A power law $U(z) = U(z_r)(z/z_r)^\alpha$ through the two lowest levels has the exponent

$$\alpha = \frac{\ln(U_{50}/U_{10})}{\ln(50/10)} = \frac{\ln(7/3)}{\ln 5} = \frac{0.847}{1.609} = 0.53,$$

already far above the neutral value of about 1/7, and extrapolated upward it gives $U_{150} = 7 \times 3^{0.53} = 12.5\,\mathrm{m\,s^{-1}}$ and $U_{300} = 7 \times 6^{0.53} = 18.0\,\mathrm{m\,s^{-1}}$. A logarithmic law $U = (u_*/\kappa)\ln(z/z_0)$ through the same two levels has $u_*/\kappa = (7-3)/\ln 5 = 2.49\,\mathrm{m\,s^{-1}}$ and $\ln(10/z_0) = 3/2.49 = 1.21$, so $z_0 = 10/e^{1.21} = 3.0\,\mathrm{m}$; it gives $U_{150} = 2.49\ln(150/3.0) = 9.7\,\mathrm{m\,s^{-1}}$ and $U_{300} = 11.5\,\mathrm{m\,s^{-1}}$. Neither fit has any physical standing: the log fit implies a roughness length of three meters and a friction velocity of $0.4 \times 2.49 = 1.0\,\mathrm{m\,s^{-1}}$, both absurd for a night over open land, which is the signature of a profile curved by stability rather than by roughness.

Figure 18.1 plots the example. The horizontal axis is wind speed and the vertical axis height above the ground. The black dots are the four measured levels, joined by straight lines because the shape between levels is not observed; the dashed blue curve is the power law and the dotted red curve the log law, both fitted to the 10 and 50 m values. Both fits agree with the data where they were fitted and depart from it above. The power law underestimates the wind at 150 m by $1.5\,\mathrm{m\,s^{-1}}$ and overestimates it at 300 m by $7\,\mathrm{m\,s^{-1}}$; the log law underestimates the core by more than $4\,\mathrm{m\,s^{-1}}$ and matches the 300 m value only by accident. Both increase without limit, so neither can turn the profile around.

Why the jet matters. The combination of weak wind at the surface and strong wind 100 to 300 m higher affects every application that uses the wind in that layer. The rotor of a wind turbine spans it, so its power and its loads depend on where the maximum sits. The conductor of a transmission line sits below it, in the weak wind, and its convective cooling depends on how much of the momentum aloft reaches it. The shear below the core produces turbulence in an otherwise quiet night; aircraft on approach cross the shear; and pollutants released into the jet are carried hundreds of kilometers overnight while those released below it stay near the source. Above all, the standard extrapolations of the wind from a measured height to another height, the log law and the power law, fail in the presence of a jet, as Figure 18.1 shows.

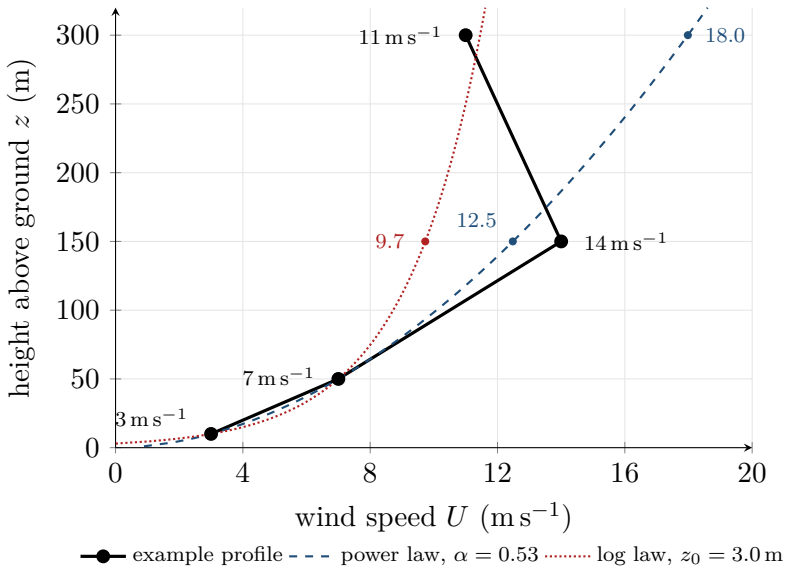


Figure 18.1: An illustrative night profile with a low-level jet, $U_{10} = 3$, $U_{50} = 7$, $U_{150} = 14$, $U_{300} = 11\,\mathrm{m\,s^{-1}}$ (dots, joined by straight lines), against the power law $U = 3\,\mathrm{m\,s^{-1}}\,(z/10\,\mathrm{m})^{0.53}$ and the log law $U = 2.49\,\mathrm{m\,s^{-1}}\,\ln(z/3.0\,\mathrm{m})$, both fitted to the two lowest levels. Colored numbers are the fits' values at 150 and 300 m.

18.1.2 The jet core and the shear below it

The *jet core* is the height of maximum wind and the speed there. In an illustrative profile with $U_{\mathrm{jet}} = 16\,\mathrm{m\,s^{-1}}$ at $z_{\mathrm{jet}} = 200\,\mathrm{m}$, the wind is weaker both above and below 200 m. Below the core the speed increases with height, $\partial U/\partial z > 0$; above it the speed decreases, $\partial U/\partial z < 0$; at the core $\partial U/\partial z = 0$. The core is therefore the one height at which the vertical shear of the speed vanishes, and the layer below it is where the jet interacts with the ground.

The shear below the core is large. With $U_{20} = 4\,\mathrm{m\,s^{-1}}$ at 20 m and $U_{\mathrm{jet}} = 16\,\mathrm{m\,s^{-1}}$ at 200 m,

$$\frac{\Delta U}{\Delta z} = \frac{16-4}{200-20}\,\frac{\mathrm{m\,s^{-1}}}{\mathrm{m}} = \frac{12}{180}\,\mathrm{s^{-1}} \approx 0.067\,\mathrm{s^{-1}}, \tag{18.1}$$

a speed change of $12\,\mathrm{m\,s^{-1}}$ over 180 m. This is a layer-mean value; the local shear is larger near the ground and smaller near the core. It is more than three times the afternoon value of about $0.02\,\mathrm{s^{-1}}$ between 10 and 100 m used in Chapter 6, and it is the shear that produces turbulence beneath the jet even in a stable layer (Section 18.3.2).

18.1.3 Strength and height of the jet

The two numbers of the core matter separately. The core speed U_{jet} says how much momentum the jet carries; the core height z_{jet} says how close that momentum is to the ground and how strong the shear below it is. A strong jet at 800 m has little immediate effect on a sensor at 20 m: the shear below it is spread over hundreds of meters, and its momentum must cross the whole stable layer to reach the sensor. A weaker jet at 80 m strongly affects the near-surface shear and the mixing: with the same $4\,\mathrm{m\,s^{-1}}$ at 20 m, a $12\,\mathrm{m\,s^{-1}}$ core at 80 m gives $(12-4)/60 = 0.13\,\mathrm{s^{-1}}$, twice the shear of equation (18.1) with a core $4\,\mathrm{m\,s^{-1}}$ weaker.

A description of a jet therefore always gives both numbers, together with the time and, where it is known, the direction at the core. A forecast or a model that has the right core speed at the wrong height is not nearly right for the near-surface wind; it can be badly wrong (Section 18.6.4).

18.1.4 A jet against a strong low-level wind

A strong wind at low levels is not by itself a jet. A profile of $5\,\mathrm{m\,s^{-1}}$ at 10 m, $10\,\mathrm{m\,s^{-1}}$ at 100 m and $15\,\mathrm{m\,s^{-1}}$ at 300 m (illustrative heights) has strong winds and strong shear, but the wind increases at every height: there is no local maximum, and the profile is an ordinary shear profile, as on a windy neutral or weakly stable day. A jet requires that the wind *decrease* somewhere above the maximum.

Figure 18.2 draws the distinction. The horizontal axis is wind speed and the vertical axis height. The solid red curve is the illustrative jet profile with its core at $16\,\mathrm{m\,s^{-1}}$ and 200 m, marked with a dot, and with the two points that define the shear of equation (18.1) marked as circles. The dashed gray curve is the strong but monotonic profile. Both have strong low-level shear; only the red one turns back toward weaker winds above the core, and only it is a jet. The curves are smooth sketches through illustrative values.

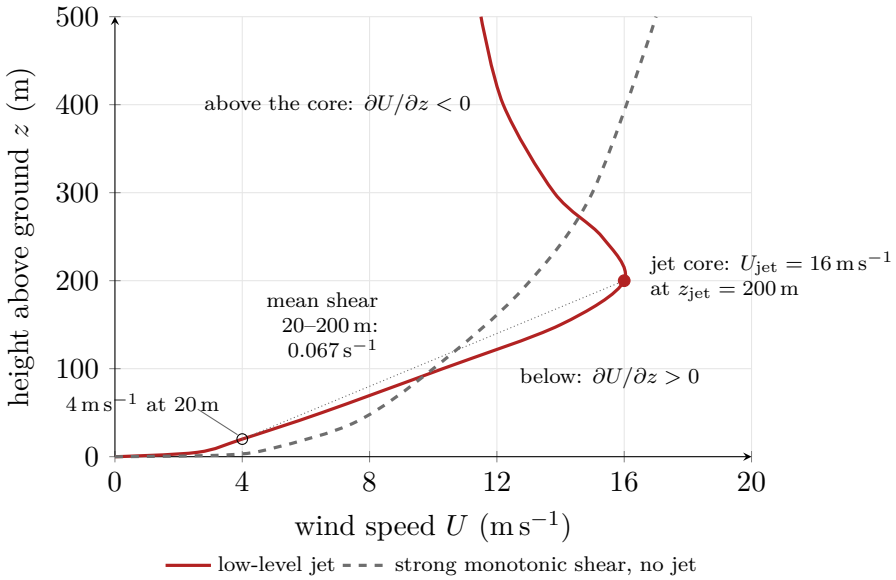


Figure 18.2: A low-level jet (solid red) against a strong low-level wind without a jet (dashed gray), illustrative smooth profiles. The jet has its core at $U_{\mathrm{jet}} = 16\,\mathrm{m\,s^{-1}}$, $z_{\mathrm{jet}} = 200\,\mathrm{m}$ (dot) and a mean shear of $(16-4)/180 = 0.067\,\mathrm{s^{-1}}$ between 20 m and the core; the monotonic profile passes through 5, 10 and $15\,\mathrm{m\,s^{-1}}$ at 10, 100 and 300 m and has no maximum.

18.2 The nocturnal inertial jet

The most common low-level jet over flat land is nocturnal, and its classic explanation rests on the momentum equation of Chapter 3 with friction switched off at sunset. This section writes the daytime balance, derives the frictionless motion of the ageostrophic wind and works an example in both hemispheres.

18.2.1 The daytime balance and decoupling at sunset

Write the horizontal momentum equation for the mean wind in the boundary layer, with the pressure-gradient force expressed through the geostrophic wind, $f\mathbf{k}\times\mathbf{V}_g = -(1/\rho)\nabla_h p$ (Chapter 3), and the friction force $\mathbf{F}$ standing for the vertical divergence of the turbulent momentum flux, $\mathbf{F} = -\partial(\overline{u'w'}, \overline{v'w'})/\partial z$ (Chapter 9). For a horizontally uniform flow, in which

advection is negligible,

$$\frac{\partial \mathbf{V}}{\partial t} = -\frac{1}{\rho}\nabla_h p - f\mathbf{k}\times\mathbf{V} + \mathbf{F} = -f\mathbf{k}\times(\mathbf{V}-\mathbf{V}_g) + \mathbf{F} = -f\mathbf{k}\times\mathbf{V}_a + \mathbf{F}. \tag{18.2}$$

Here u and v are the eastward and northward components, and $\mathbf{k}\times(a,b) = (-b,a)$. The pressure gradient enters only through $\mathbf{V}_g$, and only the ageostrophic part of the wind feels a net force from the pressure gradient and the Coriolis force together.

During the day turbulence couples the whole boundary layer to the ground, and the wind is close to a steady state in which the friction force balances the Coriolis force on the ageostrophic wind, $f\mathbf{k}\times\mathbf{V}_a = \mathbf{F}$. Taking $\mathbf{k}\times$ of both sides and using $\mathbf{k}\times(\mathbf{k}\times\mathbf{V}_a) = -\mathbf{V}_a$ gives

$$\mathbf{V}_a = -\frac{1}{f}\,\mathbf{k}\times\mathbf{F}. \tag{18.3}$$

Friction maintains an ageostrophic wind perpendicular to itself. For a friction force pointing west, against a westerly wind, $\mathbf{k}\times\mathbf{F}$ points south, and $\mathbf{V}_a$ points north for $f>0$ and south for $f<0$: toward low pressure in either hemisphere, which is the cross-isobar flow of Chapter 3. Together with the reduction of speed that the drag causes, the daytime boundary layer wind is subgeostrophic and turned toward low pressure, and the difference is a sizable ageostrophic vector.

Decoupling. After sunset the ground cools by emitting longwave radiation, a stable layer forms at the surface, and the turbulence within it weakens (Chapters 6 and 13). Above that shallow layer the turbulence of the day decays, the stress gradient becomes small, and the air of the former mixed layer, the residual layer, feels much less drag. The pressure gradient that drives it has not changed. In equation (18.2) the term $\mathbf{F}$ has collapsed while $\mathbf{V}_a$, set by the daytime balance, is still there and is no longer balanced: the air above the stable layer accelerates.

18.2.2 The frictionless ageostrophic wind

With $\mathbf{F}=0$, and with $\mathbf{V}_g$ constant in time, equation (18.2) becomes an equation for the ageostrophic wind alone, since $\partial\mathbf{V}_a/\partial t = \partial\mathbf{V}/\partial t$:

$$\frac{\partial u_a}{\partial t} = f\,v_a, \qquad \frac{\partial v_a}{\partial t} = -f\,u_a. \tag{18.4}$$

Multiplying the first equation by u_a, the second by v_a and adding gives $\frac{1}{2}\,\partial(u_a^2+v_a^2)/\partial t = f u_a v_a - f v_a u_a = 0$: the magnitude $|\mathbf{V}_a|$ is conserved. To find its direction, combine the components into the complex number $W = u_a + \mathrm{i}\,v_a$. Equations (18.4) give

$$\frac{\partial W}{\partial t} = f v_a - \mathrm{i} f u_a = -\mathrm{i} f\,(u_a + \mathrm{i}\,v_a) = -\mathrm{i} f\,W, \qquad W(t) = W(0)\,e^{-\mathrm{i}ft}. \tag{18.5}$$

In components, with (u_{a0}, v_{a0}) the ageostrophic wind at the moment friction stops,

$$u_a(t) = u_{a0}\cos ft + v_{a0}\sin ft, \qquad v_a(t) = v_{a0}\cos ft - u_{a0}\sin ft, \tag{18.6}$$

which can be checked by differentiation against equation (18.4).

The ageostrophic vector keeps its length and rotates at the angular rate $|f|$. Multiplication by $e^{-\mathrm{i}ft}$ decreases the angle of W in the (u,v) plane when $f>0$: in the Northern Hemisphere the vector turns *clockwise*, seen from above. When $f<0$ the angle increases and the vector turns *counterclockwise*. One full turn takes the inertial period $T_I = 2\pi/|f|$. The total wind

$\mathbf{V} = \mathbf{V}_g + \mathbf{V}_a$ moves on a circle of radius $|\mathbf{V}_a|$ centered on the geostrophic wind, and its speed follows from the law of cosines,

$$|\mathbf{V}|^2 = |\mathbf{V}_g|^2 + |\mathbf{V}_a|^2 + 2\,|\mathbf{V}_g|\,|\mathbf{V}_a|\cos\gamma(t), \tag{18.7}$$

where $\gamma(t)$ is the angle between $\mathbf{V}_a$ and $\mathbf{V}_g$. The speed reaches its maximum $|\mathbf{V}_g| + |\mathbf{V}_a|$ when the ageostrophic wind points along the geostrophic wind, $\gamma = 0$, and its minimum $\big||\mathbf{V}_g| - |\mathbf{V}_a|\big|$ half a period later. If γ_0 is the angle through which $\mathbf{V}_a$ must still turn, in its own sense of rotation, to reach the direction of $\mathbf{V}_g$, the maximum comes at

$$t_{\max} = \frac{\gamma_0}{|f|}. \tag{18.8}$$

This is the *inertial oscillation* of the ageostrophic wind. Chapter 3 found the special case of air released from rest, $\mathbf{V}_a(0) = -\mathbf{V}_g$, in which the speed peaks at twice the geostrophic value; here the initial vector is whatever the daytime friction left behind, and the excess over the geostrophic wind is $|\mathbf{V}_a(0)|$.

> **Principle 18.1.** *Once friction stops, the ageostrophic wind keeps its magnitude and rotates at the rate $|f|$, clockwise in the Northern Hemisphere and counterclockwise in the Southern; the wind speed peaks at $|\mathbf{V}_g| + |\mathbf{V}_a|$ when the rotating vector points along the geostrophic wind, a time $\gamma_0/|f|$ after friction stopped.*

The Blackadar mechanism. The sequence sunset, frictional decoupling of the air above the stable layer, inertial oscillation of its ageostrophic wind, and a wind maximum aloft is the Blackadar mechanism. It explains three observed features of nocturnal jets at once: the wind above the stable layer becomes supergeostrophic, it reaches its maximum some hours after sunset rather than at sunset, and it changes direction through the night as it accelerates.

18.2.3 A worked evening in both hemispheres

Take an illustrative westerly geostrophic wind $\mathbf{V}_g = (10, 0)\,\mathrm{m\,s^{-1}}$ at 40° N, where $f = 2\Omega\sin 40° = 9.37 \times 10^{-5}\,\mathrm{s^{-1}}$. In the Northern Hemisphere the low pressure lies to the north of a westerly geostrophic wind. Let the boundary-layer wind at sunset, just before decoupling, be $\mathbf{V}(0) = (6, 3)\,\mathrm{m\,s^{-1}}$: a speed of $\sqrt{36+9} = 6.7\,\mathrm{m\,s^{-1}}$, turned $\arctan(3/6) = 27°$ toward the low. Then

$$\mathbf{V}_a(0) = \mathbf{V}(0) - \mathbf{V}_g = (6-10,\ 3-0) = (-4, 3)\,\mathrm{m\,s^{-1}}, \qquad |\mathbf{V}_a(0)| = \sqrt{16+9} = 5\,\mathrm{m\,s^{-1}}.$$

- *Maximum speed.* By equation (18.7), $U_{\max} = |\mathbf{V}_g| + |\mathbf{V}_a| = 10 + 5 = 15\,\mathrm{m\,s^{-1}}$.
- *Supergeostrophic excess.* $U_{\max} - |\mathbf{V}_g| = 5\,\mathrm{m\,s^{-1}}$, half the geostrophic wind again, from a sunset wind of only $6.7\,\mathrm{m\,s^{-1}}$.
- *Time of the maximum.* $\mathbf{V}_a(0)$ points at an angle of $180° - \arctan(3/4) = 143.1°$ counterclockwise from east. Turning clockwise, it reaches the direction of $\mathbf{V}_g$ (east, angle zero) after $\gamma_0 = 143.1° = 2.498$ rad, at $t_{\max} = 2.498/(9.37 \times 10^{-5}\,\mathrm{s^{-1}}) = 26\,650\,\mathrm{s} = 7.4\,\mathrm{h}$ after sunset: about 01:25 local time for an illustrative sunset at 18:00.

The Southern Hemisphere case is the mirror image. At 30° S, $f = -7.29 \times 10^{-5}\,\mathrm{s^{-1}}$, and the low lies to the south of a westerly geostrophic wind. With the same $\mathbf{V}_g = (10, 0)\,\mathrm{m\,s^{-1}}$ and the sunset wind $\mathbf{V}(0) = (6, -3)\,\mathrm{m\,s^{-1}}$, again $6.7\,\mathrm{m\,s^{-1}}$ turned 27° toward the low, $\mathbf{V}_a(0) = (-4, -3)\,\mathrm{m\,s^{-1}}$ with magnitude $5\,\mathrm{m\,s^{-1}}$, at an angle of $-143.1°$. It turns counterclockwise through the same 143.1°, reaching the same $U_{\max} = 15\,\mathrm{m\,s^{-1}}$ after $2.498/(7.29 \times 10^{-5}\,\mathrm{s^{-1}}) =$

34 260 s = 9.5 h, about 03:30 for the same sunset. At 23° S, $|f| = 5.70 \times 10^{-5}\,\mathrm{s^{-1}}$ and the same maximum would come 12.2 h after sunset, at about 06:10, when on a twelve-hour night the sun has already risen and convective mixing is about to destroy the jet (Section 18.3.4).

Figure 18.3 draws the two oscillations as hodographs, plots of the tip of the wind vector in the (u, v) plane. In each panel the horizontal axis is the eastward component u and the vertical axis the northward component v. The black arrow from the origin is $\mathbf{V}_g$; the red arrow is the sunset wind $\mathbf{V}(0)$; the dashed arrow from the tip of $\mathbf{V}_g$ is $\mathbf{V}_a(0)$. The thick curve is the path of the wind tip during the first twelve hours, with dots and labels every two hours, ending in an arrowhead; the thin dashed circle is the rest of the idealized oscillation. The maximum is where the circle crosses the u axis on the far side, at $(15, 0)\,\mathrm{m\,s^{-1}}$. In the Northern panel the tip runs clockwise and passes the maximum between the 6 and 8 h marks; in the Southern panel it runs counterclockwise, more slowly, and passes it between 8 and 10 h.

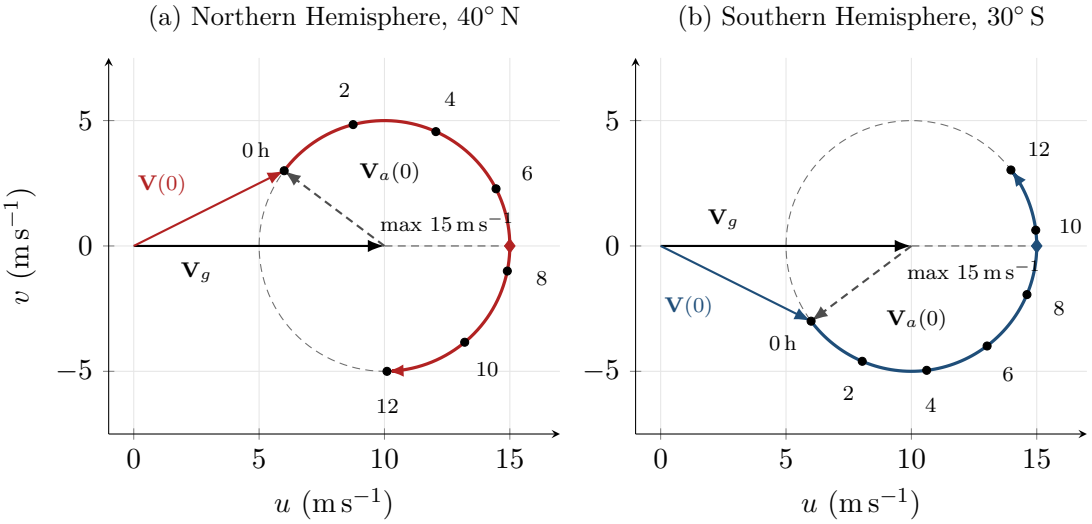


Figure 18.3: Hodographs of the frictionless inertial oscillation, equation (18.6), for an illustrative $\mathbf{V}_g = (10, 0)\,\mathrm{m\,s^{-1}}$ and $|\mathbf{V}_a(0)| = 5\,\mathrm{m\,s^{-1}}$. (a) 40° N, $f = +9.37 \times 10^{-5}\,\mathrm{s^{-1}}$, sunset wind $(6, 3)\,\mathrm{m\,s^{-1}}$: clockwise, $T_I = 18.6$ h, maximum $15\,\mathrm{m\,s^{-1}}$ at 7.4 h. (b) 30° S, $f = -7.29 \times 10^{-5}\,\mathrm{s^{-1}}$, sunset wind $(6, -3)\,\mathrm{m\,s^{-1}}$: counterclockwise, $T_I = 23.9$ h, maximum $15\,\mathrm{m\,s^{-1}}$ at 9.5 h. Dots every two hours after sunset; the diamond marks the maximum.

Figure 18.4 plots the speed of the same oscillation against time. The horizontal axis is hours after sunset and the vertical axis the wind speed from equation (18.7); the shaded band is an illustrative twelve-hour night, and the dashed horizontal line is $|\mathbf{V}_g| = 10\,\mathrm{m\,s^{-1}}$. The three curves are the same initial wind at 40° N, 30° S and 23° S, solid during the night and dotted after sunrise, when daytime mixing returns and the frictionless solution no longer applies. All three start at $6.7\,\mathrm{m\,s^{-1}}$, cross the geostrophic speed after two to three and a half hours and reach the same $15\,\mathrm{m\,s^{-1}}$; what differs is when. At 40° N the maximum falls in the middle of the night, at 30° S in its second half, and at 23° S at sunrise, so that at this latitude the night ends before the oscillation has delivered its full excess.

Direction of the jet. The rotation of $\mathbf{V}_a$ turns the wind as well as accelerating it. In the Northern Hemisphere example the wind comes from 243°, west-southwest, at sunset, from 270°, due west, at the maximum, and from about 296° after twelve hours: it veers through the night. In the Southern example it comes from 297° at sunset and backs through 270° at the maximum. Near the ground, inside the stable layer, friction still holds the wind turned toward low pressure, so at any one time the direction also changes with height. An illustrative Northern Hemisphere night profile has southeasterly wind at 10 m, southerly at 100 m and

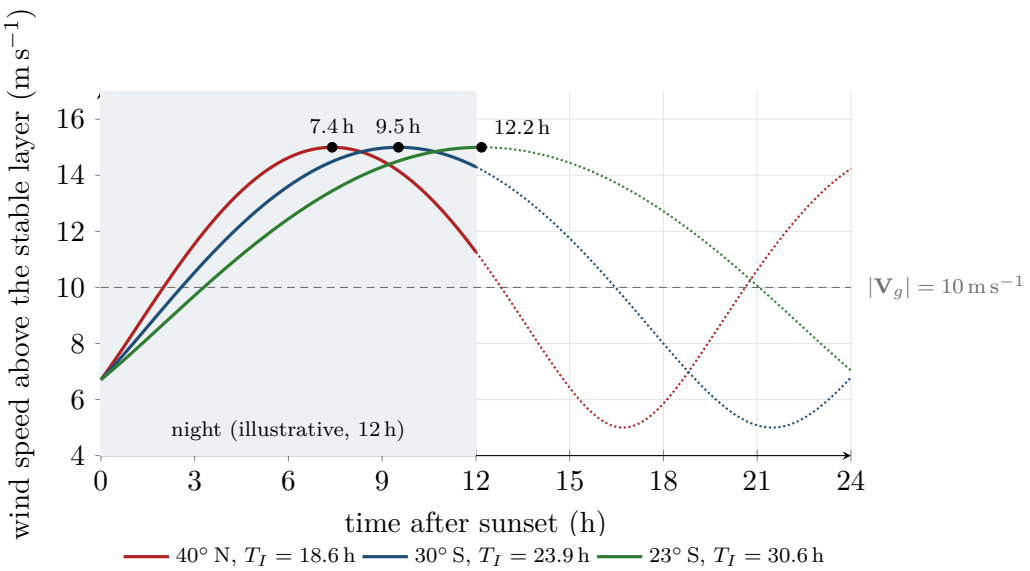


Figure 18.4: Speed of the frictionless inertial oscillation, equation (18.7) with $\gamma(t) = \gamma_0 - |f|t$, $|\mathbf{V}_g| = 10\,\mathrm{m\,s^{-1}}$, $|\mathbf{V}_a| = 5\,\mathrm{m\,s^{-1}}$ and $\gamma_0 = 143.1°$, at three latitudes. Solid during an illustrative twelve-hour night, dotted after it. Dots: maximum $15\,\mathrm{m\,s^{-1}}$ at $t_{\max} = \gamma_0/|f|$.

southwesterly at 250 m, a clockwise turning of 90° over 250 m; the Southern Hemisphere counterpart turns counterclockwise, for example northeasterly at 10 m, northerly at 100 m and northwesterly at 250 m. The jet therefore has both speed shear and directional shear. With illustrative speeds of $3\,\mathrm{m\,s^{-1}}$ at 10 m and $12\,\mathrm{m\,s^{-1}}$ at 250 m at right angles, the vector difference is $\sqrt{3^2 + 12^2} = 12.4\,\mathrm{m\,s^{-1}}$, against a speed difference of $9\,\mathrm{m\,s^{-1}}$: the directional part adds a third to the shear that a speed profile alone shows.

18.2.4 The inertial period and latitude

The time scale of the jet is the inertial period

$$T_I = \frac{2\pi}{|f|} = \frac{2\pi}{2\Omega\,|\sin\phi|}, \tag{18.9}$$

which is of order twelve to twenty-four hours in middle and high latitudes: 23.9 h at 30°, 16.9 h at 45°, 13.8 h at 60° and 12.0 h at the poles. A night of ten to twelve hours is therefore long enough for a good part of an oscillation, and the maximum of the inertial jet falls inside it. The period is the same in both hemispheres; only the sense of rotation differs.

Table 18.1 lists the period by latitude. The columns give the magnitude of the latitude, $|f|$, the inertial period, the angle through which $\mathbf{V}_a$ turns in an illustrative twelve-hour night, and the time of the maximum after sunset for the worked example, which needs a turn of 143°. At lower latitudes $|f|$ is smaller, the period longer and the oscillation slower: at 15° the night turns the vector only 93°, and the example's maximum would come eighteen hours after sunset, long after sunrise. At higher latitudes the oscillation is faster and the maximum earlier. Latitude thus changes the timing and the character of nocturnal jets. Toward the equator the inertial mechanism weakens because the night covers a small part of a slow turn; jets at low latitudes owe more to the other mechanisms of Section 18.4.

For South America the consequences are direct. At 23° S ($|f| = 5.70 \times 10^{-5}\,\mathrm{s^{-1}}$, $T_I = 30.6$ h) a twelve-hour night covers 39 % of a period, and at 30° S ($T_I = 23.9$ h) exactly half. An inertial jet at 30° S can complete the half turn that takes an ageostrophic wind from opposing to

Table 18.1: Inertial period $T_I = 2\pi/|f|$ and the inertial oscillation in a twelve-hour night, with $\Omega = 7.292 \times 10^{-5}$ rad/s. The last column is the time of the maximum of the worked example, $t_{\max} = \gamma_0/|f|$ with $\gamma_0 = 143.1°$; the same in both hemispheres.

$\lvert\phi\rvert$	$\lvert f\rvert$ ($10^{-4}\,\mathrm{s}^{-1}$)	T_I (h)	turn in 12 h	$t_{\max}$ of the example (h)
10°	0.253	68.9	63°	27.4
15°	0.377	46.2	93°	18.4
23°	0.570	30.6	141°	12.2
30°	0.729	23.9	180°	9.5
40°	0.937	18.6	232°	7.4
45°	1.031	16.9	255°	6.7
60°	1.263	13.8	313°	5.5

reinforcing the geostrophic wind; at 23° S it typically peaks near or after dawn, if the morning mixing allows it to.

18.2.5 Why the maximum is above the surface

The inertial oscillation is a property of each level separately, and the jet is the profile of its outcome. Three layers can be distinguished. Near the ground, inside the stable layer, turbulence weakens but does not vanish: the friction force remains, damps the oscillation and keeps the wind weak and turned toward low pressure. Above the stable layer, in the residual layer, the stress is weak and the air oscillates nearly freely, with the amplitude $|\mathbf{V}_a(0)|$ that the daytime drag left at that level. Higher still, above the top of the daytime boundary layer, the air never felt the ground, its ageostrophic wind was small at sunset, and it stays close to the geostrophic, free-atmosphere wind. The speed therefore increases through the stable layer, peaks just above it, where the friction has vanished but the amplitude is still large, and falls back toward the free-atmosphere wind above: a maximum in between.

In the idealized mixed layer whose stress falls linearly from the surface to the top, the friction force, and with it $\mathbf{V}_a(0)$ through equation (18.3), is the same at every height, and the whole residual layer oscillates together; the wind then falls off only near the top of the former mixed layer. In real profiles the sunset ageostrophic wind is larger in the lower part of the mixed layer, where the drag was felt most, and the maximum is sharper and lower. The core is usually found 100 to 500 m above the ground, close to the top of the surface inversion, and it rises during the night as the stable layer deepens. Some jets have their cores below 100 m, over very stable nights with shallow inversions, and some above 1 km. The height is a dynamical outcome of the depth of the stable layer and the profile of the sunset ageostrophic wind, not a fixed altitude.

18.2.6 Limits of the idealization

The frictionless solution makes four assumptions, and each fails to some degree. Friction does not vanish abruptly at sunset: the turbulence of the residual layer decays over an hour or two, and the stable layer's own stress, reaching up toward the jet, keeps damping the oscillation, so the excess over the geostrophic wind is smaller than $|\mathbf{V}_a(0)|$ and the maximum is earlier than $\gamma_0/|f|$ would give. The geostrophic wind is not constant in time: synoptic changes alter it over the night, and over sloping terrain the heating and cooling of the slope change the low-level pressure gradient with the time of day (Section 18.4.4). The geostrophic wind is not constant with height either, whenever horizontal temperature gradients are present. And the flow is not horizontally uniform: advection and terrain modify it.

The idealization is nevertheless the right first model. It explains the supergeostrophic speeds, the timing in hours after sunset, the latitude dependence, the turning of the wind through the night and the height of the core, and it says what a model must represent to produce the jet: the collapse of the friction above the stable layer at the right time and height. Observed nocturnal jets combine it with the other mechanisms of Section 18.4, which add to or subtract from the inertial excess.

18.3 The jet through the night and morning

The nocturnal jet has a life cycle from sunset to late morning. This section follows it, shows how the jet feeds turbulence back into the stable layer beneath it, and works through its breakdown when the sun heats the ground again.

18.3.1 The evolution sequence

A common conceptual sequence has six stages. At sunset the ground starts to cool and a shallow stable layer forms. In the early night the drag on the air above it weakens and the winds aloft accelerate. Around midnight the jet strengthens and turns, veering in the Northern Hemisphere and backing in the Southern. Before dawn it reaches its maximum intensity, at latitudes where the inertial timing allows. At sunrise heating of the ground starts convective turbulence near the surface. During the morning the growing convective layer mixes the jet momentum down to the ground, and the jet weakens and disappears.

Figure 18.5 draws the sequence as a schematic time-height section. The horizontal axis is local time from 18:00 to noon the next day and the vertical axis height above the ground from 0 to 1000 m. The blue line is the top of the stable boundary layer, growing through the night; the gold region is the convective boundary layer that grows after sunrise. The red shapes are isotachs, lines of equal wind speed, of the jet, labeled with illustrative speeds, and the dashed red line is the core height. The six stages are marked along the top. The jet appears above the stable layer in the early night, strengthens toward the pre-dawn hours and is cut off from below once the convective layer reaches it; the downward arrows in the convective layer stand for the momentum it carries to the ground.

18.3.2 The jet as a source of turbulence

Stability allows the jet to form, and the jet in turn produces the shear that can break the stability. The competition is measured by the Richardson number of Chapter 13. Over the layer between 20 m and the core of Section 18.1.2, the bulk Richardson number is

$$\mathrm{Ri}_B = \frac{(g/\overline{\theta})\,\Delta\theta\,\Delta z}{(\Delta U)^2}, \tag{18.10}$$

with the speed difference standing for the vector difference when the direction does not change much. With an illustrative potential temperature increase of $\Delta\theta = 3\,\mathrm{K}$ over the $\Delta z = 180\,\mathrm{m}$, $\overline{\theta} = 290\,\mathrm{K}$ and $\Delta U = 12\,\mathrm{m\,s^{-1}}$,

$$\mathrm{Ri}_B = \frac{(9.81/290)\times 3\times 180}{12^2} = \frac{0.0338\times 540}{144} = \frac{18.3}{144} = 0.13,$$

below the critical value $\mathrm{Ri}_c \approx 0.25$. Despite a stable stratification of 1.7 K per 100 m, the shear beneath the jet is strong enough to sustain turbulence. Directional shear lowers the number further.

The chain is stability, jet, shear, turbulence. The turbulence mixes jet momentum downward and slower air upward, which brings faster air toward the ground and weakens the shear that

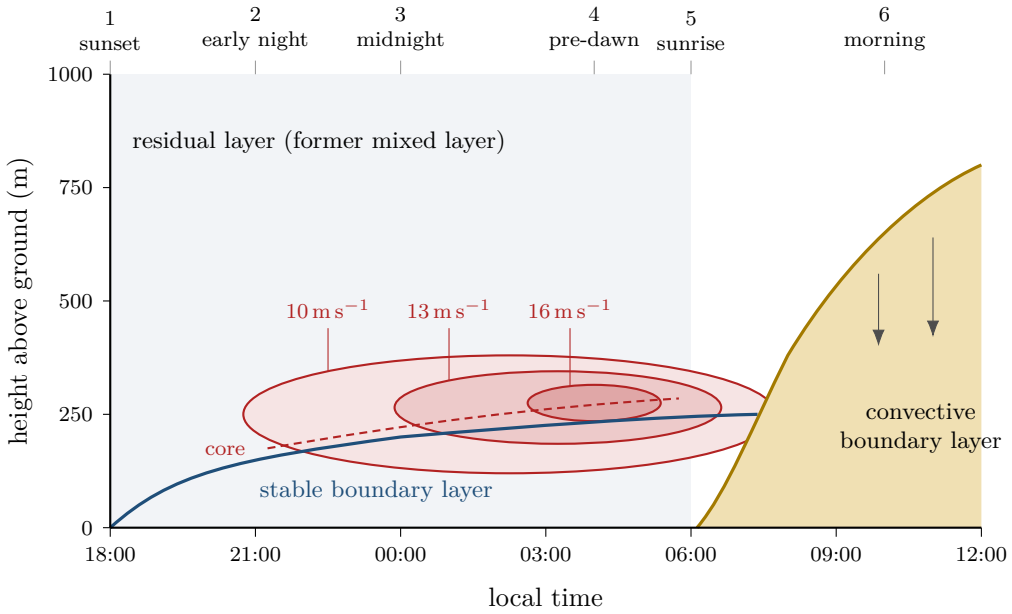


Figure 18.5: Schematic time-height section of a nocturnal low-level jet, illustrative values. Light blue band: night. Blue line: top of the stable boundary layer. Red: isotachs of the jet at 10, 13 and 16 $\mathrm{m\,s^{-1}}$, and the core height (dashed). Gold: the convective boundary layer after sunrise, which mixes the jet momentum downward (arrows). Numbers along the top: the six stages of the conceptual sequence.

produced it. The result is often intermittent: the shear builds up until the layer becomes unstable, a burst of turbulence mixes momentum down and relieves the shear, the stable layer re-forms, and the cycle repeats. Chapter 17 treats these bursts within the stable boundary layer; here their importance is that the jet is the reservoir of momentum they draw on, and that they are a mechanism of intermittent nighttime gusts at the surface.

18.3.3 Sudden increases of the night wind

Near-surface winds can increase suddenly at night without any large-scale change. Take an illustrative jet with an 18 $\mathrm{m\,s^{-1}}$ core above a surface wind of 3 $\mathrm{m\,s^{-1}}$. A turbulent burst that mixes part of the layer between them can raise the surface wind to 8 to 10 $\mathrm{m\,s^{-1}}$ or more within minutes. A rough upper bound comes from mixing completely: a speed that increases linearly from 3 $\mathrm{m\,s^{-1}}$ near the ground to 18 $\mathrm{m\,s^{-1}}$ at the core has a layer mean of $(3+18)/2 = 10.5\,\mathrm{m\,s^{-1}}$, the value the whole layer would take if its momentum were shared uniformly. Partial mixing and the drag of the ground keep the surface wind below that bound, which is why bursts of 8 to 10 $\mathrm{m\,s^{-1}}$ are typical of such a night.

For a forecaster or an operator the increase looks like a change of weather, but the pressure field and the geostrophic wind have not changed; only the vertical distribution of momentum has. A record from a 10 m station shows a step from 3 to 9 $\mathrm{m\,s^{-1}}$ and back an hour later; a profile from a remote-sensing instrument shows the same event as a temporary erosion of the jet core. Such events cannot be predicted from the surface record alone; they are predictable only in the sense that a jet with a large shear beneath it makes them likely.

18.3.4 The morning breakdown

After sunrise the ground heats, the surface heat flux turns upward and convective turbulence develops in a layer that grows from the surface (Chapter 16 treats this growth). When the

convective layer reaches the stable layer and then the jet, its thermals mix the concentrated momentum of the core through the whole depth of the layer. The maximum spreads out: the jet weakens while the surface winds strengthen. By late morning the profile is the nearly uniform profile of a mixed layer, with a speed between the former surface wind and the former core speed.

This is why many sites have their strongest near-surface winds in the late morning or early afternoon even though the strongest winds of the day occurred hundreds of meters up before dawn. It is also why a morning forecast of the surface wind depends on the overnight jet: the more momentum the jet holds and the lower its core, the larger the morning increase at the surface.

18.3.5 Momentum redistribution: a worked morning

An illustrative pair of profiles shows the redistribution. At 05:00, $U_{10} = 3\,\mathrm{m\,s^{-1}}$, $U_{200} = 16\,\mathrm{m\,s^{-1}}$ and $U_{500} = 11\,\mathrm{m\,s^{-1}}$; at 10:00, $U_{10} = 8\,\mathrm{m\,s^{-1}}$, $U_{200} = 11\,\mathrm{m\,s^{-1}}$ and $U_{500} = 10\,\mathrm{m\,s^{-1}}$. The surface wind has nearly tripled and the core has lost $5\,\mathrm{m\,s^{-1}}$. A rough check of the momentum per unit horizontal area, $\int_0^{500} U\,\mathrm{d}z$ with the density taken as constant, joins the levels by straight lines from $U = 0$ at the ground and applies the trapezoidal rule:

$$\begin{aligned}
&05{:}00: \quad \tfrac{0+3}{2}\,10 + \tfrac{3+16}{2}\,190 + \tfrac{16+11}{2}\,300 = 15 + 1805 + 4050 = 5870\,\mathrm{m^2\,s^{-1}},\\
&10{:}00: \quad \tfrac{0+8}{2}\,10 + \tfrac{8+11}{2}\,190 + \tfrac{11+10}{2}\,300 = 40 + 1805 + 3150 = 4995\,\mathrm{m^2\,s^{-1}},
\end{aligned}$$

layer means of 11.7 and $10.0\,\mathrm{m\,s^{-1}}$ over the lowest 500 m. The column did not gain momentum between 05:00 and 10:00; the morning increase at the surface was supplied from aloft.

The numbers support no more than that. Three levels are too few to close the budget: the 05:00 core may be sharper or broader than the straight lines assume, and a few meters per second of difference in the unobserved shape between 200 and 500 m changes the integral by hundreds of $\mathrm{m^2\,s^{-1}}$. The speeds are magnitudes, while the budget holds for the vector, and the jet has turned between the two times. The column also exchanges momentum with its surroundings: the ground removes it at the rate u_*^2 per unit area, which for an illustrative mean $u_* = 0.3\,\mathrm{m\,s^{-1}}$ over the five hours amounts to $0.09 \times 18\,000 = 1620\,\mathrm{m^2\,s^{-1}}$, more than the whole difference of $875\,\mathrm{m^2\,s^{-1}}$; the pressure gradient acts on any ageostrophic wind and adds or removes momentum; and entrainment exchanges it with the air above 500 m. The conclusion that survives these caveats is qualitative: the stronger surface wind of the morning needs no new forcing, because the jet held more than enough momentum above the stable layer.

Figure 18.6 plots the two profiles. The horizontal axis is wind speed and the vertical axis height above the ground. The red line is 05:00 and the gold line 10:00, each joined by straight lines as in the trapezoidal estimate; the dashed vertical lines are the two layer means. The morning profile is nearly uniform above 10 m, the night profile has its maximum at 200 m, and the surface value has risen as the core value has fallen.

Principle 18.2. *The morning increase of the surface wind after a jet night is momentum moved downward by convective mixing, not momentum added by a change of the large-scale forcing.*

18.4 Other kinds of low-level jet

A low-level jet is a flow feature, a maximum in a profile, and several distinct mechanisms produce one. This section describes the main families beside the nocturnal inertial jet, derives the thermal wind relation that underlies the baroclinic ones, and compares them in a table.

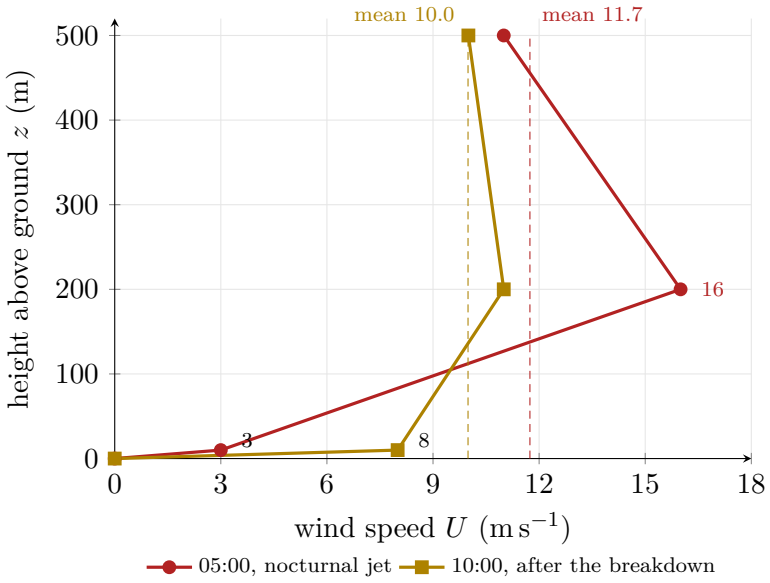


Figure 18.6: Illustrative wind profiles at 05:00 ($U_{10} = 3$, $U_{200} = 16$, $U_{500} = 11\,\mathrm{m\,s^{-1}}$) and 10:00 ($U_{10} = 8$, $U_{200} = 11$, $U_{500} = 10\,\mathrm{m\,s^{-1}}$), joined by straight lines from zero at the ground. Dashed: the layer means over 0–500 m by the trapezoidal rule, 11.7 and $10.0\,\mathrm{m\,s^{-1}}$.

18.4.1 A flow feature, not one mechanism

Not every low-level jet is a nocturnal inertial jet. Wind maxima near the ground are also produced by channeling of the flow by terrain, by strong pressure gradients confined to a shallow layer, by the temperature contrast at coastlines, by the circulations of fronts and by mountain-valley dynamics. These mechanisms can act alone or together with the inertial oscillation, and they can produce jets by day as well as by night.

The distinction matters for diagnosis and for forecasting. An inertial jet appears after sunset, peaks some hours later and breaks down in the morning, and its timing follows from the latitude. A gap flow lasts as long as the pressure difference across the gap; a coastal jet persists for days in a favorable season; a frontal jet travels with the front. Identifying a maximum in a profile is the first step; attributing it to a mechanism is the second, and it decides how the jet will evolve.

18.4.2 Terrain channeling, gap flow and valley jets

When a pressure difference drives air along a valley or through a gap in a mountain barrier, the terrain confines the flow and accelerates it. A *gap flow* is the strong wind that forms where air is forced from higher to lower pressure through a gap or a pass; a *valley jet* is a wind maximum within a valley, along its axis. Both have a low-level maximum, below the height of the surrounding ridges, and both can occur by day or by night, as long as the driving pressure difference lasts. A rough upper bound on the gap wind is obtained by converting the whole pressure difference into kinetic energy, $U \approx \sqrt{2\Delta p/\rho}$; an illustrative $\Delta p = 2\,\mathrm{hPa}$ with $\rho = 1.2\,\mathrm{kg\,m^{-3}}$ gives $\sqrt{2 \times 200/1.2} = 18\,\mathrm{m\,s^{-1}}$. Friction and mixing keep real gap winds below this bound.

The thermally driven down-valley wind of a clear night also has a jet profile, with its maximum some tens of meters above the valley floor; Chapter 19 treats it with the other thermal circulations, and Chapter 20 treats channeling, gaps and blocking as mechanically forced terrain flow. For the present purpose the point is that such maxima are tied to a place, not to a time of night: they recur at the same valley or gap whenever the driving pressure

difference recurs.

18.4.3 Coastal jets

At a coast the contrast between warm land and cool sea, or the reverse, creates horizontal temperature gradients and, through them, pressure gradients within the lowest kilometer. Combined with the Coriolis force and with topography, in particular coastal mountains and a marine inversion that confine the cool marine air to a shallow layer, these gradients produce a *coastal jet*: a low-level wind maximum blowing along the coast, near the top of the marine layer. Coastal jets are common along the eastern boundaries of the subtropical oceans, such as the coasts of California, Chile and southwestern Africa, where a cold ocean current lies beside warm land.

The physics differs from that of the nocturnal jet. The maximum is not produced by the collapse of friction and the rotation of an ageostrophic wind but by a geostrophic wind that changes with height: strong along the coast at low levels, where the land-sea pressure gradient is concentrated, and weaker above, where the temperature gradient reverses the pressure gradient. The relation between the two, the thermal wind, is derived in Section 18.4.4. Coastal jets can persist for days and show a weaker daily modulation than nocturnal jets.

18.4.4 Baroclinic forcing and the thermal wind

A horizontal temperature gradient makes the geostrophic wind change with height. The relation follows in four steps from the geostrophic and hydrostatic balances. On a pressure surface the geostrophic wind is $\mathbf{V}_g = (1/f)\,\mathbf{k}\times\nabla_p\Phi$, with Φ the geopotential (Chapter 2). The hydrostatic balance in the form $\mathrm{d}\Phi = -R_dT\,\mathrm{d}\ln p$ gives $\partial\Phi/\partial\ln p = -R_dT$. Differentiating the geostrophic wind with respect to $\ln p$ and exchanging the order of differentiation,

$$\frac{\partial\mathbf{V}_g}{\partial\ln p} = \frac{1}{f}\,\mathbf{k}\times\nabla_p\frac{\partial\Phi}{\partial\ln p} = -\frac{R_d}{f}\,\mathbf{k}\times\nabla_p T.$$

Finally, near a given height $\mathrm{d}z \approx -(R_dT/g)\,\mathrm{d}\ln p$, so $\partial/\partial z \approx -(g/R_dT)\,\partial/\partial\ln p$, and

$$\frac{\partial\mathbf{V}_g}{\partial z} \approx \frac{g}{f\,T}\,\mathbf{k}\times\nabla_h T, \qquad \frac{\partial u_g}{\partial z} \approx -\frac{g}{fT}\frac{\partial T}{\partial y}, \quad \frac{\partial v_g}{\partial z} \approx \frac{g}{fT}\frac{\partial T}{\partial x}, \tag{18.11}$$

where the gradient on a pressure surface has been replaced by the gradient at constant height, an approximation adequate in the lowest kilometers. This is the *thermal wind relation*: the vertical shear of the geostrophic wind is parallel to the isotherms, with warm air on its right in the Northern Hemisphere and on its left in the Southern. The thermal wind is not a wind but a shear, in s^{-1}, or a wind difference between two levels.

As a worked example, take a temperature that increases eastward by an illustrative 2 K per 100 km, $\partial T/\partial x = 2\times10^{-5}\,\mathrm{K\,m^{-1}}$, as over warm land east of a cool sea, with $T = 290\,\mathrm{K}$. At 40° N,

$$\frac{\partial v_g}{\partial z} = \frac{9.81}{9.37\times10^{-5}\times290}\times2\times10^{-5} = 361\times2\times10^{-5} = 7.2\times10^{-3}\,\mathrm{s^{-1}},$$

a southerly shear of $3.6\,\mathrm{m\,s^{-1}}$ per 500 m: the northward component of the geostrophic wind increases with height. At 30° S, with $f = -7.29\times10^{-5}\,\mathrm{s^{-1}}$, the same gradient gives $\partial v_g/\partial z = -464\times2\times10^{-5} = -9.3\times10^{-3}\,\mathrm{s^{-1}}$, a northerly shear of $4.6\,\mathrm{m\,s^{-1}}$ per 500 m. In both cases the shear vector has the warm land on its right in the north and on its left in the south. Over such a coast the warm land also lowers the surface pressure, giving a low-level geostrophic wind along the coast with the low on the land side: northerly in the Northern Hemisphere, southerly in the Southern. The thermal wind opposes it in both hemispheres, so the along-coast wind is

strongest near the surface and weakens with height; with friction reducing it at the ground, the result is a maximum a few hundred meters up.

Figure 18.7 draws this structure for the Northern Hemisphere. It is a vertical west-east cross section, viewed toward the north, with cool sea on the left and warm land on the right. The solid lines are four isobaric surfaces, $p_1 > p_2 > p_3 > p_4$; the circled symbols give the geostrophic wind normal to the section, a dot for a wind toward the viewer (from the north) and a cross for a wind away from the viewer (from the south), with the symbol size giving the speed. On the right a sketch of the along-coast wind against height adds the effect of friction near the ground. Because the warm column over land is thicker, the isobaric surfaces slope down toward the land near the ground, are level at mid-height and slope up aloft; the geostrophic wind is northerly and strongest at the bottom, vanishes where the surfaces are level and is southerly above. With the friction of the ground the northerly wind peaks a little above the surface: a coastal low-level jet.

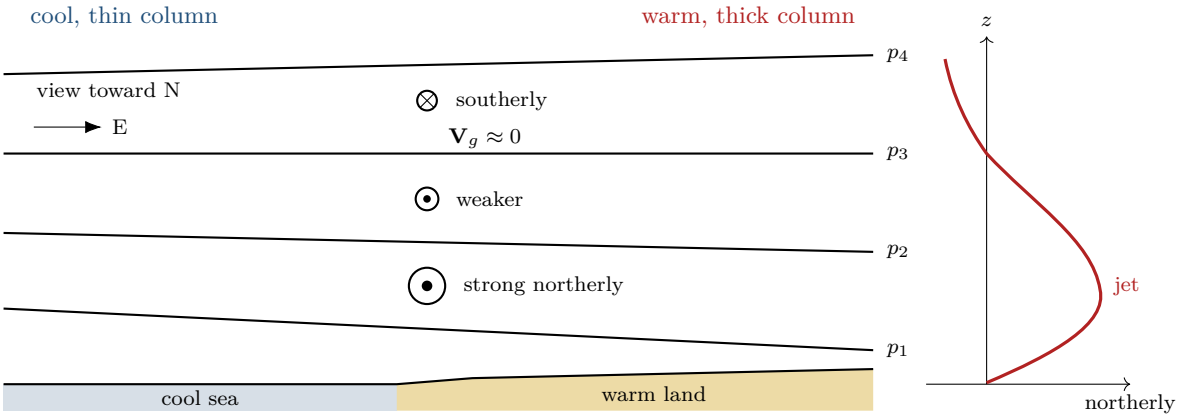


Figure 18.7: Schematic vertical cross section through a Northern Hemisphere coast with cool sea to the west and warm land to the east, viewed toward the north. Solid lines: isobaric surfaces $p_1 > p_2 > p_3 > p_4$, farther apart over the warm land. Circled dot: geostrophic wind toward the viewer (northerly); circled cross: away from the viewer (southerly); symbol size: speed. Right: the along-coast (northerly) wind against height, reduced by friction at the ground. In the Southern Hemisphere the same temperature pattern gives a southerly low-level jet.

Strong low-level temperature gradients occur at fronts, at coastlines and over sloping terrain, and each can organize a jet. Over a large sloping plain the air next to the sloping ground warms by day and cools by night relative to the air at the same height farther out over lower ground, so the low-level temperature gradient, and with it the geostrophic wind near the ground, changes with the time of day. This diurnal baroclinic forcing adds to or opposes the inertial oscillation and is one of the reasons that real nocturnal jets over sloping plains can exceed what the inertial oscillation alone predicts.

18.4.5 Baroclinicity

An atmosphere is *barotropic* when its density depends only on pressure, so that surfaces of constant pressure and surfaces of constant density coincide; then the geostrophic wind does not change with height. It is *baroclinic* when pressure and density surfaces intersect. *Baroclinicity* is the degree to which they are not parallel, and in practice it is measured by the horizontal temperature gradient on pressure surfaces, $|\nabla_p T|$, in $\mathrm{K\,m^{-1}}$ and usually quoted in kelvin per 100 km. Since at a given pressure the density is inversely proportional to the temperature, a temperature gradient along a pressure surface is the same thing as a density gradient along it, which is the intersection of the two families of surfaces. It is calculated from analyzed or

modeled temperature fields, or from pairs of stations at similar elevations.

Through equation (18.11), baroclinicity implies vertical shear of the geostrophic wind. A barotropic layer has the same geostrophic wind at every height, and a jet in it must come from friction or its removal; a baroclinic layer can have a geostrophic wind that increases and then decreases with height, and the jet is then part of the balanced flow itself. The two kinds of explanation are not exclusive, and over sloping plains or near coasts both act.

18.4.6 Mechanisms compared

Table 18.2 compares the mechanisms. The columns give the mechanism, the physical driver, the time of day at which it acts, and the typical height of the core. The heights are typical ranges, illustrative of the families rather than limits.

Real jets often combine mechanisms. A nocturnal jet over a broad plain that slopes up toward a mountain range can carry an inertial part, a diurnal baroclinic part from the slope and a channeled part where the range deflects the flow along its flank. The columns of the table are the features that separate the contributions in a record: the time of day at which the maximum appears and disappears, its persistence from one day to the next, its height, and its tie to a particular piece of terrain or coastline. A jet that follows the night at every site of a region is mostly inertial; one that stays at a gap whatever the hour is mostly channeled.

Table 18.2: Mechanisms of low-level jets. Heights are typical ranges of the core above the local ground.

Mechanism	Driver	Time of day	Typical core height
Nocturnal inertial (Blackadar)	collapse of friction above the stable layer releases the daytime ageostrophic wind	night; maximum hours after sunset, timing set by latitude	100–500 m, near the top of the inversion
Diurnal baroclinic over sloping terrain	heating and cooling of a sloping plain change the low-level geostrophic wind	night maximum, adds to the inertial jet	a few hundred meters to 1 km
Terrain channeling: valley jet, gap flow	pressure difference along a valley or across a gap, confined by terrain	day or night, while the pressure difference lasts	below ridge height, tens to a few hundred meters
Coastal jet	land-sea temperature contrast, Coriolis force, coastal mountains and the marine inversion	day and night, persisting for days; weak daily modulation	100–500 m, near the top of the marine layer
Frontal and synoptic	temperature gradient and circulation of a front; strong synoptic pressure gradient below an inversion	with the passage of a system, any time	about 500 m to 1.5 km

18.5 Observing and detecting jets

A jet is a property of the profile, so it is seen only by instruments that measure profiles or by models that compute them. This section compares the instruments, shows why a surface station misses the jet, applies a detection criterion to the chapter's profiles and examines the effect of vertical resolution.

18.5.1 Instruments

Five kinds of instrument observe low-level jets. Table 18.3 lists them with what each measures, the height range it covers and its main limits. Radiosondes, balloons carrying sensors whose drift gives the wind, deliver complete profiles of wind, temperature and humidity, but only a few times a day, usually at fixed universal times that fall at different local times at different longitudes. Sodars and Doppler lidars are ground-based remote sensors that measure the wind from the Doppler shift of sound or light scattered back by the atmosphere; radar wind profilers do the same with radio waves and reach deeper layers. Tall towers carry anemometers at fixed levels and give high-frequency, continuous records, but only up to their height.

Table 18.3: Instruments for observing low-level jets. Ranges are typical and depend on the model of instrument and the atmospheric conditions.

Instrument	What it measures	Height range	Limits
Radiosonde	wind (from the balloon's drift), temperature, humidity, pressure along the ascent	surface to the stratosphere	one profile per launch, usually twice a day; the balloon drifts; a snapshot, not a record
Sodar	wind profile from the Doppler shift of sound scattered by temperature fluctuations	about 20 to 200–500 m	limited range; noise and fixed echoes; often too shallow to see above a jet core
Doppler lidar	wind profile from the Doppler shift of laser light scattered by aerosols	about 40 m to 1–3 km	needs aerosols; fog, cloud and rain limit it; blind zone near the ground
Radar wind profiler	wind profile from radio waves scattered by refractive-index fluctuations	about 100 m to several kilometers	lowest gate and resolution of tens of meters or more; can miss or smear a low jet
Tall tower	speed and direction at fixed levels, high frequency, with temperature	to the tower top, usually 100–200 m, rarely 300 m	few levels; flow distortion by the structure; often below the core

The instruments differ in what part of the problem they solve. A radiosonde resolves the profile in detail but at one instant; a tower records continuously but only at a few heights; remote sensors combine continuity with a profile, at the cost of a minimum height, a maximum range and a vertical resolution of tens of meters. Model output fills the gaps between observations but represents the jet on its own vertical levels and with its own boundary-layer scheme (Section 18.6.5): it is a calculated, not a measured, profile.

18.5.2 The limits of a surface station

A 10 m station says almost nothing about a jet at 150 m. In the example of Figure 18.1 the station reads $3\,\mathrm{m\,s^{-1}}$ while the core holds $14\,\mathrm{m\,s^{-1}}$; on another night the same $3\,\mathrm{m\,s^{-1}}$ may sit under a $20\,\mathrm{m\,s^{-1}}$ core or under no jet at all. On a stable night the surface layer is decoupled from the air above it, and the surface measurement characterizes only the air it is in. Its low value is consistent with a jet, since decoupling is the condition for one, but it carries no information on the jet's strength, height or direction.

Characterizing the lower atmosphere therefore requires profile observations or model output. The point is the recurring distinction of this book between a point measurement and the quantity

of interest: the 10 m wind is a faithful measurement of the wind at 10 m and a poor estimate of the wind at 100 or 200 m whenever the profile is not the monotonic profile that an extrapolation assumes.

18.5.3 Detection criteria

Studies that count jets in profile records apply a *detection criterion*: a rule that decides whether a profile has a jet. A typical criterion requires a local maximum of the wind speed below a stated height, often 1 to 2 km, with a sufficient decrease above it, for example

$$U_{\text{jet}} > 10\,\text{m s}^{-1} \quad \text{and} \quad U_{\text{jet}} - U_{\text{above}} > 2\,\text{m s}^{-1}, \tag{18.12}$$

where U_{above} is the minimum speed between the core and the top of the examined layer. Some studies use a relative decrease, such as 20 % of the core speed, or different thresholds; the criteria vary, and the number and character of the jets found depend partly on the definition.

Table 18.4 applies equation (18.12) to the profiles of this chapter. The columns give the profile, its maximum and the height of the maximum, the minimum above it, the decrease and the verdict. The opening example and the 05:00 profile pass both tests. The 10:00 profile has a maximum above $10\,\text{m s}^{-1}$ but decreases by only $1\,\text{m s}^{-1}$ above it and fails; after the breakdown it is not a jet. The monotonic profile has its largest value at its top level and no decrease to test. The same opening profile seen by a sodar that reaches only 150 m would also fail, because its maximum would be the top level: detection depends on the instrument's range as well as on the threshold.

Table 18.4: Equation (18.12) applied to the chapter's illustrative profiles (speeds in m s^{-1}).

Profile	U_{jet}	z_{jet} (m)	U_{above}	decrease	jet?
Opening example (Figure 18.1)	14	150	11	3	yes
05:00 (Figure 18.6)	16	200	11	5	yes
10:00 (Figure 18.6)	11	200	10	1	no
Monotonic 5, 10, 15	15	top level	–	–	no
Opening example to 150 m only	14	top level	–	–	cannot tell

18.5.4 Vertical resolution

A jet a hundred meters thick is resolved only by levels a few tens of meters apart. A set of levels at 10, 80, 200 and 500 m samples a jet with its core at 120 m poorly; levels every 20 to 30 m do much better. The same holds for an instrument with coarse range gates and for a model with coarse vertical levels: in the lowest few hundred meters vertical resolution can matter as much as horizontal resolution.

Figure 18.8 illustrates this with an illustrative profile $U(z) = 8\,\text{m s}^{-1}\,(1 - e^{-z/20\,\text{m}}) + 7\,\text{m s}^{-1}\,e^{-((z-120\,\text{m})/50\,\text{m})^2}$, a jet of $15\,\text{m s}^{-1}$ at 120 m on an $8\,\text{m s}^{-1}$ background. The horizontal axis is wind speed and the vertical axis height. The black curve is the profile; the red squares are its values at the coarse levels, 10, 80, 200 and 500 m, joined by straight lines as a coarse model or instrument would represent it; the blue dots are its values on levels every 25 m. The coarse set sees a maximum of $11.5\,\text{m s}^{-1}$ at 80 m, $3.4\,\text{m s}^{-1}$ too weak and 40 m too low, and a shear below the core that is too weak; it still passes the criterion of equation (18.12), so the jet is detected with the wrong properties. The 25 m levels find $14.9\,\text{m s}^{-1}$ at 125 m, within $0.1\,\text{m s}^{-1}$ and 5 m of the truth.

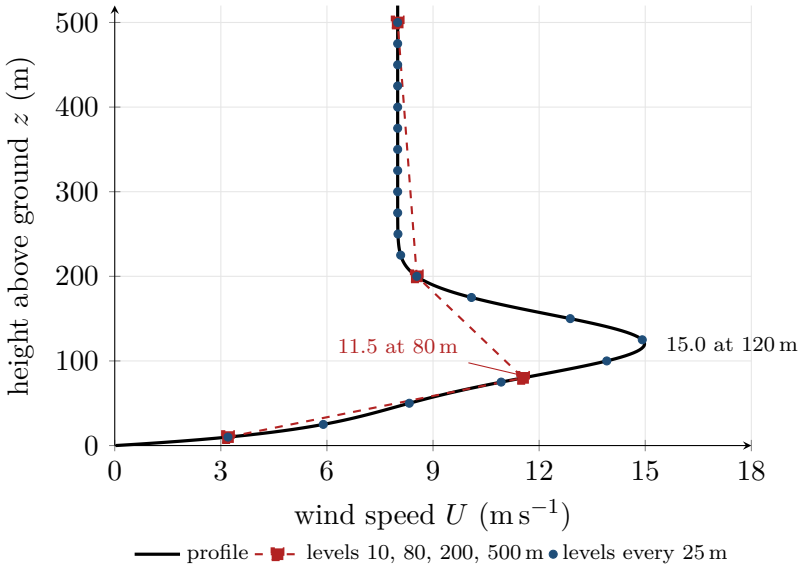


Figure 18.8: An illustrative jet, $U(z) = 8\,\mathrm{m\,s^{-1}}\,(1 - e^{-z/20\,\mathrm{m}}) + 7\,\mathrm{m\,s^{-1}}\,e^{-((z-120\,\mathrm{m})/50\,\mathrm{m})^2}$, sampled at coarse levels (10, 80, 200, 500 m; red, joined by straight lines) and at levels every 25 m (blue). The coarse levels place the maximum at 80 m with $11.5\,\mathrm{m\,s^{-1}}$; the true core is $15.0\,\mathrm{m\,s^{-1}}$ at 120 m.

18.6 Consequences for applications and forecasts

The jet changes the wind at the heights of turbines and conductors, and it is one of the harder features for models to get right. This section works through its consequences for wind energy and line rating, for profile extrapolation and for forecasts, and closes with a diagnostic.

18.6.1 Wind energy

A large modern rotor spans roughly 50 to 250 m. With a jet core inside that span, the rotor sees different speeds, directions and turbulence across its disk. In the opening example the wind is $7\,\mathrm{m\,s^{-1}}$ at 50 m, $14\,\mathrm{m\,s^{-1}}$ at 150 m and, interpolating linearly between 150 and 300 m, $12\,\mathrm{m\,s^{-1}}$ at 250 m. The available power density scales with the cube of the speed, so the bottom of the disk sees $(7/14)^3 = 1/8$ of the power density at the core. Between 50 and 150 m the shear exponent is $\ln 2/\ln 3 = 0.63$, and above the core it is negative.

The consequences are large shear across the disk, asymmetric loading of the blades as they pass from the slow bottom through the core to the top, and power variability as the core rises, turns and is eroded by bursts through the night. The directional shear of Section 18.2.3 adds a twist across the disk that the rotor cannot align with as a whole. A hub-height wind alone represents such a profile poorly, and the power estimated from it can differ from the power available across the disk. Jets also explain why nighttime production at some sites exceeds daytime production although the surface wind is weaker at night.

18.6.2 Transmission-line rating

A transmission-line conductor at 20 to 40 m sits below a jet core at about 200 m. The jet does not cool the conductor directly; the wind that cools it is the weak wind of the decoupled layer. The jet is a reservoir of momentum aloft, and when mixing increases, through a turbulent burst or the morning breakdown, part of that momentum descends to the conductor. The consequences for rating are rapid changes of the wind at the conductor, uncertainty in forecasts of those changes, and variability of the nocturnal cooling.

In the usual rating methods the forced-convection cooling grows roughly as the wind speed to a power of 0.5 to 0.6, at a fixed angle between the wind and the conductor. An illustrative burst that raises the conductor wind from 2 to 6 m s^{-1} raises the cooling by $(6/2)^{0.6} = 1.9$, nearly double, for as long as the burst lasts. The direction matters as well: the turning of the wind through the night and with height changes the angle of attack on a span of fixed orientation. A rating based on the conductor-height wind is therefore the right quantity, but on a jet night it is an intermittent one, and a forecast of its mean says little about its bursts.

18.6.3 Failure of simple extrapolation

A power law fitted to U_{10} and U_{100} and extrapolated to 300 m cannot give $U_{200} > U_{300}$, because $(z/z_r)^{\alpha}$ with $\alpha > 0$ increases at every height. With illustrative values $U_{10} = 3$ m s^{-1} and $U_{100} = 12$ m s^{-1}, the exponent is $\alpha = \log_{10}(12/3) = 0.60$, and the extrapolation gives $U_{200} = 12 \times 2^{0.60} = 18.2$ m s^{-1} and $U_{300} = 12 \times 3^{0.60} = 23.2$ m s^{-1}, a wind that keeps growing through a layer in which, on a jet night, it decreases. The log law is monotonic as well, and so is its stability-corrected form, $U = (u_*/\kappa)[\ln(z/z_0) - \psi_m]$, whose stable correction $\psi_m = -5\, z/L_{\mathrm{O}}$ only makes the increase steeper.

No surface-layer profile can produce a maximum, because surface-layer theory describes a layer of nearly constant stress whose wind is driven from above. The jet lives above that layer, in a region where the stress has collapsed and the Coriolis force on the ageostrophic wind matters, neither of which a surface-layer profile contains. On jet nights, the wind above the surface layer must come from a profile observation or from a model that represents the whole boundary layer.

18.6.4 Errors of jet height in a model

A model with the right jet strength but the wrong height can still give a poor surface wind. Take an observed core of 16 m s^{-1} at 200 m above 4 m s^{-1} at 20 m, a mean shear of 0.067 s^{-1} by equation (18.1), and a model whose core has the same 16 m s^{-1} but sits 100 m lower, at 100 m. Its mean shear is $12/80 = 0.15$ s^{-1}, more than twice as large. For the same buoyancy frequency, the gradient Richardson number scales as the inverse square of the shear and is about five times smaller, so the model's layer is far more turbulent: it mixes too much momentum down and its surface wind is too strong. A core 100 m too high errs the other way, mixes too little, and leaves the surface too calm.

The error matters most where the surface wind is used. A conductor or a 10 m forecast verified against stations sees the height error as a speed error, and a correction of the surface speed alone, without moving the jet, removes the symptom on average while leaving the timing of bursts and of the morning increase wrong. Verifying jets therefore requires comparing core heights and speeds against profile observations, not only surface winds.

18.6.5 Sensitivity to the boundary-layer scheme

Simulated jets are sensitive to the representation of stable mixing, to the surface drag, to the strength of the simulated inversion and to the vertical resolution. In a model, the jet emerges from the collapse of the parameterized stress above the stable layer, so its strength and height are as good as the scheme's turbulence in stable conditions. Too much diffusion in stable conditions smears the jet: the core is weaker, broader and higher, and the surface wind is too strong at night; this is the too-much-mixing problem of stable boundary layers treated in Chapter 17. Too little diffusion gives a jet that is too sharp or too strong, with too calm a surface beneath it.

The jet is therefore a test of boundary-layer parameterizations: a scheme that reproduces the observed core height, speed and timing over several nights represents the stable boundary

layer reasonably, and one that does not will also misplace the surface wind on those nights. Vertical resolution enters independently, as Figure 18.8 showed: a model with levels at 10, 80, 200 and 500 m cannot hold a jet 100 m thick even if its scheme is right. Weather models such as WRF, HRRR or ECMWF can be compared on this basis, configuration by configuration, against profile observations.

18.6.6 A diagnostic for nocturnal jets

Six questions decide whether a profile record shows a nocturnal inertial jet. Table 18.5 lists them with what to examine for each and what a negative answer points to. If the answers are all yes, the feature is probably a nocturnal jet of the Blackadar type; if the first two are yes and others are no, it is a jet of another mechanism of Section 18.4; if the first two are no, there is no jet, whatever the speeds.

Table 18.5: A six-question diagnostic for a nocturnal low-level jet.

	Question	What to examine	If no
1	Is there a speed maximum below about 1–2 km?	profile from a lidar, sodar, profiler, tower or model	no jet; possibly strong monotonic shear
2	Does the speed decrease above it?	speeds above the core; a criterion such as equation (18.12)	not a jet, or the instrument's range is too short
3	Is it strongest at night?	time series of the core speed over several days	a non-nocturnal mechanism: coastal, frontal, gap flow
4	Is there strong stable stratification below it?	temperature profile, $\Delta\theta$ between surface and core	decoupling is not the cause; look for terrain or baroclinic forcing
5	Does the direction rotate with height (and in time)?	direction profile; veering in the north, backing in the south	inertial rotation is weak or absent
6	Does it weaken after sunrise?	core speed and surface speed through the morning	a jet sustained by forcing that persists by day

The diagnostic is a sequence of physical checks, not a statistical test: each question asks for a feature that the Blackadar mechanism predicts, and a negative answer points to a different cause rather than merely lowering a score. It also makes explicit what a record must contain to answer the questions: a profile reaching above the core, a temperature profile, directions as well as speeds, and enough days to see the daily cycle.

The next chapter turns to the circulations driven directly by horizontal temperature contrasts at the ground, the thermal circulations of Chapter 19.

18.7 What to retain

Definition 18.1 (Low-level jet)**.** A low-level jet is a local maximum of wind speed in the lowest one to two kilometers. The nocturnal jet forms when surface cooling decouples the air above a shallow stable layer from the ground, the reduced friction lets the daytime ageostrophic wind rotate in an inertial oscillation and the wind aloft becomes supergeostrophic; after sunrise convection mixes its momentum down and the surface wind strengthens. The wind profile is not always monotonic.

Table 18.6 lists the chapter's terms with their meaning, units and the subsection that defines each.

Table 18.6: Terms of the chapter and where each is defined.

Term	Meaning	Units	Defined in
Low-level jet	local maximum of $U(z)$ in the lowest 1–2 km, with a decrease above it	–	18.1
Jet core, z_{jet}, U_{jet}	height of the maximum and the speed there	m, $\mathrm{m\,s^{-1}}$	18.1.2
Ageostrophic wind, $\mathbf{V}_a$	$\mathbf{V} - \mathbf{V}_g$; maintained by friction by day, equation (18.3)	$\mathrm{m\,s^{-1}}$	18.2.1
Inertial oscillation	rotation of $\mathbf{V}_a$ at rate $\lvert f\rvert$ with constant magnitude, equation (18.6); clockwise north, counterclockwise south	–	18.2.2
Inertial period, T_I	$2\pi/\lvert f\rvert$; 18.6 h at 40°, 23.9 h at 30°	h	18.2.4
Supergeostrophic wind	$\lvert\mathbf{V}\rvert > \lvert\mathbf{V}_g\rvert$; at most $\lvert\mathbf{V}_g\rvert + \lvert\mathbf{V}_a\rvert$	$\mathrm{m\,s^{-1}}$	18.2.2
Blackadar mechanism	sunset, decoupling, inertial oscillation, maximum aloft	–	18.2.2
Gap flow	strong wind forced through a gap from higher to lower pressure	–	18.4.2
Valley jet	low-level maximum along a valley axis	–	18.4.2
Coastal jet	along-coast maximum near the top of the marine layer, from land-sea baroclinicity, Coriolis and terrain	–	18.4.3
Thermal wind	vertical shear of $\mathbf{V}_g$, $(g/fT)\,\mathbf{k}\times\nabla_h T$	$\mathrm{s^{-1}}$	18.4.4
Baroclinicity	non-parallel pressure and density surfaces; horizontal temperature gradient on pressure surfaces	$\mathrm{K\,m^{-1}}$	18.4.5
Detection criterion	rule declaring a jet, e.g. $U_{\text{jet}} > 10\,\mathrm{m\,s^{-1}}$ and a $2\,\mathrm{m\,s^{-1}}$ decrease above	–	18.5.3

18.8 Exercises

Exercise 18.1. A lidar reports 2.5, 6, 11, 13, 10.5 and 9 m s^{-1} at 10, 40, 100, 180, 300 and 500 m. (a) Give z_{jet} and U_{jet} and the mean shear between 40 m and the core. (b) Apply the criterion of equation (18.12) to the full profile, and again to the profile truncated at 200 m as a sodar would see it. (c) Fit a power law to the 10 and 40 m values and extrapolate it to 180 and 300 m; compare with the measurements.

Exercise 18.2. At 25° S the geostrophic wind is an easterly of 8 m s^{-1}, $\mathbf{V}_g = (-8, 0)$ m s^{-1}, and the wind above the developing stable layer at sunset (18:00) is $\mathbf{V}(0) = (-5, 2)$ m s^{-1}. (a) Check that $\mathbf{V}(0)$ is turned toward low pressure. (b) Compute f, T_I and $\mathbf{V}_a(0)$, and state the sense in which $\mathbf{V}_a$ rotates. (c) Compute the maximum speed, the supergeostrophic excess and the local time of the maximum in the frictionless model. (d) Sunrise is at 06:30. Does the maximum occur during the night, and what does the answer imply for the morning wind at a conductor?

Exercise 18.3. On a coast at 35° S, the land to the east is warmer than the sea to the west by 3 K over 150 km; take $T = 288$ K. (a) Compute the thermal wind shear $\partial v_g/\partial z$ and the change of the geostrophic wind over the lowest 400 m. (b) State whether a southerly low-level geostrophic wind of 10 m s^{-1} strengthens or weakens with height, and estimate it at 400 m. (c) Repeat (a) and (b) for the same temperature pattern at 35° N with a northerly low-level wind, and explain the symmetry.

Exercise 18.4. An observed jet has 15 m s^{-1} at 200 m above 4 m s^{-1} at 20 m, with $\Delta\theta = 3$ K between the two heights and $\overline{\theta} = 290$ K. A model reproduces the 15 m s^{-1} core but places it at 100 m with the same $\Delta\theta$ between 20 m and the core. (a) Compute the mean shear and the bulk Richardson number of equation (18.10) for both. (b) Which profile mixes more, and in which direction does the model err at 20 m? (c) The model gives 7 m s^{-1} at a conductor at 30 m where 3 m s^{-1} was observed; with a forced-convection cooling proportional to $U^{0.6}$, by what factor does the model overestimate the cooling?

Chapter 19

Thermal Circulations

19.1 Differential heating as a source of wind

Chapters 16 to 18 followed the boundary layer over flat, uniform ground through the day and the night: convection by day, stable stratification and decoupling at night, and the jet that forms above a decoupled surface. Real ground is not uniform. Land lies beside water, slopes face the sun or the night sky, cities stand in farmland, and neighboring surfaces heat and cool at different rates. The question of this chapter is

how can local heating and cooling generate winds that compete with, and sometimes reverse, the wind set by the weather map?

Chapter 5 introduced the sea breeze and slope winds with first estimates of their driving force. This chapter states the mechanism in general form and derives the acceleration it produces. It then takes the circulations one family at a time: sea and land breezes with the sea-breeze front, slope, valley and drainage winds, the urban circulation, and the convergence and density currents that all of them produce. It ends with how the circulations interact with the large-scale flow and with stability, how they appear in a wind climatology, why weather models of coarse resolution miss them, and a list of questions that diagnose them at a site.

Jargon: thermal circulation, differential heating, thermal forcing, mechanical forcing, return flow, thermal low, onshore, offshore

A *thermal circulation* (thermally driven circulation) is a closed mesoscale or local circulation driven by horizontal differences of temperature, and therefore of density, near the ground; its winds are measured in m/s and it is identified by the reversal of its wind between day and night. *Differential heating* is the difference in the rate at which two neighboring surfaces, and the air above them, heat by day or cool at night, in kelvin per hour; it is measured by comparing air temperatures at the same height over the two surfaces. *Thermal forcing* is the horizontal pressure-gradient force per unit mass that differential heating creates, in $\mathrm{m\,s^{-2}}$; *mechanical forcing* is the force that arises when a background wind meets terrain or obstacles. The *return flow* is the branch of a thermal circulation aloft that carries air back over the cooler surface and closes the loop. A *thermal low* is a region of relatively low surface pressure, a fraction of a hectopascal to a few hectopascals deep, over ground that is warmer than its surroundings. *Onshore* wind blows from the sea toward the land; *offshore* wind blows from the land toward the sea.

Key idea

Differential heating → horizontal temperature and density contrast → mesoscale pressure gradient → thermal circulation. The near-surface wind is the synoptic flow plus the local thermal circulation plus the boundary layer's response to both, not a large-scale wind interpolated to the site.

19.1.1 From differential heating to a circulation

Take two neighboring columns of air with the same surface pressure p_1, one over a surface that heats (land by day) at a mean temperature T_{land}, and one over a surface that does not (the sea) at $T_{\text{sea}} < T_{\text{land}}$. The hydrostatic relation of Chapter 2, $\partial p/\partial z = -\rho g$, with the gas law $\rho = p/(R_d T)$, gives $\partial \ln p/\partial z = -g/(R_d T)$, and for a column of uniform temperature

$$p(z) = p_1 \exp\!\left(-\frac{gz}{R_d T}\right). \tag{19.1}$$

Pressure falls more slowly with height in the warm column, whose scale height $R_d T/g$ is larger. The difference between the two columns at height z follows by differentiating equation (19.1) with respect to T, $\partial p/\partial T = p\, gz/(R_d T^2)$, so that for a small contrast $\Delta T = T_{\text{land}} - T_{\text{sea}}$

$$p_{\text{land}}(z) - p_{\text{sea}}(z) \approx p(z)\,\frac{gz}{R_d T}\,\frac{\Delta T}{T}. \tag{19.2}$$

The difference is zero at the ground and grows with height. For an illustrative contrast $\Delta T = 3\,\text{K}$ at $T = 300\,\text{K}$ and $z = 1000\,\text{m}$: $gz/(R_d T) = 9810/86\,100 = 0.114$, $p(1000\,\text{m}) = 1000\,\text{hPa} \times e^{-0.114} = 892\,\text{hPa}$, and

$$p_{\text{land}} - p_{\text{sea}} \approx 892 \times 0.114 \times 0.01 \approx 1.0\,\text{hPa},$$

higher over the land. This is the result of Chapter 5, obtained there from the hypsometric thickness of the 1000 to 900 hPa layer. Aloft, air moves from the warm column toward the cool one; the mass it carries lowers the surface pressure under the warm column and raises it under the cool one; and near the ground air then moves from the cool surface toward the warm one. The loop closes with rising air over the warm surface and sinking air over the cool one.

The rate at which the loop spins up follows from the circulation theorem. Define the circulation around a closed loop of air as $C = \oint \mathbf{V}\cdot \mathrm{d}\mathbf{l}$, in $\text{m}^2\,\text{s}^{-1}$, where $\mathrm{d}\mathbf{l}$ is an element of the loop and $\mathbf{V}$ here includes the vertical velocity. Following the loop, and neglecting friction and the Coriolis force, the only acceleration is the pressure-gradient force $-\rho^{-1}\nabla p$, and

$$\frac{\mathrm{d}C}{\mathrm{d}t} = -\oint \frac{\nabla p\cdot \mathrm{d}\mathbf{l}}{\rho} = -\oint \frac{\mathrm{d}p}{\rho} = -R_d \oint T\,\mathrm{d}\ln p, \tag{19.3}$$

using $\nabla p\cdot \mathrm{d}\mathbf{l} = \mathrm{d}p$ along the loop and $1/\rho = R_d T/p$. Figure 19.1 draws the loop: a vertical cross section with the sea on the left and the heated land on the right, the lower isobar p_1 along the ground, the upper isobar p_2 raised over the warm column, and the loop in blue, made of two legs along the isobars and two vertical legs, one in each column.

Along the two isobaric legs $\mathrm{d}p = 0$ and the integrand vanishes. On the land leg, going up from p_1 to p_2 at temperature T_{land}, the contribution is $-R_d T_{\text{land}}(\ln p_2 - \ln p_1) = R_d T_{\text{land}} \ln(p_1/p_2)$; on the sea leg, going down from p_2 to p_1, it is $-R_d T_{\text{sea}} \ln(p_1/p_2)$. The sum is

$$\frac{\mathrm{d}C}{\mathrm{d}t} = R_d\,\ln\frac{p_1}{p_2}\,(T_{\text{land}} - T_{\text{sea}}), \tag{19.4}$$

positive when the land is warmer: the circulation accelerates onshore near the ground, upward over the land, offshore aloft and downward over the sea, the sea breeze. At night the contrast

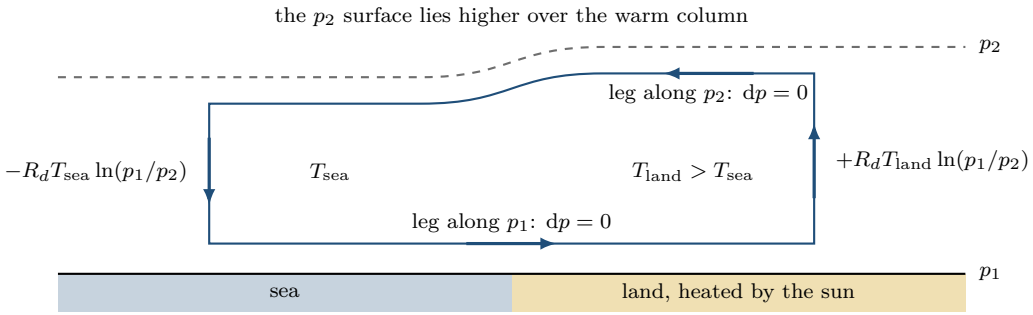


Figure 19.1: The circulation theorem applied to a land-sea contrast (schematic vertical cross section, not to scale). The blue loop runs onshore along the lower isobar p_1, up through the warm land column, offshore along the upper isobar p_2 and down through the cool sea column. Only the vertical legs contribute to $-R_d \oint T \,\mathrm{d}\ln p$; their sum, $\mathrm{d}C/\mathrm{d}t = R_d \ln(p_1/p_2)(T_{\mathrm{land}} - T_{\mathrm{sea}})$, is positive, so the circulation accelerates in the sense of the arrows.

reverses and so does the sense of the loop. For the illustrative $\Delta T = 3\,\mathrm{K}$ between $p_1 = 1000$ and $p_2 = 900\,\mathrm{hPa}$,

$$\frac{\mathrm{d}C}{\mathrm{d}t} = 287 \times \ln\frac{1000}{900} \times 3 = 287 \times 0.1054 \times 3 \approx 90.7\,\mathrm{m^2\,s^{-2}}.$$

Spread over a loop 20 km wide and about 930 m deep (the layer thickness of Chapter 5), of perimeter $2 \times 20\,000 + 925 + 934 \approx 41\,900\,\mathrm{m}$, this is a mean acceleration along the loop of $90.7/41\,900 \approx 2.2 \times 10^{-3}\,\mathrm{m\,s^{-2}}$, which unopposed for one hour would give $7.8\,\mathrm{m\,s^{-1}}$. It is half the $4.1 \times 10^{-3}\,\mathrm{m\,s^{-2}}$ that Chapter 5 obtained by placing the whole pressure difference at the surface; the circulation theorem shares it between the lower and the upper branch. Both estimates give the same order, $10^{-3}\,\mathrm{m\,s^{-2}}$.

The contrast that matters is in virtual temperature. The density of moist air is set by its virtual temperature T_v, and air over the sea is usually moister than air over land. With illustrative specific humidities of $18\,\mathrm{g\,kg^{-1}}$ over the sea and $12\,\mathrm{g\,kg^{-1}}$ over the land at 300 K, the moisture excess $T_v - T \approx 0.61\,q\,T$ is 3.3 K and 2.2 K, so a temperature contrast of 3 K is a virtual-temperature contrast of about 1.9 K. Equations (19.2) and (19.4) hold with T_v in place of T, and the circulation is driven by the smaller number.

19.1.2 Small pressure differences over short distances

A thermal circulation is driven by pressure differences of a fraction of a hectopascal to about one hectopascal. On a surface weather map, where isobars are drawn every 2 or 4 hPa, such a difference does not produce a single extra isobar, and a thermal low over a coastal plain is usually invisible on the chart. What makes it dynamically significant is the distance over which it acts. Compare, at $\rho = 1.15\,\mathrm{kg\,m^{-3}}$,

- a synoptic gradient of 10 hPa across 1000 km, that is 1 hPa per 100 km: $\rho^{-1}|\nabla_h p| = 1000/(1.15 \times 10^6) = 8.7 \times 10^{-4}\,\mathrm{m\,s^{-2}}$;
- a sea-breeze gradient of 0.95 hPa across 20 km, that is about 5 hPa per 100 km: $95/(1.15 \times 20\,000) = 4.1 \times 10^{-3}\,\mathrm{m\,s^{-2}}$.

The local gradient is about five times the synoptic one. If it were balanced geostrophically at $|f| = 10^{-4}\,\mathrm{s^{-1}}$ it would correspond to a wind of $4.1 \times 10^{-3}/10^{-4} = 41\,\mathrm{m\,s^{-1}}$. It is not balanced: the circulation lasts only hours and spans only tens of kilometers, so the Coriolis

force has no time to turn the flow parallel to the isobars (Section 19.1.4), and the air accelerates down the gradient instead. At $4.1 \times 10^{-3}\,\mathrm{m\,s^{-2}}$ the onshore wind would reach $5\,\mathrm{m\,s^{-1}}$ in $5/(4.1 \times 10^{-3}) \approx 1200\,\mathrm{s}$, twenty minutes. What holds it to a few meters per second is not a weakness of the force but friction with the surface, turbulent mixing with the air above, and the circulation itself, which moves mass and erodes the pressure difference that drives it.

A barometer at each end of the 20 km would read the difference; most surface networks are too sparse and report pressure too coarsely to resolve it. The pressure field of a thermal circulation is therefore usually inferred from its winds and temperatures, not measured directly.

19.1.3 Thermal and mechanical forcing

The winds that terrain and surface contrasts add to the large-scale flow have two kinds of origin. Thermally driven flows arise from temperature and density differences: the sea breeze, slope flows and valley circulations, the urban breeze. Mechanically driven flows arise from the background wind interacting with terrain and obstacles: gap acceleration, speed-up over ridges, channeling, wakes. Table 19.1 sets the two side by side. Its rows are the driver, examples, whether a background wind is needed, the time dependence, the weather that favors each, and how each changes direction.

Table 19.1: Thermal against mechanical forcing of local winds.

	Thermal forcing	Mechanical forcing
Driver	horizontal temperature and density contrast from differential heating or cooling	background wind meeting terrain, roughness changes or obstacles
Examples	sea and land breezes, slope and valley winds, urban breeze, cold-air drainage	speed-up over ridges, gap acceleration, channeling, wakes and sheltering
Background wind needed	no; strongest when the background wind is weak	yes; the effect scales with the background wind
Time dependence	diurnal, set by the sun	set by the synoptic wind, hours to days
Favoring weather	clear skies, slack pressure gradient, dry ground	strong pressure gradient
Change of direction	reverses between day and night	changes only when the background wind does

Real flows mix both. A valley wind may be thermally driven in the afternoon and mechanically channeled when the synoptic wind strengthens in the evening; a sea breeze crossing a coastal hill is accelerated over its crest like any other wind. The distinction is still useful, because the two respond to different inputs: a forecast of a mechanically forced wind depends mainly on the background wind and the terrain shape; a forecast of a thermally forced wind depends mainly on cloud cover, soil moisture and the time of day. Chapter 20 treats mechanical forcing; this chapter treats thermal forcing.

19.1.4 Scale and the Rossby number

The Rossby number of Chapter 5, $\mathrm{Ro} = U/(|f|L)$, says whether the Coriolis force matters over the time air takes to cross a circulation. For a sea breeze with $L = 50\,\mathrm{km}$, $U = 5\,\mathrm{m\,s^{-1}}$ and $|f| = 10^{-4}\,\mathrm{s^{-1}}$,

$$\mathrm{Ro} = \frac{5}{10^{-4} \times 5 \times 10^{4}} = 1 :$$

inertia and the Coriolis force are comparable, and the Coriolis force turns the sea breeze over the hours it blows (Section 19.2.5). For a slope flow with $L = 1\,\mathrm{km}$ and $U = 2\,\mathrm{m\,s^{-1}}$,

$$\mathrm{Ro} = \frac{2}{10^{-4} \times 10^{3}} = 20 :$$

the Coriolis force is unimportant, and the slope wind blows straight down the local pressure gradient, up or down the fall line. At lower latitude $|f|$ is smaller and Ro larger: at 23°S, $f = 2 \times 7.292 \times 10^{-5} \times \sin(-23°) = -5.70 \times 10^{-5}\,\mathrm{s^{-1}}$, and the same two flows have Ro = 1.75 and 35. Table 19.2 lists the scales of the circulations of the chapter, with their Rossby numbers at $|f| = 10^{-4}\,\mathrm{s^{-1}}$ and at 23° of latitude in either hemisphere.

Table 19.2: Scales of thermal circulations. The sea-breeze and slope values are those of the text; the others are illustrative. $\mathrm{Ro} = U/(|f|L)$, with $|f| = 5.70 \times 10^{-5}\,\mathrm{s^{-1}}$ at 23°N or 23°S.

Circulation	L	U	Depth	Time scale	Ro, $\lvert f\rvert = 10^{-4}\,\mathrm{s^{-1}}$	Ro, 23°
Sea breeze	50 km	$5\,\mathrm{m\,s^{-1}}$	0.5–1 km	afternoon	1.0	1.75
Land breeze	20 km	$2\,\mathrm{m\,s^{-1}}$	0.1–0.3 km	night	1.0	1.75
Valley wind	30 km	$4\,\mathrm{m\,s^{-1}}$	0.3–1 km	hours	1.3	2.3
Urban breeze	10 km	$2\,\mathrm{m\,s^{-1}}$	0.3–1 km	night	2.0	3.5
Slope wind	1 km	$2\,\mathrm{m\,s^{-1}}$	10–200 m	minutes to an hour	20	35

The second number that sets the behavior of the larger circulations is the ratio of the Coriolis parameter to the frequency of the daily forcing, $\omega = 2\pi/(24\,\mathrm{h}) = 7.27 \times 10^{-5}\,\mathrm{s^{-1}}$. The two are equal where $2\Omega|\sin\phi| = \omega$, at $|\phi| = 29.9°$. Linear theory of the sea breeze gives two regimes on either side of that latitude. Poleward of 30°, where $|f| > \omega$, the circulation is confined to a distance of order $Nh/\sqrt{f^2 - \omega^2}$ from the coast, with h the depth of the heated layer: about $10/(7.3 \times 10^{-5}) \approx 140\,\mathrm{km}$ at 45° for $N = 0.01\,\mathrm{s^{-1}}$ and $h = 1\,\mathrm{km}$, a scale for the whole circulation on both sides of the coast that friction reduces further. Equatorward of 30° the response is not confined and spreads away from the coast as gravity waves, and sea breezes in the tropics reach farther inland. The same ratio sets how much the sea breeze turns during the day (Section 19.2.5).

19.2 Sea and land breezes

This section takes the coastal circulation through its daily cycle: why the land heats faster than the water, how the sea breeze starts, advances behind a front, adds to the synoptic wind and turns with the Coriolis force, and how the land breeze replaces it at night.

19.2.1 Why land heats faster than water

The *sea breeze* is the daytime onshore wind, with its return flow aloft, driven by the warming of the land relative to the sea; it is measured as the onshore component of the wind at a coastal station and modeled by a weather model that resolves the coast. It exists because the same sunshine warms the two surfaces by very different amounts. Four properties of water hold its surface temperature nearly constant through the day.

- *Heat capacity.* The volumetric heat capacity of water is $4.18 \times 10^{6}\,\mathrm{J\,m^{-3}\,K^{-1}}$, about three times that of a typical soil, $1.5 \times 10^{6}\,\mathrm{J\,m^{-3}\,K^{-1}}$.
- *Vertical mixing.* Waves and currents mix the heat absorbed at the surface through an upper layer of the ocean meters to tens of meters deep.

- *Solar penetration.* Sunlight penetrates meters into clear water, so its energy is deposited in a volume rather than at a surface.
- *Evaporation.* A large part of the absorbed energy leaves the water surface as latent heat, which does not warm the air.

Land has the opposite properties: a lower heat capacity, no mixing, since heat enters the soil only by conduction, and a shallow storage depth. The depth that a daily cycle of heating reaches by conduction is $\sqrt{2\kappa_s/\omega}$, with κ_s the thermal diffusivity of the soil; for an illustrative $\kappa_s = 5 \times 10^{-7}\,\mathrm{m^2\,s^{-1}}$ it is $\sqrt{2 \times 5 \times 10^{-7}/7.27 \times 10^{-5}} = 0.12\,\mathrm{m}$.

A worked comparison. Let each surface store an illustrative $2\,\mathrm{MJ\,m^{-2}}$ in the morning. In a soil layer 0.1 m deep the temperature rise is $2 \times 10^6/(1.5 \times 10^6 \times 0.1) = 13\,\mathrm{K}$; in a water layer mixed to 10 m it is $2 \times 10^6/(4.18 \times 10^6 \times 10) = 0.05\,\mathrm{K}$. The ratio is nearly three hundred. The land surface becomes hot, the sensible heat flux H it gives the air is large, and the air above it warms by several kelvin; the sea surface and the air above it hardly change. That contrast in the air, not in the ground, is what enters equations (19.2) and (19.4). It is largest on clear days with dry soil and weak wind, and it is reduced by cloud, by wet soil, whose evaporation takes energy that would have heated the air, and by a strong wind that mixes the two air masses.

19.2.2 The daily cycle of the sea breeze

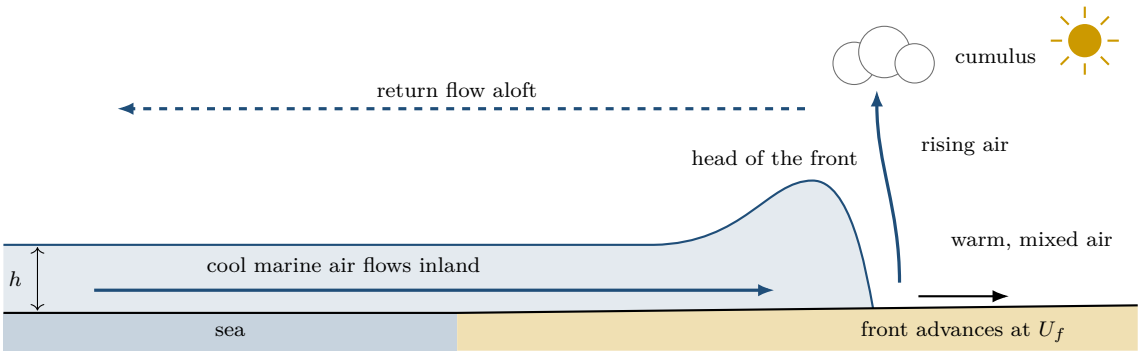
The cycle at a coastal station on a day of weak synoptic wind runs as follows. In the early morning the land is still cooler than the sea or equal to it, and the wind is light. Two to four hours after sunrise the land air becomes warmer than the marine air, the thermal low forms, and an onshore wind begins at the coast, first as a shallow flow a few hundred meters deep. Through the late morning and early afternoon it strengthens, deepens to 0.5 to 1 km, and its leading edge moves inland. The onshore wind peaks in mid-afternoon, typically 13:00 to 16:00 local time, at 3 to $7\,\mathrm{m\,s^{-1}}$, and weakens after the land stops heating in the late afternoon. After sunset the land cools below the sea and a weaker offshore land breeze takes over for the night.

Figure 19.2 draws the two halves of the cycle in a vertical cross section, sea on the left and land on the right. In panel (a), the afternoon, the shaded wedge is the cool marine air that has moved inland, of depth h; its raised leading edge is the head of the sea-breeze front; the solid arrows are the onshore flow, the rising air at the front, and the cumulus cloud that the rising air often produces; the dashed arrow is the return flow aloft. Panel (b), the night, shows the shallow layer of air cooled over the land draining offshore as the land breeze, the rising air where it meets the warmer marine air offshore, and a weak return flow above it.

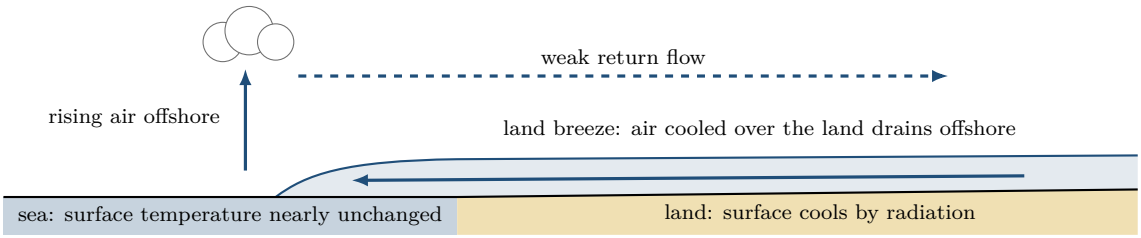
Figure 19.3 shows the same cycle as a time series at one coastal station: the horizontal axis is local time from midnight to midnight, and the vertical axis the onshore component of the wind, positive onshore and negative offshore. The solid curve is a day with no synoptic wind, an illustrative sea breeze of $5\,\mathrm{m\,s^{-1}}$ at 15:00 and a land breeze of $1.5\,\mathrm{m\,s^{-1}}$ at 03:00. The dashed curve adds a steady synoptic wind of $3\,\mathrm{m\,s^{-1}}$ offshore, discussed in Section 19.2.4. On the calm day the wind turns onshore at 09:00 and offshore at 21:00, with the daytime branch more than three times stronger than the night branch.

19.2.3 The sea-breeze front

The *sea-breeze front* is the leading edge of the cool marine air as it advances inland: a density boundary that behaves like a small cold front. Its passage at a station is recorded as a set of abrupt changes within minutes: a shift of wind direction to onshore, a drop in temperature of one to several kelvin, a rise in humidity, a jump in turbulence and gustiness, and sometimes a small rise of pressure. Ahead of it the air converges and rises, which is why a line of cumulus



(a) afternoon: sea breeze and sea-breeze front



(b) night: land breeze

Figure 19.2: Vertical cross sections of the coastal circulation (schematic, not to scale; the marine layer is typically 0.5 to 1 km deep and the front tens of kilometers inland by late afternoon; the land-breeze layer is 0.1 to 0.3 km deep). (a) Afternoon: cool marine air of depth h moves inland behind the sea-breeze front, whose head is raised and marked by rising air and often a line of cumulus. (b) Night: a shallow land breeze drains offshore, with rising air where it meets the marine air.

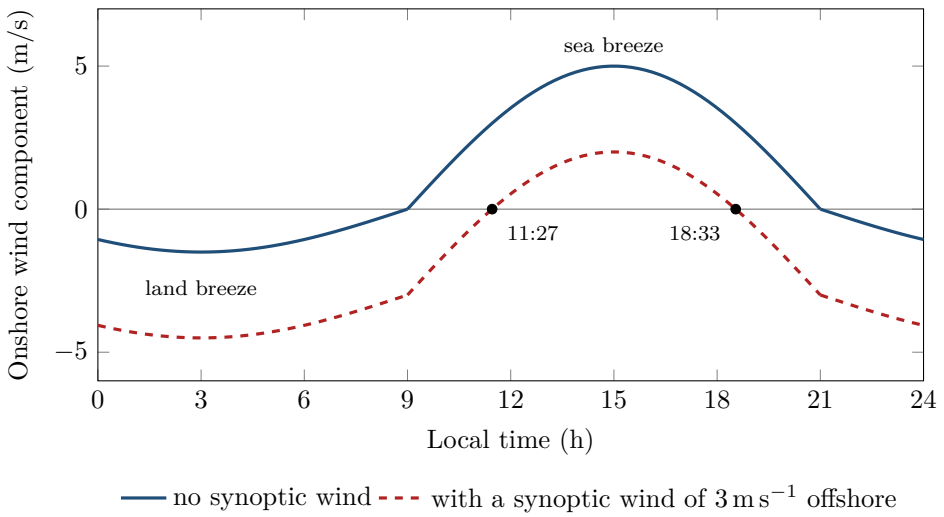


Figure 19.3: Onshore wind component at a coastal station through one day (illustrative). Solid: thermal circulation alone, $u_{\mathrm{on}}(t) = A\sin[\pi(t - 9\,\mathrm{h})/12\,\mathrm{h}]$ with $A = 5\,\mathrm{m\,s^{-1}}$ from 09:00 to 21:00 and $A = 1.5\,\mathrm{m\,s^{-1}}$ at night. Dashed: the same plus a steady synoptic component of $3\,\mathrm{m\,s^{-1}}$ offshore; the markers show when the surface wind turns onshore and back offshore.

often marks its position (Figure 19.2a). For a wind sensor or a line conductor, the front is the moment at which the near-surface wind changes direction and speed most abruptly in the whole day.

The speed of the front. The front advances as a *density current*, defined in Section 19.4.4: a layer of denser fluid spreading under lighter fluid. Its speed follows from a pressure balance. Work in a frame that moves with the front, in which the cool layer behind it is at rest and the warm air ahead approaches at the front speed U_f. Along the ground, the warm air decelerates to rest at the nose of the front. Bernoulli's relation along that streamline, for steady flow without friction, gives the pressure at the nose

$$p_{\text{nose}} = p_{\text{ahead}} + \tfrac{1}{2}\rho\, U_f^2.$$

Behind the head, the cool layer of depth h and density $\rho + \Delta\rho$ is at rest and hydrostatic, and the warm air above it is assumed at rest and hydrostatic as well, so that the pressure at the ground under the layer exceeds the pressure ahead at the same level by the extra weight of the layer,

$$p_{\text{behind}} = p_{\text{ahead}} + \Delta\rho\, g\, h.$$

The cool air at rest has the same pressure at the nose and behind it. Equating the two expressions,

$$\tfrac{1}{2}\rho\, U_f^2 = \Delta\rho\, g\, h \quad\Longrightarrow\quad U_f = \sqrt{2}\,\sqrt{g'h}, \qquad g' = g\,\frac{\Delta\rho}{\rho} = g\,\frac{\Delta\theta_v}{\theta_v}, \tag{19.5}$$

where g', in $\mathrm{m\,s^{-2}}$, is the *reduced gravity*, the gravitational acceleration multiplied by the fractional density contrast; at equal pressure the density contrast equals the contrast in virtual potential temperature $\Delta\theta_v$ between the two air masses, divided by θ_v. The factor $\sqrt{2}$ belongs to an ideal current under a deep, motionless ambient layer without mixing. Mixing at the head, friction with the ground and an ambient layer of finite depth all slow the front, and observed fronts are described by

$$U_f = k_f\sqrt{g'h}, \qquad k_f \approx 0.6 \text{ to } 1, \tag{19.6}$$

with k_f an empirical constant fitted to observations and laboratory currents, not a derived one.

For an illustrative marine layer $h = 400\,\mathrm{m}$ deep and $\Delta\theta_v = 2\,\mathrm{K}$ cooler than the land air at $\theta_v = 300\,\mathrm{K}$,

$$g' = 9.81 \times \frac{2}{300} = 0.065\,\mathrm{m\,s^{-2}}, \qquad \sqrt{g'h} = \sqrt{0.065 \times 400} = 5.1\,\mathrm{m\,s^{-1}},$$

and the front moves at $U_f = 3.1$ to $5.1\,\mathrm{m\,s^{-1}}$ relative to the air ahead of it. At $3.1\,\mathrm{m\,s^{-1}}$ for six hours it would cover 67 km; observed fronts slow down as they advance, because the marine air warms over the land and $\Delta\theta_v$ and g' fall, and they typically reach a few tens of kilometers inland in the middle latitudes and farther in the tropics. The pressure rise behind the front is $\Delta\rho\, g\, h = \rho\, g'h = 1.15 \times 0.065 \times 400 \approx 30\,\mathrm{Pa}$, 0.3 hPa, the size of the thermal pressure difference of Section 19.1.2. The head of the front is deeper than the current behind it, often one and a half to two times, and the shear at the top of the marine air produces billows of the Kelvin-Helmholtz type described in Chapter 17.

19.2.4 The synoptic wind and the sea breeze

The observed wind is the synoptic forcing and the thermal circulation together. A synoptic flow in the same direction as the sea breeze reinforces the onshore wind; an opposing flow delays, weakens or blocks it. The simplest description adds the two as vectors. Take an illustrative east-facing coast in South America at 20°S, where the onshore direction is from the east, $\beta = 90°$.

- *Opposing.* A synoptic wind of $3\,\mathrm{m\,s^{-1}}$ offshore, from 270°, and an afternoon sea breeze of $5\,\mathrm{m\,s^{-1}}$ onshore, from 90°, add to $2\,\mathrm{m\,s^{-1}}$ from 90°. The surface wind reverses direction in the afternoon: the local thermal forcing overwhelms the weak synoptic forcing.
- *Helping.* A synoptic wind of $3\,\mathrm{m\,s^{-1}}$ from 90° adds to give $8\,\mathrm{m\,s^{-1}}$ from 90°.
- *Across.* A synoptic wind of $3\,\mathrm{m\,s^{-1}}$ along the coast, from 180°, has components $u = 0$, $v = +3\,\mathrm{m\,s^{-1}}$; the breeze has $u = -5\,\mathrm{m\,s^{-1}}$, $v = 0$. The sum, $u = -5$, $v = 3\,\mathrm{m\,s^{-1}}$, is $5.8\,\mathrm{m\,s^{-1}}$ from $\beta = 121°$, by $u = -U\sin\beta$, $v = -U\cos\beta$: an east-southeasterly.

The dashed curve of Figure 19.3 is the opposing case through the day: the onshore component is the calm-day curve shifted down by $3\,\mathrm{m\,s^{-1}}$. The surface wind turns onshore only when the breeze exceeds $3\,\mathrm{m\,s^{-1}}$, when $5\sin[\pi(t-9)/12] = 3$, that is at $t = 9 + (12/\pi)\arcsin 0.6 = 11.46\,\mathrm{h}$, and back offshore at 18.54 h; the onshore period shrinks from twelve hours to seven, and the night wind is $4.5\,\mathrm{m\,s^{-1}}$ offshore instead of 1.5.

The vector sum is a first approximation, and the interaction is more than additive in three ways.

- An opposing wind holds the front back. Relative to the ground the front moves at roughly U_f plus the onshore component of the background wind; with the $U_f = 3.1$ to $5.1\,\mathrm{m\,s^{-1}}$ of Section 19.2.3 and $3\,\mathrm{m\,s^{-1}}$ offshore it advances at only 0.1 to $2.1\,\mathrm{m\,s^{-1}}$, and an offshore wind stronger than U_f holds it at the coast or offshore. A moderate offshore wind also sharpens the front, because it keeps the land air hot and piles the marine air against it.
- A helping, onshore synoptic wind advects marine air inland all day and mixes it with the land air, so the land-sea contrast and the front are weak even though the onshore wind is strong.
- A strong synoptic wind of either direction mixes the boundary layer and spreads the heating over a deep layer, and the thermal circulation is suppressed (Section 19.5.2).

19.2.5 Turning of the sea breeze by the Coriolis force

With Ro ~ 1, the Coriolis force acts on the sea breeze over the hours it blows. Chapter 5 stated the direction of the turning; a forced, damped model gives its size. Let u be the wind component toward the land and v the component 90° to the left of it (in this subsection only), let the thermal forcing be an onshore acceleration $a_0\cos\omega t$ that peaks once a day, and represent friction by the linear drag rate λ of Chapter 3. The horizontal momentum equations are

$$\frac{\mathrm{d}u}{\mathrm{d}t} - fv = a_0\cos\omega t - \lambda u, \qquad \frac{\mathrm{d}v}{\mathrm{d}t} + fu = -\lambda v. \tag{19.7}$$

Combine them into one complex equation for $\chi = u + \mathrm{i}v$: multiply the second by i and add,

$$\frac{\mathrm{d}\chi}{\mathrm{d}t} + (\lambda + \mathrm{i}f)\,\chi = a_0\cos\omega t = \frac{a_0}{2}\left(e^{\mathrm{i}\omega t} + e^{-\mathrm{i}\omega t}\right).$$

Try $\chi = c_+ e^{\mathrm{i}\omega t} + c_- e^{-\mathrm{i}\omega t}$. Substituting gives $c_\pm[\lambda + \mathrm{i}(f \pm \omega)] = a_0/2$, so the periodic solution is

$$\chi(t) = \frac{a_0}{2}\left[\frac{e^{\mathrm{i}\omega t}}{\lambda + \mathrm{i}(f+\omega)} + \frac{e^{-\mathrm{i}\omega t}}{\lambda + \mathrm{i}(f-\omega)}\right]. \tag{19.8}$$

The first term is a wind vector of fixed length rotating counterclockwise once a day, the second one rotating clockwise; their amplitudes are $A_\pm = (a_0/2)/\sqrt{\lambda^2 + (f \pm \omega)^2}$. Their sum traces an ellipse, the *hodograph* of the sea breeze, with semi-axes $A_+ + A_-$ and $|A_+ - A_-|$, and the larger term sets the sense of rotation. In the Northern Hemisphere, $f > 0$, $|f - \omega| < f + \omega$ and the

clockwise term is larger: the wind vector turns clockwise through the day, and the direction the wind blows from veers. In the Southern Hemisphere, $f < 0$, the counterclockwise term is larger: the wind vector turns counterclockwise, and the direction backs. At the equator the two terms are equal, the ellipse collapses to a line, and the wind only alternates between onshore and offshore. The result holds with or without friction and on either side of 30°; without friction the response grows without bound where $|f| = \omega$, at 30°, a resonance that friction limits.

Figure 19.4 plots equation (19.8) for an east-facing coast at 20°N and at 20°S, where $|f| = 4.99 \times 10^{-5}\,\mathrm{s}^{-1}$, with an illustrative damping time $1/\lambda = 10\,\mathrm{h}$ and a_0 scaled so that the strongest wind is $5\,\mathrm{m\,s}^{-1}$. Each panel plots the eastward component u against the northward component v of the wind vector, with north up; onshore is toward the west, the negative u axis. The markers give the wind every three hours, taking the forcing to peak at 12:00 local time, and the curved arrow inside each ellipse gives the sense of rotation.

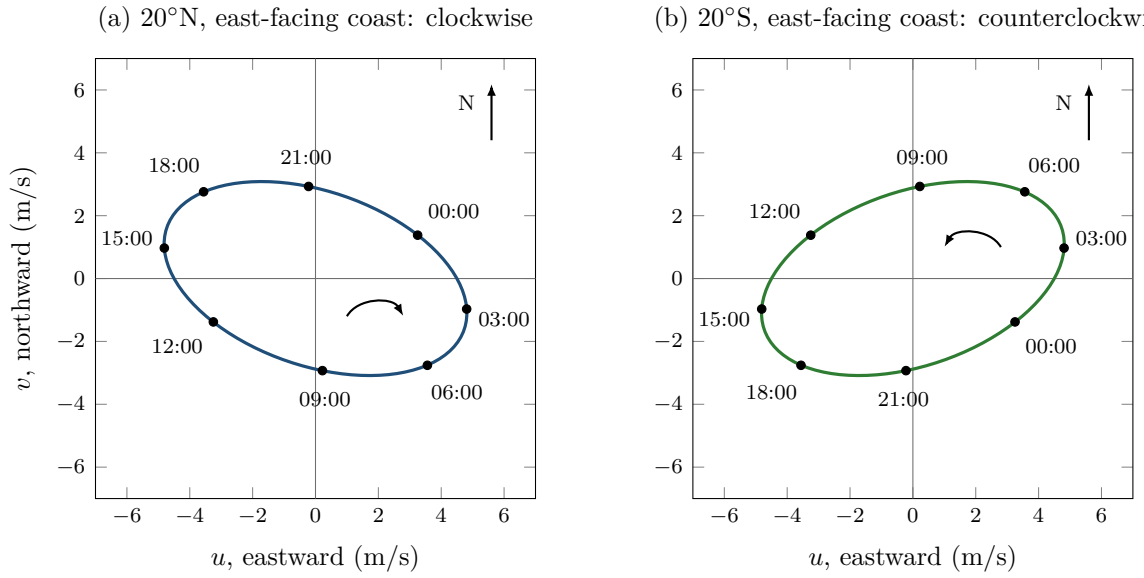


Figure 19.4: Hodographs of the sea breeze from the forced, damped model of equation (19.8): the tip of the wind vector through one day on an east-facing coast (onshore is toward negative u). Parameters: $|f| = 4.99 \times 10^{-5}\,\mathrm{s}^{-1}$ (20°), $\omega = 7.27 \times 10^{-5}\,\mathrm{s}^{-1}$, $1/\lambda = 10\,\mathrm{h}$, forcing peak at 12:00, a_0 scaled to a maximum wind of $5\,\mathrm{m\,s}^{-1}$ (illustrative). (a) Northern Hemisphere: the vector turns clockwise. (b) Southern Hemisphere: the vector turns counterclockwise. The model is linear, so its night branch is as strong as its day branch.

The ellipse has semi-axes of 5.0 and $2.8\,\mathrm{m\,s}^{-1}$, an axis ratio of 0.56 in both hemispheres. Read as wind directions, the Southern Hemisphere panel gives a wind from 113° at 12:00, from 79° at 15:00, near the onshore direction at the time of strongest wind, from 52° (northeast) at 18:00 and from 4° (north, along the coast) at 21:00: the afternoon sea breeze backs from east toward northeast and north. The Northern Hemisphere panel gives 67°, 101°, 128° and 176° at the same hours: the breeze veers from east toward southeast and south. In both, the turning between 15:00 and 18:00 is about 27°. At night the vector continues around the ellipse to offshore, the land-breeze direction, and in the morning blows along the coast the other way. The model reproduces the sense and the order of magnitude of the turning; it does not reproduce the asymmetry between day and night, which comes from stability (Section 19.2.6).

19.2.6 The land breeze

The *land breeze* is the night-time offshore wind driven by the cooling of the land below the temperature of the sea; it is measured as the offshore component of the wind at a coastal station

at night. The mechanism is the sea breeze reversed: the land surface cools by emitting infrared radiation, the air above it becomes colder and denser than the marine air, the pressure near the ground rises over the land, and air drains toward the sea (Figure 19.2b).

It is usually weaker than the sea breeze, 1 to $3\,\mathrm{m\,s^{-1}}$ against 3 to $7\,\mathrm{m\,s^{-1}}$, and shallower, 100 to 300 m against 0.5 to 1 km, for three reasons. The night-time contrast is smaller, because the land cools at night by less than it warms by day, and in the tropics the sea is often warm enough that the land barely becomes colder than it. The cooling is confined to the shallow stable layer of Chapter 17, so the pressure difference of equation (19.2), which grows with the depth of the contrast, is small. And stable air mixes momentum poorly, so the flow is retarded by friction in a thin layer. Where the land breeze meets the warmer, moister marine air offshore it converges and rises, which is why showers and cloud lines often form just off the coast late at night and in the early morning. At a station on the coast the land breeze often merges with drainage flow from nearby slopes, the subject of the next section.

19.3 Slope, valley and drainage winds

Terrain sets up thermally driven circulations at two scales, along individual slopes and along whole valleys, and at night it collects the cooled air in its low points. This section treats each, then follows a transmission line across a valley through a day and a night.

19.3.1 Anabatic and katabatic slope winds

By day the sun heats sloping ground, and the air in contact with the slope becomes warmer than the air at the same height away from it. It is buoyant, and the component of its buoyancy along the slope drives it uphill: *anabatic flow*, an upslope wind, measured as the upslope component of the wind a few meters to tens of meters above a slope. At night the slope cools by radiation, the air next to it becomes colder and denser than the air at the same height away from the slope, and it flows downhill: *katabatic flow*, a downslope or drainage wind. The pattern is upslope by day, downslope by night. Chapter 5 gave the driving acceleration along a slope of angle α,

$$a_{\parallel} = g\,\frac{\Delta T}{T}\,\sin\alpha, \tag{19.9}$$

$0.018\,\mathrm{m\,s^{-2}}$ downslope for an illustrative night with $\Delta T = -3\,\mathrm{K}$, $T = 285\,\mathrm{K}$ and $\alpha = 10^{\circ}$, about twenty times the synoptic pressure-gradient force.

The two regimes differ in structure, not only in sign.

- *Anabatic flow* lies in a convective layer: the heated air is unstable, mixes vigorously and is fed from the side and from above. The upslope layer is 50 to 200 m deep, its speed 1 to $4\,\mathrm{m\,s^{-1}}$, and the wind is turbulent and gusty. On a broad slope the upslope flow merges into the convective boundary layer of Chapter 16.

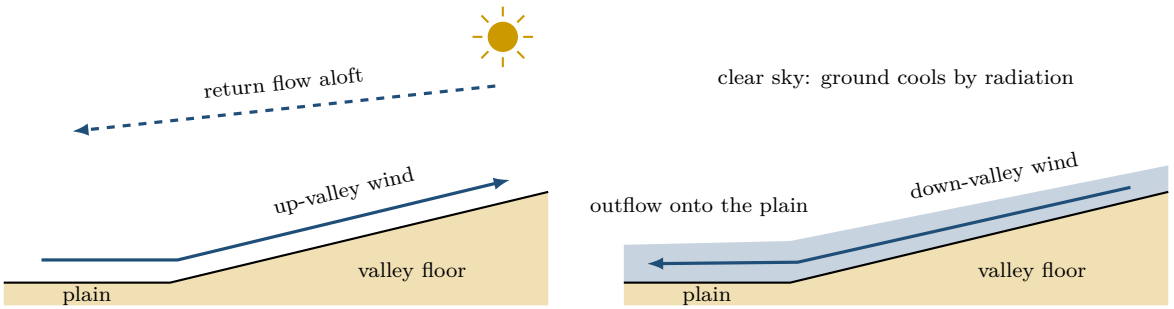
- *Katabatic flow* lies in a stable layer: the cooled air is stratified, mixes little and hugs the ground. The drainage layer is 10 to 50 m deep, with its wind maximum a few meters to about 20 m above the ground, inside the height range of a 10 m anemometer, and a speed of 1 to $3\,\mathrm{m\,s^{-1}}$, more on long, steep or snow-covered slopes. Above the maximum the speed falls off to the weak ambient wind.

Slope winds respond to the sun within tens of minutes: the upslope flow begins soon after the slope is first lit, and the downslope flow soon after it falls into shadow, so slopes facing east and west reverse at different times of day. Because $\mathrm{Ro} \gg 1$ (Table 19.2), they blow along the fall line, down the local gradient, in either hemisphere.

19.3.2 Valley winds and slope winds

A *valley wind* is the thermally driven flow along the axis of a valley: up-valley, toward higher terrain, by day, and down-valley at night. It differs from a slope wind in scale and in direction. A slope wind blows along an individual slope, across the valley axis, over distances from about 100 m to a few kilometers; a valley wind blows along the valley axis, over 10 to 100 km and more. The valley wind is deeper, often filling the valley to near ridge height, typically 3 to 6 $\mathrm{m\,s^{-1}}$ up-valley and 2 to 5 $\mathrm{m\,s^{-1}}$ down-valley, and slower to respond: it reverses hours after the slope winds, in the late morning and in the evening or later at night. Upslope flow is the small-scale branch of the daytime system and, at larger scale, helps drive up-valley flow; the return circulation of both lies above the valley.

Figure 19.5 draws the day and night system as a longitudinal section along the valley axis, with the plain on the left and the valley floor rising toward the mountains on the right. In panel (a), by day, the solid arrow is the up-valley wind near the floor and the dashed arrow the return flow aloft. In panel (b), at night, the shaded layer is the cold air draining down the valley and spreading onto the plain, and the solid arrow is the down-valley wind within it. The slope winds, perpendicular to the page, are upslope by day and downslope by night, as in the cross-valley figure of Chapter 5.



(a) day: up-valley wind (b) night: down-valley wind

Figure 19.5: The mountain-valley wind system in a longitudinal section along the valley axis (schematic, not to scale; the valley is tens of kilometers long and the flow layer a few hundred meters deep). (a) By day, air flows up the valley toward the mountains with a return flow above. (b) At night, cold air drains down the valley and out onto the plain. Slope winds across the valley, perpendicular to the page, are upslope by day and downslope at night.

Why the valley atmosphere heats more than the plain. By day the air in a valley warms more than the air at the same heights over the neighboring plain, because a valley holds less air under the same area of sunlit ground. Take a valley of width W at ridge height and depth h_m (the height of the ridges above the floor) with a V-shaped cross section. It contains a cross-sectional area $Wh_m/2$ of air below ridge height, while the plain under the same width W has Wh_m. The sun delivers about the same energy per unit horizontal area to both, so if both put the same fraction into heating the air below ridge height, the valley air warms twice as much; this ratio of air volumes is called the topographic amplification factor. If the air over the plain warms by an illustrative 4 K below a ridge height $h_m = 1000$ m, the valley air warms by 8 K, and with equal pressure at ridge height the pressure at the valley floor is lower than at the same height over the plain by $\rho\, g\, h_m\, \Delta T/T = 1.1 \times 9.81 \times 1000 \times 4/290 \approx 150$ Pa, 1.5 hPa. Spread along an illustrative valley 50 km long, this is a pressure-gradient force of $150/(1.1 \times 50\,000) = 2.7 \times 10^{-3}\ \mathrm{m\,s^{-2}}$ toward the valley head, the same order as the sea-breeze force, and it drives the up-valley wind. At night the valley air cools more than the plain air, for the same reason, and the gradient reverses. Real valleys complicate the picture: tributaries,

bends, a variable cross section, snow, and the slopes' orientation to the sun all change the timing and strength of the flow.

19.3.3 Terrain channeling

Terrain channeling is the steering of the wind along the axis of a valley by the valley's geometry, without any thermal forcing; it is identified by a wind direction in the valley that stays close to the axis while the wind above the ridges changes. Two forms are common.

- *Forced channeling*: the wind above the ridges is turned into the nearest along-valley direction, so that a valley oriented north-south sees southerly winds for any wind aloft from the southern half of the compass.
- *Pressure-driven channeling*: the along-valley component of the synoptic pressure gradient drives air along the valley from high to low pressure, with friction, not the Coriolis force, opposing it. The channeled wind then follows the pressure gradient, not the geostrophic wind, and can blow at a large angle to the wind aloft.

The second form depends on the hemisphere. Take a north-south valley under a westerly geostrophic wind. In the Northern Hemisphere the geostrophic wind keeps low pressure on its left, to the north; the pressure gradient along the valley points north, and the valley wind is southerly, at 90° to the wind aloft. In the Southern Hemisphere low pressure lies on the right of the westerly, to the south, and the valley wind is northerly. A valley wind may therefore be both thermal and mechanical, and at a given hour the two may add or oppose. Channeling, gap flow and the other mechanically forced terrain winds belong to Chapter 20.

19.3.4 Cold-air drainage and cold pools

On clear nights with weak synoptic wind the katabatic flows collect. Over open slopes the drainage is weak and shallow; in gullies and side valleys it gathers into stronger drainage currents; and where it reaches a basin, a valley floor or a closed depression it accumulates as a *cold pool*, a layer of cold, stable air, tens to a few hundred meters deep, filling the low ground. A cold pool is measured by the temperature difference between a valley-floor station and a station at the same location higher up the slope, and is modeled only where the terrain is resolved (Section 19.6.4).

The consequences for wind are strong. Inside the pool the air is stable and decoupled from the flow above, and the wind on the valley floor is often below $1\,\mathrm{m\,s^{-1}}$ and variable in direction while a ridge a few hundred meters higher sits in the background flow, at 5 to $10\,\mathrm{m\,s^{-1}}$. An illustrative clear night gives -2°C on the valley floor and $+6$°C on a ridge 300 m above it, an inversion of 8 K in 300 m; the warmest air is often on the midslope, a belt above the pool and below the ridge-top wind. A valley-floor sensor therefore differs from a nearby ridge station in temperature, speed and direction at once, and neither represents the other. Elevation alone does not determine exposure: two sites at the same elevation, one on an open slope and one in a closed hollow, can have quite different night winds. In winter, under persistent anticyclones, a cold pool can last for days, with near-calm winds on the floor throughout.

19.3.5 A transmission line across a mountain valley

The convective cooling of an overhead conductor depends on the wind speed and on the angle between the wind and the conductor: wind perpendicular to the conductor cools it most, wind parallel to it least. Take an illustrative line that crosses a valley from the floor, up a midslope, to the ridge, its spans running across the valley axis and, on the slope, straight up the fall line. Table 19.3 gives, for three spans, the regime, an illustrative speed and the angle between the wind and the conductor in the afternoon and at night.

Table 19.3: Winds on three spans of a line crossing a mountain valley (illustrative speeds and angles).

Span	Afternoon	Night	Consequence
Valley floor	up-valley wind, $3\,\mathrm{m\,s^{-1}}$, perpendicular to the conductor	cold pool, $0.5\,\mathrm{m\,s^{-1}}$ or calm, variable	good cooling by day; the least cooling of the line at night
Midslope	upslope wind, $2\,\mathrm{m\,s^{-1}}$, nearly parallel to the conductor	drainage wind, $1.5\,\mathrm{m\,s^{-1}}$, nearly parallel, maximum a few meters above the ground	modest cooling day and night; the wind angle, not the speed, limits it
Ridge	background flow, $6\,\mathrm{m\,s^{-1}}$, at about 45°	background flow, $7\,\mathrm{m\,s^{-1}}$, at about 45°, exposed above the decoupled valley	good cooling day and night

In the afternoon, upslope and up-valley flow dominate the lower spans, and the ridge span sees the stronger and differently oriented background flow. At night, drainage currents run down the slope, the valley floor is weakly ventilated in its cold pool, and the ridge is exposed to the background flow, which at night may even strengthen above the decoupled layer (Chapter 18). Spans a few hundred meters apart therefore see very different winds, and the critical span for conductor temperature changes between day and night: a single weather station, or a single model wind for the whole line, misses the span that limits the rating. The valley-floor span at night is the usual critical case, under exactly the conditions, clear sky and weak synoptic wind, in which a synoptic forecast shows nothing.

19.4 Cities, convergence and density currents

Thermal circulations also arise over cities, and every thermal circulation produces regions of converging and diverging air and, where it advances, a density current. This section treats the urban heat island and its breeze, then the continuity relation that links horizontal convergence to vertical motion, then density currents in general.

19.4.1 The urban heat island

The *urban heat island* is the excess of air temperature in a city over that of its rural surroundings, in kelvin, measured as the difference between urban and rural stations at screen height (about 2 m) at the same time. Typical mean values are 1 to 3 K; on calm, clear nights in large cities the excess reaches 5 to 10 K. It is largest at night and smallest, sometimes slightly negative, around midday. Four causes add.

- *Heat storage.* Buildings and pavement have a large heat capacity and conductivity; they store heat by day through a large surface area and release it at night.
- *Reduced evapotranspiration.* Sealed surfaces and little vegetation leave little water to evaporate, so more of the absorbed energy goes into the sensible heat flux H and less into the latent heat flux LE: the Bowen ratio $B = H/LE$ is several times larger than over vegetation.
- *Anthropogenic heat.* Heating, air conditioning, traffic and industry release heat, an illustrative 10 to $50\,\mathrm{W\,m^{-2}}$ averaged over a city and more than $100\,\mathrm{W\,m^{-2}}$ in dense centers.

- *Radiative trapping.* In street canyons the walls block part of the sky, so the surfaces lose less infrared radiation at night, and sunlight reflected between walls is partly absorbed rather than returned to the sky.

19.4.2 The urban breeze and mechanical urban effects

The warm city air has, by equation (19.2), a thermally lower surface pressure than the rural air around it. The *urban breeze* is the circulation that results: near-surface convergence from the rural surroundings toward the center, rising motion over the city, and outflow aloft, with speeds of 1 to 3 $\mathrm{m\,s^{-1}}$, measured as a systematic inflow component at stations around a city on calm nights. Figure 19.6 draws it. The upper curve is an illustrative night-time urban-minus-rural temperature against distance from the center; the lower part is a vertical cross section with the city in the middle, the inflow at the surface, the rising air over the center and the outflow aloft.

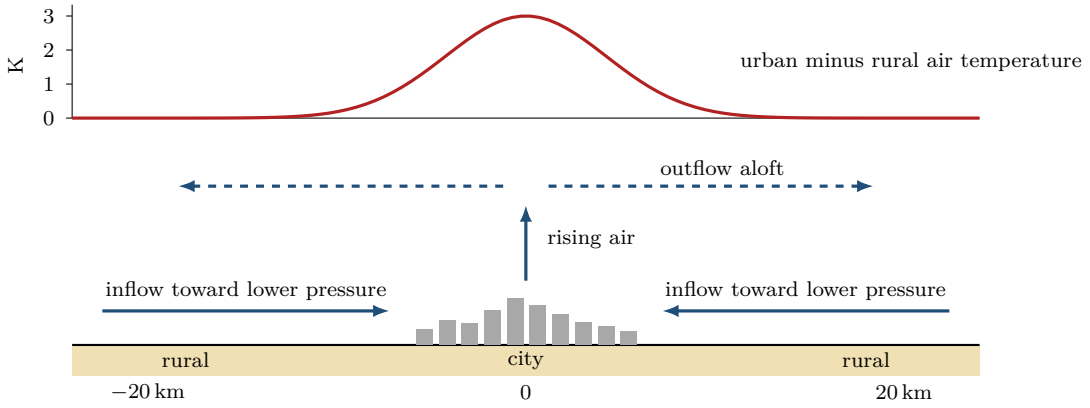


Figure 19.6: The urban breeze on a calm night (schematic). Top: urban minus rural near-surface air temperature, $\Delta T(x) = 3\,\mathrm{K}\,\exp[-(x/6\,\mathrm{km})^2]$, against distance x from the city center (illustrative). Bottom: vertical cross section with inflow toward the city near the surface, rising air over the center and outflow aloft.

The urban breeze is weak and easily overridden. A background wind of a few meters per second carries the warm air downwind as an urban plume, shifts the rising branch to the downwind edge of the city and replaces the symmetric inflow by a wind blowing through the city; the heat island itself weakens as the wind increases. The geometry of the city, its size, the layout of its streets, parks and water bodies, modifies the pattern further.

Mechanical urban effects. A city is also a large roughness element. Its buildings exert drag on the flow, with roughness lengths of the order of a meter and displacement heights of tens of meters (Chapter 11); they shed wakes and generate turbulence; and street canyons channel the wind along their axes, so that a street can carry a wind at a large angle to the wind above the roofs. The wind in a city is therefore thermal circulation and mechanical roughness together, and a sensor on a roof, in a street or in a park measures different parts of it. Urban canopies are the subject of Chapter 21.

19.4.3 Convergence and divergence

Every thermal circulation moves air horizontally toward some places and away from others. *Convergence* is a net horizontal inflow into a region, measured by a negative horizontal divergence, $\nabla_h \cdot \mathbf{V} = \partial u/\partial x + \partial v/\partial y < 0$, in $\mathrm{s^{-1}}$; *divergence* is a net horizontal outflow, $\nabla_h \cdot \mathbf{V} > 0$. Both are computed from the winds at several stations around a region, or from the wind field of a model.

Mass conservation links them to vertical motion. In the lowest kilometer the density changes little over the time and distance a circulation acts, and the continuity equation $\partial\rho/\partial t + \nabla\cdot(\rho\mathbf{u}) = 0$, with $\mathbf{u} = (u, v, w)$, reduces to

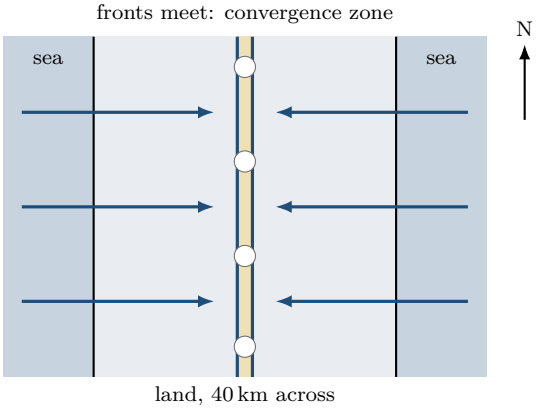
$$\frac{\partial u}{\partial x} + \frac{\partial v}{\partial y} + \frac{\partial w}{\partial z} = 0 \quad\Longrightarrow\quad \frac{\partial w}{\partial z} = -\nabla_h \cdot \mathbf{V}. \tag{19.10}$$

Integrating from the ground, where $w = 0$ over flat terrain, to the top of a layer of depth h,

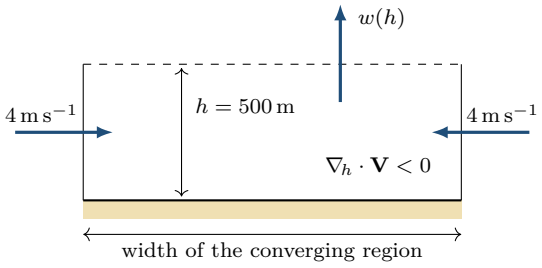
$$w(h) = -\int_0^h \nabla_h \cdot \mathbf{V}\,\mathrm{d}z \approx -(\nabla_h \cdot \mathbf{V})\,h \tag{19.11}$$

for a convergence uniform through the layer. Horizontal convergence near the ground forces rising air; divergence requires sinking air, subsidence, from above. The incompressible form neglects the decrease of density with height, an error of about ten percent over a kilometer.

Figure 19.7 shows an illustrative case. Panel (a) is a plan view of a peninsula 40 km wide running north-south, with the sea on both sides, in the Southern Hemisphere: the arrows are the sea breezes blowing inland from both coasts, the shaded strips the marine air behind the two sea-breeze fronts, and the circles the cumulus along the narrow convergence zone where the fronts meet. Panel (b) treats the converging layer as a box, with inflow through its sides and outflow through its top.



(a) plan view, Southern Hemisphere



(b) the layer as a box

Figure 19.7: Convergence of two sea breezes over a peninsula (schematic, illustrative). (a) Plan view: onshore winds from both coasts, marine air behind the two fronts (light shading), and a line of cumulus where the fronts meet. (b) The converging layer as a box of depth h: horizontal inflow through the sides must leave through the top as vertical velocity $w(h)$, equation (19.11).

A worked vertical velocity. Let the sea breezes blow inland at an illustrative $4\,\mathrm{m\,s^{-1}}$ from each side in a layer $h = 500\,\mathrm{m}$ deep. Averaged over the whole peninsula, the wind changes from $+4$ to $-4\,\mathrm{m\,s^{-1}}$ across 40 km, so

$$\nabla_h \cdot \mathbf{V} = \frac{-4-4}{40\,000} = -2\times10^{-4}\,\mathrm{s^{-1}}, \qquad w(500\,\mathrm{m}) = 2\times10^{-4}\times500 = 0.1\,\mathrm{m\,s^{-1}}.$$

When the two fronts meet, the same change of wind occurs across the narrow zone between them, an illustrative 2 km:

$$\nabla_h \cdot \mathbf{V} = \frac{-8}{2000} = -4\times10^{-3}\,\mathrm{s^{-1}}, \qquad w(500\,\mathrm{m}) = 4\times10^{-3}\times500 = 2\,\mathrm{m\,s^{-1}}.$$

Both carry the same mass upward: the inflow through the two sides, $2 \times 4\,\mathrm{m\,s^{-1}} \times 500\,\mathrm{m} = 4000\,\mathrm{m^2\,s^{-1}}$ per meter of coastline, leaves as $0.1\,\mathrm{m\,s^{-1}} \times 40\,\mathrm{km}$ or as $2\,\mathrm{m\,s^{-1}} \times 2\,\mathrm{km}$. An upward velocity of meters per second at the top of the boundary layer is enough to lift moist air to its condensation level, and sea-breeze convergence lines, as well as the convergence of upslope winds near mountain crests, are known triggers of afternoon clouds and thunderstorms. Conversely, the sinking branch over the sea in Figure 19.2(a) is divergence at the surface, and it suppresses cloud: the clear skies often seen over the coastal sea on a sea-breeze afternoon.

19.4.4 Density currents

A *density current* (gravity current) is a horizontal flow driven by gravity acting on a density difference: the denser fluid spreads beneath the lighter one. Its speed is $U_f = k_f\sqrt{g'h}$, equation (19.6), with g' the reduced gravity and h the depth of the dense layer; it is measured by the passage time of its front between stations, or by radar where the front carries insects or dust. Three atmospheric examples matter for near-surface wind.

- *Thunderstorm outflow.* Air cooled by evaporating rain sinks and spreads along the ground as a pool of cold air whose leading edge is the gust front. For an illustrative contrast $\Delta\theta_v = 8\,\mathrm{K}$ and depth $h = 1000\,\mathrm{m}$, $g' = 9.81 \times 8/300 = 0.26\,\mathrm{m\,s^{-2}}$, $\sqrt{g'h} = 16\,\mathrm{m\,s^{-1}}$, and the front moves at 10 to $16\,\mathrm{m\,s^{-1}}$, with gusts above that and a pressure jump $\rho g'h \approx 1.15 \times 0.26 \times 1000 \approx 300\,\mathrm{Pa}$, 3 hPa.
- *Sea-breeze fronts*, slower and weaker: 3 to $5\,\mathrm{m\,s^{-1}}$ and 0.3 hPa in the example of Section 19.2.3.
- *Some drainage flows*, where cold air leaving a valley spreads over a plain or a frozen surface as a shallow front.

The leading edge of any of them behaves alike: front-like, with strong horizontal gradients of temperature and humidity, convergence and rising air at the head, turbulence and billows behind it, and a sharp shift of wind direction and speed at its passage. Ahead of the edge the wind is set by the ambient flow; behind it, by the current. A station or a conductor crossed by the edge goes from one regime to the other in minutes.

19.5 Interaction with the large-scale flow and with stability

A thermal circulation never acts alone. This section places it in the hierarchy of forcings that make up the near-surface wind, states when it dominates and when it is suppressed, and shows that it changes the stability of the air as well as the direction of the wind.

19.5.1 The hierarchy of forcings

The near-surface wind at a site results from four contributions, largest in scale first: synoptic pressure forcing, which sets the background wind (Chapters 3 and 4); mesoscale thermal forcing, the subject of this chapter; boundary-layer mixing, which decides how strongly the wind aloft reaches the ground and depends on stability (Chapters 6 to 15); and terrain and roughness, which redistribute the flow locally (Chapters 11 and 20). They are not independent: the synoptic wind changes the boundary-layer mixing, the mixing changes the land-sea contrast, and the terrain shapes the thermal circulation.

The practical consequence is that the near-surface wind is not a downscaled version of the large-scale wind. Downscaling in the narrow sense, interpolating a coarse wind to the site and correcting it for height and roughness, recovers the first, third and part of the fourth contribution, but not the second: a thermal circulation is a wind that the coarse field does not

contain at all. On days when it dominates, the local wind can have a direction unrelated to the synoptic one.

19.5.2 Weak and strong synoptic days

On a day of weak synoptic forcing, a slack pressure gradient under an anticyclone with clear skies, the thermal circulations dominate. The heating contrast is large because there is no cloud, the contrast stays in place because there is no strong wind to mix it away, and the circulation's own speed, 2 to $5\,\mathrm{m\,s^{-1}}$, exceeds the background wind. The sea breeze, the slope and valley winds and the cold pools all develop fully, and the wind direction at a coastal or mountain site follows the clock.

On a day of strong synoptic forcing the thermal circulations are suppressed. A strong wind mixes the boundary layer, so the heating is spread over a deep, well-mixed layer and the near-surface contrast is small; it advects the warm and cool air across the boundary between them, erasing the contrast; and often the same weather system brings cloud, which removes the heating. The density-current relation gives a quantitative criterion at the coast: an offshore wind larger than $U_f = k_f\sqrt{g'h}$, about 3 to $5\,\mathrm{m\,s^{-1}}$ in the example of Section 19.2.3, holds the front off the land. A background wind of about 8 to $10\,\mathrm{m\,s^{-1}}$ or more typically suppresses the sea breeze, the valley winds and the urban breeze, and the local wind then follows the synoptic flow modified mechanically by terrain and roughness. Between the two the interaction of Section 19.2.4 applies, and the timing of the local regime, the onset of the breeze or the arrival of the front, shifts by hours with the synoptic wind.

19.5.3 Circulations that change the stability

Thermal circulations move air masses of different temperature, and in doing so they change the local stability as well as the wind direction. Two cases are common.

Marine air over hot land. The sea breeze brings cool marine air under the hot land air, so that near the coast the near-surface layer is stable on an afternoon that is unstable a few tens of kilometers inland. As the marine air moves over the heated ground, a convective layer grows within it from below: the thermal internal boundary layer, an internal boundary layer of the kind introduced in Chapter 7, of depth δ. Its growth follows from a heat budget. Let the marine air arrive with a stable profile $\theta(z) = \theta_s + (\mathrm{d}\theta/\mathrm{d}z)\,z$, and let the ground supply the kinematic heat flux $(\overline{w'\theta'})_0$. Ignoring entrainment, the heat added after a time t mixes a layer of depth δ to the potential temperature of the stable profile at its top, which requires $\int_0^\delta [\theta(\delta) - \theta(z)]\,\mathrm{d}z = (\mathrm{d}\theta/\mathrm{d}z)\,\delta^2/2$, so

$$\frac{\mathrm{d}\theta}{\mathrm{d}z}\,\frac{\delta^2}{2} = (\overline{w'\theta'})_0\,t \quad\Longrightarrow\quad \delta = \sqrt{\frac{2\,(\overline{w'\theta'})_0\,x}{U\,\mathrm{d}\theta/\mathrm{d}z}}, \tag{19.12}$$

with $t = x/U$ the time the air takes to travel a distance x inland at speed U. For illustrative values $(\overline{w'\theta'})_0 = 0.2\,\mathrm{K\,m\,s^{-1}}$ ($H \approx 240\,\mathrm{W\,m^{-2}}$), $\mathrm{d}\theta/\mathrm{d}z = 0.005\,\mathrm{K\,m^{-1}}$ and $U = 5\,\mathrm{m\,s^{-1}}$, $\delta = 126\,\mathrm{m}$ at $x = 1\,\mathrm{km}$ and 400 m at 10 km. A wind turbine with a hub at 150 m within the first kilometer of the coast sits above the internal boundary layer, in the stable marine air, with the strong shear and weak turbulence of stable conditions, while the wind measured at 10 m beneath it is convective. Chapter 16 gives the slab model that adds entrainment to this estimate.

Drainage air in valleys. At night the katabatic flows fill the valleys with cold air, and the cold pools of Section 19.3.4 are stable layers created by the circulation itself. They decouple the valley floor from the wind above and keep it weak, and they can persist after sunrise until the heating erodes them from below and the slopes above. The stable layers of Chapter 17,

which over flat ground form by local cooling, form in complex terrain partly by the arrival of air cooled elsewhere.

19.6 Climatology, model resolution and diagnosis

Thermal circulations leave a recognizable signature in the statistics of the wind, and they are among the first things a coarse weather model gets wrong. This section shows how to find them in a wind record, why models miss them, why their errors are errors of direction more than of speed, and closes with a list of diagnostic questions.

19.6.1 Time of day

Thermal circulations are diurnal: they blow in one direction in the afternoon and in nearly the opposite direction at night. An average over all hours mixes the two regimes and hides both. Take an illustrative coastal site with an afternoon sea breeze of $5\,\mathrm{m\,s^{-1}}$ from the east and a night land breeze of $2\,\mathrm{m\,s^{-1}}$ from the west, each half of the time. The mean speed is $3.5\,\mathrm{m\,s^{-1}}$; the mean vector, the average of $u = -5$ and $u = +2\,\mathrm{m\,s^{-1}}$, is $u = -1.5\,\mathrm{m\,s^{-1}}$, a wind of $1.5\,\mathrm{m\,s^{-1}}$ from the east. Neither describes any hour of the day: the mean speed suggests a steady moderate wind, and the mean vector a weak easterly that never blows. The remedy is to stratify the wind climatology by time of day, reporting the wind separately for each hour or for day and night, before it is averaged.

19.6.2 Wind roses

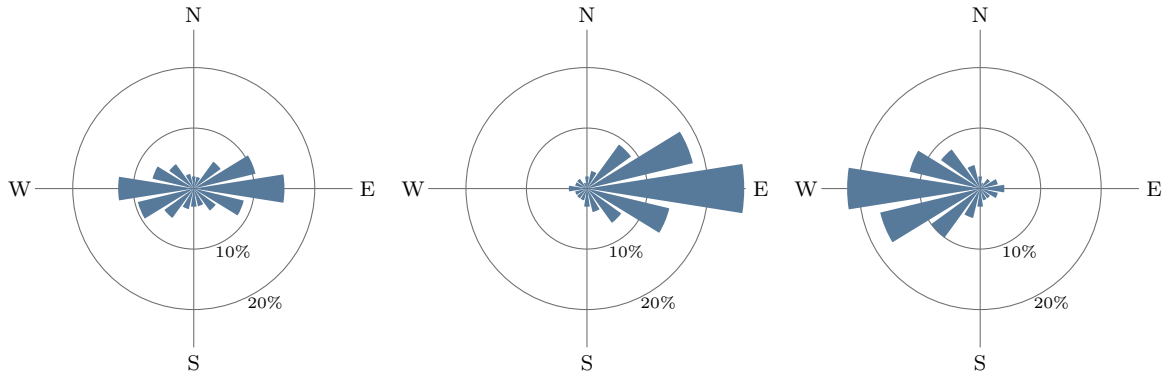
A *wind rose* is a polar diagram of the frequency with which the wind blows from each direction sector, often subdivided by speed class; it is computed from a record of measured or modeled wind direction β and speed, and drawn with each sector's bar pointing toward the direction the wind comes from. A rose reveals the prevailing synoptic flow, the signature of a sea breeze, channeling along a valley axis, and the directions from which roughness changes, $z_0(\beta)$ in the notation of Chapter 11, affect the site. A rose with two or more distinct lobes, a bimodal rose, suggests that several regimes share the record.

Figure 19.8 shows three roses for an illustrative station on an east-facing coast at 20°S, in sixteen sectors of 22.5°, with north up. The length of each bar is the percentage of hours with wind from that sector; the circles mark 10 and 20%. Panel (a) uses all hours of a year, panel (b) the hours from 09:00 to 21:00, and panel (c) the hours from 21:00 to 09:00; the two halves have equal numbers of hours, so (a) is their average.

The annual rose in panel (a) has two lobes, from the east (15% of hours from the east sector, 10.5% from east-northeast) and from the west (12.5% from west, 9.5% from west-southwest), with little from north or south. On its own it could be read as two synoptic regimes. The day and night roses in panels (b) and (c) show that it is one thermal circulation: by day 26% of hours are from the east and 18% from east-northeast, by night 22% from the west and 17% from west-southwest. The day lobe leans toward northeast, the backing of the sea breeze in the Southern Hemisphere (Section 19.2.5); at a Northern Hemisphere station on an east-facing coast it would lean toward southeast.

19.6.3 Conditional climatology

A *conditional climatology* is a set of wind statistics computed separately for subsets of the record defined by a condition: day against night, summer against winter, stable against unstable hours, or one synoptic regime against another. It is computed from the same record as the annual statistics, with each hour assigned to its class by time, by season, by a stability measure such



(a) all hours (b) 09:00 to 21:00 (c) 21:00 to 09:00

Figure 19.8: Wind roses for an illustrative station on an east-facing coast at 20°S (Southern Hemisphere; north up). Bars point toward the direction the wind comes from; bar length is the percentage of hours with wind from that sector (circles at 10 and 20%). (a) All hours: a bimodal rose with an easterly and a westerly lobe. (b) Day, 09:00 to 21:00: the sea breeze, from east to east-northeast. (c) Night, 21:00 to 09:00: the land breeze and drainage, from west to west-southwest. Frequencies illustrative.

as the sign of the heat flux or a bulk Richardson number (Chapter 13), or by the large-scale wind or pressure pattern.

Its purpose is to separate regimes that the full record mixes. A daytime easterly with a night-time westerly, as in Figure 19.8, reveals a thermal circulation hidden in the annual rose; a summer-only sea breeze shows up only in the summer subset; a nocturnal drainage wind shows up only in the stable subset; and conditioning on weak synoptic wind isolates the thermal regime from the days on which the synoptic flow dominates. The cost is sample size: each class has fewer hours, and a class of a few dozen hours does not give a stable rose. The conditions should be chosen for physical reasons, the ones listed above, not by searching many subsets for a pattern.

19.6.4 Model resolution

A weather model represents the atmosphere on a grid of spacing Δx, and it represents features well only when they span several grid lengths; a common rule of thumb places the effective resolution at five to seven times Δx. A coarse model does not resolve narrow valleys, the detailed geometry of a coastline, an urban heat island or small slope winds. It can have the synoptic field right and the local wind wrong. That is a scale mismatch, not a failure of the model's physics.

A 10 km model and a sea breeze. The sea breeze as a whole spans tens of kilometers, but its structure has kilometer scales: the front is about 1 km wide, and the bays and headlands that shape it are 1 to 5 km across. A model with $\Delta x = 10$ km smooths all of these. Each grid cell is land or sea, so the model coastline is a staircase whose position can be wrong by up to half a cell, 5 km; bays and headlands vanish; the thermal contrast in a coastal cell is a blend of land and sea; the convergence zones where breezes from different stretches of coast meet are misplaced or missing; and the front is smeared over two or three cells. At a front speed of $3\,\mathrm{m\,s^{-1}}$, a position error of 10 km is an error of $10\,000/3 \approx 3300$ s, about an hour, in the time the breeze reaches a site. Coastal wind errors therefore come from horizontal resolution as much as from the boundary-layer physics.

A smoothed mountain. The same smoothing lowers mountains and fills valleys. Take an illustrative mountain 1500 m high above sea level rising from a valley floor at 300 m over 5 km of horizontal distance, represented in a coarse model as 900 m high with the floor raised to 500 m. The relief falls from 1200 to 400 m and the slope angle from $\arctan(1200/5000) = 13.5°$ to $\arctan(400/5000) = 4.6°$; by equation (19.9) the along-slope forcing falls in the ratio $\sin 4.6°/\sin 13.5° = 0.34$. The heating geometry, the pressure distribution, the valley depth and with it the topographic amplification, the slope circulation and the channeling all change. A ridge-top station at 1500 m is 600 m above the model's ground, so the model's 10 m wind is a wind at a different altitude, inside the valley's air rather than in the flow over the ridge. Terrain representation in models is taken up in Chapter 20 and in Chapter 27.

19.6.5 Direction is harder than speed

A thermal circulation is above all a change of wind direction, and a model that misses it may still get the speed right. Take a model that forecasts the synoptic westerly at $5\,\mathrm{m\,s^{-1}}$ for an afternoon in which a sea breeze blows from the east at $5\,\mathrm{m\,s^{-1}}$. The speed error is zero. The vector error, the magnitude of the difference between the forecast and observed wind vectors, follows from the law of cosines,

$$|\mathbf{V}_\mathrm{m} - \mathbf{V}_\mathrm{o}|^2 = U_\mathrm{m}^2 + U_\mathrm{o}^2 - 2\,U_\mathrm{m}U_\mathrm{o}\cos\Delta\beta, \tag{19.13}$$

with subscripts m and o for model and observation and $\Delta\beta$ the difference of directions. For equal speeds U it reduces to $2U\sin(\Delta\beta/2)$. In the example $\Delta\beta = 180°$ and the vector error is $2 \times 5 = 10\,\mathrm{m\,s^{-1}}$, twice the wind speed; for $\Delta\beta = 90°$ it is $7.1\,\mathrm{m\,s^{-1}}$, and for 30°, $2.6\,\mathrm{m\,s^{-1}}$. A modest or zero speed error can sit on a large dynamical error: the model has the wrong regime.

What the error costs depends on the application. For transport of pollutants or smoke, the 180° error sends the plume the wrong way. For a wind farm it changes which turbines stand in the wakes of others. For a transmission conductor, whose cooling depends on the angle between wind and conductor regardless of the sense of the wind, a 180° error is harmless and a 90° error, which turns a perpendicular wind into a parallel one, is not. Verification of thermally driven winds therefore needs vector measures, or speed and direction separately and conditioned on the regime (Section 19.6.3), not speed statistics alone.

19.6.6 Diagnostic questions

Whether thermal circulations matter at a site can be decided from seven questions, in Table 19.4. Each row gives the question, what to look at to answer it, and what a yes implies for the wind.

A site with several yes answers has a wind climate made of regimes, and its wind should be modeled, measured and verified regime by regime. Questions 3 and 5 concern terrain that also forces the wind mechanically, and Chapter 20 takes up that mechanically forced flow over and around terrain.

19.7 What to retain

Definition 19.1 (Thermal circulation)**.** Differential heating creates a horizontal temperature and density contrast, the contrast a mesoscale pressure gradient, and the gradient a thermal circulation. The near-surface wind is the synoptic flow plus the local thermal circulation plus the boundary layer's response to both, not a downscaled large-scale wind.

Table 19.5 lists the terms of the chapter, their meaning, their units and the subsection that defines each.

Table 19.4: Seven diagnostic questions for thermally driven winds at a site.

	Question	What to look at	If yes
1	Is there a coastline nearby?	distance to sea or large lake; within a few tens of kilometers	expect a sea breeze, a front passage and a land breeze
2	Is there strong differential heating?	land use, soil moisture, cloud climatology	thermal circulations strong on clear, dry days
3	Are slope or valley winds possible?	terrain slopes and valley axes around the site	upslope and up-valley by day, downslope and down-valley at night
4	Does the wind change systematically with time of day?	roses and mean vectors by hour (Sections 19.6.1 and 19.6.2)	a diurnal regime; stratify all statistics by hour
5	Can a cold-air pool form?	valley floor or basin, clear calm nights, floor against slope temperatures	near-calm, decoupled nights; poor exposure at low sites
6	Is there urban heating?	distance to a city, urban against rural temperatures	urban breeze on calm nights, plus mechanical urban effects
7	Is the background wind weak enough for local circulations to dominate?	synoptic pressure gradient and wind; frequency of slack days	thermal regime on those days; a coarse model will miss it

19.8 Exercises

Exercise 19.1. On a clear afternoon the air between 1000 and 900 hPa is 4 K warmer over land than over the sea, where its mean temperature is 298 K. (a) Compute the difference of pressure between the two columns at $z = 1000$ m from equation (19.2), taking the surface pressure as 1000 hPa, and say over which surface it is higher. (b) Compute $\mathrm{d}C/\mathrm{d}t$ from equation (19.4) and the mean acceleration around a loop 30 km wide and 930 m deep. (c) Compute the Rossby number of a sea breeze with $L = 40$ km and $U = 6\,\mathrm{m\,s^{-1}}$ at 35°N and at 35°S. (d) On which side of 30° do these latitudes lie, and what does linear theory say about how far the circulation extends from the coast?

Exercise 19.2. A station stands on an east-facing coast at 23°S. On a summer afternoon the marine air behind the sea-breeze front is 3 K cooler in virtual potential temperature than the land air ($\theta_v = 303$ K) and $h = 500$ m deep. (a) Compute g', $\sqrt{g'h}$, the range of front speeds for $k_f = 0.6$ to 1 and the pressure rise behind the front at $\rho = 1.15\,\mathrm{kg\,m^{-3}}$. (b) The synoptic wind is $4\,\mathrm{m\,s^{-1}}$ from the west. Does the front advance inland, and at what speed relative to the ground? (c) At 15:00 the wind at the station blows onshore at $5\,\mathrm{m\,s^{-1}}$. Does the sea breeze turn clockwise or counterclockwise in the following hours, and from which compass sector does it blow at 18:00? Give both answers also for the same coast at 23°N. (d) Add the synoptic $4\,\mathrm{m\,s^{-1}}$ westerly to a $5\,\mathrm{m\,s^{-1}}$ easterly sea breeze as vectors and state the speed and direction of the surface wind.

Exercise 19.3. A V-shaped valley is 800 m deep and 40 km long. (a) By afternoon the air over the plain below ridge height has warmed 3 K. Using the topographic amplification factor of a V-shaped valley, compute the warming in the valley, the pressure deficit at the valley floor ($T = 293$ K, $\rho = 1.1\,\mathrm{kg\,m^{-3}}$, equal pressure at ridge height) and the along-valley pressure-gradient force. (b) At night a slope of 15° carries air 2 K colder than its surroundings at $T = 280$ K; compute the along-slope acceleration. (c) A line span on that slope runs along the fall line. Explain, using Table 19.3, why its cooling is limited by the wind angle, and name the span of the line that is most likely critical at night.

Exercise 19.4. (a) Two sea breezes blow inland at $3\,\mathrm{m\,s^{-1}}$ from opposite sides of a peninsula and meet in a convergence zone 3 km wide, within a layer 600 m deep. Compute the horizontal

Table 19.5: The terms of the chapter and where each is defined.

Term	Meaning	Units	Defined in
Thermal circulation	closed circulation driven by horizontal temperature and density differences; reverses between day and night	m/s	19.1, 19.1.1
Sea breeze	daytime onshore wind with return flow aloft, driven by land warmer than sea	m/s	19.2.1, 19.2.2
Land breeze	night-time offshore wind, land colder than sea; weaker and shallower than the sea breeze	m/s	19.2.6
Sea-breeze front	leading edge of the marine air; a density boundary with abrupt shifts of wind, temperature and humidity; speed $k_f\sqrt{g'h}$	m/s	19.2.3
Anabatic flow	upslope wind over a heated slope; convective, 50 to 200 m deep	m/s	19.3.1
Katabatic flow	downslope (drainage) wind over a cooled slope; stable, 10 to 50 m deep, maximum near the ground	m/s	19.3.1
Valley wind	thermally driven flow along a valley axis: up-valley by day, down-valley at night; 10 to 100 km	m/s	19.3.2
Terrain channeling	steering of the wind along a valley axis by its geometry, forced or pressure-driven	–	19.3.3
Cold pool	layer of cold, stable air collected in low terrain by drainage	K, m	19.3.4
Urban heat island	urban minus rural air temperature; largest on calm, clear nights	K	19.4.1
Urban breeze	inflow toward a warm city near the surface, rising air over it	m/s	19.4.2
Convergence	net horizontal inflow, $\nabla_h \cdot \mathbf{V} < 0$; forces rising air, $w(h) \approx -(\nabla_h \cdot \mathbf{V})h$	s^{-1}	19.4.3
Divergence	net horizontal outflow, $\nabla_h \cdot \mathbf{V} > 0$; requires subsidence	s^{-1}	19.4.3
Density current	flow of denser fluid spreading beneath lighter fluid under gravity; reduced gravity $g' = g\Delta\theta_v/\theta_v$	m/s	19.2.3, 19.4.4
Wind rose	polar diagram of the frequency of wind from each direction sector	%	19.6.2
Conditional climatology	wind statistics computed separately for classes of hours: time of day, season, stability, synoptic regime	–	19.6.3
Vector error	magnitude of the difference of forecast and observed wind vectors	m/s	19.6.5

divergence in the zone and the vertical velocity at the top of the layer, and check that the mass leaving through the top equals the mass entering through the sides. (b) A model forecasts $6\,\mathrm{m\,s^{-1}}$ from 250° while the observed wind is $5\,\mathrm{m\,s^{-1}}$ from 80°. Compute the speed error and the vector error from equation (19.13). (c) At a site, the wind is $4\,\mathrm{m\,s^{-1}}$ from 90° for the twelve day hours and $2\,\mathrm{m\,s^{-1}}$ from 270° for the twelve night hours. Compute the mean speed and the mean vector, and sketch the annual, day and night roses.

Chapter 20

Terrain-Induced Flow

20.1 Flow over a hill

Earlier chapters met terrain several times in passing. Chapter 4 showed that the speed-up over a ridge crossing is not a Coriolis effect; Chapter 5 explained the speed-up over a hill by continuity and by the pressure perturbations the hill creates; Chapter 12 showed that the crest profile no longer obeys the logarithmic law. The preceding chapter treated the circulations that sloping ground drives by heating and cooling. This chapter treats the mechanical effect of terrain on a wind that is already blowing. Its question is

how does terrain reshape the wind field near the surface?

Terrain accelerates the flow over crests, slows it at the foot of a slope and behind an obstacle, redirects it along valleys and through gaps, blocks it when the air is stable, makes it separate and recirculate behind steep slopes, and launches gravity waves into the stable air above. The chapter follows these responses in order: the speed-up over a single hill and its size; separation, sheltering and the turbulence terrain produces; channeling and gap flow; stratified flow, blocking and mountain waves; and finally the way terrain enters speed-up maps and numerical models.

Jargon: terrain speed-up, speed-up factor, fractional speed-up, pressure perturbation, windward, leeward, hill height, half-width

Terrain speed-up is the increase of the wind speed over a crest, ridge or hilltop relative to the wind at the same height above ground over flat terrain upstream. The *speed-up factor* S, dimensionless, is the ratio of the two speeds; the *fractional speed-up* $\Delta S = S - 1$ is the same comparison expressed as a fraction of the reference speed. Both are measured by pairs of anemometers at the same height above local ground, one on the terrain and one at an undisturbed reference site, or computed by a flow model. A *pressure perturbation* p', in pascals, is the departure of the pressure from the background pressure field that would exist without the terrain. The *windward* side of an obstacle faces the incoming wind; the *leeward* (lee) side is the downstream, sheltered side. The *hill height* h_m, in meters, is the height of the crest above the surrounding terrain; the *half-width* L_h, in meters, is the horizontal distance from the crest to the point where the terrain has fallen to half that height.

Key idea

Terrain does not squeeze a fixed wind; the background wind, the terrain geometry and the stability of the air together set up a pressure perturbation field, and that field accelerates, blocks, separates or channels the flow. The same ridge produces speed-up, sheltering, blocked flow or waves depending on the atmospheric regime.

20.1.1 A hill in a uniform wind

Consider a uniform wind of speed U_∞ approaching an isolated, smooth hill. Far upstream the streamlines, the lines everywhere tangent to the velocity, are horizontal and evenly spaced. As the air approaches the hill the streamlines are displaced upward to pass over it; the displacement is largest at the ground, where the streamline must follow the surface, and decreases with height. Because the displacement decreases upward, the streamlines over the crest lie closer together than upstream: they are compressed. The same volume of air per unit time passes between two neighboring streamlines, so where they are closer the air moves faster. Near the crest the wind therefore exceeds the upstream wind at the same height above ground, $U_{\text{crest}} > U_{\text{upstream}}$. This is terrain speed-up.

The Coriolis force plays no part in it. Chapter 5 showed that air crosses a hill a kilometer wide in about 100 s, a small fraction of the time of order $1/|f| \approx 3\,\text{h}$ the Coriolis force needs to turn the flow appreciably; the Rossby number of the flow over a hill is of order 100. For terrain up to a few tens of kilometers across, everything in this chapter except the channeling by large-scale pressure gradients in Section 20.4 is therefore the same in both hemispheres.

20.1.2 The speed-up factor

The size of the effect is expressed by comparing the wind over the terrain with a reference wind. The speed-up factor is

$$S = \frac{U_{\text{terrain}}(\Delta z)}{U_{\text{ref}}(\Delta z)}, \tag{20.1}$$

where Δz is the height above the local ground, the same for the two winds, and the reference wind is measured or computed over flat, undisturbed terrain upstream with the same roughness. The fractional speed-up is

$$\Delta S = \frac{U_{\text{terrain}} - U_{\text{ref}}}{U_{\text{ref}}} = S - 1. \tag{20.2}$$

The two measures carry the same information. The factor S is convenient for multiplying a reference wind; the fractional speed-up ΔS is convenient for theory, since it is zero without terrain and, for low hills, proportional to the terrain height. A value below one for S, or below zero for ΔS, is a slow-down.

For an illustrative case with $U_{\text{ref}} = U_0 = 8\,\text{m s}^{-1}$ upstream and $U_{\text{crest}} = 10\,\text{m s}^{-1}$ at the same height above the crest,

$$S = \frac{10\,\text{m s}^{-1}}{8\,\text{m s}^{-1}} = 1.25, \qquad \Delta S = \frac{10\,\text{m s}^{-1} - 8\,\text{m s}^{-1}}{8\,\text{m s}^{-1}} = 0.25,$$

a speed-up of 25 %. Both numbers depend on the height at which they are evaluated: Section 20.2.3 shows that the fractional speed-up is largest close to the ground and decays upward. A speed-up factor without a stated height above ground, a stated reference site and a stated wind direction is incomplete.

20.1.3 Continuity and the pressure perturbation

Two arguments explain the acceleration, and Chapter 5 gave both. The first is continuity. Over the short distances of terrain flow the air is nearly incompressible, so the volume flow through a cross-section is conserved, $A\,U \approx$ constant, and a reduced effective cross-section A over the crest gives a higher speed U. The argument is intuition, not a theory: it gives an average over the section, it needs a fixed upper lid that the atmosphere does not provide, and it says nothing about where the acceleration happens.

The second argument, more complete, is the pressure-gradient view. Write the pressure as the background pressure plus a perturbation,

$$p = p_{\text{background}} + p', \tag{20.3}$$

where $p_{\text{background}}$ is the pressure field the large-scale flow would have over flat ground and p' is the part the terrain causes. The along-wind momentum equation for steady flow near the crest, with the Coriolis force negligible and the turbulent stress set aside for the moment, is

$$U\,\frac{\partial U}{\partial x} = -\frac{1}{\rho}\,\frac{\partial p'}{\partial x},$$

since the background gradient, of order 1 Pa per kilometer, is negligible against the terrain's gradient over the same distance. Integrated along a streamline, this is Bernoulli's relation, $p' + \frac{1}{2}\rho U^2 = \text{constant}$:

$$p'_2 - p'_1 = -\tfrac{1}{2}\,\rho\,(U_2^2 - U_1^2). \tag{20.4}$$

Pressure rises on the windward side, where the air is slowed as it approaches the slope; it falls toward the crest, where the air is fastest; and it recovers downstream. The gradient from the high pressure at the windward foot to the low pressure at the crest is what accelerates the air up the slope, and the adverse gradient from the crest down the lee slope is what slows it again.

For the worked case, with $\rho = 1.2\,\mathrm{kg\,m^{-3}}$, the pressure at the crest relative to the undisturbed upstream flow is

$$p'_{\text{crest}} = -\tfrac{1}{2} \times 1.2 \times (10^2 - 8^2)\,\mathrm{Pa} = -0.6 \times 36\,\mathrm{Pa} \approx -22\,\mathrm{Pa},$$

about 0.22 hPa. A synoptic gradient of 1 hPa per 100 km changes the pressure by 1 Pa in a kilometer; locally the hill's own pressure field is twenty times stronger than the large-scale gradient that drives the wind.

The pressure perturbation is a dynamically adjusted pressure-flow system, not the synoptic wind being squeezed. The pressure field and the flow adjust to each other so that the flow satisfies continuity and momentum together, and the perturbation reaches ahead of the hill: the air begins to decelerate before it reaches the windward foot, because the raised pressure there is felt upstream. A model that took the large-scale wind and simply scaled it by an area ratio would miss this upstream influence and the lee recovery alike.

20.1.4 Windward and leeward

Figure 20.1 shows the whole pattern along a two-dimensional ridge. The horizontal axis of all three panels is the distance from the crest in units of the half-width, with the wind from the left. The top panel is a vertical cross section: the shaded shape is the ridge and the blue curves are streamlines. The middle panel is the pressure perturbation near the ground, in pascals. The bottom panel is the near-surface wind speed, with the upstream reference of $8\,\mathrm{m\,s^{-1}}$ dashed. The ridge has $h_m/L_h = 0.125$, for instance $h_m = 100\,\mathrm{m}$ and $L_h = 800\,\mathrm{m}$.

Read from left to right, the figure shows the windward deceleration, the crest acceleration and the lee recovery. The near-surface wind falls below its upstream value well ahead of the slope, reaching a minimum of $7.75\,\mathrm{m\,s^{-1}}$ at $x = -\sqrt{3}\,L_h$, about 1.4 km upwind of the crest for $L_h = 800\,\mathrm{m}$; there the pressure perturbation is at its maximum, about +2 Pa. From that point the pressure falls toward the crest and the air accelerates up the slope to $10\,\mathrm{m\,s^{-1}}$ at the crest, where $p' \approx -22\,\mathrm{Pa}$. The mean acceleration over the 1.39 km between the two points follows from the pressure difference of about 24 Pa: $24/(1.2 \times 1390) \approx 0.014\,\mathrm{m\,s^{-2}}$, the same value as the kinematic estimate $(10^2 - 7.75^2)/(2 \times 1390) \approx 0.014\,\mathrm{m\,s^{-2}}$, as Bernoulli's relation requires. Downstream of the crest the pressure rises again, the air decelerates down the lee slope and the wind returns toward its upstream value.

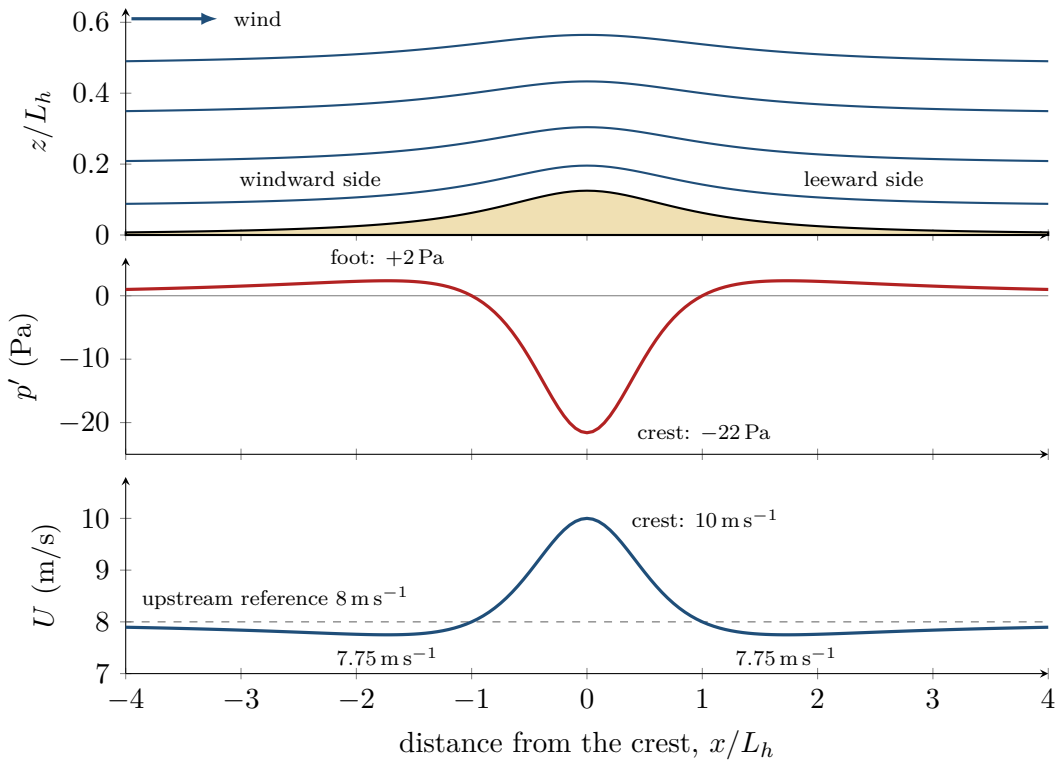


Figure 20.1: Flow over a two-dimensional ridge $h(x) = h_m/[1 + (x/L_h)^2]$ with $h_m/L_h = 0.125$ (vertical scale exaggerated about three times). Top: streamlines from linear potential flow, a streamline starting at height z_u upstream lying at $z_u + h_m\, L_h(L_h + z_u)/[(L_h + z_u)^2 + x^2]$. Bottom: near-surface speed $U = U_0[1 + \Delta S(x)]$ with $U_0 = 8\,\mathrm{m\,s^{-1}}$ and $\Delta S(x) = 0.25\,[1 - (x/L_h)^2]/[1 + (x/L_h)^2]^2$, the linear-theory shape scaled to a crest speed-up of 25 %. Middle: $p' = -\frac{1}{2}\rho(U^2 - U_0^2)$ with $\rho = 1.2\,\mathrm{kg\,m^{-3}}$. Values illustrative; the lee side of a real hill is not symmetric with the windward side.

The linear solution drawn here is symmetric about the crest. Real ridges are not: the turbulent boundary layer loses momentum on the windward slope and over the crest, so the lee flow is slower than the windward flow at the same distance, and on a steep enough lee slope it separates from the surface (Section 20.3). A ridge therefore has acceleration on the windward slope, a maximum near the crest, and deceleration or separation in the lee.

20.2 The magnitude of the speed-up

The size of the speed-up depends on the shape of the terrain, on the height at which it is evaluated and on the direction of the wind. This section gives the dimensionless ratio that controls it, a rule of thumb for the crest value, its decay with height, its dependence on direction, and the linear theory behind all three together with the conditions under which that theory fails.

20.2.1 Hill shape and aspect ratio

The flow responds to the height, slope, curvature and width of a hill and to its orientation relative to the wind. A broad, smooth hill produces an attached, accelerated flow that follows the surface; a steep, sharp ridge produces strong separation in its lee. The single number that captures most of this is the aspect ratio

$$\text{aspect ratio} = \frac{h_m}{L_h}, \tag{20.5}$$

the hill height over its half-width. A small aspect ratio, below about 0.1, describes gentle terrain with weak, nearly linear perturbations; a large one, above about 0.3 to 0.5, describes steep terrain whose flow is nonlinear and likely to separate.

The aspect ratio is tied to the slope. For the ridge profile of Figure 20.1, $h(x) = h_m/[1 + (x/L_h)^2]$, the slope is

$$\frac{\mathrm{d}h}{\mathrm{d}x} = -\frac{h_m}{L_h}\,\frac{2\,x/L_h}{[1+(x/L_h)^2]^2}.$$

Setting its derivative to zero gives $1 + (x/L_h)^2 = 4\,(x/L_h)^2$, so the steepest point lies at $x = \pm L_h/\sqrt{3}$, where the slope is

$$\left|\frac{\mathrm{d}h}{\mathrm{d}x}\right|_{\max} = \frac{2/\sqrt{3}}{(4/3)^2}\,\frac{h_m}{L_h} = \frac{9}{8\sqrt{3}}\,\frac{h_m}{L_h} \approx 0.65\,\frac{h_m}{L_h}. \tag{20.6}$$

For $h_m/L_h = 0.125$ the steepest slope is 0.081, about 4.6°: a gentle hill. Other profiles give other coefficients, but the maximum slope is always of the order of the aspect ratio.

20.2.2 A rule of thumb for the crest speed-up

For low, smooth hills in neutral flow, linear theory (Section 20.2.5) and field experiments support a simple rule of thumb for the maximum fractional speed-up near the surface at the crest:

$$\Delta S_{\max} \approx C_s\,\frac{h_m}{L_h}, \qquad C_s \approx 2 \text{ for a two-dimensional ridge}, \quad C_s \approx 1.6 \text{ for an isolated hill}. \tag{20.7}$$

The coefficient is smaller for an isolated, roughly circular hill because air can pass around its sides as well as over it, so less of it must be forced over the crest. The rule holds for aspect ratios below about 0.3, for attached flow, and for near-neutral stratification; it applies a few meters to a few tens of meters above the crest, not at the height of the hill.

For the ridge of Figure 20.1, $h_m = 100\,\mathrm{m}$ and $L_h = 800\,\mathrm{m}$, the rule gives $\Delta S_{\max} = 2 \times 0.125 = 0.25$, the 25 % of the worked case. For an illustrative second example, a ridge 60 m high with a half-width of 400 m has $h_m/L_h = 0.15$ and

$$\Delta S_{\max} \approx 2 \times 0.15 = 0.30, \qquad U_{\mathrm{crest}} \approx 1.30 \times 8\,\mathrm{m\,s^{-1}} = 10.4\,\mathrm{m\,s^{-1}};$$

an isolated hill of the same height and half-width gives $\Delta S_{\max} \approx 1.6 \times 0.15 = 0.24$ and $U_{\mathrm{crest}} \approx 9.9\,\mathrm{m\,s^{-1}}$. Doubling the height at fixed half-width doubles the predicted speed-up, while doubling the half-width at fixed height halves it: a low, narrow hill can accelerate the wind more than a high, broad one. The rule is a first estimate from linear theory for low hills, not a substitute for a measurement or a flow model.

20.2.3 Decay with height above the crest

The speed-up is concentrated near the ground and decays upward over a height of the order of the half-width. A guideline form consistent with equation (20.7) is

$$\Delta S(\Delta z) \approx \Delta S_{\max} \exp\!\left(-C_z \frac{\Delta z}{L_h}\right), \qquad C_z \approx 3 \text{ (ridge)}, \quad C_z \approx 4 \text{ (isolated hill)}, \tag{20.8}$$

with Δz the height above the crest. Over the ridge of the worked case the fractional speed-up is 0.24 at 10 m, 0.21 at 50 m, 0.17 at 100 m and 0.09 at $L_h/3 \approx 270\,\mathrm{m}$; at $\Delta z = L_h = 800\,\mathrm{m}$ it has fallen to $e^{-3} \approx 5\,\%$ of its maximum.

Figure 20.2 shows what this does to the wind profile. The left panel plots height above local ground against wind speed: the blue curve is a neutral logarithmic profile over flat ground upstream, the red curve the profile above the crest of the same ridge. The right panel plots the fractional speed-up against height for the ridge and for an isolated hill with the same aspect ratio.

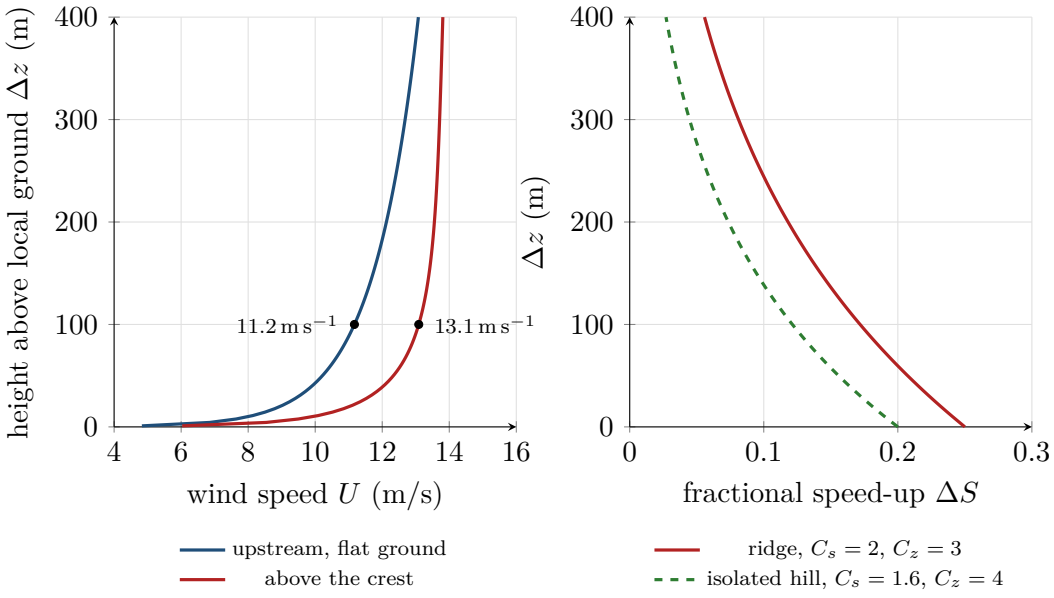


Figure 20.2: Speed-up and height. Left: upstream neutral profile $U = (u_*/\kappa)\ln(\Delta z/z_0)$ with $z_0 = 0.03\,\mathrm{m}$ and $u_* = 0.55\,\mathrm{m\,s^{-1}}$ ($8\,\mathrm{m\,s^{-1}}$ at 10 m), and the crest profile $U\,[1 + \Delta S(\Delta z)]$ from equation (20.8). Right: $\Delta S(\Delta z)$ for $h_m/L_h = 0.125$ and $L_h = 800\,\mathrm{m}$. Values illustrative; the guideline form is not valid within the lowest few meters, where friction reduces the speed-up.

The crest profile is faster than the upstream one at every height, by $1.9\,\mathrm{m\,s^{-1}}$ at 10 m and $1.9\,\mathrm{m\,s^{-1}}$ at 100 m (9.9 against $8.0\,\mathrm{m\,s^{-1}}$, and 13.1 against $11.2\,\mathrm{m\,s^{-1}}$), but the fractional

difference falls from 24 to 17 %, and above about 400 m the two profiles nearly coincide. The crest profile is therefore flatter: the ratio of the winds at 100 and 10 m is 1.40 upstream and 1.32 at the crest, equivalent to power-law exponents of 0.145 and 0.120. A shear exponent fitted on flat ground and applied at a crest overestimates the wind aloft relative to the wind near the ground.

Very close to the surface, the speed-up does not keep increasing downward. Linear theory divides the flow into an inner layer, within which turbulent stress matters and the air has time to adjust to the local surface, and an outer layer above, which behaves like inviscid flow. The depth ℓ of the inner layer is given by the standard estimate $\ell \ln(\ell/z_0) \approx 2\kappa^2 L_h$; for $L_h = 800\,\mathrm{m}$ and $z_0 = 0.03\,\mathrm{m}$ the right-hand side is $2 \times 0.16 \times 800 = 256\,\mathrm{m}$, satisfied by $\ell \approx 36\,\mathrm{m}$, since $36 \ln(1200) \approx 255$. The largest fractional speed-up lies within this layer, a few meters to a few tens of meters above the crest; below that height the surface friction reduces it.

20.2.4 Dependence on wind direction

A long ridge accelerates a wind that crosses it at right angles far more than a wind that blows along its axis. For an infinitely long ridge in linear theory the dependence follows in two lines. Let the wind of speed U make an angle γ with the ridge axis, so that its component across the ridge is $U \sin\gamma$ and its component along it is $U \cos\gamma$. The ridge varies only in the cross-ridge direction, so it perturbs only the cross-ridge component, by the fraction $\Delta S_\perp$ it would apply to a perpendicular wind: the crest wind has components $U \sin\gamma\,(1 + \Delta S_\perp)$ across and $U \cos\gamma$ along. Its speed, to first order in the small $\Delta S_\perp$, is

$$U_{\mathrm{crest}} = U\sqrt{\sin^2\gamma\,(1+\Delta S_\perp)^2 + \cos^2\gamma} \approx U\,(1 + \Delta S_\perp \sin^2\gamma), \qquad \Delta S(\gamma) \approx \Delta S_\perp \sin^2\gamma. \tag{20.9}$$

The wind also turns slightly toward the perpendicular over the crest, because only its cross-ridge component grows.

Figure 20.3 plots the fractional speed-up against the angle between the wind and the ridge axis, from 0° (wind along the ridge) to 90° (wind across it). The red curve is the long ridge of the worked case, $\Delta S_\perp = 0.25$; the green dashed line is an isolated round hill with the same aspect ratio, whose speed-up does not depend on direction.

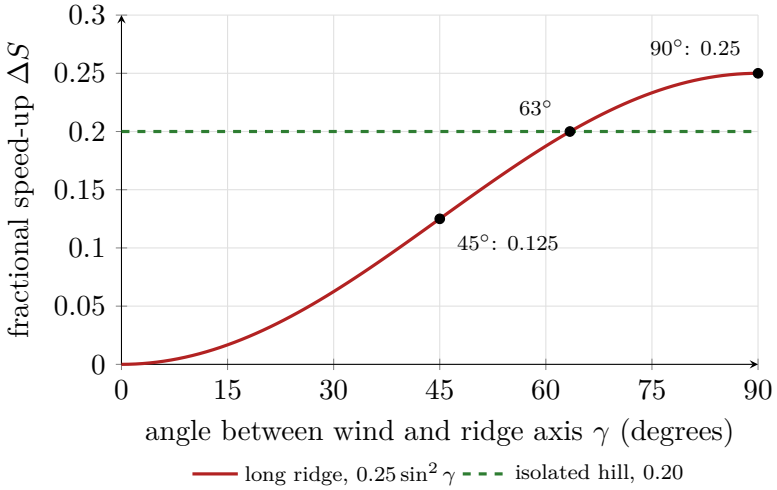


Figure 20.3: Fractional speed-up at the crest against the angle γ between the wind and the ridge axis, from equation (20.9) with $\Delta S_\perp = 0.25$ ($h_m/L_h = 0.125$, $C_s = 2$), and for an isolated round hill with $C_s = 1.6$. Values illustrative.

A wind at 45° to the ridge receives half the perpendicular speed-up, 0.125; a wind along the ridge receives none in this idealization, and a real ridge of finite length gives it a small

speed-up from its ends and its irregularities. The two curves cross at $\sin^2\gamma = 0.8$, $\gamma \approx 63°$: for winds more oblique than that, a round hill accelerates the flow more than a ridge of the same aspect ratio. For a ridge whose axis runs north–south, the angle is $\gamma = 90°$ for a westerly ($\beta = 270°$) or easterly wind, 45° for a northwesterly ($\beta = 315°$), and 0° for a northerly or southerly wind. The speed-up factor is thus a function of the wind direction, in the same way that the roughness length of a heterogeneous site is a function $z_0(\beta)$ of direction (Chapter 11). The exact expression gives 0.132 instead of 0.125 at 45°, with the wind turned 6° toward the perpendicular; the linear form is sufficient for estimates.

20.2.5 Linear theory and its limits

For low, gentle terrain the perturbations the terrain causes are small compared with the background state, and the equations of motion can be linearized: the wind perturbation is then proportional to the terrain height. The structure of the result can be derived from the outer, inviscid layer. Let $\eta(x, z)$ be the vertical displacement of the streamline that passes through (x, z), equal to the terrain height $h(x)$ at the ground. The vertical velocity is $w' = U\,\partial\eta/\partial x$, since the flow follows the streamline slope. Continuity, $\partial u'/\partial x + \partial w'/\partial z = 0$, then gives $\partial u'/\partial x = -U\,\partial^2\eta/\partial x\,\partial z$, and with $u' = 0$ far upstream,

$$u' = -U\,\frac{\partial \eta}{\partial z}. \tag{20.10}$$

A speed-up therefore requires a displacement that decreases with height. In irrotational flow the displacement obeys Laplace's equation, and a terrain component $\hat{h}\cos(kx)$ of wavenumber k produces the displacement $\hat{h}\cos(kx)\,e^{-|k|z}$, so that $u' = U\,|k|\,\hat{h}\cos(kx)\,e^{-|k|z}$. Three properties of terrain flow follow. The speed-up is positive over crests and negative over troughs. It is proportional to $|k|\,\hat{h}$, a height over a horizontal length, which is the aspect ratio of equation (20.5). And it decays with height over $1/|k|$, which for a hill is of the order of the half-width. For the ridge profile of Figure 20.1 the inviscid crest value is $\Delta S = h_m/L_h$; the turbulent inner layer roughly doubles it close to the ground, which is why the coefficient C_s of the rule of thumb is about two. This is the content of Jackson and Hunt's linear theory of flow over low hills.

Linear theory is cheap: the responses to separate terrain components add, so the speed-up over a whole landscape can be computed from the Fourier transform of its terrain in seconds. It fails where its assumptions fail: on steep hills, where the perturbation is no longer small; where the flow separates, since a separated region is not a small perturbation of anything; over complex canopies such as forests, whose drag is distributed through a layer and changes the inner layer; and in very stable, blocked flow, where buoyancy rather than inertia controls the response (Section 20.5). In those cases a nonlinear flow model is needed, the subject of Section 20.6.

20.3 Separation, sheltering and terrain-induced turbulence

Downstream of the crest the pressure rises again and the air must decelerate against it. This section describes what happens when the near-surface air cannot do so while remaining attached to the surface: separation, the recirculation zone, the sheltered region behind a hill, and the turbulence that terrain generates. It ends with a worked line of four sites across a ridge.

20.3.1 Flow separation

On the lee slope the pressure increases in the direction of flow, an adverse pressure gradient. The air in the outer flow carries enough momentum to climb it; the air close to the ground has already lost much of its momentum to surface friction. If the slope is steep enough, the pressure

rise outruns the momentum of that near-surface air, it is brought to rest, and the boundary layer detaches from the surface. This is *flow separation*: the boundary layer leaves the surface along a separation line and continues downstream as a free shear layer, with a region of reversed or recirculating flow beneath it.

A typical critical slope for the lee side of a smooth hill is about 0.3, an angle of about 17° ($\tan 17^\circ = 0.31$). Over rough surfaces such as forest the near-surface air has less momentum and separation sets in at lower slopes; stability, the upstream turbulence and the curvature of the crest change the threshold further, so the value is a typical one, not a constant. With equation (20.6), a ridge of the profile of Figure 20.1 reaches a lee slope of 0.3 when $0.65\,h_m/L_h \approx 0.3$, that is $h_m/L_h \approx 0.46$. The worked ridge, with a steepest slope of 0.081, stays attached; an illustrative hill 200 m high with a half-width of 300 m has a steepest slope of $0.65 \times 0.67 \approx 0.43$, about 23°, and separates. A sharp crest or an escarpment edge fixes the separation point at the edge itself, whatever the slope below.

20.3.2 The recirculation zone

Behind a steep ridge or obstacle the region beneath the separated shear layer is a *recirculation zone*: the mean flow near the ground may reverse and blow back up the lee slope toward the crest, closing a large eddy whose top is the shear layer. Its length is of the order of several hill heights, depending on the slope, the roughness and the stability, and downstream of it the flow reattaches to the surface. Inside it the mean wind is very low, the turbulence is high, because the shear layer above sheds eddies into it, and the wind direction varies rapidly and can reverse within minutes. A wind vane in a recirculation zone may report a direction opposite to the wind over the crest.

20.3.3 Sheltering

Downstream of a hill, whether or not the flow separates, the mean wind is reduced over a distance of many hill heights: the *sheltered* region or wake. Sheltering reduces the mean wind but not necessarily the turbulence, which may be elevated, since the wake carries the eddies produced by the shear layer and by the separation. Low mean wind is therefore not calm flow. With illustrative values, a crest wind of $11\,\mathrm{m\,s^{-1}}$ with a standard deviation $\sigma_u = 1.5\,\mathrm{m\,s^{-1}}$ has a turbulence intensity $\mathrm{TI} = 1.5/11 \approx 0.14$, while the lee site of the same ridge with $U = 4\,\mathrm{m\,s^{-1}}$ and $\sigma_u = 1.8\,\mathrm{m\,s^{-1}}$ has $\mathrm{TI} = 1.8/4 = 0.45$. A sheltered site reports a low mean wind and gusts that are large relative to it, and a model or a sensor that sees only the mean misreads it.

20.3.4 Terrain-induced turbulence

Terrain generates turbulence in four ways: by increasing the shear of the mean wind, near the surface on the windward slope and across the shear layer of a separated flow; by separation itself; by wakes behind hills and ridges; and by the breaking of mountain waves aloft (Section 20.5.3), including the rotors, turbulent eddies with horizontal axes beneath the crests of strong lee waves. Complex terrain therefore has a higher turbulence intensity than flat terrain with the same roughness. The consequences reach every application of near-surface wind: fatigue loading of wind turbines, the representativeness of an anemometer, the gust loading and the convective cooling of a transmission conductor, and the dispersion of pollutants, which is faster in the turbulent wake and can bring an elevated plume to the ground behind a hill.

20.3.5 Four sites across a ridge

Consider an illustrative background wind of $8\,\mathrm{m\,s^{-1}}$ from the west, crossing a north–south ridge, and four sites along a west–east line: an open valley floor upwind of the ridge, the windward

slope, the ridge crest and the steep lee slope. Table 20.1 lists the mean wind at each site at the same height above local ground, the speed-up factor relative to the background wind and a qualitative level of turbulence. Figure 20.4 draws the same line: the upper part is a west–east cross section of the terrain with the four sites marked and a possible recirculation in the lee; the lower part is a bar chart of the mean wind at each site, with the background $8\,\mathrm{m\,s^{-1}}$ dashed and the turbulence level written under each site name.

Table 20.1: Mean wind and turbulence at four sites along a line crossing a ridge, for a background wind of $8\,\mathrm{m\,s^{-1}}$ from the west (illustrative).

Site	Mean wind (m/s)	S	Turbulence	Reason
A: open valley	5	0.63	moderate	low elevation, upstream deceleration ahead of the ridge, surface roughness
B: windward slope	7	0.88	moderate	air still slowed by the raised windward pressure, accelerating upslope
C: ridge crest	11	1.38	low	accelerated, attached flow; turbulence small relative to the mean
D: lee slope	4	0.50	high	sheltering, separation and recirculation; eddies from the shear layer

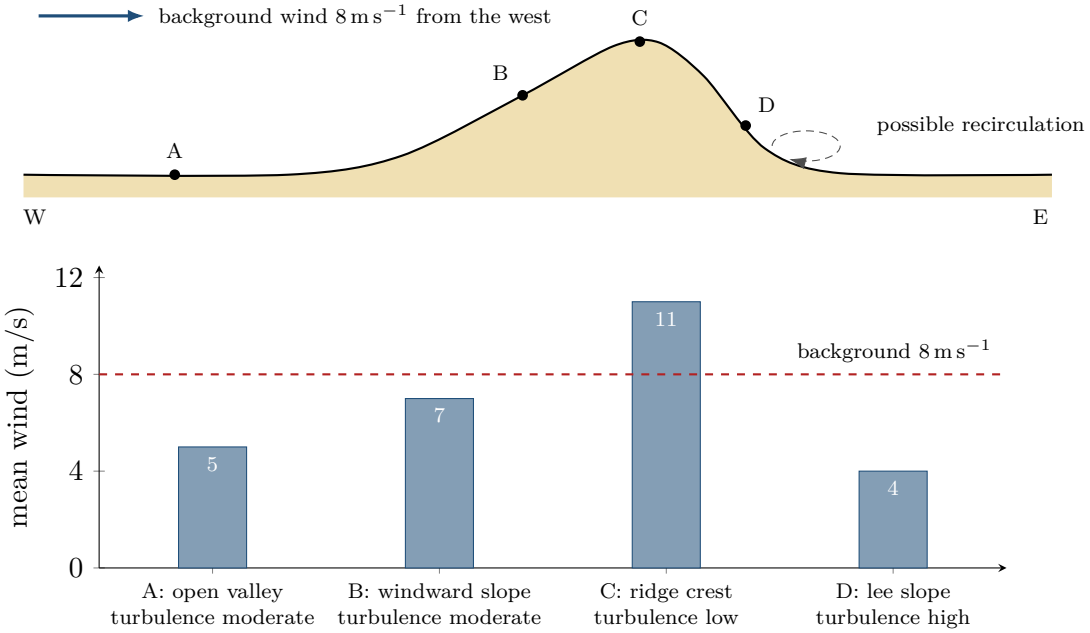


Figure 20.4: Four sites along a west–east line across a north–south ridge in a background wind of $8\,\mathrm{m\,s^{-1}}$ from the west. Top: terrain cross section (schematic, vertical scale exaggerated) with the sites A to D and a possible recirculation in the lee. Bottom: mean wind at each site at the same height above local ground, with the turbulence level under each site name. Values illustrative, from Table 20.1.

The four sites lie within a few kilometers of each other and receive the same background wind, yet their mean winds range from 4 to $11\,\mathrm{m\,s^{-1}}$, a factor of almost three. The crest is the fastest and the least turbulent site; the lee slope is the slowest and may be the most turbulent of the four. The valley and the windward slope both read below the background wind, because the ridge's raised pressure slows the flow ahead of it. A single station at any one of the four

sites would give a different picture of the same wind; Section 20.4.3 calls this the exposure of the site.

20.4 Channeling, gap flow and exposure

Terrain also changes the direction of the wind. This section describes how valleys align the flow with their axes, how gaps accelerate it, and how the position of a site relative to the surrounding terrain and the prevailing wind, its exposure, decides which of these effects it experiences.

20.4.1 Valley channeling

In a valley the wind near the floor tends to blow along the valley axis, up or down the valley, even when the large-scale wind above the ridge tops is oblique to it. This mechanical *channeling* has two forms. In forced channeling the wind above the ridges is turned by the sidewalls into the valley's direction: the cross-valley component is blocked and the along-valley component is carried down into the valley by turbulent mixing, so a southwesterly wind over a north–south valley becomes a southerly valley wind. In pressure-driven channeling the valley wind is driven by the along-valley component of the large-scale pressure gradient, from high to low pressure along the axis, and its direction is set by the pressure field rather than by the wind aloft. The thermally driven up-valley and down-valley winds, a third mechanism, belong to Chapter 19.

Pressure-driven channeling is the one case in this chapter in which the hemisphere matters, because the large-scale pressure field is in geostrophic balance. Chapter 3 gives the balance $f\,\mathbf{k}\times\mathbf{V}_g = -(1/\rho)\nabla_h p$. For a geostrophic westerly $\mathbf{V}_g = (U, 0)$, $\mathbf{k}\times\mathbf{V}_g = (0, U)$, so

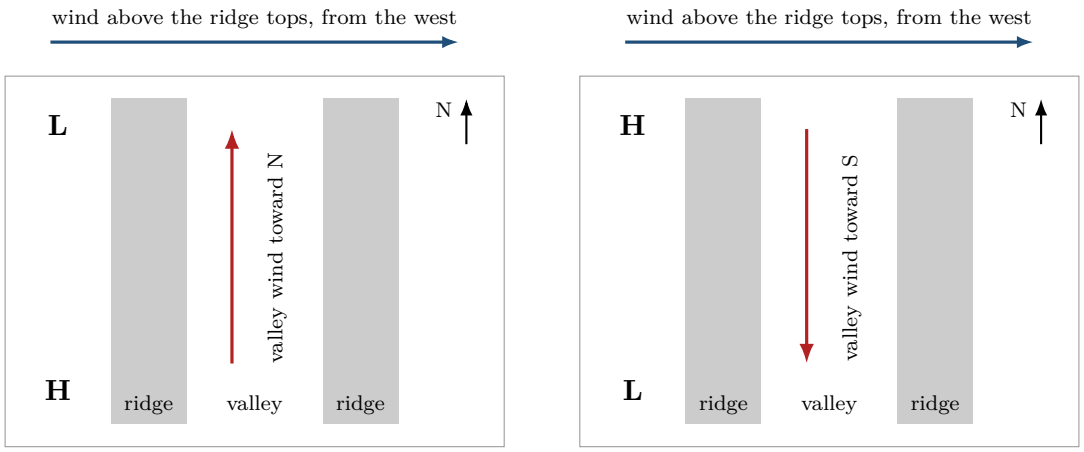
$$\frac{\partial p}{\partial y} = -\rho f U.$$

In the Northern Hemisphere, $f > 0$ and the pressure decreases toward the north: a north–south valley below a westerly wind has its low pressure at the northern end and the valley wind blows toward the north, a southerly wind, at right angles to the wind above. In the Southern Hemisphere, $f < 0$ and the pressure decreases toward the south: the same valley under the same westerly has a northerly valley wind blowing toward the south. Figure 20.5 draws the two cases as plan views with north at the top: the gray strips are the two ridges, L and H mark the low and high pressure of the large-scale field, the blue arrow above each panel is the wind above the ridge tops and the red arrow in the valley is the pressure-driven valley wind.

The size of the driving gradient follows from the balance. At 30° latitude, $|f| = 2 \times 7.292 \times 10^{-5} \times 0.5 = 7.29 \times 10^{-5}\,\mathrm{s}^{-1}$, and a geostrophic wind of $10\,\mathrm{m\,s}^{-1}$ needs $|\partial p/\partial y| = 1.2 \times 7.29 \times 10^{-5} \times 10 = 8.75 \times 10^{-4}\,\mathrm{Pa}$ per meter, 0.875 hPa per 100 km. Along a valley 50 km long the pressure difference is about 44 Pa, and equation (20.4) gives an upper bound for the valley wind of $\sqrt{2 \times 44/1.2} \approx 8.6\,\mathrm{m\,s}^{-1}$ if the air started at rest and lost nothing to friction; friction keeps the real valley wind below this. A valley wind that blows at right angles to the wind aloft is common in such valleys and is the reason a valley station cannot be used to infer the direction of the large-scale wind.

20.4.2 Gap winds

Air forced through a narrow pass or gap in a mountain barrier accelerates, often strongly. Three effects combine. A pressure difference across the barrier, high on one side and low on the other, drives the air through the gap; the gap channels the flow into its direction; and the reduced cross-section of the gap concentrates it. The result is a *gap flow*, or gap wind, which can be much faster than the wind on either side of the barrier.



(a) Northern Hemisphere, $f > 0$

(b) Southern Hemisphere, $f < 0$

Figure 20.5: Pressure-driven channeling in a north–south valley under a westerly wind above the ridge tops (plan view, north at the top, schematic). The geostrophic balance places the low pressure to the north in the Northern Hemisphere (a) and to the south in the Southern Hemisphere (b); the valley wind blows along the axis toward the low, at right angles to the wind above.

Bernoulli's relation gives the speed an air parcel reaches if the whole pressure difference Δp across the gap is converted into kinetic energy:

$$U_{\text{gap}} = \sqrt{U_{\text{up}}^2 + \frac{2\,\Delta p}{\rho}}. \tag{20.11}$$

For an illustrative difference of 3 hPa across a pass, with $\rho = 1.2\,\text{kg}\,\text{m}^{-3}$ and an upstream wind of $3\,\text{m}\,\text{s}^{-1}$,

$$U_{\text{gap}} = \sqrt{3^2 + \frac{2 \times 300}{1.2}}\,\text{m}\,\text{s}^{-1} = \sqrt{9 + 500}\,\text{m}\,\text{s}^{-1} \approx 22.6\,\text{m}\,\text{s}^{-1},$$

an upper bound that friction and mixing reduce. The pressure difference is often hydrostatic in origin: a pool of cold, dense air dammed on one side of the barrier. A cold layer of depth D and potential-temperature deficit $\Delta\theta$ raises the pressure at its base by $\rho\, g\, (\Delta\theta/\theta)\, D$ relative to the warmer side at the same level. For an illustrative $D = 600\,\text{m}$, $\Delta\theta = 4\,\text{K}$ and $\theta = 285\,\text{K}$, the excess is $1.2 \times 9.81 \times (4/285) \times 600 \approx 99\,\text{Pa}$, about 1 hPa, enough for a gap wind of $\sqrt{2 \times 99/1.2} \approx 12.9\,\text{m}\,\text{s}^{-1}$ from rest. Gap winds are therefore most frequent in stable conditions, when the stratification also prevents the cold air from flowing over the barrier (Section 20.5.1).

20.4.3 Terrain exposure

Two sites at the same elevation can have very different wind climates. A site on an exposed ridge facing the prevailing wind receives the crest speed-up of Section 20.2.2; a site at the same elevation behind an upstream ridge lies in its sheltered region and receives a reduced mean wind with elevated turbulence. What matters is not the elevation of a site but its *terrain exposure*: its position relative to the surrounding terrain, measured in the direction from which the wind comes. Exposure is a function of direction. A site exposed to westerly winds can be sheltered from easterly ones, and its wind climate is the combination of its exposures weighted by how often each direction occurs.

Exposure at several scales. Exposure depends on the scale at which the terrain is examined. A hilltop is exposed at the scale of 100 m, standing above its immediate surroundings, but may

be sheltered at the scale of 10 km if it lies inside a broad mountain basin surrounded by higher ranges. The wind at the hilltop is then the basin's reduced and channeled wind, accelerated locally by the hill. Exposure is hierarchical: an assessment of a site examines the terrain at several scales, from the obstacles within a few hundred meters to the ranges tens of kilometers away, and the speed-up factors of the scales multiply, as in the chain of influences on a single reading in Chapter 5.

20.5 Stratified flow over terrain

Everything so far assumed near-neutral air, in which a parcel lifted over a hill is neither helped nor resisted by buoyancy. In stable air lifting costs energy, and the flow may go around a hill instead of over it, or oscillate in waves downstream. This section derives the parameter that decides between the two, the Froude number, and describes blocking, mountain waves, downslope windstorms, their hydraulic analogy, and the role of the boundary-layer depth.

Jargon: blocking, Froude number, dividing-streamline height, mountain wave, downslope windstorm, hydraulic jump

Blocking is the stagnation or diversion of stable low-level air upstream of a barrier that it lacks the kinetic energy to cross. The *Froude number* $\mathrm{Fr} = U/(Nh_m)$, dimensionless, compares the inertia of the upstream wind U with the resistance of a stable stratification of buoyancy frequency N to vertical displacement over a terrain height h_m; it is computed from upstream soundings or model profiles. The *dividing-streamline height* h_d, in meters, is the upstream height below which air is blocked or diverted around a barrier and above which it passes over. A *mountain wave* (orographic gravity wave) is the oscillation of stable air displaced vertically by terrain, appearing in the vertical velocity, temperature, pressure and horizontal wind downstream and above the terrain. A *downslope windstorm* is a strong, often gusty wind down the lee slope of a mountain range, much faster than the upstream wind. A *hydraulic jump* is an abrupt transition from fast, thin (supercritical) flow to slower, deeper (subcritical) flow, with intense turbulence.

20.5.1 Blocking and flow over the top

In stable air, a parcel displaced upward is colder than its new surroundings and is pulled back down. Chapter 6 derived the restoring acceleration on a parcel displaced by δz as $-N^2\,\delta z$, with $N^2 = (g/\theta)\,\mathrm{d}\theta/\mathrm{d}z$. The work needed to lift a unit mass of air from the ground to the crest height h_m against this force is

$$\int_0^{h_m} N^2 z\,\mathrm{d}z = \tfrac{1}{2}\,N^2 h_m^2.$$

The air approaching the barrier has kinetic energy $\frac{1}{2}U^2$ per unit mass. If the kinetic energy exceeds the work, $\frac{1}{2}U^2 > \frac{1}{2}N^2h_m^2$, the air can rise over the crest; if not, the low-level air cannot cross and goes around the barrier, stagnates upstream of it, or flows through whatever gaps it offers. Neutral air, $N = 0$, crosses any barrier in this sense; the stronger the stratification, the more of the low-level flow is blocked. The argument neglects the pressure perturbations, which also do work on the parcel, but the criterion it yields is the standard one.

20.5.2 The Froude number

The condition $U > Nh_m$ is expressed by the Froude number of flow over terrain,

$$\mathrm{Fr} = \frac{U}{N\,h_m}, \tag{20.12}$$

with U the upstream wind, N the upstream buoyancy frequency and h_m the terrain height. It is the ratio of the inertia available to cross the terrain to the stability resisting the vertical displacement. For $\mathrm{Fr} \gg 1$ the flow goes over the terrain, close to the neutral behavior of the previous sections. For $\mathrm{Fr} \ll 1$ the low-level flow is blocked or diverted around it. Near $\mathrm{Fr} \approx 1$ the response is strongest: mountain waves of large amplitude and downslope winds. The same mountain under different stability gives a different wind field.

For an illustrative wind of $U = 10\,\mathrm{m\,s^{-1}}$ across a barrier $h_m = 500\,\mathrm{m}$ high, in a stratification with $N = 0.01\,\mathrm{s^{-1}}$,

$$\mathrm{Fr} = \frac{10\,\mathrm{m\,s^{-1}}}{0.01\,\mathrm{s^{-1}} \times 500\,\mathrm{m}} = 2,$$

and the air is able to cross. The buoyancy frequency of $0.01\,\mathrm{s^{-1}}$ corresponds, at $\theta = 290\,\mathrm{K}$, to $\mathrm{d}\theta/\mathrm{d}z = N^2\theta/g = 10^{-4} \times 290/9.81 \approx 3\,\mathrm{K}$ per kilometer, a typical value for the lower troposphere. With $N = 0.04\,\mathrm{s^{-1}}$ instead,

$$\mathrm{Fr} = \frac{10\,\mathrm{m\,s^{-1}}}{0.04\,\mathrm{s^{-1}} \times 500\,\mathrm{m}} = 0.5,$$

and blocking is much more likely. That buoyancy frequency corresponds to about 4.7 K per 100 m, the gradient of a strong nocturnal inversion; through a layer 500 m deep it is an extreme value, chosen to make the contrast plain. The same $\mathrm{Fr} = 0.5$ arises with ordinary values, such as a $5\,\mathrm{m\,s^{-1}}$ wind and $N = 0.02\,\mathrm{s^{-1}}$ over the same barrier. Some texts define the inverse quantity, Nh_m/U, often called the nondimensional mountain height, for which blocking corresponds to values above one; others build a Froude number on the half-width, $U/(NL_h)$, which measures a different thing, whether the hill is wide enough for the waves to be hydrostatic. The definition in use must be checked before a threshold is applied.

The dividing-streamline height. For $\mathrm{Fr} < 1$, the energy argument says which part of the upstream flow is blocked. A parcel approaching at height z_0 needs to rise only $h_m - z_0$ to clear the crest, which it can do if $U \geq N(h_m - z_0)$. The lowest height from which air passes over is therefore

$$h_d = h_m - \frac{U}{N} = h_m\,(1 - \mathrm{Fr}), \qquad \mathrm{Fr} < 1, \tag{20.13}$$

a standard estimate of the dividing-streamline height. For the worked case with $\mathrm{Fr} = 0.5$, $U/N = 10/0.04 = 250\,\mathrm{m}$ and $h_d = 500\,\mathrm{m} \times (1 - 0.5) = 250\,\mathrm{m}$: the air in the lowest 250 m upstream is blocked or diverted around the barrier, and the air above passes over its upper half. For $\mathrm{Fr} \geq 1$ the estimate gives $h_d \leq 0$ and all the air crosses.

20.5.3 Mountain waves

When stable air is lifted over terrain and descends on the other side, buoyancy does not simply return it to its original height: it overshoots and oscillates about it, with the buoyancy frequency N, while the wind carries it downstream. The oscillation, fixed in place by the terrain that forces it, is a *mountain wave*, or orographic gravity wave. It appears in every variable: the vertical velocity alternates between up and down, the temperature between cold (in the crests, where air has risen) and warm, the pressure and the horizontal wind with them.

Stable air is required. A restoring force needs $N^2 > 0$: in neutral air a displaced parcel stays where it is put, and in convective air it accelerates away, so neither supports the organized wave response. Mountain waves are therefore a feature of stable conditions, of the free troposphere above the boundary layer by day and of the whole column on stable nights.

A parcel oscillating with period $2\pi/N$ while carried at speed U travels a horizontal distance

$$\lambda = \frac{2\pi U}{N} \tag{20.14}$$

during one oscillation, a standard estimate of the horizontal wavelength of lee waves. For $U = 10\,\mathrm{m\,s^{-1}}$ and $N = 0.01\,\mathrm{s^{-1}}$, $\lambda = 2\pi \times 10/0.01\,\mathrm{m} \approx 6.3\,\mathrm{km}$; for $N = 0.02\,\mathrm{s^{-1}}$, 3.1 km. Terrain whose width is of the order of U/N, 1 km in the first case, excites such waves most strongly. Under the crests of strong lee waves rotors can form, and where waves grow large enough to overturn they break into turbulence aloft. For a mast or a turbine in the lee of a range, the waves appear as a standing pattern of strong and weak wind and of rising and sinking air that stays fixed while the upstream conditions persist.

20.5.4 Downslope windstorms and the hydraulic analogy

Under some conditions the response to stable flow over a range concentrates in a layer of fast air descending the lee slope: a downslope windstorm, with near-surface winds much faster than the upstream wind and violent gusts. Named examples include the foehn of the Alps, the chinook east of the Rocky Mountains, the bora of the Adriatic coast and the zonda on the eastern slopes of the Andes in Argentina. The mechanisms vary. In some the air arriving in the lee is warm and dry after losing its moisture on the windward side; in the bora it is cold air pouring over a barrier; in many the strong wind comes from large-amplitude or breaking mountain waves that focus the flow toward the surface.

Some of these flows behave like the flow of a shallow layer of water over an obstacle, an analogy that is useful for gap flows and downslope windstorms. Consider a stable layer of depth D under a weaker stratification aloft, with a potential-temperature step $\Delta\theta$ at its top, so that gravity acts on it through the reduced gravity $g' = g\,\Delta\theta/\theta$. For steady flow over terrain $h(x)$, continuity gives $UD = \text{constant}$, so $\mathrm{d}U/\mathrm{d}x = -(U/D)\,\mathrm{d}D/\mathrm{d}x$, and the momentum equation is $U\,\mathrm{d}U/\mathrm{d}x + g'\,\mathrm{d}(D+h)/\mathrm{d}x = 0$. Substituting the first into the second,

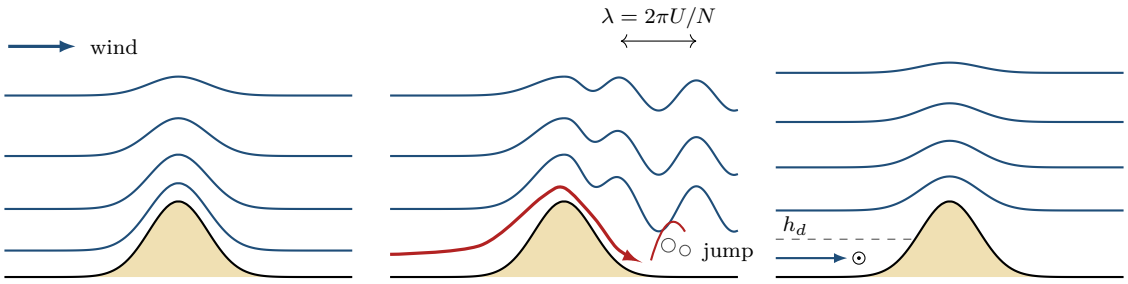
$$(1 - \mathrm{Fr}_s^2)\,\frac{\mathrm{d}D}{\mathrm{d}x} = -\frac{\mathrm{d}h}{\mathrm{d}x}, \qquad \frac{\mathrm{d}U}{\mathrm{d}x} = \frac{U}{D}\,\frac{1}{1-\mathrm{Fr}_s^2}\,\frac{\mathrm{d}h}{\mathrm{d}x}, \qquad \mathrm{Fr}_s = \frac{U}{\sqrt{g'D}}, \tag{20.15}$$

where Fr_s is the Froude number of the layer, the ratio of the flow speed to the speed $\sqrt{g'D}$ of long waves on the layer. Subcritical flow, $\mathrm{Fr}_s < 1$, accelerates and thins as it climbs the windward slope and decelerates again down the lee. Supercritical flow, $\mathrm{Fr}_s > 1$, does the opposite. If the subcritical flow accelerates enough to become critical, $\mathrm{Fr}_s = 1$, at the crest, it becomes supercritical beyond it; on the lee slope $\mathrm{d}h/\mathrm{d}x < 0$ and $1 - \mathrm{Fr}_s^2 < 0$, so $\mathrm{d}U/\mathrm{d}x > 0$ and the air keeps accelerating all the way down the slope. This is the hydraulic picture of a downslope windstorm. At the foot of the slope the fast, thin flow returns to the slow, deep state of its surroundings through a *hydraulic jump*, a sudden thickening with intense turbulence. For an illustrative layer with $\Delta\theta = 5\,\mathrm{K}$, $\theta = 290\,\mathrm{K}$ and $D = 800\,\mathrm{m}$, $g' = 9.81 \times 5/290 \approx 0.169\,\mathrm{m\,s^{-2}}$ and $\sqrt{g'D} \approx 11.6\,\mathrm{m\,s^{-1}}$; an upstream wind of $8\,\mathrm{m\,s^{-1}}$ has $\mathrm{Fr}_s \approx 0.69$, subcritical, and a crest that thins the layer enough can bring it to the critical state.

20.5.5 Stability and boundary-layer depth

The terrain effect is not set by terrain geometry alone. In neutral air a ridge produces the smooth passage and the speed-up of Section 20.2. In strongly stable air the same ridge blocks the low-level flow, channels it through gaps, launches waves, and lets the air in the valleys decouple from the flow above. Figure 20.6 draws the three regimes as vertical cross sections with the wind from the left: (a) $\mathrm{Fr} \gg 1$, with streamlines passing over the hill; (b) Fr near one, with lee waves of wavelength λ and a fast layer descending the lee slope into a jump; (c) $\mathrm{Fr} \ll 1$, with the low-level air below the dividing-streamline height stopped upstream and diverted around the hill, and only the air above it passing over.

Moving from panel (a) to panel (c) at fixed terrain is a change of stability or of wind speed alone, which is what makes a terrain effect a property of the regime and not only of the hill. The



(a) Fr $\gg 1$: flow over (b) Fr ≈ 1: waves, downslope wind (c) Fr $\ll 1$: blocked below h_d

Figure 20.6: Regimes of stable flow over a hill (vertical cross sections, wind from the left, schematic). (a) Large Froude number: the air passes over, as in neutral flow. (b) Froude number near one: lee waves of horizontal wavelength $\lambda = 2\pi U/N$ and a fast layer (red) descending the lee slope into a turbulent hydraulic jump. (c) Small Froude number: below the dividing-streamline height $h_d = h_m(1 - \mathrm{Fr})$ (dashed) the air is blocked and leaves the section around the sides of the hill (circled dot, flow out of the page); only the air above h_d crosses.

depth of the boundary layer enters the same way. A ridge $h_m = 800\,\mathrm{m}$ high is, by day, immersed in a well-mixed boundary layer 2000 m deep: the air crossing it is near-neutral, turbulent mixing couples the valleys to the crest, and the speed-up of Section 20.2.2 applies. At night the same ridge rises far above a stable boundary layer 150 m deep. The valley air is decoupled, pooled and nearly calm, while the crest stands in the stratified flow above, often in the fast residual or jet-level winds of Chapter 18, and the response is governed by the Froude number of that flow. The ridge, the valley sites and the crest sites are then in completely different regimes, and a speed-up factor measured by day says little about the night.

20.6 Terrain in models and practice

Terrain is the one ingredient of the near-surface wind that does not change, and that makes terrain corrections attractive. This section describes how terrain effects are tabulated in speed-up maps, why a single static factor fails, how linear models and computational fluid dynamics share the work, how they are coupled to weather models, and how weather models themselves represent the terrain they cannot resolve.

20.6.1 Persistence and speed-up maps

Terrain is fixed in time. For a given wind direction, stability and speed, the terrain's response is therefore repeatable: the same ridge produces the same speed-up every time the same conditions recur. This repeatability is what makes terrain corrections worth computing once and storing. What is stored cannot be one constant number per site, however; it is a set of factors indexed by the conditions.

A *speed-up map* tabulates

$$S(x, y) = \frac{U(x, y)}{U_{\mathrm{ref}}} \tag{20.16}$$

over an area, at a stated height above local ground and relative to a stated reference wind, for each direction sector and, where it matters, each stability class. Such maps show the exposed ridges with $S > 1$ and the sheltered valleys with $S < 1$; they are used to place wind turbines on the fastest sites, to place anemometers where they represent what they are meant to represent, and, for transmission lines, to give each span its own exposure, since a line crossing a ridge has spans at the crest, on the slopes and in the valleys, whose convective cooling differs with the local wind.

20.6.2 Why a static factor fails

A fixed correction such as $S = 1.25$ for a site may hold in neutral westerly flow, for which it was measured, and fail in stable northerly flow. For a site on the crest of a north–south ridge, equation (20.9) already reduces the speed-up to nearly zero for a northerly wind, which blows along the ridge; and in stable air the Froude number can move the site from the regime of panel (a) of Figure 20.6 to that of panel (c). The general dependence is

$$S = f(\beta,\ \text{stability},\ U,\ \text{terrain}), \tag{20.17}$$

with the wind direction β, a stability measure such as N or L_O, the wind speed and the terrain geometry. The dependence on speed enters through the Froude number. For an illustrative ridge $h_m = 300\,\text{m}$ high in air with $N = 0.02\,\text{s}^{-1}$, $Nh_m = 6\,\text{m}\,\text{s}^{-1}$: a night wind of $3\,\text{m}\,\text{s}^{-1}$ has $\text{Fr} = 0.5$ and is partly blocked, while a wind of $12\,\text{m}\,\text{s}^{-1}$ under the same stratification has $\text{Fr} = 2$ and crosses. A speed-up map is therefore a table in direction, stability and speed, and a single factor is a single entry of that table.

20.6.3 Linear models against computational fluid dynamics

Linear models (Section 20.2.5) are fast and adequate for gentle terrain in neutral flow. Where the flow is strongly nonlinear, over steep slopes, with separation, recirculation and strong local acceleration, computational fluid dynamics (CFD) is used. A CFD model solves the nonlinear equations of motion on a fine grid, of meters to tens of meters, and resolves the pressure perturbations, the separation, the recirculation, the local acceleration and the turbulence that terrain creates. Microscale CFD for terrain is run either as RANS (Reynolds-averaged Navier–Stokes), which computes the mean flow and parameterizes all the turbulence, or as LES (large-eddy simulation), which resolves the large turbulent eddies and parameterizes only the small ones; Chapter 29 treats these models.

CFD is not a substitute for meteorology. Its result depends on the inflow it is given: the wind direction, the vertical profile of wind speed, the stability and the turbulence at its upstream boundary. A CFD run with a neutral logarithmic inflow reproduces neutral terrain flow and nothing else; it does not know of a stable night, a low-level jet or a sea breeze unless the inflow carries them. CFD computes the local modification of a wind that something else must supply.

20.6.4 Mesoscale-to-microscale coupling

The supplier is a weather model. In *mesoscale-to-microscale coupling* a mesoscale weather model, with a grid of kilometers, computes the background wind and stability, and a microscale terrain model, linear or CFD, computes the local modification of that wind by the terrain and roughness it resolves. Figure 20.7 draws the chain from top to bottom: each box is a stage, the arrows show what passes between stages, the notes at the side list what each stage contributes, and the dashed arrow is the comparison with measurements that validates the result.

The division of labor follows the scales of Chapter 5. The weather model carries what is mesoscale and larger, the synoptic pressure field, the stability, the boundary-layer depth, the thermally driven circulations and the low-level jets; it cannot carry a ridge a few hundred meters wide. The terrain model carries that ridge and cannot generate the stable night by itself. The weather model contributes the direction, the vertical profile, the stability and possibly the turbulence; the terrain model contributes the speed-up, the sheltering and the separation.

20.6.5 Terrain smoothing in weather models

A weather model represents the terrain by its average over each grid cell, and it further smooths that average to keep its numerics stable. A narrow ridge is lowered and broadened. Figure 20.8

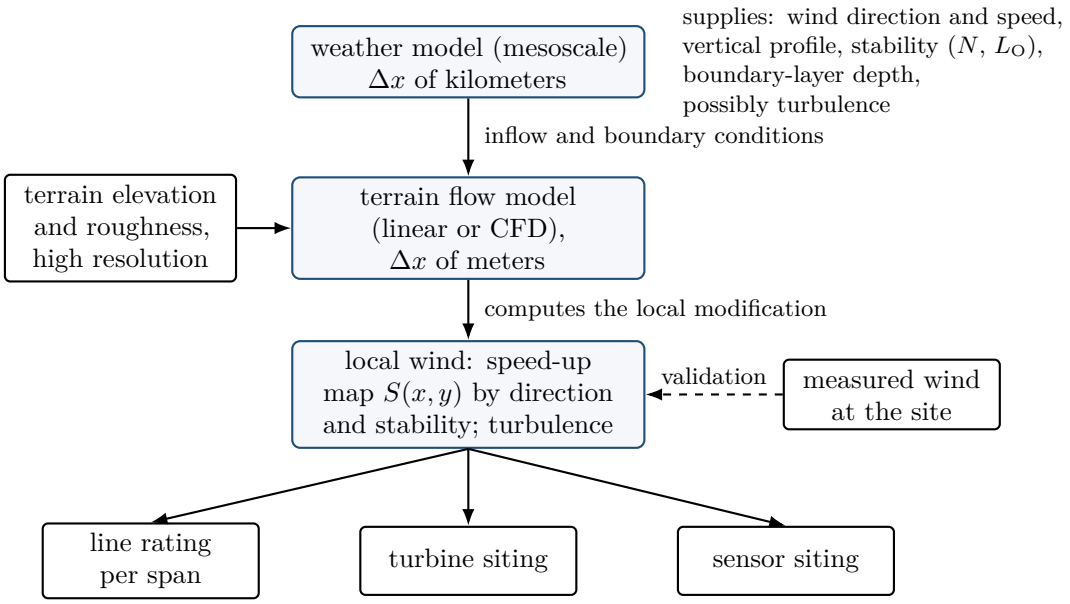


Figure 20.7: Mesoscale-to-microscale coupling (schematic). The weather model supplies the background flow and its stability; the terrain flow model computes the local modification by terrain and roughness; the resulting speed-up maps and turbulence serve line rating, turbine siting and sensor siting, and are validated against site measurements.

shows an illustrative case. The horizontal axis is distance across the ridge in kilometers and the vertical axis is height above the surrounding valley floor; the black curve is the real ridge, 1000 m high with a half-width of 3 km, and the red curve with dots is the ridge as the model represents it, 600 m high with a half-width of 5 km, the dots marking grid points 3 km apart.

The two profiles enclose the same area, as an averaging filter requires, but almost everything that drives the terrain flow has changed. The crest is 400 m lower, the steepest slope falls from $0.65 \times 1000/3000 \approx 0.22$ to $0.65 \times 600/5000 \approx 0.08$, the valleys on either side are shallower, and the pressure perturbations scale with them. The rule of thumb (20.7) gives, for the real ridge, $\Delta S_{\max} \approx 2 \times 1000/3000 \approx 0.67$, at the edge of the rule's range and thus only indicative; for the model ridge, $2 \times 600/5000 = 0.24$. The model's crest wind lacks most of the real speed-up, and it is evaluated 400 m lower in the atmosphere besides. The regime changes too: with an illustrative $U = 10\,\mathrm{m\,s^{-1}}$ and $N = 0.015\,\mathrm{s^{-1}}$, the real ridge has $\mathrm{Fr} = 10/(0.015 \times 1000) \approx 0.67$ and a dividing-streamline height of about 330 m, while the model ridge has $\mathrm{Fr} = 10/(0.015 \times 600) \approx 1.1$ and lets all the air cross. Smoothing thus produces systematic representativeness errors in mountains: underestimated crest winds, overestimated valley winds, missing blocking and misplaced waves. These are errors of the grid-cell wind against the point wind, and Chapters 27 and 28, on terrain representation and downscaling, return to them.

20.6.6 Subgrid orographic drag

Terrain smaller than the model can resolve still exerts force on the flow, and large-scale models parameterize it. Three effects are represented. Mountain-wave drag (gravity-wave drag) is the momentum that unresolved mountain waves carry upward and deposit where they break, decelerating the flow aloft. Subgrid blocking (low-level drag) is the drag of unresolved barriers on the stable low-level air that flows around rather than over them. Unresolved roughness (turbulent orographic form drag) is the drag of small hills on the boundary layer, represented by raising the effective roughness length above that of the vegetation.

The size of wave drag shows why it cannot be neglected. Linear theory gives a standard

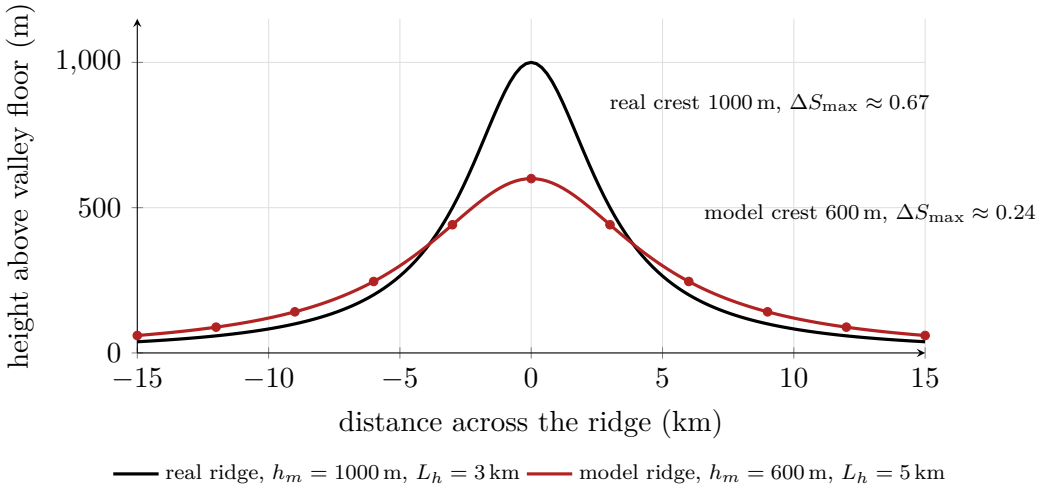


Figure 20.8: A ridge and its representation in a weather model (illustrative). Both profiles have the form $h_m/[1 + (x/L_h)^2]$ and the same cross-sectional area, $\pi h_m L_h = 3\pi \times 10^6\,\mathrm{m}^2$, as a smoothing filter preserves; dots mark model grid points 3 km apart. The speed-up values are from equation (20.7) with $C_s = 2$.

result for the drag per unit length of a long ridge of the profile of Figure 20.1 in hydrostatic flow, $(\pi/4)\,\rho N U h_m^2$. For $\rho = 1.2\,\mathrm{kg\,m^{-3}}$, $N = 0.01\,\mathrm{s^{-1}}$, $U = 10\,\mathrm{m\,s^{-1}}$ and an illustrative $h_m = 500\,\mathrm{m}$ with $L_h = 10\,\mathrm{km}$ (so that $NL_h/U = 10$ and the hydrostatic assumption holds), the drag is $0.785 \times 1.2 \times 0.01 \times 10 \times 500^2 \approx 2.4 \times 10^4\,\mathrm{N}$ per meter of ridge. Spread over a strip 40 km wide, four half-widths, it is a stress of 0.59 Pa, three times the turbulent surface stress $\rho u_*^2 = 1.2 \times 0.4^2 \approx 0.19\,\mathrm{Pa}$ of a windy day over flat land. Each of these parameterized drags is the resolved against parameterized distinction of Chapter 5 applied to terrain: what the grid cannot hold, it represents by its average effect. The next chapter turns from terrain to the vegetation and urban canopies that cover it, where the obstacles are smaller than the depth of the flow and the wind is slowed and made turbulent within and above the canopy.

20.7 What to retain

Definition 20.1 (Terrain-induced flow)**.** The background wind, the terrain geometry and the stability of the air together set up pressure perturbations that accelerate, block, separate or channel the near-surface flow. The same ridge gives speed-up, sheltering, blocked flow or waves depending on the atmospheric regime, so a terrain correction is a function of direction, stability and speed, not one number.

Table 20.2 lists the terms of the chapter, their meaning, their units and the subsection that defines each.

20.8 Exercises

Exercise 20.1. A long ridge 80 m high with a half-width of 500 m lies across a neutral wind of $7\,\mathrm{m\,s^{-1}}$ measured at 20 m over flat ground upstream. (a) Compute the aspect ratio, the steepest slope of the ridge for the profile of Figure 20.1, and say whether the lee flow is likely to separate. (b) With equations (20.7) and (20.8), compute the fractional speed-up and the wind at 20 m above the crest. (c) Estimate the pressure perturbation at the crest with Bernoulli's relation and $\rho = 1.2\,\mathrm{kg\,m^{-3}}$. (d) Repeat (b) for an isolated hill of the same height and half-width.

Table 20.2: The terms of the chapter and where each is defined.

Term	Meaning	Units	Defined in
Terrain speed-up	increase of the wind over a crest relative to the upstream wind at the same height above ground	–	20.1.1
Speed-up factor S	$U_{\text{terrain}}/U_{\text{ref}}$ at the same Δz; a function of direction, stability and speed	–	20.1.2, 20.6.2
Fractional speed-up ΔS	$S-1$; about $C_s h_m/L_h$ at a low crest, decaying with height over about L_h	–	20.1.2, 20.2.2
Pressure perturbation p'	pressure minus the background pressure; raised windward, lowered over the crest	Pa	20.1.3
Windward, leeward	the side facing the incoming wind; the downstream, sheltered side	–	20.1.4
Aspect ratio h_m/L_h	hill height over half-width; small is gentle, large is steep and nonlinear	–	20.2.1
Flow separation	detachment of the boundary layer from a lee slope steeper than about 0.3	–	20.3.1
Recirculation zone	region of reversed mean flow beneath a separated shear layer; weak wind, high turbulence	–	20.3.2
Sheltering	reduced mean wind downstream of terrain, often with elevated turbulence	–	20.3.3
Channeling	alignment of valley wind with the valley axis, forced or pressure-driven	–	20.4.1
Gap flow	acceleration through a pass driven by a pressure difference, up to $\sqrt{U^2+2\Delta p/\rho}$	m/s	20.4.2
Terrain exposure	position of a site relative to the surrounding terrain in the direction of the wind, at several scales	–	20.4.3
Blocking	stagnation or diversion of stable low-level air that cannot cross a barrier	–	20.5.1
Froude number Fr	$U/(Nh_m)$: inertia against stable resistance; over for $\text{Fr} \gg 1$, blocked for $\text{Fr} \ll 1$	–	20.5.2
Dividing-streamline height h_d	$h_m(1-\text{Fr})$ for $\text{Fr}<1$: below it air is blocked	m	20.5.2
Mountain wave	buoyancy oscillation of stable air forced by terrain; wavelength about $2\pi U/N$	m	20.5.3
Downslope windstorm	strong lee-slope wind, much faster than upstream	m/s	20.5.4
Hydraulic jump	abrupt return from fast thin to slow deep flow, with intense turbulence	–	20.5.4
Speed-up map	$S(x,y)=U(x,y)/U_{\text{ref}}$ by direction sector and stability class	–	20.6.1
Mesoscale-to-microscale coupling	weather model supplies the background flow; terrain model computes its local modification	–	20.6.4
Subgrid orographic drag	parameterized wave drag, low-level blocking drag and orographic roughness	Pa	20.6.6

Exercise 20.2. A transmission line in southern Brazil, at 30°S, crosses the crest of a long ridge whose axis runs from northeast to southwest; the perpendicular fractional speed-up at conductor height is $\Delta S_\perp = 0.3$. (a) With equation (20.9), compute the speed-up factor for winds from 315°, 270° and 225°. (b) A valley running north–south lies below a geostrophic westerly of $12\,\mathrm{m\,s^{-1}}$ nearby. Compute the Coriolis parameter and the along-valley pressure gradient, and state toward which end of the valley the pressure-driven valley wind blows. (c) Give the answer to (b) for the same valley at 30°N.

Exercise 20.3. A wind of $6\,\mathrm{m\,s^{-1}}$ approaches a range 600 m high. Take $\theta = 290\,\mathrm{K}$. (a) Compute the buoyancy frequency and the Froude number for a potential-temperature gradient of 4 K per kilometer and for one of 3 K per 100 m. (b) For the case with $\mathrm{Fr} < 1$, compute the dividing-streamline height and describe the low-level flow. (c) Compute the lee-wave wavelength in both cases. (d) Which of the two would a speed-up factor measured on a windy afternoon describe?

Exercise 20.4. (a) A pressure difference of 2.5 hPa drives air from rest through a mountain pass. Compute the Bernoulli upper bound on the gap wind with $\rho = 1.2\,\mathrm{kg\,m^{-3}}$, and the depth of a cold pool 5 K colder than its surroundings ($\theta = 285\,\mathrm{K}$) that would produce that difference. (b) A weather model represents a ridge 700 m high with a half-width of 1.5 km as a ridge 400 m high of the same profile and cross-sectional area. Compute the model ridge's half-width and the rule-of-thumb crest speed-up for both ridges. (c) For $U = 8\,\mathrm{m\,s^{-1}}$ and $N = 0.012\,\mathrm{s^{-1}}$, compute the Froude number of both ridges and say whether the model changes the regime.

Chapter 21

Vegetation and Urban Canopies

21.1 The canopy as a distributed momentum sink

The surface-layer theory of the preceding chapters treats the ground as a boundary: a plane at $z = 0$, or at the displacement height, at which the air loses its momentum, and whose effect on the flow above is summarized by a roughness length z_0. Over grass the picture is accurate. Over a forest, a field of maize or a city it is not, because the obstacles are tall enough for the wind to blow among them, and the air loses its momentum not at one level but throughout a layer tens of meters deep. The question of this chapter is

what happens to the wind when the "surface" is not a surface but a layer of obstacles?

The chapter first describes a canopy as a layer that absorbs momentum over its depth and writes the drag force that does it. It then derives the wind profile inside the canopy, joins it to the logarithmic profile above, and describes the shear layer at the canopy top and the organized turbulence it produces. It treats vegetation canopies (density, leaf area, seasons, crops, forest edges) and urban canopies (street canyons, flow regimes, frontal area, directional roughness, local acceleration and downwash, thermal effects), the ways models represent canopies, and what the turbulence near a canopy does to a measurement.

Jargon: canopy, canopy flow, canopy height, canopy drag, frontal area density, porosity

A *canopy* is a layer of the atmosphere next to the ground that is filled with obstacles: leaves, branches and stems of vegetation, crop plants, or buildings, streets and the trees between them. *Canopy flow* is the atmospheric flow within and above such a layer, where the air passes among the obstacles rather than over a closed surface. The *canopy height* h_c (m) is the characteristic height of the obstacles, the mean top of the vegetation or the mean building height; it is measured by survey, airborne laser scanning or building databases. *Canopy drag* is the loss of momentum of the air caused by the form drag of the canopy elements, distributed through the canopy depth; it is written as a force per unit volume of air, F_D (N/m^3), and represented in models by a drag coefficient and an area density. The *frontal area density* a (m^{-1}, that is, m^2 of obstacle area per m^3 of air) is the area of the obstacles projected onto a plane perpendicular to the wind, per unit volume of canopy space. *Porosity* is the fraction of the canopy volume, or of a vertical cross section through it, that is open to the air; a dense hedge has a low porosity, an orchard a high one.

Key idea

A canopy is not a rough surface but a three-dimensional momentum sink: the wind penetrates it, decays within it, and produces a strong shear layer at its top, and only well above the canopy can its whole effect be summarized by a roughness length and a displacement height.

21.1.1 The canopy concept

Over a flat, rough surface the turbulent momentum flux $-\overline{u'w'}$ is nearly constant with height through the surface layer and is delivered, all of it, to the ground and the small elements on it (Chapters 9 and 10). The surface is a sink of momentum at one level. In a canopy, the leaves, branches, stems or buildings each take part of the momentum out of the air that passes them. The sink is spread over the canopy depth: some of the momentum carried downward by the turbulence is absorbed by the upper crowns, some by the lower branches, and only a small remainder reaches the soil.

Figure 21.1 compares the two pictures. Panel (a) is a side view of a flat rough surface with the wind blowing from the left; its single arrow is the drag on the air, which acts at the ground. Panel (b) is a side view of a forest of height h_c; its arrows are the drag per unit volume at four heights in the canopy, their lengths proportional to the values computed later in the chapter for an illustrative forest. Panel (c) has on its horizontal axis the kinematic momentum flux $-\overline{u'w'}$ divided by its value above the canopy, u_*^2, and on its vertical axis the height divided by the canopy height. The solid curve is the canopy, the dashed line the flat surface.

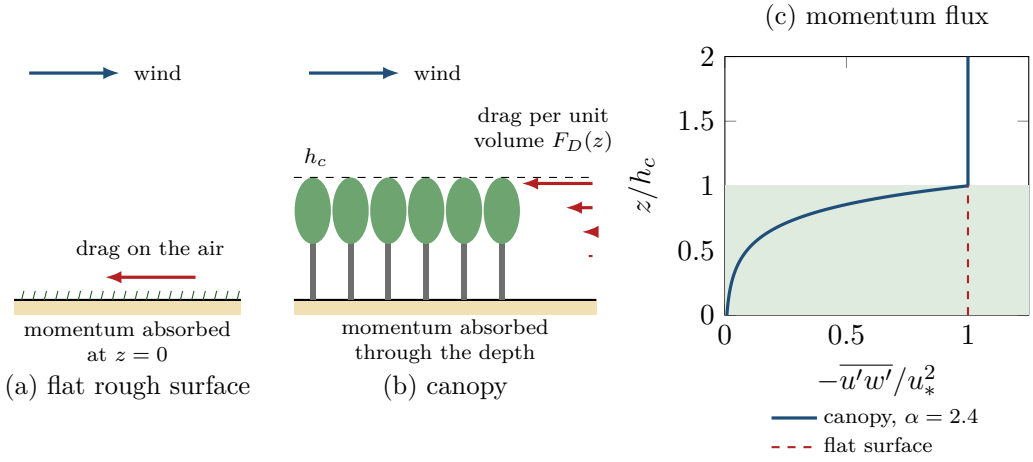


Figure 21.1: The canopy as a distributed momentum sink (schematic), wind from the left. (a) Over a flat rough surface the drag acts at the ground. (b) In a canopy it acts through the depth; arrow lengths are proportional to the drag per unit volume of the illustrative forest of Section 21.2.2 at 0.95, 0.75, 0.55 and 0.35 h_c. (c) Kinematic momentum flux relative to its value above the canopy: canopy (solid), $-\overline{u'w'}/u_*^2 = \exp[-2\alpha(1 - z/h_c)]$ with $\alpha = 2.4$, from the model of Section 21.2.2; flat surface (dashed), constant down to the ground. Above h_c the two coincide. Shaded: the canopy.

Over the flat surface the momentum flux is the same at every height down to the ground, because nothing absorbs momentum on the way. In the canopy the flux falls from u_*^2 at the top to a few percent of it in the lower half of the canopy, because each layer of foliage takes its share; in the model drawn, less than one percent reaches the ground. The shapes of the drag and the flux in panels (b) and (c) are the same function, for a reason derived in Section 21.2.2. This is the difference between a canopy and a rough surface: the momentum sink is distributed with height.

21.1.2 Canopy height

The canopy height h_c is the reference length of canopy flow. Typical values are about 1 to 3 m for crops (less for short cereals and grass), about 10 to 30 m and more for forests, and the scale of the buildings for an urban canopy, from about 5 m in a district of single-storey houses to 100 m and more among towers. Heights inside and above a canopy are usually expressed as z/h_c, and the profiles of this chapter are drawn on that axis.

The canopy height marks a change in the physics, not only in the geometry. Below $z = h_c$ the air is in direct contact with the obstacles and is slowed by their drag; above it the air feels the canopy only through the turbulence that carries momentum down to it. The flow below and above h_c therefore behaves differently, and the two regions need different descriptions.

21.1.3 Above-canopy against within-canopy flow

Above the canopy, and sufficiently far above it, the flow resembles the boundary layer over a rough wall: the momentum flux is nearly constant with height and the mean wind follows the logarithmic profile with heights counted from the displacement height, $U = (u_*/\kappa)\ln[(z-d)/z_0]$ (Chapters 7 and 11). The canopy enters only through d and z_0.

Within the canopy the wind interacts directly with the obstacles. The drag is distributed over the depth, the wakes of the individual elements overlap, and the turbulence is highly heterogeneous: it differs between a gap and a crown, between the windward and the lee side of a building, and from one moment to the next as gusts penetrate from above. The mean wind is weak and does not follow a logarithmic law; its shape is set by the vertical distribution of the drag and by the turbulence that resupplies momentum from above.

> **Principle 21.1.** *Within-canopy flow is not logarithmic flow. The logarithmic profile describes the wind above a canopy, with heights counted from the displacement height; inside the canopy the profile is set by the distribution of the drag.*

21.1.4 The drag force per unit volume

Each canopy element exerts a form drag on the air (Chapter 11). For an element of frontal area A in a wind U, the drag is $\frac{1}{2}\rho C_D A U^2$, with C_D the drag coefficient of the element, of order 0.1 to 0.3 for leaves and shoots and about 1 for a building. Summing over the elements in a volume of canopy and dividing by the volume replaces A by the frontal area per unit volume, the frontal area density a, and gives the drag force per unit volume of air,

$$F_D = \tfrac{1}{2}\,\rho\, C_D\, a\, U^2, \tag{21.1}$$

in $\mathrm{N/m^3}$, with U the local mean wind. Here C_D is the drag coefficient of the canopy elements, not the surface drag coefficient $\tau_0/(\rho U^2)$ of Chapter 10; the chapter states which one is meant wherever both appear. The force acts against the wind, at every height where there are elements, and its quadratic dependence on U means that the drag is concentrated where the wind is strongest, near the canopy top.

Take an illustrative forest with $h_c = 20\,\mathrm{m}$ and a uniform frontal area density $a = 0.2\,\mathrm{m^{-1}}$ (Section 21.3.2 relates this value to a leaf area index of 4), an element drag coefficient $C_D = 0.2$, $\rho = 1.2\,\mathrm{kg\,m^{-3}}$ and a wind at the canopy top $U_h = U(h_c) = 2.77\,\mathrm{m\,s^{-1}}$, the value that the log profile of Chapter 11 gives at h_c for $u_* = 0.8\,\mathrm{m\,s^{-1}}$, $d = 14\,\mathrm{m}$ and $z_0 = 1.5\,\mathrm{m}$: $U_h = (0.8/0.4)\ln[(20-14)/1.5]\,\mathrm{m\,s^{-1}} = 2 \times 1.386\,\mathrm{m\,s^{-1}} = 2.77\,\mathrm{m\,s^{-1}}$. At the canopy top

$$F_D = 0.5 \times 1.2 \times 0.2 \times 0.2 \times 2.77^2\,\mathrm{N\,m^{-3}} = 0.024 \times 7.69\,\mathrm{N\,m^{-3}} = 0.185\,\mathrm{N\,m^{-3}}.$$

If the wind kept this value all the way down, the canopy would remove $0.185 \times 20 = 3.69\,\mathrm{N\,m^{-2}}$ of momentum per unit time and ground area. The turbulence above the canopy supplies only the surface stress $\rho\,u_*^2 = 1.2 \times 0.8^2\,\mathrm{Pa} = 0.768\,\mathrm{Pa}$, about a fifth of that. In a steady state the canopy cannot absorb more momentum than the flow above delivers, so the wind must weaken downward until the integrated drag equals 0.77 Pa. That requirement determines the in-canopy profile, which the next section derives.

21.2 Wind inside and at the top of a canopy

This section derives the mean wind inside a canopy from a momentum balance with a simple closure, joins it to the logarithmic profile above, and describes the shear layer at the canopy top, the sweeps and ejections it produces, and the layers above the canopy in which the roughness length and the displacement height apply.

21.2.1 The momentum balance in a canopy

In a steady, horizontally homogeneous canopy, with the quantities averaged in time and over a horizontal area that contains many elements, the along-wind momentum of the air changes only through the vertical divergence of the turbulent flux and through the drag. Per unit mass,

$$0 = -\frac{\partial\,\overline{u'w'}}{\partial z} - \frac{F_D}{\rho},$$

where the pressure-gradient and Coriolis forces have been neglected against the much larger drag, as in the surface layer above. With equation (21.1),

$$\frac{\partial(-\overline{u'w'})}{\partial z} = \tfrac{1}{2}\,C_D\,a\,U^2. \tag{21.2}$$

The kinematic stress $-\overline{u'w'}$ increases upward through the canopy at a rate equal to the drag per unit mass. Integrating from the ground to the canopy top gives $u_*^2 - (-\overline{u'w'})_0 = \int_0^{h_c} \tfrac{1}{2}\,C_D\,a\,U^2\,\mathrm{d}z$: the stress above the canopy equals the drag of the whole canopy plus the small stress that reaches the ground. This is the integral of the drag per unit volume used in Chapter 11 to define the displacement height as the centroid of the drag.

Above the canopy, $a = 0$ and equation (21.2) returns the constant-flux layer of the surface layer. Inside, the equation has two unknowns, the flux and the wind, and needs a closure that relates them. The averaging over a horizontal area also produces dispersive fluxes, from the spatial variation of the time-mean wind between gaps and elements; they are small in dense canopies and are neglected here.

21.2.2 The exponential wind profile

The simplest closure is a mixing length (Chapter 8):

$$-\overline{u'w'} = K_m\,\frac{\partial U}{\partial z}, \qquad K_m = l^2\,\frac{\partial U}{\partial z}, \qquad \text{so} \qquad -\overline{u'w'} = l^2\left(\frac{\partial U}{\partial z}\right)^2. \tag{21.3}$$

Near a flat surface $l = \kappa z$, because the eddies are limited by the distance to the ground. Inside a canopy the dominant eddies are produced by the shear at the canopy top and have a size set by the canopy, not by the height above the soil; a standard simplified model therefore takes the mixing length constant with height in the canopy. It also takes the frontal area density and the element drag coefficient uniform.

Try a profile that decays exponentially downward from the canopy top,

$$U(z) = U_h \exp[\alpha(z/h_c - 1)],$$

with α a dimensionless constant. Then, step by step,

$$\frac{\partial U}{\partial z} = \frac{\alpha}{h_c}\,U, \qquad -\overline{u'w'} = l^2\,\frac{\alpha^2}{h_c^2}\,U^2, \qquad \frac{\partial(-\overline{u'w'})}{\partial z} = l^2\,\frac{\alpha^2}{h_c^2}\,2U\,\frac{\partial U}{\partial z} = 2\,l^2\,\frac{\alpha^3}{h_c^3}\,U^2.$$

Setting the last expression equal to $\frac{1}{2}\,C_D\,a\,U^2$, equation (21.2), the factor U^2 cancels: the trial profile satisfies the momentum balance at every height in the canopy, provided

$$\alpha^3 = \frac{C_D\,a\,h_c^3}{4\,l^2}. \tag{21.4}$$

The in-canopy wind is therefore

$$U(z) = U_h \exp\!\left[-\alpha\left(1 - \frac{z}{h_c}\right)\right], \qquad 0 \le z \le h_c, \tag{21.5}$$

and α is the *attenuation coefficient* of the canopy: the number of e-foldings by which the wind falls from the canopy top to the ground. The flux follows from the second step, $-\overline{u'w'} = u_*^2 \exp[-2\alpha(1 - z/h_c)]$, once the condition $-\overline{u'w'} = u_*^2$ at $z = h_c$ is imposed; it decays twice as fast as the wind and has the same shape as the drag per unit volume, which is why the two coincide in Figure 21.1.

The condition at the canopy top also eliminates the mixing length. From $u_*^2 = l^2(\alpha/h_c)^2 U_h^2$, the mixing length is $l = u_*\,h_c/(\alpha\,U_h)$; substituting it into equation (21.4) gives

$$\alpha = \frac{C_D\,a\,h_c}{4}\left(\frac{U_h}{u_*}\right)^2. \tag{21.6}$$

The attenuation is strong when the canopy is dense ($C_D\,a\,h_c$ large) and when the wind at the top is large compared with the friction velocity. For the illustrative forest, $C_D\,a\,h_c = 0.2 \times 0.2 \times 20 = 0.8$ and $U_h/u_* = 2.77/0.8 = 3.47$, so

$$\alpha = \frac{0.8}{4} \times 3.47^2 = 0.2 \times 12.0 = 2.40, \qquad l = \frac{0.8 \times 20}{2.40 \times 2.77}\,\mathrm{m} = 2.40\,\mathrm{m}.$$

The wind at mid-canopy is $U(10\,\mathrm{m}) = 2.77\,\mathrm{m\,s^{-1}} \times e^{-1.20} = 2.77 \times 0.301\,\mathrm{m\,s^{-1}} = 0.84\,\mathrm{m\,s^{-1}}$, and near the ground $U(2\,\mathrm{m}) = 2.77\,\mathrm{m\,s^{-1}} \times e^{-2.16} = 0.32\,\mathrm{m\,s^{-1}}$. The total drag is

$$\int_0^{h_c} F_D\,\mathrm{d}z = \tfrac{1}{2}\rho\,C_D\,a\,U_h^2\,\frac{h_c\,(1 - e^{-2\alpha})}{2\alpha} = 0.185 \times \frac{20 \times 0.992}{4.80}\,\mathrm{Pa} = 0.762\,\mathrm{Pa},$$

and the remaining 0.006 Pa of the 0.768 Pa supplied from above, the fraction $e^{-2\alpha} = 0.8\,\%$, reaches the ground. The profile has done what Section 21.1.4 required of it.

The model has known limits. It does not satisfy $U = 0$ at the ground; the real wind drops to zero in a thin layer at the soil that the model ignores. It assumes uniform foliage, whereas many forests have a dense crown over an open trunk space, where the wind often shows a secondary maximum. And the constant mixing length is a closure, not a law: it describes the mean profile in many canopies, but not the transport mechanism (Section 21.2.6). The exponential form is nonetheless the standard first description of the mean wind in a vegetation canopy, and other forms used in practice keep its main property: the wind decays rapidly downward into the canopy.

21.2.3 Typical attenuation coefficients

Table 21.1 lists typical ranges of the attenuation coefficient for common vegetation canopies, with typical heights and leaf area indices (defined in Section 21.3.2) and the fraction of the

Table 21.1: Typical attenuation coefficients α of the exponential in-canopy profile, equation (21.5). Ranges illustrative.

Canopy	h_c (m)	LAI	α	$U(0.5\,h_c)/U_h$ at mid-range
Cereal crop (wheat, rice)	0.5 to 1.2	3 to 6	2 to 3	0.29
Maize	2 to 3	3 to 5	2 to 3	0.29
Orchard, open woodland	3 to 8	1 to 3	0.5 to 1.5	0.61
Deciduous forest, leaf-on	15 to 30	3 to 6	2 to 3	0.29
Deciduous forest, leaf-off	15 to 30	0.5 to 1.5 (branches)	0.5 to 1.5	0.61
Dense coniferous forest	10 to 30	5 to 10	2 to 4	0.22
Tropical rain forest	25 to 40	4 to 7	2 to 4	0.22

canopy-top wind that remains at mid-canopy, $U(0.5\,h_c)/U_h = e^{-\alpha/2}$, for the middle of each range. The values are typical, not constants; they vary with the stand, the season and the wind.

A sparse canopy with $\alpha \approx 1$ keeps more than half of the canopy-top wind at mid-height; a dense one with $\alpha \approx 3$ keeps about a fifth, and near the ground, at $0.1\,h_c$, the two keep $e^{-0.9} = 0.41$ and $e^{-2.7} = 0.07$ of it. Urban canopies are not in the table: among buildings the drag is concentrated on a few large faces, the flow separates and recirculates, and no smooth profile describes the mean wind at street level (Section 21.4).

21.2.4 The full profile: canopy and log layer joined

The exponential profile inside and the logarithmic profile above meet at the canopy top. Continuity of the wind and of the stress there was used to find α; continuity of the shear is a further condition. The shear of the exponential profile at h_c is $\alpha U_h/h_c$, and that of the log profile is $u_*/[\kappa(h_c - d)]$. Equating them, and using $l = u_* h_c/(\alpha U_h)$, gives

$$l = \kappa\,(h_c - d), \qquad \alpha = \frac{h_c\,u_*}{\kappa\,(h_c - d)\,U_h}\,: \tag{21.7}$$

the in-canopy mixing length equals the mixing length of the log layer at the canopy top, the von Kármán constant times the height of the canopy top above the zero plane. For the illustrative forest, $\kappa(h_c - d) = 0.4 \times 6\,\mathrm{m} = 2.40\,\mathrm{m}$ and $\alpha = 20 \times 0.8/(0.4 \times 6 \times 2.77) = 2.40$, the same values that the drag gave. The illustrative parameters are thus consistent: the canopy drag $C_D a h_c = 0.8$, the surface parameters $d = 14\,\mathrm{m}$ and $z_0 = 1.5\,\mathrm{m}$ and the friction velocity $0.8\,\mathrm{m\,s^{-1}}$ describe one forest, with wind, stress and shear continuous at its top.

Figure 21.2 draws the result. Panel (a) has the wind speed on the horizontal axis and the height above the ground on the vertical axis, from 0 to 60 m. The solid curve is the exponential profile below $h_c = 20\,\mathrm{m}$ and the log profile above; the dashed curve continues the log profile into the canopy, where it reaches zero at $d + z_0 = 15.5\,\mathrm{m}$. The shaded band is the canopy and the dotted line the displacement height. Panel (b) has the wind relative to U_h on the horizontal axis and z/h_c on the vertical axis, and draws equation (21.5) for three attenuation coefficients that span Table 21.1.

Panel (a) shows the two halves of the canopy wind. Above the canopy the wind grows logarithmically, from $2.77\,\mathrm{m\,s^{-1}}$ at the top to $5.71\,\mathrm{m\,s^{-1}}$ at 40 m. Inside, it falls to a third of U_h at mid-canopy and to about a tenth near the ground. The dashed curve shows what the log profile would say if it were used inside the canopy: zero wind everywhere below 15.5 m, which is wrong; the canopy air moves, slowly, and is replaced by gusts from above. Panel (b) shows how strongly the canopy density controls the in-canopy wind for the same wind at the top.

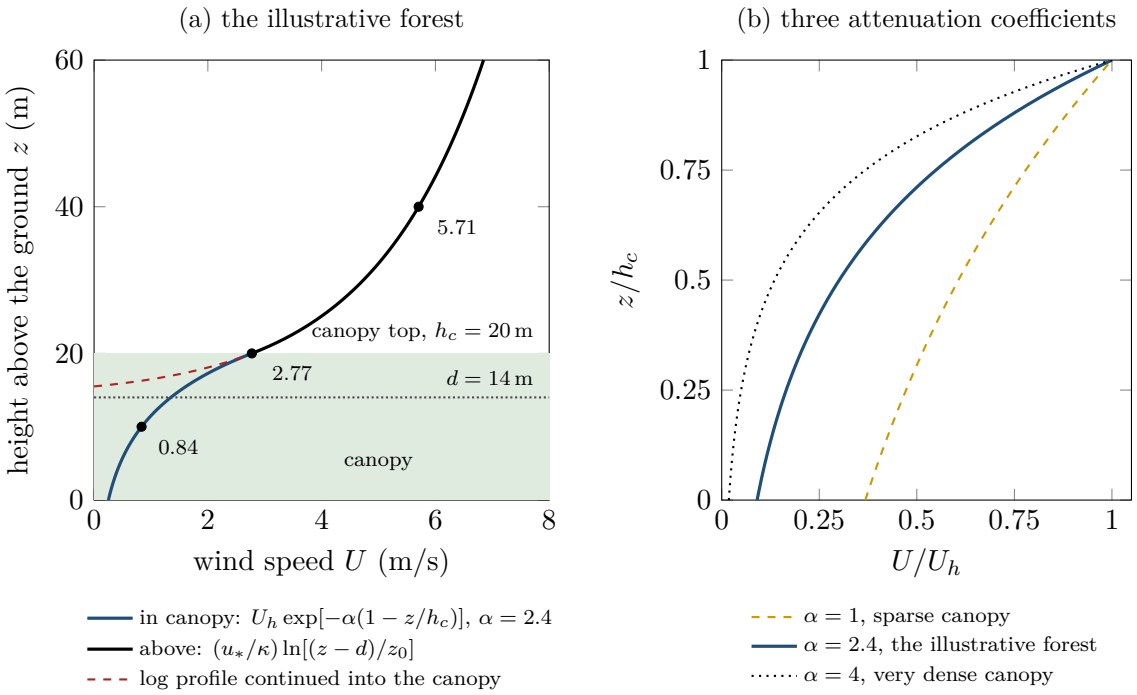


Figure 21.2: The wind inside and above a canopy. (a) Illustrative forest, $h_c = 20\,\mathrm{m}$, $d = 14\,\mathrm{m}$, $z_0 = 1.5\,\mathrm{m}$, $u_* = 0.8\,\mathrm{m\,s^{-1}}$, $\kappa = 0.4$, $U_h = 2.77\,\mathrm{m\,s^{-1}}$: equation (21.5) with $\alpha = 2.4$ below the canopy top and the log profile above (solid); the log profile continued below h_c (dashed). Points: values in m/s at 10, 20 and 40 m. (b) Equation (21.5) in dimensionless form, $U/U_h = \exp[-\alpha(1 - z/h_c)]$, for $\alpha = 1$, 2.4 and 4.

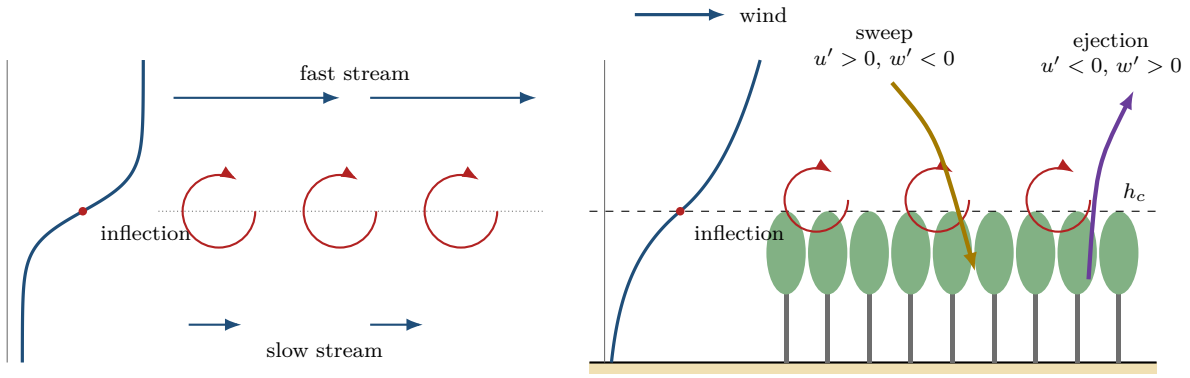
21.2.5 The canopy-top shear layer

The strongest shear in the whole profile is at the canopy top, where fast air above meets slow air below. For the illustrative forest it is $\alpha U_h/h_c = 2.40 \times 2.77/20\,\mathrm{s^{-1}} = 0.33\,\mathrm{s^{-1}}$, the shear the log profile has at only 6 m above its zero plane. A more important feature is the curvature. Inside the canopy, $\partial^2 U/\partial z^2 = (\alpha/h_c)^2 U > 0$; above it, $\partial^2 U/\partial z^2 = -u_*/[\kappa(z-d)^2] < 0$. The curvature changes sign at $z = h_c$, so the profile has an *inflection point* at the canopy top. A wind profile over a flat wall, logarithmic down to the ground, has none.

The inflection point matters because a parallel shear flow can be unstable to small inviscid disturbances only if its profile has one (the inflection-point criterion of hydrodynamic stability). A canopy-top profile meets that condition, and the shear layer there behaves like a *plane mixing layer*, the layer between two parallel streams of different speed, rather than like a wall boundary layer. A plane mixing layer rolls up into vortices with axes across the flow, by the same Kelvin–Helmholtz mechanism that Chapter 17 described for a stratified shear layer, here without stratification. Their size is set by the thickness of the shear layer, measured by the *shear length* $U_h/(\partial U/\partial z)_h$, which in the exponential model is $h_c/\alpha = 8.3\,\mathrm{m}$ for the illustrative forest. Coherent structures are observed at canopy tops with spacings along the wind of about eight shear lengths, here about 70 m, three to four canopy heights.

Figure 21.3 compares the two flows. Panel (a) is a side view of a plane mixing layer: a fast stream above and a slow stream below, with the wind from the left, the speed profile on the left with its inflection point, and the rollers along the interface. Panel (b) is a side view of a canopy, with the profile of Figure 21.2 drawn on the left, the rollers along the canopy top, and two arrows: a sweep carrying fast air down into the canopy and an ejection carrying slow canopy air up.

The two panels have the same structure: an inflection point, a layer of strong shear, and



(a) plane mixing layer (b) canopy-top shear layer

Figure 21.3: The mixing-layer analogy (schematic), wind from the left. (a) Plane mixing layer between a fast and a slow stream: a speed profile of hyperbolic-tangent shape, with its inflection point on the interface, and rollers with axes across the flow along the interface. (b) Canopy: the profile of Figure 21.2(a) (exponential below h_c, logarithmic above) with its inflection point at the canopy top, rollers along the canopy top, a sweep (gold) and an ejection (purple).

rollers of a size set by the shear layer, not by the distance to the ground. The canopy-top turbulence is therefore organized, not only random. The rollers and the larger structures that grow from them sweep air into the canopy and lift canopy air out, in events that carry most of the momentum and of the heat and gases exchanged between the canopy and the air above.

21.2.6 Sweeps and ejections at the canopy top

Chapter 9 classified the contributions to the momentum flux by the signs of the fluctuations. A *sweep* has $u' > 0$ and $w' < 0$: fast air moving down. An *ejection* has $u' < 0$ and $w' > 0$: slow air moving up. Both give a negative product $u'w'$ and both carry momentum downward. Over a flat surface the two contribute about equally, with ejections slightly larger above the roughness elements. In and just above a canopy, sweeps dominate: high-momentum air from above the canopy penetrates the crowns in short, intense events that carry most of the downward momentum flux, separated by longer quiet periods. Ejections of slow canopy air complete the exchange, and well above the canopy, at about twice the canopy height and more, they again carry the larger share.

The sweeps explain a measurement that is otherwise puzzling. In the illustrative forest the mean wind at mid-canopy is $0.84\,\mathrm{m\,s^{-1}}$, but a sweep can bring air with the speed of the canopy top, $2.8\,\mathrm{m\,s^{-1}}$, or more when the event coincides with a gust aloft, down to that height for a few seconds. A sensor at 10 m in the forest then records gusts of 3 to $4\,\mathrm{m\,s^{-1}}$, four times the mean (illustrative values). A low mean wind in a canopy does not imply low peak wind there.

The sweeps also explain why local-gradient closures, such as the mixing length of equation (21.3), perform poorly in canopies as a description of transport. A gradient closure assumes that the flux at a height is set by the gradient at that height, which holds when the eddies are small compared with the scale over which the gradient changes. The canopy-top eddies are about as large as the canopy, and a sweep carries momentum from above the canopy to deep inside it in one event, bypassing the local gradient. The clearest evidence is the trunk space of forests with an open understory: there the mean wind often has a secondary maximum, so that $\partial U/\partial z < 0$ below the crown, while the momentum flux is still downward. A gradient closure would put the flux upward, the wrong sign, and would need a negative eddy viscosity to reproduce the measurement. The exponential profile of Section 21.2.2 describes the mean wind in many canopies; it does not describe how the momentum gets there.

21.2.7 Roughness sublayer, displacement height and roughness length

Chapter 11 defined the *roughness sublayer*: the layer above the obstacles in which individual canopy elements still influence the flow, so that the wind and the turbulence vary with position at the same height and the log profile may fail. Its depth is about 2 to 5 h_c as a rough order of magnitude. Above a 20 m forest that is 40 to 100 m, and a sensor at 40 m may still be inside it. In the roughness sublayer the mixing-layer eddies of Section 21.2.5 make the mixing more efficient than surface-layer eddies of the same height, and the measured shear is smaller than the log value $u_*/[\kappa(z-d)]$; the matched profile of Figure 21.2, logarithmic right down to h_c, is therefore an idealization near the canopy top.

The *displacement height* d acquires its physical meaning in a canopy. In a dense forest most of the drag acts near the crowns, so the effective aerodynamic origin of the profile above is shifted upward, usually to $d \approx 0.6$ to $0.8\,h_c$, and the log-law height becomes $z-d$. The exponential model gives a check: the drag per unit volume is proportional to $e^{2\alpha(z/h_c-1)}$, and its centroid, the definition of d in Chapter 11, is

$$\frac{d}{h_c} = \frac{\int_0^1 s\, e^{2\alpha s}\,\mathrm{d}s}{\int_0^1 e^{2\alpha s}\,\mathrm{d}s} = \frac{e^{2\alpha}(2\alpha-1)+1}{2\alpha\,(e^{2\alpha}-1)},$$

which for $2\alpha = 4.8$ is $(121.5 \times 3.8 + 1)/(4.8 \times 120.5) = 0.80$: $d = 16$ m, at the dense end of the rule. The 14 m used for the same forest, $0.7\,h_c$, lies within the rule too; the difference of 2 m between two reasonable estimates shows how loosely d is determined by the canopy structure.

Above the roughness sublayer, in the inertial sublayer, the canopy can be represented by z_0 and d alone, and

$$U(z) = \frac{u_*}{\kappa}\ln\frac{z-d}{z_0}$$

becomes useful, but only sufficiently far above the canopy. Chapter 11 gives the values of z_0 and d for canopies, the methods of estimating them, and their dependence on the frontal area index; the rest of this chapter describes the flow that the two parameters summarize.

21.3 Vegetation canopies

Vegetation canopies differ in density, in the distribution of their foliage, in their seasonal cycle and at their edges. This section describes the parameters that measure canopy density, the changes of a canopy through the year, and the flow at forest edges and the fetch downwind of them.

21.3.1 Sparse against dense canopies

Canopy density matters as much as canopy height. A sparse forest, such as open woodland or a widely spaced plantation, lets the wind penetrate deep into the stand; a dense forest strongly suppresses the wind below the crown. Two forests of the same height can therefore behave very differently. With the same wind at the top, a sparse canopy with $\alpha = 1$ has 61 % of U_h at mid-height and 41 % at $0.1\,h_c$, and a dense one with $\alpha = 3$ has 22 % and 7 % (Figure 21.2(b)). Their roughness lengths and displacement heights differ too: the dense canopy has the higher d, and its z_0 may be larger or smaller, depending on which side of the maximum of z_0/h_c against frontal area it lies (Chapter 11).

The parameters that measure density are three. The *leaf area density* (m^2 of one-sided leaf area per m^3 of canopy, m^{-1}) is the amount of foliage per unit volume at each height. The *frontal area density* a (m^{-1}) is the area that the foliage, branches and stems present to the wind, per unit volume; it is what enters the drag, equation (21.1). The *porosity* is the open fraction of the canopy. Leaf area density and porosity can be measured, by harvesting or by optical methods; the frontal area density is usually derived from them.

21.3.2 Leaf area index

The *leaf area index* LAI (dimensionless, m^2 of leaf per m^2 of ground) is the one-sided leaf area of a canopy per unit ground area: the leaf area density integrated over the canopy depth. A value of 4 means that the leaves of the canopy, laid flat, would cover the ground four times. It is a common ecological parameter, measured by harvesting the leaves of a plot, by collecting the litter of a deciduous stand, by optical instruments that infer it from the fraction of light transmitted through the canopy, and over large areas from satellite reflectance. Typical values are 1 to 3 for grass and open woodland, 3 to 6 for crops and deciduous forest in leaf, and 5 to 10 for dense coniferous forest (for needles, one half of the total surface area).

A large LAI usually means a dense foliage canopy and strong attenuation. A common approximation sets the frontal area density equal to the leaf area density, $a \approx \mathrm{LAI}/h_c$ for uniform foliage, and folds the projection of the randomly oriented leaves onto the plane perpendicular to the wind (on average about one half) into an effective drag coefficient C_D of 0.1 to 0.3. The illustrative forest of this chapter does so: LAI = 4 over $h_c = 20\,\mathrm{m}$ gives $a = 0.2\,\mathrm{m}^{-1}$ with $C_D = 0.2$. But LAI alone does not determine the drag. Branches and stems, counted by the plant area index rather than the leaf area index, add frontal area; the clumping of leaves into shoots and crowns lets air pass between the clumps; the geometry of the crowns and their flexibility in strong wind change the frontal area that faces the flow. Two stands with the same LAI can have different α, z_0 and d.

21.3.3 Seasonal changes and crops

A deciduous forest has two aerodynamic states. In *leaf-on* the foliage gives a high drag and strong attenuation; in *leaf-off* only branches and stems remain, the drag is lower and the wind penetrates much deeper. Between the two states the attenuation coefficient falls from about 2 to 3 to about 1 (Table 21.1), so that the mid-canopy wind roughly doubles for the same wind at the top, from $e^{-1.2} = 0.30$ to $e^{-0.5} = 0.61$ of U_h in the illustrative case of $\alpha = 2.4$ against 1. The displacement height falls, because the drag then reaches deeper into the canopy. The roughness length changes less than the foliage suggests, and in either direction, because a canopy near the dense end of the z_0 curve becomes rougher, not smoother, when it thins. In temperate climates leaf-off falls in December to February in the Northern Hemisphere and in June to August in the Southern; in seasonally dry tropical climates the deciduous forests shed their leaves in the dry season instead. A static land-cover roughness, applied year-round, misses all of this.

Crops change faster still. A maize field is bare soil after sowing, a canopy 2 to 3 m tall a few months later, and stubble after harvest; its height, density, leaf area, z_0, d and α change through every growing season, and a second crop in the same year repeats the cycle. Agricultural roughness is time-varying. A field after harvest is aerodynamically very different from the same field at peak crop height: Chapter 11 found an 18 % lower 10 m wind over a mature crop with $z_0 = 0.25\,\mathrm{m}$ than over the bare field with $z_0 = 0.01\,\mathrm{m}$, for the same wind at 100 m. The calendar of the crop, not of the year, sets the season of the roughness, and it differs between the hemispheres and between crops.

21.3.4 Forest edges

A forest edge is an abrupt change of roughness and of canopy height, by two orders of magnitude in z_0 and by the full height of the trees in the obstacle layer. Flow entering a forest from open land meets the canopy drag at once and decelerates rapidly inside the canopy. Part of the air is deflected upward over the edge; at the canopy top a strong shear layer forms, the turbulence is enhanced, and an internal boundary layer of the forest grows downwind from the edge (Chapters 7 and 11).

The deceleration inside the canopy has a length scale that follows from the drag. Near the edge, where the air entering the canopy has not yet been resupplied from above, its momentum balance along the wind is approximately $\rho U\,\partial U/\partial x = -F_D = -\frac{1}{2}\rho\, C_D\, a\, U^2$, with x the distance into the forest. Dividing by ρU gives $\partial U/\partial x = -\frac{1}{2}\, C_D\, a\, U$, whose solution decays exponentially with the e-folding distance $2/(C_D\, a)$. For the illustrative forest that is $2/(0.2 \times 0.2) = 50\,\mathrm{m}$, two and a half canopy heights: within about 100 m of the edge the in-canopy wind has fallen to a seventh of its entry value and has adjusted to the interior profile. The estimate neglects the pressure gradient that the edge builds up and the momentum supplied from above, and it gives the order of magnitude only.

Flow leaving a forest does the reverse. It accelerates over the smoother surface downwind, but the forest's momentum deficit and the turbulence shed by the edge, a step 20 m high, persist far downstream, over ten to twenty canopy heights (Chapter 7), and the flow may separate from the canopy top and reattach on the clearing.

21.3.5 Fetch downwind of a forest

Consider a sensor 20 m above an open clearing, but only 100 m downwind of a forest edge with $h_c = 20\,\mathrm{m}$. The rough rule of Chapter 7, an internal boundary layer of depth $\delta \approx 0.1\,x$, puts the top of the clearing's internal boundary layer at about 10 m at the sensor, and the layer in equilibrium with the clearing at about 1 m. The sensor lies above the whole internal boundary layer: the air it measures has not yet felt the clearing at all, and it also lies in the wake of the edge, which extends 200 to 400 m. The wind there still retains the forest's influence. Assigning it the roughness length of the clearing is wrong; the upstream aerodynamic history of the air matters.

Figure 21.4 draws both transitions in side view, wind from the left, with a vertical scale exaggerated four times. Panel (a) is the entry into a forest: the in-canopy wind arrows shorten with the distance $2/(C_D a)$, the air above is deflected upward, and the forest's internal boundary layer grows from the edge. Panel (b) is the exit onto a clearing: the dashed line is the top of the clearing's internal boundary layer, $\delta = 0.1\,x$, the dotted line the top of its equilibrium layer, $0.01\,x$, the shaded region the wake of the edge, and the mast carries the sensor of this subsection.

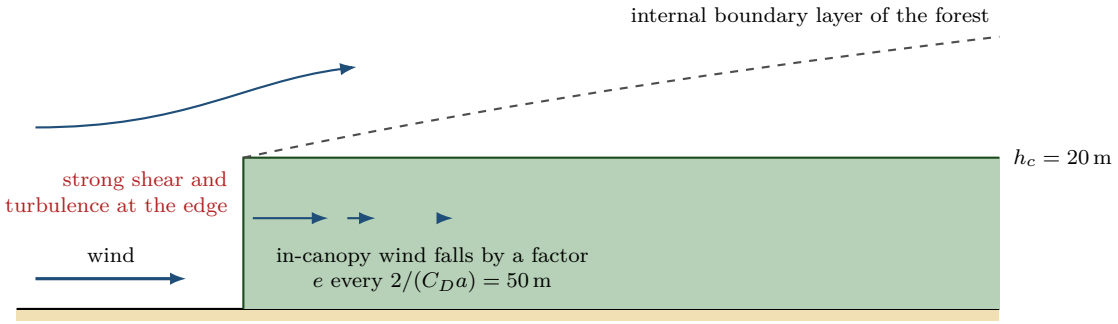
Panel (b) shows the sensor well above the dashed line, inside the shaded wake: by both criteria it measures forest-modified air. A roughness length for this sensor has to be taken from the forest and the edge for winds from the forest side, and from the clearing only for directions in which the clearing extends upwind over a fetch of about a hundred sensor heights, 2 km here.

21.4 Urban canopies

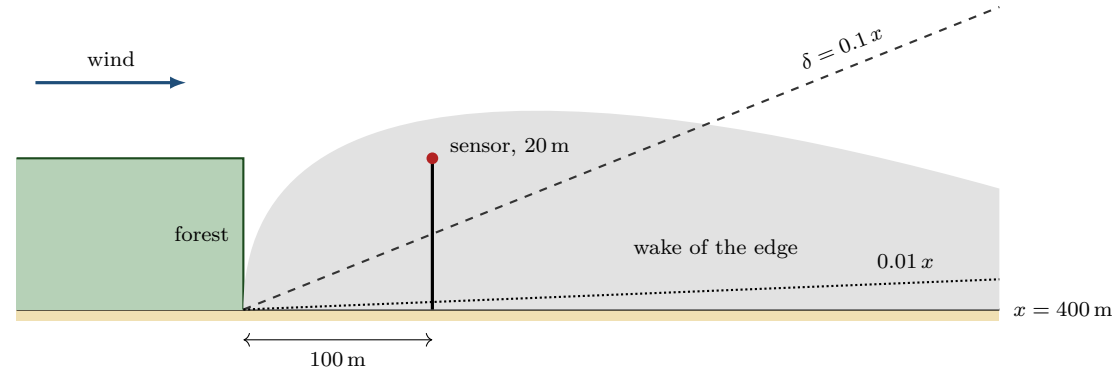
Cities are canopies of the same kind in concept, with more geometric complexity: the obstacles are large, impermeable, sharp-edged and arranged along streets. This section describes the layers of an urban canopy, the flow in street canyons, the three flow regimes that building spacing produces, the frontal area index and the directional roughness it implies, the local acceleration and downwash that buildings cause, and the separation of mechanical from thermal urban effects.

21.4.1 The urban canopy layer

An urban canopy contains buildings, streets, courtyards, trees and infrastructure such as bridges, masts and elevated roads. The wind penetrates this layer, along streets, through gaps and over low roofs, rather than flowing over a rough plane. The region from the ground to about the mean building height is the *urban canopy layer*: the air of the streets and courtyards, in direct



(a) field to forest



(b) forest to clearing

Figure 21.4: Forest edges (schematic), wind from the left; horizontal and vertical scales 1 to 4. (a) Entry into a forest with $C_D a = 0.04\,\mathrm{m}^{-1}$: in-canopy wind decaying with the e-folding distance $2/(C_D a) = 50\,\mathrm{m}$, upward deflection, the canopy-top shear layer, and the forest's internal boundary layer. (b) Exit onto a clearing: top of the clearing's internal boundary layer $\delta = 0.1\,x$ (dashed), top of its equilibrium layer $0.01\,x$ (dotted), the wake of the edge (shaded, ten to twenty canopy heights long), and a sensor at 20 m, 100 m from the edge.

contact with walls and roads, where the flow is set by the local geometry and varies from one street to the next.

Above the roofs the wind still feels individual buildings: towers shed wakes, roof edges separate the flow, and the wind at one point differs from that at another point at the same height. This layer, up to about 2 to 5 times the mean building height, is the urban roughness sublayer; in urban climatology the name usually covers the urban canopy layer too, from the ground up, and this chapter uses it for the part above the roofs, as Chapter 11 did for vegetation. Above it, an inertial sublayer may eventually emerge, in which the city acts through z_0 and d alone and the log profile holds. Over a district of uniform houses it begins a few tens of meters above the ground; over a center of towers of varied heights the roughness sublayer can reach the top of the surface layer, and the inertial sublayer is absent.

21.4.2 Street canyons

A *street canyon* is a street bounded on both sides by continuous rows of buildings. Its geometry is described by its *aspect ratio* h_c/W, the building height divided by the street width W (m). The flow in it depends on the aspect ratio and on the direction of the wind above the roofs. With the wind across the street, the air in a narrow canyon turns into a recirculating vortex driven by the flow over the roofs: at street level it blows against the roof-level wind, toward the upwind wall. With the wind along the street, the canyon channels the flow, and at its ends and at intersections the wind can accelerate. With the wind oblique, the two combine into a helical flow along the canyon. Corners produce strong local acceleration; the lee of a wall or a courtyard produces sheltered zones of weak wind.

Wind measured at street level can therefore be completely unrepresentative of the wind above the roofs: weaker by a factor of two or more, from a different direction, or reversed, and changing with the direction above in a way set by the street pattern rather than by the weather. A street-level record answers questions about that street; it cannot stand for the wind of the district.

21.4.3 Flow regimes against building spacing

How the flow interacts with an array of buildings depends mainly on their spacing relative to their height. For long rows of buildings across the wind, three regimes are recognized. Figure 21.5 draws them in side view, wind from the left, with buildings of the same height h_c and three spacings W; the dashed outlines are wakes and the circular arrows recirculating vortices. Table 21.2 lists the approximate ranges of the aspect ratio for each regime and its properties; the thresholds are approximate, and they shift for buildings of other shapes, such as cubes, and for staggered arrays.

In *isolated-roughness flow* the buildings are far enough apart for each wake to develop and reattach to the ground before the next building; each building adds its own drag. In *wake-interference flow*, at intermediate spacing, the wake of one building reaches the next and the wakes of successive buildings interact strongly; the flow between them is complex and unsteady. In *skimming flow*, in dense arrays, the flow passes largely over the building tops while a recirculating vortex occupies each street canyon; the above-roof flow and the street-level flow become partly decoupled, and the air in the streets is renewed only intermittently. The regimes are the urban form of the curve of z_0/h_c against frontal area index in Chapter 11: rising in the isolated regime, reaching its maximum in the wake-interference regime, and falling in the skimming regime. They explain why obstacle density, not only obstacle height, sets the drag of a city.

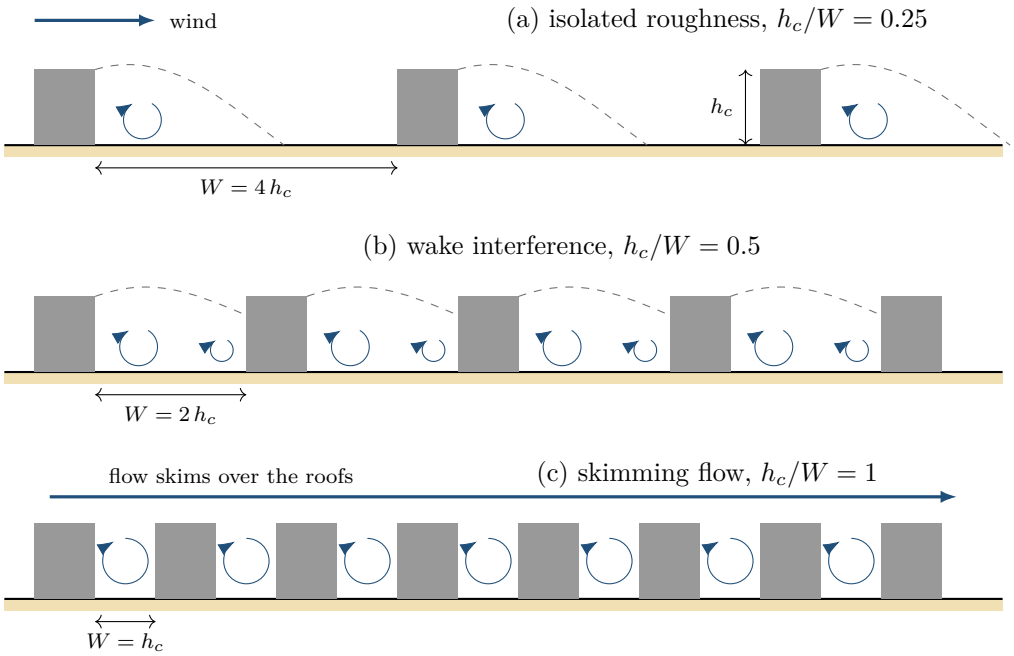


Figure 21.5: Flow regimes over rows of buildings of height h_c across the wind (schematic), wind from the left. (a) Isolated roughness, $W = 4\,h_c$: each wake reattaches before the next building. (b) Wake interference, $W = 2\,h_c$: each wake reaches the next building. (c) Skimming flow, $W = h_c$: the flow passes over the roofs and a vortex fills each street. Dashed: wakes; circular arrows: recirculation.

Table 21.2: Flow regimes over long rows of buildings across the wind. Thresholds approximate.

Regime	h_c/W	W/h_c	Flow	Street-level air and drag
Isolated roughness	below 0.3	above 3.3	each building's wake develops independently and reattaches before the next	well ventilated; drag grows in proportion to the number of buildings
Wake interference	0.3 to 0.65	1.5 to 3.3	each wake reaches the next building and interacts with its upwind vortex; complex secondary flows	intermittent exchange; drag near its maximum
Skimming flow	above 0.65	below 1.5	the flow passes over the roofs; a stable vortex fills each street	partly decoupled from the air above; z_0 falls, d rises

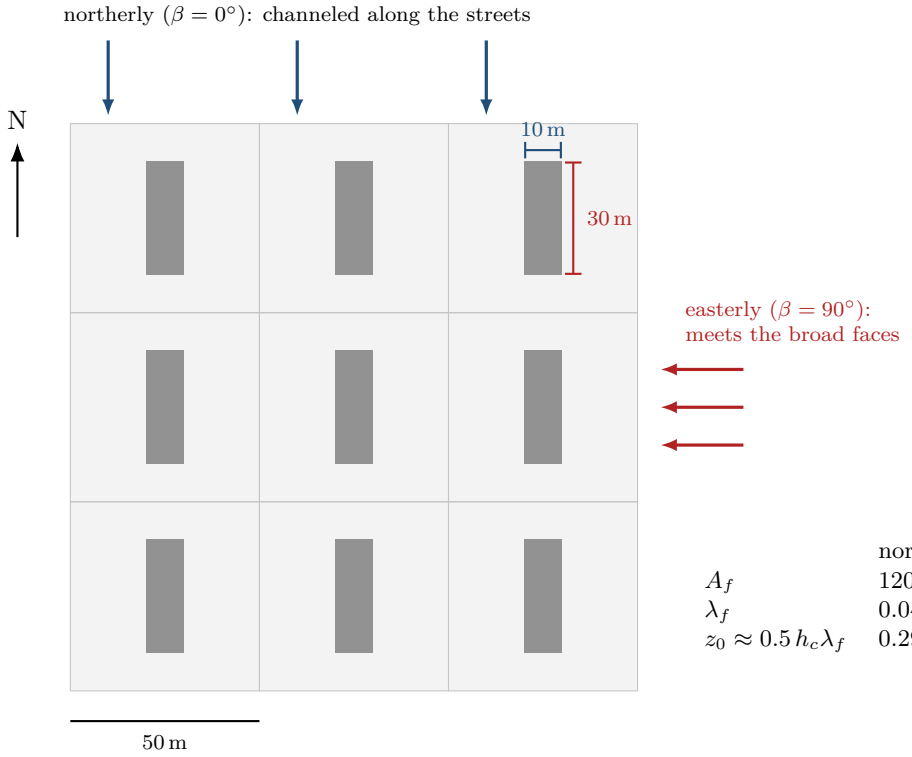
21.4.4 Frontal area index and directional urban roughness

The *frontal area index* is

$$\lambda_f = \frac{A_f}{A_T}, \tag{21.8}$$

the projected frontal area A_f of the obstacles, the area they present to a wind from a given direction, divided by the ground area A_T on which they stand (dimensionless). It is computed from building heights and footprints, from a building database or from airborne laser scanning. A higher frontal area index typically means more drag, up to the maximum of z_0 at λ_f of about 0.2 to 0.4; the rule $z_0 \approx 0.5\, h_c\, \lambda_f$ of Chapter 11 applies for sparse arrays, λ_f below about 0.2. Unlike the leaf area index, λ_f depends strongly on the wind direction, because the faces presented to the wind depend on it.

Figure 21.6 is a plan view of an illustrative district, north at the top. Buildings $h_c = 12\,\mathrm{m}$ tall have footprints of 10 m east to west by 30 m north to south, one on each plot of $50\,\mathrm{m} \times 50\,\mathrm{m}$, so that the rows of buildings and the streets between them run north to south. The arrows show a northerly and an easterly wind; the brackets mark the width of the face each wind meets. The geometry and the numbers hold in either hemisphere.



	northerly	easterly
A_f	$120\,\mathrm{m}^2$	$360\,\mathrm{m}^2$
λ_f	0.048	0.144
$z_0 \approx 0.5\, h_c \lambda_f$	0.29 m	0.86 m

Figure 21.6: Plan view of an illustrative district (valid in either hemisphere), north at the top: buildings 12 m tall with footprints 10 m × 30 m, long side north to south, one per 50 m × 50 m plot. A northerly wind meets the 10 m faces and is channeled along the north–south streets; an easterly wind meets the 30 m faces. Table: frontal area per plot, frontal area index and roughness length from the sparse-array rule.

For one plot, $A_T = 2500\,\mathrm{m}^2$. A northerly wind meets a face 10 m wide and 12 m tall, $A_f = 120\,\mathrm{m}^2$ and $\lambda_f = 120/2500 = 0.048$; an easterly wind meets a face 30 m wide, $A_f = 360\,\mathrm{m}^2$ and $\lambda_f = 0.144$. Both are in the sparse range, and the rule gives $z_0 \approx 0.5 \times 12 \times 0.048\,\mathrm{m} = 0.29\,\mathrm{m}$ for the northerly and $0.5 \times 12 \times 0.144\,\mathrm{m} = 0.86\,\mathrm{m}$ for the easterly. The district is three times rougher for the easterly wind. The northerly wind is channeled between the rows; the easterly strikes the broad building faces directly.

The consequence for the wind is computed as in Chapter 11, with the same wind aloft, $10\,\mathrm{m\,s^{-1}}$ at 150 m, in neutral air, and an illustrative displacement height $d = 4\,\mathrm{m}$ (a third of h_c, for a sparse array) for both directions. With $u_* = \kappa U(150\,\mathrm{m})/\ln[(150-d)/z_0]$,

$$z_0(0^\circ) = 0.29\,\mathrm{m}: \qquad u_* = \frac{4}{\ln(146/0.29)}\,\mathrm{m\,s^{-1}} = \frac{4}{6.22}\,\mathrm{m\,s^{-1}} = 0.64\,\mathrm{m\,s^{-1}},$$
$$U(40\,\mathrm{m}) = 10\,\mathrm{m\,s^{-1}} \times \frac{\ln(36/0.29)}{6.22} = 7.75\,\mathrm{m\,s^{-1}};$$
$$z_0(90^\circ) = 0.86\,\mathrm{m}: \qquad u_* = \frac{4}{\ln(146/0.86)}\,\mathrm{m\,s^{-1}} = \frac{4}{5.13}\,\mathrm{m\,s^{-1}} = 0.78\,\mathrm{m\,s^{-1}},$$
$$U(40\,\mathrm{m}) = 10\,\mathrm{m\,s^{-1}} \times \frac{\ln(36/0.86)}{5.13} = 7.27\,\mathrm{m\,s^{-1}}.$$

The easterly carries $(0.78/0.64)^2 = 1.47$ times the stress and a 6 % weaker wind at 40 m, a height above the roofs at which the log profile is at best approximate. The roughness length of a city is a function of the wind direction, $z_0 = z_0(\beta)$, with β the direction from which the wind blows, and the variation is larger in cities than over vegetation because buildings are elongated, aligned along streets and impermeable.

21.4.5 Building-induced acceleration and downwash

Not all buildings slow the flow. Between structures the wind can accelerate, by channeling along a street aligned with the wind, by the pressure difference between the windward and the lee side of a building, which drives air through passages and gaps, and by constriction, where continuity forces the air diverted around a group of buildings through the openings between them. Flow around the windward corners of a building separates and accelerates sharply, and the corner streams can reach 1.5 to 2 times the undisturbed wind at the same height (illustrative). Urban roughness increases the aggregate drag of a city and can create local speed-up at the same time; both are true, at different scales.

Tall buildings add *downwash*: the downward redirection of higher-momentum air along the windward face of a building. The approach wind increases with height, and with it the stagnation pressure that it exerts on the windward face, $p_\infty + \frac{1}{2}\rho U(z)^2$, with p_∞ the undisturbed static pressure. The pressure on the face is therefore highest at about two thirds to three quarters of the building height, the stagnation point, and decreases downward. Below the stagnation point the vertical pressure gradient along the face drives the air downward; it reaches the ground in front of the building, rolls into a standing vortex at its base and escapes around the corners at high speed. For an illustrative tower 100 m tall in an approach wind of $12\,\mathrm{m\,s^{-1}}$ at 100 m and $6\,\mathrm{m\,s^{-1}}$ at 10 m, the stagnation pressures differ by $\frac{1}{2} \times 1.2 \times (12^2 - 6^2)\,\mathrm{Pa} = 64.8\,\mathrm{Pa}$, the dynamic pressure of a wind of $\sqrt{2 \times 64.8/1.2}\,\mathrm{m\,s^{-1}} = 10.4\,\mathrm{m\,s^{-1}}$. That sets the scale of the downwash: winds near the base of a tower can be much stronger than the wind the same place would have without it, which is why pedestrian-wind studies are made around tall towers.

Figure 21.7 draws the mechanism in side view, wind from the left. The arrows on the left are the approach wind at four heights, their lengths proportional to the speed; the tall building is 100 m high; the dot on its windward face is the stagnation point; the arrows along the face show the flow splitting there, upward and over the roof above it, downward below it; the circular arrow is the standing vortex at the base and the arrow at the ground the high near-ground wind.

The figure shows why the near-ground wind at the foot of a tower is set by the wind at a large fraction of the tower's height, not by the wind at street level. The same building that adds drag to the district, lowering the wind averaged over it, raises the wind at a few points around its base, and a sensor or a pedestrian at those points experiences the local, not the average, effect.

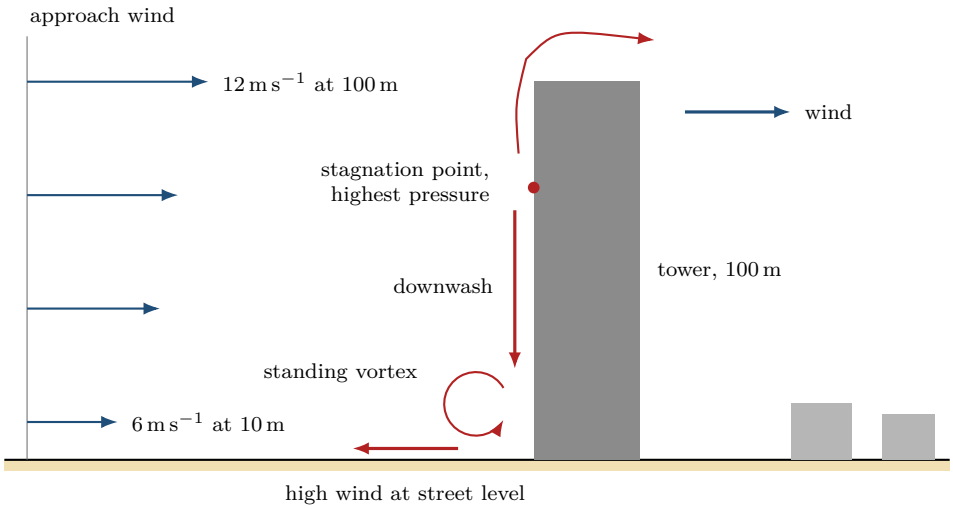


Figure 21.7: Downwash at a tall building (schematic), wind from the left. Approach wind at 10, 40, 70 and 100 m, arrow lengths proportional to the speed (illustrative: 6, 8.8, 10 and 12 m s^{-1}). The stagnation pressure $\frac{1}{2}\rho U^2$ on the windward face is largest near the stagnation point, at about 0.7 of the building height; below it the face pressure gradient drives air down to the ground, where it forms a standing vortex and a strong flow near the ground.

21.4.6 Thermal against mechanical urban effects

Cities also heat differently from the land around them. Chapter 19 described the urban heat island and the urban breeze it drives. Urban wind therefore includes two kinds of effects. *Mechanical canopy effects* come from the geometry: drag, channeling, wakes, corner streams, downwash, and the decoupling of the street air in skimming flow. *Thermal urban effects* come from the heat: the heat island lowers the surface pressure over the city and drives a convergent inflow on calm nights, and it keeps the urban boundary layer near neutral or unstable at night while the countryside around it is stable, so that more momentum is mixed down to the ground in the city.

The two should not be conflated. A city may mechanically slow the regional wind, locally accelerate the flow in some streets, and thermally generate a convergence toward its center, all at once. They differ in their dependence on the weather: the mechanical effects scale with the wind speed and act in every condition, whereas the thermal effects are strongest in light winds and clear nights and fade as the wind increases. A difference between an urban and a rural station that grows with the wind speed points to the mechanical effects; one that appears on calm, clear nights points to the thermal ones. On a calm night the mixing of the urban boundary layer can even make the near-surface wind in a city stronger than in the stable countryside, the reverse of what the drag alone would predict.

21.5 Representing canopies in models

A model represents a canopy in one of a few ways, from two numbers in the lower boundary condition to the full geometry of every building. This section states when a single roughness length is enough, compares the strategies, and describes the porous-canopy drag used in computational fluid dynamics and the urban canopy models of weather models.

21.5.1 When one roughness length is enough

A weather model may represent an urban grid cell with $z_0 = 1.5\,\mathrm{m}$ and $d = 10\,\mathrm{m}$. That may be adequate for the large-scale momentum exchange: the stress the cell exerts on the boundary layer, the wind well above the roofs, the turning of the wind toward low pressure. With $u_* = 0.8\,\mathrm{m\,s^{-1}}$ the cell's wind at 50 m is $(0.8/0.4)\ln[(50-10)/1.5]\,\mathrm{m\,s^{-1}} = 2 \times 3.28\,\mathrm{m\,s^{-1}} = 6.57\,\mathrm{m\,s^{-1}}$, a reasonable estimate of the wind averaged over the cell at that height, if 50 m lies above the roughness sublayer.

But the two parameters cannot give the wind next to a specific building. Below $d+z_0 = 11.5\,\mathrm{m}$ the profile is not defined, and the street canyon, the corner stream and the downwash of Section 21.4 do not exist in it. The same holds in a forest: z_0 and d give the wind above the roughness sublayer, not inside the stand. The division of labor is

$$z_0,\ d \ \Rightarrow\ \text{aggregate flow}, \qquad \text{explicit geometry} \ \Rightarrow\ \text{local flow}.$$

A forecast of the wind at a point inside a canopy, whether a sensor in a street or a conductor among trees, needs one of the richer representations below.

21.5.2 Parameterized against explicit canopies

There are two broad strategies. A *parameterized canopy* represents the drag statistically, by z_0 and d, or by drag coefficients and area densities distributed over height, without locating any individual obstacle. An *explicit canopy* represents the individual trees or buildings in the geometry of a computational fluid dynamics (CFD) model, with the flow resolved around each. The choice depends on the scale and the purpose: the grid spacing a model can afford, and the question it is meant to answer.

Table 21.3 compares four representations in increasing order of detail. Its columns give what each represents, the grid on which it is typically used, what it gives and what it misses. Chapter 27 treats the surface representation of weather models and Chapter 29 the CFD models in depth.

Table 21.3: Four representations of a canopy, in increasing order of detail. Grid spacings indicative.

Representation	What is represented	Typical grid	Gives	Misses
Roughness length and displacement height	canopy as a lower boundary, z_0 and d	weather model, 1 to 25 km	stress and wind above the roughness sublayer	in-canopy wind, roughness sublayer, local flow
Distributed drag (porous canopy)	$a(z)$ and C_D in the lowest levels	levels about $h_c/10$ apart	in-canopy mean profile, canopy-top shear, edges if resolved	individual trees and gaps, street-level detail
Urban canopy model	street geometry statistics, heat budgets of roofs, walls and roads, drag	weather model, 0.5 to 5 km	urban temperature, turbulence and wind averaged over the streets	a particular street or building
Explicit geometry	each building or tree in the mesh	CFD, about 1 m near the obstacles	local flow, channeling, corner streams, downwash	needs inflow from a larger model; small domains; cost

The table is ordered by cost as well as detail. A roughness length costs nothing and covers a continent; explicit geometry costs hours of computing for a few city blocks. The detail is

worth its cost only where the question is local, and a model that resolves a canopy explicitly still depends on the coarser model that supplies its inflow.

21.5.3 Porous-canopy drag in CFD

Vegetation is too detailed to resolve leaf by leaf, so CFD models represent it as a porous momentum sink: a region of the flow in which each grid cell carries the drag of the foliage it contains. The *porous-canopy model* adds to the momentum equation the force per unit volume

$$\mathbf{F}_\mathrm{c} = -\tfrac{1}{2}\,\rho\, C_D\, a\, |\mathbf{u}|\, \mathbf{u}, \tag{21.9}$$

with $\mathbf{u} = (u, v, w)$ the local mean velocity vector and $|\mathbf{u}|$ its magnitude. It is the vector form of equation (21.1): its magnitude is $\frac{1}{2}\rho C_D a |\mathbf{u}|^2$, and the product $|\mathbf{u}|\mathbf{u}$ makes it act against the local flow in any direction, including the vertical flow at an edge. The frontal area density can vary in space, $a(x, y, z)$, so a stand, a hedgerow, a single crown or a clearing can be given its own drag.

The drag also changes the turbulence. It converts the kinetic energy of the mean flow into wakes of the size of leaves and shoots, which dissipate quickly; turbulence models of the kind used in CFD, such as the k-epsilon model (whose k is the turbulent kinetic energy, written e in this book), add source and sink terms for e and its dissipation inside the canopy (Chapter 29). To resolve the exponential decay of the illustrative forest, whose wind falls by a factor e over $h_c/\alpha = 8.3\,\mathrm{m}$ and whose drag over half that distance, the mesh needs vertical spacings of about 2 m, a tenth of the canopy height, through the canopy. The porous model then reproduces the in-canopy profile, the canopy-top shear layer and the edge flow of Section 21.3.4 without resolving any leaf or branch.

21.5.4 Urban canopy models

Weather models may represent cities by urban canopy parameterizations instead of a large roughness length. Such a scheme describes each urban grid cell by statistics of its geometry, such as the mean building height, the street width, the fraction of the cell covered by roofs and the street orientations, and it computes separate heat budgets for the roofs, the walls and the roads, the drag of the buildings, and the radiation trapped between the walls of the street canyons. Single-layer schemes treat the urban canopy as one layer below the lowest model level; multilayer schemes distribute the drag and the heat exchange over several model levels within and above the buildings, in the manner of the porous-canopy drag.

These schemes can improve the model's urban temperature, its turbulence and its urban wind, and they produce the heat island and its effects on stability that a roughness length cannot. But they remain parameterizations, not explicit building-scale CFD. Their streets are statistical: they represent the average canyon of a cell, not the street in which a sensor stands, and their wind is the average over the canopy layer of the cell. A local question, such as the wind at the foot of a tower or along a particular line route through a district, still needs explicit geometry, or a measurement.

21.6 Canopies and wind measurements

The flow near a canopy makes siting a measurement critical. This section describes the turbulence that a sensor near a forest or a building records, works the example of a sensor beside a tree line, and separates the accuracy of an instrument from the representativeness of its location.

21.6.1 Turbulence near canopies

A sensor near a forest or a building may experience high turbulence intensity, large directional variability, wake effects and non-Gaussian gusts. The turbulence intensity rises toward and into a canopy, because the standard deviation of the wind stays of the order of the friction velocity while the mean wind falls. For the illustrative forest, with illustrative values of the ratio σ_u/u_*,

$$\begin{aligned} z = 40\,\mathrm{m}: &\quad \sigma_u \approx 2.4\,u_* = 1.92\,\mathrm{m\,s^{-1}}, \quad U = 5.71\,\mathrm{m\,s^{-1}}, \quad \mathrm{TI} = 0.34; \\ z = 20\,\mathrm{m}: &\quad \sigma_u \approx 2.0\,u_* = 1.60\,\mathrm{m\,s^{-1}}, \quad U = 2.77\,\mathrm{m\,s^{-1}}, \quad \mathrm{TI} = 0.58; \\ z = 10\,\mathrm{m}: &\quad \sigma_u \approx 1.0\,u_* = 0.80\,\mathrm{m\,s^{-1}}, \quad U = 0.84\,\mathrm{m\,s^{-1}}, \quad \mathrm{TI} \approx 1.0, \end{aligned}$$

against typical values of 0.15 to 0.2 at 10 m over open grass. Inside the canopy the wind direction fluctuates widely, and in the wake of a building or a crown it can reverse.

The gusts are not Gaussian. Because sweeps carry fast air down in short, strong events, the distribution of u' inside and just above a canopy is skewed toward large positive values and that of w' toward large negative values, with heavy tails. A gust estimate made from the mean and standard deviation under a Gaussian assumption underestimates the peaks there. Statistics of gusts and extremes are the subject of Chapter 24; here the point is that the canopy changes their shape, not only their size.

21.6.2 A sensor beside a tree line

Suppose a sensor stands 15 m from a tree line 20 m tall, a distance of $0.75\,h_c$. When the wind blows from the trees, the sensor is deep inside their near wake, which extends ten to twenty tree heights downwind: it records a reduced mean wind, a high turbulence intensity, gusts from sweeps and eddies shed at the tree tops, and a direction deflected by the recirculation behind the trees. When the wind blows toward the trees, the sensor is in the region of upwind blockage, where the approaching air is slowed and lifted over the obstacle. In both cases the record depends on the wind direction through the geometry of the trees.

The sensor may measure the local wake accurately. But if the purpose is the regional wind over open terrain, for a model evaluation, a wind resource estimate or the rating of a line that crosses open country, it is a bad representative location: no calibration of the instrument removes the effect of the trees. Rules for the distance from obstacles and for exposure belong to Chapter 23; the flow that makes them necessary is the canopy and wake flow of this chapter.

21.6.3 Accuracy against representativeness

The tree-line example separates two properties of a measurement. The *accuracy* of an instrument is how closely its reading matches the true wind at the point where it stands; it is set by calibration, response and mounting. The *representativeness* of a measurement is how closely the true wind at that point matches the wind the user needs: the wind over open terrain at a standard height, the wind averaged over a model grid cell, or the wind at a conductor some distance away. A sensor can be technically accurate and meteorologically unrepresentative,

$$\text{instrument accuracy} \neq \text{measurement representativeness}.$$

Near canopies the second error usually dominates the first. A well-calibrated anemometer reads the wind in a street canyon or in the wake of a forest edge to within a few percent, and that wind differs from the open-terrain wind by tens of percent, with a sign and size that change with the wind direction. The distinction runs through the next chapters, which first ask what wind instruments actually measure and how accurately, beginning with the wind measurements of Chapter 22.

21.7 What to retain

Definition 21.1 (Canopy flow)**.** Vegetation and cities are not simply rough surfaces but three-dimensional momentum sinks: the background flow meets a canopy drag distributed through the obstacle layer, which produces a shear layer at the canopy top and wakes and coherent turbulence within and above it; only sufficiently far above the canopy can the whole system be simplified into a roughness length z_0 and a displacement height d.

Table 21.4 lists the terms of the chapter, their meaning, their units and the subsection that defines each.

Table 21.4: The terms of the chapter and where each is defined.

Term	Meaning	Units	Defined in
Canopy flow	atmospheric flow within and above a layer of obstacles	–	21.1
Canopy height h_c	characteristic height of the vegetation or buildings	m	21.1.2
Canopy drag F_D	distributed momentum loss caused by the canopy elements, $\frac{1}{2}\rho C_D a U^2$ per unit volume	N/m^3	21.1.4
Frontal area density a	frontal area of the obstacles per unit volume of canopy	m^{-1}	21.1.4
Attenuation coefficient α	e-foldings of the in-canopy wind from top to ground, $U = U_h e^{-\alpha(1-z/h_c)}$	–	21.2.2
Canopy-top shear layer	layer of strongest shear, with an inflection point, at the canopy top; behaves like a plane mixing layer	–	21.2.5
Leaf area index LAI	one-sided leaf area per unit ground area	–	21.3.2
Urban canopy layer	layer from the ground to about the mean building height	m (depth)	21.4.1
Street canyon	street bounded by buildings, described by its aspect ratio h_c/W	–	21.4.2
Skimming flow	dense arrays: flow passes over the roofs, a vortex fills each street	–	21.4.3
Wake interference	intermediate spacing: wakes of successive buildings interact	–	21.4.3
Isolated roughness	sparse obstacles with relatively independent wakes	–	21.4.3
Frontal area index λ_f	projected frontal area of the obstacles per unit ground area, for a given wind direction	–	21.4.4
Downwash	downward redirection of higher-momentum air along the windward face of a tall building	–	21.4.5
Porous-canopy model	representation of vegetation by a distributed drag $-\frac{1}{2}\rho C_D a \lvert\mathbf{u}\rvert\mathbf{u}$	N/m^3	21.5.3

21.8 Exercises

Exercise 21.1. A maize crop has $h_c = 2.5\,\mathrm{m}$, a uniform leaf area index LAI $= 4$ and an effective element drag coefficient $C_D = 0.25$. Above it, $u_* = 0.35\,\mathrm{m\,s^{-1}}$ and the wind at the canopy top is $U_h = 1.12\,\mathrm{m\,s^{-1}}$. (a) Compute the frontal area density, taking $a = \mathrm{LAI}/h_c$, and the attenuation coefficient from equation (21.6). (b) Compute the wind at 1.25 m and at 0.5 m, and the fraction of the stress that reaches the ground. (c) Compute the in-canopy mixing length, the displacement height implied by equation (21.7) and the roughness length for which the log profile gives U_h at the canopy top; compare d/h_c and z_0/h_c with the rules of thumb. (d) Compute the drag per unit volume at the canopy top with $\rho = 1.2\,\mathrm{kg\,m^{-3}}$.

Exercise 21.2. A district has buildings 18 m tall with footprints 12 m east to west by 36 m north to south, one per plot of 60 m × 60 m. The projected width of a building for a wind from direction β is $12\,\mathrm{m}\,|\cos\beta| + 36\,\mathrm{m}\,|\sin\beta|$. (a) Compute λ_f and the sparse-array roughness length for northerly and easterly winds. (b) A site in the district lies at 30°S. The geostrophic wind blows from 340° and friction turns the surface wind by 20° toward low pressure. On which side of the geostrophic flow does the low pressure lie, from which direction does the surface wind blow, and what are λ_f and z_0 for it? (c) Repeat (b) for the same district at 30°N. (d) With $10\,\mathrm{m\,s^{-1}}$ at 200 m in neutral air and $d = 6\,\mathrm{m}$, compute u_* and the wind at 60 m for the two cases, and explain why the hemisphere changes the wind through the building geometry.

Exercise 21.3. A forest 25 m tall has LAI = 4 ($a = \mathrm{LAI}/h_c$) and $C_D = 0.2$. (a) Compute the e-folding distance of the in-canopy wind entering the forest from a field, and the distance over which it falls to a tenth of its entry value, by the estimate of Section 21.3.4. (b) A mast stands in a clearing 150 m downwind of the forest edge, with sensors at 10 and 30 m. Using $\delta \approx 0.1\,x$ and an equilibrium layer of $0.01\,x$, say which sensor lies in the clearing's internal boundary layer and which in its equilibrium layer, and whether either lies in the wake of the edge. (c) What fetch of clearing would the 30 m sensor need to measure a wind in equilibrium with the clearing? (d) For a wind from the forest, which roughness length would be appropriate for each sensor?

Exercise 21.4. A deciduous forest 20 m tall at 35°S has $\alpha = 2.4$ in leaf-on and $\alpha = 1.0$ in leaf-off; for the same synoptic wind the canopy-top wind is $2.8\,\mathrm{m\,s^{-1}}$ in leaf-on and $3.5\,\mathrm{m\,s^{-1}}$ in leaf-off (illustrative). A sensor is mounted at 8 m inside the stand. (a) In which months is the stand in leaf-off, and in which would it be at 35°N? (b) Compute the mean wind at the sensor in each season. (c) In leaf-on, $\sigma_u = 0.9\,\mathrm{m\,s^{-1}}$ at the sensor; compute the turbulence intensity, and the ratio to the mean of a $3\,\mathrm{m\,s^{-1}}$ sweep gust. (d) Is the record representative of the open-terrain wind at 10 m? State the two kinds of error that separate the reading from that wind, and which of them a calibration of the anemometer removes.

Chapter 22

Wind Measurements

22.1 What a wind sensor reports

Earlier chapters have used measured winds throughout: cup anemometers on masts to fit logarithmic profiles, sonic anemometers to compute fluxes and the friction velocity, lidar and tower profiles to locate the nighttime wind maximum. This chapter turns to the instruments themselves. Its question is

what does a wind sensor actually measure, and what can go wrong?

For near-surface wind, the quality of a measurement depends on much more than the accuracy of the instrument. Eight attributes decide what a recorded wind value means: the type of sensor; its sampling rate; the averaging interval of the reported value; the sensor's response time; the way it is mounted; its exposure to the surrounding terrain and obstacles; the distortion of the flow by the mounting structure; and the representativeness of the measurement point for the quantity the value is used for. The chapter follows them in order: what a sensor reports and in which conventions; the instruments that measure at a point; sampling, response and averaging; mounting and flow distortion; the instruments that measure a profile above a tower; and finally the errors, the quality-control checks and the complete description that turns a number into a usable wind value. Exposure enters here only as one item of that description; the next chapter treats it.

Jargon: anemometer, wind vane, in-situ, remote sensing, sampling rate, averaging interval, response time, flow distortion, exposure, representativeness error

An *anemometer* is an instrument that measures wind speed or wind velocity; a *wind vane* is an instrument that measures wind direction. An *in-situ* instrument measures the air at the place where the instrument stands; a *remote-sensing* instrument measures air at a distance, from light, sound or radio waves scattered back to it. The *sampling rate* f_s, in hertz (samples per second), is the number of values a data logger records per second. The *averaging interval*, in seconds or minutes, is the period over which the recorded samples are combined into one reported value, such as a ten-minute mean. The *response time*, in seconds, is the time a sensor needs to follow a change of the wind; it is a property of the physical sensor, not of the logger. *Flow distortion* is the modification of the measured flow by the sensor's own body and by the structure that holds it. *Exposure* is the situation of the sensor relative to the terrain, obstacles and surface cover around it. The *representativeness error* is the part of the difference between a measured value and the quantity it is compared with that comes from their different spatial or temporal scales, not from an error of the instrument.

Key idea

A wind value is a statistic of a three-dimensional vector, produced at one point by one instrument with its own response, sampled, averaged and mounted in a particular way. Its accuracy, how well it describes the air at that point, and its representativeness, how well that point stands for the quantity it is used for, are separate properties, and the second is often the larger source of error.

22.1.1 Wind as a vector

The air velocity at a point is a three-dimensional vector, (u, v, w), with u the eastward, v the northward and w the upward component. Its horizontal part is the wind vector $\mathbf{V} = (u, v)$, and the horizontal speed is $U = \sqrt{u^2 + v^2}$. Ideally a wind measurement would deliver all three components, at a rate fast enough to resolve the turbulence. Most standard weather stations deliver two derived quantities instead: the horizontal speed U and the horizontal direction β, each as an average over a few minutes.

Different instruments therefore measure different parts of the flow. A cup anemometer measures the horizontal speed U, a scalar, and nothing about direction or vertical motion. A wind vane measures the direction β. A propeller anemometer measures the component of the velocity along its own axis. A sonic anemometer measures the three components u, v and w. A Doppler lidar or sodar measures the component along its beam, and a radiosonde the displacement of a balloon over time. Two instruments at the same place can agree perfectly about the air and still report different numbers, because they report different quantities. Before two wind values are compared, both must be reduced to the same quantity: the same component or the same speed, at the same height, over the same averaging interval.

The vertical component deserves a separate remark. Its mean near flat ground is small, of the order of millimeters to a few centimeters per second, while its turbulent fluctuations have standard deviations of tens of centimeters per second (about $1.25\,u_*$ in neutral conditions, Chapter 8). Only an instrument that measures w itself, fast enough to follow those fluctuations, can give the vertical fluxes of Chapter 9; a mean of w is almost never a useful product of a wind measurement, and a large measured mean of w is usually a symptom of a mounting error (Section 22.4.4).

22.1.2 The direction convention

Meteorological wind direction is the direction *from* which the wind blows, in degrees measured clockwise from true north. A north wind blows from the north toward the south, $\beta = 0°$ or $360°$; a west wind blows from the west toward the east, $\beta = 270°$. The convention is the same in both hemispheres: it refers to geographic north, not to the pole that is nearer.

The convention is easy to confuse with the direction of a vector in mathematics. In Cartesian coordinates, the direction of a vector is where it points, given as an angle α_m measured counterclockwise from the positive x axis, east. Meteorology names the source instead. If the air moves eastward, $u > 0$ and $v = 0$: the vector points east, its mathematical angle is $\alpha_m = 0°$, and its meteorological direction is $\beta = 270°$, because the air comes from the west.

The general relation follows in two steps. The vector points toward the compass bearing $\beta + 180°$, the side opposite to its source. A compass bearing B, measured clockwise from north, corresponds to the mathematical angle $90° - B$, measured counterclockwise from east. Hence

$$\alpha_m = 90° - (\beta + 180°) = 270° - \beta \pmod{360°}. \tag{22.1}$$

For $\beta = 270°$ it gives $\alpha_m = 0°$, east, as above; for a north wind, $\beta = 0°$, it gives $\alpha_m = 270°$, a vector pointing south. A third convention, the direction toward which the flow goes, measured clockwise from north, is used for ocean currents and appears in some data files; it differs from

the meteorological direction by 180°. The distinction matters constantly when working with wind data: a sign error, a swapped component or a mixed convention rotates every direction in a data set by 180° or mirrors it, and the error does not show in the wind speed.

22.1.3 Components and direction: a worked case

The components follow from the speed and the meteorological direction as

$$u = -U \sin\beta, \qquad v = -U \cos\beta, \tag{22.2}$$

which Chapter 1 derived; the minus signs express that the air moves toward the side opposite to β. Dividing by U gives $\sin\beta = -u/U$ and $\cos\beta = -v/U$, so the inverse is

$$U = \sqrt{u^2 + v^2}, \qquad \beta = \operatorname{atan2}(-u, -v) \pmod{360^\circ}, \tag{22.3}$$

where the two-argument arctangent $\operatorname{atan2}(y, x)$ returns the angle whose sine is proportional to its first argument and whose cosine is proportional to its second, in the correct quadrant.

Take an illustrative wind of $U = 8\,\mathrm{m\,s^{-1}}$ from $\beta = 60^\circ$, an east-northeasterly. Equation (22.2) gives

$$u = -8 \sin 60^\circ = -8 \times 0.866 = -6.93\,\mathrm{m\,s^{-1}}, \qquad v = -8 \cos 60^\circ = -8 \times 0.500 = -4.00\,\mathrm{m\,s^{-1}},$$

both negative, because the air moves toward the west-southwest, bearing 240°. Its mathematical angle is, by equation (22.1), $\alpha_m = 270^\circ - 60^\circ = 210^\circ$, which is indeed the angle of the vector $(-6.93, -4.00)$ measured counterclockwise from east. The inverse recovers the direction: $\beta = \operatorname{atan2}(6.93, 4.00) = 60^\circ$, and $U = \sqrt{6.93^2 + 4.00^2} = 8.00\,\mathrm{m\,s^{-1}}$.

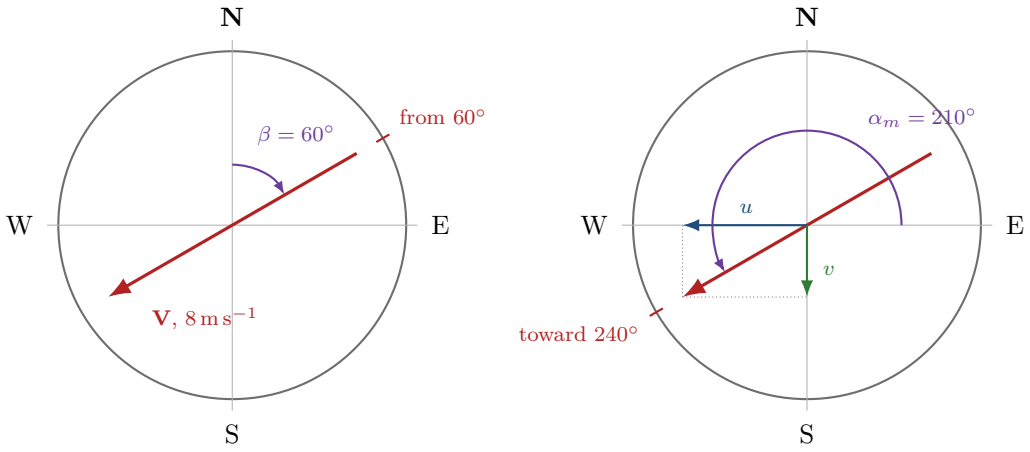
The two-argument form is necessary. A single arctangent, $\arctan(u/v) = \arctan(1.732) = 60^\circ$, gives the same answer here, but it gives it also for the opposite wind, $u = +6.93\,\mathrm{m\,s^{-1}}$ and $v = +4.00\,\mathrm{m\,s^{-1}}$, whose direction is 240°. The three usual errors produce three different wrong directions for the same wind: forgetting the minus signs gives 240°, swapping u and v gives $\operatorname{atan2}(4.00, 6.93) = 30^\circ$, and reporting the mathematical angle gives 210°.

Figure 22.1 draws the worked case in two panels, each a compass seen from above with north at the top. In both, the red arrow is the wind vector of $8\,\mathrm{m\,s^{-1}}$, pointing toward the west-southwest. Panel (a) shows the meteorological direction: the purple arc runs clockwise from north to the side the wind comes from, $\beta = 60^\circ$. Panel (b) shows the mathematical description: the blue and green arrows along the axes are the components u and v, and the purple arc runs counterclockwise from east to the side the vector points to, $\alpha_m = 210^\circ$. The same vector carries two angles that differ by neither 0° nor 180°, which is why the convention of every direction in a data set must be stated.

North and the model grid. Two further conversions sit between an instrument and equation (22.2). A vane or a sonic anemometer is aligned at installation, and a direction referenced to magnetic north must be corrected by the local magnetic declination, which reaches tens of degrees in some regions. A weather model may report u and v along the axes of its map projection, which differ from east and north away from the projection's central meridian and must be rotated before a direction is computed (Chapter 1).

22.1.4 Heights above ground and above sea level

Standard meteorological wind is referenced to 10 m above ground level over reasonably open terrain, the height of U_{10}. Above ground level, abbreviated AGL, is the height above the local ground surface. Engineering sensors are installed at other heights: 2 m at agricultural and hydrological stations, 20, 50 or 100 m on wind resource masts, the hub height of a turbine,



(a) meteorological direction (b) components and mathematical angle

Figure 22.1: One wind vector, two angles: an illustrative wind of $8\,\mathrm{m\,s^{-1}}$ from $\beta = 60°$, seen from above with north at the top (valid in either hemisphere). (a) The meteorological direction is measured clockwise from north to the side the wind comes from. (b) The components are $u = -U\sin\beta = -6.93\,\mathrm{m\,s^{-1}}$ and $v = -U\cos\beta = -4.00\,\mathrm{m\,s^{-1}}$; the mathematical angle, counterclockwise from east to the side the vector points to, is $\alpha_m = 270° - \beta = 210°$.

the height of the conductors of a transmission line. Because the wind changes with height (Chapters 12 and 14), a wind value without its measurement height cannot be compared with any other, and the height must always be recorded.

A second reference is mean sea level, abbreviated MSL: height above the mean level of the sea, the reference of topographic maps and of the elevation of a site. The two are very different quantities. An illustrative sensor 30 m AGL at a site whose ground lies 800 m MSL is at an elevation of about

$$800\,\mathrm{m} + 30\,\mathrm{m} = 830\,\mathrm{m}\ \mathrm{MSL}.$$

The word "about" is deliberate: the site elevation itself is usually known to a few meters, from a map, a survey or a satellite positioning receiver, and different elevation data sets refer to slightly different definitions of sea level.

Each height serves its own purpose. The surface-layer relations of the earlier chapters, the logarithmic profile, the stability functions and the roughness corrections, all use height above the ground, or above the displacement height $z - d$ over a canopy. Pressure, temperature lapse rates and the levels of a weather model in the free atmosphere use height above sea level or geopotential height (Chapter 2). A model's lowest levels are given above the model's own terrain, which in uneven country differs from the real ground under the sensor by tens of meters (Chapter 1). Confusing the references produces errors of the full site elevation: the 30 m sensor of the example, treated as 830 m above ground, would be extrapolated through a whole boundary layer, and treated as 30 m MSL, it would sit 770 m underground.

22.2 In-situ wind instruments

Four instruments measure the wind at the point where they stand: the cup anemometer, the propeller anemometer, the wind vane and the sonic anemometer. Each is described on the same template, its principle, what it measures, its strengths and its limits; the section ends with a comparison table and a schematic of the three main types.

22.2.1 The cup anemometer

Principle. A cup anemometer carries three, sometimes four, hemispherical or conical cups on horizontal arms around a vertical shaft. At any instant the cup whose open side faces the wind has a larger drag than the cup whose rounded back faces it; the difference produces a torque about the shaft, and the rotor turns. The rotation rate settles where the torques balance, and above a small threshold it is nearly proportional to the wind speed. A calibration in a wind tunnel against a reference speed gives the linear transfer function

$$U = a_0 + a_1\,\omega, \tag{22.4}$$

where ω is the rotation rate in revolutions per second, a_1, in meters per revolution, is the length of air that passes per revolution, and the offset a_0, in meters per second, reflects the friction of the bearings and the low-speed behavior of the rotor. With illustrative constants $a_0 = 0.25\,\mathrm{m\,s^{-1}}$ and $a_1 = 0.62\,\mathrm{m}$, a rotor turning at $\omega = 12.5$ revolutions per second indicates

$$U = 0.25\,\mathrm{m\,s^{-1}} + 0.62\,\mathrm{m} \times 12.5\,\mathrm{s^{-1}} = 0.25 + 7.75 = 8.0\,\mathrm{m\,s^{-1}}.$$

The constants are specific to the rotor type and, for accurate work, to each individual instrument; using a generic calibration instead of an individual one is itself a source of error of a percent or so (illustrative).

What it measures. The rotor responds to the magnitude of the horizontal wind, whatever its direction: a cup anemometer measures the horizontal speed U, a scalar. It gives no direction, and it does not measure the vertical wind. Its response to a wind inclined to the horizontal is not simply the horizontal part of that wind; it depends on the rotor's shape, which adds a small error in the turbulent and sloping flows where the wind is often inclined.

Strengths and limits. The cup anemometer is simple, robust, inexpensive and widely used, with a long history of calibration and comparison, and it is good for the mean wind, the ten-minute and hourly means of climatology and wind resource assessment. Its limits follow from its mechanics: mechanical inertia, which delays its response (Section 22.2.2); moving parts, whose bearings wear and raise the starting threshold with age; a bias toward high values in turbulent flow, called overspeeding (Section 22.2.3); no measurement of the vertical wind; and vulnerability to icing (Section 22.6.4).

22.2.2 Response and the distance constant

A rotor with mass cannot change its rotation rate instantly. To a first approximation the indicated speed U_m follows the true speed U as a first-order system,

$$\frac{\mathrm{d}U_m}{\mathrm{d}t} = \frac{U - U_m}{\tau_r}, \tag{22.5}$$

with a response time τ_r, the time in which U_m completes $1 - e^{-1} = 63\,\%$ of a step change of U. For a cup rotor the response time is not a constant. The aerodynamic torque on the cups scales with ρU^2 times a function of the ratio of the cup speed to the wind speed, so its sensitivity to a change of the rotation rate, which is what pulls the rotor back toward equilibrium, scales with ρU; the rotor's moment of inertia is fixed. The response time, inertia divided by that sensitivity, is therefore inversely proportional to the wind speed:

$$\tau_r = \frac{\ell_d}{U}. \tag{22.6}$$

The constant ℓ_d, in meters, is the *distance constant*: the length of air that must pass the sensor for its indication to complete 63 % of a step change. It is a property of the rotor, measured in a wind tunnel by step tests, and it is the standard response measure of cup and propeller anemometers because, unlike the response time, it is the same at every speed.

With an illustrative distance constant of $\ell_d = 3\,\mathrm{m}$, a cup responds with $\tau_r = 3/10 = 0.3\,\mathrm{s}$ in a wind of $10\,\mathrm{m\,s^{-1}}$ and with $\tau_r = 3/2 = 1.5\,\mathrm{s}$ in a wind of $2\,\mathrm{m\,s^{-1}}$. A cup is thus fastest in strong winds and slowest in the light winds of a stable night, when the fluctuations are weak and slow anyway but the mean itself may change quickly. A wind vane responds in a different way: its fin, turned by aerodynamic force against its own inertia, behaves as a second-order system that can overshoot and oscillate, and it is characterized by a damping ratio and a delay distance, the distance analog of a time constant. A sonic anemometer has no moving parts; its response is limited instead by its path length (Section 22.3.3).

22.2.3 Overspeeding

Cup anemometers respond faster to an increase of the wind than to a decrease. Equation (22.6) contains the reason: during a gust the wind is strong and the response time short, so the rotor spins up quickly; during a lull the wind is weak and the response time long, so the rotor spins down slowly. The rotor therefore spends more of its time near the high speeds than the wind does, and in a fluctuating wind its mean indication exceeds the mean wind. This positive bias in turbulent conditions is called *overspeeding*.

A deliberately extreme example shows the mechanism. Let the wind alternate abruptly between 10 and $6\,\mathrm{m\,s^{-1}}$ every half second, a square wave with a true mean of $8\,\mathrm{m\,s^{-1}}$, and let the cup have $\ell_d = 3\,\mathrm{m}$, so that $\tau_r = 0.3\,\mathrm{s}$ in the high phase and 0.5 s in the low phase. Each phase is a first-order approach toward the current wind. In the periodic state the indication rises to $9.49\,\mathrm{m\,s^{-1}}$ at the end of each high phase and falls only to $7.28\,\mathrm{m\,s^{-1}}$ at the end of each low phase, and its averages over the two phases are

$$10-(10-7.28)\,\frac{0.3}{0.5}\bigl(1-e^{-0.5/0.3}\bigr) = 8.68\,\mathrm{m\,s^{-1}}, \qquad 6+(9.49-6)\,\frac{0.5}{0.5}\bigl(1-e^{-0.5/0.5}\bigr) = 8.20\,\mathrm{m\,s^{-1}},$$

so the mean indication is $8.44\,\mathrm{m\,s^{-1}}$, $0.44\,\mathrm{m\,s^{-1}}$ or 5.5 % above the true mean. A rotor with a fixed response time of 0.375 s for both phases would follow a symmetric wave between 6.83 and $9.17\,\mathrm{m\,s^{-1}}$ whose mean is exactly $8.00\,\mathrm{m\,s^{-1}}$: the bias comes from the asymmetry of the response, not from the lag itself.

Figure 22.2 draws the example. The horizontal axis is time in seconds over two periods; the vertical axis is speed. The gray square wave is the true wind; the solid red curve is the indication of the cup with $\tau_r = \ell_d/U$; the dashed blue curve is the indication of a hypothetical sensor with a fixed response time. The horizontal dashed lines mark the true mean and the red cup's mean. The red curve climbs steeply after each rise of the wind and descends gently after each fall, and its mean sits above the true one.

Real turbulence is much gentler than this square wave: its fluctuations are continuous, and most of their variance lies at frequencies below the response of the cup, which follows them almost exactly. The bias is therefore usually small in modern instruments with small distance constants, a fraction of a percent to about a percent of the mean (illustrative). It grows with the turbulence intensity and with the distance constant, which is why it matters in turbulence studies, over rough or complex terrain, and in wind-resource work where a percent of wind speed is several percent of energy.

22.2.4 The propeller anemometer and the wind vane

Propeller anemometer. A propeller anemometer carries a helicoid propeller on a horizontal shaft. Its rotation rate is proportional to the component of the wind along the shaft, so it

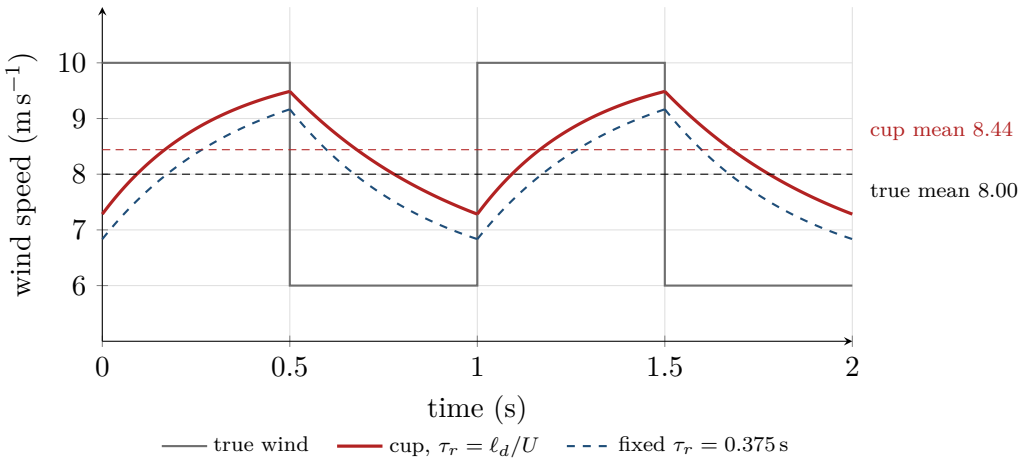


Figure 22.2: Overspeeding of a cup anemometer in an extreme, illustrative square-wave wind alternating between 10 and 6 m s^{-1} every 0.5 s. Each phase follows equation (22.5) toward the current wind. Red: $\tau_r = \ell_d/U$ with $\ell_d = 3$ m (0.3 s high, 0.5 s low), periodic between 7.28 and 9.49 m s^{-1}, mean 8.44 m s^{-1}. Blue: a fixed $\tau_r = 0.375$ s, periodic between 6.83 and 9.17 m s^{-1}, mean 8.00 m s^{-1}.

measures a component along a preferred axis rather than the speed. An ideal propeller would indicate $U_m = U \cos \gamma_p$ for a wind at an angle γ_p to its axis, the *cosine response*. Real propellers depart from it, mostly at large angles, where they under-respond and finally stall as the wind approaches the plane of the propeller. Three propellers on orthogonal shafts, one of them vertical, measure u, v and w, provided their readings are corrected for the departure from the cosine response and the shafts are aligned with the intended axes. The strengths of the propeller anemometer are its directional sensitivity and a reasonable response, with distance constants of one to a few meters (illustrative); its limits are its moving parts, the cosine-response errors and its dependence on alignment.

Propeller and vane. The propeller is often combined with a vane: a tail fin turns the whole body into the wind, so that the propeller faces the wind and measures its speed, and the angle of the body gives the direction. The combination measures speed and direction with one instrument, and the cosine errors are small because the propeller is kept nearly aligned with the wind; the alignment is imperfect when the direction changes faster than the vane can follow.

Wind vane. A wind vane measures the horizontal wind direction β as defined in Section 22.1.2. A fin on a vertical pivot is pushed by the wind until it trails downstream, and the angle of the pivot is read by a potentiometer or an optical encoder against a reference mark that is aligned with true north at installation. Every direction the vane reports carries the error of that alignment: a reference mark set 5° off north turns the whole record by 5°. A potentiometer vane has, in addition, a small sector near its zero, a few degrees wide, in which the reading is undefined. Like a cup, a vane needs a minimum wind speed to turn reliably, and in calm air it reports whatever position it last held (Section 22.6.4).

22.2.5 The sonic anemometer

Principle. A sonic anemometer measures the wind from the travel time of ultrasonic pulses between pairs of transducers. Two transducers face each other across a path of length ℓ_p, of the order of 0.1 to 0.15 m, and each alternately emits a pulse and receives the pulse of the other. Sound travels at the speed of sound c_s relative to the air, and the air itself moves along the

path with the velocity component u_ℓ. The pulse traveling with that component and the pulse traveling against it take

$$t_1 = \frac{\ell_p}{c_s + u_\ell}, \qquad t_2 = \frac{\ell_p}{c_s - u_\ell}. \tag{22.7}$$

Inverting each and taking the difference and the sum gives $1/t_1 - 1/t_2 = 2u_\ell/\ell_p$ and $1/t_1 + 1/t_2 = 2c_s/\ell_p$, so

$$u_\ell = \frac{\ell_p}{2}\left(\frac{1}{t_1} - \frac{1}{t_2}\right), \qquad c_s = \frac{\ell_p}{2}\left(\frac{1}{t_1} + \frac{1}{t_2}\right). \tag{22.8}$$

The velocity follows from the two transit times and the path length alone: the speed of sound, and with it the temperature and humidity of the air, cancels from u_ℓ. For an illustrative path of $\ell_p = 0.15\,\mathrm{m}$, $c_s = 343\,\mathrm{m\,s^{-1}}$ (air at about 20°C) and $u_\ell = 5\,\mathrm{m\,s^{-1}}$, equation (22.7) gives $t_1 = 0.15/348 = 431.03\,\mu\mathrm{s}$ and $t_2 = 0.15/338 = 443.79\,\mu\mathrm{s}$, a difference of $12.75\,\mu\mathrm{s}$; equation (22.8) returns $u_\ell = 5.00\,\mathrm{m\,s^{-1}}$ and $c_s = 343.0\,\mathrm{m\,s^{-1}}$. Since the difference of the transit times changes by about $2\ell_p/c_s^2 = 2.5\,\mu\mathrm{s}$ per meter per second, a resolution of $0.01\,\mathrm{m\,s^{-1}}$ requires timing to about 25 nanoseconds.

What it measures. Three non-parallel paths give three velocity components, which the instrument transforms into u, v and w in its own axes; it corrects internally for the small lengthening of the acoustic path by the wind across it. Sonic anemometers typically sample at 10 to 20 Hz or more. They measure the vertical fluctuation w' directly, together with the horizontal ones, and therefore the covariances $\overline{u'w'}$ and $\overline{w'T'}$ of Chapter 9. From those follow the momentum flux, the sensible heat flux, the friction velocity u_* (Chapter 10) and the turbulent kinetic energy e (Chapter 8). For micrometeorology, the study of the small-scale processes near the ground, the sonic anemometer is the central instrument: the eddy covariance method is built on it.

Strengths and limits. A sonic anemometer has no moving parts, hence no starting threshold, no overspeeding and no wear; it measures all three components fast. Its limits are of other kinds. Its own transducers and struts disturb the flow along its paths, *transducer shadowing*, which the manufacturer's calibration partly corrects. Rain, snow or ice on the transducers interrupts the pulses and produces gaps or spikes. Because it measures w, it is sensitive to small tilts (Section 22.4.4). It costs more, needs more power and produces more data than a cup: four channels at 20 Hz are 288 000 values an hour.

22.2.6 Sonic temperature

The second result of equation (22.8), the speed of sound, carries thermodynamic information. In an ideal gas the speed of sound squared is the ratio of specific heats times the gas constant times the temperature. For moist air, to a good approximation,

$$c_s^2 = \frac{c_p}{c_v}\, R_d\, T\,(1 + 0.51\,q), \tag{22.9}$$

where $c_p/c_v \approx 1.40$ is the ratio of the specific heats of dry air at constant pressure and at constant volume and q is the specific humidity. The instrument reports the *sonic temperature*

$$T_s = \frac{c_s^2}{(c_p/c_v)\, R_d} = T\,(1 + 0.51\,q), \tag{22.10}$$

with $(c_p/c_v)R_d = 1.40 \times 287 = 401.8\,\mathrm{m^2\,s^{-2}\,K^{-1}}$. For the speed of sound of the example above, $c_s = 343.0\,\mathrm{m\,s^{-1}}$, $T_s = 343.0^2/401.8 = 292.8\,\mathrm{K}$.

The sonic temperature is not the thermodynamic air temperature, because humidity changes the speed of sound. In humid tropical air at $T = 300\,\mathrm{K}$ with $q = 0.015\,\mathrm{kg\,kg^{-1}}$, $T_s =$

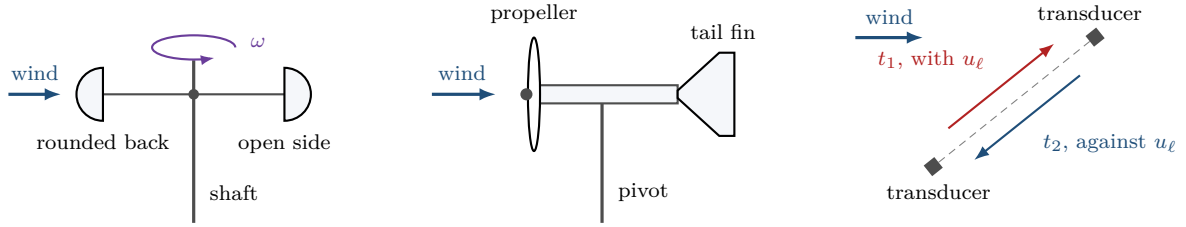
$300 \times 1.00765 = 302.3\,\mathrm{K}$, 2.3 K above T and close to the virtual temperature $T_v = T(1+0.61q) = 302.7\,\mathrm{K}$. The difference matters most for the heat flux. Writing $T_s' \approx T' + 0.51\,\overline{T}\,q'$ gives

$$\overline{w'T_s'} \approx \overline{w'T'} + 0.51\,\overline{T}\,\overline{w'q'}.$$

Over an illustrative irrigated field with a latent heat flux of $LE = 300\,\mathrm{W\,m^{-2}}$, $\overline{w'q'} = 300/(1.2 \times 2.45 \times 10^6) = 1.02 \times 10^{-4}\,\mathrm{kg\,kg^{-1}\,m\,s^{-1}}$ and the second term is $0.51 \times 300 \times 1.02 \times 10^{-4} = 0.0156\,\mathrm{K\,m\,s^{-1}}$. If the true kinematic heat flux is $0.10\,\mathrm{K\,m\,s^{-1}}$ (about $120\,\mathrm{W\,m^{-2}}$), the sonic flux is 16 % too large. Precise heat-flux work therefore corrects the sonic flux with the humidity flux measured by a fast gas analyzer beside the sonic, as Chapter 9 described.

22.2.7 Comparison of in-situ instruments

Figure 22.3 sketches the three main types side by side. Panel (a) is a cup anemometer seen from the side, with the wind from the left: the cup on the right shows its open side to the wind, the cup on the left its rounded back, and the arrow around the shaft is the rotation ω. Panel (b) is a propeller and vane on a vertical pivot: the propeller faces the wind and the fin at the tail keeps it there. Panel (c) is one acoustic path of a sonic anemometer seen from the side: the two transducers face each other across the path, the red arrow is the pulse traveling with the along-path wind component, the blue arrow the pulse traveling against it, and the wind is horizontal. The figure shows what each instrument physically responds to: a torque from a drag difference, a torque from a component along an axis, and a difference of transit times.



(a) cup anemometer: speed U from ω

(b) propeller and vane: speed and direction β

(c) one sonic path: u_ℓ and c_s from t_1, t_2

Figure 22.3: Schematic of three in-situ wind instruments (not to scale). (a) Cup anemometer: the drag difference between the open side and the rounded back of the cups turns the rotor at a rate ω related to the horizontal speed by equation (22.4). (b) Propeller and vane: the fin keeps the propeller facing the wind; the propeller gives the speed, the angle of the pivot the direction. (c) One path of a sonic anemometer, transducers ℓ_p apart: the transit times with and against the along-path wind give u_ℓ and the speed of sound by equation (22.8).

Table 22.1 collects the four instruments on the template of this section: what each measures, its typical response, its strengths and its limits. The pattern is simple. The mechanical sensors are robust and measure the mean wind well, with a response of a fraction of a second to a few seconds that lengthens in light wind; the sonic anemometer measures the turbulence itself, at the cost of more care in mounting and processing.

22.3 Sampling, response and averaging

A recorded wind value is the end of a chain: the sensor's physical response filters the flow, the logger samples the filtered signal, and processing averages the samples into a reported value. This section treats each link, and then the two averaging problems peculiar to wind: the averaging of directions, and the difference between the mean speed and the speed of the mean vector.

Table 22.1: In-situ wind instruments compared. Response values are typical orders of magnitude and illustrative.

Instrument	Measures	Response	Strengths	Limits
Cup anemometer	horizontal speed U	distance constant of a few meters; $\tau_r = \ell_d/U$	simple, robust, inexpensive, good mean wind	inertia; moving parts; overspeeding; starting threshold; no w; icing
Propeller anemometer	component along its axis	distance constant of one to a few meters	directional sensitivity; three propellers give u, v, w	moving parts; departure from cosine response; alignment
Wind vane	direction β	second order, damping ratio and delay distance	simple, robust	north alignment; dead sector; threshold; undefined in calm
Sonic anemometer	u, v, w and sonic temperature	limited by path length, 10 to 20 Hz or more	no moving parts or threshold; fluxes, u_*, e	transducer shadowing; tilt; rain and ice; cost, power, data volume

22.3.1 Sampling rate

A sensor sampled at $f_s = 1\,\mathrm{Hz}$ records one value per second; a turbulence instrument at $f_s = 20\,\mathrm{Hz}$ records twenty values per second, one every $1/f_s = 0.05\,\mathrm{s}$. The sampling rate determines which turbulent fluctuations can be observed. A fluctuation that rises and falls between two samples leaves no trace, or a false one; if the sensor is sampled too slowly, the high-frequency fluctuations are lost. Chapter 9 showed the scale of the problem: at 10 m in a wind of $8\,\mathrm{m\,s^{-1}}$ an eddy as large as the measurement height passes in about 1.25 s, and the smaller eddies that still carry flux pass in a fraction of that.

The required rate depends on the product. A ten-minute mean speed needs only enough samples for a stable average, and standard stations sample every one to three seconds (illustrative), which also allows the three-second gust to be formed. Turbulence statistics and fluxes need the eddies themselves, and eddy-covariance systems sample at 10 to 20 Hz. The price is volume: a ten-minute period at 20 Hz holds $20 \times 600 = 12\,000$ samples per channel.

22.3.2 The Nyquist frequency and aliasing

Data sampled at the frequency f_s can resolve fluctuations only up to the *Nyquist frequency*

$$f_N = \frac{f_s}{2}, \tag{22.11}$$

two samples per period of the fastest fluctuation. The reason appears when two sinusoids, one at a frequency n and one at $f_s - n$, are sampled at the times $t_k = k/f_s$:

$$\sin\Big(2\pi(f_s - n)\frac{k}{f_s}\Big) = \sin\Big(2\pi k - 2\pi n\frac{k}{f_s}\Big) = -\sin\Big(2\pi n\frac{k}{f_s}\Big).$$

At every sample the two give the same value up to a change of sign, a shift of phase, so the samples cannot tell them apart. A fluctuation at a frequency above f_N therefore appears in the record at the folded frequency $f_s - n$, below f_N. This is *aliasing*. With $f_s = 20\,\mathrm{Hz}$, $f_N = 10\,\mathrm{Hz}$: fluctuations above 10 Hz cannot be resolved reliably, and if they are present in the signal reaching the logger they reappear below it.

Figure 22.4 draws an example at a low rate where the effect is visible. The horizontal axis is time over ten seconds; the vertical axis is a fluctuation of unit amplitude. The thin blue curve is a fluctuation at $n = 0.8\,\mathrm{Hz}$; the red dots are its samples at $f_s = 1\,\mathrm{Hz}$, for which $f_N = 0.5\,\mathrm{Hz}$;

the dashed red curve is the sinusoid at $f_s - n = 0.2\,\mathrm{Hz}$, a period of five seconds, that passes through the same samples. The record shows a slow five-second oscillation that does not exist in the wind.

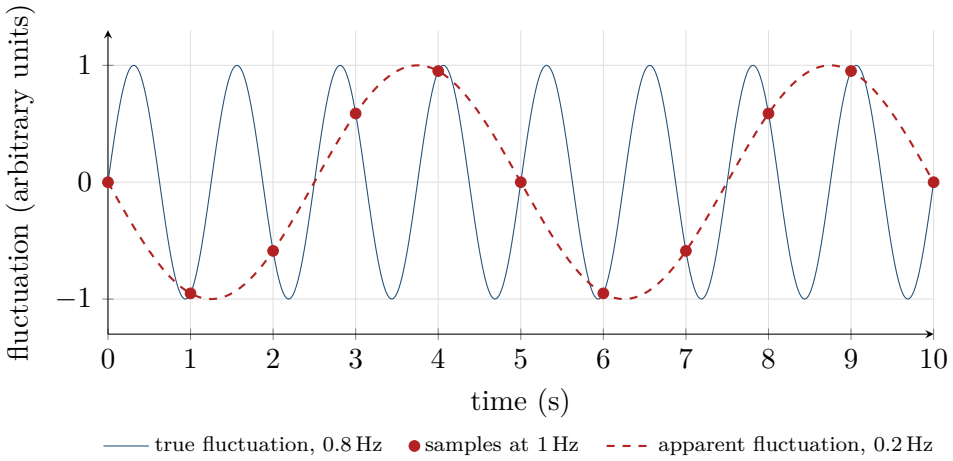


Figure 22.4: Aliasing (illustrative): a fluctuation $\sin(2\pi n t)$ with $n = 0.8\,\mathrm{Hz}$ sampled at $f_s = 1\,\mathrm{Hz}$ ($f_N = 0.5\,\mathrm{Hz}$). The samples coincide with those of $-\sin(2\pi(f_s - n)t)$, a fluctuation at 0.2 Hz.

The variance of an aliased fluctuation is not lost; it is misplaced, at a lower frequency where it adds spurious energy. In a turbulence spectrum, which falls steeply with frequency in the inertial subrange (Chapter 8), the folded energy can visibly flatten the high-frequency end. Aliasing is prevented by removing the fluctuations above f_N before sampling: by the slow response of the sensor itself, by an electronic low-pass filter, or by an instrument that averages its fast internal measurements over each output interval. A record whose sensor responds more slowly than the sampling interval does not alias, but, as the next subsection shows, it does not resolve the fast fluctuations either.

22.3.3 Response time against sampling rate

Sampling fast does not help if the physical sensor responds slowly. A sensor might be recorded at 10 Hz but have a mechanical response time of $\tau_r = 2\,\mathrm{s}$; it then cannot capture the rapid turbulence, whatever the logger does. A first-order sensor, equation (22.5), passes a sinusoidal fluctuation of frequency n with its amplitude reduced by the factor

$$\frac{1}{\sqrt{1 + (2\pi n \tau_r)^2}}, \tag{22.12}$$

which is close to one for slow fluctuations and falls as $1/n$ for fast ones; the half-power or cutoff frequency, where the variance is halved, is $n_c = 1/(2\pi\tau_r)$. For $\tau_r = 2\,\mathrm{s}$, $n_c = 0.080\,\mathrm{Hz}$, and the factor is 0.62 at 0.1 Hz, 0.16 at 0.5 Hz and 0.08 at 1 Hz. The 10 Hz record has a Nyquist frequency of 5 Hz, but it carries information only below about 0.1 Hz; its successive samples are nearly identical readings of a slowly moving needle.

Two properties must therefore be distinguished: the *sampling frequency*, a property of the logger, and the *sensor response*, a property of the physical instrument. The effective time resolution of a record is set by the slower of the two, the smaller of f_N and n_c. For a cup with $\ell_d = 3\,\mathrm{m}$ the cutoff follows from equation (22.6) as $n_c = U/(2\pi\ell_d)$: 0.42 Hz at $8\,\mathrm{m\,s^{-1}}$ and 0.11 Hz at $2\,\mathrm{m\,s^{-1}}$. A three-second gust, a fluctuation of a few tenths of a hertz, is near that cutoff, so a slow cup underestimates gusts, more so in light wind. A sonic anemometer averages the wind along its path and attenuates fluctuations whose wavelength is comparable with the

path length, at $8\,\mathrm{m\,s^{-1}}$ and $\ell_p = 0.15\,\mathrm{m}$ about $8/0.15 \approx 50\,\mathrm{Hz}$, far above the Nyquist frequency of its usual sampling rate.

22.3.4 The averaging period

Wind products are almost always averages over some interval: one second, one minute, ten minutes, an hour. A ten-minute mean speed is written $\overline{U}_{10\,\mathrm{min}}$. A gust is defined over a short interval, most often three seconds, as the highest running mean of that duration within a longer reference period. Chapter 8 showed with a sampled record how the highest value falls and the spread of values narrows as the averaging lengthens.

The numbers differ because they are different statistics, not because some are wrong. Suppose the instantaneous wind in a ten-minute period fluctuates between 4 and $14\,\mathrm{m\,s^{-1}}$. Its ten-minute mean might be $8\,\mathrm{m\,s^{-1}}$, and its maximum three-second gust $13\,\mathrm{m\,s^{-1}}$, lower than the $14\,\mathrm{m\,s^{-1}}$ peak because averaging over three seconds smooths the briefest excursions. All three numbers describe the same wind correctly. A dispatcher who reads $8\,\mathrm{m\,s^{-1}}$ and an engineer who reads $13\,\mathrm{m\,s^{-1}}$ for the same period are both right, and they are describing different quantities: the mean that drives the average cooling of a conductor or the energy of a turbine, and the short peak that loads a structure. For any wind value the first question is therefore

what averaging interval does this wind value represent?

A weather model adds a further kind: its wind is the value of a grid cell at a time step, a spatial average that corresponds roughly, not exactly, to a time average of tens of minutes at a point (Chapter 8).

22.3.5 The gust factor

The ratio of a gust to the mean of the same period is the *gust factor*,

$$G = \frac{U_{\mathrm{gust}}}{\overline{U}}. \tag{22.13}$$

For an illustrative gust of $U_{\mathrm{gust}} = 15\,\mathrm{m\,s^{-1}}$ in a period with mean $\overline{U} = 10\,\mathrm{m\,s^{-1}}$, $G = 15/10 = 1.5$; for the period of the previous subsection, $G = 13/8 = 1.63$.

The gust factor is not a constant of a site. Chapter 8 wrote it as $G = 1 + g_{\mathrm{pk}}\,\mathrm{TI}$, with TI the turbulence intensity and g_{pk} the peak factor, the excess of the gust over the mean in standard deviations; with a typical $g_{\mathrm{pk}} = 2.5$, a gust factor of 1.5 corresponds to $\mathrm{TI} = 0.2$, a value of rough land. It therefore depends on the turbulence; on the averaging intervals, since a one-second gust exceeds a three-second gust and the highest gust in an hour exceeds the highest in ten minutes; on the roughness, which raises the turbulence intensity; and on the stability, since convective afternoons are gusty and stable nights are not, apart from intermittent bursts. It depends also on the instrument, because a sensor with a slow response smooths the gust before the averaging does (Section 22.3.3). A gust factor is meaningful only with its gust duration, its reference period, its height and the response of the instrument that measured it.

22.3.6 Averaging wind direction

Wind directions must not be averaged arithmetically. Two winds from 359° and 1° both come from almost exactly north, yet their arithmetic mean is

$$\frac{359^\circ + 1^\circ}{2} = 180^\circ,$$

a wind from the south, which is completely wrong: it is the opposite of both. The scale of directions is circular, and the arithmetic mean fails whenever the values straddle the jump from 360° to 0°.

The correct procedure averages the vector components. Each direction β_i with speed U_i is converted with equation (22.2),

$$u_i = -U_i \sin\beta_i, \qquad v_i = -U_i \cos\beta_i,$$

the components are averaged, and the mean direction is reconstructed with equation (22.3), $\overline{\beta} = \operatorname{atan2}(-\overline{u}, -\overline{v})$. For the two winds, each at an illustrative $5\,\mathrm{m\,s^{-1}}$,

$$\begin{aligned} \beta_1 = 359^\circ: &\quad u_1 = -5\sin 359^\circ = +0.087\,\mathrm{m\,s^{-1}}, \quad v_1 = -5\cos 359^\circ = -4.999\,\mathrm{m\,s^{-1}}, \\ \beta_2 = 1^\circ: &\quad u_2 = -5\sin 1^\circ = -0.087\,\mathrm{m\,s^{-1}}, \quad v_2 = -5\cos 1^\circ = -4.999\,\mathrm{m\,s^{-1}}. \end{aligned}$$

The means are $\overline{u} = 0$ and $\overline{v} = -4.999\,\mathrm{m\,s^{-1}}$, so $\overline{\beta} = \operatorname{atan2}(0, 4.999) = 0^\circ$, a north wind, as it should be, with a mean vector speed of $4.999\,\mathrm{m\,s^{-1}}$.

Two variants are in use. Averaging the components weighted by speed, as above, gives the direction of the mean air motion; averaging unit vectors, $U_i = 1$, gives each observation equal weight and is the only option for a vane without an anemometer. The two differ when the direction depends on the speed, for example when strong winds come from one sector and light winds from another; both are legitimate, and a data set should state which it uses. Measures of the spread of directions, the circular counterparts of the standard deviation, belong to Chapter 24.

22.3.7 Scalar mean and vector mean

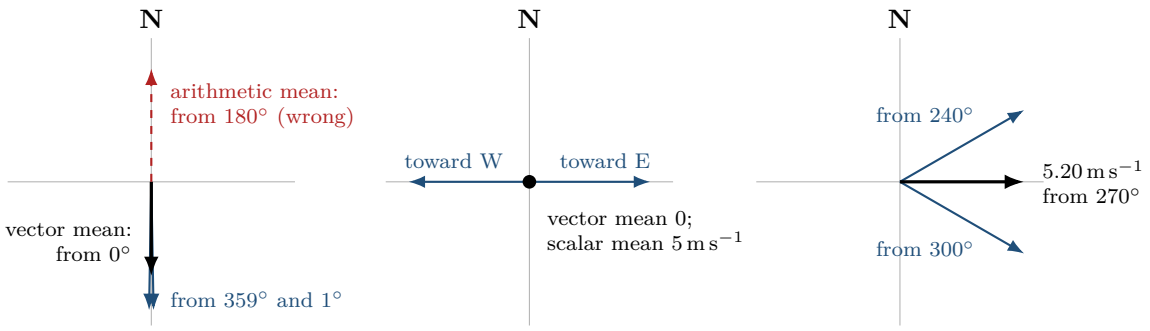
Two mean speeds can be formed from the same record. The *scalar mean speed* is the average of the speeds, $\overline{U} = \frac{1}{N}\sum U_i$; the *vector mean speed* is the magnitude of the mean vector, $\sqrt{\overline{u}^2 + \overline{v}^2}$. By the triangle inequality the length of a sum of vectors never exceeds the sum of their lengths, so the vector mean speed is never larger than the scalar mean speed, and the two are equal only when the direction is constant:

$$\text{mean speed} \neq \text{speed of the mean vector}.$$

Suppose the wind speed is always $5\,\mathrm{m\,s^{-1}}$ but the wind alternates between blowing toward the east and toward the west. The scalar mean speed is $5\,\mathrm{m\,s^{-1}}$; the components cancel, and the vector mean speed is 0. A less extreme illustrative case is a wind of $6\,\mathrm{m\,s^{-1}}$ meandering so that half the samples come from 240° and half from 300°: the scalar mean is $6\,\mathrm{m\,s^{-1}}$, while the cross-components cancel and the vector mean is $6\cos 30^\circ = 5.20\,\mathrm{m\,s^{-1}}$ from 270°, 13 % lower.

Figure 22.5 draws the three cases of this and the previous subsection, each seen from above with north at the top. Thin blue arrows are individual winds, drawn from the center in the direction the air moves; thick arrows and dots are the vector means. In panel (a), the two winds from 359° and 1° point south and almost coincide; the vector mean (black) points south as well, while the arithmetic mean of the directions, 180°, would be the dashed red arrow pointing north. In panel (b), the east and west winds cancel and the vector mean is the dot at the center. In panel (c), the two meandering winds give a vector mean (black) shorter than either.

The ratio of the vector mean speed to the scalar mean speed, 0.87 in the meander example, is a measure of the steadiness of the direction: one for a constant direction, zero for a symmetric reversal. Which mean is wanted depends on the use. The cooling of a conductor and the power of a turbine respond to the speed at each instant, and the scalar mean, or better the distribution of speeds, is the relevant quantity; the net transport of a pollutant over the period follows the vector mean. The instruments deliver different means by construction: a cup averages speeds and gives the scalar mean, while averaged sonic components or a model's averaged u and v give the vector mean. In light, variable winds, such as a stable night or a weak sea-breeze transition, a comparison of the two produces an apparent bias that is a difference of definitions, not of the wind.



(a) 359° and 1°, 5 m s^{-1} each (b) east and west, 5 m s^{-1} each (c) meander, 6 m s^{-1} each

Figure 22.5: Direction averaging and vector means, seen from above with north at the top (illustrative). Blue: individual winds, drawn toward where the air moves. Black: vector mean. (a) Component averaging gives 0°; the arithmetic mean of the directions gives 180°. (b) Opposite winds: scalar mean 5 m s^{-1}, vector mean 0. (c) Winds of 6 m s^{-1} from 240° and 300°: vector mean $6\cos 30° = 5.20$ m s^{-1} from 270°.

22.4 Mounting and flow distortion

A sensor measures the flow at its own position, and the structure that holds it is part of that flow. This section treats the distortion caused by towers and booms, the tower shadow and the choice of boom orientation, the tilt of a sonic anemometer and the coordinate rotation that corrects it.

22.4.1 Flow distortion by towers and booms

A sensor mounted on a tower does not automatically measure the undisturbed wind, because the tower itself disturbs the flow. Upstream of the tower the air is slowed as it approaches the obstacle, *blockage*; beside it the air accelerates as it is deflected around the structure; downstream lies a *wake* of reduced mean speed; and the structure sheds eddies that add turbulence to the wake. All of these modifications of the measured flow by the sensor's surroundings are called *flow distortion*. A solid tubular mast disturbs the flow more than an open lattice tower of the same width, and the boom, the clamps and the vertical pole that raises a sensor above its boom each contribute a smaller distortion of their own. The sensor's own body is part of the problem too: the transducer shadowing of a sonic anemometer (Section 22.2.5) is flow distortion at the scale of centimeters.

The disturbance decays with distance from the structure, measured in tower widths, so the length of the boom matters: a boom several tower widths long keeps the error outside the wake to about a percent of the speed (illustrative), while in the wake itself the deficit reaches tens of percent. The orientation of the boom matters as much, because it decides for which wind directions the sensor lies in the wake. The cleanest position on a mast is a sensor on a pole above the top of the tower, which no part of the structure shadows; wind-resource masts put their primary anemometer there for this reason.

22.4.2 Tower shadow

If the wind comes from behind the tower relative to the sensor, the air reaching the sensor has passed the tower first, and the instrument sits in the tower's wake. This is the *tower shadow*. In the shadow the mean speed reads low and the turbulence high, and a sonic anemometer records the eddies shed by the structure rather than those of the boundary layer. The affected range of

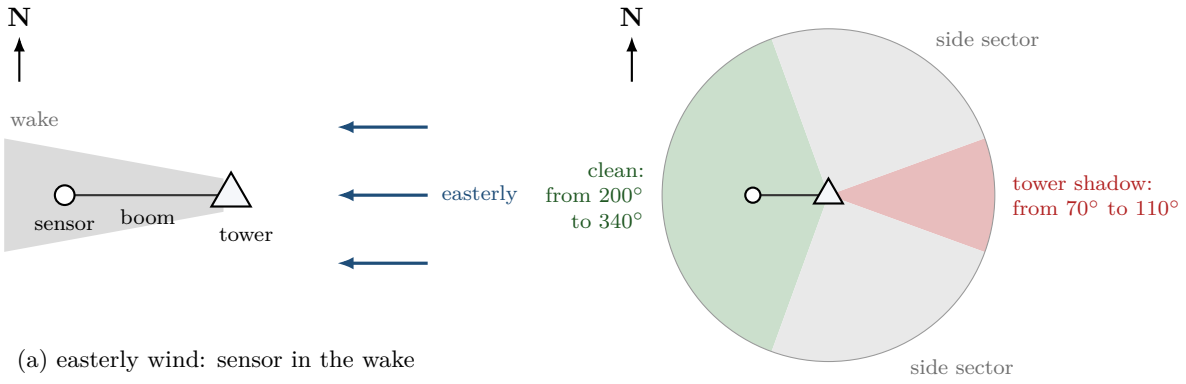
directions, the *shadow sector*, depends on the width of the tower and the length of the boom; an illustrative width is 40°, 20° on either side of the direction from the sensor to the tower.

Measurements from the shadow sector need to be filtered: flagged, excluded, or replaced by the reading of a second sensor at the same height on a boom on the opposite side of the tower, which is upwind of the tower when the first is downwind. The pair also reveals the shadow in the data. Plotted against wind direction, the ratio of the two readings is close to one for most directions and shows a pronounced dip, of tens of percent (illustrative), in each sensor's shadow sector; the width of the dips measures the sector to be filtered. Leaving the shadow in a record biases more than the shadowed hours: if the prevailing wind falls in the shadow sector, the long-term mean, the turbulence intensity and the wind rose (Chapter 19) of the whole record are biased.

22.4.3 Boom orientation

Suppose an anemometer is mounted on a boom extending west from a tower. For easterly winds the tower lies upstream of the sensor, which then sits in the wake. For westerly winds the sensor is upstream of the tower and has a cleaner exposure, affected only by the small blockage ahead of the structure. For northerly and southerly winds the sensor is beside the tower and sees a small acceleration. Instrumentation quality is thus strongly directional: the same anemometer is accurate for some directions and biased for others.

Figure 22.6 draws this mounting in plan view, north at the top. Panel (a) shows the physical cause: an easterly wind, the blue arrows from the right, meets the tower, the triangle, and the gray wake behind it engulfs the sensor at the end of the boom. Panel (b) shows the consequence as sectors of wind direction, each wedge drawn on the side from which the wind comes: the red wedge is the shadow sector, winds from about 70° to 110°; the green wedge the clean sector, winds from the west half of the compass; and the gray wedges the side sectors with small acceleration. The boundaries are illustrative.



(a) easterly wind: sensor in the wake

(b) quality by wind direction

Figure 22.6: A sensor on a boom extending west from a lattice tower, plan view, north at the top (either hemisphere). (a) In an easterly wind the sensor lies in the tower wake. (b) Wind-direction sectors, each drawn on the side the wind comes from: tower shadow, winds from about 70° to 110° (an illustrative sector 40° wide); clean, winds from about 200° to 340°, with only a small blockage; side sectors with a small acceleration.

The orientation of a boom is therefore chosen from the wind climate of the site, the wind rose of Chapter 19, so that the prevailing directions do not fall in the shadow sector. The west-pointing boom of the example suits a site in the westerlies of the middle latitudes of either hemisphere. It is the wrong choice under the trade winds, which blow from the east: from the northeast in the Northern Hemisphere and from the southeast in the Southern Hemisphere, as

along the coast of northeastern Brazil, where a boom pointing east, into the prevailing wind, would keep the common directions clean. Where the wind has no single prevailing direction, two booms on opposite sides of the tower are used, and for each direction the record is taken from the sensor that is upwind of the tower.

22.4.4 Sensor tilt

For sonic anemometers, even a small tilt matters, because the vertical wind is small. If the sensor's vertical axis is tilted by an angle γ in the direction of the wind, the measured vertical component contains the part $U \sin\gamma$ of the horizontal wind. For $U = 10\,\mathrm{m\,s^{-1}}$ and a tilt of $\gamma = 2°$,

$$U \sin\gamma = 10\,\mathrm{m\,s^{-1}} \times \sin 2° = 10 \times 0.0349 \approx 0.35\,\mathrm{m\,s^{-1}}$$

of horizontal wind leaks into the measured w. That is large compared with the typical mean vertical velocity over flat ground, millimeters to a few centimeters per second: the error is ten to a hundred times the quantity. The same tilt is negligible for the horizontal speed, which it reduces by the factor $\cos 2° = 0.99939$, less than a tenth of a percent; a 2° tilt of a cup anemometer does not matter, and the same tilt of a sonic anemometer does.

The leakage does not stay in the mean. Chapter 9 showed that a 2° tilt in an $8\,\mathrm{m\,s^{-1}}$ wind mixes part of the along-wind variance into the covariance $\overline{u'w'}$, making the momentum flux 15 % too small in magnitude and the friction velocity 8 % low. Over sloping ground the issue arises even with a perfectly level sensor: the mean flow follows the slope, so a sensor level with respect to gravity sees a mean vertical velocity relative to its axes. Leveling cannot solve both problems; a rotation of the coordinates can.

22.4.5 Coordinate rotation

For turbulence analysis the measured velocities are rotated, window by window, into coordinates in which

$$\overline{v} = 0 \qquad \text{and} \qquad \overline{w} = 0.$$

Then u is the along-wind component, v the crosswind component and w the component normal to the mean flow, called vertical. In these coordinates the covariances have their physical meaning: $\overline{u'w'}$ is the vertical flux of along-wind momentum, uncontaminated by the along-wind variance, and $\overline{v'w'}$ the crosswind stress. Chapter 9 derived the usual double rotation, a turn about the vertical axis followed by a tilt about the new crosswind axis, and the planar-fit alternative, which fits one tilted plane to the mean winds of many periods and keeps the coordinates fixed to the terrain.

The rotation changes the meaning of the symbols, and the change is a frequent source of error. After rotation, u and v are no longer the eastward and northward components of equation (22.2); a direction computed from the rotated components is meaningless. The wind direction β must be computed from the unrotated horizontal components, after they have been referred to true north with the azimuth of the sensor's axes measured at installation, and a record that stores only rotated components has lost its direction.

22.5 Wind profiling instruments

In-situ sensors measure at one height. The wind at turbine and conductor heights, and above them through the boundary layer, requires either a tall tower or an instrument that measures a profile. This section describes Doppler lidar, sodar, Doppler radar, radiosondes and tall towers, and then compares remote sensing with tower measurements.

22.5.1 Doppler lidar

Principle. A Doppler lidar (light detection and ranging) sends pulses or a focused beam of infrared laser light into the atmosphere and receives the light scattered back by aerosol particles, dust, haze and droplets, carried by the air. The motion of the particles shifts the frequency of the returned light by the Doppler effect,

$$\Delta f_D = \frac{2\,v_r}{\lambda_w}, \tag{22.14}$$

where v_r is the *radial* or line-of-sight velocity, the component of the air velocity along the beam, positive away from the instrument, and λ_w is the transmitted wavelength. For an illustrative $\lambda_w = 1.5\,\mu$m, a radial velocity of $1\,\mathrm{m\,s^{-1}}$ shifts the frequency by $2/(1.5\times10^{-6}) = 1.33\times10^{6}$ hertz. The range of each measurement follows from the travel time of the pulse or from the focus distance of the beam.

Retrieval. The lidar measures only v_r. To obtain the horizontal wind it points its beam in several directions and combines the radial velocities under an assumption about the flow. Consider two beams in the east–west plane, each tilted by the zenith angle χ from the vertical, one toward the east and one toward the west. With u and w the same at both beams,

$$v_{r,E} = u\sin\chi + w\cos\chi, \qquad v_{r,W} = -u\sin\chi + w\cos\chi, \tag{22.15}$$

and solving,

$$u = \frac{v_{r,E} - v_{r,W}}{2\sin\chi}, \qquad w = \frac{v_{r,E} + v_{r,W}}{2\cos\chi}; \tag{22.16}$$

a north–south pair gives v the same way. The assumption that u and w are the same at both beams is a *retrieval assumption*: the flow must be horizontally homogeneous over the volume the beams sample. At 100 m above the instrument with $\chi = 28^\circ$, the two beams are $2\times100\times\tan28^\circ = 106$ m apart. For a uniform wind $u = 8\,\mathrm{m\,s^{-1}}$, $w = 0$, the radial velocities are $\pm8\sin28^\circ = \pm3.76\,\mathrm{m\,s^{-1}}$, and equation (22.16) returns $8.00\,\mathrm{m\,s^{-1}}$. On a hilltop the assumption fails. If the air rises at $0.5\,\mathrm{m\,s^{-1}}$ under the upwind (west) beam and sinks at $0.5\,\mathrm{m\,s^{-1}}$ under the downwind (east) beam, illustrative values for a westerly over a rounded crest, then $v_{r,E} = 3.76 - 0.5\cos28^\circ = 3.31\,\mathrm{m\,s^{-1}}$, $v_{r,W} = -3.76 + 0.44 = -3.31\,\mathrm{m\,s^{-1}}$, and the retrieved speed is $6.63/(2\sin28^\circ) = 7.06\,\mathrm{m\,s^{-1}}$, 12 % low, with a retrieved w of zero. The instrument works perfectly and the retrieval is wrong.

Strengths and limits. The lidar is a remote-sensing instrument that needs no tower, gives vertical profiles, and reaches through hundreds of meters or more, typically from about 40 m to 1 to 3 km. Its limits are that it needs aerosols, so very clean air weakens its signal; that it measures the line-of-sight velocity, from which the wind follows only through retrieval assumptions; that its performance degrades in fog, low cloud and heavy precipitation, which attenuate the beam; that each measurement averages over a probe volume tens of meters long along the beam; and that it has a blind zone near the ground.

22.5.2 Sodar

A sodar (sound detection and ranging) sends pulses of audible sound, of a few kilohertz, upward in several tilted beams and listens for the echo. The sound is scattered by small-scale fluctuations of temperature, which change the speed of sound and so act as reflectors. The echo is Doppler shifted by the motion of the air, $\Delta f_D = 2v_r f_0/c_s$ for a transmitted frequency f_0; for $f_0 = 3000$ Hz and $v_r = 1\,\mathrm{m\,s^{-1}}$ the shift is $2\times3000/343 = 17.5$ Hz. The beam geometry and the retrieval are those of the lidar, equations (22.15) and (22.16), with the same assumption of homogeneous flow, so a sodar retrieves vertical profiles of the wind.

Its advantages are a lower cost than some lidar systems and good coverage of the lower atmosphere, typically from about 20 m to 200–500 m. Its limits are acoustic noise, from traffic, machinery and the wind itself around the antenna, which drowns the weak echo in strong winds; range limits, since sound is attenuated and the echo needs temperature fluctuations, which are weak in well-mixed neutral air; sensitivity to precipitation, which adds noise and its own scattering; and site constraints: nearby towers, trees or buildings return fixed echoes, and the audible pulses can disturb neighbors.

22.5.3 Doppler radar

A Doppler radar measures the radial velocity of scatterers in its beam from the Doppler shift of radio waves: raindrops, snow, insects, or fluctuations of the refractive index of clear air. A scanning weather radar maps the radial velocity over a region a few hundred kilometers across, and it is especially useful for the larger-scale wind structure: fronts, the outflow of convective storms, low-level jets at some height above the ground.

A standard weather radar is not, however, a point near-surface wind instrument. Its beam rises with distance, because it leaves the antenna at a small elevation angle and because the Earth curves away beneath it. With the usual allowance for refraction, which replaces the Earth's radius $R_\mathrm{E} = 6371\,\mathrm{km}$ by $\frac{4}{3}R_\mathrm{E}$, the height of the beam center at range r and elevation angle ε_b is about

$$h_b \approx r \tan \varepsilon_b + \frac{r^2}{2 \times \frac{4}{3} R_\mathrm{E}}. \tag{22.17}$$

For $\varepsilon_b = 0.5^\circ$ and $r = 50\,\mathrm{km}$, $h_b \approx 436 + 147 \approx 580\,\mathrm{m}$ above the radar, and a beam 1° wide is about 870 m wide there. Beyond a few tens of kilometers the radar observes winds hundreds of meters above the ground averaged over volumes hundreds of meters across, and only their radial component. Vertically pointing radar wind profilers use the same principle to give profiles from about 100 m to several kilometers above a site (Chapter 18).

22.5.4 Radiosondes

A *radiosonde* is a small instrument package carried aloft by a balloon, transmitting its measurements by radio. It measures pressure, temperature, humidity and, with a satellite positioning receiver, its own position. The wind is inferred from the drift of the balloon: the horizontal displacement between successive positions divided by the time between them is the horizontal wind averaged over the layer the balloon crossed. With a typical ascent rate of about $5\,\mathrm{m\,s^{-1}}$, a layer 100 m deep is crossed in 20 s, so the sounding resolves the vertical structure of the wind in detail.

A radiosonde provides excellent vertical profiles, from the surface to the stratosphere, but operationally typically only one or two launches per day at many sites, at fixed universal times that fall at different local times at different longitudes. Its temporal resolution is therefore limited: a sounding is a snapshot, and a low-level jet that forms after midnight and decays after sunrise may fall between two launches. Two further limits matter near the ground: the balloon drifts with the wind, tens of kilometers by the time it reaches the middle of the troposphere, so the profile is not vertical; and the lowest tens of meters are often poorly resolved, because the sensors are still adjusting after the launch and the launch site is surrounded by buildings.

22.5.5 Tall meteorological towers

A tall meteorological tower carries anemometers, vanes and thermometers at several fixed heights, for example 10, 30, 60, 100 and 200 m, often with sonic anemometers at some of them. Such towers are extremely valuable because they directly characterize the vertical structure of the lower boundary layer, continuously and at high frequency: the shear, the directional

turning, the stability and the turbulence. With illustrative readings of $6\,\mathrm{m\,s^{-1}}$ at 10 m and $9\,\mathrm{m\,s^{-1}}$ at 100 m, the power-law exponent of the shear is $\alpha = \ln(9/6)/\ln(100/10) = 0.18$. The directional turning is the difference of directions between two levels, computed on the circle as

$$\Delta\beta = \left[(\beta_{\mathrm{upper}} - \beta_{\mathrm{lower}} + 180^\circ) \bmod 360^\circ\right] - 180^\circ, \tag{22.18}$$

which keeps the result between -180° and $+180^\circ$; a positive value is a clockwise turning with height. In the friction layer the wind turns from its cross-isobar surface direction toward the geostrophic direction with height (Chapter 3): clockwise in the Northern Hemisphere and counterclockwise in the Southern. A Northern Hemisphere tower might read 250° at 10 m and 265° at 100 m, $\Delta\beta = +15^\circ$; a Southern Hemisphere tower might read 250° and 235°, $\Delta\beta = -15^\circ$. Temperatures at two or more levels give the stability (Chapter 13), and sonic anemometers at several levels the turbulence and the fluxes.

Tall towers are, however, expensive to build and maintain, and they are sparse; most regions have none. Their heights are fixed, their structure distorts the flow at every level (Section 22.4.1), and they rarely exceed 200 to 300 m, often below the core of a nighttime low-level jet.

22.5.6 Remote sensing against tower measurements

The two families complement each other. A tower gives a direct, local measurement, with excellent temporal resolution and without retrieval assumptions, but limited vertical extent. A lidar or sodar gives remote vertical profiling, with greater height coverage and no structure in the flow, but it requires retrieval assumptions, averages over volumes tens of meters to a hundred meters across, and misses the lowest meters. Their ten-minute mean speeds agree closely over flat, uniform terrain where the assumptions hold; their turbulence statistics do not, because the volume averaging and the scanning of a lidar filter the fluctuations differently from a point sensor. Using both together can be very powerful: a short tower checks the remote sensor at the overlapping heights and in the local terrain, and the remote sensor extends the profile above the tower.

Table 22.2 lists the profiling instruments with their typical height range, their vertical and temporal resolution and their main limits. Figure 22.7 shows the same height ranges graphically. Its horizontal axis lists the instruments; its vertical axis is height above ground on a logarithmic scale from 1 m to 30 km. Dark bars are the typical range, light bars extensions reached only under good conditions or at some ranges; the dotted lines mark the 10 m of standard wind and the 150 m upper end of the engineering heights of this book. Only the tower and the remote profilers cover the engineering range continuously, and only the remote profilers reach well above it.

22.6 Measurement errors and quality control

Every wind observation has an uncertainty, and the largest part of it often does not come from the instrument. This section lists the sources of measurement uncertainty, separates instrument error from representativeness error, treats icing and the problems of light wind, sets out the usual quality-control checks with a worked suspicious case, and ends with the complete description of a wind value.

22.6.1 Sources of measurement uncertainty

The uncertainty of a wind measurement has several sources: the calibration of the sensor; its alignment, to north for a vane and to the vertical for a sonic anemometer; its response time, which smooths gusts and turbulence; icing; electronic noise in the signal and the logger; and flow distortion by the mounting. Each can be estimated. An illustrative budget for the ten-minute

Table 22.2: Wind profiling instruments. Ranges and resolutions are typical and illustrative; they depend on the instrument and the atmospheric conditions.

Instrument	Height range	Resolution	Main limits
Tall tower	fixed levels to 100–200 m, rarely 300 m	a few levels; seconds or faster	expensive, sparse; flow distortion at each level; often below a jet core
Sodar	about 20 to 200–500 m	gates of about 10–20 m; profiles every few minutes	acoustic noise; range; precipitation; fixed echoes; retrieval assumption
Doppler lidar	about 40 m to 1–3 km	gates of about 20–30 m; profiles every seconds to minutes	needs aerosols; fog, cloud and rain; line-of-sight velocity; retrieval in complex terrain
Radar wind profiler	about 100 m to several kilometers	gates of tens of meters or more; profiles every several minutes	lowest gate high; coarse near the ground
Weather radar	hundreds of meters to about 10 km, rising with range	beam hundreds of meters wide at tens of kilometers	radial velocity only; needs scatterers; not a near-surface point wind
Radiosonde	surface to about 30 km	meters to tens of meters vertically; one or two profiles a day	snapshot; balloon drift; lowest tens of meters poorly resolved

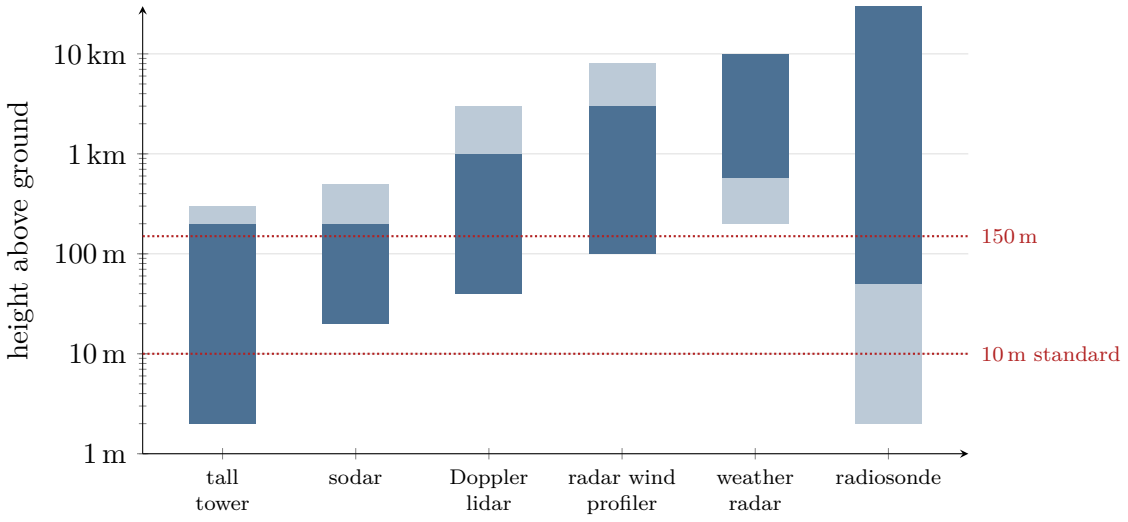


Figure 22.7: Typical height coverage of wind profiling instruments, illustrative, on a logarithmic height axis. Dark: typical range; light: reached only in good conditions (tower: the tallest towers; sodar and lidar: clean, favorable air; radar profiler: deep-reaching systems; radiosonde: lowest tens of meters poorly resolved; weather radar: lower beams near the radar, 580 m at 50 km by equation (22.17)).

mean of a well-installed cup anemometer at $8\,\mathrm{m\,s^{-1}}$ might assign 1 % to calibration, 1 % to flow distortion outside the shadow sector and 0.5 % to overspeeding and response. Independent errors add in quadrature, so the combined standard uncertainty is

$$\sqrt{1^2 + 1^2 + 0.5^2}\,\% = 1.5\,\%, \qquad 0.015 \times 8\,\mathrm{m\,s^{-1}} = 0.12\,\mathrm{m\,s^{-1}};$$

electronic noise, averaged over thousands of samples, adds almost nothing to a ten-minute mean. For a vane, an alignment uncertainty of two to five degrees (illustrative) usually dominates the direction error.

These errors are real, and a good installation keeps them small. They may nevertheless be smaller than another, larger source of error that no calibration addresses: the representativeness error.

22.6.2 Instrument error and representativeness error

Suppose an anemometer is perfectly calibrated, but it sits behind a row of trees, beside a building, or in a small valley. If its reading is compared with the wind of a weather model's grid cell 3 km across, the mismatch may be huge. That mismatch is not necessarily an error of the sensor or of the model: the two may simply represent different spatial scales, one the wind at a sheltered point and the other the average wind of a cell of nine square kilometers. The distinction is essential, and it has two names:

- *Instrument error*: the sensor measures the local wind inaccurately. Calibration, maintenance and better mounting reduce it.
- *Representativeness error*: the local wind is measured correctly, but it is not representative of the quantity being compared or inferred: the wind of a grid cell, the wind at a conductor a kilometer away, the regional wind at hub height. A better instrument does not reduce it at all.

In short,

$$\text{measurement accuracy} \neq \text{representativeness}.$$

With the budget of the previous subsection, the instrument error of a ten-minute mean at $8\,\mathrm{m\,s^{-1}}$ is about $0.12\,\mathrm{m\,s^{-1}}$. If the same anemometer stands where nearby trees reduce the wind by an illustrative 30 % relative to the open surroundings, its reading differs from the wind of the open terrain by $2.4\,\mathrm{m\,s^{-1}}$, twenty times the instrument error, with a perfect instrument. The remedies lie elsewhere: in the siting of the sensor, the subject of Chapter 23, and in modeling the difference between the point and the quantity of interest, by exposure corrections and downscaling (Chapter 28).

22.6.3 The point and the grid cell

An anemometer measures the local flow around the instrument: the air crossing a cup rotor ten or twenty centimeters across, or the 0.15 m paths of a sonic anemometer, a volume of the order of a thousandth of a cubic meter. A weather model's grid cell represents an area of 1 to $100\,\mathrm{km^2}$, grid spacings of 1 to 10 km; a cell 3 km wide with a lowest layer 20 m deep holds $9 \times 10^6\,\mathrm{m^2} \times 20\,\mathrm{m} = 1.8 \times 10^8\,\mathrm{m^3}$ of air, eleven orders of magnitude more than the sonic's volume. Time averaging narrows the gap only partly: in a ten-minute mean at $6\,\mathrm{m\,s^{-1}}$ about 3.6 km of air passes the sensor (Chapter 1), but that air is a line upstream along the wind, not the area of the cell, and it carries the imprint of the obstacles and terrain next to the sensor.

A point-to-grid comparison therefore always contains a spatial sampling difference, and direct one-to-one validation of a model against a station requires care. The comparison is fairest

when both values are brought to the same height and the same averaging interval, when the station is representative of its surroundings, and when statistics over many periods and many stations are compared rather than single values; Chapters 23 and 24 treat these steps. The same care applies in the other direction: a grid-cell value is not wrong because it does not match one point inside the cell.

22.6.4 Icing, starting threshold and calm winds

Icing. In cold, humid conditions, supercooled fog, freezing drizzle or wet snow, ice can severely affect mechanical anemometers. Rime on the cups changes their shape and adds mass and friction, so the rotor turns slower than the wind and reads low; ice in the bearings or around the rotor freezes the cups, and the anemometer reports a calm in a moderate wind; a frozen vane reports the same direction for hours, whatever the wind does. Heated instruments, with heated cups, vanes or sonic transducers, mitigate the problem at the cost of power. For operational wind monitoring, icing quality-control flags matter: a transmission-line rating computed from an iced anemometer's calm assumes far less convective cooling than the conductor actually has, and one computed from a frozen vane uses a wrong angle between the wind and the conductor. Typical flags combine an air temperature near or below 0°C and a high humidity with a symptom in the record: a speed of zero while other sensors report wind, a direction that does not change, or an unheated sensor falling below a heated one at the same height.

Starting threshold. Mechanical anemometers need a minimum wind speed before they begin rotating reliably, the *starting threshold*, illustratively a few tenths of a meter per second for a cup, and similar for a vane; the offset a_0 of equation (22.4) is related to it. Below the threshold the sensor reports zero or turns intermittently, so very low-wind measurements are biased low and the frequency of calms is overstated. The bias falls on the stable nights of Chapter 17, when the wind near the ground is weakest, and it grows with the age of the bearings. A sonic anemometer has no starting threshold, only its noise.

Direction in calm air. When $U \approx 0$, the wind direction becomes poorly defined, because equation (22.3) divides a direction out of components that are themselves near zero. A vane may point essentially arbitrarily, usually wherever it last stopped. A sonic anemometer computes a direction from components dominated by noise: with an illustrative noise of $0.02\,\mathrm{m\,s^{-1}}$ in each component and a wind of $0.05\,\mathrm{m\,s^{-1}}$, the direction is uncertain by about $\arctan(0.02/0.05) = 22°$, and at lower speeds by any amount. Calm-period direction data therefore require special treatment: below a stated speed, such as $0.5\,\mathrm{m\,s^{-1}}$ (illustrative), the direction is reported as calm or variable and excluded from direction statistics, or the directions are weighted by speed so that the calm periods carry little weight. Wind roses carry a separate calm category for this reason (Chapter 19). The detail is small and important: it decides the directions of exactly the weak-wind periods that limit the cooling of a conductor.

22.6.5 Quality-control checks

Before wind data are used, they are screened by quality control: automated and manual checks that flag values that cannot be correct, or probably are not. Table 22.3 lists the basic checks for wind, with what each detects and an example of a test; the thresholds are illustrative and are tuned to each site and instrument. The checks cover impossible values, stuck sensors, sudden unrealistic jumps, missing data, the consistency of speed and direction, the tower-wake sectors of Section 22.4.2 and icing. On a tower with several heights, the vertical consistency of the profile can also be checked, which is the most powerful test because it brings physics to bear.

Table 22.3: Basic quality-control checks for wind data. Thresholds are illustrative.

Check	Detects	Example test
Impossible values	sensor or logger faults	speed below 0 or above $75\,\mathrm{m\,s^{-1}}$ near the ground; direction outside 0–360°
Stuck sensor	frozen or failed sensor, repeated last value	speed or direction unchanged for 1 h while the speed exceeds $2\,\mathrm{m\,s^{-1}}$
Sudden jumps	spikes, electrical interference	change of more than $10\,\mathrm{m\,s^{-1}}$ between consecutive ten-minute means without a matching change at other sensors
Missing data	logger or communication gaps	fraction of valid samples in the period below 90 %
Speed–direction consistency	failed anemometer or vane	direction changing while the speed is zero; speed of zero during strong wind at nearby sensors
Tower-wake sectors	tower shadow	direction within the shadow sector of the boom; ratio of opposite-boom sensors far from one
Icing	iced cups or vane	air temperature below about 1°C, high humidity, and a stuck or falling reading
Vertical consistency	failure at one level	a level whose speed departs from the profile of its neighbors by more than physics allows

A flag records a suspicion; it does not delete the value. The raw data are kept, the flags are stored beside them, and each use of the data decides which flags exclude a value, so that a decision can be revisited when the cause of a problem becomes known.

22.6.6 A suspicious profile

Suppose three anemometers on one tower report, for the same ten-minute period,

$$U_{10} = 8\,\mathrm{m\,s^{-1}}, \qquad U_{20} = 8.5\,\mathrm{m\,s^{-1}}, \qquad U_{40} = 0.2\,\mathrm{m\,s^{-1}}.$$

The 40 m value is suspicious, and the profile of Chapter 12 quantifies why. Fitting $U = A + B \ln z$ through the two lower levels gives $B = 0.5/\ln 2 = 0.72\,\mathrm{m\,s^{-1}}$, which is u_*/κ and corresponds to $u_* = 0.4 \times 0.72 = 0.29\,\mathrm{m\,s^{-1}}$, and the extrapolation to 40 m gives

$$U_{40} \approx 8.5 + 0.72 \ln \frac{40}{20} = 8.5 + 0.50 = 9.0\,\mathrm{m\,s^{-1}}.$$

Other plausible profiles, with any stability and roughness, give values between the $8.5\,\mathrm{m\,s^{-1}}$ of no shear and about $11.2\,\mathrm{m\,s^{-1}}$, the value of a power-law exponent of 0.4 above 20 m, very strong shear. A reading of $0.2\,\mathrm{m\,s^{-1}}$ is forty-five times smaller than the extrapolated $9.0\,\mathrm{m\,s^{-1}}$; it would require the wind to fall by $8.3\,\mathrm{m\,s^{-1}}$ over twenty meters above two levels where it increases with height, a shear no boundary layer sustains.

Figure 22.8 draws the case. The horizontal axis is wind speed and the vertical axis height above ground. The blue dots are the two consistent readings, the red cross the suspicious one; the dashed curve is the logarithmic fit through the lower two levels, extended to 40 m; and the gray bar at 40 m spans the plausible range of the previous paragraph. The red cross lies far outside it.

The possible causes are instrumental: a sensor failure, such as a seized bearing; icing, which can affect the highest level first when it lies in cloud or fog; or a communication issue, a logger channel or a transmission that delivered a placeholder instead of a value. None of them is a property of the wind, and the value is flagged. Physics provides powerful quality-control

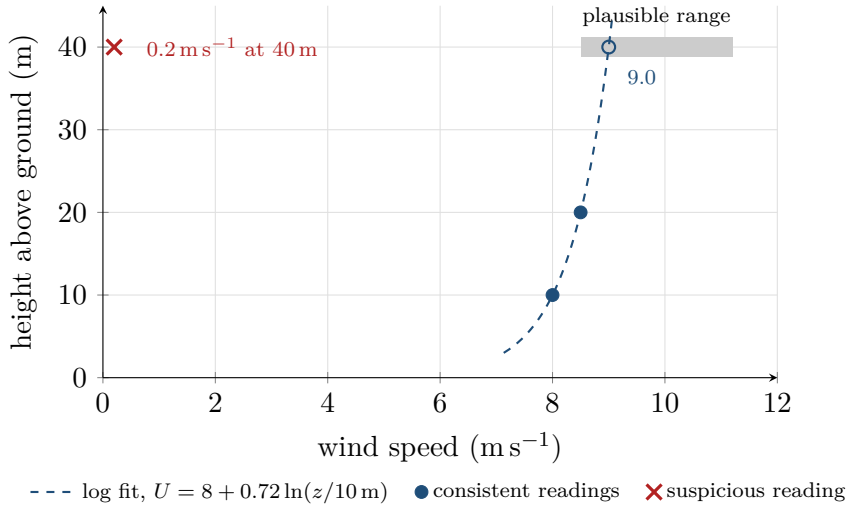


Figure 22.8: Vertical-consistency check on a three-level tower (illustrative). The logarithmic fit through $U_{10} = 8\,\mathrm{m\,s^{-1}}$ and $U_{20} = 8.5\,\mathrm{m\,s^{-1}}$, $U = 8 + 0.72\ln(z/10\,\mathrm{m})$, extrapolates to $9.0\,\mathrm{m\,s^{-1}}$ at 40 m; the gray bar spans 8.5 to $11.2\,\mathrm{m\,s^{-1}}$, the range of power-law exponents from 0 to 0.4 above 20 m. The reported $0.2\,\mathrm{m\,s^{-1}}$ is physically implausible.

constraints, because the profile relations of the earlier chapters bound what neighboring levels can report. The constraint is asymmetric: a weak wind near the ground under a strong wind aloft is common on stable nights, when the surface layer decouples (Chapter 17), and must not be flagged on that ground alone; a near calm above two levels of steady, increasing wind is not.

22.6.7 The complete description of a wind value

The checks of this section and the conventions of the whole chapter reduce to ten questions to ask of any wind observation. Table 22.4 lists them with the reason each matters and the place where this book treats it. Only after these questions have been answered should a number be treated as "the wind."

Table 22.4: Ten questions to ask of a wind observation.

	Question	Why it matters	Treated in
1	What instrument?	speed, component or vector; response, threshold, overspeeding	Section 22.2
2	What height?	wind changes with height; AGL against MSL	Section 22.1.4
3	What sampling frequency?	which fluctuations are resolved; aliasing	Section 22.3.1, 22.3.2
4	What averaging interval?	a gust, a ten-minute mean and an hourly mean differ	Section 22.3.4
5	What coordinate convention?	from or toward; true or magnetic north; rotated components	Section 22.1.2, 22.4.5
6	What is the surrounding terrain?	speed-up, sheltering, channeling	Chapters 20, 23
7	What is upstream?	obstacles, roughness changes, internal boundary layers	Chapters 11, 23
8	Is there flow distortion?	tower shadow, boom orientation, tilt	Section 22.4
9	Is the sensor inside a roughness sublayer?	the profile laws do not hold among the obstacles	Chapters 11, 21
10	What spatial scale does the value represent?	point against grid cell; representativeness error	Section 22.6.2, 22.6.3

A wind measurement is therefore never just $U = 8\,\mathrm{m\,s^{-1}}$. A physically complete description is more like

$$U = 8\,\mathrm{m\,s^{-1}} \text{ at } 20\,\mathrm{m} \text{ AGL, ten-minute scalar mean, cup anemometer sampled at } 1\,\mathrm{Hz}, \text{ on a boom with westerly exposure,}$$

together with the direction in its convention, the instrument's distance constant and the quality flags of the period. Even then, the description says how well the value describes the air at the sensor, not whether the sensor's site is representative of the place and the quantity for which the value will be used. That second question, of the measurement height, the exposure, the obstacles and the terrain around the sensor, is the subject of the next chapter, Chapter 23, on measurement height and exposure.

22.7 What to retain

Definition 22.1 (Wind measurement)**.** A wind measurement is a statistic of a vector, made at one point by one instrument with its own response, at a stated height, sampling rate, averaging interval, coordinate convention and mounting; its instrument error describes how well it measures the air at that point, and its representativeness error how well that point stands for the quantity it is used for, and the second is often the larger.

Table 22.5 lists the terms of the chapter, their meaning, their units and the subsection that defines each.

22.8 Exercises

Exercise 22.1. A coastal station in southern Brazil, at 23°S, reports three consecutive ten-minute values: $4\,\mathrm{m\,s^{-1}}$ from 350°, $6\,\mathrm{m\,s^{-1}}$ from 10° and $5\,\mathrm{m\,s^{-1}}$ from 20°. (a) Compute u and v for each value. (b) Compute the arithmetic mean of the three directions and explain why it is wrong. (c) Compute the vector mean speed and direction and the scalar mean speed, and their ratio. (d) Give the mathematical angle of the mean vector. (e) The anemometer is 10 m AGL and the ground at the station lies 15 m MSL; give the sensor's elevation above mean sea level.

Exercise 22.2. A mast in northeastern Brazil, in the trade winds, sees winds mostly from 100° to 140°. A single boom carries the main anemometer, and the tower shadow covers 20° on either side of the direction from the sensor to the tower. (a) For a boom pointing west, which wind directions are shadowed, and how much of the prevailing sector do they cover? (b) Choose a boom azimuth that keeps the prevailing sector clean and give its shadow sector. (c) A sonic anemometer on the mast is tilted by 1.5° in a wind of $12\,\mathrm{m\,s^{-1}}$; compute the horizontal wind that leaks into w and compare it with a mean vertical velocity of $0.01\,\mathrm{m\,s^{-1}}$. (d) A tall tower nearby reads 110° at 10 m and 95° at 100 m. Compute $\Delta\beta$ with equation (22.18) and say whether the sense of turning is the one expected for the friction layer in this hemisphere.

Exercise 22.3. A cup anemometer with a distance constant of 2.5 m is sampled at 1 Hz. (a) Compute its response time and cutoff frequency in winds of 4 and $12\,\mathrm{m\,s^{-1}}$. (b) Compute the Nyquist frequency of the record, and the frequency at which a fluctuation of 0.7 Hz in the sensor output would appear. (c) In which wind is the time resolution of the record limited by the logger, and in which by the sensor? (d) A ten-minute period has a mean of $9\,\mathrm{m\,s^{-1}}$ and a highest three-second gust of $13.5\,\mathrm{m\,s^{-1}}$. Compute the gust factor, and the turbulence intensity it implies with a peak factor of 2.5.

Exercise 22.4. (a) A sonic anemometer path is 0.12 m long. The transit times are $t_1 = 341.88\,\mu\mathrm{s}$ and $t_2 = 349.85\,\mu\mathrm{s}$. Compute the along-path wind component and the speed of sound. (b)

Table 22.5: The terms of the chapter and where each is defined.

Term	Meaning	Units	Defined in
Meteorological direction β	direction the wind comes from, clockwise from true north; $\alpha_m = 270^\circ - \beta$	degree	22.1.2
AGL, MSL	height above the local ground; height above mean sea level	m	22.1.4
Cup anemometer	mechanical sensor of horizontal speed using rotating cups, $U = a_0 + a_1\omega$	m/s	22.2.1
Distance constant ℓ_d	length of air for 63 % of a step response; $\tau_r = \ell_d/U$	m	22.2.2
Overspeeding	positive bias of a cup in turbulence, from faster response to rising wind	m/s	22.2.3
Propeller anemometer	axis-sensitive mechanical sensor with a cosine response	m/s	22.2.4
Wind vane	instrument measuring wind direction	degree	22.2.4
Sonic anemometer	ultrasonic instrument measuring u, v, w from transit times	m/s	22.2.5
Sonic temperature T_s	$c_s^2/((c_p/c_v)R_d) = T(1 + 0.51q)$, close to T_v	K	22.2.6
Sampling rate f_s	number of recorded values per second	Hz	22.3.1
Nyquist frequency f_N	$f_s/2$, highest resolvable frequency	Hz	22.3.2
Aliasing	appearance of fluctuations above f_N at $f_s - n$	–	22.3.2
Response time τ_r	physical time for a sensor to follow a change of the wind	s	22.2.2, 22.3.3
Averaging interval	period over which wind statistics are computed	s, min	22.3.4
Gust factor G	gust speed divided by the mean wind of the period	–	22.3.5
Scalar and vector mean	mean of speeds; magnitude of the mean vector, never larger	m/s	22.3.7
Flow distortion	modification of the measured flow by the sensor and its mounting	–	22.4.1
Tower shadow	distorted flow in the tower's wake, in a sector of directions	–	22.4.2
Coordinate rotation	rotation to $\overline{v} = 0$, $\overline{w} = 0$ before computing covariances	–	22.4.5
Lidar	laser-based remote wind profiler, line-of-sight velocity	m/s	22.5.1
Sodar	acoustic remote wind profiler	m/s	22.5.2
Radiosonde	balloon-borne profile instrument; wind from the drift	–	22.5.4
Instrument error	error of the sensor in measuring the local wind	m/s	22.6.2
Representativeness error	difference caused by mismatched spatial or physical scales	m/s	22.6.2
Starting threshold	minimum speed at which a mechanical sensor turns reliably	m/s	22.6.4
Quality control	checks that flag values that cannot be, or probably are not, correct	–	22.6.5

Compute the sonic temperature and, for a specific humidity of $0.018\,\mathrm{kg\,kg^{-1}}$, the air temperature. (c) A tower reads $5.0\,\mathrm{m\,s^{-1}}$ at 10 m, $6.2\,\mathrm{m\,s^{-1}}$ at 30 m, $6.9\,\mathrm{m\,s^{-1}}$ at 60 m and $0.0\,\mathrm{m\,s^{-1}}$ at 100 m, with the 100 m vane fixed at 215° for the past three hours and an air temperature of $-2\,^{\circ}\mathrm{C}$ in fog. Fit a logarithmic profile through the two lowest levels, extrapolate it to 60 and 100 m, and decide which checks of Table 22.3 the 100 m value fails and what the most likely cause is.

Chapter 23

Measurement Height and Exposure

23.1 Height and the standard measurement

Chapter 22 treated the instruments: how cups, vanes, sonic anemometers and remote sensors measure, with what response, and with what instrument error. A perfectly calibrated instrument can still report a wind that represents the flow of interest poorly, because what it reports depends on where it stands: at what height, above what surface, behind which obstacles and on what part of the terrain. The question of this chapter is

when does a wind sensor measure the wind that is actually wanted?

The answer is a matter of siting, and it is as important as the accuracy of the instrument. The chapter follows the siting problem outward from the sensor: the measurement height and the standard surface wind; the obstacles, the fetch and the footprint upwind of the sensor; the terrain around it; the representativeness of a point reading for an area, a height or a flow regime; the comparison of a station with a weather model, with the corrections that can and cannot be made; and the metadata, homogeneity and network design that make a wind record interpretable.

Jargon: exposure, siting, height above ground level, mean sea level, standard surface wind, open terrain, representativeness

Exposure is the degree to which a sensor samples the undisturbed flow it is intended to represent: how freely it interacts with the approaching air, given the obstacles, the surface and the terrain around it. It has no unit; it is described by the surroundings of the sensor in each direction and, operationally, by an exposure class. *Siting* is the choice of the location and height of a sensor. *Height above ground level* (AGL), in meters, is the vertical distance from the local ground to the sensor; the elevation of the ground itself is given above *mean sea level* (MSL). The *standard surface wind* is the wind measured at about 10 m AGL over *open terrain*, ground with few obstacles and low vegetation over a long distance in every direction; it is written U_{10}. *Representativeness* is the degree to which a measurement stands for the quantity it is used for: the wind over an area, at another height, or in another flow regime.

Key idea

A wind sensor does not measure a universal quantity called the local wind. It measures the wind at one height, at one point, with one directional exposure, under one terrain and roughness regime. Before a measurement is compared with a model, with another station or with the wind at an engineering asset, the first question is whether the two quantities represent the same flow.

23.1.1 Measurement height

Near the surface the mean wind usually increases with height, because the surface removes momentum from the air and turbulence carries that loss upward (Chapters 7 and 12). In the surface layer, therefore,

$$U(z_2) > U(z_1) \qquad \text{for} \quad z_2 > z_1. \tag{23.1}$$

The exceptions are local and known: above the core of a low-level jet the speed decreases with height (Chapter 18), and inside a canopy, a recirculation zone or the wake of an obstacle the profile can be inverted over a few meters. A 10 m, a 20 m and a 50 m wind are therefore different physical quantities, not three estimates of one.

The neutral logarithmic profile of Chapter 12, $U(z) = (u_*/\kappa)\ln(z/z_0)$, makes the difference concrete. Dividing the profile at z_2 by the profile at z_1 removes the friction velocity:

$$\frac{U(z_2)}{U(z_1)} = \frac{\ln(z_2/z_0)}{\ln(z_1/z_0)}. \tag{23.2}$$

Take an illustrative open grass site with $z_0 = 0.03\,\mathrm{m}$ and $U_{10} = 6\,\mathrm{m\,s^{-1}}$ in neutral air. The friction velocity is $u_* = 0.4 \times 6/\ln(333) = 2.4/5.809 = 0.41\,\mathrm{m\,s^{-1}}$, and equation (23.2) gives

$$U(2\,\mathrm{m}) = 6\,\mathrm{m\,s^{-1}} \times \frac{\ln 66.7}{\ln 333} = 4.34\,\mathrm{m\,s^{-1}}, \quad U(20\,\mathrm{m}) = 6\,\mathrm{m\,s^{-1}} \times \frac{\ln 667}{\ln 333} = 6.72\,\mathrm{m\,s^{-1}},$$

$$U(50\,\mathrm{m}) = 6\,\mathrm{m\,s^{-1}} \times \frac{\ln 1667}{\ln 333} = 7.66\,\mathrm{m\,s^{-1}}, \quad U(100\,\mathrm{m}) = 6\,\mathrm{m\,s^{-1}} \times \frac{\ln 3333}{\ln 333} = 8.38\,\mathrm{m\,s^{-1}}.$$

Figure 23.1 draws this profile. The horizontal axis is the mean wind speed and the vertical axis the height above ground; the solid curve is the neutral profile with the five values marked, and the dashed curve is a stable profile with the same 10 m wind, drawn up to 50 m.

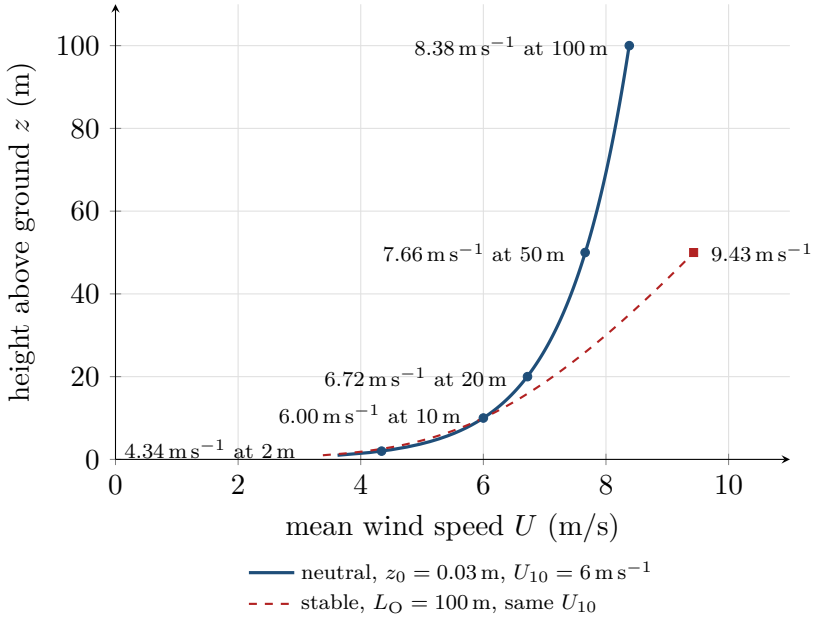


Figure 23.1: Mean wind speed against height over open grass. Solid: neutral logarithmic profile $U(z) = (u_*/\kappa)\ln(z/z_0)$ with $z_0 = 0.03\,\mathrm{m}$, $\kappa = 0.4$ and $u_* = 0.41\,\mathrm{m\,s^{-1}}$, so that $U_{10} = 6\,\mathrm{m\,s^{-1}}$. Dashed: stable profile $U(z) = (u_*/\kappa)[\ln(z/z_0) + 5z/L_O]$ with $L_O = 100\,\mathrm{m}$ and the same 10 m wind ($u_* = 0.38\,\mathrm{m\,s^{-1}}$), drawn to 50 m. Values illustrative.

The 100 m wind is 40 % larger than the 10 m wind over the same ground at the same moment. For a wind turbine with a hub at 100 m, whose power in the operating range grows roughly with

the cube of the speed, the factor $1.40^3 \approx 2.7$ separates the energy implied by the station from the energy available at the hub. A transmission-line sensor at a conductor height of 20 m sees 12 % more wind than the station, and the convective cooling of the conductor depends on that wind, not on the 10 m value. The ratio is not fixed: in the stable case of the figure the 50 m wind is $9.43\,\mathrm{m\,s^{-1}}$, 1.57 times the 10 m wind against 1.28 in neutral air, because stable stratification suppresses the mixing that couples the levels (Chapter 14). A wind value is incomplete without its height, and the height that belongs with it is the height above ground level.

23.1.2 The standard 10 m wind

Meteorological surface wind is conventionally measured at about 10 m AGL over reasonably open terrain. The convention provides a degree of standardization: two stations that follow it measure the same kind of quantity, so their records can be compared, mapped and combined, and a weather model can report its near-surface wind at the same nominal height (Chapter 12 showed how a model diagnoses that value from its lowest level).

The convention fixes the height, not the exposure. A 10 m sensor surrounded by buildings is not aerodynamically equivalent to a 10 m sensor over open grass:

$$\text{same height} \neq \text{same exposure}. \tag{23.3}$$

An illustrative calculation shows the size of the difference. Let the wind at a blending height of 60 m, above which the two surfaces no longer leave separate traces (Chapter 11), be the same over an open field and over a suburb. Over the field, with $z_0 = 0.03$ m and no displacement, the neutral profile gives $U(10\,\mathrm{m})/U(60\,\mathrm{m}) = \ln 333/\ln 2000 = 5.809/7.601 = 0.764$. Over the suburb, with an illustrative $z_0 = 0.5$ m and displacement height $d = 4$ m, it gives $\ln[(10-4)/0.5]/\ln[(60-4)/0.5] = \ln 12/\ln 112 = 2.485/4.718 = 0.527$. The suburban 10 m wind is $0.527/0.764 = 0.69$ of the open value, about 30 % lower, under the same wind aloft. And this is the optimistic estimate: with buildings 8 m tall the suburban sensor sits at 1.25 building heights, inside the roughness sublayer, where the reading depends on the sensor's position relative to individual buildings and the logarithmic profile does not hold at all (Chapter 11).

23.1.3 Exposure

Exposure describes how freely the sensor interacts with the approaching atmospheric flow. Good exposure generally means:

- few nearby obstacles;
- an adequate upwind fetch over a uniform surface;
- no strong local wake at the sensor;
- terrain representative of the area the measurement stands for;
- a sensor high enough above the roughness elements.

Poor exposure may involve buildings, trees, ridges, the sensor's own tower structure, and abrupt land-cover transitions upwind.

Exposure is not a property of the instrument. It is a relation between the sensor, its surroundings, the flow and the quantity the measurement is meant to represent. Its effects are also of a different size from instrument error: a calibrated anemometer is typically accurate to a few tenths of a meter per second (Chapter 22), while the examples of this section change the reading by tens of percent. This is why exposure matters as much as accuracy. Exposure is described by the surroundings in each direction, and the parts of this chapter supply its ingredients: the obstacles and fetch (Section 23.2), the terrain (Section 23.3), and the exposure classes in which networks record it (Section 23.6).

23.1.4 Upwind and downwind surroundings

A wind sensor responds primarily to the surface and the obstacles that the air encountered before reaching it. The air arriving at the sensor carries the momentum deficit, the turbulence and the profile it acquired upwind, because the mean wind advects them downstream faster than turbulence can erase them (Chapter 7). If the wind is from the west, the landscape that matters is the one west of the sensor. When the wind shifts to the east, the landscape that matters becomes the one east of it, and the relevant exposure changes with it.

The downwind surroundings are not irrelevant, only less important. An obstacle downwind of the sensor raises the pressure on its windward face, and that pressure perturbation slows and deflects the approaching air over a distance of about one to two obstacle heights upwind of the obstacle, as the raised windward pressure of a hill does on a larger scale (Chapter 20). A sensor a few meters in front of a wall is therefore disturbed, while a sensor ten obstacle heights in front of it is not. Beyond that short distance, exposure is set by what lies upwind, and it is a function of wind direction.

23.1.5 Directional exposure

Because exposure follows the upwind direction, a single station can have good exposure in one sector and poor exposure in another. Figure 23.2 is a plan view of an illustrative station, with north at the top. The mast is at the center; the four sectors are separated by the diagonal lines; the dashed circle has a radius of about 300 m. West and north of the mast lies an open field; east of it, a forest with trees about 20 m tall begins about 150 m away; south of it, a group of buildings stands about 60 m away. The geometry holds in either hemisphere.

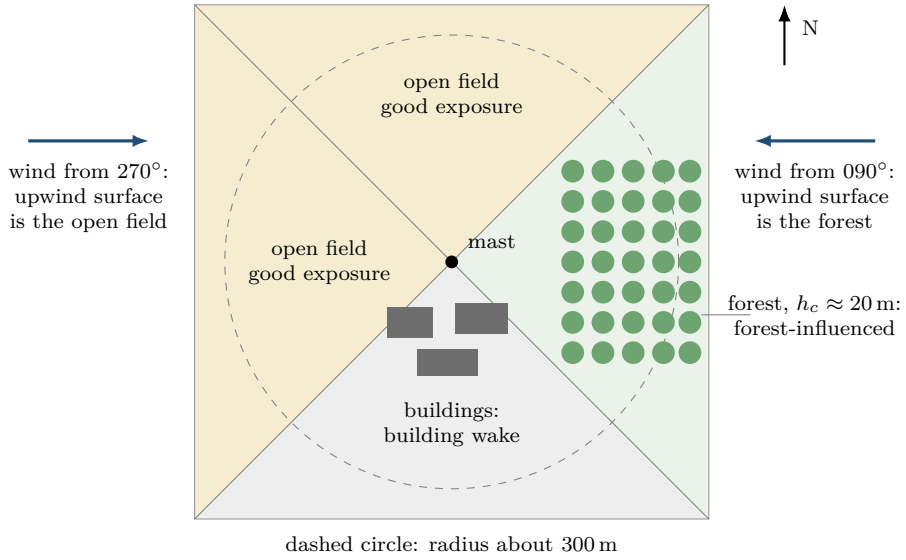


Figure 23.2: Directional exposure of an illustrative station (plan view, north at the top, schematic, valid in either hemisphere). The diagonal lines divide the surroundings into four sectors of 90°; the dashed circle has a radius of about 300 m. The exposure of the mast depends on which sector lies upwind.

The figure shows one mast with three exposures. For winds from the west sector, 225° to 315°, and from the north, the upwind surface is the open field and the exposure is good. For winds from the east sector the air has just crossed the forest edge: the reading is forest-influenced, lower and more turbulent than the open-field value. For winds from the south sector the mast lies about three building heights downwind of the buildings (for buildings about 20 m tall), inside their wake. The station therefore produces a record of mixed quality, and the mixture

depends on the wind climate. If, for illustration, the wind blows from the west and north 65 % of the time, from the east 20 % and from the south 15 %, then about a third of the record is compromised, and it is compromised systematically: east and south winds read low. The prevailing directions themselves depend on the climate and the hemisphere; the trade winds, for example, blow from the northeast north of the equator and from the southeast south of it, so the same mast geometry would yield a different mixture in the two hemispheres.

Station metadata should therefore record exposure by direction sector, and a wind record from such a station should be analyzed by sector, with the poorly exposed sectors flagged or corrected, rather than averaged over all directions. The wind roses of Chapter 19 are the natural tool: a rose of the record next to a rose of the exposure classes shows how much of the climatology rests on which surroundings.

23.2 Obstacles, fetch and footprint

The surroundings that set the exposure act on the flow in three ways: individual obstacles shed wakes, changes of surface leave the flow partly adjusted to the old surface, and the measurement integrates the influence of an upwind source area whose size depends on height and stability. This section treats the three in turn, with the ratios and rules of thumb used to site a sensor.

23.2.1 Obstacle wakes

Behind an obstacle the mean wind is reduced and the turbulence is increased. The region of reduced wind is the obstacle's *wake*. Consider a building of height $h_c = 20\,\mathrm{m}$; the obstacle height is written h_c, as for a canopy, and all distances in this section are measured in units of it. The wake of such a building extends several multiples of h_c downstream. A sensor only $2\,h_c = 40\,\mathrm{m}$ behind the building can therefore be strongly distorted: it may sit in the recirculation zone directly behind the building, where the mean flow is weak or reversed and the direction fluctuates rapidly (Chapter 20 described the same zone behind a steep ridge).

Figure 23.3 shows the structure of a wake in a vertical cross section along the wind. The horizontal axis is the distance x from the downwind face of the obstacle in units of h_c; the gray block is the obstacle, one height deep. The upper part marks the displacement zone upwind of the obstacle, the recirculation cavity behind it, the near wake and the far wake, with the dashed curve as the top of the wake. The lower part plots an illustrative fractional reduction of the mean wind, $\Delta U/U_0$, at the height of a sensor at half the obstacle height, against the same distance; the sensor positions at 2, 10 and $20\,h_c$ are marked in both parts.

Read along the wind, the figure shows four regions. Upwind of the obstacle, over about one to two heights, the air is slowed by the raised pressure on the windward face. Behind the obstacle, the flow separates at the upwind edges and a recirculation cavity forms; for a compact building it reaches about one to three heights downstream, and for a long wall or a dense shelterbelt it is longer. Downstream of the cavity lies the near wake, where the deficit is large and the turbulence high, and then the far wake, where turbulent mixing refills the deficit with momentum from above and the wind recovers gradually; the wake grows upward to about twice the obstacle height. In the illustrative curve the deficit is 11 % at $10\,h_c$ and 1 % at $20\,h_c$. The sensor at $2\,h_c$ lies in the cavity, where its reading has little to do with the approaching wind.

The exact wake length depends on geometry and atmospheric stability. A wide obstacle across the wind produces a longer wake than a narrow one, because the air cannot pass around its sides; a porous obstacle such as a row of trees produces a smaller deficit that persists further; and a stable boundary layer, whose weak turbulence refills the deficit slowly, lengthens the wake, while convective mixing shortens it.

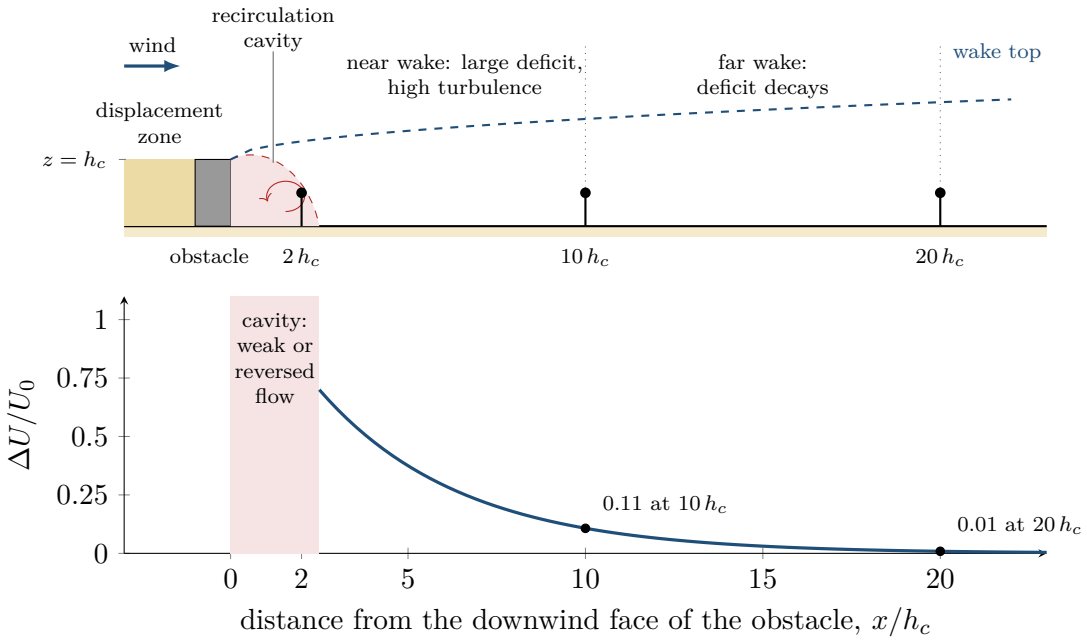


Figure 23.3: The wake of a solid obstacle of height h_c (schematic, vertical scale exaggerated). Top: vertical cross section along the wind with the displacement zone upwind, the recirculation cavity, the near and far wake, and three sensors at height $h_c/2$. Bottom: fractional reduction of the mean wind at the sensor height outside the cavity, $\Delta U/U_0 = 0.7\exp[-(x/h_c - 2.5)/4]$, an illustrative shape whose length depends on the obstacle's width and porosity and on the stability of the air.

23.2.2 Sensor height relative to obstacle height

A useful dimensionless measure of how an obstacle affects a sensor is the ratio of the sensor height to the obstacle height,

$$\frac{z}{h_c}. \tag{23.4}$$

If the ratio is small, individual obstacles matter strongly: the sensor is within, or just above, the layer in which the flow is organized by particular buildings or trees. If the sensor is many obstacle heights above the surface, the effects of the individual obstacles have merged, and aggregate roughness concepts, the roughness length z_0 and the displacement height d, become appropriate.

This is the distinction between the roughness sublayer and the inertial sublayer of Chapter 11. The roughness sublayer extends to about 2 to $5\,h_c$ above the ground. An illustrative 10 m sensor among 8 m buildings has $z/h_c = 1.25$ and is inside it; the same sensor raised to 40 m has $z/h_c = 5$ and is at or above its top, where a profile with z_0 and d can describe the flow. A 10 m sensor beside 20 m trees has $z/h_c = 0.5$: it measures within the height range of the obstacles themselves, and no aggregate roughness length describes its reading. In the rough picture of Figure 23.3, where the wake grows to about $2\,h_c$, an obstacle lower than about half the sensor height sends little of its wake up to the sensor, while an obstacle taller than the sensor buries it.

23.2.3 Distance to an obstacle

For siting, the second dimensionless measure is the horizontal distance from the obstacle in units of its height,

$$\frac{x}{h_c}, \tag{23.5}$$

where x is the horizontal distance between the sensor and the obstacle and h_c the obstacle height. A tree 20 m tall at 20 m from the sensor gives $x/h_c = 1$. That is very close aerodynamically: the sensor is in the displacement zone if the tree is downwind and in the cavity or near wake if it is upwind. The same tree 400 m away gives $x/h_c = 20$; its direct wake influence is much smaller, about 1 % in the illustrative curve of Figure 23.3.

A common siting rule of thumb. A widely used rule of thumb for standard exposure places the anemometer at a distance of at least about ten times the height of any obstacle,

$$x \gtrsim 10\, h_c, \tag{23.6}$$

and a stricter version asks for about $20\, h_c$ in the prevailing wind directions. It is a rule of thumb, not a physical law: it corresponds to the end of the near wake in Figure 23.3, where the deficit has fallen to about a tenth, and it does not account for a long wall, a stable night or a sensor below the obstacle top. For the 20 m building and the 20 m tree above, it asks for 200 m; for a 6 m shed, 60 m. The rule applies to each obstacle separately and in each direction, and it is one criterion among several: a sensor can be ten heights from every obstacle and still be in the internal boundary layer of the nearest forest edge.

23.2.4 Fetch and internal boundary layers

The *fetch* is the upwind distance over a reasonably uniform surface (Chapter 7). Adequate fetch allows the boundary layer to adjust to the local roughness, so that the profile at the sensor is the profile of the surface beneath it. If the fetch is too short, the wind profile retains a memory of the upstream terrain. This matters most downwind of forest edges, coastlines, urban boundaries and crop transitions.

Chapter 7 gave the rough rules: downwind of a change of surface an internal boundary layer grows to a height $\delta \approx 0.1\, x$, and only its lowest tenth, about $0.01\, x$, is in equilibrium with the new surface. A sensor at height z therefore needs a fetch of about $100\, z$ of uniform surface to measure an equilibrium profile: about 1 km for a 10 m sensor.

Suppose the wind moves from a forest onto grass. Near the surface the flow starts adjusting to the grass immediately, accelerating as the smoother surface removes less momentum; higher levels still reflect the forest profile. The internal boundary layer grows downstream. For an illustrative 10 m sensor 200 m downwind of the edge of a 20 m forest, $x/h_c = 10$ and the obstacle rule of equation (23.6) is met, but

$$\delta \approx 0.1 \times 200\,\mathrm{m} = 20\,\mathrm{m}, \qquad \text{equilibrium layer} \approx 0.01 \times 200\,\mathrm{m} = 2\,\mathrm{m}.$$

The sensor lies inside the internal boundary layer and five times above its equilibrium part. It lies over grass but measures a partially forest-adjusted flow: a wind lower than the equilibrium grass value at 10 m, with more turbulence, and a profile that a grass roughness length does not describe. The rules of thumb are for near-neutral air; in stable air the internal boundary layer grows far more slowly and the memory of the forest lasts longer.

23.2.5 The measurement footprint

The fetch argument leads to a more general concept. A near-surface measurement is influenced by an upwind region of the surface, not just by the point directly beneath the sensor. That region is the measurement's *source area* or *footprint*; the *footprint function* gives the relative weight with which each part of the upwind surface contributes to the measured quantity, per unit upwind distance. The concept was developed for fluxes measured by eddy covariance (Chapter 9), where the flux must be attributed to a surface; the wind at a sensor, which reflects the surface stress upwind, has a source area of the same nature and order of size.

A simple analytical form shows how the footprint scales. Near the ground the eddy diffusivity for a scalar is $K_h = \kappa u_* z/\phi_h$ (Chapter 14), so an influence released at the surface spreads upward at a speed of about $K_h/z = \kappa u_*/\phi_h$ and reaches the sensor height z after a time $t \approx z\,\phi_h/(\kappa u_*)$. During that time the mean wind carries it a distance

$$x_{\mathrm{fp}} = \frac{z\,U(z)\,\phi_h}{\kappa\,u_*} = \frac{z\,\phi_h}{\kappa^2}\left[\ln\frac{z}{z_0} - \psi_m\right], \tag{23.7}$$

the footprint length scale, with ϕ_h and ψ_m evaluated at z/L_{O}. A diffusion model with a constant wind and this diffusivity gives the crosswind-integrated footprint function

$$\mathcal{F}(x) = \frac{x_{\mathrm{fp}}}{x^2}\,\exp\!\left(-\frac{x_{\mathrm{fp}}}{x}\right), \qquad \mathcal{C}(x) = \int_0^x \mathcal{F}(x')\,\mathrm{d}x' = \exp\!\left(-\frac{x_{\mathrm{fp}}}{x}\right), \tag{23.8}$$

where x is the upwind distance from the sensor, $\mathcal{F}$ (per meter) integrates to one, and the cumulative footprint $\mathcal{C}(x)$ is the fraction of the influence that comes from within the distance x. Setting $\mathrm{d}\mathcal{F}/\mathrm{d}x = 0$ gives the most influential distance, $x_{\mathrm{fp}}/2$; the distance from within which a fraction P of the influence comes is $x_{\mathrm{fp}}/\ln(1/P)$.

For the open-grass sensor of Section 23.1.1, $z = 10\,\mathrm{m}$ and $z_0 = 0.03\,\mathrm{m}$, in neutral air ($\phi_h = 1$, $\psi_m = 0$):

$$x_{\mathrm{fp}} = \frac{10 \times 5.809}{0.16}\,\mathrm{m} = 363\,\mathrm{m}, \qquad \text{peak at } 182\,\mathrm{m},$$

$$50\,\%\ \text{within}\ \frac{363}{\ln 2}\,\mathrm{m} = 524\,\mathrm{m}, \qquad 80\,\%\ \text{within}\ \frac{363}{\ln 1.25}\,\mathrm{m} = 1.63\,\mathrm{km}.$$

The 80 % distance is about 160 sensor heights, the same order as the fetch of $100\,z$ of the internal-boundary-layer rule: the two arguments describe the same physics. A higher sensor generally has a larger upwind footprint. At $z = 50\,\mathrm{m}$ over the same grass, $x_{\mathrm{fp}} = 50 \times 7.419/0.16 = 2.32\,\mathrm{km}$ and 80 % of the influence comes from within 10.4 km. A rougher surface shortens the footprint, because the stronger turbulence relative to the wind, a smaller U/u_*, carries the influence upward faster: with $z_0 = 0.3\,\mathrm{m}$ the 10 m sensor has $x_{\mathrm{fp}} = 219\,\mathrm{m}$ and 80 % within 0.98 km. The footprint thus depends on the measurement height, the stability, the roughness and the wind speed. The wind speed acts mainly through stability: in neutral air U/u_* is fixed by z/z_0 and the footprint does not depend on the speed, but strong winds keep the air near neutral and light winds let it become stable at night or unstable by day.

23.2.6 Stability and the footprint

Stability changes the footprint strongly. Under unstable conditions, strong vertical mixing by large convective eddies connects the sensor to the surface close to it on all sides: the footprint is short in the upwind direction and broad across the wind. Under stable conditions, vertical mixing is weaker and the influence of the surface reaches the sensor only after a long horizontal journey: the footprint becomes elongated far upstream and narrow. The measurement footprint depends on stability.

With the Businger–Dyer forms (Chapter 14) the change can be computed from equation (23.7). For the 10 m grass sensor with an illustrative $L_{\mathrm{O}} = -50\,\mathrm{m}$, $z/L_{\mathrm{O}} = -0.2$, $\phi_h = (1 - 16\,z/L_{\mathrm{O}})^{-1/2} = 0.49$ and $\psi_m = 0.46$; with $L_{\mathrm{O}} = 50\,\mathrm{m}$, $z/L_{\mathrm{O}} = 0.2$, $\phi_h = 1 + 5\,z/L_{\mathrm{O}} = 2.0$ and $\psi_m = -5\,z/L_{\mathrm{O}} = -1.0$. Then

$$x_{\mathrm{fp}}^{\mathrm{unstable}} = \frac{10 \times 0.49 \times (5.809 - 0.46)}{0.16}\,\mathrm{m} = 163\,\mathrm{m},$$

$$x_{\mathrm{fp}}^{\mathrm{stable}} = \frac{10 \times 2.0 \times (5.809 + 1.0)}{0.16}\,\mathrm{m} = 851\,\mathrm{m},$$

and the 80 % distances are 0.73 km and 3.8 km, against 1.63 km in neutral air: a factor of five between a sunny afternoon and a clear night at the same mast.

Figure 23.4 draws these footprints. In the left panel the horizontal axis is the upwind distance from the sensor and the vertical axis the footprint function $\mathcal{F}$, per kilometer, for the 10 m sensor in the three stability states. In the right panel the horizontal axis is the upwind distance on a logarithmic scale and the vertical axis the cumulative footprint $\mathcal{C}$, for the 10 m sensor in neutral and stable air and for a 50 m sensor in neutral air; the dashed line marks 80 %.

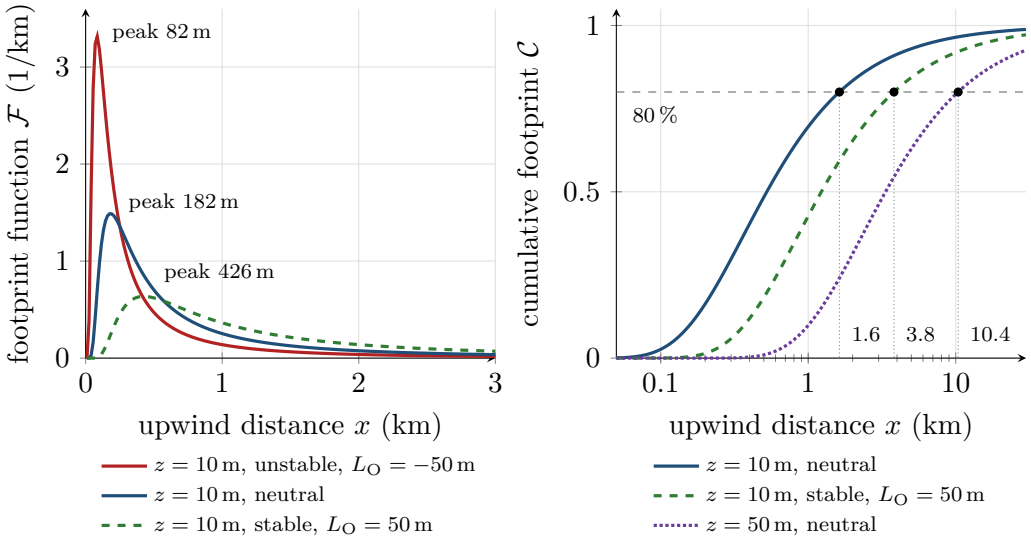


Figure 23.4: Footprint of a wind or flux sensor over open grass, $z_0 = 0.03$ m, from equation (23.8) with the length scale of equation (23.7): $x_{fp} = 163$ m (unstable, $L_O = -50$ m), 363 m (neutral) and 851 m (stable, $L_O = 50$ m) at $z = 10$ m, and 2.32 km at $z = 50$ m in neutral air. Left: footprint function per kilometer of upwind distance. Right: fraction of the influence from within the distance x. Simplified analytical model; values illustrative.

The left panel shows the unstable footprint concentrated within a few hundred meters, with its peak at 82 m, and the stable footprint spread over kilometers, with a peak at 426 m that is low and broad. In the right panel the three cumulative curves reach 80 % at 1.6, 3.8 and 10.4 km. The consequence for siting is that a single sensor looks at different surfaces at different times of day: a forest edge 1.5 km upwind is almost invisible to the 10 m sensor in the afternoon and a large part of its source area at night. The analytical form is a simplification: it assumes a constant wind with height and a flat, uniform surface, and it gives only the crosswind-integrated weight. Its scalings with height, roughness and stability are the robust part. The footprint is especially important for flux measurements, whose purpose is to attribute an exchange to a surface; for the wind, it is the quantitative form of the fetch requirement.

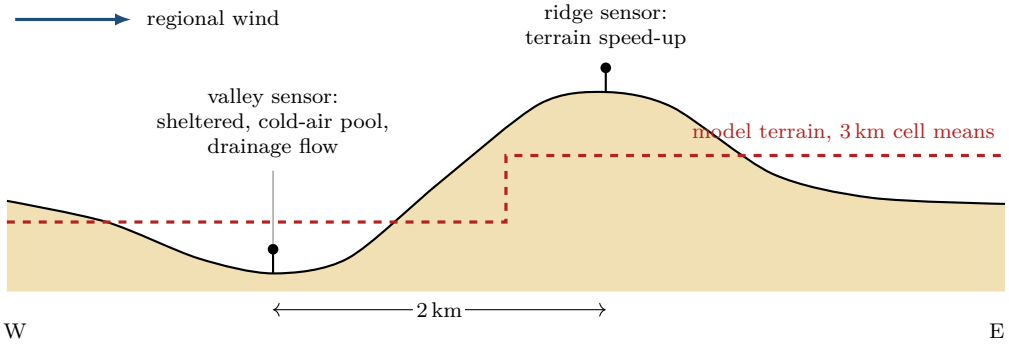
23.3 Terrain exposure

Obstacles and roughness changes act over hundreds of meters; terrain acts over kilometers and produces the largest differences between nearby sensors. This section applies the terrain flow of Chapter 20 to the siting question: ridge-top and valley sensors, their comparison with a coarse model, and the meaning of the measurement height on a slope.

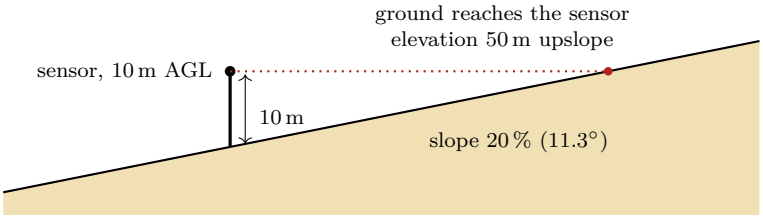
23.3.1 Two sensors two kilometers apart

A ridge-top sensor may be exposed to flow accelerated by the terrain; a nearby valley sensor may be sheltered. Two sensors separated by only 2 km can therefore measure very different winds. Neither is necessarily wrong: they represent different *terrain exposures*, the position of each site relative to the surrounding terrain, measured in the direction from which the wind comes (Chapter 20).

Figure 23.5 illustrates the situation. Panel (a) is a west–east vertical cross section, 6 km long, with elevation above an arbitrary datum on the vertical axis (exaggerated). The shaded profile is the real terrain: a valley floor and, 2 km east of it, a ridge crest about 300 m higher, with a sensor at each. The dashed steps are the terrain of a weather model with 3 km grid cells, each step the mean elevation of its cell. Panel (b) is a closer cross section of a slope, drawn without vertical exaggeration, and is discussed in Section 23.3.4.



(a) ridge and valley sensors against model terrain



(b) a sensor on a slope (no vertical exaggeration)

Figure 23.5: Terrain exposure (schematic). (a) West–east cross section with a valley sensor and a ridge-crest sensor 2 km apart, both 40 m above local ground in the drawing for visibility; vertical scale exaggerated about seven times. The dashed steps are the terrain of a model with 3 km grid cells. (b) A mast on a uniform 20 % slope: the ground 50 m upslope lies at the elevation of the 10 m sensor. Elevations illustrative.

Panel (a) shows two features that recur through the rest of the chapter. The two sensors sit in different flow regimes, the ridge sensor in the accelerated flow over the crest and the valley sensor in the sheltered low ground. And the model's terrain is neither: its cell containing the valley sensor is about 85 m above the valley floor, and its cell containing the ridge sensor is about 100 m below the crest. The model sees a gentle step where the real terrain has a valley and a ridge.

23.3.2 Ridge-top measurements

A ridge-top sensor may measure

$$U_{\text{ridge}} > U_{\text{regional}} \tag{23.9}$$

because of terrain speed-up. Chapter 20 gave the rule of thumb for the fractional speed-up near the crest of a low two-dimensional ridge, $\Delta S \approx 2\,h_m/L_h$. For an illustrative ridge with $h_m = 150\,\mathrm{m}$ and $L_h = 1\,\mathrm{km}$, $\Delta S \approx 0.30$, and a regional wind of $7\,\mathrm{m\,s^{-1}}$ at sensor height becomes about $9.1\,\mathrm{m\,s^{-1}}$ at the crest.

If that measurement is compared directly with a coarse weather-model grid cell, the model may appear biased low. Chapter 5 showed that a model with $\Delta x = 3\,\mathrm{km}$ represents features only down to an effective resolution of about 15 to 30 km; a ridge with a half-width of 1 km is absent from its terrain or survives as a broad, low bump. If the model's version of the ridge is, say, 60 m high with a half-width of 3 km, the same rule gives $\Delta S \approx 0.04$ and a model wind of about $7.3\,\mathrm{m\,s^{-1}}$, 20 % below the measurement. The issue may be representativeness rather than model error: the grid-cell mean terrain does not contain the same ridge acceleration, so the model is not predicting the quantity the sensor measures.

23.3.3 Valley measurements

Likewise, a valley sensor may measure weak winds because of sheltering by the surrounding ridges (Chapter 20), cold-air pooling on clear nights, when the cold, dense air that collects on the valley floor decouples the surface from the flow above (Chapter 17), and drainage flow, the slow downslope and down-valley wind of cooled air (Chapter 19). A coarse model may predict the stronger regional flow. At night the valley sensor may report 1 to $2\,\mathrm{m\,s^{-1}}$ from the down-valley direction while the model reports $7\,\mathrm{m\,s^{-1}}$ from the synoptic direction. Again,

$$\text{point–grid mismatch} \neq \text{model error, automatically.} \tag{23.10}$$

The mismatch at a valley station also varies with the time of day: small on a windy, mixed afternoon, when the valley air is coupled to the flow above, and large on a calm night. In a verification it therefore appears as a diurnal cycle of error, which is easily mistaken for an error in the model's boundary-layer scheme.

23.3.4 Sensor height over sloping terrain

Even the meaning of "10 m AGL" becomes subtle on a slope. A sensor may be 10 m vertically above the local ground, but nearby terrain can intersect the flow at a similar elevation. Panel (b) of Figure 23.5 shows the geometry. On a uniform slope of 20 %, an angle $\gamma = \arctan 0.2 = 11.3°$, the distance from the sensor to the ground measured perpendicular to the slope is $10\,\mathrm{m} \times \cos\gamma = 9.8\,\mathrm{m}$, close to the vertical value. The larger effect is horizontal: the ground rises to the sensor's elevation only $z/\tan\gamma = 10\,\mathrm{m}/0.2 = 50\,\mathrm{m}$ upslope.

The consequence depends on the wind direction relative to the slope. For a wind blowing down the slope, the air reaching the sensor was in contact with the ground 50 m earlier, about two seconds at $5\,\mathrm{m\,s^{-1}}$, and carries the low speed and high turbulence of near-surface air; the sensor reads lower than its nominal height suggests. For a wind blowing up the slope, the air at the sensor's elevation was higher above the ground upwind, and the slope itself accelerates the flow toward the crest; the sensor reads higher. The effective exposure therefore depends on the surrounding three-dimensional terrain and on the wind direction, not just on the local vertical distance, and a height correction that assumes a logarithmic profile over flat ground does not apply on the slope.

23.4 Representativeness

Whether a sensor is well sited depends on what its reading is meant to represent. This section separates standard from application-specific siting, distinguishes three kinds of representativeness, explains why no fixed radius describes a sensor, and quantifies the difference between a point value and an area average.

23.4.1 Standard against application-specific siting

There are two different siting goals. A meteorological station aims to represent the regional surface weather: the wind that a large area experiences, comparable with other stations and with weather models. Its siting therefore seeks open, standardized exposure, at 10 m over open terrain, away from obstacles, on terrain typical of the region.

An engineering sensor may aim instead to measure the actual local condition at an asset. A transmission-line sensor should measure the wind that cools the conductor, at the conductor's height and position, even if that wind is locally modified by the terrain; a wind turbine's assessment mast should measure the wind at hub height at the turbine location. These are different objectives, and a site that serves one can fail the other. The objective has to be stated before the quality of a site can be judged.

23.4.2 Representative against intentionally local

A sensor beside a transmission line in a ridge gap may be a poor meteorological reference station. The gap accelerates and channels the flow (Chapter 20), so the sensor reads faster than the regional wind and from a direction set by the gap's axis; used as a regional reference, it would bias a model verification and distort a regional wind map. The same sensor may be an excellent asset-specific sensor: the conductor in the gap is cooled by exactly the gap wind, and a regional station 15 km away, however well exposed, would misrepresent the conductor's cooling in both speed and direction.

"Good exposure" therefore depends on the measurement objective. A sensor is *representative* when it stands for an area, a height or a regime larger than its own site; it is *intentionally local* when it stands for the conditions at one asset. Both are legitimate. The error is to use one as if it were the other, which is why the objective belongs in the metadata of every sensor (Section 23.6.1).

23.4.3 Three kinds of representativeness

It is useful to separate three questions that the word "representativeness" tends to merge. *Spatial representativeness* asks whether the sensor represents the surrounding region: how well a point stands for an area. *Vertical representativeness* asks whether the measurement height represents the level of interest: how well the measurement height matches the target height. *Dynamical representativeness* asks whether the site experiences the same physical regime as the quantity to be inferred: a valley sensor may not represent ridge flow even if the two are geographically close, because at night one is in a decoupled cold pool and the other in the flow above it. Table 23.1 sets the three side by side with an example of each and the means of reducing the mismatch.

The three kinds fail independently. A ridge-crest sensor at conductor height on the same ridge as a transmission line can be vertically and dynamically representative of the line while being spatially unrepresentative of the region; a well-exposed 10 m station can be spatially representative and vertically unrepresentative of a turbine hub. Stating which of the three a use requires is the first step of any comparison.

23.4.4 The representativeness radius

There is no universal statement of the form "a wind sensor represents 1 km". The distance over which a sensor is representative, its *representativeness radius*, depends on the height of the sensor, the terrain, the roughness, the stability and the wind direction. The footprint of Section 23.2.5 gives one measure of it over flat ground: for one 10 m sensor over grass the distance that supplies 80 % of the influence ranges from 0.7 km on an unstable afternoon to

Table 23.1: Three kinds of representativeness, with an illustrative example of each.

Kind	Question	Example of a failure	Means of reducing the mismatch
Spatial	Does the point represent the surrounding area?	a 10 m sensor in a forest clearing compared with a 3 km grid cell of mixed farmland: the clearing is sheltered, the cell is not	several sensors, an area-average model value, a roughness correction (Section 23.5.5)
Vertical	Does the measurement height represent the level of interest?	a 10 m station used for a 100 m hub: a factor 1.40 in neutral air and more on stable nights (Figure 23.1)	measure at the target height, or extrapolate with stated stability
Dynamical	Does the site experience the regime of the target?	a valley sensor used for a ridge-crest conductor: decoupled cold pool at night against accelerated flow aloft	a sensor in the target regime; stratify by regime

3.8 km on a stable night, and it is 10 km for a 50 m sensor. In complex terrain representativeness can be extremely local: the valley and ridge sensors of Figure 23.5 are 2 km apart and differ by a factor of two or more, and on a slope a few tens of meters change the exposure.

The radius also depends on the quantity. A daily or monthly mean wind varies more smoothly in space than an hourly mean, because some of the local effects change sign with direction and average out over time; gusts and turbulence intensity, set by the nearest obstacles and slopes, vary over shorter distances still. A representativeness radius is therefore a property of a sensor, a site, a condition and a statistic together, and it should be estimated, for example from the correlation between neighboring sensors, rather than assumed.

23.4.5 Point value against area average

A model may approximate an area-representative wind, the average over an area A,

$$\langle U \rangle_A = \frac{1}{A} \int_A U(x, y)\, \mathrm{d}A, \tag{23.11}$$

while the sensor measures the point value $U(x_0, y_0)$. Write the point value as the area average plus a local deviation, $U(x_0, y_0) = \langle U \rangle_A + U''(x_0, y_0)$. In heterogeneous terrain the local deviation is not zero, and

$$U(x_0, y_0) \neq \langle U \rangle_A. \tag{23.12}$$

This difference can remain even with a perfect model and a perfect sensor: the model may compute $\langle U \rangle_A$ exactly and the sensor may measure $U(x_0, y_0)$ exactly, and the two still differ by U''.

The size of the difference follows from the statistics of the spatial field. Treat the wind at one moment as a field with spatial standard deviation σ_s about its regional mean and a spatial correlation $\varrho(r)$ between points a distance r apart, falling from one at $r = 0$ over a correlation length ℓ_s. The variance of the area average is the average of the covariances of all pairs of points in the area:

$$\mathrm{Var}\big(\langle U \rangle_A\big) = \frac{\sigma_s^2}{A^2} \int_A \int_A \varrho(r)\, \mathrm{d}A\, \mathrm{d}A' = \mathcal{R}\, \sigma_s^2. \tag{23.13}$$

If the area consisted of N independent patches, ϱ would be one within a patch and zero between patches, and $\mathcal{R} = 1/N$: the area average is smoother than any point by the factor N in variance. This is the variance reduction of an area mean. The variance of the representativeness difference

also involves the covariance between the point and the average, $\mathcal{Q}\,\sigma_s^2$:

$$\mathrm{Var}\big(U(x_0,y_0)-\langle U\rangle_A\big)=\sigma_s^2\,(1+\mathcal{R}-2\mathcal{Q})=\mathcal{D}\,\sigma_s^2. \tag{23.14}$$

Along a transect of length L with an exponential correlation $\varrho(r)=e^{-r/\ell_s}$ and the point at its center, the integrals give, with $s=L/\ell_s$,

$$\mathcal{R}=\frac{2}{s^2}\big(s-1+e^{-s}\big),\qquad \mathcal{Q}=\frac{2}{s}\big(1-e^{-s/2}\big). \tag{23.15}$$

Figure 23.6 plots the two variance ratios against the length of the averaging transect in units of the correlation length, on a logarithmic axis. The solid curve is $\mathcal{R}$, the variance of the average relative to that of a point; the dashed curve is $\mathcal{D}$, the variance of the point-minus-average difference; the dotted line is the large-s limit $2/s$ of $\mathcal{R}$.

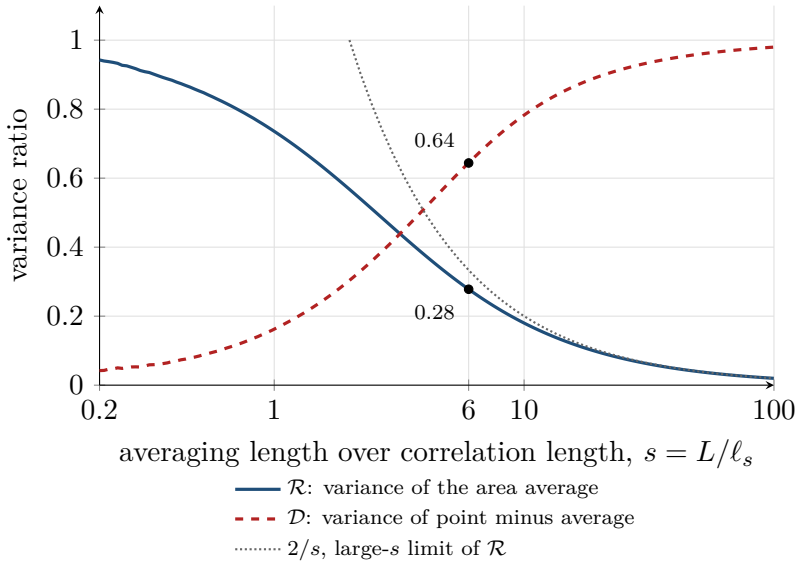


Figure 23.6: Variance ratios of equations (23.13) to (23.15) for an average along a transect of length L through a field with exponential spatial correlation of length ℓ_s, the point at the center of the transect. Points: $s=6$, a 3 km grid cell with $\ell_s=500$ m. Values illustrative.

For averages over less than a correlation length the two ratios behave as expected: the average is almost the point value, $\mathcal{R}$ is near one and $\mathcal{D}$ near zero. As the averaging length grows, $\mathcal{R}$ falls toward $2/s$ and $\mathcal{D}$ rises toward one: the average becomes smooth, and the point deviates from it by almost the full point variability. For an illustrative 3 km cell over terrain whose local wind deviations have $\sigma_s=1.5\,\mathrm{m\,s^{-1}}$ and $\ell_s=500$ m, $s=6$, $\mathcal{R}=0.28$, $\mathcal{Q}=0.32$ and $\mathcal{D}=0.64$, so the representativeness difference has a standard deviation of $1.5\,\mathrm{m\,s^{-1}}\times\sqrt{0.64}=1.2\,\mathrm{m\,s^{-1}}$. Over a two-dimensional cell the variance of the average falls faster still, to about $2\pi\ell_s^2/A=0.17$ of the point variance for this cell in the large-area limit, which leaves the difference even closer to the full point variability. For a single fixed station the local deviation U'' is not purely random: part of it is a systematic offset by direction sector and stability class, the ridge always faster and the valley always slower, and only the rest varies from case to case. The statistical picture describes the spread over many stations or many conditions; the metadata of Section 23.6.1 describe the systematic part at one station.

23.5 Comparing a station with a model

The most common use of a station is to judge a weather model, and the most common mistake is to treat the difference between the two as model error. This section lists what a grid cell

represents, quantifies the elevation and roughness mismatches, works a height and an exposure correction, states what such corrections cannot fix, and draws the consequence for statistical models trained on stations.

23.5.1 The grid cell and the point

Suppose the model resolution is $\Delta x = 3\,\mathrm{km}$. The grid cell represents an effective elevation, an effective roughness, an effective land use and an effective wind: values that stand for the whole cell (Chapters 25 and 27). A point station samples the air within centimeters to meters of the instrument: the rotor of a cup anemometer or the acoustic path of a sonic anemometer is a few tenths of a meter across. The ratio of the areas is about $(3000\,\mathrm{m})^2/(1\,\mathrm{m})^2 \approx 10^7$; the scale difference is enormous.

Time averaging narrows the gap only partly. During a 10-minute average at $6\,\mathrm{m\,s^{-1}}$, about 3.6 km of air passes the sensor, so the average samples a streak of the flow along the wind and removes most of the turbulent sampling noise (Chapter 8). It does not remove the effects that are fixed to the site, the wake of the nearby building, the speed-up of the crest, the roughness of the upwind field, because every parcel in the streak passes the same obstacles and the same terrain on its way to the sensor. A comparison of a model with an observation should therefore carry, besides the uncertainty of the sensor, a *representativeness uncertainty*. If the three sources are independent, the expected squared difference between the model value and the observation is

$$\sigma^2_{\mathrm{diff}} = \sigma^2_{\mathrm{instr}} + \sigma^2_{\mathrm{rep}} + \sigma^2_{\mathrm{model}}, \tag{23.16}$$

where σ_{instr} is the instrument uncertainty, σ_{rep} the standard deviation of the representativeness difference and σ_{model} the model's own error. With an illustrative $\sigma_{\mathrm{instr}} = 0.2\,\mathrm{m\,s^{-1}}$ and the $\sigma_{\mathrm{rep}} = 1.2\,\mathrm{m\,s^{-1}}$ of the previous section, a perfect model would still differ from the station by $\sqrt{0.04 + 1.44}\,\mathrm{m\,s^{-1}} = 1.22\,\mathrm{m\,s^{-1}}$, and the instrument would account for less than 3 % of that variance. Chapter 24 develops the verification measures; the budget states what part of them the model can be held to.

23.5.2 Elevation mismatch

Suppose a station stands at 1200 m MSL but the model grid elevation of its cell is 850 m. The model's atmospheric level structure is then referenced to terrain 350 m lower: the model's 10 m wind is a wind at 860 m MSL, the station's a wind at 1210 m MSL. This *elevation mismatch*, the difference between the actual and the modeled terrain elevation, affects every near-surface variable:

- temperature: with an illustrative lapse rate of 6.5 K per kilometer the model surface air is about $0.35 \times 6.5 = 2.3\,\mathrm{K}$ warmer than the air at the station's elevation, and on a night with an inversion the sign can reverse;
- pressure: the hydrostatic difference is $\rho g\,\Delta z \approx 1.1 \times 9.81 \times 350\,\mathrm{Pa} \approx 3.8 \times 10^3\,\mathrm{Pa}$, about 38 hPa, so model surface pressure cannot be compared with station pressure without reduction (Chapter 2);
- stability: the model surface may sit in a smoothed valley whose cold pool the real station, 350 m higher on a slope or crest, lies above;
- wind: the station is exposed to flow that, in the model, lies 360 m above the model ground, where the wind is stronger and less affected by surface friction.

Neither of the obvious ways of comparing the two is right. Comparing at the same height above ground, the model's 10 m wind with the station's, matches the surface friction but places

the model wind 350 m lower in the atmosphere. Comparing at the same altitude, the model wind 360 m above its ground with the station, matches the atmospheric level but removes the friction of the surface the station actually stands on. The ridge of Figure 23.5 is the typical case. Elevation mismatch is a major issue in complex terrain, and how models represent and smooth terrain is the subject of Chapter 27.

23.5.3 Roughness mismatch

Likewise, the roughness length at the station generally differs from the roughness length of the model cell,

$$z_{0,\mathrm{station}} \neq z_{0,\mathrm{model}}, \tag{23.17}$$

a *roughness mismatch*. A model cell may represent mixed farmland with one effective roughness length, an area average of the drag of fields, hedges and farm buildings (Chapter 11). The station may sit in a forest clearing, where the 10 m sensor is below the top of the surrounding 20 m trees, at $z/h_c = 0.5$, and measures the sheltered flow of the clearing. Or it may sit in an open corridor along a road, smoother than the cell. Then even at identical height, $U_{10,\mathrm{model}}$ and $U_{10,\mathrm{obs}}$ are not strictly equivalent: they are winds over two different surfaces. The roughness that matters at the station is, in addition, the roughness upwind in the current wind direction over the footprint of Section 23.2.5, which differs by sector.

23.5.4 Height correction

Observations are sometimes adjusted to a common reference height, for example from a 20 m mast to the 10 m standard, $U_{20} \to U_{10}$. Under neutral, homogeneous conditions equation (23.2) gives

$$U_{10} = U_{20}\,\frac{\ln(10/z_0)}{\ln(20/z_0)}, \tag{23.18}$$

with heights in meters. For an illustrative $U_{20} = 7.0\,\mathrm{m\,s^{-1}}$ and $z_0 = 0.05\,\mathrm{m}$,

$$U_{10} = 7.0\,\mathrm{m\,s^{-1}} \times \frac{\ln 200}{\ln 400} = 7.0 \times \frac{5.298}{5.991}\,\mathrm{m\,s^{-1}} = 6.19\,\mathrm{m\,s^{-1}}.$$

The correction is moderately sensitive to the roughness length: $z_0 = 0.01\,\mathrm{m}$ gives $6.36\,\mathrm{m\,s^{-1}}$ and $z_0 = 0.5\,\mathrm{m}$ gives $5.68\,\mathrm{m\,s^{-1}}$, a range of $\pm 5\,\%$ for a factor of fifty in z_0. It is more sensitive to stability. With the stability-corrected profile,

$$U_{10} = U_{20}\,\frac{\ln(10/z_0) - \psi_m(10/L_\mathrm{O})}{\ln(20/z_0) - \psi_m(20/L_\mathrm{O})},$$

an illustrative stable $L_\mathrm{O} = 50\,\mathrm{m}$ ($\psi_m = -1.0$ at 10 m and -2.0 at 20 m) gives $7.0 \times 6.298/7.991 = 5.52\,\mathrm{m\,s^{-1}}$, 11 % below the neutral value, and an unstable $L_\mathrm{O} = -50\,\mathrm{m}$ ($\psi_m = 0.46$ and 0.70) gives $6.40\,\mathrm{m\,s^{-1}}$. If stability or terrain effects are important, the neutral correction can introduce a substantial error, and the error grows with the ratio of the two heights: the step from 20 to 10 m is short, while the step from 10 to 100 m of Figure 23.1 multiplies the wind by 1.40 in neutral air and by much more on a stable night. On a slope or a crest the profile is not logarithmic at all, because the speed-up decays with height (Chapter 20), and the correction does not apply.

23.5.5 Exposure correction

Correcting exposure is harder than correcting height. A height correction moves a wind along one profile; an exposure correction moves it from the profile of one surface to the profile of another, and it may have to account for directional roughness, terrain speed-up, obstacle wakes

and stability. The simplest case, a change of roughness under a common flow, can be handled with the blending-height idea of Chapter 11: at a blending height z_b the wind is taken to be the same over both surfaces, and each surface carries its own friction velocity below it.

Consider an illustrative station whose anemometer is at $z_s = 20\,\mathrm{m}$ over open grass, $z_{0,s} = 0.03\,\mathrm{m}$ in the current wind sector, and which reads $7.4\,\mathrm{m\,s^{-1}}$. The model cell, mixed farmland with $z_{0,m} = 0.15\,\mathrm{m}$, reports $U_{10,\mathrm{model}} = 6.0\,\mathrm{m\,s^{-1}}$, in neutral conditions. To compare like with like, the observation is first carried up the station's own profile to the blending height and then down the model surface's profile to 10 m:

$$U_m(10\,\mathrm{m}) = U_s(z_s)\,\frac{\ln(z_b/z_{0,s})}{\ln(z_s/z_{0,s})}\,\frac{\ln(10\,\mathrm{m}/z_{0,m})}{\ln(z_b/z_{0,m})}. \tag{23.19}$$

With $z_b = 60\,\mathrm{m}$,

$$U_s(60\,\mathrm{m}) = 7.4\,\mathrm{m\,s^{-1}} \times \frac{\ln 2000}{\ln 667} = 7.4 \times \frac{7.601}{6.502}\,\mathrm{m\,s^{-1}} = 8.65\,\mathrm{m\,s^{-1}},$$

$$U_m(10\,\mathrm{m}) = 8.65\,\mathrm{m\,s^{-1}} \times \frac{\ln 66.7}{\ln 400} = 8.65 \times \frac{4.200}{5.991}\,\mathrm{m\,s^{-1}} = 6.06\,\mathrm{m\,s^{-1}}.$$

The choice of blending height matters little: 40 m gives $6.16\,\mathrm{m\,s^{-1}}$ and 100 m gives $5.96\,\mathrm{m\,s^{-1}}$. Table 23.2 follows the comparison step by step, and Figure 23.7 draws the two profiles.

Table 23.2: Station against model, step by step (illustrative, neutral air, $\kappa = 0.4$, no displacement).

Comparison	Station value (m/s)	Model (m/s)	Apparent model error
Raw: station at 20 m against model U_{10}	7.40	6.0	−19 %
Height corrected over the station's own surface, equation (23.18) with $z_0 = 0.03\,\mathrm{m}$	6.61	6.0	−9 %
Height and exposure corrected to the model's surface, equation (23.19) with $z_b = 60\,\mathrm{m}$	6.06	6.0	−1 %

The raw comparison makes the model appear 19 % too slow. Height correction alone removes half of the apparent error, and the exposure correction removes almost all the rest: the model's 10 m wind over its farmland surface agrees with what the station implies for that surface. In the figure the two profiles cross at the blending height and diverge below it, by $0.55\,\mathrm{m\,s^{-1}}$ at 10 m; that divergence is the roughness mismatch. The correction can be applied in either direction: the observation carried to the model's surface, as here, to verify the model, or the model carried to the station's surface, with the inverse factor, to predict the wind at the site. The calculation assumes neutral air, a blending height above which the two surfaces share one wind, and a fetch long enough for the station's surface to have set its own stress (Chapter 11); its result is a statement about the roughness mismatch only.

23.5.6 Limits of correction

A roughness correction moves a wind between two logarithmic profiles. Several common exposure problems are not of that form:

- obstacle wakes, in which the flow at the sensor is not on any logarithmic profile (Figure 23.3);

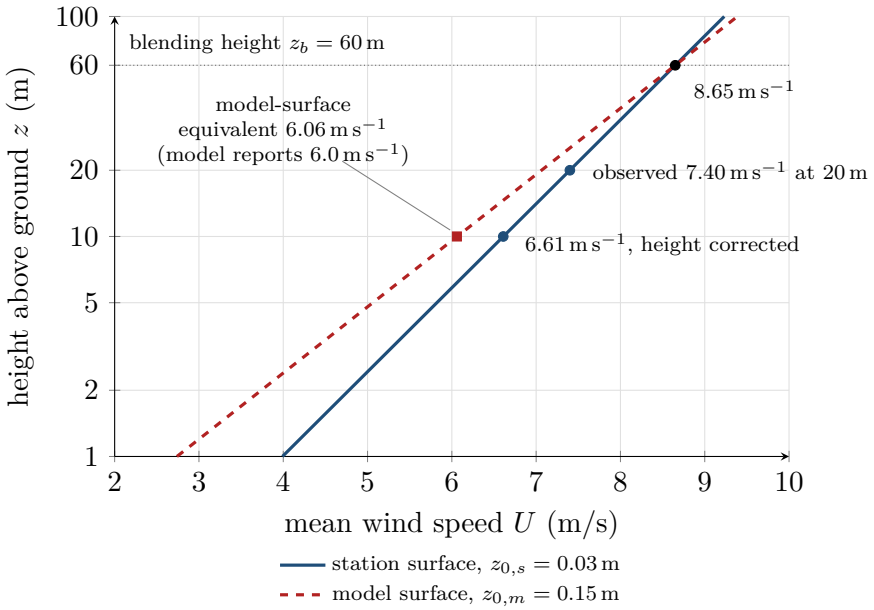


Figure 23.7: Height and exposure correction with a blending height. Neutral logarithmic profiles $U(z) = (u_*/\kappa)\ln(z/z_0)$ over the station's surface ($z_{0,s} = 0.03\,\mathrm{m}$, through the observed $7.40\,\mathrm{m\,s^{-1}}$ at 20 m) and over the model cell's surface ($z_{0,m} = 0.15\,\mathrm{m}$), both passing through the same $8.65\,\mathrm{m\,s^{-1}}$ at $z_b = 60\,\mathrm{m}$, equation (23.19). Values illustrative.

- terrain speed-up and sheltering, which depend on the wind direction, the stability and the height above the crest (Chapter 20);
- stability, which changes both the profile and the footprint and so changes the correction from hour to hour;
- directional roughness, which requires a correction for each sector rather than one factor;
- exposure that changes with time, as trees grow or buildings are added (Section 23.6.2).

A correction factor fitted to a station can absorb the average of these effects, but not their dependence on direction, stability and time, and the remaining random part of the representativeness difference cannot be corrected at all. At some point a microscale flow model of the site, run for each sector and stability class (Chapter 29), becomes more defensible than a simple correction factor, because it computes the wakes, the speed-up and the sheltering from the geometry instead of fitting them as one number.

23.5.7 Consequences for model training

The same issues reach statistical models. Suppose a statistical downscaling model is trained to predict the wind at one station from weather-model output. The model may learn that station's terrain exposure, its roughness and its obstacle effects, as well as the weather model's errors. It may perform very well there. But those learned corrections may not generalize to a site 20 km away. If the training station is on a ridge crest with a speed-up of 1.3, the learned mapping multiplies the weather-model wind by about 1.3 in the directions where the crest is exposed; applied at a valley site, the same mapping would overpredict the valley wind by that factor and more. A site-specific bias correction is therefore not automatically a general atmospheric model. It is a model of one station's exposure combined with one weather model's errors, and it transfers only to sites with the same exposure. Chapter 28 treats the methods and their pitfalls;

the siting consequence is that training data from several exposures, with their metadata, are needed before a learned correction can be expected to generalize.

23.6 Station metadata, homogeneity and network design

A wind record is interpretable only together with a description of where and how it was measured, and that description changes over the life of a station. This section lists the metadata, explains homogeneity and the station-history problem, works a practical example of three disagreeing stations, and ends with the design of a sensor network and a decomposition of an observed wind.

23.6.1 Station metadata

Station metadata are the information describing the sensor, the site and the exposure. For serious wind analysis they should include the items of Table 23.3; the table gives, for each, what to record and why it matters for interpreting the wind. The first nine items are the core list; the last three follow from the earlier sections of the chapter.

Table 23.3: Station metadata for a wind sensor.

Item	What to record	Why it matters
Latitude and longitude	position, with its datum and precision	locates the model cell, the terrain and the land cover
Ground elevation	elevation of the ground at the mast, m MSL	elevation mismatch with the model (Section 23.5.2)
Sensor height	height of each sensor, m AGL	vertical representativeness; height correction
Instrument type	sensor type, model, averaging and sampling	response, overspeeding, direction averaging (Chapter 22)
Calibration history	dates and results of calibrations and replacements	instrument drift and steps in the record
Boom orientation	direction of each boom from the mast	sectors disturbed by the mast's own wake
Nearby obstacles	height, width and distance of each, by direction	z/h_c and x/h_c; wake-affected sectors
Surrounding roughness	land cover and z_0 by direction sector, with season	roughness mismatch; height and exposure correction
Terrain class	flat, rolling, ridge, valley, slope, coastal	terrain exposure and dynamical representativeness
Directional exposure	exposure quality for each sector	stratified analysis (Section 23.1.5)
Siting objective	standard reference or intentionally local, and for which asset	which use of the record is legitimate
History of changes	date and description of every change above	homogeneity of the record

Without metadata a wind time series is much harder to interpret. A record of hourly speeds with no height, no exposure and no history can still be averaged, but no one can say whether its mean is the regional wind, the wind behind a building or the wind on a crest, and the corrections of the previous section cannot be made. Photographs of the surroundings taken from the mast in each direction, repeated every few years, are among the most informative and cheapest metadata.

23.6.2 Changes over time and homogeneity

Exposure can change while the station stays where it is. Trees grow; buildings are constructed; crops change with the season and with land use; the sensor height is changed when a mast is replaced; the tower hardware, the booms or the instrument type change. A 20-year wind record may therefore not be homogeneous even if the instrument remains at the same coordinates. Reconstructing what the exposure was at each time is the *station-history problem*.

A climatological record is *homogeneous* when the changes in the data reflect weather and climate rather than changes in instrumentation or exposure; *station homogeneity* is the consistency of the measurement conditions through time. A station relocation, a new building or a growing shelterbelt creates an artificial shift in the mean wind, abrupt or gradual. Because the atmosphere varies from year to year, a shift of a few percent is hard to see in the record of one station alone; it becomes visible against a neighboring reference station that shares the same weather. The ratio of the two records removes most of the common climate variation and leaves the changes that belong to one site.

Figure 23.8 shows an illustrative case. The upper panel plots the annual mean wind speed of a candidate station and of a neighboring reference station over 20 years. The lower panel plots the ratio of the candidate to the reference. During years 4 to 11 a shelterbelt grows in the candidate's prevailing upwind sector; in year 12 the candidate is moved to a more exposed position nearby.

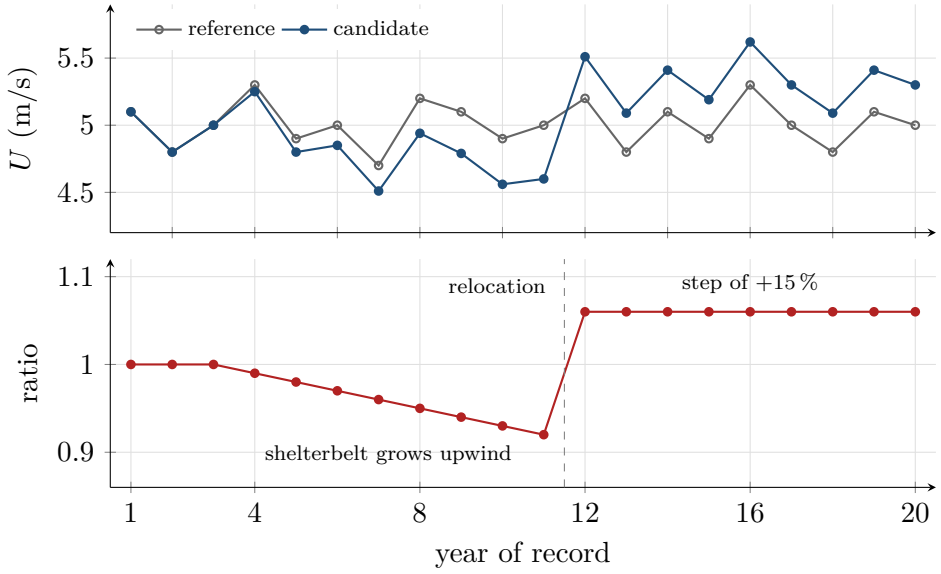


Figure 23.8: An inhomogeneous wind record (illustrative). Top: annual mean wind speed at a candidate station and at a neighboring reference station. Bottom: ratio of the two; it declines by 1 % per year from year 4 to year 11 as a shelterbelt grows upwind of the candidate, and jumps from 0.92 to 1.06 when the candidate is relocated in year 12.

In the upper panel the two records look alike: both vary by about $\pm 0.3\,\mathrm{m\,s^{-1}}$ from year to year, and the candidate's changes are hidden in that variation. The ratio in the lower panel separates them. The gradual decline from 1.00 to 0.92 is the growing shelterbelt, an 8 % loss of wind that a trend analysis of the candidate alone would report as a decline of the regional wind; the step from 0.92 to 1.06, a 15 % increase, is the relocation. The raw candidate record has a mean of $4.84\,\mathrm{m\,s^{-1}}$ over its first 11 years and $5.32\,\mathrm{m\,s^{-1}}$ over its last 9, a 10 % rise that the atmosphere did not produce: the reference changed by less than 0.5 %. For wind energy, a 15 % step in speed is a factor of $1.15^3 \approx 1.5$ in the cube of the speed. Long-term wind trends therefore require a careful review of the metadata, and the reference station must itself be

checked for homogeneity, since a change at the reference would appear in the ratio with the opposite sign.

23.6.3 Sensitivity of wind to siting

Temperature can often remain reasonably representative within a broad area. Air temperature near the ground is set by the surface energy balance and by the air mass, both of which vary smoothly over flat terrain in well-mixed conditions, and a few meters of displacement or a nearby building change it little. Wind is much more sensitive to obstacles, terrain and roughness, because each of them sets up its own pressure perturbation and momentum sink at the scale of the obstacle, tens to hundreds of meters, and the wind responds directly to both. The examples of this chapter, a 30 % difference between an open and a suburban 10 m sensor, a factor of two between a valley and a ridge 2 km apart, a wake that removes most of the wind $2\,h_c$ behind a building, have no counterpart of that size in daytime temperature over the same distances. Wind is therefore one of the most spatially heterogeneous of the routinely measured meteorological variables, and this is why station siting matters so much for it. (At night the contrast narrows: cold-air pools make the temperature heterogeneous in complex terrain too.)

Exposure classes. Operational networks sometimes classify stations according to exposure quality. A high-quality reference station might require open terrain, a large separation from obstacles (for example the ten-heights rule of thumb of equation (23.6) or more) and the standard height; lower classes accept closer obstacles or shorter fetch, with a stated expected error. Engineering networks may use a different standard, because the local asset exposure is itself the quantity of interest: a conductor-height sensor in a ridge gap is the best possible sensor for that span and a poor class for a reference network. This distinction should always be explicit, in the exposure class and in the siting objective recorded in the metadata.

23.6.4 Three stations in one region

Suppose three nearby stations report, for the same hour,

$$U_A = 4\,\mathrm{m\,s^{-1}}, \qquad U_B = 7\,\mathrm{m\,s^{-1}}, \qquad U_C = 10\,\mathrm{m\,s^{-1}}.$$

Before concluding that two of the sensors are wrong, inspect their sites. Station A is on a valley floor, station B on an open plain and station C on a ridge crest. Those values may all be physically consistent. Relative to the open-plain value, the ridge reads 1.43 times higher, the speed-up of a ridge with an aspect ratio $h_m/L_h \approx 0.21$ by the rule of thumb of Chapter 20; the valley reads 0.57 times the plain, consistent with sheltering and a partly decoupled valley atmosphere. Table 23.4 lists the three stations with an illustrative decomposition of each reading into the contributions of Section 23.6.6.

Table 23.4: Three nearby stations and an illustrative decomposition of each reading (m/s), with a regional wind of $7\,\mathrm{m\,s^{-1}}$ at sensor height.

Station	U_{regional}	$\Delta U_{\mathrm{terrain}}$	$\Delta U_{\mathrm{roughness}}$	$\Delta U_{\mathrm{obstacle}}$	$\Delta U_{\mathrm{instr}}$	U_{obs}
A: valley floor	7.0	−2.4	−0.4	−0.1	−0.1	4.0
B: open plain	7.0	0.0	+0.1	−0.1	0.0	7.0
C: ridge crest	7.0	+3.1	0.0	0.0	−0.1	10.0

The table makes the diagnosis explicit. The spread of $6\,\mathrm{m\,s^{-1}}$ among the stations is almost entirely terrain: $5.5\,\mathrm{m\,s^{-1}}$ of it comes from the terrain column, and the instrument column contributes $0.1\,\mathrm{m\,s^{-1}}$ at most. A quality-control procedure that flagged A and C as outliers

against the regional mean of $7\,\mathrm{m\,s^{-1}}$ would discard two correct measurements of two real flow regimes.

23.6.5 Sensor network design

To characterize a region rather than one site, multiple sensors may be needed, deliberately placed in different regimes: a ridge, a valley, an open plain, a forest edge. With simultaneous records from such a network, the regional forcing and the local terrain response can be separated much more effectively than with one sensor. The component common to all the sites, for example the open-plain record or the common variation across sites, estimates the regional forcing; the ratio of each site to it, stratified by direction sector and stability class, estimates that site's local response. With a single sensor the two are confounded: a low reading may be a weak regional wind or a sheltered site, and nothing in the record distinguishes them.

The design follows from the earlier sections. Each sensor's exposure should be documented by sector; the network should span the regimes in which the quantity of interest will be needed, so that the dynamical representativeness of Table 23.1 is covered; at least one sensor should meet the standard exposure, so that the network connects to weather models and to other networks; and sensors for an asset should be placed at the asset's height and in its regime, labeled as intentionally local.

23.6.6 A decomposition of an observed wind

A useful conceptual decomposition of a measured wind is

$$U_{\mathrm{obs}} = U_{\mathrm{regional}} + \Delta U_{\mathrm{terrain}} + \Delta U_{\mathrm{roughness}} + \Delta U_{\mathrm{obstacle}} + \Delta U_{\mathrm{instr}}, \tag{23.20}$$

where U_{regional} is the wind the region would have at the sensor height over standard open terrain, the three ΔU terms are the modifications by the terrain, the local roughness and the nearby obstacles, and $\Delta U_{\mathrm{instr}}$ is the instrument error. The decomposition is conceptual rather than strictly additive: terrain speed-up multiplies a wind that roughness has already reduced, and a wake reduces whatever wind arrives. A multiplicative form, $U_{\mathrm{obs}} \approx U_{\mathrm{regional}}\, S_{\mathrm{terrain}}\, S_{\mathrm{roughness}}\, S_{\mathrm{obstacle}} + \Delta U_{\mathrm{instr}}$, is often closer to the physics, and its logarithm is additive. Either way it is a good diagnostic framework: each term has its own section in this chapter, its own metadata and its own correction or model. The important point is that the instrument error may be only a small part of the difference between a measurement and a model or between two stations, as in Table 23.4. The next chapter turns to the statistics of the wind values that such sensors record: means and vector means, distributions, gusts and extremes, and the measures by which a model is verified against them.

23.7 What to retain

Definition 23.1 (Measurement height and exposure)**.** A wind sensor measures the wind at one height, at one point, with one directional exposure, under one terrain and roughness regime. Before a measurement is compared with a model, another station or an engineering asset, the two quantities must be shown to represent the same flow; otherwise their difference is representativeness, not error.

Table 23.5 lists the terms of the chapter, their meaning, their units and the subsection that defines each.

Table 23.5: The terms of the chapter and where each is defined.

Term	Meaning	Units	Defined in
Exposure	degree to which a sensor samples the undisturbed flow it is intended to represent	–	23.1.3
Height AGL	height of the sensor above the local ground; always attached to a wind value	m	23.1.1
Standard surface wind U_{10}	wind at about 10 m AGL over open terrain	m/s	23.1.2
Directional exposure	exposure as a function of the upwind sector	–	23.1.5
Wake	region of reduced mean wind and increased turbulence behind an obstacle	–	23.2.1
Height ratio z/h_c	sensor height over obstacle height; small means individual obstacles matter	–	23.2.2
Distance ratio x/h_c	distance to an obstacle over its height; rule of thumb $\gtrsim 10$	–	23.2.3
Fetch	upwind distance over a relatively uniform surface; about $100\,z$ for equilibrium	m	23.2.4
Measurement footprint	upwind region influencing a measurement; length scale x_{fp}, longer with height and in stable air	m	23.2.5
Terrain exposure	degree to which a location is open or sheltered relative to the flow	–	23.3.1
Spatial representativeness	how well a point represents an area	–	23.4.3
Vertical representativeness	how well the measurement height matches the target height	–	23.4.3
Dynamical representativeness	whether the site experiences the target flow regime	–	23.4.3
Representativeness radius	distance over which a sensor stands for its surroundings; not fixed	m	23.4.4
Representativeness uncertainty	spread of point minus area average, $\sqrt{\mathcal{D}}\,\sigma_s$	m/s	23.4.5, 23.5.1
Elevation mismatch	difference between actual and modeled terrain elevation	m	23.5.2
Roughness mismatch	difference between local and modeled aerodynamic roughness	m	23.5.3
Height correction	move a wind along one profile to another height	–	23.5.4
Exposure correction	move a wind from one surface's profile to another's, via a blending height	–	23.5.5
Station metadata	information describing sensor, site and exposure	–	23.6.1
Station homogeneity	consistency of measurement conditions through time	–	23.6.2
Exposure class	network grade of a station's exposure quality	–	23.6.3

23.8 Exercises

Exercise 23.1. An anemometer at 25 m above open grass, $z_0 = 0.05\,\mathrm{m}$, reads $8.0\,\mathrm{m\,s^{-1}}$ in neutral air. (a) With equation (23.2), compute the wind at 10 m, and repeat with $z_0 = 0.2\,\mathrm{m}$ to see the sensitivity to the roughness length. (b) Repeat the 10 m value for a stable surface layer with $L_O = 60\,\mathrm{m}$, using $\psi_m = -5\,z/L_O$. (c) The weather-model cell containing the mast has $z_{0,m} = 0.4\,\mathrm{m}$ and reports $U_{10} = 5.8\,\mathrm{m\,s^{-1}}$. With equation (23.19), the station's $z_0 = 0.05\,\mathrm{m}$ and $z_b = 60\,\mathrm{m}$, compute the model-surface equivalent of the observation and the apparent model error before and after the correction. (d) Name two effects that this correction would not remove.

Exercise 23.2. A 10 m mast is planned on open grass ($z_0 = 0.03\,\mathrm{m}$), 120 m east of a row of trees 15 m tall. (a) Compute x/h_c and z/h_c, and the distance required by the rule of thumb of equation (23.6). (b) For a west wind in neutral air, compute the footprint length scale x_{fp}, the most influential upwind distance and the fraction of the influence that comes from within 120 m of the mast, that is, from the grass between the mast and the trees. (c) Repeat (b) for a stable night with $L_O = 50\,\mathrm{m}$ ($\phi_h = 1 + 5\,z/L_O$). (d) What do (b) and (c) imply for the use of this mast as a grass-surface reference in west winds?

Exercise 23.3. A station in southern Brazil at 30°S has open pasture in the sector 200° to 280°, a eucalyptus plantation 25 m tall at 150 m in the sector 280° to 340°, and buildings in the sector 340° to 020°. Above the boundary layer the geostrophic wind blows from 270°, and the 10 m wind is turned by 20° toward low pressure. (a) Compute the Coriolis parameter, state on which side of the geostrophic flow the low pressure lies, and give the direction β of the 10 m wind. (b) Which exposure sector lies upwind of the 10 m sensor, and which would lie upwind if the surface wind blew from the geostrophic direction? (c) Repeat (a) and (b) for a station with the same surroundings at 30°N. (d) Compute x/h_c for the plantation and say how the readings in case (a) should be treated.

Exercise 23.4. (a) Local wind deviations in a region have $\sigma_s = 1.2\,\mathrm{m\,s^{-1}}$ and a correlation length $\ell_s = 1\,\mathrm{km}$. With equation (23.15), compute $\mathcal{R}$, $\mathcal{Q}$, $\mathcal{D}$ and the standard deviation of the representativeness difference for transects of 2 km and 10 km. (b) With an instrument uncertainty of $0.15\,\mathrm{m\,s^{-1}}$ and a perfect model, compute the expected root-mean-square difference between model and station for both transects with equation (23.16), and the fraction of its variance due to the instrument. (c) The ratio of a station's annual mean wind to a neighbor's is 0.98 for 12 years and 0.86 afterward, when a warehouse 15 m tall is built 60 m west of the mast. Compute x/h_c, the step in percent, and the corresponding change in the cube of the speed, and state what the metadata should record.

Chapter 24

Wind Statistics

24.1 Means and variability of the wind

A wind record is never one number. A sonic anemometer sampled twenty times a second, a cup anemometer logged every ten minutes and a weather model written out every hour all produce series that rise and fall on every time scale, and the series must be reduced to a few numbers before it can inform a design, a rating or a forecast evaluation. Depending on the application, the number wanted is a mean speed, a mean vector, a gust, a variance, a turbulence intensity, a frequency of directions, a probability of exceeding a threshold or an extreme value that occurs once in decades. The question of this chapter is

how should a wind field that is always fluctuating be summarized, and which statistic answers which question?

The chapter first treats means and variability; then the statistics of wind direction, which is a circular quantity; the probability distribution of wind speed and the Weibull distribution; exceedance probabilities, quantiles, return periods and extreme values; the structure of a record in time, through its autocorrelation, integral scales and spectrum; and finally the metrics used to compare a modeled wind with an observed one. Turbulence intensity, gusts and averaging periods (Chapter 8), variance, covariance and correlation (Chapter 9), and wind roses and conditional climatology (Chapter 19) were introduced earlier; they are recalled briefly here and carried further.

Jargon: statistic, sample, scalar mean speed, vector mean wind, variance, standard deviation, averaging period, temporal resolution

A *statistic* is a number computed from a record that summarizes one property of it. A *sample* is one value of the record: $U_1, U_2, \ldots, U_N$ are N samples of the horizontal wind speed U, in m/s. The *scalar mean speed* $\overline{U}$ is the average of the speeds, ignoring direction. The *vector mean wind* is the average of the wind vectors, computed from the averages $\overline{u}$ and $\overline{v}$ of the eastward and northward components; its magnitude U_{vec} is the *mean-vector speed*. The *variance* σ_U^2, in m^2/s^2, is the mean squared departure from the mean, and the *standard deviation* σ_U, in m/s, is its square root. The *averaging period* is the length of time over which a stored or reported value is averaged (three seconds, one minute, ten minutes, one hour); the *temporal resolution* of a record is the interval between its stored values, set by the sampling frequency f_s of the instrument or the output interval of a model.

Key idea

There is no single statistic called "the wind". A mean speed, a vector mean, a gust, a variance, a return level and a frequency of directions are different statistics of the same fluctuating, directional and multiscale flow; the statistic must be chosen to match the physical question, and a sound analysis usually needs more than one.

In this section and in the sections on direction and verification, u and v are the eastward and northward components of the wind and β is the direction from which it blows, clockwise from north, so that $u = -U\sin\beta$ and $v = -U\cos\beta$. In Section 24.5, which treats the fluctuations within a single record, u' is the along-wind fluctuation, as in Chapters 8 and 9.

24.1.1 Scalar mean speed and vector mean wind

The scalar mean speed of N samples is

$$\overline{U} = \frac{1}{N}\sum_{i=1}^{N} U_i, \tag{24.1}$$

which is what is usually meant by "the average wind speed". It ignores direction: a sample of $5\,\mathrm{m\,s^{-1}}$ from the west and one of $5\,\mathrm{m\,s^{-1}}$ from the east count the same. Averaging the components instead,

$$\overline{u} = \frac{1}{N}\sum_{i=1}^{N} u_i, \qquad \overline{v} = \frac{1}{N}\sum_{i=1}^{N} v_i, \qquad U_{\mathrm{vec}} = \sqrt{\overline{u}^2 + \overline{v}^2}, \tag{24.2}$$

gives the vector mean wind and its speed, and the direction of the vector mean is the angle β_{vec} with $\sin\beta_{\mathrm{vec}} = -\overline{u}/U_{\mathrm{vec}}$ and $\cos\beta_{\mathrm{vec}} = -\overline{v}/U_{\mathrm{vec}}$. Because the length of a sum of vectors never exceeds the sum of their lengths, $U_{\mathrm{vec}} \le \overline{U}$ always, with equality only when every sample has the same direction. The ratio $U_{\mathrm{vec}}/\overline{U}$, between zero and one, is the *steadiness* of the wind: one for a wind of constant direction, near zero for a wind that blows from all directions or reverses.

Figure 24.1 draws two cases. In both panels north is up, every arrow is a wind vector drawn from the origin in the direction toward which the air moves, with a length proportional to its speed, and the red arrow, where there is one, is the vector mean. In panel (a) the wind is $5\,\mathrm{m\,s^{-1}}$ from the west for half the period ($u = +5\,\mathrm{m\,s^{-1}}$) and $5\,\mathrm{m\,s^{-1}}$ from the east for the other half ($u = -5\,\mathrm{m\,s^{-1}}$). The scalar mean speed is

$$\overline{U} = \tfrac{1}{2}\,(5 + 5) = 5\,\mathrm{m\,s^{-1}},$$

while the components cancel, $\overline{u} = \tfrac{1}{2}\,(5 - 5) = 0$ and $\overline{v} = 0$, so $U_{\mathrm{vec}} = 0$ and the steadiness is zero. Both numbers are correct; they answer different questions. The scalar mean says how fast the air moves past the sensor on average, which is what matters for the energy in the wind or the cooling of a conductor. The vector mean says how far, and in which direction, the air is carried on average, which is what matters for the transport of a pollutant plume or of moisture: over the period, air from this site goes nowhere. In panel (b) three samples of $5\,\mathrm{m\,s^{-1}}$ come from 240°, 270° and 300°. Their components are $(u, v) = (4.33, 2.50)$, $(5.00, 0)$ and $(4.33, -2.50)\,\mathrm{m\,s^{-1}}$, so $\overline{u} = 4.55\,\mathrm{m\,s^{-1}}$, $\overline{v} = 0$ and the vector mean is $4.55\,\mathrm{m\,s^{-1}}$ from 270°, against a scalar mean of $5\,\mathrm{m\,s^{-1}}$: a steadiness of 0.91. A spread of ±30° in direction costs only nine percent of the mean-vector speed.

24.1.2 Variance and standard deviation

The strength of the fluctuations about the mean is measured by the variance of the speed,

$$\sigma_U^2 = \overline{(U - \overline{U})^2} = \frac{1}{N}\sum_{i=1}^{N}(U_i - \overline{U})^2, \qquad \sigma_U = \sqrt{\sigma_U^2}, \tag{24.3}$$



(a) $\overline{U} = 5\,\mathrm{m\,s^{-1}}$, $U_{\mathrm{vec}} = 0$ (b) $\overline{U} = 5\,\mathrm{m\,s^{-1}}$, $U_{\mathrm{vec}} = 4.55\,\mathrm{m\,s^{-1}}$

Figure 24.1: Scalar mean speed and vector mean wind (schematic, either hemisphere; north up). Arrows point toward where the air moves, with length proportional to speed. (a) $5\,\mathrm{m\,s^{-1}}$ from the west half the time and $5\,\mathrm{m\,s^{-1}}$ from the east the other half: the vectors cancel. (b) Three samples of $5\,\mathrm{m\,s^{-1}}$ from 240°, 270° and 300°: the vector mean (red) is $4.55\,\mathrm{m\,s^{-1}}$ from 270°, a steadiness of 0.91.

the mean squared departure and its square root, the standard deviation, which has the units of the speed. A large σ_U means that the wind varies strongly about its mean. Expanding the square gives the form used in data loggers, which accumulate sums as the samples arrive: $\sigma_U^2 = \overline{U^2} - \overline{U}^2$. For a turbulence record of thousands of samples the divisor N is used; for a short series, such as twenty annual maxima, the unbiased divisor $N - 1$ is preferred, and the difference is then a few percent. The variance and the covariance of a record, and the fluctuation $U' = U - \overline{U}$ whose mean square the variance is, were defined in Chapter 9.

The variance of the speed is not the same as the variance of the components. When the direction meanders, the components fluctuate across the mean wind while the speed may hardly change, and σ_U then understates the motion: a wind that turns slowly through 90° at a constant $3\,\mathrm{m\,s^{-1}}$ has $\sigma_U = 0$ but large variances of u and v. The difference is small in a strong wind, where the fluctuations are mostly along the wind, and large in a light and variable one.

24.1.3 Turbulence intensity and its behavior at low wind speed

The turbulence intensity of Chapter 8,

$$\mathrm{TI} = \frac{\sigma_U}{\overline{U}}, \tag{24.4}$$

normalizes the variability by the mean speed. For $\overline{U} = 10\,\mathrm{m\,s^{-1}}$ and $\sigma_U = 2\,\mathrm{m\,s^{-1}}$, $\mathrm{TI} = 0.20 = 20\,\%$. The normalization is useful where loads or power scale with the mean: two sites with the same TI have fluctuations of the same relative size.

At low wind speed the ratio misleads. Take an illustrative night-time record with $\overline{U} = 1\,\mathrm{m\,s^{-1}}$ and $\sigma_U = 0.8\,\mathrm{m\,s^{-1}}$:

$$\mathrm{TI} = \frac{0.8\,\mathrm{m\,s^{-1}}}{1\,\mathrm{m\,s^{-1}}} = 0.80 = 80\,\%.$$

The number suggests violent turbulence, but the absolute fluctuations are modest: $0.8\,\mathrm{m\,s^{-1}}$ is less than half the $2\,\mathrm{m\,s^{-1}}$ of the windy record above, whose TI is a quarter as large. The ratio is also unstable. An error of only $\pm 0.2\,\mathrm{m\,s^{-1}}$ in the mean, well within the uncertainty of a cup anemometer near its starting threshold (Chapter 22), moves TI between $0.8/1.2 = 67\,\%$ and $0.8/0.8 = 100\,\%$; as $\overline{U}$ approaches zero, TI grows without bound whatever the turbulence. And at low speed the meandering of the direction makes σ_U itself a poor measure of the fluctuations (Section 24.1.2). The practical rule is to inspect σ_U and $\overline{U}$ together, to report TI only above a

stated minimum mean speed, and, for a light wind, to describe the fluctuations by σ_U, σ_v and σ_w directly.

24.1.4 Gusts and the gust factor

A *gust* is a short-duration maximum of the wind speed: the highest value, within a reference period, of the speed averaged over a short gust duration (Chapter 8). A station might report, for each ten minutes, the mean speed and the highest three-second running mean; then $U_{\text{gust}} > \overline{U}$, and both values are statistics of the same record. The exact definition, the gust duration, the reference period and the response of the instrument, depends on the observing standard, and two networks that call different statistics "the gust" are not comparable without conversion.

The *gust factor* is the ratio of the gust to the mean of the same reference period,

$$G = \frac{U_{\text{gust}}}{\overline{U}} = 1 + g_{\text{pk}}\,\text{TI}, \tag{24.5}$$

dimensionless, where the second form uses the peak factor $g_{\text{pk}} = (U_{\text{gust}} - \overline{U})/\sigma_U$ of Chapter 8. For an illustrative gust of $18\,\text{m s}^{-1}$ in a ten-minute mean of $12\,\text{m s}^{-1}$,

$$G = \frac{18\,\text{m s}^{-1}}{12\,\text{m s}^{-1}} = 1.5,$$

which corresponds, for example, to $\text{TI} = 0.20$ and $g_{\text{pk}} = 2.5$: $12 \times (1 + 2.5 \times 0.20) = 18\,\text{m s}^{-1}$. The second form shows what the gust factor depends on. It grows with the turbulence intensity, and therefore with the roughness of the upwind surface: with the same peak factor, a TI of 0.08 over open water gives $G = 1.2$ and a TI of 0.25 over a suburb gives $G = 1.6$. It depends on stability: convective downdrafts raise it, and stable nights lower TI but may produce isolated bursts that set the maximum. And it depends on the averaging periods: a longer reference period samples more extreme fluctuations and raises g_{pk}, while a longer gust duration smooths them and lowers it, so a three-second gust in an hour gives a larger G than a three-second gust in ten minutes, and a one-minute gust a smaller one.

24.1.5 Averaging period and temporal resolution

The same record averaged over 1 s, 10 s, 1 min and 10 min gives four series. As the averaging period grows, the short turbulent fluctuations are filtered out, and the variance of the averaged values decreases: in the ten-minute record of Chapter 8, the standard deviation fell from $1.98\,\text{m s}^{-1}$ for the raw samples to $1.12\,\text{m s}^{-1}$ for one-minute means, and the highest value from $16.0\,\text{m s}^{-1}$ to $11.4\,\text{m s}^{-1}$. The standard deviation is therefore a function of the averaging scale,

$$\sigma_U = \sigma_U(\text{averaging period}), \tag{24.6}$$

and there is no context-free "wind variability". How fast it falls depends on how long the turbulent structures persist, a dependence made quantitative in Section 24.5.4.

The averaging period and the temporal resolution are different properties. A sonic anemometer sampled at $f_s = 20\,\text{Hz}$ resolves fluctuations up to the Nyquist frequency $f_N = f_s/2 = 10\,\text{Hz}$ (Chapter 22), but if the logger stores only ten-minute means, the stored product resolves nothing shorter than ten minutes: the raw data captured the turbulence and the product discarded it. Loggers usually store, for each period, the mean, the standard deviation and the maximum gust, so that some of the information survives as statistics. For model validation the first question about an observation is therefore which kind it is:

- an *instantaneous* value, one sample at one time;
- a *high-frequency raw* record, from which any statistic can still be computed;

- an *averaged product*, such as a ten-minute or hourly mean, with or without its standard deviation and gust.

A model's output has the same ambiguity: a value written every hour may be the grid-cell wind at that instant or an average over the hour, and in either case it is a spatial average over the grid cell (Chapter 5). Comparing an hourly snapshot of a grid-cell wind with a ten-minute mean at a point, or with a three-second gust, mixes three different statistics.

24.2 Statistics of wind direction

Wind direction is an angle, and the arithmetic of ordinary numbers fails on it. This section defines the circular mean and a circular measure of spread, recalls the wind rose and what a single rose hides, and introduces conditional and directional statistics.

24.2.1 Circular mean and circular spread

Direction is circular: 359° is 2° from 1°, not 358°, and 0° and 360° are the same direction. The arithmetic mean of 359° and 1° is 180°, the opposite of both. Ordinary statistics are therefore inappropriate for direction, and *circular statistics* are used instead: each direction is replaced by a unit vector, the vectors are averaged, and the direction of the average is the mean direction. With the unit vector pointing toward the direction the wind comes from, its eastward and northward components are $\sin\beta$ and $\cos\beta$, and

$$\overline{S} = \frac{1}{N}\sum_{i=1}^{N} \sin\beta_i, \qquad \overline{C} = \frac{1}{N}\sum_{i=1}^{N} \cos\beta_i, \qquad \overline{\beta} = \operatorname{atan2}(\overline{S}, \overline{C}), \tag{24.7}$$

where atan2 is the two-argument arctangent, which returns the angle in the correct quadrant, here converted to the range 0° to 360°. The length of the averaged unit vector,

$$\overline{R}_\beta = \sqrt{\overline{S}^2 + \overline{C}^2}, \qquad 0 \le \overline{R}_\beta \le 1, \tag{24.8}$$

the *mean resultant length*, measures concentration: one when all directions are equal, zero when they are spread evenly or cancel. Two measures of spread follow from it: the *circular variance* $1 - \overline{R}_\beta$, between zero and one, and the *circular standard deviation*

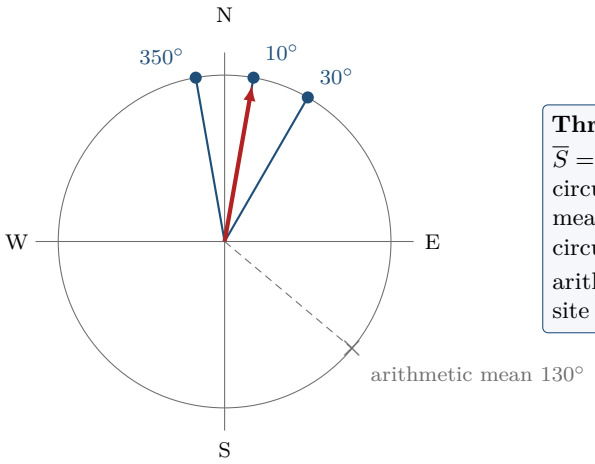
$$s_\beta = \sqrt{-2\ln \overline{R}_\beta}, \tag{24.9}$$

in radians, which for a narrow spread reduces to the ordinary standard deviation of the angles and grows without bound as $\overline{R}_\beta$ falls to zero.

Figure 24.2 works an example. The circle is the unit circle, north up; the blue dots on it are three illustrative ten-minute directions, 350°, 10° and 30°, with their unit vectors drawn from the center; the red arrow is their circular mean; and the gray cross is the arithmetic mean. The sums give

$$\overline{S} = \tfrac{1}{3}\,(-0.1736 + 0.1736 + 0.5000) = 0.1667, \qquad \overline{C} = \tfrac{1}{3}\,(0.9848 + 0.9848 + 0.8660) = 0.9452,$$

so $\overline{\beta} = \operatorname{atan2}(0.1667, 0.9452) = 10.0°$, $\overline{R}_\beta = \sqrt{0.1667^2 + 0.9452^2} = 0.960$, a circular variance of 0.040, and $s_\beta = \sqrt{-2\ln 0.960} = 0.286\,\text{rad} = 16.4°$. The directions lie −20°, 0° and +20° from the mean, whose ordinary root-mean-square is 16.3°, so the circular standard deviation reproduces the intuitive spread. The arithmetic mean, $(350 + 10 + 30)/3 = 130°$, points to the southeast, nearly opposite to every sample.



Three directions: 350°, 10°, 30°
$\overline{S} = 0.1667$, $\overline{C} = 0.9452$
circular mean $\overline{\beta} = 10.0°$ (red arrow)
mean resultant length $\overline{R}_\beta = 0.960$
circular standard deviation $s_\beta = 16.4°$
arithmetic mean 130°: wrong, nearly opposite every sample

Figure 24.2: Circular mean of three wind directions (illustrative, either hemisphere; north up). Each direction is a unit vector toward where the wind comes from; the red arrow is their average, of length $\overline{R}_\beta = 0.960$ (drawn to scale) and direction 10°. The arithmetic mean of the angles, 130°, is meaningless.

Unit-vector and vector-mean directions. The mean direction of equation (24.7) weights every sample equally. The direction β_{vec} of the vector mean wind of equation (24.2) weights each sample by its speed. The two agree when speed and direction are unrelated and differ when the strong winds come from one side and the light winds from another; the vector-mean direction is the one relevant to transport, the unit-vector direction the one relevant to the frequency of directions. Neither is defined when the wind is calm, and samples below a stated speed are usually excluded from direction statistics. How an instrument averages direction within its own sampling period is a question of measurement, treated in Chapter 22.

24.2.2 Wind roses and what one rose hides

A *wind rose* (Chapter 19) summarizes how frequently the wind comes from each direction sector, commonly sixteen sectors of 22.5° or twelve of 30°, often subdivided by speed class, with calms below a stated threshold counted separately. It identifies prevailing directions, channeling along a valley axis, sea-breeze regimes, and the sectors from which a change of roughness, $z_0(\beta)$, affects the site (Chapter 11).

A single rose can hide the physics. If the wind at a coastal site is easterly by day and westerly by night, the annual rose is simply bimodal, with an east lobe and a west lobe, and could be read as two synoptic regimes. Stratified by time of day, the two lobes separate into a day rose and a night rose, and the mechanism, a sea breeze and a land breeze, becomes obvious. The day lobe on an east-facing coast also carries the Coriolis turning of the sea breeze: it leans toward the northeast in the Southern Hemisphere and toward the southeast in the Northern Hemisphere, as the day and night roses of Chapter 19 showed for a station at 20°S. The annual rose hides the timing, the seasonal rose hides the diurnal cycle, and every rose hides the dependence of speed on direction unless it is drawn with speed classes. Wind climatology should therefore often be conditional.

24.2.3 Conditional and directional statistics

A *conditional statistic* is computed only over the samples that satisfy a stated condition. Writing $\mathcal{P}(U)$ for the probability density of wind speed (Section 24.3.1), useful conditional densities

include

$$\mathcal{P}(U \mid \text{daytime}), \quad \mathcal{P}(U \mid \text{stable}), \quad \mathcal{P}(U \mid 255^\circ \le \beta < 285^\circ), \quad \mathcal{P}(U \mid \text{winter}),$$

the distribution of speed by day, in stable hours, in the westerly sector and in winter. Conditioning on direction uses a sector rather than a single angle, because a measured direction is never exactly 270°. Each conditional distribution is often far more informative than the one unconditional distribution, because it separates mechanisms that the full record mixes; its cost, as Chapter 19 noted, is a smaller sample in each class.

Directional statistics condition on the wind direction. Take an illustrative site at 30°S whose mean speed is

$$\overline{U}\,(\text{westerly sector}) = 8\,\mathrm{m\,s^{-1}}, \qquad \overline{U}\,(\text{easterly sector}) = 4\,\mathrm{m\,s^{-1}}.$$

A factor of two between opposite sectors may reflect the terrain (a ridge that shelters the site from the east), the roughness (open water to the west, forest or town to the east) or the exposure of the sensor itself (a building close to the mast on its east side). The three causes are distinguished by comparing the sector ratio with the roughness map, with a terrain model and with a second sensor, and the distinction matters for modeling: a model with a single effective roughness for the grid cell cannot produce a factor of two between sectors, and a correction from model to site must be computed sector by sector, $z_0(\beta)$ and a speed-up factor $S(\beta)$ in the terms of Chapters 11 and 20. Directional statistics are therefore among the most useful inputs to local wind modeling, and the siting questions they raise are taken up in Chapter 23.

24.3 The distribution of wind speed

A mean and a standard deviation do not say how often the wind is calm or strong; the whole distribution does. This section describes the histogram and the probability density, the Weibull distribution with the meaning of its two parameters, its moments and the mean of the cube of the speed, the cases in which a Weibull fit fails, and the difference between mean and median.

24.3.1 Histogram and probability density

A *histogram* counts the samples whose speed falls in each class of a chosen width ΔU. Dividing each count by $N\,\Delta U$ gives an estimate of the *probability density* $\mathcal{P}(U)$, in s/m, defined so that $\mathcal{P}(U)\,\mathrm{d}U$ is the probability that the speed lies between U and $U + \mathrm{d}U$ and $\int_0^\infty \mathcal{P}\,\mathrm{d}U = 1$. Its integral from zero is the *cumulative distribution* $\mathcal{F}(U) = \Pr(\text{speed} \le U)$, dimensionless, rising from zero to one.

The distribution of wind speed has two general properties. Speed is non-negative, $U \ge 0$, so the density is bounded at zero. And it is usually skewed to the right rather than symmetric: most hours have light to moderate wind and a few have strong wind, so the right tail is long. A Gaussian distribution, symmetric and unbounded in both directions, is a poor model for it, although the individual velocity components within a short turbulent record are often close to Gaussian (Section 24.5.6). A common empirical model of the speed distribution is the Weibull distribution.

24.3.2 The Weibull distribution

The Weibull distribution is most easily stated through its cumulative form,

$$\mathcal{F}(U) = 1 - \exp\left[-\left(\frac{U}{c}\right)^{k}\right], \qquad U \ge 0, \tag{24.10}$$

with two parameters: the *scale parameter* $c > 0$, in m/s, and the *shape parameter* $k > 0$, dimensionless. (In this chapter only, k is the Weibull shape; elsewhere in the book k is a wavenumber.) Differentiating with respect to U by the chain rule, $\mathrm{d}(U/c)^k/\mathrm{d}U = (k/c)(U/c)^{k-1}$, gives the density

$$\mathcal{P}(U) = \frac{k}{c}\left(\frac{U}{c}\right)^{k-1} \exp\left[-\left(\frac{U}{c}\right)^{k}\right], \tag{24.11}$$

and the probability that the speed exceeds U is simply $1 - \mathcal{F}(U) = \exp[-(U/c)^k]$, the form used in Section 24.4.1. The distribution is especially common in wind-energy climatology, where it is fitted to a year or more of ten-minute or hourly mean speeds at hub height.

Three fitting methods are in common use. The *method of moments* chooses c and k so that the fitted mean and standard deviation equal those of the sample; a convenient empirical approximation for the shape is

$$k \approx \left(\frac{\sigma_U}{\overline{U}}\right)^{-1.086}, \tag{24.12}$$

after which c follows from the mean (equation (24.13)). *Maximum likelihood* chooses the parameters that make the observed sample most probable. A *Weibull plot* uses the fact that $\ln[-\ln(1-\mathcal{F})] = k\ln U - k\ln c$ is a straight line in $\ln U$, with slope k, and fits it by least squares. The ratio $\sigma_U/\overline{U}$ in equation (24.12) is the coefficient of variation of the ten-minute or hourly means over the whole record, a climatological spread of order 0.5; it is not the turbulence intensity, which is the same ratio computed within one ten-minute period from the raw samples.

24.3.3 Scale and shape

The scale parameter c sets the characteristic magnitude of the wind: at $U = c$ the cumulative distribution is $1 - \mathrm{e}^{-1} = 0.632$ whatever the shape, so 63 % of the samples lie below c, and the mean is close to $0.89\,c$ for the usual shapes (Table 24.1). A larger c means a windier climate. The shape parameter k controls the spread and the form: a small k gives a broad, variable distribution with many calm hours and a long tail; a large k gives a distribution tightly concentrated about its mean. For $k > 1$ the density vanishes at $U = 0$ and has its mode at $c\,[(k-1)/k]^{1/k}$; for $k = 1$ it is the exponential distribution, largest at zero.

The special case $k = 2$ is the *Rayleigh distribution*, and it has a physical origin. If the two horizontal components u and v are independent, Gaussian, of zero mean and of equal standard deviation σ, their joint density is $(2\pi\sigma^2)^{-1}\exp[-(u^2+v^2)/(2\sigma^2)]$. Changing to polar coordinates, $u^2 + v^2 = U^2$ and $\mathrm{d}u\,\mathrm{d}v = U\,\mathrm{d}U\,\mathrm{d}\beta$; integrating over the direction multiplies by 2π and gives

$$\mathcal{P}(U) = \frac{U}{\sigma^2}\exp\left(-\frac{U^2}{2\sigma^2}\right),$$

which is equation (24.11) with $k = 2$ and $c = \sqrt{2}\,\sigma$. A Rayleigh distribution of speed is what a wind with no prevailing direction and Gaussian components produces; wind climates with a dominant direction or with a steady trade wind have larger shapes, and climates with many calms smaller ones. Shapes from about 1.5 to 3 cover most sites, with larger values where one steady wind dominates.

Figure 24.3 plots equation (24.11). The horizontal axis is the wind speed and the vertical axis the probability density in s/m. The three solid curves share the scale $c = 8\,\mathrm{m\,s^{-1}}$ and have shapes 1.5, 2 and 3; the dashed curve has $k = 2$ and the smaller scale $c = 6\,\mathrm{m\,s^{-1}}$. At fixed scale, raising the shape moves the mode from 3.8 to 5.7 and $7.0\,\mathrm{m\,s^{-1}}$ and narrows the peak; the $k = 1.5$ curve has the most hours below $3\,\mathrm{m\,s^{-1}}$ and the most above $15\,\mathrm{m\,s^{-1}}$. At fixed shape, lowering the scale from 8 to $6\,\mathrm{m\,s^{-1}}$ compresses the whole curve toward zero and raises its peak, so that the area stays one.

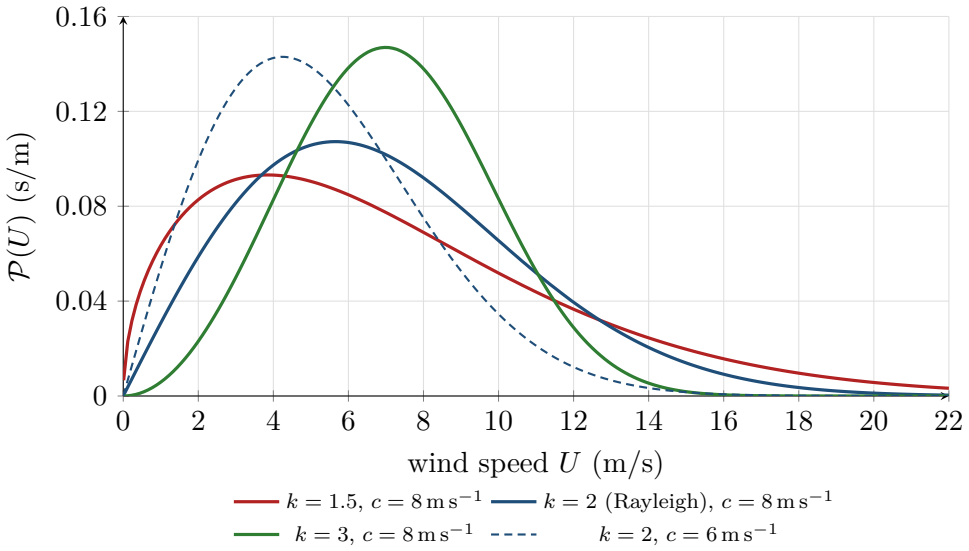


Figure 24.3: Weibull probability densities, $\mathcal{P}(U) = (k/c)(U/c)^{k-1}\exp[-(U/c)^k]$, for three shapes at the scale $c = 8\,\mathrm{m\,s^{-1}}$ (solid) and for $k = 2$ at $c = 6\,\mathrm{m\,s^{-1}}$ (dashed). Parameters illustrative.

24.3.4 Moments and the mean of the cube

The mean of any power of the speed follows from one substitution. With $x = (U/c)^k$, so that $U = c\,x^{1/k}$ and $\mathrm{d}x = (k/c)(U/c)^{k-1}\mathrm{d}U$, the nth moment is

$$\overline{U^n} = \int_0^\infty U^n\,\mathcal{P}(U)\,\mathrm{d}U = \int_0^\infty c^n\,x^{n/k}\,\mathrm{e}^{-x}\,\mathrm{d}x = c^n\,\Gamma\!\left(1+\frac{n}{k}\right), \tag{24.13}$$

where $\Gamma(z) = \int_0^\infty x^{z-1}\mathrm{e}^{-x}\,\mathrm{d}x$ is the gamma function, with $\Gamma(1) = 1$, $\Gamma(z+1) = z\,\Gamma(z)$ and $\Gamma(\tfrac{1}{2}) = \sqrt{\pi}$. The mean is $\overline{U} = c\,\Gamma(1+1/k)$, the variance $c^2[\Gamma(1+2/k) - \Gamma^2(1+1/k)]$, and the median, from $\mathcal{F} = \tfrac{1}{2}$ in equation (24.10), $c\,(\ln 2)^{1/k}$.

The third moment matters because the kinetic energy carried through a unit area per unit time is $\tfrac{1}{2}\rho U^3$, so the mean power density of the wind is $\tfrac{1}{2}\rho\,\overline{U^3}$, not $\tfrac{1}{2}\rho\,\overline{U}^3$. For an illustrative Rayleigh climate with $c = 8\,\mathrm{m\,s^{-1}}$ and $k = 2$, using $\Gamma(1.5) = \sqrt{\pi}/2 = 0.8862$ and $\Gamma(2.5) = 1.5 \times 0.8862 = 1.3293$,

$$\overline{U} = 8 \times 0.8862 = 7.09\,\mathrm{m\,s^{-1}}, \qquad \overline{U^3} = 8^3 \times 1.3293 = 680.6\,\mathrm{m^3\,s^{-3}},$$
$$\overline{U}^3 = 7.09^3 = 356.4\,\mathrm{m^3\,s^{-3}}.$$

The mean of the cube is 1.91 times the cube of the mean. With $\rho = 1.225\,\mathrm{kg\,m^{-3}}$, the power density is $\tfrac{1}{2} \times 1.225 \times 680.6 = 417\,\mathrm{W\,m^{-2}}$, while the cube of the mean speed would suggest $218\,\mathrm{W\,m^{-2}}$: using the mean speed alone underestimates the energy by almost half. The ratio $\overline{U^3}/\overline{U}^3 = \Gamma(1+3/k)/\Gamma^3(1+1/k)$ depends only on the shape, and Table 24.1 lists it with the other shape-dependent ratios. For each shape the columns give the mean and the median as fractions of the scale, their ratio, the coefficient of variation $\sigma_U/\overline{U}$ and the cube ratio. The broader the distribution, the larger the cube ratio: 2.72 for $k = 1.5$, 1.40 for $k = 3$.

The opposite bias applies to a process that responds less than linearly to the speed. The forced-convection cooling of a conductor grows roughly as $U^{0.6}$, a concave function, and its mean is then smaller than its value at the mean speed: for the same climate, $\overline{U^{0.6}} = 8^{0.6}\,\Gamma(1.3) = 3.482 \times 0.8975 = 3.13$, against $\overline{U}^{0.6} = 7.09^{0.6} = 3.24$, a cooling overestimated by 3.5 % if the mean speed is used. In both cases the mean speed is the wrong summary: the statistic must be the mean of the quantity that matters.

The table also checks equation (24.12): the coefficients of variation 0.679, 0.523 and 0.363 give $k \approx 1.52$, 2.02 and 3.00.

Table 24.1: Shape-dependent properties of the Weibull distribution, from equation (24.13). The mean and median are fractions of the scale c; the last column is the ratio of the mean of the cube to the cube of the mean.

Shape k	Mean/c	Median/c	Mean/median	$\sigma_U/\overline{U}$	$\overline{U^3}/\overline{U}^3$
1.5	0.903	0.783	1.153	0.679	2.72
2 (Rayleigh)	0.886	0.833	1.064	0.523	1.91
3	0.893	0.885	1.009	0.363	1.40

24.3.5 Limits of the Weibull fit

A Weibull distribution fits many wind-speed climatologies reasonably well, but it is an empirical form with one mode, and real distributions can be multimodal, regime-dependent and terrain-dependent. A site with both calm nocturnal drainage flow and strong daytime synoptic flow has two populations of hours, and a single Weibull fitted to both represents neither.

Figure 24.4 shows such a case. The bars are the histogram, in bins of $0.5\,\mathrm{m\,s^{-1}}$ and normalized as a density, of a synthetic year of 8760 hourly speeds at an illustrative site with two regimes: 44 % of the hours (drawn with probability 0.45) come from a light-wind regime with $c = 2\,\mathrm{m\,s^{-1}}$, $k = 1.8$, the calm nights with weak drainage, and the rest from a windy regime with $c = 8\,\mathrm{m\,s^{-1}}$, $k = 2.4$, the daytime mixing of the synoptic wind. The dashed curve is the true two-regime density, and the solid red curve is one Weibull fitted to the whole year by maximum likelihood, as a routine resource study would do, with $c = 5.18\,\mathrm{m\,s^{-1}}$ and $k = 1.30$. The dotted vertical lines mark the median and the mean of the sample.

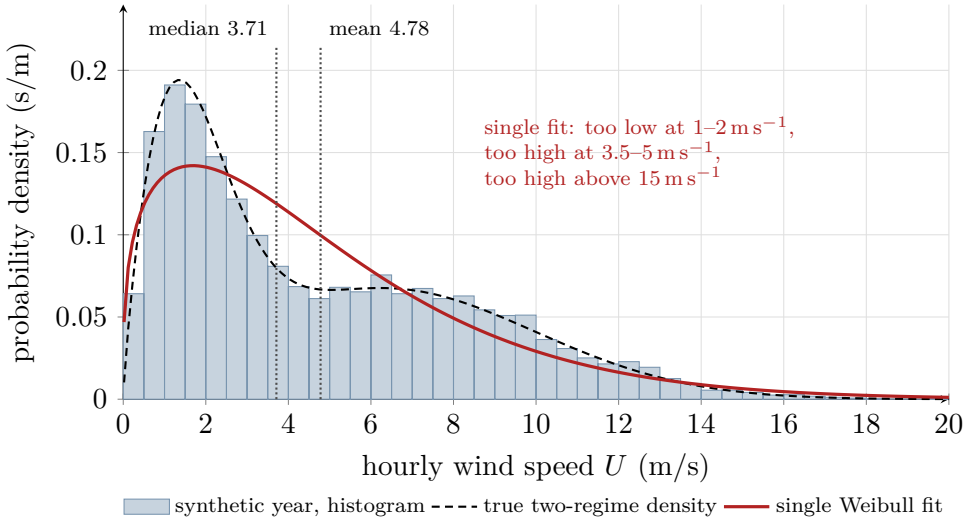


Figure 24.4: A synthetic year of 8760 hourly speeds from two regimes, illustrative (script `scripts/ch24_data.py`, seed 24): 45 % probability of a light-wind regime with $c = 2\,\mathrm{m\,s^{-1}}$, $k = 1.8$ and 55 % of a windy regime with $c = 8\,\mathrm{m\,s^{-1}}$, $k = 2.4$. Bars: histogram as a density. Dashed: the true mixture density. Red: one Weibull fitted by maximum likelihood, $c = 5.18\,\mathrm{m\,s^{-1}}$, $k = 1.30$.

The fit reproduces the mean, $4.78\,\mathrm{m\,s^{-1}}$ against the sample's $4.78\,\mathrm{m\,s^{-1}}$, and the probability of an hour below $1\,\mathrm{m\,s^{-1}}$, 11.1 % against 11.4 %, but both agreements are coincidences of a smooth curve crossing an irregular one. It misses the shape. The histogram has a sharp peak at 1 to $2\,\mathrm{m\,s^{-1}}$, where the fit is about 25 % too low, and a trough at 3.5 to $5\,\mathrm{m\,s^{-1}}$, where the fit is 45 to 65 % too high. The probability of an hour below $2\,\mathrm{m\,s^{-1}}$, which for a conductor is the probability of poor cooling, is 29.9 % in the sample and 25.1 % in the fit. In the tail, the

probability above $15\,\mathrm{m\,s^{-1}}$ is 0.67 % in the sample and 1.85 % in the fit, nearly three times too high, because the single broad Weibull with $k = 1.30$ must reach both the calms and the strong winds with one long tail. The mean of the cube is $337\,\mathrm{m^3\,s^{-3}}$ in the sample and $375\,\mathrm{m^3\,s^{-3}}$ in the fit, an 11 % overestimate of the power density. A goodness-of-fit test on a year of data may still accept the fit, and the figure shows that a good fit is not a physical mechanism: the two regimes are visible only when the hours are separated by time of day or stability (Section 24.2.3), and each regime is then well described by its own Weibull.

24.3.6 Mean and median

For a right-skewed distribution the mean exceeds the median, because a few high-wind hours pull the mean upward while the median, the speed exceeded half of the time, is set by the order of the values alone. For the Rayleigh climate of Section 24.3.4 the median is $8 \times (\ln 2)^{1/2} = 6.66\,\mathrm{m\,s^{-1}}$ against a mean of $7.09\,\mathrm{m\,s^{-1}}$; for the two-regime year of Figure 24.4, the median is $3.71\,\mathrm{m\,s^{-1}}$ and the mean $4.78\,\mathrm{m\,s^{-1}}$, 29 % higher. Half the hours of that year have less than $3.7\,\mathrm{m\,s^{-1}}$, a fact the mean of $4.8\,\mathrm{m\,s^{-1}}$ conceals. The median therefore often describes "typical" conditions better, while the mean is the correct summary for a quantity that is additive over time, such as the distance air travels or, through the mean of the cube, the energy. The right statistic again depends on the question.

24.4 Exceedance, quantiles and extremes

Many engineering questions concern thresholds rather than averages: how often the wind exceeds a design speed, how often it falls below the speed needed to cool a conductor, and how strong the strongest gust in fifty years will be. This section defines the exceedance probability, quantiles and the return period, introduces extreme-value distributions, and states the caution that applies to every estimate beyond the length of the record.

24.4.1 Exceedance probability

The *exceedance probability* of a threshold speed U_{th} is the fraction of time the speed is above it,

$$\Pr(U > U_{\mathrm{th}}) = 1 - \mathcal{F}(U_{\mathrm{th}}) = \exp\left[-\left(\frac{U_{\mathrm{th}}}{c}\right)^{k}\right], \tag{24.14}$$

the second form for a Weibull distribution. Typical questions are the probability that the wind exceeds $10\,\mathrm{m\,s^{-1}}$, the probability that the cooling wind falls below $1\,\mathrm{m\,s^{-1}}$, $\Pr(U < 1\,\mathrm{m\,s^{-1}}) = \mathcal{F}(1\,\mathrm{m\,s^{-1}})$, and the probability that a gust exceeds a design threshold. Such probabilities are often more useful than the mean: a conductor rating is limited by the hours of weak wind, not by the average.

For the Rayleigh climate with $c = 8\,\mathrm{m\,s^{-1}}$,

$$\Pr(U > 10\,\mathrm{m\,s^{-1}}) = \exp\left[-\left(\tfrac{10}{8}\right)^{2}\right] = \mathrm{e}^{-1.5625} = 0.210,$$

$$\Pr(U < 1\,\mathrm{m\,s^{-1}}) = 1 - \exp\left[-\left(\tfrac{1}{8}\right)^{2}\right] = 0.0155,$$

so the wind exceeds $10\,\mathrm{m\,s^{-1}}$ for 21 % of the year, about 1840 hours, and is below $1\,\mathrm{m\,s^{-1}}$ for 1.6 %, about 136 hours. With the broader shape $k = 1.5$ and the same scale, the second probability is $1 - \exp(-0.125^{1.5}) = 4.3$ %, nearly three times larger: the shape parameter, not the mean, decides how often a conductor is poorly cooled.

Figure 24.5 plots equation (24.14) on a logarithmic vertical axis for the three shapes of Figure 24.3, all with $c = 8\,\mathrm{m\,s^{-1}}$. The horizontal axis is the threshold speed; the vertical axis is

the fraction of time above it, from one down to 10^{-7}. The three distributions have nearly the same mean, 7.22, 7.09 and 7.14 m s^{-1}, and exceedances at 10 m s^{-1} within a factor of two of one another, 0.25, 0.21 and 0.14, but their tails diverge. At 20 m s^{-1} the exceedance is 1.9×10^{-2} for $k = 1.5$, 1.9×10^{-3} for $k = 2$ and 1.6×10^{-7} for $k = 3$: 168 hours, 17 hours and five seconds a year. Three distributions that agree on the mean disagree by five orders of magnitude on the strong-wind tail, and the tail of a Weibull fit is set by a shape that was chosen to fit the bulk of the hours.

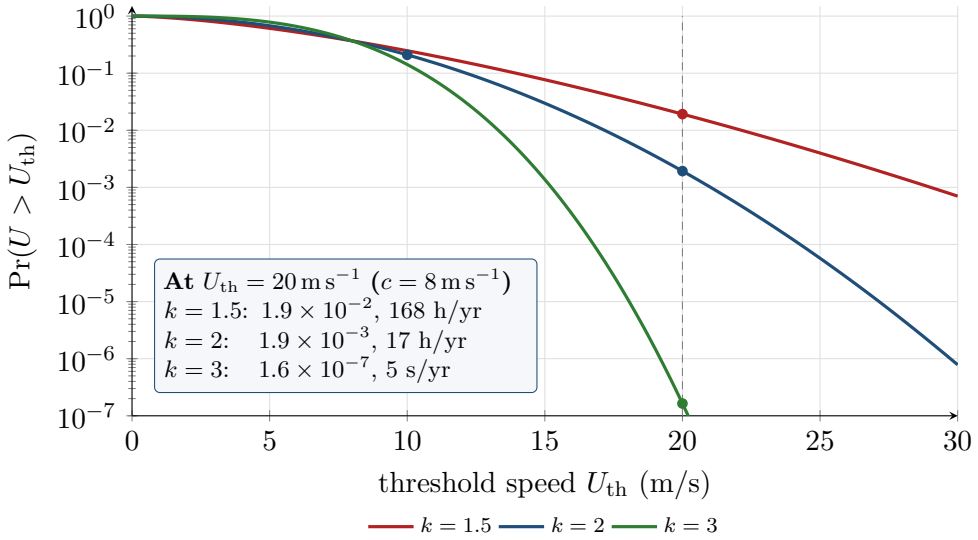


Figure 24.5: Weibull exceedance probability, $\Pr(U > U_{\mathrm{th}}) = \exp[-(U_{\mathrm{th}}/c)^k]$, for $c = 8\,\mathrm{m\,s^{-1}}$ and three shapes, on a logarithmic axis (illustrative). The dot at 10 m s^{-1} is the worked value 0.21 for $k = 2$; the dots on the dashed line are the values at 20 m s^{-1}.

24.4.2 Quantiles

A *quantile* reverses the question: the speed U_p below which a fraction p of the samples lies, $\mathcal{F}(U_p) = p$. Instead of a mean alone, a distribution can be reported by $U_{0.10}$, $U_{0.50}$ (the median) and $U_{0.90}$; in this book the probability is written as a fraction in the subscript, because U_{10} is the wind at 10 m. A value $U_{0.90} = 12\,\mathrm{m\,s^{-1}}$ means that 90 % of the winds are at or below 12 m s^{-1}. For a Weibull distribution, solving equation (24.10) for U gives

$$U_p = c\,[-\ln(1-p)]^{1/k}, \tag{24.15}$$

and for the Rayleigh climate with $c = 8\,\mathrm{m\,s^{-1}}$, $U_{0.10} = 8\sqrt{0.105} = 2.60\,\mathrm{m\,s^{-1}}$, $U_{0.50} = 6.66\,\mathrm{m\,s^{-1}}$ and $U_{0.90} = 8\sqrt{2.303} = 12.1\,\mathrm{m\,s^{-1}}$, the value just quoted. From a record, quantiles are read from the sorted samples without any assumed distribution. Quantiles are the natural output of probabilistic wind modeling: a forecast that gives $U_{0.10}$, $U_{0.50}$ and $U_{0.90}$ states its uncertainty in the units of the wind, and the low quantile is the one a conservative conductor rating uses.

24.4.3 Return period

Extreme-wind design is expressed through the *return period* T_R, in years: the mean interval between years in which a given level is exceeded. If P_a is the probability that the level is exceeded in any one year and the years are independent, the number of years until the first exceedance follows a geometric distribution, whose mean is $1/P_a$; hence

$$T_R = \frac{1}{P_a}, \qquad \Pr(\text{at least one exceedance in } N_y \text{ years}) = 1 - (1 - P_a)^{N_y}, \tag{24.16}$$

the second because the probability of no exceedance in N_y independent years is $(1 - P_a)^{N_y}$. A 50-year return wind has an annual exceedance probability of $1/50 = 0.02$. (If the return period is instead defined as the mean interval between individual events, counted as a Poisson process, then $P_a = 1 - \mathrm{e}^{-1/T_R} = 0.0198$; for long return periods the two definitions agree, which is the sense of the usual statement that P_a is "roughly" $1/T_R$.)

A 50-year wind does not occur once every 50 years. The probability of at least one exceedance is

$$1 - 0.98^{1} = 2\,\% \text{ in one year}, \qquad 1 - 0.98^{25} = 40\,\% \text{ in 25 years},$$
$$1 - 0.98^{50} = 64\,\% \text{ in 50 years}, \qquad 1 - 0.98^{100} = 87\,\% \text{ in 100 years}.$$

A structure with a 50-year design life designed for the 50-year wind has nearly a two-in-three chance of meeting it, and a fair chance of meeting it more than once. The return period is a statement of probability per year, not a schedule.

24.4.4 Extreme-value distributions

Extreme winds are modeled with distributions from extreme-value theory, which describe the maximum of many values rather than the values themselves. Three are in common use. The *generalized extreme value* (GEV) distribution describes the largest value in each block of time, usually the annual maximum; its cumulative form is $\exp\{-[1 + \xi\,(x - \mu_G)/\sigma_G]^{-1/\xi}\}$, with a location μ_G, a scale σ_G, both in m/s, and a dimensionless shape ξ that governs the tail. The *Gumbel* distribution is its special case $\xi = 0$, the limiting form for maxima of variables whose tails decay exponentially or faster, which includes the Weibull and the Gaussian. The *generalized Pareto* distribution describes not annual maxima but all the excesses over a high threshold (the peaks-over-threshold method), which uses more of the record. These differ fundamentally from fitting the ordinary distribution of wind speed: they are fitted to the extremes alone and say nothing about the typical hours, and a Weibull fitted to all hours says little about the extremes.

The Gumbel distribution of the annual maximum gust $U_{\max}$ is

$$\mathcal{F}_G(U_{\max}) = \exp\left\{-\exp\left[-\frac{U_{\max} - \mu_G}{\sigma_G}\right]\right\}. \tag{24.17}$$

The level exceeded with annual probability $P_a = 1/T_R$ follows by setting $\mathcal{F}_G = 1 - 1/T_R$ and taking the logarithm twice:

$$U_{T_R} = \mu_G + \sigma_G\, y_G, \qquad y_G = -\ln\left[-\ln\left(1 - \frac{1}{T_R}\right)\right], \tag{24.18}$$

where y_G is the *reduced variate*. For an illustrative site whose annual maximum three-second gusts have $\mu_G = 25\,\mathrm{m\,s^{-1}}$ and $\sigma_G = 3\,\mathrm{m\,s^{-1}}$, the 50-year return level has $y_G = -\ln(-\ln 0.98) = -\ln 0.02020 = 3.902$, so

$$U_{50} = 25 + 3 \times 3.902 = 36.7\,\mathrm{m\,s^{-1}},$$

and the 100-year level, with $y_G = 4.600$, is $38.8\,\mathrm{m\,s^{-1}}$. Doubling the return period adds only $2.1\,\mathrm{m\,s^{-1}}$, because the Gumbel tail is exponential. (Here U_{50} denotes the 50-year return level, as is customary; it is not a height.)

Equation (24.18) is a straight line in y_G, which gives the Gumbel plot of Figure 24.6. The horizontal axis is the reduced variate, with the corresponding return periods marked along the top; the vertical axis is the annual maximum gust. The dots are an illustrative record of 20 annual maxima, sorted and plotted at the reduced variate of the plotting position $\mathcal{F}_i = i/(N+1)$ for the ith smallest of $N = 20$. The solid line is the least-squares fit, $\mu_G = 25.0\,\mathrm{m\,s^{-1}}$ and $\sigma_G = 3.0\,\mathrm{m\,s^{-1}}$; the dashed line is a method-of-moments fit to the same twenty values, $\mu_G = 25.1\,\mathrm{m\,s^{-1}}$ and $\sigma_G = 2.54\,\mathrm{m\,s^{-1}}$. The shaded region lies beyond the largest plotting position of the record, $y_G = 3.02$, a return period of 21 years.

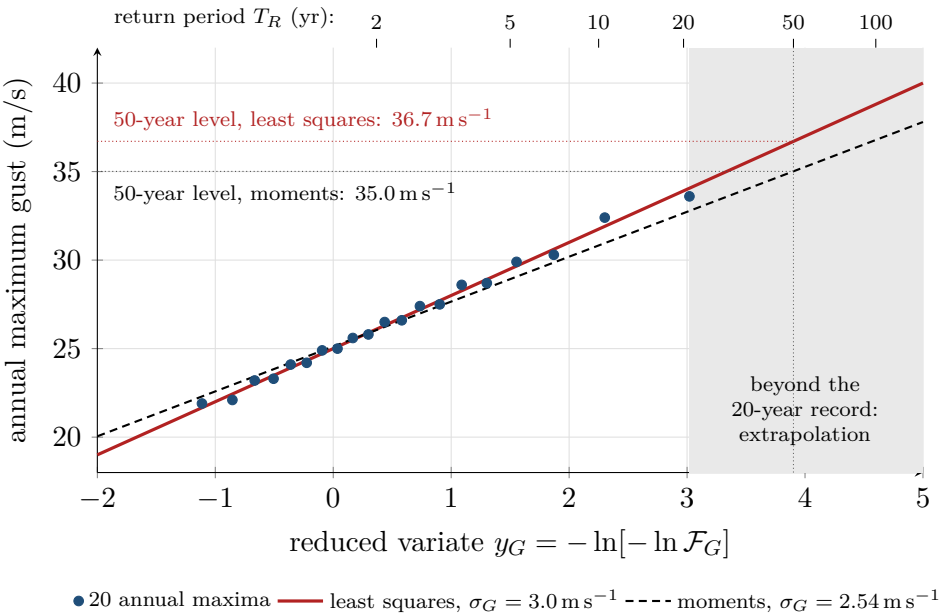


Figure 24.6: Gumbel plot of 20 illustrative annual maximum gusts. Line: $U_{\max} = \mu_G + \sigma_G\, y_G$ (equation (24.18)) fitted by least squares ($\mu_G = 25.0\,\mathrm{m\,s^{-1}}$, $\sigma_G = 3.0\,\mathrm{m\,s^{-1}}$, solid) and by the method of moments ($\mu_G = 25.1\,\mathrm{m\,s^{-1}}$, $\sigma_G = 2.54\,\mathrm{m\,s^{-1}}$, dashed). Shaded: return periods longer than the record.

24.4.5 Extrapolation beyond the record

The figure shows the central difficulty of extreme-value estimation. The two fits agree within the record, where the data constrain them, and diverge beyond it: at 50 years the least-squares line gives $36.7\,\mathrm{m\,s^{-1}}$ and the method of moments $35.0\,\mathrm{m\,s^{-1}}$, and neither is wrong in any sense the twenty points can decide. Since wind loads grow with the square of the speed, the difference is $(36.7/35.0)^2 = 1.10$, a 10 % difference in design load from the choice of fitting method alone. The sampling uncertainty of the fitted parameters adds more: a different twenty years at the same site would give a different slope.

Several cautions follow. A return level for a period much longer than the record is an extrapolation of the fitted form, and its uncertainty should be stated with it. A Weibull fitted to all hours should not be used to estimate rare extremes without justification: its tail is set by the moderate hours (Figure 24.5), and consecutive hours of one storm are not independent samples. A site whose extremes come from two mechanisms, such as the gusts of thunderstorm downdrafts and those of large-scale storms, has two populations of maxima, and one distribution fitted to both misrepresents the tail, as one Weibull misrepresented the two regimes of Figure 24.4. And the record itself must be homogeneous: a change of instrument, mounting or surroundings during the twenty years changes the maxima for reasons that have nothing to do with the climate (Chapter 23).

24.5 Structure in time

The statistics so far treat a record as a set of values whose order does not matter. The order does matter: the wind remembers its recent past, and how long it remembers sets the size of the eddies, the reliability of a mean and the way variance is spread over frequency. This section treats the autocorrelation, the integral time and length scales, the number of independent samples in a record and the sampling error of a mean, the power spectral density, and intermittent, non-Gaussian fluctuations.

24.5.1 Covariance, correlation and root-mean-square

For two fluctuating variables, such as the along-wind and vertical velocity fluctuations u' and w' of a turbulence record, the covariance $\overline{u'w'}$ carries both the magnitude of the fluctuations and their units, $\mathrm{m}^2/\mathrm{s}^2$, while the correlation coefficient

$$r_{uw} = \frac{\overline{u'w'}}{\sigma_u\,\sigma_w}, \qquad -1 \le r_{uw} \le 1, \tag{24.19}$$

is dimensionless and measures the strength of the association alone (Chapter 9, where a typical near-surface value of about -0.3 was derived). For a zero-mean fluctuation the *root-mean-square*, the term common in the turbulence literature, is the standard deviation:

$$u_{\mathrm{rms}} = \sqrt{\overline{u'^2}} = \sigma_u.$$

The rest of this section applies the same idea, a covariance normalized into a correlation, to one variable and itself at two times.

24.5.2 Autocorrelation and the integral time scale

The *autocovariance* of the along-wind fluctuation at a time lag Δt is

$$R_{uu}(\Delta t) = \overline{u'(t)\,u'(t+\Delta t)}, \qquad r_{uu}(\Delta t) = \frac{R_{uu}(\Delta t)}{\sigma_u^2}, \tag{24.20}$$

and r_{uu}, its normalized form, is the *autocorrelation*: the correlation of the signal with itself shifted by Δt. It equals one at zero lag, lies between -1 and 1, and is the same for positive and negative lags in a stationary record. It measures the memory of the wind: if r_{uu} remains high for several seconds, the turbulent structures passing the sensor persist over that time, and a value now predicts the value a few seconds later. It is computed from a high-frequency record, by averaging the product of the fluctuation with its own shifted copy.

The area under the autocorrelation defines the *integral time scale*,

$$\mathcal{T}_u = \int_0^\infty r_{uu}(\Delta t)\,\mathrm{d}\Delta t, \tag{24.21}$$

in seconds, the characteristic persistence time of the turbulence: the length of a rectangle of height one with the same area as the autocorrelation. A simple and often adequate model is the exponential, $r_{uu} = \exp(-\Delta t/\mathcal{T}_u)$, for which the integral is exactly $\mathcal{T}_u$ and the autocorrelation falls to $1/\mathrm{e} = 0.37$ at $\Delta t = \mathcal{T}_u$. In a measured record the autocorrelation does not decay cleanly: slow trends and mesoscale motions keep it from reaching zero, and the integral is usually taken to the first zero crossing. Near the ground, integral time scales of a few seconds to a few tens of seconds are usual.

Figure 24.7 draws the exponential autocorrelation for an illustrative $\mathcal{T}_u = 5\,\mathrm{s}$. The horizontal axis is the lag in seconds and the vertical axis the autocorrelation. The shaded area under the curve equals the area of the dashed red rectangle of height one and width $\mathcal{T}_u$; the dot marks the lag at which the correlation has fallen to 0.37. After about three integral time scales, 15 s, the correlation is below 0.05: values more than fifteen seconds apart are nearly independent.

24.5.3 The integral length scale and Taylor's hypothesis

A sensor at a fixed point measures in time, but eddies have sizes. *Taylor's frozen-turbulence hypothesis* links the two: if the turbulent structures are carried past the sensor by the mean

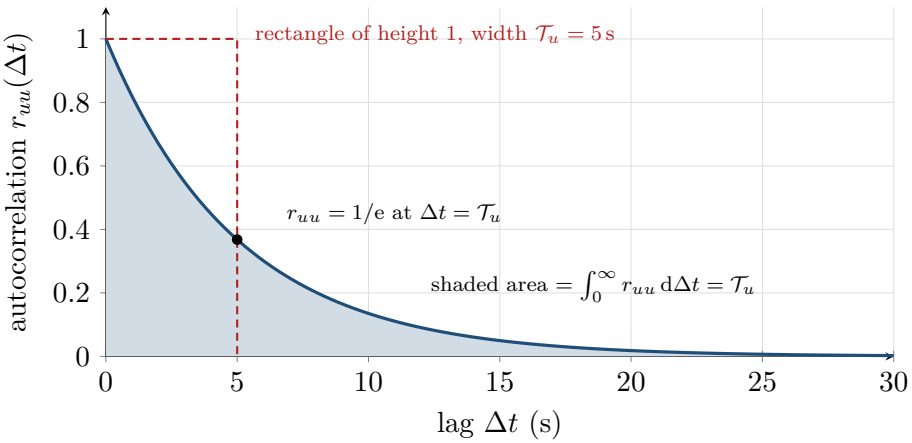


Figure 24.7: Exponential autocorrelation $r_{uu} = \exp(-\Delta t/\mathcal{T}_u)$ with $\mathcal{T}_u = 5\,\mathrm{s}$ (illustrative). The area under the curve equals the area of the rectangle of height one and width $\mathcal{T}_u$.

wind faster than they evolve, the record at a point is a spatial transect through a frozen pattern, and a time interval t corresponds to a distance

$$x \approx \overline{U}\, t.$$

Chapter 8 used the same idea to convert a wavenumber into a frequency. Applied to the integral time scale, it gives the *integral length scale*

$$\Lambda_u \approx \overline{U}\, \mathcal{T}_u, \tag{24.22}$$

in meters, an approximate size of the energy-containing eddies in the along-wind direction. For $\overline{U} = 10\,\mathrm{m\,s^{-1}}$ and $\mathcal{T}_u = 5\,\mathrm{s}$,

$$\Lambda_u \approx 10\,\mathrm{m\,s^{-1}} \times 5\,\mathrm{s} = 50\,\mathrm{m},$$

eddies comparable in size to a transmission tower or a turbine rotor.

The hypothesis works best when the mean advection is strong compared with the turbulent evolution, which in practice means a small turbulence intensity; a common working criterion is TI below about 0.5. It fails in light winds, where the eddies evolve as fast as they are carried (the night-time record of Section 24.1.3, with TI = 0.8, is an example), in free convection, where the thermals rise more than they drift, and in the recirculation behind an obstacle, where the mean wind itself reverses. In those cases a time scale measured at a point cannot be converted into a length.

24.5.4 Independent samples and the sampling error of a mean

Successive samples of a turbulent record are not independent, and the integral time scale says how many independent values a record contains. The mean of a record of length T_{avg} is $\overline{u}_T = T_{\mathrm{avg}}^{-1}\int_0^{T_{\mathrm{avg}}} u\,\mathrm{d}t$, and its variance about the true mean, for a stationary record, is the double integral of the autocovariance,

$$\sigma_{\overline{u}}^2 = \frac{1}{T_{\mathrm{avg}}^2}\int_0^{T_{\mathrm{avg}}}\!\!\int_0^{T_{\mathrm{avg}}} R_{uu}(t_2 - t_1)\,\mathrm{d}t_1\,\mathrm{d}t_2 = \frac{2}{T_{\mathrm{avg}}}\int_0^{T_{\mathrm{avg}}}\left(1 - \frac{\Delta t}{T_{\mathrm{avg}}}\right) R_{uu}(\Delta t)\,\mathrm{d}\Delta t,$$

where the second form groups the pairs of times by their separation Δt: on the square of side T_{avg}, the pairs with separation between Δt and $\Delta t + \mathrm{d}\Delta t$ occupy two strips of total area $2(T_{\mathrm{avg}} - \Delta t)\,\mathrm{d}\Delta t$. When the record is much longer than the integral time scale, the factor

in parentheses is close to one wherever R_{uu} is not negligible, and the integral is $\sigma_u^2 \mathcal{T}_u$ by equation (24.21). Hence

$$\sigma_{\overline{u}} = \sigma_u \sqrt{\frac{2\,\mathcal{T}_u}{T_{\mathrm{avg}}}} = \frac{\sigma_u}{\sqrt{N_{\mathrm{eff}}}}, \qquad N_{\mathrm{eff}} = \frac{T_{\mathrm{avg}}}{2\,\mathcal{T}_u}, \tag{24.23}$$

which has the form of the standard error of a mean of N_{eff} independent values: the record contains one independent sample per two integral time scales, however fast it was sampled.

For a ten-minute record with $\sigma_u = 2\,\mathrm{m\,s^{-1}}$ and $\mathcal{T}_u = 5\,\mathrm{s}$, $N_{\mathrm{eff}} = 600/10 = 60$ and

$$\sigma_{\overline{u}} = 2\,\mathrm{m\,s^{-1}} \times \sqrt{\frac{2 \times 5}{600}} = 2 \times 0.129 = 0.26\,\mathrm{m\,s^{-1}},$$

even though the record holds 12 000 samples at 20 Hz. A ten-minute mean of $10\,\mathrm{m\,s^{-1}}$ measured by a perfect instrument is therefore uncertain by about $0.26\,\mathrm{m\,s^{-1}}$, 2.6 %, simply because ten minutes contain only sixty independent samples of the turbulence. A one-minute mean contains six and is uncertain by about $0.8\,\mathrm{m\,s^{-1}}$. This sampling error sets a floor under any comparison of a model with a short-period mean: no model can be verified more precisely than the observation is defined.

The same calculation gives the standard deviation of a series of block means, the quantity of equation (24.6). For the exponential autocorrelation, the integral can be done exactly, and the variance of block means of length T_{avg}, divided by σ_u^2, is $2x\,[1 - x\,(1 - \mathrm{e}^{-1/x})]$ with $x = \mathcal{T}_u/T_{\mathrm{avg}}$. Table 24.2 evaluates it for $\sigma_u = 2\,\mathrm{m\,s^{-1}}$ and $\mathcal{T}_u = 5\,\mathrm{s}$. Its columns are the averaging period, the number of independent samples it contains, the ratio of the standard deviation of the block means to σ_u, and that standard deviation. Averaging over one second removes almost nothing, because one second is short compared with $\mathcal{T}_u$; averaging over ten minutes removes nearly all of the turbulent variance. In a real record the standard deviation of ten-minute means over a day is larger than the table's $0.26\,\mathrm{m\,s^{-1}}$, because the wind also varies on time scales of hours that a single integral time scale does not describe; the table describes only the turbulence.

Table 24.2: Standard deviation of block means of a stationary record with an exponential autocorrelation, $\sigma_u = 2\,\mathrm{m\,s^{-1}}$ and $\mathcal{T}_u = 5\,\mathrm{s}$ (illustrative). N_{eff} is $T_{\mathrm{avg}}/(2\mathcal{T}_u)$; the ratio is exact for the exponential model.

Averaging period	N_{eff}	Std. dev. of means/σ_u	Std. dev. of means (m/s)
1 s	0.1	0.97	1.94
10 s	1	0.75	1.51
1 min	6	0.39	0.78
10 min	60	0.13	0.26

24.5.5 Power spectral density

A record can also be analyzed in frequency rather than in time. The *power spectral density* $E_u(n)$, in $\mathrm{m^2\,s^{-2}}$ per hertz, distributes the variance over frequency n, in hertz (the letter f is the Coriolis parameter in this book): $E_u(n)\,\mathrm{d}n$ is the variance contributed by fluctuations with frequencies between n and $n + \mathrm{d}n$, and

$$\int_0^\infty E_u(n)\,\mathrm{d}n = \sigma_u^2. \tag{24.24}$$

The spectrum and the autocovariance are a Fourier-transform pair, so they contain the same information arranged differently; in particular the spectrum at zero frequency is $E_u(0) = 4\,\sigma_u^2\,\mathcal{T}_u$,

so a long integral time scale means a spectrum concentrated at low frequencies. It is computed from a high-frequency record by a fast Fourier transform, averaged over segments to reduce its scatter, and it is the frequency-domain form of the wavenumber spectrum of Chapter 8, related to it by Taylor's hypothesis.

A spectrum identifies features that no single statistic shows: the *large eddies*, as the low-frequency peak of the premultiplied spectrum $n\,E_u(n)$ used below, near $0.15/\mathcal{T}_u$ for the model form of Figure 24.8; the *inertial subrange*, where $E_u \propto n^{-5/3}$; *instrument noise*, as a flat floor at high frequency, which is white noise; and *periodic motions*, as narrow spikes, for example the shedding of vortices from a mast or waves in a stable layer. It also shows what an instrument or an averaging period removes: a cup anemometer cuts off the high frequencies, and a ten-minute mean keeps only the variance below about $1/600\,\mathrm{Hz}$.

Why spectra matter. Two records can have the same $\overline{U}$ and the same σ_U and yet different spectra. Figure 24.8 plots two such spectra in premultiplied form, $n\,E_u(n)$ against n on a logarithmic frequency axis, a form in which equal areas under the curves mean equal variances. Both records have $\overline{U} = 10\,\mathrm{m\,s^{-1}}$ and $\sigma_u = 2\,\mathrm{m\,s^{-1}}$, so both have $\mathrm{TI} = 0.2$ and the same area. Both use a standard model form of the along-wind spectrum, given in the caption. The blue record has $\mathcal{T}_u = 30\,\mathrm{s}$, an integral length scale of 300 m, and its variance is concentrated near 0.005 Hz: slow, large gusts lasting minutes. The red record has $\mathcal{T}_u = 1.5\,\mathrm{s}$, an integral length scale of 15 m, and its variance is near 0.1 Hz: rapid, small-scale turbulence. At high frequency both curves fall as $n^{-2/3}$, the premultiplied form of the $-5/3$ law. The engineering consequences differ. Large, slow gusts load a whole structure or a whole span of conductor at once and are coherent over hundreds of meters; small, fast eddies buffet a part of it and average out over a long span. A conductor, whose temperature responds over minutes, follows the slow variations of the first record and filters out those of the second. Variance alone does not characterize the turbulence.

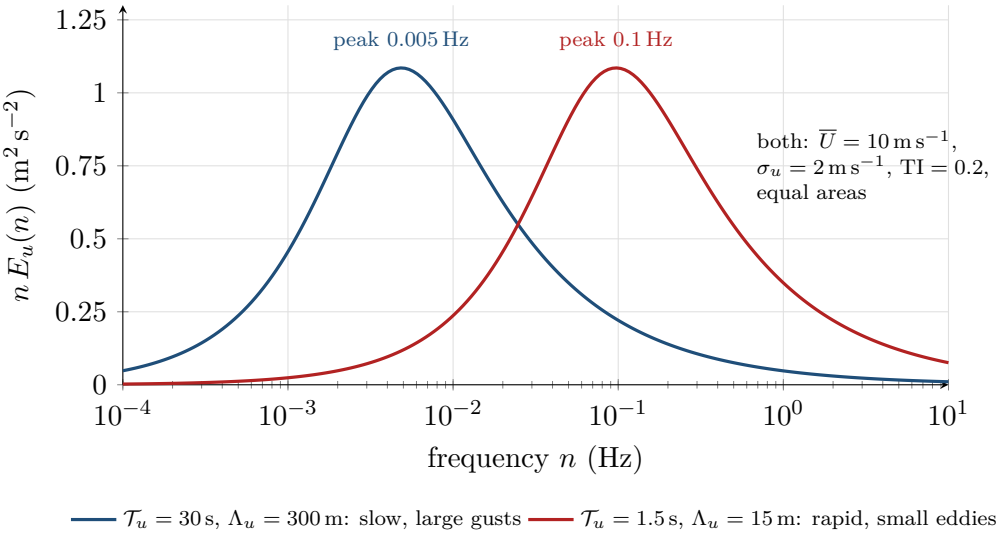


Figure 24.8: Premultiplied along-wind spectra of two records with the same mean and variance (illustrative), from the von Kármán form $nE_u(n)/\sigma_u^2 = 4\,n\mathcal{T}_u/[1 + 70.8\,(n\mathcal{T}_u)^2]^{5/6}$ with $\sigma_u = 2\,\mathrm{m\,s^{-1}}$ and $\mathcal{T}_u = 30$ and $1.5\,\mathrm{s}$ ($\Lambda_u = \overline{U}\mathcal{T}_u$ at $\overline{U} = 10\,\mathrm{m\,s^{-1}}$).

24.5.6 Intermittency and non-Gaussian fluctuations

Every statistic so far assumes that the record is stationary, that its statistics do not change within the averaging period. Wind statistics often are not. A stable night may alternate between

calm periods with almost no turbulence and bursts of turbulence lasting minutes, as the shear builds up and is released (Chapter 17). This is *intermittency*: the alternation between distinct turbulence states within one record. The overall variance of such a record may be moderate while the process is highly intermittent, and its mean and variance then describe a state that never occurs.

Intermittency shows in the higher moments. The *skewness* and the *kurtosis* of a fluctuation,

$$\mathrm{Sk}_u = \frac{\overline{u'^3}}{\sigma_u^3}, \qquad \mathrm{Ku}_u = \frac{\overline{u'^4}}{\sigma_u^4}, \tag{24.25}$$

both dimensionless, measure the asymmetry of the distribution and the weight of its tails; a Gaussian distribution has $\mathrm{Sk} = 0$ and $\mathrm{Ku} = 3$. Take an illustrative intermittent ten-minute record that is calm, with Gaussian fluctuations of standard deviation $0.1\,\mathrm{m\,s^{-1}}$, for 80 % of the time, and turbulent, with Gaussian fluctuations of $1.0\,\mathrm{m\,s^{-1}}$, for 20 %. Its variance is the weighted mean of the two, $0.8 \times 0.1^2 + 0.2 \times 1.0^2 = 0.208\,\mathrm{m^2\,s^{-2}}$, so $\sigma_u = 0.46\,\mathrm{m\,s^{-1}}$, an unremarkable value. Its fourth moment, with $\overline{u'^4} = 3\sigma^4$ for each Gaussian part, is $3\,(0.8 \times 0.1^4 + 0.2 \times 1.0^4) = 0.600\,\mathrm{m^4\,s^{-4}}$, and

$$\mathrm{Ku}_u = \frac{0.600}{0.208^2} = 13.9,$$

more than four times the Gaussian value. The tail is where the difference matters: the probability of a fluctuation larger than three standard deviations, $|u'| > 1.37\,\mathrm{m\,s^{-1}}$, is 0.27 % for a Gaussian of the same variance and 3.4 % for the intermittent record, all of it in the bursts, almost thirteen times more.

Velocity components in neutral, horizontally uniform turbulence are approximately Gaussian over the central range of their values. Gust extremes, canopy turbulence (Chapter 21), separated flow behind hills and buildings, and stable intermittency can be strongly non-Gaussian, and the vertical velocity in a convective boundary layer is positively skewed, with narrow strong updrafts and broad weak downdrafts (Chapter 16). For loads, gust statistics and exceedances, the tail behavior matters, and a Gaussian estimate based on the standard deviation alone can understate it by an order of magnitude.

24.6 Verification of modeled wind

A modeled wind is judged by comparing it with observations, and the comparison is itself a set of statistics with the same need to match the question. This section defines the bias, the mean absolute error and the root-mean-square error, decomposes the mean square error, shows why correlation is not accuracy, treats direction and vector errors, and closes with a table of statistics by purpose.

24.6.1 Bias, mean absolute error and root-mean-square error

For N pairs of modeled and observed speeds, $U_{\mathrm{m},i}$ and $U_{\mathrm{o},i}$, with errors $e_i = U_{\mathrm{m},i} - U_{\mathrm{o},i}$, the three common metrics, all in m/s, are

$$\mathrm{Bias} = \frac{1}{N}\sum_{i=1}^{N} e_i, \qquad \mathrm{MAE} = \frac{1}{N}\sum_{i=1}^{N} |e_i|, \qquad \mathrm{RMSE} = \sqrt{\frac{1}{N}\sum_{i=1}^{N} e_i^2}. \tag{24.26}$$

They describe different properties of the error. The *bias* is the systematic part: positive when the model is too fast on average, with positive and negative errors cancelling. The *mean absolute error* is the typical size of an error regardless of sign. The *root-mean-square error* squares before averaging, so it weights large errors more and is the metric most sensitive to occasional large misses. They are always ordered, $|\mathrm{Bias}| \le \mathrm{MAE} \le \mathrm{RMSE}$, the first because the absolute value

of a sum is at most the sum of absolute values and the second because a mean square is at least the square of the mean.

For five illustrative hourly errors $e = (+2, -1, +3, 0, +1)\,\mathrm{m\,s^{-1}}$: Bias $= 5/5 = 1.0\,\mathrm{m\,s^{-1}}$; MAE $= 7/5 = 1.4\,\mathrm{m\,s^{-1}}$; and the mean square error is $(4 + 1 + 9 + 0 + 1)/5 = 3.0\,\mathrm{m^2\,s^{-2}}$, so RMSE $= \sqrt{3.0} = 1.73\,\mathrm{m\,s^{-1}}$.

24.6.2 Decomposition of the mean square error

Writing each error as its mean plus a departure, $e_i = \mathrm{Bias} + (e_i - \mathrm{Bias})$, squaring and averaging, the cross term vanishes because the departures average to zero, and

$$\mathrm{RMSE}^2 = \mathrm{Bias}^2 + \sigma_e^2, \tag{24.27}$$

where σ_e^2 is the variance of the errors about their mean, the random part. In the example, $3.0 = 1.0^2 + 2.0$: one third of the mean square error is systematic and two thirds random. The distinction matters because a bias can be removed by a simple correction (Chapter 28) and a random error cannot. The error variance decomposes further. Since $e = U_\mathrm{m} - U_\mathrm{o}$, its variance is that of a difference,

$$\sigma_e^2 = \sigma_\mathrm{m}^2 + \sigma_\mathrm{o}^2 - 2\,r\,\sigma_\mathrm{m}\sigma_\mathrm{o}, \tag{24.28}$$

with σ_m and σ_o the standard deviations of the modeled and observed series and r their correlation. The random error is small only if the model has both the right timing (r near one) and the right amplitude (σ_m near σ_o).

The amplitude that minimizes the error. Differentiating equation (24.28) with respect to σ_m and setting the result to zero gives $\sigma_\mathrm{m} = r\,\sigma_\mathrm{o}$. When the timing is uncertain, $r < 1$, the forecast that minimizes the root-mean-square error has less variability than the observations. A model or a statistical correction tuned to minimize RMSE therefore produces a wind that is too smooth: it underestimates both the calm hours and the strong ones, and with them the exceedance probabilities of Section 24.4.1. A low RMSE and a correct distribution are different goals.

24.6.3 Correlation is not accuracy

A model may have a high correlation with the observations and a large bias, and a low bias with a poor correlation. Figure 24.9 shows three forecasts of an illustrative day. The horizontal axis is the hour and the vertical axis the wind speed. The observed wind (black) follows a daily cycle, $U_\mathrm{o} = 6 + 3\sin[2\pi(t - 9\,\mathrm{h})/24\,\mathrm{h}]$ m/s, peaking at 15 h. Forecast A (red) tracks every rise and fall perfectly but is always $3\,\mathrm{m\,s^{-1}}$ too fast. Forecast B (blue, dashed) has the right mean and amplitude but peaks six hours late. Forecast C (gray, dotted) is the constant daily mean, $6\,\mathrm{m\,s^{-1}}$.

The metrics, over the 24 hourly values, separate the three. Forecast A has $r = 1$, a perfect correlation, and Bias = MAE = RMSE $= 3.0\,\mathrm{m\,s^{-1}}$: its error is entirely systematic, and equation (24.27) gives $9 = 3^2 + 0$. Forecast B has Bias $= 0$ and $r = \cos 90^\circ = 0$; with $\sigma_\mathrm{m} = \sigma_\mathrm{o} = 3/\sqrt{2} = 2.12\,\mathrm{m\,s^{-1}}$, equation (24.28) gives $\sigma_e^2 = 4.5 + 4.5 - 0 = 9$, so RMSE $= 3.0\,\mathrm{m\,s^{-1}}$ as well, and MAE $= 2.7\,\mathrm{m\,s^{-1}}$: its error is entirely random. The two forecasts have the same RMSE for opposite reasons, and correlation alone would rank A perfect and B useless. Forecast C has an undefined correlation, since it has no variance, and the lowest RMSE, $3/\sqrt{2} = 2.1\,\mathrm{m\,s^{-1}}$, because it never commits to a timing; it is penalized once for missing the cycle, while B is penalized twice, once for the peak it forecasts at the wrong time and once for the peak it misses. Model evaluation therefore needs several metrics, at least the bias, a random-error measure and the correlation, and for some purposes a comparison of distributions.

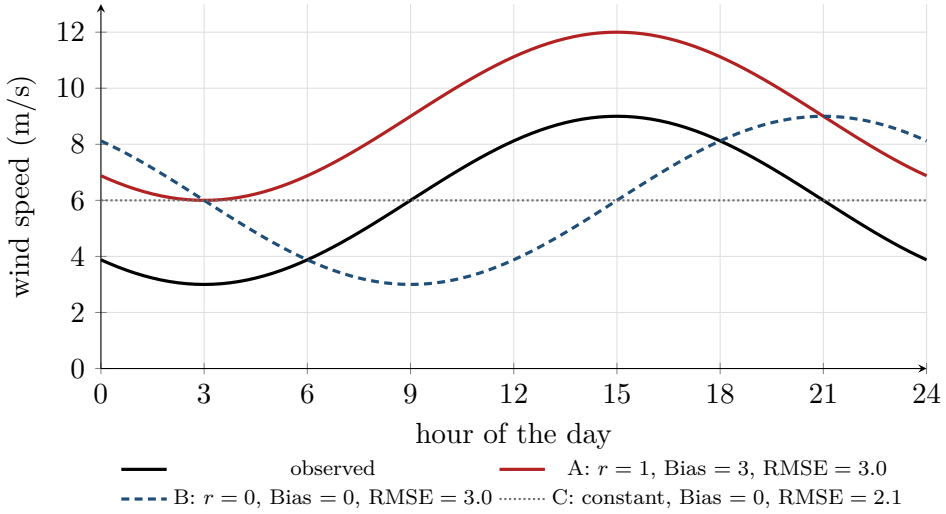


Figure 24.9: Three forecasts of an illustrative daily cycle of wind speed, $U_\mathrm{o} = 6{+}3\sin[2\pi(t{-}9)/24]$ m/s with t in hours. A: $U_\mathrm{o} + 3$; B: the same cycle six hours late; C: the constant $6\,\mathrm{m\,s^{-1}}$. Metrics over the 24 hourly values, in m/s.

24.6.4 Errors of wind direction

A forecast direction of 359° against an observed 1° is an error of 2°, not 358°, and a direction error must be computed as a circular difference,

$$\Delta\beta = \left[(\beta_\mathrm{m} - \beta_\mathrm{o} + 180^\circ) \bmod 360^\circ\right] - 180^\circ, \tag{24.29}$$

which lies between −180° and +180°. For the example, $[(358{+}180) \bmod 360]{-}180 = 178{-}180 = -2^\circ$: the forecast is 2° counterclockwise of the observation. Taking plain differences is a common data-processing mistake, and its effect is large: for directions scattered about north, many of the plain differences are near ±360°, and a mean absolute direction error of 20° can be reported as two hundred. Two further rules apply. Direction is undefined in a calm and erratic in a light wind, so direction errors are computed only for hours above a stated speed, often 1 to $2\,\mathrm{m\,s^{-1}}$. And the relevant error depends on the use: for a transmission conductor, whose cooling depends on the angle between wind and conductor but not on the sense of the wind, a direction error is taken modulo 180°, as Chapter 19 noted.

24.6.5 Vector wind error

A clean alternative to separate speed and direction metrics is to compare the components directly, through RMSE_u and RMSE_v computed by equation (24.26) with u and v in place of U. Their quadrature sum is the root-mean-square *vector error*,

$$\mathrm{RMSE}_\mathbf{V} = \sqrt{\frac{1}{N}\sum_{i=1}^{N} \left|\mathbf{V}_{\mathrm{m},i} - \mathbf{V}_{\mathrm{o},i}\right|^2} = \sqrt{\mathrm{RMSE}_u^2 + \mathrm{RMSE}_v^2}, \tag{24.30}$$

the root-mean-square length of the difference vector. It needs no circular arithmetic, it is defined in calm hours, and it weights a direction error by the speed at which it occurs, which is the weight that matters for transport. For one pair, the magnitude of the difference follows from the law of cosines of Chapter 19, $|\mathbf{V}_\mathrm{m} - \mathbf{V}_\mathrm{o}|^2 = U_\mathrm{m}^2 + U_\mathrm{o}^2 - 2U_\mathrm{m}U_\mathrm{o}\cos\Delta\beta$. A forecast of $8\,\mathrm{m\,s^{-1}}$ from 270° against an observation of $8\,\mathrm{m\,s^{-1}}$ from 300° has zero speed error and a direction error of −30°, and a vector error of $2 \times 8 \times \sin 15^\circ = 4.1\,\mathrm{m\,s^{-1}}$, half the wind speed. The price of the vector metric is that it mixes speed and direction errors, so a large value must still be traced to its source by the speed and direction metrics.

24.6.6 A hierarchy of statistics by purpose

The chapter's statistics can be arranged by the question each answers. Table 24.3 lists five purposes; for each, its columns give the statistics that matter, the reason, and the subsections that define them. For energy resources and conductor cooling the mean, the mean of the relevant power of the speed and the exceedance probabilities on both sides matter. For structural loading the gusts and the extreme return levels matter. For turbulence the standard deviation, the turbulence intensity, the spectrum and the integral scales matter. For the mechanism of the flow the direction, the wind roses and the conditional statistics matter. For model verification the bias, the random error, the correlation and the direction and vector errors matter. The statistic should follow the physical question.

Table 24.3: Statistics of wind by purpose.

Purpose	Statistics	Why	Defined in
Resource and cooling	$\overline{U}$, $\overline{U^3}$ or $\overline{U^{0.6}}$, $\Pr(U < U_{\text{th}})$, $\Pr(U > U_{\text{th}})$, low quantiles	energy goes as U^3; ratings are limited by the hours of weak wind	24.3.4, 24.4.1, 24.4.2
Structural loading	U_{gust}, G, return levels from an extreme-value fit	loads are set by rare maxima, not by the bulk	24.1.4, 24.4.4
Turbulence	σ_U, TI, spectra, $\mathcal{T}_u$, Λ_u, kurtosis	fatigue and buffeting depend on amplitude, scale and tails	24.1.3, 24.5.2, 24.5.5
Flow mechanism	β, circular mean and spread, wind roses, conditional and directional statistics	regimes and their causes are separated only by conditioning	24.2.1, 24.2.2, 24.2.3
Model verification	Bias, MAE, RMSE, r, circular direction error, vector error	systematic and random errors, timing and direction need separate measures	24.6.1 to 24.6.5

The modeled winds verified with these statistics come from numerical weather prediction, whose structure, variables and meaning of a "10 m wind" are the subject of Chapter 25.

24.7 What to retain

Definition 24.1 (Wind statistics)**.** There is no single statistic called the wind: mean speed, vector mean, gust, variance, turbulence intensity, frequency of directions, exceedance probability and return level are different statistics of one directional, nonstationary and multiscale flow, each answering a different question, and a sound analysis chooses the statistic from the physical question and usually needs more than one.

Table 24.4 lists the terms of the chapter, their meaning, their units and the subsection that defines each.

24.8 Exercises

Exercise 24.1. A station on an east-facing coast at 23°S records, on a day of weak synoptic forcing, 12 hours of wind at $6\,\mathrm{m\,s^{-1}}$ from 70° (the sea breeze) and 12 hours at $3\,\mathrm{m\,s^{-1}}$ from 250° (the land breeze). (a) Compute the scalar mean speed, the eastward and northward components of each wind, the vector mean wind (speed and direction) and the steadiness. (b) Compute the unit-vector mean direction and the mean resultant length of the 24 directions, and explain why the unit-vector mean is undefined while the vector mean is not. (c) At a station on an east-facing coast at 23°N with otherwise the same circulation, would the sea-breeze direction be

Table 24.4: The terms of the chapter and where each is defined.

Term	Meaning	Units	Defined in
Scalar mean speed	average of the speeds, $\overline{U} = N^{-1}\sum U_i$	m/s	24.1.1
Vector mean wind	average of the wind vectors; speed $U_{\mathrm{vec}} = (\overline{u}^2 + \overline{v}^2)^{1/2} \le \overline{U}$	m/s	24.1.1
Variance, standard deviation	mean squared departure from the mean, σ_U^2; its root σ_U	$\mathrm{m}^2/\mathrm{s}^2$, m/s	24.1.2
Turbulence intensity	$\mathrm{TI} = \sigma_U/\overline{U}$; inflated and unstable at low speed	–	24.1.3
Gust factor	$G = U_{\mathrm{gust}}/\overline{U} = 1 + g_{\mathrm{pk}}\mathrm{TI}$	–	24.1.4
Circular mean, circular standard deviation	direction of the averaged unit vector; $s_\beta = (-2\ln \overline{R}_\beta)^{1/2}$	degree	24.2.1
Wind rose	frequency of directions by sector, often by speed class	–	24.2.2
Conditional statistic	statistic of the samples that satisfy a condition (time, stability, sector, season)	as statistic	24.2.3
Weibull distribution	$\mathcal{F} = 1 - \exp[-(U/c)^k]$; scale c, shape k	m/s, –	24.3.2
Rayleigh distribution	Weibull with $k = 2$, $c = \sqrt{2}\,\sigma$	–	24.3.3
Exceedance probability	$\Pr(U > U_{\mathrm{th}}) = \exp[-(U_{\mathrm{th}}/c)^k]$	–	24.4.1
Quantile	speed U_p with $\mathcal{F}(U_p) = p$	m/s	24.4.2
Return period	$T_R = 1/P_a$, mean interval between exceedances	yr	24.4.3
Gumbel distribution	extreme-value distribution of annual maxima; $U_{T_R} = \mu_G + \sigma_G y_G$	m/s	24.4.4
Autocorrelation	$r_{uu}(\Delta t) = \overline{u'(t)u'(t+\Delta t)}/\sigma_u^2$	–	24.5.2
Integral time scale	$\mathcal{T}_u = \int_0^\infty r_{uu}\,\mathrm{d}\Delta t$, persistence of turbulence	s	24.5.2
Integral length scale	$\Lambda_u \approx \overline{U}\mathcal{T}_u$ by Taylor's hypothesis	m	24.5.3
Sampling error of a mean	$\sigma_u(2\mathcal{T}_u/T_{\mathrm{avg}})^{1/2}$; one independent sample per $2\mathcal{T}_u$	m/s	24.5.4
Power spectral density	$E_u(n)$, variance per unit frequency; integral σ_u^2	$\mathrm{m}^2\,\mathrm{s}^{-2}/\mathrm{Hz}$	24.5.5
Intermittency	alternation between distinct turbulence states in one record	–	24.5.6
Skewness, kurtosis	third and fourth normalized moments; 0 and 3 for a Gaussian	–	24.5.6
Bias, MAE, RMSE	mean, mean absolute and root-mean-square error; $\mathrm{RMSE}^2 = \mathrm{Bias}^2 + \sigma_e^2$	m/s	24.6.1, 24.6.2
Vector error	root-mean-square length of $\mathbf{V}_{\mathrm{m}} - \mathbf{V}_{\mathrm{o}}$	m/s	24.6.5

expected to lean north or south of east? (d) A transmission line at the station runs north–south. Compute the angle between each wind and the line, and state whether the 180° difference between the two winds matters for the cooling of the conductor.

Exercise 24.2. A site has hourly mean speeds that follow a Weibull distribution with $c = 7\,\mathrm{m\,s^{-1}}$ and $k = 2.2$. Use $\Gamma(1.455) = 0.8856$ and $\Gamma(2.364) = 1.2134$. (a) Compute the mean, the median and the mean of the cube of the speed, and the ratio of the mean of the cube to the cube of the mean. (b) Compute the fraction of hours above $12\,\mathrm{m\,s^{-1}}$ and below $1\,\mathrm{m\,s^{-1}}$, and the quantile $U_{0.90}$. (c) A second site has the same mean speed but $k = 1.6$ (so $c = 6.91\,\mathrm{m\,s^{-1}}$, with $\Gamma(1.625) = 0.8966$ and $\Gamma(2.875) = 1.7877$). Compute its mean of the cube and its fraction of hours below $1\,\mathrm{m\,s^{-1}}$, and state which site has more wind energy and which has more poorly cooled hours. (d) Equation (24.14) at the first site gives $\Pr(U > 25\,\mathrm{m\,s^{-1}}) = 7 \times 10^{-8}$. Explain why this number should not be used to estimate the 50-year wind.

Exercise 24.3. A sonic anemometer at 20 m records, over ten minutes, $\overline{U} = 8\,\mathrm{m\,s^{-1}}$ and $\sigma_u = 1.6\,\mathrm{m\,s^{-1}}$, and the autocorrelation of u' falls exponentially to 1/e at a lag of 4 s. (a) Compute TI, the integral time scale and the integral length scale, and state whether Taylor's hypothesis is reasonable. (b) Compute the number of independent samples and the sampling error of the ten-minute mean and of a one-minute mean. (c) The annual maximum three-second gusts at the same site over 25 years fit a Gumbel distribution with $\mu_G = 22\,\mathrm{m\,s^{-1}}$ and $\sigma_G = 2.8\,\mathrm{m\,s^{-1}}$. Compute the 50- and 100-year return levels and the probability that the 50-year level is exceeded at least once in a 30-year service life. (d) Which of the two return levels is the more uncertain, and why?

Exercise 24.4. A model is compared with an anemometer at a station at 30°S for five hours of winds from the northwest to the northeast:

Hour	1	2	3	4	5
Model speed (m/s), direction	7, 350°	6, 10°	5, 40°	8, 330°	4, 5°
Observed speed (m/s), direction	6, 20°	5, 345°	6, 30°	6, 300°	3, 355°

(a) Compute the bias, MAE and RMSE of the speed, and split the mean square error into its systematic and random parts. (b) Compute the direction errors with equation (24.29) and their mean absolute value, and compare it with the mean absolute value of the plain differences. (c) Compute the vector error of hour 4 and the root-mean-square vector error over the five hours, using $u = -U\sin\beta$ and $v = -U\cos\beta$. (d) The correlation of the modeled and observed speeds is 0.73. State what the results of (a) to (c) show that the correlation does not.

Chapter 25

Numerical Weather Prediction for Near-Surface Wind

25.1 What a weather model solves

Most near-surface wind forecasts, and most of the wind data used to assess sites without long measurements, come from numerical weather prediction models. Earlier chapters met these models several times: Chapter 5 separated resolved from parameterized processes and introduced effective resolution and the gray zone, Chapter 12 and Chapter 14 showed how a model diagnoses its 10 m wind from its lowest level, and Chapter 20 showed how a model smooths the terrain it cannot resolve. This chapter treats the weather model as a whole system. Its question is

how does a numerical weather prediction model actually produce a near-surface wind forecast?

The answer is a chain of steps, and each step can introduce its own error. The chapter first states what the model solves and which of its variables are forecast and which are computed from others; it then describes the grid on which the model works, the representation of the surface and of the boundary layer, the way a forecast is started and bounded, the interactions and limits that shape the near-surface wind, and finally how a model's wind is read and its error traced to a stage of the chain.

Jargon: NWP, model level, lowest model level, AGL, ASL, scheme, prognostic variable, diagnostic variable

Numerical weather prediction (NWP) is the forecasting of the atmosphere by integrating the equations of motion, thermodynamics and moisture forward in time on a three-dimensional grid, from an estimate of the present state. A *model level* is one of the discrete surfaces in the vertical on which the model stores its variables; the *lowest model level*, at height z_1 in meters, is the lowest of them above the ground. Heights are given *above ground level* (AGL), measured from the local surface, or *above sea level* (ASL). A *scheme*, or parameterization scheme, is the part of a model that computes the average effect of one class of unresolved processes, such as boundary-layer turbulence or radiation, from the resolved variables. A *prognostic variable* is a quantity whose evolution the model integrates explicitly forward in time from its own equation. A *diagnostic variable* is a quantity the model computes at each time from other model variables, without an equation of its own for its rate of change.

Key idea

A weather model does not forecast the 10 m wind directly. It solves the atmospheric state on a three-dimensional grid, and then infers the wind near the ground from that state through its boundary-layer and surface-layer physics. A wrong 10 m wind is therefore a question of which stage of that chain went wrong, not only of how large the error is.

25.1.1 The governing equations

A weather model advances in time a small set of conservation laws: momentum, energy (in the form of temperature or potential temperature), moisture, and mass (in the form of pressure, density or the mass of an air column), and, in some models, turbulence variables. The horizontal momentum equations, written schematically for the grid-cell averaged wind, are

$$\frac{\mathrm{D}u}{\mathrm{D}t} = -\frac{1}{\rho}\frac{\partial p}{\partial x} + f\,v + F_u, \tag{25.1}$$

$$\frac{\mathrm{D}v}{\mathrm{D}t} = -\frac{1}{\rho}\frac{\partial p}{\partial y} - f\,u + F_v, \tag{25.2}$$

where the rate of change following the air,

$$\frac{\mathrm{D}}{\mathrm{D}t} = \frac{\partial}{\partial t} + u\,\frac{\partial}{\partial x} + v\,\frac{\partial}{\partial y} + w\,\frac{\partial}{\partial z}, \tag{25.3}$$

contains the advection of momentum by the wind itself. Each term has a name and a physical role. The term $-(1/\rho)\,\partial p/\partial x$ is the pressure-gradient force per unit mass of Chapter 2, the forcing that drives all wind. The terms fv and $-fu$ are the Coriolis force of Chapter 3; they apply in both hemispheres with the sign of $f = 2\Omega\sin\phi$, positive in the Northern Hemisphere and negative in the Southern, so the same equations turn the wind to the right of its motion in the north and to the left in the south. The advection terms in equation (25.3) carry momentum from one place to another. The terms F_u and F_v collect everything the grid does not resolve: chiefly the vertical divergence of the turbulent momentum flux, $F_u \approx -\partial\overline{u'w'}/\partial z$ and $F_v \approx -\partial\overline{v'w'}/\partial z$ (Chapter 8), together with horizontal subgrid mixing and the drag of unresolved terrain. Setting the time derivative, the advection and F to zero recovers the geostrophic balance of Chapter 3, $fv = (1/\rho)\,\partial p/\partial x$.

The rest of the system is named here without derivation. A vertical momentum equation either reduces to hydrostatic balance, $\partial p/\partial z = -\rho g$, in models whose grid is too coarse to resolve vertical accelerations, or keeps the full vertical acceleration in nonhydrostatic models, which are needed at grid spacings of a few kilometers and below. The continuity equation conserves mass. The thermodynamic equation advances the potential temperature θ with sources from radiation, from the latent heat of condensation and evaporation, and from the divergence of the turbulent heat flux. A moisture equation advances the specific humidity q, and further equations advance cloud water, rain, ice and snow. The equation of state, $p = \rho\,R_d\,T_v$, closes the system. The model is therefore solving

$$\text{pressure forcing} + \text{rotation} + \text{advection} + \text{turbulent transport}$$

over time, and the near-surface wind is one consequence of how those four terms balance in the lowest part of the grid.

25.1.2 Prognostic and diagnostic variables

The distinction between prognostic and diagnostic variables decides how a number in a model's output was obtained. The wind components u and v, the potential temperature and the specific

humidity at the model levels are prognostic: each has its own equation, and the model adds the rate of change times the time step to the old value at every step. A diagnostic variable is evaluated from the prognostic ones whenever it is needed. Near-surface variables such as the 10 m wind U_{10} and the 2 m temperature are often partly diagnostic: the model computes them from the lowest-level values and the surface state, as Section 25.2.2 describes. Table 25.1 lists common examples. Its columns give the variable, whether it is usually prognostic or diagnostic, and how it is obtained; the assignment differs between models, and the table describes a typical one.

Table 25.1: Prognostic and diagnostic variables in a typical regional weather model. The assignment differs between models.

Variable	Kind	How it is obtained
u, v at model levels	prognostic	momentum equations (25.1) and (25.2)
w	prognostic or diagnostic	its own equation in nonhydrostatic models; from continuity in hydrostatic ones
θ, q, cloud water and ice	prognostic	thermodynamic, moisture and microphysics equations
Surface pressure or column mass	prognostic	mass continuity
Turbulent kinetic energy e	prognostic in some schemes	its budget equation, in turbulent-kinetic-energy closures
Soil temperature and soil moisture	prognostic	equations of the land-surface model
U_{10}, 2 m temperature and humidity	diagnostic	surface-layer similarity from the lowest model level and the surface state
u_*, L_{O}, surface fluxes H and LE	diagnostic	surface-layer scheme, every time step
Boundary-layer depth z_i	diagnostic	a criterion on the profiles, such as a bulk Richardson number
K_m, K_h	diagnostic	boundary-layer scheme, from shear, stability and a length scale
Gusts	diagnostic	empirical formulas from the mean wind, turbulence and stability

The distinction matters for interpretation. A prognostic variable carries the memory of the model's whole integration, of its initial state, its forcing and every scheme that touched it. A diagnostic variable adds the assumptions of the formula that produced it on top of that memory. Two models with the same wind at 60 m can report different 10 m winds because their diagnostic formulas differ, and neither difference is visible in the 10 m field alone.

25.1.3 The model as a set of components

A weather model is not one equation solver but a set of components that exchange information at every time step. Figure 25.1 draws them. The central box is the dynamical core, which integrates the resolved equations of Section 25.1.1: advection, pressure gradients, the Coriolis force. The boxes in the row below it are the physics schemes, each computing the tendency (the rate of change) that one class of unresolved processes adds to the resolved variables. The box at the bottom is the land-surface model. The two boxes at the top supply the information that starts and bounds the forecast, and the box at the right is the diagnosed near-surface output. Arrows show which component passes information to which.

At each time step the core advances the resolved variables, the schemes compute their tendencies from the new state, and the sum of all tendencies updates the state for the next step. Two features of the figure shape everything that follows. First, the near-surface wind is produced at the end of the chain on the right: it depends on the core, which delivers the

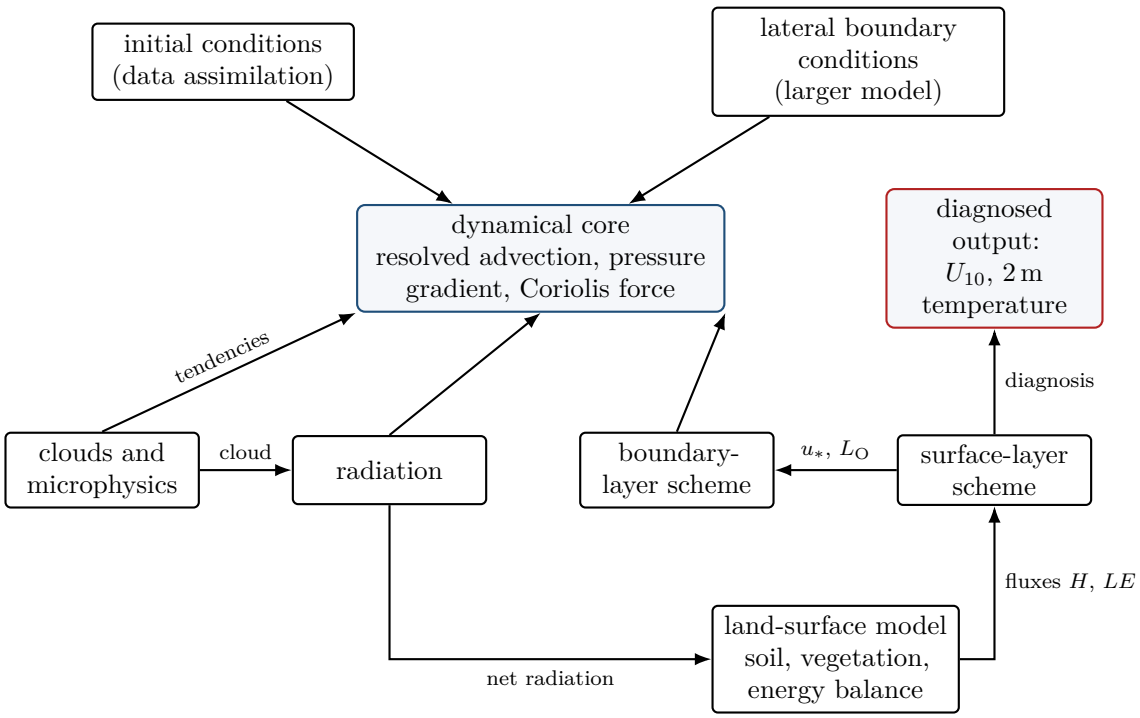


Figure 25.1: A weather model as a set of interacting components (schematic). The dynamical core advances the resolved state; the physics schemes return tendencies of the resolved variables; the land-surface model closes the surface energy balance; the surface-layer scheme supplies the surface fluxes to the boundary-layer scheme and diagnoses the near-surface output. The state passes back from the core to every scheme at every time step (arrows omitted).

wind aloft, on the boundary-layer scheme, which carries momentum down, on the surface-layer scheme, which diagnoses the 10 m value, and through the surface fluxes on the land-surface model, the radiation and the clouds. Second, the schemes are connected to each other, so an error in one, such as a misplaced cloud, reaches the wind through several others (Section 25.5.1).

25.2 The model grid

The atmosphere is continuous; the model represents it on a finite set of points. This section describes the vertical levels and their heights, the way the lowest level is connected to the ground, the horizontal grid spacing and what it resolves, the terrain-following coordinates most regional models use and their errors, the relative importance of vertical and horizontal resolution, and, from all of these, what the 10 m wind of a model is.

25.2.1 Discrete vertical levels

The model stores its variables on discrete vertical levels $z_1, z_2, z_3, \ldots$, closely spaced near the ground and progressively wider apart above. The height of the lowest level differs from model to model and from configuration to configuration. Illustrative values are: about 10 m AGL or lower in a configuration built for boundary-layer studies; 20 to 50 m AGL in many regional and global models; and 100 m or more in older or coarser configurations. Above the lowest level the spacing typically grows from a few tens of meters near the ground to several hundred meters in the middle troposphere and more than a kilometer near the model top, which lies at tens of kilometers.

Engineering applications usually ask for the wind at 10 m, the standard height of surface

anemometers, or at heights between 10 and 150 m, for conductors, hub heights and masts. Except by coincidence, neither height is a model level. Where the lowest level lies above 10 m, the model must connect the lowest-level wind to 10 m by a relation for the layer below it; where a requested height lies between two levels, the model or the user interpolates between them, and the interpolation itself assumes a profile shape.

25.2.2 From the lowest level to the ground

The relation that connects the lowest level to the ground is the surface-layer similarity theory of Chapter 12 and Chapter 14. Within the surface layer the wind profile is

$$U(z) = \frac{u_*}{\kappa}\left[\ln\!\left(\frac{z-d}{z_0}\right) - \psi_m\!\left(\frac{z-d}{L_{\mathrm{O}}}\right)\right], \tag{25.4}$$

with the friction velocity u_*, the roughness length z_0, the displacement height d (zero in most models) and the stability correction ψ_m of the Obukhov length L_{O}. The model knows the wind at its lowest level, the roughness length it has assigned to the cell, and the surface heat flux and temperature from its land-surface model; from these its surface-layer scheme solves equation (25.4) together with its temperature counterpart for u_* and L_{O}, iteratively because L_{O} depends on u_* (Chapter 14). Evaluating the same profile at 10 m with $d = 0$ and dividing by its value at z_1 gives the diagnosed wind

$$U_{10} = U_1 \,\frac{\ln(10\,\mathrm{m}/z_0) - \psi_m(10\,\mathrm{m}/L_{\mathrm{O}})}{\ln(z_1/z_0) - \psi_m(z_1/L_{\mathrm{O}})}, \tag{25.5}$$

where U_1 is the wind speed at the lowest level. The 10 m wind is therefore often parameterization-dependent: it is the lowest-level wind carried down by an assumed profile, with an assumed roughness and a modeled stability, rather than a resolved state variable. In models whose lowest level lies below 10 m, the value at 10 m is interpolated between levels; the levels themselves are then shaped by the same surface-layer and boundary-layer schemes, so the dependence remains.

The consequence is that a correct wind aloft does not guarantee a correct 10 m wind. Chapter 14 worked the case of a lowest level at $z_1 = 30\,\mathrm{m}$ with $U_1 = 6\,\mathrm{m\,s^{-1}}$ and $z_0 = 0.05\,\mathrm{m}$: the diagnosed 10 m wind is $4.97\,\mathrm{m\,s^{-1}}$ in neutral air and $4.41\,\mathrm{m\,s^{-1}}$ with $L_{\mathrm{O}} = +100\,\mathrm{m}$. If the real roughness upwind of a station is $z_0 = 0.5\,\mathrm{m}$, the same lowest-level wind gives

$$U_{10} = 6\,\mathrm{m\,s^{-1}} \times \frac{\ln(10/0.5)}{\ln(30/0.5)} = 6\,\mathrm{m\,s^{-1}} \times \frac{2.996}{4.094} = 4.39\,\mathrm{m\,s^{-1}}$$

in neutral air and $3.75\,\mathrm{m\,s^{-1}}$ with $L_{\mathrm{O}} = +100\,\mathrm{m}$. A model that got its lowest-level wind exactly right can thus be wrong at 10 m by 0.6 to $1.2\,\mathrm{m\,s^{-1}}$, from the roughness and the stability alone. Errors in the roughness length, in the stability, in the friction velocity, in the surface fluxes that set the stability, and in the stability functions themselves all enter at this last step. A near-surface wind error does not by itself imply a poor large-scale wind solution.

25.2.3 Horizontal grid spacing and effective resolution

The model also divides the horizontal atmosphere into cells. Typical grid spacings are $\Delta x = 9\,\mathrm{km}$ for a coarse regional model, 3 km for a convection-permitting regional model, and 1 km or less for a local model. Every cell carries one effective value of each surface property: terrain height, land use, soil state, roughness and vegetation. The real world inside a cell of $3\,\mathrm{km} \times 3\,\mathrm{km}$ may hold a ridge and a valley, a forest and a clearing, a town and a lake, none of which the cell distinguishes.

Chapter 5 showed that grid spacing is not resolvable scale. A feature needs several grid cells to be represented with its shape and amplitude, and the working rule is $L_{\mathrm{resolved}} \gtrsim 5$ to $10\,\Delta x$.

The effective resolution of the three grids above is therefore about 45 to 90 km, 15 to 30 km and 5 to 10 km. A valley 5 km wide is absent from the 9 km model, damped in the 3 km model and only roughly represented at 1 km. Horizontal resolution sets which terrain and which mesoscale circulations, such as sea breezes, slope and valley winds and gap flows, the model can produce at all.

25.2.4 Terrain-following coordinates

Many regional models do not place their levels on flat surfaces of constant height. They use *terrain-following coordinates*, in which the lowest levels follow the shape of the ground and the levels become gradually flatter with height until they are horizontal at the model top. A simple height-based form defines the vertical coordinate s of a point at height z above a surface of elevation z_s, under a flat model top at z_{top}, by

$$z = z_s + s\left(1 - \frac{z_s}{z_{\text{top}}}\right), \qquad 0 \le s \le z_{\text{top}}, \tag{25.6}$$

so that $s = 0$ is the ground everywhere and $s = z_{\text{top}}$ is the top. A model level is a surface of constant s, and its height above the local ground is $s\,(1 - z_s/z_{\text{top}})$. Other models define the coordinate from pressure instead of height, with the same effect. Figure 25.2 draws such levels across a mountain. The horizontal axis is distance in kilometers and the vertical axis height above sea level; the shaded shape is the terrain, the blue curves are levels of constant s, and the dashed line is a surface of constant height. The model top has been lowered to 3.5 km so that the flattening of the levels is visible.

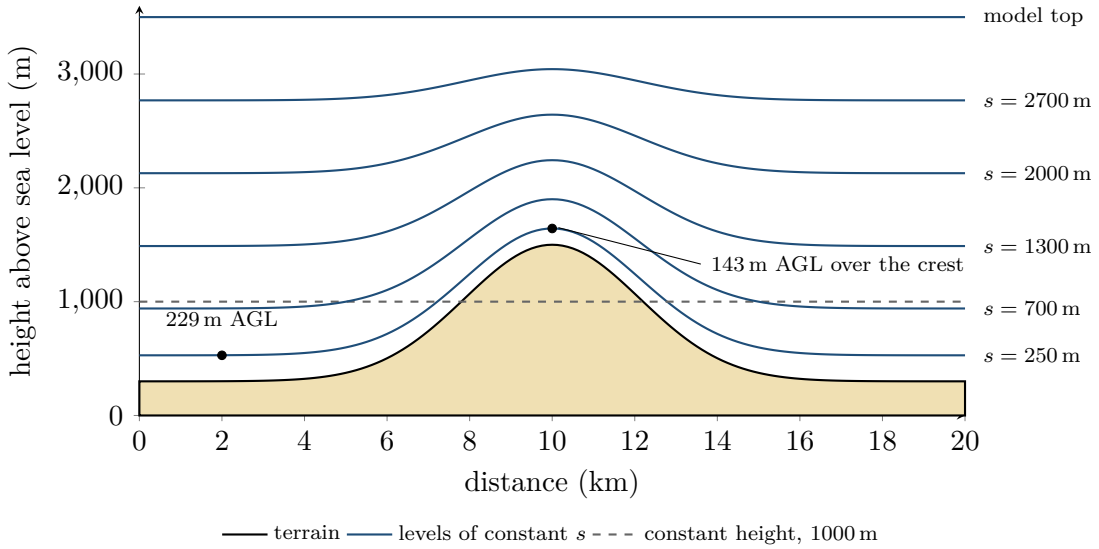


Figure 25.2: Terrain-following levels over a mountain (schematic). Terrain $z_s(x) = 300\,\text{m} + 1200\,\text{m}\,\exp\{-[(x - 10\,\text{km})/3\,\text{km}]^2\}$; levels of constant s from equation (25.6) with $z_{\text{top}} = 3.5\,\text{km}$, lowered from a realistic value of tens of kilometers to make the flattening visible. The dots mark the level $s = 250\,\text{m}$ over the plain and over the crest.

Near the ground the levels follow the terrain closely; higher up they flatten, and the top is horizontal. The same level $s = 250\,\text{m}$ lies 229 m above the plain, at 529 m above sea level, and 143 m above the crest, at 1643 m above sea level: the layer between the ground and a given level is compressed over the mountain. With a realistic model top the compression near the ground is small. For $z_{\text{top}} = 20\,\text{km}$, a lowest level at $s = 30\,\text{m}$ lies $30 \times (1 - 300/20\,000) = 29.6\,\text{m}$ above a plain at 300 m and $30 \times (1 - 1500/20\,000) = 27.8\,\text{m}$ above a crest at 1500 m. “First model

level at 30 m" therefore means approximately 30 m above the local ground, while the geometric height of the same level above sea level varies with the terrain by more than a kilometer. In models whose coordinate is defined from pressure, the height of a level also changes slightly with time, as the surface pressure and the temperature of the column change. The coordinate gives the model a fine, uniform resolution of the lowest atmosphere over mountains and plains alike, which a set of flat levels could not do: flat levels would intersect the mountain, and the lowest level above the crest could lie hundreds of meters above the ground.

25.2.5 Errors of terrain-following coordinates

Over steep terrain the levels become strongly sloped, and the coordinate then introduces numerical errors, chiefly in the horizontal pressure gradient and in advection. The pressure-gradient error follows from a change of variables. The force needs the horizontal derivative of pressure at constant height, but the model holds its values along sloping levels of constant s. The chain rule, applied along a level, gives

$$\left.\frac{\partial p}{\partial x}\right|_z = \left.\frac{\partial p}{\partial x}\right|_s - \frac{\partial p}{\partial z}\left.\frac{\partial z}{\partial x}\right|_s = \left.\frac{\partial p}{\partial x}\right|_s + \rho\, g\left.\frac{\partial z}{\partial x}\right|_s , \tag{25.7}$$

using hydrostatic balance $\partial p/\partial z = -\rho g$ in the second step. Near the ground the slope of a level is about the slope of the terrain. Over a slope of 0.2, with $\rho = 1.2\,\mathrm{kg\,m^{-3}}$ and $g = 9.81\,\mathrm{m\,s^{-2}}$, the second term is $1.2 \times 9.81 \times 0.2 = 2.35\,\mathrm{Pa}$ per meter: along the level the pressure falls by about 2.35 Pa for every meter traveled uphill, simply because the level rises. The large-scale gradient that drives the wind is about 1 hPa per 100 km, or 0.001 Pa per meter. The model must therefore compute a small difference of two terms each about 2400 times larger than the result. An error of only 0.1 % in either term, from the discretization of a curved level on a finite grid, gives a spurious gradient of 0.0024 Pa per meter, more than twice the real one. Unopposed, it accelerates the air at $0.0024/1.2 = 0.002\,\mathrm{m\,s^{-2}}$, or $7\,\mathrm{m\,s^{-1}}$ per hour.

The same slope causes errors in advection, because a flow that is horizontal crosses sloped levels and the vertical and horizontal transports must be computed between levels of different heights. Models reduce these errors in several ways: by coordinates whose levels flatten more quickly with height than equation (25.6) does, by discretizations of the pressure gradient designed for sloped levels, and by smoothing the steepest terrain (Section 25.3.1). Even the choice of vertical coordinate can therefore matter for the wind in complex terrain.

25.2.6 Vertical against horizontal resolution

Attention usually goes to the horizontal grid spacing Δx, but for the near-surface wind the vertical resolution matters at least as much. Consider a stable nighttime boundary layer only 100 m deep, with a low-level jet near its top (Chapter 17 and Chapter 18). Figure 25.3 plots height against wind speed for an illustrative profile of this kind, drawn as the black curve, with the stable layer shaded. The blue dots are the values at the levels of a fine vertical grid, with its lowest level at 10 m; the red squares are the values at the levels of a coarse grid, with its lowest level at 40 m. The straight segments between the symbols are what each grid can hold.

The fine grid has five levels inside the stable layer and follows the profile closely: the strong shear between 10 and 45 m, about $7\,\mathrm{m\,s^{-1}}$ over 35 m, and the jet core of $12.0\,\mathrm{m\,s^{-1}}$ near 91 m. The coarse grid has a single level inside the layer. Even if its values were exactly right at its levels, it would place its maximum at 150 m with $10.7\,\mathrm{m\,s^{-1}}$, 60 m too high and $1.3\,\mathrm{m\,s^{-1}}$ too weak, and it holds no information on the shear below 40 m. The real loss is larger than this sampling picture suggests, because the coarse model computes its turbulent fluxes from differences across layers 100 m thick, which smear the inversion and erode the jet. A model with one or two levels inside a shallow stable layer cannot represent the strong shear, the strength of the inversion or the low-level jet.

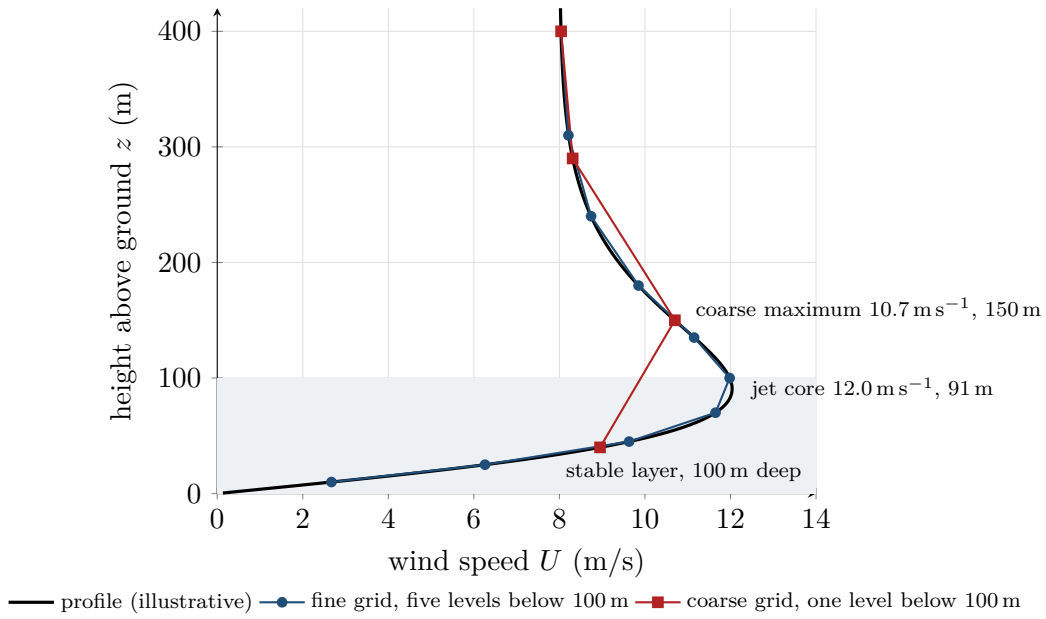


Figure 25.3: A shallow stable boundary layer with a low-level jet, $U(z) = 8\,\mathrm{m\,s^{-1}}\,[1 - e^{-z/30\,\mathrm{m}}] + 4.5\,\mathrm{m\,s^{-1}}\,(z/80\,\mathrm{m})^2\,e^{2(1-z/80\,\mathrm{m})}$ (illustrative), sampled at the levels of a fine grid (10, 25, 45, 70, 100, 135, 180, 240, 310, 400 m) and of a coarse grid (40, 150, 290, 400 m). The segments between levels are linear interpolation.

The two resolutions therefore do different work. Horizontal resolution determines the terrain and the mesoscale structure the model can carry. Vertical resolution determines the shear, the stability, the jet structure and the vertical gradients that drive the turbulence. Their costs also differ. Refining Δx from 3 to 1 km multiplies the number of columns by nine and, because the stable time step shrinks with the grid spacing, the number of time steps by about three: about 27 times the computation. Adding twenty levels to a grid of fifty multiplies the cost by about 1.4, provided the thinner layers do not shorten the time step. For the near-surface wind in stable conditions the second change is often the more useful one.

25.2.7 The meaning of the 10 m wind

The preceding subsections define what a model's 10 m wind is. A useful working definition is

$$U_{10,\mathrm{model}} = \text{the model-consistent wind at 10 m above the model's effective surface,} \tag{25.8}$$

that is, the wind of a grid cell, diagnosed by the model's surface-layer scheme from its lowest-level wind, 10 m above a smoothed terrain height with one effective roughness and one stability for the whole cell. It is not necessarily the wind at a particular sensor location 10 m above the real terrain. The two differ by everything the cell average and the diagnosis leave out: the local terrain, the upwind roughness of the sensor, and its local stability. The comparison of model and station is a comparison of a grid-cell value with a point value, as defined in the vocabulary, and the difference between them is partly representativeness error, not model error (Section 25.5.3).

The direction carries the same caveat. Many surface-layer schemes give the 10 m wind the direction of the lowest level. The real wind near the ground is turned further toward low pressure by the surface stress, by a few degrees across the surface layer and more in stable air. In the Northern Hemisphere the wind turns counterclockwise as height decreases, so its direction β decreases toward the ground; in the Southern Hemisphere it turns clockwise and β increases. A model that reports 040° at 10 m in southern Brazil, copied from a lowest level at

30 m, may correspond to a real surface wind from about 043°, and in a stable night from 050° or more. For a transmission conductor, whose convective cooling depends on the angle between the wind and the line, a direction error of ten degrees can matter as much as a speed error.

25.3 The surface and the boundary layer in the model

The near-surface wind is shaped by the surface beneath it and by the turbulence that couples it to the wind aloft. This section describes how the model represents the terrain and the land use of a cell, how its land-surface model closes the surface energy balance, how the soil moisture reaches the wind, how the boundary-layer scheme represents turbulent transport, and how the division between resolved and parameterized turbulence changes with the grid spacing.

25.3.1 Effective terrain and smoothing

Each grid cell has one terrain height. Consider a cell 3 km wide in steep mountain terrain, containing a valley floor at 400 m and a ridge at 1200 m above sea level. Figure 25.4 draws a cross section through it: the horizontal axis is distance across the cell, the vertical axis is height above sea level, the shaded shape is the real terrain, and the red dashed line at 750 m is the terrain height the model assigns to the whole cell. The figure also carries the land cover and the winds used in Section 25.5.3.

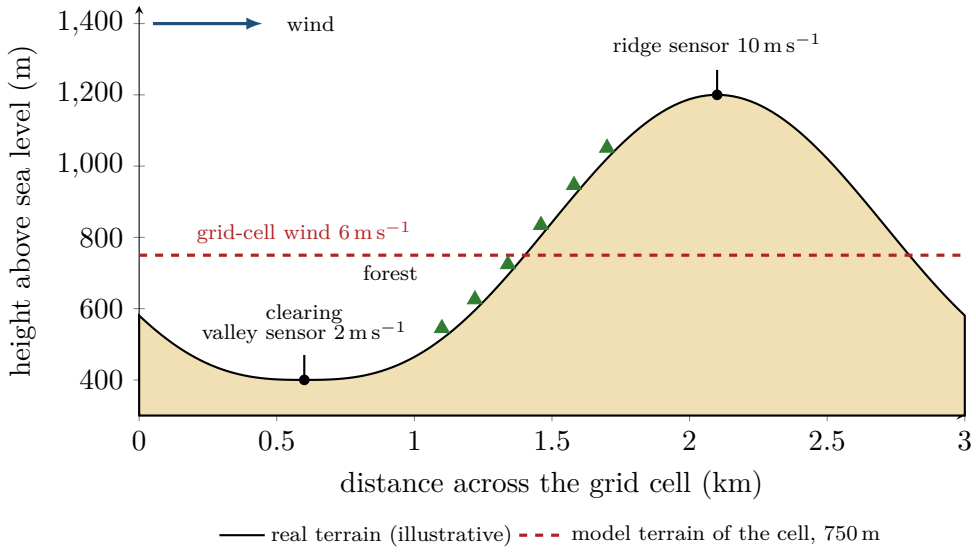


Figure 25.4: Cross section through a grid cell 3 km wide (illustrative). Real terrain $h(x) = 400\,\text{m} + 800\,\text{m}\,\{[1 - \cos(2\pi(x - 0.6\,\text{km})/3\,\text{km})]/2\}^{1.4}$, whose area average over the cell is 750 m; the model carries the cell at that height. One grid-scale wind of 6 m s^{-1} represents a valley sensor reading 2 m s^{-1} and a ridge sensor reading 10 m s^{-1}.

The model's surface lies 350 m above the valley floor and 450 m below the crest. The flow in the model therefore does not experience the real slopes, the ridge crest or the depth of the valley: it blows over a flat cell at 750 m, or over a gentle undulation formed with the neighboring cells. The speed-up over the crest, the sheltering of the valley and the channeling along it are absent from the resolved flow. Model terrain is not real terrain.

Beyond the averaging, models deliberately smooth the topography to avoid numerical instability and the errors of steep slopes described in Section 25.2.5. Chapter 20 showed the consequences with a ridge 1000 m high: mountains become too low, valleys too shallow and ridges too broad. The result is a systematic weakening of terrain speed-up, channeling, blocking

and gap flow, the effects that dominate the surface wind in complex terrain. Surface winds in mountains are therefore among the most difficult to forecast. Chapter 27, on how the surface is represented in models, treats terrain smoothing, subgrid orography and their remedies in detail.

25.3.2 Land-use representation

The model assigns each cell a set of land-surface properties, usually from a land-use or land-cover class looked up in a table: the roughness length z_0, the vegetation fraction, the albedo (the fraction of incoming sunlight the surface reflects), the leaf area index LAI, and parameters of the soil that govern its moisture. These properties feed the surface momentum budget, through z_0 and the surface stress, and the surface energy budget, through the albedo, the vegetation and the soil water.

Land-cover errors therefore become wind errors. With the diagnosis (25.5) and the same lowest-level wind of $8\,\mathrm{m\,s^{-1}}$ at 30 m in neutral air, Chapter 12 found a 10 m wind of $6.46\,\mathrm{m\,s^{-1}}$ for $z_0 = 0.1$ m, $6.73\,\mathrm{m\,s^{-1}}$ for a smoother $z_0 = 0.03$ m and $5.85\,\mathrm{m\,s^{-1}}$ for a rougher $z_0 = 0.5$ m. A cell classified as cropland that is really half forest has the wrong roughness, and its diagnosed 10 m wind is wrong by several tenths of a meter per second even with a perfect wind aloft. The same error reaches the wind a second way, through the energy budget, which the next two subsections follow. How land-use classes, mosaics within a cell and the effective roughness of a heterogeneous cell are built is the subject of Chapter 27.

25.3.3 The land-surface model and the surface energy balance

Weather models couple the atmosphere to a *land-surface model*: a model of the soil, the vegetation and the exchange of energy and water between them and the air. It carries prognostic soil temperature and soil moisture in several layers, computes the temperature of the surface, and from these the sensible and latent heat fluxes that the surface passes to the atmosphere. Those fluxes set the stability of the surface layer and drive the turbulence of the boundary layer, so the near-surface wind is coupled to the land-surface energy balance.

The balance is the one of Chapter 16,

$$R_n = H + LE + G_s, \tag{25.9}$$

with every term in $\mathrm{W\,m^{-2}}$: the net radiation R_n, positive into the surface; the sensible heat flux H and the latent heat flux LE, both positive upward; and the ground heat flux G_s, positive into the soil. The land-surface model computes all four. The radiation scheme supplies the incoming sunlight and longwave radiation; the albedo and the surface temperature set what is reflected and emitted; the soil conductivity sets G_s; and the availability of water in the soil and the opening of the plants' stomata decide how the available energy $R_n - G_s$ divides between H and LE. The partition, expressed by the Bowen ratio $B = H/LE$, strongly affects the stability: energy that goes into evaporation does not heat the air. The stability in turn controls the vertical mixing of momentum, and with it the wind near the ground.

25.3.4 Soil moisture and the surface wind

Suppose the soil in the model is too dry. More of the available energy then goes into sensible heat. With an illustrative midday $R_n - G_s = 450\,\mathrm{W\,m^{-2}}$, a correctly moist surface with $B = 0.3$ gives $H = 450 \times 0.3/1.3 = 104\,\mathrm{W\,m^{-2}}$, and a model surface dried to $B = 2$ gives $H = 450 \times 2/3 = 300\,\mathrm{W\,m^{-2}}$. Divided by $\rho\, c_p = 1.2 \times 1004\,\mathrm{J\,m^{-3}\,K^{-1}}$, the kinematic heat fluxes are 0.086 and $0.249\,\mathrm{K\,m\,s^{-1}}$. The three consequences follow in order.

Stronger convection. With $u_* = 0.4\,\mathrm{m\,s^{-1}}$ and $\overline{\theta} = 300\,\mathrm{K}$, the Obukhov length $L_\mathrm{O} = -u_*^3\,\overline{\theta}/(\kappa\, g\,\overline{w'\theta'})$ is $-0.064 \times 300/(0.4 \times 9.81 \times 0.086) = -57\,\mathrm{m}$ for the moist surface and $-20\,\mathrm{m}$ for the dry one: the dry model is much more unstable.

Deeper mixing. The stronger heating grows a deeper mixed layer. With illustrative depths of $z_i = 1500\,\mathrm{m}$ and $2500\,\mathrm{m}$, the convective velocity scale $w_* = (g\,\overline{w'\theta'}\,z_i/\overline{\theta})^{1/3}$ of Chapter 16 is $(9.81 \times 0.086 \times 1500/300)^{1/3} = 1.6\,\mathrm{m\,s^{-1}}$ and $(9.81 \times 0.249 \times 2500/300)^{1/3} = 2.7\,\mathrm{m\,s^{-1}}$.

Stronger downward transport of momentum. Two effects raise the surface wind. Within the surface layer, the more unstable profile is more uniform: from the same $9\,\mathrm{m\,s^{-1}}$ at $50\,\mathrm{m}$ over $z_0 = 0.1\,\mathrm{m}$, equation (25.5) applied between 50 and 10 m with the standard unstable ψ_m of Chapter 14 gives $7.29\,\mathrm{m\,s^{-1}}$ for $L_\mathrm{O} = -57\,\mathrm{m}$ and $7.48\,\mathrm{m\,s^{-1}}$ for $L_\mathrm{O} = -20\,\mathrm{m}$. Above the surface layer, a deeper mixed layer spreads the surface drag over more air, so the mixed-layer wind lies closer to the geostrophic wind. A slab model of the mixed layer, in which the Coriolis force on the ageostrophic wind balances the surface drag spread over the depth z_i,

$$f\,\mathbf{k} \times (\mathbf{V}_m - \mathbf{V}_g) = -\frac{C_D\,U_m}{z_i}\,\mathbf{V}_m, \qquad U_m = \frac{U_g}{\sqrt{1+r^2}}, \quad r = \frac{C_D\,U_m}{|f|\,z_i},$$

with the mixed-layer wind $\mathbf{V}_m$ of speed U_m, gives, for $U_g = 10\,\mathrm{m\,s^{-1}}$, $C_D = 0.003$ and $|f| = 7.29 \times 10^{-5}\,\mathrm{s^{-1}}$ at 30° latitude, $U_m = 9.67\,\mathrm{m\,s^{-1}}$ for $z_i = 1500\,\mathrm{m}$ and $9.87\,\mathrm{m\,s^{-1}}$ for $z_i = 2500\,\mathrm{m}$. The second relation follows from the first by writing the vectors as complex numbers, $\mathbf{V}_m = \mathbf{V}_g\,i/(r+i)$ for $f > 0$. The mixed-layer wind is also turned toward low pressure by $\arctan r$, 14.8° and 9.2°: to the left of the geostrophic wind in the Northern Hemisphere and to the right in the Southern.

Together the two effects make the 10 m wind of the dry model about 5 % stronger, $0.35\,\mathrm{m\,s^{-1}}$ on a wind of $7.3\,\mathrm{m\,s^{-1}}$, and turn it about 6° less, although the large-scale pressure field is the same in both. The error is small on any one afternoon but systematic: it recurs every sunny day over the region where the soil is too dry. Soil moisture can therefore make the surface wind too strong, and a bias of this kind points to the land surface, not to the dynamics.

25.3.5 The boundary-layer parameterization

Boundary-layer turbulence is far smaller than the grid of most weather models, so the model represents its effect with a *boundary-layer scheme*, or PBL scheme (from planetary boundary layer): the parameterization of the vertical turbulent transport of momentum, heat, moisture and other quantities through the boundary layer. The scheme computes the eddy diffusivities K_m and K_h, the boundary-layer depth z_i, the turbulent fluxes, and in some schemes the turbulent kinetic energy e; it receives the surface fluxes and u_* from the surface-layer scheme. Different schemes make different assumptions, and two models with the same large-scale forecast can produce different surface winds because of them. This chapter gives an overview; Chapter 26 treats the schemes in depth.

Local and nonlocal closure. A *local* closure makes the flux at a height depend on the gradient at that height,

$$-\overline{u'w'} = K_m\,\frac{\partial U}{\partial z}, \tag{25.10}$$

in along-wind coordinates, the flux-gradient relation of Chapter 8. A *nonlocal* closure adds the transport by large eddies that span the boundary layer and carry air from the surface layer to the top of the mixed layer in one motion, which no local gradient can represent. In the convective boundary layer of Chapter 16, where the mean gradients in the mixed layer are nearly zero while the fluxes are not, the distinction is essential; nonlocal schemes add a term

that does not depend on the local gradient, or a profile of K_m shaped over the whole layer. Local and nonlocal schemes can therefore produce different daytime wind profiles from the same surface fluxes.

First-order closure. A *first-order* closure relates the flux directly to the mean gradient through an eddy diffusivity,

$$\text{flux} = -\text{eddy diffusivity} \times \text{gradient},$$

as in equation (25.10). The difficulty is in computing K_m, which depends on a mixing length, on the stability and on the shear. A common form is $K_m = l^2 \, |\partial U/\partial z| \, f_m(\mathrm{Ri})$, with the mixing length l and a stability function f_m of the Richardson number that equals one in neutral air. With the neutral surface-layer values $l = \kappa z = 40\,\mathrm{m}$ at $z = 100\,\mathrm{m}$ and a shear $\partial U/\partial z = u_*/(\kappa z) = 0.01\,\mathrm{s}^{-1}$ for $u_* = 0.4\,\mathrm{m\,s}^{-1}$, $K_m = 40^2 \times 0.01 = 16\,\mathrm{m}^2\,\mathrm{s}^{-1}$, equal to $\kappa z\, u_*$ as surface-layer theory requires.

Turbulent-kinetic-energy closure. Some schemes carry the turbulent kinetic energy

$$e = \tfrac{1}{2}\left(\overline{u'^2} + \overline{v'^2} + \overline{w'^2}\right) \tag{25.11}$$

as a prognostic variable, with its own budget of shear production, buoyancy production or destruction, transport and dissipation (Chapter 8), and relate the diffusivity to it, $K_m = c\, l\, e^{1/2}$, with a constant c of order one half. The literature often writes this energy as k; this book keeps e. With $c = 0.5$, $l = 40\,\mathrm{m}$ and an illustrative $e = 0.64\,\mathrm{m}^2\,\mathrm{s}^{-2}$, four times u_*^2, again $K_m = 0.5 \times 40 \times 0.8 = 16\,\mathrm{m}^2\,\mathrm{s}^{-1}$. The two closures agree in this neutral case by construction; they differ when the turbulence is not in local equilibrium with the shear, as in the evening collapse of mixing or in the turbulence carried up from the surface, because only the second gives the model an explicit turbulence state with a memory. Table 25.2 arranges the two distinctions. Its rows are local and nonlocal closures, its columns first-order and turbulent-kinetic-energy closures, and each cell states how such a scheme obtains its fluxes.

Table 25.2: Two distinctions among boundary-layer schemes (overview; Chapter 26 treats the schemes in depth).

	First-order closure	Turbulent-kinetic-energy closure
Local	flux from the local gradient; K_m from mixing length, shear and Richardson number	prognostic e; flux from the local gradient with $K_m = c\, l\, e^{1/2}$
Nonlocal	prescribed K_m profile over the boundary layer, plus a term for transport by large eddies	prognostic e combined with an explicit transport by large eddies

25.3.6 Resolved and parameterized turbulence

Whether turbulence is resolved or parameterized depends on the grid spacing relative to the size of the energy-carrying eddies, which is comparable to the boundary-layer depth (Chapter 5). At $\Delta x = 10\,\mathrm{km}$ almost all boundary-layer turbulence is parameterized. At $\Delta x = 1\,\mathrm{km}$ some of the larger motions, such as convective rolls and the largest thermals, begin to be partly resolved. At $\Delta x = 50\,\mathrm{m}$ the large eddies are explicitly represented and only the small ones are parameterized, as in the large-eddy simulation of Chapter 5. The transition between these regimes is not clean.

Figure 25.5 shows it with an illustrative function. The horizontal axis is the grid spacing on a logarithmic scale and the vertical axis is the fraction of the vertical turbulent flux carried

by resolved motions. The red curve is a convective boundary layer 1000 m deep, the blue dashed curve a stable boundary layer 200 m deep, and the shaded band is the gray zone of the convective case.

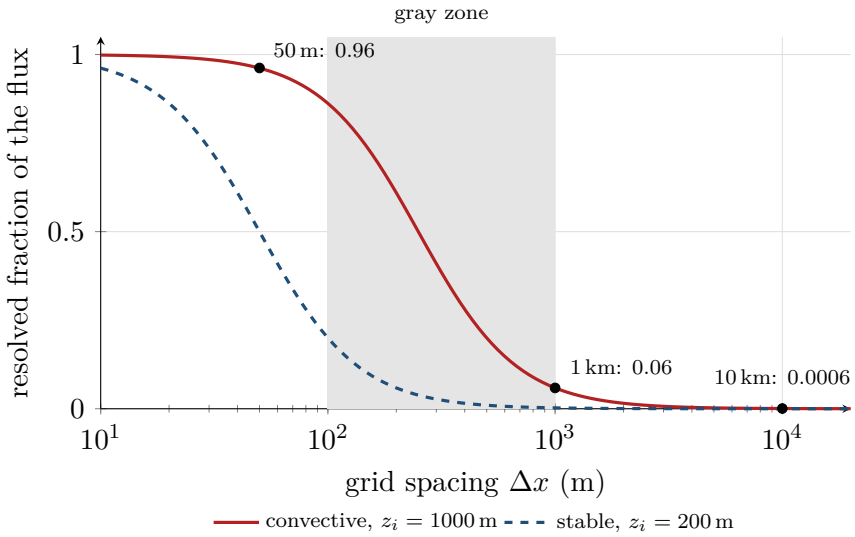


Figure 25.5: Illustrative resolved fraction of the boundary-layer turbulent flux, $1/[1 + (\Delta x/\lambda)^2]$ with $\lambda = 0.25\, z_i$, for a convective layer ($z_i = 1000$ m) and a stable layer ($z_i = 200$ m). The functional form is a schematic of the transition, not a property of any particular model.

For the convective layer, 96 % of the flux is resolved at 50 m, 6 % at 1 km and almost none at 10 km, the three regimes of the first paragraph. Between about 100 m and 1 km the fraction falls from 86 to 6 %: in this range the grid partly resolves the large turbulent structures while the boundary-layer scheme, built for entirely unresolved turbulence, still represents all of them. This is the gray zone, approximately 100 m to 1 km for a convective boundary layer, and its position depends on the conditions: for the shallow stable layer the same transition lies between about 10 and 200 m, and a grid that fully parameterizes stable turbulence by night can sit in the gray zone by day. Three failures are possible there. The same transport may be counted twice, once by the resolved eddies and once by the scheme; the scheme may suppress the resolved eddies and the flow be under-mixed until they grow; or the two together may over-mix. *Scale-aware* boundary-layer schemes try to handle this transition by reducing the parameterized part as the resolved part grows with decreasing grid spacing; Chapter 26 returns to them.

25.4 Starting and bounding the forecast

A forecast needs a starting state and, for a regional model, the state of the atmosphere at the edges of its domain throughout the run. This section describes the initial conditions, the data assimilation that produces them, the lateral boundary conditions and the nesting of models inside each other, and the spin-up of a model after it starts.

Jargon: initial conditions, data assimilation, background, analysis, lateral boundary conditions, nesting, spin-up

The *initial conditions* are the values of every prognostic variable at every grid point at the start of a forecast. *Data assimilation* is the procedure that estimates them by combining observations with a short previous forecast, weighted by the error statistics of each. The previous forecast is the *background*, and the resulting estimate of the present state is the *analysis*. The *lateral boundary conditions* are the values a regional model receives at the edges of its domain, usually from a larger-scale model. *Nesting* is the running of a finer model inside a coarser one, which supplies its boundary conditions. *Spin-up* is the time a model needs after its start for the resolved structures and turbulence of its own grid to develop.

25.4.1 Initial conditions

A forecast must start from an estimate of the atmospheric state, and its quality depends strongly on how well that state is known: the equations of Section 25.1.1 amplify small errors in the initial state over days. The observations available to build the estimate are surface stations, radiosondes (balloon-borne soundings of wind, temperature and humidity), aircraft reports, satellites (radiances, which constrain temperature and humidity, and winds derived from cloud motion and from the sea surface), and radar. They are irregular in space and time and much sparser than the grid: a model with $\Delta x = 3\,\mathrm{km}$ over a region of $1500\,\mathrm{km} \times 1500\,\mathrm{km}$ has 250 000 columns, each with fifty or more levels, while the region may have a few hundred surface stations and a few radiosondes twice a day. The initial state must therefore be estimated, not measured, and the procedure that estimates it is data assimilation.

25.4.2 Data assimilation

Data assimilation combines three ingredients: the observations, a previous short forecast valid at the same time, and the error statistics of both. The forecast supplies a complete, physically consistent first guess at every grid point; the observations correct it where they exist; the error statistics decide how far to trust each.

The principle appears in the simplest case: one scalar, such as the wind speed at one point, with a background value U_b of error standard deviation σ_b and an observation U_o of error standard deviation σ_o. Both errors are assumed unbiased and independent. A weighted combination

$$U_a = (1 - W)\, U_b + W\, U_o = U_b + W\, (U_o - U_b) \tag{25.12}$$

with a weight W between zero and one has error variance

$$\sigma_a^2 = (1 - W)^2\, \sigma_b^2 + W^2\, \sigma_o^2,$$

since the cross term vanishes for independent errors. Setting the derivative with respect to W to zero, $-2(1 - W)\, \sigma_b^2 + 2W\, \sigma_o^2 = 0$, gives the weight of least error variance and the variance it achieves:

$$W = \frac{\sigma_b^2}{\sigma_b^2 + \sigma_o^2}, \qquad \sigma_a^2 = (1 - W)\, \sigma_b^2 = \frac{\sigma_b^2\, \sigma_o^2}{\sigma_b^2 + \sigma_o^2}, \tag{25.13}$$

or, equivalently, $1/\sigma_a^2 = 1/\sigma_b^2 + 1/\sigma_o^2$. The analysis moves from the background toward the observation by the fraction W, which is large when the background is uncertain and small when the observation is; and the analysis is more precise than either ingredient, since the precisions, the inverse variances, add.

For an illustrative case, let the background wind be $U_b = 6\,\mathrm{m\,s^{-1}}$ with $\sigma_b = 2\,\mathrm{m\,s^{-1}}$ and the observation $U_o = 9\,\mathrm{m\,s^{-1}}$ with $\sigma_o = 1\,\mathrm{m\,s^{-1}}$. Then

$$W = \frac{4}{4+1} = 0.8, \qquad U_a = 6 + 0.8 \times 3 = 8.4\,\mathrm{m\,s^{-1}}, \qquad \sigma_a = \sqrt{0.2 \times 4} = 0.89\,\mathrm{m\,s^{-1}}.$$

Figure 25.6 draws the three distributions. The horizontal axis is wind speed, the vertical axis probability density; the gray curve is the background, the blue curve the observation and the red curve the analysis.

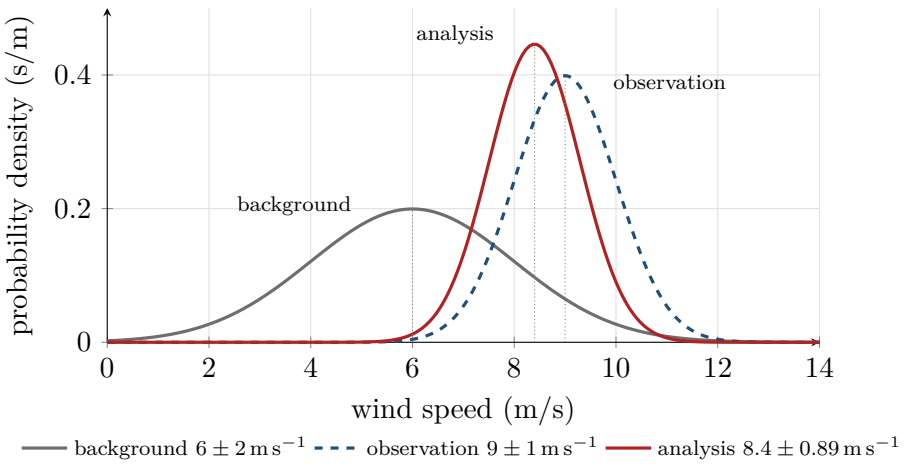


Figure 25.6: Scalar data assimilation (illustrative): Gaussian background error, $\sigma_b = 2\,\mathrm{m\,s^{-1}}$; observation error, $\sigma_o = 1\,\mathrm{m\,s^{-1}}$; and the analysis of equations (25.12) and (25.13), $W = 0.8$, $\sigma_a = 0.89\,\mathrm{m\,s^{-1}}$.

The analysis lies close to the observation, which is the more precise of the two, and its distribution is narrower than both. The observation error σ_o includes the error of the instrument and the representativeness error: the difference between what one station measures and the grid-cell value the model represents. A station in a sheltered valley that reads $9\,\mathrm{m\,s^{-1}}$ with an instrument error of $0.3\,\mathrm{m\,s^{-1}}$ may represent its grid cell only to within $3\,\mathrm{m\,s^{-1}}$; with $\sigma_o = 3\,\mathrm{m\,s^{-1}}$, $W = 4/13 = 0.31$, the analysis is $6.9\,\mathrm{m\,s^{-1}}$ and $\sigma_a = 1.66\,\mathrm{m\,s^{-1}}$. Assimilation therefore trusts a poorly exposed station less, by design.

The real problem has millions of variables instead of one, and the scalar weight becomes a matrix built from the error covariances of the background. Those covariances spread the influence of one observation to nearby grid points and to other variables, in ways consistent with the balances of Chapter 3: a pressure observation also corrects the wind. The methods in operational use differ in how they compute the combination. Three-dimensional variational assimilation (3D-Var) finds the state that best fits the background and the observations at one time by minimizing a weighted misfit. Four-dimensional variational assimilation (4D-Var) does the same over a time window, requiring the state to evolve by the model's equations through the window. Ensemble Kalman filters estimate the background error covariances from an ensemble of forecasts, so that the weights change with the weather of the day. Hybrid methods combine fixed and ensemble covariances.

For the near-surface wind, the limitation is coverage. Observations that constrain the boundary layer, such as profiles of wind in the lowest kilometer, are sparse, and surface stations represent their cells poorly in complex terrain, so they receive small weights. The local structure of the boundary layer, a shallow inversion, a valley cold pool or a jet, can therefore be poorly constrained at the start of a forecast even when the large-scale state is well analyzed.

25.4.3 Lateral boundary conditions and nesting

A global model has no lateral edges. A regional model covers only part of the globe and needs the state of the atmosphere at the edges of its domain throughout the forecast, which it receives from a larger-scale model, usually a global one. Regional models are therefore run nested:

$$\text{global model} \;\rightarrow\; \text{regional model} \;\rightarrow\; \text{local model},$$

each supplying the boundary conditions of the next, and errors can propagate down this chain. Figure 25.7 shows an illustrative chain in plan view: the outer rectangle is part of a global model with $\Delta x = 25\,\text{km}$, the middle one a regional domain with $\Delta x = 3\,\text{km}$, and the inner one a local domain with $\Delta x = 500\,\text{m}$. The grid lines indicate the relative fineness of each grid, not its true spacing, and the arrows show the boundary conditions passed inward.

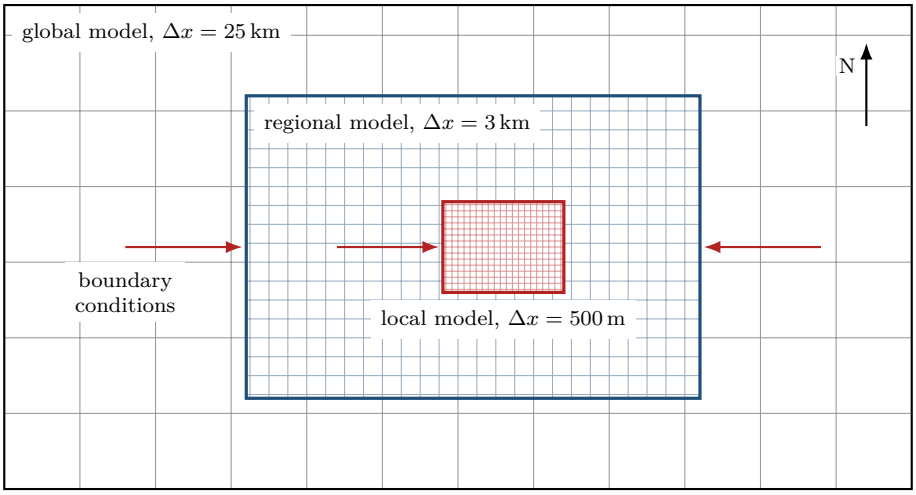


Figure 25.7: An illustrative nesting chain in plan view (schematic; grid lines indicate relative fineness, not true spacing). Each model receives its lateral boundary conditions from the one outside it. The arrangement is the same in either hemisphere.

The inner model receives its broad-scale forcing from the outer one and adds what the outer grid cannot carry: finer terrain and the mesoscale circulations it drives. Its effective resolution, by the rule of Section 25.2.3, is about 2.5 to 5 km, against 15 to 30 km for the regional model and 125 to 250 km for the global one. The jump in grid spacing between neighbors here is about eight and six; in practice nests are often stepped by ratios of three to five, with intermediate domains where needed, so that the inner model receives features it can represent. The local domain at 500 m also lies in the gray zone of Section 25.3.6 for a convective day.

The inner model cannot completely correct a badly wrong large-scale pattern. Its boundaries keep feeding it the outer model's state, and the air inside is replaced by inflow within a crossing time. A local domain 60 km wide with a wind of $10\,\text{m}\,\text{s}^{-1}$ is crossed in $60\,000/10 = 6000\,\text{s}$, about 1.7 h; a regional domain 1500 km wide is crossed in about 42 h at the same speed and in about 10 h by a jet-stream wind of $40\,\text{m}\,\text{s}^{-1}$. After a few hours the interior of a local model is determined by its boundaries, and a front placed 100 km wrong by the global model is placed 100 km wrong in the local one, now with sharp terrain detail. Nesting adds local detail; it does not add large-scale skill.

25.4.4 Spin-up

A model started from an analysis, or from the fields of a coarser model interpolated to its grid, does not begin in balance with its own resolution and physics. Turbulence and the local

structure of the boundary layer need time to develop. A model at 500 m initialized from 3 km fields starts with smooth fields that contain none of the eddies its grid can carry, and the convective eddies need several turnover times to grow. One turnover takes z_i/w_*, about $1500\,\mathrm{m}/1.6\,\mathrm{m\,s^{-1}} \approx 16\,\mathrm{min}$ in the moist case of Section 25.3.4, so the resolved turbulence takes of the order of an hour to reach equilibrium. The same applies at the inflow boundaries, where smooth air enters and needs a fetch of several kilometers, a few turnover times multiplied by the wind speed, before its turbulence is realistic. Mesoscale circulations such as sea breezes, slope winds and valley winds take hours, and the soil moisture of the land-surface model, if initialized inconsistently, adjusts over weeks.

This adjustment is called spin-up, and during it the model may have unrealistic turbulence: too little at first, then sometimes an overshoot. The first several hours of a simulation are therefore less reliable than the hours that follow, and a common practice is to discard them, or to start each run early enough that the hours of interest come after the spin-up.

25.5 Interactions and limits

The components of Figure 25.1 do not fail in isolation, and the grid imposes limits that no scheme can remove. This section follows an error through the chain of schemes, explains why a model's wind bias often differs between day and night, and shows why a single grid-scale wind cannot represent a whole valley.

25.5.1 Parameterization interaction

The near-surface wind depends on interactions among several schemes: the boundary-layer scheme, the land-surface model, the radiation, the cloud physics and the surface layer. An error in one travels through the others. A typical chain is

$$\text{cloud error} \rightarrow \text{radiation error} \rightarrow \text{surface heat-flux error} \rightarrow \text{stability error} \rightarrow \text{wind error}.$$

Consider an illustrative night under an overcast sky that the model forecasts as clear. Under the observed cloud, the cloud base returns much of the longwave radiation the ground emits; the net radiation loss is small, the surface cools slowly, and the stable layer stays weak, with an Obukhov length of about $L_\mathrm{O} = +200\,\mathrm{m}$. Under the model's clear sky the net longwave loss is several times larger, the surface cools faster and the stable layer strengthens, with $L_\mathrm{O} = +50\,\mathrm{m}$. From the same $8\,\mathrm{m\,s^{-1}}$ at 30 m over $z_0 = 0.1\,\mathrm{m}$, the diagnosis (25.5) with the stable correction $\psi_m = -5z/L_\mathrm{O}$ gives

$$L_\mathrm{O} = +200\,\mathrm{m}: \quad U_{10} = 8\,\mathrm{m\,s^{-1}} \times \frac{4.605 + 0.25}{5.704 + 0.75} = 6.02\,\mathrm{m\,s^{-1}},$$
$$L_\mathrm{O} = +50\,\mathrm{m}: \quad U_{10} = 8\,\mathrm{m\,s^{-1}} \times \frac{4.605 + 1.0}{5.704 + 3.0} = 5.15\,\mathrm{m\,s^{-1}}.$$

The cloud error has lowered the 10 m wind by $0.9\,\mathrm{m\,s^{-1}}$ through the surface-layer diagnosis alone. In the resolved flow the stronger stability also decouples the surface from the air above, which weakens the wind at the lowest level and strengthens the low-level jet aloft, so the full error is larger. The chain can be indirect: the error is in the clouds, the symptom is in the wind, and a correction applied to the wind, such as a change of roughness, would hide the cause without removing it.

25.5.2 Regime-dependent bias

Suppose a model performs well during the day but overpredicts the wind at night. That pattern points to an issue that depends on the regime, not to a uniform error. Likely causes are excessive mixing in stable conditions (the too-much-mixing problem of Chapter 17), an incorrect roughness, whose effect on the diagnosis grows in stable air, and a poor representation of the inversion, often from a coarse vertical grid (Section 25.2.6).

A single overall score hides such a pattern. Table 25.3 gives an illustrative verification of a model's 10 m wind against a station, split into day and night with equal numbers of hours. Its columns give the mean error (the bias), the standard deviation of the error about the bias, and the root-mean-square error, related by $\mathrm{RMSE}^2 = \mathrm{bias}^2 + \text{standard deviation}^2$; the verification measures themselves are defined in Chapter 24.

Table 25.3: Illustrative verification of a model's 10 m wind, stratified by regime (equal numbers of day and night hours).

Sample	Bias (m/s)	Std. dev. (m/s)	RMSE (m/s)	Reading
Day	−0.1	1.20	1.2	nearly unbiased, random error only
Night	+1.8	1.43	2.3	systematic overprediction
All hours	+0.85	1.63	1.83	a moderate error with no visible cause

The day and night values of RMSE follow from the bias and the standard deviation, for example $\sqrt{1.8^2 + 1.43^2} = 2.3\,\mathrm{m\,s^{-1}}$ at night. The overall RMSE is the square root of the average mean-square error, $\sqrt{(1.2^2 + 2.3^2)/2} = 1.83\,\mathrm{m\,s^{-1}}$, and the overall bias is the average of the two, $0.85\,\mathrm{m\,s^{-1}}$. Read alone, the last row describes a model with a moderate, slightly positive error; the first two rows show a good daytime model with a large nighttime bias, a different diagnosis with a different remedy. Verification should therefore be stratified by regime: by day and night, by stability class, by wind speed, by direction sector and by season.

25.5.3 One grid cell for a whole valley

Return to the grid cell of Figure 25.4, which covers $3\,\mathrm{km} \times 3\,\mathrm{km} = 9\,\mathrm{km}^2$ and contains a ridge, a valley, a forest and a clearing. The model produces one effective grid-scale wind for the whole cell. A sensor on the valley floor measures $2\,\mathrm{m\,s^{-1}}$; a sensor on the ridge measures $10\,\mathrm{m\,s^{-1}}$. A grid value of $6\,\mathrm{m\,s^{-1}}$ could be quite reasonable at the model's scale, if it matches the average of the real wind over the cell. Against the valley sensor the model is $4\,\mathrm{m\,s^{-1}}$ too high; against the ridge sensor it is $4\,\mathrm{m\,s^{-1}}$ too low. Neither difference is an error of the model in the sense of a wrong forecast of what the model represents: both are representativeness error, the difference caused by comparing a grid-cell value with a point value. A direct point comparison can therefore mislead, in either direction, and its sign depends on where the station stands.

Two refinements keep the comparison honest. The grid-cell average of the real wind is itself not directly measured, so the statement that $6\,\mathrm{m\,s^{-1}}$ is reasonable needs either several stations or a terrain flow model of the cell. And the average of wind speeds is not the speed of the average wind when the directions differ across the cell, as they do when the valley channels its flow and the ridge does not; a model's cell wind is closer to the second. Chapter 23 treats the kinds of representativeness, and Chapter 28 the methods that map a grid-cell wind to a point.

25.6 Reading model wind

The preceding sections show that a model's near-surface wind is the end of a chain, and that its error can enter at any link. This section gives an order in which to examine the links, a decomposition of the error into sources, a worked example of the diagnosis, and the chain itself as the summary of the chapter.

25.6.1 Hierarchical interpretation

When a model predicts a poor 10 m wind, the conclusion that the weather model is wrong is premature. A more informative procedure examines the stages of the chain in order, from the largest scale down:

1. Is the large-scale pressure pattern correct?
2. Is the wind aloft correct?
3. Is the boundary-layer depth correct?
4. Is the stability correct?
5. Is the roughness correct?
6. Is the terrain resolved?
7. Is the station representative?

Figure 25.8 places the questions beside the stages they test. The boxes on the left are the stages of the forecast chain, from the large-scale pressure field at the top to the comparison with a station at the bottom; the numbered notes on the right are the questions, and the labels between them name the error term of Section 25.6.2 that each stage contributes.

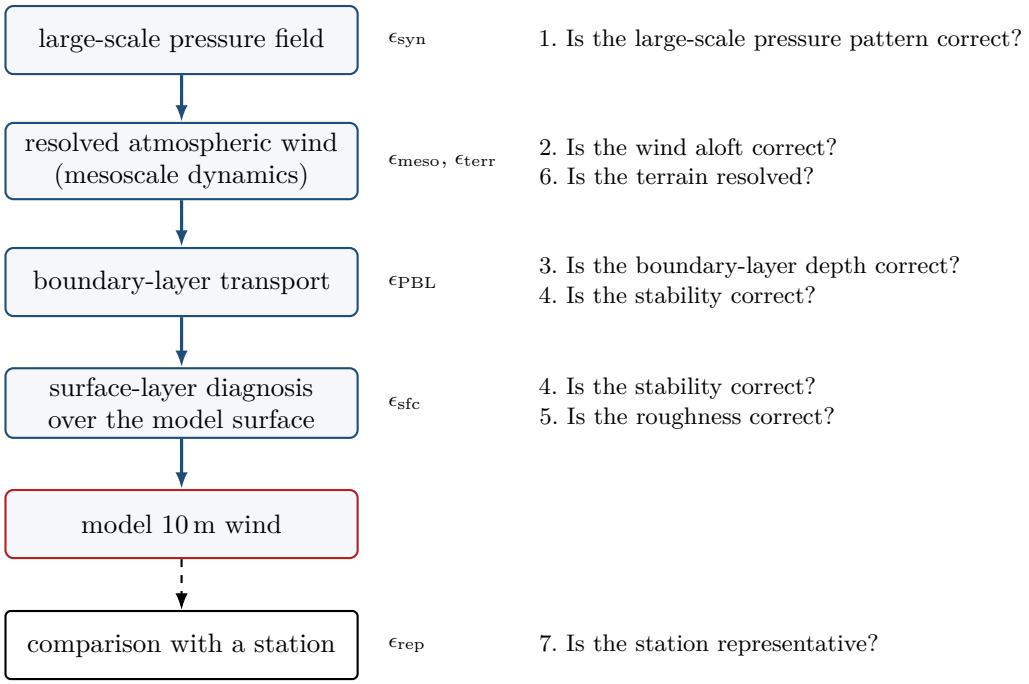


Figure 25.8: The forecast chain of a model's near-surface wind (left), the error term each stage contributes (middle) and the question that tests it (right). Stability enters both the boundary-layer transport and the surface-layer diagnosis.

Each question is answered by a different kind of evidence: analyses and surface pressure for the first, soundings, profilers, lidars, aircraft or tall towers for the second, profiles of temperature and backscatter for the third, the observed surface inversion, the heat flux or the Obukhov length for the fourth, the upwind land cover of the station for the fifth, the model terrain against a terrain map for the sixth, and the station's exposure and metadata for the seventh. Working from the top down stops at the first stage that fails, and attributes the error there rather than to the last link, where it becomes visible.

25.6.2 A decomposition of forecast wind error

The hierarchy suggests a conceptual decomposition of the error of the model's 10 m wind into contributions from the stages of the chain:

$$\epsilon_{U_{10}} = \epsilon_{\mathrm{syn}} + \epsilon_{\mathrm{meso}} + \epsilon_{\mathrm{PBL}} + \epsilon_{\mathrm{sfc}} + \epsilon_{\mathrm{terr}} + \epsilon_{\mathrm{rep}}, \tag{25.14}$$

with the synoptic, mesoscale, boundary-layer, surface, terrain and representativeness contributions. Table 25.4 lists them. Its columns give the source, what it is, a typical symptom, and the evidence that isolates it.

Table 25.4: Sources of error in a model's 10 m wind.

Source	What it is	Typical symptom	Evidence that isolates it
Synoptic ϵ_{syn}	wrong pressure pattern: position or strength of a system or front	wind wrong at all heights, over a wide area, with timing errors	analyses, surface pressure, upper-air winds
Mesoscale ϵ_{meso}	missing or misplaced sea breeze, jet, gap flow or convective outflow	regional errors at particular hours or directions	profilers, station networks, satellite
Boundary layer ϵ_{PBL}	wrong vertical mixing, depth or stability	wind aloft right, near-surface wrong; regime-dependent bias	towers, lidars, soundings by regime
Surface ϵ_{sfc}	wrong roughness, surface fluxes or similarity functions	lowest level right, 10 m wrong	flux stations, upwind land cover, two-height ratios
Terrain ϵ_{terr}	smoothed terrain: missing speed-up, sheltering, channeling	direction-dependent errors in complex terrain	model against real terrain, terrain flow models
Representativeness ϵ_{rep}	point against grid-cell value	errors fixed by site and direction, persisting under any model	neighboring stations, exposure metadata

The decomposition is not strictly additive. The stages act in sequence and multiply rather than add: the 10 m wind is roughly the wind aloft times a series of factors, one for the boundary-layer transport, one for the surface-layer diagnosis, one for the terrain and one for the exposure of the station. Taking logarithms turns that product into a sum, so the decomposition (25.14) holds for the relative errors when they are small, $\delta U_{10}/U_{10} \approx \sum \delta a_j/a_j$ over the factors a_j, and acquires cross terms when they are large. The stages also interact, as the cloud chain of Section 25.5.1 showed. The decomposition is a way of organizing the diagnosis, not an identity to be solved term by term.

25.6.3 A worked diagnosis

Suppose a model predicts a wind of $12\,\mathrm{m\,s^{-1}}$ at 500 m, and an observation-derived estimate at that height, from a wind profiler, is also $12\,\mathrm{m\,s^{-1}}$. At 10 m the model predicts $U_{10,\mathrm{model}} = 8\,\mathrm{m\,s^{-1}}$, while the station measures $U_{10,\mathrm{obs}} = 4\,\mathrm{m\,s^{-1}}$. The error at 10 m is $+4\,\mathrm{m\,s^{-1}}$, a factor of two.

The agreement at 500 m strongly suggests that the main error is not the synoptic forcing: the pressure pattern and the resolved wind aloft are right, so ϵ_{syn} and most of ϵ_{meso} are small. The error lies between 500 and 10 m. The ratio of the two winds shows how much. The model's ratio is $8/12 = 0.67$, the observed ratio $4/12 = 0.33$. Expressed as the exponent α of a power law $U(z) \propto z^{\alpha}$ (Chapter 12),

$$\alpha_{\text{model}} = \frac{\ln(8/12)}{\ln(10/500)} = 0.10, \qquad \alpha_{\text{obs}} = \frac{\ln(4/12)}{\ln(10/500)} = 0.28.$$

The model's profile is that of well-mixed air over smooth ground; the observed one is that of a stable night or of rough or sheltered ground. The candidates are therefore too much vertical mixing in the model, a roughness representation that is too smooth, local sheltering of the station, and an error in the stable boundary layer, the contributions ϵ_{PBL}, ϵ_{sfc} and ϵ_{rep}.

Figure 25.9 draws one split of the $+4\,\text{m s}^{-1}$ that is consistent with this evidence, as a waterfall: the horizontal axis lists the sources of equation (25.14) and the total; each bar starts where the previous one ended and adds its contribution, and the last bar is the total error.

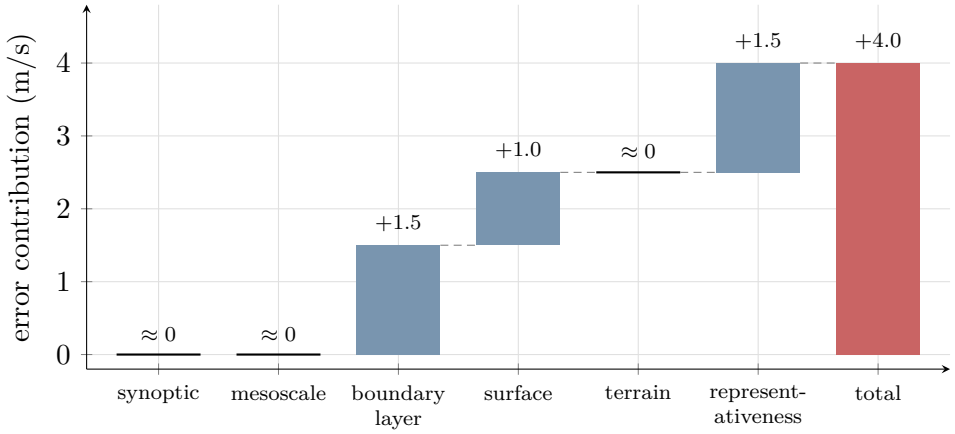


Figure 25.9: One decomposition of the $+4\,\text{m s}^{-1}$ error of the worked diagnosis into the terms of equation (25.14) (illustrative). The profiler fixes the first two bars and the station fixes the total; the split among the boundary-layer, surface and representativeness bars is a hypothesis that further evidence must test.

The figure makes the limit of the evidence explicit. The profiler and the station determine that the synoptic and mesoscale bars are near zero and that the total is $+4\,\text{m s}^{-1}$; they do not determine how the total divides among the three remaining bars. The diagnosis is nonetheless much sharper than "the model is $4\,\text{m s}^{-1}$ too windy". The next evidence follows from the candidates: the time of day and the stability of the error cases, which separate a stable-layer mixing error from the others; a tower or lidar at 50 to 100 m, which locates the excess between the boundary layer and the surface layer; the roughness upwind of the station in the direction of the wind; and a nearby exposed station, whose agreement with the model would point to sheltering of the first.

25.6.4 The forecast chain

Near-surface wind forecasting is therefore a chain,

$$\text{large-scale pressure field} \to \text{resolved atmospheric wind} \to \text{boundary-layer transport} \to \text{surface-layer diagnosis} \to U_{10},$$

the left column of Figure 25.8, and each stage can introduce error. Expressed by the physics that governs each link, it runs from the synoptic forcing through the mesoscale dynamics and the

boundary-layer parameterization to the surface-layer theory that produces the 10 m wind. When the 10 m wind is wrong, the useful question is not only how large the bias is but which stage of the chain is wrong; the answer decides whether the remedy lies in the large-scale forecast, in the vertical grid, in the boundary-layer scheme, in the land surface, in the roughness, or in the choice and exposure of the station. The link in which models differ most from one another, and whose assumptions shape the near-surface wind most directly, is the boundary-layer parameterization, which the next chapter (Chapter 26) compares scheme by scheme.

25.7 What to retain

Definition 25.1 (Numerical weather prediction of near-surface wind)**.** A weather model's near-surface wind is not one direct calculation but the end product of a chain: synoptic forcing, mesoscale dynamics, boundary-layer parameterization and surface-layer theory, evaluated over the model's effective surface. When it is wrong, the question is which stage of the chain is wrong.

Table 25.5 lists the terms of the chapter, their meaning, their units and the subsection that defines each.

25.8 Exercises

Exercise 25.1. A model's lowest level is at $s = 40\,\mathrm{m}$ in the terrain-following coordinate of equation (25.6), with $z_{\mathrm{top}} = 20\,\mathrm{km}$. (a) Compute the height of the level above the ground at a station at 2000 m above sea level and at one at sea level. (b) At the sea-level station the model gives $U_1 = 7\,\mathrm{m\,s^{-1}}$ at the lowest level. With equation (25.5), $d = 0$ and neutral air, compute the diagnosed 10 m wind for $z_0 = 0.1\,\mathrm{m}$ and for $z_0 = 0.5\,\mathrm{m}$. (c) Repeat (b) for $z_0 = 0.1\,\mathrm{m}$ with $L_{\mathrm{O}} = +80\,\mathrm{m}$ and $\psi_m = -5z/L_{\mathrm{O}}$. (d) The station measures $4.8\,\mathrm{m\,s^{-1}}$. Which of the three diagnoses agrees, and why does that agreement not prove the model's lowest-level wind correct?

Exercise 25.2. A regional model assimilates a wind observation at a station at 35°S. The background wind at the station's grid point is $U_b = 7\,\mathrm{m\,s^{-1}}$ with $\sigma_b = 1.5\,\mathrm{m\,s^{-1}}$; the station reads $U_o = 4\,\mathrm{m\,s^{-1}}$, with an instrument error of $0.5\,\mathrm{m\,s^{-1}}$. (a) Compute the weight, the analysis and its standard deviation if the representativeness error is ignored. (b) The station stands in a sheltered valley and represents its cell only to within $2\,\mathrm{m\,s^{-1}}$. Combining the two independent errors in quadrature, compute the observation error and repeat (a). (c) A local domain 45 km wide is nested inside the regional model. How long does a wind of $9\,\mathrm{m\,s^{-1}}$ take to cross it, and what does that imply for the effect of the assimilated observation on the local model after six hours?

Exercise 25.3. A model at 25°S reports a 10 m wind of $9\,\mathrm{m\,s^{-1}}$ from 020°, copied in direction from its lowest level. In the stable night the real wind turns 12° toward low pressure between that level and the ground. (a) Is the low pressure to the left or to the right of the wind, looking downwind, and does the direction β increase or decrease toward the ground? Give the expected surface wind direction. (b) A transmission line runs from 135° to 315°. Compute the angle between the line and the wind for the model direction and for the expected surface direction. (c) Answer (a) for the same situation at 25°N. (d) The model's clear-sky forecast under an observed overcast changes L_{O} from +200 to +50 m; with $8\,\mathrm{m\,s^{-1}}$ at 30 m and $z_0 = 0.1\,\mathrm{m}$, by how much does the diagnosed 10 m wind change?

Exercise 25.4. A verification of a model's 10 m wind gives, for daytime hours, a bias of $+0.3\,\mathrm{m\,s^{-1}}$ and an error standard deviation of $1.1\,\mathrm{m\,s^{-1}}$, and for nighttime hours a bias of $-1.4\,\mathrm{m\,s^{-1}}$ and a standard deviation of $1.3\,\mathrm{m\,s^{-1}}$, with equal numbers of hours. (a) Compute

Table 25.5: The terms of the chapter and where each is defined.

Term	Meaning	Units	Defined in
NWP	numerical weather prediction: integrating the atmospheric equations forward on a 3-D grid from an estimated present state	–	25.1
Prognostic variable	quantity integrated forward in time by its own equation, such as u, v, θ, q at model levels	as variable	25.1.2
Diagnostic variable	quantity computed from other model variables, such as U_{10}, u_*, z_i	as variable	25.1.2
Lowest model level z_1	lowest level above the ground on which the model stores its variables	m	25.2.1
Model 10 m wind	model-consistent wind 10 m above the model's effective surface, diagnosed from the lowest level	m/s	25.2.2, 25.2.7
Terrain-following coordinates	vertical coordinate whose levels follow the terrain near the ground and flatten with height	m	25.2.4
Effective model terrain	one smoothed terrain height per grid cell	m	25.3.1
Land-surface model	model of soil, vegetation and surface exchange of energy and water	–	25.3.3
Surface energy balance	$R_n = H + LE + G_s$	W/m^2	25.3.3
PBL scheme	parameterization of vertical turbulent transport in the boundary layer	–	25.3.5
Local, nonlocal closure	flux from the local gradient; flux including transport by boundary-layer-scale eddies	–	25.3.5
First-order, turbulent-kinetic-energy closure	K_m from mixing length, shear and stability; $K_m = c\,l\,e^{1/2}$ with prognostic e	m^2/s	25.3.5
Gray zone	grid spacing, about 100 m to 1 km for a convective layer, at which turbulence is only partly resolved	m	25.3.6
Data assimilation	combination of observations and a background forecast, weighted by their error statistics, to estimate the present state	–	25.4.2
Analysis weight W	$\sigma_b^2/(\sigma_b^2+\sigma_o^2)$: fraction by which the analysis moves toward the observation	–	25.4.2
Lateral boundary conditions	state supplied at the edges of a regional domain by a larger model	–	25.4.3
Nesting	running finer models inside coarser ones	–	25.4.3
Spin-up	time for model-resolved structures and turbulence to develop after the start	h	25.4.4
Representativeness error	difference caused by the point-against-grid-cell mismatch	m/s	25.5.3
Error decomposition	conceptual split of the 10 m error into synoptic, mesoscale, boundary-layer, surface, terrain and representativeness terms	m/s	25.6.2

the RMSE of each regime and of all hours together, and the overall bias. (b) Which statement would the overall numbers alone support, and which do the stratified ones support? (c) On one night the model gives $10\,\mathrm{m\,s^{-1}}$ at $300\,\mathrm{m}$ and $5\,\mathrm{m\,s^{-1}}$ at $10\,\mathrm{m}$; a lidar gives $10\,\mathrm{m\,s^{-1}}$ at $300\,\mathrm{m}$ and the station $7\,\mathrm{m\,s^{-1}}$. Compute the power-law exponent of each profile, state which terms of equation (25.14) are implicated, and name the evidence that would separate them.

Chapter 26

Boundary-Layer Parameterizations

26.1 The task of a boundary-layer scheme

Chapter 25 described the weather model as a system: a grid, prognostic variables, initial and boundary conditions, and a set of parameterizations for the processes the grid cannot carry. Chapters 8 and 9 introduced the closure problem and the flux–gradient relation, and Chapters 16 and 17 showed, at the level of concepts, why convective transport is nonlocal and why stable mixing is hard to represent. This chapter takes the one parameterization that matters most for the near-surface wind and treats it as a method. Its question is

how does a weather model represent the turbulence it cannot resolve?

The answer has two parts that never separate: the model predicts the resolved mean flow, and a formula supplies the unresolved turbulent transport,

$$\text{resolved mean flow} \;+\; \text{unresolved turbulent transport.}$$

The model's equations carry the mean wind, temperature and humidity of each grid cell, but the turbulence inside the cell keeps moving momentum, heat and moisture vertically, and its effect on the mean must be computed from the mean itself.

The chapter first writes the equations a boundary-layer scheme solves and reduces the scheme to the estimation of one coefficient profile. It then describes the orders of closure, from the mixing length to the prognostic turbulent kinetic energy; the treatment of convection by nonlocal schemes, with the diagnosis of the boundary-layer depth; the treatment of stable layers; the place of the scheme in the model, next to the surface-layer scheme, and what it does to the 10 m wind; and finally what happens as the grid becomes fine enough to resolve part of the turbulence.

Jargon: planetary boundary layer, PBL scheme, boundary-layer scheme, parameterization, closure, eddy diffusivity, PBLH

The *planetary boundary layer* (PBL) is another name for the atmospheric boundary layer of Chapter 6, the layer that responds to the surface within about an hour. A *PBL scheme*, also called a PBL parameterization or, in this book, a *boundary-layer scheme*, is the part of a weather model that computes the vertical turbulent transport of momentum, heat and moisture in each grid column from the column's resolved profiles; the three names mean the same thing. A *parameterization* in general is a formula that returns the average effect of processes smaller than the grid as a function of the resolved variables. A *closure* is the particular relation that expresses the unknown turbulent covariances, such as $\overline{u'w'}$, in terms of known resolved quantities. An *eddy diffusivity* is the coefficient of a closure that writes a turbulent flux as minus a coefficient times the gradient of a mean: K_m for momentum and K_h for heat, in $\mathrm{m^2\,s^{-1}}$. It is a property of the turbulence, not of the air; a model computes it, and a measurement can only infer it, as a measured flux divided by a measured gradient. *PBLH* (planetary boundary-layer height) is the model's diagnosed boundary-layer depth z_i, in meters, reported as an output field.

Key idea

For the wind, a boundary-layer scheme reduces to one quantity, the eddy diffusivity for momentum K_m as a function of height: given the resolved state, it decides how strongly the slow air near the ground is coupled to the fast air aloft, and two models with the same large-scale forecast can produce different winds at 10 m because they decide differently.

26.1.1 Resolved mean flow and unresolved transport

A regional weather model with a grid spacing of a few kilometers carries one value of each variable per grid cell and model level. Boundary-layer eddies are much smaller: near the ground they are meters across, the largest thermals of a convective afternoon are about as wide as the boundary layer is deep, one to two kilometers, and the eddies of a stable night are tens of meters. Chapter 5 showed that a model represents a feature well only if it spans several grid lengths, so even the largest thermals fall well below the effective resolution of a 3 km grid. Operational weather prediction cannot resolve the eddies that produce the vertical flux of momentum $\overline{u'w'}$.

Those eddies nevertheless control the vertical profile of the mean wind: the shear $\partial U/\partial z$ near the ground is what the downward momentum flux leaves behind once it has carried momentum from the faster air above toward the surface, where it is lost to friction. The model therefore needs an approximation for the four kinematic fluxes

$$\overline{u'w'}, \qquad \overline{v'w'}, \qquad \overline{w'\theta'}, \qquad \overline{w'q'},$$

the vertical fluxes of the two horizontal momentum components, in $\mathrm{m^2\,s^{-2}}$, of potential temperature, in $\mathrm{K\,m\,s^{-1}}$, and of specific humidity, in $\mathrm{m\,s^{-1}}$ (kilograms of water per kilogram of air times meters per second). These four quantities are what a boundary-layer scheme represents. They are covariances of fluctuations (Chapter 9): an eddy-covariance station measures them at one point; a weather model never sees the fluctuations and must compute them from the means.

26.1.2 The column equations a scheme solves

Take one grid column, ignore horizontal advection for the moment (the model's dynamics supply it), and write the horizontally averaged equations for the mean wind components $\overline{u}$ (eastward) and $\overline{v}$ (northward), the mean potential temperature and the mean specific humidity. With the

geostrophic wind (u_g, v_g) standing for the pressure-gradient force (Chapter 3),

$$\frac{\partial \overline{u}}{\partial t} = f\,(\overline{v} - v_g) - \frac{\partial \overline{u'w'}}{\partial z}, \qquad \frac{\partial \overline{v}}{\partial t} = -f\,(\overline{u} - u_g) - \frac{\partial \overline{v'w'}}{\partial z}, \tag{26.1}$$

$$\frac{\partial \overline{\theta}}{\partial t} = -\frac{\partial \overline{w'\theta'}}{\partial z} + \dots, \qquad \frac{\partial \overline{q}}{\partial t} = -\frac{\partial \overline{w'q'}}{\partial z} + \dots, \tag{26.2}$$

where the dots stand for radiation, condensation and the other processes of the model. The turbulence enters every equation in the same way, as the vertical divergence of a flux: a layer gains a quantity when more of it enters through the bottom than leaves through the top, or the reverse. Substituting the down-gradient closure of Section 26.1.4, $\overline{u'w'} = -K_m\,\partial\overline{u}/\partial z$, turns the turbulence term into a vertical diffusion term,

$$\frac{\partial \overline{u}}{\partial t} = f\,(\overline{v} - v_g) + \frac{\partial}{\partial z}\left(K_m \frac{\partial \overline{u}}{\partial z}\right), \tag{26.3}$$

and likewise for $\overline{v}$ with K_m and for $\overline{\theta}$ and $\overline{q}$ with K_h. Equation (26.3) is the equation a boundary-layer scheme actually solves for the mean wind, column by column and time step by time step: a diffusion equation with a coefficient $K_m(z,t)$ that the scheme must supply.

Figure 26.1 shows how the equation is discretized. The vertical axis is height above the ground, not to scale. The model stores the mean wind and potential temperature at the *full levels* (solid lines, with the blue wind arrows), the lowest at $z_1 = 30\,\mathrm{m}$; the scheme computes the diffusivity and the flux at the *interfaces* between them (dashed lines, with the red flux arrows). The flux through the ground, at the bottom, is not computed by the boundary-layer scheme but supplied by the surface-layer scheme of Section 26.5.1.

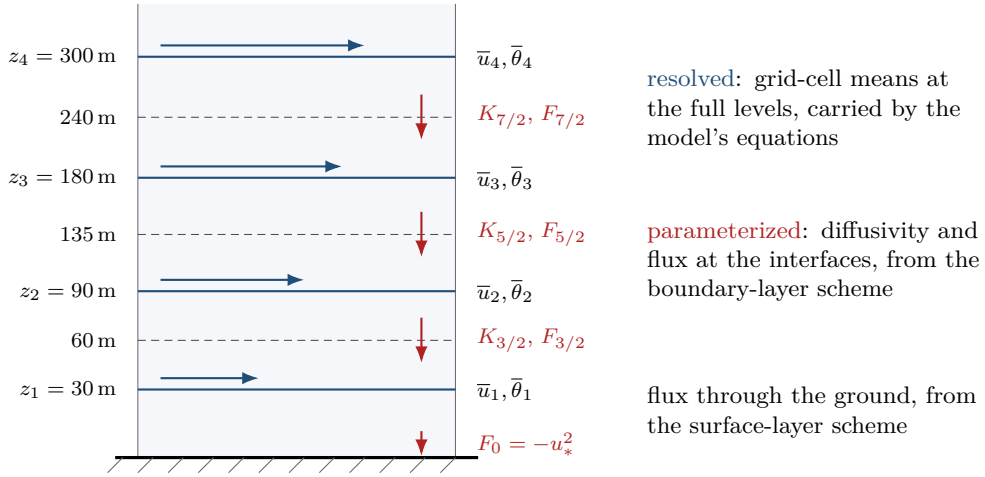


Figure 26.1: A model column as a boundary-layer scheme sees it (schematic, heights illustrative). Blue: mean wind at the full levels, increasing with height. Red: downward momentum flux at the interfaces, computed as $F_{k+1/2} = -K_{k+1/2}\,(\overline{u}_{k+1} - \overline{u}_k)/(z_{k+1} - z_k)$, and at the ground, $F_0 = -u_*^2$, from the surface-layer scheme.

The tendency of the wind at a full level is the difference between the fluxes through its upper and lower interfaces divided by the layer's depth. Take, illustratively, an eastward wind with $\overline{u}_1 = 7.0\,\mathrm{m\,s^{-1}}$ at 30 m and $\overline{u}_2 = 7.9\,\mathrm{m\,s^{-1}}$ at 90 m, a diffusivity $K_{3/2} = 8\,\mathrm{m^2\,s^{-1}}$ at the 60 m interface, and a surface friction velocity $u_* = 0.4\,\mathrm{m\,s^{-1}}$. The interface flux is

$$F_{3/2} = -8 \times \frac{7.9 - 7.0}{60} = -8 \times 0.015 = -0.12\,\mathrm{m^2\,s^{-2}},$$

downward, and the surface flux is $F_0 = -u_*^2 = -0.16\,\mathrm{m^2\,s^{-2}}$. The lowest layer, 0 to 60 m, receives $0.12\,\mathrm{m^2\,s^{-2}}$ of momentum flux from above and loses 0.16 to the ground, so the turbulence alone changes its wind at the rate

$$\frac{\partial \overline{u}_1}{\partial t} = -\frac{F_{3/2} - F_0}{60\,\mathrm{m}} = -\frac{-0.12 + 0.16}{60} = -6.7 \times 10^{-4}\,\mathrm{m\,s^{-2}},$$

$-2.4\,\mathrm{m\,s^{-1}}$ per hour. In a steady boundary layer this deceleration is balanced by the pressure-gradient and Coriolis terms of equation (26.1), through the ageostrophic wind; the scheme's diffusivity decides how large the turbulent term is, and with it the wind that achieves the balance.

26.1.3 The closure problem

Chapters 8 and 9 derived why the column equations cannot be solved as they stand. Reynolds averaging of the equations of motion leaves covariances such as $\overline{u'w'}$ in every averaged equation, and the averaging supplies no equation for them. Equations for the covariances can be derived, but they contain higher-order correlations, which need further equations, and at every level the unknowns outnumber the equations. This is the *closure problem.*

A boundary-layer scheme ends the hierarchy at some level by a relationship between resolved quantities and unresolved turbulent fluxes,

$$\text{resolved quantities (means, gradients, surface fluxes, } z_i) \longrightarrow \text{unresolved turbulent fluxes.}$$

The relationship is not derived from the equations alone. It contains assumptions about the eddies, a length scale, constants calibrated on measurements, and a decision about which conditions it is meant for. Different schemes make different assumptions, and the rest of the chapter is about those assumptions and their consequences for the wind.

26.1.4 Down-gradient diffusion and its sign

The simplest closure, already used in equation (26.3), treats turbulent transport like molecular diffusion:

$$\overline{u'w'} = -K_m \frac{\partial \overline{u}}{\partial z}, \qquad \overline{w'\theta'} = -K_h \frac{\partial \overline{\theta}}{\partial z}, \tag{26.4}$$

with K_m the eddy diffusivity for momentum (also called the eddy viscosity) and K_h the eddy diffusivity for heat; moisture is treated with K_h or with a diffusivity of its own. The analogy is with Fourier's law of heat conduction and with molecular viscosity, in which a flux runs down the gradient of the transported quantity in proportion to it. Turbulence transports quantities down their gradients, but with coefficients of order 1 to $100\,\mathrm{m^2\,s^{-1}}$, about 10^5 to 10^7 times the molecular value, because eddies, not molecules, do the carrying.

The minus sign follows from what the eddies do. Suppose the wind increases upward, $\partial\overline{u}/\partial z > 0$. An eddy that moves air downward ($w' < 0$) brings air from above, which carries the larger wind of its level ($u' > 0$); one that moves air upward ($w' > 0$) brings slower air ($u' < 0$). Both give $u'w' < 0$, so $\overline{u'w'} < 0$: momentum is transported downward, toward the ground where it is lost. With $K_m > 0$, the right side $-K_m\,\partial\overline{u}/\partial z$ is negative too, and the sign is correct. Likewise, if $\partial\overline{\theta}/\partial z < 0$, an unstable stratification, the rising air is warmer than its new surroundings ($w' > 0$, $\theta' > 0$) and the sinking air cooler, so $\overline{w'\theta'} > 0$: heat moves upward, again in agreement with $-K_h\,\partial\overline{\theta}/\partial z > 0$. In a stable layer, $\partial\overline{\theta}/\partial z > 0$, the flux is downward. None of these signs depends on the hemisphere: the vertical fluxes follow the vertical gradients, not the Coriolis parameter, so the same closure serves both hemispheres.

26.1.5 The eddy diffusivity as the central unknown

Once the flux is written as

$$\text{flux} = -K \times \text{gradient},$$

the whole difficulty moves into one question: how large should K be, at each height and time? A large K_m means strong mixing: the column is tightly coupled, the wind profile is nearly uniform, and the fast air aloft is brought close to the ground. A small K_m means weak vertical coupling: the column can carry strong shear, and the low levels are left slow.

The size of the effect follows from the flux the column must carry. In the example of Section 26.1.2, suppose the 60 m interface has to carry the whole surface stress, $0.16\,\mathrm{m^2\,s^{-2}}$. With $K_m = 8\,\mathrm{m^2\,s^{-1}}$ the required shear is $0.16/8 = 0.020\,\mathrm{s^{-1}}$, a wind difference of $1.2\,\mathrm{m\,s^{-1}}$ between 30 and 90 m; with $K_m = 2\,\mathrm{m^2\,s^{-1}}$ it is $0.080\,\mathrm{s^{-1}}$, a difference of $4.8\,\mathrm{m\,s^{-1}}$. If the wind at 90 m is held by the forcing aloft, the second column has a wind at 30 m $3.6\,\mathrm{m\,s^{-1}}$ lower than the first. That one choice, the size of K_m, strongly affects the near-surface wind, and every scheme in this chapter is a different way of making it.

26.2 Orders of closure

Closures differ in how much of the turbulence they carry as variables of their own. This section builds the mixing-length closure, generalizes it to first-order closure with a stability function, adds a prognostic equation for the turbulent kinetic energy, explains what that equation gains, and compares the orders in one table.

26.2.1 The mixing-length closure

Chapter 7 introduced Prandtl's argument: an eddy displaces air vertically by a typical distance l, the mixing length, before the air mixes with its new surroundings. A parcel displaced by l arrives with a velocity excess $u' \sim l\,\partial\overline{u}/\partial z$, and the vertical velocity of the eddy that moved it is of the same size, $|w'| \sim l\,|\partial\overline{u}/\partial z|$. Their correlated product gives $-\overline{u'w'} \sim l^2\,|\partial\overline{u}/\partial z|\,\partial\overline{u}/\partial z$, and comparison with equation (26.4) gives

$$K_m = l^2 \left| \frac{\partial \mathbf{V}}{\partial z} \right|, \tag{26.5}$$

where $|\partial\mathbf{V}/\partial z|$ is the magnitude of the vector shear (Chapter 17), so that a change of direction with height counts as shear as much as a change of speed. Near the ground the eddies are limited by the distance to the surface, and $l = \kappa z$. In the neutral surface layer the shear is $u_*/(\kappa z)$, so equation (26.5) gives $K_m = \kappa^2 z^2\, u_*/(\kappa z) = \kappa\, u_*\, z$, the surface-layer diffusivity of Chapter 9: the closure reproduces the logarithmic profile it was built from.

Across the full boundary layer the mixing length cannot keep growing as κz; the eddies are limited by the depth of the turbulent layer and by the stratification. A common form blends the two limits,

$$\frac{1}{l} = \frac{1}{\kappa z} + \frac{1}{l_\infty}, \tag{26.6}$$

with an asymptotic length l_∞, in meters, that a scheme may fix or scale with z_i. With an illustrative $l_\infty = 80$ m, $l = 1/(1/4{+}1/80) = 3.8$ m at $z = 10$ m, close to κz; $l = 1/(1/40{+}1/80) = 26.7$ m at 100 m; and $l = 1/(1/400 + 1/80) = 66.7$ m at 1000 m, close to the limit. Stability reduces the length further, which is the subject of the stability functions of the next subsection and of Section 26.4.1. Real boundary-layer schemes therefore use the mixing length as one ingredient of more elaborate forms rather than on its own.

26.2.2 First-order closure and stability functions

A scheme that relates each flux directly to a mean gradient,

$$F_\chi = \overline{w'\chi'} = -K_\chi \frac{\partial \overline{\chi}}{\partial z}, \tag{26.7}$$

for a momentum component or a scalar χ (here χ stands for u, v, θ or q), is a *first-order closure*. The name counts statistical moments: the model carries prognostic equations only for the first moments, the means, and expresses the second moments, the fluxes, through first derivatives of those means. Equation (26.5) is a first-order closure for neutral air. For stratified air the diffusivity is multiplied by a *stability function* of the gradient Richardson number,

$$K_m = l^2 \left|\frac{\partial \mathbf{V}}{\partial z}\right| F_m(\mathrm{Ri}_g), \qquad K_h = l^2 \left|\frac{\partial \mathbf{V}}{\partial z}\right| F_h(\mathrm{Ri}_g), \tag{26.8}$$

with $F_m = F_h = 1$ in neutral air, $F > 1$ in unstable air and $F < 1$ in stable air. Ri_g is computed from the model's own resolved profiles, level by level.

The stability function implied by similarity theory. The surface layer fixes F_m near the ground. Monin–Obukhov theory (Chapter 14) gives $\partial U/\partial z = u_*\phi_m/(\kappa z)$ and $K_m = \kappa u_* z/\phi_m$; equation (26.8) with $l = \kappa z$ gives $K_m = \kappa^2 z^2\, u_*\phi_m/(\kappa z)\, F_m = \kappa u_* z\, \phi_m F_m$. The two agree only if

$$F_m = \frac{1}{\phi_m^2}.$$

Chapter 14 showed that with the standard Businger–Dyer forms $\mathrm{Ri}_g = z/L_\mathrm{O}$ in unstable air and $\mathrm{Ri}_g = z/L_\mathrm{O}/(1 + 5\, z/L_\mathrm{O})$, that is $z/L_\mathrm{O} = \mathrm{Ri}_g/(1 - 5\,\mathrm{Ri}_g)$, in stable air. Substituting:

$$F_m = (1 - 16\,\mathrm{Ri}_g)^{1/2} \quad (\mathrm{Ri}_g < 0), \qquad F_m = (1 - 5\,\mathrm{Ri}_g)^2 \quad (0 \le \mathrm{Ri}_g < 0.2), \tag{26.9}$$

the second because $1 + 5\, z/L_\mathrm{O} = 1/(1 - 5\,\mathrm{Ri}_g)$. In unstable air F_m grows with $|\mathrm{Ri}_g|$: at $\mathrm{Ri}_g = -0.5$ it is 3. In stable air it falls to zero at $\mathrm{Ri}_g = 0.2$, the limit at which the log-linear profile stops representing the layer. The same steps give $F_h = 1/(\phi_m\phi_h)$.

Figure 26.2 draws two illustrative stable-side forms that represent the two families used in practice. The horizontal axis is the gradient Richardson number from 0 to 1; the vertical axis is the factor F_m by which stability multiplies the neutral diffusivity. The dashed vertical line marks the critical value $\mathrm{Ri}_c = 0.25$.

Both curves start at one and fall with Ri_g, but they part company early. At $\mathrm{Ri}_g = 0.15$ the short-tail function, of the same family as the similarity form (26.9), has already removed 84 % of the neutral mixing ($F_m = 0.16$), and at Ri_c it removes all of it; the long-tail function keeps 0.40 at $\mathrm{Ri}_g = 0.15$, 0.17 at $\mathrm{Ri}_g = 0.5$ and 0.09 at $\mathrm{Ri}_g = 1$, and never reaches zero. The difference between the curves above $\mathrm{Ri}_g \approx 0.2$ is the difference between a model whose stable layer can decouple completely and one that always keeps some mixing. Section 26.4.2 follows what each does to the nighttime wind.

26.2.3 Higher-order closure and the turbulent kinetic energy

Instead of diagnosing all turbulence from the local gradients at each time step, a scheme can carry turbulence quantities as prognostic variables of their own. The most common choice is the turbulent kinetic energy per unit mass, e, in $\mathrm{m^2\,s^{-2}}$. The diffusivity is then built from it,

$$K_m = c_m\, l\, \sqrt{e}, \qquad K_h = \frac{K_m}{\mathrm{Pr}_t}, \tag{26.10}$$

a velocity scale $\sqrt{e}$ times a length scale l, with a dimensionless constant c_m. This is a *TKE closure*. It is called a one-and-a-half-order closure: it carries one second-moment quantity, e,

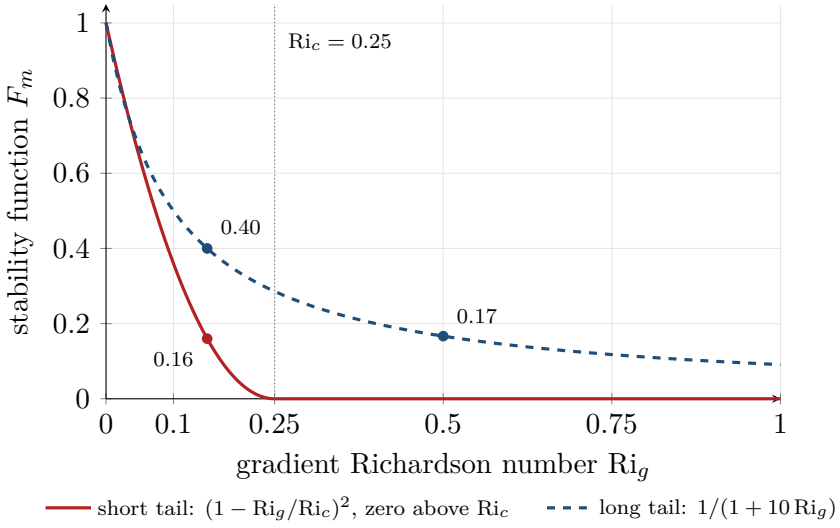


Figure 26.2: Two illustrative stable stability functions, the factor by which stability multiplies the neutral diffusivity $l^2|\partial\mathbf{V}/\partial z|$. Short tail (solid): $F_m = (1 - \mathrm{Ri}_g/\mathrm{Ri}_c)^2$ for $\mathrm{Ri}_g < \mathrm{Ri}_c = 0.25$ and zero above. Long tail (dashed): $F_m = 1/(1 + 10\,\mathrm{Ri}_g)$. Illustrative forms of the two families, not the functions of a particular model.

prognostically, but still diagnoses the individual fluxes with equation (26.7). A *second-order closure* carries prognostic equations for all the fluxes and variances and closes at the third moments.

The prognostic equation is the budget of Chapter 8, with each unknown term replaced by a closure:

$$\frac{\partial e}{\partial t} = \underbrace{K_m \left|\frac{\partial \mathbf{V}}{\partial z}\right|^2}_{P_s} \underbrace{-K_h\, N^2}_{P_b} + \underbrace{\frac{\partial}{\partial z}\left(K_e \frac{\partial e}{\partial z}\right)}_{\mathrm{Tr}} \underbrace{-c_\varepsilon \frac{e^{3/2}}{l}}_{-\varepsilon}. \tag{26.11}$$

Term by term: shear production $P_s = -\overline{u'w'}\,\partial\overline{u}/\partial z - \overline{v'w'}\,\partial\overline{v}/\partial z$ becomes $K_m|\partial\mathbf{V}/\partial z|^2$ when both momentum fluxes are written with equation (26.4), and is never negative. Buoyancy production $P_b = (g/\overline{\theta_v})\,\overline{w'\theta_v'}$ becomes $-K_h N^2$, with $N^2 = (g/\overline{\theta_v})\,\partial\overline{\theta_v}/\partial z$: a source in unstable air ($N^2 < 0$) and a sink in stable air. Transport Tr, the redistribution of e between heights by the eddies and by pressure fluctuations, is modeled as a diffusion of e itself with a diffusivity K_e of the order of K_m; it creates and destroys nothing. Dissipation is modeled by a dimensional argument: an eddy of size l and velocity $\sqrt{e}$ hands its energy e to smaller eddies in about one turnover time $l/\sqrt{e}$, so $\varepsilon \sim e/(l/\sqrt{e}) = e^{3/2}/l$, with a constant c_ε. All terms are in $\mathrm{m^2\,s^{-3}}$.

Constants from the surface layer. The constants are not free. In the neutral surface layer, with $l = \kappa z$ in both places, production balances dissipation: $u_*^2 \cdot u_*/(\kappa z) = c_\varepsilon e^{3/2}/(\kappa z)$, and the diffusivity must equal $\kappa u_* z$: $c_m \kappa z \sqrt{e} = \kappa u_* z$. The second gives $\sqrt{e} = u_*/c_m$, and the first then gives $c_\varepsilon = c_m^3$. With $c_m = 0.4$, $c_\varepsilon = 0.064$ and $e = u_*^2/c_m^2 = 6.3\,u_*^2$, near the upper end of the range of about 3 to 6 times u_*^2 observed near the ground in neutral air. These values are illustrative; schemes use different length scales for mixing and for dissipation and calibrate their own constants.

Local equilibrium. When storage and transport are small, equation (26.11) reduces to production equals dissipation. Write $\mathcal{S} = |\partial\mathbf{V}/\partial z|$ and use $K_h = K_m/\mathrm{Pr}_t$: $P_s + P_b = K_m\mathcal{S}^2(1 - \mathrm{Ri}_g/\mathrm{Pr}_t) = K_m\mathcal{S}^2(1 - \mathrm{Ri}_f)$, with $\mathrm{Ri}_f = \mathrm{Ri}_g/\mathrm{Pr}_t$ the flux Richardson number (Chapter 13).

Setting this equal to $c_\varepsilon e^{3/2}/l$ with $K_m = c_m l\sqrt{e}$ gives $e = (c_m/c_\varepsilon)\, l^2\mathcal{S}^2(1-\mathrm{Ri}_f)$, and then

$$K_m = c_m\sqrt{\frac{c_m}{c_\varepsilon}}\, l^2\mathcal{S}\,\sqrt{1-\mathrm{Ri}_f} = l^2\mathcal{S}\,\sqrt{1-\mathrm{Ri}_f} \qquad (c_\varepsilon = c_m^3). \tag{26.12}$$

In equilibrium the TKE closure is the mixing-length closure with a stability function $F_m = (1-\mathrm{Ri}_g/\mathrm{Pr}_t)^{1/2}$, which reaches zero only at $\mathrm{Ri}_f = 1$, where buoyancy destroys all that shear produces. The two closures differ only out of equilibrium, which is the subject of the next subsection.

26.2.4 The memory of the turbulence

Turbulence has its own energy budget, and a prognostic e gives it physical memory: the diffusivity at a given time depends on the production and dissipation of the recent past, and through the transport term on production at other heights, not only on the local gradient at that instant. A first-order closure responds instantly: change the gradient, and K_m changes in the same time step.

The size of the memory follows from the dissipation term alone. With production switched off, equation (26.11) becomes $\mathrm{d}e/\mathrm{d}t = -c_\varepsilon e^{3/2}/l$. Writing it for $e^{-1/2}$, $\mathrm{d}(e^{-1/2})/\mathrm{d}t = c_\varepsilon/(2l)$, and integrating from e_0 at $t = 0$,

$$e(t) = \frac{e_0}{(1+a\,t)^2}, \qquad K_m(t) = \frac{K_m(0)}{1+a\,t}, \qquad a = \frac{c_\varepsilon\sqrt{e_0}}{2\,l}. \tag{26.13}$$

With illustrative values $e_0 = 1\,\mathrm{m^2\,s^{-2}}$, $l = 40\,\mathrm{m}$ and $c_\varepsilon = 0.064$, $a = 0.064/80 = 8.0\times10^{-4}\,\mathrm{s^{-1}}$. The initial time scale $e_0/\varepsilon_0 = l/(c_\varepsilon\sqrt{e_0}) = 625\,\mathrm{s}$ is about ten minutes; the energy halves after $(\sqrt{2}-1)/a = 518\,\mathrm{s}$, about nine minutes; after thirty minutes $1 + a\,t = 2.44$, so e has fallen to $0.17\,e_0$ and the diffusivity to 0.41 of its initial value.

Figure 26.3 draws this decay. The horizontal axis is time after production stops, from 0 to 60 minutes; the vertical axis is the ratio of each quantity to its initial value. The solid and dashed curves are e/e_0 and $K_m/K_m(0)$ from equation (26.13); the dotted line is what a first-order closure does with the same change, a drop of K_m to the value of the new local state, here zero, in one time step.

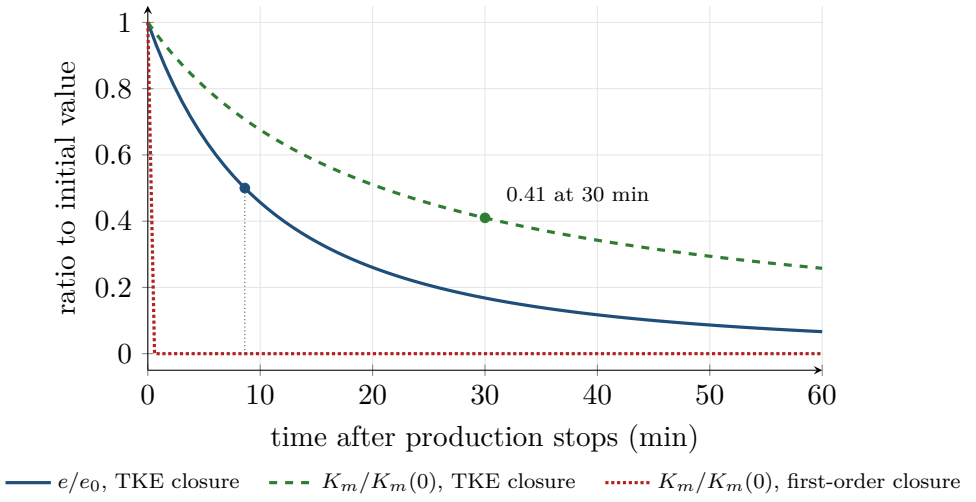


Figure 26.3: Memory of a TKE closure (illustrative). Decay of the turbulent kinetic energy and of the diffusivity after production stops, $e/e_0 = (1+at)^{-2}$ and $K_m/K_m(0) = (1+at)^{-1}$ with $a = c_\varepsilon\sqrt{e_0}/(2l) = 8.0\times10^{-4}\,\mathrm{s^{-1}}$ ($c_\varepsilon = 0.064$, $e_0 = 1\,\mathrm{m^2\,s^{-2}}$, $l = 40\,\mathrm{m}$); blue dot: the half-life of e, 8.6 min. Dotted red: a first-order closure, whose diffusivity follows the local state at once.

The diffusivity of the TKE closure falls slowly: more than a third of the initial mixing is still active half an hour after its source has gone, and a quarter after an hour. The first-order closure keeps none. The case is the evening transition of Chapter 6 in its simplest form: the surface heating stops near sunset, buoyancy production vanishes and then turns negative, and the real turbulence decays over tens of minutes, not instantly. A prognostic e follows that decay (negative buoyancy production in equation (26.11) makes it faster than the curve), and its transport term keeps turbulence alive in the upper part of a layer where the local production is small. The model can represent shear production, buoyancy, dissipation and turbulent transport separately, which a first-order closure cannot.

26.2.5 Comparison of closure orders

Table 26.1 compares the closures met in boundary-layer schemes. Its rows are the closures; its columns give the turbulence variables the scheme carries in time, how it obtains the diffusivity or the flux, and its main strength and weakness for the near-surface wind. The nonlocal rows are treated in Section 26.3.

Table 26.1: Closures used in boundary-layer schemes. Order counts the highest statistical moment carried by a prognostic equation.

Closure	Carried in time	Diffusivity or flux from	Strength	Weakness
First-order local	means only	$l^2\lvert\partial\mathbf{V}/\partial z\rvert\, F(\mathrm{Ri}_g)$	simple, cheap, robust; good in shear-driven and weakly stable air	no memory; cannot carry flux without a local gradient
First-order nonlocal (K-profile)	means only	prescribed $K(z)$ scaled by u_*, w_*, z_i, plus a counter-gradient term	daytime mixing and depth well represented	needs a diagnosed z_i; prescribed shape
One-and-a-half order (TKE)	means and e	$c_m l\sqrt{e}$	memory, transport, buoyancy and shear separately	length scale l still prescribed; local in convection unless augmented
Second order	means, all fluxes and variances	prognostic fluxes; third moments closed	anisotropy, counter-gradient fluxes from physics	many constants; cost; numerical delicacy
Eddy diffusivity plus mass flux	means (and often e)	$-K\,\partial\overline{\chi}/\partial z$ plus a plume term $M(\chi_u-\overline{\chi})$	thermals represented explicitly	plume model and its constants; more cost

The table reads from simple to elaborate, but not from worse to better: each level adds assumptions and constants, as Chapter 8 noted, and the right choice depends on the regime. Operational models mostly use the first-order nonlocal and the TKE rows, often combined, and add the mass-flux term in schemes built for convective afternoons.

26.3 Convective mixing and nonlocal schemes

A closure that looks only at the local gradient fails exactly where the daytime boundary layer is most energetic. This section defines local closure and where it works, shows why it fails in convection, builds the nonlocal diffusivity profile with its counter-gradient term and the mass-flux alternative, connects nonlocal mixing to the daytime wind, treats the diagnosis of the boundary-layer depth on which nonlocal schemes depend, and closes with two models that differ only in that depth.

26.3.1 Local closure

A *local closure* assumes that the turbulence at a level depends primarily on conditions at that level:

$$K_m(z) = \mathcal{F}\left(\mathrm{Ri}_g(z),\ l(z),\ |\partial \mathbf{V}/\partial z|\,(z)\right),$$

the first-order form (26.8) being the standard example. It is attractive because it is simple and physically intuitive: mixing is strong where the shear is strong and the stratification weak. The TKE closure is local in the same sense in its production and dissipation, though not in its transport.

Local closure works when the eddies that carry the flux are small compared with the distance over which the gradients change, so that an eddy samples one gradient during its excursion. That is the case in shear-driven turbulence near the ground, where $l = \kappa z$ is smaller than z itself, and in stable layers, where the stratification keeps the eddies small (Section 26.4.1). It therefore works reasonably well in stable conditions and in windy, near-neutral, shear-driven conditions.

26.3.2 Failure of local closure in convection

A thermal that leaves the surface layer rises through the mixed layer to about the boundary-layer top, illustratively 1000 m. It carries its excess heat over that whole distance, in roughly one convective time z_i/w_*, about eight minutes for $w_* = 2\,\mathrm{m\,s^{-1}}$. At midlevel the local potential-temperature gradient is nearly zero, because the thermals themselves have mixed it away, yet the heat flux there is still about 40 % of its surface value (the linear flux profile of Chapter 16). In the upper third of the mixed layer the gradient is slightly stable, $\partial\overline{\theta}/\partial z > 0$, while the flux is still upward. A local closure gives no flux where the gradient is zero and a downward flux where it is positive, the wrong answer in both places; to reproduce the measured flux it would need an infinite K_h at midlevel and a negative one above.

The statement is general:

> large convective eddies can transport quantities without a strong local gradient.

The flux at a height is set by eddies that start near the ground and span the layer, so it depends on the surface heating and on the depth, not on the local gradient. This violates the assumption behind every local diffusion form, and no choice of a positive local K_h repairs it.

26.3.3 The nonlocal diffusivity profile and the counter-gradient term

A *nonlocal closure* makes the transport depend on the structure of the whole boundary layer. Its most common form, the K-profile, has three ingredients. First, the depth z_i is diagnosed (Section 26.3.5). Second, the diffusivity is prescribed as a profile across the layer, small at the ground, large inside the turbulent layer and small again near and above the top; a conceptual and widely used shape is

$$K_m(z) = \kappa\, w_s\, z \left(1 - \frac{z}{z_i}\right)^2, \qquad 0 \le z \le z_i, \tag{26.14}$$

with w_s a velocity scale, close to u_*/ϕ_m near the ground and of the order of the convective velocity scale w_* in a convective layer, and with K_h from the same profile divided by Pr_t. Exact formulas vary between schemes. Third, a counter-gradient term is added to the flux,

$$F_\chi = -K_\chi \left(\frac{\partial \overline{\chi}}{\partial z} - \gamma_\chi\right), \qquad \gamma_\theta = C\,\frac{(\overline{w'\theta'})_0}{w_s\, z_i}, \tag{26.15}$$

where γ_χ is the nonlocal correction for the quantity χ, in units of its gradient, and for heat it is proportional to the surface kinematic heat flux $(\overline{w'\theta'})_0$, with a dimensionless coefficient C of

about 6.5 (Chapter 16). The extra term allows an upward flux even where $\partial\overline{\theta}/\partial z \approx 0$. Some schemes apply a similar term to momentum; many also prescribe the flux at the top of the layer, the entrainment flux, as a fraction of the surface flux.

The profile (26.14) has its maximum where its derivative, proportional to $(1-z/z_i)(1-3z/z_i)$, vanishes: at $z = z_i/3$, with $K_m = \kappa w_s (z_i/3)(2/3)^2 = (4/27)\,\kappa w_s z_i$. The nonlocal flux at mid-depth, $K_h\gamma_\theta$ with $w_s = w_*$ and $\mathrm{Pr}_t = 1$, is $\kappa w_* (z_i/2)(1/4) \times 6.5\,(\overline{w'\theta'})_0/(w_* z_i) = 0.325\,(\overline{w'\theta'})_0$, independent of the depth and of w_*. Take an illustrative afternoon with $(\overline{w'\theta'})_0 = 0.20\,\mathrm{K\,m\,s^{-1}}$ ($H \approx 240\,\mathrm{W\,m^{-2}}$) and $\overline{\theta} = 300\,\mathrm{K}$, and two depths. For $z_i = 1400\,\mathrm{m}$, $w_* = (9.81/300 \times 0.20 \times 1400)^{1/3} = 2.09\,\mathrm{m\,s^{-1}}$, the maximum diffusivity is $0.148 \times 0.4 \times 2.09 \times 1400 = 174\,\mathrm{m^2\,s^{-1}}$ at 467 m, and $\gamma_\theta = 6.5 \times 0.20/(2.09 \times 1400) = 4.4 \times 10^{-4}\,\mathrm{K\,m^{-1}}$. For $z_i = 700\,\mathrm{m}$, $w_* = 1.66\,\mathrm{m\,s^{-1}}$, the maximum is $69\,\mathrm{m^2\,s^{-1}}$ at 233 m, and $\gamma_\theta = 1.1 \times 10^{-3}\,\mathrm{K\,m^{-1}}$.

Figure 26.4 draws both cases. Panel (a) has the diffusivity on the horizontal axis and height on the vertical, for the two depths, with the dotted lines marking each z_i and the dots the maxima. Panel (b) uses dimensionless axes: height divided by z_i, and heat flux divided by the surface flux. Its solid line is a linear total flux with an entrainment ratio of 0.2 (Chapter 16), $\overline{w'\theta'}/(\overline{w'\theta'})_0 = 1 - 1.2\,z/z_i$; its dashed line is the nonlocal part $K_h\gamma_\theta$, which for the profile (26.14) with $w_s = w_*$ is $2.6\,(z/z_i)(1 - z/z_i)^2$ times the surface flux; its dotted line is the remainder, the part the local term $-K_h\,\partial\overline{\theta}/\partial z$ must carry.

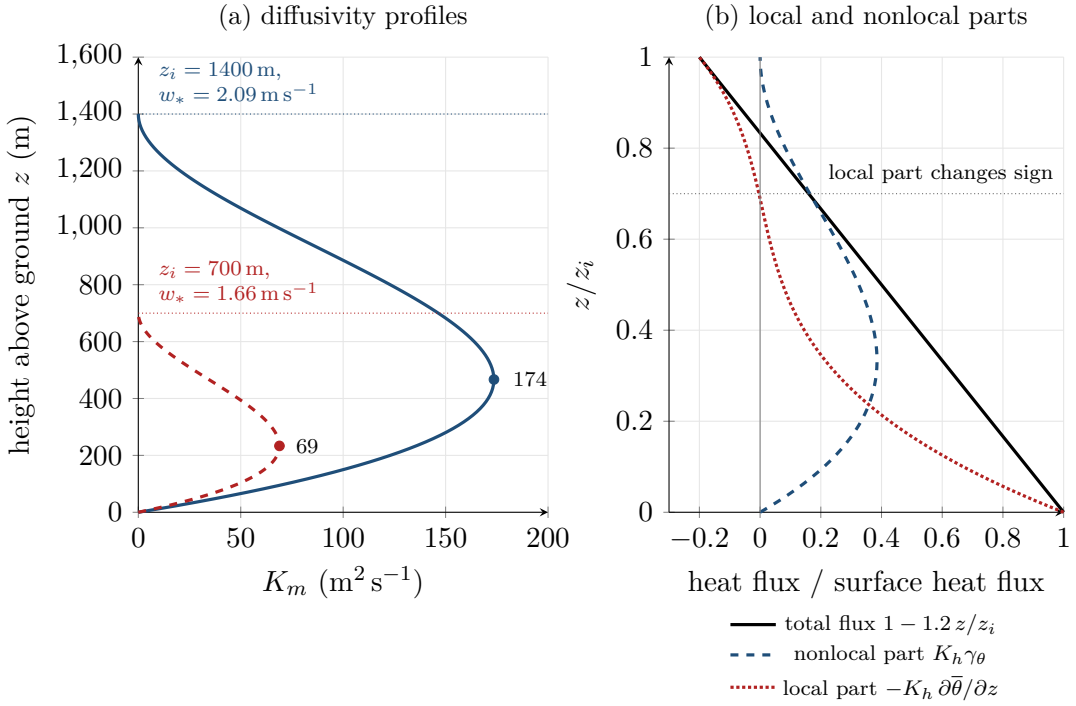


Figure 26.4: The nonlocal K-profile (illustrative). (a) $K_m = \kappa w_* z(1 - z/z_i)^2$ with $(\overline{w'\theta'})_0 = 0.20\,\mathrm{K\,m\,s^{-1}}$, $\overline{\theta} = 300\,\mathrm{K}$, $\kappa = 0.4$, for two depths; dots: maxima at $z_i/3$. (b) Decomposition of a linear heat flux with entrainment ratio 0.2 into the nonlocal part $K_h\gamma_\theta = 2.6\,(z/z_i)(1 - z/z_i)^2\,(\overline{w'\theta'})_0$ ($C = 6.5$, $\mathrm{Pr}_t = 1$) and the local remainder.

Panel (a) shows that a deeper layer is not only taller: its diffusivity is larger everywhere above the surface layer, because both w_* and z_i grow, and at 467 m the deep layer mixes with $174\,\mathrm{m^2\,s^{-1}}$ where the shallow one, near its own top, mixes with $\kappa \times 1.66 \times 467 \times (1 - 467/700)^2 = 34\,\mathrm{m^2\,s^{-1}}$. Panel (b) shows why the counter-gradient term is needed. Near the ground the local part carries most of the flux, through the steep superadiabatic gradient of the surface layer. At mid-depth the nonlocal part carries 0.325 of the surface flux out of a total of 0.40, and the local part only the rest. Above about $0.7\,z_i$ the local part is negative: the gradient there is slightly stable, the

local term carries heat down, and the nonlocal term alone keeps the total flux upward. This is the counter-gradient region of Chapter 9, represented.

Mass-flux schemes. A second family represents the thermals explicitly. Divide the grid column into updrafts, occupying a small area fraction a_u with vertical velocity w_u and value χ_u of the transported quantity, and an environment that occupies the rest. Since the mean vertical velocity is zero, the environment sinks at $w_e = -a_u w_u/(1-a_u)$, and the flux carried by this organized circulation works out, after the averaging over both parts, to $a_u w_u(\chi_u - \overline{\chi})/(1-a_u)$, or for a small updraft fraction $M(\chi_u - \overline{\chi})$, with $M = a_u w_u$ the kinematic mass flux, in $\mathrm{m\,s^{-1}}$. The scheme writes the total flux as

$$F_\chi = -K_\chi \frac{\partial \overline{\chi}}{\partial z} + M\,(\chi_u - \overline{\chi}),$$

small eddies by diffusion, thermals by the mass flux, and computes w_u and χ_u with a model of a plume rising from the surface layer and mixing with its surroundings. Illustratively, updrafts on 10 % of the area rising at $1.5\,\mathrm{m\,s^{-1}}$ and 0.4 K warmer than the mean carry $0.1 \times 1.5 \times 0.4 = 0.06\,\mathrm{K\,m\,s^{-1}}$, most of the $0.08\,\mathrm{K\,m\,s^{-1}}$ at mid-depth of the example above. Either way, by a counter-gradient term or by a mass flux, the scheme adds to the local diffusion a transport that responds directly to the surface heating.

26.3.4 Nonlocal mixing and the daytime wind

The same thermals carry momentum. Their downdrafts bring fast air from the upper mixed layer toward the surface, where it is slowed, and their updrafts carry slow air up; the result is the nearly uniform mixed-layer wind and the strong surface coupling of convective afternoons (Chapter 16). A purely local scheme sees almost no shear in the mixed layer and computes a small diffusivity from it: with $l = 67\,\mathrm{m}$ and an illustrative mixed-layer shear of $0.002\,\mathrm{s^{-1}}$, $l^2\mathcal{S} = 9\,\mathrm{m^2\,s^{-1}}$, and an unstable stability function of 2 to 4 raises it only to about 20 to $40\,\mathrm{m^2\,s^{-1}}$, against $150\,\mathrm{m^2\,s^{-1}}$ in the middle of the deep K-profile of Figure 26.4. The local diffusivity is also self-limiting: the mixing destroys the shear on which it depends.

A purely local scheme may therefore underestimate the downward transport of momentum by day and predict U_{10} too weak during convective afternoons, with a mixed-layer wind too fast and too much shear near the top of the surface layer. A nonlocal scheme, whose mixing depends on the heating and on z_i rather than on the shear, produces stronger surface coupling. For a wind farm or a transmission line the difference is in the afternoon wind at 10 to 150 m, the hours of strongest convective cooling of conductors.

26.3.5 Diagnosing the boundary-layer depth

Many schemes diagnose z_i at every time step and build the diffusivity profile on it, so that the diffusivity is small at the ground, large within the turbulent layer, and small again near or above the top. The model must therefore decide where the turbulence effectively ends, and the turbulence is not one of its variables. Table 26.2 lists the four usual methods. Its columns give the method, the height it returns as z_i, where it works best and its main weakness.

The bulk Richardson method is the most common. It computes, for each model level,

$$\mathrm{Ri}_B(z) = \frac{g}{\theta_{v,s}} \frac{\left[\overline{\theta_v}(z) - \theta_{v,s}\right] z}{\overline{u}(z)^2 + \overline{v}(z)^2}, \tag{26.16}$$

the ratio of the buoyancy difference between height z and the surface to the squared wind at z (taken relative to zero wind at the ground), and returns as z_i the lowest height at which Ri_B reaches a critical value Ri_{Bc}, interpolating between levels. The reference $\theta_{v,s}$ is the lowest-level

Table 26.2: Methods of diagnosing the boundary-layer depth in a model.

Method	z_i is the lowest height where	Works best	Weakness
Bulk Richardson number	Ri_B computed from the surface (or lowest level) reaches a critical value, 0.25 to 0.5	day and night; common default	depends on the critical value and on any thermal excess
TKE threshold	e falls below a threshold or a small fraction of its near-surface value	TKE schemes	threshold is arbitrary; residual turbulence aloft
Inversion strength	$\partial\overline{\theta_v}/\partial z$ is largest, or exceeds a threshold	convective layer with a sharp cap	ill-defined in stable or smooth profiles
Parcel method	a parcel rising from the surface with its θ_v (plus an excess) meets equal $\overline{\theta_v}$	convective layer	undefined at night; sensitive to the surface value

virtual potential temperature, sometimes with a thermal excess proportional to the surface heat flux added in convective conditions, to represent the warmer air that thermals carry.

Figure 26.5 applies the method to an illustrative afternoon profile. Panel (a) shows $\overline{\theta_v}$, panel (b) the wind speed, both against height from 0 to 2000 m; panel (c) shows Ri_B from equation (26.16) without (solid) and with (dashed) a thermal excess of 0.5 K, the dotted vertical lines marking two critical values, 0.25 and 0.5, and the dots the four resulting depths.

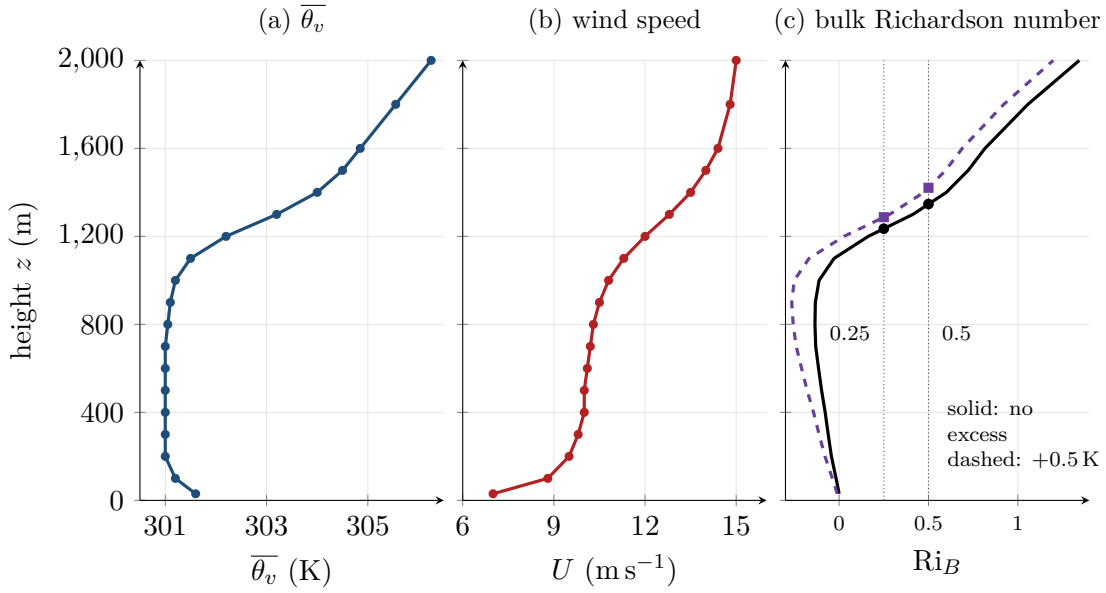


Figure 26.5: Bulk Richardson diagnosis of the boundary-layer depth on an illustrative afternoon profile (values at model levels, joined by straight lines). Ri_B from equation (26.16) with $g = 9.81\,\mathrm{m\,s^{-2}}$ and $\theta_{v,s} = 301.6\,\mathrm{K}$ (solid) or 302.1 K (dashed, thermal excess 0.5 K). Dots: diagnosed z_i for critical values 0.25 and 0.5.

The profile has a superadiabatic surface layer (301.6 K at 30 m), a mixed layer at 301.0 K up to about 900 m, a capping inversion that gains 3 K between 1100 and 1400 m, and a wind that is nearly uniform at $10\,\mathrm{m\,s^{-1}}$ in the mixed layer and rises to $15\,\mathrm{m\,s^{-1}}$ above. In the mixed layer $\overline{\theta_v} < \theta_{v,s}$ and Ri_B is negative; it turns positive in the inversion and climbs steeply. At 1300 m, without excess,

$$\mathrm{Ri}_B = \frac{9.81}{301.6} \times \frac{(303.2 - 301.6) \times 1300}{12.8^2} = 0.0325 \times \frac{2080}{163.8} = 0.413,$$

and at 1200 m it is 0.163, so $\mathrm{Ri}_{Bc} = 0.25$ is reached at $1200 + 100 \times (0.25 - 0.163)/(0.413 - 0.163) = 1235$ m. With $\mathrm{Ri}_{Bc} = 0.5$ the depth is 1347 m; with the thermal excess, 1287 and 1421 m. The parcel method on the same profile gives 1114 m without excess and 1186 m with it (the heights at which $\overline{\theta_v}$ reaches 301.6 and 302.1 K). Six defensible choices spread the depth over more than 300 m, a quarter of its value, on one and the same profile; on a stable night, where Ri_B grows gradually rather than across a sharp inversion, the spread can be a factor of two. Different schemes therefore diagnose different z_i, and with it a different volume over which momentum is mixed.

26.3.6 Two models with the same wind aloft

Suppose two models predict the same large-scale state, with a wind of $15\,\mathrm{m\,s^{-1}}$ above both boundary layers, at 2000 m for example. Model A diagnoses $z_i = 1400$ m and strong daytime mixing; model B diagnoses $z_i = 700$ m. Model A mixes high-momentum air down from a deeper layer, and the two might predict, illustratively,

$$U_{10,A} = 9\,\mathrm{m\,s^{-1}}, \qquad U_{10,B} = 6\,\mathrm{m\,s^{-1}}.$$

The large-scale forecasts are almost identical; the boundary-layer solutions are not.

A slab model of the mixed layer shows the part of this difference that the depth alone explains. Treat the mixed layer as one slab of depth z_i with a uniform wind $\mathbf{V}$, driven by the pressure gradient (through $\mathbf{V}_g$) and slowed by a surface stress $C_D|\mathbf{V}|\mathbf{V}$ spread over the depth, with C_D a drag coefficient for the mixed-layer wind and the stress at the top neglected. In steady state,

$$0 = -f\,\mathbf{k} \times (\mathbf{V} - \mathbf{V}_g) - \frac{C_D\,|\mathbf{V}|\,\mathbf{V}}{z_i}.$$

The Coriolis term on the ageostrophic wind $\mathbf{V}_a = \mathbf{V} - \mathbf{V}_g$ balances the drag, so $\mathbf{k} \times \mathbf{V}_a$ is parallel to $\mathbf{V}$: $\mathbf{V}_a$ is perpendicular to $\mathbf{V}$, and the three vectors form a right triangle with $\mathbf{V}_g$ as hypotenuse. Taking magnitudes, $|f|\,|\mathbf{V}_a| = C_D U^2/z_i$ and $U_g^2 = U^2 + |\mathbf{V}_a|^2$, so

$$U_g^2 = U^2 + r^2 U^4, \qquad r = \frac{C_D}{|f|\,z_i}, \qquad \tan\alpha = \frac{|\mathbf{V}_a|}{U} = r\,U, \tag{26.17}$$

with α the angle between the mixed-layer wind and the geostrophic wind. With $U_g = 15\,\mathrm{m\,s^{-1}}$, $|f| = 1.0 \times 10^{-4}\,\mathrm{s^{-1}}$ and an illustrative $C_D = 0.004$, model A has $r = 0.0286\,\mathrm{s\,m^{-1}}$; solving the quadratic in U^2, $U^2 = [-1 + (1 + 4r^2U_g^2)^{1/2}]/(2r^2) = 194$, so $U = 13.9\,\mathrm{m\,s^{-1}}$ and $\alpha = 21.7°$. Model B, with half the depth, has $r = 0.0571\,\mathrm{s\,m^{-1}}$, $U = 12.3\,\mathrm{m\,s^{-1}}$ and $\alpha = 35.1°$. The shallower layer carries the same surface drag in half the mass of air, so its wind is slower and crosses the isobars at a larger angle. The turning is toward low pressure: to the left of $\mathbf{V}_g$, counterclockwise, in the Northern Hemisphere, and to the right, clockwise, in the Southern Hemisphere, where $f < 0$ and low pressure lies on the right of the flow.

The depth alone thus explains a difference of $1.6\,\mathrm{m\,s^{-1}}$ in the mixed-layer wind and of 13° in direction. The rest of the example's $3\,\mathrm{m\,s^{-1}}$ at 10 m is in the strength of the mixing between the mixed layer and the ground, the "strong daytime mixing" of model A: its U_{10} is $9/13.9 = 0.65$ of its mixed-layer wind, model B's only $6/12.3 = 0.49$. Both effects are boundary-layer effects, and neither appears in the large-scale fields. The direction difference matters as much as the speed for a transmission line, whose cooling depends on the angle between the wind and the conductor.

26.4 Stable boundary-layer closures

At night the question a scheme must answer changes: not how far the thermals carry heat, but how much mixing should survive under stable stratification. This section describes stable

closure, the rate at which it should reduce the diffusivity, the minimum diffusivity that many models impose, the processes no local closure can represent, the role of the turbulent Prandtl number, and what all of this does to low-level jets.

26.4.1 Stable closure

Under stable stratification a local scheme reduces K_m as the Richardson number increases, through a stability function (Figure 26.2),

$$\text{more stable} \;\longrightarrow\; \text{larger } \mathrm{Ri}_g \;\longrightarrow\; \text{smaller } K_m.$$

A TKE scheme reaches the same result in two ways: the buoyancy term $-K_h N^2$ of equation (26.11) destroys turbulent kinetic energy, and the length scale is limited by the stratification. The second follows from energy. An eddy with vertical velocity of order $\sqrt{e}$ in a layer of buoyancy frequency N feels the restoring acceleration $N^2 s$ at a displacement s (Chapter 17), so its kinetic energy $e/2$ per unit mass is spent after $N^2 s^2/2 = e/2$, at $s = \sqrt{e}/N$. Schemes therefore limit the mixing length by a length of the form $l \le c_N \sqrt{e}/N$, with a coefficient c_N of order one half to one. With $e = 0.1\,\mathrm{m^2\,s^{-2}}$ and $N = 0.04\,\mathrm{s^{-1}}$, a moderate nocturnal inversion, $\sqrt{e}/N = 0.316/0.04 = 7.9\,\mathrm{m}$: the eddies of a stable layer are a few meters to tens of meters, whatever the height.

Small eddies are what make local closure suitable at night (Section 26.3.1). The difficulty of stable closure is therefore not its form but the amount of mixing it allows, which the next three subsections take up.

26.4.2 The rate of collapse of the diffusivity

How quickly K_m should fall with increasing stability is one of the hard parts of boundary-layer modeling. Take an illustrative stable layer at 25 m with the blended mixing length of equation (26.6), $l = 1/(1/10 + 1/80) = 8.9\,\mathrm{m}$, a shear $\mathcal{S} = 0.08\,\mathrm{s^{-1}}$ and $\mathrm{Ri}_g = 0.3$, so that $N^2 = 0.3 \times 0.08^2 = 1.92 \times 10^{-3}\,\mathrm{s^{-2}}$ and $\partial\overline{\theta}/\partial z = N^2\,\overline{\theta}/g = 0.056\,\mathrm{K\,m^{-1}}$ with $\overline{\theta} = 285\,\mathrm{K}$. The neutral diffusivity would be $l^2\mathcal{S} = 79 \times 0.08 = 6.3\,\mathrm{m^2\,s^{-1}}$. The short-tail function of Figure 26.2 gives zero: the layer is above the critical value and the model's turbulence is off. The long-tail function gives $F_m = 1/(1+3) = 0.25$ and $K_m = 1.6\,\mathrm{m^2\,s^{-1}}$, a momentum flux $1.6 \times 0.08 = 0.13\,\mathrm{m^2\,s^{-2}}$, $u_* = 0.36\,\mathrm{m\,s^{-1}}$, and with $\mathrm{Pr}_t = 1$ a heat flux $\overline{w'\theta'} = -1.6 \times 0.056 = -0.088\,\mathrm{K\,m\,s^{-1}}$, that is $H = 1205 \times (-0.088) = -106\,\mathrm{W\,m^{-2}}$ with $\rho c_p = 1205\,\mathrm{J\,m^{-3}\,K^{-1}}$.

The second result is not sustainable. A clear night removes about $60\,\mathrm{W\,m^{-2}}$ from the surface by net longwave radiation (Chapter 17), and only part of it is drawn from the air; a downward heat flux of $106\,\mathrm{W\,m^{-2}}$ would warm the surface air faster than radiation cools it. The model therefore cannot hold this gradient: its inversion erodes, its shear weakens, and it settles into a weaker, deeper, better-mixed stable layer. The first result has the opposite problem: with no mixing, nothing brings heat down to the cooling surface or momentum down to the slowing wind, and the model's surface layer decouples.

The consequences come in pairs, because one choice moves heat and momentum together. If K_m falls too rapidly, the surface wind becomes too weak, the inversion too strong and the near-surface temperature too cold. If K_m stays too large, the surface wind becomes too strong, the inversion too weak and the surface too warm. Chapter 17 tabulated the full pattern of these paired errors. The tradeoff between the two is the classic problem of stable boundary-layer modeling, and the real layer, with its intermittent turbulence, lies between the two curves of Figure 26.2 rather than on either.

26.4.3 Background diffusion

Some models impose a minimum diffusivity,

$$K_m \geq K_{\min} > 0,$$

called *background diffusion*. It prevents the model's turbulence from disappearing entirely. Numerically and operationally that improves robustness: without it, a model surface layer can cool without limit, its shear can grow until the numerics struggle, and the larger-scale forecast degrades.

The minimum is also a physical statement, and on very stable nights it is often too large. Take an illustrative very stable layer with shear $0.05\,\mathrm{s^{-1}}$ and $\partial\overline{\theta}/\partial z = 0.08\,\mathrm{K\,m^{-1}}$, $\mathrm{Ri}_g = (9.81/285 \times 0.08)/0.05^2 = 1.1$. With $K_{\min} = 1\,\mathrm{m^2\,s^{-1}}$ applied to both momentum and heat, the momentum flux is $0.05\,\mathrm{m^2\,s^{-2}}$, an apparent u_* of $0.22\,\mathrm{m\,s^{-1}}$, and the heat flux $-0.08\,\mathrm{K\,m\,s^{-1}}$, $-96\,\mathrm{W\,m^{-2}}$: far more than a very stable layer carries. With $K_{\min} = 0.1\,\mathrm{m^2\,s^{-1}}$ they are $0.005\,\mathrm{m^2\,s^{-2}}$ ($u_* = 0.07\,\mathrm{m\,s^{-1}}$) and $-9.6\,\mathrm{W\,m^{-2}}$, close to what such a night shows. A floor chosen for robustness can thus maintain too much mixing during very stable nights and produce the nighttime wind overprediction of Section 26.5.5. Background diffusion is a major modeling compromise: the model is kept stable at the price of a systematic bias in the weakest-wind nights.

26.4.4 Missing processes in the stable layer

Real stable boundary layers include intermittent turbulence, gravity waves, drainage flows, low-level jets and nonstationarity (Chapters 17 and 18). A local eddy-diffusivity model in a horizontally uniform column cannot represent all of that. Gravity waves carry momentum without much heat and without being turbulence; drainage flows are driven by horizontal pressure gradients over slopes that the model's smoothed terrain may not contain; the low-level jet is an inertial oscillation of the whole layer above the inversion; and intermittent turbulence is a sequence of bursts and quiet periods that no steady flux–gradient relation describes.

Intermittency also defeats averaging. Suppose, illustratively, that a half-hour contains a ten-minute burst at $\mathrm{Ri}_g = 0.1$ and twenty quiet minutes at $\mathrm{Ri}_g = 0.5$. With the short-tail function the burst mixes at $F_m = 0.36$ and the quiet period not at all, so the average mixing over the half-hour is $0.36/3 = 0.12$ of the neutral value. A scheme that sees the half-hour's mean state, $\mathrm{Ri}_g \approx (0.1 \times 10 + 0.5 \times 20)/30 = 0.37$, computes zero. Because the stability function is nonlinear, the flux of the mean state is not the mean of the fluxes. Stable boundary-layer parameterization is therefore not just a calibration problem: there are genuine missing processes, and no choice of constants in a local closure supplies them.

26.4.5 The turbulent Prandtl number

Momentum and heat need not mix at the same rate. The ratio

$$\mathrm{Pr}_t = \frac{K_m}{K_h} \tag{26.18}$$

is the turbulent Prandtl number, dimensionless, measured as the ratio of the two diffusivities inferred from a flux and gradient measurement of each and set in a model by the scheme. Chapter 14 showed that similarity theory with the standard forms gives $\mathrm{Pr}_t = \phi_h/\phi_m = 1$ in stable air and less than one in unstable air, where coherent plumes carry heat more efficiently than momentum; in very stable air, observations suggest values above one, because waves and pressure fluctuations still transport momentum when the transport of heat has nearly stopped. Its value may therefore depend on stability, and a model can mix wind and temperature differently.

The consequence is in the energy budget. The flux Richardson number is $\mathrm{Ri}_f = -P_b/P_s = K_h N^2/(K_m \mathcal{S}^2) = \mathrm{Ri}_g/\mathrm{Pr}_t$ (Chapter 13), and continuous turbulence requires that buoyancy not destroy everything shear produces, $\mathrm{Ri}_f < 1$, with values well below one in practice. A layer with Pr_t increasing with stability keeps Ri_f moderate while Ri_g exceeds 0.25: with an illustrative $\mathrm{Pr}_t = 1 + 4\,\mathrm{Ri}_g$, a layer at $\mathrm{Ri}_g = 0.5$ has $\mathrm{Pr}_t = 3$ and $\mathrm{Ri}_f = 0.17$. This is the physical basis of long-tail schemes: if heat is mixed less than momentum, turbulence can survive at gradient Richardson numbers above the critical value.

Why it matters for wind. Suppose $K_m > K_h$. Momentum then mixes more efficiently than heat: the wind profile is smoothed while the inversion that suppresses the mixing is retained. The relations among wind shear, temperature gradient and Richardson number change. In the layer of Section 26.4.2, with $\mathrm{Pr}_t = 1 + 4 \times 0.3 = 2.2$ instead of one, the long-tail heat flux falls from -106 to $-106/2.2 = -48\,\mathrm{W\,m^{-2}}$, a value the surface energy budget can supply, while the momentum flux, and the coupling of the surface wind to the wind aloft, stay the same. The wind and thermal structures are coupled but not identical, and a model tuned for its 2 m temperature through K_h is not thereby tuned for its 10 m wind through K_m.

26.4.6 Mixing and the low-level jet

A nocturnal low-level jet depends on decoupling (Chapter 18): once the mixing below collapses, the air above the inversion is freed of surface friction and its ageostrophic wind turns with the inertial oscillation, of period $T_I = 2\pi/|f|$, to give a supergeostrophic maximum some hours after sunset. A boundary-layer scheme that keeps too much mixing does two things: it smears the jet vertically, spreading its momentum over a deeper layer with a weaker, higher maximum, and it keeps bringing that momentum down, so the surface winds are too strong. A scheme with too little mixing leaves the jet too sharp, too strong and too low, over a surface that is too calm.

A diffusion time sets the scale of the effect. Mixing with diffusivity K_m smooths a layer of depth h in a time of order h^2/K_m. For an illustrative jet layer $h = 200\,\mathrm{m}$ deep, h^2/K_m is 56 h with $K_m = 0.2\,\mathrm{m^2\,s^{-1}}$, 11 h with $1\,\mathrm{m^2\,s^{-1}}$ and 2.2 h with $5\,\mathrm{m^2\,s^{-1}}$. At 35° of latitude, north or south, $|f| = 8.37 \times 10^{-5}\,\mathrm{s^{-1}}$ and $T_I = 20.9$ h, and the jet needs several hours of undisturbed oscillation to reach its maximum. With the first value the oscillation runs nearly free; with the last it is damped within a few hours, before the jet can form. Low-level jet structure is therefore very sensitive to the stable formulation of the scheme, including its background diffusion, and the height and speed of a modeled jet are as much a property of the scheme as of the atmosphere.

26.5 The boundary-layer scheme inside the weather model

A boundary-layer scheme does not work alone. This section separates it from the surface-layer scheme beneath it, states what happens when the two disagree, follows both into the model's 10 m wind, interprets a daytime and a nighttime wind error, and treats the boundary-layer height as an output field.

26.5.1 Surface-layer scheme and boundary-layer scheme

The two terms are easy to confuse. The *surface-layer scheme* handles the lowest part of the column, between the ground and the lowest model level z_1. It applies Monin–Obukhov similarity (Chapter 14) to the wind and potential temperature at z_1, the roughness length of the grid cell and the surface temperature, and solves iteratively for the surface stress, the heat and moisture fluxes, u_*, θ_* and L_O; it also diagnoses the 10 m wind and the 2 m temperature. The *boundary-layer scheme* handles turbulent vertical transport through the deeper layer above, from

the lowest interface to z_i and beyond, with the surface fluxes as its lower boundary condition. The surface-layer scheme relates surface stress, heat flux, roughness and near-surface variables; the boundary-layer scheme relates the resolved profiles to the fluxes in between.

Figure 26.6 shows how the two are connected inside the model's time step. Each box is a component of the model; each arrow is a quantity passed from one to the other. The loop runs clockwise from the land-surface model at the upper left; the two boxes at the bottom are output fields that users receive.

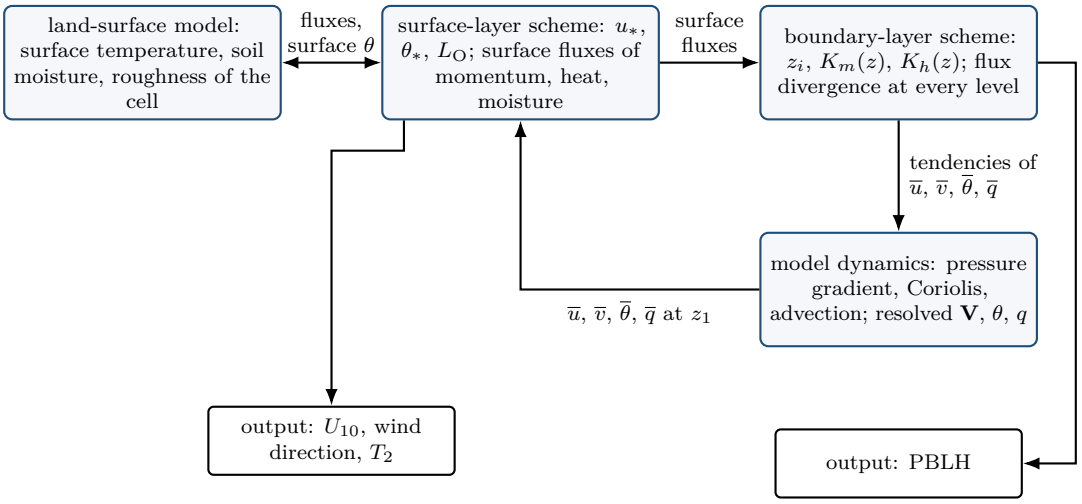


Figure 26.6: Coupling of the surface-layer scheme and the boundary-layer scheme in one model time step (schematic). The surface-layer scheme turns the lowest-level state into surface fluxes and the diagnosed near-surface fields; the boundary-layer scheme turns the surface fluxes and the resolved profiles into tendencies; the dynamics update the resolved state.

The figure makes two points. The 10 m wind leaves the model from the surface-layer scheme, not from the boundary-layer scheme, but the lowest-level wind it is computed from has just been updated with the boundary-layer tendencies. And the depth z_i, reported as PBLH, is an internal variable of one scheme, made visible. Both points return in the subsections that follow.

26.5.2 Consistency between the two schemes

The two schemes must work together consistently. Suppose the surface-layer scheme predicts a strong stress, $u_* = 0.6\,\mathrm{m\,s^{-1}}$, a surface flux of $-0.36\,\mathrm{m^2\,s^{-2}}$, while the boundary-layer scheme mixes weakly above, with $K_m = 2\,\mathrm{m^2\,s^{-1}}$ at the 60 m interface and a shear of $0.03\,\mathrm{s^{-1}}$ there, a flux of $-0.06\,\mathrm{m^2\,s^{-2}}$. The lowest layer then loses $0.36\,\mathrm{m^2\,s^{-2}}$ through the ground and receives only 0.06 from above, and its wind changes at $-(-0.06 + 0.36)/60 = -5.0 \times 10^{-3}\,\mathrm{m\,s^{-2}}$, $-18\,\mathrm{m\,s^{-1}}$ per hour. Within minutes the lowest-level wind collapses, the stress the surface-layer scheme computes from it falls, and the profile develops a kink between the first and second levels that neither scheme intended. Momentum transfer is inconsistent across the interface between the two schemes.

The condition for consistency is that the two describe the same turbulence where they meet: near the lowest level, the boundary-layer diffusivity should approach the surface-layer value, $K_m(z) \to \kappa u_* z/\phi_m(z/L_O)$; here $\kappa u_* z = 0.4 \times 0.6 \times 60 = 14\,\mathrm{m^2\,s^{-1}}$ in neutral air, seven times what the boundary-layer scheme supplied. The stability seen by the two must also agree: a surface-layer scheme that finds $L_O = 50\,\mathrm{m}$, stable, under a boundary-layer scheme that computes a negative Richardson number at the first interface produces fluxes of opposite tendency on either side of z_1. Models therefore usually pair surface-layer and boundary-layer formulations designed to work together, and a configuration that mixes a surface-layer scheme from one

family with a boundary-layer scheme from another needs checking.

26.5.3 How the two schemes set the 10 m wind

The 10 m wind of a model depends on both schemes. The surface-layer scheme diagnoses it from the lowest level (Chapters 12 and 14),

$$U_{10} = U(z_1)\,\frac{\ln(10\,\mathrm{m}/z_0) - \psi_m(10\,\mathrm{m}/L_\mathrm{O})}{\ln(z_1/z_0) - \psi_m(z_1/L_\mathrm{O})}, \tag{26.19}$$

with the direction usually taken from the lowest level. The lowest-level wind $U(z_1)$ is itself the product of boundary-layer mixing: it is the wind that the column's diffusivity profile leaves at z_1 between the momentum brought down from aloft and the momentum lost to the ground.

With $z_1 = 30\,\mathrm{m}$ and $z_0 = 0.1\,\mathrm{m}$, the neutral ratio is $\ln 100/\ln 300 = 4.605/5.704 = 0.807$. If the boundary-layer scheme leaves $U(z_1) = 8\,\mathrm{m\,s^{-1}}$, $U_{10} = 6.46\,\mathrm{m\,s^{-1}}$; if a less mixed column leaves $6\,\mathrm{m\,s^{-1}}$, $U_{10} = 4.84\,\mathrm{m\,s^{-1}}$. If instead the surface-layer scheme finds a stable $L_\mathrm{O} = 50\,\mathrm{m}$, with $\psi_m = -5z/L_\mathrm{O}$, the ratio becomes $(4.605+1.0)/(5.704+3.0) = 0.644$, and the same $8\,\mathrm{m\,s^{-1}}$ gives $5.15\,\mathrm{m\,s^{-1}}$. A difference of 1.3 to $1.6\,\mathrm{m\,s^{-1}}$ at 10 m can therefore come from either scheme, and U_{10} contains information from both parameterizations. Comparing a model with a mast at z_1 separates them: the boundary-layer scheme is tested by the wind at z_1, the surface-layer scheme by the ratio.

26.5.4 A daytime underprediction

Suppose observations show $U_{10} = 9\,\mathrm{m\,s^{-1}}$ on a sunny afternoon, the model predicts $5\,\mathrm{m\,s^{-1}}$, and the model's wind at 300 m is accurate, say $11\,\mathrm{m\,s^{-1}}$ against $11\,\mathrm{m\,s^{-1}}$ observed. The observed ratio $U_{10}/U_{300} = 0.82$ is typical of a well-mixed convective layer; the model's 0.45 is typical of a weakly mixed one. With the wind aloft right, the large-scale forcing is not the cause. A possible interpretation is

insufficient downward momentum mixing,

with three potential causes, each checkable. The diagnosed boundary layer may be too shallow, which a radiosonde, lidar or ceilometer profile can test against the model's z_i. The nonlocal mixing may be too weak, as with the local scheme of Section 26.3.4. Or the surface heat flux may be too small, from a soil that is too wet or a cloud cover that is wrong: since $w_* \propto [(\overline{w'\theta'})_0 z_i]^{1/3}$ and the K-profile is proportional to w_*, halving the heat flux lowers w_* and the diffusivity by a factor $2^{1/3} = 1.26$, about 21 %, before the shallower growth of the layer is counted.

Table 26.3 sets this case beside the nighttime case of the next subsection. Its rows are the symptom, the interpretation, the likely causes and the checks; its two columns are the two cases.

26.5.5 A nighttime overprediction

Suppose now that on a clear night the observed U_{10} is $2\,\mathrm{m\,s^{-1}}$, the model gives $6\,\mathrm{m\,s^{-1}}$, and the model's wind at 200 m is about right, say $10\,\mathrm{m\,s^{-1}}$. The observed shear between 10 and 200 m is $(10-2)/190 = 0.042\,\mathrm{s^{-1}}$, the modeled one half of it, $(10-6)/190 = 0.021\,\mathrm{s^{-1}}$. The pattern suggests

too much stable mixing,

rather than wrong synoptic forcing: the momentum aloft is right, and the model has brought too much of it down. The confirming evidence is the paired error of Section 26.4.2: a 2 m temperature too warm and an inversion too weak in the same hours. The usual suspects are a long-tail stability function, a background diffusivity of the size of Section 26.4.3, or a stable layer diagnosed too deep.

Table 26.3: Two characteristic wind errors of a boundary-layer scheme (illustrative numbers).

	Sunny afternoon	Clear night
Symptom	U_{10} observed $9\,\mathrm{m\,s^{-1}}$, modeled $5\,\mathrm{m\,s^{-1}}$; U_{300} accurate	U_{10} observed $2\,\mathrm{m\,s^{-1}}$, modeled $6\,\mathrm{m\,s^{-1}}$; U_{200} accurate
Interpretation	insufficient downward momentum mixing	too much stable mixing
Likely causes	boundary layer too shallow; nonlocal mixing too weak; surface heat flux too small	long-tail stability function; background diffusion; stable layer too deep
Checks	model z_i against a sounding or lidar; model H against a flux station; shear between 10 and 300 m	2 m temperature too warm; inversion too weak; shear between 10 and 200 m too weak
Not the cause	synoptic forcing (wind aloft is right)	synoptic forcing (wind aloft is right)

The two examples show the method of reading a boundary-layer error: fix the wind aloft first, then compare the ratio of the near-surface wind to it, then look for the paired error in temperature. An error in U_{10} that comes with a correct wind aloft and a matching error in the near-surface temperature belongs to the mixing; an error in U_{10} without either belongs elsewhere, to the forcing, the roughness or the representativeness of the station (Chapter 23).

26.5.6 Boundary-layer height as a model output

Models often provide PBLH, the planetary boundary-layer height, as an output field. It is useful: it measures the depth of mixing, the volume into which surface emissions are diluted, and the height below which the wind is coupled to the surface. But PBLH is scheme-dependent. Two models can produce different heights from similar atmospheres because they use different definitions: a critical bulk Richardson number of 0.25 or 0.5, with or without a thermal excess, a TKE threshold, an inversion or a parcel criterion. On the profile of Figure 26.5 the definitions of Table 26.2 give heights from 1114 to 1421 m.

PBLH is therefore not always a directly comparable physical observable. Observed depths are scheme-dependent too: a lidar or ceilometer detects the top of the aerosol layer, a radiosonde the base of the inversion, a sodar or a wind profiler the top of the turbulence, and on a stable night or in the morning transition the three can differ by hundreds of meters. A fair comparison applies the same definition to both, for example the model's own bulk Richardson algorithm to an observed radiosonde profile, or the observational criterion to the model's profiles.

26.6 Grid resolution and scale awareness

Everything so far assumed that the grid resolves none of the boundary-layer turbulence. This section compares the closure philosophies, introduces schemes that adapt to the grid spacing, separates convection-permitting from turbulence-resolving grids, describes the approach to large-eddy simulation and the gray zone between, explains why a parameterization is not a defect, and closes with a diagnostic hierarchy for two configurations that disagree.

26.6.1 Closure philosophies compared

Three philosophies run through the chapter. Figure 26.7 draws each as a chain from what the scheme reads to the flux it returns. Each row is one philosophy; each box is a step, and the arrows give the order.

Rows (a) and (b) both end in a diffusivity and a down-gradient flux; they differ in what lies between, an instantaneous diagnosis against a budget with memory. Row (c) differs in where it

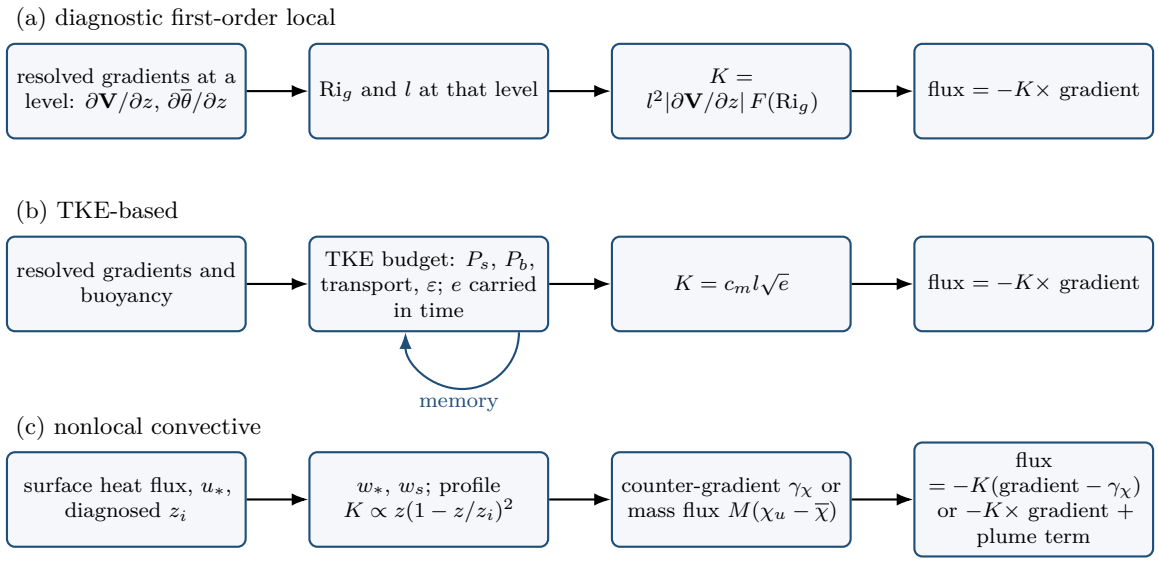


Figure 26.7: Three closure philosophies (schematic). (a) A diagnostic first-order local closure turns local gradients into a diffusivity at each time step. (b) A TKE closure passes through a prognostic turbulent kinetic energy that carries memory from one time step to the next. (c) A nonlocal convective closure builds the transport from the surface forcing and the depth of the layer, adding large-eddy transport over substantial vertical distances.

starts: at the surface and the top of the layer, not at the local gradient, and its last box admits a flux with no local gradient at all. Many modern schemes combine aspects of these approaches: a TKE closure for the stable and shear-driven parts of the column with a nonlocal or mass-flux term for convective conditions, switching or blending according to the sign of the surface heat flux.

26.6.2 Scale-aware schemes

As the grid spacing becomes finer, part of the turbulence becomes explicitly resolved, and the parameterization should contribute less; otherwise the same transport is counted twice. A *scale-aware* scheme makes its diffusivity, or its other subgrid effects, depend on the grid spacing:

$$\Delta x \text{ decreases} \longrightarrow \text{more turbulence resolved} \longrightarrow \text{less turbulence parameterized.}$$

A simple way to write it multiplies the diffusivity of a conventional scheme by a partition function, $K_{\mathrm{sg}} = \mathcal{P}(\Delta x/z_i)\,K$, with $\mathcal{P}$ the fraction of the turbulent transport that is subgrid, near one for $\Delta x \gg z_i$ and near zero for $\Delta x \ll z_i$. The natural argument is $\Delta x/z_i$, because the energy-carrying eddies of the boundary layer have the size of its depth.

Figure 26.8 draws an illustrative partition function. The horizontal axis is the ratio $\Delta x/z_i$ on a logarithmic scale, from 0.01 to 100; the vertical axis is a fraction of the turbulent transport. The solid curve is the subgrid fraction $\mathcal{P}$, the dashed curve the resolved fraction $1 - \mathcal{P}$, and the shaded band the range in which neither is below 10 %. The marked points are five combinations of grid spacing and depth discussed below.

With a daytime depth of 1400 m, a 3 km grid has $\Delta x/z_i = 2.1$ and parameterizes 98 % of the transport; a 500 m grid has 0.36 and parameterizes 59 %; a 100 m grid has 0.07 and parameterizes 5 %. At night, with $z_i = 200$ m, the same 100 m grid has $\Delta x/z_i = 0.5$ and still parameterizes 74 %: a grid that nearly resolves the afternoon's thermals is in the middle of the gray zone at night. Doing this smoothly is difficult. The function in the figure is a smooth curve, but the resolved turbulence is not guaranteed to appear just because the grid could carry

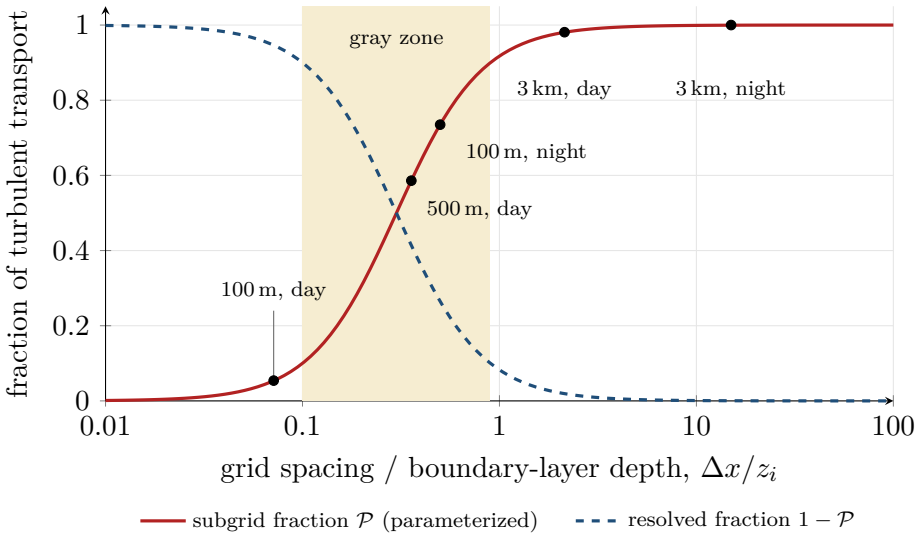


Figure 26.8: An illustrative partition between parameterized and resolved boundary-layer transport, $\mathcal{P} = (x/0.3)^2/[1 + (x/0.3)^2]$ with $x = \Delta x/z_i$. Shaded: $0.1 < x < 0.9$, where both fractions exceed 10 %. Points: grid spacings of 100 m, 500 m and 3 km with a daytime depth $z_i = 1400$ m and a nighttime depth $z_i = 200$ m.

it: resolved eddies take time to develop from the model's initial state and its numerics damp the smallest of them. A scheme that reduces its diffusivity on schedule can then leave transport missing, and one that does not can count it twice.

26.6.3 Convection-permitting and turbulence-resolving grids

A model with $\Delta x = 3$ km may represent deep thunderstorms explicitly rather than through a convection scheme: their updrafts are several kilometers wide and the storms span ten kilometers or more, so the grid carries them, coarsely. Such a model is called *convection-permitting*: it permits deep convection, without fully resolving its internal structure.

It still cannot resolve most boundary-layer turbulent eddies. The largest thermals are about z_i wide, one to two kilometers, below the grid spacing itself and far below the effective resolution of several grid lengths (Chapter 5); the eddies near the ground are smaller still. Figure 26.8 places the 3 km grid at $\mathcal{P} = 0.98$ by day and 1.0 at night: the boundary-layer scheme is in full use. So

$$\text{convection permitting} \neq \text{boundary-layer turbulence resolving},$$

a distinction that matters whenever a convection-permitting model is assumed to have resolved the near-surface wind's turbulence and its gusts. It has resolved the storms, not the boundary layer.

26.6.4 The approach to large-eddy simulation

At sufficiently fine resolution, perhaps $\Delta x \sim 10$ to 100 m depending on the problem, the large boundary-layer eddies begin to be explicitly represented, and the model moves toward large-eddy simulation (LES; Chapter 5) rather than a conventional boundary-layer parameterization. Its subgrid model then represents only the small eddies, often with a subgrid turbulent kinetic energy, and the role of the boundary-layer scheme ends.

The range follows from comparing the grid spacing with the boundary-layer depth. An eddy is represented reasonably only if it spans several grid lengths, five to ten. The energy-carrying

eddies of a convective layer are about z_i across, so resolving them needs $\Delta x \lesssim z_i/10$: about 140 m for $z_i = 1400$ m, the upper end of the range. Those of a stable layer 200 m deep are tens of meters, which needs a few meters, below the lower end. Near the ground the eddies scale with the height itself, so the lowest meters stay subgrid at any practical spacing and need a surface model even in LES. The transition is gradual: which eddies are resolved depends on the regime, the height and the time of day, not on the grid alone.

26.6.5 The gray zone

At $\Delta x \sim 100$ to 1000 m some large eddies may be resolved, but not adequately: they are present on the grid, distorted by it, with sizes set partly by the grid spacing rather than by the physics. Chapter 5 called this range the gray zone, and Figure 26.8 shades it. A conventional boundary-layer scheme still assumes that all the turbulence is unresolved, and its full diffusivity mixes away the gradients that would drive the resolved thermals, or coexists with them and counts their transport twice. The mismatch can produce unrealistic behavior: convective rolls and cells whose spacing is a few grid lengths, a mixed layer that grows too fast or too slowly, and a near-surface wind whose variability depends on the grid.

High-resolution near-surface wind modeling is therefore not simply a matter of making the grid smaller. A run at 500 m is not a better version of the same model at 3 km; it is a model in a different regime, whose boundary-layer scheme must know what part of the turbulence the grid now carries.

26.6.6 Parameterization as the average effect of unresolved processes

A common misconception holds that resolved physics is real and parameterized physics is fake. It is not so. A parameterization is an attempt to represent the average effect of unresolved processes on the resolved state, and at operational weather-prediction scales it is unavoidable: no grid of kilometers can carry eddies of meters, and the column equations (26.1) need the flux divergence whether the grid resolves the eddies or not. Even an LES parameterizes its smallest eddies, and an anemometer's ten-minute mean is itself an average over turbulence it does not report. The resolved field of any model is a filtered representation of the atmosphere, and the parameterization supplies what the filter removed.

The relevant question about a scheme is therefore not whether it is real but

whether its assumptions are appropriate for the regime and the resolution.

A K-profile with a counter-gradient term is a good assumption for a convective afternoon on a 3 km grid and a poor one for a very stable night; a short-tail local closure is the reverse; any conventional scheme is a poor assumption in the gray zone. The errors of Sections 26.5.4 and 26.5.5 are errors of applicability, not proofs that parameterization fails.

26.6.7 A diagnostic hierarchy

If two weather-model configurations differ in their near-surface wind, the chapter's chain gives an order in which to compare them. Table 26.4 lists it. Its rows run from the large scale to the turbulence; its columns give what to compare and what a difference at that step implies.

The order matters. Steps 1 and 2 rule the forcing in or out, as in the two examples of Section 26.5; steps 3 to 7 locate the difference in the depth, the coupling, the surface forcing or the regime; step 8, the diffusivity profile, is reached last because differences in all the other quantities change K_m even when the closures are identical. Followed in order, the comparison can often identify why two forecasts differ, not only by how much. The surface beneath the column, its terrain height, roughness and land cover, enters steps 5 to 7 through the surface-layer scheme and is the subject of the next chapter, on terrain and land-surface representation in weather models (Chapter 27).

Table 26.4: A diagnostic hierarchy for two configurations whose near-surface winds differ. Stop at the first step that shows a material difference.

	Quantity	Compare	A difference means
1	Large-scale pressure field	sea-level pressure and geopotential gradients; geostrophic wind	the forcing differs; the boundary layer is not the first suspect
2	Wind above the boundary layer	wind at a level above both z_i	the forcing reaching the boundary layer differs
3	Boundary-layer height	PBLH, with each model's definition stated	the depth over which momentum is mixed differs (Section 26.3.6)
4	Vertical wind shear	U at z_1, 100, 300 m; ratio U_{10}/U aloft	the coupling of the surface to the flow aloft differs
5	Surface heat flux	H and $(\overline{w'\theta'})_0$	the convective forcing differs (by day) or the cooling (by night)
6	Friction velocity u_*	surface-layer output	the surface stress or the roughness differs
7	Stability	L_{O}, Ri_g near the ground	the regime each model sees differs
8	Eddy diffusivity K_m	profile of K_m through the layer	the closure itself differs for the same state

26.7 What to retain

Definition 26.1 (Boundary-layer parameterization)**.** A boundary-layer scheme answers one question: given the resolved state, how much momentum and heat should turbulence transport vertically? For the wind this reduces to estimating $K_m(z)$ correctly: too much mixing couples the surface too strongly to the winds aloft, too little leaves it too decoupled, which is why two models with nearly identical synoptic forecasts can produce very different near-surface winds.

Table 26.5 lists the terms of the chapter, their meaning, their units and the subsection that defines each.

26.8 Exercises

Exercise 26.1. A model column has full levels at 30 and 90 m, where the eastward wind is 6.0 and 7.5 $\mathrm{m\,s^{-1}}$ (no northward component), and an interface at 60 m. The surface friction velocity from the surface-layer scheme is 0.35 $\mathrm{m\,s^{-1}}$. (a) Compute the mixing length at 60 m with equation (26.6) and $l_\infty = 80$ m, and the neutral diffusivity there. (b) Compute the momentum flux at the interface; state its sign and what it means. (c) Compute the tendency of the wind of the lowest layer (0 to 60 m) due to turbulence alone, in $\mathrm{m\,s^{-1}}$ per hour, and explain why it is positive. (d) With $\mathrm{Ri}_g = 0.15$ at the interface, recompute the diffusivity and the flux with the short-tail and the long-tail functions of Figure 26.2.

Exercise 26.2. On a clear night a layer between 10 and 50 m has a wind difference of 4 $\mathrm{m\,s^{-1}}$ in one direction and $\Delta\theta = 2$ K, with $\overline{\theta} = 285$ K, $l = 8$ m and $\rho c_p = 1205\,\mathrm{J\,m^{-3}\,K^{-1}}$. (a) Compute $\mathcal{S}$, N^2 and Ri_g. (b) Compute K_m, the momentum flux and the apparent u_* with each stability function of Figure 26.2. (c) Compute the sensible heat flux H with $\mathrm{Pr}_t = 1$ for each, and with $\mathrm{Pr}_t = 1 + 4\,\mathrm{Ri}_g$ for the long tail; compare with a net longwave loss of 60 $\mathrm{W\,m^{-2}}$ and state which results the surface can sustain. (d) The model imposes $K_{\min} = 1\,\mathrm{m^2\,s^{-1}}$. Which of the results of (b) changes, and to what?

Exercise 26.3. An afternoon has $H = 300\,\mathrm{W\,m^{-2}}$, $\rho c_p = 1205\,\mathrm{J\,m^{-3}\,K^{-1}}$ and $\overline{\theta} = 303$ K. (a) For $z_i = 1200$ m compute $(\overline{w'\theta'})_0$ and w_*. (b) With equation (26.14) and $w_s = w_*$, compute the

Table 26.5: The terms of the chapter and where each is defined.

Term	Meaning	Units	Defined in
Boundary-layer (PBL) parameterization	model of unresolved boundary-layer turbulent transport in each grid column	–	26.1
Closure	relationship used to estimate unresolved turbulent terms from resolved quantities	–	26.1.3
Eddy diffusivity K_m, K_h	effective turbulent mixing coefficients, flux $= -K\times$ gradient	$\mathrm{m^2\,s^{-1}}$	26.1.4
Mixing length l	eddy excursion length; κz near the ground, limited aloft	m	26.2.1
First-order closure	fluxes modeled from local mean gradients; only the means carried in time	–	26.2.2
Stability function F_m	factor multiplying the neutral diffusivity, a function of Ri_g; short or long tail	–	26.2.2
TKE closure	scheme that predicts e and builds $K_m = c_m l\sqrt{e}$	–	26.2.3
Local closure	turbulence determined mainly from local conditions	–	26.3.1
Nonlocal closure	includes transport by eddies across substantial vertical distances	–	26.3.3
Counter-gradient term γ_χ	nonlocal correction allowing flux without a local gradient	units of the gradient	26.3.3
Mass flux M	$a_u w_u$: area fraction times vertical velocity of the updrafts of a plume model	$\mathrm{m\,s^{-1}}$	26.3.3
Background diffusion	minimum imposed turbulent mixing, $K_{\min}$	$\mathrm{m^2\,s^{-1}}$	26.4.3
Turbulent Prandtl number Pr_t	K_m/K_h; may depend on stability	–	26.4.5
Surface-layer scheme	similarity solution between the ground and z_1; surface fluxes, U_{10}, T_2	–	26.5.1
Scale-aware scheme	parameterization that adapts to the model resolution through $\Delta x/z_i$	–	26.6.2
Convection-permitting	grid that carries deep convection explicitly but not boundary-layer eddies	–	26.6.3
PBLH	diagnosed planetary boundary-layer height; scheme-dependent	m	26.3.5, 26.5.6

maximum diffusivity and its height, and the diffusivity at $z_i/2$. (c) Compute γ_θ with $C = 6.5$, and the heat flux carried by the nonlocal term at $z_i/2$; compare it with the linear flux profile of Figure 26.4(b). (d) A model's lowest level has $\overline{\theta_v} = 300.8\,\mathrm{K}$; above, it has $\overline{\theta_v} = 301.0$, 302.4 and 303.6 K with wind speeds 10, 12 and $13\,\mathrm{m\,s^{-1}}$ at 1100, 1300 and 1500 m. Compute Ri_B at the three heights with equation (26.16) and diagnose z_i for $\mathrm{Ri}_{Bc} = 0.25$ and 0.5. Which value is closer to the 1200 m of part (a), and what does the difference do to the diffusivity profile?

Exercise 26.4. A site at 30°S lies under a geostrophic wind of $15\,\mathrm{m\,s^{-1}}$ from 090°. A transmission line runs east–west past the site. Two model configurations diagnose afternoon depths of 1400 and 700 m. (a) Compute $|f|$, and with the slab model of equation (26.17) and $C_D = 0.004$ the mixed-layer wind speed and the angle α for each depth. (b) In which sense, clockwise or counterclockwise, is the mixed-layer wind turned from the geostrophic wind in this hemisphere? Give the direction from which it blows in each configuration. (c) Compute the angle between the wind and the conductor in each case, and state which configuration gives the larger convective cooling at the same speed. (d) If both models have $U_{10}/U_{\mathrm{ML}} = 0.7$, compute U_{10} for each, and state which step of Table 26.4 would first reveal the cause of the difference.

Chapter 27

Terrain and Land-Surface Representation in Weather Models

27.1 The effective surface of a grid cell

A weather model computes the wind over a surface it has to be told about: the height of the ground, the drag of what stands on it, and how it heats and moistens the air. It cannot be told about the real surface in full, because the real surface varies on every scale down to single trees and buildings and the model holds one value of each property per grid cell. Chapter 5 showed terrain averaged over grid cells of two sizes; Chapter 11 defined the effective roughness of a mixed grid cell; Chapter 20 showed a ridge lowered and broadened by a weather model and the drag of terrain the model cannot resolve. This chapter brings these results together and extends them to the whole land surface. Its question is

how does a numerical weather model represent real terrain and surface heterogeneity on a finite grid, and what does that representation do to the near-surface wind it computes?

The question matters for near-surface wind because the model does not see the hill, the forest edge, the road or the valley that an instrument sees. It sees a grid-scale approximation of them, and the wind it computes is the wind over that approximation. The chapter first describes what one grid cell holds; it then treats the terrain, the land cover, the terrain too small to resolve, and the thermal state of the surface, and ends with the consequences for validating and correcting model winds.

Jargon: effective surface, terrain smoothing, effective elevation, land-use class, land-surface model, mosaic representation, land-sea mask, subgrid orography, orographic drag, representation mismatch

The *effective surface* of a grid cell is the set of single values a model assigns to the cell in place of the real surface it covers: terrain height, roughness length, land-use class, vegetation fraction and the soil and thermal properties that go with them. *Terrain smoothing* is the loss of topographic detail when real terrain is averaged over grid cells and further filtered for numerical reasons. The *effective elevation* (m above sea level) is the one terrain height the model gives a cell. A *land-use class* is a surface category, such as cropland or forest, from which the model takes a set of surface parameters. The *land-surface model* is the part of a weather model that computes the temperature, moisture and energy exchange of the ground and vegetation. A *mosaic* (or tile) *representation* divides a cell into fractions of different surface types and computes the surface fluxes of each separately. The *land-sea mask* is the field that says which cells, or which fraction of each cell, are land or water. *Orography* is the relief of the land surface; *subgrid orography* is the part of it smaller than the model resolves, and *orographic drag* (Pa) is the force per unit area that terrain exerts on the flow, as distinct from the roughness drag of vegetation and buildings. A *representation mismatch* is a difference between a model value and an observation that arises because the two describe different surfaces or different locations, not because the model's atmosphere is wrong.

Key idea

A weather-model grid cell does not contain the real surface; it contains an effective representation of it, and the model wind is the wind over that representation. A near-surface wind error can therefore come from the atmospheric dynamics or from how the model represents the surface, and the two are different problems with different remedies.

27.1.1 What one grid cell holds

Take a model with a grid spacing of $\Delta x = 3\,\mathrm{km}$. Each grid cell covers about $3\,\mathrm{km} \times 3\,\mathrm{km} = 9\,\mathrm{km}^2$. Inside that area there may be forest, farms, buildings, roads, water, hills and valleys, each of which changes the wind near it: the forest by its drag, the hill by the pressure perturbation it creates, the water by its low roughness and its different temperature. The atmospheric model cannot resolve any of these explicitly. Instead it uses effective grid-cell properties: a terrain height z_{model}, a roughness length z_0, a land-use class and a vegetation fraction, together with the albedo, the leaf area index and the soil properties attached to the class.

Figure 27.1 sets one such cell beside its model counterpart. The left square is the real surface, 3 km on a side, drawn in plan view with north up: forest covers the northern 40 %, with a hill marked by contour lines; farmland covers 40 % across the middle and the southeast, with a stream along a shallow valley; a town covers the southwestern 20 %; a road crosses the cell from south to north; a triangle marks an anemometer at the edge of the farmland. The printed elevations and roughness lengths are those of the real surface at the places marked. The right square is the same cell as the model holds it: one color, one class and one value of each property. The numbers are illustrative.

The model surface is an abstraction. Its terrain height of 520 m is the mean of ground that runs from 430 m at the stream to 640 m on the hill; its roughness length is that of farmland, although forest and town, with roughness lengths ten times larger, cover 60 % of the cell; and its single class says nothing of the hill, the stream or the town. None of these simplifications is an error of the model. Each is the price of a finite grid, and each changes the wind the model computes.

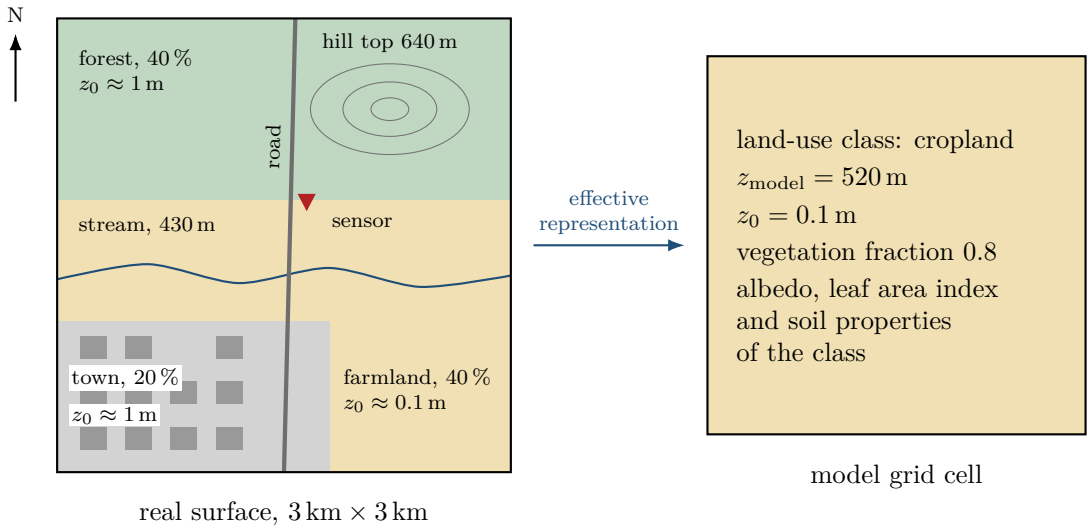


Figure 27.1: A real 3 km grid cell (left, plan view, north up) and the effective surface a model gives it (right). The real cell holds forest with a hill, farmland with a stream, a town, a road and a sensor; the model cell holds one land-use class, one terrain height, one roughness length and one vegetation fraction. Values illustrative.

27.1.2 Effective grid-cell properties

Every surface quantity the model uses is a grid-cell property of this kind. The terrain height sets the bottom boundary of the model's atmosphere and, through it, the pressure perturbations that terrain creates (Chapter 20). The roughness length and displacement height set the surface stress through the surface-layer scheme (Chapters 11 and 14). The land-use class, the vegetation fraction and the soil properties set, through the land-surface model, the partition of the available energy between sensible and latent heat and therefore the stability of the air near the ground (Chapter 16). Chapter 25 describes these components as parts of the model system; this chapter is concerned with the surface values they are given and with what is lost when a heterogeneous surface is reduced to one value per cell.

The reduction runs along a chain:

$$\text{real terrain and land use} \longrightarrow \text{grid-scale terrain, roughness and heat flux} \longrightarrow \text{model wind.}$$

The first arrow is the representation of the surface; the second is the model's dynamics and physics acting on that representation. A model can carry out the second step correctly and still produce a near-surface wind that disagrees with an instrument, because the first step gave it a surface that is not the instrument's surface.

27.1.3 Two sources of near-surface wind error

The chain separates two kinds of error. An error of the *atmospheric dynamics* is an error in how the model evolves the flow over the surface it was given: a misplaced front, a wrong large-scale pressure gradient, too much or too little turbulent mixing in its boundary-layer scheme. An error of *surface representation* is an error that arises because the surface the model was given differs from the real one, or from the part of the real one that affects a particular site: smoothed terrain, a wrong land-use class, an isotropic roughness where the real roughness depends on direction, a shifted coastline, too dry a soil.

The two kinds call for different remedies. A dynamical error is reduced by better initial conditions, better parameterizations or a better model. A representation error is reduced by a better surface description, by finer grids where the feature is resolvable, or by a correction that

maps the grid-cell wind onto the local surface. Treating one as the other is costly: tuning a boundary-layer scheme to remove a bias that comes from a wrong roughness length makes the wind right for the wrong reason and breaks it elsewhere. The rest of the chapter describes the representation side of the chain, component by component, and closes with a decomposition that separates the two in practice (Section 27.6.6).

27.2 Terrain in the model

This section follows the terrain from the real ground to the model's lower boundary: how it is smoothed and why, what smoothing does to the wind, how the model's single elevation differs from a station's, how that difference appears as model error, and how far finer horizontal and vertical grids reduce the problem.

27.2.1 Terrain smoothing

Suppose the real terrain contains a narrow ridge whose crest is at 1200 m above mean sea level, with valleys on either side at 400 m. A coarse model may represent the whole region with a terrain elevation closer to 700 m. The ridge becomes lower, broader and smoother; the valleys become higher and shallower. This is *terrain smoothing*. It has two causes. The first is averaging: a grid cell holds the mean height of the ground it covers, and a feature narrower than a cell is averaged with its surroundings. The second is filtering: models smooth the averaged field further, between neighboring cells, for the numerical reasons of Section 27.2.2.

The effect of a simple filter can be computed exactly. A common choice replaces each cell's height z_j by a weighted mean of itself and its two neighbors, $\tilde{z}_j = (z_{j-1} + 2z_j + z_{j+1})/4$. Applied to a terrain wave $z_j = \cos(kx_j)$ of wavenumber $k = 2\pi/\lambda$ on grid points $x_j = j\,\Delta x$, it gives

$$\begin{aligned} \tilde{z}_j &= \frac{\cos(kx_j - k\Delta x) + 2\cos(kx_j) + \cos(kx_j + k\Delta x)}{4} \\ &= \cos(kx_j)\,\frac{1 + \cos(k\Delta x)}{2} = \cos(kx_j)\,\cos^2\!\left(\frac{\pi\Delta x}{\lambda}\right), \end{aligned} \tag{27.1}$$

using $\cos(a-b) + \cos(a+b) = 2\cos a\cos b$ and $1 + \cos 2c = 2\cos^2 c$. The filter multiplies each terrain wave by $\cos^2(\pi\Delta x/\lambda)$: by 0 at $\lambda = 2\Delta x$, which it removes entirely; by 0.5 at $\lambda = 4\Delta x$; by 0.90 at $\lambda = 10\Delta x$. It keeps the broad terrain and removes the narrow, which is what the numerics require and what the near-surface wind does not.

Figure 27.2 shows the two steps on an illustrative transect. The horizontal axis is distance along the transect in kilometers, the vertical axis terrain height above sea level. The thin black curve is the real terrain: a main ridge with its crest at 1200 m, valley floors near 400 m about 6 km on either side, two lower side ridges, and, at 17.5 km, a small hill about 100 m across and 40 m high. The three stepped curves are the terrain as models with $\Delta x = 9$, 3 and 1 km hold it: the mean over each cell followed by one pass of the filter of equation (27.1).

On the 9 km grid the ridge becomes a cell at 688 m, close to the 700 m of the example, and the cells over the valleys sit at 585 and 599 m: the whole region lies between about 590 and 690 m, and the 800 m of relief between crest and valley floor has become about 100 m. On the 3 km grid the crest is 871 m and the valleys about 510 m; on the 1 km grid they are 1133 m and 409 m, close to the real terrain. Chapter 20 showed the same lowering and broadening for a ridge represented at one resolution, with the cross-sectional area preserved; the transect adds the dependence on grid spacing and shows the valleys filling as the ridge falls.

27.2.2 Reasons for smoothing

Models do not smooth terrain carelessly. If the terrain changes too sharply from one grid cell to the next, three problems arise.

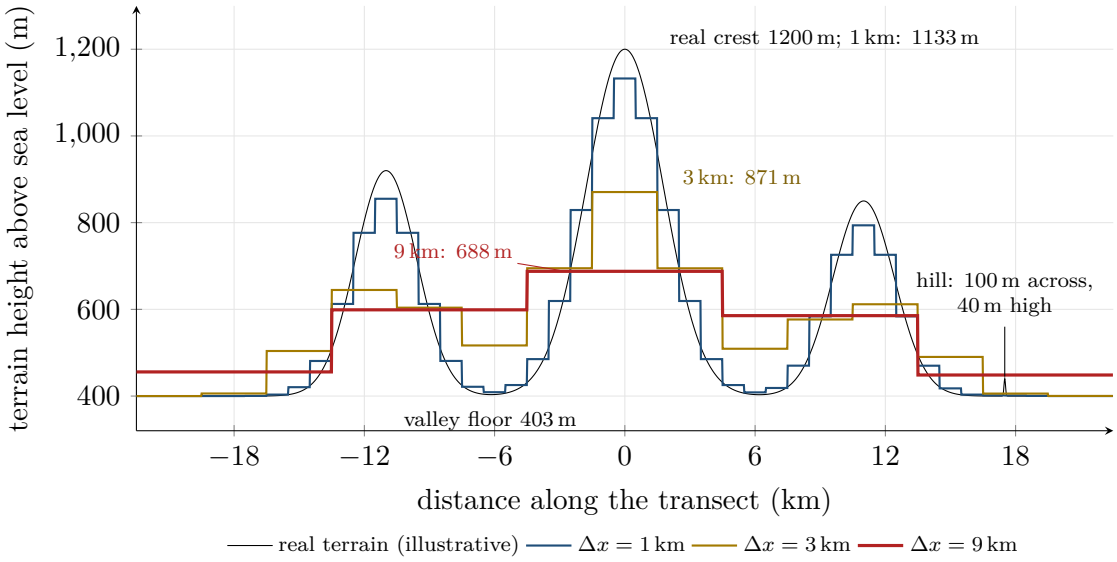


Figure 27.2: An illustrative terrain transect (thin black) and its representation on grids of 9, 3 and 1 km: the mean over each cell followed by one pass of the filter $\tilde{z}_j = (z_{j-1} + 2z_j + z_{j+1})/4$ (equation (27.1)). Data generated by `scripts/ch27_data.py`.

Numerical instability. Terrain features one or two cells wide force flow features of the same width, waves of $2\Delta x$ to $4\Delta x$ that the model's difference equations represent badly (Chapter 5) and that grow into grid-scale noise. Steep slopes also force large vertical velocities in the model's lowest layers: air following a slope of 0.5 at $20\,\mathrm{m\,s^{-1}}$ rises at $10\,\mathrm{m\,s^{-1}}$, and with a layer 20 m thick and a time step of 10 s it would cross $10 \times 10/20 = 5$ layers per step, more than an explicit vertical advection scheme can handle stably (its Courant number must stay below about one).

Pressure-gradient errors. Most models use *terrain-following coordinates*: model levels that follow the ground near the surface and flatten with height. The horizontal pressure-gradient force must then be computed from pressures on sloping levels. Let σ label a level and $z(x, \sigma)$ its height. By the chain rule, the change of pressure along the level is the change at constant height plus the change due to the level's rise, $\partial p/\partial x|_\sigma = \partial p/\partial x|_z + (\partial p/\partial z)\,\partial z/\partial x|_\sigma$, and with the hydrostatic relation $\partial p/\partial z = -\rho g$,

$$-\frac{1}{\rho}\left.\frac{\partial p}{\partial x}\right|_z = -\frac{1}{\rho}\left.\frac{\partial p}{\partial x}\right|_\sigma - g\left.\frac{\partial z}{\partial x}\right|_\sigma . \tag{27.2}$$

The force the flow feels, on the left, is the difference of two terms on the right that are each large over steep terrain. On a level with a slope of 0.13 the second term is $9.81 \times 0.13 \approx 1.3\,\mathrm{m\,s^{-2}}$, while the pressure-gradient force that drives a $10\,\mathrm{m\,s^{-1}}$ geostrophic wind at $|f| = 10^{-4}\,\mathrm{s^{-1}}$ is $|f|U_g = 10^{-3}\,\mathrm{m\,s^{-2}}$, about a thousand times smaller. An error of 0.1 % in either large term, from the discretization of the slope or of the pressure, produces a spurious force as large as the real one. The error grows with the slope, so smoother terrain gives smaller errors.

Distorted vertical coordinates. Over steep terrain the lowest model levels are strongly tilted and the grid boxes near the ground become skewed, so that a box's neighbors in the model grid are at quite different heights above sea level. The numerical approximations assume nearly level, nearly rectangular boxes and lose accuracy as the skew grows. Figure 27.3 in Section 27.2.6 draws such levels over a ridge.

Some smoothing is therefore necessary. But it changes the meteorology: the model computes a correct flow over terrain that is not the real terrain.

27.2.3 Effects of smoothing on the wind

Smoothing weakens every terrain effect of Chapter 20, because each depends on the height, slope or narrowness that the filter removes. It weakens the *ridge speed-up*, which scales with the aspect ratio h_m/L_h; the *channeling* of valley winds, which needs valley walls high enough to confine the flow; *terrain blocking*, which needs a barrier high enough that stable air cannot cross it; *gap winds*, which need a pass narrower than the barrier it cuts; and *flow separation*, which needs a lee slope steeper than about 0.3. Conceptually, smoothed terrain gives a smoothed local wind field. The model may predict the large-scale wind correctly and still miss the local terrain amplification.

Table 27.1 quantifies this for the main ridge of Figure 27.2. Each row is one representation; the columns give the crest height, the valley height, the relief between them, the steepest slope between neighboring grid points (for the real terrain, the steepest slope of the ridge), and the Froude number $\mathrm{Fr} = U/(Nh_m)$ of Chapter 20 for an illustrative stable flow with $U = 10\,\mathrm{m\,s^{-1}}$ and $N = 0.015\,\mathrm{s^{-1}}$, taking the relief as the obstacle height.

Table 27.1: The main ridge of Figure 27.2 at four resolutions. Froude number for $U = 10\,\mathrm{m\,s^{-1}}$, $N = 0.015\,\mathrm{s^{-1}}$ and the relief as obstacle height. Values illustrative.

Representation	Crest (m)	Valley (m)	Relief (m)	Steepest slope	Fr
Real terrain	1200	403	797	0.27	0.84
$\Delta x = 1\,\mathrm{km}$	1133	409	724	0.21	0.92
$\Delta x = 3\,\mathrm{km}$	871	513	358	0.06	1.86
$\Delta x = 9\,\mathrm{km}$	688	592	96	0.016	6.9

The real ridge, with $\mathrm{Fr} = 0.84$, blocks the lowest air: by the dividing-streamline relation of Chapter 20 the layer below $h_m(1 - \mathrm{Fr}) = 797 \times 0.16 \approx 130\,\mathrm{m}$ above the valley floor cannot cross. Its steepest slope, 0.27, is close to the separation threshold, and over forest the lee flow may separate. On the 3 km grid the Froude number is 1.86 and all the air crosses; on the 9 km grid the ridge is a bump of 96 m over 9 km, with a slope of 0.016, and the flow passes over it almost undisturbed. A wind forecast for a transmission line in either valley would, from the coarse models, show neither the blocking that leaves the valley air stagnant nor the channeling that the valley walls impose; a forecast for the crest would lack most of the speed-up and would be evaluated hundreds of meters lower in the atmosphere.

27.2.4 Effective elevation

A model grid cell uses one representative terrain elevation, z_{model}. A real station stands at its own elevation, z_{stn}. If, for example, $z_{\mathrm{stn}} - z_{\mathrm{model}} = 400\,\mathrm{m}$, the model and the observation are not describing the same location in the atmosphere, even when both are labeled "10 m above ground". The difference affects every variable.

Pressure. Integrating the hydrostatic relation over the 400 m with a scale height $H = R_d T/g = 287 \times 285/9.81 \approx 8340\,\mathrm{m}$ for an illustrative $T = 285\,\mathrm{K}$ gives $p(z_{\mathrm{stn}}) = p(z_{\mathrm{model}})\, e^{-400/8340}$. With 930 hPa at the model's ground, the station's pressure is lower by $930 \times (1 - e^{-0.048}) = 43.6\,\mathrm{hPa}$.

Temperature. Under a typical environmental lapse rate of 6.5 K per kilometer the station is 2.6 K cooler. Under a nighttime valley inversion it may instead be several kelvin warmer, because the cold air pools below it.

Wind. The station's 10 m wind is taken 410 m above the model's ground, where in the model the flow is in the upper part of a nighttime boundary layer, or even above it; and the station's

surface has its own friction, which the model's air at that height does not feel.

Stability. At night the station may sit above the stable layer that the model places at its own 10 m, in air that is mixed and windy while the model's near-surface air is calm and stratified; or a ridge station may be exposed to a low-level jet that the model's lower surface leaves above it (Chapter 18).

Models correct the temperature and pressure for such differences with standard lapse-rate and hydrostatic adjustments. No comparably simple correction exists for the wind, which depends on exposure as well as on height.

27.2.5 Elevation mismatch as apparent model error

Suppose a station sits on a ridge and the model grid cell is much lower. The model may predict a weaker wind simply because its terrain is less exposed. The apparent forecast error then partly reflects a representation mismatch rather than an error of the atmospheric dynamics. The worked case below shows how large the representation part can be.

Example 27.1 (A ridge station in a low grid cell)**.** A station stands on the crest of a long ridge at $z_{\mathrm{stn}} = 1100\,\mathrm{m}$, with valleys at 400 m on either side, so the real ridge has $h_m = 700\,\mathrm{m}$ above the valleys and, say, a half-width $L_h = 3.5\,\mathrm{km}$. The model cell containing the station has $z_{\mathrm{model}} = 700\,\mathrm{m}$: the model's ridge rises only 300 m above its valleys, with a half-width of about 6 km. In neutral cross-ridge flow the model's 10 m wind at the cell is $6.0\,\mathrm{m\,s^{-1}}$; the station measures $9.0\,\mathrm{m\,s^{-1}}$. The apparent error is $6.0 - 9.0 = -3.0\,\mathrm{m\,s^{-1}}$, a third of the observation.

Estimate the representation part with the rule of thumb of Chapter 20 for the crest speed-up of a two-dimensional ridge, $\Delta S_{\max} \approx 2\,h_m/L_h$, valid in neutral flow for aspect ratios below about 0.3:

$$\text{real ridge: } \Delta S = 2 \times \frac{700}{3500} = 0.40, \qquad \text{model ridge: } \Delta S = 2 \times \frac{300}{6000} = 0.10.$$

The model's $6.0\,\mathrm{m\,s^{-1}}$ already contains its own speed-up of 10 %, so the upstream wind it implies at 10 m above the valley floor is $U_{\mathrm{ref}} = 6.0/1.10 = 5.45\,\mathrm{m\,s^{-1}}$. The real ridge would raise that wind to $5.45 \times 1.40 = 7.64\,\mathrm{m\,s^{-1}}$ at the crest. Of the apparent error of $3.0\,\mathrm{m\,s^{-1}}$, $7.64 - 6.0 = 1.64\,\mathrm{m\,s^{-1}}$, or 55 %, is the missing terrain: a representation mismatch that no improvement of the atmospheric dynamics would remove. The remaining $9.0 - 7.64 = 1.36\,\mathrm{m\,s^{-1}}$ is what the investigation should examine for other causes: roughness, stability, the large-scale wind itself.

Reading the model at the station's altitude instead, 400 m above its ground, does not make the comparison clean either: that wind belongs to the free part of the model's boundary layer and feels none of the crest's surface friction, so it would overstate the crest wind rather than understate it. Neither the model's 10 m wind nor its wind at the station's altitude is the quantity the station measures.

27.2.6 Vertical resolution over terrain

Terrain realism depends on the vertical grid as well as the horizontal one. Suppose a ridge is 500 m high and the model has only a few levels below that height. It may then represent poorly the acceleration of the wind over the crest, which is concentrated within a few tens of meters of the ground (Chapter 20); the blocking of stable air, whose dividing-streamline height must be located between levels; and the interaction of the flow with an inversion near crest height, which decides whether the air flows over the ridge or around it and whether lee waves form.

Figure 27.3 shows an illustrative case. The horizontal axis is distance across a ridge 500 m high with a half-width of 2.5 km; the vertical axis is height above the valley floor. The thin

curves are model levels at nominal heights of 25, 75, 150, 250, 400, 600, 850 and 1150 m above the ground, following the terrain near the surface and flattening with height. The shaded band is an inversion between 350 and 450 m above the valley floor.

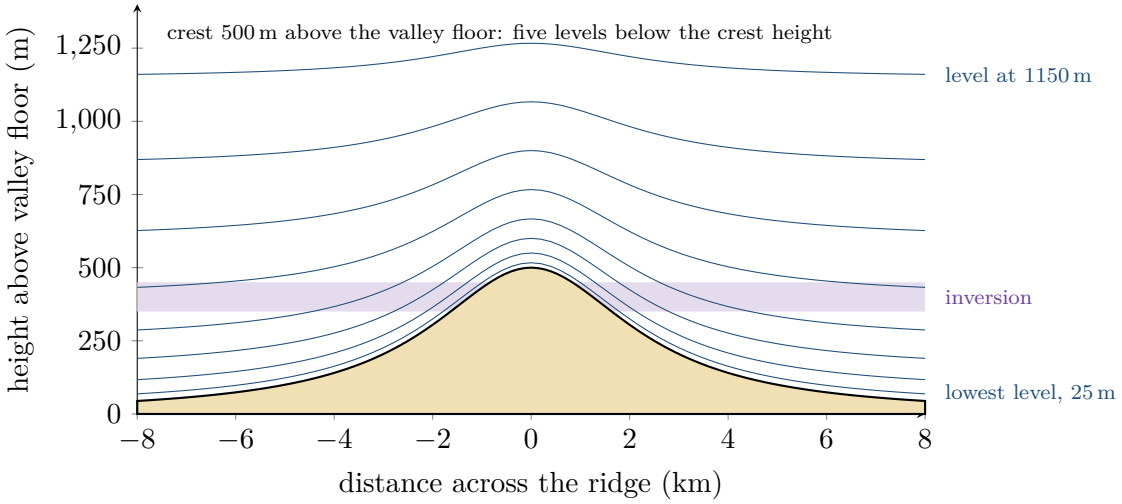


Figure 27.3: Terrain-following model levels over a ridge $500/[1+(x/2.5\,\mathrm{km})^2]$ m high (illustrative). Each level is drawn at its nominal height above the ground plus the terrain height reduced linearly to zero at 1500 m. The shaded band is an inversion 100 m thick, at 350 to 450 m above the valley floor.

Five levels lie below the crest height. The lowest, 25 m above the ground, sits above most of the layer in which the crest speed-up is largest, so the model's wind at its lowest level carries part of the speed-up and its 10 m wind is extrapolated from there. A blocked layer 130 m deep, as for the real ridge of Table 27.1, spans two level intervals. The inversion, 100 m thick, falls inside the single interval between the levels at 250 and 400 m over the valley, so the model smears it over about 150 m and weakens its gradient. On the upper slopes, where the ground is 350 to 450 m high, the inversion meets the terrain and lies within the lowest one or two levels, and the crest stands above it: whether the model places a crest above or below an inversion decides whether the crest wind belongs to the stable air below or to the flow above, and a few tens of meters of error in either the terrain or the inversion height can reverse it. Near the ground the levels slope with the terrain, by up to 0.13 on this ridge, which is the slope that enters equation (27.2). A model represents terrain flow through the pair $(\Delta x, \Delta z)$, not through the horizontal resolution alone.

27.2.7 Horizontal resolution and effective resolution

Refining the grid from 9 km to 3 km to 1 km resolves the terrain progressively better. Figure 27.2 shows it: the main ridge's relief grows from about 100 m to 358 m to 724 m of its real 797 m, and with it the model captures more of the major ridges, the valleys and the coastlines. But a hill 100 m across is still unresolved at 1 km: in the figure the 1 km grid holds about 2 m of the hill's 40 m, because a 1 km cell averages the hill with 900 m of flat ground around it. Higher resolution improves the representation gradually; each refinement brings a new range of features into the model and leaves everything smaller outside it.

The grid spacing also overstates what the model resolves. By the rule of Chapter 5, a model represents features of about 5 to 10 Δx and larger with their shape and amplitude. With $\Delta x = 1$ km the smallest well-resolved feature is closer to 5 to 10 km. A hill 1 km across therefore appears numerically in the model's topography field, as one raised cell, but the flow response to it, the windward deceleration, the crest speed-up and the lee wake, is carried by flow features

one or two cells wide and is damped and distorted by the model's numerics. The distinction is between the terrain the model contains and the terrain whose flow it resolves.

> **Principle 27.1.** *Higher resolution improves the representation of terrain gradually. A model with grid spacing Δx contains terrain features down to about Δx but resolves their flow only down to about 5 to $10\,\Delta x$; everything smaller reaches the model wind through smoothing and parameterization.*

The temptation to overinterpret fine grids. A 1 km model map looks detailed. It shows narrow valleys, local ridges and localized wind maxima a few kilometers across, and that detail invites a confidence it has not earned. Many of those structures lie at or below the model's effective resolution limit: a wind maximum 2 km across on a 1 km grid spans two grid points, where the model's flow is inaccurate in amplitude and position and may be partly numerical noise. Visual detail is not physical reliability. A fine-grid wind map is to be read with its effective resolution in mind, and a local feature is trusted only when it is several times larger than the grid spacing or is confirmed by observation.

27.3 Land cover in the model

The second component of the effective surface is the land cover: what stands on the ground and how it exchanges momentum, heat and moisture with the air. This section describes how models classify land cover, what a single class hides, how mosaic schemes recover part of it, how roughness is averaged, what is lost when roughness depends on direction, how cities are represented, and how vegetation acts on the wind through two pathways.

27.3.1 Land-use classes

A model assigns each grid cell a land-use category, taken from a land-cover map: cropland, forest, urban, water, grassland and others. Each category implies a set of values: the roughness length z_0, the albedo (the fraction of incoming solar radiation the surface reflects), the vegetation fraction (the fraction of the ground covered by vegetation), the leaf area index LAI (one-sided leaf area per unit ground area), and soil properties such as the soil type and its capacity to hold water. These values feed directly into the surface-layer scheme, which computes the stress and the turbulent fluxes from the roughness and the stability, and into the land-surface model, which computes the surface temperature and the partition of the available energy.

Table 27.2 lists illustrative values for five classes. Its columns give the class, its roughness length, its albedo, its vegetation fraction and its leaf area index. The roughness lengths are within the ranges of Chapter 11; actual models use their own tables, often with seasonal values.

Table 27.2: Surface parameters a model may attach to five land-use classes. Values illustrative.

Land-use class	z_0 (m)	Albedo	Vegetation fraction	LAI
Cropland	0.1	0.18	0.8	3
Forest	1.0	0.12	0.9	5
Urban	1.0	0.15	0.1	0.5
Water	0.0002	0.08	0	0
Grassland	0.03	0.20	0.8	2

27.3.2 Heterogeneity hidden by one class

Suppose a grid cell is 40 % forest, 40 % farmland and 20 % urban, the cell of Figure 27.1. A simple model classifies it by its dominant category. Forest and farmland tie here, so the class depends on how the tie is broken or on a percent of difference in the land-cover map; if it falls to cropland, the cell receives $z_0 = 0.1\,\mathrm{m}$, the albedo of crops and a vegetation fraction of 0.8. The 60 % of the cell that is forest or town, with roughness lengths ten times larger, disappears from the model.

The effective roughness of the cell is then badly different from the local environment of a sensor in it, and in a direction that depends on where the sensor stands. A sensor in the farmland sees roughly the cropland surface the model assumed; a sensor at the forest edge or in the town sees a much rougher one. Neither sees the cell as a whole. The classification error is not random: it always removes the minority surfaces, and when those are the rough ones the model's cell is systematically too smooth.

27.3.3 Mosaic representation

Some land-surface models use a *mosaic representation*, in which the different surface fractions of a cell are kept separately. With area fractions χ_i summing to one,

$$\chi_{\mathrm{forest}} = 0.4, \qquad \chi_{\mathrm{crop}} = 0.4, \qquad \chi_{\mathrm{urban}} = 0.2,$$

the model computes the surface temperature, the stress and the heat fluxes of each surface type, called a *tile*, from that tile's own parameters, and passes the area-weighted mean flux to the atmosphere:

$$\tau_0 = \sum_i \chi_i\, \tau_{0,i}, \qquad H = \sum_i \chi_i\, H_i. \tag{27.3}$$

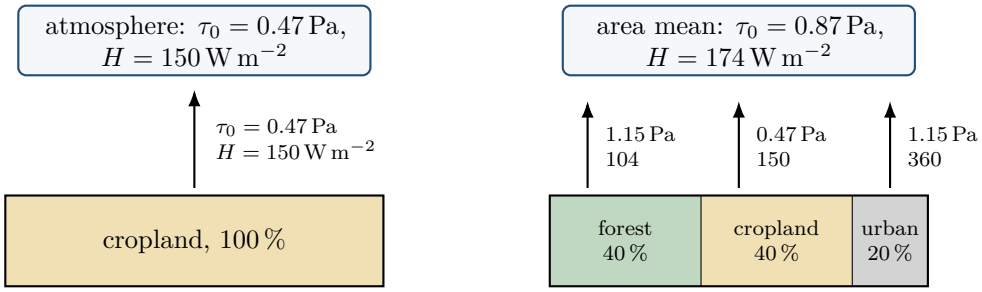
The averaging is of fluxes, not of parameters. This improves realism, because each flux is a nonlinear function of its parameters and the mean of the fluxes differs from the flux of the mean parameters. But the atmospheric column above the cell still sees one grid-scale result: one stress and one heat flux, one wind profile and one boundary layer. The mosaic gives the atmosphere better averages; it does not give it the local wind over each tile.

Figure 27.4 compares the two treatments of the cell. Panel (a) is the dominant-class cell, all cropland; panel (b) is the mosaic, with its three tiles drawn as strips in proportion to their area. Each upward arrow carries the surface stress τ_0 and the sensible heat flux H of the surface below it; in panel (b) the box at the top is the area-weighted mean of equation (27.3) that the atmosphere receives. The stress is computed for a common wind of $10\,\mathrm{m\,s^{-1}}$ at a blending height $z_b = 60\,\mathrm{m}$, with $\tau_{0,i} = \rho\,[\kappa U(z_b)/\ln(z_b/z_{0,i})]^2$, $\rho = 1.2\,\mathrm{kg\,m^{-3}}$ and the roughness lengths of Table 27.2, displacement neglected. The heat flux is computed for an available energy of $450\,\mathrm{W\,m^{-2}}$ at midday and illustrative Bowen ratios $B = 0.3$ for the forest, 0.5 for the crops and 4 for the town, with $H = [B/(1+B)] \times 450\,\mathrm{W\,m^{-2}}$ (Chapter 16).

The drag coefficients at 60 m are $(0.4/\ln 60)^2 = 0.00954$ for the forest and the town and $(0.4/\ln 600)^2 = 0.00391$ for the crops. The mosaic's mean drag coefficient is $0.4 \times 0.00954 + 0.4 \times 0.00391 + 0.2 \times 0.00954 = 0.00729$, and its stress $1.2 \times 0.00729 \times 10^2 = 0.87\,\mathrm{Pa}$, 1.86 times the dominant-class value of 0.47 Pa; the friction velocities are 0.85 and $0.63\,\mathrm{m\,s^{-1}}$. The mosaic's heat flux is $0.4 \times 104 + 0.4 \times 150 + 0.2 \times 360 = 174\,\mathrm{W\,m^{-2}}$, 16 % more than the dominant class gives, nearly all of it from the town. The mean of the fluxes is not the flux of the mean parameters: averaging the Bowen ratios first, $0.4 \times 0.3 + 0.4 \times 0.5 + 0.2 \times 4 = 1.12$, would give $H = (1.12/2.12) \times 450 = 238\,\mathrm{W\,m^{-2}}$, an overestimate of 37 %.

The near-surface wind over each tile tells the same story from the sensor's side. With the common wind at 60 m, the neutral 10 m wind over a surface of roughness z_0 is

$$U(10\,\mathrm{m}) = U(z_b)\,\frac{\ln(10\,\mathrm{m}/z_0)}{\ln(z_b/z_0)}, \tag{27.4}$$



(a) dominant class (b) mosaic of three tiles

Figure 27.4: Surface stress and sensible heat flux of one grid cell (illustrative) as a dominant-class cell (a) and as a mosaic (b). Stress from $\rho\,[\kappa U(z_b)/\ln(z_b/z_0)]^2$ with $U(z_b) = 10\,\mathrm{m\,s^{-1}}$ at $z_b = 60\,\mathrm{m}$; heat flux from $[B/(1+B)] \times 450\,\mathrm{W\,m^{-2}}$ with $B = 0.3$, 0.5 and 4. Tile heat fluxes in $\mathrm{W\,m^{-2}}$. The atmosphere receives the area-weighted mean.

which gives $5.62\,\mathrm{m\,s^{-1}}$ over the forest and the town and $7.20\,\mathrm{m\,s^{-1}}$ over the crops. The dominant-class model gives the cell $7.20\,\mathrm{m\,s^{-1}}$, which matches a sensor in the crop field and is $1.6\,\mathrm{m\,s^{-1}}$ too high for a sensor at the forest edge; the mosaic gives the cell the stress of an effective surface (Section 27.3.4) whose 10 m wind is $6.18\,\mathrm{m\,s^{-1}}$, which matches neither. The dominant-class model agrees with the crop sensor for the wrong reason.

27.3.4 Effective roughness

The model needs one aerodynamic roughness z_0 for the column above the cell, and averaging roughness is not trivial. The arithmetic mean $(z_{0,1} + z_{0,2})/2$ of two surfaces is not in general the correct effective roughness, because the drag depends nonlinearly on z_0 through $\ln(z/z_0)$. The surface stress of a patch under a common wind $U(z_b)$ is

$$\tau_{0,i} = \rho \left[\frac{\kappa\, U(z_b)}{\ln(z_b/z_{0,i})} \right]^2 , \tag{27.5}$$

and it is the stresses that add over patches, as in equation (27.3). The effective roughness length is the one whose stress equals the mean, $[\ln(z_b/z_{0,\mathrm{eff}})]^{-2} = \sum_i \chi_i\,[\ln(z_b/z_{0,i})]^{-2}$, which is the blending rule of Chapter 11. For the cell of Section 27.3.3,

$$\ln \frac{60}{z_{0,\mathrm{eff}}} = \frac{0.4}{\sqrt{0.00729}} = 4.68, \qquad z_{0,\mathrm{eff}} = 60\,\mathrm{m} \times e^{-4.68} = 0.55\,\mathrm{m}.$$

The arithmetic mean of the three roughness lengths is $0.4 \times 1.0 + 0.4 \times 0.1 + 0.2 \times 1.0 = 0.64\,\mathrm{m}$; the geometric mean, the average of $\ln z_0$, is 0.40 m; the dominant class gives 0.1 m. The effective value lies between the two means, as it did for the half-forest, half-grass cell of Chapter 11 (0.37 m against 0.515 and 0.17 m). The dominant class is the furthest from it, by a factor of five.

Two further points complete the picture. The effective roughness is a grid-scale property: the roughness of a uniform surface that would exert the cell's mean stress, not the roughness at any sensor in the cell. And it may include more than vegetation and buildings: some models raise it above the land-cover value to represent the turbulent drag of small unresolved hills, an orographic roughness that mixes terrain and roughness on purpose (Section 27.4).

27.3.5 Directional roughness

Real roughness depends on the direction the wind comes from. A site with open fields to the west and forest to the east has $z_0 = z_0(\beta)$, low for westerly winds and high for easterly ones,

where β is the wind direction. A weather model usually uses one isotropic z_0 for the whole grid cell, the same for every direction, and directional exposure effects are lost. The result is a bias that depends on wind direction.

The size of the bias follows from equation (27.4). Take open fields with $z_0 = 0.03\,\mathrm{m}$ to the west, forest with $z_0 = 1.0\,\mathrm{m}$ to the east, and a model cell with the isotropic effective value $0.37\,\mathrm{m}$ of the half-and-half cell of Chapter 11. Under a common neutral wind at $60\,\mathrm{m}$ the ratio of the $10\,\mathrm{m}$ wind to the $60\,\mathrm{m}$ wind is

$$\begin{aligned} \text{west (open fields):} \quad & \frac{\ln(10/0.03)}{\ln(60/0.03)} = \frac{5.81}{7.60} = 0.764, \\ \text{east (forest):} \quad & \frac{\ln(10/1.0)}{\ln(60/1.0)} = \frac{2.30}{4.09} = 0.562, \\ \text{model, any direction:} \quad & \frac{\ln(10/0.37)}{\ln(60/0.37)} = \frac{3.30}{5.09} = 0.648. \end{aligned}$$

For westerly winds the model's $10\,\mathrm{m}$ wind is $0.648/0.764 = 0.85$ of the real one, 15 % too low; for easterly winds it is $0.648/0.562 = 1.15$ of it, 15 % too high. The mean bias over a year of mixed directions may be near zero while the error in each direction is large. A bias whose sign changes with the wind direction is the signature of directional roughness, and it is checked by sorting the model errors by direction sector before averaging them (Chapter 11 gives the roughness rose that describes such a site).

27.3.6 Urban representation

A simple model represents a city merely as a rough surface, $z_0 = 1\,\mathrm{m}$ or similar, with an urban albedo and little vegetation. The roughness reproduces part of the drag of the buildings on the wind well above them, and nothing else: no displacement of the wind profile by the building height, no heat stored in walls and roads during the day and released at night, no shading, no trapping of radiation in street canyons.

A more advanced *urban canopy model* represents the city by its geometry and materials: roofs, walls and roads as separate surfaces, the street-canyon geometry (building height, street width and orientation), and the heat storage of the building materials. That changes both of the ways the city acts on the wind. It changes the drag, which now depends on the building heights and frontal areas and on the wind direction relative to the streets; and it changes the thermal forcing, because the stored heat keeps the urban surface warmer at night, weakens the nighttime stable layer and keeps the near-surface air more mixed than over the surrounding countryside. Urban wind is therefore very sensitive to the land-surface formulation: two models with the same grid and the same city, one with a roughness length and one with an urban canopy model, can disagree on the nighttime wind in the streets by more than either disagrees with the countryside. The flow within and above urban canopies is the subject of Chapter 21.

27.3.7 Vegetation fraction and the two pathways

Vegetation influences the near-surface wind in several ways at once: by its aerodynamic drag, by evapotranspiration (the transfer of soil water to the air through plants), by shading the ground, and through all three by the surface temperature. An error in the vegetation fraction or in the land-use class that sets it therefore reaches the wind through two pathways. The *momentum pathway* runs through the roughness length and the displacement height to the surface stress and the wind profile. The *thermal pathway* runs through the albedo, the Bowen ratio and the surface temperature to the sensible heat flux, the stability and the depth of mixing, and from there to the wind profile again.

Figure 27.5 draws the two pathways. Boxes on the left are surface inputs that a model takes from its land-cover and surface data; the gray bar collects them, since each can act on

both pathways; the upper row of boxes is the momentum pathway, the lower row the thermal pathway; both converge on the model's near-surface wind on the right. Each arrow means "sets" or "changes".

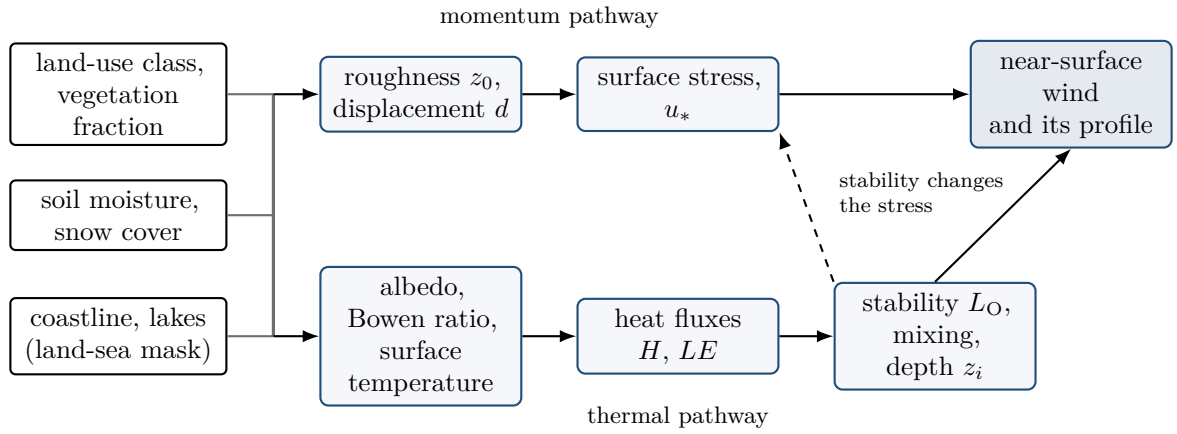


Figure 27.5: The two pathways by which the surface description reaches the near-surface wind in a weather model. Momentum pathway (upper row): roughness and displacement set the stress. Thermal pathway (lower row): radiation and moisture properties set the heat fluxes, which set the stability and the mixing. The dashed arrow marks the coupling: the stability changes the stress the roughness produces.

Too little vegetation in a cell, for example, lowers its roughness and raises the near-surface wind through the upper row; it also lowers the evapotranspiration, raises the Bowen ratio and the daytime sensible heat flux, deepens the mixing and raises the afternoon wind again through the lower row. The two effects can add or partly cancel, and they act at different times of day: the momentum pathway at all hours, the thermal pathway mainly in the afternoon and at night. That is why land-use datasets matter so much for wind: a land-cover map that is out of date, too coarse or wrong about a single class changes the modeled wind through both pathways at once.

27.4 Subgrid terrain

Terrain too small for the grid is not simply absent from a model. This section describes how its bulk effects are represented: the statistics of subgrid orography, the drag of mountain waves, the blocking of stable low-level flow, and the difference between orographic drag and the roughness drag of the land cover.

27.4.1 Subgrid orography

The terrain removed by averaging and filtering still exerts forces on the real flow. Models represent its bulk effect through *subgrid orographic parameterizations*, which compute the force the unresolved terrain would exert from statistics of that terrain within each cell: the standard deviation of the subgrid height σ_h (m), its anisotropy (how elongated the ridges are), their orientation and their mean slope. These statistics come from a high-resolution terrain map and are fixed fields of the model, like the terrain height itself. For the 9 km cell over the main ridge of Figure 27.2, the real terrain inside the cell runs from about 430 to 1200 m with a mean of 790 m and a standard deviation $\sigma_h = 266$ m, while the cell's filtered height is 688 m; the parameterization works with the 266 m of subgrid relief that the resolved terrain has lost.

The parameterizations represent three effects: mountain-wave drag, flow blocking, and unresolved roughness. Unresolved terrain therefore still influences the model, indirectly, through

forces added to the model's momentum equations. Figure 27.6 shows the three in one schematic cross section of a grid cell. The thin black line is the real terrain with several hills; the thick red line is the smooth terrain the model resolves, with σ_h marking the spread of the real heights about it. The wind comes from the left. Above the hills, the wavy blue lines are mountain waves, which carry momentum upward and deposit it where they break; at low levels, on the upstream side, stable air is held back by the hills and diverted around them; near the ground, the small circles are turbulent eddies in the lee of the smaller hills.

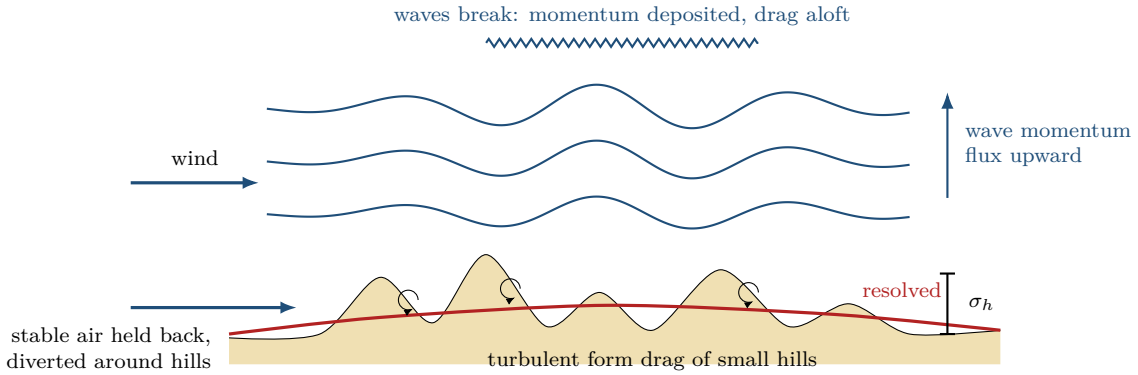


Figure 27.6: Subgrid orography in one grid cell (schematic, vertical scale exaggerated). Real terrain (thin black) and the smooth resolved terrain (thick red); σ_h is the standard deviation of the real heights about the resolved ones. The parameterized effects are mountain-wave drag (upper, waves breaking aloft), flow blocking (low levels, upstream) and turbulent orographic form drag (near the ground).

27.4.2 Mountain-wave drag

Large-scale stable flow over unresolved mountains generates gravity waves, the mountain waves of Chapter 20. Those waves transport momentum vertically. The *wave stress* $\tau_w = -\rho\,\overline{u'w'}$, with the covariance taken over the wave, is the downward flux of the along-wind momentum; for a wave launched by a mountain it equals the drag the mountain exerts on the flow. In a wave that neither grows nor dissipates, τ_w is the same at every height: the wave carries the momentum deficit upward without depositing it. Where the wave breaks, because it has grown steep in the thinning air or met a level where the wind turns or weakens, τ_w falls to zero over a layer and the deficit is deposited there. The change of the mean flow in that layer is

$$\frac{\partial U}{\partial t} = -\frac{1}{\rho}\frac{\partial\,(\rho\,\overline{u'w'})}{\partial z} = \frac{1}{\rho}\frac{\partial \tau_w}{\partial z}, \tag{27.6}$$

which is negative, a deceleration, where τ_w decreases with height. A coarse model cannot resolve every wave, so it parameterizes their aggregate drag as *orographic gravity-wave drag*, from the subgrid statistics of Section 27.4.1, the wind and the stability.

The order of magnitude shows why it matters. Chapter 20 estimated the wave drag of an illustrative ridge as a stress of about 0.6 Pa. If a wave stress of 0.5 Pa falls to zero across a layer 5 km deep where $\rho \approx 0.5\,\mathrm{kg\,m^{-3}}$, then $\partial\tau_w/\partial z \approx -0.5/5000\,\mathrm{Pa\,m^{-1}}$ and by equation (27.6) the deceleration is $0.5/(0.5 \times 5000) = 2 \times 10^{-4}\,\mathrm{m\,s^{-2}}$, about $0.7\,\mathrm{m\,s^{-1}}$ per hour or $17\,\mathrm{m\,s^{-1}}$ per day. A model that omits it lets the winds aloft over mountains run far too fast within days, which is why the parameterization is important especially in global models, whose grids leave most mountain waves unresolved. Its effect on the near-surface wind is indirect, through the large-scale flow and the pressure field it shapes.

27.4.3 Flow blocking

Stable low-level flow may be unable to cross unresolved terrain. The real atmosphere then goes around it, and the air below the dividing-streamline height is held back or diverted (Chapter 20). The model's smoothed terrain is too low to block anything, so a model represents the effect through a *subgrid flow-blocking* parameterization: a drag on the low-level flow, applied in the layer that the unresolved terrain would block, rather than through explicit terrain geometry.

The blocked depth is estimated from the subgrid statistics and the Froude number. Treat the subgrid relief of the crest cell of Section 27.4.1 as an obstacle of effective height $h_{\text{eff}} = 2\sigma_h \approx 530\,\text{m}$ (an illustrative choice; schemes take h_{eff} proportional to σ_h). In air with $N = 0.015\,\text{s}^{-1}$, a wind of $10\,\text{m}\,\text{s}^{-1}$ gives $\text{Fr} = 10/(0.015 \times 530) = 1.26$ and nothing is blocked; a wind of $5\,\text{m}\,\text{s}^{-1}$ gives $\text{Fr} = 0.63$ and a blocked layer $h_{\text{eff}}(1 - \text{Fr}) = 530 \times 0.37 \approx 200\,\text{m}$ deep, in which the scheme removes momentum from the low-level flow. Again the parameterized terrain physics matters even where the mountain itself is not resolved: without it, the model's stable low-level wind over mountainous terrain is too strong and too uniform.

27.4.4 Roughness drag and orographic drag

Two kinds of surface drag must be kept apart. *Surface roughness drag* comes from vegetation, buildings and small obstacles: the skin friction and form drag of elements that stand within the surface layer. *Orographic drag* comes from hills, mountains, terrain-induced waves and blocking: the pressure difference across terrain features and the momentum carried away by the waves they launch. Both remove momentum from the flow, but through different physical mechanisms, at different heights and with different dependence on stability.

Table 27.3 compares them. Its rows are the two kinds of drag; its columns give the source, the mechanism, where in the vertical the momentum is removed, the dependence on stability, how a model represents it, and an illustrative magnitude.

Table 27.3: Surface roughness drag and orographic drag. Magnitudes illustrative.

	Surface roughness drag	Orographic drag
Source	vegetation, buildings, small obstacles	hills, mountains, terrain-induced waves, blocking
Mechanism	skin friction and form drag of elements in the surface layer, passed upward by turbulence	pressure difference across terrain; momentum flux of gravity waves; deceleration of blocked air
Where removed	at the surface, felt through the boundary layer	near the surface (blocking, form drag) and aloft where waves break
Stability	reduced in stable air, enhanced in convective air through mixing	waves and blocking exist only in stable air; set by Fr
Representation	z_0 and d in the surface-layer scheme	gravity-wave drag, blocking and orographic-roughness schemes using σ_h, anisotropy and orientation
Magnitude	$\rho u_*^2 \approx 0.2\,\text{Pa}$ for $u_* = 0.4\,\text{m}\,\text{s}^{-1}$	about 0.6 Pa for a ridge 500 m high in stable flow

The distinction matters when a model's near-surface wind is too strong over mountainous terrain. Raising the roughness length reduces it by increasing the drag in the surface layer at all hours; the real cause may be missing low-level blocking, which acts only in stable air, or missing wave drag, which acts aloft. Each fix makes the near-surface wind smaller, and only the right one makes it right in the right conditions. The physics of flow over terrain that these parameterizations approximate is the subject of Chapter 20.

27.5 The thermal state of the surface

The surface acts on the wind through its temperature and moisture as well as through its shape and drag. This section follows errors in the land-surface temperature, the soil moisture, the coastline, the lakes and the snow cover through the heat fluxes to the wind, and collects them in one table.

27.5.1 Land-surface temperature

Suppose the model surface is too warm during the daytime. The sensible heat flux follows the difference between the surface temperature T_s and the air temperature T_a above it. In the bulk form used by surface-layer schemes,

$$H = \rho\, c_p\, C_H\, U\, (T_s - T_a), \tag{27.7}$$

with C_H a dimensionless transfer coefficient for heat at the reference height of U and T_a. With illustrative values $\rho = 1.2\,\mathrm{kg\,m^{-3}}$, $c_p = 1004\,\mathrm{J\,kg^{-1}\,K^{-1}}$, $C_H = 0.004$ and $U = 5\,\mathrm{m\,s^{-1}}$, each kelvin of surface-temperature error changes H by $1.2 \times 1004 \times 0.004 \times 5 = 24\,\mathrm{W\,m^{-2}}$. A surface 2 K too warm raises a true $150\,\mathrm{W\,m^{-2}}$ to about $200\,\mathrm{W\,m^{-2}}$.

The larger heat flux produces too much convective mixing: the mixed layer grows deeper and its convective velocity scale $w_* \propto (H\, z_i)^{1/3}$ grows (Chapter 16). With the depth growing as the square root of the accumulated heat input, a 32 % larger flux deepens the layer by $\sqrt{1.32} = 1.15$ and raises w_* by $(1.32 \times 1.15)^{1/3} = 1.15$. The stronger mixing brings more of the faster wind aloft down to the surface, and U_{10} may become too high. Near-surface wind is thus sensitive to surface-temperature errors that originate in the land-surface physics, far from the dynamics of the wind itself.

27.5.2 Soil moisture

Soil moisture errors act through the same chain. If the model's soil moisture is underestimated, less water is available for evaporation: the latent heat flux LE falls and the sensible heat flux H rises. With the available energy of $450\,\mathrm{W\,m^{-2}}$ of Section 27.3.3, a cropland whose real Bowen ratio is 0.5 has $H = 150$ and $LE = 300\,\mathrm{W\,m^{-2}}$; if the model's dry soil gives it $B = 1.5$, it computes $H = 270$ and $LE = 180\,\mathrm{W\,m^{-2}}$. That strengthens the daytime convection, deepens the mixed layer and raises the afternoon near-surface wind. The chain is

$$\text{soil-moisture error} \longrightarrow \text{heat-flux error} \longrightarrow \text{boundary-layer error} \longrightarrow \text{wind error},$$

and an overestimated soil moisture runs it in the opposite direction: too little sensible heat, a shallow layer and an afternoon wind too weak under a correct wind aloft (Chapter 16). It is a clear example of coupled model physics: the wind error appears in the momentum field, and its cause lies in the soil-water budget of the land-surface model, which in turn depends on the model's rainfall of the preceding days or weeks.

27.5.3 Coastlines

Coastlines are resolution-sensitive. Suppose a coastal grid cell contains 60 % land and 40 % water. The model must decide how to represent it: as a land cell, because land is the larger fraction; as a mixed cell, with land and water tiles whose fluxes are averaged as in equation (27.3); or, in the simplest models, by a fixed threshold of the land-sea mask that turns every cell entirely to land or to water. Each choice places the model's coastline somewhere other than the real one.

Figure 27.7 shows a land-sea mask on a 3 km grid over an illustrative east-facing coast in the Southern Hemisphere, north up. Each square is a grid cell. The thick black line is the real coastline, with land to the west and sea to the east; the shading is the model's mask, a cell

counting as land (gold) when more than half its area is land and as sea (blue) otherwise; the thick red staircase is the coastline the model sees. The outlined cell at the bottom is the 60 % land cell of the text.

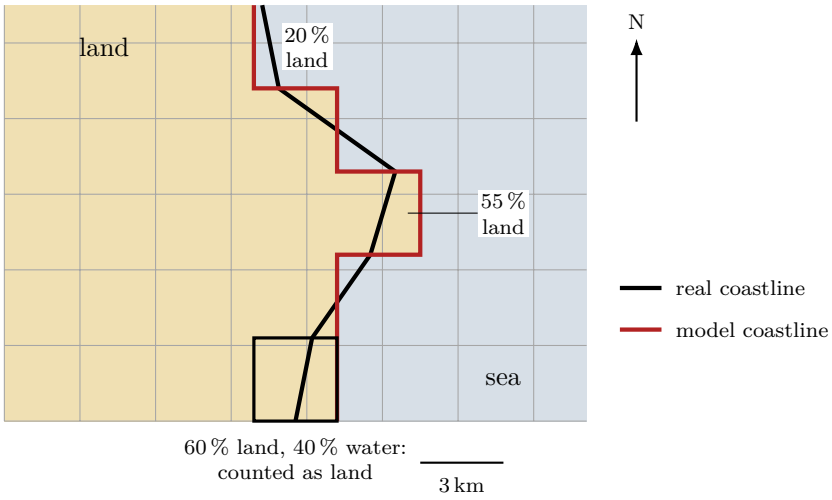


Figure 27.7: A land-sea mask on a 3 km grid (illustrative east-facing coast in the Southern Hemisphere, north up). Cells with more than half their area on land are land (gold), the others sea (blue). The model coastline (red) departs from the real one (black) by up to about half a cell, and by about 0.7 cell where the coast turns; coastal cells mix land and water fractions that the mask does not show.

The model coastline departs from the real one by up to half a cell along most of its length and by about 0.7 of a cell, 2 km, where the real coast turns; the headland in the middle of the figure becomes a single land cell protruding a full cell into the sea, and the coast north of it a straight step. A coastline shifted by such distances changes four things. It changes the timing of the sea breeze: a breeze front advancing at $3\,\mathrm{m\,s^{-1}}$ reaches a site 1.5 km inland about $1500/3 = 500\,\mathrm{s}$, some 8 minutes, earlier or later, and the shift of the whole circulation can be larger (Chapter 19). It moves the roughness transition from water to land, where the internal boundary layer of Chapter 7 starts. It moves the change of heat capacity between land, which heats and cools quickly, and water, which hardly changes temperature in a day. And it changes the surface temperature of the mixed cells, a blend of land and sea that neither surface has. Coastal wind can therefore be sensitive to geographic errors that look small on a map. Where the breeze turns during the day, it turns clockwise in the Northern Hemisphere and counterclockwise in the Southern (Chapter 19); a misplaced coastline shifts that rotation in time and space.

27.5.4 Lakes

Large lakes generate local breezes, change the stability of the air above and downwind of them, and create roughness transitions. A lake is smooth: with $z_0 = 0.0002\,\mathrm{m}$ against 0.1 m for the surrounding cropland, the neutral 10 m wind under a common wind at 60 m is $\ln(50\,000)/\ln(300\,000) = 0.858$ of the 60 m wind over the water against 0.720 over the land, about 19 % faster. The lake's large heat capacity keeps its surface cooler than the land by day and warmer by night, so the air over it is stable in the afternoon, with a lake breeze toward the shore, and unstable at night, with mixing that keeps the night wind over and just downwind of the lake stronger than over the surrounding stable land.

A lake 2 km × 4 km on a 3 km grid covers parts of two to four cells and may fill none of them by more than half; with a threshold mask it vanishes from the model or shrinks to one water

cell. If a model omits or shrinks a lake, the local wind can change materially: the roughness, the stability and the breeze all revert to those of the surrounding land. This is especially relevant in regions with many inland water bodies and reservoirs, where the lakes are individually small and collectively a large part of the surface.

27.5.5 Snow cover

Snow changes the surface dramatically, in four properties at once. It changes the albedo: fresh snow reflects about 0.8 of the incoming solar radiation against about 0.2 for grass, so under $600\,\mathrm{W\,m^{-2}}$ of sunshine the surface absorbs 120 instead of $480\,\mathrm{W\,m^{-2}}$. It changes the roughness: snow fills the spaces between grass and crop stems and lowers the roughness length to about 0.001 m, which by itself raises the neutral 10 m wind under a common wind at 60 m from 0.764 to 0.837 of that wind, by about 10 %, compared with grass of $z_0 = 0.03\,\mathrm{m}$. It changes the temperature: a melting or snow-covered surface cannot rise above 0°C. And it changes the heat flux: with little absorbed energy and a capped surface temperature, the sensible heat flux is small or negative even by day, and the air near the ground is stable.

The net effect on the wind depends on which change dominates. The lower roughness raises the near-surface wind; the stable stratification decouples the surface air from the flow aloft and lowers it, especially in light winds and at night (Chapter 17). A snow-cover error, snow the model has and the ground does not or the reverse, can therefore affect the near-surface wind indirectly and in either direction, and again shows that the wind is coupled to the full land-surface system.

27.5.6 Surface errors traced to the wind

Table 27.4 collects the surface errors of this section and the previous one. Each row is one error of the model's surface description; the columns give the mechanism by which it reaches the wind and the symptom it produces in the modeled near-surface wind, the clue by which it can be recognized in a comparison with observations.

The table is a diagnostic tool as much as a summary. A bias that appears only in the afternoon points to the thermal pathway, one that appears at all hours to the momentum pathway, one that changes sign with direction to directional roughness, and one confined to a coastal band to the land-sea mask. Reading the error by time of day, by direction and by location narrows its source before any model physics is changed.

27.6 Consequences for validation and correction

The representation of the surface decides what a model wind can be compared with and how it can be corrected. This section shows how grid-cell averaging erases local extremes, how validation should separate model error from scale mismatch, how statistical, dynamical and microscale methods correct the representation, why a correction should depend on the state of the atmosphere, why finer grids alone do not solve the problem, and how a wrong local forecast can be diagnosed.

27.6.1 Grid-cell averaging and local extremes

Suppose the real wind in a grid cell is $U_{\mathrm{ridge}} = 12\,\mathrm{m\,s^{-1}}$ on an exposed ridge and $U_{\mathrm{valley}} = 3\,\mathrm{m\,s^{-1}}$ in a sheltered valley beside it. A coarse model may produce $U_{\mathrm{grid}} = 7\,\mathrm{m\,s^{-1}}$ for the cell. That may be a reasonable grid-scale value. But neither the ridge nor the valley experiences $7\,\mathrm{m\,s^{-1}}$. The averaging that represents the cell removes the local extremes, which are often what matters: the ridge wind for the cooling of a transmission line crossing the crest, or for a turbine there; the

Table 27.4: Surface errors, their mechanism and their symptom in the modeled near-surface wind.

Surface error	Mechanism	Wind symptom
Surface too warm by day	H too large; too much convective mixing	afternoon U_{10} too high; boundary layer too deep
Soil too dry	LE too small, H too large	as above; bias grows through a dry spell
Soil too wet	H too small; shallow, weak mixing	afternoon U_{10} too low with the wind aloft correct
Roughness too low (wrong class, missing forest or town)	stress too small	U_{10} too high at all hours; u_* too low
Isotropic roughness at a site with directional roughness	one z_0 for all directions	bias whose sign changes with wind direction
Vegetation fraction wrong	momentum and thermal pathways together	mixed: day and night biases of different size or sign
City as roughness only	no heat storage or canyon geometry	nighttime urban wind and mixing too weak
Coastline shifted	roughness transition, heat capacity and breeze source moved	sea-breeze onset early or late; coastal wind wrong in a band about a cell wide
Lake omitted or shrunk	roughness, stability and breeze of land instead of water	wind near the lake too low, especially at night; no lake breeze
Snow missing or spurious	albedo, roughness, surface temperature and stability all change	bias in either direction; largest in light winds and at night

valley wind for the dispersion of what is emitted in it. This loss is *representativeness smoothing*: the reduction of the spatial range of a variable when it is represented by grid-cell values.

Figure 27.8 draws such a cell. The horizontal axis is distance across a 3 km cell whose center is a ridge crest and whose edges are valley floors, as the inset terrain profile at the top shows; the vertical axis is the near-surface wind. The blue curve is an illustrative real wind, $U(x) = 7.5 + 4.5\cos(2\pi x/3\,\mathrm{km})$ in m/s, which is $12\,\mathrm{m\,s^{-1}}$ at the crest and $3\,\mathrm{m\,s^{-1}}$ at the valley floors; the dashed line is its mean over the cell, $7.5\,\mathrm{m\,s^{-1}}$; the red line is the model's $7\,\mathrm{m\,s^{-1}}$. The two dots mark a ridge sensor and a valley sensor.

The real wind passes through $7\,\mathrm{m\,s^{-1}}$ only on the two slopes; the places where a sensor would be installed, the crest and the valley floors, are far from it. The model value is a good estimate of the cell mean, which is the quantity a grid-cell value represents, and a poor estimate of the wind at any chosen point.

27.6.2 Model error and scale mismatch in validation

If the model's $7\,\mathrm{m\,s^{-1}}$ is compared with the $12\,\mathrm{m\,s^{-1}}$ of the ridge sensor, the model appears to underpredict by $5\,\mathrm{m\,s^{-1}}$. But some fraction of that is expected, because the grid cell cannot represent the ridge. In Figure 27.8 the decomposition is exact: the model differs from the cell mean of the real wind by $7.0 - 7.5 = -0.5\,\mathrm{m\,s^{-1}}$, and the cell mean differs from the ridge wind by $7.5 - 12 = -4.5\,\mathrm{m\,s^{-1}}$. The first part is model error, the error the model makes in the quantity it represents; the second is scale mismatch, the difference between the cell mean and the point value, which the model is not designed to reproduce. Here 90 % of the apparent error is scale mismatch. Against the valley sensor the same model appears to overpredict by $4\,\mathrm{m\,s^{-1}}$, with the same $-0.5\,\mathrm{m\,s^{-1}}$ of model error inside it.

Validation should therefore distinguish model error from scale mismatch. In practice the

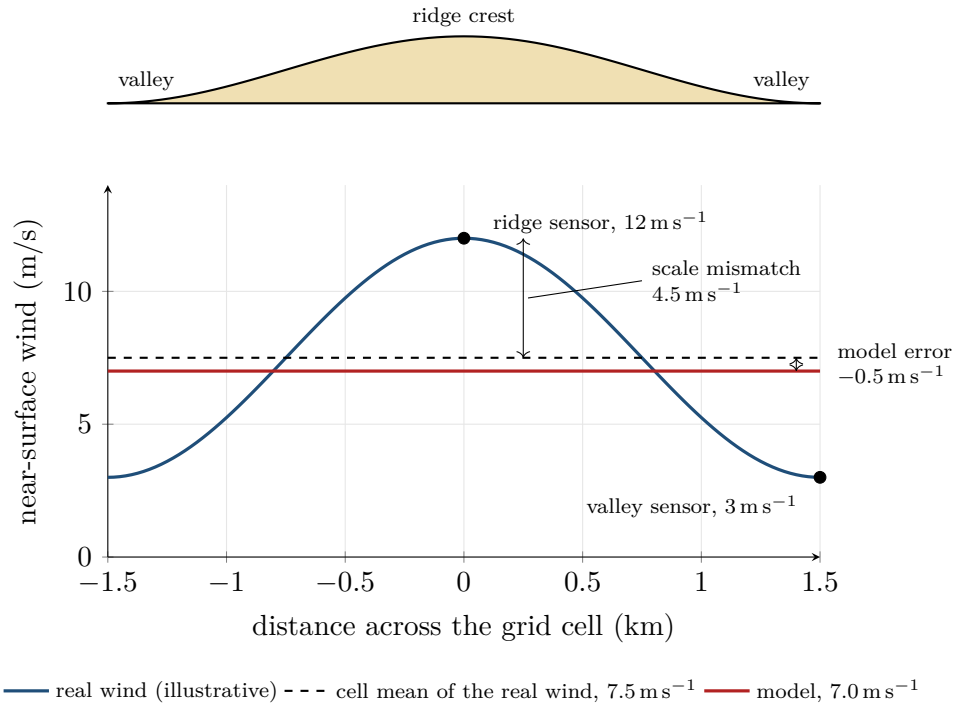


Figure 27.8: Representativeness smoothing in one 3 km grid cell. Real wind $U(x) = 7.5 + 4.5\cos(2\pi x/3\,\mathrm{km})$ (illustrative), its cell mean and the model's grid-cell value; the inset at the top is the terrain profile. Against the ridge sensor, the model's $-5\,\mathrm{m\,s^{-1}}$ splits into a model error of $-0.5\,\mathrm{m\,s^{-1}}$ and a scale mismatch of $4.5\,\mathrm{m\,s^{-1}}$.

cell mean of the real wind is not measured, and the split has to be estimated: from several sensors in the cell, from a terrain flow model that gives the ratio of the point wind to the cell mean (the speed-up factors of Chapter 20), or at least from the sensor's exposure relative to the cell. A validation statistic that mixes stations on crests, slopes and valley floors without such a correction mostly measures the terrain, not the model. Chapter 23 treats the representativeness of a station and Chapter 24 the verification statistics themselves.

> **Principle 27.2.** *A difference between a grid-cell wind and a point measurement is the sum of model error and scale mismatch. Validation that attributes the whole difference to the model judges the model on a quantity it does not represent.*

27.6.3 Statistical, dynamical and microscale correction

Three families of methods carry a grid-cell wind to a site. They are the subject of Chapters 28 and 29; here each is described by what it does with the surface representation.

Statistical downscaling. If a model systematically underpredicts a ridge station, a statistical correction can be learned from a record of model winds and observations, for example the linear regression

$$U_{\mathrm{local}} = b_0 + b_1\, U_{\mathrm{NWP}}, \tag{27.8}$$

with coefficients fitted to the record; illustrative values $b_0 = 0.6\,\mathrm{m\,s^{-1}}$ and $b_1 = 1.6$ turn a model wind of $7\,\mathrm{m\,s^{-1}}$ into $11.8\,\mathrm{m\,s^{-1}}$. This can work very well at that site. But it does not necessarily recover the correct physics: it may simply learn the local exposure relationship, the average ratio of the crest wind to the grid-cell wind over the conditions in the record, and it says nothing about why the ratio is what it is or how it changes in conditions the record lacks.

Dynamical downscaling. Alternatively, a finer atmospheric model can be run nested inside the coarse one: the coarse model supplies the forcing at the boundaries of a smaller domain, the finer model carries finer terrain and land cover, and it computes a more detailed local wind. This is *dynamical downscaling*. It preserves more physical structure than a statistical correction, because the finer model computes the terrain flow it resolves. It costs more computation: refining the grid spacing by a factor r multiplies the number of columns by r^2 and, through the time step that must shrink with the grid spacing, the number of steps by r, so a nest from 3 km to 1 km costs about $3^3 = 27$ times as much per unit area and time.

Microscale correction. At even smaller scales, the weather model is combined with a terrain flow model: computational fluid dynamics (CFD), linearized terrain models, or empirical speed-up factors (Chapter 20). The chain then becomes

$$\text{global model} \longrightarrow \text{regional weather model} \longrightarrow \text{local terrain model} \longrightarrow \text{site wind},$$

each stage carrying the scales the one above cannot. This is often necessary for site-specific wind prediction, because the terrain and obstacles that set the wind at a span or a turbine are tens to hundreds of meters across, far below the effective resolution of any weather model.

27.6.4 Static and state-dependent correction

A static correction assumes a fixed relation, for example

$$U_{\text{site}} = 1.2\, U_{\text{NWP}}.$$

But the real terrain response depends on the wind direction β, the stability and the wind speed U (Chapter 20). A better conceptual model is

$$U_{\text{site}} = \mathcal{F}(U_{\text{NWP}},\ \beta,\ \text{stability},\ \text{terrain}), \tag{27.9}$$

a function of the state of the atmosphere for a given terrain, not one fixed multiplier. For a crest site, illustrative values might be a factor of 1.2 in neutral flow across the ridge, about 1.0 in flow along it, and 0.7 in weak stable flow that the ridge blocks below the site's height. The constant 1.2 is the first entry of that table, applied to all of it. The same reasoning applies to the regression of equation (27.8): its coefficients fitted over all conditions are an average of a state-dependent relation, and they are reliable only where the mix of conditions stays the same.

27.6.5 Resolution and parameterization

Higher resolution does not eliminate parameterizations. Even if the grid is refined from 3 km to 500 m, vegetation, buildings, most of the turbulence and small terrain remain unresolved, and parameterizations remain necessary for all of them. Only the partition between resolved and parameterized physics changes: at 500 m the hills of a few kilometers and the larger valleys move into the resolved part, and the hills of a few hundred meters, the forest edges and the buildings stay in the parameterized part, as roughness, subgrid drag and surface fluxes.

"Just use a finer weather model" is therefore an incomplete answer. Increasing the resolution can improve the terrain, the coastlines and the mesoscale circulations, such as sea breezes, valley winds and gap flows. But it can also enter the turbulence gray zone, the range of grid spacing near the size of the largest boundary-layer eddies, of the order of the boundary-layer depth, where the eddies are partly resolved and partly parameterized and both treatments are compromised (Chapter 5); a grid of a few hundred meters in a convective layer 1 km deep is inside it. It increases the sensitivity to land-surface details, because each cell now holds fewer surface types and an error in one class affects a larger share of the cell. It increases numerical noise over steep terrain, which a finer grid resolves with steeper slopes, and with it the pressure-gradient errors of Section 27.2.2. And it exposes deficiencies in parameterizations that were designed and tuned for coarser grids. Finer is not automatically better in every regime.

27.6.6 A diagnostic decomposition

When a local wind forecast is wrong, five questions often identify the real source of the error. Table 27.5 lists them. Each row is one candidate source; the columns give the question to ask, the evidence that answers it, and the symptom that points to it. The first three rows are the surface representation of this chapter; the fourth is the boundary-layer physics (Chapter 26); the fifth is the comparability of model and measurement.

Table 27.5: A diagnostic decomposition of a local wind-forecast error.

Source	Question	Evidence	Typical symptom
Terrain	Is the real topography represented?	$z_{\mathrm{stn}} - z_{\mathrm{model}}$; model against real relief; speed-up factor of the site	bias at exposed or sheltered sites, larger in cross-ridge directions
Roughness	Is the land-cover drag realistic?	model z_0 and class against the site's roughness by direction	bias at all hours; sign changes with direction
Thermal surface	Are the surface temperature and heat flux reasonable?	model against observed surface temperature, H, Bowen ratio, soil moisture, snow	bias mainly in the afternoon or at night; drifts with dry and wet spells
Boundary layer	Is the mixing correct?	modeled against observed z_i, wind shear and inversion strength	night wind too high near the surface, too low aloft; jet misplaced
Scale	Is the model quantity comparable with the point measurement?	cell mean against point value; sensor exposure; averaging time	large error with near-zero error of the cell mean

The rows are not exclusive: a crest station in a model cell that is too low, too smooth and too wet can carry three of them at once, as Example 27.1 carried a terrain part and a remainder. Working through them in order turns "the model is wrong by $3\,\mathrm{m\,s^{-1}}$" into a set of statements about which part of the error belongs to the surface representation, which to the atmospheric physics and which to the comparison itself, and each part has its own remedy. The next chapter takes up the remedies that act on the model output, the statistical and dynamical downscaling methods that convert a coarse model wind into a site-specific wind forecast (Chapter 28).

27.7 What to retain

Definition 27.1 (Effective surface representation)**.** A weather-model grid cell does not contain the real surface but an effective representation of it: smoothed terrain, one land-use class or a mosaic of tiles, one effective roughness and one thermal state. The near-surface wind is computed over that representation, so its errors come either from the atmospheric dynamics or from how the model represents the surface, and the two are different problems with different remedies.

Table 27.6 lists the terms of the chapter, their meaning, their units and the subsection that defines each.

27.8 Exercises

Exercise 27.1. A wind station stands at $z_{\mathrm{stn}} = 950\,\mathrm{m}$ on the crest of a long ridge rising from valleys at 350 m, with a half-width of 3 km. The model cell containing it has $z_{\mathrm{model}} = 620\,\mathrm{m}$; the model's ridge rises 270 m above its valleys with a half-width of 6 km. (a) With $T = 288\,\mathrm{K}$

Table 27.6: The terms of the chapter and where each is defined.

Term	Meaning	Units	Defined in
Effective surface	the single values of terrain, roughness, class and thermal properties a model gives a grid cell	–	27.1.1
Terrain smoothing	reduction of real topographic detail by cell averaging and numerical filtering; ridges lowered, valleys raised	–	27.2.1
Effective elevation z_{model}	the one representative terrain height of a grid cell	m	27.2.4
Representation mismatch	difference between model and observation caused by different surfaces or locations, not by the model's atmosphere	as variable	27.2.5
Land-use class	surface category from which a model takes z_0, albedo, vegetation fraction, LAI and soil properties	–	27.3.1
Land-surface mosaic	fractional representation of several surface types in one cell, each with its own fluxes, averaged for the atmosphere	–	27.3.3
Effective roughness	grid-scale roughness length whose stress equals the area-mean stress of the cell	m	27.3.4
Momentum and thermal pathways	the routes by which the surface reaches the wind: through the stress, and through the heat fluxes and stability	–	27.3.7
Subgrid orography	terrain smaller than the model resolves, described by σ_h, anisotropy and orientation	m	27.4.1
Mountain-wave drag	parameterized momentum loss from unresolved terrain-generated gravity waves, deposited where they break	Pa	27.4.2
Flow blocking	diversion or stagnation of stable low-level flow by terrain; parameterized as low-level drag	–	27.4.3
Orographic drag	momentum loss caused by terrain, as distinct from roughness drag	Pa	27.4.4
Land-sea mask	field giving the land or water status, or fraction, of each cell	–	27.5.3
Effective resolution	smallest scale a model represents reliably, about 5 to 10 Δx	m	27.2.7
Representativeness smoothing	loss of local extremes when a variable is represented by grid-cell values	–	27.6.1
Dynamical downscaling	finer weather model driven by a coarser model's output	–	27.6.3

and 940 hPa at the model's ground, compute the hydrostatic pressure difference between the model's ground and the station, and the temperature difference under a lapse rate of 6.5 K per kilometer. (b) In neutral cross-ridge flow the model's 10 m wind is $5.5\,\mathrm{m\,s^{-1}}$ and the station measures $8.5\,\mathrm{m\,s^{-1}}$. With $\Delta S_{\max} \approx 2\,h_m/L_h$, estimate the crest wind the model would give over the real ridge and split the apparent error into a representation part and a remainder. (c) Check that both ridges lie within the range of the rule.

Exercise 27.2. A grid cell is 50 % grassland ($z_0 = 0.03\,\mathrm{m}$), 30 % forest ($z_0 = 1.0\,\mathrm{m}$) and 20 % water ($z_0 = 0.0002\,\mathrm{m}$). Take a blending height of 60 m, a wind of $10\,\mathrm{m\,s^{-1}}$ there, $\rho = 1.2\,\mathrm{kg\,m^{-3}}$ and neutral air, displacement neglected. (a) Compute the stress of each tile, the mosaic stress, and the effective roughness length. (b) Compare it with the dominant-class value and with the arithmetic and geometric means of the roughness lengths. (c) Compute the neutral 10 m wind over each tile and over the effective surface. (d) With an available energy of $400\,\mathrm{W\,m^{-2}}$ and Bowen ratios of 1.0 (grass), 0.4 (forest) and 0.1 (water), compute the mosaic sensible heat flux and the flux obtained by averaging the Bowen ratios first.

Exercise 27.3. A transmission line in southern Brazil, at 30°S, runs past a site with open fields ($z_0 = 0.03\,\mathrm{m}$) in the sector from 270° to 360° and forest ($z_0 = 1.0\,\mathrm{m}$) in the sector from 180° to 270°. The weather model uses an isotropic $z_0 = 0.37\,\mathrm{m}$. (a) The geostrophic wind blows from 250°, and surface friction turns the surface wind by 25° toward low pressure. Give the surface wind direction at 30°S and, for comparison, at 30°N. (b) Which surface lies upwind of the site in each case? (c) For a common neutral wind of $10\,\mathrm{m\,s^{-1}}$ at 60 m, compute the real and the modeled 10 m wind in each case and the model's relative error. (d) Explain why a bias averaged over all directions could be close to zero at this site.

Exercise 27.4. (a) A 3 km cell contains an exposed ridge where the wind is $13\,\mathrm{m\,s^{-1}}$ over 30 % of the cell and sheltered ground where it is $4\,\mathrm{m\,s^{-1}}$ over the rest. The model gives $6.0\,\mathrm{m\,s^{-1}}$. Compute the cell mean of the real wind and split the model's apparent error against a ridge sensor into model error and scale mismatch. (b) On a 3 km grid the model coastline lies 1.2 km seaward of the real one. A sea-breeze front advances inland at $2.5\,\mathrm{m\,s^{-1}}$. By roughly how long is its arrival at a site 10 km inland shifted, and in which direction? (c) A nest refines the grid from 3 km to 1 km and then to 333 m. Give the effective resolution of each grid with the rule of 5 to $10\,\Delta x$, and the cost of each refinement relative to the previous one.

Chapter 28

Statistical and Dynamical Downscaling

28.1 The downscaling problem

The three preceding chapters described the weather model as a system, its boundary-layer schemes and the way it represents the surface. Each ended at the same place: the model produces a wind that belongs to a grid cell over smoothed terrain with an effective roughness, while an engineering application needs the wind at one point, at one height, over the real surface. This chapter treats the methods that bridge the two. Its question is

how is a coarse-grid weather forecast turned into a useful site-specific wind forecast?

There are two families of answers. *Statistical downscaling* learns the relationship between the model output and local observations from a historical record. *Dynamical downscaling* runs a finer atmospheric or flow model that solves more of the local physics explicitly. A third route, *hybrid downscaling*, chains the two. The chapter states the problem and its target, then follows the statistical methods from the simplest correction to regression and machine learning together with the ways they fail, then the dynamical and microscale methods, and closes with the choice between them, their combination and the representation of uncertainty.

Jargon: downscaling, statistical downscaling, dynamical downscaling, hybrid downscaling, predictor, predictand, training record

Downscaling is any method that estimates a local, fine-scale atmospheric quantity, here the wind speed or velocity at a site, in meters per second, from the coarser output of a weather model. *Statistical downscaling* does so with a relationship fitted to past pairs of model output and site observations. *Dynamical downscaling* does so by running another physical model, a weather model on a finer grid or a microscale terrain or flow model, driven by the coarse model. *Hybrid downscaling* applies a physical model first and a statistical correction to its result. A *predictor* is an input variable of a statistical model, such as the model wind speed or the hour of the day; the *predictand* is the quantity it predicts, here the site wind. The *training record* is the set of past predictor and predictand values from which a statistical model is fitted.

Key idea

Downscaling translates a grid-scale atmospheric state into a site-scale one. Statistical methods learn that translation from data, dynamical methods compute more of it from physics, and both are judged only against an explicitly defined target.

28.1.1 Why downscaling is needed

Consider a regional weather model with a grid spacing of $\Delta x = 3\,\mathrm{km}$ and a site that sits on a ridge, at a forest edge, on a valley floor or along a transmission corridor that crosses all three. The model wind is the wind of an effective grid-cell flow: an average over a cell 3 km wide, over terrain smoothed to the model's effective resolution of about 15 to 30 km (Chapter 5), with a single effective roughness length for the cell (Chapter 11), and with its 10 m value diagnosed from the lowest model level by surface-layer similarity (Chapter 12). The ridge that accelerates the wind, the forest edge that slows it and the valley that decouples at night are smaller than the cell; the model either smooths them away or represents them by their average effect.

The site wind is therefore a function of the model wind and of everything the model does not resolve:

$$U_{\mathrm{site}} = F(U_{\mathrm{NWP}},\ \beta,\ \text{stability},\ \text{terrain},\ \text{roughness}), \tag{28.1}$$

where U_{site} is the wind speed at the site and target height, U_{NWP} the model wind speed at the corresponding model point and height, β the wind direction, measured clockwise from north as the direction the wind comes from, the stability is expressed for instance by the stability parameter z/L_{O} of Chapter 14, and terrain and roughness describe the site's surroundings. Downscaling is the estimation of the function F. The weather model supplies the first arguments; the method of downscaling decides how the rest enter.

28.1.2 Statistical, dynamical and hybrid routes

Figure 28.1 draws the three routes from the grid-cell wind to the site wind. The top box is the forecast of the coarse model; the three boxes in the middle row are the three families of methods, each with the techniques it contains; the bottom box is the site wind at an explicit target. Solid arrows carry the forecast, and the dashed arrows show where a training record of site observations enters.

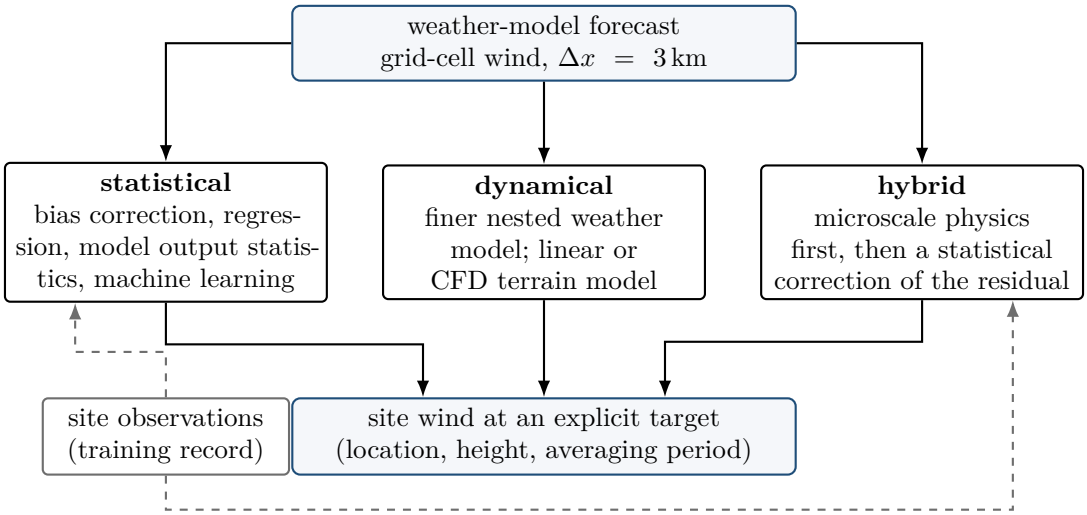


Figure 28.1: Three routes from the grid-cell wind of a weather model to the wind at a site (schematic). Solid arrows carry the forecast; dashed arrows show where site observations train the statistical part of a method.

The statistical route needs a training record at the site and costs little to run once fitted. The dynamical route needs no site record but needs a physical model, its setup and its computing time; it can produce winds at sites where nothing is measured. The hybrid route needs both: the physical model computes the part of the local wind that physics can predict, and the statistical model learns the residual from observations. The three routes are compared in Section 28.6.

28.1.3 The target must be explicit

A downscaling method cannot be judged without knowing what it is meant to predict. Four plausible targets near the same transmission line are the 10 m wind over open, flat terrain; the wind at conductor height, perhaps 20 to 30 m, along a span; the wind on the ridge the line crosses; and the wind at the anemometer of the nearest station. They are different quantities. The first is the standard reference exposure used to compare stations (Chapter 23); the second is what sets the convective cooling of the conductor and thus its rating; the third includes the terrain speed-up of Chapter 20; the fourth includes whatever the instrument and its mounting do to the flow (Chapter 22).

A target is specified by its location, its height above local ground, its averaging period (a 10-minute mean, an hourly mean or a gust) and, for statistical methods, by the instrument that defines it. A method trained to reproduce one of these targets and evaluated against another acquires an error that is a property of the mismatch, not of the method. The target is therefore fixed first, and every comparison in the rest of the chapter is made against a stated target.

28.1.4 Downscaling as a translation between scales

The core of the problem is a translation from a grid-scale atmospheric state to a site-scale atmospheric state. The coarse model carries the synoptic pressure field, the stability, the boundary-layer depth and the mesoscale circulations; the site adds its terrain, roughness, obstacles and exposure. The task is to decide, for each local effect, which of four kinds it is. A *predictable* effect follows from the resolved state by known physics, such as the speed-up over a mapped ridge for a given direction and stability. A *systematic* effect repeats in the record and can be learned from it, such as a constant underestimate of the night wind at a sheltered station. An *unresolved* effect depends on structure the grid and the predictors do not carry, such as a single tree upwind of the mast. An *uncertain* effect varies from case to case with no predictor that explains it, such as the turbulent fluctuation of a 10-minute mean.

The methods of this chapter differ in which of these they handle. Physical models address the predictable part; statistical models address the systematic part; neither removes the unresolved and uncertain parts, which a good downscaling system represents as a stated uncertainty rather than hides inside a single number.

28.2 Simple statistical corrections

The simplest statistical methods correct the model wind with one or two fitted numbers. This section derives the general linear correction, treats its two special cases, the additive and the multiplicative correction, makes the correction depend on direction and stability, and shows with a worked example how a single correction fails when the site has two regimes.

28.2.1 The linear correction

Statistical downscaling learns a relationship between large-scale predictors, taken from the model, and local observations. The simplest such relationship is a straight line,

$$U_{\mathrm{site}} = a + b\,U_{\mathrm{NWP}}, \tag{28.2}$$

with an intercept a, in meters per second, and a dimensionless slope b, both fitted from a training record of n pairs $(U_{\mathrm{NWP},i},\, U_{\mathrm{obs},i})$ of model wind and observed site wind at the same times. Least squares chooses a and b to minimize the sum of squared errors $\sum_i (U_{\mathrm{obs},i} - a - b\,U_{\mathrm{NWP},i})^2$. Setting the derivatives with respect to a and b to zero gives two equations, whose solution is

$$b = \frac{\sum_i (U_{\mathrm{NWP},i} - \overline{U}_{\mathrm{NWP}})(U_{\mathrm{obs},i} - \overline{U}_{\mathrm{obs}})}{\sum_i (U_{\mathrm{NWP},i} - \overline{U}_{\mathrm{NWP}})^2}, \qquad a = \overline{U}_{\mathrm{obs}} - b\,\overline{U}_{\mathrm{NWP}}, \tag{28.3}$$

where the overbars are means over the training record. The slope is the covariance of the two winds divided by the variance of the model wind; the intercept makes the fitted line pass through the point of the two means.

The line contains the two simplest corrections as special cases. With $b = 1$ it shifts the model wind by a constant, the additive bias correction. With $a = 0$ it scales the model wind by a constant, the multiplicative correction. The two describe different physical situations, and the next two subsections take them in turn.

28.2.2 Additive bias correction

A *bias* is the systematic part of a model error: the mean, over a record, of the model value minus the observed value, in meters per second for wind speed. A *bias correction* removes it. Suppose the model systematically predicts $U_{\mathrm{NWP}} = 8\,\mathrm{m\,s^{-1}}$ when the site typically measures $U_{\mathrm{obs}} = 6\,\mathrm{m\,s^{-1}}$; the bias is $+2\,\mathrm{m\,s^{-1}}$, and the additive correction is

$$U_{\mathrm{corrected}} = U_{\mathrm{NWP}} - 2\,\mathrm{m\,s^{-1}}. \tag{28.4}$$

The correction is easy to fit, needing only the mean of the differences, and easy to apply.

It assumes that the bias is the same at every wind speed, direction, hour and season, and usually it is not. At low wind the additive form also fails on its own terms: a model wind of $1.5\,\mathrm{m\,s^{-1}}$ becomes $-0.5\,\mathrm{m\,s^{-1}}$, an impossible speed, so the corrected value must be clipped at zero. A constant offset is appropriate when the error comes from a cause that does not scale with the wind, such as an anemometer threshold or a model that never quite becomes calm at night; it is inappropriate when the error is a fraction of the wind, which is the usual case for terrain and roughness effects.

28.2.3 Multiplicative correction

When the site wind is a fixed fraction of the model wind, the appropriate correction is a factor,

$$U_{\mathrm{site}} = S_c\, U_{\mathrm{NWP}}, \tag{28.5}$$

where S_c, dimensionless, is the *correction factor*. For a site on a ridge, with $S_c = 1.25$ and $U_{\mathrm{NWP}} = 8\,\mathrm{m\,s^{-1}}$, $U_{\mathrm{site}} = 1.25 \times 8\,\mathrm{m\,s^{-1}} = 10\,\mathrm{m\,s^{-1}}$. The factor resembles the terrain speed-up factor S of Chapter 20, and for a ridge much narrower than the grid cell it is dominated by it; the two are not identical, because S is measured against the undisturbed upstream wind, while S_c is measured against the model wind and therefore also absorbs the model's own errors. The multiplicative form keeps a calm model wind calm and scales errors with the wind, as terrain and roughness effects do. A simple fit is the ratio of the means, $S_c = \overline{U}_{\mathrm{obs}}/\overline{U}_{\mathrm{NWP}}$, which preserves the mean wind.

Table 28.1 shows when each correction is appropriate. Its first column is the model wind at three illustrative times; the next three columns belong to site A, whose observed wind is the model wind minus $2\,\mathrm{m\,s^{-1}}$, and give the observation and the values corrected by the additive and the multiplicative fit; the last three columns do the same for site B, a ridge site whose observed wind is 1.25 times the model wind.

At site A the mean difference, model minus observed, is $+2\,\mathrm{m\,s^{-1}}$, so the additive fit is $U_{\mathrm{NWP}} - 2\,\mathrm{m\,s^{-1}}$ and reproduces every observation; the ratio of the means is $18/24 = 0.75$, and the multiplicative fit overpredicts at low wind and underpredicts at high wind by $1\,\mathrm{m\,s^{-1}}$. At site B the mean difference is $-2\,\mathrm{m\,s^{-1}}$, and the additive fit $U_{\mathrm{NWP}} + 2\,\mathrm{m\,s^{-1}}$ makes the opposite errors, while the ratio of the means, $30/24 = 1.25$, reproduces every observation. Both wrong fits remove the mean bias and both leave a root-mean-square error of $\sqrt{(1^2 + 0^2 + 1^2)/3} \approx 0.82\,\mathrm{m\,s^{-1}}$. The general line (28.2) with (28.3) recovers $a = -2\,\mathrm{m\,s^{-1}}$, $b = 1$ at site A and $a = 0$, $b = 1.25$ at site B, so it fits both; which special case applies is a question about the physics of the error, and a scatter plot of the training record answers it.

Table 28.1: Additive and multiplicative corrections fitted at two illustrative sites. Site A: $U_{\mathrm{obs}} = U_{\mathrm{NWP}} - 2\,\mathrm{m\,s^{-1}}$; site B: $U_{\mathrm{obs}} = 1.25\,U_{\mathrm{NWP}}$. All values in m/s.

	Site A (constant offset)			Site B (ridge, constant ratio)		
U_{NWP}	observed	offset −2	factor 0.75	observed	offset +2	factor 1.25
4	2	2	3	5	6	5
8	6	6	6	10	10	10
12	10	10	9	15	14	15
RMSE		0	0.82		0.82	0

28.2.4 Direction- and stability-dependent correction

One constant factor is too simple for a site in terrain, because the terrain the wind crosses depends on where the wind comes from. A more realistic model lets the factor depend on direction,

$$U_{\mathrm{site}} = S_c(\beta)\,U_{\mathrm{NWP}}. \tag{28.6}$$

For a site on a north–south ridge with a sheltering hill to its north, illustrative values are $S_c(270^\circ) = 1.3$ for westerly flow across the ridge and $S_c(0^\circ) = 0.9$ for northerly, sheltered flow. In practice the factor is fitted separately for each direction sector of the model wind, often twelve sectors of 30°, or as a smooth function of direction (Section 28.3.2). This already captures the directional terrain effects of Chapter 20 and the directional roughness $z_0(\beta)$ of Chapter 11.

Terrain response and vertical mixing also depend on stability, so a physically more defensible model is

$$U_{\mathrm{site}} = S_c(\beta, z/L_{\mathrm{O}})\,U_{\mathrm{NWP}}, \tag{28.7}$$

with the stability parameter z/L_{O} taken from the model's surface layer (the literature often writes it ζ; this book reserves ζ for the relative vorticity). For the westerly sector of the ridge, neutral flow has the strong crest speed-up, say $S_c = 1.3$; strongly stable flow, with a Froude number below one (Chapter 20), may be blocked, so that the crest wind falls below the model wind, say $S_c = 0.6$; and unstable flow mixes momentum through a deep layer, which reduces the contrast between the site and the cell and brings the factor closer to one, say $S_c = 1.1$ (all illustrative). In practice the stability is binned into a few classes and the factor is tabulated by sector and class, the same structure as the speed-up maps of Chapter 20. Each added dimension divides the training record among more cells, and a cell with few samples has a poorly determined factor; this cost returns in Section 28.6.5.

28.2.5 One correction for two regimes

Suppose a site has two regimes of roughly equal frequency and similar model winds. In westerly, near-neutral flow the site wind is $U_{\mathrm{site}} = 1.3\,U_{\mathrm{NWP}}$; in easterly, stable flow it is $U_{\mathrm{site}} = 0.6\,U_{\mathrm{NWP}}$. A single factor fitted to the whole record by least squares through the origin is $S_c = \sum U_{\mathrm{NWP}} U_{\mathrm{obs}} / \sum U_{\mathrm{NWP}}^2$, which is the average of the two regime factors weighted by each regime's share of $\sum U_{\mathrm{NWP}}^2$; with equal shares,

$$S_c = \tfrac{1}{2}(1.3 + 0.6) = 0.95.$$

Figure 28.2 plots the situation. The horizontal axis is the model wind and the vertical axis the observed site wind; the blue circles are illustrative westerly neutral hours, the red squares easterly stable hours, the two thin lines the regime relations, and the dashed black line the single fitted correction. The vertical arrows mark the errors of the single fit at a model wind of $8\,\mathrm{m\,s^{-1}}$.

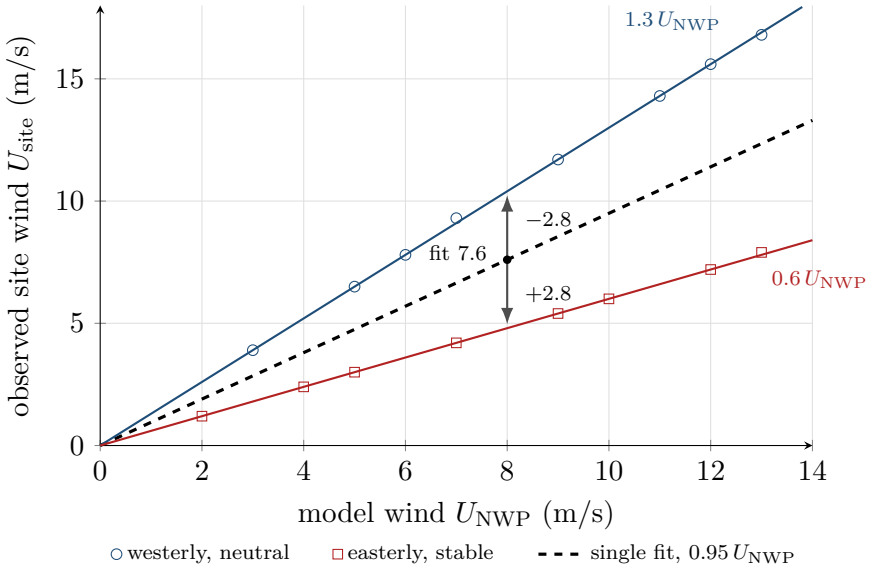


Figure 28.2: A site with two regimes (illustrative): westerly near-neutral hours follow $U_{\text{site}} = 1.3\,U_{\text{NWP}}$, easterly stable hours $U_{\text{site}} = 0.6\,U_{\text{NWP}}$. The single factor fitted to both, 0.95, has zero mean error over the record and is wrong in both regimes; arrows show its errors at $U_{\text{NWP}} = 8\,\text{m s}^{-1}$.

The single fit lies between the two clouds of points and passes through neither. At a model wind of $8\,\text{m s}^{-1}$ it predicts $7.6\,\text{m s}^{-1}$; the westerly site wind is $10.4\,\text{m s}^{-1}$, so the fit is $2.8\,\text{m s}^{-1}$ or 27 % too low, and the easterly site wind is $4.8\,\text{m s}^{-1}$, so the fit is $2.8\,\text{m s}^{-1}$ or 58 % too high. Averaged over the record the errors cancel: the mean bias is zero and the correction looks perfect by that measure, while its root-mean-square error at this model wind is $2.8\,\text{m s}^{-1}$. The consequence is not symmetric for an application. For a transmission line, whose rating rises with the wind that cools the conductor, the stable easterly error overstates the cooling wind by more than half on exactly the nights when the wind is weakest, and the rating computed from it is unsafe. A conditional model, with one factor per regime, removes both errors; Section 28.3.5 builds such models.

28.3 Regression and model output statistics

The corrections of the previous section use one predictor, the model wind, with the direction and stability entering only through binning. This section adds more predictors in a regression, shows how a circular variable such as direction must be encoded, describes the meteorological method of model output statistics, adds terrain descriptors, builds regime-dependent models and explains why predicting wind components can be better than predicting speed and direction.

28.3.1 Multiple linear regression

A multiple linear regression predicts the site wind from several predictors at once:

$$U_{\text{site}} = a_0 + a_1\,U_{\text{NWP}} + a_2\,x_\beta + a_3\,T + a_4\,\text{Ri}_B + \cdots + \delta, \tag{28.8}$$

where the a_j are fitted coefficients (written a because β is the wind direction in this book), x_β stands for an encoding of the model wind direction (Section 28.3.2), T is the model temperature, Ri_B is the bulk Richardson number between two model levels (Chapter 13), and δ is the residual, the part of the site wind the predictors do not explain. Each coefficient has the units of the site wind divided by those of its predictor: a_1 is dimensionless, a_3 is in $\text{m s}^{-1}\,\text{K}^{-1}$.

With n training times and n_p predictors, the predictor values form an $n \times (n_p + 1)$ matrix $\mathbf{X}$ whose first column is ones, the observations form a vector $\mathbf{y}$, and the coefficients a vector $\mathbf{a}$. Least squares minimizes $\|\mathbf{y} - \mathbf{X}\mathbf{a}\|^2$; setting its gradient to zero gives the normal equations and their solution,

$$\mathbf{X}^\top \mathbf{X}\,\mathbf{a} = \mathbf{X}^\top \mathbf{y}, \qquad \mathbf{a} = (\mathbf{X}^\top \mathbf{X})^{-1} \mathbf{X}^\top \mathbf{y}, \tag{28.9}$$

of which equation (28.3) is the case $n_p = 1$. The model is linear in its coefficients, not necessarily in the physics: a predictor may be a product such as $U_{\mathrm{NWP}} \sin\beta$, so that the direction effect scales with the wind as a speed-up does, and the fitted function is then a direction-dependent factor of the kind of equation (28.6).

28.3.2 Encoding direction

Direction cannot enter a regression as a number of degrees. The directions 359° and 1° are two degrees apart, but as numbers they differ by 358; a term $a_2\beta$ with an illustrative $a_2 = 0.001\,\mathrm{m\,s^{-1}}$ per degree predicts site winds that differ by $0.36\,\mathrm{m\,s^{-1}}$ for two nearly identical northerly winds, and it places a jump at north that does not exist in the atmosphere. Direction is a circular variable, and it is encoded by the two coordinates of a point on the unit circle,

$$x_\beta = \cos\beta, \qquad y_\beta = \sin\beta, \tag{28.10}$$

which vary continuously all the way around: $\cos\beta$ is the northward and $\sin\beta$ the eastward coordinate of the point from which the wind comes.

Figure 28.3 contrasts the two encodings. The left panel places directions on a number line from 0 to 360°; the right panel places them on the unit circle, with the eastward coordinate $\sin\beta$ horizontal, the northward coordinate $\cos\beta$ vertical and north at the top. The directions 1° and 359° are marked in both, and 181° is marked as a direction that is truly far from them.

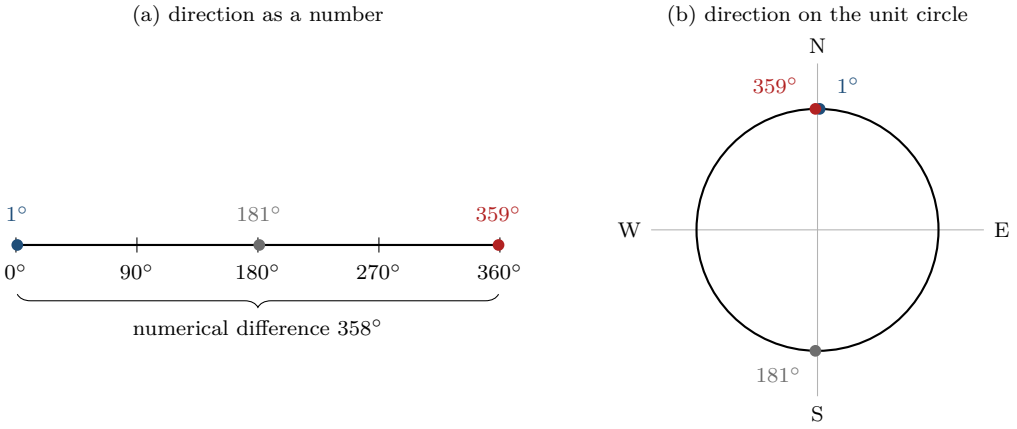


Figure 28.3: Two encodings of wind direction. (a) As a number of degrees, 1° and 359° lie at opposite ends of the scale. (b) As the point $(\sin\beta, \cos\beta)$ on the unit circle, with $\sin\beta$ horizontal (eastward), $\cos\beta$ vertical (northward) and north at the top, they are neighbors, 0.035 apart, while 181° lies across the circle, 2.0 away.

On the number line the two northerly directions are as far apart as two directions can be, and 181°, a southerly, sits halfway between them. On the circle the order is right. The worked numbers are $\cos 359° = \cos 1° = 0.99985$ and $\sin 359° = -0.01745$, $\sin 1° = +0.01745$, so the two points differ only in their eastward coordinate, by $0.0349 = 2\sin 1°$, the chord of a 2° arc; the point for 181° lies at a distance of 2.0, a diameter, from both. Circular continuity is preserved.

The encoding also gives the fitted direction effect a physical shape. A regression with the terms $a_s \sin\beta + a_c \cos\beta$ fits

$$a_s \sin\beta + a_c \cos\beta = A\cos(\beta - \beta_0), \qquad A = \sqrt{a_s^2 + a_c^2}, \quad \cos\beta_0 = a_c/A,\ \sin\beta_0 = a_s/A, \tag{28.11}$$

a single smooth wave around the compass with its maximum at the direction β_0 and its minimum opposite. For the factor of Section 28.2.4, the illustrative fit $S_c(\beta) = 1.1 - 0.2\sin\beta - 0.2\cos\beta$ reproduces $S_c(270°) = 1.1 + 0.2 = 1.3$ and $S_c(0°) = 1.1 - 0.2 = 0.9$; its amplitude is $A = 0.28$ and its maximum, 1.38, lies at $\beta_0 = 225°$, with the minimum, 0.82, at 45°. A ridge accelerates winds from both sides, so its factor peaks twice around the compass; the terms $\sin 2\beta$ and $\cos 2\beta$, the second harmonic, represent that, just as the $\sin^2$ dependence on the crossing angle in Chapter 20 equals $\frac{1}{2}(1 - \cos 2\gamma)$. The same encoding applies to every circular predictor: the hour of the day, t in hours, enters as $\sin(2\pi t/24)$ and $\cos(2\pi t/24)$, the day of the year as the sine and cosine of 2π times its fraction of the year, and the aspect of a slope like a direction.

28.3.3 Model output statistics

Model output statistics (MOS) is the classic meteorological form of statistical downscaling: a regression, fitted separately for each site, each forecast lead time and often each season, that learns the systematic relationships between the output of a weather model and the weather observed at the site. Its goal is to correct known model biases statistically. For wind, typical predictors are the model wind, the model pressure gradient, a stability measure, the temperature, the cloud cover, the time of day and the season; the predictand is the observed wind at the station. Because the relationship is fitted to the forecasts of the model at the lead time it will be applied to, MOS corrects both the model's representation error and its forecast error at that lead time.

The difference from a raw bias correction is the conditioning. A bias correction might say only $U_{\text{corrected}} = U_{\text{NWP}} - 1\,\text{m s}^{-1}$ for every forecast. MOS writes

$$U_{\text{corrected}} = f(U_{\text{NWP}},\ \beta,\ \text{Ri}_B,\ \text{hour},\ \text{season}), \tag{28.12}$$

with f usually a multiple linear regression with the encodings of the previous subsection. It can therefore learn regime-dependent errors: a model that overestimates the wind at a sheltered station by $2\,\text{m s}^{-1}$ on stable nights and by nothing on windy afternoons gets a correction of $2\,\text{m s}^{-1}$ at night and none in the afternoon, where a single bias correction would subtract $1\,\text{m s}^{-1}$ from both and be wrong by $1\,\text{m s}^{-1}$ each time. The pressure-gradient predictor is a reminder that the hemisphere enters the physics of a predictor: Section 28.4.7 shows that the same gradient implies opposite wind directions in the two hemispheres.

28.3.4 Terrain-aware predictors

A regression fitted at one site learns that site's corrections without knowing why they arise. One way to give a statistical model some knowledge of the cause, and thereby some ability to work at other sites, is to add physical descriptors of the site as predictors: elevation, slope, aspect (the direction a slope faces, encoded like a wind direction), curvature (whether the ground is convex, as on a crest, or concave, as in a hollow), ridge exposure (the height of the site above its surroundings within a stated radius, the exposure of Chapter 20), roughness, and distance to the coast. These descriptors are computed from elevation and land-cover maps, and they are constant at a given site.

Because they are constant at one site, terrain predictors carry no information in a single-site regression; they act only when the model is trained on many sites at once, where the variation among sites reveals how, for instance, the correction factor grows with ridge exposure. They are most useful in products with the wind direction: exposure matters for the winds that cross the

ridge, so a predictor such as the elevation difference toward the upwind direction carries more information than the elevation alone. The model then has some information about why the local wind differs from the grid-cell wind, which is the condition for transferability (Section 28.4.7).

28.3.5 Regime-dependent models

The example of Section 28.2.5 suggests a strong approach: classify the atmospheric state first, then use a separate downscaling relationship in each class. A *regime-dependent model* is such a set of relationships with a classification rule that selects one of them from the predictors available at forecast time. It reflects the fact that different physics dominate in different regimes: terrain speed-up in strong, well-mixed flow; decoupling and blocking on stable nights; deep mixing on convective days; local thermal circulations when the synoptic forcing is weak.

Table 28.2 lists five regimes and an illustrative classification. Each row gives the regime, the conditions in the model output that select it, and the physics that governs the site wind in it. The rules are applied in the order of the table, so that a strong synoptic wind takes precedence over the time of day, and the hours that match no rule fall into a near-neutral default class.

Table 28.2: An illustrative regime classification for a coastal site with nearby terrain. Thresholds are examples; each site needs its own.

Regime	Selected when (model output)	Dominant physics at the site
Strong synoptic	wind at 100 m above $10\,\mathrm{m\,s^{-1}}$	near-neutral, mechanically mixed; terrain speed-up by direction
Sea breeze	daytime, wind at 100 m below $5\,\mathrm{m\,s^{-1}}$, land warmer than sea, onshore direction	thermally driven onshore flow (Chapter 19); direction turns through the day
Drainage	night, $z/L_\mathrm{O} > 0.1$, wind at 100 m below $3\,\mathrm{m\,s^{-1}}$, downslope direction	cold air flowing down slopes and valleys; weak, shallow, direction fixed by terrain
Convective day	daytime, $z/L_\mathrm{O} < -0.1$	deep mixing; site wind close to the cell wind, gusty
Stable night	night, $z/L_\mathrm{O} > 0.1$	decoupling, blocking, sheltering; site wind well below the model wind

The classification uses only model quantities, so it can be applied when a forecast is issued. The sea-breeze row shows why a rule keyed on direction must respect the hemisphere: the sea-breeze wind vector turns clockwise through the day in the Northern Hemisphere and counterclockwise in the Southern Hemisphere (Chapter 19), so the direction sector that marks the afternoon sea breeze on an east-facing coast lies south of east in the Northern Hemisphere and north of east in the Southern Hemisphere. The cost of regimes is data: five regimes divide the training record five ways, and a rare regime, such as drainage on a site where it occurs on a few nights a month, may have too few independent events for a reliable fit. Merging rare regimes with a physically similar one, or sharing coefficients across regimes except those the physics says differ, keeps each fit determined.

28.3.6 Predicting wind components

Instead of predicting the speed U and the direction β, a statistical model can predict the eastward and northward components u and v of the wind and recover the speed and direction from them:

$$U = \sqrt{u^2 + v^2}, \qquad u = -U \sin\beta, \quad v = -U \cos\beta, \tag{28.13}$$

so that β is the angle whose sine is $-u/U$ and whose cosine is $-v/U$, between 0° and 360°. The minus signs appear because β is the direction the wind comes from, while u and v point where it goes. For predicted components $u = 3\,\mathrm{m\,s^{-1}}$ and $v = -4\,\mathrm{m\,s^{-1}}$, the speed is $5\,\mathrm{m\,s^{-1}}$; the wind

blows toward the east and south, so it comes from the northwest, and indeed $\sin\beta = -0.6$, $\cos\beta = 0.8$ give $\beta = 323°$. Check: $-5\sin 323.1° = 3.0$ and $-5\cos 323.1° = -4.0$.

Components avoid the circular-direction problem entirely, since u and v are ordinary real numbers, and they behave more smoothly in a statistical model: near calm, where the direction is undefined and jumps erratically, the components simply pass through zero. They have one trap. A model fitted by least squares predicts the conditional mean of u and of v, and the speed of a mean vector is smaller than the mean of the speeds whenever the direction is uncertain. If a forecast is equally likely to be $6\,\mathrm{m\,s^{-1}}$ from 250° or $6\,\mathrm{m\,s^{-1}}$ from 290°, the mean vector has a speed of $6\cos 20° = 5.64\,\mathrm{m\,s^{-1}}$, 6 % below the speed of either case. Speed derived from predicted components is therefore biased low where the direction is uncertain, and either the speed is predicted as a separate predictand or the components are used to set the direction only.

28.4 Machine-learning downscaling

Machine learning extends statistical downscaling from fitted lines to flexible functions of many predictors. This section describes what such models add, how they learn the wrong thing, why they extrapolate poorly, how they must be validated on autocorrelated records, and the data problems that decide whether they work: leakage, the calibration period, the quality of the observations and the step from one site to another.

28.4.1 Nonlinear conditional relationships

Modern statistical downscaling may use random forests, gradient boosting or neural networks to fit

$$U_{\mathrm{site}} = f_{\mathrm{ML}}(\mathbf{x}), \tag{28.14}$$

where $\mathbf{x}$ is a vector of possibly dozens of predictors: the model wind at several heights, its direction, the stability, the boundary-layer depth, pressure gradients, terrain descriptors and land cover. A random forest averages many regression trees, each of which splits the training record repeatedly on one predictor at a time and predicts, in each final group, the mean observed wind of that group; gradient boosting adds trees one after another, each fitted to the errors left by the previous ones; a neural network composes many weighted sums passed through nonlinear functions. All three are fitted by minimizing an error over the training record, as the regression was.

They work well because the local bias is often nonlinear and conditional: ridge speed-up only for certain directions, valley decoupling mainly at night, a sea breeze only under weak synoptic flow. A linear regression represents such effects only through products of predictors chosen in advance. A tree finds them by itself: a split on direction followed by a split on stability isolates the westerly neutral hours of Section 28.2.5, and the tree predicts for them a wind near $1.3\,U_{\mathrm{NWP}}$ without having been told that such a regime exists.

28.4.2 Learning the wrong thing

A flexible model fits whatever is in its training record, including what will not recur. If the record contains mostly westerly flow, the model is well determined for westerlies and poorly determined for the rare easterly events, which may be exactly the stable, blocked cases of Figure 28.2; its errors in those events can be large while its overall score is good. If the sensor was moved, or a tree grew beside it, during the record, the model learns a mixture of two sites and applies it to neither. The model may have learned site-specific quirks of the record rather than physics.

Hence a principle that applies to every statistical method and most strongly to the flexible ones.

Principle 28.1. *An excellent fit to the historical record is not the same as robust physical generalization; a statistical downscaling model is trusted only for conditions its training record represents, and only after a test on data it has not seen.*

28.4.3 Extrapolation

Statistical models perform best inside the range of conditions they were trained on. Suppose the model winds in the training record never exceeded $15\,\mathrm{m\,s^{-1}}$ and a storm forecast gives $30\,\mathrm{m\,s^{-1}}$. The model is then extrapolating beyond its evidence, and how it does so depends on its form. A linear regression continues its fitted line, which is right only if the physics stays the same at twice the wind. A tree-based model cannot extrapolate at all: each of its predictions is an average of training observations, so it can never predict a wind above the largest wind in its training groups.

Figure 28.4 shows this. The horizontal axis is the model wind and the vertical axis the predicted site wind; the shaded band is the range of the training record, the dashed line the true relation $U_{\mathrm{site}} = 1.25\,U_{\mathrm{NWP}}$ of the ridge site of Table 28.1, and the red steps the prediction of a regression tree with bins $1.5\,\mathrm{m\,s^{-1}}$ wide fitted inside the band.

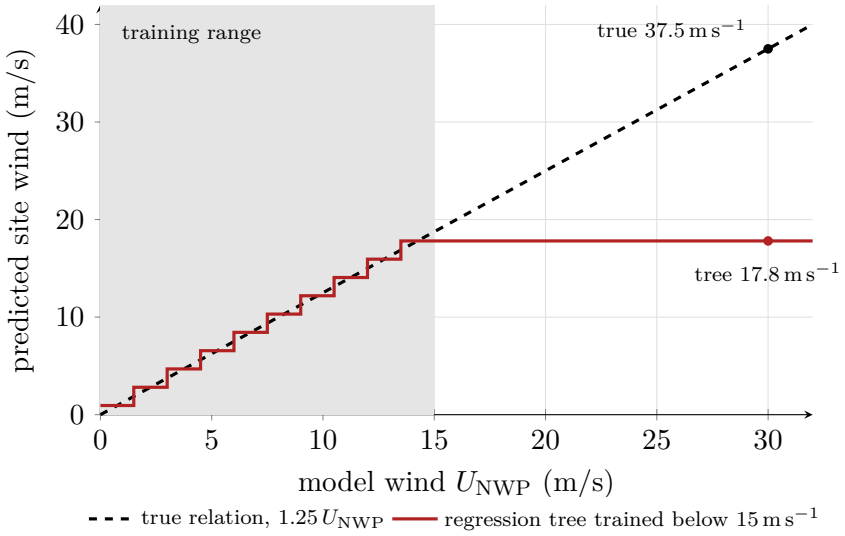


Figure 28.4: Extrapolation by a regression tree (illustrative). True relation $U_{\mathrm{site}} = 1.25\,U_{\mathrm{NWP}}$; the tree predicts in each bin of width $1.5\,\mathrm{m\,s^{-1}}$ the mean of the training observations, 1.25 times the bin center, and beyond the training range it repeats the value of its last bin.

Inside the band the steps follow the true line closely. Beyond $15\,\mathrm{m\,s^{-1}}$ the tree repeats the value of its last bin, $1.25 \times 14.25 \approx 17.8\,\mathrm{m\,s^{-1}}$, so at a model wind of $30\,\mathrm{m\,s^{-1}}$ it predicts $17.8\,\mathrm{m\,s^{-1}}$ against a true $37.5\,\mathrm{m\,s^{-1}}$, an error of 53 %. The danger matters most for extremes, which are rare in any record and are often what the application cares about: the design gust of a structure, the peak load on a turbine. It applies at the low end as well: a record with few calm nights gives a poor model of the weak winds that limit a conductor's rating. A model that extrapolates is flagged, and the forecast in that range comes from physics, from a method fitted to extremes (Chapter 24) or from a stated wider uncertainty.

28.4.4 Cross-validation for autocorrelated records

Cross-validation estimates how well a model predicts data it has not seen by fitting it on part of the record, the training set, and scoring it on the rest, the test set, repeated over several such splits. The common default draws the test times at random. For wind records that

default is wrong, because the record is strongly autocorrelated: consecutive hours belong to the same weather event. With an illustrative lag-one correlation of $r_1 = 0.9$ between consecutive hourly values and the exponential decay of a first-order autoregressive process, the correlation is $0.9^{24} \approx 0.08$ after a day and $0.9^{48} \approx 0.006$ after two. A randomly chosen test hour at 14:00 has its neighbors at 13:00 and 15:00, each correlated 0.9 with it, in the training set; the model then interpolates within an event it has already seen, and the score measures that interpolation, not a forecast.

The autocorrelation also reduces the information in the record. For a first-order autoregressive record of n values the effective number of independent values is $n_{\text{eff}} \approx n\,(1 - r_1)/(1 + r_1)$; a year of hourly data, $n = 8760$, with $r_1 = 0.9$ carries the information of $n_{\text{eff}} \approx 8760 \times 0.1/1.9 \approx 460$ independent hours. A model with dozens of predictors fitted to 460 effective samples can overfit even when 8760 rows look like plenty.

Figure 28.5 contrasts three splits of a two-year record. Each row is the record divided into 48 half-month blocks, with time running from left to right; blue blocks are training data, red blocks test data and gray blocks a buffer left out of both.

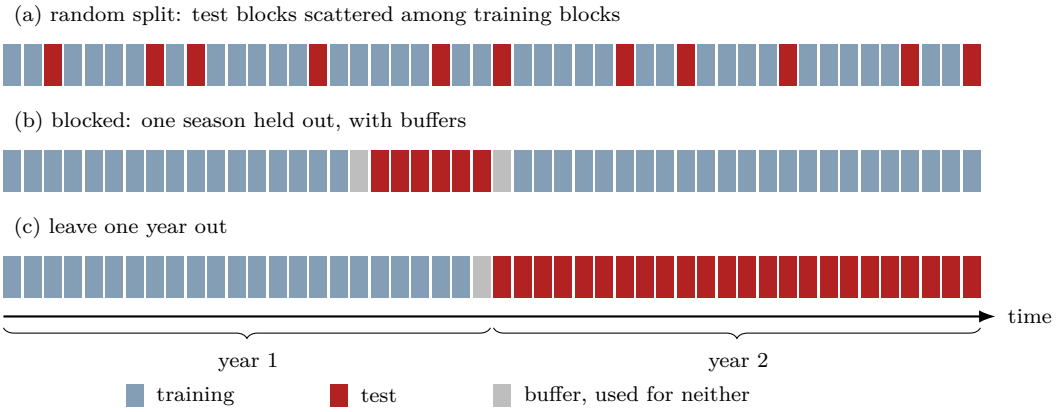


Figure 28.5: Three ways to split a two-year record into training and test data (schematic; each block is half a month). A random split (a) puts every test block next to correlated training blocks; a blocked split (b) holds out a contiguous season with a buffer on each side; leaving a whole year out (c) tests the model on a year it has never seen.

In row (a) nearly every test block touches a training block on both sides, and the weather of the test block is known to the model through its neighbors; at the finer, hourly scale at which random splits are usually drawn, this is the interpolation described above. In row (b) the test season is contiguous, and the buffers, each half a month and longer than the decay time of the correlation, keep the edges of the training data from being near-copies of the edges of the test data. Row (c) asks the hardest question, whether a model trained on one year forecasts another. The appropriate designs are therefore blocked validation, leave-one-season-out, leave-one-year-out, and event-based holdout, in which whole events of a kind, such as every storm or every blocked easterly night, are held out together. Each tests the model on future-like unseen conditions, not on the neighbors of samples it was trained on, and each gives a larger and more honest error than a random split.

28.4.5 Leakage

Leakage is the use, in fitting or testing a model, of information that would not be available when a real forecast is issued. The standard example is a predictor such as the local temperature observed at the forecast valid time: in the historical record it is there beside the wind, and it carries information about the stability at that hour, so the model uses it and scores well.

When a forecast is issued a day ahead, that observation does not yet exist, the model must run without it or with a substitute, and its operational performance is far worse than its test score.

Leakage has subtler forms. A random cross-validation split on an autocorrelated record leaks the test period through its neighbors (Section 28.4.4). A model trained on the weather model's analyses, its best estimate of the current state, and applied to its 24-hour forecasts has learned a relationship to a predictor that is more accurate in training than in use. Scaling the predictors with means and variances computed over the whole record, including the test period, passes a little information from test to training. Every predictor must therefore satisfy one condition: it is available, with the accuracy it had in training, at the time the forecast is issued.

28.4.6 Calibration period and observation quality

The *calibration period* is the span of time the training record covers. A model trained on a single year learns that year's weather, and that year may not contain rare storms, an unusual drought that dried the soil and changed the stability, extreme stability episodes or atypical wind directions. The model then has no evidence for those conditions and extrapolates when they come (Section 28.4.3). Longer and more diverse calibration data generally improve robustness; several years that include a range of seasons and regimes are worth more than more predictors fitted to one year.

The observations matter as much as their span. If the site sensor suffers tower shadow in one sector, poor exposure behind a building, or surroundings that change as trees grow or a structure is built, the statistical model learns those effects as part of the site wind (Chapters 22 and 23). That may be acceptable when the objective is to reproduce that sensor, for instance to forecast what a protection relay will read. It is not acceptable when the objective is the wind of the broader local atmosphere, such as the wind along a span a kilometer away. The quality and exposure of the training observations are therefore part of the target definition of Section 28.1.3: the model predicts what its observations measure, flaws included.

28.4.7 Site-specific and transferable models

A model trained at one site can be very accurate there and useless at the next. Another site may differ in terrain, roughness and exposure, and the correction factors learned for the first site encode its particular ridge and its particular trees. A site-specific correction is not a universal downscaling model. *Transferability*, the ability of a model to work at locations or in regimes not represented in its training record, is a separate problem with its own test: the model is trained on some sites and scored on others it has never seen, a leave-one-site-out validation.

Transferability requires that the predictors explain why the wind differs, through the terrain-aware predictors of Section 28.3.4, and that the relationships involve physics that is the same at the new site. The hemisphere is an example of physics that is not. A model that uses the north–south pressure gradient as a predictor of the wind direction relies on the geostrophic balance of Chapter 3, which for a westerly geostrophic wind of speed U_g gives $\partial p/\partial y = -\rho f U_g$. At 30° latitude, $|f| = 2 \times 7.292 \times 10^{-5} \times \sin 30^\circ = 7.29 \times 10^{-5}\,\mathrm{s}^{-1}$, and a westerly of $10\,\mathrm{m\,s}^{-1}$ needs a gradient of magnitude $1.2 \times 7.29 \times 10^{-5} \times 10 = 8.75 \times 10^{-4}\,\mathrm{Pa}$ per meter, 0.875 hPa per 100 km. In the Northern Hemisphere, $f > 0$, the pressure falls toward the north; in the Southern Hemisphere, $f < 0$, it falls toward the south. A model trained in the Northern Hemisphere and applied in southern Brazil would read a gradient with pressure falling toward the south as an easterly and predict the wrong direction. The remedy is a physically defined predictor, such as the geostrophic wind components computed with the local f, rather than a raw gradient whose meaning depends on the sign of f.

28.5 Dynamical and microscale downscaling

Instead of learning a statistical correction, dynamical downscaling computes the local wind with another physical model at finer resolution. This section describes what finer resolution adds, how nested grids pass information, where dynamical downscaling still falls short, and the microscale models, linearized terrain models and computational fluid dynamics, that continue the chain below the weather model, together with the two ways of coupling them to it.

28.5.1 A finer atmospheric model

Dynamical downscaling runs a weather model on a finer grid over a limited area, driven at its boundaries by a coarser model. An illustrative chain is

$$25\,\mathrm{km} \longrightarrow 3\,\mathrm{km} \longrightarrow 500\,\mathrm{m},$$

from a global model to a regional model to a fine local domain; in practice the grid spacing is usually reduced by a factor of three to five per step, so a jump from 25 to 3 km passes through an intermediate grid. The finer model explicitly solves more of the local dynamics. It resolves mountains, valleys and coastlines that the coarse grid smoothed away; it develops the thermal circulations of Chapter 19, the sea breeze and the slope and valley winds, which need the land–sea and slope contrasts to be on the grid; and it computes the local pressure gradients that drive channeling and gap flow. The local wind changes are then generated dynamically, by the equations of motion, rather than statistically.

The price is computing time. Halving the grid spacing doubles the number of points in each horizontal direction and, through the stability limit on the time step, halves the time step, so the cost of a fixed domain grows as Δx^{-3}. Refining from 3 km to 500 m over the same area multiplies the cost by $6^3 = 216$, which is why fine domains are small and nested inside coarser ones. The weather model as a system, with its grids, nesting and spin-up, is the subject of Chapter 25.

28.5.2 One-way and two-way nesting

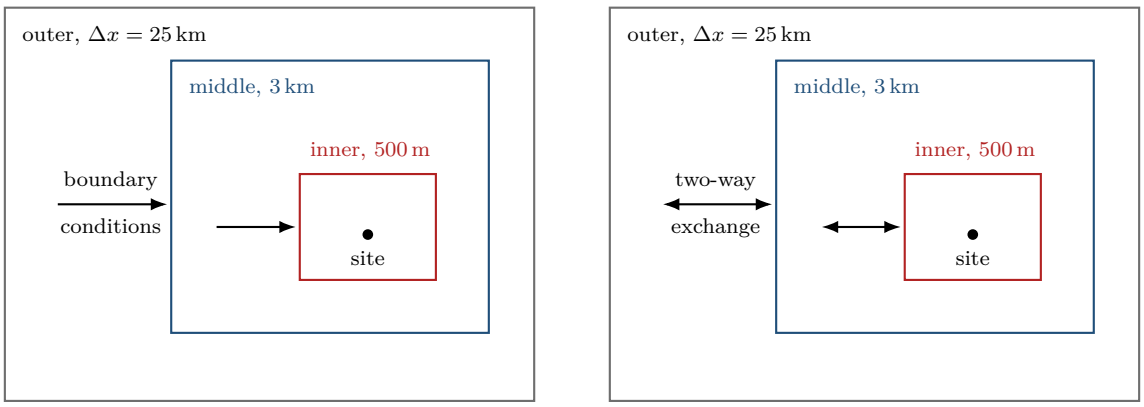
A nested model places a fine grid inside a coarse one. In *one-way nesting* the outer model provides the boundary conditions of the inner model, the wind, temperature, humidity and pressure along the inner domain's edges at each coupling time, and the inner model does not feed information back outward. The coarse forecast can even be run first and the fine one afterward. This is common and computationally convenient. In *two-way nesting* the two grids run together and exchange information in both directions: the inner solution replaces or adjusts the outer solution over the area they share, so that the fine grid's better-resolved terrain and circulations influence the coarser grid.

Figure 28.6 draws the two arrangements. Each panel is a plan view of three nested domains with the illustrative grid spacings of the chain above and the site marked by a dot; the arrows across the domain edges show the direction in which information passes.

In panel (a) information flows only inward, from the global scale down to the site; an error at the outer level propagates inward and nothing inside corrects it. In panel (b) the inner domains also send their solution outward, so that, for instance, a sea breeze resolved on the 3 km grid modifies the flow the 25 km grid carries along the coast. Two-way nesting improves the consistency between the grids but is more complex to run and to diagnose. For site wind forecasting, whose interest is the innermost domain, one-way nesting is often sufficient.

28.5.3 Limits of dynamical downscaling

Dynamical downscaling does not remove the downscaling problem; it moves it to a smaller scale. A weather model run at 500 m still leaves unresolved the buildings, the trees, the hills smaller



(a) one-way nesting (b) two-way nesting

Figure 28.6: Nested domains in plan view (schematic; illustrative grid spacings). (a) One-way nesting: each outer domain supplies the boundary conditions of the next inner domain and receives nothing back. (b) Two-way nesting: information also passes from each inner domain back to the domain that contains it.

than a few grid lengths, which with an effective resolution of five to ten grid lengths means hills smaller than about 2.5 to 5 km, and the turbulence. And at 500 m the model has entered the gray zone of Chapter 5, roughly 100 m to 1 km for the boundary layer, in which the largest convective eddies are partly resolved and partly parameterized, so that the boundary-layer scheme of Chapter 26 is used outside the range for which it was designed.

The resulting site wind can therefore still be biased: by the terrain and roughness below its effective resolution, by its boundary-layer and surface-layer schemes (Chapter 27), and by the errors of the coarser model that drives it, which the fine grid inherits through its boundaries. A dynamically downscaled wind is a better estimate of the local flow, not an observation of it, and it is usually followed by a statistical correction when site observations exist (Section 28.6.2).

28.5.4 Microscale downscaling with linearized terrain models

Below the mesoscale weather model the chain continues with a microscale model, one with a grid of meters to tens of meters that resolves the terrain and roughness around the site. *Microscale downscaling* is the use of such a model, driven by the weather model, to compute the site wind:

$$\text{weather model} \longrightarrow \text{microscale terrain model} \longrightarrow \text{site wind.}$$

Examples are linearized terrain models, computational fluid dynamics with the Reynolds-averaged equations (RANS), and large-eddy simulation (LES). The approach is especially common in wind engineering, where it produces the speed-up maps of Chapter 20.

A linearized terrain model treats the wind perturbation caused by gentle terrain as a small, linear response to the topography, as derived in Chapter 20: the speed-up is proportional to the terrain height over its horizontal length, and the responses to separate terrain components add. Its advantages are speed, low computing cost and the ease of computing many wind directions, so that a full set of direction-dependent speed-up factors for a site costs seconds. Its limitations follow from its assumptions: it is poor where the flow separates, behind lee slopes steeper than about 0.3; in steep terrain, where the perturbation is no longer small; and in strongly blocked stable flow, with a Froude number well below one, where buoyancy rather than inertia controls the response.

28.5.5 CFD downscaling

Computational fluid dynamics (CFD) with the RANS equations solves the nonlinear equations of motion on a fine three-dimensional mesh around the site, with a turbulence closure for the unresolved eddies. It explicitly computes the local terrain-induced pressure and flow structures, and so represents what the linear model cannot: the crest speed-up of steep ridges, wakes, separation and recirculation, and the effects of individual obstacles such as buildings or a forest edge. LES goes further and resolves the large turbulent eddies themselves, at a much higher cost.

A CFD model needs boundary conditions: the wind and turbulence profiles entering its domain, the stability, and the conditions at its top and sides. Those come most often from the weather model. CFD is therefore not a replacement for the weather model; it is a downstream local model that adds the microscale structure to a mesoscale state it cannot generate itself, since a domain a few kilometers wide holds neither the synoptic pressure field nor the diurnal cycle of the boundary layer. Its methods, closures and limits are the subject of Chapter 29.

28.5.6 Offline and online coupling

The weather model and the microscale model can be joined in two ways. In *offline coupling* the weather model is run first, its profiles of wind, temperature and turbulence are saved at the boundaries of the microscale domain, and the microscale model is run afterward with them as input:

$$\text{run the weather model} \longrightarrow \text{save profiles} \longrightarrow \text{run CFD afterward.}$$

The two models do not interact during the run. A common form precomputes the microscale flow for a set of inflow directions and stability classes, a lookup library, and at forecast time picks or interpolates the precomputed case that matches the weather model's state. This is simpler and fast in operation.

In *online coupling* the mesoscale and microscale domains run together and exchange information during the simulation, as in two-way nesting: the microscale domain receives evolving boundary conditions at every coupling step and may return its effect on the flow. This can be more physically consistent, since the microscale flow follows the weather as it changes rather than a sequence of steady snapshots, but it is substantially more complex and more expensive. For operational forecasting, offline approaches are more common.

28.6 Choosing and combining methods

No single method is best for every site and purpose. This section compares statistical and dynamical downscaling, describes the hybrid methods that combine them, and turns from a single predicted wind to a predicted distribution: the sources of downscaling uncertainty and the use of ensembles to carry it to the site.

28.6.1 Statistical against dynamical downscaling

Table 28.3 compares the two families aspect by aspect: computing cost, data needs, performance at an observed site, performance at an unobserved site, behavior in conditions outside experience, the bias that remains, operational complexity and the typical way each fails.

The two columns are close to complements. Statistical downscaling is fast, needs observations, excels at a known site, extrapolates poorly and learns the local bias; dynamical downscaling is expensive, needs a physical model, works at unobserved sites, can capture new regimes and keeps its own model bias. Neither is universally superior, and the choice follows from the data available and the question asked: a forecast at a long-instrumented station favors statistics, a map of the wind along a new corridor favors physics.

Table 28.3: Statistical and dynamical downscaling compared.

Aspect	Statistical	Dynamical
Computing cost	small; fitting and applying a regression or a trained model	large; a finer weather model or a CFD run per case or per library entry
Data needs	a long, good-quality record of observations at the site	terrain and land-cover maps and a physical model setup; no site record needed
At an observed site	excellent; learns the local bias of model and sensor	good, but the local bias of its schemes remains
At an unobserved site	poor unless trained on many sites with terrain predictors	works; the physics applies wherever the model is run
Outside experience	may extrapolate poorly in rare regimes and extremes	may capture new regimes physically
Remaining bias	small within the training conditions	model bias from schemes, resolution and the driving model
Operations	easy to deploy and update	more complex: runs, boundary data, monitoring
Typical failure	learns the record's quirks; leakage; extrapolation	gray zone, unresolved obstacles, inherited driving errors

28.6.2 Hybrid downscaling

Because the strengths are complementary, a practical strategy chains them:

$$\text{weather model} \longrightarrow \text{microscale physics} \longrightarrow \text{statistical correction.}$$

The regional weather model provides the atmospheric forcing; a terrain model estimates the local speed-up for the forecast direction and stability; and a statistical or machine-learning model corrects the residual bias against site observations. In multiplicative form,

$$U_{\text{site}} = r(\mathbf{x})\; S(\beta, z/L_{\text{O}})\; U_{\text{NWP}}, \tag{28.15}$$

where S is the speed-up factor computed by the terrain model with the weather-model wind as its reference, and r, dimensionless, is the residual ratio learned from the observations, close to one when the physics is right. With illustrative values, a westerly model wind of $8\,\mathrm{m\,s^{-1}}$, a terrain-model speed-up of 1.3 and a residual ratio of 0.93 learned for that sector give $U_{\text{site}} = 0.93 \times 1.3 \times 8\,\mathrm{m\,s^{-1}} = 9.7\,\mathrm{m\,s^{-1}}$.

The division of labor is what makes hybrids attractive. Physics handles the terrain, the stability dependence and the directional effects, which it computes from first principles for every direction and stability, including those rare in the record. Statistics handles what physics leaves: the unresolved biases of the models, sensor-specific corrections and the remaining imperfections of the schemes. The statistical model is not asked to learn the whole function F of equation (28.1) from scratch but only a residual close to one, which needs fewer data and fails more gracefully: where the residual model has no evidence, it can fall back to $r = 1$ and leave the physics in charge. This is how the hybrid escapes the extrapolation trap of Figure 28.4.

28.6.3 Deterministic and probabilistic downscaling

Most simple downscaling produces one value, such as $\hat{U}_{\text{site}} = 7.3\,\mathrm{m\,s^{-1}}$: a point estimate, *deterministic downscaling*. The local wind uncertainty may be substantial, and one number hides it. *Probabilistic downscaling* predicts instead the conditional distribution $p(U_{\text{site}} \mid \mathbf{x})$ of the site wind given the predictors, or a set of its quantiles. The quantile Q_q, in meters per second, is the wind below which the site wind falls with probability q; an illustrative forecast is

$$Q_{10} = 5.2\,\mathrm{m\,s^{-1}}, \qquad Q_{50} = 7.1\,\mathrm{m\,s^{-1}}, \qquad Q_{90} = 9.8\,\mathrm{m\,s^{-1}},$$

where the subscripts are q in percent. The forecast states that the site wind lies between 5.2 and 9.8 $\mathrm{m\,s^{-1}}$ with probability 0.8, and is equally likely to fall above or below 7.1 $\mathrm{m\,s^{-1}}$. That expresses the uncertainty explicitly. A quantile is fitted by minimizing the pinball loss, $q\,(y-Q)$ when the observation y exceeds the prediction Q and $(1-q)\,(Q-y)$ otherwise, which penalizes misses on each side in the proportion that makes a fraction q of observations fall below Q.

Figure 28.7 shows a distribution consistent with these numbers. The horizontal axis is the site wind and the vertical axis the probability density; the shaded area is the central 80 % interval between Q_{10} and Q_{90}, the solid red line is the median and the dashed black line the mean, which is the deterministic forecast.

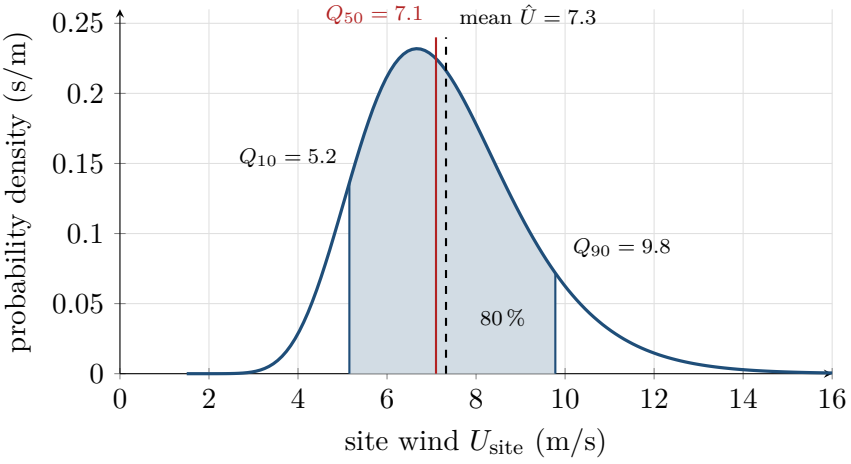


Figure 28.7: A probabilistic site-wind forecast (illustrative): a lognormal density with median 7.1 $\mathrm{m\,s^{-1}}$ and logarithmic standard deviation 0.25, $p(U) = \exp\{-[\ln(U/7.1)]^2/(2\times 0.25^2)\}/(0.25\,U\sqrt{2\pi})$. Its quantiles are $Q_{10} = 5.15$, $Q_{50} = 7.1$ and $Q_{90} = 9.78\,\mathrm{m\,s^{-1}}$ and its mean is 7.33 $\mathrm{m\,s^{-1}}$.

The distribution is skewed to the right, as wind-speed distributions are: Q_{90} lies 2.7 $\mathrm{m\,s^{-1}}$ above the median and Q_{10} only 1.9 $\mathrm{m\,s^{-1}}$ below it, the most probable wind, $7.1\,e^{-0.0625} \approx 6.7\,\mathrm{m\,s^{-1}}$, lies below the median, and the mean, $7.1\,e^{0.25^2/2} \approx 7.33\,\mathrm{m\,s^{-1}}$, lies above it. The deterministic 7.3 $\mathrm{m\,s^{-1}}$ is the mean of this distribution, and the median 7.1 $\mathrm{m\,s^{-1}}$ is a different summary of the same forecast; the difference is not an inconsistency. For a decision the distribution carries what the point estimate cannot: a line rating set at the wind exceeded with probability 0.9 uses $Q_{10} = 5.2\,\mathrm{m\,s^{-1}}$, not 7.3 $\mathrm{m\,s^{-1}}$.

28.6.4 Sources of uncertainty

The uncertainty of a downscaled wind has several sources: the uncertainty of the weather forecast itself, the terrain and obstacles the methods do not resolve, the error of the downscaling model, and the error of the measurements against which the model was trained and is verified. Downscaling should represent at least some of them, and a deterministic correction hides all of them inside one number.

The sources combine as variances when they are independent, not as standard deviations. With an illustrative spread of 1.0 $\mathrm{m\,s^{-1}}$ from the forcing and a downscaling residual of 1.2 $\mathrm{m\,s^{-1}}$, the total standard deviation is

$$\sigma_{\mathrm{total}} = \sqrt{\sigma_f^2 + \sigma_d^2} = \sqrt{1.0^2 + 1.2^2}\,\mathrm{m\,s^{-1}} = \sqrt{2.44}\,\mathrm{m\,s^{-1}} \approx 1.56\,\mathrm{m\,s^{-1}},$$

where σ_f is the standard deviation from the forcing and σ_d that from the downscaling; adding the two standard deviations would give 2.2 $\mathrm{m\,s^{-1}}$ and overstate the uncertainty. The measurement

error enters twice: once as noise in the training observations, which inflates the fitted residual, and once in the verification, which makes a perfect forecast look imperfect (Chapter 24).

28.6.5 Ensemble downscaling

A weather-model ensemble is a set of forecasts from perturbed initial conditions or model formulations whose spread represents the uncertainty of the large-scale forecast (Chapter 25). With 20 ensemble members, each member can be downscaled separately to give

$$U_{\text{site}}^{(1)},\ U_{\text{site}}^{(2)},\ \ldots,\ U_{\text{site}}^{(20)},$$

a local forecast distribution. This *ensemble downscaling* carries the large-scale forecast uncertainty into the site forecast: a front whose timing differs among the members gives site winds that differ accordingly. With an illustrative ensemble of model winds with mean $8.0\,\mathrm{m\,s^{-1}}$ and standard deviation $0.8\,\mathrm{m\,s^{-1}}$, downscaled by a factor of 1.25, the site members have mean $10.0\,\mathrm{m\,s^{-1}}$ and standard deviation $1.0\,\mathrm{m\,s^{-1}}$, the forcing part of the previous subsection. Twenty members estimate the central quantiles reasonably but the tails poorly: Q_{10} falls between the second and third of the sorted members.

Even with a perfect ensemble, the downscaling function itself is uncertain. A factor $S_c(\beta, z/L_{\mathrm{O}})$ fitted from a training record is well constrained in common regimes and poorly constrained in rare ones: with an illustrative residual scatter of 0.2 in the factor, a westerly neutral class with 400 independent events determines it to $0.2/\sqrt{400} = 0.01$, while an easterly stable class with 25 determines it only to $0.2/\sqrt{25} = 0.04$, and its residual scatter about the fit, the $1.2\,\mathrm{m\,s^{-1}}$ above, is not in the ensemble at all. The total uncertainty is therefore not just the ensemble spread; conceptually,

$$\text{total uncertainty} = \text{forcing uncertainty} + \text{downscaling uncertainty}, \tag{28.16}$$

where the sum is of variances for independent parts. Ensemble downscaling that passes every member through one deterministic function represents only the first term; adding to each member a residual drawn from the downscaling model's error distribution, or passing the members through several plausible fits of the function, represents the second. The microscale part of these methods, the flow model that computes the terrain and obstacle effects from the inflow the weather model supplies, is the subject of the next chapter on computational fluid dynamics and microscale wind modeling, Chapter 29.

28.7 What to retain

Definition 28.1 (Downscaling)**.** Downscaling maps a coarse atmospheric state to the wind at a particular site and a stated target: statistical methods learn that mapping from data, dynamical methods solve more of the physics explicitly, and the most robust operational systems are often hybrid, a weather model followed by a physical local correction and a statistical correction of the residual, with the uncertainty stated rather than hidden.

Table 28.4 lists the terms of the chapter, their meaning, their units and the subsection that defines each.

28.8 Exercises

Exercise 28.1. A training record at a station gives the pairs of model wind and observed wind $(3, 2.4)$, $(6, 4.8)$, $(9, 7.2)$ and $(12, 9.6)$, in m/s. (a) Compute the additive bias correction and the ratio-of-means multiplicative correction, and apply each to the four model winds. (b) Compute

Table 28.4: The terms of the chapter and where each is defined.

Term	Meaning	Units	Defined in
Downscaling	estimation of a site wind from coarse weather-model output, the function F	m/s	28.1.1
Statistical downscaling	a relationship from large-scale predictors to local observations, fitted to a training record	m/s	28.2.1
Bias correction	removal of the systematic model error, model minus observed, by an offset	m/s	28.2.2
Correction factor S_c	ratio of site wind to model wind; a function of direction and stability	–	28.2.3, 28.2.4
MOS	model output statistics: regression of site observations on model output, by site and lead time	m/s	28.3.3
Regime-dependent model	separate downscaling relationships for different physical states, selected by a rule	–	28.3.5
Leakage	use of information that is unavailable when a real forecast is issued	–	28.4.5
Transferability	ability of a model to work at new locations or in new regimes	–	28.4.7
Dynamical downscaling	running a finer physical atmospheric model driven by a coarser one	m/s	28.5.1
One-way nesting	outer model drives inner model through its boundaries, without feedback	–	28.5.2
Two-way nesting	inner and outer models exchange information in both directions	–	28.5.2
Microscale downscaling	linear terrain, RANS or LES models below the weather-model scale	m/s	28.5.4
Hybrid downscaling	physical local correction followed by a statistical residual correction	m/s	28.6.2
Probabilistic downscaling	prediction of the local wind distribution $p(U_{\text{site}} \mid \mathbf{x})$ or its quantiles Q_q	m/s	28.6.3
Ensemble downscaling	downscaling of each ensemble member to carry forcing uncertainty to the site	m/s	28.6.5

the root-mean-square error of each fit and say which form of error the station has. (c) Fit the line (28.2) with equation (28.3) and compare. (d) What does the additive correction predict for a model wind of $1\,\mathrm{m\,s^{-1}}$?

Exercise 28.2. A transmission corridor in southern Brazil, at 30°S, crosses a ridge. A regression gives the correction factor $S_c(\beta) = 1.05 + 0.15\sin\beta - 0.10\cos\beta$. (a) Compute S_c for winds from 0°, 90°, 180° and 270°, and the direction and value of its maximum with equation (28.11). (b) A forecast gives $U_{\mathrm{NWP}} = 9\,\mathrm{m\,s^{-1}}$ with components $u = -5.4\,\mathrm{m\,s^{-1}}$ and $v = 7.2\,\mathrm{m\,s^{-1}}$. Compute the direction β, say from which quadrant the wind comes, and compute the site wind. (c) The model's geostrophic wind there is a westerly of $10\,\mathrm{m\,s^{-1}}$. Compute the Coriolis parameter and the north–south pressure gradient, and state toward which pole the pressure falls. (d) Give the answer to (c) at 30°N.

Exercise 28.3. A site has two regimes. In 70 % of the hours (westerly, near neutral) $U_{\mathrm{site}} = 1.2\,U_{\mathrm{NWP}}$; in 30 % (easterly, stable) $U_{\mathrm{site}} = 0.5\,U_{\mathrm{NWP}}$; the model winds have the same distribution in both. (a) Compute the single factor fitted through the origin by least squares. (b) For a model wind of $6\,\mathrm{m\,s^{-1}}$, compute the error of the single fit in each regime, in m/s and in percent, and its mean error over the record. (c) A conductor's rating is computed from the downscaled wind. In which regime is the single fit unsafe, and why?

Exercise 28.4. (a) An hourly wind record of three years has a lag-one autocorrelation of 0.85. Compute the effective number of independent hours, the correlation after 12 and after 48 h, and propose a buffer length for a blocked cross-validation. (b) A 20-member ensemble of model winds has mean $7.0\,\mathrm{m\,s^{-1}}$ and standard deviation $1.2\,\mathrm{m\,s^{-1}}$; the downscaling factor is 1.15 and the downscaling residual has a standard deviation of $0.9\,\mathrm{m\,s^{-1}}$. Compute the mean and the forcing spread of the site members and the total standard deviation. (c) Assuming the total is normally distributed, compute Q_{10} and Q_{90} of the site wind ($z_{0.9} = 1.2816$). (d) Say what the ensemble alone would give for the same quantiles and why it is too narrow.

Chapter 29

CFD and Microscale Wind Modeling

29.1 Computational fluid dynamics for local wind

Chapter 5 placed computational fluid dynamics at the bottom of the modeling hierarchy, below the weather models; Chapter 8 introduced the two ways it treats turbulence, Reynolds averaging and large-eddy simulation, and the closure problem both must solve; Chapter 20 showed the flow features over terrain that only a nonlinear model reproduces: separation, recirculation, strong local acceleration. This chapter treats the method itself. Its question is

what can computational fluid dynamics add to a weather model, and where can computational fluid dynamics itself go wrong?

The method is useful where the wind depends strongly on local geometry: hills, ridges, valleys, buildings, forests and the corridors of transmission lines. The chapter follows it from the equations to the prediction: why every eddy cannot be computed and what the three families of method resolve instead; the Reynolds-averaged models and their closures; large-eddy simulation; the setup of a terrain simulation, from the domain and the inlet to the wall treatment and the mesh; the physics beyond neutral flow; and the steps that turn a set of simulations into a site wind prediction, including validation and uncertainty.

Jargon: CFD, NWP, microscale model, mesh, cell, boundary condition, DNS, RANS, LES

Computational fluid dynamics (CFD) is the numerical solution of the equations of fluid flow, the Navier–Stokes equations, on a discrete set of points around a specified geometry. *Numerical weather prediction* (NWP) integrates the equations of the atmosphere forward in time on a grid of kilometers from an observed initial state (Chapter 5). A *microscale model* is any model that resolves flow features below about one kilometer: a CFD model in this chapter. The *mesh* (or computational grid) is the subdivision of the flow domain into small volumes, the *cells*, in each of which the model carries one value of each variable; the cell size, in meters, is the model's grid spacing Δx horizontally and Δz vertically. A *boundary condition* is the value or the flux of a variable prescribed on the edge of the domain: the inflowing wind at the inlet, the drag at the ground. *DNS* (direct numerical simulation) solves the Navier–Stokes equations with every turbulent eddy resolved; *RANS* (Reynolds-averaged Navier–Stokes) solves the averaged equations and models all turbulence; *LES* (large-eddy simulation) resolves the large eddies and models the small ones.

Key idea

A weather model supplies the atmospheric environment: the wind aloft, its direction, the stability and the depth of the boundary layer. CFD resolves how the local geometry modifies that environment. CFD is therefore a physical model of the local modification, with its own uncertainty from inflow, roughness, mesh and turbulence model, and not a source of ground truth.

29.1.1 The local-flow problem

Consider an illustrative weather-model forecast of $U = 8\,\mathrm{m\,s^{-1}}$ from the west over a grid cell a few kilometers across. The cell contains a steep ridge, a forest edge and a cluster of buildings. The grid-cell value is a spatial average over all of them (Chapter 5); the wind at individual points can be $5\,\mathrm{m\,s^{-1}}$ in the lee of the forest edge, $10\,\mathrm{m\,s^{-1}}$ over open ground and $14\,\mathrm{m\,s^{-1}}$ on the ridge crest. Relative to the grid-cell value these are speed-up factors (Chapter 20) of

$$S = \frac{5}{8} = 0.63, \qquad \frac{10}{8} = 1.25, \qquad \frac{14}{8} = 1.75,$$

a range of almost a factor of three within one cell. For a transmission line crossing the cell the difference is not academic: the convective cooling of the conductor grows roughly as the wind speed to a power of about 0.5 to 0.6 (Chapter 8), so the crest span is cooled $(14/5)^{0.6} \approx 1.9$ times as strongly as the sheltered span at the same angle of attack.

CFD tries to resolve these spatial differences. Its grid spacing is of meters to tens of meters, small enough to represent the ridge, the forest edge and the buildings as geometry rather than as an effective roughness. The division of labor is then

$$\text{weather model: the atmospheric environment} \;\rightarrow\; \text{CFD: the local flow modification.}$$

The rest of the chapter examines what each half of that statement requires.

29.1.2 The governing equations

CFD is not a separate physical system. It solves the same fluid equations as a weather model, on a finer grid and usually with fewer processes. For the microscale the air can be treated as incompressible. Density changes produced by the motion itself are of the order of the square of the Mach number, $(U/c)^2$, with $c \approx 340\,\mathrm{m\,s^{-1}}$ the speed of sound; for $U = 15\,\mathrm{m\,s^{-1}}$ this is $(15/340)^2 \approx 0.002$, two tenths of a percent. The changes that matter are those produced by temperature differences, which act through buoyancy and are treated in Section 29.5.2. With the velocity vector $\mathbf{u} = (u, v, w)$, x along the inflow direction, z upward and a constant reference density ρ_0, the momentum equation is

$$\frac{\partial \mathbf{u}}{\partial t} + (\mathbf{u}\cdot\nabla)\,\mathbf{u} = -\frac{1}{\rho_0}\nabla p + \nu\,\nabla^2\mathbf{u} + \mathbf{F}, \tag{29.1}$$

and conservation of mass reduces to the continuity equation

$$\nabla\cdot\mathbf{u} = \frac{\partial u}{\partial x} + \frac{\partial v}{\partial y} + \frac{\partial w}{\partial z} = 0. \tag{29.2}$$

Written out, the along-flow component of equation (29.1) is

$$\frac{\partial u}{\partial t} + u\frac{\partial u}{\partial x} + v\frac{\partial u}{\partial y} + w\frac{\partial u}{\partial z} = -\frac{1}{\rho_0}\frac{\partial p}{\partial x} + \nu\left(\frac{\partial^2 u}{\partial x^2} + \frac{\partial^2 u}{\partial y^2} + \frac{\partial^2 u}{\partial z^2}\right) + F_x,$$

and the v and w components have the same form. Term by term: the local rate of change of the velocity, plus its advection by the flow itself, equals the pressure-gradient force, plus molecular diffusion of momentum, plus the remaining forces per unit mass $\mathbf{F}$.

In the vertical equation, p is the departure of the pressure from a hydrostatic reference state, so that gravity and the hydrostatic part of the vertical pressure gradient have already cancelled; what remains of gravity is the buoyancy of air that is warmer or colder than the reference. $\mathbf{F}$ collects that buoyancy, the Coriolis force, the drag of a canopy that is not resolved as geometry (Chapter 21) and any imposed large-scale forcing. The advection term $(\mathbf{u}\cdot\nabla)\mathbf{u}$ is quadratic in the velocity: it is the nonlinearity that makes the flow separate behind a steep ridge, that the linear models of Chapter 20 omit, and that makes the flow turbulent. A weather model solves a compressible equivalent of the same equations, with moisture, radiation and the Coriolis force kept everywhere; CFD is a finer-scale numerical solution of the same fluid dynamics.

29.1.3 The cost of resolving every eddy

Equations (29.1) and (29.2) hold for the instantaneous turbulent flow, and solving them with every eddy resolved is direct numerical simulation. It is impossible for the atmosphere because the Reynolds number, $\mathrm{Re} = UL/\nu$ (Chapter 8), is enormous: with $U = 10\,\mathrm{m\,s^{-1}}$, $\nu = 1.5\times10^{-5}\,\mathrm{m^2\,s^{-1}}$ and L from 10 m to 1 km, it lies between about 10^7 and 10^9, and larger for deeper flows.

The Reynolds number fixes how many grid points DNS needs. The largest eddies have a size L and a velocity u_0 and dissipate energy at the rate $\varepsilon \sim u_0^3/L$; the smallest have the Kolmogorov length $\eta_K = (\nu^3/\varepsilon)^{1/4}$ (Chapter 8). The ratio of the two is

$$\frac{L}{\eta_K} = L\left(\frac{u_0^3}{L\,\nu^3}\right)^{1/4} = \left(\frac{u_0 L}{\nu}\right)^{3/4} = \mathrm{Re}^{3/4}, \tag{29.3}$$

with Re formed from the velocity and size of the large eddies. A grid that resolves the smallest eddies across a cube of side L needs about $(L/\eta_K)^3 = \mathrm{Re}^{9/4}$ points. For eddies of $u_0 = 1\,\mathrm{m\,s^{-1}}$ and $L = 1\,\mathrm{km}$, the size of the boundary layer, $\mathrm{Re} = 1\times1000/(1.5\times10^{-5}) = 6.7\times10^7$, $\mathrm{Re}^{3/4}\approx 7.4\times10^5$ and $\eta_K \approx 1.4\,\mathrm{mm}$, and the cube alone needs $\mathrm{Re}^{9/4}\approx 4\times10^{17}$ points. Across the range of Re above, $\mathrm{Re}^{9/4}$ runs from $(10^7)^{9/4}\approx 6\times10^{15}$ to $(10^9)^{9/4}\approx 2\times10^{20}$.

An illustrative terrain domain 6 km long, 4 km wide and 1.5 km deep, $3.6\times10^{10}\,\mathrm{m^3}$, at a spacing of 1 mm would hold

$$N = \frac{3.6\times10^{10}\,\mathrm{m^3}}{(10^{-3}\,\mathrm{m})^3} = 3.6\times10^{19}$$

cells. At five variables of eight bytes each, the state alone would occupy about 1.4×10^{21} bytes, and the time step, limited to the time the flow takes to cross one cell, $10^{-3}\,\mathrm{m}/10\,\mathrm{m\,s^{-1}} = 10^{-4}\,\mathrm{s}$, would require 3.6×10^7 steps per simulated hour. DNS is used for low-Reynolds-number flows in research and is out of reach for any realistic atmospheric site. CFD for the wind therefore also needs a turbulence model.

29.1.4 Three approaches

The three approaches differ in where they draw the line between resolved and modeled motion. Table 29.1 compares them. Its columns give the approach, what it resolves, what it models, an illustrative grid spacing for an atmospheric site, the cell count for the $3.6\times10^{10}\,\mathrm{m^3}$ domain above, and what its output contains. RANS models all turbulence statistically and solves for the mean flow. LES resolves the large turbulent eddies explicitly and models the small ones. DNS resolves every scale. For atmospheric engineering, RANS and LES are the practical choices.

Table 29.1: The three approaches to turbulent flow in CFD. Grid spacings and cell counts are illustrative, for a domain of $6 \times 4 \times 1.5\,\mathrm{km}$; RANS meshes are stretched, so their count is not the volume divided by the cube of one spacing.

Approach	Resolves	Models	Δx	Cells	Output
DNS	every eddy, down to η_K	nothing	about 1 mm	3.6×10^{19}	the complete turbulent field
LES	eddies larger than the filter, about the grid spacing	subgrid eddies	2 to 20 m	4.5×10^{6} to 4.5×10^{9}	time series, gusts, coherent structures, statistics
RANS	the mean flow around the geometry	all turbulence	5 to 50 m, finer near the site and the ground	10^{6} to 10^{7}	mean speed-up and turning; modeled e and ε

Figure 29.1 shows the same division on the energy spectrum of Chapter 8. The upper panel plots a model spectrum $E(k)$ against the wavenumber k on log-log axes, from eddies of kilometers on the left to millimeters on the right; the spectrum peaks at eddies of about 100 m and falls with slope $-5/3$ through the inertial subrange. The shaded part is the energy an LES with a filter width of 10 m resolves, everything to the left of the cutoff wavenumber $k_c = \pi/(10\,\mathrm{m}) = 0.31\,\mathrm{rad\,m^{-1}}$. The lower panel has one bar per approach on the same wavenumber axis: blue where the approach resolves the motion, gray where it models it. DNS is blue up to π/η_K; LES is blue to the left of k_c and gray to the right; RANS is gray across the whole spectrum, since only the mean flow is computed. With this spectrum the LES resolves about 62 % of the turbulent kinetic energy and models the remaining 38 %.

The figure states the trade-off of the chapter. Moving the boundary between resolved and modeled motion to the right buys realism at a cost that grows with the third power of the inverse grid spacing; moving it to the left buys speed at the price of a closure that must represent eddies carrying most of the energy. Neither choice removes the model: it decides how much of the turbulence the model is responsible for.

29.2 Reynolds-averaged models

Reynolds-averaged models solve for the mean flow and represent every eddy by a closure. This section writes the averaged equations, the eddy-viscosity closure, the two-equation models in common use, what their output contains and what it does not, and the difference between steady and unsteady solutions.

29.2.1 The averaged equations

RANS starts from the Reynolds decomposition of every variable into a mean and a fluctuation, $u = \overline{u} + u'$ (Chapter 8). In index notation, with $u_1, u_2, u_3 = u, v, w$ and $x_1, x_2, x_3 = x, y, z$ and a sum over repeated indices, averaging equations (29.1) and (29.2) gives

$$\frac{\partial \overline{u}_i}{\partial t} + \overline{u}_j \frac{\partial \overline{u}_i}{\partial x_j} = -\frac{1}{\rho_0}\frac{\partial \overline{p}}{\partial x_i} + \nu \frac{\partial^2 \overline{u}_i}{\partial x_j \partial x_j} - \frac{\partial \overline{u_i' u_j'}}{\partial x_j} + \overline{F}_i, \qquad \frac{\partial \overline{u}_j}{\partial x_j} = 0. \tag{29.4}$$

Every term has the form of the instantaneous equation except one: the average of the nonlinear advection leaves behind the divergence of the correlations $\overline{u_i' u_j'}$, and $-\rho_0\,\overline{u_i' u_j'}$ are the Reynolds stresses. Near the ground over flat terrain the only important one is $-\rho_0\,\overline{u'w'}$, the turbulent

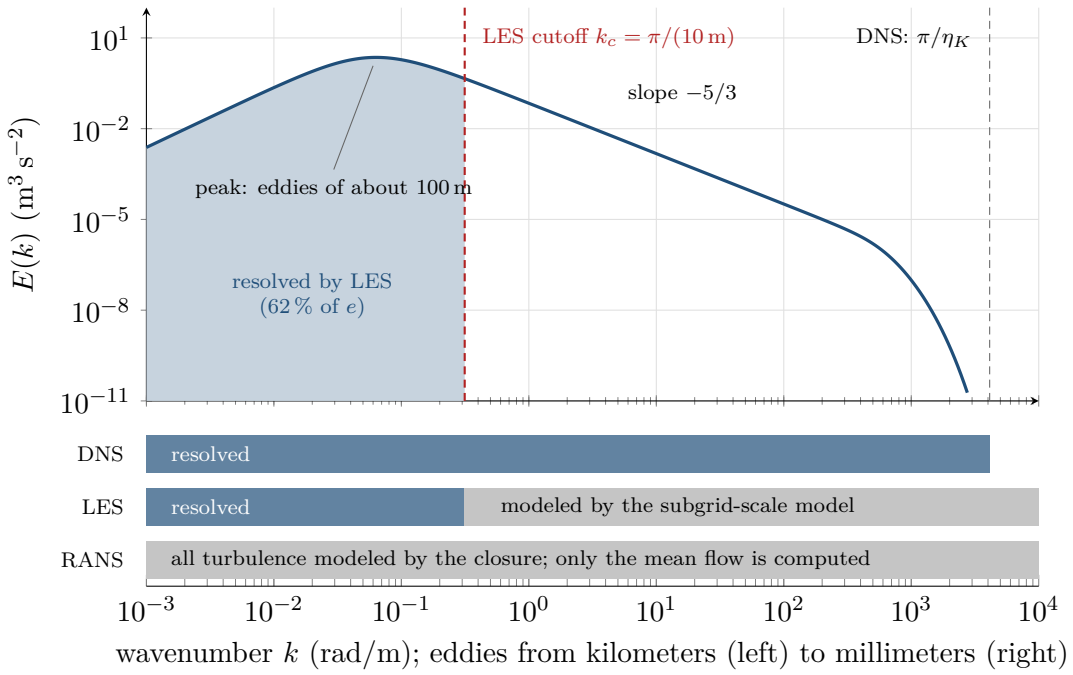


Figure 29.1: What each approach resolves, on a model energy spectrum (illustrative). Top: $E(k) = C_K \varepsilon^{2/3} k^{-5/3} f_L(kL) f_\eta(k\eta_K)$ with $C_K = 1.5$, $\varepsilon = 0.01\,\mathrm{m^2\,s^{-3}}$, a large-eddy length $L = 45\,\mathrm{m}$ (peak at a wavelength of about 100 m), $\eta_K = 0.76\,\mathrm{mm}$, and the shape functions $f_L = [kL/((kL)^2 + 6.78)^{1/2}]^{11/3}$ and $f_\eta = \exp\{-5.2[((k\eta_K)^4 + 0.4^4)^{1/4} - 0.4]\}$; shaded, the part resolved by an LES with a 10 m filter. Bottom: resolved (blue) and modeled (gray) ranges of DNS, LES and RANS.

shear stress τ of the surface layer; over terrain and around buildings the normal stresses and the horizontal shear stresses matter as well.

The four equations (29.4) have four mean unknowns, three velocity components and the pressure, and six further unknowns, the independent Reynolds stresses, for which the averaging provides no equation. This is the closure problem of Chapter 8 again. A RANS model is defined by how it closes it, and its mean wind is only as good as that closure.

29.2.2 Eddy-viscosity closure

The most common closure treats turbulent momentum transport as an enhanced diffusion. The Reynolds stresses are set proportional to the mean rate of strain,

$$-\overline{u_i' u_j'} = \nu_t \left(\frac{\partial \overline{u}_i}{\partial x_j} + \frac{\partial \overline{u}_j}{\partial x_i} \right) - \frac{2}{3} e\, \delta_{ij}, \tag{29.5}$$

where ν_t, in $\mathrm{m^2\,s^{-1}}$, is the *eddy viscosity*, the effective turbulent momentum diffusivity, and δ_{ij} is one for $i = j$ and zero otherwise. The last term is needed for consistency: summing the diagonal, $i = j$, the left-hand side gives $-(\overline{u'^2} + \overline{v'^2} + \overline{w'^2}) = -2e$, while the strain term sums to $2\nu_t\, \partial \overline{u}_i / \partial x_i$, which is zero by continuity; without $-\frac{2}{3} e\, \delta_{ij}$ the turbulent kinetic energy would vanish. The schematic form often quoted without this term describes only the shear stresses, $i \neq j$.

Relation (29.5) is the eddy-viscosity hypothesis, in the literature also called the Boussinesq hypothesis; it has nothing to do with the Boussinesq approximation for buoyancy of Section 29.5.2. For a horizontally uniform surface layer, with only $\partial \overline{u}/\partial z$ nonzero, it reduces to $-\overline{u'w'} = \nu_t\, \partial \overline{u}/\partial z$, which is the eddy diffusivity K_m of Chapter 8 under the name that CFD uses; in the

neutral surface layer $\nu_t = \kappa u_* z$. Like K_m, the eddy viscosity is a property of the turbulence, not of the air, and the closure is complete only once ν_t is known everywhere. The two-equation models below compute it from two transported turbulence quantities.

29.2.3 The k–ε model

The classic RANS model carries two prognostic equations, one for the turbulent kinetic energy and one for its dissipation rate. In its name, k is the turbulent kinetic energy, written e in this book; the model is called the k–ε model, and in its equations below the book's symbols are used. In the standard high-Reynolds-number form,

$$\frac{\mathrm{D}e}{\mathrm{D}t} = \frac{\partial}{\partial x_j}\left[\left(\nu + \frac{\nu_t}{\sigma_e}\right)\frac{\partial e}{\partial x_j}\right] + P_s - \varepsilon, \tag{29.6}$$

$$\frac{\mathrm{D}\varepsilon}{\mathrm{D}t} = \frac{\partial}{\partial x_j}\left[\left(\nu + \frac{\nu_t}{\sigma_\varepsilon}\right)\frac{\partial \varepsilon}{\partial x_j}\right] + C_{\varepsilon 1}\frac{\varepsilon}{e}P_s - C_{\varepsilon 2}\frac{\varepsilon^2}{e}, \tag{29.7}$$

where $\mathrm{D}/\mathrm{D}t$ follows the mean flow and $P_s = -\overline{u_i' u_j'}\,\partial \overline{u}_i/\partial x_j$ is the shear production of Chapter 8, computed from the modeled stresses. In words, equation (29.6) says: the rate of change of the turbulent kinetic energy carried with the mean flow equals its spreading by turbulent and molecular diffusion, plus its production by the shear of the mean flow, minus its dissipation into heat. It is the budget of Chapter 8 with its turbulent transport modeled as diffusion. Equation (29.7) has the same structure for the dissipation rate: diffusion; a source proportional to the production of turbulent kinetic energy, scaled by the inverse time ε/e of the energy-containing eddies; and a sink proportional to ε^2/e. Unlike the first, the second equation is not derived term by term from the Navier–Stokes equations; it is a model, built by analogy with the first and calibrated on measurements.

From the two quantities, the eddy viscosity is

$$\nu_t = C_\mu \frac{e^2}{\varepsilon}, \tag{29.8}$$

the only combination of e and ε with units of $\mathrm{m^2\,s^{-1}}$: e^2/ε has units $\mathrm{m^4\,s^{-4}}/(\mathrm{m^2\,s^{-3}}) = \mathrm{m^2\,s^{-1}}$. It is a velocity scale $e^{1/2}$ times a length scale $e^{3/2}/\varepsilon$, the size of the energy-containing eddies. The standard constants are $C_\mu = 0.09$, $C_{\varepsilon 1} = 1.44$, $C_{\varepsilon 2} = 1.92$, $\sigma_e = 1.0$ and $\sigma_\varepsilon = 1.3$.

The value of C_μ follows from a layer of constant stress in which production balances dissipation. There $-\overline{u'w'} = u_*^2$ and $\nu_t = u_*^2/(\partial\overline{u}/\partial z)$; production is $P_s = u_*^2\,\partial\overline{u}/\partial z = \varepsilon$; substituting both into equation (29.8),

$$\frac{u_*^2}{\partial\overline{u}/\partial z} = C_\mu \frac{e^2}{u_*^2\,\partial\overline{u}/\partial z} \quad\Longrightarrow\quad C_\mu = \left(\frac{u_*^2}{e}\right)^2.$$

The standard value corresponds to $u_*^2/e = 0.3$, the ratio measured in engineering shear flows. Chapter 8 gave $e \approx 5.5\,u_*^2$ for the neutral atmospheric surface layer, which by the same relation gives $C_\mu \approx (1/5.5)^2 \approx 0.033$. Some atmospheric applications therefore use a smaller C_μ, with the other constants adjusted to match; with the standard value the model underestimates the turbulent kinetic energy of the surface layer by about forty percent while still giving the right stress.

For an illustrative neutral surface layer with $u_* = 0.5\,\mathrm{m\,s^{-1}}$ at $z = 10\,\mathrm{m}$ over $z_0 = 0.05\,\mathrm{m}$, the equilibrium values of Section 29.4.2 are $e = u_*^2/\sqrt{C_\mu} = 0.25/0.3 = 0.833\,\mathrm{m^2\,s^{-2}}$ and $\varepsilon = u_*^3/(\kappa(z+z_0)) = 0.125/(0.4\times 10.05) = 0.0311\,\mathrm{m^2\,s^{-3}}$, so

$$\nu_t = 0.09 \times \frac{0.833^2}{0.0311} = 2.01\,\mathrm{m^2\,s^{-1}} = \kappa u_*(z+z_0) = 0.4\times 0.5\times 10.05.$$

The model is widely used because it is robust, numerically forgiving, inexpensive and familiar, with decades of experience in engineering flows.

29.2.4 The k–ω and SST models

A second family replaces the dissipation rate by the *specific dissipation rate*

$$\omega = \frac{\varepsilon}{C_\mu\, e}, \tag{29.9}$$

in s^{-1}: the rate of dissipation per unit of turbulent kinetic energy, an inverse time scale of the energy-containing eddies. Again k in the name k–ω is the turbulent kinetic energy. The eddy viscosity becomes $\nu_t = e/\omega$, identical to equation (29.8) after substituting equation (29.9). For the worked surface layer, $\omega = 0.0311/(0.09 \times 0.833) = 0.415\,\mathrm{s}^{-1}$ and $\nu_t = 0.833/0.415 = 2.01\,\mathrm{m}^2\,\mathrm{s}^{-1}$, the same value. The two models differ not in their equilibrium but in how their transport equations behave away from it: the k–ω model is better behaved near walls and more sensitive to adverse pressure gradients, which make the flow decelerate, but its solution depends on the value of ω prescribed in the free stream, far from the wall.

The *SST* model (shear-stress transport) blends the two: it uses the k–ω equations near the surface and switches to the k–ε behavior away from it, and it limits the eddy viscosity so that the modeled shear stress does not exceed about $0.3\,e$, the same ratio $u_*^2/e = \sqrt{C_\mu}$ as above. Where the flow decelerates against a rising pressure, production exceeds dissipation and the unlimited k–ε model produces too much eddy viscosity, which carries momentum down to the slowing near-wall air and keeps it attached. The limiter removes that excess. SST therefore often performs better in flows with strong adverse pressure gradients and separation, which are exactly the flows behind steep terrain and around buildings (Section 29.5.1).

29.2.5 What RANS gives and what it does not

RANS produces a mean wind field, usually a steady one, at modest cost. That is what is needed when the question is the expected mean wind at a location for a given inflow, and it is how RANS is used: terrain speed-up maps, wind-energy siting, and engineering flow studies around buildings, industrial sites and line corridors. Its output is the mean velocity, the mean pressure and the modeled turbulence quantities e, ε or ω, and ν_t, everywhere in the domain.

RANS does not simulate the time-varying eddies. It cannot reproduce individual gusts, coherent eddies such as those shed from a building corner, or intermittent turbulence; it predicts statistical quantities only:

$$\text{RANS} = \text{mean flow} + \text{modeled turbulence statistics.}$$

Even its turbulence statistics are partial. A turbulence intensity estimated from the modeled e assumes a split of the energy among the three components, and the isotropic split, $\sigma = \sqrt{2e/3}$, gives for the worked layer $\sqrt{2 \times 0.833/3} = 0.75\,\mathrm{m\,s}^{-1}$, against the along-wind $\sigma_u = 2.4\,u_* = 1.2\,\mathrm{m\,s}^{-1}$ of the anisotropic surface layer of Chapter 8. A gust or a turbulence intensity from RANS is therefore an estimate built on two modeling assumptions, the closure and the split, and is to be validated separately from the mean wind.

29.2.6 Steady and unsteady solutions

Three kinds of solution are in use. *Steady RANS* solves equations (29.4) with $\partial/\partial t = 0$ and returns one stationary mean flow. *Unsteady RANS* (URANS) keeps the time derivative and allows the mean flow to change in time: it can represent large, organized, slow structures such as periodic vortex shedding behind an obstacle, provided their time scale is well separated from that of the turbulence that the closure represents. In the atmosphere that separation is weak, and URANS results are to be read with that in mind. LES is transient by nature: its resolved field changes at every time step.

Figure 29.2 compares what the three report at one point in the wake of an illustrative building 30 m across in a wind of $10\,\mathrm{m\,s^{-1}}$. The horizontal axis is time over five minutes; the vertical axis is the along-wind speed at the point. Vortex shedding behind a bluff body has a Strouhal number $f_{\mathrm{sh}}b/U \approx 0.2$, with f_{sh} the shedding frequency and b the width of the obstacle, so the shedding frequency is $0.2 \times 10/30 = 0.067\,\mathrm{Hz}$, a period of 15 s. Steady RANS reports one number, $4\,\mathrm{m\,s^{-1}}$. URANS reports the shedding as a regular oscillation between 3 and $5\,\mathrm{m\,s^{-1}}$. LES reports a record with the shedding, its irregular phase and the resolved turbulence: over the five minutes its mean is $4.0\,\mathrm{m\,s^{-1}}$, its standard deviation $1.2\,\mathrm{m\,s^{-1}}$, its range 0.7 to $7.4\,\mathrm{m\,s^{-1}}$, and its highest three-second mean $6.9\,\mathrm{m\,s^{-1}}$, a gust neither RANS solution contains. If the question is a mean speed-up factor, steady RANS may be enough; if unsteady wakes and gusts matter, LES may be necessary.

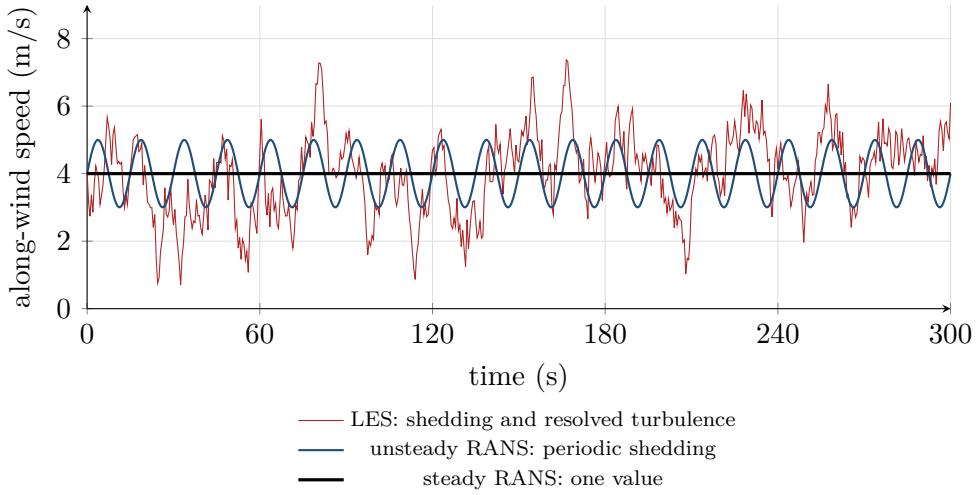


Figure 29.2: Along-wind speed at one point in the wake of a 30 m obstacle as reported by steady RANS, unsteady RANS and LES (synthetic, illustrative). Mean $4\,\mathrm{m\,s^{-1}}$; shedding period 15 s (Strouhal number 0.2, $U = 10\,\mathrm{m\,s^{-1}}$); the LES record adds a wandering shedding phase and first-order autoregressive turbulence with a standard deviation of $1.2\,\mathrm{m\,s^{-1}}$ and an integral time of 4 s. Generated by `scripts/ch29_data.py`.

29.3 Large-eddy simulation

Large-eddy simulation computes the large turbulent eddies directly and models only the small ones. This section describes the filtering that separates them, why the result can be more realistic than RANS, the subgrid-scale model that remains, the grid resolution the method requires and its cost compared with RANS.

29.3.1 Filtering and the resolved field

LES separates the flow by size rather than by averaging in time. The velocity is filtered in space,

$$\widetilde{u}_i(\mathbf{x},t) = \int \mathcal{G}(\mathbf{x}-\mathbf{x}')\,u_i(\mathbf{x}',t)\,\mathrm{d}\mathbf{x}', \tag{29.10}$$

with a filter kernel $\mathcal{G}$ of width Δ_f, in practice about the grid spacing: $\widetilde{u}_i$ is a local average over a volume of size Δ_f, and the eddies smaller than Δ_f are removed from it. Filtering equations (29.1) gives equations for $\widetilde{u}_i$ of the same form as equations (29.4), with the Reynolds stresses replaced by the *subgrid-scale stresses*

$$\tau_{ij}^{\mathrm{sgs}} = \widetilde{u_i u_j} - \widetilde{u}_i\,\widetilde{u}_j, \tag{29.11}$$

the momentum transport by eddies smaller than the filter. The structure is the same as in RANS; the difference is in what the unknown term represents. In RANS it is all the turbulence; in LES it is only the part smaller than the grid, and the resolved field $\widetilde{u}_i$ remains turbulent, three-dimensional and time-dependent.

LES is attractive for near-surface wind because the large eddies are the ones that depend on the flow's surroundings. They are produced by the terrain, through separation and wakes; by the shear of the mean wind; and by convection, as thermals as deep as the boundary layer (Chapter 16). The small eddies of the inertial subrange have largely forgotten their source (Chapter 8), and a generic model represents them adequately. LES computes the part of the turbulence that is specific to the site and models the part that is universal.

29.3.2 Why LES can be more realistic

The large atmospheric eddies hold most of the turbulent kinetic energy and carry most of the momentum and heat; they are also anisotropic, shaped by the shear, the ground and gravity. RANS compresses all of them into the single scalar ν_t of equation (29.5), which aligns the stresses with the mean strain and has no memory of how the eddies were produced. LES simulates their evolution: they are generated, advected, stretched and broken up by the resolved equations themselves.

LES can therefore capture what RANS represents only on average or not at all: wake shedding behind buildings and ridges; coherent structures, such as the rolls of a sheared layer and the plumes of a convective one; turbulent bursts, short episodes in which fast air from above reaches the ground; and recirculation zones that change size and position in time. These are the features that produce gusts and the extreme loads on structures and conductors. The price is computational: an LES must be run at fine resolution, for long enough to accumulate statistics, and it needs a turbulent inflow. A smooth mean profile at the inlet of an LES produces turbulence only after a long fetch, so the inflow is taken from a separate precursor simulation of the upstream boundary layer or generated synthetically with the right spectra.

29.3.3 The subgrid-scale model

The subgrid-scale stresses (29.11) are unknown, and a *subgrid-scale* (SGS) model supplies them. The common approach reuses the eddy-viscosity form (29.5) with the filtered strain rate $\widetilde{S}_{ij} = \tfrac{1}{2}(\partial\widetilde{u}_i/\partial x_j + \partial\widetilde{u}_j/\partial x_i)$ and a subgrid eddy viscosity ν_{sgs}. In the Smagorinsky model,

$$\nu_{\mathrm{sgs}} = (C_{\mathrm{smag}}\,\Delta_f)^2\,|\widetilde{S}|, \qquad |\widetilde{S}| = \sqrt{2\,\widetilde{S}_{ij}\widetilde{S}_{ij}}, \tag{29.12}$$

with C_{smag} about 0.1 to 0.2: a length, the filter width, times a velocity, the filter width times the resolved strain. Atmospheric codes often carry instead a prognostic subgrid turbulent kinetic energy e_{sgs} and set $\nu_{\mathrm{sgs}} = C_k\,\Delta_f\,e_{\mathrm{sgs}}^{1/2}$ with a constant C_k of about 0.1, which lets buoyancy act on the subgrid energy in stable and convective layers.

Two consequences follow. First, LES does not remove parameterization; it moves it to smaller scales. Where the filter lies in the inertial subrange, the modeled part carries little energy and less flux, and the result is insensitive to the model's details. Second, the condition fails near the ground. At height z the energy-containing eddies are of size of order z (Chapter 8), so in the first few cells above the surface the filter is as large as the eddies, the subgrid model carries most of the stress, and LES there is no better than its subgrid and wall models. LES is most reliable well above the first cells, and least reliable at the heights of a 10 m anemometer unless the grid near the ground is fine.

29.3.4 Grid resolution

To resolve an eddy the grid must be considerably smaller than the eddy. A dominant turbulence scale of 100 m is not resolved by a grid of 100 m: a wave of wavelength 100 m sampled every 100 m shows the same value at every point and vanishes from the grid, and the shortest wave a grid can carry at all has a wavelength of $2\Delta x$. Spacings of 10 to 20 m, five to ten points per wavelength, or finer, are needed.

The inertial-subrange spectrum gives the energy left to the subgrid model. Integrating $E(k) = C_K \varepsilon^{2/3} k^{-5/3}$ from the cutoff $k_c = \pi/\Delta_f$ to infinity,

$$e_{\mathrm{sgs}} = \int_{k_c}^{\infty} C_K\, \varepsilon^{2/3}\, k^{-5/3}\, \mathrm{d}k = \frac{3}{2}\, C_K\, \varepsilon^{2/3}\, k_c^{-2/3} = \frac{3}{2}\, C_K\, \varepsilon^{2/3} \left(\frac{\Delta_f}{\pi}\right)^{2/3}, \tag{29.13}$$

valid while k_c lies in the inertial subrange. For the spectrum of Figure 29.1, with $\varepsilon = 0.01\,\mathrm{m^2\,s^{-3}}$ and $\Delta_f = 10\,\mathrm{m}$, $e_{\mathrm{sgs}} = 1.5 \times 1.5 \times 0.0464 \times (10/\pi)^{2/3} = 2.25 \times 0.0464 \times 2.16 = 0.226\,\mathrm{m^2\,s^{-2}}$, 39 % of the total turbulent kinetic energy of $0.586\,\mathrm{m^2\,s^{-2}}$, close to the 38 % of the exact integral. Halving Δ_f reduces the subgrid energy only by $2^{2/3} = 1.59$, because the $-5/3$ spectrum falls slowly.

Figure 29.3 plots the resolved fraction of the turbulent kinetic energy of that spectrum against the filter width, on a logarithmic horizontal axis; the dashed line marks 80 %, a common working criterion for a well-resolved LES, and the labels give the cell count of the $6 \times 4 \times 1.5$ km domain at three spacings. A 100 m grid resolves 3 % of the energy; 20 m resolves 42 %; 10 m, 62 %; and 80 % requires about 4 m. The momentum flux is less demanding than the energy: its spectrum, the cospectrum of u' and w', falls as $k^{-7/3}$ in the inertial subrange, so its unresolved part falls as $k_c^{-4/3}$ rather than $k_c^{-2/3}$. A filter five times smaller than the peak wavelength leaves about $5^{-2/3} = 0.34$ of the energy unresolved but only about $5^{-4/3} = 0.12$ of the flux. A 10 to 20 m grid thus resolves most of the transport of momentum by 100 m eddies while leaving a large share of their energy to the subgrid model; LES resolution can become computationally demanding quickly, and the requirement depends on which quantity is wanted.

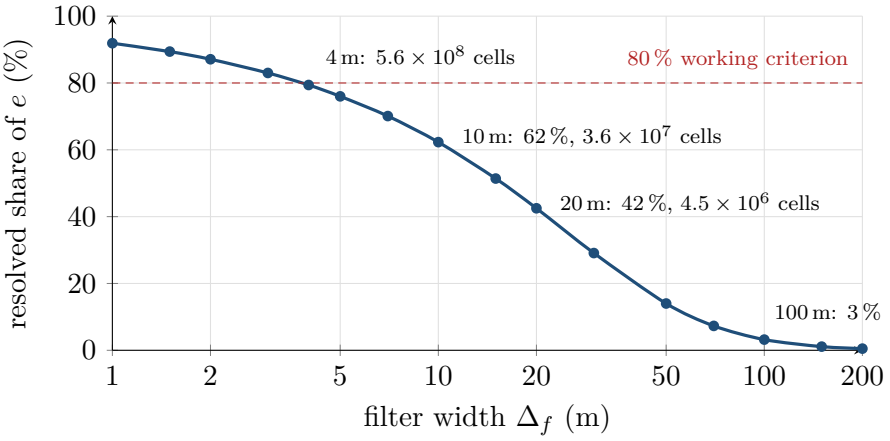


Figure 29.3: Share of the turbulent kinetic energy resolved by an LES with a sharp spectral filter at $k_c = \pi/\Delta_f$, for the model spectrum of Figure 29.1 (energy peak at a wavelength of about 100 m; illustrative). Cell counts are for a domain of $6 \times 4 \times 1.5$ km at uniform spacing.

29.3.5 Cost compared with RANS

Take the illustrative domain of 6 km by 4 km by 1.5 km at a uniform LES spacing of 10 m: $600 \times 400 \times 150 = 3.6 \times 10^7$ cells. The time step is limited by the condition that the flow cross less

than about half a cell per step; with a maximum speed of $15\,\mathrm{m\,s^{-1}}$, $\Delta t \approx 0.5 \times 10\,\mathrm{m}/15\,\mathrm{m\,s^{-1}} = 0.33\,\mathrm{s}$. The run must first let the turbulence develop and wash out the initial state, about two flow-through times of $6000\,\mathrm{m}/10\,\mathrm{m\,s^{-1}} = 600\,\mathrm{s}$ each, and then accumulate one hour of statistics: 4800 s in all, or 14 400 steps. The total is about $3.6 \times 10^7 \times 1.44 \times 10^4 = 5.2 \times 10^{11}$ cell updates.

A steady RANS run of the same domain uses a stretched mesh, about 10 m near the site and coarser toward the boundaries, of $300 \times 200 \times 40 = 2.4 \times 10^6$ cells, and converges in a few thousand iterations: about $2.4 \times 10^6 \times 2000 = 4.8 \times 10^9$ cell updates, roughly a hundred times fewer, if the cost per update is taken as similar. A library of 12 wind directions and 3 stability classes, 36 RANS runs, costs about 1.7×10^{11} updates, a third of the single LES. Refining the LES to 5 m multiplies its cells by eight and its time steps by two, its cost by sixteen (Chapter 5). The comparison sets the roles of the two methods: RANS for sweeps over many conditions, LES for the few conditions in which the eddies themselves are the answer.

29.4 Domain, boundary conditions and mesh

A CFD result depends as much on how the simulation is set up as on the turbulence model. This section describes the computational domain, the inlet and its turbulence, the requirement that the inflow be preserved across an empty domain, the treatment of the ground, the terrain mesh, and the test of mesh convergence.

29.4.1 The computational domain

A microscale simulation needs a finite domain, and its boundaries must be far enough from the site that they do not influence the flow there. For terrain the domain typically spans several kilometers horizontally and 1 to 3 km vertically. Figure 29.4 draws a vertical section through a domain in the direction of the inflow: the inlet on the left with its wind profile, the terrain with the region of interest boxed around the hill, the outlet on the right, the top boundary, and the ground with its wall treatment. The arrows below the ground and at the right give rule-of-thumb extents, in units of the hill height h_m; the band under the top marks the damping layer used in stable cases (Section 29.5.3).

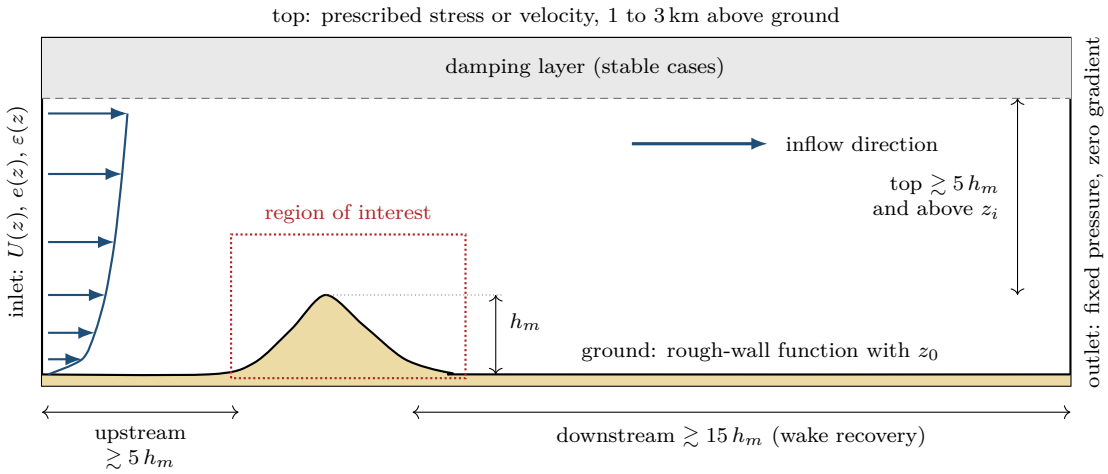


Figure 29.4: Vertical section through a terrain CFD domain along the inflow direction (schematic, not to scale). Boundary conditions are written at each boundary; extents are rules of thumb in units of the hill height h_m. The lateral boundaries, not shown, are periodic or symmetry planes.

The rules of thumb, labeled as such because they vary between practice guides and must be checked for each case, are: the inlet at least about five hill heights upstream of the first

significant terrain, so that the flow ahead of the hill can decelerate freely; the outlet at least about fifteen hill heights downstream, so that the wake has recovered before the outflow condition is imposed; the top at least about five hill heights above the highest terrain and above the boundary-layer depth z_i; the lateral boundaries at least about five hill heights to each side of the region of interest; and a blockage ratio, the frontal area of the terrain or obstacles divided by the cross-section of the domain, below about three percent. For an illustrative isolated hill with $h_m = 200\,\mathrm{m}$ and a base 1.2 km wide, they give at least 1 km upstream, 3 km downstream and 1 km of depth; the frontal area of the hill, about $\frac{1}{2} \times 200\,\mathrm{m} \times 1200\,\mathrm{m} = 1.2 \times 10^5\,\mathrm{m}^2$, is 2 % of the cross-section of a domain 4 km wide and 1.5 km deep, $6 \times 10^6\,\mathrm{m}^2$, which passes the blockage test.

The reason for the margins is continuity. A rigid top forces all the air entering the domain to pass between the hill and the top; for a long two-dimensional ridge under a lid at height D, the speed averaged over the column above the crest is exactly $D/(D - h_m)$ times the upstream average, 1.25 for $D = 5\,h_m$ and 1.11 for $D = 10\,h_m$. Part of that acceleration is physical, since the streamlines over a real hill are also lifted; the error is the part a free atmosphere would relieve by lifting them higher, and it shrinks as the top rises. An inlet too close to the terrain, likewise, prescribes the flow where the hill already slows it. Boundaries that are too close produce speed-ups the site does not have.

29.4.2 The inlet profile

CFD needs the incoming wind as a boundary condition, the *inlet profile*: the prescribed atmospheric state entering the domain. A simplistic inlet prescribes a speed uniform with height, for example $U = 10\,\mathrm{m\,s^{-1}}$ at every level. The atmospheric wind is not uniform: it increases with height through the surface layer, and the shape of the profile sets how strongly the near-surface air responds to the terrain. A uniform inlet develops a boundary layer only after it meets the ground, so the flow arriving at the hill has a profile set by the fetch inside the domain, not by the atmosphere. A better inlet prescribes $U(z)$ together with the turbulence quantities. For neutral flow the profile is the logarithmic law of Chapter 12,

$$U(z) = \frac{u_*}{\kappa} \ln\!\left(\frac{z - d}{z_0}\right), \tag{29.14}$$

which CFD codes, with z measured from the wall and $d = 0$, usually write as $(u_*/\kappa)\ln((z + z_0)/z_0)$, so that the speed is zero at the wall itself; for $z \gg z_0$ the two are the same.

A physically consistent inlet, the *atmospheric boundary-layer inlet*, also specifies $e(z)$ and $\varepsilon(z)$, or the equivalent $\omega(z)$, such that the three profiles satisfy the turbulence model in a horizontally uniform, neutral, constant-stress layer. With $z' = z + z_0$, the log profile has the shear $\partial U/\partial z = u_*/(\kappa z')$ and the stress $-\overline{u'w'} = u_*^2$, so the eddy viscosity is $\nu_t = u_*^2/(\partial U/\partial z) = \kappa u_* z'$. In equilibrium, production equals dissipation:

$$\varepsilon = P_s = \nu_t \left(\frac{\partial U}{\partial z}\right)^2 = \kappa u_* z' \frac{u_*^2}{\kappa^2 z'^2} = \frac{u_*^3}{\kappa z'}.$$

Equation (29.8) then gives $e^2 = \nu_t\,\varepsilon/C_\mu = \kappa u_* z' \cdot u_*^3/(\kappa z')/C_\mu = u_*^4/C_\mu$. The standard equilibrium inlet is therefore

$$U(z) = \frac{u_*}{\kappa} \ln\!\left(\frac{z + z_0}{z_0}\right), \qquad e = \frac{u_*^2}{\sqrt{C_\mu}}, \qquad \varepsilon(z) = \frac{u_*^3}{\kappa(z + z_0)}, \tag{29.15}$$

with a turbulent kinetic energy constant with height and a dissipation rate that falls inversely with height. For $u_* = 0.5\,\mathrm{m\,s^{-1}}$ and $z_0 = 0.05\,\mathrm{m}$ the inlet has $U = 4.64$, 6.63 and $9.50\,\mathrm{m\,s^{-1}}$ at 2, 10 and 100 m, $e = 0.833\,\mathrm{m^2\,s^{-2}}$ at every height, and $\varepsilon = 0.031\,\mathrm{m^2\,s^{-3}}$ at 10 m and $0.0031\,\mathrm{m^2\,s^{-3}}$ at 100 m. The challenge is to make these profiles consistent with the wall treatment, the top boundary and the model constants; otherwise the profile changes before it reaches the terrain.

29.4.3 Preservation of the inlet profile

Suppose a log profile is prescribed at the inlet. If the turbulence model, the wall roughness and the top boundary are not consistent with it, the model modifies the profile over flat terrain, and by the time the flow reaches the hill the inflow is already wrong: the speed-up is computed for a wind that the inlet did not specify. The test is *inlet-profile preservation*: an empty domain, flat and with the same roughness as the inlet, is run first, and the profiles at its outlet are compared with those at its inlet. They should be identical. Three requirements must hold together:

inlet profile + turbulence model + wall model must be consistent.

Figure 29.5 shows a typical failure. The axes are wind speed and height over the lowest 100 m. The black curve is the inlet, equation (29.15) with $u_* = 0.5\,\mathrm{m\,s^{-1}}$ and $z_0 = 0.05\,\mathrm{m}$; the dots on it are the profile 1 km downstream in a consistent setup, unchanged. The red curve is the same distance downstream when the wall function was given a roughness thirty times too small, the error of Section 29.4.4 with the effective $z_0 = 0.0017\,\mathrm{m}$. An internal boundary layer (Chapter 7) grows from the inlet, about 40 m deep after 1 km by the rule of that chapter; inside it the smoother wall lets the air accelerate. At 10 m the wind has risen from 6.63 to $7.21\,\mathrm{m\,s^{-1}}$, by 9 %; at 2 m from 4.64 to $5.88\,\mathrm{m\,s^{-1}}$, by 27 %; the surface stress has fallen to $(0.331/0.5)^2 = 44\,\%$ of its inlet value. A hill placed at that distance would be computed in an inflow with too little shear near the ground, and its speed-up factors would be wrong in the layer where they are largest.

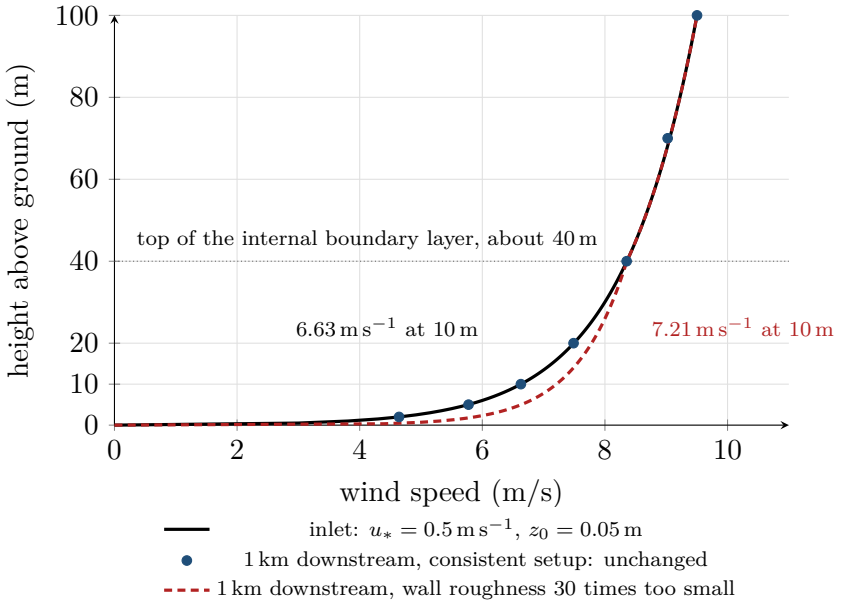


Figure 29.5: Inlet-profile preservation over an empty, flat domain (illustrative). Black: the neutral inlet $U = (u_*/\kappa)\ln((z+z_0)/z_0)$ with $u_* = 0.5\,\mathrm{m\,s^{-1}}$, $z_0 = 0.05\,\mathrm{m}$, $\kappa = 0.4$. Red: the profile 1 km downstream when the wall behaves as $z_0 = 0.0017\,\mathrm{m}$, modeled as an internal boundary layer 40 m deep with $u_* = 0.331\,\mathrm{m\,s^{-1}}$ below it and the inlet profile above.

Two further sources of drift come from the model and the top boundary. In the ε equation (29.7), the equilibrium profiles (29.15) are an exact steady solution only if the constants satisfy

$$\sigma_\varepsilon = \frac{\kappa^2}{(C_{\varepsilon 2} - C_{\varepsilon 1})\sqrt{C_\mu}}, \tag{29.16}$$

which follows from substituting the profiles into the equation: the production and destruction terms leave a residual $(C_{\varepsilon 2} - C_{\varepsilon 1})\varepsilon^2/e$ that the diffusion term, $u_*^4/(\sigma_\varepsilon z'^2)$, must balance. With

the standard constants and $\kappa = 0.4$ the right-hand side is $0.16/(0.48 \times 0.3) = 1.11$, not the standard 1.3, and the dissipation profile drifts unless one constant is adjusted. The top boundary matters as well: the log profile requires the stress $\rho_0 u_*^2$ at every height, so a frictionless top, which forces the stress to zero there, cannot sustain it, and the profile relaxes toward a channel flow. A consistent setup prescribes the stress at the top, or the inlet values there, or drives the flow with a pressure gradient that accounts for the decrease of stress with height (Section 29.5.5). The real boundary layer is not a constant-stress layer 1.5 km deep, and inlets built from a weather model's profiles of U, e and θ face the same test.

29.4.4 Wall functions and aerodynamic roughness

Near a surface the velocity changes rapidly with height, and resolving the layer next to the wall would need a very fine mesh. Over a smooth wall that layer is the viscous sublayer, about $5\nu/u_*$ thick: $5 \times 1.5 \times 10^{-5}/0.5 = 0.15\,\mathrm{mm}$ for $u_* = 0.5\,\mathrm{m\,s^{-1}}$. Atmospheric surfaces are not smooth: the roughness Reynolds number $u_* z_0/\nu = 0.5 \times 0.05/(1.5 \times 10^{-5}) \approx 1700$ is far above the value of about 2.5 at which a surface becomes aerodynamically fully rough, so the viscous sublayer is broken up by the roughness elements, grass blades, stones, crops, which no terrain mesh resolves either. The near-wall layer is therefore never resolved; RANS, and LES near the ground, use a *wall function*: a near-wall parameterization that imposes a known relation between the velocity at the first cell and the surface stress. In atmospheric applications it is the log law. With the first cell center at height z_p, the turbulent kinetic energy there gives the friction velocity, $u_* = C_\mu^{1/4} e_p^{1/2}$, the log law gives the expected velocity, $U_p = (u_*/\kappa)\ln((z_p + z_0)/z_0)$, and the wall stress $\rho_0 u_*^2$ and the value $\varepsilon_p = u_*^3/(\kappa(z_p + z_0))$ are imposed. For the worked layer with $z_p = 2\,\mathrm{m}$, $u_* = 0.09^{1/4} \times 0.833^{1/2} = 0.548 \times 0.913 = 0.50\,\mathrm{m\,s^{-1}}$, $U_p = 1.25\ln(41) = 4.64\,\mathrm{m\,s^{-1}}$ and the wall stress is $1.2 \times 0.25 = 0.30\,\mathrm{Pa}$.

CFD codes specify the surface roughness in different ways: as an *equivalent sand-grain roughness* k_s, the diameter of tightly packed sand grains that would produce the same drag, inherited from pipe-flow engineering; as the aerodynamic roughness length z_0; or as other roughness-height parameters. These are not interchangeable. For a fully rough sand-grain wall the log law reads $U/u_* = (1/\kappa)\ln(z/k_s) + 8.5$; setting it equal to $(1/\kappa)\ln(z/z_0)$ gives

$$k_s = z_0\, e^{8.5\kappa} \approx 30\, z_0 \tag{29.17}$$

for $\kappa = 0.4$ (about $33\, z_0$ for $\kappa = 0.41$; the exact factor depends on the constants a code uses). Entering a roughness length where the code expects k_s makes the wall thirty times too smooth, which is the error of Figure 29.5; entering k_s where it expects z_0 makes it thirty times too rough. Many sand-grain wall functions also require the first cell center to lie above k_s. For grass with $z_0 = 0.05\,\mathrm{m}$, $k_s = 1.5\,\mathrm{m}$ and the first cell must be at least 3 m tall; for forest with $z_0 = 1\,\mathrm{m}$, $k_s = 30\,\mathrm{m}$, and a first cell 60 m tall would leave nothing of the profile at the heights of interest. Codes intended for the atmosphere therefore use wall functions written directly in z_0, or represent the forest as a canopy drag (Chapter 21). The conversion is a frequent source of hidden error: the simulation runs, converges and looks plausible, and its near-ground winds are wrong by a fixed fraction.

29.4.5 The terrain mesh

Complex terrain must be discretized into cells that follow the ground. The quality of that mesh is set by five properties: the horizontal spacing, which decides which terrain features exist in the model; the vertical spacing, which decides how well the profile near the ground is represented; the aspect ratio of the cells, their horizontal size over their vertical size, which is large near the ground and degrades the accuracy of the solver when extreme; the skewness, the departure of the cells from right angles where the mesh is forced to follow steep slopes; and

the refinement near the ground, usually a first cell of one to a few meters with each cell above taller by a fixed growth ratio. A first cell of 1 m with a growth ratio of 1.15 reaches 1.5 km in n cells with $1\,\mathrm{m} \times (1.15^n - 1)/0.15 = 1500\,\mathrm{m}$, so $1.15^n = 226$ and $n = \ln 226/\ln 1.15 \approx 39$; the topmost of them is about 200 m tall. Stretching makes the vertical resolution cheap; the horizontal resolution is what drives the cell count.

If the mesh is too coarse, terrain slopes are smoothed. A ridge with a half-width $L_h = 300\,\mathrm{m}$ is described by only six points across its central 600 m at $\Delta x = 100\,\mathrm{m}$; its crest is cut and its slopes are reduced, and with them the pressure perturbations and the speed-up (Chapter 20). Ten or more cells per half-width is a common working target. The elevation data themselves have a resolution and an error, and a mesh cannot be finer in effect than the terrain model it is built from. CFD can thus reproduce the problem of coarse NWP, terrain that is lower and smoother than the real one, only at a smaller scale.

29.4.6 Mesh convergence

A result is more trustworthy if it is reasonably insensitive to refinement of the mesh: this is *mesh convergence*, the stability of the solution under grid refinement. The test runs the same case on a sequence of meshes refined by a constant ratio r, for example $\Delta x = 40$, 20 and 10 m with $r = 2$, and follows a quantity of interest. Suppose the predicted crest wind is $U_\mathrm{c} = 10.0$, $U_\mathrm{m} = 11.5$ and $U_\mathrm{f} = 11.7\,\mathrm{m\,s^{-1}}$ on the coarse, medium and fine meshes. The successive changes are 1.5 and $0.2\,\mathrm{m\,s^{-1}}$; their ratio, 7.5, measures how fast the error shrinks. For a scheme whose error falls as Δx^n, the ratio is r^n, so the observed order of convergence is

$$n = \frac{\ln[(U_\mathrm{m} - U_\mathrm{c})/(U_\mathrm{f} - U_\mathrm{m})]}{\ln r} = \frac{\ln 7.5}{\ln 2} = 2.9,$$

and the extrapolation to zero spacing, Richardson extrapolation, is

$$U_0 \approx U_\mathrm{f} + \frac{U_\mathrm{f} - U_\mathrm{m}}{r^n - 1} = 11.7 + \frac{0.2}{7.5 - 1} = 11.73\,\mathrm{m\,s^{-1}}.$$

The fine-mesh value lies 0.3 % below the extrapolated one; a common form of the error band, 1.25 times that relative difference, is 0.33 %, about $\pm 0.04\,\mathrm{m\,s^{-1}}$. The solution is approaching convergence. An observed order of 2.9 is higher than the second order of most solvers, a sign that the three meshes may not yet be in the range where the error behaves as a single power; with $n = 2$ the extrapolation would be $11.7 + 0.2/3 = 11.77\,\mathrm{m\,s^{-1}}$. Either way, the converged crest wind lies within about one percent of the fine-mesh value.

Figure 29.6 plots the test. The horizontal axis is the grid spacing, with refinement toward the left; the vertical axis is the predicted crest wind. The blue points are the three runs, the curve through them the fitted power law, and the open circle at zero spacing the extrapolated value. The gray squares are a contrasting sequence, 10.0, 11.5 and $12.9\,\mathrm{m\,s^{-1}}$, whose changes, 1.5 and $1.4\,\mathrm{m\,s^{-1}}$, hardly shrink: if the prediction keeps changing like this, the mesh is insufficient and no extrapolation is meaningful. Convergence is also a property of a quantity at a place: a crest wind may be converged while the length of the recirculation zone in the lee is not, and each quantity that is reported needs its own test.

29.5 Separation, stability and large-scale forcing

The setups of the previous section are neutral, non-rotating and driven by an inlet. This section treats the physics that the neutral setup leaves out or handles poorly: separated and recirculating flow, buoyancy and its approximation, stable and unstable layers, the Coriolis force at the microscale, and the large-scale forcing that keeps the air moving.

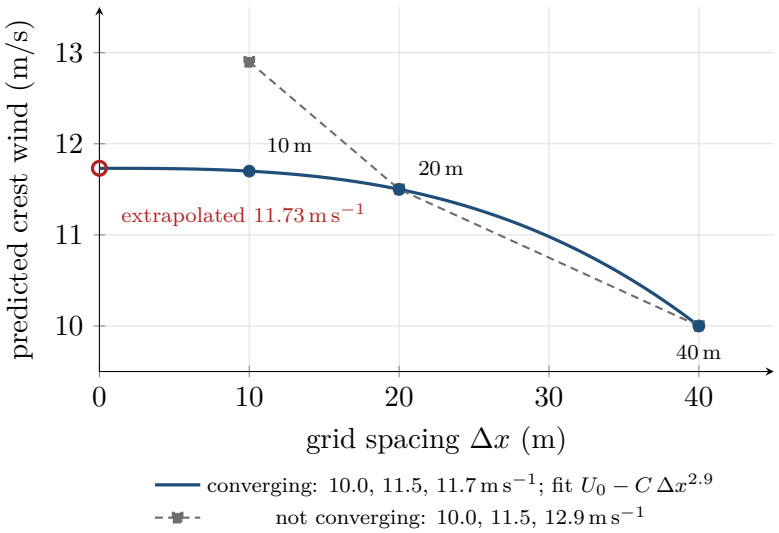


Figure 29.6: Mesh-convergence test for a predicted crest wind on three meshes refined by $r = 2$ (illustrative). Blue: a converging sequence with the power law $U = 11.731 - 3.81 \times 10^{-5}\,\Delta x^{2.91}$ through the three points and the Richardson extrapolation at $\Delta x = 0$. Gray: a sequence that does not converge.

29.5.1 Separation and recirculation

For a smooth, gentle hill the flow stays attached, the speed-up is set by the pressure perturbation over the crest, and RANS may do well. For steep terrain the flow separates on the lee slope (Chapter 20), where the near-ground air, slowed by friction, cannot climb the rising pressure. Where it separates, and where it reattaches, depend on the balance between that pressure rise and the momentum that turbulence brings down to the near-ground air, which is exactly what the closure computes. The choice of turbulence model therefore becomes much more important: a closure with too much eddy viscosity in the decelerating flow, such as the standard k–ε model, delays separation or suppresses it, and shortens the recirculation zone; the stress limiter of SST (Section 29.2.4) separates the flow earlier; and LES computes an unsteady separation line that moves with the passing eddies. Different closures can produce different answers for the same ridge, and predicting exactly where flow separates and reattaches is difficult.

Behind a ridge, CFD may predict $U < 0$ relative to the background direction: reversed mean flow, the near-ground air blowing back up the lee slope toward the crest. The size of the recirculation zone depends on the slope, the roughness, the stability and the turbulence model. These are difficult validation targets. A recirculation zone is a few hill heights long, its mean wind is small and its direction variable, a single mast samples one point of it, and a lidar's assumption of a horizontally uniform flow across its scanning cone fails inside it (Chapter 22). A lee site is where models disagree most and measurements constrain them least.

29.5.2 Buoyancy and the Boussinesq approximation

So far the flow has implicitly been neutral, but atmospheric flow can be stable, neutral or unstable. To represent stability, CFD solves a transport equation for the potential temperature (Chapter 13),

$$\frac{\mathrm{D}\overline{\theta}}{\mathrm{D}t} = \frac{\partial}{\partial x_j}\left(\frac{\nu_t}{\mathrm{Pr}_t}\frac{\partial \overline{\theta}}{\partial x_j}\right)$$

in RANS form, with the turbulent heat diffusivity written as the eddy viscosity over a turbulent Prandtl number, and buoyancy then appears in the momentum equations. The common way

to include it is the *Boussinesq approximation*: density variations are neglected everywhere except where they multiply gravity. The density is the constant ρ_0 in the inertia, continuity and pressure-gradient terms, and the buoyancy force per unit mass is

$$\mathbf{F}_b = -\frac{\rho - \rho_0}{\rho_0}\, g\, \mathbf{k} = g\, \frac{\theta - \theta_0}{\theta_0}\, \mathbf{k}, \tag{29.18}$$

upward for air lighter than the reference. The second form follows from the ideal gas law at nearly constant pressure, $\rho = p/(R_d T)$, for which $(\rho - \rho_0)/\rho_0 \approx -(T - T_0)/T_0$, and from the fact that θ is proportional to T at a given pressure; with moist air, θ_v replaces θ.

The approximation works well for most atmospheric microscale flows, whose density variations are small. Air 3 K colder than a reference of 300 K differs in density by one percent and feels a buoyancy of $9.81 \times (-3/300) = -0.098\,\mathrm{m\,s^{-2}}$, downward: a large force compared with the accelerations of terrain flow, while the neglected change of its inertia is a one-percent correction. The turbulence model needs the same term: the turbulent kinetic energy equation (29.6) gains the buoyancy production $P_b = (g/\theta_0)\,\overline{w'\theta'} = -(g/\theta_0)(\nu_t/\mathrm{Pr}_t)\,\partial\overline{\theta}/\partial z$ of Chapter 8, negative in stable air, and the ε equation a corresponding term whose constant is much less settled than the neutral ones. Stable RANS solutions inherit that uncertainty.

29.5.3 Stable and unstable flow

Under stable conditions, $\partial\theta/\partial z > 0$, vertical motion is suppressed, and terrain effects shift from flow over the hill toward blocking, channeling and gravity waves (Chapter 20). The controlling number is the Froude number $\mathrm{Fr} = U/(N h_m)$. A night gradient of $\partial\theta/\partial z = 0.012\,\mathrm{K\,m^{-1}}$ at $\theta = 300\,\mathrm{K}$ gives $N^2 = (9.81/300) \times 0.012 = 3.9 \times 10^{-4}\,\mathrm{s^{-2}}$, $N = 0.020\,\mathrm{s^{-1}}$. Over a hill with $h_m = 200\,\mathrm{m}$, a wind of $4\,\mathrm{m\,s^{-1}}$ has $\mathrm{Fr} = 1$ and a wind of $2\,\mathrm{m\,s^{-1}}$ has $\mathrm{Fr} = 0.5$, for which the air below a dividing-streamline height of about $h_m(1 - \mathrm{Fr}) = 100\,\mathrm{m}$ flows around the hill rather than over it. A neutral simulation has $N = 0$ and $\mathrm{Fr} = \infty$: all the air crosses the crest. A neutral CFD solution may therefore be badly wrong for a strongly stable night. Stable simulations also carry gravity waves, of wavelength $2\pi U/N$, about 2.5 km for $U = 8\,\mathrm{m\,s^{-1}}$; the domain must contain several wavelengths downstream, and the top needs the damping layer of Figure 29.4, which absorbs the waves instead of reflecting them back down onto the terrain.

Under unstable conditions, $\partial\theta/\partial z < 0$ near the ground, buoyant turbulence enhances vertical mixing. It weakens some terrain-induced shear patterns, since the near-ground air is constantly replaced by air mixed down from above, and it creates large convective eddies, thermals and their downdrafts as deep as the boundary layer, 1 to 2 km on a summer afternoon (Chapter 16). Their transport is nonlocal, which an eddy viscosity represents poorly, and their size requires a domain several times z_i wide. LES is particularly useful for convective cases: it resolves the thermals directly, at spacings of tens of meters, and returns the intermittent wind that a site experiences as they pass.

29.5.4 Coriolis at the microscale

For a small domain the Coriolis force may be negligible. The Rossby number $\mathrm{Ro} = U/(|f|L)$ (Chapter 5) compares inertia with the Coriolis force. For $L = 1\,\mathrm{km}$ and $U = 10\,\mathrm{m\,s^{-1}}$ at 45°N, $f = 2 \times 7.292 \times 10^{-5} \times \sin 45^\circ = 1.03 \times 10^{-4}\,\mathrm{s^{-1}}$ and $\mathrm{Ro} = 10/(1.03 \times 10^{-4} \times 1000) = 97$; at 23°S, $f = -5.70 \times 10^{-5}\,\mathrm{s^{-1}}$ and $\mathrm{Ro} = 10/(5.70 \times 10^{-5} \times 1000) = 175$. With $\mathrm{Ro} \gg 1$ the rotation is weak: air crosses the domain in 100 s, a small fraction of $1/|f|$, which is 2.7 and 4.9 h at the two latitudes. For a domain of 20 km at 45°N, $\mathrm{Ro} \approx 4.8$, and for flows that persist for hours in weak winds, such as stable valley flows, the Coriolis force may need to be included.

The inflow is a separate matter. The wind entering the domain has already been turned by the Coriolis force over the whole depth of the boundary layer: in the Northern Hemisphere it veers (turns clockwise) with height, in the Southern Hemisphere it backs (turns counterclockwise),

typically by tens of degrees between the surface and the top of the boundary layer (Chapter 6). An inlet that prescribes such a turning profile while the domain omits both the Coriolis force and the large-scale pressure gradient has nothing that maintains it, and the directional shear diffuses away downstream. For a conductor at 15 m and a turbine hub at 100 m, whose winds may differ in direction by ten degrees or more, that loss matters.

29.5.5 Pressure-gradient forcing

A local CFD domain still needs the large-scale forcing that keeps the air moving against surface drag. It can be imposed through the inlet wind alone, through a pressure gradient, or through a geostrophic wind. An inlet alone sustains the flow only as long as the momentum it brings in lasts; in a long domain the near-ground air decelerates. A uniform pressure gradient, added as a constant source in the momentum equation, balances the surface stress over the depth D of the domain:

$$-\frac{1}{\rho_0}\frac{\partial p}{\partial x} = \frac{u_*^2}{D},$$

for $u_* = 0.5\,\mathrm{m\,s^{-1}}$ and $D = 1500\,\mathrm{m}$ a source of $1.7 \times 10^{-4}\,\mathrm{m\,s^{-2}}$, a gradient of $1.2 \times 1.7 \times 10^{-4} = 2.0 \times 10^{-4}\,\mathrm{Pa\,m^{-1}}$, or $0.2\,\mathrm{Pa}$ per kilometer. The stress then decreases linearly from $\rho_0 u_*^2$ at the ground to zero at the top, the profile is logarithmic only near the ground, and the inconsistency with a frictionless top of Section 29.4.3 disappears.

With rotation, the physically consistent forcing is geostrophic. The pressure gradient is specified through the geostrophic wind $\mathbf{V}_g$ that balances it, $-(1/\rho_0)\nabla_h p = f\mathbf{k} \times \mathbf{V}_g$ (Chapter 3), and together with the Coriolis force on the horizontal wind $\mathbf{V}$ the horizontal forcing is

$$-\frac{1}{\rho_0}\nabla_h p - f\mathbf{k} \times \mathbf{V} = -f\mathbf{k} \times (\mathbf{V} - \mathbf{V}_g), \tag{29.19}$$

which vanishes where the wind is geostrophic and turns the slowed near-ground wind toward low pressure, to the left of $\mathbf{V}_g$ in the Northern Hemisphere ($f > 0$) and to the right in the Southern ($f < 0$), producing the turning with height of the previous subsection. A geostrophic wind of $10\,\mathrm{m\,s^{-1}}$ at 45°N corresponds to a pressure gradient of $\rho_0 f U_g = 1.2 \times 1.03 \times 10^{-4} \times 10 = 1.2 \times 10^{-3}\,\mathrm{Pa\,m^{-1}}$, six times the gradient of the non-rotating channel above: in the atmosphere most of the pressure gradient is balanced by the Coriolis force, and only a small part by friction. For realistic atmospheric CFD, specifying a geostrophic pressure-gradient forcing can be more physically consistent than prescribing only an inlet speed.

29.6 From simulation to site prediction

A single CFD solution describes one flow regime; a site prediction needs every regime the site experiences. This section describes the coupling to weather models, the libraries that make CFD usable in operation, the conditions under which a speed-up factor scales with the wind, validation and uncertainty, a worked ridge in two regimes, and the choice among RANS, LES and no CFD at all.

29.6.1 Coupling to weather models

A weather model can supply what CFD cannot generate: the wind profile, the temperature profile, the depth of the boundary layer, the stability, and the geostrophic forcing. CFD can then resolve what the weather model cannot: the terrain speed-up, the local sheltering behind forests and ridges, and the building wakes. The typical chain is

$$\text{NWP} \;\rightarrow\; \text{CFD} \;\rightarrow\; \text{site wind},$$

the mesoscale-to-microscale coupling of Chapter 20. The coupling is usually one way: the weather model drives the CFD and does not feel its result. It can be offline, the CFD run for idealized conditions taken from the weather model's climatology, or online, the CFD inflow updated from each forecast.

Two consistency problems arise at the interface. The weather model's grid cell already contains a smoothed version of the terrain (Chapter 20), so its wind already includes part of the terrain's effect; a speed-up computed relative to an undisturbed inflow and applied to that wind counts the resolved part twice. A speed-up for coupling is better computed relative to the wind the weather model represents, for instance the CFD wind averaged over the weather model's grid cell at the same height. And the two models represent turbulence in different ways, with a boundary-layer scheme of a kilometer-scale column in one and a three-dimensional closure in the other, so the profiles handed over are not automatically a steady state of the CFD model, which is the preservation problem of Section 29.4.3 again.

29.6.2 Lookup and speed-up libraries

One CFD run is not a forecast system. A simulation of $10\,\mathrm{m\,s^{-1}}$ from the west under neutral conditions gives one flow regime. Operational forecasting must cover every combination of speed, direction and stability the site experiences, and a full simulation for each forecast hour is rarely affordable. The options are many simulations computed in advance, or a reduced-order representation of them. The practical approach precomputes a *lookup library*: cases for the wind direction $\beta = 0°, 30°, \ldots, 330°$, twelve sectors, each with several stability classes, for example five, sixty runs in all; three speed classes for the stable cases, where the Froude number matters, raise the number further. In operation the procedure is: first, obtain the weather model's condition at the site, its direction, speed at a reference height and stability class; second, select the nearest library cases or interpolate between them; third, produce the local correction.

The library rarely stores full fields. It stores a *speed-up factor*, the ratio of the local wind to a reference wind,

$$S(x, y, \beta, \text{stability}) = \frac{U_{\text{local}}}{U_{\text{ref}}}, \qquad U_{\text{local}} = S\, U_{\text{NWP}}, \tag{29.20}$$

at each point and height of interest, together with the local change of direction, since channeling turns the wind as well as accelerating it. This is computationally efficient: one multiplication per forecast value. It assumes some degree of linear scaling with the background speed, the subject of the next subsection.

Figure 29.7 shows a library for one point, the crest of an illustrative north–south ridge, at 50 m above ground. The horizontal axis is the inflow direction in degrees, the vertical axis the speed-up factor; the blue curve is the neutral class and the red curve a stable class, each through its twelve stored sectors. Both are largest for winds across the ridge, from the west and the east, and close to one for winds along it; the stable class is lower in every sector, because blocking sends less air over the crest. Suppose the weather model gives $U_{\text{NWP}} = 9\,\mathrm{m\,s^{-1}}$ at 50 m from $\beta = 280°$. Between the stored sectors 270°, $S = 1.30$, and 300°, $S = 1.18$, linear interpolation with weight $(280 - 270)/30 = 1/3$ gives

$$S = 1.30 + \tfrac{1}{3}(1.18 - 1.30) = 1.26, \qquad U_{\text{local}} = 1.26 \times 9\,\mathrm{m\,s^{-1}} = 11.3\,\mathrm{m\,s^{-1}}$$

in the neutral class, and with $S = 1.10 + \tfrac{1}{3}(1.04 - 1.10) = 1.08$, $9.7\,\mathrm{m\,s^{-1}}$ in the stable class: a difference of $1.6\,\mathrm{m\,s^{-1}}$ from the stability class alone. Interpolation between 330° and 0° must wrap around north.

29.6.3 Linear scaling with wind speed

A speed-up factor is useful when the local wind is proportional to the background wind, $U_{\text{local}} \propto U_{\text{background}}$, and for neutral flow this holds for a reason that can be shown. Measure

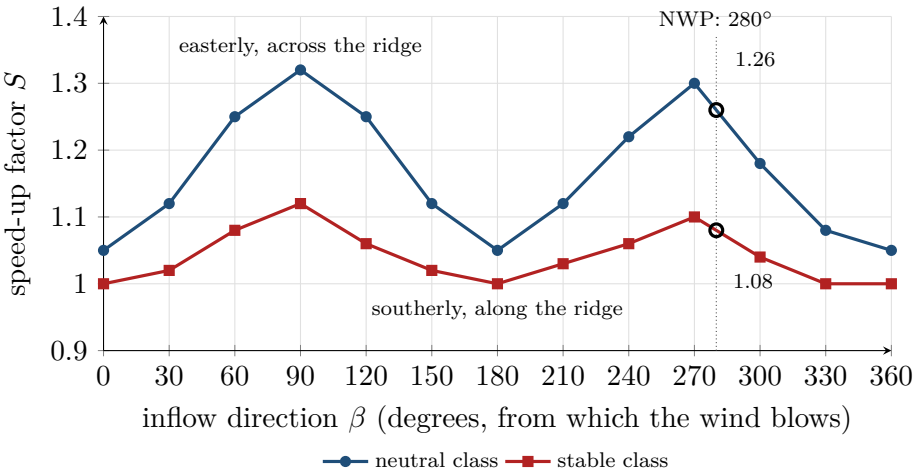


Figure 29.7: Speed-up library at the crest of a north–south ridge, 50 m above ground, for twelve inflow sectors and two stability classes (illustrative values). The open circles are the values interpolated for an inflow from 280°.

lengths in a terrain scale L, velocities in U_{ref}, pressure in $\rho_0 U_{\text{ref}}^2$ and time in L/U_{ref}. The neutral RANS equations then contain only one parameter with U_{ref} in it, the molecular term $1/\text{Re}$, which is negligible over a fully rough surface; the modeled turbulence scales the same way, $e \propto U_{\text{ref}}^2$, $\varepsilon \propto U_{\text{ref}}^3/L$ and $\nu_t \propto U_{\text{ref}} L$; and the wall function depends on z_0/L, not on the speed. The scaled solution is therefore the same for every U_{ref}, and so is S: one neutral run serves all speeds for its direction.

The argument fails as soon as a second parameter contains the speed. Buoyancy adds the Froude number $U/(Nh_m)$ and rotation the Rossby number $U/(|f|L)$; with them, the scaled solution changes with U_{ref} and the flow response becomes nonlinear in the background speed. Over the hill of Section 29.5.3 with $N = 0.02\,\text{s}^{-1}$, a wind of $4\,\text{m s}^{-1}$ has $\text{Fr} = 1$ and a wind of $12\,\text{m s}^{-1}$ has $\text{Fr} = 3$: the same direction and stability class give two different regimes, and a fixed factor fits at most one. Separation adds sensitivity of another kind. In neutral, fully rough flow even a separated solution scales with the speed by the argument above, but the recirculation is sensitive to small changes of direction and, in real air, to the stability that usually accompanies weak winds, so its factors carry larger errors. Blocking is the Froude-number effect itself. Fixed speed-up factors therefore have limits: they are most reliable for neutral, attached, strong-wind flow, which is also the regime of most interest for wind energy and for the cooling of lines at high load in windy weather, and least reliable in light winds at night.

29.6.4 Validation and uncertainty

A CFD result should be compared against measurements: meteorological masts, lidar profiles and scans (Chapter 22), wind-tunnel measurements on a scale model of the terrain, and field campaigns that instrument a hill or a valley with many masts at once. Speed-up factors are often compared rather than speeds, since a ratio between two measured points removes much of the inflow uncertainty. Without validation, a detailed flow visualization can look convincing while being quantitatively wrong, and this is one of the main dangers of CFD. A CFD animation can show detailed vortices; that does not show the solution is correct. The questions to be answered before a result is used are five: is it mesh independent; is the turbulence model appropriate for the flow, attached or separated, neutral or stratified; are the boundary conditions realistic, including the inflow profile and its preservation; is the roughness correct, in the units the code expects; and has the model been validated at this site or a similar one? A detailed flow field is not validated physics.

The uncertainty of a CFD prediction has five sources: the inflow, the roughness, the terrain data, the turbulence model and the numerics. Table 29.2 lists them for an illustrative crest wind, with an example of each, an illustrative size in percent and a means of reducing it. The roughness entry follows from the log profile: with the wind at 100 m fixed, doubling z_0 from 0.05 to 0.1 m changes the ratio $U(10\,\mathrm{m})/U(100\,\mathrm{m})$ from $\ln 200/\ln 2000 = 0.697$ to $\ln 100/\ln 1000 = 0.667$, by about 4.5 %. If the five are independent they add in quadrature, $\sqrt{10^2 + 4.5^2 + 2^2 + 5^2 + 0.3^2} \approx 12\,\%$, so a predicted crest wind of $13\,\mathrm{m\,s^{-1}}$ carries about $\pm 1.6\,\mathrm{m\,s^{-1}}$. The numerical part, the one that mesh convergence measures, is the smallest; the inflow and the turbulence model dominate. This is often overlooked: CFD is not deterministic truth because its equations are deterministic.

Table 29.2: Sources of uncertainty in a CFD crest wind (illustrative sizes, one standard deviation, in percent of the predicted wind).

Source	Example	Size	Reduced by
Inflow	weather-model wind wrong by $1\,\mathrm{m\,s^{-1}}$ in $10\,\mathrm{m\,s^{-1}}$; wrong stability class	10	better forcing, site measurements, ensembles of inflows
Roughness	z_0 uncertain by a factor of two; k_s and z_0 confused	4.5	land-cover survey, measured profiles, unit checks
Terrain	elevation-data error and smoothing of steep slopes	2	finer elevation data, mesh following the data
Turbulence model	closures differ on attached flow; far more in separated lee flow	5	comparison of closures, LES for key cases
Numerics	finite mesh and iteration error	0.3	mesh convergence, tighter convergence criteria

29.6.5 A ridge in two regimes

Suppose a weather model gives $U = 10\,\mathrm{m\,s^{-1}}$ at 100 m from the west over a north–south ridge with a valley on its upwind side. A neutral CFD simulation predicts, at the same height above local ground, $6\,\mathrm{m\,s^{-1}}$ in the valley, $9\,\mathrm{m\,s^{-1}}$ on the windward slope, $13\,\mathrm{m\,s^{-1}}$ at the crest and $3\,\mathrm{m\,s^{-1}}$ in the lee recirculation, where the near-ground mean flow may be reversed. That is exactly the local spatial structure a weather model does not resolve. Now change the regime from neutral to strongly stable, with the same $10\,\mathrm{m\,s^{-1}}$ aloft. The result changes in four ways: more blocking, so less air crosses the crest; stronger channeling, so the valley wind turns to blow along the valley axis; slower flow on the windward slope, where the blocked air stagnates; and a different lee structure, either a stagnant pool of cold air or, when the Froude number is near one, a downslope wind faster than anything upstream (Chapter 20).

Table 29.3 sets the two regimes side by side. Its columns give the location, the neutral wind and its speed-up factor, the stable wind and its factor, and the mechanism of the change; the stable values are illustrative. The factor at the crest falls from 1.3 to 1.0, and in the lee it can end anywhere between 0.1 and 1.2. The local wind is therefore a function of the regime,

$$\mathbf{u}_{\mathrm{local}} = F\left(\mathbf{u}_{\mathrm{NWP}},\ \text{stability},\ \text{terrain},\ \text{roughness}\right), \tag{29.21}$$

and not a terrain multiplier.

29.6.6 Choosing RANS, LES or no CFD

Table 29.4 summarizes the practical differences between the two methods. Its rows are cost, what is computed, the cases each suits, what each depends on most, its fitness for parameter sweeps and its typical product. RANS is chosen when the main goal is a mean terrain correction,

Table 29.3: Wind at four locations across a ridge for $10\,\mathrm{m\,s^{-1}}$ from the west at 100 m, in neutral and strongly stable conditions (illustrative).

Location	Neutral (m/s)	S	Stable (m/s)	S	Mechanism of the change
Valley	6	0.6	4, along the valley	0.4	channeling turns and slows the flow
Windward slope	9	0.9	5	0.5	blocked air decelerates and turns
Crest	13	1.3	10	1.0	less air crosses the crest
Lee	3, possibly reversed	0.3	1 (cold pool) or 12 (downslope wind)	0.1 to 1.2	depends on the Froude number

steady flow around buildings, many wind directions or computational efficiency, and above all when the mean field matters more than the instantaneous turbulence. LES is chosen when wake dynamics, intermittent turbulence, coherent eddies, transient gusts or convective boundary layers matter, and when the computational resources and the validation data justify it.

Table 29.4: RANS and LES in practice.

	RANS	LES
Cost	cheap: about 10^9 to 10^{10} cell updates per case	expensive: about 10^{11} to 10^{13} cell updates per case
Computes	the mean flow	time-varying eddies
Suits	many steady cases	turbulence structure
Depends most on	the closure	the resolution and the subgrid model
Parameter sweeps	easy: libraries of tens of cases	harder to run operationally
Typical product	speed-up maps	gusts, coherent structures, wake loads

CFD may also be unnecessary. If the terrain is flat and homogeneous and the site is well represented by the weather model's grid cell, CFD adds little, because there is no local modification to resolve. If the main uncertainty is the synoptic forecast itself, microscale CFD will not reduce it: with an illustrative forecast error of $2\,\mathrm{m\,s^{-1}}$ at 100 m and a local terrain effect of $0.3\,\mathrm{m\,s^{-1}}$ that CFD could remove, the combined error falls only from $\sqrt{2^2 + 0.3^2} = 2.02\,\mathrm{m\,s^{-1}}$ to $2\,\mathrm{m\,s^{-1}}$, one percent. CFD should solve a real, unresolved local-flow problem.

Figure 29.8 places the method in the scale hierarchy of near-surface wind modeling,

$$\text{global forecast} \;\rightarrow\; \text{regional NWP} \;\rightarrow\; \text{microscale CFD} \;\rightarrow\; \text{sensor or asset}.$$

Its horizontal axis is length on a logarithmic scale, from 0.1 m to 100 000 km. Each bar spans one level, from its grid spacing (or, for the sensor, the instrument's size) on the left to its domain on the right, and the text above each bar states what that level supplies. The diamonds on the bottom row mark three feature sizes. A building of 30 m and a ridge of 500 m fall inside the CFD bar and below the grid spacing of both weather models; a coastline circulation of 50 km falls inside the regional model. Each level answers a different part of the problem: the global model the large-scale state, the regional model the mesoscale flow and the stability, CFD the local geometry, and the sensor or asset model the relation between the modeled flow and the place where the wind is measured or used. Chapter 30 assembles these levels, from synoptic forcing to validation, into a procedure for building a defensible site wind model and deciding how much of this complexity a site justifies.

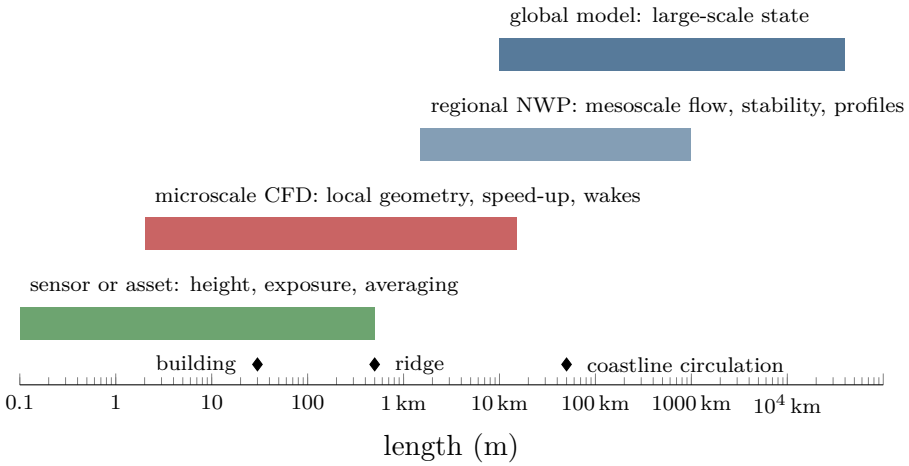


Figure 29.8: The scale hierarchy of near-surface wind modeling (illustrative). Each bar runs from a level's grid spacing, or the instrument's size, to its domain: global model about 10 km to the circumference of the Earth; regional NWP 1.5 km to 1000 km; microscale CFD 2 m to 15 km; sensor or asset 0.1 m to a line span of 500 m. Diamonds mark a 30 m building, a 500 m ridge and a 50 km coastline circulation.

29.7 What to retain

Definition 29.1 (CFD for site wind)**.** CFD adds the local spatial physics a weather model cannot resolve: the weather model supplies the atmospheric forcing, CFD the local geometry, and together they give a site-scale wind field. CFD is only as good as its inflow, roughness, mesh, turbulence model and validation, and it is a physical model with uncertainty, not ground truth.

Table 29.5 lists the terms of the chapter, their meaning, their units and the subsection that defines each.

29.8 Exercises

Exercise 29.1. A wind study covers a domain 5 km long, 3 km wide and 1 km deep. The largest eddies have a size of 500 m and a velocity of $1\,\mathrm{m\,s^{-1}}$; take $\nu = 1.5 \times 10^{-5}\,\mathrm{m^2\,s^{-1}}$. (a) Compute the Reynolds number of the large eddies, the ratio of the largest to the smallest eddy size and the Kolmogorov length. (b) Compute the number of cells a DNS of the domain would need at a spacing equal to the Kolmogorov length. (c) An LES uses a uniform spacing of 8 m. Compute its cell count, its time step for a maximum speed of $12\,\mathrm{m\,s^{-1}}$ and a crossing of at most half a cell per step, and the number of steps for two flow-through times at $8\,\mathrm{m\,s^{-1}}$ plus one hour of statistics. (d) By what factor does the cost grow if the spacing is halved, and what share of the turbulent kinetic energy of an inertial-subrange spectrum moves from the subgrid model to the resolved field when it is?

Exercise 29.2. A neutral inlet has $u_* = 0.45\,\mathrm{m\,s^{-1}}$ over $z_0 = 0.1$ m; use $\kappa = 0.4$ and $C_\mu = 0.09$. (a) From the equilibrium inlet (29.15), compute U, e, ε and ν_t at 10 and 80 m, and check that $\nu_t = \kappa u_* (z + z_0)$. (b) The code specifies roughness as an equivalent sand-grain roughness and requires the first cell center above it. Compute k_s and the minimum height of the first cell. (c) With $C_\mu = 0.033$ instead, compute e and compare it with $5.5\,u_*^2$. (d) A user enters 0.1 m in the sand-grain field. What effective z_0 does the wall then have, and in which direction does the near-ground wind drift across an empty domain?

Table 29.5: The terms of the chapter and where each is defined.

Term	Meaning	Units	Defined in
CFD	computational fluid dynamics: numerical solution of the Navier–Stokes equations around a geometry	–	29.1
DNS	direct numerical simulation: every eddy resolved; needs about $\mathrm{Re}^{9/4}$ points	–	29.1.3
RANS	Reynolds-averaged Navier–Stokes: mean flow solved, all turbulence modeled	–	29.2.1
LES	large-eddy simulation: eddies larger than the filter resolved, smaller ones modeled	–	29.3.1
Eddy viscosity	ν_t, effective turbulent momentum diffusivity in $-\overline{u_i' u_j'} = \nu_t(\dots) - \frac{2}{3} e \delta_{ij}$	m^2/s	29.2.2
k–ε model	RANS model transporting e and ε; $\nu_t = C_\mu e^2/\varepsilon$, $C_\mu = 0.09$	–	29.2.3
k–ω model	RANS model transporting e and the specific dissipation rate $\omega = \varepsilon/(C_\mu e)$	ω: $1/\mathrm{s}$	29.2.4
SST	shear-stress transport: blend of k–ω near walls and k–ε away, with a stress limiter; useful for separation	–	29.2.4
SGS model	subgrid-scale model of LES, e.g. $\nu_{\mathrm{sgs}} = (C_{\mathrm{smag}} \Delta_f)^2 \lvert\widetilde{S}\rvert$	m^2/s	29.3.3
Inlet profile	prescribed atmospheric state entering the domain: $U(z)$, $e(z)$, $\varepsilon(z)$	$\mathrm{m/s}$, $\mathrm{m}^2/\mathrm{s}^2$, $\mathrm{m}^2/\mathrm{s}^3$	29.4.2
Inlet-profile preservation	inlet profiles unchanged across an empty, flat domain	–	29.4.3
Wall function	near-wall parameterization imposing the log law between the first cell and the surface stress	–	29.4.4
Equivalent sand-grain roughness	$k_s \approx 30\, z_0$; not interchangeable with z_0	m	29.4.4
Mesh convergence	stability of the solution under grid refinement; Richardson extrapolation	–	29.4.6
Boussinesq approximation	density variations retained only in the buoyancy term, $g(\theta - \theta_0)/\theta_0$	m/s^2	29.5.2
Lookup library	precomputed cases by direction, stability (and speed), interpolated in operation	–	29.6.2
Speed-up factor	$S = U_{\mathrm{local}}/U_{\mathrm{ref}}$; fixed only for neutral, strong-wind flow	–	29.6.2, 29.6.3

Exercise 29.3. The crest wind of a ridge is computed on meshes of 30, 15 and 7.5 m: 12.2, 13.4 and 13.7 m s^{-1}. (a) Compute the observed order of convergence, the extrapolated crest wind and the error band $1.25\,|U_{\mathrm{f}} - U_{\mathrm{m}}|/(U_{\mathrm{f}}(r^{n} - 1))$. (b) At a point in the lee the same meshes give -0.5, 1.2 and 0.4 m s^{-1}. Can this sequence be extrapolated? What does it say about the mesh for the lee? (c) Which of the two quantities would a line-rating study at the lee span depend on, and what should be done before using it?

Exercise 29.4. A transmission line runs north–south across the crest of the ridge of Figure 29.7, at 28°S. In neutral conditions the weather model gives, upstream of the ridge, 12 m s^{-1} from 255° at 100 m and 7.5 m s^{-1} from 268° at the conductor height of 15 m. Assume the library of the figure applies at 15 m, and that at 100 m it stores $S(240^{\circ}) = 1.10$ and $S(270^{\circ}) = 1.14$. (a) Does the wind back or veer with height, and is that what the Southern Hemisphere leads one to expect? (b) Compute the local wind at the conductor and at a 100 m turbine hub on the crest. (c) Compute the component of the conductor wind perpendicular to the line; then repeat (b) and (c) for the conductor if the 100 m direction had been used for the lookup, and state the error. (d) Compute the Coriolis parameter and the Rossby number of a 4 km domain at 12 m s^{-1}, and say whether the Coriolis force is needed inside the domain and whether the inflow's turning is.

Chapter 30

Building a Defensible Site Wind Model

30.1 The site wind problem and its target

The preceding chapters followed the wind from the pressure field that drives it, through the boundary layer that couples it to the ground, to the terrain, roughness and obstacles that reshape it locally, and then to the instruments that measure it and the models that predict it. This last chapter assembles those pieces into a procedure. Its question is

how is a local wind model built that is physically credible, useful, and honest about its uncertainty?

The answer is not to pick the highest-resolution model available. A model of fine resolution can be wrong for the target, wrong in the regime that matters, or right for the wrong reason, and its detail does not reveal which. A defensible site wind model is instead a chain of steps, each of which can be examined and tested on its own. The chapter first fixes the target of the model in quantity, space and time; it then builds the physical hierarchy from the large-scale forcing down through the boundary-layer regime to the site and its observations; it establishes a baseline and climbs a ladder of complexity only as far as the evidence requires; it validates the result by regime, direction and height and diagnoses the errors physically; and it closes with the statement of uncertainty, the validation against the engineering decision, the report of the model and a synthesis of the book.

Jargon: site wind model, target variable, baseline model, regime validation, decision metric

A *site wind model* is any procedure that produces the wind, in meters per second (and its direction, in degrees), at a particular place and height from larger-scale information such as a weather-model forecast, local observations and a description of the terrain. The *target variable* is the exact wind quantity the model is intended to predict: a stated speed or velocity component, at a stated location and height above ground, over a stated averaging period, in stated units. A *baseline model* is a simple reference model, fitted and tested before anything more complex, against which every added complexity is measured. *Regime validation* is the evaluation of a model's performance separately in each physical state of the atmosphere, such as convective, near-neutral and stable conditions, rather than only over the whole record. A *decision metric* is the quantity that directly affects the engineering decision the model serves, such as the probability that the wind across a conductor falls below a cooling threshold; it may differ from the wind speed itself.

Key idea

A defensible site wind model is not a high-resolution wind prediction. It is the correct physical hierarchy at the appropriate scale, fed by good observations, validated independently by regime, and stated with an explicit uncertainty. The question to ask of such a model is not only whether it is accurate, but why it is accurate.

30.1.1 A chain of models and its weakest link

A site wind prediction passes through a sequence of physical stages, each with its own model:

large-scale forcing → boundary-layer state → surface and terrain modification → site wind → validation → uncertainty.

Figure 30.1 draws the chain vertically. The four upper boxes are the physical stages, from the pressure field at the top to the wind at the stated target; the two lower boxes are the steps that judge the prediction and state its reliability. The notes on the right give, for each stage, the quantities that describe it, the chapters that treat it, and the kind of uncertainty that enters there.

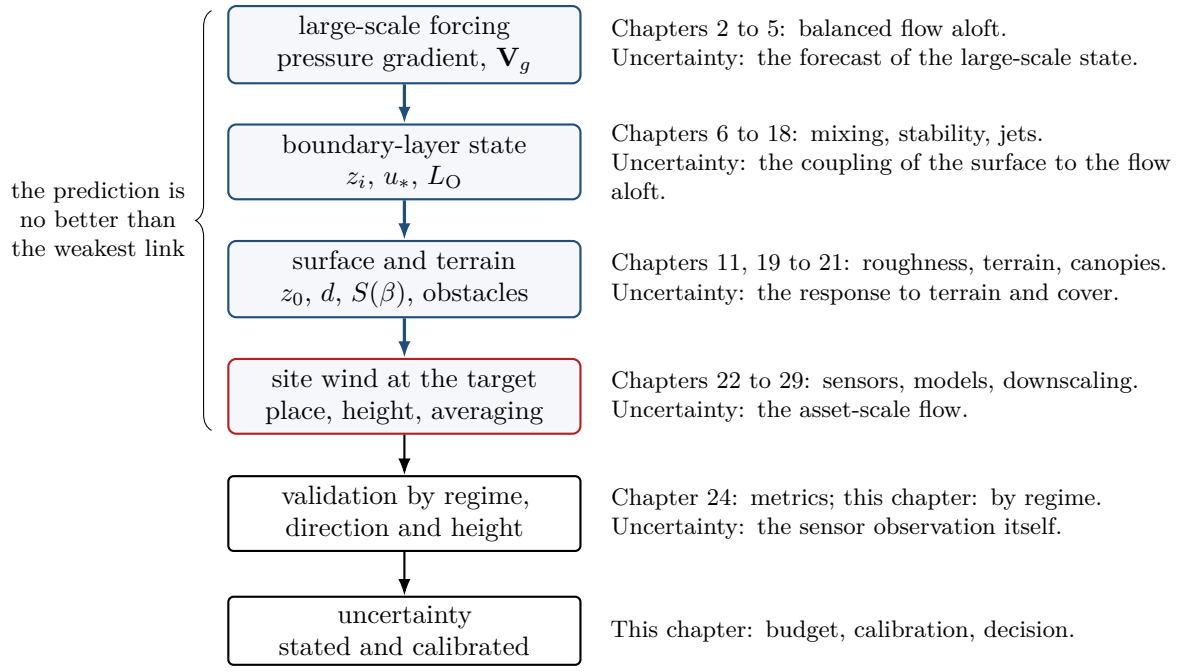


Figure 30.1: The chain of a site wind model (schematic). The four upper stages are physical; the two lower ones judge the prediction. The notes give the chapters that treat each stage and the uncertainty that enters there.

The quality of the final prediction is limited by the weakest link of the chain. A perfect terrain model downstream of a wrong forecast of the pressure field reproduces the wrong wind faithfully; a perfect forecast interpreted with the wrong stability gives the wrong surface wind; and a correct site wind validated against a sheltered sensor looks wrong. Each link therefore needs its own evidence, and the improvement of one link helps only if it is the weakest. The rest of the chapter takes the links in order, and the uncertainty notes on the right of the figure return in Section 30.6 as the terms of an uncertainty budget.

30.1.2 The quantity before the model

Before a model is chosen, the target is defined. "The wind at the site" names at least seven different problems:

- the 10 m wind over open terrain, the standard reference exposure of Chapter 23;
- the wind at a conductor, at its height and along its span;
- the wind at the hub height of a turbine, perhaps 80 to 150 m;
- the 3-second gust, which loads structures;
- the hourly mean, used in energy and market applications;
- the probability that the wind falls below $2\,\mathrm{m\,s^{-1}}$, which limits the cooling of a line;
- the maximum credible wind, which sets a design load.

Table 30.1 sets them side by side. Its columns give the target, its spatial support (the place or area it describes), its averaging period, the application that needs it and the statistic that the application uses.

Table 30.1: Seven targets that are all called "the wind at the site".

Target	Spatial support	Averaging	Application	Statistic used
10 m open-terrain wind	a point at standard exposure	10 min	comparison of stations and models	mean, bias
Conductor wind	a span, 100 to 500 m, at 15 to 40 m	10 min	line rating	low quantiles, $\Pr(U_\perp < U_{\mathrm{th}})$
Hub-height wind	a rotor disk at 80 to 150 m	10 min to 1 h	energy yield	$\overline{U^3}$, distribution
3-second gust	a point or a member	3 s	structural loading	maxima, return levels
Hourly mean	a point or a cell	1 h	energy and market forecasts	mean, RMSE
$\Pr(U < 2\,\mathrm{m\,s^{-1}})$	a point or a span	10 min	cooling limit of a line	probability, reliability
Maximum credible wind	a point	gust or 10 min	design load	extreme-value quantile

These are very different problems. A model that predicts the hourly mean well may say nothing about the 3-second gust, whose ratio to the mean, the gust factor G of Chapter 24, depends on the turbulence; a model that predicts the mean speed well may be poor at the low quantiles that limit a conductor, because a model tuned to minimize the root-mean-square error produces a wind that is too smooth (Chapter 24); and a model of the 10 m wind over open terrain is not a model of the wind on a ridge-top span. The first rule of the chapter is therefore the following.

> **Principle 30.1.** *Define the quantity before defining the model: the target variable, its location, its height above ground, its averaging period and the statistic the application uses.*

30.1.3 The spatial target

The target also has a spatial support. It may be a point or an area average, and the two are different quantities. A sensor represents a few meters of local flow, or, through its footprint, a distance upwind of a few hundred meters to a few kilometers that depends on height and stability (Chapter 23). A weather-model grid cell represents an area kilometers wide, over terrain smoothed to the model's effective resolution (Chapters 25 and 27). A transmission span

may require an effective wind along 100 to 500 m of conductor: the conductor heats or cools as a whole, and a single gap in the wind at one point along it matters less than a lull over most of the span.

These are not interchangeable. The point wind varies more than the area average, because the averaging over space removes the small-scale variability, just as averaging over time removes the turbulence (Chapter 24). A model trained on a point sensor and used for a span transfers the point's variability to the span and overstates the probability of a lull along the whole conductor; a model of a grid cell used for a point understates the extremes at the point. The relation between the two, which Chapter 23 called the point value against the area average, is part of the target definition and returns as the representativeness term of the uncertainty budget in Section 30.6.2.

30.1.4 The temporal target

The averaging period is equally part of the target. The 3-second, the 1-minute, the 10-minute and the hourly means,

$$U_{3\,\mathrm{s}}, \qquad U_{1\,\mathrm{min}}, \qquad U_{10\,\mathrm{min}}, \qquad U_{1\,\mathrm{h}},$$

are different quantities: the shorter the period, the more of the turbulence the value contains, and the wider its distribution about the longer mean (Chapter 24). The relevant period is set by the time over which the engineering system responds. For the thermal rating of a conductor it is about 10 minutes, because the conductor's thermal inertia smooths shorter gusts; for structural loading short gusts may matter much more, because a structure feels the instantaneous pressure, which grows as the square of the wind.

The conductor's smoothing follows from its heat balance. The conductor temperature T_c changes as the heat stored in it, per meter of conductor, responds to the difference between the heating by the current and the sun and the cooling by convection and radiation. Linearized about a steady state, a small fluctuation T_c' obeys $\tau_c \, \mathrm{d}T_c'/\mathrm{d}t = -T_c' + A_c U'$, where U' is the wind fluctuation, A_c a sensitivity in kelvin per meter per second, and τ_c the thermal time constant: the heat capacity per meter divided by the rate at which the cooling changes with the conductor temperature, typically 5 to 20 minutes. For a wind fluctuation of period P the solution oscillates with an amplitude reduced by the gain

$$G(P) = \frac{1}{\sqrt{1 + (2\pi\tau_c/P)^2}}, \tag{30.1}$$

the response of a first-order low-pass filter. Figure 30.2 plots it. The horizontal axis is the period of the wind fluctuation on a logarithmic scale, from one second to about three hours; the vertical axis is the gain; the blue curve is a conductor with $\tau_c = 10$ minutes and the red curve an element that responds within $\tau_c = 1\,\mathrm{s}$, standing for a structure loaded by gusts. The dotted lines mark the four averaging periods.

For the conductor, a gust lasting a few seconds passes with a gain of 8×10^{-4}, a one-minute fluctuation with 0.016, a ten-minute fluctuation with 0.16 and an hourly one with 0.69: the conductor follows the hourly changes of the wind, sees a sixth of the ten-minute ones and ignores the gusts. For the fast element the 3-second gust still passes with a gain of 0.43 and everything slower passes almost entirely. The ten-minute mean is therefore a natural target for line rating, and the gust for structures. The nonlinearity of the cooling does not change this: with cooling proportional to $U^{0.6}$ (Chapter 8), a second-order expansion gives the mean cooling over a ten-minute period as $\overline{U}^{0.6}[1 + \tfrac{1}{2}(0.6)(0.6 - 1)\,\mathrm{TI}^2]$, which for a turbulence intensity of 0.2 is 0.995 of the cooling of the mean wind, a difference of half a percent. The physics of the model should match the time scale of the engineering problem.

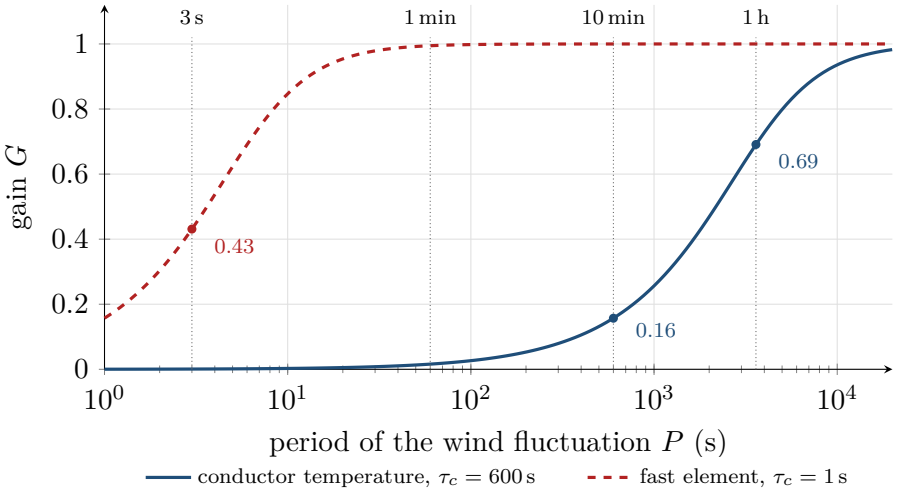


Figure 30.2: Gain of a first-order thermal response to a sinusoidal wind fluctuation, $G = [1 + (2\pi\tau_c/P)^2]^{-1/2}$, for a conductor with $\tau_c = 600\,\mathrm{s}$ and for a fast element with $\tau_c = 1\,\mathrm{s}$ (illustrative time constants).

30.2 The physical hierarchy and the atmospheric regime

With the target fixed, the model is built from the large scale down; the first two steps of the analysis are the large-scale forcing and the boundary-layer regime. This section decomposes the site wind into the physics of its scales, examines the large-scale forcing, diagnoses the boundary-layer regime with the stability measures of the earlier chapters, and shows why the regime decides how the wind aloft reaches the target.

30.2.1 Decomposition by scale

A useful conceptual decomposition writes the site wind vector as a function of the large-scale wind and of the layers and surfaces that modify it:

$$\mathbf{V}_{\text{site}} = F(\mathbf{V}_{\text{synoptic}},\ \text{boundary layer},\ \text{terrain},\ \text{roughness},\ \text{obstacles}). \tag{30.2}$$

Each argument has its own physics. The *synoptic forcing* is the pressure gradient and the free-atmospheric wind it balances (Chapters 3 and 4). The *boundary layer* sets the stability and the vertical transport of momentum (Chapters 6 to 18). The *terrain* produces speed-up, blocking, channeling and separation (Chapter 20). The *roughness* sets the surface drag and modifies the wind profile (Chapters 11 and 12). The *obstacles*, trees, buildings and infrastructure, add wakes and sheltering (Chapters 21 and 23).

The decomposition prevents one model from being asked to do everything. A weather model is good at the first two arguments and poor at the last three; a terrain model is good at the third and needs the first two as input; a statistical correction can learn the last two at a measured site but cannot create the first. Writing the site wind as equation (30.2) assigns each argument to the model that resolves it and makes visible which argument a given method leaves to another. As Chapters 25 and 23 noted for their own decompositions, the dependence is closer to a product than a sum: roughly, the site wind is the wind aloft times a factor for the boundary layer, one for the terrain, one for the roughness and one for the obstacles, so that relative errors of the factors add.

30.2.2 The large-scale forcing

The first step looks above the local surface influence. Useful variables are the wind at about 500 m above ground, $U_{500\,\mathrm{m}}$, which lies above most of the surface layer by day and above the nocturnal inversion on many nights; the wind at the 850 hPa level, U_{850}, about 1.5 km above sea level, which is near the top of or above the boundary layer over low terrain; the geostrophic wind $\mathbf{V}_g$; and the horizontal pressure gradient $\nabla_h p$. Four questions organize them. Is the synoptic wind strong or weak? From which direction does it blow? Is a front passing? Is the pressure forcing steady?

Each answer has consequences for the site. A strong synoptic wind, say a geostrophic wind above about $10\,\mathrm{m\,s^{-1}}$, keeps the boundary layer mechanically mixed day and night, so the regime is near neutral and the site wind follows the wind aloft; a weak one lets the diurnal cycle, thermal circulations and drainage control the site (Chapters 19 and 17). The direction decides which terrain and which exposure sector lie upwind. A passing front changes the direction abruptly, and the sense of the change depends on the hemisphere: behind a cold front the wind veers, turning clockwise, in the Northern Hemisphere (from southwest to northwest) and backs, turning counterclockwise, in the Southern Hemisphere (from northwest to southwest), because the pressure trough that the front marks is crossed in mirror-image geometry. Steady forcing allows the boundary layer to approach equilibrium; rapidly changing forcing leaves it lagging, and inertial oscillations follow (Chapter 18).

The geostrophic relation of Chapter 3 turns the pressure gradient into a wind with the sign of f. At 30°S, $f = 2 \times 7.292 \times 10^{-5} \times \sin(-30^\circ) = -7.29 \times 10^{-5}\,\mathrm{s^{-1}}$; a gradient of 1 hPa per 100 km, 10^{-3} Pa per meter, with $\rho = 1.2\,\mathrm{kg\,m^{-3}}$ balances a geostrophic wind of $10^{-3}/(1.2 \times 7.29 \times 10^{-5}) = 11.4\,\mathrm{m\,s^{-1}}$. If the pressure falls toward the south, the wind is a westerly in the Southern Hemisphere and an easterly at 30°N. If the large-scale forcing is wrong, local corrections cannot rescue the forecast: a terrain factor multiplies whatever wind arrives, and a statistical correction fitted to the usual forcing has nothing to say about a pressure pattern the model misplaced.

30.2.3 Diagnosing the boundary-layer regime

The second step asks what kind of boundary layer the site is in: convective, near neutral, weakly stable or strongly stable. The answer says how strongly the surface wind is coupled to the winds aloft. Five diagnostics, each from an earlier chapter, carry the answer. The boundary-layer depth z_i (Chapters 6 and 16) gives the thickness over which momentum is mixed: 1 to 2 km on a convective afternoon, tens to a few hundred meters at night. The Obukhov length L_O and the stability parameter z/L_O (Chapters 14 and 15) measure the importance of buoyancy at the target height z (the literature writes the parameter as ζ; this book keeps ζ for the relative vorticity). The Richardson numbers, the gradient number Ri_g and the bulk number Ri_B (Chapter 13), compare buoyancy with shear across a layer and are available above the surface layer, where z/L_O is not defined. The friction velocity u_* (Chapter 10) measures the surface stress and thus the vigor of mechanical mixing.

A useful classification of each period, in terms of the stability parameter at the target height, is the following. *Convective day*: $z/L_\mathrm{O} < 0$, in practice below about -0.1, with strong mixing by buoyant plumes. *Near neutral*: $|z/L_\mathrm{O}| \ll 1$, in practice $|z/L_\mathrm{O}|$ below about 0.1, with mechanical mixing by shear, typical of windy or overcast conditions. *Stable night*: $z/L_\mathrm{O} > 0$, in practice between about 0.1 and 1, with continuous but weakened turbulence, the weakly stable regime of Chapter 17. *Very stable or decoupled*: large z/L_O, above about 1, or Ri_g above the critical value of about 0.25, with weak and intermittent turbulence and the surface nearly decoupled from the flow above. The thresholds need not be perfect, and each site may move them; their purpose is to separate physically different regimes, in which the same model wind means different site winds. The classification uses the model's or the site's own stability

estimate, which carries its own error, so periods near a boundary are treated as uncertain rather than forced into one class.

30.2.4 Regime and the coupling to the wind aloft

Suppose a weather model predicts $U_{200} = 12\,\mathrm{m\,s^{-1}}$ at 200 m. During a convective afternoon that momentum strongly influences the wind at 20 m, U_{20}: the plumes of Chapter 16 mix it down through the whole layer. During a strongly stable night it may not: the inversion isolates the surface layer, the wind at 200 m may even accelerate into a low-level jet (Chapter 18) while the wind at 20 m falls toward calm. The mapping $U_{200} \to U_{20}$ therefore depends critically on the regime.

Figure 30.3 shows that dependence as the distribution of the ratio U_{20}/U_{200} in each of the four classes, for an illustrative site over grass. Each box spans the middle half of the hours of its class, from the lower to the upper quartile; the line inside the box is the median, and the whiskers reach the 5th and 95th percentiles. The dashed line is the ratio a single regression fitted to all hours would use.

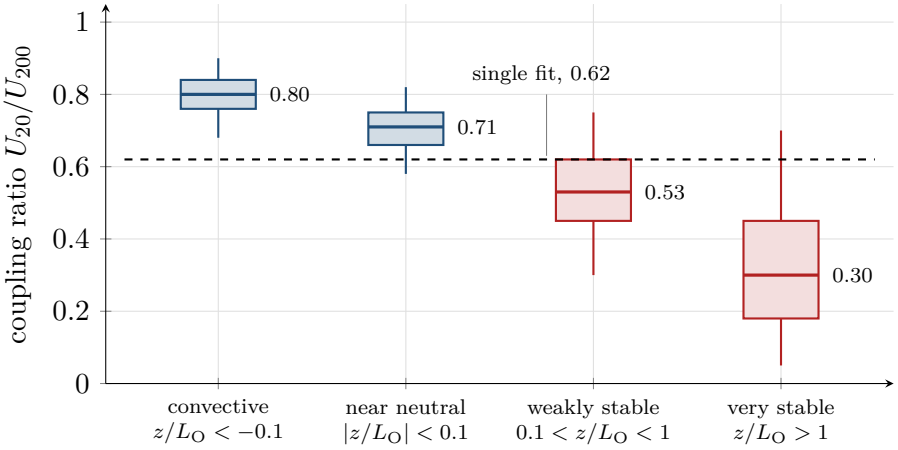


Figure 30.3: Distribution of the coupling ratio U_{20}/U_{200} by stability class at an illustrative site over grass. Boxes: lower to upper quartile; inner line: median; whiskers: 5th and 95th percentiles. Dashed: the ratio of a single regression over all hours (illustrative values).

Two features stand out. The median ratio falls from 0.80 in convective hours to 0.30 in very stable ones, so that $U_{200} = 12\,\mathrm{m\,s^{-1}}$ means $U_{20} \approx 9.6\,\mathrm{m\,s^{-1}}$ on a convective afternoon and $3.6\,\mathrm{m\,s^{-1}}$ on a very stable night. Expressed as the exponent of a power law between 20 and 200 m, $\alpha = -\ln(\text{ratio})/\ln 10$, the medians correspond to $\alpha = 0.10$, 0.15, 0.28 and 0.52, the range of profiles met in Chapters 8 and 12. And the spread grows with stability: the convective ratios lie within 0.68 to 0.90, the very stable ones anywhere from 0.05 to 0.70, because the decoupled surface wind depends on drainage, intermittent bursts and local sheltering that the wind at 200 m does not carry. A single regression with the ratio 0.62 blurs these behaviors together: it predicts $7.4\,\mathrm{m\,s^{-1}}$ for every hour, about $2\,\mathrm{m\,s^{-1}}$ too low by day and nearly $4\,\mathrm{m\,s^{-1}}$ too high on very stable nights, with a zero mean error. The regime is therefore not a refinement of the model; it selects the model.

30.3 Site characterization and observations

The third and fourth steps describe the physical location and examine the measurements that will train and test the model. This section gives the site an aerodynamic context, organizes

that context by wind direction, audits the observations and writes the measurement equation that separates the instrument from the place.

30.3.1 The aerodynamic context of a site

A site is described by more than its coordinates (x, y, z). It needs an aerodynamic context: the elevation, which sets its height relative to the surrounding terrain and to the cold pools that collect at night; the slope, the inclination of the ground, which governs speed-up and separation (Chapter 20); the aspect, the direction the slope faces, which governs its heating and the onset of slope winds (Chapter 19); the terrain curvature, convex on a crest and concave in a hollow, which separates exposed from sheltered positions; the surrounding roughness, and its displacement height where tall vegetation or buildings are present (Chapter 11); the forests and buildings themselves, as obstacles with a height and a distance (Chapters 21 and 23); and the upstream exposure by direction.

The elevation, slope, aspect and curvature come from an elevation model at a resolution finer than the features of interest, tens of meters for a ridge; the roughness and obstacles from land-cover maps, aerial images and a site visit. Each descriptor answers a physical question. A crest with a slope of 0.2 and a half-width of a few hundred meters produces a speed-up of tens of percent in neutral flow; a lee slope steeper than about 0.3 separates; a convex position cools less at night than a concave one. The same descriptors become predictors of a statistical model in Section 30.4.2.

30.3.2 Directional exposure

The most useful single description of a site divides the compass into sectors and records the exposure of each, as Chapter 23 did for a sensor. Table 30.2 gives an illustrative example for a site on a ridge. Its columns are the sector, the surface upwind of the site in that sector, the expected effect on the wind and the correction factor, the ratio of the site wind to the model wind, fitted below.

Table 30.2: Directional exposure of an illustrative ridge site and the correction factor $S_c(\beta) = U_{\text{site}}/U_{\text{NWP}}$ of the smooth fit in Figure 30.4.

Sector	Exposure	Expected effect	S_c
W (270°)	open ridge	speed-up across the crest	1.22
NW (315°)	forested slope	crest speed-up reduced by the forest's drag	1.07
N (0°)	valley axis	channeling along the valley; little speed-up	1.07
E (90°)	sheltered	lee of a higher hill; wake and, at night, cold air	0.69
S (180°)	buildings	building wakes and roughness	0.79

With such a map the local correction becomes naturally direction-dependent. That is much more useful than one generic site roughness, which would average a ridge, a forest, a valley and a group of buildings into a single number that describes none of them. Figure 30.4 shows how the factors are obtained from a training record. The horizontal axis is the model wind direction β, the vertical axis the correction factor S_c; the black circles are the ratios of the mean site wind to the mean model wind in twelve sectors of 30°, with bars of plus and minus two standard errors; the blue curve is a smooth fit of three harmonics, of the form of Chapter 28,

$$S_c(\beta) = 0.942 + 0.109\cos\beta - 0.201\sin\beta - 0.013\cos 2\beta + 0.026\sin 2\beta + 0.030\cos 3\beta + 0.068\sin 3\beta.$$

The labels at the top name the exposure of each sector.

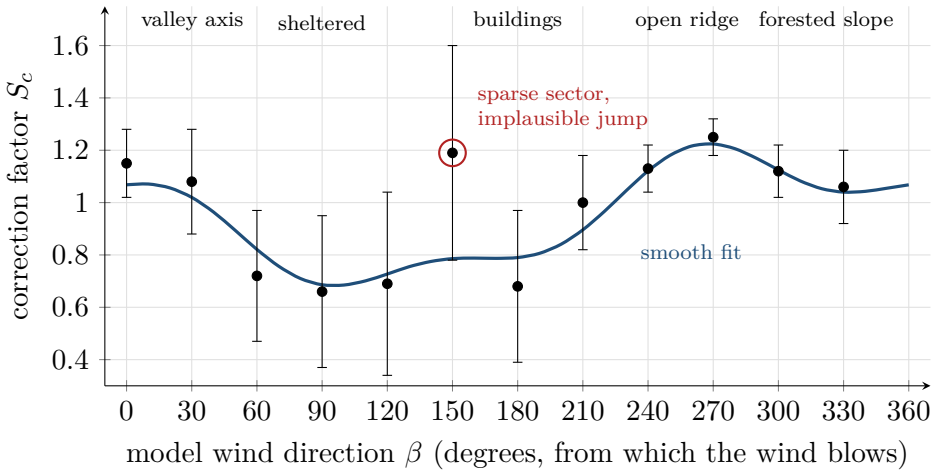


Figure 30.4: Directional correction factor at an illustrative ridge site. Circles: ratio of mean site wind to mean model wind in twelve sectors, with bars of ±2 standard errors, which are wide where the record has few independent events. Curve: three-harmonic fit given in the text.

The fit peaks at 1.22 near 270°, the open ridge, and falls to 0.69 near 90°, the sheltered sector. The bars show where the record is informative: the westerly sectors, which prevail, are determined to within about ±0.07, the easterly and southerly ones, which are rare, only to within ±0.3 to 0.4. One sector, 150°, has a ratio of 1.19 between two neighbors near 0.7. Terrain and roughness vary continuously with direction, and a jump of 0.5 between adjacent sectors that share the same buildings and hill is not physical; with ±0.41 the estimate is also consistent with the smooth curve. The smooth fit therefore uses the well-determined sectors to constrain the poorly determined ones, which is one of the physical consistency checks of Section 30.5.8. A model wind of $8\,\mathrm{m\,s^{-1}}$ gives a site wind of $1.22 \times 8 = 9.8\,\mathrm{m\,s^{-1}}$ from the west and $0.69 \times 8 = 5.5\,\mathrm{m\,s^{-1}}$ from the east.

30.3.3 Auditing the observations

Before anything is fitted, the measurements are checked for whether they can be trusted. The audit covers the sensor type, which fixes its threshold, response and overspeeding (Chapter 22); its height above ground and above the displacement height; its sampling period, the interval between readings, and its averaging period, which must match the target; tower shadow, the wake of the mast in one sector; nearby obstacles and their changes over time (Chapter 23); missing data, and whether the gaps fall preferentially in one regime, such as calm nights when a cup anemometer stalls or icing days when it freezes; and the calibration, its date and its traceability.

The audit matters because a statistical model will faithfully learn bad data too. A mast whose easterly sector lies in its own tower shadow yields a correction factor that is low for easterlies; the model reproduces that shadow in every forecast and attributes it to the atmosphere. A record whose calm hours are missing yields a model that has never seen a calm and underestimates the probability of the lulls that limit a conductor. A sensor raised from 10 to 12 m halfway through the record yields a step that the model absorbs as a change of climate. Each defect is cheaper to find before fitting than to diagnose afterward, and each is recorded with the model so that its consequences can be traced.

30.3.4 The measurement equation

The audit is organized by a measurement equation. Conceptually, an observation is

$$y_{\text{obs}} = y_{\text{true}} + \epsilon_{\text{instrument}} + \epsilon_{\text{representativeness}}, \tag{30.3}$$

where y_{true} is the target quantity, the true wind at the target place, height and averaging period; $\epsilon_{\text{instrument}}$ is the instrument error, the difference between the reading and the true wind at the sensor; and $\epsilon_{\text{representativeness}}$ is the difference between the true wind at the sensor and the true wind of the target, the mismatch of place, height, exposure and spatial support that Chapter 23 separated into spatial, vertical and dynamical kinds. Both errors are in meters per second.

The instrument error is often much smaller than the representativeness error, especially in complex terrain. For a calibrated cup anemometer with an illustrative uncertainty of $0.1\,\text{m s}^{-1}$ plus one percent, a reading of $6\,\text{m s}^{-1}$ is uncertain by about $0.16\,\text{m s}^{-1}$. If the same mast stands 150 m downwind of a forest edge in its easterly sector, the easterly readings are lower than the open-terrain wind of the target by perhaps 20 to 30 percent, 1.2 to $1.8\,\text{m s}^{-1}$: ten times the instrument error, and a hundred times its variance. "Sensor uncertainty" should therefore not mean calibration uncertainty alone; it includes the question of what the sensor represents, which is a property of the place, not of the instrument.

30.4 Baselines, predictors and model complexity

The fifth and sixth steps fit a model. This section starts from a simple baseline, chooses physically meaningful predictors, recommends predicting wind components, asks whether physical downscaling is needed, and arranges the candidate models on a ladder of complexity whose rungs are climbed only when the evidence demands.

30.4.1 The baseline

Every model starts simple. Two baselines cover most sites. The statistical baseline is the linear correction of the model wind,

$$U_{\text{site}} = a + b\,U_{\text{NWP}}, \tag{30.4}$$

with the intercept a and the slope b fitted by least squares (Chapter 28). The physical baseline is the logarithmic profile through the model's or the site's friction velocity,

$$U(z) = \frac{u_*}{\kappa}\,\ln\!\left(\frac{z-d}{z_0}\right), \tag{30.5}$$

with the displacement height d and the roughness length z_0 of the site's upwind surface (Chapter 12), and its stability-corrected form where the regime is not neutral (Chapter 14).

A baseline is needed to determine whether added complexity actually helps. A complicated model can look impressive, with maps, many predictors and fine detail, without adding value; only its score against the baseline, on the same independent test data, shows whether it does. A useful summary is the skill score $1 - \text{RMSE}^2_{\text{model}}/\text{RMSE}^2_{\text{baseline}}$, the fraction of the baseline's mean square error that the model removes: a model with $\text{RMSE} = 1.5\,\text{m s}^{-1}$ against a baseline of $1.8\,\text{m s}^{-1}$ has a skill of $1 - 2.25/3.24 = 0.31$. A skill near zero means the complexity added nothing that the test data can detect.

30.4.2 Physically meaningful predictors

Good predictors are quantities with a physical reason to affect the site wind. Among the outputs of a weather model they include the model wind speed U_{NWP} and its components u_{NWP} and v_{NWP}, which carry the direction; the stability parameter z/L_{O}; the boundary-layer depth, often

labeled PBLH (planetary boundary-layer height) in model output, the z_i of this book; the wind at 200 m, U_{200}, which measures the momentum available aloft; a temperature difference between two heights, ΔT, which measures the stratification near the ground; and the potential temperature θ. Site descriptors add the slope, the aspect and the roughness length z_0, or their direction-dependent forms, which act when a model is trained on several sites (Chapter 28). A model built from such predictors is interpretable: each coefficient or dependence can be checked against the physics it is meant to represent.

Wind speed alone is not enough. Suppose the model wind is $U_{\mathrm{NWP}} = 8\,\mathrm{m\,s^{-1}}$ in two cases. In case A it is a westerly wind over the exposed ridge; in case B an easterly wind behind the forest. The local wind can be completely different: with the factors of Table 30.2, $9.8\,\mathrm{m\,s^{-1}}$ in case A and $5.5\,\mathrm{m\,s^{-1}}$ in case B, a ratio of 1.8. In heterogeneous terrain, therefore,

$$U_{\mathrm{site}} \neq F(U_{\mathrm{NWP}}) \text{ alone;}$$

the direction and the stability enter as arguments, as in equation (30.2). A model of speed alone fits the average of the two cases, $7.7\,\mathrm{m\,s^{-1}}$, which is wrong in both.

30.4.3 Wind components

Instead of predicting the speed alone, a model can predict the eastward and northward components of the site wind, u_{site} and v_{site}, and compute the speed from them,

$$U_{\mathrm{site}} = \sqrt{u_{\mathrm{site}}^2 + v_{\mathrm{site}}^2}, \tag{30.6}$$

and the direction from $u = -U\sin\beta$, $v = -U\cos\beta$. This naturally preserves the direction, which the conductor application of Section 30.6.5 needs, and avoids the problems of circular statistics: there is no discontinuity at north and no undefined direction in calm (Chapter 24). The components carry one trap, shown in Chapter 28: a least-squares model predicts the mean vector, whose speed is lower than the mean speed when the direction is uncertain, so the speed is either predicted separately or corrected for that bias.

30.4.4 When physical downscaling is needed

Whether a statistical correction is enough depends on the terrain. If the terrain is simple, flat or gently rolling with homogeneous cover, a statistical correction may be enough: the site differs from the grid cell by a roughly constant factor per direction and regime, which the record determines. If the terrain strongly controls the flow, with ridges, valleys, steep slopes or abrupt changes of cover inside the grid cell, a terrain-aware or dynamical correction is used. The possibilities are a linearized terrain model, valid for gentle slopes and attached flow (Chapter 20); RANS CFD, for steep terrain, separation and obstacles (Chapter 29); a finer weather model, for thermal circulations and gap flows that need the mesoscale dynamics (Chapter 28); or a hybrid approach that applies the physics first and a statistical correction to its residual.

Complexity must be justified by a real unresolved process. Three indications are useful. First, the errors of the statistical model are organized by direction and stability in a way that matches the terrain, for instance large in the sectors that cross a steep lee slope. Second, the target lies where no observations exist, so nothing can be learned statistically, as for the spans of a new line. Third, the regimes of interest are rare in the record, so the statistical model would extrapolate. Conversely, when the main uncertainty is the large-scale forecast, microscale physics does not reduce it: with a forecast error of $2\,\mathrm{m\,s^{-1}}$ and a local terrain error of $0.3\,\mathrm{m\,s^{-1}}$ that a flow model could remove, the combined error falls only from $\sqrt{2^2 + 0.3^2} = 2.02\,\mathrm{m\,s^{-1}}$ to $2\,\mathrm{m\,s^{-1}}$ (Chapter 29).

30.4.5 The complexity ladder

The candidate models form a ladder of increasing complexity. Level 0 is the raw weather-model wind, interpolated to the site and height. Level 1 is a bias correction, additive, multiplicative or linear. Level 2 is a statistical model that depends on direction and stability, such as the factor $S_c(\beta, z/L_{\mathrm{O}})$ of Chapter 28 or a regime-dependent regression. Level 3 adds terrain predictors, and with them some ability to transfer to unmeasured places. Level 4 couples the weather model to a microscale physical model, linear or CFD, with a statistical correction of its residual. Level 5 is a time-dependent high-resolution approach, such as large-eddy simulation driven by the weather model. A model moves upward only when the simpler model demonstrably fails, and the failure is demonstrated on independent test data.

Figure 30.5 shows an illustrative climb. The horizontal axis is the level; the vertical axis is the root-mean-square error of the site wind on a held-out test year, for all hours (blue circles) and for the stable hours alone (red squares). The bars are plus and minus two standard errors of each RMSE, estimated from the effective number of independent cases, about 400 for all hours and 120 for the stable hours, with $\mathrm{SE(RMSE)} \approx \mathrm{RMSE}/\sqrt{2n_{\mathrm{eff}}}$ for normally distributed errors.

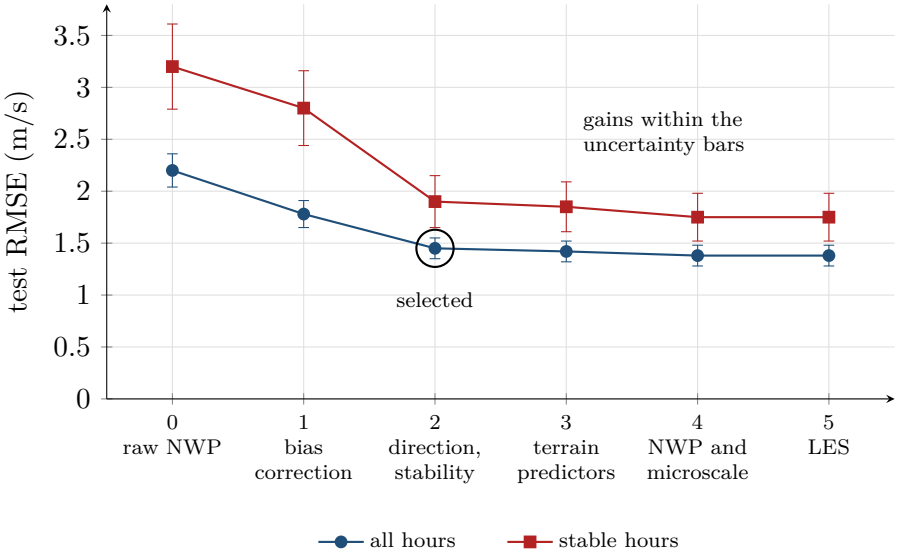


Figure 30.5: Test error of models on the complexity ladder at an illustrative site, for all hours and for stable hours, with bars of ±2 standard errors. Level 5 adds cost but no measurable gain.

The bias correction of level 1 removes the systematic error and lowers the RMSE from 2.20 to $1.78\,\mathrm{m\,s^{-1}}$, but the stable hours remain at $2.80\,\mathrm{m\,s^{-1}}$; Section 30.5.1 shows that they contribute three quarters of its mean square error. Level 2, which lets the correction depend on direction and stability, lowers the stable error to $1.90\,\mathrm{m\,s^{-1}}$ and the overall error to $1.45\,\mathrm{m\,s^{-1}}$, far more than the bars. Beyond level 2 the gains, 0.03 to $0.07\,\mathrm{m\,s^{-1}}$ overall and 0.05 to $0.15\,\mathrm{m\,s^{-1}}$ in stable hours, are smaller than the uncertainty of the scores. A paired comparison of two models on the same test hours has a smaller uncertainty than either score, because the two models' errors are correlated, but here it too fails to separate them. Level 2 is selected, and level 4 is held in reserve for the day the line is extended to spans without observations.

30.4.6 Model selection

The climb is a model-selection problem, and its answer has a precise form. The correct model is not the most complicated model available. It is the simplest model that resolves the processes

relevant to the question. That is a stronger engineering principle than "use the best model", because it can be tested: a process is relevant if leaving it out produces an error, in the regime and the statistic that the target defines, larger than the uncertainty of the test.

Principle 30.2. *Choose the simplest model that resolves the processes relevant to the question, and move up the complexity ladder only when the simpler model demonstrably fails on independent data in a regime that matters.*

The principle has three consequences. A more complex model must earn its place by an improvement on the test set, not by its appearance. The comparison is made in the regime and statistic of the target: a model that improves the overall RMSE but not the low quantiles on stable nights does not help a line rating. And a model higher on the ladder has more parameters, more inputs and more ways to fail, so that an unproven gain is a net loss of robustness.

30.5 Validation and physical diagnosis

The seventh and eighth steps test the model. This section breaks the errors down by regime, direction and height, validates whole profiles, separates calibration from testing with chronological and event holdout, diagnoses errors physically, exposes compensating errors, and lists the physical consistency checks and the out-of-distribution test that guard the model in operation.

30.5.1 Validation by regime

An overall RMSE is not enough. Performance is broken down by day and night, by stability, by wind direction, by wind speed and by season, and each breakdown asks whether a part of the physics is weak. Table 30.3 gives the breakdown by stability for the level-1 model of Figure 30.5. Its columns are the regime, its share of the test hours, the bias (model minus observed), the RMSE, the random part of the error $\sigma_e = (\mathrm{RMSE}^2 - \mathrm{Bias}^2)^{1/2}$ (Chapter 24) and the share of the total mean square error that the regime contributes.

Table 30.3: Validation of the level-1 model by stability regime on a test year (illustrative). Errors in m/s.

Regime	Share	Bias	RMSE	σ_e	Share of mean square error
Convective	30 %	−0.3	1.2	1.16	14 %
Neutral	40 %	+0.1	1.0	0.99	13 %
Stable	30 %	+1.9	2.8	2.06	74 %
All hours	100 %	+0.52	1.78	1.71	100 %

The overall line combines the regimes by their shares: the mean square error is $0.3 \times 1.2^2 + 0.4 \times 1.0^2 + 0.3 \times 2.8^2 = 0.432 + 0.400 + 2.352 = 3.184\,\mathrm{m^2\,s^{-2}}$, so RMSE $= 1.78\,\mathrm{m\,s^{-1}}$, and the bias is $0.3(-0.3) + 0.4(0.1) + 0.3(1.9) = +0.52\,\mathrm{m\,s^{-1}}$. The breakdown immediately shows where the physics is weak. The convective and neutral regimes are good, with errors of about $1\,\mathrm{m\,s^{-1}}$ and small biases. The stable regime has an RMSE of $2.8\,\mathrm{m\,s^{-1}}$, a bias of $+1.9\,\mathrm{m\,s^{-1}}$, the model too fast at night, and three quarters of the total mean square error. The positive bias points at too much mixing or too weak decoupling in the stable boundary layer (Chapters 17 and 26), and the large random part, $2.06\,\mathrm{m\,s^{-1}}$, at the intermittency and local drainage that the model does not represent. The overall $1.78\,\mathrm{m\,s^{-1}}$ says only that the model is mediocre; the table says which part of it to fix.

30.5.2 Validation by direction

The same breakdown by direction exposes the site. Suppose, at a second illustrative site, the error of westerly winds is $\mathrm{RMSE_W} = 0.8\,\mathrm{m\,s^{-1}}$ and that of easterly winds $\mathrm{RMSE_E} = 3.5\,\mathrm{m\,s^{-1}}$. That suggests a site or exposure problem, such as forest sheltering of the sensor or unresolved terrain in the easterly sector, rather than a problem of the weather model, whose forcing errors would not depend so strongly on the side from which the wind arrives. An overall $\mathrm{RMSE} = 1.6\,\mathrm{m\,s^{-1}}$ would hide it. With the two sectors making up the record, the overall mean square error is $w\,0.8^2 + (1-w)\,3.5^2$ for a westerly share w; setting it to $1.6^2 = 2.56$ gives $w = (12.25 - 2.56)/(12.25 - 0.64) = 0.83$. The westerlies, 83 percent of the hours, dominate the overall score, and the easterlies, 17 percent, carry an error four times larger that the score dilutes.

The breakdown also says what to do. An error confined to one sector is addressed by the exposure description of Section 30.3.2: a direction-dependent factor, a terrain model for that sector, or a second sensor whose exposure in that sector is good. Direction errors themselves are computed as circular differences, and the vector error combines speed and direction errors in one number (Chapter 24); for a conductor the direction error is taken modulo 180°, since the sense of the wind along the line does not change its cooling.

30.5.3 Validation by height and of profiles

If measurements exist at several heights, for instance at 10, 50 and 100 m, every level is compared. Suppose the wind at 100 m, U_{100}, is good but the wind at 10 m, U_{10}, is poor. That suggests a surface or boundary-layer problem, not necessarily a synoptic error: the momentum aloft is right, and its transfer to the ground is wrong. The two-height ratio U_{10}/U_{100} then locates the problem more closely, as the exponent α did in the diagnosis of Chapter 25: a ratio too large means too much mixing or too smooth a surface, a ratio too small the opposite. Multi-height observations are diagnostically powerful because they separate the forcing from the coupling, which a single height mixes.

The comparison extends to whole profiles: the wind profile $U(z)$ and, where available, the potential temperature profile $\theta(z)$, from a tower, a lidar or a sounding. A model can match U_{10} for the wrong reason. Too much roughness and too much vertical mixing, for example, act in opposite directions on the 10 m wind and can accidentally cancel there; a full profile reveals the cancellation, as Section 30.5.7 shows with numbers. A profile of θ adds the stratification, which decides the regime and which no wind measurement shows directly.

30.5.4 Calibration against testing

One period is used to fit the model, the *calibration* or training period, and another, independent period to test it. The model is never judged on the observations used for fitting, because a model with enough freedom can reproduce its training data closely while failing on any other. For a time series the split is chronological: for example, the years 2024 and 2025 for training and 2026 for testing. A chronological holdout tests the model as it will be used, on a future it has not seen, and it also exposes drift: a sensor replaced, a forest grown, a weather model upgraded between the two periods. The principle is to test on genuinely unseen conditions. Its limit is the content of the test year: a single year may not contain the rare regimes of interest, a severe storm or a long windless heat wave, and a score on that year says nothing about them.

30.5.5 Event holdout

For high-wind or low-wind events the test is stronger if whole events are held out. Suppose the record contains 30 storms of about 24 hours each, 720 storm hours. Adjacent hours within

one storm are highly correlated, with a lag-one correlation near 0.95, so a random split of the timestamps puts hours of the same storm into both the training and the test sets; the two sets are then almost identical, and the model is scored on its interpolation within storms it has seen, which produces an optimistic validation (Chapter 28). Holding out entire storms, one at a time or in groups, tests the model on storms it has not seen.

Event holdout also states honestly how much evidence the test contains. With the first-order autoregressive estimate of Chapter 28, $n_{\mathrm{eff}} \approx n(1 - r_1)/(1 + r_1)$, the 720 storm hours with $r_1 = 0.95$ carry the information of about $720 \times 0.05/1.95 \approx 18$ independent values: fewer than the number of storms, so that each storm contributes roughly one independent sample. The sampling uncertainty of an RMSE follows: for normally distributed errors its relative standard error is about $1/\sqrt{2(n-1)}$, which is 2.6 percent for $n = 720$ and 13 percent for $n = 30$. A storm RMSE of $2.0\,\mathrm{m\,s^{-1}}$ is therefore uncertain by about $\pm 0.26\,\mathrm{m\,s^{-1}}$, not $\pm 0.05\,\mathrm{m\,s^{-1}}$, and two models whose storm scores differ by $0.1\,\mathrm{m\,s^{-1}}$ cannot be ranked by them.

30.5.6 Physical diagnosis of errors

The breakdowns turn validation into scientific diagnosis. Suppose the observed wind is much weaker than predicted. Four questions, in order, locate the cause. Is the wind aloft wrong? If yes, the error is in the forcing, and no local correction will fix it. Is the wind aloft right but the surface wind wrong? Then the error is in the coupling between the boundary layer and the surface. Does the error occur only for one direction? Then it is terrain or exposure. Does the error occur only at night? Then it is a stable-boundary-layer problem. The order follows the chain of Figure 30.1 from the top, as the hierarchical interpretation of Chapter 25 did, and stops at the first stage whose evidence fails.

Each question has a test with numbers. The first compares the model wind at 100 to 500 m with a lidar, a tall mast or a sounding: an illustrative agreement within $0.5\,\mathrm{m\,s^{-1}}$ at $12\,\mathrm{m\,s^{-1}}$ clears the forcing. The second compares the ratio U_{10}/U_{100} of the model with the observed ratio: 0.67 against 0.50 places the excess wind in the lowest hundred meters. The third sorts the errors by the sectors of Table 30.2: an error of $+2.5\,\mathrm{m\,s^{-1}}$ in the sheltered sector and $+0.3\,\mathrm{m\,s^{-1}}$ elsewhere names the exposure. The fourth sorts them by the stability classes of Section 30.2.3: a bias of $+1.9\,\mathrm{m\,s^{-1}}$ at night and near zero by day, as in Table 30.3, names the stable boundary layer. Several answers can be yes at once, since a sheltered sector is often worse at night, and the breakdown is then made jointly, by sector and class.

30.5.7 Compensating errors

Compensating errors are two or more model errors that accidentally cancel in the validated quantity. Suppose a model has too much boundary-layer mixing and too much roughness. On a stable night the excess mixing carries momentum down and raises the wind near the ground; the excess roughness extracts momentum and lowers it. The two may cancel at 10 m and give the right answer there, and a validation at 10 m alone would rate the model excellent. At 100 m it fails badly.

Figure 30.6 shows such a case. The left panel plots height against wind speed and the right panel height against potential temperature, both up to 120 m; the black curves are the observed night profiles, the red dashed curves the model's, and the black dots the measurements of a mast at 10, 50 and 100 m. The observed wind follows $U = 8\,\mathrm{m\,s^{-1}}\,(z/100\,\mathrm{m})^{0.25}$, a stable profile; the model wind follows $U = 4.5\,\mathrm{m\,s^{-1}}\,(z/10\,\mathrm{m})^{0.125}$, a well-mixed one.

At 10 m both winds are $4.5\,\mathrm{m\,s^{-1}}$: the model has no error there. At 50 m the model gives $5.5\,\mathrm{m\,s^{-1}}$ against $6.7\,\mathrm{m\,s^{-1}}$, and at 100 m it gives $6.0\,\mathrm{m\,s^{-1}}$ against $8.0\,\mathrm{m\,s^{-1}}$, 25 percent too low; a turbine hub or a high conductor would be badly mispredicted. The temperature panel shows why: the observed inversion is 5 K over 100 m, the model's only 2 K, and the model's surface air is 2 K too warm, the signature of excess mixing, which spreads the surface cooling

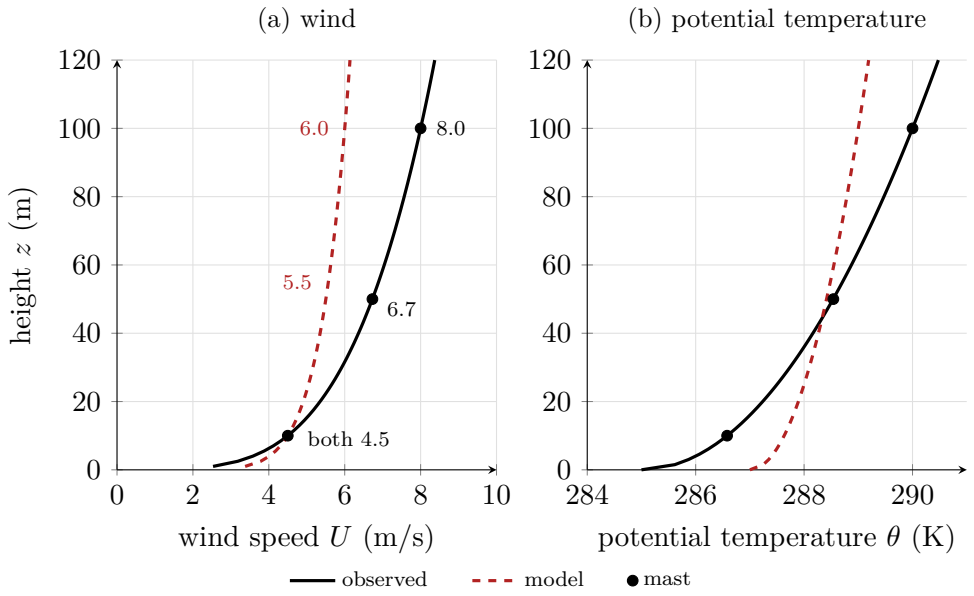


Figure 30.6: Compensating errors on a stable night (illustrative). Observed: $U = 8\,(z/100)^{0.25}$ m/s, $\theta = 285 + 5\,(z/100)^{1/2}$ K. Model with too much mixing and too much roughness: $U = 4.5\,(z/10)^{0.125}$ m/s, $\theta = 287 + 2\,(z/100)^{1/2}$ K. The two agree at 10 m only.

through a deeper layer and drains the momentum aloft. The roughness error is hidden in the low end of the profile: for a neutral log profile, raising z_0 from 0.05 to 0.2 m lowers U_{10}/U_{100} from $\ln 200/\ln 2000 = 0.70$ to $\ln 50/\ln 500 = 0.63$, about ten percent, which offsets the excess wind that the mixing brings down. Fixing only one of the two errors would make the 10 m wind worse, and a tuning judged at 10 m would reject the fix. This is why physical validation, of profiles and of the regime, matters in addition to statistical validation at one height.

30.5.8 Physical consistency and out-of-distribution conditions

A defensible model obeys basic physics, and *physical consistency* is the compliance of its predictions with the governing physical constraints. Four checks catch many failures of statistical models. Wind speed cannot be negative, which an additive correction can violate at low wind (Chapter 28). The response to stability should be plausible: the ratio of the surface wind to the wind aloft should decrease from convective to stable conditions, as in Figure 30.3, and a model in which it increases needs a physical reason such as a low-level jet. Terrain speed-up should vary smoothly with direction, as in Figure 30.4, since the terrain seen by two winds 30° apart overlaps. And a predicted profile should not behave impossibly: a wind that decreases with height in the surface layer over flat open ground, with no canopy, jet or obstacle to explain it, or a shear exponent far outside the range of about 0.05 to 0.6, flags an error. These constraints are cheap to evaluate on every prediction.

Out-of-distribution conditions. A prediction is *out of distribution* when the conditions it is asked about are unlike those used to build or validate the model. Suppose the model was trained on winds of 0 to 15 m s^{-1} and receives 25 m s^{-1}. That is out of distribution, and the prediction is not trusted blindly: a regression continues its line, which is right only if the physics does not change, and a tree-based model repeats the value of its last bin (Chapter 28). The same applies to rare combinations whose parts are each common: easterly winds and very stable conditions may each be frequent, while easterly very stable hours are rare, say 25 independent events, and the factor for that cell is poorly determined. A simple test counts the independent

training events in the cell of the predictors that the forecast falls into, sector by stability class by speed class, and flags the forecast when the count is below a threshold, for instance 20.

Silence can be better than false precision. When the model is outside its calibrated domain, a defensible system may state that the uncertainty is too large for a reliable site correction, rather than produce a number such as $12.73\,\mathrm{m\,s^{-1}}$. It can fall back to a simpler, better-founded level of the ladder, such as the physical baseline or the raw weather-model wind with a wide stated uncertainty, and say so. That is better scientific practice than unjustified numerical precision, and it is better engineering practice too, because a flagged forecast leads a user to caution where a confident wrong one leads to error.

30.6 Uncertainty, decisions and the model report

The ninth and tenth steps state the uncertainty and check it, and the last validates the decision itself. This section writes a prediction with its uncertainty, combines the sources in a budget, tests the probabilistic calibration, validates against the decision with the example of transmission-line cooling, assembles the workflow and the report, and ends with the complete model of near-surface wind that the book has built.

30.6.1 A prediction with its uncertainty

A site wind estimate should not be a bare number such as $U = 7.3\,\mathrm{m\,s^{-1}}$. It should look more like

$$U = 7.3\,\mathrm{m\,s^{-1}}, \qquad [5.8,\ 9.1]\,\mathrm{m\,s^{-1}},$$

a central value with an interval of stated probability, or better, the whole conditional distribution $p(U \mid \text{data})$ of the site wind given the information available. The interval in the example is wider above the central value, $1.8\,\mathrm{m\,s^{-1}}$, than below it, $1.5\,\mathrm{m\,s^{-1}}$, as a wind-speed distribution skewed to the right gives; on a logarithmic scale it is nearly symmetric, $\ln(5.8/7.3) = -0.23$ and $\ln(9.1/7.3) = +0.22$, which for an 80 percent interval corresponds to a lognormal distribution with a logarithmic standard deviation of $0.225/1.2816 = 0.18$. The interval is needed because the uncertainty comes from several sources, which the next subsection separates, and because the decision often depends on the tail of the distribution, not on its center.

30.6.2 An uncertainty budget

A useful decomposition of the variance of the error of a site wind prediction is

$$\sigma^2_{\text{total}} = \sigma^2_{\text{forecast}} + \sigma^2_{\text{downscaling}} + \sigma^2_{\text{measurement}} + \sigma^2_{\text{representation}}, \tag{30.7}$$

conceptually at least. It follows from writing the error as a sum of four parts and taking the variance: the variance of a sum is the sum of the variances plus twice the covariances, and the covariances vanish only if the parts are independent. They are not always independent; a forecast that misses the evening transition also mis-specifies the stability that the downscaling uses, so the forecast and downscaling errors are correlated on stable evenings. The decomposition nonetheless forces the question of where the uncertainty originates.

The four terms follow the hierarchy of uncertainty of Figure 30.1, from the large-scale atmosphere through the boundary-layer transport and the terrain and roughness response to the asset-scale flow and the sensor observation; uncertainty can enter at every level, which is why near-surface wind is intrinsically a probabilistic problem.

Forecast uncertainty. This is the uncertainty in the future atmospheric state: the pressure pattern, the timing of a front, the wind direction. Weather-model ensembles are particularly useful here, because the spread of their members estimates it (Chapters 25 and 28).

Downscaling uncertainty. Even if the weather model were perfect, the mapping from the grid wind to the site wind is uncertain: the terrain correction, the roughness and the stability effects are each known imperfectly. This term is estimated from historical residuals, the scatter of the observed site wind about the downscaled prediction when the downscaling is driven by analyses rather than forecasts, or from probabilistic models fitted to those residuals.

Measurement uncertainty. This includes the calibration, the instrument response and the alignment of the sensor, whose error in north alignment becomes an error of direction. It is usually comparatively small for good sensors, but it still matters: it enters the training data, where it inflates the fitted residual, and the verification, where it makes a perfect prediction look imperfect.

Representativeness uncertainty. This is the uncertainty due to the spatial and physical mismatch between what is measured or modeled and the target, and it is often the hardest term. Does a point sensor represent the site, the conductor, the model grid cell or the surrounding terrain? The answer can be estimated, from two sensors at different points of the same span or from a flow model, but rarely removed completely. It should be acknowledged explicitly, with a number.

Table 30.4 gives an illustrative budget for the 30 m wind on the ridge span of Section 30.6.7. Its columns are the source, what produces it, how it is estimated, its standard deviation in m/s and its share of the total variance.

Table 30.4: Uncertainty budget of the 30 m wind on a ridge span (illustrative; one standard deviation).

Source	Produced by	Estimated from	σ (m/s)	Variance share
Forecast	pressure pattern, frontal timing, direction	ensemble spread mapped to the site	0.9	46 %
Downscaling	terrain factor, roughness, stability correction	residuals of the downscaling driven by analyses	0.7	28 %
Measurement	calibration, response, alignment, sampling of the 10-min mean	calibration certificate; sampling error	0.3	5 %
Representation	mast against the span average	two sensors on a span; flow model	0.6	21 %
Total	in quadrature	equation (30.7)	1.32	100 %

The total is $\sqrt{0.9^2 + 0.7^2 + 0.3^2 + 0.6^2} = \sqrt{0.81 + 0.49 + 0.09 + 0.36} = \sqrt{1.75} = 1.32\,\mathrm{m\,s^{-1}}$; adding the standard deviations instead would give $2.5\,\mathrm{m\,s^{-1}}$ and nearly double the stated uncertainty. The forecast dominates, the measurement is the smallest term, and the representation is three quarters of the downscaling term. The table also shows what a historical residual measures. The residuals of past forecasts against the mast contain the forecast, downscaling and measurement errors, $\sqrt{0.81 + 0.49 + 0.09} = 1.18\,\mathrm{m\,s^{-1}}$, about $1.2\,\mathrm{m\,s^{-1}}$, but not the mismatch between the mast and the span, because the mast is the reference. Used alone for the span, the residual understates the uncertainty, 1.2 against $1.32\,\mathrm{m\,s^{-1}}$; the representativeness term must be added from other evidence.

30.6.3 Probabilistic calibration

A probability forecast is checked against frequencies. *Probabilistic calibration*, or reliability, is the agreement between forecast probabilities and observed frequencies. If a model predicts $\Pr(U < 3\,\mathrm{m\,s^{-1}}) = 20$ percent many times, then roughly 20 percent of those cases should have $U < 3\,\mathrm{m\,s^{-1}}$. Suppose the model issued that forecast on 500 occasions and the wind was below $3\,\mathrm{m\,s^{-1}}$ on 140, 28 percent. If the occasions were independent, the standard error of the observed frequency would be $\sqrt{0.2 \times 0.8/500} = 0.018$, and 28 percent lies 4.5 standard errors above 20. The occasions are hours, and consecutive hours are correlated; with an illustrative 150 independent situations among them the standard error is $\sqrt{0.16/150} = 0.033$, and the discrepancy is 2.4 standard errors: smaller evidence, but still a miscalibration.

Figure 30.7 generalizes the check to all probabilities in a *reliability diagram*. The horizontal axis is the forecast probability of the event, grouped in bins of 0.1; the vertical axis is the observed frequency of the event in each bin. A calibrated forecast lies on the diagonal. The blue circles are a calibrated model; the red squares an overconfident one, whose observed frequencies follow $0.35 + 0.5\,(p - 0.35)$; the dotted line is the climatological frequency of the event, 0.35.

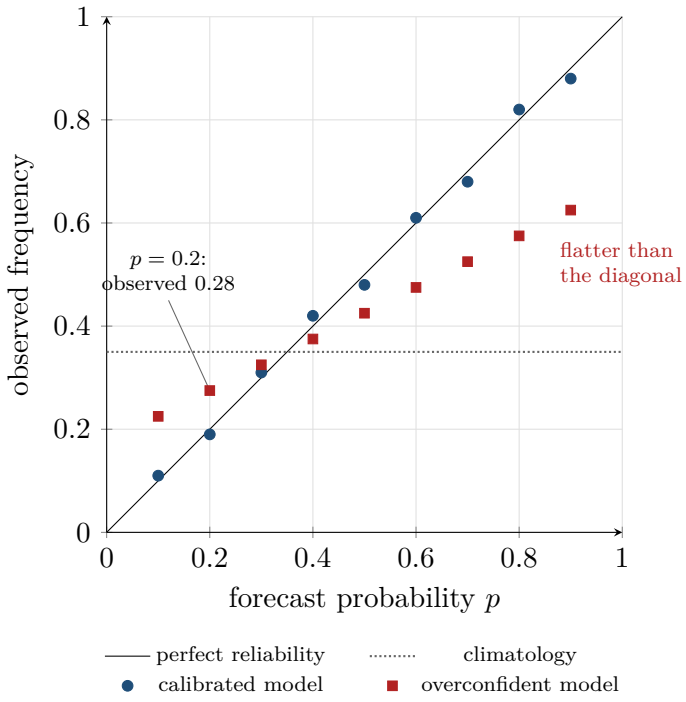


Figure 30.7: Reliability diagram of probability forecasts of an event such as $U < 3\,\mathrm{m\,s^{-1}}$ (illustrative). Calibrated forecasts lie on the diagonal; the overconfident forecasts, observed frequency $0.35 + 0.5(p - 0.35)$, are too extreme on both sides of the climatological frequency 0.35.

The overconfident model is too extreme on both sides. When it forecasts 0.9 the event happens only 62 percent of the time; when it forecasts 0.1, 22 percent; its curve is flatter than the diagonal and crosses it at the climatological frequency. Its 20 percent forecasts are the 28 percent of the text. A forecast distribution that is too narrow is *overconfident* in exactly this sense, even if its mean prediction is good: it puts too little probability in the tails, so the events it calls unlikely happen too often.

Coverage of prediction intervals. The same check applies to intervals. An 80 percent interval should contain 80 percent of the observations, and the fraction it actually contains is

its *coverage*. Coverage is computed by regime, because an overall coverage can be right while every regime is wrong. Table 30.5 shows it for the regimes of Table 30.3, with an interval of $\pm 1.2816\,\sigma$ about the prediction using a single predictive standard deviation $\sigma = 1.5\,\mathrm{m\,s^{-1}}$ in all regimes. Its columns are the regime, its share, its RMSE, the coverage if the errors are normal with standard deviation equal to the RMSE, $2\Phi(1.2816 \times 1.5/\mathrm{RMSE}) - 1$ with Φ here the standard normal distribution function (not the geopotential), and the factor by which the regime's σ would have to be multiplied to restore 80 percent coverage.

Table 30.5: Coverage of 80 % prediction intervals built with one predictive standard deviation, $1.5\,\mathrm{m\,s^{-1}}$, for all regimes (illustrative; errors taken as normal with zero mean and standard deviation equal to the regime's RMSE).

Regime	Share	RMSE (m/s)	Coverage	Factor for σ
Convective	30 %	1.2	0.89	0.80
Neutral	40 %	1.0	0.95	0.67
Stable	30 %	2.8	0.51	1.87
All hours	100 %	1.78	0.80	–

The overall coverage is $0.3 \times 0.89 + 0.4 \times 0.95 + 0.3 \times 0.51 = 0.80$, exactly the nominal value, and a check of all hours would pass the model. By regime, the intervals are too wide by day, where they contain 89 and 95 percent of the observations, and far too narrow at night, where they contain only half. The factor in the last column follows from inverting the coverage: an interval of half-width $h = 1.2816\,\sigma$ has coverage c when $h/\sigma_{\mathrm{true}} = \Phi^{-1}[(1+c)/2]$, so $\sigma_{\mathrm{true}}/\sigma = 1.2816/\Phi^{-1}[(1+c)/2]$; for $c = 0.508$, $\Phi^{-1}(0.754) = 0.687$ and the factor is 1.87, which is the ratio 2.8/1.5. With the stable bias of $+1.9\,\mathrm{m\,s^{-1}}$ included, the stable coverage falls further, to 0.47. A regime-dependent σ, 1.2, 1.0 and $2.8\,\mathrm{m\,s^{-1}}$, restores the coverage in each regime, and the stable intervals become wide enough to admit what is not known about the night.

30.6.4 Decision-oriented validation

The best metric depends on the downstream use. Suppose the decision is based on whether the wind falls below $2\,\mathrm{m\,s^{-1}}$. Then the overall RMSE is not enough, because it is dominated by the errors of the common, moderate winds, and a model can have a low RMSE while missing most of the low-wind hours. The evaluation counts instead the four outcomes of the decision, in a contingency table: *hits*, events forecast and observed; *misses*, events observed but not forecast; *false alarms*, events forecast but not observed; and correct negatives. Two summaries follow: the probability of detection, hits divided by observed events, and the false-alarm ratio, false alarms divided by forecast events. The probability forecasts near the threshold, for $2\,\mathrm{m\,s^{-1}}$ here, are checked for calibration as in Figure 30.7. The model is validated against the actual engineering decision.

Table 30.6 compares two illustrative models of the low-wind event on 2000 test hours, of which 180 are events. Model A minimizes the RMSE; model B has a higher RMSE but a regime-dependent distribution whose low quantiles are calibrated at night. The columns give the RMSE, the four counts, the two summaries and the expected cost when a missed event costs ten times as much as an unnecessary action.

Model A detects half the events; model B detects four in five, with a slightly lower false-alarm ratio. With the stated costs, model A costs $(90 + 40) \times 1 + 90 \times 10 = 1030$ and model B $(144 + 60) \times 1 + 36 \times 10 = 564$, so the model with the worse RMSE is the better model for this decision. The costs also set the probability at which to act. If acting costs C_a whether or not the event occurs, and an unprotected event costs C_m, the expected cost is C_a when acting and

Table 30.6: Two models of a low-wind event on 2000 test hours with 180 events (illustrative). Cost: 1 per action (hit or false alarm), 10 per miss.

Model	RMSE (m/s)	Hits	Misses	False alarms	Correct neg.	Detect. prob.	False-alarm ratio	Cost
A	1.3	90	90	40	1780	0.50	0.31	1030
B	1.5	144	36	60	1760	0.80	0.29	564

$p\,C_m$ when not, for an event probability p; acting is cheaper when $p > C_a/C_m$, here $p > 0.1$. A calibrated probability is what makes this rule work: an overconfident model that says 0.05 when the true frequency is 0.2 withholds the action exactly when it is needed.

30.6.5 Transmission-line cooling

Suppose the thermal risk of a conductor becomes significant when the wind perpendicular to it falls below $1.5\,\mathrm{m\,s^{-1}}$, $U_\perp < 1.5\,\mathrm{m\,s^{-1}}$. Then the important quantity is not the mean wind speed but the probability $\Pr(U_\perp < 1.5\,\mathrm{m\,s^{-1}})$, the decision metric of this application, which is a much more targeted modeling problem. The perpendicular component follows from the geometry. Let the conductor run along the azimuth β_ℓ, measured clockwise from north (the line has no sense, so β_ℓ and $\beta_\ell + 180^\circ$ are the same line), and let $\gamma = \beta - \beta_\ell$ be the angle between the wind direction and the conductor. The unit vector along the line has eastward and northward components $(\sin\beta_\ell, \cos\beta_\ell)$, and the wind vector is $(u, v) = (-U\sin\beta, -U\cos\beta)$. The component along the line is their scalar product, $-U\cos(\beta - \beta_\ell)$, and the component across it is the magnitude of their cross product, $|u\cos\beta_\ell - v\sin\beta_\ell| = U|\sin(\beta_\ell - \beta)|$, so

$$U_\perp = U\,|\sin\gamma|, \qquad U_\parallel = U\,|\cos\gamma|. \tag{30.8}$$

The absolute values make the result independent of the sense of the wind and of the line. (The angle is often written ϕ elsewhere; this book reserves ϕ for latitude.)

Figure 30.8 shows the geometry and its consequence. Panel (a) is a plan view, north at the top, of a north–south conductor in the Southern Hemisphere with a wind from 345° and its two components. Panel (b) plots the wind speed against the angle γ; the curve $U = 1.5\,\mathrm{m\,s^{-1}}/\sin\gamma$ separates the shaded region, where $U_\perp < 1.5\,\mathrm{m\,s^{-1}}$, from the region of adequate cross-wind, and the numbered points mark the cases discussed below.

Wind direction therefore matters for conductor cooling. A wind of $10\,\mathrm{m\,s^{-1}}$ nearly parallel to the conductor, $\gamma = 5^\circ$, has $U_\perp = 10\sin 5^\circ = 0.9\,\mathrm{m\,s^{-1}}$ and lies in the shaded region (point 1), while a wind of $4\,\mathrm{m\,s^{-1}}$ perpendicular to it has $U_\perp = 4\,\mathrm{m\,s^{-1}}$ (point 2). Equation (30.8) overstates the contrast, because a wind along the conductor still cools it through the turbulence it carries and the flow it drives along the surface: common rating methods multiply the cooling of a perpendicular wind by an angle factor $K(\gamma) = 1.194 - \cos\gamma + 0.194\cos 2\gamma + 0.368\sin 2\gamma$, which is 1 at $\gamma = 90^\circ$ and 0.39, not zero, for a parallel wind. Even so, with the forced-convection cooling growing as $U^{0.6}$, a parallel wind of $10\,\mathrm{m\,s^{-1}}$ cools as $0.388 \times 10^{0.6} = 1.54$ in relative units and a perpendicular wind of $4\,\mathrm{m\,s^{-1}}$ as $4^{0.6} = 2.30$: the faster wind removes a third less heat. Forecasting the speed alone may therefore be insufficient. The perpendicular component is a conservative decision variable, since it ignores the cooling that remains in parallel wind, and its threshold is set with that in mind.

A Southern Hemisphere example. Consider a north–south line, $\beta_\ell = 0^\circ$, at 30°S, under a prefrontal wind from the north-northwest that the weather model gives as $9\,\mathrm{m\,s^{-1}}$ from 345° at 100 m; at the conductor height of 20 m on a stable evening the speed is $6\,\mathrm{m\,s^{-1}}$. Taken at the 100 m direction, $\gamma = 15^\circ$ and $U_\perp = 6\sin 15^\circ = 1.55\,\mathrm{m\,s^{-1}}$, just above the threshold (point

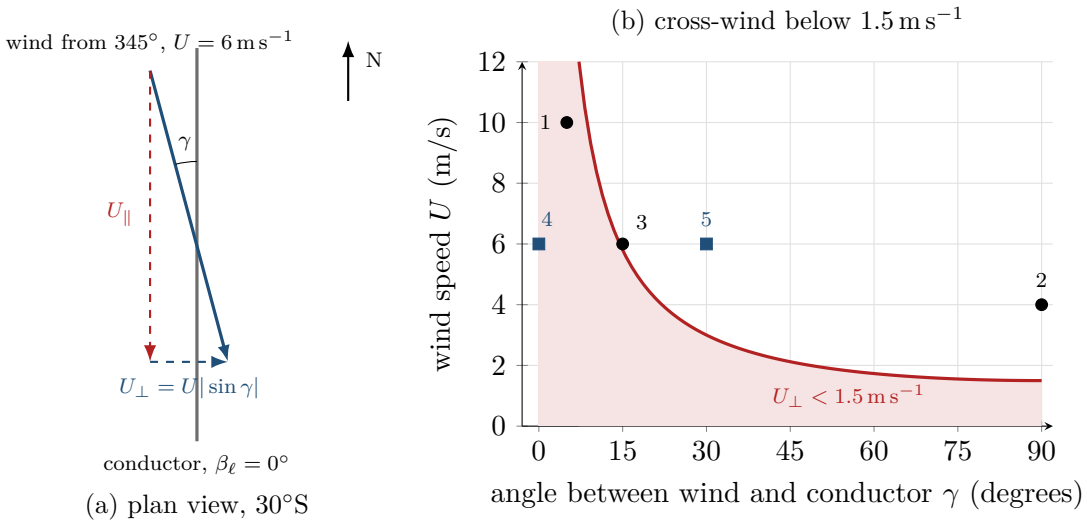


Figure 30.8: Cross-wind on a conductor. (a) Plan view of a north–south conductor at 30°S with a wind of $6\,\mathrm{m\,s^{-1}}$ from 345°, $\gamma = 15°$, and its components along and across the line. (b) Region where $U_\perp = U|\sin\gamma|$ is below $1.5\,\mathrm{m\,s^{-1}}$ (shaded), bounded by $U = 1.5/\sin\gamma$. Points (illustrative): 1, $10\,\mathrm{m\,s^{-1}}$ at 5°, $U_\perp = 0.9\,\mathrm{m\,s^{-1}}$; 2, $4\,\mathrm{m\,s^{-1}}$ at 90°, $4.0\,\mathrm{m\,s^{-1}}$; 3, $6\,\mathrm{m\,s^{-1}}$ at the 100 m direction, 15°, $1.55\,\mathrm{m\,s^{-1}}$; 4, the same wind at conductor height in the Southern Hemisphere, 0°, 0; 5, in the Northern Hemisphere, 30°, $3.0\,\mathrm{m\,s^{-1}}$.

3 of Figure 30.8). But the wind turns with height in the boundary layer, by an illustrative 15° between 100 and 20 m on such an evening, and the sense of the turning depends on the hemisphere (Chapter 3): the near-surface wind is turned toward low pressure, which lies to the right of the flow in the Southern Hemisphere and to its left in the Northern Hemisphere. In the Southern Hemisphere the 20 m wind is therefore turned clockwise, to 0°, exactly along the line, and $U_\perp = 0$ (point 4); the same geometry at 30°N would turn it counterclockwise, to 330°, with $\gamma = 30°$ and $U_\perp = 3.0\,\mathrm{m\,s^{-1}}$ (point 5). The hemisphere alone moves the cross-wind from zero to twice the threshold. Near parallel the sensitivity to direction is greatest: $\mathrm{d}U_\perp/\mathrm{d}\gamma = U\cos\gamma$, so at $8\,\mathrm{m\,s^{-1}}$ and $\gamma = 10°$ a direction error of 10° changes $U_\perp$ by about $8 \times 0.985 \times 0.175 = 1.4\,\mathrm{m\,s^{-1}}$, nearly the whole threshold. A model for this decision must predict direction at conductor height, not only at the model's levels, and its direction error must be validated in the near-parallel cases.

Site wind modeling is multivariable. The useful state of the site is therefore not the speed U alone but a vector such as

$$\mathbf{x} = (U,\ \beta,\ T,\ \text{stability},\ \text{terrain regime}),$$

with the direction β (written θ in some texts; this book keeps θ for potential temperature), the air temperature T, a stability measure and the terrain regime, for instance attached flow, blocked flow or a cold pool. The engineering model then maps that state into the quantity it needs: the cooling of a conductor, which depends on the speed, the angle and the air temperature; the loading of a structure, which depends on the gust and the direction; the energy production of a turbine, which depends on the hub wind, the shear and the turbulence; or the dispersion of a release, which depends on the direction, the speed and the stability.

30.6.6 The workflow and the model report

The steps of the chapter form a practical workflow. It regroups the ten steps of the preceding sections into nine and places the audit of the measurements before the site and the regime, because a flawed record distorts every later diagnosis. Figure 30.9 draws it. The nine boxes are the steps in order; the notes on the right give the chapters that supply the tools of each step; the arrows on the left are the two feedback loops, from a regime that fails validation back to the choice of correction, and from a decision metric that is not met back to the definition of the target.

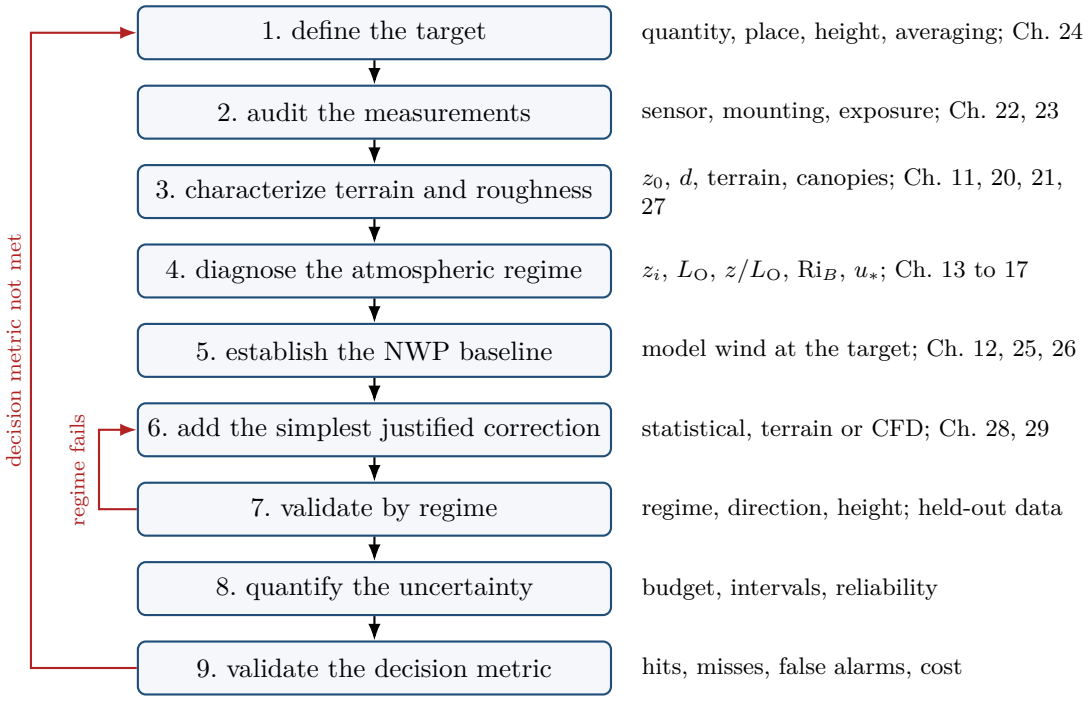


Figure 30.9: A defensible site-wind workflow. Boxes: the nine steps; notes: the quantities and chapters each step uses; red arrows: the feedback from a failed regime to the correction and from an unmet decision metric to the target.

A strong model report records the workflow so that the result can be reproduced and defended. At minimum it states the target variable; the sensor and site description; the input data; the terrain and roughness characterization; the model assumptions; the calibration period; the independent test period; the performance by regime; the uncertainty; and the limitations. Table 30.7 lists these items with what each must contain and the question it answers for a reader.

How a result is stated. A statement such as "the wind at the site will be $7.6\,\mathrm{m\,s^{-1}}$" is avoided: it names no target and no uncertainty. A better statement is: "the modeled 10-minute mean wind at 20 m above ground is $7.6\,\mathrm{m\,s^{-1}}$, with the main uncertainty arising from stable-boundary-layer coupling and easterly terrain sheltering." It states the quantity, the averaging period, the height and the physical sources of the uncertainty, and an interval of stated probability completes it. It is a much stronger scientific statement, because every part of it can be checked.

Table 30.7: Minimum contents of a site wind model report.

Item	Contents	Question answered
Target variable	quantity, place, height, averaging period, statistic	what exactly is predicted?
Sensor and site	instrument, height, mounting, exposure by sector	what do the observations represent?
Input data	weather model, levels, lead times, period	what drives the model?
Terrain and roughness	elevation data, $z_0(\beta)$, d, obstacles	what local physics is included?
Model assumptions	form, predictors, regimes, ladder level	why this model and not a simpler one?
Calibration period	dates, data removed by the audit	what was the model fitted to?
Independent test period	dates, holdout design, events held out	was the test genuinely unseen?
Performance by regime	bias, RMSE, coverage by regime, direction, height	where is the model weak?
Uncertainty	budget, intervals, reliability	how far can the numbers be trusted?
Limitations	out-of-distribution conditions, unresolved processes	where must the model not be used?

30.6.7 The complete problem and a final example

The near-surface wind problem that the preceding chapters have built can now be written as one function:

$$\mathbf{V}_{\text{site}}(t) = \mathcal{F}\big[\mathbf{V}_g,\ z_i,\ u_*,\ L_{\text{O}},\ z_0,\ d,\ \text{terrain},\ \text{canopy},\ \text{local observations}\big], \tag{30.9}$$

where $\mathbf{V}_g$ represents the large-scale forcing, z_i the boundary-layer depth, u_* the surface stress, L_{O} the stability, z_0 and d the aerodynamic properties of the surface, and the terrain, the canopy and the local observations the rest. That is essentially the whole near-surface wind modeling problem: each argument has a chapter, and the methods of the last chapters are ways of evaluating $\mathcal{F}$.

A worked site estimate. Suppose the wind is needed at 30 m above ground on the ridge of Table 30.2. The weather model predicts $U_{100} = 9\,\text{m}\,\text{s}^{-1}$ from the west. The atmosphere is moderately unstable, with $z/L_{\text{O}} = -0.2$ at 100 m, so $L_{\text{O}} = -500\,\text{m}$, and the upwind roughness length is $z_0 = 0.25\,\text{m}$. The surface-layer correction from 100 to 30 m uses the stability-corrected profile of Chapter 14 with the unstable Businger–Dyer form, $\psi_m = 2\ln[(1+x)/2] + \ln[(1+x^2)/2] - 2\arctan x + \pi/2$ with $x = (1 - 16\,z/L_{\text{O}})^{1/4}$: at 100 m, $x = 1.432$ and $\psi_m = 0.461$; at 30 m, $z/L_{\text{O}} = -0.06$, $x = 1.183$ and $\psi_m = 0.190$. The ratio of the winds is

$$\frac{U_{30}}{U_{100}} = \frac{\ln(30/0.25) - 0.190}{\ln(100/0.25) - 0.461} = \frac{4.787 - 0.190}{5.991 - 0.461} = 0.831,$$

so the background wind at 30 m is $U_{30,\text{background}} = 0.831 \times 9 = 7.5\,\text{m}\,\text{s}^{-1}$, against $7.2\,\text{m}\,\text{s}^{-1}$ for neutral air, since the unstable layer mixes more momentum down; the friction velocity is $\kappa U_{100}/5.530 = 0.65\,\text{m}\,\text{s}^{-1}$. A terrain model gives a westerly speed-up of $S(270^\circ) = 1.25$ at 30 m on the crest, which is consistent with the statistical factor of Table 30.2. The terrain correction gives

$$U_{30,\text{site}} = 1.25 \times 7.5\,\text{m}\,\text{s}^{-1} = 9.4\,\text{m}\,\text{s}^{-1}.$$

The historical residual standard deviation of this chain against the mast is $\sigma = 1.2\,\text{m}\,\text{s}^{-1}$, and the budget of Table 30.4 adds the representation of the span, for $1.32\,\text{m}\,\text{s}^{-1}$. A much more

informative forecast than a single number is therefore

$$U_{30} \approx 9.4\,\mathrm{m\,s^{-1}}, \qquad \text{uncertainty about } \pm 1 \text{ to } 2\,\mathrm{m\,s^{-1}},$$

or, as an 80 percent interval with the full budget, $9.4 \pm 1.2816 \times 1.32 = [7.7,\ 11.1]\,\mathrm{m\,s^{-1}}$, rather than a pretended exact $9.375\,\mathrm{m\,s^{-1}}$, the product 1.25×7.5 carried to four digits. The number of digits a model prints is not its precision; its validation is.

The chain of ideas. The book can be condensed into one chain, each link of which is a step of the workflow:

pressure gradients create wind → the Coriolis force organizes large-scale flow
→ boundary-layer turbulence connects that flow to the surface
→ stability controls the strength of that coupling
→ terrain and roughness reshape the local flow
→ measurements observe one local realization
→ models must reconcile all of these scales.

Table 30.8 maps each link to the chapters that develop it and to the step of the workflow of Figure 30.9 that uses it. Its columns are the link, its physical content, the chapters and the workflow steps.

Table 30.8: The chain of ideas of the book, the chapters that develop each link and the workflow steps that use it.

Link	Physical content	Chapters	Workflow steps
Pressure gradients create wind	pressure-gradient force, geopotential, the wind system	1, 2	4, 5
Coriolis organizes large-scale flow	geostrophic and gradient balance, scales of motion	3 to 5	4, 5
Turbulence connects the flow to the surface	boundary layer, surface layer, fluxes, u_*, log profile	6 to 10, 12	3, 5
Stability controls the coupling	stratification, similarity theory, L_{O}, convective and stable layers, jets	13 to 18	4, 7
Terrain and roughness reshape the flow	roughness, thermal circulations, terrain flow, canopies	11, 19 to 21	3, 6
Measurements observe one realization	instruments, exposure, statistics	22 to 24	1, 2, 7
Models reconcile the scales	weather models, schemes, surface, downscaling, CFD, the site model	25 to 30	5 to 9

A defensible site wind model, then, is not simply a high-resolution wind prediction. It combines the correct physical hierarchy, the appropriate scale, good observations, independent validation and an explicit uncertainty. The most important habit it requires is to ask not only whether a model is accurate but why it is accurate, because a model that is right for a reason can be trusted where it has not yet been tested, and one that is right by accident cannot. That habit is what separates a useful local wind model from a fitted number generator, and it is the thread that runs through every chapter of this book, from the pressure gradient that sets the air in motion to the sensor that records one gust of it.

30.7 What to retain

Definition 30.1 (Defensible site wind model)**.** A defensible site wind model predicts an explicitly defined target through the correct physical hierarchy, from large-scale forcing through

the boundary-layer regime to terrain, roughness and obstacles; it is the simplest model that resolves the relevant processes, is validated on independent data by regime, direction and height and against the decision it serves, and states a calibrated uncertainty.

Table 30.9 lists the terms of the chapter, their meaning, their units and the subsection that defines each.

Table 30.9: The terms of the chapter and where each is defined.

Term	Meaning	Units	Defined in
Target variable	exact wind quantity the model predicts: quantity, place, height, averaging, statistic	m/s	30.1, 30.1.2
Baseline model	simple reference model fitted and tested before adding complexity	m/s	30.4.1
Complexity ladder	levels 0 to 5, from raw NWP to LES, climbed only on demonstrated failure	–	30.4.5
Regime validation	evaluation of performance separately by physical state	m/s	30.5.1
Event holdout	testing on whole events withheld from fitting	–	30.5.5
Measurement equation	$y_{\text{obs}} = y_{\text{true}} + \epsilon_{\text{instrument}} + \epsilon_{\text{representativeness}}$	m/s	30.3.4
Representativeness uncertainty	uncertainty due to the spatial or physical mismatch between measurement or model and target	m/s	30.3.4, 30.6.2
Uncertainty budget	σ^2_{total} as the sum of forecast, downscaling, measurement and representation variances	m/s	30.6.2
Out-of-distribution	conditions unlike those used to build or validate the model	–	30.5.8
Probabilistic calibration	agreement between forecast probabilities and observed frequencies; coverage of intervals	–	30.6.3
Decision metric	quantity that directly affects the engineering decision, e.g. $\Pr(U_\perp < 1.5\,\text{m s}^{-1})$	–	30.6.4, 30.6.5
Cross-wind $U_\perp$	wind component perpendicular to a conductor, $U\lvert\sin\gamma\rvert$	m/s	30.6.5
Compensating errors	several model errors that accidentally cancel in the validated quantity	–	30.5.7
Physical consistency	compliance of predictions with governing physical constraints	–	30.5.8

30.8 Exercises

Exercise 30.1. A model is validated on a test year by regime. Convective hours (25 percent) have a bias of $-0.2\,\text{m s}^{-1}$ and an RMSE of $1.1\,\text{m s}^{-1}$; neutral hours (45 percent) a bias of 0 and an RMSE of $0.9\,\text{m s}^{-1}$; stable hours (30 percent) a bias of $+1.5\,\text{m s}^{-1}$ and an RMSE of $2.5\,\text{m s}^{-1}$. (a) Compute the overall bias and RMSE, and the share of the mean square error contributed by the stable hours. (b) Compute the random part σ_e in the stable regime and say which physical causes the bias and the random part point to. (c) At the same site the westerly error is $0.9\,\text{m s}^{-1}$ and the easterly error $3.0\,\text{m s}^{-1}$. What westerly share of the hours makes the overall RMSE equal to $1.5\,\text{m s}^{-1}$, if these two sectors make up the record? (d) Which of the two breakdowns calls for a terrain or exposure correction, and which for a change in the boundary-layer treatment?

Exercise 30.2. The uncertainty of a hub-height wind has a forecast part of $1.1\,\text{m s}^{-1}$, a downscaling part of $0.5\,\text{m s}^{-1}$, a measurement part of $0.2\,\text{m s}^{-1}$ and a representation part of $0.4\,\text{m s}^{-1}$. (a) Compute the total standard deviation in quadrature and the linear sum, and the

variance share of each part. (b) Compute an 80 percent interval about a prediction of $9.0\,\mathrm{m\,s^{-1}}$ ($z_{0.9} = 1.2816$). (c) Historical residuals against the mast give $1.2\,\mathrm{m\,s^{-1}}$. Which parts does that residual contain, and what does it omit? (d) The model's 80 percent intervals, built with the overall σ, cover 0.92 of the observations by day and 0.58 at night. Compute the factor by which each regime's σ must be multiplied ($\Phi^{-1}(0.96) = 1.751$, $\Phi^{-1}(0.79) = 0.806$).

Exercise 30.3. A transmission line at 25°S runs along the azimuth $\beta_\ell = 20°$. The weather model gives $8\,\mathrm{m\,s^{-1}}$ from 10° at 100 m; at the conductor height of 20 m the speed is $5.5\,\mathrm{m\,s^{-1}}$ and the wind is turned by 12° relative to 100 m. (a) Compute γ and $U_\perp$ using the 100 m direction. (b) Decide the sense of the turning in the Southern Hemisphere and compute γ and $U_\perp$ at 20 m; repeat for the same geometry at 25°N. (c) For each case, is the cross-wind below $1.5\,\mathrm{m\,s^{-1}}$? (d) With the angle factor $K(\gamma)$ of Section 30.6.5 and cooling proportional to $U^{0.6}$, compare the cooling in the Southern Hemisphere case with that of a $3\,\mathrm{m\,s^{-1}}$ wind perpendicular to the line. (e) Compute $\mathrm{d}U_\perp/\mathrm{d}\gamma$ at 20 m in the Southern Hemisphere case and the change of $U_\perp$ for a direction error of 8°.

Exercise 30.4. A site model predicts the wind at a 40 m conductor on a crest. The weather model gives $U_{100} = 11\,\mathrm{m\,s^{-1}}$ from the west in neutral air over $z_0 = 0.1$ m, and a terrain model gives $S(270°) = 1.2$ at 40 m. (a) Compute the background wind at 40 m with the neutral log profile and the site wind. (b) Repeat (a) for a stable evening with $L_\mathrm{O} = +200$ m and the Businger–Dyer form $\psi_m = -5\,z/L_\mathrm{O}$, keeping the speed-up unchanged, and say why that assumption is doubtful on a stable evening. (c) A low-wind model is scored on 1500 hours with 120 events: 84 hits, 36 misses and 50 false alarms. Compute the probability of detection, the false-alarm ratio and the cost with 1 per action and 8 per miss, and the probability above which acting is cheaper. (d) The 120 events come from 15 calm nights. Compute the relative standard error of an RMSE estimated from 120 independent values and from 15, and say which applies.